New Strategies in Oxidative Bond Formation

By

Karina Targos

A dissertation submitted in partial fulfillment of

the requirements for the degree of

Doctor of Philosophy

(Chemistry)

at the

UNIVERSITY OF WISCONSIN-MADISON

2023

Date of final oral examination: 12/13/23

The dissertation is approved by the following members of the Final Oral Committee:

Zachary K. Wickens, Professor, Organic Chemistry

Samuel H. Gellman, Professor, Organic Chemistry, Chemical Biology, Materials Chemistry, Physical Chemistry

Daniel J. Weix, Professor, Organic Chemistry, Inorganic Chemistry

Clark R. Landis, Professor, Organic Chemistry, Inorganic Chemistry

Acknowledgements

Graduate school has been an unexpected journey filled with challenges and triumphs. I am thankful for the collaborative spirit within the chemistry department at UW-Madison. Even when several buildings were shut down for months due to construction, our colleagues ensured continuity in our research by opening their lab spaces to us. I would like to express my appreciation to the dedicated staff at the Paul Bender Chemical Instrument Center (CIC). They played a crucial role in navigating the challenges imposed by both COVID-19 measures and persistent building construction. The seamless operation from the CIC was indispensable for sustaining research momentum over these strange few years.

I am sincerely grateful for the unique experience of being a part of the Wickens group during its formative years. It's been a privilege to witness the evolution of the group with each passing year and each new cohort of wonderful people. Through all its changes, the group has maintained a commitment to cultivating a supportive research environment. I appreciate this commitment as it has played a pivotal role in shaping my perspectives and enriching my overall graduate school journey. I am especially thankful to Sara Alektiar, a trusted confidant whose relentless dedication to intellectual rigor propelled me forward not only in scientific pursuits but also nudged me towards personal growth.

To Zach, my deepest gratitude. His constant support and belief in me shaped me as a scientist and as a human. From the moment he took a chance on me by welcoming me into the group, I've been continually amazed by his impossible patience and immense encouragement. It's unbelievable that he's put up with me all this time. From him, I learned the intricacies of conducting impactful scientific research. Beyond academia, he taught me the importance of extending kindness to others and, perhaps most crucially, treating myself with grace. I consider myself so fortunate to have had Zach as a mentor and I eagerly anticipate the continued growth of our relationship beyond graduate school. Zach, your impact on my journey is immeasurable, and for that, I am forever grateful. Thank you for your guidance and the invaluable lessons that will undoubtedly resonate throughout my career and personal life.

Most importantly, to my husband, Joey– I am filled with overwhelming love. Your support has been my anchor, and I truly couldn't have accomplished anything without you. Your unwavering encouragement

and understanding have been the driving force behind my academic successes. I am profoundly blessed to have you by my side and am so excited for the next chapter of our lives together.

To everyone who has been a part of this academic journey, I am thankful for the foundation you have laid, and I am excited about the possibilities that lie ahead.

Philippians 4:13

Table of Contents

Acknowledgements ii

Table of Contents iv

Research Summary viii

Chapter 1

New Approaches to Oxidative Alkene Functionalization Unlocked by Thianthrenation

1.1 Overview 1

1.2 Introduction 2

1.3 Alkenes as alkenyl cation equivalents 3

1.4 Alkenes as vicinal dication equivalents 10

1.5 Alkenes as *Z*-allyl cation equivalents 15

1.6 Conclusion and Outlook 21

1.7 Acknowledgements 22

1.8 References 23

Chapter 2

Electrochemical Synthesis of Allylic Amines from Terminal Alkenes and Secondary Amines

2.1 Abstract 28

2.2 Introduction 28

2.3 Results and Discussion 31

2.4 Conclusion 37

2.5 Acknowledgements 38

2.6 References 39

Chapter 3

Unraveling the Mechanism of Z*-selective Allylic Functionalization* via *Thianthrenium Salts*

3.1 Abstract 46

3.2 Introduction 47

3.3 Results and Discussion 48

3.4 Conclusion 56

3.5 Acknowledgements 57

3.6 References 57

Chapter 4

General Z*-Selective Allylic Functionalization of Alkenes* via *Thianthrenium Salts*

4.1 Abstract 62

4.2 Introduction 62

4.3 Results and Discussion 64

4.4 Conclusion 68

4.5 Acknowledgements 68

4.6 References 68

Chapter 5

Catalytic Base Enabled 1,2-Addition of N*-Nucleophiles into Alkenylthianthrenium Salts*

5.1 Abstract 70

5.2 Introduction 71

5.3 Results and Discussion 73

5.4 Conclusion 83

5.5 Acknowledgements 83

5.6 References 83

Chapter 6

Diastereoselective Synthesis of Cyclopropanes from Carbon Pronucleophiles and Alkenes

6.1 Abstract 88

6.2 Introduction 88

6.3 Results and Discussion 91

6.4 Conclusion 97

6.5 Acknowledgements 97

6.6 References 98

Chapter 7

Electrochemical Z-selective C(sp^2)–H Functionalization of Alkenes

7.1 Abstract 106

7.2 Introduction 107

7.3 Results and Discussion 108

7.4 Conclusion 116

7.5 Acknowledgements 117

7.6 References 117

Chapter 8

Unveiling Potent Photooxidation Behavior of Catalytic Photoreductants

8.1 Abstract 119

8.2 Introduction 120

8.3 Results and Discussion 122

8.4 Conclusion 128

8.5 Acknowledgements 129

8.6 References 130

Appendix A: Supporting Information for Chapter 2 *(Electrochemical Synthesis of Allylic Amines from Terminal Alkenes and Secondary Amines)* 136

Appendix B: Supporting Information for Chapter 3 *(Unraveling the Mechanism of* Z*-selective Allylic Functionalization* via *Thianthrenium Salts)* 186

Appendix C: Supporting Information for Chapter 4 *(General* Z*-Selective Allylic Functionalization of Alkenes* via *Thianthrenium Salts)* 286

Appendix D: Supporting Information for Chapter 5 *(Catalytic Base Enabled 1,2-Addition of* N-*Nucleophiles into Alkenylthianthrenium Salts)* 291

Appendix E: Supporting Information for Chapter 6 *(Diastereoselective Synthesis of Cyclopropanes from Carbon Pronucleophiles and Alkenes)* 308

Appendix F: Supporting Information for Chapter 7 *(Electrochemical Z-selective C(sp^2)–H Functionalization of Alkenes)* 398

Appendix G: Supporting Information for Chapter 8 *(Unveiling Potent Photooxidation Behavior of Catalytic Photoreductants)* 409

Research Summary

Hydrocarbon feedstocks are plentiful and new methods to engage them in oxidative bond forming reactions are an important frontier of organic synthesis. While photochemistry and electrochemistry offer appealing energy inputs for transforming these feedstocks into value-added products, existing strategies to directly engage unsaturated precursors in bond forming reactions are limited due to the high oxidation potentials required (>2 V vs. SCE). This not only limits functional group tolerance, but also poses nucleophile compatibility challenges. My dissertation work has focused on the development of new activation modes to engage hydrocarbons in oxidative bond forming reactions that overcome the limitations of conventional photoredox and electrosynthetic strategies.

The first portion of this thesis is an overview of recent developments in oxidative alkene functionalization (**Chapter 1**). In particular, the introductory discussion will focus on cationic synthons unlocked by alkene thianthrenation. Recently, our group has developed the electrogeneration of meta-stable dicationic adducts between thianthrene and alkenes under mild anodic oxidation. In my work, we leveraged this alkene activation for allylic bond forming reactions with a range of nucleophiles, such as oxidatively sensitive alkyl amines (**Chapter 2**). We then outlined a detailed mechanistic study that explains this reactivity and the origin of *Z*-selectivity (**Chapter 3**). Unpublished investigations of the scope of *Z*-selective allylic functionalization will be presented (**Chapter 4**), as well as insights into diverting the reactivity of alkenylthianthrenium salts from allylic pathways towards difunctionalization reactions (**Chapter 5**). Additionally, we have leveraged thianthrenium electrophiles for cyclopropane strained-ring synthesis (**Chapter 6**). Finally, a new electrochemical *Z*-selective transformation of alkene-thianthrenium adducts will be presented with a focus on outlining the stereodetermining step of this process (**Chapter 7**).

The final chapter will describe another engine to drive oxidative bond formation using visible light energy (**Chapter 8**). *N*-phenylphenothiazine—a conventional photoreductant—was coaxed into potent photooxidant behavior in the presence of O_2 and lithium cation co-catalyst. This photocatalytic system enables oxidation of benzene for C–N bond formation with nitrogen-containing heterocycles using simple LEDs.

Taken together, these two new strategies offer distinct and powerful advantages relative to the state-of-the-art in oxidative construction of new bonds from unsaturated precursors.

Chapter 1: New Approaches to Oxidative Alkene Functionalization Unlocked by Thianthrenation

A minireview by Min Ji Kim,[†] **Karina Targos**,[†] Dylan E. Holst, Diana J. Wang, and Zachary K. Wickens. [†]M.K. and K.T. contributed equally.

1.1 Overview

Oxidative alkene functionalization reactions are a fundamental class of complexity-building organic transformations. However, the majority of established approaches rely on electrophilic reagents that limit the diversity of groups that can be installed. Recent advances have established a new approach that instead relies on the transformation of alkenes into thianthrene-derived cationic electrophiles. These linchpin intermediates can be generated selectively and undergo a diverse array of mechanistically distinct reactions with abundant nucleophiles. Taken together, this unlocks a suite of net oxidative alkene transformations that have been elusive using conventional strategies. This minireview describes these advances and is organized around the three distinct synthons formally accessible from alkenes *via* thianthrenation: 1) alkenyl cations; 2) vicinal dications; 3) allyl cations. Throughout the minireview, we illustrate how thianthrenium salts address key limitations endemic to classic alkene-derived electrophiles and highlight the mechanistic origins of these distinctions wherever possible.

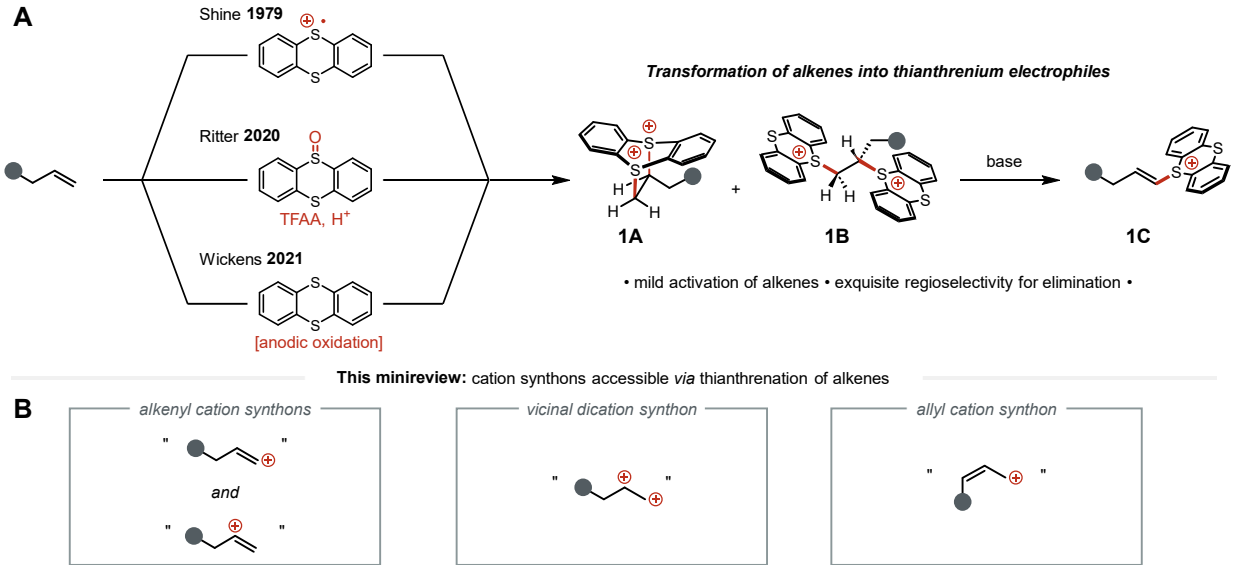

Figure 1.1. Overview of minireview. (A) Preparation of thianthrenium salt electrophiles from alkenes. (B) Three reactivity manifolds discussed in this chapter.

1.2 Introduction

Oxidative alkene functionalization is a premier tactic for the synthesis of densely functionalized molecules.[1–3] Decades of research in this area have focused on leveraging high energy species derived from either common nucleophiles (*e.g.* amines, alcohols, etc.) or the alkene itself (Figure 1.1).[4,5] Tremendous progress has been made by exploiting electrophilic reagents, wherein the formerly nucleophilic coupling partner is incorporated into an oxidant. For example, peroxides are used for alkene epoxidation rather than water.[6] The alkene can alternatively be transformed into a versatile electrophile that can be directly engaged with widely available nucleophiles. For example, epoxidation of alkenes sets the stage for nucleophilic ring opening to prepare a diverse array of alcohol-containing products.[7] In principle, an implementation of this strategy wherein the alkene-derived electrophile does not dictate the functional groups present in the final product would be particularly appealing. While alkenes can be transformed into a variety of traceless electrophiles through halogenation (*e.g.* dihalides and allylic halides), translation of this reactivity manifold into a general tactic for alkene functionalization has been stymied by selectivity challenges in the synthesis of requisite electrophilic intermediates as well as the downstream nucleophilic displacement.[5,8–11]

Recent advances in the transformation of alkenes into thianthrenium electrophiles have set the stage for a new approach to oxidative alkene functionalization. These efforts are part of an emerging area leveraging thianthrenium salts broadly in synthesis, which have been recently reviewed.[12–14] Studies regarding thianthrenium salts date back to the late 1970s with extensive early investigations from Shine and co-workers.[15–17] In the context of alkenes, these studies revealed that treatment of alkenes with thianthrene radical cation provides two distinct dicationic thianthrene-alkene adducts (**1A** and **1B**).[18] Further studies illustrated that these adducts undergo elimination to alkenylthianthrenium salts (**1C**).[15,19] While these early observations were intriguing, their translation into synthetic methods remained largely unexplored until efficient protocols were introduced decades later to access these key intermediates. First, Ritter and co-workers built on their prior work in arene thianthrenation[20] and introduced an operationally simple approach to transform alkenes into analogous adducts by deoxygenative activation of thianthrene S-oxide (TT S-oxide). Subsequently, Wickens and co-workers advanced an approach to prepare these adducts *via* anodic

oxidation of thianthrene (TT) in service of a new electrochemical alkene aziridination method.[21] Taken together, these two protocols provide a new means to transform alkenes into versatile sulfonium electrophiles that expands beyond prior approaches that were restricted to activated vinylarene substrates.[13,22–24]

This minireview will provide an overview of the oxidative alkene functionalization reactions unlocked by the modern protocols to transform alkenes into thianthrenium electrophiles. These species have been found to offer distinct reactivity and selectivity advantages relative to conventional halide-based electrophiles. The review is organized around the three distinct electrophilic identities that have been exploited from the thianthrenium-alkene adducts: (1) alkenyl electrophiles, (2) vicinal dielectrophiles, and (3) allylic electrophiles. Throughout this review, comparisons will be made to conventional halide-based electrophiles that are, in many cases, also accessible from alkenes. Of note, alkene thianthrenation has facilitated the translation of the well-established reactivity of vinylsulfonium salts[12,13,25–27] derived from 1,2-bromosulfonium ethane into a diverse array of alkene functionalization transformations. Further distinctions between thianthrenium salts and other sulfonium electrophiles will be discussed where the relevant comparisons have been made. Finally, we will offer our perspective on future opportunities regarding the use of thianthrene to enable novel oxidative alkene functionalization reactions.

1.3 Alkenes as alkenyl cation equivalents

Alkenylthianthrenium salts have been leveraged as alkenyl electrophiles in mechanistically diverse transformations. These new reactions take advantage of distinct reactivity of alkenylthianthrenium salts towards (1) transition metal catalysts via oxidative addition into the C(sp^2)–S bond, as well as (2) polar nucleophiles *via* conjugate addition to form a sulfonium ylide intermediate (Figure 1.2). Overall, these reactivity patterns enable the use of alkenes as an alkenyl cation synthon at either of the alkene C(sp^2)-sites.

There are two key distinctions between alkenylthianthrenium salts and the corresponding alkenylhalide: the alkenylthianthrenium salts are (1) more straightforward to access directly from alkenes and (2) amenable to more diverse reactivity manifolds. While the thianthrene-alkene dicationic adducts

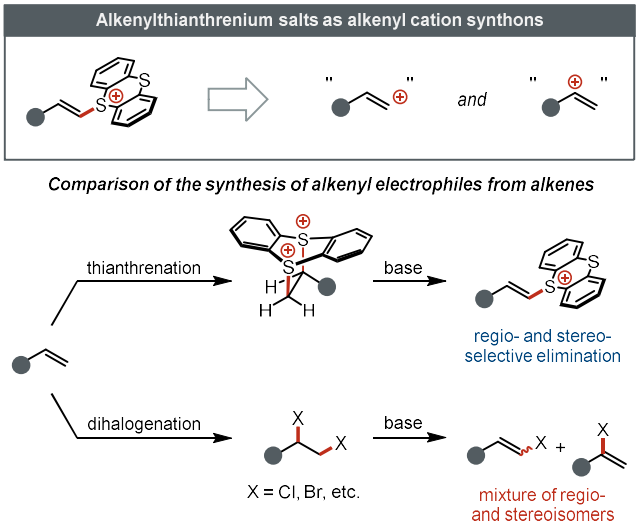

Figure 1.2. Alkenylthianthrenium electrophiles allow alkenes to be used as alkenyl cation synthons.

resemble dihalides, their elimination behavior–and thus their utility in accessing alkenyl electrophiles–is distinct (Figure 1.2). Elimination of dicationic thianthrenium salts provides exclusively the linear regioisomer with high selectivity for the *E*-stereoisomer. In contrast, elimination of vicinal dihalides to alkenylhalides suffers from both poor regio- and stereoselectivity, yielding difficult to separate mixtures.[28–30] To circumvent this problem, alkenylhalides are more commonly prepared from the corresponding alkynes rather than alkenes.[31–33] Furthermore, reactions have been developed to substitute alkenylthianthrenium salts at both the *ipso*- and *cine*-positions, offering a stark contrast to the *ipso*-substitution chemistry of alkenylhalides.

In 2020, Ritter and co-workers reported the first general synthesis of alkenylthianthrenium salts and provided important initial insight into their synthetic utility (Scheme 1.1).[20] The authors illustrated how this enables formal alkenyl C(sp^2)–H activation using a variety of metal-catalyzed coupling reactions. Specifically, a model alkenylthianthrenium salt **1.1** was shown to be competent as an electrophile in C–C

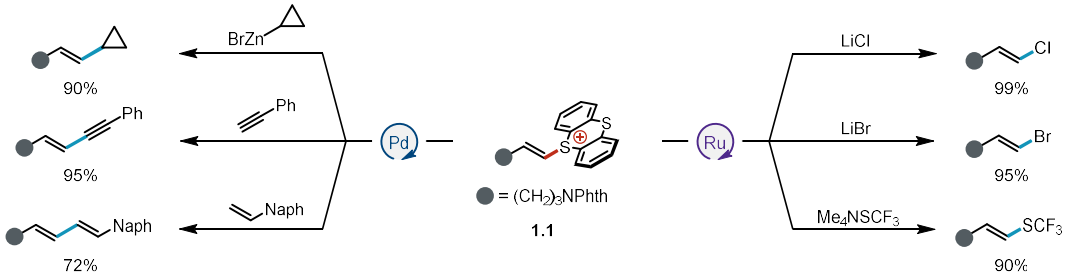

Scheme 1.1. Cross-coupling reactions using thianthrenium electrophiles reported by Ritter and co-workers.[20]

bond forming reactions including Negishi, Sonogashira, and Heck cross-couplings.[34–37] These cross-coupling reactions each generated the desired products in high yield with an *E*-stereochemical configuration. In addition to palladium-catalyzed couplings, the thianthrenium electrophile was engaged using ruthenium catalysts that often suffer from lack of reactivity with alkenylhalides due to slow oxidative addition. This enables a collection of functional group interconversion processes that replace the thianthrenium moiety with halogens as well as a trifluorothioether.

In 2021, Ritter and co-workers showed that an inexpensive feedstock, ethylene, can be broadly employed as a formal vinylating agent *via* transformation into a vinylthianthrenium salt. (Scheme 1.2).[38] This work focused on the utility of vinylthianthrenium salt as a practical replacement of vinylhalides, which are often toxic and carcinogenic gases.[39] First, the authors benchmarked the reactivity of this

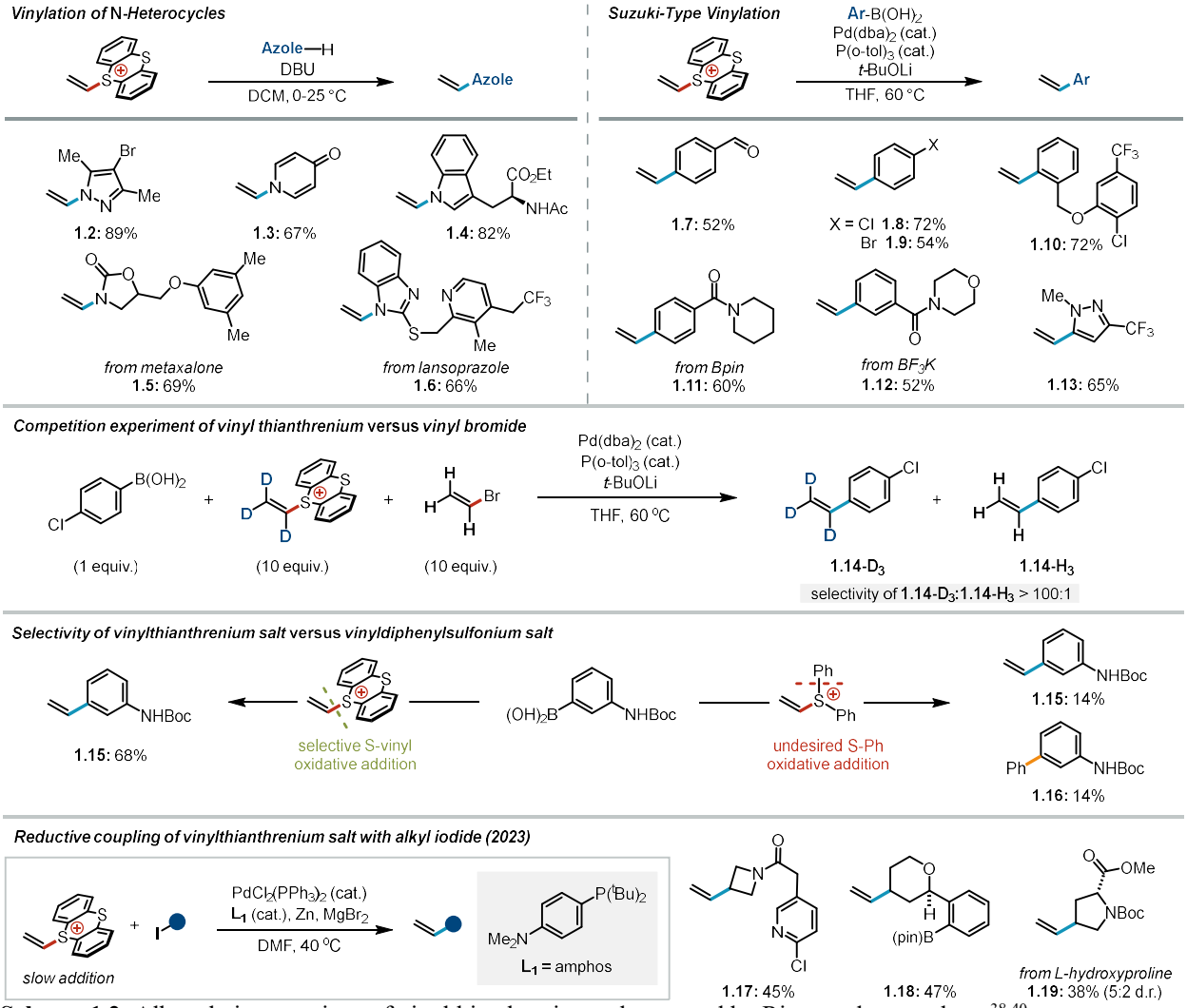

Scheme 1.2. Alkenylation reactions of vinylthianthrenium salt reported by Ritter and co-workers.[38,40]

vinylthianthrenium salt in established annulation reactions of vinyldiphenylsulfonium salts and found that this new reagent furnishes the desired products in similar or improved yields. Next, they illustrated that vinylthianthrenium salts can be employed as vinyl electrophiles under Suzuki-type coupling conditions across a wide range of (hetero)aryl boronic acids. Beyond transition-metal-catalyzed processes, this reagent can be employed in *N*-vinylation of azacycles such as indoles, pyrazoles, pyridones, and cyclic carbamates via conjugate addition and elimination. In this study, Ritter and co-workers also demonstrated the distinct advantages of vinylthianthrenium salts relative to established vinyl electrophiles. One-pot competition experiments illustrated that the vinylthianthrenium salt is a more reactive electrophile than vinylbromide in the Suzuki-type cross-coupling reaction. This observation rationalizes the tolerance of various other C(sp^2) electrophiles (*e.g.* arylbromides) in the scope of the Suzuki-type vinylation. In addition to their reactivity advantages over vinylhalides, the vinylthianthrenium salts also addressed the substantial oxidative addition selectivity problems that have precluded the use of vinyldiphenylsulfonium salts in cross-coupling chemistry. While this minireview was under review, Ritter and co-workers reported an exciting expansion of this reactivity to include reductive cross coupling with alkyl iodides using a palladium catalyst.[40]

In 2021, Huang and co-workers illustrated that alkenylthianthrenium salts undergo copper-catalyzed silylation and borylation at the *ipso*-position (Scheme 1.3).[41] Alkenylthianthrenium salts derived from aliphatic terminal, internal, or cyclic alkenes were each successfully functionalized with consistent >9:1 *E*-selectivity. Styrenyl substrates were converted into the corresponding silane or boronic ester products cleanly with high stereoselectivity (≥20:1 *E*:*Z*). Remarkably, a sterically hindered alkenylthianthrenium salt derived from a trisubstituted alkene afforded fully substituted alkene final products **1.22** and **1.31**, albeit in diminished yield. Furthermore, both methods tolerated a range of functional groups, such as alkylbromides, phthalimides and esters. Similar to previous observations from Ritter,[20] the reaction was found to be stereoretentive based on formation of **1.25** from the *E*-alkenylthianthrenium salt and stereoisomeric **1.26** from the *Z*-alkenylthianthrenium salt. Both reactions were shown to be amenable to scale up without change to the reaction conditions.

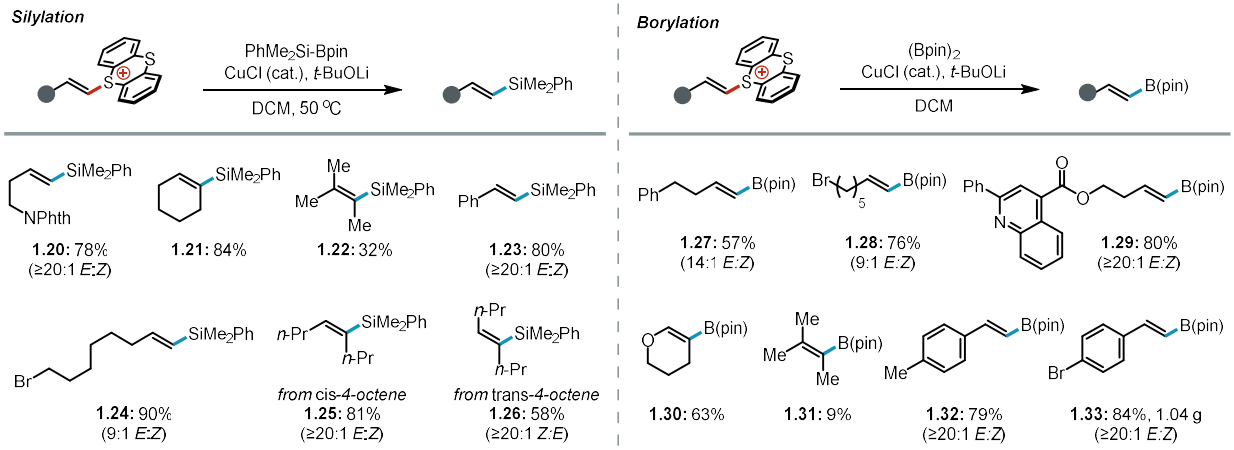

Scheme 1.3. Silylation and borylation using thianthrenium electrophiles reported by Huang and co-workers.[41]

In 2022, Huang and co-workers continued to explore the *ipso*-substitution reactivity of alkenylthianthrenium salts by developing a palladium-catalyzed C(sp^2)–P bond forming reaction with biarylphosphines (Scheme 1.4).[42] Alkenylthianthrenium salts derived from both cyclic and acyclic aliphatic alkenes as well as vinylarenes were found to be competent electrophiles. Furthermore, a variety of pendant functional groups such as alkylhalides, arylhalides, and phthalimides were well-tolerated. Typically, the authors treated the reactions with elemental sulfur to transform the resultant phosphine into the corresponding phosphine sulfide to facilitate isolation and characterization. The reaction was performed on gram scale and gave **1.41** in high yield.

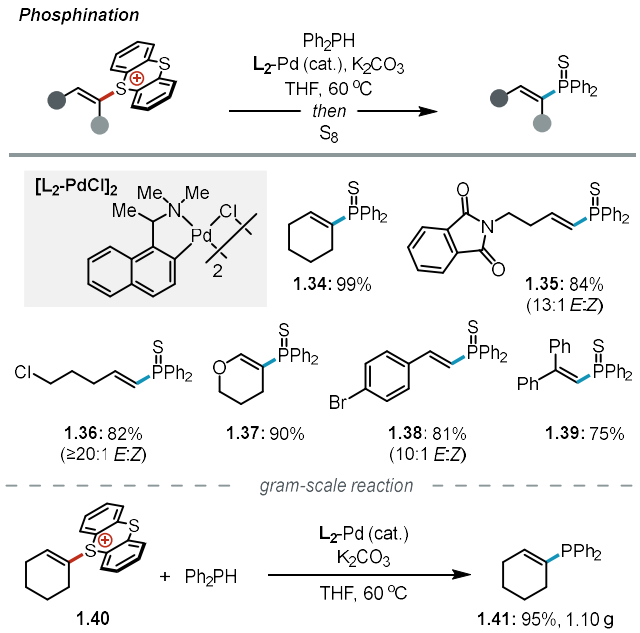

Scheme 1.4. Phosphination of thianthrenium electrophiles reported by Huang and co-workers.[42]

Later the same year, Huang and co-workers reported the regiodivergent arylation of alkenylthianthrenium salts *via* ligand-controlled rhodium catalysis (Scheme 1.5).[43] Use of a diene ligand **L$_3$** yielded *cine*-arylated 1,1-disubstituted alkenes, while use of a bisphosphine ligand **L$_4$** yielded *ipso*-arylated internal alkenes. This regiodivergent methodology clearly highlights the versatility of the alkenylthianthrenium electrophile relative to its halide counterpart. The optimal conditions with the diene ligand gave high regioselectivity for *cine*-substitution for most alkenylthianthrenium salts, though styrenylthianthrenium salts underwent the desired reaction in diminished regioselectivity. In contrast, with the optimal phosphine ligand, *ipso*-selectivity was observed for the coupling of most alkenylthianthrenium salts with arylboroxine partners. The authors proposed that *cine*-substitution pathway involves a reversible rhodium-catalyzed β-hydride elimination and re-insertion of [Rh]–H; they supported this hypothesis with deuterium labeling experiments.

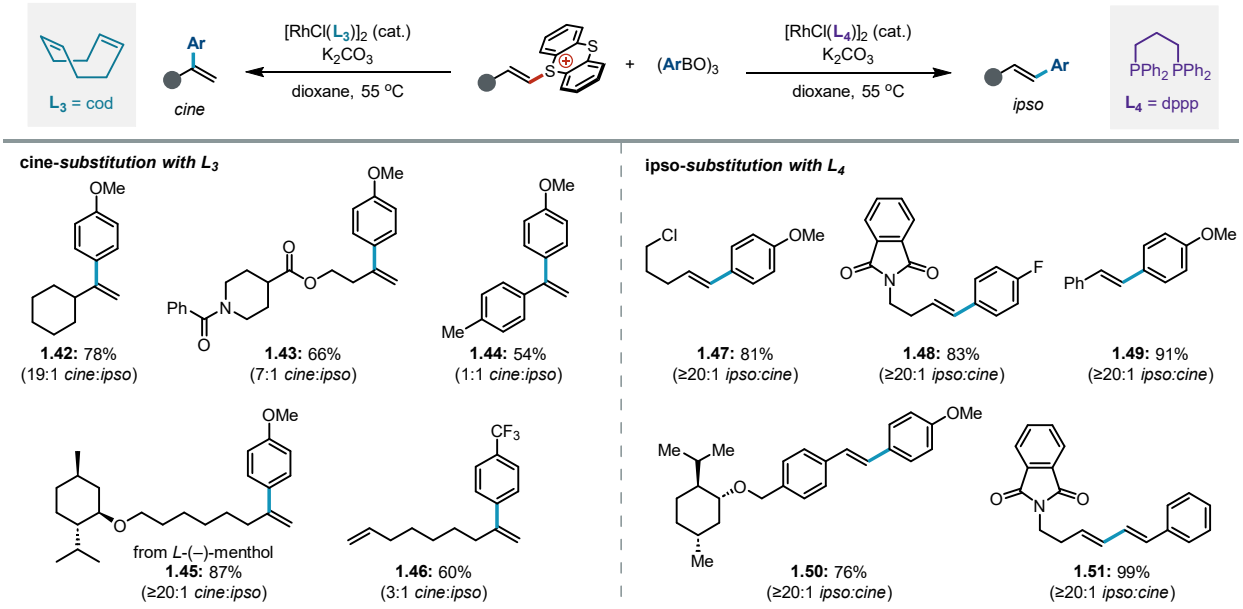

Scheme 1.5. Regiodivergent functionalization using thianthrenium electrophiles reported by Huang and co-workers.[43]

In 2023, Shu and co-workers uploaded a manuscript disclosing a metal-free, heck-type *cine*-functionalization of alkenylthianthrenium salts (Scheme 1.6).[44] Under basic conditions, treatment of alkenyl thianthrenium salts with sulfur, carbon, and nitrogen nucleophiles afforded formal C(sp^2)–H functionalization products *via* conjugate addition and elimination sequences. The authors initially

optimized this reactivity for the synthesis of alkenylsulfones using aryl- and alkylsulfinates as nucleophiles. The reactivity was next translated to the analogous C–C and C–N bond formation: cyanide was used for the preparation of alkenylnitriles and electron-deficient nitrogen nucleophiles such as sulfonamide furnished enamides. Notably, heteroaryl groups such as imidazoles and indoles were competent nucleophiles and furnished *N*-alkenylated products. Various alkenylthianthrenium salts derived from terminal and internal aliphatic alkenes, styrenes, and gaseous alkenes were all competent electrophiles for the *cine*-alkenylation reaction. The authors demonstrated the scalability of this protocol in the context of the sulfonylation reaction. The practicality of the method was demonstrated in a one-pot procedure to access an alkenylimidazole from alkene.

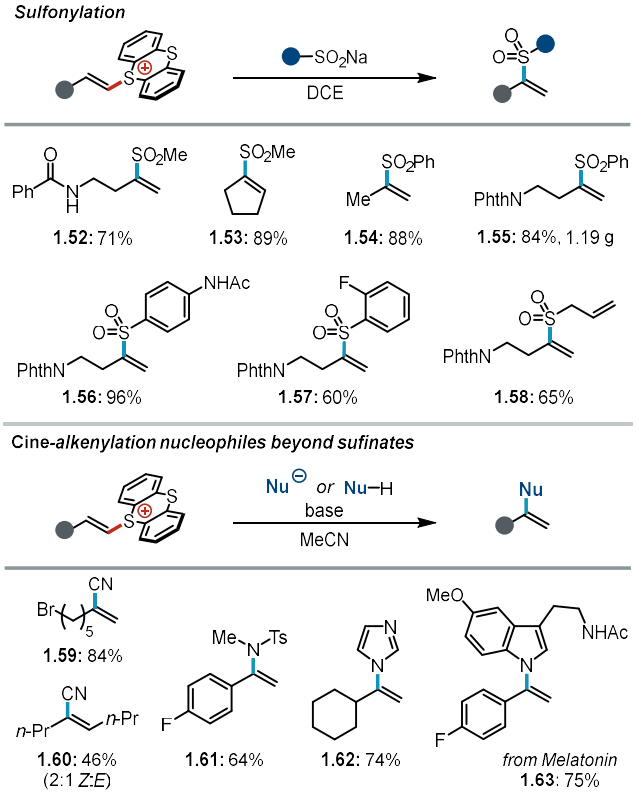

Scheme 1.6. Metal-free *cine* alkenylation of alkenylthianthrenium salt reported by Shu and co-workers.[44]

1.4 Alkenes as vicinal dication equivalents

In this section, the use of thianthrenium electrophiles to enable net alkene difunctionalization reactions will be discussed. These methods have leveraged abundant nucleophiles to generate either strained three-membered rings or vicinal aminofunctionalized products. In principle, either thianthrenium dicationic adducts or alkenylthianthrenium salts could serve as the dielectrophilic species. Overall, this reactivity pattern allows alkenes to be viewed as a formal vicinal dication synthon (Figure 1.3).

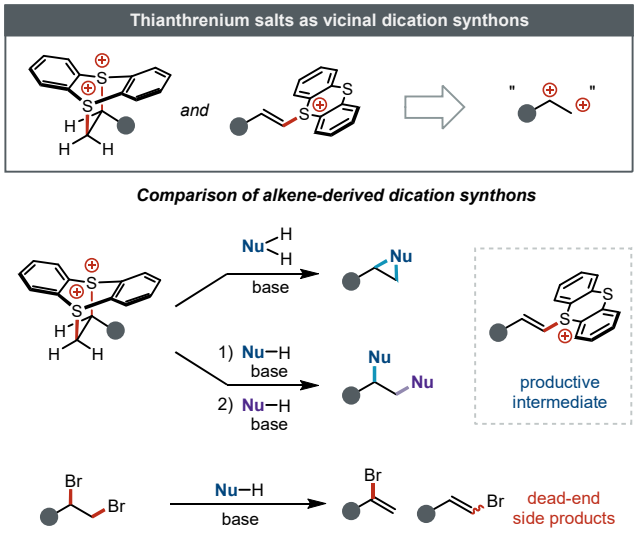

Figure 1.3. Vicinal difunctionalization of alkenes *via* thianthrenium electrophiles.

The reactivity of thianthrenium dielectrophiles is distinct from that of classic analogs (Figure 1.3). While vicinal dihalides can also be readily accessed from alkenes, attempts to leverage these species as dielectrophiles beyond simple 1,2-dihaloethane systems typically result in elimination rather than the desired substitution.[45] This challenge has previously motivated the development of multistep sequences to prepare alternative dielectrophiles that favor substitution over elimination.[46,47] In contrast, the dicationic thianthrenium adducts undergo highly selective formal substitution because their elimination products remain active electrophiles for conjugate-addition-type mechanisms. Furthermore, reactions have been developed to selectively engage each electrophilic site of thianthrenium salts in a sequential fashion, enabling net substitution by two distinct nucleophiles and offering contrast to even the dielectrophilic species that circumvent elimination (*e.g.* cyclic sulfates and bromonium ions).

In 2021, Wickens and co-workers developed an alkene aziridination reaction via the formal coupling of primary amines and terminal alkenes (Scheme 1.7).[21] In this report, a new electrochemical preparation of dicationic adducts was developed by anodic oxidation of thianthrene in the presence of an alkene substrate. Then, in a one-pot manner, substitution of adducts with a primary amine nucleophile under basic conditions (Cs_2CO_3) afforded a diverse set of *N*-alkyl aziridine products. Alkenes bearing proximal and distal functional groups, as well as the gaseous alkene propene, were effectively engaged in the electrochemical aziridination protocol. Amines bearing functional groups that would be challenging to introduce using classic pre-activated, electrophilic nitrogen reagents (*e.g.* oxidatively sensitive groups) underwent efficient aziridination. This protocol enabled improved access to an aziridine drug intermediate **1.68** as well as an array of new analogs (**1.69** and **1.70**). The overall one-pot, two-step procedure was scaled using a commercially-available flow reactor to generate multiple grams of aziridine product **1.71**. This initial report indicated that the formal substitution of the dicationic adducts could occur by either direct substitution or an elimination-conjugate addition pathway that proceeds *via* an alkenylthianthrenium

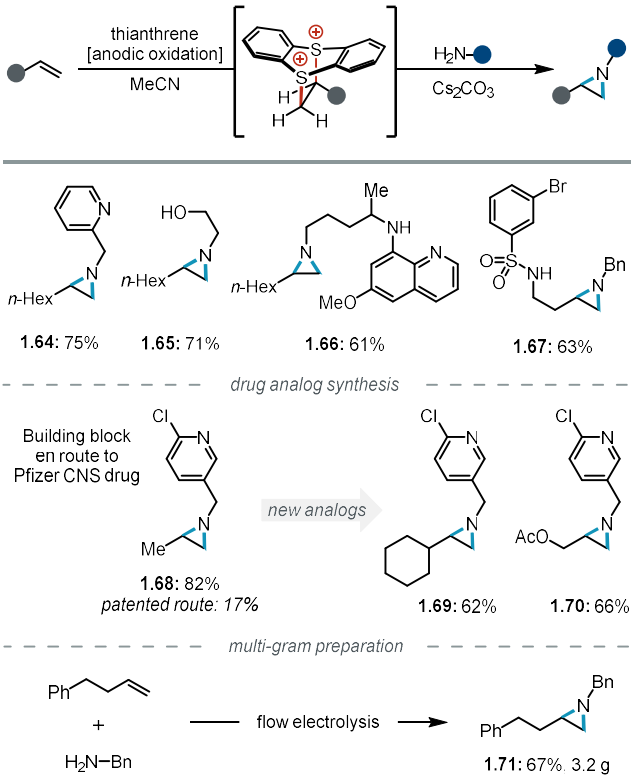

Scheme 1.7. Aziridination of alkenes reported by Wickens and co-workers.[21]

intermediate. Authors from the same research group in a later report (*vide infra*) settled on the elimination-based alkenylthianthrenium pathway as the more likely mechanism.[48]

In 2022, Shu and co-workers developed a unified protocol for three-membered ring synthesis that directly engaged alkenylthianthrenium salts with a variety of nitrogen and carbon nucleophiles (Scheme 1.8).[49] Under basic conditions (K_2CO_3), a range of nitrogen nucleophiles including alkylamines, sulfonamides, carbamates, and amides were converted into the corresponding aziridines in synthetically useful yields. In the same report, the authors leveraged acidic carbon pronucleophiles under basic conditions to enable cyclopropanation of alkenylthianthrenium salts. Disubstituted pronucleophiles, such as malononitrile and malonic esters, were selectively converted into cyclopropane products. With these methodologies, biologically-relevant nitrogen nucleophiles and carbon pronucleophiles were converted into complex aziridines and cyclopropanes, respectively. Alkenylthianthrenium salts derived from both terminal and 1,2-disubstituted alkenes were converted to the desired three-membered ring products. Furthermore, the authors illustrated that this methodology could be adapted to an overall one-pot, two-step protocol starting from the corresponding alkene with minimal loss in yield.

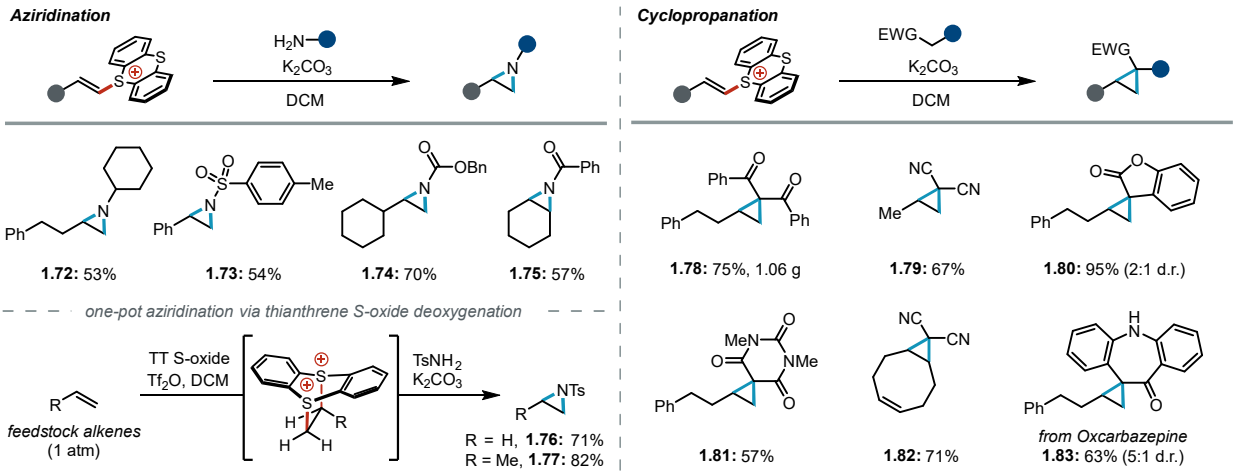

Scheme 1.8. Aziridination and cyclopropanation of alkenylthianthrenium salts reported by Shu and co-workers.[49]

In 2023, Wickens and co-workers reported a formal alkene cyclopropanation protocol that leverages the reactivity of thianthrenium intermediates (Scheme 1.9).[48] In this report, treatment of

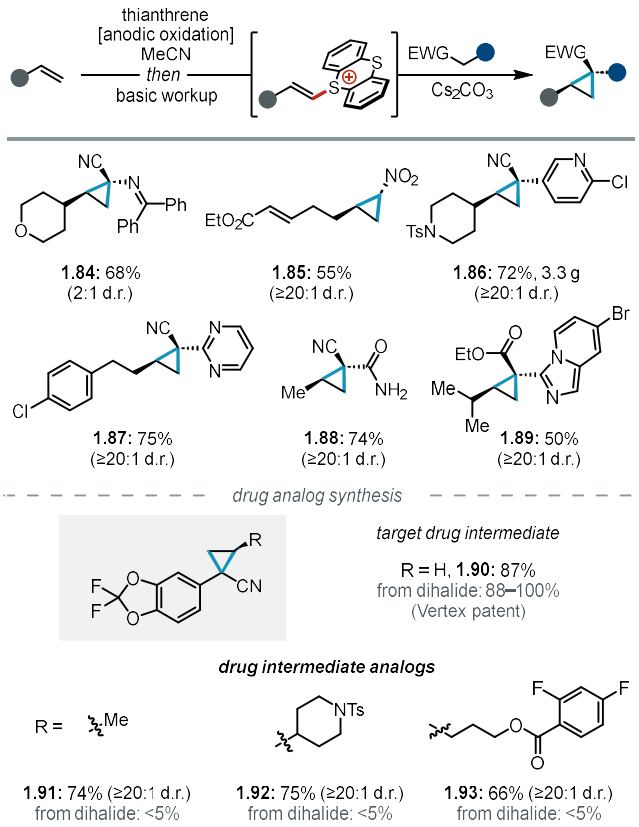

Scheme 1.9. Cyclopropanes of alkenes reported by Wickens and co-workers.[48]

electrochemically-generated thianthrenium electrophiles with diverse carbon pronucleophiles and a base (Cs_2CO_3) afforded substituted cyclopropane products. Of note, basic heterocycles, such as pyridines and pyrimidines, served as suitable secondary electron-withdrawing groups on the carbon coupling partner. The authors found that steric differentiation between the two electron-withdrawing groups conferred substantial diastereoselectivity. For example, organonitrile pronucleophiles typically resulted in highly diastereoselective cyclopropanation (≥20:1 d.r.). Furthermore, a suite of cyclopropane building blocks were synthesized from gaseous feedstock alkenes. The utility of the method was illustrated through the synthesis of substituted derivatives (**1.92–1.93**) of cyclopropane-containing drug intermediate **1.90** that were inaccessible using established methods that relied on dihalide substitution. Mechanistic studies revealed that an alkenylthianthrenium species, generated from elimination of the dicationic adducts, was a key intermediate *en route* to the cyclopropane products. These observations prompted a similar series of experiments regarding the authors' prior work on aziridination, which supported an analogous mechanism.

In 2023, Wickens and co-workers reported a distinct reactivity pattern for thianthrenium electrophiles that expanded beyond strained-ring synthesis and introduced a suite of net alkene aminofunctionalization processes (Scheme 1.10).[50] The key observation of this work was that treatment of dicationic adducts with potassium phthalimide generated a 1,2-phthalimidosulfonium salt as a single constitutional isomer. The resultant alkylthianthrenium intermediate could be isolated by precipitation. These electrophilic salts were subsequently substituted by a diverse array of second nucleophiles, including carboxylates, thiolates, and amines. This reactivity was adapted to a one-pot procedure wherein phthalimide and various amine nucleophiles are formally delivered across the alkene to accomplish net diamination. Mechanistic studies provided a plausible rationale for the apparent regiospecific substitution. The dicationic adducts were found to eliminate *in situ* to an alkenylthianthrenium intermediate **1.99** that undergoes attack at the β-position by potassium phthalimide in a conjugate-addition-type mechanism. Consistent with the

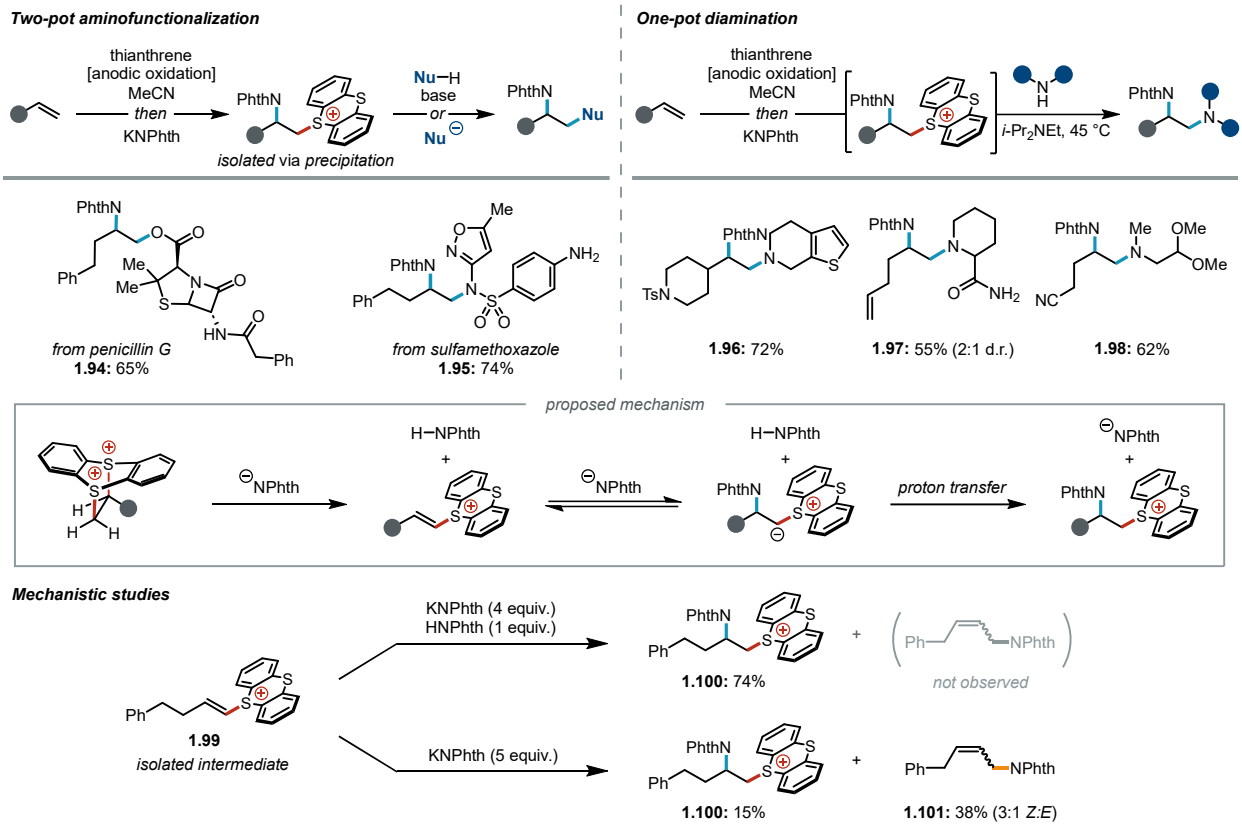

Scheme 1.10. Aminofunctionalization *via* thianthrenium salts and mechanistic studies reported by Wickens and co-workers.[50]

proposed mechanism, isolated alkenylthianthrenium salt **1.99** is kinetically competent in the reaction as long as the proton liberated through adduct elimination is restored by addition of phthalimide alongside potassium phthalimide.

1.5 Alkenes as *Z*-allyl cation equivalents

The reactivity manifolds discussed thus far involve addition of a new functional group directly at the carbons of the alkene. Transformation of alkenes into thianthrenium electrophiles, however, offers a third distinct reactivity pattern: net allylic C(sp^3)–H functionalization (Figure 1.4). This reactivity typically proceeds with exquisite regioselectivity for linear over branched allylic products, and furthermore, exhibits a preference for formation of *Z*-alkene products. This transformation offers a complementary platform for allylic functionalization to established metal-catalyzed approaches as well as recent advances.[51–56] Overall, this reactivity pattern of thianthrenium electrophiles enables use of alkenes as *Z*-allylic cation synthons.

The allylic functionalization reactivity accessed from thianthrenium electrophiles is distinct from that of classic allylic electrophiles (*e.g.* allylbromides). In contrast to the selectivity for linear product formation using the thianthrene-based approaches, the regioselectivity observed using halogenation sequences is often diminished by two distinct problems: (1) synthesis of allylic halides from alkenes can be poorly regioselective, and (2) substitution can produce a mixture of linear and branched allylic products due to competition between S_N2 versus S_N2' pathways. Furthermore, dibromination byproducts are often

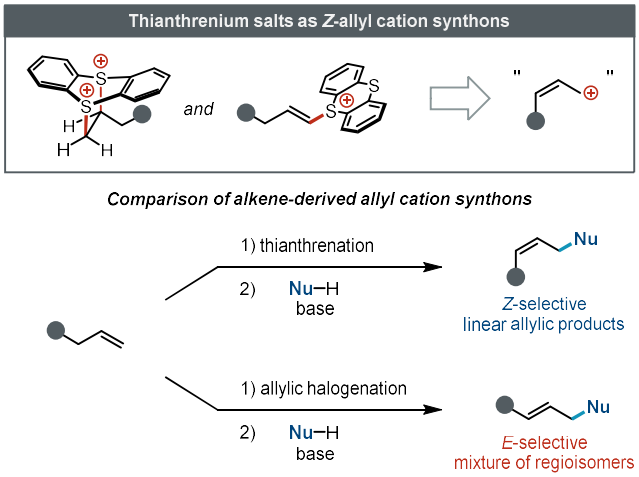

Figure 1.4. Allylic functionalization of alkenes *via* thianthrenium electrophiles.

observed in allylic halogenation processes using electrophilic bromine reagents, such as *N*-bromosuccinimide (NBS).[57] The *Z*-selectivity typically observed using thianthrenium salts offers another major distinction (Figure 1.4). The corresponding *Z*-allylic electrophiles are inaccessible from alkene precursors. Instead, classic *Z*-allylic electrophiles are typically accessed via a multistep sequence involving alkynol semi-hydrogenation followed by transformation of the alcohol into a leaving group.

In 2021, Wickens and co-workers developed an allylic amination method wherein terminal alkenes and amines are formally coupled (Scheme 1.11).[58] In this report, electrochemically-generated alkene-thianthrene dicationic adducts were treated with base (*i*-Pr_2NEt) and a secondary aliphatic amine nucleophile in a one-pot protocol to afford allylic amine products. Feedstock alkenes were amenable to electrochemical activation and subsequent allylic amination. Notably, dicationic adducts derived from 1-butene underwent allylic substitution to afford *Z*-crotylamines in high *Z*-selectivity (≥9:1 *Z:E*). The reaction was effective for both cyclic and acyclic secondary amines, including those embedded within complex

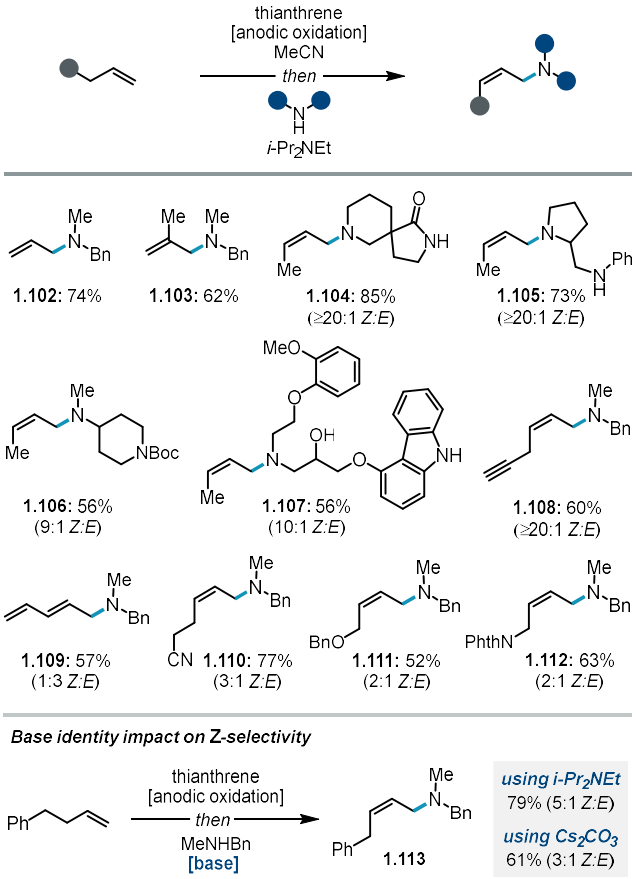

Scheme 1.11. Allylic amination of alkenes with secondary amines reported by Wickens and co-workers.[58]

biologically-active molecules. Alkenes bearing a variety of proximal functional groups were converted to the corresponding allylic amine building blocks, albeit in diminished *Z*-selectivity (1:1 to 6:1 *Z:E*). The Brønsted base used to promote the reaction was identified as the key to maximizing the *Z*-selectivity of the processes, with sterically hindered trialkylamine bases proving optimal. The authors advanced a working hypothesis that the reaction proceeds through isomerization of the alkenylthianthrenium salt to an allylic thianthrenium intermediate, but this species was not directly observed.

Contemporaneously to the report described above, Shu and co-workers developed a related allylic functionalization procedure enabled by transformation of alkenes into alkenylthianthrenium salts (Scheme 1.12).[59] In this report, the alkenylthianthrenium salts, upon treatment with K_2CO_3 base, underwent allylic functionalization with diverse oxygen, nitrogen, and sulfur nucleophiles. The authors found that a wide variety of carboxylic acids were amenable to the process, from simple acetic acid to more complex bioactive acids. Carboxylic acids were also found to engage thianthrenium salts derived from cyclic internal alkenes of various sizes in formal allylic functionalization reactivity. With alkenylthianthrenium salts derived from

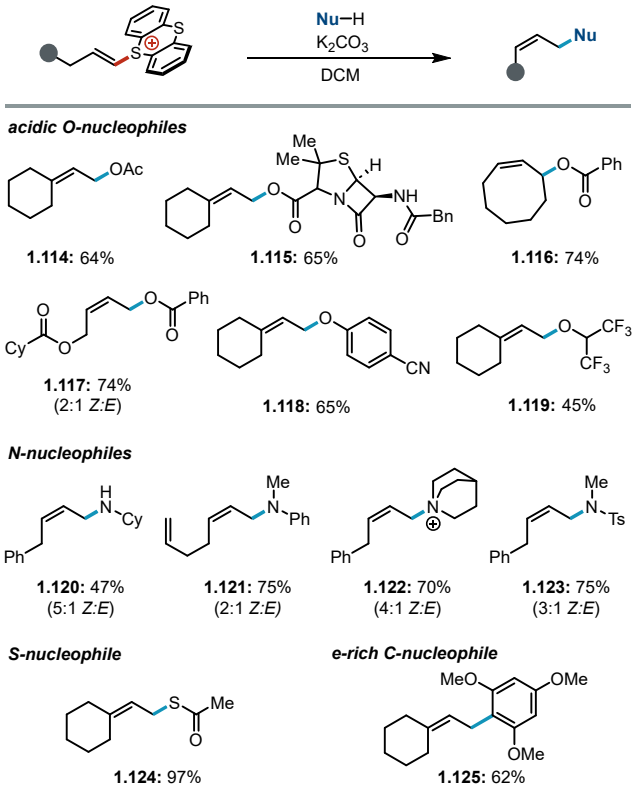

Scheme 1.12. Allylic functionalization of alkenylthianthrenium salts reported by Shu and co-workers.[59]

terminal alkenes, modest *Z*-selectivity was observed in the allylic ester products, typically between 2:1 and 3:1 *Z:E*. However, the authors noted that, in some cases, replacing carbonate with an amine base improved *Z:E*, albeit in diminished yield.[60] Primary, secondary, and tertiary amines were each demonstrated to be viable for allylic amination giving *Z*-allylic amine products in 2:1 to 5:1 *Z:E*. The authors advanced a working hypothesis in which the dicationic adducts are transiently formed from alkenylthianthrenium salts and proceed to allylic products through a substitution-elimination sequence.

In 2023, Soós, Varga, and co-workers exploited the allylation reactivity of thianthrenium salts to deliver *Z*-α,β-unsaturated carbonyl compounds from alkenes (Scheme 1.13).[61] To accomplish this, the authors engaged alkenylthianthrenium salts using weakly nucleophilic dimethyl sulfoxide or *N*-methylmorpholine *N*-oxide under basic conditions (K_2CO_3), which tap into reactivity analogous to the Kornblum oxidation. This yielded α,β-unsaturated carbonyl compounds as the final products across a broad range of alkene starting materials and, where relevant, enal products were obtained with *Z*-selectivity (typically 4:1 to 6:1 *Z:E*).[62] In addition to examining a new nucleophile class, the authors expanded the nature of the products that could be accessed through variations to the alkene as well. Of note, terminal alkenes bearing pendant electrophilic functionalities such as aldehydes, alkylbromides, and alkyltosylates were suitable substrates for this transformation, illustrating the high relative electrophilicity of the thianthrenium handle. This new transformation could be exploited in one-pot syntheses of natural products from alkene starting materials using both the chemical and electrochemical methods to generate the requisite thianthrenium electrophile (Scheme 1.14). While thianthrenium salts derived from terminal alkenes underwent linear-selective functionalization, those derived from 1,2-disubstituted alkenes underwent allylic functionalization with poor regioselectivity (Scheme 1.13). The authors attributed this observation to competition between S_N2 and S_N2' processes from a putative allylic thianthrenium intermediate. Indeed, in their mechanistic studies, the authors illustrated that an aryl stabilized allylic thianthrenium salt can be isolated and was shown to be kinetically competent, albeit without any stereochemical readout. Intriguingly, the S_N2' product was favored when an exceptionally hindered alkenylthianthrenium salt was employed (**1.135**).

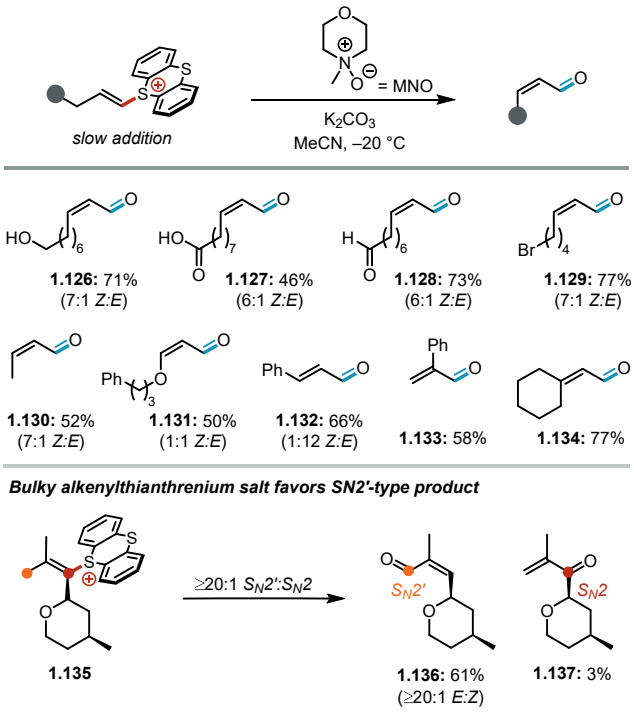

Scheme 1.13. α,β-unsaturated carbonyls from alkenyl thianthrenium salts *via* tandem allylic functionalization and Kornblum/Ganem oxidation reported by Soos, Varga, and co-workers.[61]

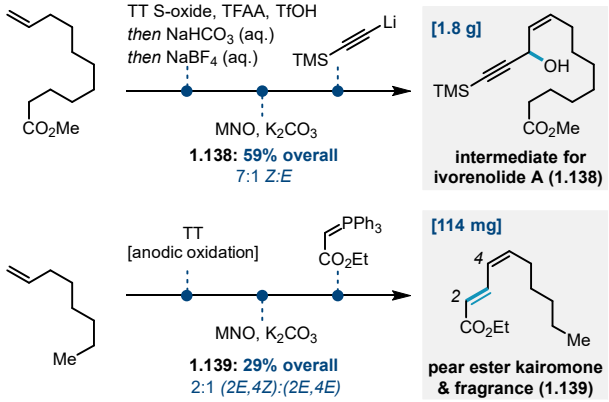

Scheme 1.14. Selected examples of streamlined synthesis of natural products *via* allylation reactivity by Soos, Varga, and co-workers.[61]

Wickens and Gutierrez uploaded a manuscript describing a detailed mechanistic study of the unusual allylic functionalization reactivity of thianthrenium salts (Scheme 1.15, see Chapter 3). All mechanistic experiments in the previously described reports focused on establishing kinetic competence of various thianthrenium species. However, the elementary steps and origin of *Z*-selectivity remained unclear

because these data were consistent with several distinct mechanisms. In this new mechanistic study, the authors used reaction kinetics, kinetic isotope effects, isotopic labeling, and detailed density functional theory calculations to distinguish between the prior mechanistic hypotheses and provide a model to explain the observed stereoselectivity. These studies indicate that the dicationic adducts initially undergo exergonic elimination to an alkenylthianthrenium species. Following elimination, allylic deprotonation of this alkenylthianthrenium salt was determined to be both rate- and stereodetermining. Calculations indicate that endergonic deprotonation occurs with *Z*-selectivity, consistent with experimental observations. Intriguingly, the kinetic *Z*-selectivity appears to arise from a late transition structure, which reflects the increased thermodynamic stability of the *Z*-allylic ylide relative to the E-isomer.[63–66] The resultant *Z*-allylic ylide was found to be configurationally stable and rapidly protonated to form an allylic thianthrenium electrophile. This *Z*-allylic electrophile is then substituted with high S_N2 regioselectivity to provide the final allylic product. This mechanistic model is fully consistent with all data reported to date and rationalizes the observed reactivity and stereoselectivity.

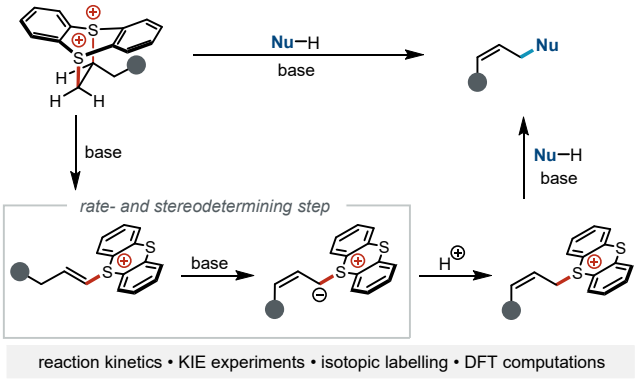

Scheme 1.15. Elementary steps of *Z*-selective allylic functionalization from thianthrenium salts reported by the Wickens and Gutierrez groups.

1.6 Conclusion and Outlook

This chapter highlights the diverse formal oxidative alkene functionalization reactions unlocked by transformation of alkenes into linchpin thianthrenium electrophiles. The recent burst of interest in this approach has been driven by new methods to access thianthrenium electrophiles from alkenes: (1) deoxygenation of thianthrene S-oxide, and (2) anodic oxidation of thianthrene. Overall, these strategies has enabled the development of an array of methods that collectively allow alkenes to be viewed as formal alkenyl cations, vicinal dications, and *Z*-allylic cations.

The transformation of alkenes into alkenylthianthrenium salts has enabled a suite of new formal regioselective C(sp^2)–H functionalization reactions. The regio- and stereoselective synthesis of alkenylthianthrenium salts from alkenes distinguishes these species from classic alkenylhalide electrophiles, which are typically accessed from less abundant precursors. These thianthrenium salts participate in multiple reactivity manifolds, which enables both *ipso*- and *cine*-substitution processes with a wide range of nucleophiles. We envision future efforts will introduce new strategies to promote regiodivergent coupling that expand upon seminal reports in this arena.

Alkene thianthrenation has unlocked a new approach to alkene difunctionalization that leverages abundant nucleophiles as coupling partners. These thianthrenium species favor net-disubstitution reactivity, in stark contrast to classic halide dielectrophiles that often suffer from the formation of dead-end elimination side products. Initial investigation into this reactivity focused on the introduction of modular routes to strained three-membered rings. We envision that future work in this area will expand this platform to enable the synthesis of larger ring systems alongside new approaches to control stereochemistry. Furthermore, these dielectrophiles were shown to undergo a single, regiospecific substitution with phthalimide to furnish 1,2-phthalimidosulfonium intermediates that are en route to vicinally functionalized products, such as diamines. We expect that further mechanistic understanding will enable generalization of this reactivity beyond phthalimide and unlock a new platform for vicinal alkene difunctionalization.

Generation of thianthrenium electrophiles from aliphatic alkenes has revealed a new mechanism to promote the formal C(sp^3)–H allylic functionalization of alkenes. This reaction manifold is exquisitely

selective for linear products over the branched isomer and offers intriguing *Z*-selectivity. These observations offer a complement to the corresponding allylic halide electrophiles that can be similarly accessed from alkenes but with high *E*-selectivity. Unlike the other two reaction manifolds wherein the structures of the thianthrenium electrophiles are evocative of the observed reactivity, this allylic functionalization transformation was substantially less obvious. Indeed, at least in our studies, these products were initially observed as unexpected side products when attempting other transformations. At this stage, seminal reports in this area have established that many nucleophiles participate in this mechanistic manifold albeit with variable *Z*-selectivity. A recently disclosed mechanistic study offered the first detailed model to rationlize both this reactivity and the origin of *Z*-selectivity. We envision these mechanistic insights will aid in the development of new methods that enforce high *Z*-selectivity across a broad range of nucleophiles.

Despite the rapid synthetic advances exploiting alkene-derived thianthrenium salts over the past four years, numerous areas for further development remain. For example, while internal alkenes can be readily transformed into the corresponding thianthrenium salts, the reactivity of these more substituted electrophiles remains underexplored. We suspect that tuning thianthrene structure will offer a new avenue to expand upon the reactions developed to date. Indeed, in other contexts, structural modifications to sulfonium electrophiles have proven essential to control reactivity and selectivity.[67–69] Additionally, while thianthrene and thianthrene S-oxide are each inexpensive stoichiometric activating groups, rendering these processes catalytic would nonetheless be attractive and promote development enantioselective variants. Overall, the unique reactivity and selectivity profiles of thianthrenium electrophiles offer a fertile ground for the development of formal oxidative alkene functionalization reactions that will continue to be enriched by future discoveries.

1.7 Acknowledgements

This work was financially supported by the NIH (R01GM149674-01). This material is based upon work supported by the National Science Foundation Graduate Research Fellowship Program under grant no. DGE-1747503 (K.T.). Any opinions, findings, and conclusions or recommendations expressed in this

material are those of the author(s) and do not necessarily reflect the views of the National Science Foundation.

All authors contributed to the outline and content of the literature review. M.K. and K.T. contributed equally to the preparation of the minireview manuscript. D.E.H. provided a first draft of the introduction and vicinal dication synthon section. D.J.W. provided a preliminary draft of the allyl cation section.

1.8 References

(1) Patel, M.; Desai, B.; Sheth, A.; Dholakiya, B. Z.; Naveen, T. Recent Advances in Mono- and Difunctionalization of Unactivated Olefins. *Asian Journal of Organic Chemistry* **2021**, *10* (12), 3201–3232.

(2) Bary, G.; Jamil, M. I.; Arslan, M.; Ghani, L.; Ahmed, W.; Ahmad, H.; Zaman, G.; Ayub, K.; Sajid, M.; Ahmad, R.; Huang, D.; Liu, F.; Wang, Y. Regio- and Stereoselective Functionalization of Alkenes with Emphasis on Mechanistic Insight and Sustainability Concerns. *Journal of Saudi Chemical Society* **2021**, *25* (7), 101260.

(3) Yao, H.; Hu, W.; Zhang, W. Difunctionalization of Alkenes and Alkynes via Intermolecular Radical and Nucleophilic Additions. *Molecules* **2021**, *26* (1), 105.

(4) Lee, J. H.; Choi, S.; Hong, K. B. Alkene Difunctionalization Using Hypervalent Iodine Reagents: Progress and Developments in the Past Ten Years. *Molecules* **2019**, *24* (14), 2634.

(5) Denmark, S. E.; Kuester, W. E.; Burk, M. T. Catalytic, Asymmetric Halofunctionalization of Alkenes—A Critical Perspective. *Angewandte Chemie International Edition* **2012**, *51* (44), 10938–10953.

(6) Effenberger, F. Electrophilic Reagents—Recent Developments and Their Preparative Application. *Angewandte Chemie International Edition in English* **1980**, *19* (3), 151–171.

(7) Crotti, P.; Pineschi, M. Epoxides in Complex Molecule Synthesis. In *Aziridines and Epoxides in Organic Synthesis*; John Wiley & Sons, Ltd, 2006; pp 271–313.

(8) Chemler, S. R.; Bovino, M. T. Catalytic Aminohalogenation of Alkenes and Alkynes. *ACS Catal.* **2013**, *3* (6), 1076–1091.

(9) Song, L.; Luo, S.; Cheng, J.-P. Catalytic Intermolecular Haloamidation of Simple Alkenes with N-Halophthalimide as Both Nitrogen and Halogen Source. *Org. Lett.* **2013**, *15* (22), 5702–5705.

(10) Ashtekar, K. D.; Vetticatt, M.; Yousefi, R.; Jackson, J. E.; Borhan, B. Nucleophile-Assisted Alkene Activation: Olefins Alone Are Often Incompetent. *J. Am. Chem. Soc.* **2016**, *138* (26), 8114–8119.

(11) Zhang, J.; Wang, J.; Qiu, Z.; Wang, Y. Highly Regio- and Diastereoselective Halohydroxylation of Olefins: A Facile Synthesis of Vicinal Halohydrins. *Tetrahedron* **2011**, *67* (36), 6859–6867.

(12) Meng, H.; Liu, M.-S.; Shu, W. Organothianthrenium Salts: Synthesis and Utilization. *Chem. Sci.* **2022,** *13*, 13690-13707.

(13) Kozhushkov, S. I.; Alcarazo, M. Synthetic Applications of Sulfonium Salts. *Eur J Inorg Chem* **2020**, *2020* (26), 2486–2500.

(14) van Dalsen, L.; Brown, R. E.; Rossi-Ashton, J. A.; Procter, D. J. Sulfonium Salts as Acceptors in Electron Donor-Acceptor Complexes. *Angewandte Chemie International Edition* **2023**, *62* (29), e202303104.

(15) Shine, H. J.; Zhao, B.; Qian, D.-Q.; Marx, J. N.; Guzman-Jimenez, I. Y.; Thurston, J. H.; Ould-Ely, T.; Whitmire, K. H. Adducts of Phenoxathiin and Thianthrene Cation Radicals with Alkenes and Cycloalkenes. *J. Org. Chem.* **2003**, *68* (23), 8910–8917.

(16) Lee, W. K.; Liu, B.; Park, C. W.; Shine, H. J.; Whitmire, K. H. Addition of Thianthrene Cation Radical to Cycloalkenes. An Unexpected Monoadduct. *J. Org. Chem.* **1999**, *64* (25), 9206–9210.

(17) Rangappa, P.; Shine, H. J. An Overview of Some Reactions of Thianthrene Cation Radical. Products and Mechanisms of Their Formation. *Journal of Sulfur Chemistry* **2006**, *27* (6), 617–664.

(18) Shine, H. J.; Bandlish, B. K.; Mani, S. R.; Padilla, A. G. Ion Radicals. 43. Addition of Thianthrene and Phenoxathiin Cation Radicals to Alkenes and Alkynes. *J. Org. Chem.* **1979**, *44* (6), 915–917.

(19) Qian, D.-Q.; Shine, H. J.; Guzman-Jimenez, I. Y.; Thurston, J. H.; Whitmire, K. H. Mono- and Bisadducts from the Addition of Thianthrene Cation Radical Salts to Cycloalkenes and Alkenes. *J. Org. Chem.* **2002**, *67* (12), 4030–4039.

(20) Chen, J.; Li, J.; Plutschack, M. B.; Berger, F.; Ritter, T. Regio- and Stereoselective Thianthrenation of Olefins To Access Versatile Alkenyl Electrophiles. *Angewandte Chemie International Edition* **2020**, *59* (14), 5616–5620.

(21) Holst, D. E.; Wang, D. J.; Kim, M. J.; Guzei, I. A.; Wickens, Z. K. Aziridine Synthesis by Coupling Amines and Alkenes via an Electrogenerated Dication. *Nature* **2021**, *596* (7870), 74–79.

(22) Matsuo, J.; Yamanaka, H.; Kawana, A.; Mukaiyama, T. A Convenient Method for the Synthesis of 2-Arylaziridines from Styrene Derivatives via 2-Arylethenyl(Diphenyl)Sulfonium Salts. *Chem. Lett.* **2003**, *32* (4), 392–393.

(23) Nenaidenko, V. G.; Balenkova, E. S. New Synthetic Capabilities of Sulfonium Salts. *Russian Journal of Organic Chemistry* **2003**, *39* (3), 291–330.

(24) Matlock, J. V.; Fritz, S. P.; Harrison, S. A.; Coe, D. M.; McGarrigle, E. M.; Aggarwal, V. K. Synthesis of α-Substituted Vinylsulfonium Salts and Their Application as Annulation Reagents in the Formation of Epoxide- and Cyclopropane-Fused Heterocycles. *J. Org. Chem.* **2014**, *79* (21), 10226–10239.

(25) Kaiser, D.; Klose, I.; Oost, R.; Neuhaus, J.; Maulide, N. Bond-Forming and -Breaking Reactions at Sulfur(IV): Sulfoxides, Sulfonium Salts, Sulfur Ylides, and Sulfinate Salts. *Chem. Rev.* **2019**, *119* (14), 8701–8780.

(26) Yar, M.; McGarrigle, E. M.; Aggarwal, V. K. An Annulation Reaction for the Synthesis of Morpholines, Thiomorpholines, and Piperazines from β-Heteroatom Amino Compounds and Vinyl Sulfonium Salts. *Angewandte Chemie International Edition* **2008**, *47* (20), 3784–3786.

(27) Mondal, M.; Chen, S.; Kerrigan, N. J. Recent Developments in Vinylsulfonium and Vinylsulfoxonium Salt Chemistry. *Molecules* **2018**, *23* (4), 738.

(28) Kutsumura, N.; Kubokawa, K.; Saito, T. TBAF-Promoted Dehydrobrominations of Vicinal Dibromides Having an Adjacent O-Functional Group. *Synlett* **2010**, *2010* (18), 2717–2720.

(29) Buchanan, G. S.; Cole, K. P.; Li, G.; Tang, Y.; You, L.-F.; Hsung, R. P. Constructing the Architecturally Distinctive ABD-Tricycle of Phomactin A through an Intramolecular Oxa-[3+3] Annulation Strategy. *Tetrahedron* **2011**, *67* (52), 10105–10118.

(30) Križková, P. M.; Lindner, W.; Hammerschmidt, F. Improved Synthesis of Racemate and Enantiomers of Taniguchi Lactone and Conversion of Their C–C Double Bonds into Triple Bonds. *Synthesis* **2018**, *50* (3), 651–657.

(31) Brown, H. C.; Subrahmanyam, C.; Hamaoka, T.; Ravindran, N.; Bowman, D. H.; Misumi, S.; Unni, M. K.; Somayaji, V.; Bhat, N. G. Vinylic Organoboranes. 13. A Convenient Stereospecific Synthesis of (Z)-1-Halo-1-Alkenes from 1-Alkynes via (E)-1-Alkenylborane Derivatives with Halogens. *J. Org. Chem.* **1989**, *54* (26), 6068–6075.

(32) Zweifel, George.; Whitney, C. C. Novel Method for the Synthesis of Isomerically Pure Vinyl Halides from Alkynes via the Hydroalumination Reaction. *J. Am. Chem. Soc.* **1967**, *89* (11), 2753–2754.

(33) Brown, H. C.; Gupta, S. K. Catecholborane (1,3,2-Benzodioxaorole) as a New, General Monohydroboration Reagent for Alkynes. Convenient Synthesis of Alkeneboronic Esters and Acids from Alkynes via Hydroboration. *J. Am. Chem. Soc.* **1972**, *94* (12), 4370–4371.

(34) This reactivity builds upon prior efforts employing alkenyl- and vinylsulfonium electrophiles in transition metal cross-coupling. For representative examples, see refs 35–37.

(35) Aukland, M. H.; Talbot, F. J. T.; Fernández-Salas, J. A.; Ball, M.; Pulis, A. P.; Procter, D. J. An Interrupted Pummerer/Nickel-Catalysed Cross-Coupling Sequence. *Angewandte Chemie International Edition* **2018**, *57* (31), 9785–9789.

(36) Srogl, J.; Allred, G. D.; Liebeskind, L. S. Sulfonium Salts. Participants Par Excellence in Metal-Catalyzed Carbon−Carbon Bond-Forming Reactions. *J. Am. Chem. Soc.* **1997**, *119* (50), 12376–12377.

(37) Lin, H.; Dong, X.; Li, Y.; Shen, Q.; Lu, L. Highly Selective Activation of Vinyl C–S Bonds Over Aryl C–S Bonds in the Pd-Catalyzed Coupling of (E)-(β-Trifluoromethyl)Vinyldiphenylsulfonium Salts: Preparation of Trifluoromethylated Alkenes and Dienes. *European Journal of Organic Chemistry* **2012**, *2012* (25), 4675–4679.

(38) Juliá, F.; Yan, J.; Paulus, F.; Ritter, T. Vinyl Thianthrenium Tetrafluoroborate: A Practical and Versatile Vinylating Reagent Made from Ethylene. *J. Am. Chem. Soc.* **2021**, *143* (33), 12992–12998.

(39) IARC. *1,3-Butadiene, Ethylene Oxide and Vinyl Halides (Vinyl Fluoride, Vinyl Chloride and Vinyl Bromide)*.

(40) Lansbergen, B.; Tewari, S.; Tomczyk, I.; Seemann, M.; Buchholz, H. L.; Chamier Cieminski, D.; Rippegarten, M.; Julia, F.; Ritter, T. Reductive Cross-Coupling of a Vinyl Thianthrenium Salt and Secondary Alkyl Iodides. *Angewandte Chemie International Edition n/a* (n/a), e202313659.

(41) Xie, R.; Zhu, J.; Huang, Y. Cu-Catalyzed Highly Selective Silylation and Borylation of Alkenylsulfonium Salts. *Org. Chem. Front.* **2021**, *8* (20), 5699–5704.

(42) Zhu, J.; Ye, Y.; Huang, Y. Palladacycle-Catalyzed Olefinic C–P Cross-Coupling of Alkenylsulfonium Salts with Diarylphosphines to Access Alkenylphosphines. *Organometallics* **2022**, *41* (16), 2342–2348.

(43) Ye, Y.; Zhu, J.; Xie, H.; Huang, Y. Rhodium-Catalyzed Divergent Arylation of Alkenylsulfonium Salts with Arylboroxines. *Angewandte Chemie International Edition* **2022**, *61* (49), e202212522.

(44) Shu, W.; Liu, M.-S.; Meng, H. Unified Metal-Free Intermolecular Heck-Type Sulfonylation, Cyanation, Amination, Amidation of Alkenes by Thianthrenation. ChemRxiv July 3, 2023. https://doi.org/10.26434/chemrxiv-2023-xsgh1.

(45) Since failed reactions are rarely reported in the literature, our group has prepared substituted vicinal dibromides to evaluate their substitution with nucleophiles and explain the paucity of examples of this reactivity. See refs 21 and 48.

(46) Lohray, B. B.; Gao, Y.; Sharpless, K. B. One Pot Synthesis of Homochiral Aziridines and Aminoalcohols from Homochiral 1,2-Cyclic Sulfates. *Tetrahedron Letters* **1989**, *30* (20), 2623–2626.

(47) Gao, Yun.; Sharpless, K. Barry. Vicinal Diol Cyclic Sulfates. Like Epoxides Only More Reactive. *J. Am. Chem. Soc.* **1988**, *110* (22), 7538–7539.

(48) Kim, M. J.; Wang, D. J.; Targos, K.; Garcia, U. A.; Harris, A. F.; Guzei, I. A.; Wickens, Z. K. Diastereoselective Synthesis of Cyclopropanes from Carbon Pronucleophiles and Alkenes. *Angewandte Chemie International Edition* **2023**, *62* (21), e202303032.

(49) Liu, M.-S.; Du, H.-W.; Cui, J.-F.; Shu, W. Intermolecular Metal-Free Cyclopropanation and Aziridination of Alkenes with XH2 (X=N, C) by Thianthrenation**. *Angewandte Chemie International Edition* **2022**, *61* (41), e202209929.

(50) Holst, D. E.; Dorval, C.; Winter, C. K.; Guzei, I. A.; Wickens, Z. K. Regiospecific Alkene Aminofunctionalization via an Electrogenerated Dielectrophile. *J. Am. Chem. Soc.* **2023**, *145* (15), 8299–8307.

(51) Liu, G.; Wu, Y. Palladium-Catalyzed Allylic C–H Bond Functionalization of Olefins. In *C-H Activation*; Yu, J.-Q., Shi, Z., Eds.; Topics in Current Chemistry; Springer: Berlin, Heidelberg, 2010; pp 195–209.

(52) Kazerouni, A. M.; McKoy, Q. A.; Blakey, S. B. Recent Advances in Oxidative Allylic C–H Functionalization via Group IX-Metal Catalysis. *Chem. Commun.* **2020**, *56* (87), 13287–13300.

(53) Cheng, Q.; Chen, J.; Lin, S.; Ritter, T. Allylic Amination of Alkenes with Iminothianthrenes to Afford Alkyl Allylamines. *J. Am. Chem. Soc.* **2020**, *142* (41), 17287–17293.

(54) Ali, S. Z.; Budaitis, B. G.; Fontaine, D. F. A.; Pace, A. L.; Garwin, J. A.; White, M. C. Allylic C–H Amination Cross-Coupling Furnishes Tertiary Amines by Electrophilic Metal Catalysis. *Science* **2022**, *376* (6590), 276–283.

(55) Jin, Y.; Jing, Y.; Li, C.; Li, M.; Wu, W.; Ke, Z.; Jiang, H. Palladium-Catalysed Selective Oxidative Amination of Olefins with Lewis Basic Amines. *Nat. Chem.* **2022**, *14* (10), 1118–1125.

(56) Wang, S.; Gao, Y.; Liu, Z.; Ren, D.; Sun, H.; Niu, L.; Yang, D.; Zhang, D.; Liang, X.; Shi, R.; Qi, X.; Lei, A. Site-Selective Amination towards Tertiary Aliphatic Allylamines. *Nat Catal* **2022**, *5* (7), 642–651.

(57) Dauben, H. J.; McCoy, L. L. N-Bromosuccinimide. I. Allylic Bromination, a General Survey of Reaction Variables [1-3]. *J. Am. Chem. Soc.* **1959**, *81* (18), 4863–4873.

(58) Wang, D. J.; Targos, K.; Wickens, Z. K. Electrochemical Synthesis of Allylic Amines from Terminal Alkenes and Secondary Amines. *J. Am. Chem. Soc.* **2021**, *143* (51), 21503–21510.

(59) Liu, M.-S.; Du, H.-W.; Shu, W. Metal-Free Allylic C–H Nitrogenation, Oxygenation, and Carbonation of Alkenes by Thianthrenation. *Chem. Sci.* **2022**, *13* (4), 1003–1008.

(60) This observation is in-line with allylic amination by the Wickens group (see ref. 58), in which base identity was optimized for *Z*-selectivity.

(61) Angyal, P.; Kotschy, A. M.; Dudás, Á.; Varga, S.; Soós, T. Intertwining Olefin Thianthrenation with Kornblum/Ganem Oxidations: Ene-Type Oxidation to Furnish α,β-Unsaturated Carbonyls. *Angewandte Chemie International Edition* **2023**, *62* (2), e202214096.

(62) One particularly useful application of this method is the tunability between the kinetically preferred *Z*-enal and the thermodynamically preferred *E*-enal simply by simply increasing temperature and reaction time.

(63) Hoffmann, R.; Olofson, R. A. The Dependence of Conformational and Isomer Stability on the Number of Electrons in Extended π Systems. *J. Am. Chem. Soc.* **1966**, *88* (5), 943–946.

(64) Schleyer, P. v. R.; Dill, J. D.; Pople, J. A.; Hehre, W. J. Geometrical Preferences of the Crotyl Anion, Radical and Cation. *Tetrahedron* **1977**, *33* (19), 2497–2501. https://doi.org/10.1016/0040-4020(77)80071-9.

(65) Schleyer, P. von R.; Kaneti, J.; Yun-Dong, W.; Chandrasekhar, J. The Preference of 1-Methylallyl Polar Organometallics and Carbanions for Cis Rather than for Trans Geometries. *Journal of Organometallic Chemistry* **1992**, *426* (2), 143–157.

(66) Janesko, B. G.; Villegas, H. Attractive Nonbonded Interactions Help Stabilize the Z Form of Alkenyl Anions. *J. Org. Chem.* **2018**, *83* (15), 8208–8213.

(67) Paul, S.; Filippini, D.; Silvi, M. Polarity Transduction Enables the Formal Electronically Mismatched Radical Addition to Alkenes. *J. Am. Chem. Soc.* **2023**, *145* (5), 2773–2778.

(68) Berger, F.; Plutschack, M. B.; Riegger, J.; Yu, W.; Speicher, S.; Ho, M.; Frank, N.; Ritter, T. Site-Selective and Versatile Aromatic C−H Functionalization by Thianthrenation. *Nature* **2019**, *567* (7747), 223–228.

(69) Unthank, M. G.; Hussain, N.; Aggarwal, V. K. The Use of Vinyl Sulfonium Salts in the Stereocontrolled Asymmetric Synthesis of Epoxide- and Aziridine-Fused Heterocycles: Application to the Synthesis of (−)-Balanol. *Angewandte Chemie International Edition* **2006**, *45* (42), 7066–7069.

Chapter 2: Electrochemical Synthesis of Allylic Amines from Terminal Alkenes and Secondary Amines

This chapter has been published and adapted with permission from:

Diana J. Wang, **Karina Targos**, and Zachary K. Wickens. Electrochemical Synthesis of Allylic Amines from Terminal Alkenes and Secondary Amines. *J. Am. Chem. Soc.* **2021**, 143, 51, 21503–21510.

2.1 Abstract

Allylic amines are valuable synthetic targets *en route* to diverse biologically active amine products. Current allylic C–H amination strategies remain limited with respect to the viable *N*-substituents. Herein we disclose a new electrochemical process to prepare aliphatic allylic amines by coupling two abundant starting materials: secondary amines and unactivated alkenes. This oxidative transformation proceeds *via* electrochemical generation of an electrophilic adduct between thianthrene and the alkene substrates. Treatment of these adducts with aliphatic amine nucleophiles and base provides allylic amine products in high yield. This synthetic strategy is also amenable to functionalization of feedstock gaseous alkenes at one atmosphere. In the case of 1-butene, high *Z*-selective crotylation is observed. This strategy, however, is not limited to the synthesis of simple building blocks; complex biologically active molecules are suitable as both alkene and amine coupling partners.

2.2 Introduction

Aliphatic amines are prevalent in pharmaceuticals, natural products, and other biologically active molecules.[1–3] Thus, the development of strategies to rapidly construct C–N bonds is of longstanding synthetic importance. Allylic amines are particularly valuable building blocks due to their synthetic versatility.[4–8] A deceptively simple strategy to prepare alkyl allylic amines would be the oxidative coupling

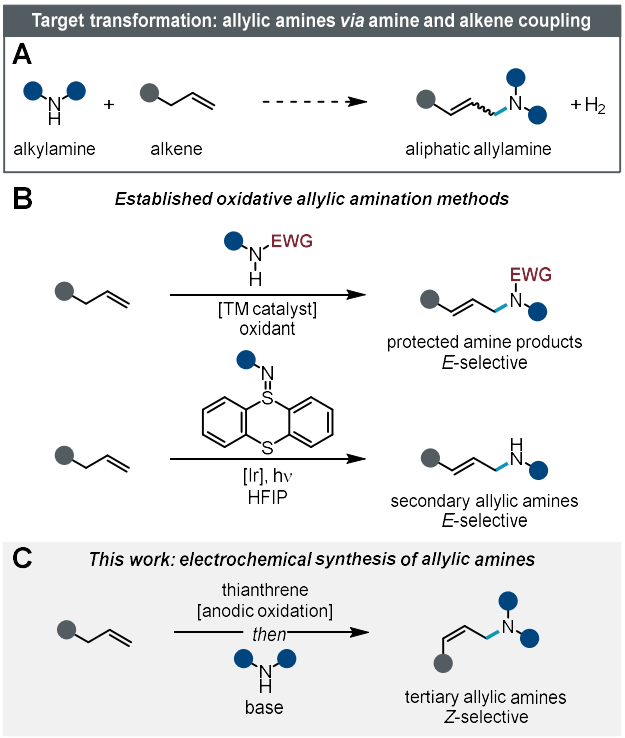

Figure 2.1. Project overview. (A) Idealized transformation to access aliphatic allylic amines. (B) Representative established allylic C–H amination reactions. (C) Schematic overview of this work.

of alkenes and aliphatic amines (Figure 2.1A). Such a reaction would be an attractive complement to classic amine allylation strategies such as S_N2[9–16] and π-allyl substitution reactions[17–24] that rely on prefunctionalized electrophiles.[25] However, successful realization of such a transformation requires a strategy to promote the desired oxidative C–N bond-forming process without undesired oxidation of the aliphatic amine starting materials or the aliphatic allylic amine products (0.8 – 1.1 V *vs.* SCE).[26] As a consequence, generation of aliphatic allylic amines by oxidative coupling of alkenes and amines has remained elusive.[27–36] Instead, pioneering reports have established powerful C–H functionalization protocols to construct allylic C–N bonds using oxidatively stable nitrogen sources in diverse intermolecular amination reactions.[37–46] These reaction manifolds primarily take advantage of electronically deactivated nitrogen pronucleophiles[47–59] and nitrene precursors.[60–74] As a direct result, these established approaches offer limited access to aliphatic allylic amine products and instead furnish products with electron-deficient nitrogen atoms, such as allylic sulfonamides and carbamates (Figure 2.1B).

Despite the significant progress in other oxidative amination reactions,[75–80] to date, there is a single intermolecular allylic C−H amination reaction that directly furnishes aliphatic allylic amine products.[27] This strategy, reported by Ritter and co-workers in 2020, exploits photochemically-activated sulfilimine reagents as nitrogen sources. While this is a landmark report in allylic C–H amination, installation of different *N*-substituents in the product requires preparation of unique electrophilic reagents. Additionally, this reagent design strategy is not readily amenable to tertiary amine synthesis. Accordingly, a complementary synthetic technology that generates allylic amines *via* an oxidative coupling of unactivated amine nucleophiles and alkenes remains poised to have a significant impact on organic synthesis. Such an approach would directly translate the >4 million commercially available aliphatic amines into versatile allylic amine building blocks.[81]

We recently developed an electrochemical strategy to engage oxidatively sensitive nucleophiles in net oxidative alkene difunctionalization reactions.[80] Our approach draws inspiration from Yoshida's pioneering cation pool work[82–84] and contributes to a rapidly growing body of literature exploiting oxidized thianthrene derivatives as synthetic intermediates.[85–92] Specifically, we leveraged electrochemistry to cleanly generate dicationic adducts between unactivated alkenes and thianthrene (**TT**),[93,94] a safe[95] and inexpensive[96] reagent. This strategy circumvents the need for oxidatively stable coupling partners in net oxidative alkene functionalization reactions; the oxidative alkene activation event is decoupled from nucleophilic substitution. In our first report, we leveraged this approach to enable the formal coupling of primary amine nucleophiles with alkenes to furnish aziridine products through a one-pot, two-operation process. Herein, we report an electrochemical strategy to prepare linear, tertiary allylic amine products from aliphatic amines and alkenes with contrathermodynamic *Z*-selectivity (Figure 2.1C). This is accomplished by diverting the reactivity of the dicationic alkene-thianthrene adducts down a formal substitution-elimination pathway.

2.3 Results and Discussion

Our development of an allylic amination process began with an unexpected observation during the study of our dication pool aziridination reaction. We found that, upon exposure to excess *tert*-butylamine, the electrogenerated mixture of dicationic electrophiles **2.1** and **2.2** was transformed into the linear allylic amine product **2.3** in 3:1 *Z:E* ratio rather than the expected *N*-*tert*-butylaziridine (Scheme 2.1). We suspected this net substitution-elimination process may be a consequence of the increased steric bulk about the nitrogen nucleophile. This rationalization suggested that secondary amine nucleophiles may proceed down an analogous allyic amination pathway rather than forming aziridinium intermediates expected to lead to diamination products.[97] Such a reaction would furnish tertiary *Z*-allylic amine products and serve as an ideal complement to the recent secondary *E*-allylic amine synthesis developed by Ritter and co-workers.[27] To probe this hypothesis, we exposed an electrogenerated mixture of **2.1** and **2.2** to an excess of *N*-methylbenzylamine. To our delight, this resulted in conversion of the adduct to the corresponding allylic amine product **2.4** with 4:1 *Z*-selectivity. Next, we aimed to identify a suitable stoichiometric base to lower the necessary equivalents of amine (Table 2.1). We surveyed a range of bases and found *i*-Pr_2NEt promoted the desired allylic functionalization in 79% yield with a 1:1 stoichiometry of amine and alkene starting materials. Increasing the steric bulk of the amine base to triisobutylamine resulted in formation of a alkenylthianthrenium salt **2.5** alongside a reduced yield of allylic amine product (entry 2). Smaller amine bases, such as triethylamine, also resulted in reduced yield (40%) of the desired allylic amine product **2.4** due to competitive formation of an allylic ammonium salt **2.6** derived from the triethylamine base (entry 3). Alternative bases, such as Cs_2CO_3, promoted the desired allylic functionalization albeit in diminished

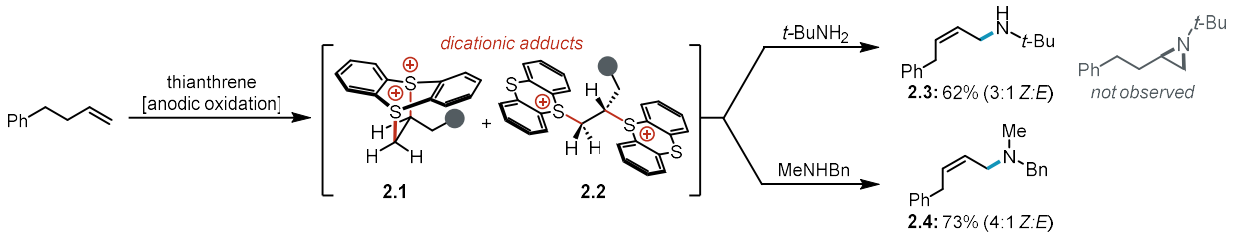

[a]Reactions were conducted using alkene (0.15 mmol), thianthrene (0.23 mmol), 3 mL MeCN (0.2 M n-Bu_4NPF_6), **I** = 4.0 mA, 2.5 **h** (2.5 F mol^{-1} alkene); then amine (1.2 mmol), 16 h. Yields and *Z:E* ratios were determined by ^1H NMR analysis. See appendix A for details.

Scheme 2.1. Initial observations of allylic amination from electrogenerated dicationic adducts.[a]

Table 2.1. Base Evaluation for the Allylic Amination Reaction.[a,b]

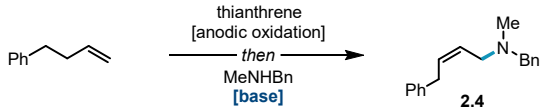

entry	base	yield **2.4** (%) (*Z*:*E*)	yield **2.5** (%)
1	*i*-Pr_2NEt	79 (6:1)	n.d.
2	*i*-Bu_3N	27 (5:1)	52[c]
3	Et_3N	40 (3:1)	n.d.
4	Cs_2CO_3	61 (3:1)	n.d.
5	$NaHCO_3$	<5	67[d]

observed side products:

[a]Reactions were conducted using alkene (0.15 mmol), thianthrene (0.23 mmol), 3 mL MeCN (0.2 M *n*-Bu_4NPF_6), I = 4.0 mA, 2.5 h (2.5 F mol^{-1} alkene); then base (1.1 mmol), amine (0.30 mmol), 16 h. Yields and *Z*:*E* ratios were determined by ^1H NMR analysis. See the appendix A for details. [b]n.d. = not detected. [c]1:5 *Z*:*E*. [d]1:6 *Z*:*E*.

Z- selectivity (entry 4). Weaker inorganic bases, such as $NaHCO_3$, provided alkenylthianthrenium product **2.5** alongside traces of the desired allylic amine (entry 5). Overall, this method provides an appealing one-pot synthesis of allylic amine building blocks.

With optimized conditions in hand, we next investigated the alkene scope for this allylic amination process, employing *N*-methylbenzylamine as a model secondary amine nucleophile (Table 2.2). Allylic amination of 4-phenyl-1-butene and an aryl bromide derivative provided the desired *Z*-allylic amine products (**2.4**, **2.7**) without detectable arene thianthrenation. Likewise, selective alkene functionalization in the presence of an unconjugated alkyne was obtained with high *Z*-selectivity (**2.8**). This result, alongside with tolerance of aromatic substrates (**2.4**, **2.7**), illustrates the exquisite chemoselectivity for adduct formation between oxidized thianthrene and alkene over previously observed thianthrenation of arenes[85] and alkynes.[98] Unconjugated dienes underwent selective monofunctionalization to provide *Z*-unconjugated diene **2.9** and *E*-conjugated diene **2.10** building blocks. Alkenes bearing a variety of proximal functional groups, such as nitrile (**2.11**), acetate (**2.12**), ether (**2.13**), and phthalimide (**2.14**) each efficiently delivered the desired allylic amine products. These examples illustrate the viability of accessing allylic amine building blocks with a secondary homoallylic (**2.11**, **2.12**) or allyic (**2.13**, **2.14**) functional group handle for further elaboration. Allylcyclohexane underwent allylic amination to furnish the sterically hindered

Table 2.2. Scope of Alkenes for Allylic Amination *via* Dication Pool Strategy.[a,b]

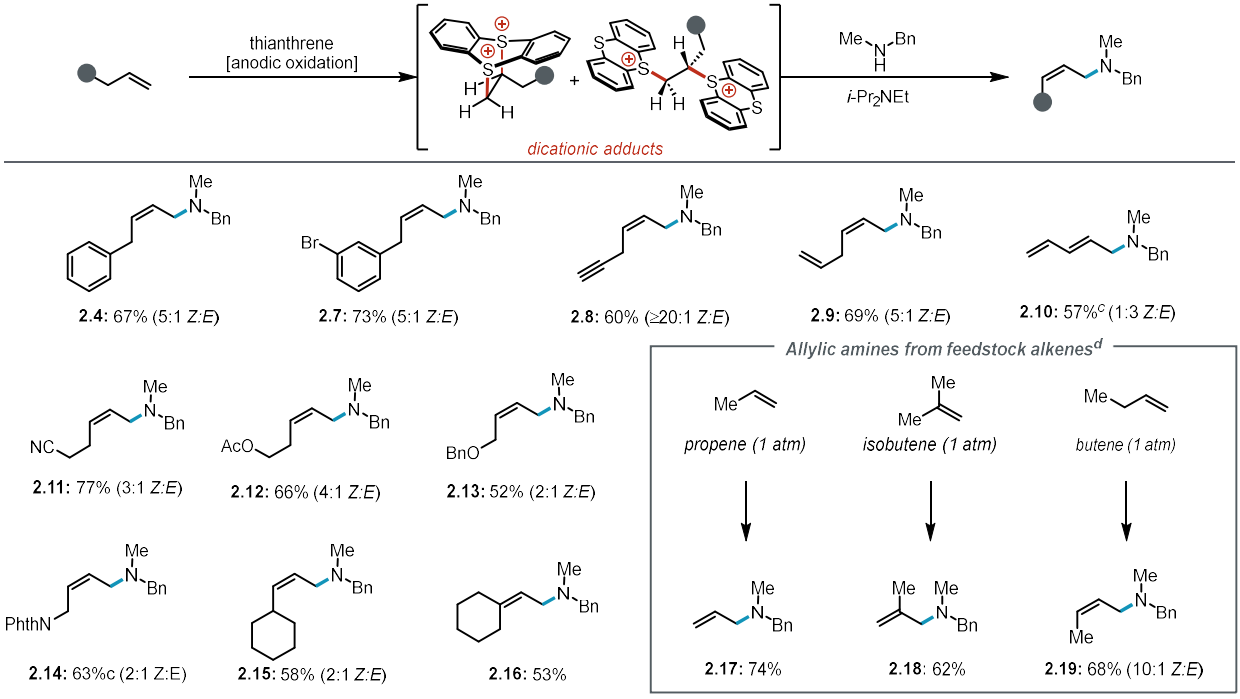

[a]Reactions were conducted using alkene (0.4 mmol), thianthrene (0.6 mmol), 8 mL MeCN (0.2 M n-Bu_4NPF_6), I = 12.0 mA, 2.2 h (2.5 F mol^{-1} alkene); then i-Pr_2NEt (2.8 mmol), amine (0.8 mmol), 16 h. Yields and *Z*:*E* ratios are of the purified product unless otherwise noted. See the appendix A for further details. [b]Isolated yield (*Z*:*E*). [c]NMR yield. [d]Reactions were conducted using alkene (1 atm), thianthrene (1.0 mmol), 4 mL MeCN (0.2 M n-Bu_4NPF_6), I = 60.0 mA, 45 min (1.7 F mol^{-1} thianthrene); then i-Pr_2NEt (3.2 mmol), amine (0.4 mmol), 3 h.

vinylcyclohexane product **2.15**.[99] Finally, vinylcyclohexane underwent allylic amination to form trisubstituted allylic amine **2.16**.[100]

We next probed whether this oxidative coupling strategy is also amenable to functionalization of commodity feedstock alkenes derived from steam cracking and related petroleum refinery processes (Table 2.2).[101,102] Electrolysis of thianthrene under one atmosphere of propene and isobutene each generated the desired dicationic adducts. Treatment of these reaction mixtures with i-Pr_2NEt and *N*-methylbenzylamine resulted in allyl- and methallylamine products (**2.17**, **2.18**) in high yields relative to the amine starting material. Traditional methods to produce these products rely on S_N2 displacement of the corresponding allylic halides, which are carcinogenic and also industrially derived from the same feedstock alkenes through a multistep oxidation-halogenation sequence.[103,104] In contrast, this electrochemical method offers an appealing alternative protocol that produces H_2 gas as the stoichiometric byproduct since thianthrene can be recycled and reused.[105] Notably, 1-butene—the simplest alkene to form stereoisomeric allylic amine products—gave allylic amine **2.19** with high *Z*-selectivity. This highlights the value of this new

transformation beyond a green chemistry context; crotylhalides are only readily available as an *E*-dominant mixture.

Next, we probed the scope of the amine nucleophile, employing 1-butene as the alkene coupling partner (Table 2.3). These transformations furnish synthetically attractive *Z*-crotylamine building blocks that are not straightforward to access using conventional alkylation chemistry. Simple, acyclic dialkylamines (**2.20–2.23**) resulted in high yields and *Z*-selectivity. Of note, even sterically hindered amines delivered the corresponding *Z*-crotylamine product **2.21**, albeit with a diminished yield. Heteroaromatic and saturated heterocycles are tolerated both as pendant functional groups (**2.22**, **2.23**) or as the nucleophile itself (**2.24–2.28**). Amine nucleophiles bearing potential competing nucleophiles were also selectively transformed into *Z*-allylic amine products (**2.24**, **2.26**), preserving the unprotected functional groups for further derivatization. In addition to spirocyclic piperidine (**2.24**), other bicyclic heterocycles with morpholine (**2.27**) and piperazine (**2.28**) cores underwent *Z*-selective crotylation.

Table 2.3. Scope of Z-Crotylamine Building Blocks.[a,b]

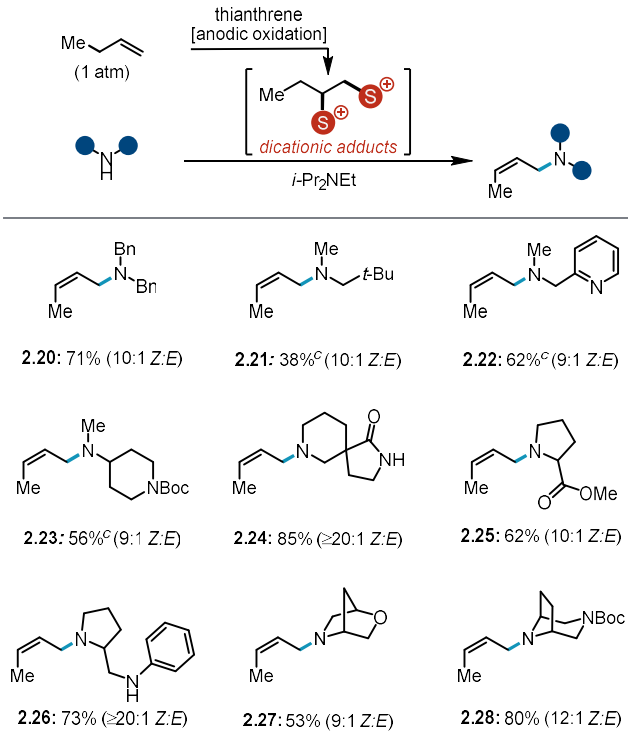

[a]Reactions were conducted using butene (1 atm), thianthrene (1.0 mmol), 4 mL MeCN (0.2 M n-Bu_4NPF_6), **I** = 60.0 mA, 45 min (1.7 F mol^{-1} thianthrene); then i-Pr_2NEt (3.2 mmol), amine (0.4 mmol), 3 h. Yields and *Z*:*E* ratios are of the purified product unless otherwise noted. See the appendix A for further experimental details. [b]Isolated yield (*Z*:*E*). [c]NMR yield.

In addition to the efficient formation of simple, allylic amine building blocks, we envisioned that this newly realized oxidative allylic amination methodology would also streamline the synthesis of more complex amine products (Table 2.4). With this in mind, we next evaluated a range of drug-like compounds as both alkene and amine coupling partners. Due to their structural complexity, these substrates each contain numerous functional groups expected to be liabilities for typical oxidative allylic amination procedures. Lewis basic heterocycles, such as pyridine (**2.29**) and pyrazole (**2.30**) as well as oxidatively sensitive electron-rich aromatic systems (**2.31–2.33**),[26] each delivered the desired allylic amine products. Additionally, allylic amines could be obtained from substrates bearing a variety of saturated heterocycles, including piperidine (**2.29**), morpholine (**2.30**), homopiperazine (**2.34**), and piperizine (**2.35**). Of note, the homopiperazine (**2.34**) and piperizine substrates (**2.35**), each contain a competent tertiary amine nucleophile yet produce the desired allylic amine products in synthetically useful yield. This chemoselectivity extended to other nucleophilic functional groups; unprotected alcohols and arylamines (**2.31**, **2.32**) did not compete with the secondary amine under these allylation conditions, leaving them as synthetic handles for further functionalization. An array of different aryl halides were well tolerated, including both medicinally relevant

Table 2.4. Oxidative Coupling of Complex Bioactive Molecules.[a,b]

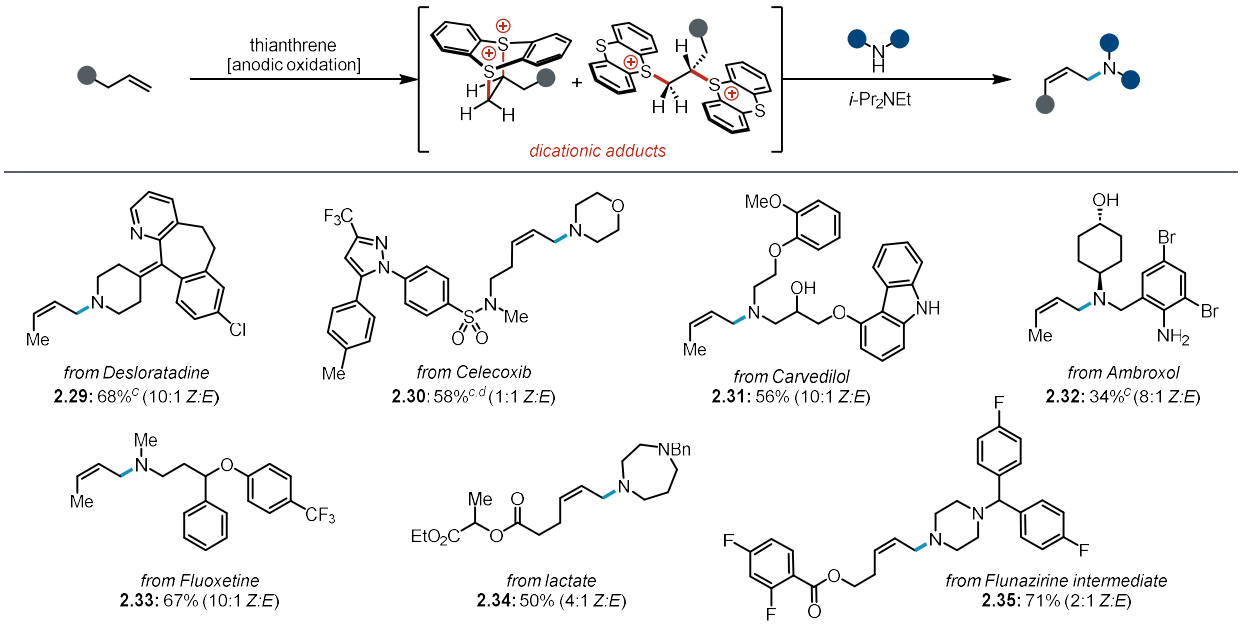

[a]Limiting amine reactions were conducted using alkene (1 atm), thianthrene (1.0 mmol), 4 mL MeCN (0.2 M n-Bu_4NPF_6), I = 60.0 mA, 45 min (1.7 F mol^{-1} thianthrene); then i-Pr_2NEt (3.2 mmol), amine (0.4 mmol), 3 h. Limiting alkene reactions were conducted using alkene (0.4 mmol), thianthrene (0.6 mmol), 8 mL MeCN (0.2 M n-Bu4NPF_6), I = 12.0 mA, 2.2 h (2.5 F mol^{-1} alkene); then i-Pr_2NEt (2.8 mmol), amine (0.4 mmol), 16 h. Yields and *Z*:*E* ratios are of the purified product unless otherwise noted. See the apprendix A for further details. [b]Isolated yield (*Z*:*E*). [c]NMR yield. [d]0.8 mmol amine.

fluorinated groups (**2.30**, **2.33**, **2.35**) as well as aryl bromides (**2.32**) and chlorides (**2.29**) that readily participate in cross-coupling reactions.

During our investigation of the alkene scope for allylic amination, we observed saturated heterocyclic products when using alkenes bearing a tethered pronucleophile (Table 2.5). Under basic conditions, intramolecular cyclization would furnish an alkylthianthrenium salt that can undergo substitution with the secondary amine nucleophile. From the NH sulfonamide precursors, pyrrolidine (**2.36**) and piperidine (**2.**37) were formed in high yields. Methylation of the sulfonamide moiety eliminated this cyclization pathway to enable allylic amination reactivity (**2.30**). Tetrahydrofuran **2.38** was obtained from several ether starting materials, including an L-menthol alkene derivative. These observations are part of a broader ongoing investigation by a current graduate student in the Wickens group that aims to generalize cyclization transformations of thianthrenium salts to generate a suite of saturated heterocycles.

Table 2.5. Scope of Cyclized Products from Alkenes with Tethered Nucleophiles.[a]

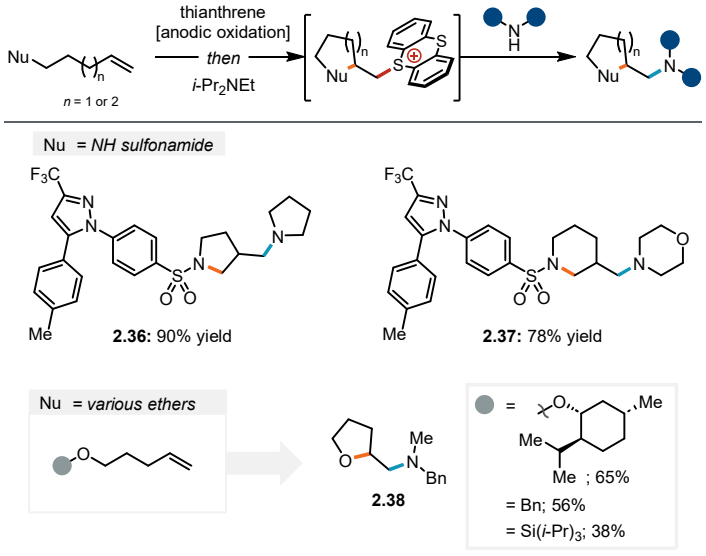

[a]Reactions were conducted using alkene (0.4 mmol), thianthrene (0.6 mmol), 8 mL MeCN (0.2 M n-Bu_4NPF_6), I = 12.0 mA, 2.2 h (2.5 F mol^{-1} alkene); then i-Pr_2NEt (2.8 mmol), amine (0.8 mmol), 16 h. NMR yields reported. See the appendix A for further details.

Next, we aimed to provide some preliminary mechanistic insight into this new process. Monitoring the transformation of dicationic adducts to allylic amine over time revealed that the adducts are rapidly consumed and an alkenylthianthrenium salt is generated. Given the basic conditions, we suspected that the alkenylthianthrenium salt was likely a key intermediate *en route* to the observed allylic amine product rather

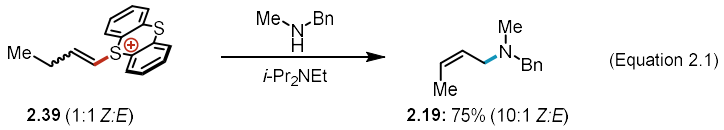

2.39 (1:1 *Z*:*E*) **2.19**: 75% (10:1 *Z*:*E*) (Equation 2.1)

than an off-cycle reservoir. To probe this specific question, we directly prepared alkenylthianthrenium salt **2.39** by base-induced elimination of the electrochemically generated dicationic adducts between 1-butene and thianthrene. We then subjected this isolated alkenylthianthrenium **2.39** to otherwise standard substitution conditions (see appendix A for experimental details). Under these conditions, the allyic amine product **2.19** was formed in 75% yield and identical stereoselectivity to what is observed under standard conditions (Equation 2.1). This is consistent with the alkenylthianthrenium salt serving as an on pathway intermediate. Based on these data, we have constructed a working mechanistic model wherein the alkenylthianthrenium salt undergoes a base-induced isomerization to an allylic thianthrenium intermediate. This species is then rapidly trapped with the amine nucleophile. Indeed, there is a single report of alkenylsulfonium salts being converted to allylic amines.[106] Studies were underway to clarify the mechanistic details of this reaction, particularly the stereodetermining step for the process (see Chapter 3). Beyond the mechanistic implications, however, these data also indicate that alkenylthianthrenium salts prepared through chemical means[86] can be engaged as an electrophile for this transformation. We envision this may be valuable for practicing synthetic chemists in a small-scale research and development setting where electrochemistry offers a less significant advantage relative to more traditional synthetic tactics.

2.4 Conclusion

Overall, we developed an electrochemical synthesis of allylic amines from terminal alkenes and secondary amines. This represents the first example of a formal C–H functionalization approach to furnish tertiary aliphatic allylic amines as well as the first example of a strategy for oxidative allylic C–H functionalization that provides *Z*-selectivity. This linear-selective process exhibits good functional group tolerance and is attractive for substrates ranging from feedstock gas functionalization to derivatization of complex molecules. Furthermore, the conditions are operationally simple; no precautions to exclude air or moisture are necessary. Preliminary mechanistic studies indicate that alkenylthianthrenium salts are key

intermediates. We anticipate that this new electrochemical transformation will find immediate application in organic synthesis given the established synthetic utility of allylic amine building blocks. Moreover, we anticipate that the results reported herein set the stage for the development of a wide range of *Z*-selective allylic functionalization reactions that remain challenging to accomplish *via* more conventional approaches.

2.5 Acknowledgements

We thank Prof. Mark Levin for helpful discussions regarding this manuscript. We thank the Weix, Stahl, Yoon and Schomaker groups for sharing their chemical inventories. In addition, we would like to thank Prof. Samuel Gellman and the entire Gellman group for hosting the authors of this work during a temporary closure of our labs. Along this line, we also thank the staff of the Paul Bender Chemistry Instrumentation Center for enabling NMR and MS sample analysis during building construction. B. J. Thompson is acknowledged for his assistance with the design and fabrication of the power supply. T. Drier is acknowledged for the fabrication of electrochemical glassware. We also acknowledge support and suggestions from all members of the Wickens group throughout the investigation of this project. This work was financially supported by the Office of the Vice Chancellor for Research and Graduate Education at the University of Wisconsin-Madison, with funding from the Wisconsin Alumni Research Foundation. This material is based upon work supported by the National Science Foundation Graduate Research Fellowship Program under Grant No. DGE-1747503 (K.T.). Any opinions, findings, and conclusions or recommendations expressed in this material are those of the author(s) and do not necessarily reflect the views of the National Science Foundation. Spectroscopic instrumentation was supported by a generous gift from Paul J. and Margaret M. Bender, the National Science Foundation (CHE-1048642), and the National Institutes of Health (S10OD012245 and 1S10OD020022-1).

Z.K.W. and D.J.W. designed the project. K.T. designed and executed the investigation of the alkene scope. D.J.W. designed the crotylation. All authors performed the experiments and collected the data. D.J.W. implemented the mechanistic experiments that all authors designed. K.T. implemented the base identity experiments that all authors designed. All authors contributed to writing the manuscript.

2.6 References

(1) Trowbridge, A.; Walton, S. M.; Gaunt, M. J. New Strategies for the Transition-Metal Catalyzed Synthesis of Aliphatic Amines. *Chem. Rev.* **2020**, *120*, 2613–2692.

(2) Richter, M. F.; Drown, B. S.; Riley, A. P.; Garcia, A.; Shirai, T.; Svec, R. L.; Hergenrother, P. J. Predictive Compound Accumulation Rules Yield a Broad-Spectrum Antibiotic. *Nature* **2017**, *545* (7654), 299–304.

(3) Vitaku, E.; Smith, D. T.; Njardarson, J. T. Analysis of the Structural Diversity, Substitution Patterns, and Frequency of Nitrogen Heterocycles among U.S. FDA Approved Pharmaceuticals. *J. Med. Chem.* **2014**, *57* (24), 10257–10274.

(4) For examples of synthetic strategies that exploit allylic amines as key intermediates, see references 5–8.

(5) Johannsen, M.; Jørgensen, K. A. Allylic Amination. *Chem. Rev.* **1998**, *98* (4), 1689–1708.

(6) Wang, M.; Xiao, F.; Bai, Y.; Hu, X. Reactions of Tertiary Allylic Amines and Dichlorocarbenes. *Synth. Commun.* **2015**, *45* (19), 2259–2265.

(7) DeLuca, R. J.; Sigman, M. S. Anti-Markovnikov Hydroalkylation of Allylic Amine Derivatives via a Palladium-Catalyzed Reductive Cross-Coupling Reaction. *J. Am. Chem. Soc.* **2011**, *133* (30), 11454–11457.

(8) Weiner, B.; Baeza, A.; Jerphagnon, T.; Feringa, B. L. Aldehyde Selective Wacker Oxidations of Phthalimide Protected Allylic Amines: A New Catalytic Route to B3-Amino Acids. *J. Am. Chem. Soc.* **2009**, *131* (27), 9473–9474.

(9) Allylic S_N2 reactions can suffer from numerous problems such as poor regioselectivity between branched and linear products. In the case of amination, competitive overallylation of tertiary amine products can be a major challenge. For specific examples of these issues, see references 10–12.

(10) Mitsunobu, O. In *Comprehensive Organic Synthesis*; Trost, B. M., Fleming, I., Winterfeldt, E., Eds.; Pergamon Press: Oxford, 1991; Vol. 6, pp 22-28.

(11) Sen, S. E.; Roach, S. L. A Convenient Two-Step Procedure for the Synthesis of Substituted Allylic Amines from Allylic Alcohols. *Synthesis* **1995**, *1995* (07), 756–758.

(12) Solomons, T.W.G.S.; Fryhle, C.B.; Snyder S. A. In *Organic Chemistry*; Wiley: New York, 2016, pp 901-908.

(13) For selected successful examples of SN_2-type reactions, see references 14–16.

(14) Roughley, S. D.; Jordan, A. M. The Medicinal Chemist's Toolbox: An Analysis of Reactions Used in the Pursuit of Drug Candidates. *J. Med. Chem.* **2011**, *54* (10), 3451–3479.

(15) Brown, D. G.; Boström, J. Analysis of Past and Present Synthetic Methodologies on Medicinal Chemistry: Where Have All the New Reactions Gone? Miniperspective. *J. Med. Chem.* **2016**, *59* (10), 4443–4458.

(16) Taylor, A. R.; Katritzky, R. J. K. In *Comprehensive Organic Functional Group Transformations II.*; Elsevier; pp 255–300.

(17) For examples of amination of transition metal π-allyl intermediates derived from allylic electrophiles, see references 18–24.

(18) Trost, B. M.; Van Vranken, D. L. Asymmetric Transition Metal-Catalyzed Allylic Alkylations. *Chem. Rev.* **1996**, *96* (1), 395–422.

(19) Graening, T.; Schmalz, H.-G. Pd-Catalyzed Enantioselective Allylic Substitution: New Strategic Options for the Total Synthesis of Natural Products. *Angew. Chem. Int. Ed.* **2003**, *42* (23), 2580–2584.

(20) Grange, R. L.; Clizbe, E. A.; Evans, P. A. Recent Developments in Asymmetric Allylic Amination Reactions. *Synthesis* **2016**, *48* (18), 2911-2968.

(21) Yamashita, Y.; Gopalarathnam, A.; Hartwig, J. F. Iridium-Catalyzed, Asymmetric Amination of Allylic Alcohols Activated by Lewis Acids. *J. Am. Chem. Soc.* **2007**, *129* (24), 7508–7509.

(22) You, S.-L.; Zhu, X.-Z.; Luo, Y.-M.; Hou, X.-L.; Dai, L.-X. Highly Regio- and Enantioselective Pd-Catalyzed Allylic Alkylation and Amination of Monosubstituted Allylic Acetates with Novel Ferrocene P,N-Ligands. *J. Am. Chem. Soc.* **2001**, *123* (30), 7471–7472.

(23) Takeuchi, R.; Ue, N.; Tanabe, K.; Yamashita, K.; Shiga, N. Iridium Complex-Catalyzed Allylic Amination of Allylic Esters. *J. Am. Chem. Soc.* **2001**, *123* (39), 9525–9534.

(24) Sundararaju, B.; Achard, M.; Bruneau, C. Transition Metal Catalyzed Nucleophilic Allylic Substitution: Activation of Allylic Alcohols via π-Allylic Species. *Chem. Soc. Rev.* **2012**, *41* (12), 4467–4483.

(25) While reductive amination is a classic approach for the synthesis of aliphatic amines, the reductive amination α,β-unsaturated aldehydes is substantially less common, presumably due to rapid 1,4-addition processes.

(26) Roth, H.; Romero, N.; Nicewicz, D. Experimental and Calculated Electrochemical Potentials of Common Organic Molecules for Applications to Single-Electron Redox Chemistry. *Synlett* **2015**, *27* (05), 714–723.

(27) Cheng, Q.; Chen, J.; Lin, S.; Ritter, T. Allylic Amination of Alkenes with Iminothianthrenes to Afford Alkyl Allylamines. *J. Am. Chem. Soc.* **2020**, *142* (41), 17287–17293.

(28) Substantial progress has been made in redox-neutral hydroamination processes that furnish aliphatic amine products. See references 29–36.

(29) Wiese, S.; Badiei, Y. M.; Gephart, R. T.; Mossin, S.; Varonka, M. S.; Melzer, M. M.; Meyer, K.; Cundari, T. R.; Warren, T. H. Catalytic C–H Amination with Unactivated Amines through Copper(II) Amides. *Angew. Chem. Int. Ed.* **2010**, *49* (47), 8850–8855.

(30) Beller, M.; Trauthwein, H.; Eichberger, M.; Breindl, C.; Herwig, J.; Müller, T. E.; Thiel, O. R. The First Rhodium-Catalyzed Anti-Markovnikov Hydroamination: Studies on Hydroamination and Oxidative Amination of Aromatic Olefins. *Chem. - Eur. J.* **1999**, *5* (4), 1306–1319.

(31) Utsunomiya, M.; Hartwig, J. F. Intermolecular, Markovnikov Hydroamination of Vinylarenes with Alkylamines. *J. Am. Chem. Soc.* **2003**, *125* (47), 14286–14287.

(32) Al-Masum, M.; Meguro, M.; Yamamoto, Y. The Two Component Palladium Catalyst System for Intermolecular Hydroamination of Allenes. *Tetrahedron Lett.* **1997**, *38* (34), 6071–6074.

(33) Kuchenbeiser, G.; Shaffer, A. R.; Zingales, N. C.; Beck, J. F.; Schmidt, J. A. R. Palladium(II) 3-Iminophosphine (3IP) Complexes: Active Precatalysts for the Intermolecular Hydroamination of 1,2-Dienes (Allenes) and 1,3-Dienes with Aliphatic Amines under Mild Conditions. *J. Organomet. Chem.* **2011**, *696* (1), 179–187.

(34) Ickes, A. R.; Ensign, S. C.; Gupta, A. K.; Hull, K. L. Regio- and Chemoselective Intermolecular Hydroamination of Allyl Imines for the Synthesis of 1,2-Diamines. *J. Am. Chem. Soc.* **2014**, *136* (32), 11256–11259.

(35) Liu, R. Y.; Buchwald, S. L. CuH-Catalyzed Olefin Functionalization: From Hydroamination to Carbonyl Addition. *Acc. Chem. Res.* **2020**, *53* (6), 1229–1243.

(36) Gui, J.; Pan, C.-M.; Jin, Y.; Qin, T.; Lo, J. C.; Lee, B. J.; Spergel, S. H.; Mertzman, M. E.; Pitts, W. J.; La Cruz, T. E.; Schmidt, M. A.; Darvatkar, N.; Natarajan, S. R.; Baran, P. S. Practical Olefin Hydroamination with Nitroarenes. *Science* **2015**, *348* (6237), 886–891.

(37) Ramirez, T. A.; Zhao, B.; Shi, Y. Recent Advances in Transition Metal-Catalyzed sp^3 C–H Amination Adjacent to Double Bonds and Carbonyl Groups. *Chem. Soc. Rev.* **2012**, *41* (2), 931–942.

(38) Liron, F.; Oble, J.; Lorion, M. M.; Poli, G. Direct Allylic Functionalization Through Pd-Catalyzed C-H Activation: Direct Allylic Functionalization by Pd-Catalyzed C-H Activation. *Eur. J. Org. Chem.* **2014**, *2014* (27), 5863–5883.

(39) Fernandes, R. A.; Nallasivam, J. L. Catalytic Allylic Functionalization *via* π-Allyl Palladium Chemistry. *Org. Biomol. Chem.* **2019**, *17* (38), 8647–8672.

(40) Wang, R.; Luan, Y.; Ye, M. Transition Metal–Catalyzed Allylic C(sp_3)–H Functionalization via η^3-Allylmetal Intermediate. *Chin. J. Chem.* **2019**, *37* (7), 720–743.

(41) Fix, S. R.; Brice, J. L.; Stahl, S. S. Efficient Intramolecular Oxidative Amination of Olefins through Direct Dioxygen-Coupled Palladium Catalysis. *Angew. Chem. Int. Ed.* **2002**, *41* (1), 164–166.

(42) As an alternative to employing oxidatively stable nitrogen sources, a handful of examples have exploited amine oxidation (typically of *N*-aryl amines) to generate an iminium intermediate that undergoes a subsequent trapping with vinyl nucleophiles in a one-pot process. For examples, see references 43–46.

(43) Muramatsu, W.; Nakano, K.; Li, C.-J. Direct sp^3 C–H Bond Arylation, Alkylation, and Amidation of Tetrahydroisoquinolines Mediated by Hypervalent Iodine(III) under Mild Conditions. *Org. Biomol. Chem.* **2014**, *12* (14), 2189–2192.

(44) Barham, J. P.; John, M. P.; Murphy, J. A. One-Pot Functionalisation of N-Substituted Tetrahydroisoquinolines by Photooxidation and Tunable Organometallic Trapping of Iminium Intermediates. *Beilstein J. Org. Chem.* **2014**, *10* (1), 2981–2988.

(45) Franz, J. F.; Kraus, W. B.; Zeitler, K. No Photocatalyst Required – Versatile, Visible Light Mediated Transformations with Polyhalomethanes. *Chem. Commun.* **2015**, *51* (39), 8280–8283.

(46) Barham, J. P.; John, M. P.; Murphy, J. A. Contra-Thermodynamic Hydrogen Atom Abstraction in the Selective C–H Functionalization of Trialkylamine N-CH_3 Groups. *J. Am. Chem. Soc.* **2016**, *138* (47), 15482–15487.

(47) Burman, J. S.; Blakey, S. B. Regioselective Intermolecular Allylic C−H Amination of Disubstituted Olefins via Rhodium/π-Allyl Intermediates. *Angew. Chem. Int. Ed.* **2017**, *56* (44), 13666–13669.

(48) Ma, R.; White, M. C. C–H to C–N Cross-Coupling of Sulfonamides with Olefins. *J. Am. Chem. Soc.* **2018**, *140* (9), 3202–3205.

(49) Lei, H.; Rovis, T. Ir-Catalyzed Intermolecular Branch-Selective Allylic C–H Amidation of Unactivated Terminal Olefins. *J. Am. Chem. Soc.* **2019**, *141* (6), 2268–2273.

(50) Liu, G.; Yin, G.; Wu, L. Palladium-Catalyzed Intermolecular Aerobic Oxidative Amination of Terminal Alkenes: Efficient Synthesis of Linear Allylamine Derivatives. *Angew. Chem. Int. Ed.* **2008**, *47* (25), 4733–4736.

(51) Reed, S. A.; Mazzotti, A. R.; White, M. C. A Catalytic, Brønsted Base Strategy for Intermolecular Allylic C−H Amination. *J. Am. Chem. Soc.* **2009**, *131* (33), 11701–11706.

(52) Pattillo, C. C.; Strambeanu, I. I.; Calleja, P.; Vermeulen, N. A.; Mizuno, T.; White, M. C. Aerobic Linear Allylic C–H Amination: Overcoming Benzoquinone Inhibition. *J. Am. Chem. Soc.* **2016**, *138* (4), 1265–1272.

(53) Yin, G.; Wu, Y.; Liu, G. Scope and Mechanism of Allylic C−H Amination of Terminal Alkenes by the Palladium/PhI(OPiv)$_2$ Catalyst System: Insights into the Effect of Naphthoquinone. *J. Am. Chem. Soc.* **2010**, *132* (34), 11978–11987.

(54) Harris, R. J.; Park, J.; Nelson, T. A. F.; Iqbal, N.; Salgueiro, D. C.; Bacsa, J.; MacBeth, C. E.; Baik, M.-H.; Blakey, S. B. The Mechanism of Rhodium-Catalyzed Allylic C–H Amination. *J. Am. Chem. Soc.* **2020**, *142* (12), 5842–5851.

(55) Lei, H.; Rovis, T. A Site-Selective Amination Catalyst Discriminates between Nearly Identical C–H Bonds of Unsymmetrical Disubstituted Alkenes. *Nat. Chem.* **2020**, *12* (8), 725–731.

(56) Ide, T.; Feng, K.; Dixon, C. F.; Teng, D.; Clark, J. R.; Han, W.; Wendell, C. I.; Koch, V.; White, M. C. Late-Stage Intermolecular Allylic C–H Amination. *J. Am. Chem. Soc.* **2021**, *143* (37), 14969–14975.

(57) Gephart III, R. T.; Huang, D. L.; Aguila, M. J. B.; Schmidt, G.; Shahu, A.; Warren, T. H. Catalytic C–H Amination with Aromatic Amines. *Angew. Chem. Int. Ed.* **2012**, *51* (26), 6488–6492.

(58) Wilken, M.; Ortgies, S.; Breder, A.; Siewert, I. Mechanistic Studies on the Anodic Functionalization of Alkenes Catalyzed by Diselenides. *ACS Catal.* **2018**, *8* (11), 10901–10912.

(59) Souto, J. A.; Zian, D.; Muñiz, K. Iodine(III)-Mediated Intermolecular Allylic Amination under Metal-Free Conditions. *J. Am. Chem. Soc.* **2012**, *134* (17), 7242–7245.

(60) Roizen, J. L.; Harvey, M. E.; Du Bois, J. Metal-Catalyzed Nitrogen-Atom Transfer Methods for the Oxidation of Aliphatic C–H Bonds. *Acc. Chem. Res.* **2012**, *45* (6), 911–922.

(61) Starkov, P.; Jamison, T. F.; Marek, I. Electrophilic Amination: The Case of Nitrenoids. *Chem. – Eur. J.* **2015**, *21* (14), 5278–5300.

(62) Dauban, P.; Dodd, R. H. Iminoiodanes and C-N Bond Formation in Organic Synthesis. *Synlett* **2003**, *2003* (11), 1571–1586.

(63) Shimbayashi, T.; Sasakura, K.; Eguchi, A.; Okamoto, K.; Ohe, K. Recent Progress on Cyclic Nitrenoid Precursors in Transition-Metal-Catalyzed Nitrene-Transfer Reactions. *Chem. – Eur. J.* **2019**, *25* (13), 3156–3180.

(64) Scriven, E. F. V.; Turnbull, K. Azides: Their Preparation and Synthetic Uses. *Chem. Rev.* **1988**, *88* (2), 297–368.

(65) Shin, K.; Kim, H.; Chang, S. Transition-Metal-Catalyzed C–N Bond Forming Reactions Using Organic Azides as the Nitrogen Source: A Journey for the Mild and Versatile C–H Amination. *Acc. Chem. Res.* **2015**, *48* (4), 1040–1052.

(66) Lebel, H.; Huard, K.; Lectard, S. *N*-Tosyloxycarbamates as a Source of Metal Nitrenes: Rhodium-Catalyzed C−H Insertion and Aziridination Reactions. *J. Am. Chem. Soc.* **2005**, *127* (41), 14198–14199.

(67) Hennessy, E. T.; Betley, T. A. Complex N-Heterocycle Synthesis via Iron-Catalyzed, Direct C–H Bond Amination. *Science* **2013**, *340* (6132), 591–595.

(68) Hennessy, E. T.; Liu, R. Y.; Iovan, D. A.; Duncan, R. A.; Betley, T. A. Iron-Mediated Intermolecular N-Group Transfer Chemistry with Olefinic Substrates. *Chem. Sci.* **2014**, *5* (4), 1526–1532.

(69) Liang, C.; Collet, F.; Robert-Peillard, F.; Müller, P.; Dodd, R. H.; Dauban, P. Toward a Synthetically Useful Stereoselective C−H Amination of Hydrocarbons. *J. Am. Chem. Soc.* **2008**, *130* (1), 343–350.

(70) Collet, F.; Lescot, C.; Liang, C.; Dauban, P. Studies in Catalytic C–H Amination Involving Nitrene C–H Insertion. *Dalton Trans.* **2010**, *39* (43), 10401–10413.

(71) Fantauzzi, S.; Gallo, E.; Caselli, A.; Ragaini, F.; Casati, N.; Macchi, P.; Cenini, S. The Key Intermediate in the Amination of Saturated C–H Bonds: Synthesis, X-Ray Characterization and Catalytic Activity of $Ru(TPP)(NAr)_2$ (Ar = 3,5-$(CF_3)_2C_6H_3$). *Chem. Commun.* **2009**, No. 26, 3952–3954.

(72) Leveraging ene reactions rather than nitrene insertion, other high oxidation state nitrogen sources have been used for allylic amination. See references 73–74.

(73) Bao, H.; Tambar, U. K. Catalytic Enantioselective Allylic Amination of Unactivated Terminal Olefins via an Ene Reaction/[2,3]-Rearrangement. *J. Am. Chem. Soc.* **2012**, *134* (45), 18495–18498.

(74) Bayeh, L.; Le, P. Q.; Tambar, U. K. Catalytic Allylic Oxidation of Internal Alkenes to a Multifunctional Chiral Building Block. *Nature* **2017**, *547* (7662), 196–200.

(75) New strategies for alkene oxidation strategies towards *N*-alkyl aziridine synthesis have been recently developed, see references 76–80. In stark contrast, the synthesis of allylic amine building blocks from alkenes via net $C(sp^3)$–H amination transformations remains limited.

(76) Falk, E.; Makai, S.; Delcaillau, T.; Gürtler, L.; Morandi, B. Design and Scalable Synthesis of *N*-Alkylhydroxylamine Reagents for the Direct Iron-Catalyzed Installation of Medicinally Relevant Amines. *Angew. Chem. Int. Ed.* **2020**, *59* (47), 21064–21071.

(77) Jat, J. L.; Paudyal, M. P.; Gao, H.; Xu, Q.-L.; Yousufuddin, M.; Devarajan, D.; Ess, D. H.; Kürti, L.; Falck, J. R. Direct Stereospecific Synthesis of Unprotected N–H and N–Me Aziridines from Olefins. *Science* **2014**, *343* (6166), 61–65.

(78) Ošeka, M.; Laudadio, G.; Leest, N. P. van; Dyga, M.; Bartolomeu, A. de A.; Gooßen, L. J.; Bruin, B. de; Oliveira, K. T. de; Noël, T. Electrochemical Aziridination of Internal Alkenes with Primary Amines. *Chem* **2021**, *7* (1), 255–266.

(79) Govaerts, S.; Angelini, L.; Hampton, C.; Malet-Sanz, L.; Ruffoni, A.; Leonori, D. Photoinduced Olefin Diamination with Alkylamines. *Angew. Chem. Int. Ed.* **2020**, *59* (35), 15021–15028.

(80) Holst, D. E.; Wang, D. J.; Kim, M. J.; Guzei, I. A.; Wickens, Z. K. Aziridine Synthesis by Coupling Amines and Alkenes via an Electrogenerated Dication. *Nature* **2021**, *596* (7870), 74–79.

(81) 2,490,000 primary amines and 1,888,500 secondary amines, which totals 4,378,500 commerical amines to give aliphatic amine products. eMolecules (eMolecules Inc, accessed 7 November 2021); https://www.emolecules.com.

(82) Yoshida, J.; Shimizu, A.; Hayashi, R. Electrogenerated Cationic Reactive Intermediates: The Pool Method and Further Advances. *Chem. Rev.* **2018**, *118* (9), 4702–4730.

(83) Hayashi, R.; Shimizu, A.; Yoshida, J. The Stabilized Cation Pool Method: Metal- and Oxidant-Free Benzylic C–H/Aromatic C–H Cross-Coupling. *J. Am. Chem. Soc.* **2016**, *138* (27), 8400–8403.

(84) Yoshida, J.; Suga, S. Basic Concepts of "Cation Pool" and "Cation Flow" Methods and Their Applications in Conventional and Combinatorial Organic Synthesis. *Chem. – Eur. J.* **2002**, *8* (12), 2650–2658.

(85) Berger, F.; Plutschack, M. B.; Riegger, J.; Yu, W.; Speicher, S.; Ho, M.; Frank, N.; Ritter, T. Site-Selective and Versatile Aromatic C−H Functionalization by Thianthrenation. *Nature* **2019**, *567* (7747), 223–228.

(86) Chen, J.; Li, J.; Plutschack, M. B.; Berger, F.; Ritter, T. Regio- and Stereoselective Thianthrenation of Olefins To Access Versatile Alkenyl Electrophiles. *Angew. Chem. Int. Ed.* **2020**, *59* (14), 5616–5620.

(87) Alvarez, E. M.; Plutschack, M. B.; Berger, F.; Ritter, T. Site-Selective C–H Functionalization-Sulfination Sequence to Access Aryl Sulfonamides. *Org. Lett.* **2020**, *22* (12) 4593–4596.

(88) Juliá, F.; Yan, J.; Paulus, F.; Ritter, T. Vinyl Thianthrenium Tetrafluoroborate: A Practical and Versatile Vinylating Reagent Made from Ethylene. *J. Am. Chem. Soc.* **2021**, *143* (33), 12992–12998.

(89) Chen, C.; Wang, M.; Lu, H.; Zhao, B.; Shi, Z. Enabling the Use of Alkyl Thianthrenium Salts in Cross-Coupling Reactions by Copper Catalysis. *Angew. Chem. Int. Ed.* **2021**, *60* (40), 21756–21760.

(90) Chen, C.; Wang, Z.-J.; Lu, H.; Zhao, Y.; Shi, Z. Generation of Non-Stabilized Alkyl Radicals from Thianthrenium Salts for C–B and C–C Bond Formation. *Nat. Commun.* **2021**, *12* (1), 4526.

(91) Jia, H.; Häring, A. P.; Berger, F.; Zhang, L.; Ritter, T. Trifluoromethyl Thianthrenium Triflate: A Readily Available Trifluoromethylating Reagent with Formal CF_3^+, CF_3•, and CF_3^- Reactivity. *J. Am. Chem. Soc.* **2021**, *143* (20), 7623–7628.

(92) Antoni, P. W.; Mackenroth, A. V.; Mulks, F. F.; Rudolph, M.; Helmchen, G.; Hashmi, A. S. K. Dibenzothiophenesulfilimines: A Convenient Approach to Intermolecular Rhodium-Catalysed C−H Amidation. *Chem. – Eur. J.* **2020**, *26* (37), 8235–8238.

(93) Shine, H. J.; Bandlish, B. K.; Mani, S. R.; Padilla, A. G. Ion Radicals. 43. Addition of Thianthrene and Phenoxathiin Cation Radicals to Alkenes and Alkynes. *J. Org. Chem.* **1979**, *44* (6), 915–917.

(94) Shine, H. J.; Zhao, B.; Qian, D.-Q.; Marx, J. N.; Guzman-Jimenez, I. Y.; Thurston, J. H.; Ould-Ely, T.; Whitmire, K. H. Adducts of Phenoxathiin and Thianthrene Cation Radicals with Alkenes and Cycloalkenes. *J. Org. Chem.* **2003**, *68* (23), 8910–8917.

(95) Mitchell, S. C.; Waring, R. H. Fate of Thianthrene in Biological Systems. *Xenobiotica* **2017**, *47* (8), 731–740.

(96) The cost of thianthrene is less than 0.15 USD $mmol^{-1}$.

(97) When base was omitted from previously reported thianthrene-based aziridination conditions (reference 80), diamination was observed rather than aziridination. Preliminary mechanistic evidence suggests this product proceeds via an aziridinium intermediate. Additionally, for a recent strategy generating diamine products via generation of aziridinium salts from secondary amines, see reference 79.

(98) Alkyne thianthrenation by chemically-generated thianthrene radical cation has been previously observed, see: Rangappa, P.; Shine, H. J.; Marx, J. N.; Ould-Ely, T.; Kelly, A. T.; Whitmire, K. H. Adducts of Thianthrene- and Phenoxathiin Cation Radical Tetrafluoroborates to 1-Alkynes. Structures and Formation of 1-(5-Thianthreniumyl)-

and 1-(10-Phenoxathiiniumyl)Alkynes on Alumina Leading to α-Ketoylides and α-Ketols. *J. Org. Chem.* **2005**, *70* (24), 9764–9770.

(99) While stereoselectivity was attenuated in these examples bearing proximal branching or functional groups, the thermodynami-cally disfavored *Z*-isomer was still observed.

(100) Currently, this methodology is restricted to terminal alkenes. While adducts could be formed readily from internal alkenes, these adducts provided an intractable mixture upon treatment with the amine nucleophile (see appendix A for details).

(101) Zimmermann, H. Propene. In *Ullmann's Encyclopedia of Industrial Chemistry*; American Cancer Society, 2013; pp 00–00.

(102) Geilen, F. M. A.; Stochniol, G.; Peitz, S.; Schulte-Koerne, E. Butenes. In *Ullmann's Encyclopedia of Industrial Chemistry*; American Cancer Society, 2014; pp 1–13.

(103) Krähling, L.; Krey, J.; Jakobson, G.; Grolig, J.; Miksche, L. Allyl Compounds. In *Ullmann's Encyclopedia of Industrial Chemistry*; American Cancer Society, 2000.

(104) By avoiding use of allylic halides, this method also obviates need for disposal of halide waste.

(105) Our previous report shows 76% thianthrene recovery following substitution of the dicationic adducts upon scaleup. See reference 80.

(106) Yamanaka, H.; Matsuo, J.; Kawana, A.; Mukaiyama, T. A Convenient Method for the Synthesis of β,γ-Unsaturated Amines from Alkenes via α,β-Unsaturated Diphenylsulfonium Salts. *Chem. Lett.* **2003**, *32* (7), 626–627.

Chapter 3: Unraveling the Mechanism of *Z*-selective Allylic Functionalization *via* Thianthrenium Salts

A collaboration with Achyut R. Gogoi, Angel Rentería-Gómez, Min Ji Kim, Osvaldo Gutierrez, and Zachary K. Wickens

3.1 Abstract

A detailed mechanistic study of the *Z*-selective allylic functionalization of thianthrenium salts is presented. We have leveraged kinetic analysis and deuterium labelling to concretely determine the elementary steps involved. We find that the reaction proceeds *via* a rate- and stereodetermining allylic deprotonation of an alkenylthianthrenium species. Intriguingly, computational studies uncover a pronounced kinetic bias towards the generation of the *Z*-allylic thianthrenium ylide in this step. We have identified stabilizing non-bonding interactions that contribute to the observed stereoselectivity. Overall, the *Z*-configuration of the ylide is effectively locked through a sequence of subsequent fast and irreversible steps: protonation to a *Z*-allylic thianthrenium electrophile followed by regioselective substitution by the nucleophile. While a few isolated reports have noted the thermodynamic preference of freely rotating *Z*-allylic anions, the *Z*-selective allylic functionalization of thianthrenium salts marks the first method wherein this phenomenon has been exploited in a more general synthetic context.

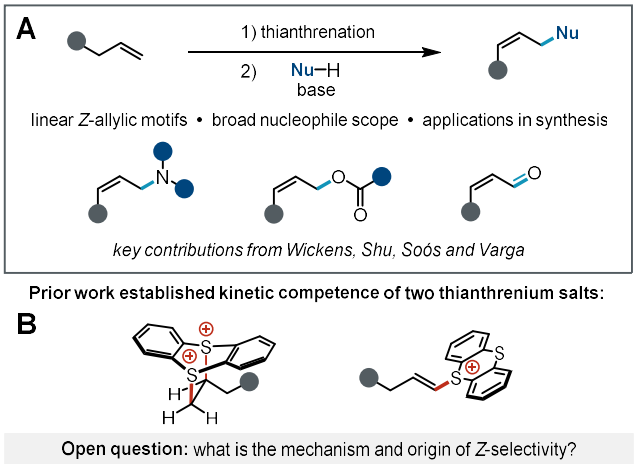

Figure 3.1. Overview of Z-selective allylic functionalization from thianthrenium salts. (A) Synthetic advances. (B) Prior mechanistic work.

3.2 Introduction

Stereoselective methods to make alkenes have proven to be valuable tools for the synthesis of complex molecules.[1,2] However, established approaches to prepare alkenes are skewed towards *E*-selective methods and preparation of *Z*-alkenes remains generally more challenging. Indeed, *Z*-alkenes cannot be generated selectively *via* thermodynamically-controlled processes since the *E*-stereoisomer is often more thermodynamically stable due to minimization of steric interactions.[3] This restriction can be circumvented by kinetically-controlled processes, but successful approaches must either offset the energetic penalty from 1,3-allylic strain in *Z*-alkene-forming transition structure or introduce new impediments to the *E*-alkene-forming pathway.[4] While several *Z*-selective methods to prepare alkenes have been established (*e.g.* Wittig olefination and semi-hydrogenation), the development of new protocols to access *Z*-alkenes remains an area of considerable contemporary interest.[5–8] As new distinct approaches to synthesize *Z*-alkenes continue to emerge, elucidating the origin of stereocontrol in these processes is of significant importance.[9–14] In addition to establishing a fundamental mechanistic understanding of these new transformations, identification of the factors that control reactivity and selectivity in these processes can, in turn, provide a blueprint for rational improvements to reaction conditions.[15,16]

Recently, independent reports from our group alongside Shu and co-workers introduced a new class of transformations to prepare an array of *Z*-alkene products (Figure 3.1).[17,18] In these methods, alkenes are first transformed into thianthrenium electrophiles[19–21] which are then treated with base and a nucleophile to furnish allylic functionalized products with exquisite regioselectivity and surprising *Z*-selectivity. These initial reports have led to further exciting developments made by others that cleverly exploit this allylic functionalization in new synthetic contexts.[22,23] Taken together, these advances suggest this new reactivity manifold will ultimately lead to a general platform for formal *Z*-selective allylic C(sp^3)–H functionalization. However, the mechanism of this process remains unknown. Confoundingly, the minimal mechanistic data presented to date are consistent with multiple mechanisms because the focus of the experiments has been establishing kinetic competence of thianthrenium species that could potentially interconvert. This leaves the elementary steps of the reaction opaque and ultimately precludes the elucidation of the origin of

stereocontrol.[24,25] Overall, we posit that constructing a detailed mechanistic model for this reaction will be a requisite step to translate this reactivity into a new broadly-applicable strategy in *Z*-alkene synthesis. Herein, we present an experimental mechanistic investigation that uncovers the elementary steps of the allylic functionalization of thianthrenium salts using amine nucleophiles.

3.3 Results and Discussion

A complete mechanism that is consistent with experimental and computational investigations (*vide infra*) is presented in Figure 3.2. Allylic functionalization proceeds through an isolable alkenylthianthrenium intermediate **3B** that is generated upon base-induced elimination of dicationic adducts **3A**.[17,20,26–28] The first step of the allylic functionalization process is the rate-determining deprotonation of an allylic C–H bond of the alkenylthianthrenium salt **3B**. The resultant allylic thianthrenium ylide **3C** is then rapidly protonated; under reaction conditions, this step is rendered irreversible as the corresponding allylic thianthrenium electrophile **3D** undergoes regioselective substitution with the nucleophile. The outcome of this step affords *Z*-allylic products (**3P**). Below, we will delineate the experimental and computational results and analyses that lead to the conclusion of these outlined elementary steps.

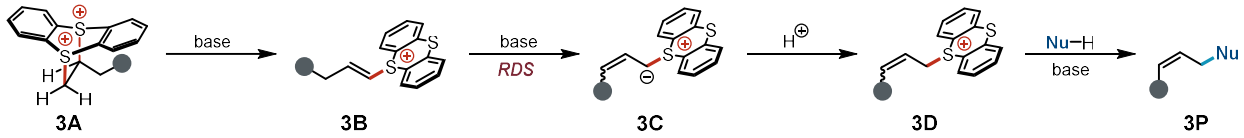

Figure 3.2. Elementary steps of *Z*-selective allylic functionalization from thianthrenium salts determined through experimental and computational studies.

Since both dicationic adducts and alkenylthianthrenium salts have been established as kinetically competent for allylic functionalization,[17,18] we first monitored the allylic amination reaction in order to identify which thianthrenium species to employ for our subsequent mechanistic studies. To this end, we electrochemically-generated a pool of meta-stable dicationic adducts **3.1** and **3.2** using 4-phenyl-1-butene and thianthrene (Scheme 3.1). Upon treatment with base in the absence of amine nucleophile, we observed rapid and quantitative elimination of dicationic adducts **3.1** and **3.2** to a solution-stable alkenylthianthrenium intermediate **3.3**.[29] When *N*-methylbenzylamine was added to the solution, the

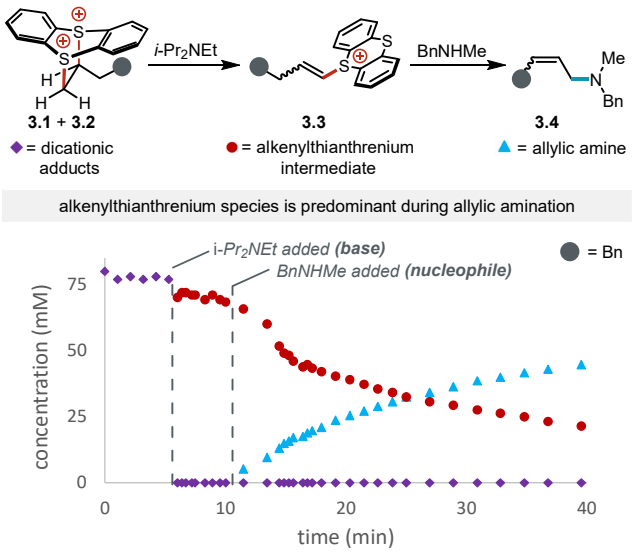

[a]Electrogenerated adducts were prepared using 4-phenyl-1-butene (0.2 mmol), thianthrene (0.3 mmol), 2 mL MeCN-d_3 (0.4 M KPF_6), I = 6.0 mA, 2.2 h (2.5 F mol^{-1} alkene); then *i*-Pr_2NEt (1.6 mmol); then amine (0.3 mmol). CH_2Br_2 was used as an internal standard. Only *mono*-adduct **3.1** is depicted. See appendix B for details.

Scheme 3.1. Monitoring speciation of thianthrenium salts.[a]

conversion of **3.3** corresponded to the formation of allylic amine product **3.4**. Furthermore, alkenylthianthrenium salt **3.3** was the only thianthrenium species detected by ^{1}H NMR spectroscopy during the allylic amination reaction. No detectable steady-state concentration of other thianthrenium species was observed (*e.g.* dicationic adducts **3A,** or allylic thianthrenium salt **3D**). Crucially however, these data do not exclude that transient thianthrenium electrophiles may be generated during allylic amination. These observations are consistent with the alkenylthianthrenium salt being a convergent intermediate as proposed in previous mechanistic hypotheses.[17,18] With these initial mechanistic insights, we opted to skip the exothermic elimination step (ΔH = –27.0 kJ/mol) of dicationic precursors to simplify the reaction conditions.[30,31] Thus, we conducted our experimental investigations using bench-stable alkenylthianthrenium salt **3.3** to streamline subsequent mechanism analyses (Scheme 3.2).

We next set out to identify model amine nucleophile for the allylic amination of alkenylthianthrenium salts that would enable the clearest mechanistic analysis. We recognized that a secondary aliphatic amine may serve a possible dual role as both nucleophile and base.[32] Indeed, when alkenylthianthrenium salt **3.3** was treated with *N*-methylbenzylamine in the absence of exogenous base, we

observed allylic amine product **3.4** in 52% yield and 5:1 *Z:E* (Scheme 3.2). We hypothesized that a non-basic aryl amine would deconvolute the kinetic behavior of the nucleophile for allylic amination. To test this hypothesis, we treated **3.3** with *N*-methylaniline with and without base (*i*-Pr_2NEt). These experiments revealed that in the absence of exogenous base, no allylic amination of **3.3** was observed. Under allylic amination conditions using *i*-Pr_2NEt base, we achieved a 57% yield of **3.5** with 6:1 *Z:E* selectivity, which is a similar outcome to secondary amine reactivity (Scheme 3.2). Taken together, these results indicate that aniline acts only as a nucleophile and *i*-Pr_2NEt is the sole base that promotes the allylic functionalization process. Overall, we identified the simplest components necessary for a mechanistic study of the reaction: alkenylthianthrenium salt, *N*-methylaniline nucleophile,[33] and base (*i*-Pr_2NEt).[34]

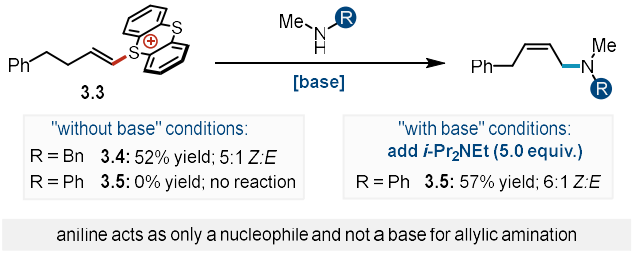

[a]Reactions conducted using alkenylthianthrenium salt (0.05 mmol), nucleophile (0.05 mmol), 0.5 mL MeCN, 6 h. [b]yields and *Z:E* determined by NMR.

Scheme 3.2. Model amine selection for experimental mechanistic studies of *Z*-selective allylic amination from thianthrenium salts.[a,b]

With a model reaction in hand, we set out to elucidate the elementary steps of the allylic amination reaction using kinetic experiments. Using *N*-methylaniline, we found zero-order dependence of the initial reaction rate on the nucleophile concentration (Figure 3.3A). Thus, we concluded that the rate-determining step for the allylic functionalization occurs prior to nucleophilic substitution. Next, kinetic experiments revealed a first-order dependence on the alkenylthianthrenium **3.3** (Figure 3.3B) as well as a first-order dependence on trialkylamine base (*i*-Pr_2NEt) (Figure 3.3C). These data altogether are consistent with rate-determining allylic deprotonation of the alkenylthianthrenium salt. We recognized the potential for various ylide intermediates to be formed; in particular, the reformation of dicationic adducts upon protonation. We questioned if the conjugate acid of *i*-Pr_2NEt, accumulated during the allylic amination, plays any kinetic role. When varying the concentration of exogenous *i*-Pr_2NHEtPF_6, we observed no impact on the initial rate

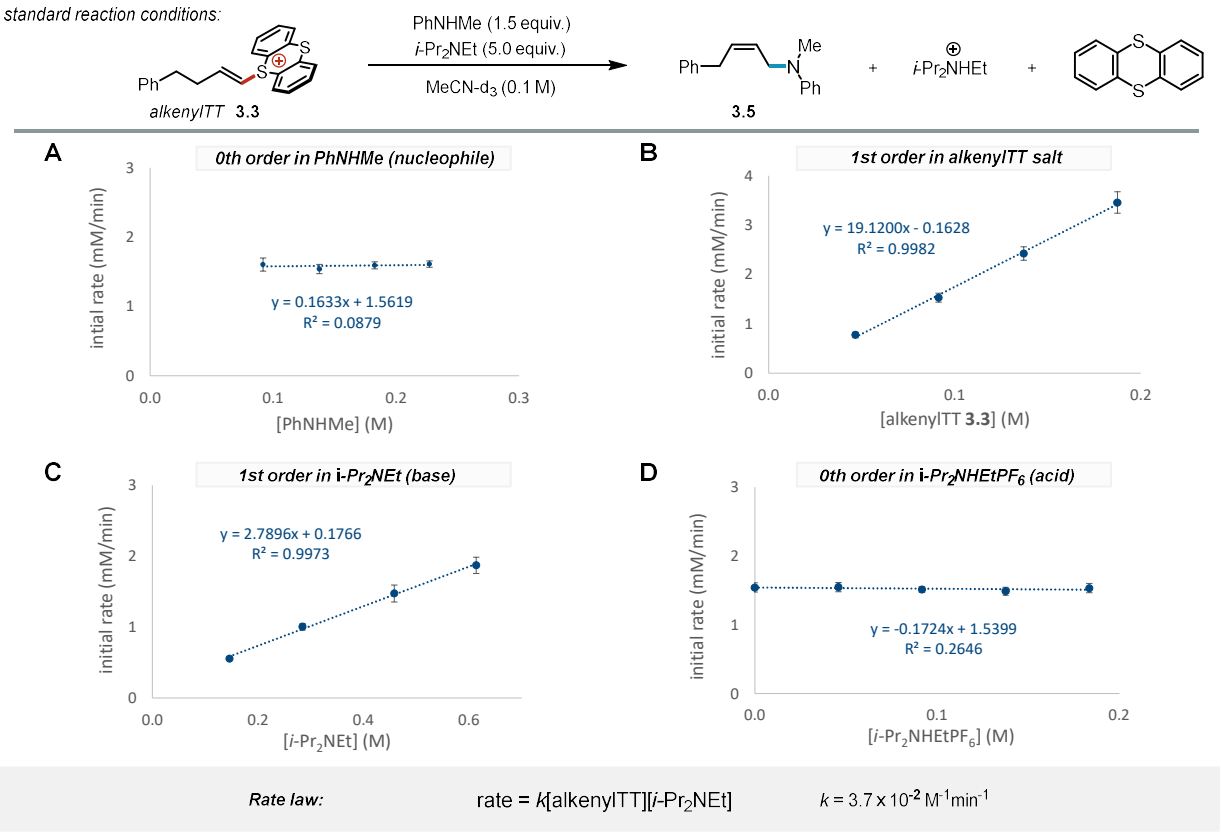

Figure 3.3. Reaction kinetics for allylic amination of alkenylthianthrenium salt and summary of rate law. (A) 0th order in aniline nucleophile, (B) 1st order in alkenythianthrenium salt, (C) 1st order in trialkylamine base, (D) 0th order in conjugate acid of amine. See appendix B for experimental details.

of allylic amine formation (Figure 3.3D). These observations are inconsistent with mechanisms in which dicationic adduct is transiently formed from alkenylthianthrenium salts followed by nucleophilic substitution or elimination (see appendix B for details).[35] Overall, these data are support deprotonation of the alkenylthianthrenium species being involved in the rate-determining step. Kinetic analyses afford a calculated experimental rate constant of 3.7±0.8 x 10^{-2} $M^{-1}mol^{-1}$ for this reaction.

Next, we conducted deuterium labelling experiments to support the rate-determining allylic deprotonation of the alkenylthianthrenium species by the base. A primary kinetic isotope effect (KIE) of 7.46±0.53 was observed in a two-pot competition experiment between **3.3** and **3.3-*d*$_2$** (Scheme 3.3A). This large primary KIE was consistent with the KIE value of 7.31±1.26 obtained in a one-pot competition experiment (Table B18). These results support that allylic C(sp^3)–H/D bond breaking is involved in the rate-determining step for the allylic functionalization of alkenylthianthrenium salts.[36] These KIEs combined

with reactant orders are inconsistent with conjugate-addition-type mechanisms, which have been observed with alkenylthianthrenium salts in other synthetic context (see appendix B for details).[37,38] To probe the irreversibility of this key allylic deprotonation step, the allylic amination reaction was conducted with an excess of deuterium oxide as a deuterium source (Scheme 3.3B).[39,40] We reasoned that an irreversible allylic deprotonation would give no deuterium incorporation into the corresponding alkenyl position of the allylic amine product. Experimentally, no deuterium was detected in the site of initial C(sp^3)–H bond breaking, consistent with the allylic deprotonation being irreversible under allylic substitution conditions (Scheme 3.3B). Furthermore, this result is inconsistent with a Curtin-Hammett scenario involving rapid isomerization between the alkenylthianthrenium salt and an allylic thianthrenium tautomer.[41]

Having identified the rate-determining step of the allylic functionalization process, we next probed each subsequent elementary step to establish a complete mechanistic picture. First, to probe the formation of the ylide **3D** intermediate, we examined the allylic amine product formed with the addition of deuterium oxide to the reaction conditions. The site that corresponds to the generated allylic thianthrenium ylide exhibited 53% deuterium incorporation (Scheme 3.3B).[42] The approximately 50% incorporation is consistent with irreversible ylide **3D** protonation due to fast nucleophilic substitution of the resultant allylic

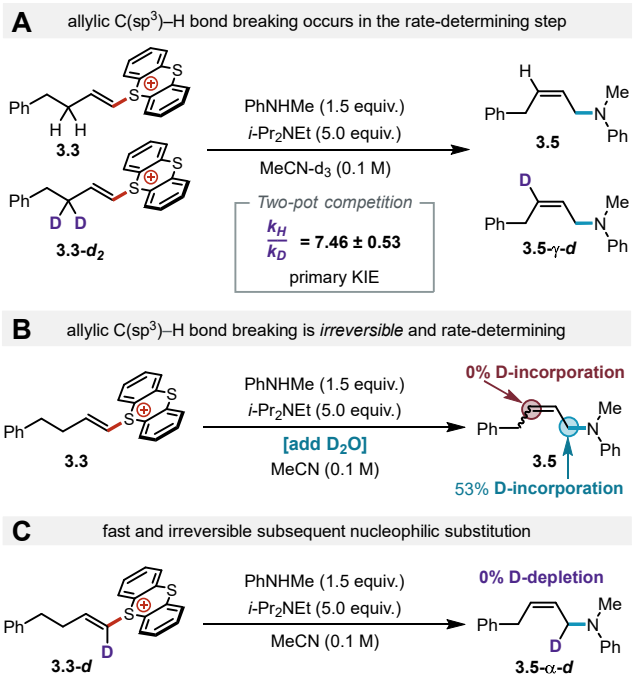

Scheme 3.3. Kinetic isotope effect (KIE) and deuterium-labelling experiments. See appendix B for experimental details.

thianthrenium electrophile **3E**. To further support this proposal, we subjected α-deuterated alkenylthianthrenium salt **3.3-*d*** to the allylic amination conditions (Scheme 3.3C). Allylic amine product **3.5-α-*d*** derived from deuterium-labelled alkenylthianthrenium salt **3.3-*d*** shows no deuterium depletion at the corresponding position. Taken together, these results are consistent with the non-stabilized allylic thianthrenium salt[43] formed upon ylide protonation being rapidly and irreversibly trapped by the amine nucleophile.

The elementary steps validated in this mechanistic study invoke the substitution of an allylic thianthrenium electrophile despite no observation of branched allylic products that are common side products for allylic halide substitution reactions. Notably, allylic amination of thianthrenium salts is consistently regioselective for linear products, with only isolated exceptions with thianthrenium salts derived from sterically hindered alkene precursors.[44] To evaluate whether substitution behavior of the proposed allylic thianthrenium species is consistent with these observations,[45] we conducted dispersion-corrected density functional theory (DFT) calculations (see appendix B for details). The DFT computations support high regioselectivity for S_N2 over S_N2' substitution for the *Z*-allylic thianthrenium electrophile (Figure 3.4, $\Delta\Delta G^{\ddagger}$ = 3.2 kcal/mol).[46,47] These computational data are consistent with the experimental observations and, accordingly, support the intermediacy of an allylic thianthrenium intermediate.

With a complete set of the elementary steps in hand,[48] we wanted to build and validate a computational model of the process with the ultimate goal of identifying the stereodetermining step. Our computational studies predict that the allylic deprotonation has the highest energetic barrier, consistent with

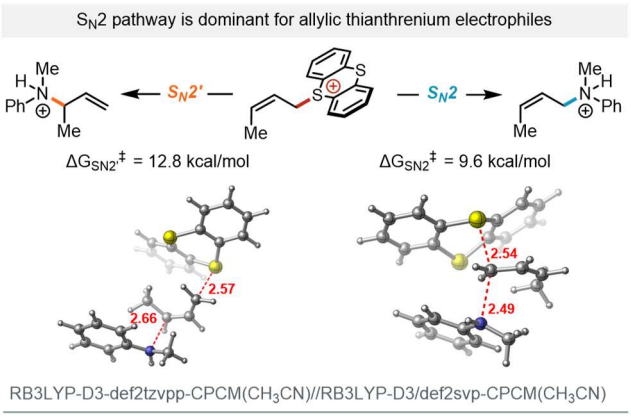

Figure 3.4. Computations to probe the nucleophilic substitution of postulated allylic thianthrenium intermediate.

experimental analyses that assign this as the rate-determining step (Figure 3.5). After deprotonation, the subsequent elementary steps are each favorable and ultimately rendered irreversible by highly exergonic nucleophilic displacement of the allylic thianthrenium intermediate. Intriguingly, these calculations indicate that the deprotonation to form the allylic thianthrenium ylide occurs with *Z*-selectivities that are consistent with experimental observations ($\Delta\Delta G^{\ddagger}$ = 2.3 kcal/mol). While the computational model appears to identify ylide formation as stereodetermining, we recognized that this would be an unusual scenario because it requires that the allylic anion is configurationally stable. However, in stark contrast to the low rotational barriers of simpler allylic anions, our calculations predict an unsurmountable barrier (*i.e.* 56 kcal/mol) for *Z/E*-isomerization of the allylic thianthrenium ylides. This high rotational barrier precludes isomerization between **3C_Z** and **3C_E** at room temperature (Figure 3.5). The origin of this high barrier is the direct consequence of localized alkene and ylide character as opposed to the anion being fully delocalized through the π-system (see appendix B for details). Overall, these data indicate that allylic deprotonation of the alkenylthianthrenium species sets the stereochemistry of the final allylic functionalized product. This stereodetermining step is a rare example of *Z*-selective deprotonation that enables *Z*-alkene synthesis.

To establish the origin of *Z*-selectivity, we next took a closer look at the allylic deprotonation that ultimately leads to the formation of *Z*-alkene or *E*-alkene. Given that the key deprotonation step is highly endergonic (~15 kcal/mol uphill in energy), we reasoned that, according to Hammond's postulate, the energy of the late transition state would be controlled more by the factors influencing the allylic ylide stability than the alkenylthianthrenium starting material. In fact, calculations show that the *Z*-isomer of the allylic thianthrenium ylide is more thermodynamically stable than the *E*-allylic ylide.[49] This energetic preference for the *Z*-isomer reflects the conformational landscape of simpler, freely-rotating allylic anions, which have an established preference for the *Z*-conformation.[50–55] Previous studies into those systems have put forward various explanations that invoke either electrostatic-based considerations[56] or nonbonding interactions,[57–60] although other possibilities cannot be ruled out.[61] Natural bond orbital (NBO) analysis of the competing ylide-forming transitions states (**TS3-1_E** and **TS3-1_Z**) revealed that the *Z*-forming transition state has more overall stabilizing interactions than the *E*-forming transition state (Figure 3.6).

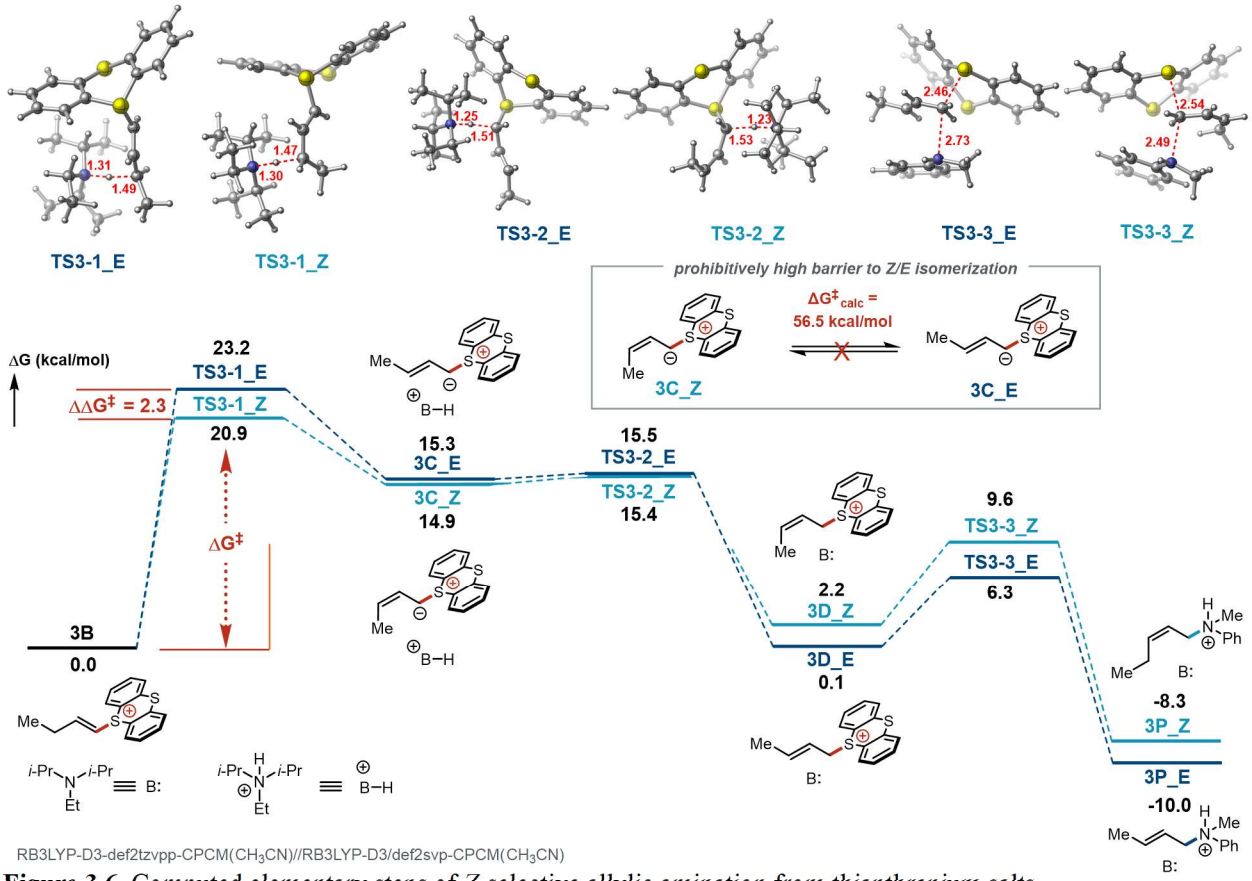

Figure 3.6. Computed elementary steps of *Z*-selective allylic amination from thianthrenium salts.

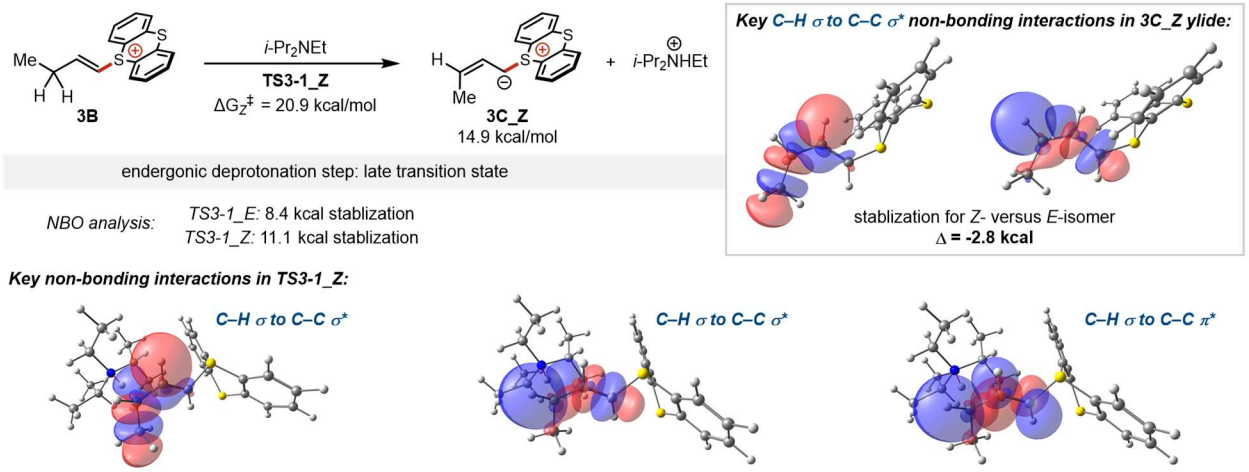

Figure 3.5. Computations to probe the origin of Z-selectivity in the rate-determining and stereodetermining allylic deprotonation step.

Specifically, we identified several C–H σ to C–C σ* or C–C π*non-bonding interactions that are present only in the transition structure that leads to the *Z*-allylic ylide. Furthermore, the resultant Z-allylic ylide product still possesses the majority of these NBO interactions. This suggests that the kinetic selectivity for

Z-allylic ylide formation is intimately tied to the factors that influence stability of the *Z*-allylic thianthrenium ylide.

3.4 Conclusion

In conclusion, we have outlined a detailed mechanistic model of the *Z*-selective allylic functionalization in the context of amine nucleophiles and thianthrenium salts derived from aliphatic alkenes. For the first time, the elementary steps of this reaction and the rate-determining step have been elucidated through kinetic analyses and deuterium labelling. Upon rate- and stereodetermining allylic deprotonation of the alkenylthianthrenium salt, a *Z*-allylic thianthrenium ylide is generated. Relative to an all-carbon allylic system, the thianthrenium ylide stereochemistry is locked due to high barrier for C–C double bond rotation. Protonation of the *Z*-allylic thianthrenium ylide affords an allylic thianthrenium electrophile that is regioselectively trapped by a nucleophile. Mechanistic data are all consistent with the allylic deprotonation being overall irreversible and stereodetermining. We anticipate these findings can lead to design of allylation methodologies that improve the selectivity for other alkenes and nucleophile classes.

More broadly, we have uncovered a distinct way to enforce *Z*-selectivity. A typical mechanistic manifold to impart high *Z*-selectivity is reagent or catalyst design that introduces a new steric clash to disfavor the formation of *E*-alkene. In contrast, the origin of *Z*-selectivity of the allylic functionalization of thianthrenium salts arises from a late transition state that exhibits the kinetic preference for *Z*-allylic thianthrenium ylide formation. Given that the elements (*e.g*. allylic deprotonation,[62] *Z*-allylic ylide thermodynamic preference,[63] high allylic anion rotational barriers[64]) are not unique to thianthrenium salts, we anticipate the findings in this mechanistic study to be generalizable in controlling Z-selectivity of a broader array of allylic functionalization reactions. These insights into a new origin of control are anticipated to inspire the design of new reactions that add to toolbox of *Z*-selective transformations in alkene synthesis.

3.5 Acknowledgements

This material is based upon work supported by the National Science Foundation Graduate Research Fellowship Program under grant no. DGE-1747503 (K.T.). Any opinions, findings, and conclusions or recommendations expressed in this material are those of the author(s) and do not necessarily reflect the views of the National Science Foundation. Spectroscopic instrumentation was supported by a generous gift from Paul J. and Margaret M. Bender, the National Science Foundation (CHE-1048642), and the National Institutes of Health (S10OD012245 and 1S10OD020022-1). O.G. acknowledges the NIGMS NIH (R35GM137797), Camille and Henry Dreyfus Foundation, and the Welch Foundation (A-2102-20220331) for funding and Texas A&M University HPRC resources (https://hprc.tamu.edu). B. J. Thompson is acknowledged for his assistance with the design and fabrication of the power supply. T. Drier is acknowledged for the fabrication of electrochemical glassware.

Z.K.W. and K.T. designed the project. K.T. designed and executed the mechanistic experiments. A.R.G. and A. R.-G. performed the computations. All authors contributed to the writing of the manuscript in preparation.

3.6 References

(1) Saicic, R. N. Protecting Group-Free Syntheses of Natural Products and Biologically Active Compounds. *Tetrahedron* **2014**, *70* (44), 8183–8218.

(2) Zhao, H.; Brånalt, J.; Perry, M.; Tyrchan, C. The Role of Allylic Strain for Conformational Control in Medicinal Chemistry. *J. Med. Chem.* **2023**, *66* (12), 7730–7755.

(3) Hoffmann, R. W. Allylic 1,3-Strain as a Controlling Factor in Stereoselective Transformations. *Chem. Rev.* **1989**, *89* (8), 1841–1860.

(4) Siau, W.-Y.; Zhang, Y.; Zhao, Y. Stereoselective Synthesis of Z-Alkenes. In *Stereoselective Alkene Synthesis*; Wang, J., Ed.; Topics in Current Chemistry; Springer: Berlin, Heidelberg, 2012; pp 33–58.

(5) Meek, S. J.; O'Brien, R. V.; Llaveria, J.; Schrock, R. R.; Hoveyda, A. H. Catalytic Z-Selective Olefin Cross-Metathesis for Natural Product Synthesis. *Nature* **2011**, *471* (7339), 461–466.

(6) Koh, M. J.; Khan, R. K. M.; Torker, S.; Yu, M.; Mikus, M. S.; Hoveyda, A. H. High-Value Alcohols and Higher-Oxidation-State Compounds by Catalytic Z-Selective Cross-Metathesis. *Nature* **2015**, *517* (7533), 181–186.

(7) Metternich, J. B.; Gilmour, R. A Bio-Inspired, Catalytic E → Z Isomerization of Activated Olefins. *J. Am. Chem. Soc.* **2015**, *137* (35), 11254–11257.

(8) Molloy, J. J.; Schäfer, M.; Wienhold, M.; Morack, T.; Daniliuc, C. G.; Gilmour, R. Boron-Enabled Geometric Isomerization of Alkenes via Selective Energy-Transfer Catalysis. *Science* **2020**, *369* (6501), 302–306.

(9) Vedejs, E.; Fleck, T. J. Kinetic (Not Equilibrium) Factors Are Dominant in Wittig Reactions of Conjugated Ylides. *J. Am. Chem. Soc.* **1989**, *111* (15), 5861–5871.

(10) Vedejs, E.; Marth, C. F. Mechanism of the Wittig Reaction: The Role of Substituents at Phosphorus. *J. Am. Chem. Soc.* **1988**, *110* (12), 3948–3958.

(11) Robiette, R.; Richardson, J.; Aggarwal, V. K.; Harvey, J. N. Reactivity and Selectivity in the Wittig Reaction: A Computational Study. *J. Am. Chem. Soc.* **2006**, *128* (7), 2394–2409.

(12) Oger, C.; Balas, L.; Durand, T.; Galano, J.-M. Are Alkyne Reductions Chemo-, Regio-, and Stereoselective Enough To Provide Pure (*Z*)-Olefins in Polyfunctionalized Bioactive Molecules? *Chem. Rev.* **2013**, *113* (3), 1313–1350.

(13) Liu, P.; Xu, X.; Dong, X.; Keitz, B. K.; Herbert, M. B.; Grubbs, R. H.; Houk, K. N. Z-Selectivity in Olefin Metathesis with Chelated Ru Catalysts: Computational Studies of Mechanism and Selectivity. *J. Am. Chem. Soc.* **2012**, *134* (3), 1464–1467.

(14) Neveselý, T.; Wienhold, M.; Molloy, J. J.; Gilmour, R. Advances in the E → Z Isomerization of Alkenes Using Small Molecule Photocatalysts. *Chem. Rev.* **2022**, *122* (2), 2650–2694.

(15) Sperger, T.; Sanhueza, I. A.; Schoenebeck, F. Computation and Experiment: A Powerful Combination to Understand and Predict Reactivities. *Acc. Chem. Res.* **2016**, *49* (6), 1311–1319.

(16) Keitz, B. K.; Endo, K.; Patel, P. R.; Herbert, M. B.; Grubbs, R. H. Improved Ruthenium Catalysts for Z-Selective Olefin Metathesis. *J. Am. Chem. Soc.* **2012**, *134* (1), 693–699.

(17) Wang, D. J.; Targos, K.; Wickens, Z. K. Electrochemical Synthesis of Allylic Amines from Terminal Alkenes and Secondary Amines. *J. Am. Chem. Soc.* **2021**, *143* (51), 21503–21510.

(18) Liu, M.-S.; Du, H.-W.; Shu, W. Metal-Free Allylic C–H Nitrogenation, Oxygenation, and Carbonation of Alkenes by Thianthrenation. *Chem. Sci.* **2022**, *13* (4), 1003–1008.

(19) A variety of practical methods have been recently advanced to prepare these thianthrenium salts, see: refs 20 and 21.

(20) Chen, J.; Li, J.; Plutschack, M. B.; Berger, F.; Ritter, T. Regio- and Stereoselective Thianthrenation of Olefins To Access Versatile Alkenyl Electrophiles. *Angewandte Chemie* **2020**, *132* (14), 5665–5669.

(21) Holst, D. E.; Wang, D. J.; Kim, M. J.; Guzei, I. A.; Wickens, Z. K. Aziridine Synthesis by Coupling Amines and Alkenes via an Electrogenerated Dication. *Nature* **2021**, *596* (7870), 74–79.

(22) Soós and Varga have coupled the allylic reactivity of alkenylthianthrenium salts with Kornblum oxidation to afford Z-α,β-unsaturated carbonyl compounds that are leveraged for natural product syntheses. See ref. 23.

(23) Angyal, P.; Kotschy, A. M.; Dudás, Á.; Varga, S.; Soós, T. Intertwining Olefin Thianthrenation with Kornblum/Ganem Oxidations: Ene-Type Oxidation to Furnish α,β-Unsaturated Carbonyls. *Angewandte Chemie International Edition* **2023**, *62* (2), e202214096.

(24) Recent mechanistic work on the process that generates aryl thianthrenium salts have revealed the origins of the exquisite para-selectivity that characterizes those reactions. For details, see ref. 25.

(25) Juliá, F.; Shao, Q.; Duan, M.; Plutschack, M. B.; Berger, F.; Mateos, J.; Lu, C.; Xue, X.-S.; Houk, K. N.; Ritter, T. High Site Selectivity in Electrophilic Aromatic Substitutions: Mechanism of C–H Thianthrenation. *J. Am. Chem. Soc.* **2021**, *143* (39), 16041–16054.

(26) Shine, H. J.; Zhao, B.; Qian, D.-Q.; Marx, J. N.; Guzman-Jimenez, I. Y.; Thurston, J. H.; Ould-Ely, T.; Whitmire, K. H. Adducts of Phenoxathiin and Thianthrene Cation Radicals with Alkenes and Cycloalkenes. *J. Org. Chem.* **2003**, *68* (23), 8910–8917.

(27) Qian, D.-Q.; Shine, H. J.; Guzman-Jimenez, I. Y.; Thurston, J. H.; Whitmire, K. H. Mono- and Bisadducts from the Addition of Thianthrene Cation Radical Salts to Cycloalkenes and Alkenes. *J. Org. Chem.* **2002**, *67* (12), 4030–4039.

(28) Juliá, F.; Yan, J.; Paulus, F.; Ritter, T. Vinyl Thianthrenium Tetrafluoroborate: A Practical and Versatile Vinylating Reagent Made from Ethylene. *J. Am. Chem. Soc.* **2021**, *143* (33), 12992–12998.

(29) These results are consistent with qualitative observations in our previous work wherein we isolated and re-subjected the alkenylthianthrenium species to support its kinetic competence.

(30) For example, we recognized that one-pot allylic functionalization from dicationic adducts would result in inaccurate quantification of base concentration necessary for kinetic analyses. See ref. ref. 31.

(31) Kim, M. J.; Wang, D. J.; Targos, K.; Garcia, U. A.; Harris, A. F.; Guzei, I. A.; Wickens, Z. K. Diastereoselective Synthesis of Cyclopropanes from Carbon Pronucleophiles and Alkenes. *Angewandte Chemie International Edition* **2023**, *62* (21), e202303032.

(32) We found that the initial rate of the reaction exhibited a first-order dependence on the secondary amine concentration (see appendix B for details).

(33) Allylic amination with PhNHMe and 4-Ph-1-butene-derived alkenylTT salt also enables *in situ* monitoring of *Z:E* ratios.

(34) In addition to *i*-Pr_2NEt being a suitable homogeneous base for monitoring *in situ* reaction kinetics, our group and others have observed superior *Z*-selectivity with trialkylamine bases than with heterogeneous bases such as carbonate.

(35) Consistent with our prior work, we observe rapid and quantitative elimination of dicationic adducts to alkenylthianthrenium salt. The rate of elimination is significantly faster than that of allylic amination.

(36) Simmons, E. M.; Hartwig, J. F. On the Interpretation of Deuterium Kinetic Isotope Effects in C□H Bond Functionalizations by Transition-Metal Complexes. *Angewandte Chemie International Edition* **2012**, *51* (13), 3066–3072.

(37) Holst, D. E.; Dorval, C.; Winter, C. K.; Guzei, I. A.; Wickens, Z. K. Regiospecific Alkene Aminofunctionalization via an Electrogenerated Dielectrophile. *J. Am. Chem. Soc.* **2023**, *145* (15), 8299–8307.

(38) Shu, W.; Liu, M.-S.; Meng, H. Unified Metal-Free Intermolecular Heck-Type Sulfonylation, Cyanation, Amination, Amidation of Alkenes by Thianthrenation. ChemRxiv July 3, 2023. https://doi.org/10.26434/chemrxiv-2023-xsgh1.

(39) We expect exchange between deuterium from D_2O and the conjugate acid of the amine base would be rapid where complete scrambling is to be observed. Under these conditions, deuteration of anionic intermediates should be feasible.

(40) Perrin, C. L.; Dwyer, T. J.; Baine, P. Two-Dimensional NMR Exchange Spectroscopy Study of Proton Exchange in Aqueous Ammonium Ion: H/D Primary Kinetic Isotope Effect for Direct Nitrogen-to-Nitrogen Proton Transfer. *J. Am. Chem. Soc.* **1994**, *116* (9), 4044–4049.

(41) Our data are inconsistent with a plausible Curtin-Hammett explanation for the origin of *Z*-selectivity recently suggested by Soós and coworkers. See ref. 23.

(42) Deuterium incorporation is close to 50% for *Z*-isomer of the allylic product. Curiously, lesser %D-incorporation was observed for the *E*-isomer product. We tentatively attribute this discrepancy to contributions from molecular dynamics. See appendix B for details.

(43) Stabilized allylic sulfonium and thianthrenium salts have been made but not with Z-stereochemistry. We suspect that non-stablized aliphatic allylic thianthrenium species are too reactive electrophiles to be isolated under the basic conditions used for their generation. .

(44) For regioselectivity with sterically hindered alkenylthianthrenium salts, see ref. 23.

(45) To probe the formation of a transient allylic thianthrenium electrophile, we aimed to alter the energetic landscape of allylic amination by using a bulky trialkylamine base as the nucleophile. In situ monitoring under these modified conditions revealed a new allylic intermediate during the allylic amination. We postulate the identity of this transient intermediate as the allylic thianthrenium tautomer (see appendix B for details), consistent with the mechanism put forward.

(46) A similar energy difference was observed between the S_N2 and S_N2' transition states leading to the *E*-allylic product.

(47) We reasoned that the nucleophilic substitution is stereoretentive in the pathways calculated given they are stereoretentive in allylic substitution with other allylic electrophiles.

(48) We considered a diverse array of possible alternative mechanisms, including each of those previously proposed in literature. None of the other mechanisms are consistent with new experimental details disclosed in this study. See appendix B for details.

(49) This is counter to the well-established thermodynamic preference for the *E*-configuration of neutral alkenes. Indeed, the alkenylthianthrenium starting material, allylic thianthrenium intermediate, and allylic products were more stable in the *E*-configuration.

(50) Young, W. G.; Winstein, S.; Prater, A. N. Allylic Rearrangements. II. Crotyl and Methylvinylcarbinylmagnesium Bromides [1]. *J. Am. Chem. Soc.* **1936**, *58* (2), 289–291.

(51) Haag, W. O.; Pines, H. The Kinetics of Carbanion-Catalyzed Isomerization of Butenes and 1-Pentene [1-3]. *J. Am. Chem. Soc.* **1960**, *82* (2), 387–391.

(52) Bank, S.; Schriesheim, A.; Rowe, C. A. An Understanding of the Stereoselectivity of Base-Catalyzed Olefin Isomerization Based on a Thermodynamically More Stable Cis-Allylic Anion. *J. Am. Chem. Soc.* **1965**, *87* (14), 3244–3245.

(53) Thompson, T. B.; Ford, W. T. Rotational Barriers of Allyl Anions in Solution. *J. Am. Chem. Soc.* **1979**, *101* (19), 5459–5464.

(54) McDonald, R. T.; Bywater, S. Cis-Trans Isomerization of Alkyl-Substituted Allylic Ion Pairs. 1. Isomerization of (Neopentylallyl)Lithium, -Sodium, and -Potassium in Tetrahydrofuran. *Organometallics* **1986**, *5* (8), 1529–1532.

(55) Schlosser, M.; Hartmann, J. 2-Alkenyl Anions and Their Surprising Endo Preference. Facile and Extreme Stereocontrol over Carbon-Carbon Linking Reactions with Organometallics of the Allyl Type. *J. Am. Chem. Soc.* **1976**, *98* (15), 4674–4676.

(56) Bank, S. Thermodynamic Stability of Allylic Intermediates. *J. Am. Chem. Soc.* **1965**, *87* (14), 3245–3246.

(57) Hoffmann, R.; Olofson, R. A. The Dependence of Conformational and Isomer Stability on the Number of Electrons in Extended π Systems. *J. Am. Chem. Soc.* **1966**, *88* (5), 943–946.

(58) Schleyer, P. v. R.; Dill, J. D.; Pople, J. A.; Hehre, W. J. Geometrical Preferences of the Crotyl Anion, Radical and Cation. *Tetrahedron* **1977**, *33* (19), 2497–2501.

(59) Schleyer, P. von R.; Kaneti, J.; Yun-Dong, W.; Chandrasekhar, J. The Preference of 1-Methylallyl Polar Organometallics and Carbanions for Cis Rather than for Trans Geometries. *Journal of Organometallic Chemistry* **1992**, *426* (2), 143–157.

(60) Janesko, B. G.; Villegas, H. Attractive Nonbonded Interactions Help Stabilize the Z Form of Alkenyl Anions. *J. Org. Chem.* **2018**, *83* (15), 8208–8213.

(61) For example, we have formed an initial hypothesis that the energy difference may also involve changes in the relative contribution of allylic $A^{1,2}$ and $A^{1,3}$ strain (for a computational analysis, see appendix B for details).

(62) Excitingly, we suspect that stereodetermining allylic deprotonation to a *Z*-allylic thianthrenium ylide has been unlocked by recent advances in the thianthrenation of aliphatic alkenes

(63) Intriguingly, we found that the *Z*-configuration preference was not unique to the allylic thianthrenium ylide—computational studies revealed *Z*-preference for a variety of allylic anions. See appendix B for details. Given that these characteristics seem to extend beyond allylic thianthrenium ylides, computational studies are underway to understand the physical details of this *Z*-allylic anion preference in other systems.

(64) Furthermore, when we then compared the ylide localization and rotational barriers to other ylides, we found these characteristics to be common among substituted allylic motifs relative to hydrocarbon allylic systems, indicating these may be generalizable features for locking the carbon-carbon bond *Z*-configuration.

Chapter 4: General *Z*-Selective Allylic Functionalization of Alkenes *via* Thianthrenium Salts

A study by **Targos, K.**; Wickens, Z. K.

4.1 Abstract

The realization of a *Z*-selective allylic C–H functionalization is a long-standing challenge. Herein, we have developed a collection of transformations to access various *Z*-allylic products based around thianthrenium electrophiles prepared from alkenes. In our work, we leveraged this alkene activation for allylic bond forming reactions with a range of acidic nucleophiles, such as sulfonamides and carboxylic acids. We discovered base identity and slow addition of nucleophile was crucial for maintaining *Z*-selectivity of this formal C–H allylic functionalization process. Overall, we have enabled a general allylic functionalization platform that affords high *Z*-selectivity across diverse alkene and nucleophile classes to furnish a suite of *Z*-allylic products.

4.2 Introduction

Allylic C–H functionalization of alkenes is an attractive transformation to streamline the organic synthesis of versatile allylic moieties. Traditional allylic C–H functionalization reactions of alkenes involve C–H activation to form an electrophilic metal-π-allyl complex, followed by nucleophilic substitution.[1–3] While the synthetic utility of such methods is undisputed, stereochemical outcomes are dominated by thermodynamic control, leading to the formation of products with *E*-selectivity.[4] In contrast, the realization of a general *Z*-selective allylic C–H functionalization is challenging, and examples are rare.[5–7] Recently, we developed a strategy where electrogenerated dicationic adducts between aliphatic alkenes and thianthrene, a safe and inexpensive reagent, are leveraged for the formal coupling of oxidatively sensitive secondary amines with alkenes to furnish linear, tertiary allylic amine products with *Z*-selectivity.[8] The unusual approach provides access to desirable *Z*-allylamine derivatives that are not directly accessible by other C−H functionalization reactions.[9] However, our allylic amination provided poor-to-modest *Z*-selectivity depending on alkene structure (Chapter 2). In fact, this stereoselectivity challenge persists across the handful of reports that also leverage allylic functionalization from alkenylthianthrenium salts.[10,11] Recently,

our group has elucidated the elementary steps of this process in a detailed mechanistic study and we revealed that allylic deprotonation of the alkenylthianthrenium species is rate- and stereodetermining during the allylic functionalization process (Chapter 3). Given this key step does not involve the nucleophile, I recognized that we could exploit this platform more broadly to develop a general, *Z*-selective allylic functionalization of alkenes.

More broadly, we hypothesize that base selection to access anionic nucleophiles from weakly acidic pronucleophiles is crucial for maintaining high *Z*-selectivity since the stereodetermining step of the allylic functionalization process is dependent on base identity. We noted that reported methods for allylic C–H amination using thianthrenium salts typically require nucleophilic nitrogen sources to maintain high *Z*-selectivity (*e.g.* secondary aliphatic amines); use of acidic N–H pronucleophiles such as sulfonamides has not been amenable to high *Z*-selective allylic functionalization.[10] We posit this is due to these nucleophiles requiring deprotonation prior to engaging with an electrophile. We envisioned that identifying appropriate conditions for achieving high *Z*-selectivity with sulfonamides[12] would inform the development of a general

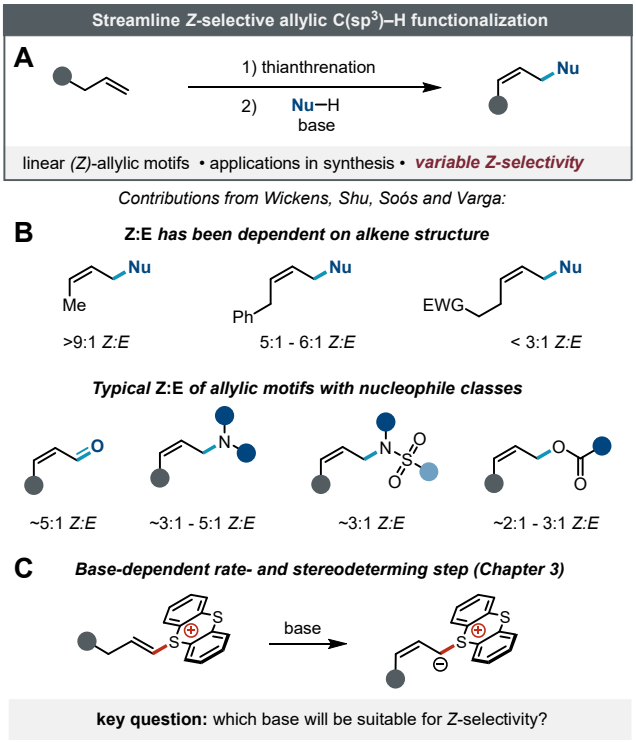

Figure 4.1. Project overview. (A) Recently discovered *Z*-selective allylic functionalization reaction. (B) Variable *Z*-selectivity challenges. (C) Stereoselective allylic deprotonation.

Z-selective allylic functionalization of alkenes. Herein, we outline a detailed study to improve the *Z*-selectivity across varying alkene structures and a broad range of nucleophiles.

4.3 Results and Discussion

We focused our study initially on the *Z*-crotylation[13] of *N*-nucleophiles with the ultimate goal of gaining insights to improve the *Z*-selectivity of this allylic C–H functionalization method beyond amination. First, we wanted to map out which *N*-nucleophiles can be engaged in allylic functionalization with *Z*-crotylation using alkenylthianthrenium salt **4.1** derived from 1-butene. Decoupling the nucleophilicity versus basicity for allylic amination is important for establishing a system to study since base promotes the stereoselective allylic deprotonation. We recognized that appropriate selection of an activating group for primary amine and sulfonamide nucleophiles would not only eliminate aziridination pathways,[14,15] but also deactivate them for allylic functionalization without exogenous base. We found that trifluoroacetate-protected amines can undergo allylic amination with **4.1** using Cs_2CO_3 base to afford protected secondary allylic amine product **4.3** but with poor 2:1 *Z:E*. Although a wide range of sulfonamide-protected *N*-alkylamines could also be engaged in allylic amination with **4.1** to afford *Z*-crotylsulfonamides **4.4–4.9** in high yields (>90%), all optimization efforts did not improve the *Z:E* above 5:1 with 1-butene parent alkene. Furthermore, the *Z*-selectivity of allylic sulfonamides **4.10–4.16** obtained using this nucleophile class was even lower when employing alkenylthianthrenium salt **4.2** derived from 4-phenyl-1-butene. This observation is consistent with alkene-dependence noted in our previous allylic amination protocol with aliphatic secondary amines.[8] More acidic sulfonamides could be engaged with Cs_2CO_3 base or 1 equivalent of *i*-Pr_2NEt amine to furnish *N*-aryl (**4.17, 4.18**) and *N*-carbonyl (**4.19–4.21**) substituted allylic products. We noted that in some instances, the Z-selectivity was higher with the trialkylamine base than carbonate. Notably, we found that higher Z-selectivity with these sulfonamide nucleophiles could be achieved by increasing the *i*-Pr_2NEt loading; however, selectivity remained modest and yields were often diminished compared to when using carbonate base (see Appendix C for details).

Table 4.1. Scope of Allylic Amination of Alkenylthianthrenium Salts Using Acidic N–H Pronucleophiles.

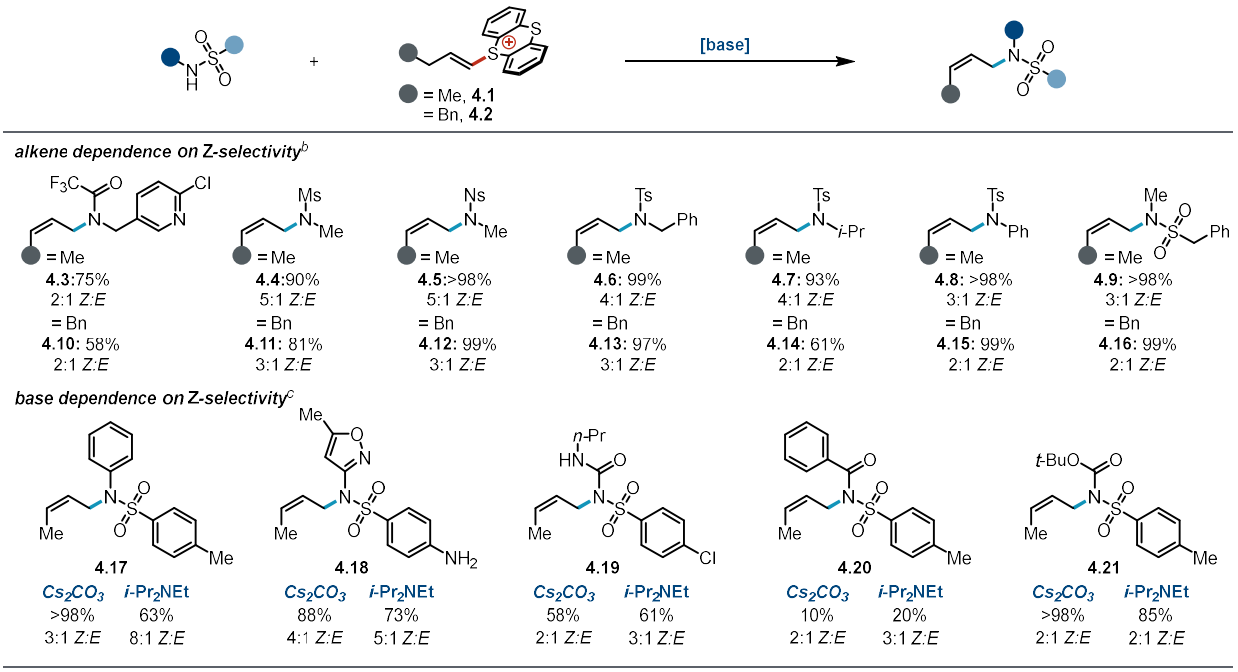

[a]Reactions conducted using alkenylthianthrenium salt (0.05 mmol), nucleophile (0.05 mmol), 0.5 mL MeCN, 3 h. NMR yields and *Z*:*E*. See the appendix C for further experimental details. [b]Cs_2CO_3 (0.15 mmol). [c]Cs_2CO_3 (0.15 mmol) or *i*-Pr_2NEt (0.05 mmol).

To further study this substitution reaction from alkenylthianthrenium salts and improve the *Z*-selectivity, we selected BocNHTs as a differentially-protected ammonia surrogate and representative nucleophile class to enable synthetically valuable preparation of *Z*-allylamines. We noted that 1-butene worked decently with this nucleophile and excess *i*-Pr_2NEt base already to give **4.21** in 93% yield, 7:1 *Z:E* (see Appendix C). Thus, for these investigations, we opted to use a phthalimide-functionalized alkenylthianthrenium salt **4.22**, which under our allylic amination conditions gave low 2:1 *Z:E* for allylamine. We hypothesized that the deprotonated sulfonamide might attenuate *Z*-selectivity by acting as a poorly *Z*-selective base. Consistent with this proposal, when the potassium salt of the sulfonamide nucleophile was used in the absence of exogenous base, the allylic sulfonamide product **4.23** exhibited slight *E*-selectivity (Figure 4.2). One equivalent of with inorganic bases such as Cs_2CO_3 or trialkylamine bases such as N(*i*-Pr)(*t*-Bu)Me gave poor diastereoselectivity comparable to the sulfonamide anion itself. Based on our allylic deprotonation model for achieving stereocontrol (Chapter 3), we hypothesized that base identity was key for promoting the *Z*-selectivity. Indeed, our group and others have observed a base-dependence on the *Z*-selectivity. For example, inorganic bases such as Cs_2CO_3 decrease *Z*-selectivity for

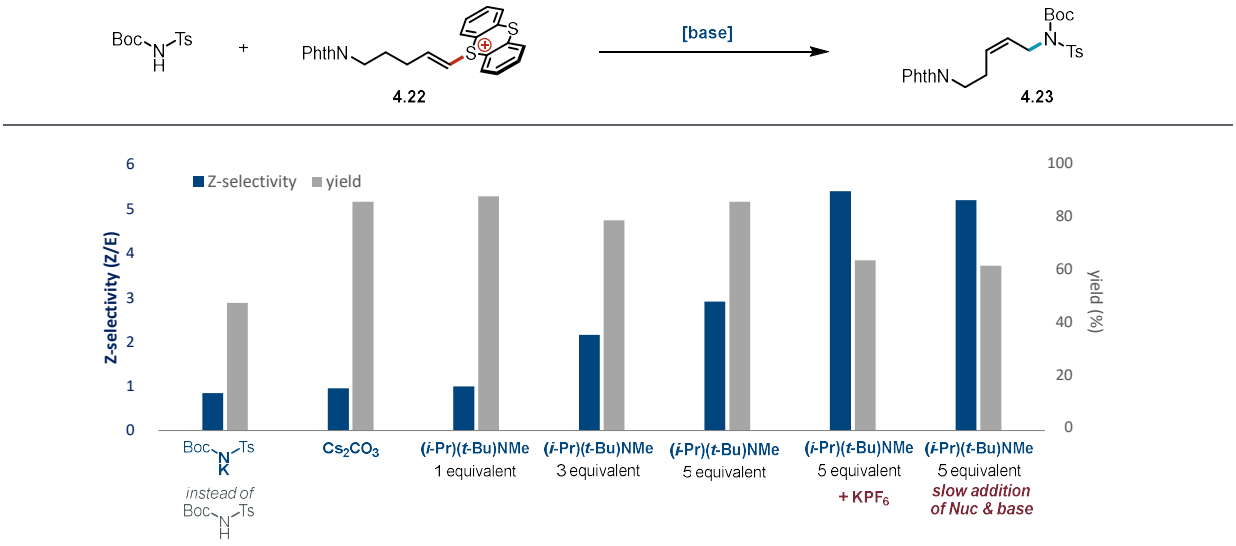

[a]Reactions conducted using alkenylthianthrenium salt (0.05 mmol), nucleophile (0.05 mmol), 0.5 mL MeCN, 3 h. NMR yields and *Z:E*. See the appendix C for further experimental details.

Figure 4.2. Improving *Z*-selectivity of sulfonamide nucleophile by controlling base identity and concentrations.

secondary amine[8] and carboxylate[10] nucleophiles compared to trialkylamine bases such as *i*-Pr_2NEt. We wondered if trialkylamine bases could promote allylic functionalization of sulfonamide nucleophiles in high *Z*-selectivity. Our key insight was to mitigate the sulfonamide acting as a poorly *Z*-selective base by (a) employing an excess of amine base, which improved the *Z*-selectivity of allylic product, and (b) the addition of a potassium salt to decrease the anion solubility (Figure 4.3). Consistent with our proposal for potassium decreasing the sulfonamide solubility, the yield and *Z*-selectivity could be recapitulated by slow addition of sulfonamide nucleophile (Figure 4.2).

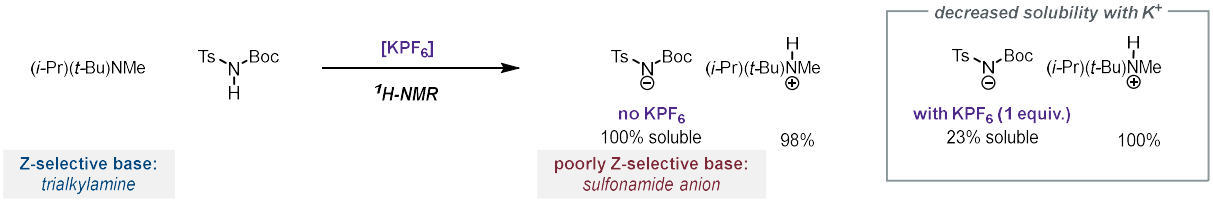

Figure 4.3. Experimental support for working model for improved *Z*-selectivity with anionic nucleophiles.

We next investigated the alkene structure impact on *Z:E* using either (a) isolated alkenylthianthrenium salt with added KPF_6 salt, or (b) electrochemically-prepared alkenylthianthrenium intermediates carried through basic quench without purification of KPF_6 electrolyte. Under either conditions, allylic sulfonamides **4.23–4.27** in >5:1 *Z:E* were prepared from various alkenes and Boc-

protected sulfonamides. Each alkene investigated showed a notable improvement in the *Z*-selectivity compared to our allylic amination study with aliphatic secondary amines.[8] Notably, *Z*-crotylation of BocNHTs using feedstock 1-butene derived alkenylthianthrenium salt **4.1** afforded the protected allylic amine **4.28** in high ≥20:1 *Z*-selectivity. Furthermore, triflylsulfonamide-protected primary amines and anilines were able to undergo *Z*-selective functionalization using trialkylamine base, enabling access to secondary *Z*-allylamines upon deprotection. Complex N−H sulfonamides were amenable to the allylation reaction using thianthrenium electrophiles in excellent 7:1 to 11:1 *Z*-selectivity (**4.30, 4.31**). Excitingly, these principles were not unique to acidic *N*-nucleophiles; carboxylic acids undergo allylic functionalization with alkenylthianthrenium salts to furnish allylic esters **4.32** and **4.33** in high 10:1 *Z:E* under these optimized potassium salt and trialkylamine base conditions. Lastly, we found that water was a competent nucleophile for the formation of synthetically useful *Z*-allylic alcohols from alkenylthianthrenium salts (**4.34**).

Table 4.2. Z-Selective Allylation of Anionic Nucleophiles Using Alkenylthianthrenium Salts or Electrochemical Thianthrenation of Alkene Starting Materials.

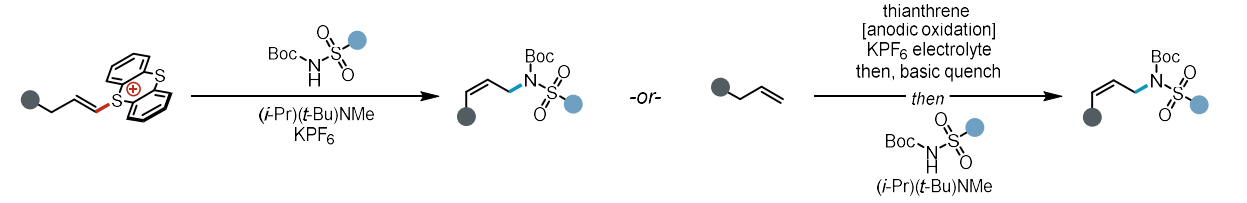

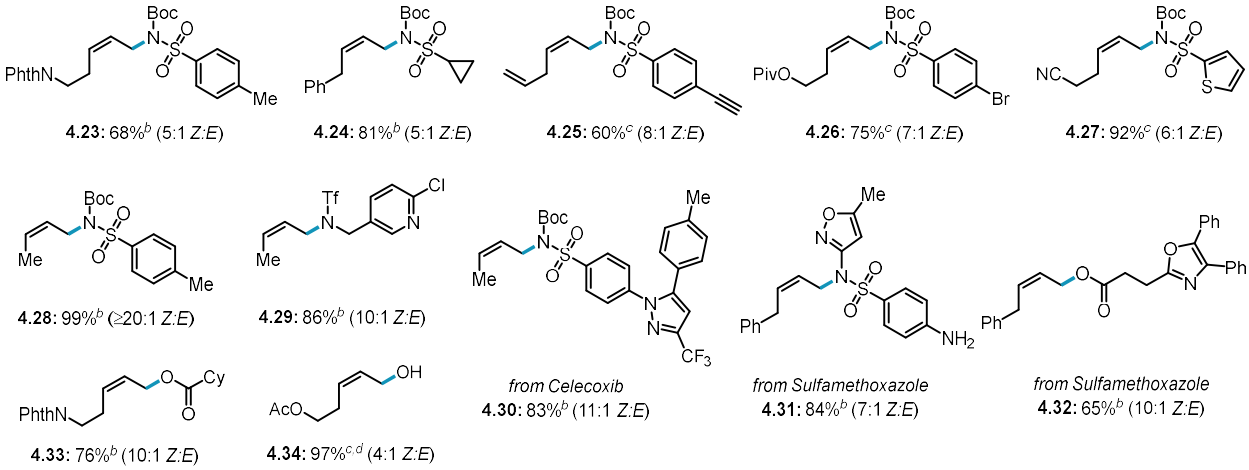

4.23: 68%[b] (5:1 *Z:E*)
4.24: 81%[b] (5:1 *Z:E*)
4.25: 60%[c] (8:1 *Z:E*)
4.26: 75%[c] (7:1 *Z:E*)
4.27: 92%[c] (6:1 *Z:E*)
4.28: 99%[b] (≥20:1 *Z:E*)
4.29: 86%[b] (10:1 *Z:E*)
from Celecoxib
4.30: 83%[b] (11:1 *Z:E*)
from Sulfamethoxazole
4.31: 84%[b] (7:1 *Z:E*)
from Sulfamethoxazole
4.32: 65%[b] (10:1 *Z:E*)
4.33: 76%[b] (10:1 *Z:E*)
4.34: 97%[c, d] (4:1 *Z:E*)

[a]NMR yields and *Z:E*. See the appendix C for further experimental details. [b]Reactions conducted using alkenylthianthrenium salt (0.05 mmol), nucleophile (0.05 mmol), (*i*-Pr)(*t*-Bu)NMe (0.25 mmol), 0.25 mL MeCN (2.4 M KPF_6), 3 h. [c]Reactions were conducted using alkene (0.15 mmol), thianthrene (0.225 mmol), MeCN (0.3 M KPF_6), **I** = 5.4 mA, 2.2 h (2.5 F mol^{-1} alkene); then alumina quench; then nucleophile (0.10 mmol), (*i*-Pr)(*t*-Bu)NMe (0.50 mmol), 4 h. [d]$CsHCO_3$ (0.90 mmol).

4.4 Conclusion

Overall, we have expanded the scope of amenable *N*- and *O*-nucleophiles that can undergo base-induced allylic functionalization with alkenylthianthrenium salts to furnish a suite of *Z*-allylic products. We have found that anionic nucleophiles can act as poorly *Z*-selective bases for the overall allylation transformation. Our key insight was that slow addition of nucleophile and use of trialkylamine bases enable high *Z*-selectivity across a range of alkene structures. We anticipate this *Z*-selective net C–H allylic functionalization of alkenes will streamline organic synthesis of versatile allylic moieties amenable for further diversification.

4.5 Acknowledgements

Z.K.W. and K.T. designed the study. K.T. performed the experiments and collected the data.

4.6 References

(1) Reed, S. A.; White, M. C. Catalytic Intermolecular Linear Allylic C−H Amination via Heterobimetallic Catalysis. *J. Am. Chem. Soc.* **2008**, *130* (11), 3316–3318.

(2) Liu, G.; Yin, G.; Wu, L. Palladium-Catalyzed Intermolecular Aerobic Oxidative Amination of Terminal Alkenes: Efficient Synthesis of Linear Allylamine Derivatives. *Angew. Chem. Int. Ed.* **2008**, *47* (25), 4733–4736.

(3) Reed, S. A.; Mazzotti, A. R.; White, M. C. A Catalytic, Brønsted Base Strategy for Intermolecular Allylic C−H Amination. *J. Am. Chem. Soc.* **2009**, *131* (33), 11701–11706.

(4) Yin, G.; Wu, Y.; Liu, G. Scope and Mechanism of Allylic C−H Amination of Terminal Alkenes by the Palladium/PhI(OPiv)2 Catalyst System: Insights into the Effect of Naphthoquinone. *J. Am. Chem. Soc.* **2010**, *132* (34), 11978–11987.

(5) Takeuchi, R.; Shiga, N. Complete Retention of Z Geometry in Allylic Substitution Catalyzed by an Iridium Complex. *Org. Lett.* **1999**, *1* (2), 265–268.

(6) Guo, W.; Martínez-Rodríguez, L.; Kuniyil, R.; Martin, E.; Escudero-Adán, E. C.; Maseras, F.; Kleij, A. W. Stereoselective and Versatile Preparation of Tri- and Tetrasubstituted Allylic Amine Scaffolds under Mild Conditions. *J. Am. Chem. Soc.* **2016**, *138* (36), 11970–11978.

(7) Martínez-Gualda, A. M.; Cano, R.; Marzo, L.; Pérez-Ruiz, R.; Luis-Barrera, J.; Mas-Ballesté, R.; Fraile, A.; de la Peña O'Shea, V. A.; Alemán, J. Chromoselective Access to Z- or E- Allylated Amines and Heterocycles by a Photocatalytic Allylation Reaction. *Nat Commun* **2019**, *10* (1), 2634.

(8) Wang, D. J.; Targos, K.; Wickens, Z. K. Electrochemical Synthesis of Allylic Amines from Terminal Alkenes and Secondary Amines. *J. Am. Chem. Soc.* **2021**, *143* (51), 21503–21510.

(9) Cheng, Q.; Chen, J.; Lin, S.; Ritter, T. Allylic Amination of Alkenes with Iminothianthrenes to Afford Alkyl Allylamines. *J. Am. Chem. Soc.* **2020**, *142* (41), 17287–17293.

(10) Liu, M.-S.; Du, H.-W.; Shu, W. Metal-Free Allylic C–H Nitrogenation, Oxygenation, and Carbonation of Alkenes by Thianthrenation. *Chem. Sci.* **2022**, *13* (4), 1003–1008.

(11) Angyal, P.; Kotschy, A. M.; Dudás, Á.; Varga, S.; Soós, T. Intertwining Olefin Thianthrenation with Kornblum/Ganem Oxidations: Ene-Type Oxidation to Furnish α,β-Unsaturated Carbonyls. *Angewandte Chemie International Edition* **2023**, *62* (2), e202214096.

(12) Nobuta, T.; Kawabata, T. Catalyst-Controlled Site-Selective Asymmetric Epoxidation of Nerylamine and Geranylamine Derivatives. *Chem. Commun.* **2017**, *53* (67), 9320–9323.

(13) Several protocols for Z-crotylation are available, for example by S_N2 or other allylic alkylation reactions such as the Tsuji−Trost reaction. However, the requisite crotylhalides electrophiles are only readily available as an *E*-dominant mixture and the synthesis of *Z*-crotylhalides requires multistep preparation.

(14) Holst, D. E.; Wang, D. J.; Kim, M. J.; Guzei, I. A.; Wickens, Z. K. Aziridine Synthesis by Coupling Amines and Alkenes via an Electrogenerated Dication. *Nature* **2021**, *596* (7870), 74–79.

(15) Liu, M.-S.; Du, H.-W.; Cui, J.-F.; Shu, W. Intermolecular Metal-Free Cyclopropanation and Aziridination of Alkenes with XH2 (X=N, C) by Thianthrenation**. *Angewandte Chemie International Edition* **2022**, *61* (41), e202209929.

Chapter 5: Catalytic Base Enabled 1,2-Addition of *N*-Nucleophiles into Alkenylthianthrenium Salts

A collaboration with Dr. Céline Dorval, Adrian D. Matthews, Dylan E. Holst, Sara N. Alektiar, Tom Tan, and Zachary K. Wickens; Dr. Rik Oost, Dr. José Enrique Gomez Pulido, Dr. Matthew Horwitz, Dr. Justin Dicciann, Dr. Mikko Muuronen

5.1 Abstract

Recent synthetic advances have facilitated the transformation of alkenes into alkenylthianthrenium electrophiles. From this one common intermediate, both allylic functionalization and net heterofunctionalization reactions can be achieved. However, factors that dictate these reaction pathways are not fully understood and achieving precise control remains a challenge. Herein, we describe catalytic base conditions that divert reaction selectivity from elimination processes towards conjugate-like addition. Under stoichiometric Cs_2CO_3 base conditions, sulfonamide nucleophiles react with alkenylthianthrenium salts to form allylic products, while 5 mol % Cs_2CO_3 conditions promote addition of the sulfonamide into the internal, β-position to generate 1,2-sulfonamidosulfonium salts. Mechanistic studies using stoichiometric proton-sponge (1,8-dimethylamino naphthalene) reveal an equilibrium mixture of alkenylthianthrenium salt, sulfonamide nucleophile, and alkylthianthrenium product that is mediated by facile proton transfers. Sulfonamide deprotonation is implicated as the rate-determining step of the 1,2-addition transformation. These insights have been leveraged for *N*-alkylation of azoles. Catalytic base conditions enable efficient single addition of azoles into alkenylthianthrenium salts to form 1,2-azolothianthrenium electrophiles that can undergo subsequent substitution to prepare vicinal motifs. Exquisite *N*-regioselectivity is achieved by the reversibility of the conjugate-type addition and sulfonium ylide protonation sequence. This azole alkylation methodology was used to engage alkenylthianthrenium salts derived from 1,2-disubstituted and 1,1-disubstituted alkenes.

5.2 Introduction

Oxidative alkene functionalization reactions are a fundamental class of synthetic transformations that rapidly increase molecular complexity.[1,2] A unified strategy to provide different types of building blocks from simple aliphatic alkenes would be an appealing approach for the modular synthesis of diverse scaffolds. This building-block-oriented platform would ideally engage several nucleophile classes in a simple protocol. Recent synthetic advances in the transformation of alkenes into thianthrenium electrophiles have set the stage for a new approach to oxidative alkene functionalization.[3,4] The versatility of these thianthrenium salts has unlocked distinct synthons formally accessible from alkenes *via* thianthrenation

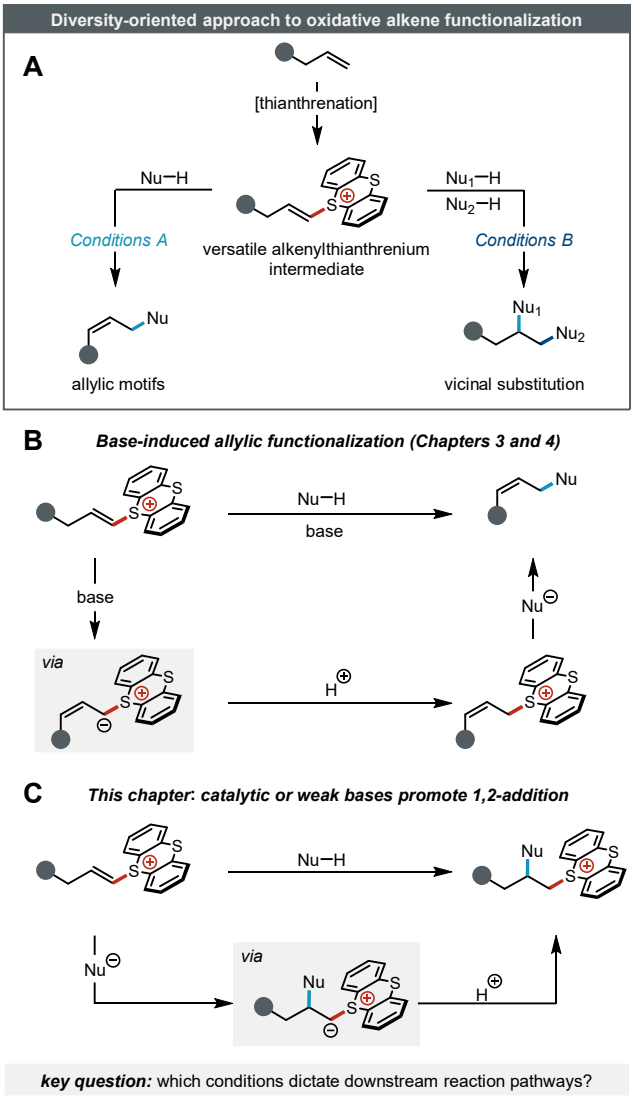

Figure 5.1. Overview of a building-block approach to oxidative alkene functionalization. (A) Divergent reactivity of alkenylthianthrenium Salts. (B) Allylic ylide pathway. (C) conjugate-addition pathway.

(see Chapter 1). In particular, both vicinal dication and allyl cation reactivity have been revealed from a common alkenylthianthrenium salt intermediate which has been leveraged for either allylic functionalization and heterofunctionalization processes.[5–8] We envision that alkenylthianthrenium electrophiles could be a particularly well-suited reagent for a modular synthesis of a suite of building blocks simply by changing reaction conditions that tap into these distinct reactivity manifolds (Figure 5.1A). Conditions that promote allylic cation reactivity would generate *Z*-allylic motifs bearing an alkene for further elaboration,[9–22] while conditions that enable vicinal dication reactivity would furnish net heterofunctionalized products using two unique nucleophiles. However, while the synthetic utility of alkenylthianthrenium salts is currently well-recognized, achieving precise control over product formation remains largely underexplored.

The key to the diverse reactivity of alkenylthianthrenium salts lies in their ability to form two distinct sulfonium ylides. For allylation pathways, we have found that allylic deprotonation of the alkenylthianthrenium salt by a suitable base generates a *Z*-allylic thianthrenium ylide (Figure 5.1B, also see Chapter 3). Upon protonation, the allylic thianthrenium electrophile undergoes irreversible S_N2 substitution. Another distinct reactivity pattern of alkenylthianthrenium salts is difunctionalization. For this pathway, 1,2-addition of a first nucleophile into the internal, β-position of the alkenylthianthrenium salt generates a sulfonium ylide (Figure 5.1C). Upon protonation, the resultant alkylthianthrenium electrophile can be substituted by a second nucleophile. Recently, our group has shown thianthrenium salts can successfully undergo this 1,2-addition mechanism with phthalimide as the first nucleophile.[8] Our hypothesis is that treatment of electrogenerated dicationic adducts with potassium phthalimide generates a proton necessary for the ylide quenching. In principle, this alkylthianthrenium intermediate could be accessed by conjugate-type addition of alkenylthianthrenium species by any nucleophile. In practice, selective single addition into alkenylthianthrenium salts of nucleophiles beyond phthalimide remains elusive. We have identified that the difficulty in leveraging alkenylthianthrenium electrophiles for selective conjugate-type addition lies in controlling the reactivity of the labile thianthrenium moiety which is prone to both over-substitution and elimination pathways. We suspected that careful selection of reaction conditions may *bias* which sulfonium

ylide is generated from alkenylthianthrenium reagents. If successful, nucleophilic substitution of the resultant 1,2-alkylthianthrenium salts obtained with various polar nucleophiles would grant access to an unexplored chemical space of vicinal motifs that are complementary to the those accessible *via* nucleophilic opening of strained rings.[23–28] This chapter will focus on enabling selective conjugate-type addition of *N*-nucleophiles into alkenylthianthrenium salts.

5.3 Results and Discussion

5.3.1 *N*-alkyl Sulfonamide Nucleophiles

We have gained some insights into reaction conditions that promote allylic functionalization pathways (see Chapter 4). When alkenylthianthrenium salt **5.1** was treated with stoichiometric Cs_2CO_3 base and *N*-methyltosylamine, allylic sulfonamide **5.2** was formed in quantitative yield and 4:1 *Z:E* (Figure 5.2A). We wondered if decreasing the equivalents of base would promote selective conjugate-type addition of the sulfonamide nucleophile into the alkenylthianthrenium salt, or simply furnish allylic products in lower yield. Our working model for how substoichiometric base could promote the 1,2-addition pathway is as follows: (1) sulfonamide anion is initially formed in low concentration, (2) sulfonamide anion then undergoes selective single addition into the alkenylthianthrenium salt, (3) the resultant sulfonium ylide deprotonates more sulfonamide, (4) this deprotonation step re-generates competent anionic nucleophile for selective single addition. Excitingly, we uncovered that use of certain weaker bases or substoichiometric amounts of bases did indeed alter the reaction pathway to give 1,2-sulfonamidosulfonium salts rather than allylic sulfonamides (Figure 5.2B). We hypothesize that because the overall base concentration is low under these conditions, allylic functionalization is mitigated. This key insight of base loading control on elimination *versus* conjugate-type addition pathways has had implications for more broadly manipulating reaction selectivity from alkenylthianthrenium salts (*vide infra*). The observation of reaction selectivity of sulfonamide nucleophiles under altered reaction conditions merited further study and is described below. In this chapter, we describe an experimental investigation of the divergent reactivity of sulfonamide nucleophiles with alkenylthianthrenium salts—with an emphasis on promoting 1,2-addition products—and

attempt to extract generalizable aspects to aid in the design of new heterofunctionalization chemistry. These findings have informed an ongoing project that expands the conjugate-type addition reactivity to azole nucleophiles.

In the context of sulfonamide nucleophiles, we found catalytic base conditions with more deactivated *N*-methylnosylamine afforded alkylthianthrenium product **5.4** in lower 49% yield and 11% of the corresponding allylic sulfonamide side product (see Appendix D). Concurrent work in the Wickens group leveraged proton-sponge (1,8-dimethylamino naphthalene) to promote regioselective addition of pyrazole and imidazole to electrogenerated thianthrene-alkene dicationic adducts. We hypothesized that replacing catalytic Cs_2CO_3 with proton-sponge would minimize the allylation pathway since we found it is not an effective base for allylic functionalization of alkenylthianthrenium salts.[29] While no allylic sulfonamide was detected when using one equivalent of proton-sponge, the yield of desired alkylthianthrenium **5.4** did not increase (Figure 5.2C). Overall, base identity and concentration are key to controlling selective single addition over base-induced allylic functionalization pathways.

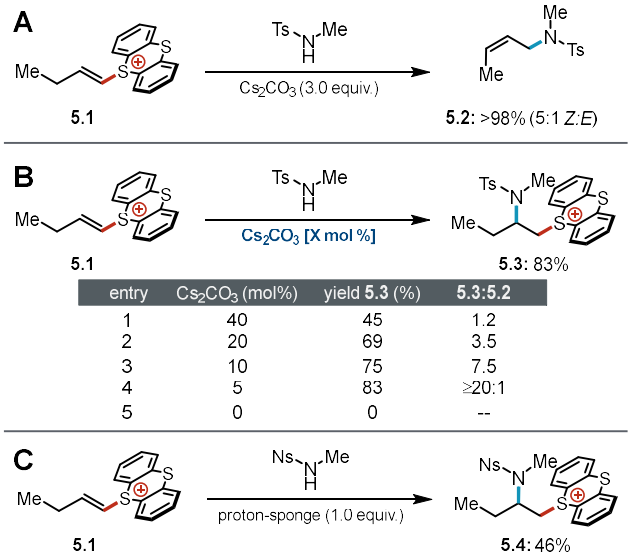

entry	Cs_2CO_3 (mol%)	yield **5.3** (%)	**5.3**:**5.2**
1	40	45	1.2
2	20	69	3.5
3	10	75	7.5
4	5	83	≥20:1
5	0	0	--

Figure 5.2. Initial observations of base dependent conditions for divergent (A) allylic functionalization, *versus* (B) 1,2-addition of sulfonamide nucleophiles with alkenylthianthrenium electrophiles using catalytic base and (C) proton sponge.

Table 5.1. Preliminary Scope of 1,2-Sulfonamidosulfonium Salts.[a]

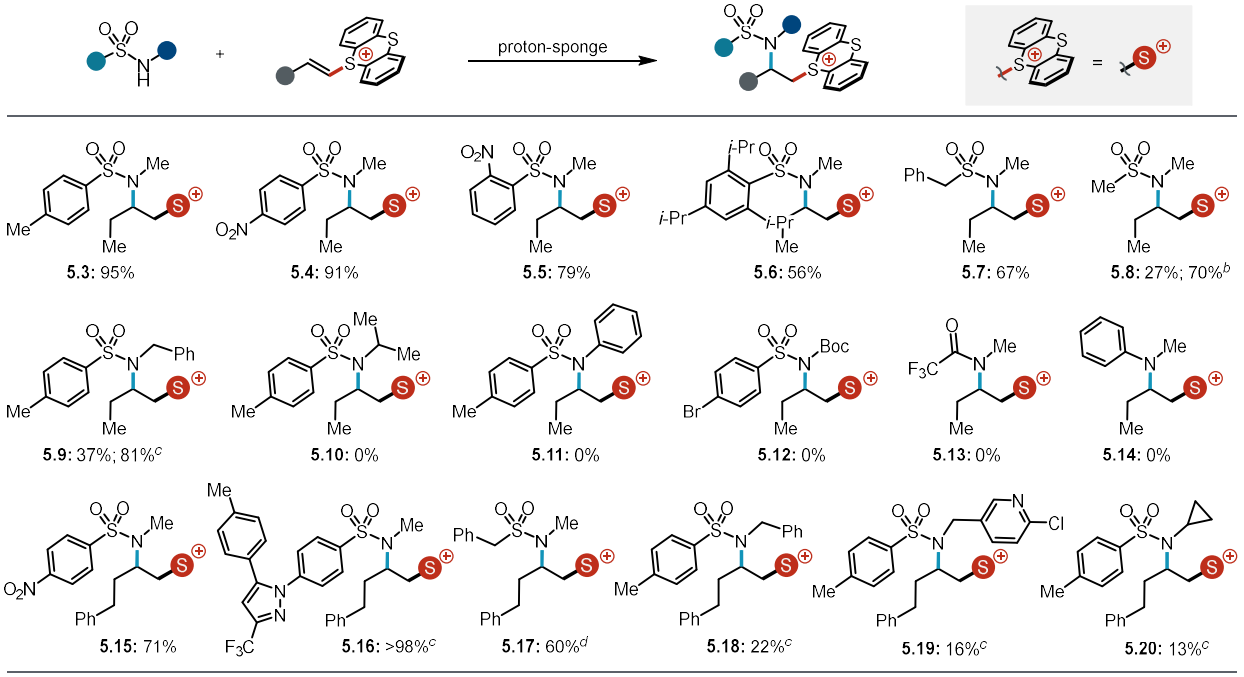

[a]Reactions conducted using alkenylthianthrenium salt (0.05-0.08 mmol), nucleophile (0.05-0.1 mmol), proton-sponge (0.05-0.08 mmol), 0.1-0.2 mL MeCN, 3 h. NMR yields. See the appendix D for further experimental details. yields. [b]5 mol % Cs2CO3 base. [c] >2.0 equivalents of alkenylthianthrenium salt and 3.0 equivalents of proton sponge. [d]16 h.

With conditions to *bias* sulfonamide nucleophiles towards conjugate-type addition in hand, we probed the preliminary scope of 1,2-sulfonamidothianthrenium products (Table 5.1). With alkenylthianthrenium salt **5.1** derived from 1-butene, corresponding adducts were formed by selective single addition of *S*-aryl sulfonamides with electron-donating (**5.3**), electron-withdrawing (**5.4**, **5.5**), and even exceptionally sterically-hindered groups (**5.6**). *S*-alkyl substitution on the sulfonamide nucleophile was tolerated (**5.7**, **5.8**). Replacing *N*-methyl with other *N*-alkyl substitutents rendered the sulfonamide nucleophile ineffective in undergoing this addition reactivity with alkenylthianthrenium reagents. For example, while *N*-benzyltosylamine could be engaged to form **5.9** in diminished 37% yield, *N*-isopropyltosylsamine and *N*-phenyltosylamine did not react. Other *N*-protecting groups (*e.g.* TFA) were not amenable under these conditions and no conversion of the alkenylthianthrenium salt was observed. When using an alkenylthianthrenium salt derived from 4-phenyl-1-butene, conjugate-addition products (**5.15–5.17**) were selectively formed using a variety of *S*-substituted sulfonamides. However, a similar sensitivity to *N*-alkyl substituent of the sulfonamide was observed and alkylthianthrenium product yields suffered (**5.18–5.20**). Overall, while the preliminary scope of sulfonamides appears to be broad for the formation of

1,2-sulfonamidosulfonium salts, the yields suffer with *N*-alkyl substitution other than *N*-methyl sulfonamides as well as when employing more complex alkenylthianthrenium salts.

We conducted mechanistic studies to understand the low reactivity of *N*-alkyl substituted sulfonamide nucleophiles for 1,2-addition into alkenylthianthrenium salts. To this end, we monitored the reaction of *N*-methylnosylamine and *N*-benzyltosylamine with alkenylthianthrenium salt **5.1** in the presence of proton-sponge base (Figure 5.3A). The formation of *N*-benzyl substituted product **5.9** was notably disfavored compared to *N*-methyl substituted sulfonamide **5.5**. In both cases, the reaction profiles resembled equilibration curves, which suggests product formation is dictated by an equilibrium mixture of alkylthianthrenium adduct, sulfonamide, and alkenylthianthrenium salt mediated by facile proton transfers. Consistent with this hypothesis, increasing the reaction concentration to drive the solution from bimolecular towards unimolecular dramatically increased the yield of alkylsulfonium **5.3** (Figure 5.3B). Ongoing projects in the Wickens group are developing systems that drive this equilibrium by introduction of a subsequent irreversible reaction with the disfavored alkylthianthrenium intermediate. For example, a variety of one-pot nucleophilic substitutions have been used to trap transient 1,2-sulfonamidothianthrenium adducts and prepare a suite of saturated heterocycles (for an example, see Chapter **2**).

To further probe the mechanism, we varied the relative concentration of each reaction component and monitored the impact on the formation of 1,2-sulfonamidothianthreniuim salt **5.9** (Figure 5.3C, Table 5.2). We found that increasing the alkenylthianthrenium salt **5.1** concentration increased the overall yield of **5.9** but not the yield after 3 hours (entries 1 and 3). Increasing the concentration of *N*-benzyltosylamine increased the final **5.9** yield as well as the initial yield (entries 1, 4–5). Lastly, increasing the loading of proton-sponge did not affect final yield but increased the initial rate of **5.9** formation (entries 1–2, 5–6). Taken together, these data are consistent with deprotonation of sulfonamide being the overall rate determining step in the formation of 1,2-sulfonamidosulfonnium products (Figure 5.3D). Using these mechanistic insights, the yield of **5.9** was improved from 37% to 81% by driving the alkylthianthrenium salt equilibrium with excess alkenylthianthrenium reagent and proton-sponge base (see appendix D). Given the reversibility of alkylthianthrenium salt formation, future work in the Wickens group will elucidate the

interplay of nucleophilicity and basicity for various nucleophile classes in order to understand and manipulate the relative rates of the 1,2-addition reaction *versus* competitive base-induced allylic deprotonation pathways.

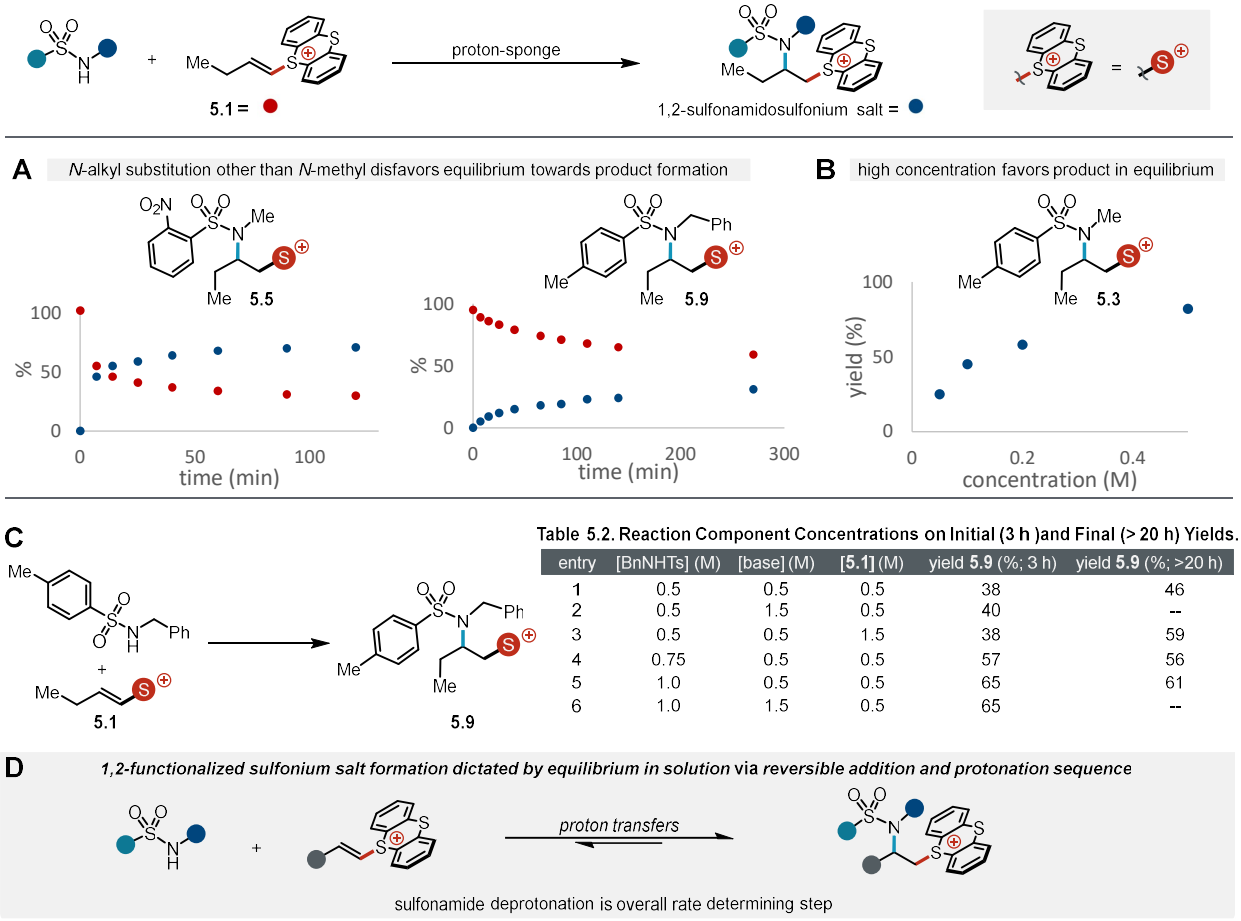

Table 5.2. Reaction Component Concentrations on Initial (3 h)and Final (> 20 h) Yields.

entry	[BnNHTs] (M)	[base] (M)	[**5.1**] (M)	yield **5.9** (%; 3 h)	yield **5.9** (%; >20 h)
1	0.5	0.5	0.5	38	46
2	0.5	1.5	0.5	40	--
3	0.5	0.5	1.5	38	59
4	0.75	0.5	0.5	57	56
5	1.0	0.5	0.5	65	61
6	1.0	1.5	0.5	65	--

Figure 5.3. Mechanistic studies of 1,2-sulfonamidosulfonium salt formation. (A) Reaction profiles. (B) Concentration optimization. (C) Reaction concentration components on initial and final yield. (D) Data are consistent with an equilibrium solution with mediated proton transfers.

5.3.2 Azole Nucleophiles

The observations outlined above have informed a parallel project conducted by a postdoctoral researcher that aims to develop a new azole *N*-alkylation platform. Azoles are essential scaffolds in the pharmaceutical and agrochemical industries.[30–36] However, medicinally relevant *N*-alkylated azoles are notably limited to a handful of specific substructures despite the enormous potential for diversity of sp^3 scaffolds.[37–39] We suspected that the restricted chemical space covered by *N*-alkylated azole products is a

direct result of the limitations of established approaches to construct these motifs. While *de novo* ring synthesis is effective for generating azole cores,[40,41] these methods lack high modularity and prevent rapid access to large *N*-alkylated azole libraries. In principle, the construction of a new C–N bond using the nucleophilic nitrogen of readily accessible azoles should offer high modularity.[42–45] In practice, this modular substitution approach is hampered by the intrinsic substrate limitations of current *N*-alkylation methods. For example, alkyl (pseudo)halide substitution only readily achieves primary *N*-alkylated azoles;[46–48] whereas, the Mitsunobu reaction fails at delivering alkylated pyrazoles and imidazoles, two of the most prevalent azole classes.[49,50] Additionally, efficient access to *N*-alkylated unsymmetrical azole products is stymied by the variable *N*-regioselectivity of these methods. Accordingly, the development of modular approaches that overcomes these limitations is poised to unlock uncharted *N*-alkylated azole chemical space.

Given the versatility of alkylthianthrenium salts, we envisioned *N*-alkylated azole alkylthianthrenium salts would provide valuable building blocks for the preparation of previously inaccessible azole sp^3 scaffolds (Figure 5.4A). A modular approach to access this sulfonium intermediate leverages conjugate-type addition of azole nucleophiles into alkenylthianthrenium salts derived from alkene precursors. Subsequent substitution of the 1,2-azolothianthrenium species enables access to secondary vicinal *N*-azole constitutional isomers that are elusive using conventional substitution chemistry (*e.g.* epoxide ring opening under basic conditions, Figure 5.4B). Excitingly, azole addition into alkenylthianthrenium salts was rendered more efficient by taking advantage of catalytic base insights that enabled alkylthianthrenium salt formation with sulfonamides. Analogous to prior studies described above, we found that substoichiometric Cs_2CO_3 loading increased the selectivity of azole conjugate-addition over base-induced elimination pathways (Figure 5.4C). To evaluate the *N*-regioselectivity of our *N*-alkylation system, we chose ethyl 1H-pyrazole-3-carboxylate **5.21** as our model substrate since this unsymmetrical azole typically exhibits moderate to poor *N*-regioselectivity in *N*-alkylation reactions using alkylhalides. A new insight in this project was that the identity of catalytic base had a significant effect on *N*-regioselectivity of the transformation. For example, when catalytic Cs_2CO_3 base was used, **5.24** was formed in high yield

and ≥20:1 N^1:N^2(Figure 5.4C). Replacing Cs_2CO_3 base with 10 mol % of *i*-Pr_2NEt provided the same yield outcome but with significantly diminished *N*-regioselectivity of 3:1 N^1:N^2 (see Appendix D for details). To gain some mechanistic insights into the origin of high *N*-regioselectivity, the minor N^2-isomer was isolated and re-subjection to catalytic base. Under these conditions, the N^2- isomer converted quantitatively to the

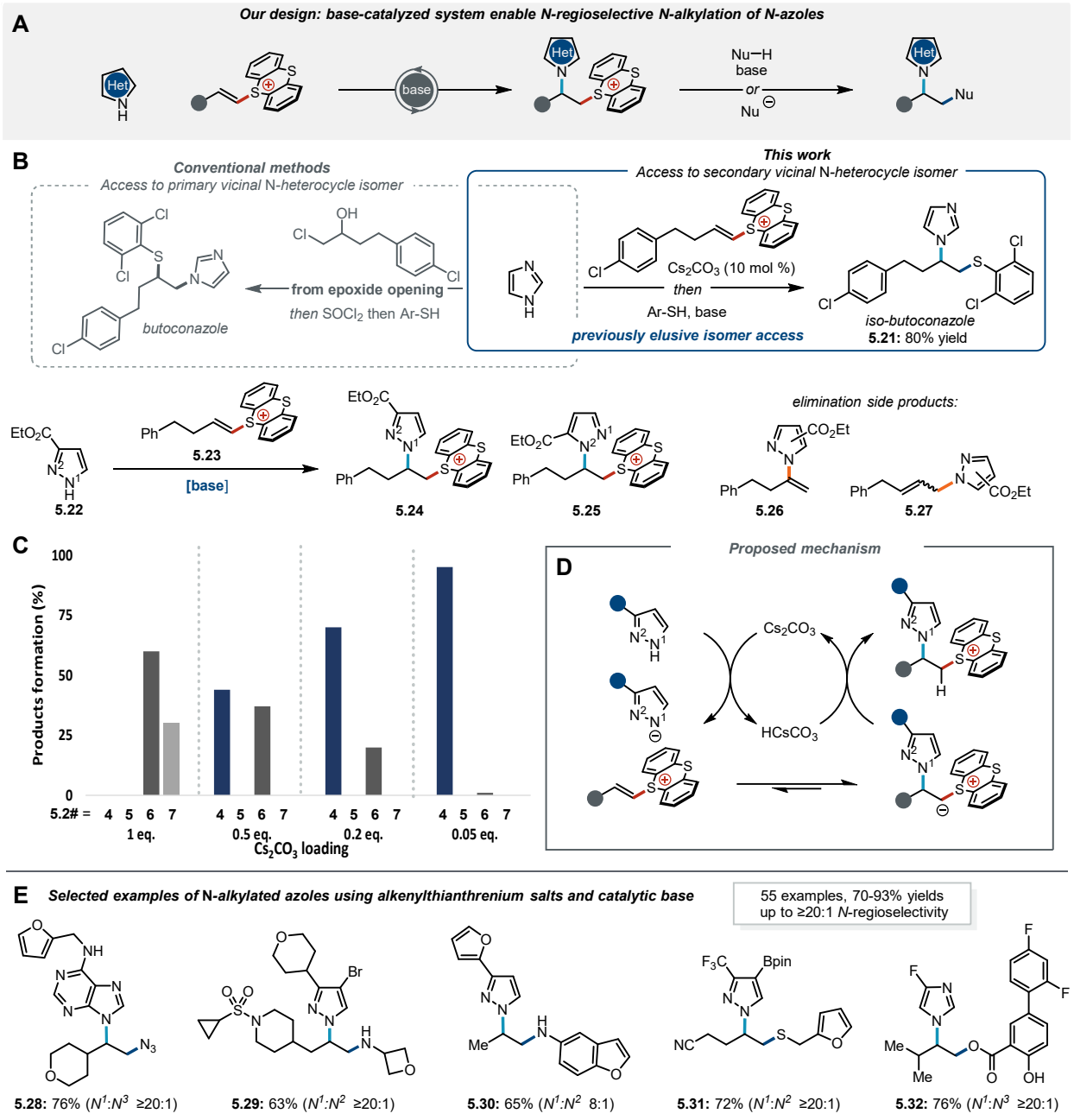

Figure 5.4. Azole *N*-alkylation project overview. (A) Schematic overview of this work. (B) Net heterofunctionalization of alkenylthianthrenium salts enable access to new *N*-alkylated azole chemical space. (C) Catalytic base conditions engender selective conjugate-type addition and high *N*-regioselectivity. (D) Proposed mechanism to achieve *N*-regioselectivity. (E) Selected scope examples.

N^1-regioisomer (see Appendix D for details). Based on these data, we propose that base identity controls the relative rates of reversible conjugate-type addition and protonation sequences which renders the transformation under either kinetic (N^2-selective) or thermodynamic (N^1-selective) control (Figure 5.4D).[51] Overall, these studies lead to a general *N*-regioselective azole alkylation method that can engage a wide range of heterocycle classes with excellent functional group tolerance and high *N*-regioselectivity (Figure 5.4E).

Inspired by the reversibility of alkylthianthrenium salt formation that gives rise to high *N*-regioselectivity, we wondered if this thermodynamic control could be leveraged to achieve a diastereoselective transformation. We hypothesized that nucleophilic addition into an alkenylthianthrenium salt with a chiral center adjacent to the site of conjugate-type addition may be engender diastereoselectivity if there is a thermodynamic energy difference between the two diastereomeric alkylthianthrenium products. To probe this hypothesis, we prepared a series of such alkenylthianthrenium salts and treated them to trifluoromethyl-substituted azole **5.33** under catalytic base conditions (Table 5.3). While alkylsulfonium products **5.34**–**5.36** were formed in moderate-to-high yields, all exhibited low diastereoselectivity (up to

Table 5.3. Investigation of Diastereoselective Azole Addition.

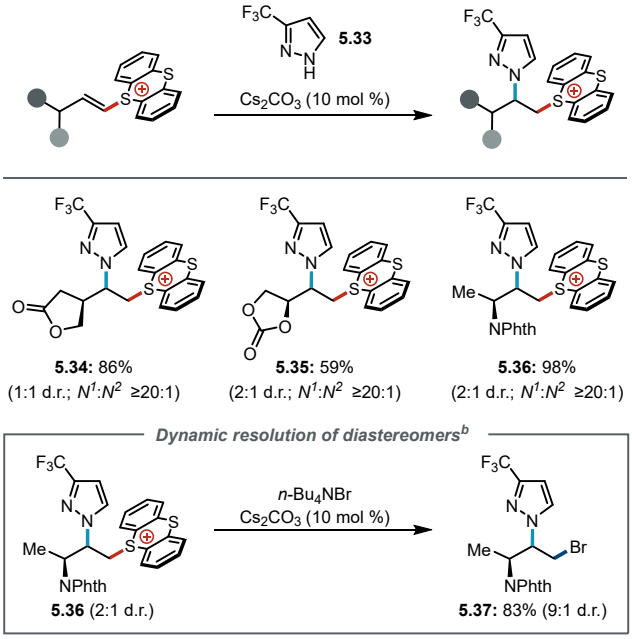

[a]Reactions conducted using alkenylthianthrenium salt (0.1 mmol), azole (0.1 mmol), Cs_2CO_3 (0.01 mmol), 2 mL MeCN, 3 h. NMR yields. See the appendix D for further experimental details. [b]DMF solvent.

2:1 d.r.). We noted that addition of half an equivalent of bromide nucleophile to the diastereomeric mixture of **5.36** consumed one diastereomer selectively over the other (see appendix D). We envisioned that, upon addition of a second nucleophile, dynamic diastereomeric resolution facilitated by the reversibility of alkylsulfonium formation would result in high diastereoselectivity of heterofunctionalization products. Indeed, under optimized conditions, alkylsulfonium intermediate **5.36** (2:1 d.r.) was converted to disubstituted product **5.37** with improved diastereoselectivity (9:1 d.r., Table 5.3). We anticipate that the thermodynamically controlled process can be exploited more broadly in new synthetic contexts.

In principle, conjugate-type addition of nucleophiles is not mechanistically limited to alkenylthianthrenium salts derived from terminal alkenes. We next focused on engaging more sterically hindered alkenylthianthrenium salts in this reactivity manifold. If successful, heterocycle conjugate-type addition into these electrophiles would furnish densely functionalized scaffolds. First, we investigated the reactivity of alkenylthianthrenium salts derived from symmetric 1,2-disubstituted alkenes with pyrazole **5.33** under catalytic base conditions (Table 5.4). Using a cyclic alkenylthianthrenium salt, product **5.38** was formed in low 10% yield with high remaining alkenylthianthrenium starting material. The conjugate-addition was more effective with acyclic alkenylthianthrenium salts and afforded products **5.39** and **5.40** in up to *ca.* 50% yields.[52] Taken together, these data suggest that conformational flexibility of the resultant 1,2-azolosulfonium salts is necessary for achieving high yields. As such, the equilibrium of alkylthianthrenium product formation is disfavored when employing alkenylthianthrenium salts derived

Table 5.4. 1,2-Azolothianthrenium Salts from Internal Alkenes.

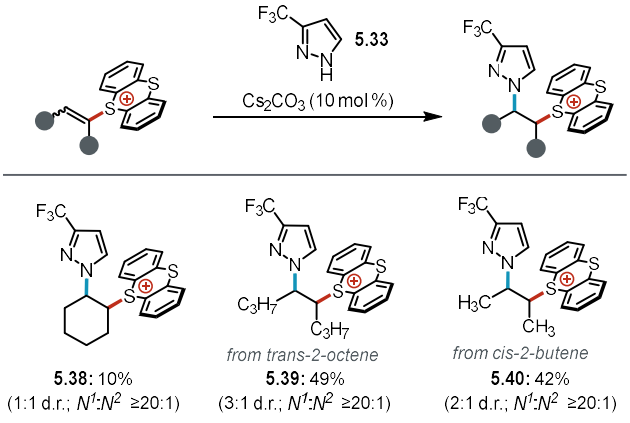

[a]Reactions conducted using alkenylthianthrenium salt (0.1 mmol), azole (0.1 mmol), Cs_2CO_3 (0.01 mmol), 2 mL MeCN, 3 h. NMR yields.

from internal alkenes. Nonetheless, *in situ* substitution with a second nucleophile may drive the formation of difunctionalized products from these hindered alkylthianthrenium salts.[53,54]

Next, we electrochemically prepared alkenylthianthrenium salt **5.41** derived from a 1,1-disubstited alkene: isobutene. Excitingly, we found that heterocycles undergo efficient conjugate-addition with this hindered alkenylthianthrenium salt to form α-tertiary azoles under either catalytic Cs_2CO_3 or stoichiometric *i*-Pr_2NEt conditions (Table 5.5). Preparation of this azole motif is exceptionally challenging with conventional methods due to the sterically-hindered site of nucleophilic substitution. However, we observed that these 1,2-azolosulfonium products are still prone to base-induced elimination pathways. Treatment of *N*-alkyl azole **5.42** with stoichiometric Cs_2CO_3 base resulted in quantitative elimination to an allylic functionalized azole (see appendix D). This irreversible allylic pathway was a dominant issue when attempting substitution of the alkylsulfonium electrophile **5.41** with basic nucleophiles (*e.g.* acetate, secondary aliphatic amine, Table 5.5). We found that non-basic nucleophiles were competent for substitution of the 1,2-azolothianthrenium intermediates and **5.47**, formed upon subsequent addition of a thiolate nucleophile, was isolated in 88% yield with exceptional *N*-regioselectivity (≥20:1 N^1:N^2). We anticipate future work in the Wickens group will explore thianthrenium structures that may promote substitution pathways over elimination pathways to generate vicinal motifs.

Table 5.5. 1,2-Azolothianthrenium Salts and Second Substitution from 1,1-Disubstituted Alkenes.

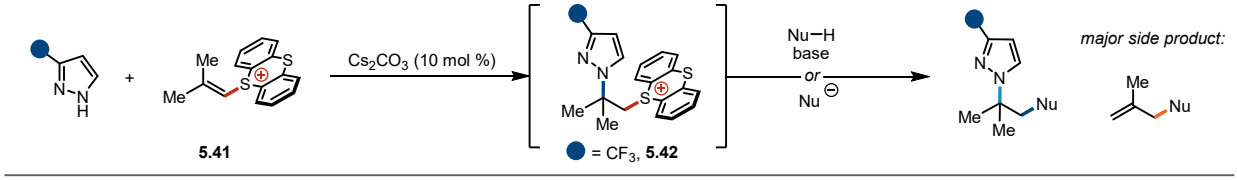

[a]Reactions conducted using alkenylthianthrenium salt (0.1 mmol), azole (0.1 mmol), Cs_2CO_3 (0.01 mmol), 2 mL MeCN, 3 h. NMR yields. See the appendix D for further experimental details. [b]*n*-Bu_4NBr (0.3 mmol). [b]*n*-Bu_4NN_3 (0.1 mmol). [b]KOAc (0.1 mmol). [b]BnNHMe (0.1 mmol), *i*-Pr_2NEt (0.1 mmol). [b]alkenylthianthrenium salt (0.2 mmol), azole (0.2 mmol), Cs_2CO_3 (0.02 mmol), 4 mL MeCN, 3 h; then thiolate (0.3 mmol), 48 h. Isolated yield.

5.4 Conclusion

Overall, we have identified conditions that divert nucleophilic substitution of alkenylthianthrenium salts towards net alkene heterofunctionalization reactions. While use of stoichiometric base often promotes allylic functionalization, substoichiometric base loadings have enabled selective conjugate-type addition of several nucleophile classes. Mechanistic studies revealed that 1,2-sulfonamidosulfonium formation is dictated by a proton-transfer-mediated equilibrium solution of sulfonamide, alkenylthianthrenium salt, and alkylsulfonium product. These insights were leveraged in the *N*-alkylation of azoles using alkenylthianthrenium salts. Key to this new methodology was achieving base-dependent reversibility of the conjugate-addition and ylide protonation sequence that renders the overall reaction highly *N*-regioselective. We anticipate that this modular approach to generate vicinal motifs will find immediate application in organic synthesis given the established importance of *N*-alkylated azoles in the pharmaceutical and agrochemical industries. Moreover, continued examination of reaction conditions that promote conjugate-type addition *versus* allylic functionalization is anticipated to dramatically expand the scope of engageable nucleophiles that remain challenging to leverage in both reactivity manifolds.

5.5 Acknowledgements

K.T. performed the sulfonamide nucleophile experiments and collected the data. Z.K.W. and C.D. designed the azole project. All authors performed the azole nucleophile experiments and collected the data. C.D. designed and executed the azole mechanistic experiments. All authors contributed to writing the azole manuscript in preparation.

5.6 References

(1) Patel, M.; Desai, B.; Sheth, A.; Dholakiya, B. Z.; Naveen, T. Recent Advances in Mono- and Difunctionalization of Unactivated Olefins. *Asian Journal of Organic Chemistry* **2021**, *10* (12), 3201–3232.

(2) Yao, H.; Hu, W.; Zhang, W. Difunctionalization of Alkenes and Alkynes via Intermolecular Radical and Nucleophilic Additions. *Molecules* **2021**, *26* (1), 105.

(3) Chen, J.; Li, J.; Plutschack, M. B.; Berger, F.; Ritter, T. Regio- and Stereoselective Thianthrenation of Olefins To Access Versatile Alkenyl Electrophiles. *Angewandte Chemie International Edition* **2020**, *59* (14), 5616–5620.

(4) Holst, D. E.; Wang, D. J.; Kim, M. J.; Guzei, I. A.; Wickens, Z. K. Aziridine Synthesis by Coupling Amines and Alkenes via an Electrogenerated Dication. *Nature* **2021**, *596* (7870), 74–79.

(5) Wang, D. J.; Targos, K.; Wickens, Z. K. Electrochemical Synthesis of Allylic Amines from Terminal Alkenes and Secondary Amines. *J. Am. Chem. Soc.* **2021**, *143* (51), 21503–21510.

(6) Liu, M.-S.; Du, H.-W.; Shu, W. Metal-Free Allylic C–H Nitrogenation, Oxygenation, and Carbonation of Alkenes by Thianthrenation. *Chem. Sci.* **2021**.

(7) Angyal, P.; Kotschy, A. M.; Dudás, Á.; Varga, S.; Soós, T. Intertwining Olefin Thianthrenation with Kornblum/Ganem Oxidations: Ene-Type Oxidation to Furnish α,β-Unsaturated Carbonyls. *Angewandte Chemie International Edition* **2023**, *62* (2), e202214096.

(8) Holst, D. E.; Dorval, C.; Winter, C. K.; Guzei, I. A.; Wickens, Z. K. Regiospecific Alkene Aminofunctionalization via an Electrogenerated Dielectrophile. *J. Am. Chem. Soc.* **2023**, *145* (15), 8299–8307.

(9) Johannsen, M.; Jørgensen, K. A. Allylic Amination. *Chem. Rev.* **1998**, *98* (4), 1689–1708.

(10) Evans, P. A.; Robinson, J. E.; Nelson, J. D. Enantiospecific Synthesis of Allylamines via the Regioselective Rhodium-Catalyzed Allylic Amination Reaction [*J. Am. Chem. Soc.* **1999** , *121* , 6761−6762]. *J. Am. Chem. Soc.* **1999**, *121* (51), 12214–12214.

(11) Weiner, B.; Baeza, A.; Jerphagnon, T.; Feringa, B. L. Aldehyde Selective Wacker Oxidations of Phthalimide Protected Allylic Amines: A New Catalytic Route to B3-Amino Acids. *J. Am. Chem. Soc.* **2009**, *131* (27), 9473–9474.

(12) Moosophon, P.; Baird, M. C.; Kanokmedhakul, S.; Pyne, S. G. Total Synthesis of Calystegine B4. *European Journal of Organic Chemistry* **2010**, *2010* (17), 3337–3344.

(13) Carroll, A. W.; Savaspun, K.; Willis, A. C.; Hoshino, M.; Kato, A.; Pyne, S. G. Total Synthesis of Natural Hyacinthacine C5 and Six Related Hyacinthacine C5 Epimers. *J. Org. Chem.* **2018**, *83* (10), 5558–5576.

(14) Miller, K. E.; Wright, A. J.; Olesen, M. K.; Hovey, M. T.; Scheerer, J. R. Stereoselective Synthesis of (+)-Loline Alkaloid Skeleton. *J. Org. Chem.* **2015**, *80* (3), 1569–1576.

(15) Ichikawa, Y.; Ito, T.; Isobe, M. Stereoselective Allyl Amine Synthesis through Enantioselective Addition of Diethylzinc and [1,3]-Chirality Transfer: Synthesis of Lentiginosine and Polyoxamic Acid Derivative. *Chemistry – A European Journal* **2005**, *11* (6), 1949–1957.

(16) Skoda, E. M.; Davis, G. C.; Wipf, P. Allylic Amines as Key Building Blocks in the Synthesis of (E)-Alkene Peptide Isosteres. *Org. Process Res. Dev.* **2012**, *16* (1), 26–34.

(17) White, J. D.; Kim, T.-S.; Nambu, M. Absolute Configuration and Total Synthesis of (+)-Curacin A, an Antiproliferative Agent from the Cyanobacterium Lyngbya Majuscula. *J. Am. Chem. Soc.* **1997**, *119* (1), 103–111.

(18) Gao, Y.; Klunder, J. M.; Hanson, R. M.; Masamune, H.; Ko, S. Y.; Sharpless, K. B. Catalytic Asymmetric Epoxidation and Kinetic Resolution: Modified Procedures Including in Situ Derivatization. *J. Am. Chem. Soc.* **1987**, *109* (19), 5765–5780.

(19) Jeong, J. U.; Tao, B.; Sagasser, I.; Henniges, H.; Sharpless, K. B. Bromine-Catalyzed Aziridination of Olefins. A Rare Example of Atom-Transfer Redox Catalysis by a Main Group Element. *J. Am. Chem. Soc.* **1998**, *120* (27), 6844–6845.

(20) Herlé, B.; Späth, G.; Schreyer, L.; Fürstner, A. Total Synthesis of Mycinolide IV and Path-Scouting for Aldgamycin N. *Angewandte Chemie International Edition* **2021**, *60* (14), 7893–7899.

(21) Hara, S.; Makino, K.; Hamada, Y. Total Synthesis of Halipeptin A, a Potent Anti-Inflammatory Cyclodepsipeptide from a Marine Sponge. *Tetrahedron Letters* **2006**, *47* (7), 1081–1085.

(22) Mikami, K.; Azuma, K.-I.; Nakai, T. [2,3]-Wittig Sigmatropic Rearrangement of Crotyl Propargyl Ether System. An Emerging Tool for Control of Acyclic Stereochemistry. *Tetrahedron* **1984**, *40* (12), 2303–2308.

(23) Thirumalaikumar, M. Ring Opening Reactions of Epoxides. A Review. *Organic Preparations and Procedures International* **2022**, *54* (1), 1–39.

(24) Curthbertson, E.; O'Brien, P.; Towers, T. D. Practical One-Step Synthesis of Koga's Chiral Bases. *Synthesis* **2001**, *2001* (5), 693–695.

(25) Moschona, F.; Savvopoulou, I.; Tsitopoulou, M.; Tataraki, D.; Rassias, G. Epoxide Syntheses and Ring-Opening Reactions in Drug Development. *Catalysts* **2020**, *10* (10), 1117.

(26) Cheng, M.; De, B.; Almstead, N. G.; Pikul, S.; Dowty, M. E.; Dietsch, C. R.; Dunaway, C. M.; Gu, F.; Hsieh, L. C.; Janusz, M. J.; Taiwo, Y. O.; Natchus, M. G.; Hudlicky, T.; Mandel, M. Design, Synthesis, and Biological Evaluation of Matrix Metalloproteinase Inhibitors Derived from a Modified Proline Scaffold. *J. Med. Chem.* **1999**, *42* (26), 5426–5436.

(27) Hu, X. E. Nucleophilic Ring Opening of Aziridines. *Tetrahedron* **2004**, *60* (12), 2701–2743.

(28) Akhtar, R.; Naqvi, S. A. R.; Zahoor, A. F.; Saleem, S. Nucleophilic Ring Opening Reactions of Aziridines. *Mol Divers* **2018**, *22* (2), 447–501.

(29) The pKa of the conjugate acid of proton-sponge is 7.5 in DMSO.

(30) Maertens, J. A. History of the Development of Azole Derivatives. *Clin Microbiol Infect* **2004**, *10 Suppl 1*, 1–10.

(31) Kim, J. H.; Cheng, L. W.; Land, K. M. Advances in Antifungal Development: Discovery of New Drugs and Drug Repurposing. *Pharmaceuticals (Basel)* **2022**, *15* (7), 787.

(32) Kane, A.; Carter, D. A. Augmenting Azoles with Drug Synergy to Expand the Antifungal Toolbox. *Pharmaceuticals* **2022**, *15* (4), 482.

(33) Jørgensen, L. N.; Heick, T. M. Azole Use in Agriculture, Horticulture, and Wood Preservation – Is It Indispensable? *Frontiers in Cellular and Infection Microbiology* **2021**, *11*.

(34) Kerru, N.; Gummidi, L.; Maddila, S.; Gangu, K. K.; Jonnalagadda, S. B. A Review on Recent Advances in Nitrogen-Containing Molecules and Their Biological Applications. *Molecules* **2020**, *25* (8), 1909.

(35) Tran, T. N.; Henary, M. Synthesis and Applications of Nitrogen-Containing Heterocycles as Antiviral Agents. *Molecules* **2022**, *27* (9), 2700.

(36) Li, X.; Yu, Y.; Tu, Z. Pyrazole Scaffold Synthesis, Functionalization, and Applications in Alzheimer's Disease and Parkinson's Disease Treatment (2011–2020). *Molecules* **2021**, *26* (5), 1202.

(37) Shafiei, M.; Peyton, L.; Hashemzadeh, M.; Foroumadi, A. History of the Development of Antifungal Azoles: A Review on Structures, SAR, and Mechanism of Action. *Bioorganic Chemistry* **2020**, *104*, 104240.

(38) Cernak, T.; Dykstra, K. D.; Tyagarajan, S.; Vachal, P.; Krska, S. W. The Medicinal Chemist's Toolbox for Late Stage Functionalization of Drug-like Molecules. *Chem. Soc. Rev.* **2016**, *45* (3), 546–576.

(39) Vitaku, E.; Smith, D. T.; Njardarson, J. T. Analysis of the Structural Diversity, Substitution Patterns, and Frequency of Nitrogen Heterocycles among U.S. FDA Approved Pharmaceuticals: Miniperspective. *J. Med. Chem.* **2014**, *57* (24), 10257–10274.

(40) Ameziane El Hassani, I.; Rouzi, K.; Assila, H.; Karrouchi, K.; Ansar, M. Recent Advances in the Synthesis of Pyrazole Derivatives: A Review. *Reactions* **2023**, *4* (3), 478–504.

(41) Nandurkar, D.; Danao, K.; Rokde, V.; Shivhare, R.; Mahajan, U.; Kumari, P.; Patel, A. B. Pyrazole Scaffold: Strategies toward the Synthesis and Their Applications. In *Strategies for the Synthesis of Heterocycles and Their Applications*; IntechOpen, 2022.

(42) Chen, S.-J.; Golden, D. L.; Krska, S. W.; Stahl, S. S. Copper-Catalyzed Cross-Coupling of Benzylic C–H Bonds and Azoles with Controlled N-Site Selectivity. *J. Am. Chem. Soc.* **2021**, *143* (36), 14438–14444.

(43) Liang, Y.; Zhang, X.; MacMillan, D. W. C. Decarboxylative Sp3 C–N Coupling via Dual Copper and Photoredox Catalysis. *Nature* **2018**, *559* (7712), 83–88.

(44) Li, P.; Zbieg, J. R.; Terrett, J. A. The Direct Decarboxylative N-Alkylation of Azoles, Sulfonamides, Ureas, and Carbamates with Carboxylic Acids via Photoredox Catalysis. *Org. Lett.* **2021**, *23* (24), 9563–9568.

(45) Sheng, T.; Zhang, H.-J.; Shang, M.; He, C.; Vantourout, Julien. C.; Baran, Phil. S. Electrochemical Decarboxylative N-Alkylation of Heterocycles. *Org. Lett.* **2020**, *22* (19), 7594–7598.

(46) Huang, A.; Wo, K.; Lee, S. Y. C.; Kneitschel, N.; Chang, J.; Zhu, K.; Mello, T.; Bancroft, L.; Norman, N. J.; Zheng, S.-L. Regioselective Synthesis, NMR, and Crystallographic Analysis of N1-Substituted Pyrazoles. *J. Org. Chem.* **2017**, *82* (17), 8864–8872.

(47) Norman, N. J.; Bao, S. T.; Curts, L.; Hui, T.; Zheng, S.-L.; Shou, T.; Zeghibe, A.; Burdick, I.; Fuehrer, H.; Huang, A. Highly Selective N-Alkylation of Pyrazoles: Crystal Structure Evidence for Attractive Interactions. *J. Org. Chem.* **2022**, *87* (15), 10018–10025.

(48) Iškauskienė, M.; Ragaitė, G.; Sløk, F. A.; Šačkus, A. Facile Synthesis of Novel Amino Acid-like Building Blocks by N-Alkylation of Heterocyclic Carboxylates with N-Boc-3-Iodoazetidine. *Mol Divers* **2020**, *24* (4), 1235–1251.

(49) Swamy, K. C. K.; Kumar, N. N. B.; Balaraman, E.; Kumar, K. V. P. P. Mitsunobu and Related Reactions: Advances and Applications. *Chem. Rev.* **2009**, *109* (6), 2551–2651.

(50) Kim, E. J.; Ko, S. Y.; Dziadulewicz, E. K. Mitsunobu Alkylation of Imidazole: A Convenient Route to Chiral Ionic Liquids. *Tetrahedron Letters* **2005**, *46* (4), 631–633.

(51) Horváth, A. Catalysis and Regioselectivity in the Michael Addition of Azoles. Kinetic vs. Thermodynamic Control. *Tetrahedron Letters* **1996**, *37* (25), 4423–4426.

(52) Increasing the alkenylthianthrenium salt equivalents improved the yield up to 65%, but deleterious side reactions remained problematic (see appendix D).

(53) Liu, M.-S.; Du, H.-W.; Cui, J.-F.; Shu, W. Intermolecular Metal-Free Cyclopropanation and Aziridination of Alkenes with XH2 (X=N, C) by Thianthrenation**. *Angewandte Chemie International Edition* **2022**, *61* (41), e202209929.

(54) Shu, W.; Liu, M.-S.; Meng, H. Unified Metal-Free Intermolecular Heck-Type Sulfonylation, Cyanation, Amination, Amidation of Alkenes by Thianthrenation. ChemRxiv July 3, 2023. https://doi.org/10.26434/chemrxiv-2023-xsgh1.

Chapter 6: Diastereoselective Synthesis of Cyclopropanes from Carbon Pronucleophiles and Alkenes

This chapter has been reproduced as published:

Min Ji Kim, Diana J. Wang, **Karina Targos**, Uriel A. Garcia, Alison F. Harris, Ilia A. Guzei, Zachary K. Wickens. Diastereoselective Synthesis of Cyclopropanes from Carbon Pronucleophiles and Alkenes. *Angew. Chem. Int. Ed.* **2023**, e202303032.

6.1 Abstract

Cyclopropanes are desirable structural motifs with valuable applications in drug discovery and beyond. Established alkene cyclopropanation methods give rise to cyclopropanes with a limited array of substituents, are difficult to scale, or both. Herein, we disclose a new cyclopropane synthesis through the formal coupling of abundant carbon pronucleophiles and unactivated alkenes. This strategy exploits dicationic adducts derived from electrolysis of thianthrene in the presence of alkene substrates. We find that these dielectrophiles undergo cyclopropanation with methylene pronucleophiles via alkenyl thianthrenium intermediates. This protocol is scalable, proceeds with high diastereoselectivity, and tolerates diverse functional groups on both the alkene and pronucleophile coupling partners. To validate the utility of this new procedure, we prepared an array of substituted analogs of an established cyclopropane that is en route to multiple pharmaceuticals.

6.2 Introduction

Cyclopropanes are important structural motifs with diverse applications as synthetic intermediates, mechanistic probes, and design elements of bioactive molecules.[1–10] In the context of medicinal chemistry, these three-membered carbocyclic rings are employed to increase potency, reduce off-target effects, and fine-tune metabolic stability.[10–12] Recognition of these strategic benefits has driven the number of approved small molecule drugs containing cyclopropanes to double over the last ten years.[13] Recently, other

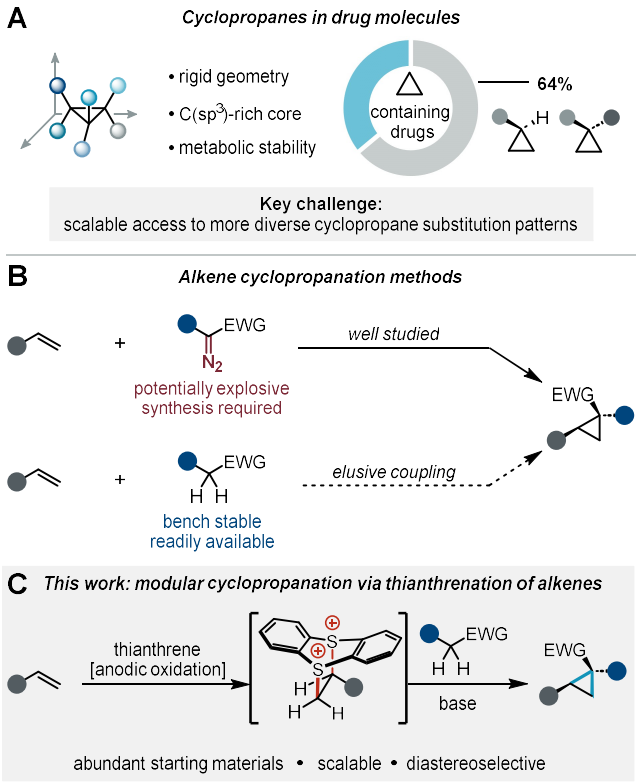

Figure 6.1. Project overview. (A) Cyclopropanes in drug molecules. (B) Alkene cyclopropanation methods. (C) overview of this work.

structurally rigid ring systems are emerging as an appealing design strategy to precisely control the 3D molecular geometry of drug candidates.[11,14–20] While in principle cyclopropanes offer a myriad of 3D shapes, 64% of the cyclopropane rings in active pharmaceutical ingredients are substituted at only a single carbon (Figure 6.1A).[13,21] This overrepresentation of a narrow subset of possible substitution patterns is, in part, due to the reactions used to construct cyclopropane rings. For example, cyclopropanes substituted at one carbon are straightforward to access on large scale via enolate alkylation using 1,2-dihaloethane dielectrophiles. However, vicinal dihalides bearing any additional substituents suffer inextricable elimination reactions, limiting access to more substituted analogs through this intermolecular disconnection.[22–25] The Corey–Chaykovsky reaction offers an alternative method for that allows synthesis of more substituted cyclopropanes but requires activated electron-deficient π-systems (*e.g.* α,β-unsaturated carbonyl compounds).[26–29] The most well-studied approach to prepare more substituted cyclopropanes from a broader range of alkenes remains cyclopropanation based on metal carbenoid reactivity (Figure 6.1B).[30–

[40] While indisputably effective, the modularity of these methods is limited by the requisite synthesis of unique carbene precursors to deliver each distinct substituent. Furthermore, hazardous diazo compounds are commonly required, which further complicates broad implementation due to safety concerns.[41–57] Despite these varied approaches to prepare cyclopropanes, development of new approaches to prepare cyclopropane products is an area of contemporary interest.[58–63] Overall, a modular annulative cyclopropane synthesis that couples two abundant building blocks has remained elusive and is poised to substantially impact synthetic chemistry.

A deceptively straightforward strategy to access cyclopropanes in a modular fashion would be through the direct intermolecular oxidative coupling of carbon pronucleophiles and alkenes. Unfortunately, this idealized reaction has remained elusive.[64–66] In principle, the net transformation could be accomplished through conversion of an alkene to a dielectrophile that undergoes iterative substitution with a methylene pronucleophile rather than deleterious elimination. No established dielectrophile possesses the requisite selectivity profile to accomplish this in a general fashion.

Recent work has begun to explore the diverse and unique electrophilic reactivity of thianthrenium salts.[67–76] Our group recently developed an electrochemical strategy to generate dicationic adducts between unactivated alkenes and thianthrene (**TT**) that serve as dielectrophiles.[67,68,77–79,72] Specifically, we found these species underwent substitution by primary amine nucleophiles without deleterious elimination, unlocking a new approach to prepare *N*-alkyl aziridine products.[80–82] Very recently, Shu and co-workers reported a related method of preparing aziridines through the reaction of isolated alkenyl thianthrenium salt with nitrogen nucleophiles.[83] Additionally, this study extended the alkenyl sulfonium reactivity to cyclopropane synthesis from a handful of malonates and similarly acidic carbon pronucleophiles. Concurrently, we were exploring the use of alkene-derived thianthrenium salts to enable a new approach to cyclopropanation. In contrast to Shu's studies, however, our investigations focused on examining the diastereoselectivity of such a process alongside the strategic advantages offered by such an approach in the synthesis of heteroaryl-substituted cyclopropanes. Herein, we report the results of these investigations into the reactivity of dicationic thianthrene-alkene adducts with carbon pronucleophiles (Figure 6.1C). This led

to a modular and diastereoselective approach to prepare heteroaryl-substituted cyclopropanes from abundant precursors as well as key insights into the dicationic adduct substitution mechanism that transcends cyclopropanation processes.

6.3 Results and Discussion

We initiated our investigations using nitrile pronucleophile **6.3**. This model pronucleophile was selected for two primary reasons: (1) we suspected that sterically differentiated carbanion stabilizing groups would maximize diastereoselectivity, and (2) basic nitrogen heterocycles are pervasive in medicinal chemistry but their coordinating ability can challenge many established alkene cyclopropanation procedures.[84–86] After initial optimization of reaction conditions (see appendix E for details), we found this pronucleophile underwent base-promoted cyclopropanation with dicationic adducts (**6.1** and **6.2**) in high yield (Scheme 6.1). Consistent with our hypothesis, small nitrile substituent promotes high diastereoselectivity (≥20:1 d.r.). Indeed, conducting the same procedure with an analog of **6.3**, wherein the nitrile is replaced with an ester, furnished the product in diminished diastereoselectivity (2:1 d.r., see appendix E for details). Although these initial conditions were effective, they required a substantial excess of Cs_2CO_3 base (10 equiv.) to favor the desired cyclopropane over the elimination product, an alkenylthianthrenium salt (**6.5**). Given that initially we anticipated increased formation of elimination byproducts upon increasing base equivalents, we suspected that a more complex mechanistic pathway might be occurring rather than simple iterative substitution.

To investigate the mechanism of cyclopropanation, we monitored the substitution of dicationic adducts by ^{1}H NMR (Scheme 6.1). Intriguingly, the dicationic adducts are rapidly consumed to form alkenylthianthrenium salt **6.5**. This elimination product is subsequently converted to cyclopropane product **6.4**. Overall, this time course analysis suggests that an alkenylthianthrenium **6.5** is a key intermediate en route to cyclopropanation. This proposal is consistent with prior work on vinylsulfonium salts, which undergo cyclopropanation reactions with malonates and related pronucleophiles. However, these previously reported transformations have been predominantly limited to unsubstituted vinylsulfonium salts.[87–94] Only

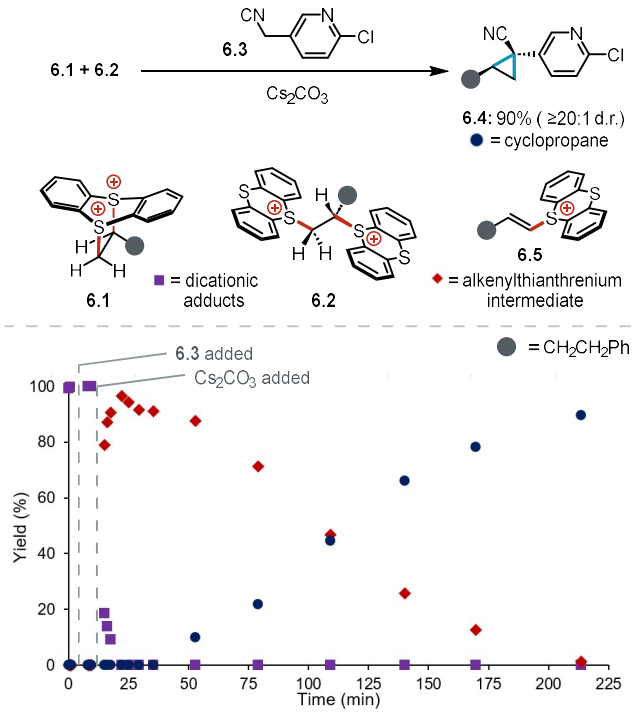

[a]Electrogenerated adducts were prepared using alkene (0.15 mmol), thianthrene (0.225 mmol), 3 mL of MeCN-d_3 (0.2 M KPF_6); then pronucleophile (0.15 mmol), Cs_2CO_3 (1.5 mmol), 2.5 h. See appendix E for further details.

Scheme 6.1. Initial experiments investigating cyclopropanation.[a]

a handful of alkenylsulfonium salts have been found to undergo cyclopropanation.[94–100] Given the relatively limited examples of cyclopropanation from unactivated alkenylsulfonium salts similar to **6.5**, we validated this potential mechanism by isolating **6.5** and resubjecting it to the substitution conditions. This experiment afforded the cyclopropane product **6.4** in 89% yield, validating the kinetic competency of this species as an intermediate in cyclopropanation. This electrophilic elimination product also offers a plausible explanation for the distinct reactivity profile of the dicationic adducts relative to conventional dihalide dielectrophiles, since alkenylhalides do not undergo addition with nucleophiles. With this mechanism in mind, we streamlined access to the key alkenylthianthrenium intermediate by passing the dicationic adduct solution through a short pad of basic alumina prior to addition of the pronucleophile and base. This modified procedure furnished the desired cyclopropane product **6.4** in 81% yield relative to alkene as a single diastereomer using one equivalent of pronucleophile and two equivalents of Cs_2CO_3.

With an optimized procedure in hand, we next examined the scope of this new cyclopropanation protocol. We found that this process enabled the formal coupling of a wide range of carbon pronucleophiles and unactivated alkenes (Table 6.1). First, we probed a range of nitrile pronucleophiles substituted with a second strong electron withdrawing group. Alkylnitriles bearing amide (**6.6, 6.7**), ester (**6.8**), sulfone (**6.9**), benzophenone imine (**6.10**), and phosphonate (**6.11**) α-substituents each underwent efficient cyclopropanation. High diastereoselectivity was observed across the majority of these substrates and in several cases relative configuration was unambiguously verified by X-ray crystallography.[101] These stereochemically defined cyclopropane building blocks each bear distinct synthetic handles for further diversification. Furthermore, acidic cyclic pronucleophiles were converted into a range of architecturally complex spirocyclic building blocks (**6.12–6.14**) from simple precursors. Symmetrical pronucleophiles such as malonate and malononitrile were also suitable coupling partners and afforded the expected

Table 6.1. Scope of Cyclopropanation *via* Electrogenerated Sulfonium Dielectrophiles.[a]

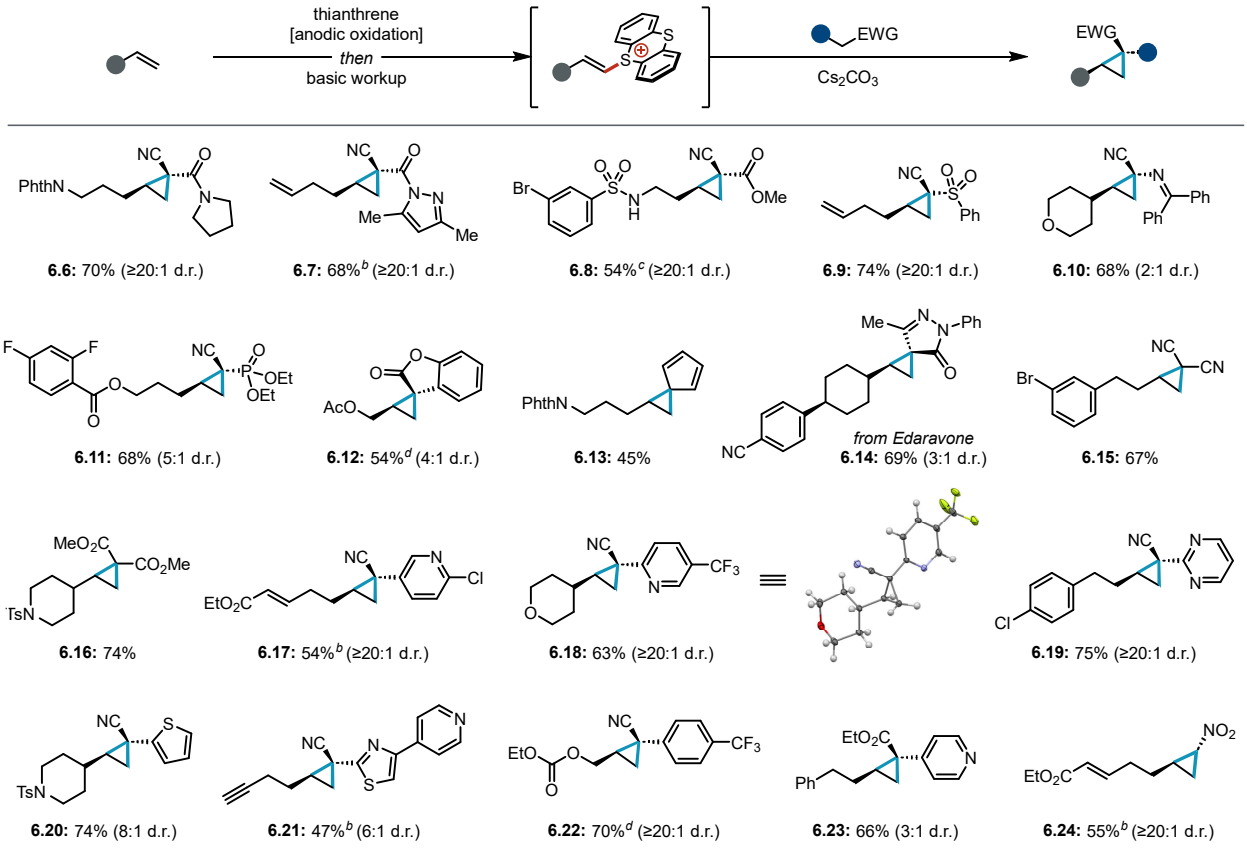

[a]Reactions were conducted using alkene (0.4 mmol), thianthrene (0.6 mmol), 8 mL of MeCN (0.2 M n-Bu_4NPF_6); then pronucleophile (0.4 mmol), Cs_2CO_3 (1.0 mmol), 2 h. Yields and d.r. are of the purified product as a racemate unless otherwise noted. See appendix E for further experimentla details. [b]NMR yield. [c]Alkene (0.6 mmol), thianthrene (0.9 mmol), 8 mL of MeCN (0.2 M n-Bu_4NPF_6). [d]Alkene (0.8 mmol), thianthrene (1.2 mmol), 8 mL of MeCN (0.2 M n-Bu_4NPF_6).

cyclopropane products (**6.15, 6.16**). We next explored the scope of this methodology with respect to less acidic pronucleophiles bearing diverse and medicinally-relevant (hetero)arenes as secondary withdrawing groups. We found that alkylnitrile pronucleophiles substituted with pyridines (**6.17, 6.18**), pyrimidines (**6.19**), thiophenes (**6.20**), thiazoles (**6.21**), and trifluorotoluene derivatives (**6.22**) each underwent efficient and diastereoselective cyclopropanation. Of note, established carbene-transfer-based approaches to related products deliver the opposite relative stereochemistry.[85] Hetereoarene substituted pronucleophiles with an ester instead of a nitrile furnished the final cyclopropane product in high yield, albeit with diminished diastereoselectivity (**6.23**). We also found that nitromethane, an inexpensive commodity chemical, could be employed to prepare 1,2-disubstituted cyclopropane (**6.24**) with high selectivity for the trans product. Less acidic pronucleophiles bearing a weaker single electron withdrawing group failed to deliver more than traces of cyclopropane products (see appendix E for details). Throughout these studies, we found that variation of the alkene coupling partner provided access to cyclopropane building blocks bearing diverse pendant functional groups, such as acetates (**6.12**), carbonates (**6.22**), nitriles (**6.14**), phthalimides (**6.6, 6.13**), and sulfonamides (**6.8**). Additionally, steric hindrance about the alkene was well tolerated (**6.10, 6.14, 6.16, 6.18, 6.20**). Notably, unconjugated dienes (**6.7, 6.9**) and ene-ynes (**6.21**) both underwent selective cyclopropanation at a single site, leaving a pendant unsaturated π-system for subsequent derivatization. An alkene substrate containing an α,β-unsaturated ester (**6.17, 6.24**) underwent selective cyclopropanation at the more electron-rich alkene. This demonstrates high selectivity both in the generation of the key electrophilic alkenyl thianthrenium intermediate as well as for cyclopropanation over enolate 1,4-addition. Taken together, these data validate that this modular cyclopropanation strategy is amenable to the synthesis of diverse and complex cyclopropanes that would have been difficult to prepare using more conventional methods.

We next evaluated the viability of performing this process on preparative scale (Scheme 6.2). We synthesized product **6.25** on multigram scale (3.3 g, 72% yield, 7.9 mmol, ≥20:1 d.r.) using a 1:1 stoichiometry of the alkene and pronucleophile coupling partners. This representative example is illustrative of the power of this protocol in the synthesis of versatile cyclopropane building blocks. Specifically,

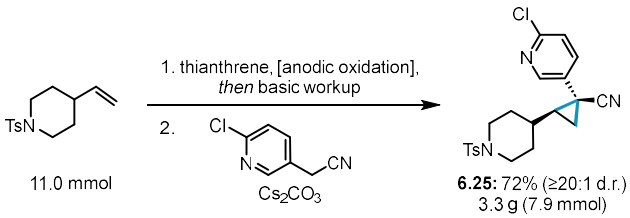

[a]Reaction was conducted using alkene (11.0 mmol), thianthrene (16.5 mmol), 110 mL of MeCN (0.2 M n-Bu_4NPF_6); then pronucleophile (11.0 mmol), Cs_2CO_3 (27.5 mmol), 16 h. Yield and d.r. are of the purified product.

Scheme 6.2. Preparative scale cyclopropanation.[a]

compound **6.25** bears orthogonal handles for further functionalization using robust reactions, such as S_NAr and Grignard addition. Of note, this practical batch electrolysis reaction setup is comprised of a DC power supply, inexpensive electrodes, and a divided cell and does not require any precautions to exclude air or moisture. Combined with the low cost,[102] low toxicity,[103] and recyclability[67] of the thianthrene promoter, these results demonstrate the scalability of this electrochemical cyclopropanation protocol.

We recognized that use of feedstock alkenes would enable access to cyclopropane building blocks from exceptionally inexpensive starting materials. Anodic oxidation of thianthrene under 1 atm of ethylene, propene, 1-butene, and 2-methyl-1-butene each delivered dicationic adducts that could be subsequently converted to the desired cyclopropane products (Table 6.2). When relevant, these reactions proceeded with

Table 6.2. Cyclopropane building blocks from feedstock alkenes.[a]

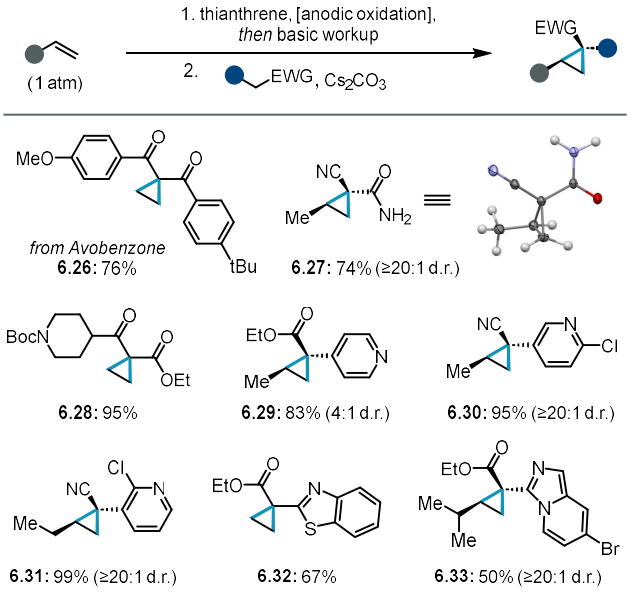

[a]Reactions were conducted using alkene (1 atm), thianthrene (1.0 mmol), 4 mL of MeCN (0.4 M n-Bu_4NPF_6); then pronucleophile (0.4 mmol), Cs_2CO_3 (1.0 mmol), 14–16 h. Yields and d.r. are of the purified product.See appendix E futher details

high diastereoselectivity even in the case of propene (**6.27**, **6.29**, **36.0**), which bears a relatively small methyl substituent. These data illustrate how the high functional group tolerance of this method can be leveraged to prepare diverse cyclopropane building blocks for drug discovery from simple precursors.

We envisioned that this newly realized oxidative cyclopropanation methodology would have immediate utility through both the preparation of established cyclopropane targets as well as previously unknown derivatives. As an illustrative example, we prepared cyclopropane **6.34** from a commercially available benzylic nitrile and ethylene (1 atm) in high yield (Scheme 6.3). Compound **6.34** is an established intermediate in the synthesis of two distinct small molecule components in the most common cystic fibrosis drugs (lumacaftor and tezacaftor; total sales in 2021 amounted to $6.9 B USD).[104] The established route to **6.34** constructs the cyclopropane ring through an enolate dialkylation using 1,2-dihaloethane.[105,106] While circumventing this carcinogenic dihalide may offer strategic advantages in synthesis of **6.34**, we anticipated that the true power of this oxidative coupling route would lie in the synthesis of new structural analogs to this key intermediate. Indeed, no analogs of intermediate **6.34** bearing additional substituents on the cyclopropane moiety have been previously reported, presumably due to the limitations associated with substituted dihalide dielectrophiles. To this end, we prepared a series of substituted analogs of **6.34** by

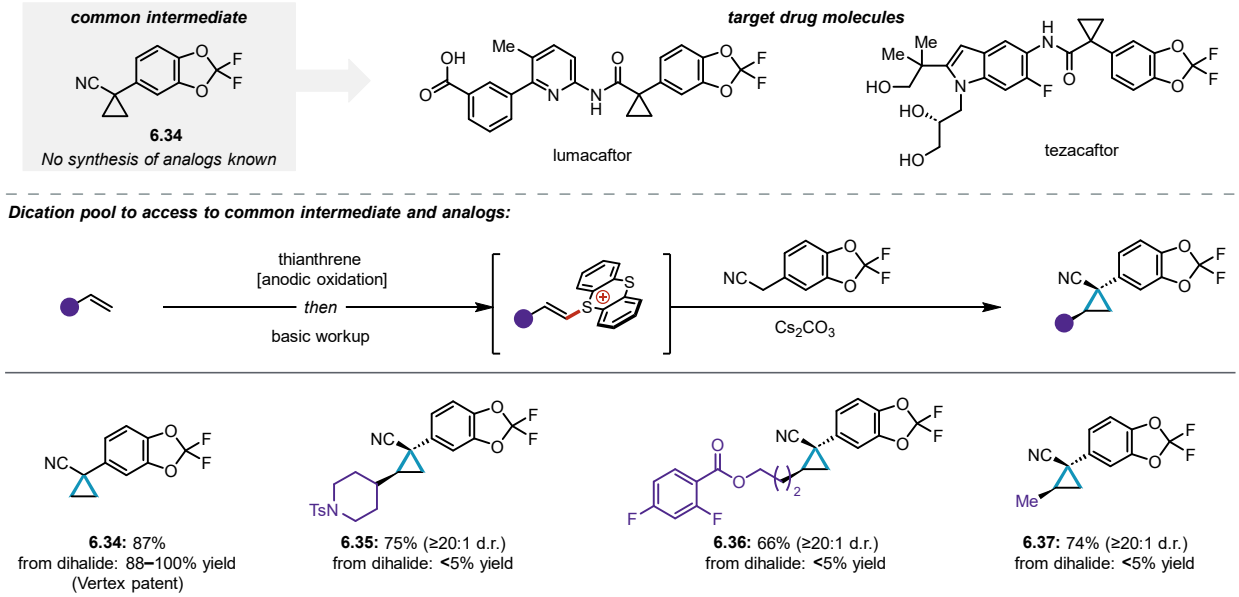

[a]Gaseous alkene reactions were conducted using alkene (1 atm), thianthrene (1.0 mmol), 4 mL of MeCN (0.4 M *n*-Bu_4NPF_6); then pronucleophile (0.4 mmol), Cs_2CO_3 (1.0 mmol), 14–16 h. Reactions with non-gaseous alkenes were conducted using alkene (0.4 mmol), thiathrene (0.6 mmol), 8 mL of MeCN (0.2 M *n*-Bu_4NPF_6); then pronucleophile (0.4 mmol), Cs_2CO_3 (1.0 mmol), 2 h. Yields and d.r. are of the purified product.See the appendix E for further experimental details.

Scheme 6.3. Synthesis of drug intermediate and analogs.[a]

varying the alkene coupling partner (**6.35–6.37**). This approach enabled both large structural changes, such as replacement of a cyclopropyl hydrogen with a piperidine ring (**6.35**), as well as small perturbations, accessing methylated analog **6.37**. Attempts to access the same products from analogous vicinal dihalide starting materials resulted in at most trace product. Taken together, these results illustrate how this new technology can impact the cyclopropane compounds prepared and studied in medicinal chemistry.

6.4 Conclusion

Overall, we have developed a modular procedure to prepare cyclopropanes from abundant carbon pronucleophiles and alkenes *via* electrochemically-generated thianthrenium salts. Mechanistic studies revealed that the dicationic adducts underwent rapid elimination under the reaction conditions to form an alkenylthianthrenium salt, which serves as a key electrophilic intermediate *en route* to cyclopropanes. This approach is amenable to generation of diverse cyclopropanes bearing medicinally-relevant functional groups and handles for further elaboration. This cyclopropanation strategy allows for highly diastereoselective synthesis of nitrile-substituted cyclopropanes and furnishes complementary relative stereochemistry when compared to conventional metal-catalyzed approaches. This method expands the scope of readily accessible cyclopropane building blocks using inexpensive coupling partners and reagents. We anticipate that this new transformation will find broad application in organic synthesis given the growing interest in cyclopropanes in medicinal chemistry and beyond.

6.5 Acknowledgements

We thank the Stahl, Weix, Yoon, and Schomaker groups for sharing their chemical inventory. This work was financially supported by the Office of the Vice Chancellor for Research and Graduate Education at the University of Wisconsin–Madison with funding from the Wisconsin Alumni Research Foundation. Spectroscopic instrumentation was supported by a generous gift from Paul J. and Margaret M. Bender, NSF (CHE-1048642), and NIH (S10OD012245 and 1S10OD020022-1). The Bruker D8 VENTURE Photon III X-ray diffractometer was partially funded by NSF Award #CHE-1919350 to the UW–Madison Department

of Chemistry. This material is based upon work supported by the National Science Foundation Graduate Research Fellowship Program under grant no. DGE-1747503 (K.T.). Any opinions, findings, and conclusions or recommendations expressed in this material are those of the author(s) and do not necessarily reflect the views of the National Science Foundation. A.F.H. was supported by a Nicholas O'Connor Research Fellowship.

Z.K.W. and M.K. designed the project. All authors performed the experiments and collected the data. M.K. designed and implemented the mechanistic experiments. I.A.G. collected and analyzed X-ray data to provide crystal structures. Z.K.W., M.K, K.T., D.J.W., and U.A.G. contributed to writing the manuscript.

6.6 References

(1) Wong, H. N. C.; Hon, M. Y.; Tse, C. W.; Yip, Y. C.; Tanko, J.; Hudlicky, T. Use of Cyclopropanes and Their Derivatives in Organic Synthesis. *Chem. Rev.* **1989**, *89*, 165–198.

(2) Griller, D.; Ingold, K. U. Free-Radical Clocks. *Acc. Chem. Res.* **1980**, *13*, 317–323.

(3) Pirenne, V.; Muriel, B.; Waser, J. Catalytic Enantioselective Ring-Opening Reactions of Cyclopropanes. *Chem. Rev.* **2021**, *121*, 227–263.

(4) Ebner, C.; Carreira, E. M. Cyclopropanation Strategies in Recent Total Syntheses. *Chem. Rev.* **2017**, *117*, 11651–11679.

(5) Faust, R. Fascinating Natural and Artificial Cyclopropane Architectures. *Angewandte Chemie International Edition* **2001**, *40*, 2251–2253.

(6) Wessjohann, L. A.; Brandt, W.; Thiemann, T. Biosynthesis and Metabolism of Cyclopropane Rings in Natural Compounds. *Chem. Rev.* **2003**, *103,* 1625–1648.

(7) Lamberth, C. Small Ring Chemistry in Crop Protection. *Tetrahedron* **2019**, *75*, 4365–4383.

(8) Ghosh, K.; Das, S. Recent Advances in Ring-Opening of Donor Acceptor Cyclopropanes Using C-Nucleophiles. *Org. Biomol. Chem.* **2021**, 19 (5), 965–982.

(9) Schneider, T. F.; Kaschel, J.; Werz, D. B. A New Golden Age for Donor–Acceptor Cyclopropanes. *Angewandte Chemie International Edition* **2014**, 53 (22), 5504–5523.

(10) Talele, T. T. The “Cyclopropyl Fragment” Is a Versatile Player That Frequently Appears in Preclinical/Clinical Drug Molecules. *J. Med. Chem.* **2016**, 59 (19), 8712–8756.

(11) Taylor, R. D.; MacCoss, M.; Lawson, A. D. G. Rings in Drugs. *J. Med. Chem.* **2014**, 57 (14), 5845–5859.

(12) Novakov, I. A.; Babushkin, A. S.; Yablokov, A. S.; Nawrozkij, M. B.; Vostrikova, O. V.; Shejkin, D. S.; Mkrtchyan, A. S.; Balakin, K. V. Synthesis and Structure—Activity Relationships of Cyclopropane-Containing Analogs of Pharmacologically Active Compounds. *Russ Chem Bull* **2018**, 67 (3), 395–418.

(13) Wishart, D. S.; Feunang, Y. D.; Guo, A. C.; Lo, E. J.; Marcu, A.; Grant, J. R.; Sajed, T.; Johnson, D.; Li, C.; Sayeeda, Z.; Assempour, N.; Iynkkaran, I.; Liu, Y.; Maciejewski, A.; Gale, N.; Wilson, A.; Chin, L.; Cummings, R.; Le, D.; Pon, A.; Knox, C.; Wilson, M. DrugBank 5.0: A Major Update to the DrugBank Database for 2018. *Nucleic Acids Res* **2018**, 46 (D1), D1074–D1082.

(14) Hung, A. W.; Ramek, A.; Wang, Y.; Kaya, T.; Wilson, J. A.; Clemons, P. A.; Young, D. W. Route to Three-Dimensional Fragments Using Diversity-Oriented Synthesis. *Proceedings of the National Academy of Sciences* **2011**, 108 (17), 6799–6804.

(15) Carreira, E. M.; Fessard, T. C. Four-Membered Ring-Containing Spirocycles: Synthetic Strategies and Opportunities. *Chem. Rev.* **2014**, 114 (16), 8257–8322.

(16) Zheng, Y.; Tice, C. M.; Singh, S. B. The Use of Spirocyclic Scaffolds in Drug Discovery. *Bioorganic & Medicinal Chemistry Letters* **2014**, 24 (16), 3673–3682.

(17) Mykhailiuk, P. K. Saturated Bioisosteres of Benzene: Where to Go Next? *Org. Biomol. Chem.* **2019**, 17 (11), 2839–2849.

(18) Zhao, J.-X.; Chang, Y.-X.; He, C.; Burke, B. J.; Collins, M. R.; Del Bel, M.; Elleraas, J.; Gallego, G. M.; Montgomery, T. P.; Mousseau, J. J.; Nair, S. K.; Perry, M. A.; Spangler, J. E.; Vantourout, J. C.; Baran, P. S. 1,2-Difunctionalized Bicyclo[1.1.1]Pentanes: Long–Sought-after Mimetics for Ortho/Meta-Substituted Arenes. *Proceedings of the National Academy of Sciences* **2021**, 118 (28), e2108881118.

(19) Zhang, X.; Smith, R. T.; Le, C.; McCarver, S. J.; Shireman, B. T.; Carruthers, N. I.; MacMillan, D. W. C. Copper-Mediated Synthesis of Drug-like Bicyclopentanes. *Nature* **2020**, 580 (7802), 220–226.

(20) Gianatassio, R.; Lopchuk, J. M.; Wang, J.; Pan, C.-M.; Malins, L. R.; Prieto, L.; Brandt, T. A.; Collins, M. R.; Gallego, G. M.; Sach, N. W.; Spangler, J. E.; Zhu, H.; Zhu, J.; Baran, P. S. Strain-Release Amination. *Science* **2016**, 351 (6270), 241–246.

(21) Analysis was conducted using the DrugBank database (accessed January 2023), see reference 13 for DrugBank details.

(22) Lavoisier, T.; Rodriguez, J. Practical Large Scale Preparation of Activated Cyclopropanes. *Synthetic Communications* **1996**, 26 (3), 525–530.

(23) Časar, Z. Synthetic Approaches to Contemporary Drugs That Contain the Cyclopropyl Moiety. *Synthesis* **2020**, 52 (09), 1315–1345.

(24) To circumvent these elimination issues, a multistep protocol has been developed involving initial dihydroxylation followed by sequential activation and substitution steps, see: Jakubowska, A.; Żuchowski, G.; Kulig, K. Cyclic Sulfates as Useful Tools in the Asymmetric Synthesis of 1-Aminocyclopropane-1-Carboxylic Acid Derivatives. *Tetrahedron Asymmetry* **2015**, 26 (21), 1261–1267.

(25) Since failed experiments are not often reported, we validated the challenge of elimination by subjecting a substituted vicinal dibromide to malonate and base. These experiments resulted in formation of exclusively elimination products. See appendix E for details.

(26) Gololobov, Yu. G.; Nesmeyanov, A. N.; lysenko, V. P.; Boldeskul, I. E. Twenty-Five Years of Dimethylsulfoxonium Ethylide (Corey's Reagent). *Tetrahedron* **1987**, 43 (12), 2609–2651.

(27) Li, A.-H.; Dai, L.-X.; Aggarwal, V. K. Asymmetric Ylide Reactions: Epoxidation, Cyclopropanation, Aziridination, Olefination, and Rearrangement. *Chem. Rev.* **1997**, 97 (6), 2341–2372.

(28) Caiuby, C. A. D.; Furniel, L. G.; Burtoloso, A. C. B. Asymmetric Transformations from Sulfoxonium Ylides. *Chem. Sci.* **2022**, 13 (5), 1192–1209.

(29) Beutner, G. L.; George, D. T. Opportunities for the Application and Advancement of the Corey–Chaykovsky Cyclopropanation. *Org. Process Res. Dev.* **2022**.

(30) Chen, D. Y.-K.; Pouwer, R. H.; Richard, J.-A. Recent Advances in the Total Synthesis of Cyclopropane-Containing Natural Products. *Chem. Soc. Rev.* **2012**, 41 (13), 4631–4642.

(31) Davies, H. M. L.; Antoulinakis, E. G. Intermolecular Metal-Catalyzed Carbenoid Cyclopropanations. In *Organic Reactions*; American Cancer Society, **2004**; pp 1–326.

(32) Charette, A. B.; Beauchemin, A. Simmons-Smith Cyclopropanation Reaction. In *Organic Reactions*; American Cancer Society, **2004**; pp 1–415.

(33) Gurmessa, G. T.; Singh, G. S. Recent Progress in Insertion and Cyclopropanation Reactions of Metal Carbenoids from α-Diazocarbonyl Compounds. *Res Chem Intermed* **2017**, 43 (11), 6447–6504.

(34) Wu, W.; Lin, Z.; Jiang, H. Recent Advances in the Synthesis of Cyclopropanes. *Org. Biomol. Chem.* **2018**, 16 (40), 7315–7329.

(35) Lebel, H.; Marcoux, J.-F.; Molinaro, C.; Charette, A. B. Stereoselective Cyclopropanation Reactions. *Chem. Rev.* ***2003***, 103 (4), 977–1050.

(36) Brookhart, Maurice.; Studabaker, W. B. Cyclopropanes from Reactions of Transition Metal Carbene Complexes with Olefins. *Chem. Rev.* **1987**, 87 (2), 411–432.

(37) Ford, A.; Miel, H.; Ring, A.; Slattery, C. N.; Maguire, A. R.; McKervey, M. A. Modern Organic Synthesis with α-Diazocarbonyl Compounds. *Chem. Rev.* **2015**, 115 (18), 9981–10080.

(38) Doyle, M. P.; Forbes, D. C. Recent Advances in Asymmetric Catalytic Metal Carbene Transformations. *Chem. Rev.* **1998**, 98 (2), 911–936.

(39) Maas, G. Ruthenium-Catalysed Carbenoid Cyclopropanation Reactions with Diazo Compounds. *Chem. Soc. Rev.* **2004**, 33 (3), 183–190.

(40) Simmons, H. E.; Smith, R. D. A NEW SYNTHESIS OF CYCLOPROPANES FROM OLEFINS. *J. Am. Chem. Soc.* **1958**, 80 (19), 5323–5324.

(41) Green, S. P.; Wheelhouse, K. M.; Payne, A. D.; Hallett, J. P.; Miller, P. W.; Bull, J. A. Thermal Stability and Explosive Hazard Assessment of Diazo Compounds and Diazo Transfer Reagents. *Org. Process Res. Dev.* **2020**, 24 (1), 67–84.

(42) In some cases, diazo compounds can be generated in situ, for selected examples, see refs 43–46.

(43) Day, A. C.; Raymond, P.; Southam, R. M.; Whiting, M. C. The Preparation of Secondary Aliphatic Diazo-Compounds from Hydrazones. *J. Chem. Soc. C* **1966**, No. 0, 467–469.

(44) Morandi, B.; Carreira, E. M. Iron-Catalyzed Cyclopropanation in 6 M KOH with in Situ Generation of Diazomethane. *Science* **2012**, 335 (6075), 1471–1474.

(45) Fulton, J. R.; Aggarwal, V. K.; de Vicente, J. The Use of Tosylhydrazone Salts as a Safe Alternative for Handling Diazo Compounds and Their Applications in Organic Synthesis. *European Journal of Organic Chemistry* **2005**, 2005 (8), 1479–1492.

(46) Liu, Z.; Sivaguru, P.; Zanoni, G.; Bi, X. N-Triftosylhydrazones: A New Chapter for Diazo-Based Carbene Chemistry. *Acc. Chem. Res.* **2022**, 55 (12), 1763–1781.

(47) Alkene cyclopropanation using diazo compounds has been successfully executed for large scale manufacturing though numerous safety concerns must be considered, for selected examples, see: 48–52.

(48) Simpson, J. H.; Kotnis, A. S.; Deshpande, R. P.; Kacsur, D. J.; Hamm, J.; Kodersha, G.; Merkl, W.; Domina, D.; Wang, S. Y. Development of a Multi-Kilogram Procedure To Prepare, Use, and Quench Ethyl Diazoacetate. In Managing Hazardous Reactions and Compounds in Process Chemistry; ACS Symposium Series; American Chemical Society, 2014; Vol. 1181, pp 235–244. https://doi.org/10.1021/bk-2014-1181.ch009.

(49) Proctor, L. D.; Warr, A. J. Development of a Continuous Process for the Industrial Generation of Diazomethane1. *Org. Process Res. Dev.* **2002**, 6 (6), 884–892.

(50) Anthes, R.; Bello, O.; Benoit, S.; Chen, C.-K.; Corbett, E.; Corbett, R. M.; DelMonte, A. J.; Gingras, S.; Livingston, R.; Sausker, J.; Soumeillant, M. Kilogram Synthesis of a Selective Serotonin Reuptake Inhibitor. *Org. Process Res. Dev.* **2008**, 12 (2), 168–177.

(51) Lathrop, S. P.; Mlinar, L. B.; Manjrekar, O. N.; Zhou, Y.; Harper, K. C.; Sacia, E. R.; Higgins, M.; Bogdan, A. R.; Wang, Z.; Richter, S. M.; Gong, W.; Voight, E. A.; Henle, J.; Diwan, M.; Kallemeyn, J. M.; Sharland, J. C.; Wei, B.; Davies, H. M. L. Continuous Process to Safely Manufacture an Aryldiazoacetate and Its Direct Use in a Dirhodium-Catalyzed Enantioselective Cyclopropanation. *Org. Process Res. Dev.* **2022**.

(52) Bien, J.; Davulcu, A.; DelMonte, A. J.; Fraunhoffer, K. J.; Gao, Z.; Hang, C.; Hsiao, Y.; Hu, W.; Katipally, K.; Littke, A.; Pedro, A.; Qiu, Y.; Sandoval, M.; Schild, R.; Soltani, M.; Tedesco, A.; Vanyo, D.; Vemishetti, P.; Waltermire, R. E. The First Kilogram Synthesis of Beclabuvir, an HCV NS5B Polymerase Inhibitor. *Org. Process Res. Dev.* **2018**, 22 (10), 1393–1408.

(53) Accessing metal carbenoid reactivity without diazo compounds is an area of considerable contemporary interest. For recent examples of progress in this domain, see: 54–57.

(54) Zhang, L.; DeMuynck, B. M.; Paneque, A. N.; Rutherford, J. E.; Nagib, D. A. Carbene Reactivity from Alkyl and Aryl Aldehydes. *Science* **2022**.

(55) Cao, L.-Y.; Wang, J.-L.; Wang, K.; Wu, J.-B.; Wang, D.-K.; Peng, J.-M.; Bai, J.; Zhuo, C.-X. Catalytic Asymmetric Deoxygenative Cyclopropanation Reactions by a Chiral Salen-Mo Catalyst. *J. Am. Chem. Soc.* **2023**.

(56) Herndon, J. W. The Chemistry of the Carbon-Transition Metal Double and Triple Bond: Annual Survey Covering the Year 2017. *Coordination Chemistry Reviews* **2018**, 377, 86–190.

(57) Zhu, D.; Ma, J.; Luo, K.; Fu, H.; Zhang, L.; Zhu, S. Enantioselective Intramolecular C−H Insertion of Donor and Donor/Donor Carbenes by a Nondiazo Approach. *Angewandte Chemie International Edition* **2016**, 55 (29), 8452–8456

(58) Johnson, J. D.; Teeples, C. R.; Akkawi, N. R.; Wilkerson-Hill, S. M. Efficient Synthesis of Orphaned Cyclopropanes Using Sulfones as Carbene Equivalents. *J. Am. Chem. Soc.* **2022**, 144 (32), 14471–14476.

(59) Phelan, J. P.; Lang, S. B.; Compton, J. S.; Kelly, C. B.; Dykstra, R.; Gutierrez, O.; Molander, G. A. Redox-Neutral Photocatalytic Cyclopropanation via Radical/Polar Crossover. *J. Am. Chem. Soc.* **2018**, 140 (25), 8037–8047.

(60) Fischer, D. M.; Lindner, H.; Amberg, W. M.; Carreira, E. M. Intermolecular Organophotocatalytic Cyclopropanation of Unactivated Olefins. *J. Am. Chem. Soc.* **2023**, 145 (2), 774–780.

(61) Jie, L.-H.; Guo, B.; Song, J.; Xu, H.-C. Organoelectrocatalysis Enables Direct Cyclopropanation of Methylene Compounds. *J. Am. Chem. Soc.* **2022**, 144 (5), 2343–2350.

(62) Herraiz, A. G.; Suero, M. G. New Alkene Cyclopropanation Reactions Enabled by Photoredox Catalysis via Radical Carbenoids. *Synthesis* **2019**, 51 (14), 2821–2828.

(63) Chen, Z.-L.; Xie, Y.; Xuan, J. Visible Light-Mediated Cyclopropanation: Recent Progress. *European Journal of Organic Chemistry* **2022**, 2022 (44), e202201066.

(64) For progress towards this direct oxidative coupling, see: refs 65 and 66.

(65) Cotugno, P.; Monopoli, A.; Ciminale, F.; Milella, A.; Nacci, A. Palladium-Catalyzed Cross-Coupling of Styrenes with Aryl Methyl Ketones in Ionic Liquids: Direct Access to Cyclopropanes. *Angewandte Chemie International Edition* **2014**, 53 (49), 13563–13567.

(66) Manna, S.; Antonchick, A. P. Copper-Catalyzed (2+1) Annulation of Acetophenones with Maleimides: Direct Synthesis of Cyclopropanes. *Angewandte Chemie International Edition* **2015**, 54 (49), 14845–14848.

(67) Holst, D. E.; Wang, D. J.; Kim, M. J.; Guzei, I. A.; Wickens, Z. K. Aziridine Synthesis by Coupling Amines and Alkenes via an Electrogenerated Dication. *Nature* **2021**, 596 (7870), 74–79.

(68) Wang, D. J.; Targos, K.; Wickens, Z. K. Electrochemical Synthesis of Allylic Amines from Terminal Alkenes and Secondary Amines. *J. Am. Chem. Soc.* **2021**, 143 (51), 21503–21510.

(69) Berger, F.; Plutschack, M. B.; Riegger, J.; Yu, W.; Speicher, S.; Ho, M.; Frank, N.; Ritter, T. Site-Selective and Versatile Aromatic C−H Functionalization by Thianthrenation. *Nature* **2019**, 567 (7747), 223–228.

(70) Meng, H.; Liu, M.-S.; Shu, W. Organothianthrenium Salts: Synthesis and Utilization. *Chem. Sci.* **2022**, 13 (46), 13690–13707.

(71) Tang, S.; Zhao, X.; Yang, L.; Li, B.; Wang, B. Copper-Catalyzed Carboxylation of Aryl Thianthrenium Salts with CO2. *Angewandte Chemie International Edition* **2022**, 61 (47), e202212975..

(72) Chen, J.; Li, J.; Plutschack, M. B.; Berger, F.; Ritter, T. Regio- and Stereoselective Thianthrenation of Olefins To Access Versatile Alkenyl Electrophiles. *Angewandte Chemie International Edition* **2020**, 59 (14), 5616–5620.

(73) Liu, M.-S.; Du, H.-W.; Shu, W. Metal-Free Allylic C–H Nitrogenation, Oxygenation, and Carbonation of Alkenes by Thianthrenation. *Chem. Sci.* **2022**, 13 (4), 1003–1008.

(74) Angyal, P.; Kotschy, A. M.; Dudás, Á.; Varga, S.; Soós, T. Intertwining Olefin Thianthrenation with Kornblum/Ganem Oxidations: Ene-Type Oxidation to Furnish α,β-Unsaturated Carbonyls. *Angewandte Chemie International Edition* **2023**, 62 (2), e202214096.

(75) Chen, C.; Wang, Z.-J.; Lu, H.; Zhao, Y.; Shi, Z. Generation of Non-Stabilized Alkyl Radicals from Thianthrenium Salts for C–B and C–C Bond Formation. *Nat Commun* **2021**, 12 (1), 4526.

(76) Chen, C.; Wang, M.; Lu, H.; Zhao, B.; Shi, Z. Enabling the Use of Alkyl Thianthrenium Salts in Cross-Coupling Reactions by Copper Catalysis. *Angewandte Chemie International Edition* **2021**, 60 (40), 21756–21760.

(77) Prior to our work, these dicationic adducts had been prepared and characterized from both thianthrene radical cation and thianthrene S-oxide. See refs 78, 79, and 72.

(78) Shine, H. J.; Bandlish, B. K.; Mani, S. R.; Padilla, A. G. Ion Radicals. 43. Addition of Thianthrene and Phenoxathiin Cation Radicals to Alkenes and Alkynes. *J. Org. Chem.* **1979**, 44 (6), 915–917.

(79) Lee, W. K.; Liu, B.; Park, C. W.; Shine, H. J.; Whitmire, K. H. Addition of Thianthrene Cation Radical to Cycloalkenes. An Unexpected Monoadduct. *J. Org. Chem.* **1999**, 64 (25), 9206–9210.

(80) For alternative strategies to prepare aziridines from alkenes and primary amines using anodic oxidation, see refs 81 and 82.

(81) Oseka, M.; Laudadio, G.; van Leest, N. P.; Dyga, M.; de Andrade Bartolomeu, A.; Goossen, L.; de Bruin, B.; Thiago de Oliveira, K.; Noel, T. Electrochemical Aziridination of Internal Alkenes with Primary Amines. **2020**. https://doi.org/10.26434/chemrxiv.12824135.v1.

(82) Zeng, D.; Gu, L.; Zhang, L.; Li, G.; He, Y. Synthesis of Aziridines by Electrochemical Oxidative Annulation of Chalcones with Primary Amines. *Tetrahedron Letters* **2021**, 87, 153413.

(83) Liu, M.-S.; Du, H.-W.; Cui, J.-F.; Shu, W. Intermolecular Metal-Free Cyclopropanation and Aziridination of Alkenes with XH2 (X=N, C) by Thianthrenation. *Angewandte Chemie International Edition* **2022**, 61 (41), e202209929.

(84) For an example of transition metal-catalyzed cyclopropanation that tolerates Lewis basic heterocycles as well as a discussion of associated challenges, see: refs 85 and 86.

(85) Sharland, J. C.; Wei, B.; Hardee, D. J.; Hodges, T. R.; Gong, W.; Voight, E. A.; Davies, H. M. L. Asymmetric Synthesis of Pharmaceutically Relevant 1-Aryl-2-Heteroaryl- and 1,2-Diheteroarylcyclopropane-1-Carboxylates. *Chem. Sci.* **2021**, 12 (33), 11181–11190.

(86) Ye, Q.-S.; Li, X.-N.; Jin, Y.; Yu, J.; Chang, Q.-W.; Jiang, J.; Yan, C.-X.; Li, J.; Liu, W.-P. Synthesis, Crystal Structures and Catalytic Activity of Tetrakis(Acetato)Dirhodium(II) Complexes with Axial Picoline Ligands. *Inorganica Chimica Acta* **2015**, 434, 113–120.

(87) Juliá, F.; Yan, J.; Paulus, F.; Ritter, T. Vinyl Thianthrenium Tetrafluoroborate: A Practical and Versatile Vinylating Reagent Made from Ethylene. *J. Am. Chem. Soc.* **2021**, 143 (33), 12992–12998..

(88) Mondal, M.; Chen, S.; Kerrigan, N. J. Recent Developments in Vinylsulfonium and Vinylsulfoxonium Salt Chemistry. *Molecules* **2018**, 23 (4), 738.

(89) Zhou, M.; En, K.; Hu, Y.; Xu, Y.; Shen, H. C.; Qian, X. Zinc Triflate-Mediated Cyclopropanation of Oxindoles with Vinyl Diphenyl Sulfonium Triflate: A Mild Reaction with Broad Functional Group Compatibility. *RSC Adv.* **2017**, 7 (7), 3741–3745.

(90) Zhou, M.; Hu, Y.; En, K.; Tan, X.; Shen, H. C.; Qian, X. Efficient Cyclopropanation of Aryl/Heteroaryl Acetates and Acetonitriles with Vinyl Diphenyl Sulfonium Triflate. *Tetrahedron Letters* **2018**, 59 (14), 1443–1445.

(91) Nambu, H.; Ono, N.; Hirota, W.; Fukumoto, M.; Yakura, T. An Efficient Method for the Synthesis of 2′,3′-Nonsubstituted Cycloalkane-1,3-Dione-2-Spirocyclopropanes Using (2-Bromoethyl)Diphenylsulfonium Trifluoromethanesulfonate. *Chemical and Pharmaceutical Bulletin* **2016**, 64 (12), 1763–1768.

(92) Qin, H.; Miao, Y.; Zhang, K.; Xu, J.; Sun, H.; Liu, W.; Feng, F.; Qu, W. A Convenient Cyclopropanation Process of Oxindoles via Bromoethylsulfonium Salt. *Tetrahedron* **2018**, 74 (47), 6809–6814.

(93) Xie, C.; Han, D.; Hu, Y.; Liu, J.; Xie, T. Synthesis of Pyrrolidin-2-Ones via Tandem Reactions of Vinyl Sulfonium Salts under Mild Conditions. *Tetrahedron Letters* **2010**, 51 (40), 5238–5241.

(94) Mao, Z.; Qu, H.; Zhao, Y.; Lin, X. A General Access to 1,1-Cyclopropane Aminoketones and Their Conversion into 2-Benzoyl Quinolines. *Chem. Commun.* **2012**, 48 (79), 9927–9929.

(95) Gosselck, J.; Béress, L.; Schenk, H. Reactions of Substituted Vinylsulfonium Salts with CH-Acidic Compounds. – A New Route to Polysubstituted Cyclopropanes. *Angewandte Chemie International Edition in English* **1966**, 5 (6), 596–597.

(96) Braun, H.; Huber, G. Reaktionen von Butadienylsulfoniumsaltzen Mit Carbonionen. *Tetrahedron Letters* **1976**, 17 (25), 2121–2124.

(97) Takaki, K.; Agawa, T. Synthesis of Acylcyclopropanes and Oxiranes from Vinylsulfonium Salts and Lithium Enolates. *J. Org. Chem.* **1977**, 42 (20), 3303–3304.

(98) Lin, H.; Shen, Q.; Lu, L. β-(Trifluoromethyl)Vinyl Sulfonium Salts: Preparation and Reactions with Active Methylene and Methenyl Compounds. *J. Org. Chem.* **2011**, 76 (18), 7359–7369.

(99) Guo, S.; Zhang, N.; Tang, X.; Mao, Z.; Zhang, X.; Yan, M.; Xuan, Y. Cyclopropanation of Active Methylene Compounds with β-Alkoxycarbonyl Vinylsulfonium Salts. *Chinese Chemical Letters* **2019**, 30 (2), 406–408.

(100) Matlock, J. V.; Fritz, S. P.; Harrison, S. A.; Coe, D. M.; McGarrigle, E. M.; Aggarwal, V. K. Synthesis of α-Substituted Vinylsulfonium Salts and Their Application as Annulation Reagents in the Formation of Epoxide- and Cyclopropane-Fused Heterocycles. *J. Org. Chem*. **2014**, 79 (21), 10226–10239.

(101) Deposition Numbers 2237193 (for compound **6.18**), 2237194 (for compound **6.27**), and 2237195 (for compound **6.14**) contain the supplementary crystallographic data for the X-ray structures. These data are provided free of charge by the joint Cambridge Crystallographic Data Centre and Fachinformationszentrum Karlsruhe Access Structures service.

(102) Cost of thianthrene is less than 0.15 USD/mmol (Ambeed, Jan 2023).

(103) Mitchell, S. C.; Waring, R. H. Fate of Thianthrene in Biological Systems. *Xenobiotica* **2017**, 47 (8), 731–740. http

(104) McGrath, N. A.; Brichacek, M.; Njardarson, J. T. A Graphical Journey of Innovative Organic Architectures That Have Improved Our Lives. *J. Chem. Educ.* **2010**, 87 (12), 1348–1349.

(105) Ruah, S. H.; Hamilton, M.; Miller, M.; Grootenhuis, P. D. J.; Bear, B.; Mccarthy, J.; Zhou, J. *Heterocyclic Modulators of Atp-Binding Cassette Transporters.* WO2007056341A1, May 18, **2007**. https://patents.google.com/patent/WO2007056341A1/en (accessed 2023-01-16).

(106) Tanoury, G. J.; Harrison, C.; Littler, B. J.; Rose, P. J.; Hughes, R. M.; Jung, Y. C.; Siesel, D. A.; Lee, E. C.; Belmont, D. T. *Process of Producing Cycloalkylcarboxamido-Indole Compounds.* WO2011133751A2, October 27, **2011**. https://patents.google.com/patent/WO2011133751A2/en?oq=WO+2011133751 (accessed 2023-01-16).

Chapter 7: Electrochemical *Z*-selective C(sp^2)–H Functionalization of Alkenes

A collaboration with Peter J. Varardi, Tetsuya Inagaki, Remy F. Lalisse, Poulami Mukherjee, Osvaldo Gutierrez, and Zachary K. Wickens

7.1 Abstract

Herein, we describe the development of an electrochemical system that achieves *Z*-selective net alkene C(sp^2)–H functionalization. This oxidative transformation proceeds *via* electrochemical generation of *Z*-alkenylthianthrenium salts from thianthrene and unactivated alkenes. These stereodefined electrophiles can be engaged in a suite of stereoselective cross coupling reactions to furnish *Z*-alkene products. Mechanistic studies are consistent with base-induced elimination of electrogenerated thianthrene-alkene dicationic adducts being the stereodetermining step. Progress is ongoing in the exploration of the scope of alkenes and coupling partners for these overall *Z*-selective transformations, as well as rationalization of the origin of *Z*-selectivity.

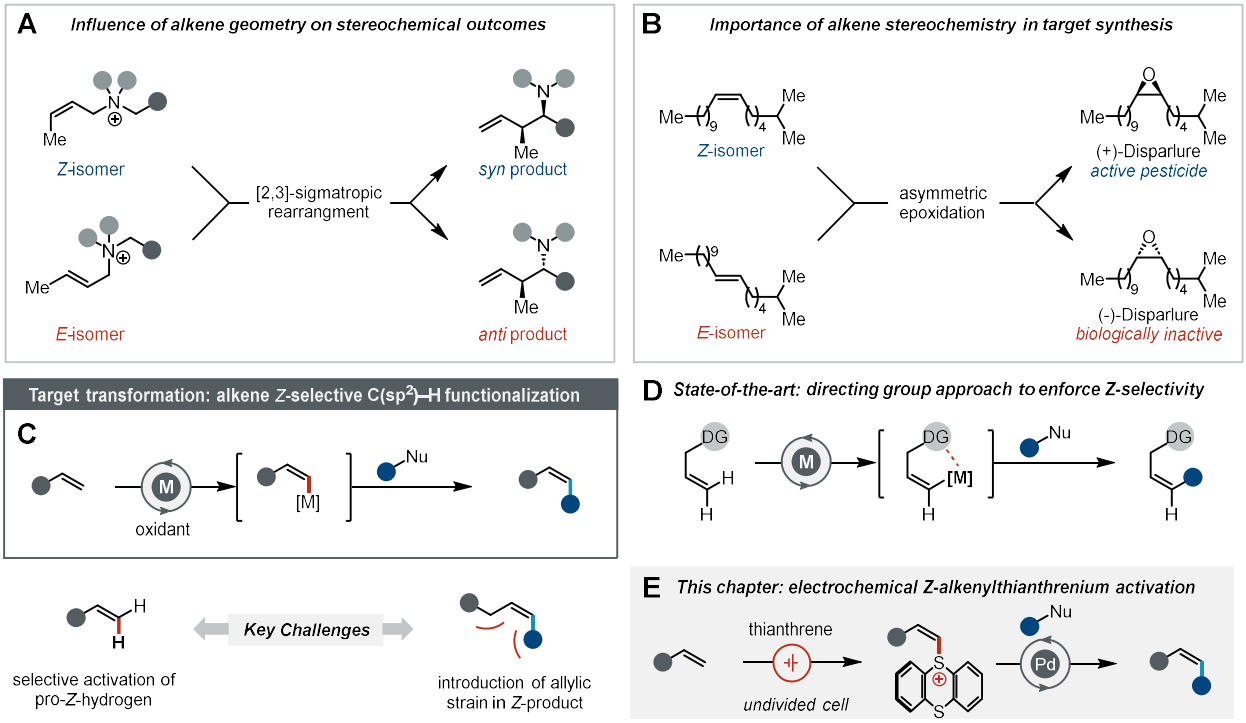

Figure 7.1. Project overview. (A) Alkene Z/E geometry controls stereochemical outcomes. (B) *Z*-alkenes in synthesis. (C) Idealized transformation to access Z-alkenes. (D) Representative established *Z*-selective alkene C(sp^2)–H functionalization. (E) Schematic overview of this work.

7.2 Introduction

Alkenes are versatile building blocks in the preparation of valuable small molecules such as agrochemicals, pharmaceuticals, and fragrances. Control over stereochemistry of the final products is intimately tied to the geometrical (E/Z) configuration of the alkene starting material (Figure 7.1A).[1–4] For example, E/Z control is paramount in the enantioselective synthesis of Disparlure, the primary sex pheromone of the globally invasive insect species, Gypsy Moth.[5] The two enantiomers of Disparlure exhibit different biological properties: the (+) enantiomer is bioactive and therefore a valuable pesticide, whereas the (-) enantiomer exhibits no bioactivity. The (+) enantiomer is prepared selectively from a *Z*-alkene, whereas the (-) enantiomer is prepared from its *E*-isomer (Figure 7.1B). Exploitation of these geometric properties in such a synthetic context requires precise stereocontrol over the alkenylation event. While olefination reactions are a cornerstone of organic synthesis, there are notably fewer methods amenable to the preparation of *Z*-alkenes.[6] An ideal yet unrealized approach to form structurally-diverse *Z*-alkenes is the *Z*-selective C(sp^2)–H functionalization of terminal alkenes in metal-catalyzed cross-couplings (Figure 7.1C).[7] However, achieving high *Z*-selectivity from unactivated alkenes a formidable challenge due to: (1) electronic similarities between the two pro-stereogenic hydrogens of the alkene, and (2) the requirement to place the activating group in a position that results in significant 1,3-allylic strain, ultimately leading to the formation of the less thermodynamically favorable product. To address these challenges, state-of-the-art approaches to C(sp^2)–H functionalization utilize directing groups to differentiate hydrogens and enforce *Z*-selectivity (Figure 7.1D).[8–12] While effective, these directing group approaches fundamentally limit the pool of available alkene substrates for C(sp^2)–H functionalization; to-date, no general *Z*-selective C(sp^2)–H functionalization of aliphatic alkenes exists.

A step towards the ideal transformation would be *Z*-selective installation of a thianthrenium moiety on an unactivated alkene precursor. Growing reports have established alkenylthianthrenium reagents as versatile electrophiles in a variety of alkenylation reactions (see Chapter 1). In particular, the Ritter group has developed a powerful net C(sp^2)–H functionalization of aliphatic alkenes in which alkenylthianthrenium electrophiles—prepared with near-perfect *E*-selectivity—are subsequently engaged

in a suite of stereospecific metal-catalyzed cross coupling.[13] Curiously, we noticed a discrepancy in the *E:Z* stereochemistry of alkenylthianthrenium salts generated from thianthrene S-oxide deoxygenation *versus* electrochemical oxidation of thianthrene protocols. In this chapter, we describe the study of electrochemical parameters that favor *Z*-selectivity. Based on these insights, we questioned whether electrochemical cell design could divert thianthrenium adduct selectivity to develop a net *Z*-selective C(sp^2)–H alkenylation reaction that proceeds *via* a *Z*-alkenylthianthrenium electrophile that can be used in stereoselective couplings (Figure 7.1E). Realization of this approach encompasses two key challenges: (1) *Z*-selective preparation of alkenylthianthrenium salts from alkenes, (2) preservation of the stereochemistry in subsequent coupling reactions with these new *Z*-electrophiles. If these challenges are successfully addressed, this innovative method is poised to dramatically expand the scope of engageable terminal alkenes for *Z*-selective cross-coupling-based olefinations and preparation of valuable *Z*-alkene building blocks. Herein, we describe the discovery of this stereoselective transformation and mechanistic experiments to elucidate the stereodetermining step of the process.

7.3 Results and Discussion

Our development of a *Z*-selective C(sp^2)–H alkenylation process began with an unexpected observation during the study of our allylic amination reaction. We found that upon exposure to base, the electrogenerated mixture of dicationic adducts **7.1** and **7.2** was transformed into a mixture of *E*- and *Z*-alkenylthianthrenium salt **7.3** in poor *E:Z* (Figure 7.1A; also see Chapter 2). We noted that *mono*-dicationic adduct has been shown to convert with high *E*-selectivity (≥20:1 *E:Z*) to the alkenylthianthrenium salt upon treatment with base.[13,14] Thus, we suspected that the *Z*-isomer of **7.3** was a consequence of the elimination of electrogenerated *bis*-dicationic adduct **7.2**. A working model for the formation of these two dicationic adducts has previously been proposed.[13,15,16] Upon anodic oxidation of thianthrene (**TT**), iterative thianthrene radical cation ($\mathbf{TT}^{\bullet+}$) addition to the alkene substrate generates *bis*-adduct (Figure 7.2B). In a divided cell, enough charge may be passed to oxidize all the neutral thianthrene (**TT**) to its radical cation congener $\mathbf{TT}^{\bullet+}$. At low **TT** concentrations, kinetically-relevant disproportionation of $\mathbf{TT}^{\bullet+}$ to form

thianthrene dication ($\mathbf{TT^{2+}}$) takes place in which the resultant $\mathbf{TT^{2+}}$ undergoes fast and irreversible cycloaddition with alkene to generate *mono*-adduct (Figure 7.2C).[17]

With this mechanistic model in hand, we investigated divided cell electrochemical parameters to favor *bis*-adduct **7.5** formation (Figure 7.2D), which we posit ultimately leads to the formation of *Z*-alkenylthianthrenium salt **7.6**. The greatest impact on dicationic adduct distribution was thianthrene loading. When doubling the thianthrene loading to 3 equivalents, the *mono:bis* selectivity of the dicationic adduct mixture **7.4** and **7.5** was inverted from *mono*-selective (5:1 *mono:bis)* to *bis*-selective (1:2 *mono:bis*). We noted that, upon treatment with base, *bis*-dominant adduct solutions resulted in *Z*-selective mixtures of alkenylthianthrenium salt **7.6**.[14] Decreasing the electrolysis current from 0.45 mmol e^-/hour to 0.14 mmol e^-/hour led to an increase in the *bis*-selectivity of the two adducts formed. Lastly, using excess thianthrene under slow constant current electrolysis, dilution of the electrochemical reaction decreased the overall reaction rates to give lower yield of adducts **7.4** and **7.5** but with comparable *mono:bis*. These data are all consistent with the working model for adduct generation. Taken together, changes to divided cell parameters that led to an increase in the *bis*-selectivity of the adducts can be rationalized by favoring the generation of $\mathbf{TT^{\bullet+}}$ and promoting the radical reactivity with alkene.

Given these divided cell insights, we hypothesized two crucial elements of undivided cell electrolysis would keep neutral **TT** concentration high and maximize contributions from radical pathways that favor formation of *bis*-adduct intermediate: (1) *bis*-adduct elimination by electrogenerated base to liberate **TT**, and (2) access to cathodic reduction of $\mathbf{TT^{2+}}$ or $\mathbf{TT^{\bullet+}}$. We first compared the electrochemical setup with 1-butene, for which the divided cell conditions afforded alkenylthianthrenium species **7.3** in 1:1 *Z:E* when meta-stable dicationic adducts **7.1** and **7.2** were treated with base. Gratifyingly, adapting electrolysis of 1-butene to an undivided cell generated alkenylthianthrenium **7.3** in 72% yield and 3:1 *Z:E* (Figure 7.3). However, we were worried the modest *Z*-selectivity may be unique to the small substituent of 1-butene given our prior observations in *Z*-selective allylic functionalization (see Chapters 2 and 4). Excitingly, the *Z*-selectivity of this electrochemical process translated to 4-phenyl-1-butene to furnish **7.6** in 81% yield with comparable 3:1 *Z:E*. An attractive feature of undivided cell electrolysis is the scalability.

Accordingly, these conditions were performed on 13.00 mmol (1.7 g) scale to prepare *Z*-alkenylthianthrenium salt **7.6** in 28% yield and ≥20:1 *Z:E* (Figure 7.3). While the isolation procedure requires further optimization, the purified Z-alkenylthianthrenium electrophile has been demonstrated to engage in a suite of stereoselective coupling reactions (*e.g.* Suzuki, Negishi, Heck couplings). This initial

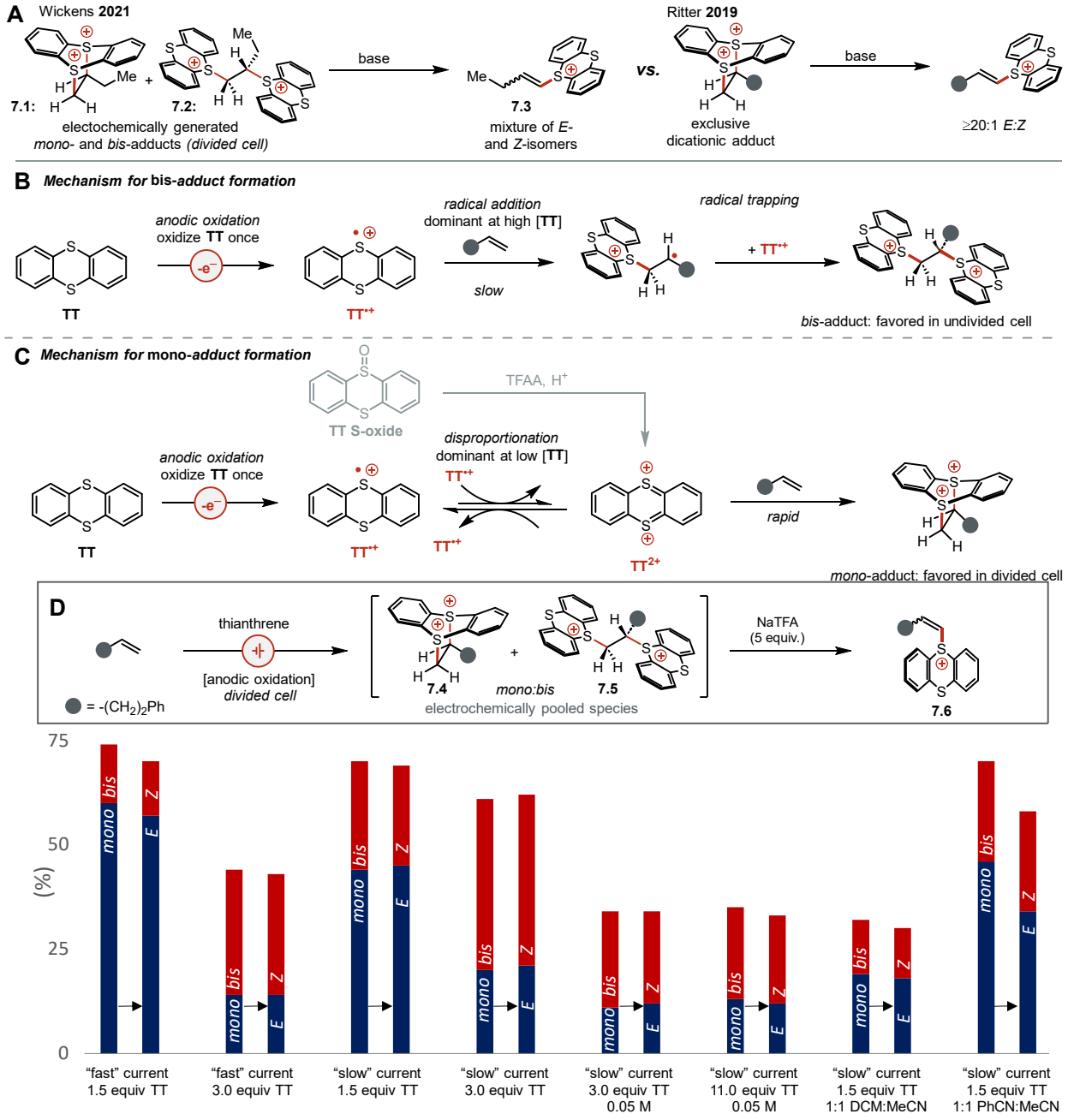

[a]Reactions were conducted using alkene (0.2 mmol), MeCN (0.4 M KPF_6), I = 6.0 mA, 2.2 h (2.5 F mol^{-1} alkene) or I = 1.9 mA, 7.0 h (2.5 F mol^{-1} alkene); then sodium trifluoroacetate (1.0 mmol), 5 min. NMR yields and *Z:E*. See the appendix F for additional experimental details.

Figure 7.2. Background context for the project. (A) Observation of *Z*-alkenylthianthrenium salt formation. (B) *Bis*-adduct formation mechanism. (C) *Mono*-adduct formation mechanism. (D) Dicationic pool studies observing *mono:bis* impact on *E:Z* after base treatment.[a]

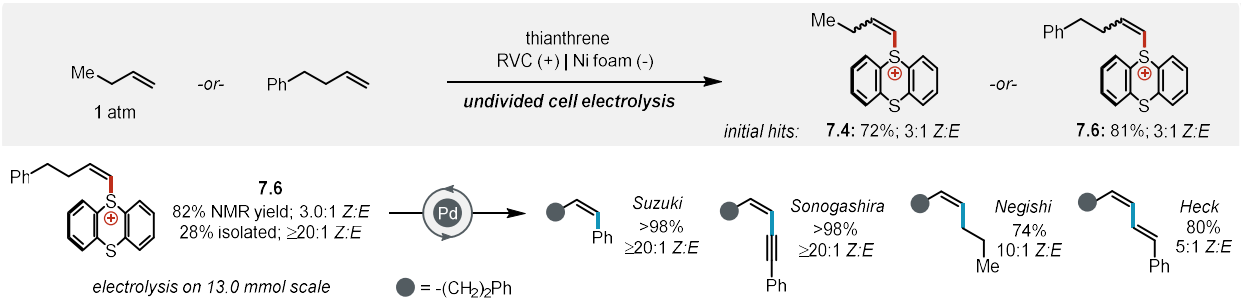

Figure 7.3. Summary of data that inspired the electrochemical *Z*-selective C(sp^2)–H functionalization of alkenes.

undivided cell reactivity is being further investigated and optimized by a current graduate student in the Wickens group as an ongoing project to establish the scope of these new stereodefined reagents.

Next, we sought to identify the stereodetermining step in the electrochemical generation of *E*- and *Z*-alkenylthianthrenium salts. Upon completion of electrolysis in an undivided cell setup, no dicationic adducts are observed. We presume that base electrogenerated upon proton reduction for the cathodic counter reaction may eliminate the dicationic adducts *in situ* to the alkenylthianthrenium product. Indeed, when employing an acid that lacks a competent conjugate base (*e.g.* HBF_4), low amounts of unreacted dicationic adducts were detected. Thus, we propose that alkenylthianthrenium salt formation proceeds *via* electrochemical dicationic adduct generation and elimination.[18] To study the stereoselectivity of the thianthrene-alkene adduct elimination, meta-stable dicationic adduct **7.4** and **7.5** solutions were pooled using divided cell electrolysis and subsequently treated with trifluoroacetate to afforded alkenylthianthrenium species **7.6**. We observed that in all cases, the *E:Z* ratio of these elimination products roughly corresponds to the original *mono:bis* ratio of the dicationic adduct mixtures (Figure 7.2D). The stereoselectivity of this base-induced elimination was insensitive to solvent identity (see Appendix F for details). Lastly, the apparent selectivity of the elimination step is base-dependent. Adducts *mono:bis* ratio was well-preserved in the alkenylthianthrenium species *E:Z* ratio when using weaker bases for the elimination whereas erosion of Z-selectivity was observed with stronger bases such as carbonate (see Appendix F for details). This could be a consequence of either changing the stereoselectivity of the elimination step, or isomerization of *Z*-isomer to *E*-isomer *via* reversible conjugate addition of nucleophilic bases (see Chapter 5), and more mechanistic experiments will need to be conducted to distinguish the two

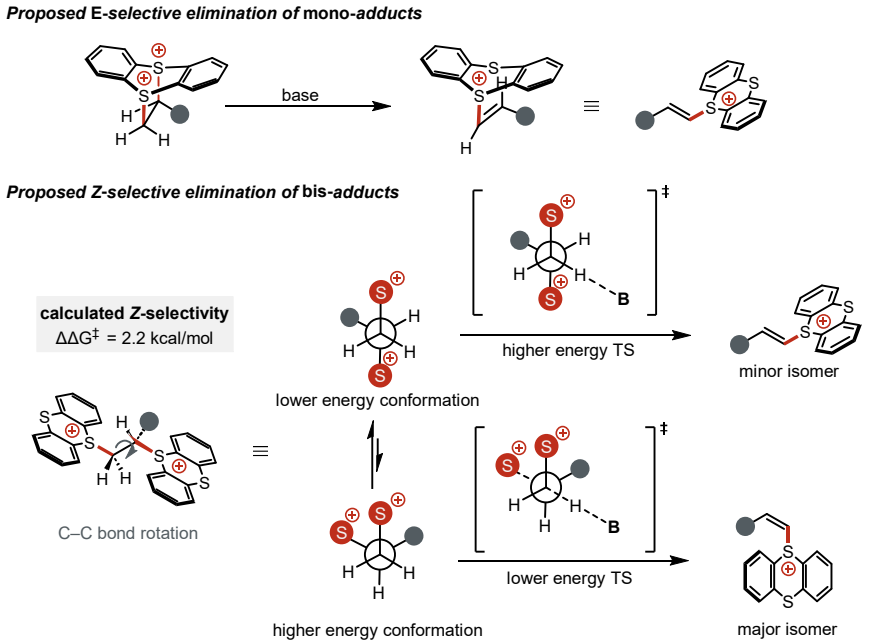

Figure 7.4. Identification of stereodetermining step and working model for *E*-selective *mono*-adduct elimination and *Z*-selective *bis*-adduct elimination.

possibilities. Taken together, these data support that base-induced elimination of the dicationic adducts is the stereodetermining step, in which *mono*-adduct eliminates with ≥20:1 *E*-selectivity and *bis*-adduct eliminates with ≥20:1 *Z*-selectivity (Figure 7.4).

With a working model in hand for the observed stereoselective formation of alkenylthianthrenium salts, we wanted to build and validate a computational model of the process that rationalizes the *bis*-adduct elimination with *Z*-selectivity. Preliminary calculations by the Gutierrez group support a Curtin-Hammett scenario of the *bis*-adduct elimination out of the higher energy gauche conformation that leads to *Z*-alkenylthianthrenium salt formation ($\Delta\Delta G^{\ddagger}$ = 2.2 kcal/mol; Figure 7.4). To rationalize this, we have formed a preliminary hypothesis that the kinetic selectivity for deprotonation of this higher-energy conformation may arise form a gauche effect of the polarized C–S σ* hyperconjugation with the two σ C–H bonds that stabilize the *Z*-alkene forming transition state.[19,20] Continued efforts in validating the computational model and explaining the kinetic selectivity of the gauche elimination is underway.

With the stereodetermining step identified as dicationic adduct elimination, we next investigated the impact of alkene structure on the stereoselectivity of alkenylthianthrenium salt formation (Table 7.1). For these studies, divided cell electrolysis conditions that have favored *bis*-adduct formation were used to generate the dicationic adduct mixtures. After near-quantitative adduct quenching by subsequent treatment with trifluoroacetate, the *bis*-adduct elimination *Z*-selectivity was determined by back-calculating the *E*-alkenylthianthrenium salt yield arising from *mono*-adduct elimination (≥20:1 *E*-selectivity). For example, adducts **7.10** and **7.11** derived from allylcyclohexane in 1:1.1 *bis:mono* eliminated quantitatively to alkenylthianthrenium salt **7.12** in comparable 1:1.1 *Z:E*, indicating ≥20:1 *Z*-selectivity for the *bis*-adduct elimination. We found that steric effects were not the major factor promoting the overall *Z*-selectivity; adducts **7.16** and **7.17** (1.3:1 *bis:mono*) derived from propylene—the smallest alkene with a substituent that could give stereoselectivity—furnished alkenylthianthrenium salt **7.18** in 1.8:1 *Z:E* selectivity. Curiously, this *Z*-enrichment of the alkenylthianthrenium product indicates that *mono*-adduct elimination may be stereoselective rather than stereospecific. We found that with more hindered α-methiene the *Z*-selectivity

Table 7.1. Dication Pool to Study Alkene Structure on the Elimination Stereoselectivity.[a]

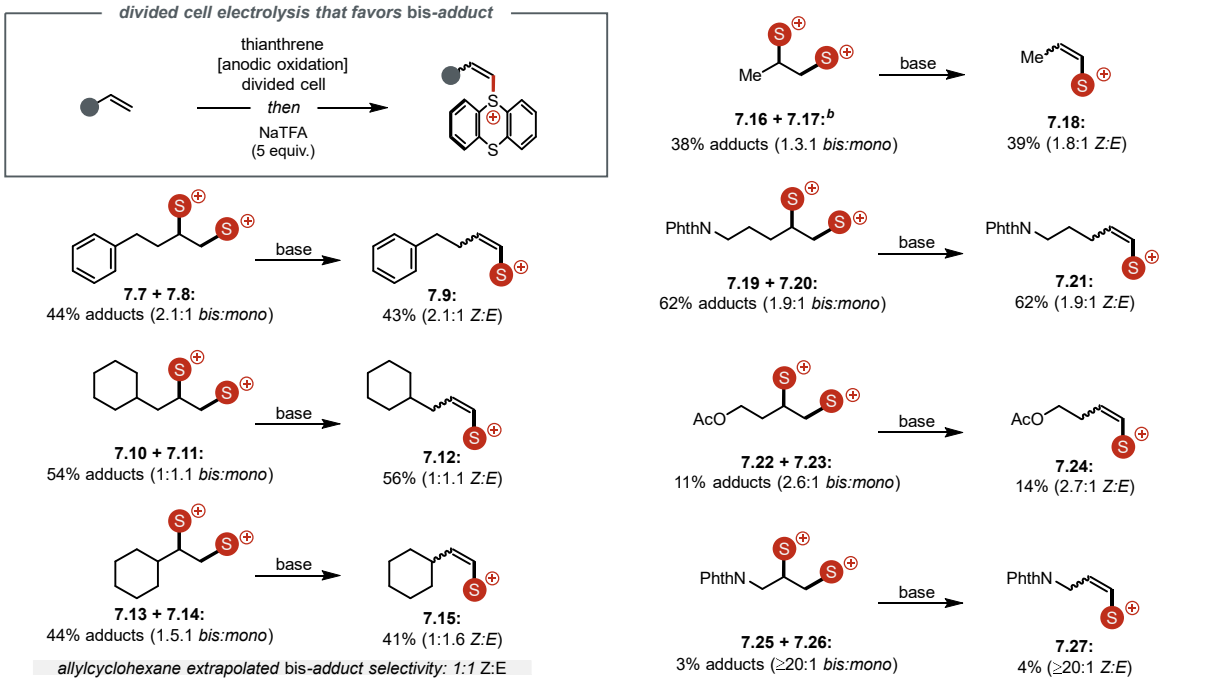

[a]Reactions were conducted using alkene (0.2 mmol), thianthrene (0.6 mmol), 2 mL MeCN (0.4 M $KNPF_6$), I = 6.0 mA, 2.2 h (2.5 F mol^{-1} alkene); then sodium trifluoroacetate (1.0 mmol), 5 min. NMR yields and *Z:E*. [d]Reactions were conducted using alkene (1 atm), thianthrene (1.0 mmol), 4 mL MeCN (0.15 M KPF_6), I = 60.0 mA, 45 min (1.7 F mol^{-1} thianthrene); then sodium trifluoroacetate (1.0 mmol), 5 min.

was obliterated; adducts **7.13** and **7.14** prepared from vinylcyclohexane afforded the corresponding alkenylthianthrenium salt **7.15** with an extrapolated 1:1 *Z:E* selectivity of the *bis*-adduct quenching. Lastly, *bis*-dominant mixtures of adducts derived from alkenes bearing both distal and proximal electron-withdrawing groups undergo stereoselective elimination with high *Z*-selectivity. Taken together, these studies indicate that electronics and modest steric effects are not crucial for achieving Z-selectivity, and that stereoselectivity of the elimination process is inherent to the thianthrenium moieties. However, reactivity with thianthrene radical cation significantly diminishes as alkenes with proximal polar functionalities become more deactivated.

Next, we studied divided cell dicationic adduct formation with thianthrene analogs to understand how to possibly favor *bis*-selectivity, and the subsequent elimination stereoselectivity (Table 7.2).[21] Compared to parent thianthrene, a sterically-hindered tetramethyl-substituted analog generated dicationic adducts **7.28** and **7.29** in high *mono*-selectivity (≥20:1 *mono:bis*). We suspect that the steric hindrance of the tetrasubstituted thianthrenium core disfavors the radical addition pathway leading to *bis*-adduct formation. These adducts eliminate to the corresponding alkenylsulfonium salts **7.30** in 9:1 *E:Z*, indicating that steric bulk of the thianthrenium motif decrease stereoselectivity of the *mono*-adduct elimination. A dimethoxy-substituted thianthrene analog performed comparably to thianthrene for dicationic adduct generation. Curiously, the *E:Z* ratio of the resultant alkenylsulfonium salt **7.33** is significantly greater than the *mono:bis* of electrogenerated adducts **7.28** and **7.29**, which is consistent with a decrease in *bis*-adduct elimination *Z*-selectivity. Lastly, a fluorinated analog of thianthrene furnished adducts **7.34** and **7.35** in higher *mono:bis* compared to parent thianthrene. This result was unintuitive since we anticipated that *bis*-adduct formation would be favored due to this thianthrene radical cation to be more electrophilic for radical addition with alkene. To rationalize the high *mono*-adduct selectivity with the fluorinated thianthrene, we hypothesize that the rate of disproportionation of fluorinated thianthrene radical cation to fluorinated thianthrene dication is increased relative to parent thianthrene, which would favor *mono*-adduct formation. The impact of thianthrene structure on disproportionation and dicationic adduct formation is an ongoing investigation in the Wickens group. The diminished 4.5:1 *E:Z* of alkenylsulfonium salt **7.36** upon base

Table 7.2. Sulfonium Activating Group Structure on Dicationic Adduct Generation and Stereoselectivity of Subsequent Elimination to Alkenylsulfonium Species.[a]

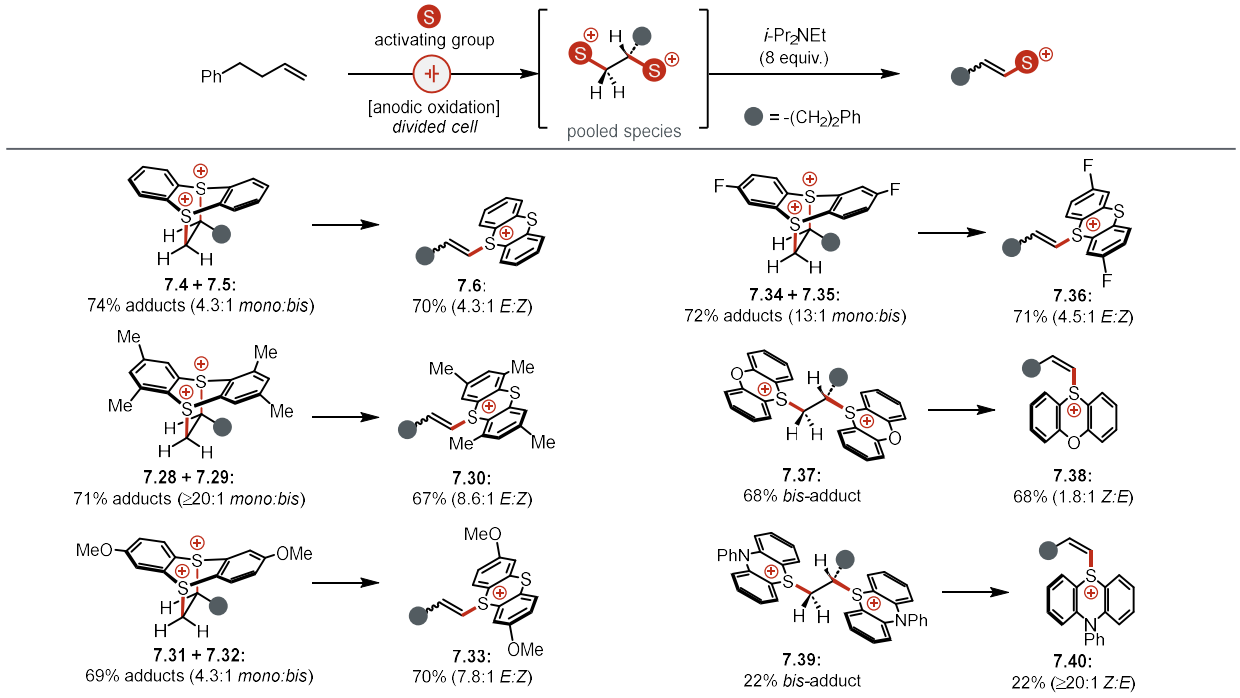

[a]Reactions were conducted using alkene (0.15 mmol), sulfide heterocycle (0.225 mmol), MeCN (0.4 M KPF_6), I = 6.0 mA, 2.2 h (2.5 F mol^{-1} alkene); then *i*-Pr_2NEt (1.2 mmol), 5 min. NMR yields and *Z*:*E*.

addition to the electrogenerated adducts **7.34** and **7.35** (13:1 *mono:bis)* suggests that the *E*-selectivity of the fluorinated analog *mono*-adduct is lower than that of parent thianthrene. Overall, these data do not indicate a clear direction for optimal electronics and steric of thianthrene analogs that could provide a straightforward solution to selective *bis*-adduct generation coupled with high *Z*-selective elimination for alkenylthianthrenium salt preparation.

We wondered if replacing thianthrene with phenoxathiin would promote the desired transformation with high *Z*-selectivity by removing the cycloaddition pathway for *mono*-adduct formation. Indeed, divided cell electrolysis with phenoxathiin in the presence of 4-phenyl-1-butene exclusively furnished exclusively *bis*-adduct **7.37** (Table 7.2). Surprisingly however, this *bis*-adduct eliminated to (10-phenoxathiiniumyl)alkene **7.38** with poor *Z*-selectivity (2:1 *Z:E)*. This observation is consistent with prior studies of phenoxathiin radical cation by the Shine group,[22] as well as the same poor stereoselectivity (2:1 *Z:E*) for alkenylphenoxathiinium species acquired in undivided cell electrolysis. Unlike thianthrenium dicationic adducts, the elimination stereoselectivity of these charged dicationic salts could be notably

impacted by solvent (see Appendix F for details). The poor *Z*-selectivity of phenoxathiine *bis*-dicationic adducts led us to question if this *Z*-selective transformation is unique to thianthrene, or if it could be extended to other sulfonium salts. To further probe the stereoselectivity of *bis*-sulfonium adduct elimination, we employed phenothiazine as another sulfur-heterocycle that would, in principle, only generate *bis*-adduct. Under divided cell electrolysis conditions, *N*-phenylphenothiazine formed *bis*-adduct **7.39** with 4-phenyl-1-butene in low 22% yield. Excitingly, this adduct eliminated to *Z*-alkenylsulfonium salt **7.40** in ≥20:1 *Z:E*. Taken together, these results indicate *Z*-selective elimination is not unique to thianthrenium *bis*-adducts, and that sulfonium structures that afford exclusive *bis*-adducts may be able to furnish *Z*-alkenylsulfonium electrophiles in high *Z*-selectivity. Future work in this electrochemical *Z*-alkenylation project area will be to explore sulfonium structures to favor *bis*-adduct formation during undivided cell electrolysis while maintaining high *Z*-selectivity upon elimination to furnish *Z*-alkenylsulfonium reagents.

7.4 Conclusion

Overall, we have developed an electrochemical preparation of *Z*-alkenylthianthrenium electrophiles from aliphatic alkenes that can be engaged in a suite of stereoselective coupling reactions. This represents the first example of net *Z*-selective C(sp^2)–H functionalization of terminal alkenes without the need for directing groups on the substrate. Key to this strategy was electrochemical cell design in which undivided cell electrolysis was crucial to (1) promote radical pathways that favor the generation of *bis*-adduct, and (2) electrogenerate an *in situ* base for the elimination of adducts to the *Z*-alkenylthianthrenium species. Divided cell electrolysis studies revealed the stereodetermining step to be elimination of *bis*-dicationic adducts to *Z*-alkenylthianthrenium species. Preliminary computations suggest a Curtin-Hammett scenario is operative in achieving stereocontrol for this *Z*-selective process. We anticipate that this new electrochemical transformation will find immediate application in organic synthesis given the established utility of *Z*-alkenes. Moreover, we anticipate continued examination of reaction conditions that favor *bis*-

adduct generation will dramatically expand the scope of engageable alkenes for *Z*-selective cross-coupling-based olefinations that remain challenging to accomplish *via* more conventional approaches.

7.5 Acknowledgements

Z.K.W., P.J.V., and K.T. designed the project. P.J.V. and T.I. performed the experiments and collected the data. K.T. designed and executed the mechanistic experiments. R.F.L. and P.M. performed the computations. All authors contributed to writing the manuscript in preparation.

7.6 References

(1) Saicic, R. N. Protecting Group-Free Syntheses of Natural Products and Biologically Active Compounds. *Tetrahedron* **2014**, *70* (44), 8183–8218.

(2) Zhao, H.; Brånalt, J.; Perry, M.; Tyrchan, C. The Role of Allylic Strain for Conformational Control in Medicinal Chemistry. *J. Med. Chem.* **2023**, *66* (12), 7730–7755.

(3) Hoffmann, R. W. Allylic 1,3-Strain as a Controlling Factor in Stereoselective Transformations. *Chem. Rev.* **1989**, *89* (8), 1841–1860.

(4) Meek, S. J.; O'Brien, R. V.; Llaveria, J.; Schrock, R. R.; Hoveyda, A. H. Catalytic Z-Selective Olefin Cross-Metathesis for Natural Product Synthesis. *Nature* **2011**, *471* (7339), 461–466.

(5) Wang, Z.; Zheng, J.; Huang, P. Asymmetric Synthesis of Both Enantiomers of Disparlure. *Chinese Journal of Chemistry* **2012**, *30* (1), 23–28.

(6) Siau, W.-Y.; Zhang, Y.; Zhao, Y. Stereoselective Synthesis of Z-Alkenes. In *Stereoselective Alkene Synthesis*; Wang, J., Ed.; Topics in Current Chemistry; Springer: Berlin, Heidelberg, 2012; pp 33–58.

(7) Lu, M.-Z.; Goh, J.; Maraswami, M.; Jia, Z.; Tian, J.-S.; Loh, T.-P. Recent Advances in Alkenyl Sp2 C–H and C–F Bond Functionalizations: Scope, Mechanism, and Applications. *Chem. Rev.* **2022**, *122* (24), 17479–17646.

(8) Liang, Q.-J.; Yang, C.; Meng, F.-F.; Jiang, B.; Xu, Y.-H.; Loh, T.-P. Chelation versus Non-Chelation Control in the Stereoselective Alkenyl Sp2 C−H Bond Functionalization Reaction. *Angewandte Chemie International Edition* **2017**, *56* (18), 5091–5095.

(9) Sun, Q.; Zhang, H.; Wang, Q.; Qiao, T.; He, G.; Chen, G. Stereoselective Synthesis of C-Vinyl Glycosides via Palladium-Catalyzed C−H Glycosylation of Alkenes. *Angewandte Chemie International Edition* **2021**, *60* (36), 19620–19625.

(10) Luo, Y.-C.; Yang, C.; Qiu, S.-Q.; Liang, Q.-J.; Xu, Y.-H.; Loh, T.-P. Palladium(II)-Catalyzed Stereospecific Alkenyl C–H Bond Alkylation of Allylamines with Alkyl Iodides. *ACS Catal.* **2019**, *9* (5), 4271–4276.

(11) Zhu, Y.; Chen, F.; Cheng, D.; Chen, Y.; Zhao, X.; Wei, W.; Lu, Y.; Zhao, J. Rhodium(III)-Catalyzed Alkenyl C–H Functionalization to Dienes and Allenes. *Org. Lett.* **2020**, *22* (22), 8786–8790.

(12) Parella, R.; Babu, S. A. Pd(II)-Catalyzed, Picolinamide-Assisted, Z-Selective γ-Arylation of Allylamines To Construct Z-Cinnamylamines. *J. Org. Chem.* **2017**, *82* (13), 6550–6567.

(13) Chen, J.; Li, J.; Plutschack, M. B.; Berger, F.; Ritter, T. Regio- and Stereoselective Thianthrenation of Olefins To Access Versatile Alkenyl Electrophiles. *Angewandte Chemie International Edition* **2020**, *59* (14), 5616–5620.

(14) Zhao, B.-J.; Shine, H. J.; Marx, J. N.; Kelly, A. T.; Hofmann, C.; Whitmire, K. H. Addition of Thianthrene Cation Radical to Non-Conjugated Dienes—Part I: Addition to One Double Bond. *Journal of Sulfur Chemistry* **2006**, *27* (2), 127–138.

(15) Holst, D. E.; Wang, D. J.; Kim, M. J.; Guzei, I. A.; Wickens, Z. K. Aziridine Synthesis by Coupling Amines and Alkenes via an Electrogenerated Dication. *Nature* **2021**, *596* (7870), 74–79.

(16) Qian, D.-Q.; Shine, H. J.; Guzman-Jimenez, I. Y.; Thurston, J. H.; Whitmire, K. H. Mono- and Bisadducts from the Addition of Thianthrene Cation Radical Salts to Cycloalkenes and Alkenes. *J. Org. Chem.* **2002**, *67* (12), 4030–4039.

(17) This mechanism is consistent with work by Ritter, where thianthrene S-oxide deoxygenation methods deliver exclusive mono-adduct formation and subsequent treatment with base provides alkenylthianthrenium electrophiles in high E-selectivity (>20:1 *E:Z*).

(18) Control experiments validate that: (1) the conversion of bis-adduct to mono-adduct occurs at an appreciably slow rate, (2) alkenylthianthrenium deprotonation by trifluoroacetate is facile and irreversible, (3) trifluoroacetate anion does not isomerize the alkenylthianthrenium product.

(19) Thiehoff, C.; Rey, Y. P.; Gilmour, R. The Fluorine Gauche Effect: A Brief History. *Israel Journal of Chemistry* **2017**, *57* (1–2), 92–100.

(20) Freitas, M. P.; Rittner, R. Is There a General Rule for the Gauche Effect in the Conformational Isomerism of 1,2-Disubstituted Ethanes? *J. Phys. Chem. A* **2007**, *111* (30), 7233–7236.

(21) N-Ethyldiisopropylamine was used as the base for the adduct elimination step. Our base identity studies with adducts derived from 1-butene support this trialkylamine base does not isomerize the resultant alkenylthianthrenium salt stereochemistry. See appendix F for details.

(22) Zhao, B.-J.; Shine, H. J.; Marx, J. N.; Hofmann, C.; Whitmire, K. H. Addition of the Phenoxathiin Cation Radical to Alkenes and Nonconjugated Dienes. Formation of (E)- and (Z)-(10-Phenoxathiiniumyl)Alkenes and (E)- and (Z)-(10-Phenoxathiiniumyl)Dienes on Basic Alumina. *J. Org. Chem.* **2007**, *72* (16), 6154–6161.

Chapter 8: Unveiling Potent Photooxidation Behavior of Catalytic Photoreductants

This chapter has been published and adapted with permission from:

Karina Targos,† Oliver P. Williams,† and Zachary K. Wickens. Unveiling Potent Photooxidation Behavior of Catalytic Photoreductants. *J. Am. Chem. Soc.* **2021**, 143, 11, 4125–4132. †K.T. and O.P.W. contributed equally.

8.1 Abstract

We describe a photocatalytic system that reveals latent photooxidant behavior from one of the most reducing conventional photoredox catalysts, *N*-phenylphenothiazine (**PTH**). This aerobic photochemical reaction engages difficult to oxidize feedstocks, such as benzene, in C(sp^2)–N coupling reactions through direct oxidation. Mechanistic studies are consistent with activation of **PTH** *via* photooxidation and that Lewis acid co-catalysts scavenge inhibitors formed upon catalyst activation.

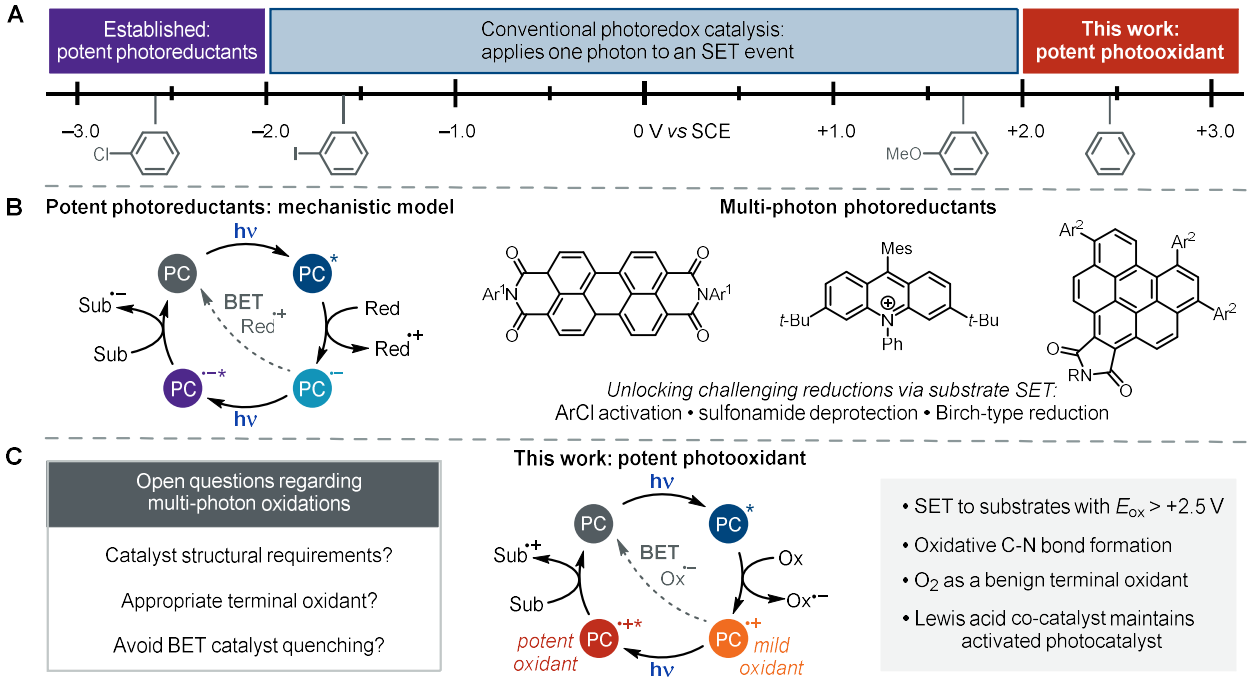

Figure 8.1. (A) Overview of redox potentials in photoredox catalysis. (B) Overview of reduced doublet photocatalysts accessed through conPET. Full catalyst structures available in appendix G. (C) Overview of research described herein.

8.2 Introduction

Reactions driven by single electron transfer (SET) are pervasive in organic chemistry. Consequently, new strategies to induce redox events are poised to profoundly impact synthetic chemistry.[1–4] Photoredox catalysis has unlocked a broad range of attractive new transformations through conversion of energy from readily accessible LEDs into chemical redox potential.[5–8] However, only a portion of this energy[9] can be harnessed due to inevitable energy losses from vibrational relaxation, internal conversion, and intersystem crossing.[10] Despite tremendous effort in photoredox catalyst design,[10–17] excited state potentials beyond roughly –2 and +2 V *vs.* SCE remain difficult to achieve using conventional photocatalyst design principles wherein a single photon from commercial LEDs is used as the primary energy source (Figure 8.1A).[18–22] Unfortunately, this redox window excludes numerous abundant hydrocarbon feedstocks from facile photoinduced electron transfer.[23]

To overcome the energetic limitations intrinsic to conventional photoredox catalysis, König and coworkers recently designed a photocatalytic system that drives challenging reductive SET events using the energy of two photons rather than one. This consecutive photoninduced electron transfer (conPET)[24,25] strategy relies on a catalytic photooxidant and sacrificial reductant that, upon irradiation, result in a potent radical anion photoreductant (Figure 8.1B). Despite its mechanistic complexity, this approach is practical and operationally simple; it leverages inexpensive and safe LEDs to accomplish reactions that otherwise require UV photoreactors or harsh chemical reductants. Following proof-of-concept aryl halide reductions,[24,26–33] this approach has enabled photochemical alternatives to alkali metal reductants in reactions such as Birch reductions[34] and sulfonamide cleavage.[35]

In contrast to the progress in photoreductions, oxidations driven by the consumption of multiple photons have remained elusive. We suspect that this is the consequence of two inextricable challenges: (1) the catalyst must be a competent photocatalyst in both the closed shell and radical cation states[5,25] and (2) the terminal oxidant must efficiently activate the catalyst but not otherwise interfere with the reaction (Figure 8.1C).[36] Given the difficulty applying multiple photons towards a challenging SET oxidation,

photoredox reactions initiated by SET oxidation are typically limited to electron-rich hydrocarbon substrates.[37–42,6]

We questioned whether conventional photoreductants, which typically possess persistent radical cation states, could be repurposed as strong photooxidants using a conPET strategy.[43] We hypothesized photochemical conditions designed to drive these photocatalysts towards their oxidized congeners could reveal potent photooxidation behavior. To probe this hypothesis, we targeted cyclic triarylamine photoreductants. These are a well-established and modular family of photocatalysts[21,44] and photophysical studies conducted by Wasilewski and coworkers indicate that their radical cation congeners exhibit photochemical activity.[45] Furthermore, intriguing studies from Wagenknecht and coworkers have implicated photoexcitation of triarylamine radical cations formed *via* SF_6 reduction in alkene pentafluorosulfonylation processes.[46,47] We envisioned that photochemically accessing these radical cations using a bystanding oxidant would offer an ideal avenue to explore the potency of these radical cation photooxidants.

We selected the Nicewicz-type[41] oxidative coupling of arenes and *N*-heterocyclic nucleophiles as a model reaction. This synthetically valuable transformation is representative of the general challenges in oxidative photoredox catalysis. It has been predominantly limited to electron-rich arene substrates, such as anisole derivatives[48] and also requires a bystanding terminal oxidant. Difficult to oxidize arene substrates, such as benzene, typically mandate high energy UV light (UVB or shorter)[18] or strong ground state oxidants (*e.g.* DDQ) that absorb visible light.[49,50] Recent progress by Lambert and coworkers has introduced an alternative electrophotocatalytic approach that employs electrochemistry and photochemistry in concert to accomplish this energetically demanding oxidation.[51–53] However, while electrophotocatalysis is an exciting emerging area of research,[51,52,54–63] these reactions require specialized electrochemical equipment (*e.g.* divided cells, electrodes, and power supplies) and are technically complex relative to purely photochemical processes.[59] Thus, we envisioned that promoting this transformation using a bench stable and commercially available photocatalyst simply with inexpensive LEDs would be a synthetically useful complement to existing methods. Accordingly, this constitutes an appealing context for our proof-of-concept experiments.

8.3 Results and Discussion

First, we examined three distinct photoreductants[21,65,66] and a range of oxidants for activity in the oxidative coupling of benzene (E_{ox} = 2.5 V *vs.* SCE)[67] and pyrazole **8.1** (Table 8.1). We initially aimed to generate the catalyst radical cation congener *via* photoreduction of reagents that undergo irreversible decomposition after SET to avoid catalyst deactivation *via* back electron transfer (BET). Excitingly, these data revealed that *N*-phenylphenothiazine (**PTH**), the most reducing photocatalyst of the series, could promote this challenging oxidative coupling in low yield using organohalides as the oxidant. A sufficiently strong oxidant to oxidize each catalyst to the corresponding radical cation without additional energy from light, $NOPF_6$,[68] provided low yield of benzene oxidation products using all three catalysts. However, under one atmosphere of O_2, **PTH** promoted oxidative coupling in promising yield (14%). Given the enhanced stability of radical cations in fluorinated alcohol solvents,[19,53,69–71] we substituted acetonitrile (MeCN) for trifluoroethanol (TFE). This resulted in a modest increase in reaction yield with **PTH** but only traces of product with the other two catalysts. Of note, while most photoredox catalysts undergo rapid intersystem

Table 8.1. Survey of Oxidants and Photoreductants.[a-d]

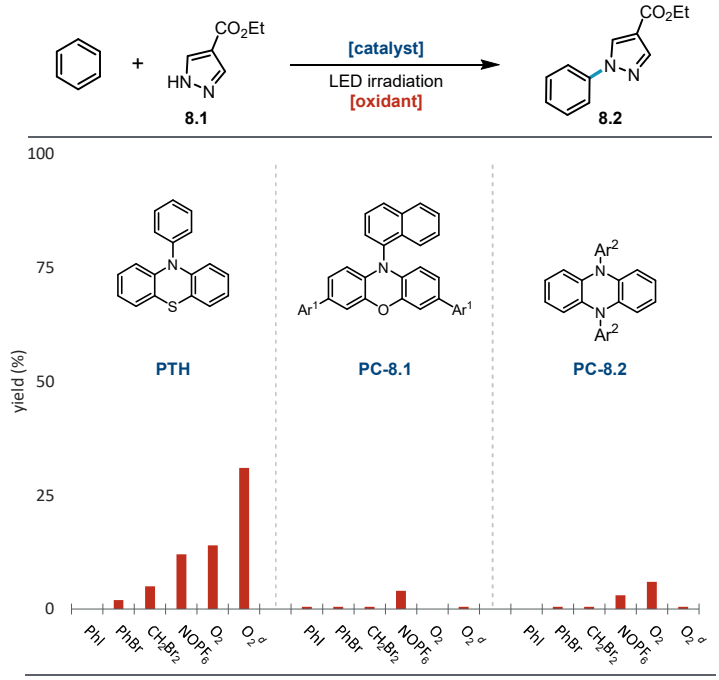

[a]Reactions were conducted on a 0.05 mmol scale in 1:1 MeCN:PhH for 24 h, unless noted otherwise, using 2.0 equiv oxidant or 1 atm O_2. Ar^1 = 4-biphenyl. Ar^2 = 2-naphthyl. [b]**PTH** irradiated using 390 nm Kessil lamp. [c]**PC-8.1** and **PC-8.2** irradiated using Tuna Blue Kessil lamp. [d]1:1 TFE:PhH.

crossing to a long-lived triplet,[5,13] **PTH** is a singlet excited state reductant.[72] This property circumvents photocatalyst deactivation by triplet-triplet annihilation with O_2.

We suspected that BET between **PTH** radical cation and superoxide[73] might attenuate reactivity under these conditions (Figure 8.2).[74] Indeed, when synthetically prepared **PTH** radical cation is treated with KO_2, we observe a rapid color change and reformation of **PTH** by ^{1}H-NMR. Given that superoxide

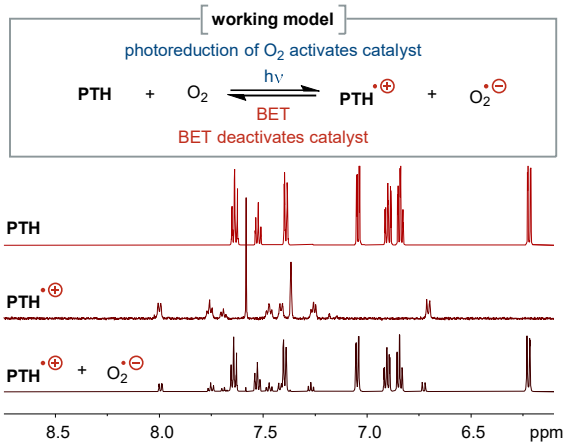

Figure 8.2. ^{1}H NMR spectroscopic evidence supporting working model for catalyst deactivation pathways.

generation is inextricable from aerobic catalyst activation, this observation could account for the modest reactivity of this catalytic system (Table 8.2, entry 1). As expected, addition of 5 mol % KO_2 to the reaction mixture completely suppressed product formation (entry 2). We hypothesized that additives capable of sequestering or scavenging this inhibitor would enhance the observed reactivity. Guided by this model, we found addition of one equivalent of an inexpensive, redox innocent Lewis acid, $LiClO_4$, dramatically improved the yield of oxidative coupling product (entry 3). Reduction of the $LiClO_4$ loading to a substoichiometric quantity (20 mol %) retained the benefits of the additive, suggesting a co-catalytic role for $LiClO_4$ rather than it purely sequestrating stoichiometric byproducts (entry 4). In principle, the lithium co-catalyst could mitigate BET by promoting superoxide disproportionation.[75,76] Consistent with this proposed Lewis acidic role, alkylammonium salts had no impact on the reaction (entry 5); whereas, other Lewis acidic lithium salts retained the catalytic effect (entries 6 and 7). Final tuning of the reaction

Table 8.2. Reaction Optimization.[a]

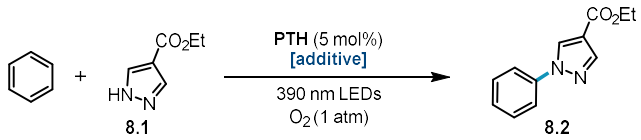

entry	additive	yield (%)
1	none	31
2	KO_2 (5 mol %)	<2
3	$LiClO_4$ (1 equiv)	86
4	$LiClO_4$ (20 mol %)	73
5	*n*-Bu_4NClO_4 (20 mol %)	29
6	$LiPF_6$ (20 mol %)	64
7	LiOTf (20 mol %)	56
8	$LiClO_4$ (20 mol %)[b]	89
9	**PC-8.1** (5 mol %), $LiClO_4$ (20 mol %)[b,c]	<2
10	**PC-8.2** (5 mol %), $LiClO_4$ (20 mol %)[b,c]	<2
11	$Ir(ppy)_3$ (1 mol %), $LiClO_4$ (20 mol %)[b,c]	<2

[a]Reactions were conducted on a 0.05 mmol scale in 1:1 TFE:PhH for 24 h. See appendix G for details. [b]9:1:10 TFE:HFIP:PhH solvent mixture. [c]Tuna Blue Kessil lamp irradiation.

parameters revealed adjusting the solvent mixture to include a small amount of hexafluoroisopropanol (HFIP) delivered the desired product in 89% yield (entry 8). Substitution of **PTH** with other triarylamine photoreductants or a classic metal-based photoreductant, $Ir(ppy)_3$, resulted in only trace yield of oxidation product under these otherwise optimal conditions (entries 9–11).

Having identified a promising catalytic system, we examined the scope of this new process (Table 8.3). Pyrazole nucleophiles bearing a range of electron-withdrawing moieties, including ketones (**8.3**), aldehydes (**8.4**), nitriles (**8.5**), and trifluoromethyl groups (**8.6**) were oxidatively coupled to benzene. Halogenated pyrazoles (**8.7** and **8.8**) were also productively coupled despite the fact that **PTH** is a potent photoreductant. Prior approaches capable of oxidizing benzene have not been readily amenable to the arylation of neutral heterocyclic substrates.[77] In contrast, we observed coupling of both parent pyrazole (**8.9**) and even an electron-rich analog (**8.10**), albeit in diminished yield relative to the electron deficient heterocyclic coupling partners. In addition to pyrazole derivatives, we found that 1,2,3-triazoles (**8.11** and **8.12**) were amenable to oxidative coupling with benzene. Even an exceptionally challenging to oxidize electron-deficient arene, chlorobenzene, could be engaged in productive $C(sp^2)$–N coupling *via* arene photooxidation (**8.13**). To probe the limits of what this catalytic system can oxidize, we evaluated acetophenone as an arene substrate and detected at most traces of oxidative coupling products. This result

Table 8.3. Scope of Arene C–H Amination.[a,b]

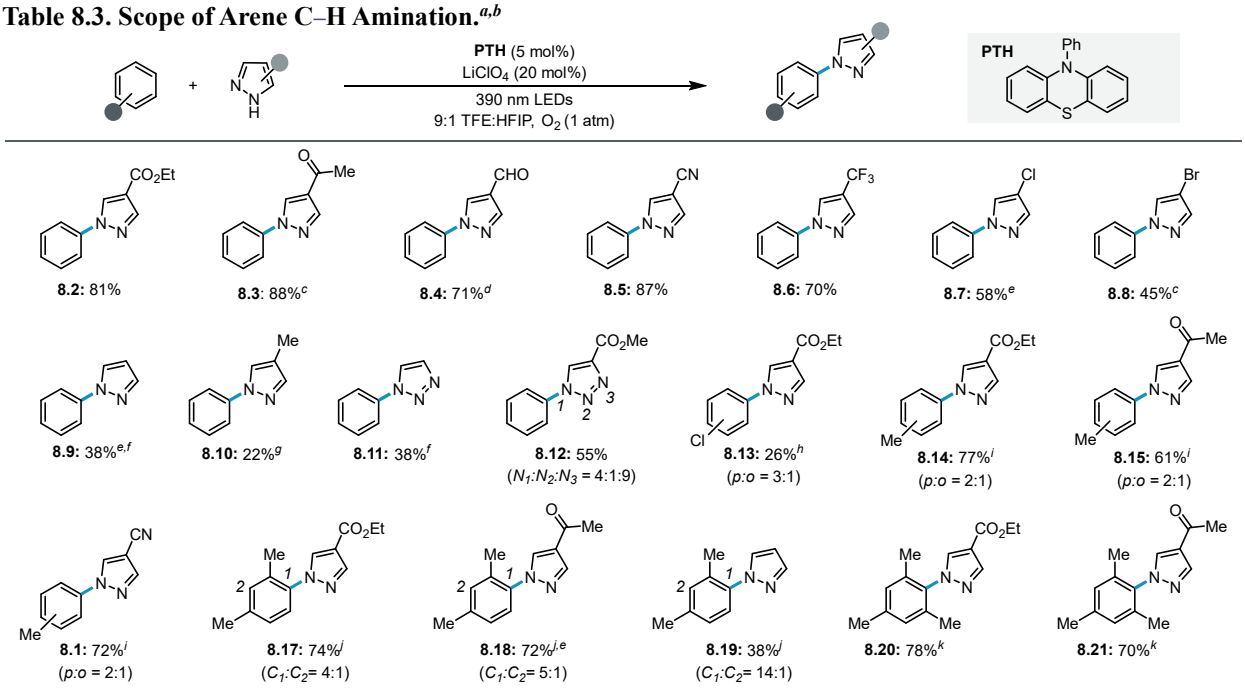

[a]Reactions conducted using 0.4 mmol of heterocycle, 8 mL of arene, and irradiated with two 390 nm Kessil lamps for 24 h with fan cooling. See the appendix G for further experimental details. [b]Isolated yields. [c]20 mol % $LiPF_6$. [d]1:1 HFIP:PhH solvent. [e]NMR yield. [f]0% pyrazole starting material remaining. [g]31% pyrazole starting material remaining. [i]1:1:2 MeCN:HFIP:arene solvent with 10 mol % *t*-dodecyl mercaptan. [j]10.0 equiv. arene, 0.1 M in 1:1 MeCN:HFIP, 10 mol% *t*-dodecyl mercaptan. [k]5.0 equiv. arene, 0.1 M in 1:1 MeCN:HFIP, 10 mol % *t*-dodecyl mercaptan.

indicates that this arene is too electronically deactivated for oxidation under these conditions. We recognized that benzylic C–H bonds could be a liability under these aerobic conditions; however, we found reasonable C(sp^2)–N coupling yields could be obtained from toluene using our standard conditions and these yields could be further improved by tuning the reaction conditions to mitigate benzylic oxidation processes.[78] Under these modified conditions, **PTH** promoted the photochemical coupling of toluene, *m*-xylene, and mesitylene with pyrazole derivatives in high yield (**8.14** to **8.21**). The oxidation of *m*-xylene and mesitylene could be achieved using a smaller excess of arene, presumably due to the significantly lower oxidation potential relative to benzene.[79] Of note, while the scope and reagent stoichiometries required for this approach are similar to prior electrophotocatalytic systems, these photocatalytic conditions exclusively require commercially available catalysts and no specialized equipment outside of LED lamps. Furthermore, this simple photocatalytic system delivers coupling products with substantially shorter reaction times.[80] Overall, these data illustrate that the scope of this photochemical process described herein is on par with complementary electrophotocatalytic approaches.[51,52]

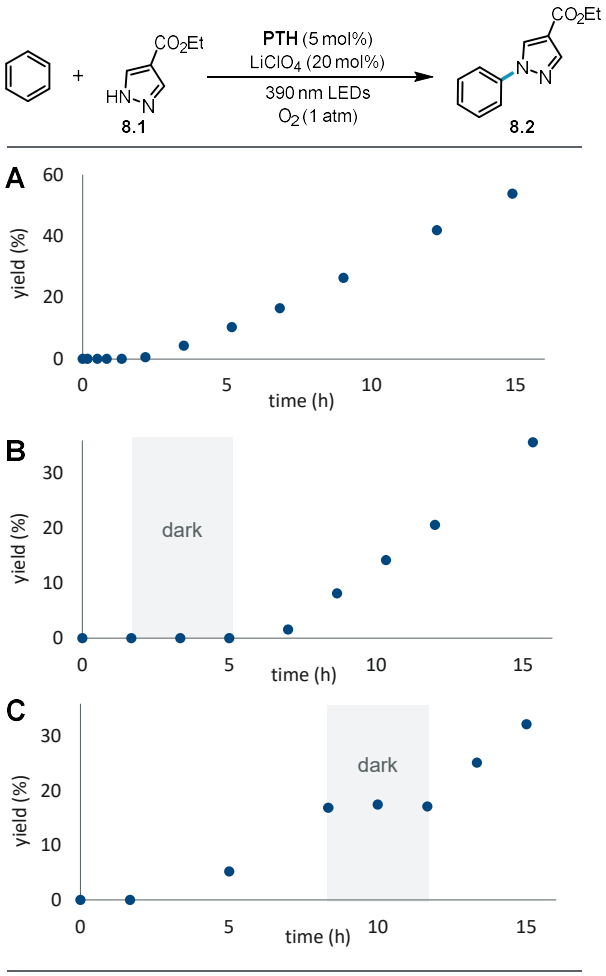

[a]Reactions were conducted on a 0.05 mmol scale in 9:1:10 TFE:HFIP:PhH. See the appendix G for overlays of total irradiation time.

Scheme 8.1. Light-dependence on induction period and product formation regimes: (A) standard reaction profile with continuous irradiation; (B) suspended irradiation during induction period; (C) suspended irradiation during product formation.[a]

Next, we aimed to uncover preliminary mechanistic insight into this new and unusually oxidizing photocatalytic system. First, we collected the full reaction profile by monitoring the yield of coupling product **8.2** as a function of time (Scheme 8.1A). These data revealed an induction period, wherein only a trace amount of product is formed, followed by 0^{th} order formation of product that continues until nearly all of the pyrazole is consumed (see appendix G for complete reaction profile). If irradiation is temporarily suspended during the induction period, the onset of product formation is correspondingly delayed (Scheme 8.1B). Similarly, when irradiation is halted during the product-forming regime, the reaction ceases until irradiation resumes (Scheme 8.1C). Overall, these data are consistent with a mechanism involving an initial

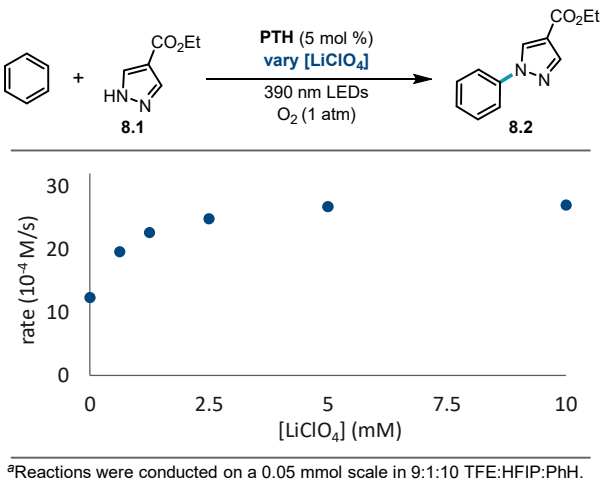

[a]Reactions were conducted on a 0.05 mmol scale in 9:1:10 TFE:HFIP:PhH.

Scheme 8.2. Saturation in lithium co-catalyst.[a]

photochemical catalyst activation step (*e.g.* photooxidation of **PTH** to the radical cation) followed by a product-forming regime with either rate-limiting catalyst oxidation or benzene oxidation, given both benzene and O_2 are present in excess throughout the reaction. Additionally, we determined the O_2 stoichiometry of the reaction by measuring gas consumption within a sealed reaction vessel equipped with a pressure transducer (Figure G16).[81] These data indicate that just over two equivalents of O_2 are consumed over the course of the reaction, consistent with O_2 acting as only a one-electron oxidant.[82] As anticipated, we found that only minimal oxygen is consumed during the induction period.

Given the initially unanticipated co-catalytic role of $LiClO_4$ in this system, we next carefully investigated the origin of its impact on the reaction. Omission of this additive resulted in a modest elongation of the induction period and, subsequently, slower product formation (see appendix G for details). Systematic variation of the concentration of $LiClO_4$ revealed that the impact of this reaction component on rate saturates at roughly 20 mol % (Scheme 8.2). These data are consistent with our working model wherein $LiClO_4$ catalytically scavenges inhibitory reactive oxygen species produced through photochemical O_2 reduction. Once the inhibitor is scavenged at a sufficiently rapid rate, its steady state concentration will approach zero and additional increase in co-catalyst loading is expected to have no impact on the process. When the reaction is charged with 5 mol % KO_2 shortly after the induction period, we observe that the

reaction halts thereafter in the absence of $LiClO_4$. In stark contrast, a reaction containing 2 equivalents of $LiClO_4$ was unperturbed by direct addition of this inhibitor (Scheme 8.3).[83]

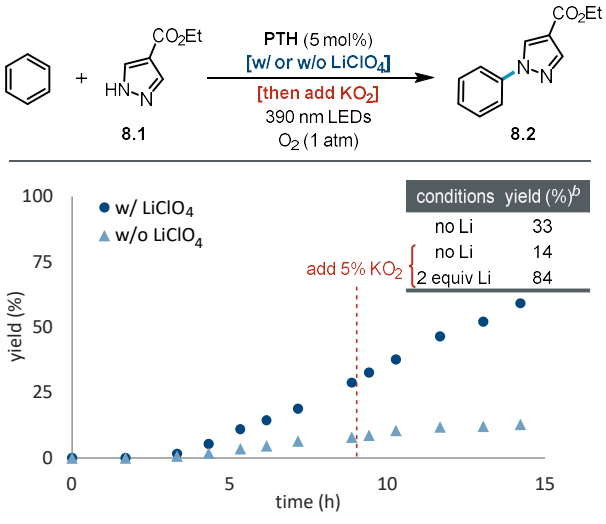

[a]Reactions were conducted on a 0.05 mmol scale in 9:1:10 TFE:HFIP:PhH. See the appendix G for further details. [b]final yield after 22 h.

Scheme 8.3. Impact of added substoichiometric KO_2 on rate with and without $LiClO_4$.[a]

Based on the data presented herein, we have constructed a plausible mechanistic model, which involves: (1) initial oxidative activation of **PTH** *via* photoreduction of O_2; (2) photoexcitation of a triarylamine radical cation to oxidize the arene substrate;[84,85] (3) trapping of arene radical cation with pyrazole nucleophile. While lithium salts are not mechanistically necessary to promote the photocatalytic transformation, we suspect that these Lewis acidic co-catalysts accelerate the reaction by promoting the disproportionation of superoxide, an inhibitor inextricably formed in the aerobic catalyst activation step. We envision the lithium co-catalyst is turned over by protonation of Li_2O_2 by HFIP.[86]

8.4 Conclusion

Overall, we have identified a catalytic system that unlocks potent photooxidant behavior from one of the most reducing conventional photoredox catalysts, **PTH**. This approach enables oxidative C(sp^2)–N coupling *via* photooxidation of arene substrates outside of the redox window of reported photoredox approaches. Preliminary mechanistic studies are fully consistent with photocatalyst activation *via*

photoreduction of O_2. Intriguingly, we found that Lewis acid co-catalysts could promote and maintain catalyst activation. Beyond providing the first example of purely photochemical benzene oxidation using inexpensive LEDs, this study provides a roadmap to exploit known photocatalysts in new and unconventional ways. We anticipate that continued examination of reaction conditions that force photocatalysts into destabilized oxidation states will dramatically expand the scope of oxidative photoredox catalysis.[87–89]

8.5 Acknowledgements

We thank Prof. Tehshik Yoon and Prof. Alison Wendlandt for helpful suggestions and manuscript proofreading. We thank the Stahl, Weix, Yoon and Schomaker groups for sharing their chemical inventory. We thank Dr. Chase Salazar and Dr. Jack Twilton (Stahl lab) for assistance measuring O_2 uptake. This work was financially supported by the Office of the Vice Chancellor for Research and Graduate Education at the University of Wisconsin–Madison with funding from the Wisconsin Alumni Research Foundation. Acknowledgment is made to the Donors of the American Chemical Society Petroleum Research Fund for partial funding of this research (60677-DNI1). This material is based upon work supported by the National Science Foundation Graduate Research Fellowship Program under Grant No. DGE-1747503 (K.T.). Any opinions, findings, and conclusions or recommendations expressed in this material are those of the author(s) and do not necessarily reflect the views of the National Science Foundation. Spectroscopic instrumentation was supported by a generous gift from Paul. J. and Margaret M. Bender, NSF (CHE-1048642), and NIH (S10OD012245 and 1S10OD020022-1).

Z.K.W., K.T., and O.P.W. designed the project. All authors performed the experiments and collected the data. All authors contributed to writing the manuscript.

8.6 References

(1) Girard, P.; Namy, J. L.; Kagan, H. B. Divalent Lanthanide Derivatives in Organic Synthesis. 1. Mild Preparation of Samarium Iodide and Ytterbium Iodide and Their Use as Reducing or Coupling Agents. *J. Am. Chem. Soc.* **1980**, *102* (8), 2693–2698.

(2) Eberson, L. Electron-Transfer Reactions in Organic Chemistry. In *Advances in Physical Organic Chemistry*; Gold, V., Bethell, D., Eds.; Academic Press, **1982**; Vol. 18, pp 79–185.

(3) Zhang, N.; Samanta, S. R.; Rosen, B. M.; Percec, V. Single Electron Transfer in Radical Ion and Radical-Mediated Organic, Materials and Polymer Synthesis. *Chem. Rev.* **2014**, *114* (11), 5848–5958.

(4) Ashby, E. C. Single-Electron Transfer, a Major Reaction Pathway in Organic Chemistry. An Answer to Recent Criticisms. *Acc. Chem. Res.* **1988**, *21* (11), 414–421.

(5) Romero, N. A.; Nicewicz, D. A. Organic Photoredox Catalysis. *Chem. Rev.* **2016**, *116* (17), 10075–10166.

(6) Prier, C. K.; Rankic, D. A.; MacMillan, D. W. C. Visible Light Photoredox Catalysis with Transition Metal Complexes: Applications in Organic Synthesis. *Chem. Rev.* **2013**, *113* (7), 5322–5363.

(7) Shaw, M. H.; Twilton, J.; MacMillan, D. W. C. Photoredox Catalysis in Organic Chemistry. *J. Org. Chem.* **2016**, *81* (16), 6898–6926.

(8) Marzo, L.; Pagire, S. K.; Reiser, O.; König, B. Visible-Light Photocatalysis: Does It Make a Difference in Organic Synthesis? *Angew. Chem. Int. Ed.* **2018**, *57* (32), 10034–10072.

(9) Photoredox methodologies commonly employ wavelengths between 390 nm and 540 nm due to the widespread availability of inexpensive and safe LEDs in this range. These wavelengths correspond to a maximum energy of 3.2 and 2.3 eV, respectively.

(10) Arias-Rotondo, D. M.; McCusker, J. K. The Photophysics of Photoredox Catalysis: A Roadmap for Catalyst Design. *Chem. Soc. Rev.* **2016**, *45* (21), 5803–5820.

(11) Vega-Peñaloza, A.; Mateos, J.; Companyó, X.; Escudero-Casao, M.; Dell'Amico, L. A Rational Approach to Organo-Photocatalysis: Novel Designs and Structure-Property Relationships. *Angew. Chem. Int. Ed.* **2021**, *60*, 1082**.**

(12) Speckmeier, E.; Fischer, T. G.; Zeitler, K. A Toolbox Approach To Construct Broadly Applicable Metal-Free Catalysts for Photoredox Chemistry: Deliberate Tuning of Redox Potentials and Importance of Halogens in Donor–Acceptor Cyanoarenes. *J. Am. Chem. Soc.* **2018**, *140* (45), 15353–15365.

(13) Sartor, S. M.; McCarthy, B. G.; Pearson, R. M.; Miyake, G. M.; Damrauer, N. H. Exploiting Charge-Transfer States for Maximizing Intersystem Crossing Yields in Organic Photoredox Catalysts. *J. Am. Chem. Soc.* **2018**, *140* (14), 4778–4781.

(14) Joshi-Pangu, A.; Lévesque, F.; Roth, H. G.; Oliver, S. F.; Campeau, L.-C.; Nicewicz, D.; DiRocco, D. A. Acridinium-Based Photocatalysts: A Sustainable Option in Photoredox Catalysis. *J. Org. Chem.* **2016**, *81* (16), 7244–7249.

(15) Lee, Y.; Kwon, M. S. Emerging Organic Photoredox Catalysts for Organic Transformations. *Eur. J. Org. Chem.* **2020**, *38*, 6028–6043.

(16) Singh, V. K.; Yu, C.; Badgujar, S.; Kim, Y.; Kwon, Y.; Kim, D.; Lee, J.; Akhter, T.; Thangavel, G.; Park, L. S.; Lee, J.; Nandajan, P. C.; Wannemacher, R.; Milián-Medina, B.; Lüer, L.; Kim, K. S.; Gierschner, J.; Kwon, M. S. Highly Efficient Organic Photocatalysts Discovered via a Computer-Aided-Design Strategy for Visible-Light-Driven Atom Transfer Radical Polymerization. *Nat. Catal.* **2018**, *1* (10), 794–804.

(17) Glaser, F.; Wenger, O. S. Recent Progress in the Development of Transition-Metal Based Photoredox Catalysts. *Coord. Chem. Rev.* **2020**, *405*, 213129.

(18) For an example of UV light promoted oxidation of benzene, see: Ohkubo, K.; Kobayashi, T.; Fukuzumi, S. Direct Oxygenation of Benzene to Phenol Using Quinolinium Ions as Homogeneous Photocatalysts. *Angew. Chem.* **2011**, *123* (37), 8811–8814.

(19) For a recent advance in redox neutral reactions triggered by photocatalytic oxidation of arenes, see: Pistritto, V. A.; Schutzbach-Horton, M. E.; Nicewicz, D. A. Nucleophilic Aromatic Substitution of Unactivated Fluoroarenes Enabled by Organic Photoredox Catalysis. *J. Am. Chem. Soc.* **2020**, *142* (40), 17187–17194.

(20) Matsubara, R.; Yabuta, T.; Md Idros, U.; Hayashi, M.; Ema, F.; Kobori, Y.; Sakata, K. UVA- and Visible-Light-Mediated Generation of Carbon Radicals from Organochlorides Using Nonmetal Photocatalyst. *J. Org. Chem.* **2018**, *83* (16), 9381–9390.

(21) Treat, N. J.; Sprafke, H.; Kramer, J. W.; Clark, P. G.; Barton, B. E.; Read de Alaniz, J.; Fors, B. P.; Hawker, C. J. Metal-Free Atom Transfer Radical Polymerization. *J. Am. Chem. Soc.* **2014**, *136* (45), 16096–16101.

(22) Although not a conventional photoredox catalyst due to its highly oxidizing ground state, DDQ has been employed as an exceptionally potent photooxidant (>3 V *vs.* SCE). For a recent review, see: Natarajan, P.; König, B. Excited-State 2,3-Dichloro-5,6-Dicyano-1,4-Benzoquinone (DDQ*) Initiated Organic Synthetic Transformations under Visible-Light Irradiation. *Eur. J. Org. Chem* https://doi.org/10.1002/ejoc.202100011.

(23) For a compilation of potentials of common organic molecules, see: Roth, H.; Romero, N.; Nicewicz, D. Experimental and Calculated Electrochemical Potentials of Common Organic Molecules for Applications to Single-Electron Redox Chemistry. *Synlett* **2015**, *27* (05), 714–723.

(24) For the seminal example of the conPET strategy, see: Ghosh, I.; Ghosh, T.; Bardagi, J. I.; Konig, B. Reduction of Aryl Halides by Consecutive Visible Light-Induced Electron Transfer Processes. *Science* **2014**, *346* (6210), 725–728.

(25) For a recent review of work in conPET, see: Glaser, F.; Kerzig, C.; Wenger, O. S. Multi-Photon Excitation in Photoredox Catalysis: Concepts, Applications, Methods. *Angew. Chem. Int. Ed.* **2020**, *59* (26), 10266–10284.

(26) Neumeier, M.; Sampedro, D.; Májek, M.; de la Peña O'Shea, V. A.; Jacobi von Wangelin, A.; Pérez-Ruiz, R. Dichromatic Photocatalytic Substitutions of Aryl Halides with a Small Organic Dye. *Chem. - Eur. J.* **2018**, *24* (1), 105–108.

(27) Ghosh, I.; König, B. Chromoselective Photocatalysis: Controlled Bond Activation through Light-Color Regulation of Redox Potentials. *Angew. Chem. Int. Ed.* **2016**, *55* (27), 7676–7679.

(28) Bardagi, J. I.; Ghosh, I.; Schmalzbauer, M.; Ghosh, T.; König, B. Anthraquinones as Photoredox Catalysts for the Reductive Activation of Aryl Halides: Anthraquinones as Photoredox Catalysts for the Reductive Activation of Aryl Halides. *Eur. J. Org. Chem.* **2018**, *2018* (1), 34–40.

(29) Kerzig, C.; Wenger, O. S. Reactivity Control of a Photocatalytic System by Changing the Light Intensity. *Chem. Sci.* **2019**, *10* (48), 11023–11029.

(30) Connell, T. U.; Fraser, C. L.; Czyz, M. L.; Smith, Z. M.; Hayne, D. J.; Doeven, E. H.; Agugiaro, J.; Wilson, D. J. D.; Adcock, J. L.; Scully, A. D.; Gómez, D. E.; Barnett, N. W.; Polyzos, A.; Francis, P. S. The Tandem Photoredox Catalysis Mechanism of $[Ir(ppy)_2$ (dtb-bpy)$]^+$ Enabling Access to Energy Demanding Organic Substrates. *J. Am. Chem. Soc.* **2019**, *141* (44), 17646–17658.

(31) Naumann, R.; Lehmann, F.; Goez, M. Micellized Tris(Bipyridine)Ruthenium Catalysts Affording Preparative Amounts of Hydrated Electrons with a Green Light-Emitting Diode. *Chem. - Eur. J.* **2018**, *24* (50), 13259–13269.

(32) Qiao, Y.; Yang, Q.; Schelter, E. J. Photoinduced Miyaura Borylation by a Rare-Earth-Metal Photoreductant: The Hexachlorocerate(III) Anion. *Angew. Chem. Int. Ed.* **2018**, *57* (34), 10999–11003.

(33) Majek, M.; Faltermeier, U.; Dick, B.; Pérez-Ruiz, R.; Jacobi von Wangelin, A. Application of Visible-to-UV Photon Upconversion to Photoredox Catalysis: The Activation of Aryl Bromides. *Chem. - Eur. J.* **2015**, *21* (44), 15496–15501.

(34) Cole, J. P.; Chen, D.-F.; Kudisch, M.; Pearson, R. M.; Lim, C.-H.; Miyake, G. M. Organocatalyzed Birch Reduction Driven by Visible Light. *J. Am. Chem. Soc.* **2020**, *142* (31), 13573–13581.

(35) MacKenzie, I. A.; Wang, L.; Onuska, N. P. R.; Williams, O. F.; Begam, K.; Moran, A. M.; Dunietz, B. D.; Nicewicz, D. A. Discovery and Characterization of an Acridine Radical Photoreductant. *Nature* **2020**, *580* (7801), 76–80.

(36) While trialkylamines are commonly employed reductants in both conventional and conPET photoredox processes, the oxidants employed in photoredox catalysis are typically incorporated into the final product and examples of bystanding terminal oxidants in photoredox catalysis are less common.

(37) Margrey, K. A.; Nicewicz, D. A. A General Approach to Catalytic Alkene Anti-Markovnikov Hydrofunctionalization Reactions via Acridinium Photoredox Catalysis. *Acc. Chem. Res.* **2016**, *49* (9), 1997–2006.

(38) Prier, C. K.; MacMillan, D. W. C. Amine α-Heteroarylation via Photoredox Catalysis: A Homolytic Aromatic Substitution Pathway. *Chem. Sci.* **2014**, *5* (11), 4173–4178.

(39) Terrett, J. A.; Clift, M. D.; MacMillan, D. W. C. Direct β-Alkylation of Aldehydes via Photoredox Organocatalysis. *J. Am. Chem. Soc.* **2014**, *136* (19), 6858–6861.

(40) Zuo, Z.; Ahneman, D. T.; Chu, L.; Terrett, J. A.; Doyle, A. G.; MacMillan, D. W. C. Merging Photoredox with Nickel Catalysis: Coupling of α-Carboxyl Sp^3-Carbons with Aryl Halides. *Science* **2014**, *345* (6195), 437–440.

(41) Romero, N. A.; Margrey, K. A.; Tay, N. E.; Nicewicz, D. A. Site-Selective Arene C-H Amination via Photoredox Catalysis. *Science* **2015**, *349* (6254), 1326–1330.

(42) Niu, L.; Yi, H.; Wang, S.; Liu, T.; Liu, J.; Lei, A. Photo-Induced Oxidant-Free Oxidative C–H/N–H Cross-Coupling between Arenes and Azoles. *Nat. Commun.* **2017**, *8* (1), 14226.

(43) Nicewicz and coworkers recently illustrated that acridinium photooxidants can be transformed into potent photoreductants through photoreduction to the acridine radical. However, it remains unclear whether this inversion of available redox potentials–from a photooxidant to a photoreductant–is a unique feature of acridinium photocatalysts or whether the behavior of other photocatalysts could be similarly manipulated by careful selection of reaction conditions.

(44) Du, Y.; Pearson, R. M.; Lim, C.-H.; Sartor, S. M.; Ryan, M. D.; Yang, H.; Damrauer, N. H.; Miyake, G. M. Strongly Reducing, Visible-Light Organic Photoredox Catalysts as Sustainable Alternatives to Precious Metals. *Chem. – Eur. J.* **2017**, *23* (46), 10962–10968.

(45) Christensen, J. A.; Phelan, B. T.; Chaudhuri, S.; Acharya, A.; Batista, V. S.; Wasielewski, M. R. Phenothiazine Radical Cation Excited States as Super-Oxidants for Energy-Demanding Reactions. *J. Am. Chem. Soc.* **2018**, *140* (15), 5290–5299.

(46) Rombach, D.; Wagenknecht, H.-A. Photoredox Catalytic Activation of Sulfur Hexafluoride for Pentafluorosulfanylation of α-Methyl- and α-Phenyl Styrene. *ChemCatChem* **2018**, *10* (14), 2955–2961.

(47) Rombach, D.; Wagenknecht, H.-A. Photoredox Catalytic a-Methyl- and a-Phenylstyrene Using SF_6. *Angew. Chem. Int. Ed.* **2020**, *59* (1), 300–303.

(48) Chan, C.-M.; Chow, Y.-C.; Yu, W.-Y. Recent Advances in Photocatalytic C–N Bond Coupling Reactions. *Synthesis* **2020**, *52*, (20), 2899–2921.

(49) For examples of DDQ excitation promote the oxidation of benzene, see: Ohkubo, K.; Fujimoto, A.; Fukuzumi, S. Visible-Light-Induced Oxygenation of Benzene by the Triplet Excited State of 2,3-Dichloro-5,6-Dicyano- *p* -Benzoquinone. *J. Am. Chem. Soc.* **2013**, *135* (14), 5368–5371.

(50) Das, S.; Natarajan, P.; König, B. Teaching Old Compounds New Tricks: DDQ-Photocatalyzed C−H Amination of Arenes with Carbamates, Urea, and N-Heterocycles. *Chem. – Eur. J.* **2017**, *23* (72), 18161–18165.

(51) Huang, H.; Strater, Z. M.; Rauch, M.; Shee, J.; Sisto, T. J.; Nuckolls, C.; Lambert, T. H. Electrophotocatalysis with a Trisaminocyclopropenium Radical Dication. *Angew. Chem. Int. Ed.* **2019**, *58* (38), 13318–13322.

(52) During the review of this manuscript, a second electrophotocatalytic strategy to accomplish this strategy was reeported, see: Wu, S.; Žurauskas, J.; Domański, M.; Hitzfeld, P. S.; Butera, V.; Scott, D. J.; Rehbein, J.; Kumar, A.; Thyrhaug, E.; Hauer, J.; Barham, J. P. Hole-Mediated Photoredox Catalysis: Tris(*p*-Substituted)Biarylaminium Radical Cations as Tunable, Precomplexing and Potent Photooxidants. *Org. Chem. Front.* **2021**, 10.1039.D0QO01609H. https://doi.org/10.1039/D0QO01609H.

(53) Photoanodes have also been used to promote the oxidative coupling of pyrazoles and arenes, however, this approach has an analogous scope to conventional photoredox catalysts and examples are limited to electron-rich systems. For an example, see: Zhang, L.; Liardet, L.; Luo, J.; Ren, D.; Grätzel, M.; Hu, X. Photoelectrocatalytic Arene C–H Amination. *Nat. Catal.* **2019**, *2* (4), 366–373.

(54) Wang, F.; Stahl, S. S. Merging Photochemistry with Electrochemistry: Functional-Group Tolerant Electrochemical Amination of C(Sp^3)−H Bonds. *Angew. Chem. Int. Ed.* **2019**, *58* (19), 6385–6390.

(55) Yan, H.; Hou, Z.-W.; Xu, H.-C. Photoelectrochemical C−H Alkylation of Heteroarenes with Organotrifluoroborates. *Angew. Chem. Int. Ed.* **2019**, *58* (14), 4592–4595.

(56) Kim, H.; Kim, H.; Lambert, T. H.; Lin, S. Reductive Electrophotocatalysis: Merging Electricity and Light To Achieve Extreme Reduction Potentials. *J. Am. Chem. Soc.* **2020**, *142* (5), 2087–2092.

(57) Cowper, N. G. W.; Chernowsky, C. P.; Williams, O. P.; Wickens, Z. K. Potent Reductants via Electron-Primed Photoredox Catalysis: Unlocking Aryl Chlorides for Radical Coupling. *J. Am. Chem. Soc.* **2020**. *142*, 5, 2093–2099.

(58) Costentin, C.; Fortage, J.; Collomb, M.-N. Electrophotocatalysis: Cyclic Voltammetry as an Analytical Tool. *J. Phys. Chem. Lett.* **2020**, *11* (15), 6097–6104.

(59) Zhang, W.; Carpenter, K. L.; Lin, S. Electrochemistry Broadens the Scope of Flavin Photocatalysis: Photoelectrocatalytic Oxidation of Unactivated Alcohols. *Angew. Chem. Int. Ed.* **2020**, *59* (1), 409–417.

(60) Shen, T.; Lambert, T. H. Electrophotocatalytic Diamination of Vicinal C–H Bonds. *Science* **2021**, *371* (6529), 620–626.

(61) Capaldo, L.; Quadri, L. L.; Ravelli, D. Merging Photocatalysis with Electrochemistry: The Dawn of a New Alliance in Organic Synthesis. *Angew. Chem. Int. Ed.* **2019***, 58*, (49), 17508–17510.

(62) Liu, J.; Lu, L.; Wood, D.; Lin, S. New Redox Strategies in Organic Synthesis by Means of Electrochemistry and Photochemistry. *ACS Cent. Sci.* **2020**, *6* (8), 1317–1340.

(63) Barham, J. P.; König, B. Synthetic Photoelectrochemistry. *Angew. Chem. Int. Ed.* **2020**, *59* (29), 11732–11747.

(64) Kingston, C.; Palkowitz, M. D.; Takahira, Y.; Vantourout, J. C.; Peters, B. K.; Kawamata, Y.; Baran, P. S. A Survival Guide for the "Electro-Curious." *Acc. Chem. Res.* **2020**, *53* (1), 72–83.

(65) Pearson, R. M.; Lim, C.-H.; McCarthy, B. G.; Musgrave, C. B.; Miyake, G. M. Organocatalyzed Atom Transfer Radical Polymerization Using *N* -Aryl Phenoxazines as Photoredox Catalysts. *J. Am. Chem. Soc.* **2016**, *138* (35), 11399–11407.

(66) Theriot, J. C.; Lim, C.-H.; Yang, H.; Ryan, M. D.; Musgrave, C. B.; Miyake, G. M. Organocatalyzed Atom Transfer Radical Polymerization Driven by Visible Light. *Science* **2016**, *352* (6289), 1082–1086.

(67) Merkel, P. B.; Luo, P.; Dinnocenzo, J. P.; Farid, S. Accurate Oxidation Potentials of Benzene and Biphenyl Derivatives via Electron-Transfer Equilibria and Transient Kinetics. *J. Org. Chem.* **2009**, *74* (15), 5163–5173.

(68) Connelly, N. G.; Geiger, W. E. Chemical Redox Agents for Organometallic Chemistry. *Chem. Rev.* **1996**, *96* (2), 877–910.

(69) Colomer, I.; Chamberlain, A. E. R.; Haughey, M. B.; Donohoe, T. J. Hexafluoroisopropanol as a Highly Versatile Solvent. *Nat. Rev. Chem.* **2017**, *1* (11), 1–12.

(70) Shida, N.; Imada, Y.; Nagahara, S.; Okada, Y.; Chiba, K. Interplay of Arene Radical Cations with Anions and Fluorinated Alcohols in Hole Catalysis. *Commun. Chem.* **2019**, *2* (1), 1–8.

(71) Eberson, L.; Hartshorn, M. P.; Persson, O.; Radner, F. Making Radical Cations Live Longer. *Chem. Commun.* **1996**, No. 18, 2105.

(72) Discekici, E. H.; Treat, N. J.; Poelma, S. O.; Mattson, K. M.; Hudson, Z. M.; Luo, Y.; Hawker, C. J.; de Alaniz, J. R. A Highly Reducing Metal-Free Photoredox Catalyst: Design and Application in Radical Dehalogenations. *Chem. Commun.* **2015**, *51* (58), 11705–11708.

(73) Based on our working model, superoxide would be formed after O_2 reduction. Other reduced oxygen species could also act as inhibitors for the reaction through either BET or another mechanism.

(74) For redox potentials of various reactive oxygen species, see: Krumova, K.; Cosa, G.; Chapter 1. *Overview of Reactive Oxygen Species.* 1–21.

(75) Lu, Y.-C.; Gallant, B. M.; Kwabi, D. G.; Harding, J. R.; Mitchell, R. R.; Whittingham, M. S.; Shao-Horn, Y. Lithium–Oxygen Batteries: Bridging Mechanistic Understanding and Battery Performance. *Energy Environ. Sci.* **2013**, *6* (3), 750.

(76) Sawyer, D. T.; Chiericato, Glaico.; Angelis, C. T.; Nanni, E. J.; Tsuchiya, Tohru. Effects of Media and Electrode Materials on the Electrochemical Reduction of Dioxygen. *Anal. Chem.* **1982**, *54* (11), 1720–1724.

(77) For an example of photochemical coupling of benzene and pyrazole in 22% yield, see: ref. 50

(78) We found that blending MeCN back into the solvent mixture reduced the activity of the system. This change improved the yields for these easier to oxidize substrates. Additionally, *t*-dodecyl mercaptan was employed as a co-catalyst in place of lithium salts, we suspect this co-catalyst could either function similarly by hydrogen atom transfer to superoxide or through an alternative mechanism. See appendix G for details.

(79) While benzene possesses an oxidation potential of 2.5 V *vs.* SCE, *m*-xylene and mesitylene possess oxidation potentials of 2.05 and 2.1 *vs.* SCE respectively. For further information, see ref. 67.

(80) Typical reaction times were 48–72 h in the electrophotocatalytic approaches reported in ref. 51 and ref. 52

(81) For a recent example using the gas uptake apparatus employed herein, see: Ryan, M. C.; Kim, Y. J.; Gerken, J. B.; Wang, F.; Aristov, M. M.; Martinelli, J. R.; Stahl, S. S. Mechanistic Insights into Copper-Catalyzed Aerobic Oxidative Coupling of N–N Bonds. *Chem. Sci.* **2020**, *11* (4), 1170–1175.

(82) In principle, O_2 can accept between one and four electrons in oxidative processes, see: Stahl, S. S. Palladium Oxidase Catalysis: Selective Oxidation of Organic Chemicals by Direct Dioxygen-Coupled Turnover. *Angew. Chem. Int. Ed.* **2004**, *43* (26), 3400–3420.

(83) Adding $LiClO_4$ could also recover a reaction inhibited by KO_2 (5 mol %) addition. See appendix G for details.

(84) While the expected excited state lifetime of the **PTH** radical cation is <1 ns and likely too short for intermolecular photocatalysis requiring diffusion (based on ref. 45). Pre-association between the catalyst and the arene may be responsible for photochemical activity. However, preliminary UV-Vis data exclude favorable formation of a charge transfer complex (Figure G22–24). Neither endothermic pre-association nor decomposition of **PTH** to a photocatalyst with a longer excited state lifetime can be excluded. Studies are ongoing into the nature of the active catalytic photooxidant.

(85) Catalyst decomposition to an active photocatalyst has been suggested as a mechanistic revision in other conPET systems and cannot be excluded here. For an example, see: Marchini, M.; Gualandi, A.; Mengozzi, L.; Franchi, P.; Lucarini, M.; Cozzi, P. G.; Balzani, V.; Ceroni, P. Mechanistic Insights into Two-Photon-Driven Photocatalysis in Organic Synthesis. *Phys. Chem. Chem. Phys.* **2018**, *20* (12), 8071–8076.

(86) The pK_a of HFIP is 9.3 and the pK_a of H_2O_2 is 11.6.

(87) Li, P.; Deetz, A. M.; Hu, J.; Meyer, G. J.; Hu, K. Chloride Oxidation by One- or Two-Photon Excitation of N-Phenylphenothiazine. *J. Am. Chem. Soc.* **2022**, *144* (38), 17604–17610.

(88) Obertík, R.; Chudoba, J.; Šturala, J.; Tarábek, J.; Ludvíková, L.; Slanina, T.; König, B.; Cibulka, R. Highly Chemoselective Catalytic Photooxidations by Using Solvent as a Sacrificial Electron Acceptor. *Chemistry – A European Journal* **2022**, *28* (67), e202202487.

(89) Li, P.; Liu, R.; Zhao, Z.; Niu, F.; Hu, K. Lignin C–C Bond Cleavage Induced by Consecutive Two-Photon Excitation of a Metal-Free Photocatalyst. *Chem. Commun.* **2023**, *59* (13), 1777–1780.

Appendix A: Supporting Information for Chapter 2 (Electrochemical Synthesis of Allylic Amines from Terminal Alkenes and Secondary Amines)

A1. General Methods and Materials

MeCN, DMF, and DCM were dried by passing through activated alumina columns. Tetrabutylammonium hexafluorophosphate was recrystallized three times from EtOAc prior to use. All liquid amines were distilled from CaH_2 prior to use. Thianthrene was recrystallized from acetone prior to use. Unless otherwise noted, other commercially-available reagents were used as received. Crude mixtures were evaluated by thin-layer chromatography using EMD/Merck silica gel 60 F254 pre-coated plates (0.25 mm) and were visualized by UV, Seebach, and/or $KMnO_4$ staining. Flash chromatography was performed with a Biotage Isolera One automated chromatography system with re-packed silica columns (technical grade silica, pore size 60 Å, 230-400 mesh particle size, 40-63 particle size) or pre-packed Biotage SNAP Ultra and Biotage Sfär Silica HC columns unless otherwise noted. Purified materials were dried in vacuo (0.050 Torr) to remove trace solvent. ^{1}H, ^{13}C, ^{19}F Spectra were taken using a Bruker Avance-400 with a BBFO Probe, a Bruker Avance-500 with a DCH Cryoprobe. NMR data are reported relative to residual $CHCl_3$ (^{1}H, δ = 7.26 ppm), $CDCl_3$ (^{13}C, δ = 77.16 ppm). Data for ^{1}H NMR spectra are reported as follows: chemical shift (δ ppm) (multiplicity, coupling constant (Hz), integration). Multiplicity and qualifier abbreviations are as follows: s = singlet, d = doublet, t = triplet, q = quartet, m = multiplet, br = broad. All NMR yields were determined via reference against an internal standard (dibromomethane or mesitylene for ^{1}H NMR). Mass spectrometry data was collected on a Thermo Scientific Q Exactive Plus Mass Spectrometer and a Waters Acquity^{TM} LCMS.

Abbreviations: Bn—benzyl, Boc—tert-butyl carbamate, *t*-Bu—tert-butyl, DCM—dichloromethane, DIPEA—N,N-Diisopropylethylamine, DMF—dimethyl formamide, EtOAc—ethyl acetate, MeCN—acetonitrile, MeOH—methanol, RVC—reticulated vitreous carbon, Ph—phenyl, TEA—triethylamine, TFA—trifluoroacetic acid.

Electrochemical Methods and Materials

All chronoamperometric and chronopotentiometric measurements were performed at room temperature using a Pine WaveNowXV. Chronoamperometric and chronopotentiometric measurements were carried out in divided cells with RVC (8 × 6 × 6 mm, Ultramet, 80 ppi) as working electrodes affixed to a graphite pencil/silver wire assembly and with nickel foam (1.4 mm x 1.4 mm, MTI Corporation, Surface density: 350g/m^2) as counter electrodes affixed to stainless steel wire (see below). The potentials were measured versus an $Ag/AgNO_3$ (0.01 M in MeCN with 0.1 M n-Bu_4N•PF_6) reference electrode (all electrodes from Pine Research) and externally referenced via the ferrocene/ferrocenium couple. Bulk constant current electrolysis experiments were driven with a Dr. Meter HY3005M-L DC Power Supply or a custom–made low current power supply (see Scheme below) which was externally calibrated with a multimeter using a 10 or 1–Ohm resistor.

Divided cell fabricated in-house. Glass frit purchased from Ace Glass (7176-36). Anode electrode assembled via affixing end of the silver wire (Belden Hook-Up wire, item no. 83005 007100) around the pencil (JuneGold 2B graphite 2 mm) using conductive graphite adhesive (Alfa Aesar, 42465), wrapping in teflon tape to prevent exposure, then piercing RVC with pencil. Solvent exposed electrode surface area (2.1 cm^2) was calculated via manufacturer-supplied surface area/volume ratio measurements. PTFE tubing (Cole-Parmer; 1/32” ID, 1/16” OD, item number EW-06407-41) connects both sides of the divided cell to normalize pressure. Septa inner diameter 16 mm. Stainless steel purchased from Grainger; stainless steel lockwire, 0.025" diameter, item number 16Y043.

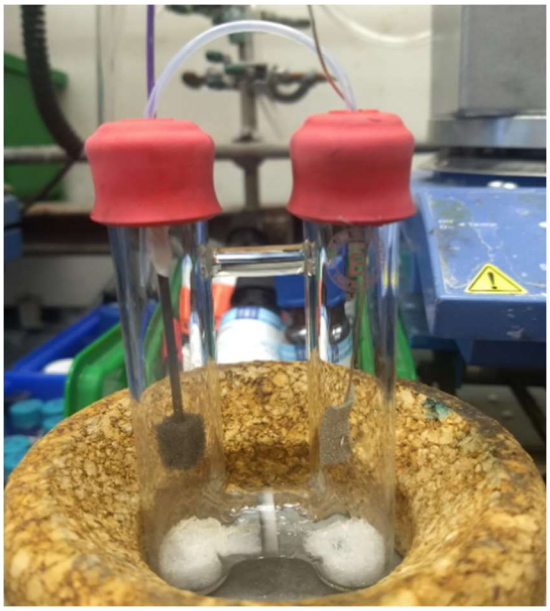

Figure A1. Large divided cell with electrodes.

Low-current Power Supply: Original design and fabrication by Dr. Blaise J. Thompson. Provides an operational range of ±0.01– 14.99 mA, tunable by variable resistor, delivering power to banana socket pair. The power supply is limited to ±15 V for bulk electrolysis and is powered by an 18 V wall wart. Circuitry is housed within an aluminum enclosure. For additional specifications, see: *J. Am. Chem. Soc.* **2020** 142, 2093–2099 and *Nature* **2021** 596, 74–79.

A2. Reaction Optimization

Experimental Procedure – To an oven-dried divided electrochemical cell equipped with magnetic stir bars was added thianthrene (48.7 mg, 0.225 mmol, 1.5 equiv) to the anode compartment and *n*-Bu_4NPF_6 (232 mg, 0.6 mmol) to both compartments. The cell was equipped with two septa containing a stainless steel wire/Ni foam cathode assembly and a pencil/RVC anode assembly connected together with a teflon tubing to equalize pressure. MeCN (3 mL) was added to the cathode and anode compartments. Alkene (0.15 mmol, 1 equiv) was added to the anode compartment. Trifluoroacetic acid (116 µL, 1.5 mmol, 10 equiv) was added to the cathode compartment and both sides of the cell were stirred at ambient temperature and electrolyzed under a constant current of 4.0 mA (5.8 mA/cm^2) for 2.5 h (2.5 F/mol). At completion of electrolysis, the electrode leads were disconnected, septa removed, and the anode RVC was pushed off the pencil into the reaction mixture. Base (1.05 mmol, 7 equiv) was added to the anode compartment followed by amine (either 0.4 mmol, 1 equiv or 0.8 mmol, 2 equiv). To the anode compartment was added a septum pierced with a needle to prevent pressurizing. After pressure equilibration, the needle was removed, and the cathode solution was removed from the cell via pipette. The anode solution was stirred in the cell for 16 h.
For NMR analyses – Following electrolysis, add dibromomethane internal standard to the anodic compartment. Upon substitution reaction completion, take up the solution in an NMR tube. Allylic amine coupling product yield was determined via ^{1}H NMR using dibromomethane as an internal standard.

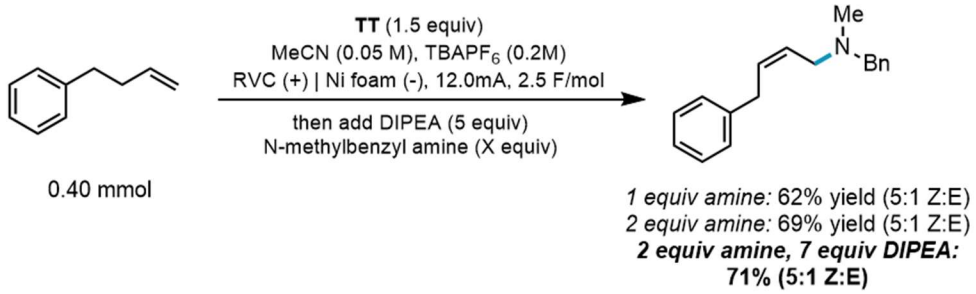

Scheme A1. Amine nucleophile and base equivalent optimization for limiting alkene 0.40 mmol scale reactions.

Internal Alkene Adduct Formation and Attempted Allylic Amination

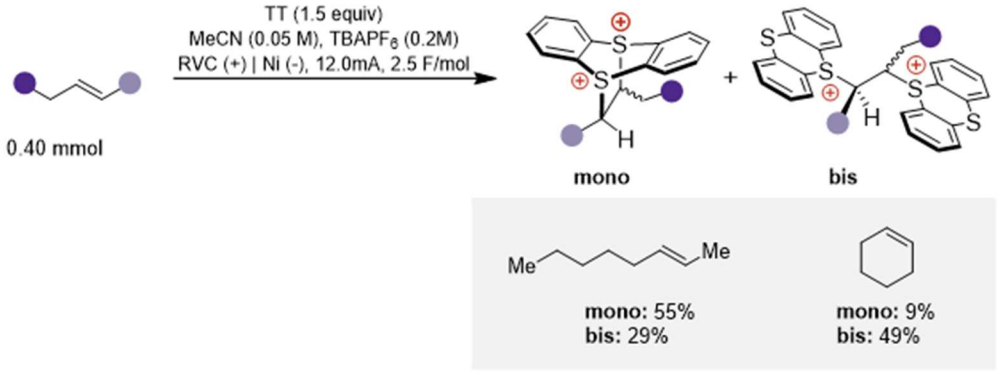

Fig. A2. 1,2-Disubstituted alkenes, which can form both mono- and bis- adduct under electrolysis in the presence of thianthrene, give intractable mixtures of products or eliminate to the internal vinylthianthrenium salt but do not react further when subjected to standard allylic amination conditions. Reactions performed on 0.4 mmol scale.

A3. Substrate Preparations

((but-3-en-1-yloxy)methyl)benzene (A1). To a suspension of NaH (60 % dispersion in mineral oil, 1.49 g, 37.2 mmol, 2 equiv) in DMF (30 mL) at 0°C was added but-3-en-1-ol (1.34 g, 15.0 mmol, 1.60 mL, 1 equiv) under inert atmosphere. After stirring for 45 min, (bromomethyl)benzene (2.5 g, 16.5 mmol, 2.43 mL, 1.1 equiv) was added dropwise. The temperature was slowly increased to room temperature and the reaction was stirred overnight (16 h). The reaction was then quenched with saturated NH_4Cl solution (~30 mL), diluted with water (~80 mL), and extracted with Et_2O (2x ~80 mL). The combined organic layer were washed with brine solution (~50 mL), dried over anhydrous MgSO4, filtered, and concentrated under reduced pressure. The residue was purified via flash column chromatography (EtOAc/hexanes) to give 1.92 g (64% yield) of **A1** as an oil. **^{1}H NMR** (500 MHz, $CDCl_3$) δ 7.39 (m, 4H), 7.32 (ddd, J = 8.7, 4.6, 2.2 Hz, 1H), 5.95 – 5.82 (m, 1H), 5.16 (dq, J = 17.2, 1.9 Hz, 1H), 5.13 – 5.07 (m, 1H), 4.57 (s, 2H), 3.58 (td, J = 6.7, 1.5 Hz, 2H), 2.43 (qd, J = 6.8, 1.6 Hz, 2H); consistent with reported spectra (*J. Am. Chem. Soc.* **2018**, 140, 49, 16976–16981).

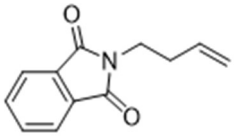

2-(but-3-en-1-yl)isoindoline-1,3-dione (A2). To a mixture of potassium phthalimide (741 mg, 4.0 mmol, 1 equiv) in DMF (8 mL) was added 4-bromo-1-butene (406 µL, 4 mmol, 1 equiv). The reaction mixture was heated to 60 °C and stirred overnight (16 h). At completion, the mixture was cooled to rt and poured into a saturated aqueous NaCl solution (~50 mL). The aqueous layer was extracted with Et2O (3 x 100 mL). The combined organic layers were washed with aqueous 10% LiCl solution (2 x 10 mL), dried over anhydrous MgSO4, filtered, and concentrated under reduced pressure. The residue was purified via flash column chromatography (EtOAc/hexanes) to give 492 mg (61% yield) of **A2** as a solid. **^{1}H NMR** (500 MHz, $CDCl_3$) δ 7.84 (dd, J = 5.4, 3.1 Hz, 2H), 7.71 (dd, J = 5.4, 3.0, 2H), 5.79 (ddt, J = 17.2, 10.2, 6.9 Hz, 1H), 5.07 (dd, J = 17.1, 1.7 Hz, 1H), 5.02 (dd, J = 10.3, 1.7 Hz, 1H), 3.77 (t, J = 7.1 Hz, 2H), 2.45 (q, J = 7.0 Hz, 2H); consistent with reported spectra (*J. Am. Chem. Soc.* **2017**, 139, 12153–12156).

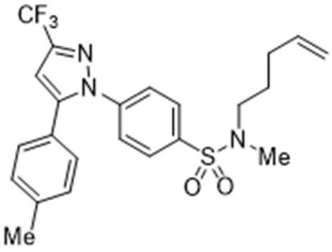

N-methyl-N-(pent-4-en-1-yl)-4-(5-(p-tolyl)-3-(trifluoromethyl)-1H-pyrazol-1-yl)benzenesulfonamide (A3). 4-(3-(p-tolyl)-5-(trifluoromethyl)-3H-2l4-pyrazol-2-yl)benzenesulfonamide (765 mg, 2.0 mmol, 1.0 equiv), 5-bromopent-1-ene (328 mg, 2.2 mmol, 261 µL, 1.1 equiv), K_2CO_3 (553 mg, 4.0 mmol, 2.0 equiv) were combined and placed under an atmosphere of nitrogen. The solids were then dissolved in acetone (2 mL) and reaction mixture was stirred at 60 ºC. Upon completion of the reaction (12 h), the solution was cooled to room temperature, filtered, rinsed with EtOAc, and concentrated under reduced pressure. The residue was purified via flash column chromatography (EtOAc/hexanes) to give 620.5 mg (69% yield) of N-(pent-4-en-1-yl)-4-(3-(p-tolyl)-5-(trifluoromethyl)-3H-2l4-pyrazol-2-yl)benzenesulfonamide as a solid. **^{1}H NMR** (500 MHz, $CDCl_3$) δ 7.86 – 7.82 (m, 2H), 7.51 – 7.43 (m, 2H), 7.20 – 7.15 (m, 2H), 7.13 – 7.08 (m, 2H), 6.74 (s, 1H), 5.71 (ddt, J = 17.0, 10.2, 6.7 Hz, 1H), 5.00 (dq, J = 12.2, 1.5 Hz, 1H), 4.98 – 4.96 (m, 1H), 4.40 (t, J = 6.2 Hz, 1H), 3.03 – 2.91 (m, 2H), 2.38 (s, 3H), 2.17 – 1.96 (m, 2H), 1.65 – 1.53 (m, 2H); consistent with reported spectra (*J. Am. Chem. Soc.* **2021**, 143, 29, 11251–11261).

N-(pent-4-en-1-yl)-4-(3-(p-tolyl)-5-(trifluoromethyl)-3H-2l4-pyrazol-2-yl)benzenesulfonamide (430 mg, 957 µmol, 1.0 equiv) was dissolved in DMF (3.2 mL) and potassium carbonate (264 mg, 1.9 mmol, 2.0 equiv) was added, followed by methyl iodide (149 mg, 1.1 mmol, 65.5 µL, 1.1 equiv). The solution was heated to 50 °C in a vial without a vent and stirred at that temperature overnight (16 h). Upon completion, the reaction mixture was partitioned between 20 mL water and 10 mL EtOAc. The layers were separated, and the aqueous phase was extracted with EtOAc. The combined organic phases were washed 3x with 10% LiCl solution, dried over $MgSO_4$, and concentrated under reduced pressure. The residue was purified via flash column chromatography (EtOAc/hexanes) to give 421.2 mg (95% yield) of **A3** as a solid. **^{1}H NMR** (500 MHz, $CDCl_3$) δ 7.94 – 7.89 (m, 2H), 7.66 – 7.60 (m, 2H), 7.35 – 7.29 (m, 2H), 7.28 – 7.22 (m, 2H), 6.90 (s, 1H), 5.93 (ddt, J = 16.9, 10.2, 6.6 Hz, 1H), 5.19 (dq, J = 17.1, 1.7 Hz, 1H), 5.14 (dq, J = 10.2, 1.4 Hz, 1H), 3.18 – 3.12 (m, 2H), 2.87 (s, 3H), 2.53 (s, 3H), 2.28 – 2.20 (m, 2H), 1.78 (p, J = 7.4 Hz, 2H). **^{13}C NMR** (126 MHz, $CDCl_3$) δ 145.41, 144.26 (q, J = 38.5 Hz), 142.56, 139.95, 137.40, 129.88, 128.85, 128.45, 125.80, 125.73, 121.20 (q, J = 269.1 Hz), 115.65, 106.35, 106.33, 49.81, 34.80, 30.66, 26.94, 21.45. **^{19}F NMR** (377 MHz, $CDCl_3$) δ -62.44. **HRMS** (ESI+) Calc: $[M+H]^+$ ($C_{23}H_{25}F_3N_3O_2S$) 464.1614; measured: 464.1609 = 1.1 ppm difference.

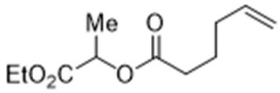

1-ethoxy-1-oxopropan-2-yl hex-5-enoate (A4). A mixture of hex-5-enoic acid (970 mg, 8.5 mmol, 1.00 mL, 1 equiv), N-(3-Dimethylaminopropyl)-N′-ethylcarbodiimide hydrochloride (2.12 g, 11.1 mmol, 1.3 equiv), and 4-(dimethylamino)pyridine (104 mg, 0.85 mmol, 0.1 equiv) in DCM (32 mL) was stirred at 0 °C for 20 min. Ethyl (R)-2-hydroxypropanoate (1.20 g, 10.2 mmol, 1.17 mL, 1.1 equiv) was added and the reaction mixture was allowed to warm to room temperature. At completion as monitored by TLC, the mixture was diluted with DCM and extracted with 1M HCl solution (~80 mL). The organic layer was washed with brine solution (~50 mL), dried over anhydrous MgSO4, filtered, and concentrated under reduced pressure. The residue was purified via flash column chromatography (EtOAc/hexanes) to give 1.17 g (64% yield) of **A4** as an oil. **^{1}H NMR** (500MHz, $CDCl_3$) δ 5.76 (ddt, J = 17.0, 10.2, 6.7 Hz, 1H), 5.04 (q, J = 7.1 Hz, 1H), 5.01 (dq, J = 16.4, 1.6 Hz, 1H), 4.97 (ddt, J = 10.2, 2.1, 1.2 Hz, 1H), 4.18 (qd, J = 7.2, 1.0 Hz, 2H), 2.45 – 2.30 (m, 2H), 2.10 (dtt, J = 7.9, 6.6, 1.4 Hz, 2H), 1.80 – 1.68 (m, 2H), 1.46 (d, J = 7.1 Hz, 3H), 1.25 (t, J = 7.1 Hz, 3H). **^{13}C NMR** (126 MHz, $CDCl_3$) δ 173.02, 170.95, 137.71, 115.51, 68.58, 61.38, 33.29, 33.02, 24.04, 17.01, 14.18. **HRMS** (ESI+) Calc: $[M+H]^+$ ($C_{11}H_{19}O_4$) 215.1278; measured: 215.1275 = 1.3 ppm difference.

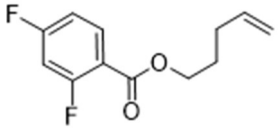

Pent-4-en-1-yl 2,4-difluorobenzoate (A5). A mixture of 2,4-difluorobenzoic acid (1.11 g, 7.0 mmol, 1 equiv), N-(3-Dimethylaminopropyl)-N′-ethylcarbodiimide hydrochloride (1.74 g, 9.1 mmol, 1.3 equiv), and 4-(dimethylamino)pyridine (86 mg, 0.7 mmol, 0.1 equiv) in DCM (28 mL) was stirred at 0 °C for 20 min. Pent-4-en-1-ol (724 mg, 8.4 mmol, 0.87 mL, 1.1 equiv) was added and the reaction mixture was allowed to warm to room temperature. At completion as monitored by TLC, the mixture was diluted with DCM and extracted with 1M HCl solution (~80 mL). The organic layer was washed with brine solution (~50 mL), dried over anhydrous MgSO4, filtered, and concentrated under reduced pressure. The residue was purified via flash column chromatography (EtOAc/hexanes) to give 1.14 g (72% yield) of **A5** as an oil. **^{1}H NMR** (500MHz, $CDCl_3$) δ 7.95 (td, J = 8.5, 6.5 Hz, 1H), 6.91 (dddd, J = 8.7, 7.6, 2.5, 1.0 Hz, 1H), 6.85 (ddd, J = 11.1, 8.9, 2.5 Hz, 1H), 5.82 (ddt, J = 16.9, 10.2, 6.6 Hz, 1H), 5.05 (dq, J = 17.1, 1.7 Hz, 1H), 5.01 – 4.96 (m, 1H), 4.32 (t, J = 6.5 Hz, 2H), 2.24 – 2.15 (m, 2H), 1.84 (dq, J = 8.1, 6.6 Hz, 2H). **^{13}C NMR** (126 MHz, $CDCl_3$) δ 165.74 (dd, J = 256.1, 11.9 Hz), 163.64 (d, J = 4.2 Hz), 162.92 (dd, J = 263.2, 12.6 Hz), 137.43, 133.97 (dd, J = 10.4, 2.4 Hz), 115.51 (dd, J = 10.5, 3.7 Hz), 115.49, 111.60 (dd, J = 21.5, 4.0 Hz), 105.27 (dd, J = 26.2, 25.2 Hz), 64.82, 30.13, 27.87. **^{19}F NMR** (377 MHz, $CDCl_3$) δ -102.21 (d, J = 12.6 Hz), -103.89 (d, J = 12.3 Hz). **HRMS** (ESI+) Calc: $[M+H]^+$ ($C_{12}H_{13}F_2O_2$) 227.0878; measured: 227.0875 = 1.4 ppm difference.

A4. General Experimental Procedures

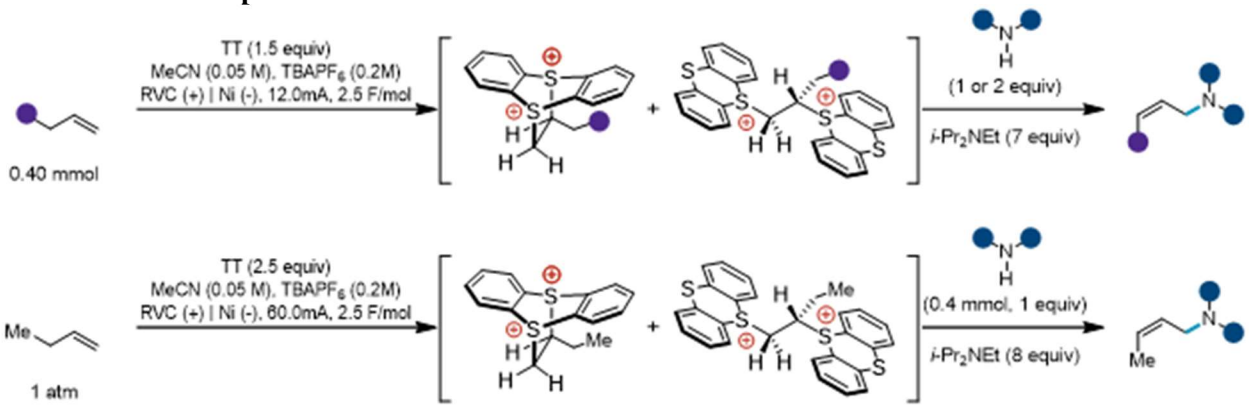

Fig. A3. Limiting amine (bottom, General Procedure B, 1-butene as representative alkene) and limiting alkene (top, General Procedure A) conditions for tertiary allylic amine formation.

CAUTION: Although there is no known toxicology data on these dicationic adducts and no issues were encountered during these experiments, we suspect, based on analogy to other dielectrophiles, that these adducts are extremely toxic. Isolation or storage of the adducts was avoided, and all substitutions were carried out *in situ*.

Note on reproducibility of conditions: undistilled DIPEA was used for substitution reactions. We found distilling both base and amine nucleophile resulted in quantitative conversion of alkene adduct to vinyl thianthrenium with no detected allylic amine product. Addition of 1 equivalent of water to distilled materials can recapitulate reactivity. We hypothesize that the role of water involves quenching of excess thianthrene radical cation. Mechanistic studies are ongoing.

General Procedure A: Limiting Alkene

To an oven-dried divided electrochemical cell equipped with magnetic stir bars was added thianthrene (130 mg, 0.6 mmol, 1.5 equiv) to the anode compartment and *n*-Bu_4NPF_6 (620 mg, 1.6 mmol) to both compartments. The cell was equipped with two septa containing a stainless steel wire/Ni foam cathode assembly and a pencil/RVC anode assembly connected together with a teflon tubing to equalize pressure. MeCN (8 mL) was added to the cathode and anode compartments. Alkene (0.4 mmol, 1 equiv) was added to the anode compartment. Trifluoroacetic acid (308 µL, 4.0 mmol, 10 equiv) was added to the cathode compartment and both sides of the cell were stirred at 30 °C and electrolyzed under a constant current of 12.0 mA (5.8 mA/cm^2) for 2.2 h (2.5 F/mol). Average cell resistance = 0.9 kΩ. At completion of electrolysis, the electrode leads were disconnected, septa removed, and the anode RVC was pushed off the pencil into the reaction mixture. DIPEA (488 µL, 2.8 mmol, 7 equiv) was added to the anode compartment followed by amine (0.8 mmol, 2 equiv). To the anode compartment was added a septum pierced with a needle to prevent pressurizing. After pressure equilibration, the needle was removed, and the cathode solution was removed from the cell via pipette. The anode solution was stirred in the cell for 16 h. At completion, either workup A or workup B was followed to yield the pure allylamine product.

General Procedure B: Limiting Amine

To an oven-dried divided electrochemical cell equipped with magnetic stir bars was added thianthrene (216 mg, 1.0 mmol, 2.5 equiv) to the anode compartment and *n*-Bu_4NPF_6 (310 mg, 0.8 mmol) to both compartments. The cell was equipped with two septa containing a stainless steel wire/Ni foam cathode assembly and a pencil/RVC anode assembly connected together with a teflon tubing to equalize pressure. In a separate 25 mL-round bottom flask, MeCN (8mL) was sparged with a balloon of gaseous alkene for 8 mins. Alkene-saturated MeCN (4mL) was delivered to the cathode and anode compartments via Teflon cannula. Trifluoroacetic acid (460 µL, 6.0 mmol, 15 equiv) was added to the cathode compartment and both

sides of the cell were stirred at ambient temperature and electrolyzed under a constant current of 60.0 mA (29 mA/cm^2) for 45 min (1.7 F/mol **TT**). Average cell resistance = 1.6 kΩ. At completion of electrolysis, the electrode leads were disconnected, septa removed, and the anode RVC was pushed off the pencil into the reaction mixture. DIPEA (560 µL, 3.2 mmol, 8 equiv) was added to the anode compartment followed by amine (0.4 mmol, 1 equiv). To the anode compartment was added a septum pierced with a needle to prevent pressurizing. After pressure equilibration, the needle was removed, and the cathode solution was removed from the cell via pipette. The anode solution was stirred in the cell for 3 h. At completion, two different workup procedures were followed depending on product sensitivity to acid.
Hydrochloride salts of amines (with an additional equivalent of DIPEA) were also used directly for substitution of electrochemically generated dicationic adducts.

Workup A:
The reaction mixture was diluted with ether (100 mL) and 6M HCl (30 mL). The organic layer was washed with 6M HCl (20 mL x 2). The combined aqueous layers were neutralized slowly with NaOH and extracted with DCM (60 mL x 3). The combined organic layers were dried with anhydrous $MgSO_4$, filtered, and concentrated under reduced pressure. The residue was purified via flash column chromatography to yield the pure allylamine product.

Workup B:
The reaction mixture was diluted with DCM (~60 mL) and 1M NaOH (150 mL). The aqueous layer was extracted with DCM (60 mL x 3). The combined organic layers were dried with anhydrous $MgSO_4$, filtered, and concentrated under reduced pressure. The residue was purified via flash column chromatography to yield the pure allylamine product.

Workup C:
The reaction mixture was diluted with DCM (~60 mL) and sat. $NaHCO_3$ (150 mL). The aqueous layer was extracted with DCM (60 mL x 3). The combined organic layers were dried with anhydrous $MgSO_4$, filtered, and concentrated under reduced pressure. The residue was purified via flash column chromatography to yield the pure allylamine product.

General Procedure C: Limiting Alkene NMR Yield
Following General Procedure B, but with the following modification: following stirring with *N*-benzylmethylamine and DIPEA for 16 h, allylamine product yield was determined via ^{1}H NMR using mesitylene or dibromomethane as an internal standard.

General Procedure D: Limiting Amine NMR Yield
Following General Procedure A, but with the following modification: following stirring with amine and DIPEA for 3 h, allylic amine product yield was determined via NMR using dibromomethane as an internal standard.

Determination *Z:E* Selectivity – reported selectivity ratios were determined by ^{1}H NMR analysis of isolated or partially isolated compounds. See details below regarding assignment of major stereoisomer.

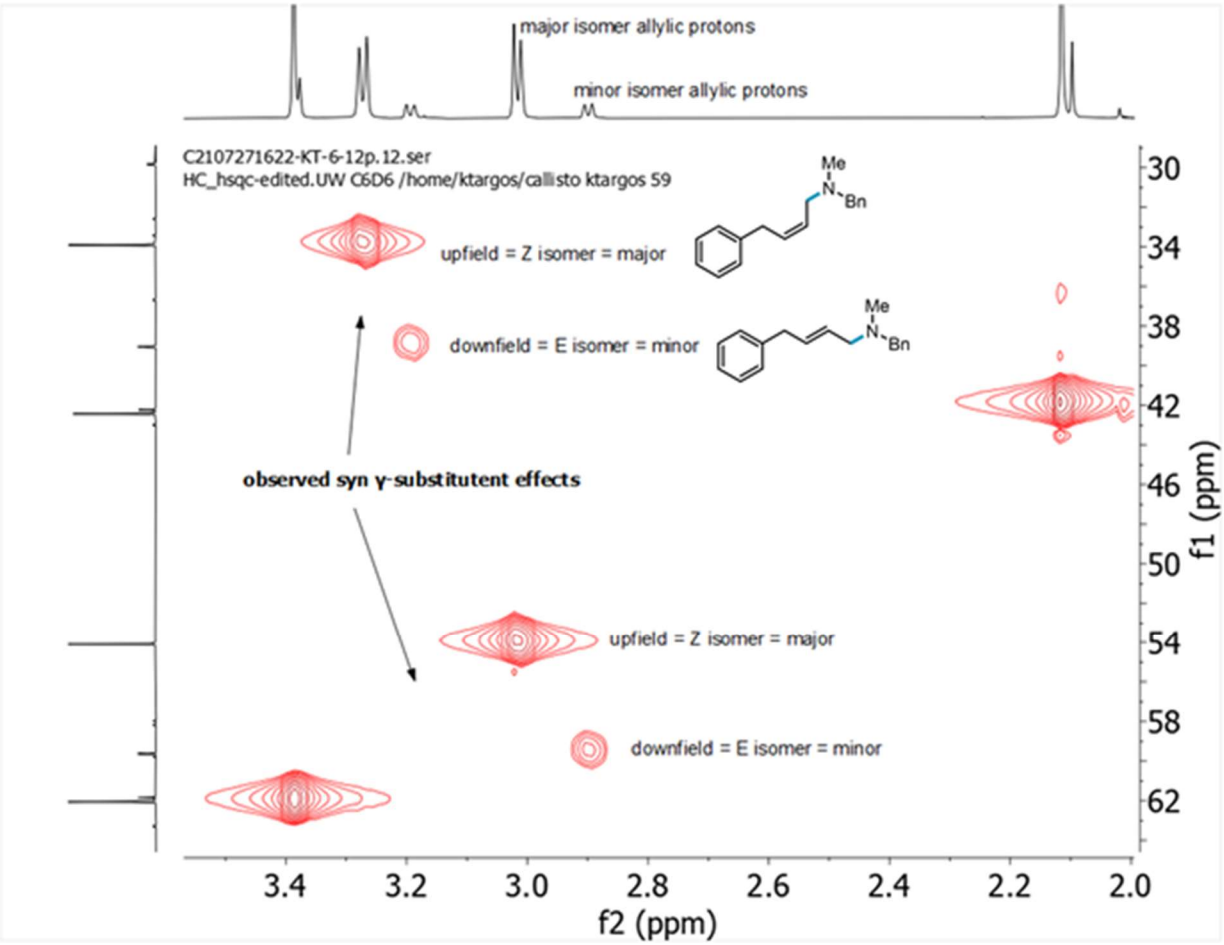

Fig. A4. Assignment was validated by ^{13}C-^{1}H NMR experiments using the correlation of the allylic protons to allylic carbon signal for which syn γ-substitutent effects of allylic carbon signals from *cis* isomers of alkenes are lower frequency (upfield). For a theoretical analysis see: Kleinpeter, E.; Seidl, P. R. *J. Phys. Org. Chem.* **2005**, 18, 272.

Additionally, authentic (Z)-N-benzyl-N-methylnon-2-en-1-amine was synthesized following literature precedent (*J. Am. Chem. Soc.* 2001, *123* (39), 9525–9534.).

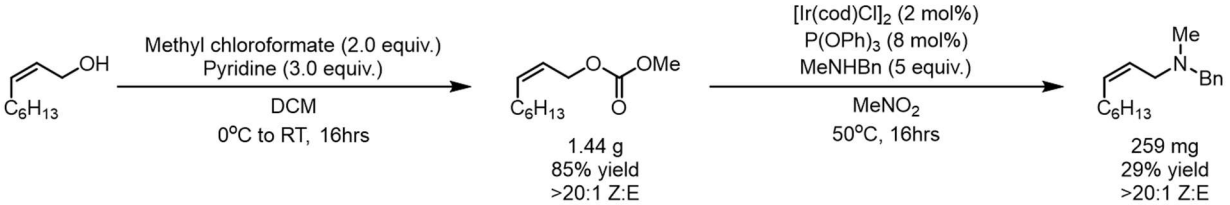

The synthesized authentic sample was doped into a crude reaction mixture of thianthrene promoted allylic amination coupling nonene and N-methylbenzylamine. Via ^{1}H NMR, observation of growth of major allylic signal confirms (Z)-allylic amine as major stereoisomer formed (see Figure **A5**).

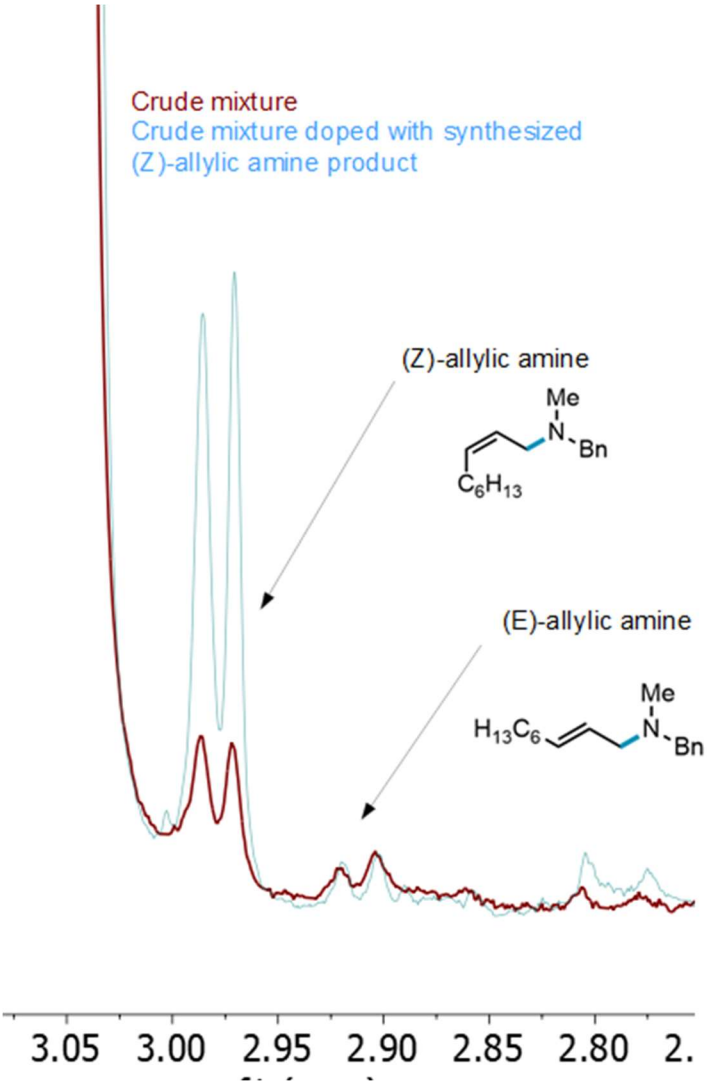

Fig. A5. Doping experiment to confirm *Z*-selective allylic amination.

A5. Allylamine Product Isolation and Characterization

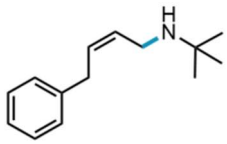

(Z)-N-(tert-butyl)-4-phenylbut-2-en-1-amine (2.3). Prepared from but-3-en-1-ylbenzene and tert-butylamine; 62% NMR yield (3:1 Z:E) obtained by following General Procedure C (using excess *tert*-butylamine in place of DIPEA). **HRMS** (ESI+) Calc: $[M+H]^+$ ($C_{14}H_{21}N$) 204.1747; measured: 204.1744 = 1.5 ppm difference.

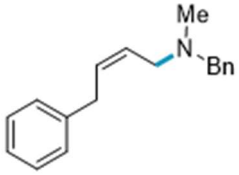

(Z)-N-benzyl-N-methyl-4-phenylbut-2-en-1-amine (2.4). Prepared from but-3-en-1-ylbenzene and N-methyl-1-phenylmethanamine; 67.8 mg (67% yield, 5:1 Z:E) obtained as an oil following General Procedure A and Workup B. **^{1}H NMR** (500 MHz, $CDCl_3$) δ 7.29 – 7.14 (m, 7H), 7.14 – 7.04 (m, 3H), 5.72 – 5.64 (m, 1H), 5.64 – 5.57 (m, 1H), 3.44 (s, 2H), 3.33 (d, J = 7.2 Hz, 2H), 3.07 (dd, J = 6.6, 1.4 Hz, 2H), 2.15 (s, 3H). Distinct minor *(E)*-isomer signals observed at δ 5.57 – 5.49 (m, 1H), 3.40 (s, 2H), 3.30 (d, J = 6.8 Hz, 2H), 2.92 (dd, J = 6.6, 1.2 Hz, 2H), 2.10 (s, 3H). **^{13}C NMR** (126 MHz, $CDCl_3$) δ 140.79, 139.19, 131.17, 129.21, 128.57, 128.44, 128.35, 128.10, 127.09, 126.08, 62.06, 54.09, 42.42, 33.90. Distinct minor *(E)*-isomer signals observed at δ 140.57, 139.21, 132.65, 128.97, 128.64, 128.53, 128.32, 127.04, 126.13, 61.85, 59.62, 42.22, 39.04. **HRMS** (ESI+) Calc: $[M+H]^+$ ($C_{18}H_{22}N$) 252.1747; measured: 252.1744 = 1.1 ppm difference.

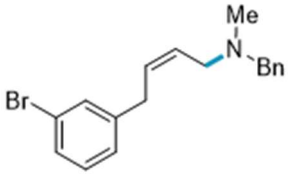

(Z)-N-benzyl-4-(3-bromophenyl)-N-methylbut-2-en-1-amine (2.7). Prepared from 1-bromo-3-(but-3-en-1-yl)benzene and N-methyl-1-phenylmethanamine; 95.9 mg (73% yield, 5:1 Z:E) obtained as an oil following General Procedure A and Workup A. **^{1}H NMR** (500 MHz, CDCl3) δ 7.28 – 7.23 (m, 6H), 7.19 (td, J = 5.8, 5.1, 2.8 Hz, 1H), 7.10 – 7.00 (m, 2H), 5.70 – 5.60 (m, 2H), 3.45 (s, 2H), 3.32 (d, J = 5.7 Hz, 2H), 3.06 (d, J = 5.2 Hz, 2H), 2.17 (s, 3H). Distinct minor *(E)*-isomer signals observed at δ 5.59 – 5.52 (m, 2H), 3.42 (s, 2H), 3.28 (d, J = 6.6 Hz, 2H), 2.95 (dd, J = 6.5, 1.2 Hz, 2H), 2.13 (s, 3H). **^{13}C NMR** (126 MHz, $CDCl_3$) δ 13C NMR (126 MHz, CDCl3) δ 143.12, 139.08, 131.54, 130.22, 130.11, 129.23, 129.22, 128.85, 128.39, 127.16, 127.10, 122.66, 62.11, 54.00, 42.45, 33.49. Distinct minor *(E)*-isomer signals observed at δ 142.92, 139.10, 131.73, 131.67, 130.09, 129.76, 129.29, 128.36, 127.32, 122.63, 61.90, 59.49, 42.25, 38.61. **HRMS** (ESI+) Calc: $[M+H]^+$ ($C_{18}H_{21}BrN$) 330.0852; measured: 330.0847 = 1.5 ppm difference.

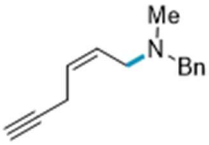

(Z)-N-benzyl-N-methylhex-2-en-5-yn-1-amine (2.8). Prepared from hex-1-en-5-yne and N-methyl-1-phenylmethanamine; 48.0 mg (60% yield, >20:1 Z:E) obtained as an oil following General Procedure A and Workup A. **^{1}H NMR** (500 MHz, $CDCl_3$) δ 7.37 – 7.30 (m, 4H), 7.29 – 7.22 (m, 1H), 5.73 – 5.53 (m, 2H), 3.51 (s, 2H), 3.06 (d, J = 6.2 Hz, 2H), 2.98 (dd, J = 6.0, 2.4 Hz, 2H), 2.22 (s, 3H), 2.00 (t, J = 2.7 Hz, 1H). Distinct minor *(E)*-isomer signals observed at δ 5.95 – 5.80 (m, 2H), 2.21 (s, 3H). **^{13}C NMR** (126 MHz, $CDCl_3$) δ 139.02, 129.27, 129.20, 128.37, 127.15, 126.67, 82.44, 68.41, 61.97, 53.79, 42.37, 17.34. Distinct minor *(E)*-isomer signals observed at δ 129.70 128.34, 70.30, 61.86, 59.20, 42.22. **HRMS** (ESI+) Calc: $[M+H]^+$ ($C_{14}H_{18}N$) 200.1434 measured: 200.1433 = 0.5 ppm difference.

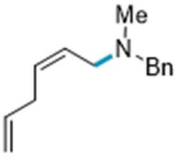

(Z)-N-benzyl-N-methylhexa-2,5-dien-1-amine (2.9). Prepared from hexa-1,5-diene and N-methyl-1-phenylmethanamine; 48.5 mg (69% yield, 5:1 Z:E) obtained as an oil following General Procedure A and Workup A. **^{1}H NMR** (500 MHz, $CDCl_3$) δ 7.31 – 7.26 (m, 4H), 7.24 – 7.17 (m, 1H), 5.86 – 5.71 (m, 1H), 5.00 (dq, J = 17.2, 1.8 Hz, 1H), 4.95 (dq, J = 10.2, 1.7 Hz, 1H), 5.08 – 4.85 (m, 2H), 3.45 (s, 2H), 3.02 (d, J = 6.0 Hz, 2H), 2.79 (t, J = 6.3 Hz, 2H), 2.16 (s, 3H). Distinct minor *(E)*-isomer signals observed at δ 2.97 (d, J = 5.8 Hz, 2H), 2.15 (s, 3H). **^{13}C NMR** (126 MHz, $CDCl_3$) δ 139.21, 136.60, 129.80, 129.21, 128.32, 128.31, 128.22, 128.17, 127.06, 115.03, 61.97, 53.97, 42.35, 31.89. Distinct minor *(E)*-isomer signals observed at δ 139.25, 136.92, 131.50, 128.64, 127.02, 115.34, 61.81, 59.70, 42.16, 36.67. **HRMS** (ESI+) Calc: $[M+H]^+$ ($C_{14}H_{20}N$) 202.1590; measured: 202.1590 = <0.1 ppm difference.

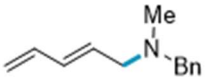

(E)-N-benzyl-N-methylpenta-2,4-dien-1-amine (2.10). Prepared from penta-1,4-diene and N-methyl-1-phenylmethanamine; 57% NMR yield (1:3 Z:E) obtained by following General Procedure C and Workup B. Peaks assigned partial isolation and ^{1}H-^{1}H COSY NMR analysis; stereochemistry determined using vinyl proton J_{HH} coupling values and ^{13}C-^{1}H HSQC NMR analysis. **HRMS** (ESI+) Calc: $[M+H]^+$ ($C_1H_{18}N$) 188.1434; measured: 188.1432 = 1.1 ppm difference.

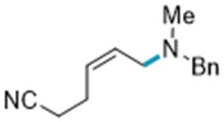

(Z)-6-(benzyl(methyl)amino)hex-4-enenitrile (2.11). Prepared from hex-5-enenitrile and N-methyl-1-phenylmethanamine; 66.0 mg (77% yield, 3:1 Z:E) obtained as an oil following General Procedure A and Workup B. **^{1}H NMR** (500 MHz, $CDCl_3$) δ 7.33 – 7.27 (m, 4H), 7.26 – 7.21 (m, 1H), 5.76 – 5.64 (m, 1H), 5.64 – 5.49 (m, 1H), 3.48 (s, 2H), 3.03 (dd, J = 6.9, 1.6 Hz, 2H), 2.41 – 2.29 (m, 4H), 2.19 (s, 3H). Distinct minor *(E)*-isomer signals observed at δ 3.02 – 2.98 (m, 2H), 2.18 (s, 3H). **^{13}C NMR** (126 MHz, $CDCl_3$) δ 138.90, 130.80, 129.11, 128.34, 128.11, 127.15, 119.29, 62.06, 53.78, 42.36, 23.62, 17.43. Distinct minor *(E)*-isomer signals observed at δ 138.96, 131.08, 129.12, 128.31, 127.07, 61.84, 59.21, 42.17, 28.26, 17.50. **HRMS** (ESI+) Calc: $[M+H]^+$ ($C_{14}H_{19}N_2$) 215.1543 measured: 215.1541 = 0.8 ppm difference.

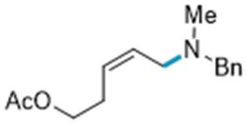

(Z)-5-(benzyl(methyl)amino)pent-3-en-1-yl acetate (2.12). Prepared from pent-4-en-1-yl acetate and N-methyl-1-phenylmethanamine; 65.7 mg (66% yield, 4:1 Z:E) obtained as an oil following General Procedure A and Workup B. **^{1}H NMR** (500 MHz, $CDCl_3$) δ 7.30 – 7.23 (m, 4H), 7.23 – 7.18 (m, 1H), 5.69 – 5.60 (m, 1H), 5.57 – 5.46 (m, 1H), 4.03 (t, J = 6.9 Hz, 2H), 3.45 (s, 2H), 3.01 (dd, J = 6.8, 1.6 Hz, 2H), 2.45 – 2.30 (m, 2H), 2.15 (s, 3H), 1.98 (s, 3H). Distinct minor *(E)*-isomer signals observed at δ 4.07 (t, J = 6.9 Hz, 2H), 3.44 (s, 2H), 2.98 – 2.92 (m, 2H), 2.13 (s, 3H). **^{13}C NMR** (126 MHz, $CDCl_3$) δ 171.12, 139.08, 130.02, 129.15, 128.32, 127.64, 127.08, 63.79, 61.97, 54.03, 42.29, 27.23, 21.02. Distinct minor *(E)*-isomer signals observed at δ 130.38, 129.02, 128.30, 127.04, 63.84, 61.71, 59.56, 42.09, 31.89, 23.69, 19.67. **HRMS** (ESI+) Calc: $[M+H]^+$ ($C_{15}H_{22}NO_2$) 248.1645 measured: 248.1643 = 0.8 ppm difference.

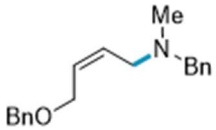

(Z)-N-benzyl-4-(benzyloxy)-N-methylbut-2-en-1-amine (2.13). Prepared from ((but-3-en-1-yloxy)methyl)benzene (**S1**) and N-methyl-1-phenylmethanamine; 58.5 mg (52% yield, 2:1 Z:E) obtained as an oil following General Procedure A and Workup B. **^{1}H NMR** (500 MHz, $CDCl_3$) δ 7.43 – 7.23 (m, 10H), 5.89 – 5.73 (m, 2H), 4.52 (s, 2H), 4.10 (d, J = 5.4 Hz, 2H), 3.49 (s, 2H), 3.05 (d, J = 5.7 Hz, 2H), 2.21 (s, 3H). Distinct minor *(E)*-isomer signals observed at δ 4.53 (s, 2H), 4.05 (d, J = 5.2 Hz, 2H), 3.52 (s, 2H), 3.07 (d, J = 5.8 Hz, 2H), 2.22 (s, 3H). **^{13}C NMR** (126 MHz, $CDCl_3$) δ 138.91, 138.30, 130.48, 129.67, 129.10, 128.43, 128.26, 127.80, 127.66, 127.05, 72.31, 65.90, 61.88, 54.06, 42.24. Distinct minor *(E)*-isomer signals observed at δ 139.00, 138.37, 131.15, 129.67, 129.16, 129.08, 128.41, 127.78, 127.61, 127.00, 72.07, 70.46, 61.79, 59.19, 42.19. **HRMS** (ESI+) Calc: $[M+H]^+$ ($C_{19}H_{24}NO$) 282.1852 measured: 282.1852 = <0.1 ppm difference.

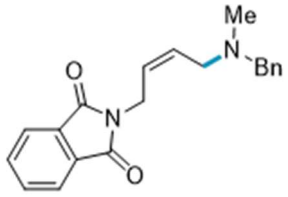

(Z)-2-(4-(benzyl(methyl)amino)but-2-en-1-yl)isoindoline-1,3-dione (2.14). Prepared from 2-(but-3-en-1-yl)isoindoline-1,3-dione (**A2**) and N-methyl-1-phenylmethanamine; 63% NMR yield (2:1 Z:E) obtained by following General Procedure C and Workup B. Peaks assigned by analogy to **2.13**.

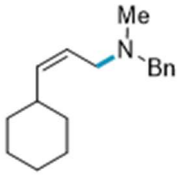

(Z)-N-benzyl-3-cyclohexyl-N-methylprop-2-en-1-amine (2.15). Prepared from allylcyclohexane and N-methyl-1-phenylmethanamine; 56.8 mg (58% yield, 2:1 Z:E) obtained as an oil following General Procedure A and Workup A. **^{1}H NMR** (500 MHz, $CDCl_3$) δ 7.32 – 7.20 (m, 4H), 7.20 – 7.14 (m, 1H), 5.40 – 5.28 (m, 2H), 3.42 (s, 2H), 2.98 (d, J = 5.7 Hz, 2H), 2.22 – 2.15 (m, 1H), 2.13 (s, 3H), 1.63 (ddt, J = 12.9, 6.8, 3.2 Hz, 2H), 1.59 – 1.49 (m, 2H), 1.25 – 1.14 (m, 3H), 1.13 – 1.05 (m, 1H), 1.05 – 0.93 (m, 2H). Distinct minor *(E)*-isomer signals observed at δ 5.56 – 5.40 (m, 2H), 3.41 (s, 2H), 2.90 (d, J = 6.3 Hz, 2H), 2.10 (s, 3H). **^{13}C NMR** (126 MHz, $CDCl_3$, mixture of major and minor stereoisomers) δ 140.40, 139.13,

138.99, 129.21, 129.14, 128.21, 128.20, 126.95, 126.93, 124.75, 124.29, 61.74, 61.48, 59.78, 54.15, 42.20, 41.92, 40.55, 36.55, 33.16, 33.01, 26.22, 26.06, 26.03, 25.89. **HRMS** (ESI+) Calc: $[M+H]^+$ ($C_{17}H_{26}N$) 244.2060 measured: 244.2058 = 0.7 ppm difference.

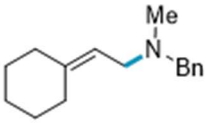

N-benzyl-2-cyclohexylidene-N-methylethan-1-amine (2.16). Prepared from vinylcyclohexane and N-methyl-1-phenylmethanamine; 48.4 mg (53% yield) obtained as an oil following a modified General Procedure A (4.0 mA instead of 12.0 mA current, and add 2 equiv of TFA to the anodic chamber) and Workup B. **^{1}H NMR** (500 MHz, $CDCl_3$) δ 7.36 – 7.27 (m, 4H), 7.27 – 7.22 (m, 1H), 5.25 (tt, J = 7.1, 1.2 Hz, 1H), 3.49 (s, 2H), 3.00 (d, J = 7.1 Hz, 2H), 2.18 (s, 3H), 2.15 (ddd, J = 14.7, 7.3, 3.3 Hz, 4H), 1.67 – 1.46 (m, 6H). **^{13}C NMR** (126 MHz, $CDCl_3$) δ 143.24, 139.39, 129.13, 128.17, 126.85, 118.39, 61.81, 54.02, 42.12, 37.35, 28.97, 28.67, 27.70, 26.86. **HRMS** (ESI+) Calc: $[M+H]^+$ ($C_{16}H_{24}N$) 230.1903 measured: 230.1901 = 1.0 ppm difference.

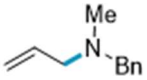

N-benzyl-N-methylprop-2-en-1-amine (2.17). Prepared from propene and N-methyl-1-phenylmethanamine; 47.9 mg (74% yield) obtained as an oil following General Procedure B and Workup B. **^{1}H NMR** (500 MHz, $CDCl_3$) δ 7.37 – 7.30 (m, 4H), 7.25 (m, J = 5.4, 4.2, 3.6 Hz, 1H), 5.92 (ddt, J = 16.8, 10.2, 6.4 Hz, 1H), 5.21 (m, 1H), 5.16 (ddt, J = 10.2, 2.2, 1.2 Hz, 1H), 3.50 (s, 2H), 3.04 (d, J = 6.5 Hz, 1H), 2.20 (s, 3H). **^{13}C NMR** (126 MHz, $CDCl_3$) δ 139.18, 136.09, 129.21, 128.35, 127.08, 117.59, 61.82, 60.68, 42.22. **HRMS** (ESI+) Calc: $[M+H]^+$ ($C_{11}H_{15}N$) 162.1277; measured: 162.1275 = 1.2 ppm difference.

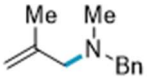

N-benzyl-N,2-dimethylprop-2-en-1-amine (2.18). Prepared from isobutene and N-methyl-1-phenylmethanamine; 43.3 mg (62% yield) obtained as an oil following General Procedure B and Workup B. **^{1}H NMR** (500 MHz, $CDCl_3$) δ 7.37 – 7.29 (m, 4H), 7.28 – 7.21 (m, 1H), 4.93 (dd, J = 2.3, 1.1 Hz, 1H), 4.90 – 4.82 (m, 1H), 3.45 (s, 2H), 2.90 (s, 2H), 2.14 (s, 3H), 1.79 (s, 3H). **^{13}C NMR** (126 MHz, $CDCl_3$) δ 143.82, 139.62, 128.82, 128.17, 126.80, 112.69, 64.62, 61.75, 42.24, 20.73. **HRMS** (ESI+) Calc: $[M+H]^+$ ($C_{12}H_{18}N$) 176.1434; measured: 176.1434 = <0.1 ppm difference.

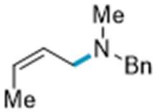

(Z)-*N*-Benzyl-*N*-methyl-1-buten-1-ylamine (2.19). Prepared from butene and N-methyl-1-phenylmethanamine; 47.9 mg (68% yield, 12:1 Z:E) obtained as an oil following General Procedure B and Workup A. **^{1}H NMR** (500 MHz, $CDCl_3$) δ 7.27 – 7.22 (m, 4H), 7.34 – 7.28 (m, 4H), 5.69 – 5.53 (m, 2H), 3.50 (s, 3H), 3.05 (dt, J = 6.7, 1.2 Hz, 2H), 2.20 (s, 3H), 1.66 – 1.62 (m, 3H). Distinct minor *(E)*-isomer signals observed at δ 3.48 (s, 3H), 2.97 (dd, J = 6.4, 1.31 Hz, 2H), 2.17 (s, 3H), 1.70 – 1.72 (m, 3H). **^{13}C NMR** (126 MHz, $CDCl_3$) δ 139.24, 129.27, 128.32, 127.73, 127.13, 127.05, 61.94, 53.72, 42.29, 13.27. Distinct minor *(E)*-isomer signals observed at δ 135.71, 128.86, 128.83, 128.52, 127.80, 127.59.83, 01, 61.76, 42.11, 17.96. **HRMS** (ESI+) Calc: $[M+H]^+$ ($C_{12}H_{17}N$) 176.1434; measured: 176.1433 = 0.6 ppm difference.

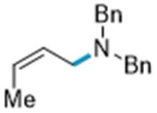

(Z)-N,N-dibenzylbut-2-en-1-amine (2.20). Prepared from butene and dibenzylamine; 71.6 mg (71% yield, 10:1 Z:E) obtained as an oil following General Procedure B and Workup A. **^{1}H NMR** (500 MHz, $CDCl_3$) δ 7.40 (d, J = 6.6 Hz, 4H), 7.33 (t, J = 7.6 Hz, 4H), 7.25 (ddt, J = 8.8, 6.7, 1.5 Hz, 2H), 5.69 – 5.58 (m, 2H), 3.59 (s, 4H), 3.10 (d, J = 6.2 Hz, 2H), 1.60 (dd, J = 6.2, 1.2 Hz, 3H). Distinctive minor *(E)*-isomer signals observed at δ 3.57 (s, 4H), 3.03 (d, J = 6.2 Hz, 2H), 1.72 (dd, J = 5.9, 1.1 Hz, 3H). **^{13}C NMR** (126 MHz, $CDCl_3$) δ 139.96, 128.96, 128.27, 127.91, 127.08, 126.89, 58.09, 49.783 13.33. Distinctive minor *(E)*-isomer signals observed at δ 140.03, 128.91, 126.85, 57.80, 55.63, 18.02. **HRMS** (ESI+) Calc: $[M+H]^+$ ($C_{18}H_{21}N$) 252.1747; measured: 252.1744 = 1.2 ppm difference.

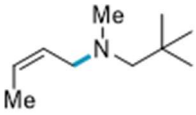

(Z)-N-methyl-N-neopentylbut-2-en-1-amine (2.21). Prepared from butene and N,2,2-trimethylpropan-1-amine; 38% NMR yield (10:1 Z:E) obtained by following General Procedure D and Workup A. **HRMS** (ESI+) Calc: $[M+H]^+$ ($C_{10}H_{21}N$) 156.1747; measured: 156.1746 = 0.6 ppm difference.

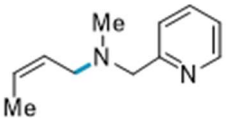

(Z)-N-methyl-N-(pyridin-2-ylmethyl)but-2-en-1-amine (2.22). Prepared from butene and N-methyl-1-(pyridin-2-yl)methanamine; 62% NMR yield (9:1 Z:E) obtained by following General Procedure D and Workup A. **HRMS** (ESI+) Calc: $[M+H]^+$ ($C_{11}H_{16}N_2$) 177.1386; measured: 177.1385 = 0.6 ppm difference.

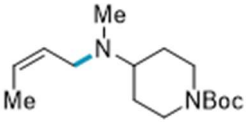

tert-butyl (Z)-4-(but-2-en-1-yl(methyl)amino)piperidine-1-carboxylate (2.23). Prepared from butene and tert-butyl 4-(methylamino)piperidine-1-carboxylate; 56% NMR yield (9:1 Z:E) obtained following General Procedure D and Workup B. **HRMS** (ESI+) Calc: $[M+H]^+$ ($C_{15}H_{28}N_2O_2$) 269.2224; measured: 269.2219 = 1.9 ppm difference.

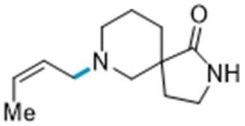

(Z)-8-(but-2-en-1-yl)-1,8-diazaspiro[4.5]decan-2-one (2.24). Prepared from butene and 1,8-diazaspiro[4.5]decan-2-one HCl salt; 71.1 mg (85% yield, >20:1 Z:E) obtained as an oil following General Procedure B and Workup C. **^{1}H NMR** (500 MHz, $CDCl_3$) δ 7.20 (br s, 1H), 5.61 – 5.53 (m, 1H), 5.43 – 5.36 (m, 1H), 3.27 (dt, J = 8.8, 5.6 Hz, 2H), 3.01 – 2.91 (m, 2H), 2.84 (d, J = 10.3 Hz, 1H), 2.59 (d, J = 11.1 Hz, 1H), 2.25 (ddd, J = 13.4, 8.0, 5.7 Hz, 1H), 2.05 (d, J = 11.1 Hz, 1H), 2.01 – 1.92 (m, 2H), 1.65 – 1.54 (m, 6H), 1.48 – 1.42 (m, 1H). **^{13}C NMR** (126 MHz, $CDCl_3$) δ 181.71, 127.38, 126.91, 58.58, 55.09, 54.00, 53.48, 44.60, 39.27, 31.82, 30.71, 22.33, 13.19. **HRMS** (ESI+) Calc: $[M+H]^+$ ($C_{12}H_{20}N_2O$) 209.1648; measured: 209.1645 = 1.4 ppm difference.

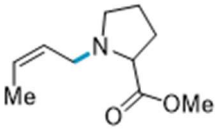

Methyl (Z)-but-2-en-1-yl-L-prolinate (2.25). Prepared from butene and methyl L-prolinate; 45.3 mg (62% yield, 10:1 Z:E) obtained as an oil following General Procedure B and Workup C. **^{1}H NMR** (500 MHz, Acetone-d_6) δ 5.48 – 5.28 (m, 2H), 3.50 (s, 3H), 3.24 – 3.14 (m, 1H), 3.06 (dd, J = 8.9, 5.6 Hz, 1H), 3.02 – 2.97 (m, 1H), 2.87 (ddd, J = 8.7, 7.3, 3.7 Hz, 1H), 2.28 (dt, J = 8.7, 7.7 Hz, 1H), 1.98 – 1.85 (m, 3H), 1.82 – 1.55 (m, 3H), 1.55 – 1.41 (m, 3H). Distinctive minor *(E)*-isomer signals observed at δ 3.49 (s, 3H). **^{13}C NMR** (126 MHz, $CDCl_3$) δ 174.71, 128.54, 126.78, 65.43, 58.52, 53.56, 51.53, 50.47, 23.87, 13.12. Distinctive minor *(E)*-isomer signals observed at δ 129.72, 128.07, 65.35, 56.72, 51.50, 29.80, 17.81. **HRMS** (ESI+) Calc: $[M+H]^+$ ($C_{10}H_{17}NO_2$) 184.1332; measured: 184.1331; 0.5 ppm difference.

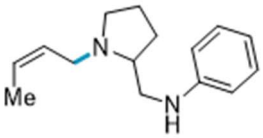

(Z)-N-((1-(but-2-en-1-yl)pyrrolidin-2-yl)methyl)aniline (2.26). Prepared from butene and (S)-N-(pyrrolidin-2-ylmethyl)aniline; 66.8 mg (73% yield, >20:1 Z:E) obtained as an oil following General Procedure B and Workup C. **^{1}H NMR** (500 MHz, $CDCl_3$) δ 7.25 – 7.15 (m, 2H), 6.72 (tt, J = 7.3, 1.1 Hz, 1H), 6.68 – 6.58 (m, 2H), 5.75 – 5.51 (m, 2H), 4.27 (s, 1H), 3.41 (dd, J = 13.7, 5.9 Hz, 0H), 3.30 – 3.11 (m, 3H), 3.02 (dd, J = 13.6, 7.2 Hz, 1H), 2.76 (dtd, J = 8.9, 5.4, 3.0 Hz, 1H), 2.39 – 2.25 (m, 1H), 2.06 – 1.88 (m, 1H), 1.87 – 1.74 (m, 3H), 1.71 – 1.64 (m, 3H). **^{13}C NMR** (126 MHz, $CDCl_3$) δ 148.97, 129.36, 127.57, 126.61, 117.01, 112.86, 62.61, 54.43, 50.24, 45.46, 28.83, 22.90, 13.21. **HRMS** (ESI+) Calc: $[M+H]^+$ ($C_{15}H_{22}N_2$) 231.1856; measured: 231.1853; 1.3 ppm difference.

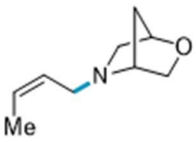

(1R,4R)-5-((Z)-but-2-en-1-yl)-2-oxa-5-azabicyclo[2.2.1]heptane (2.27). Prepared from butene and (1R,4R)-2-oxa-5-azabicyclo[2.2.1]heptane HCl salt; 32.4 mg (53% yield, 9:1 Z:E) obtained as an oil following General Procedure B and Workup B. **^{1}H NMR** (500 MHz, Acetone-d_6) δ 6.06 – 5.98 (m, 1H), 5.78 – 5.68 (m, 1H), 4.76 (t, J = 2.1 Hz, 1H), 4.59 (t, J = 2.3 Hz, 1H), 4.30 (dd, J = 10.0, 1.1 Hz, 1H), 4.18 (dd, J = 13.8, 7.3 Hz, 1H), 4.02 (dd, J = 13.7, 7.3 Hz, 1H), 3.89 (dd, J = 10.0, 2.0 Hz, 1H), 3.48 – 3.39 (m, 1H), 2.50 (d, *J* = 11.9 Hz, 2H), 2.22 (dt, J = 11.9, 2.6 Hz, 1H), 1.78 (dd, J = 7.0, 1.8 Hz, 3H). Distinct minor *(E)*-isomer signals observed at δ 2.43 (d, *J* = 12.1 Hz, 2H). **^{13}C NMR** (126 MHz, $CDCl_3$) δ 135.21, 127.94, 118.52, 114.09, 74.72, 63.79, 63.73, 55.61, 13.52. Distinct minor *(E)*-isomer signals observed at δ 119.49, 61.75, 56.12, 12.58. **HRMS** (ESI+) Calc: $[M+H]^+$ ($C_9H_{16}NO$) 154.1226; measured: 154.1226 = <0.1 ppm difference.

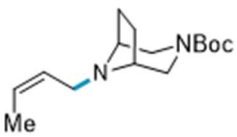

***tert*-butyl (1R,5S)-8-((Z)-but-2-en-1-yl)-3,8-diazabicyclo[3.2.1]octane-3-carboxylate (2.28).** Prepared from butene and *tert*-butyl (1R,5S)-3,8-diazabicyclo[3.2.1]octane-3-carboxylate; 85.6 mg (80% yield, 12:1 Z:E) obtained as an oil following General Procedure B and Workup B. **^{1}H NMR** (500 MHz, $CDCl_3$) δ 5.63 – 5.53 (m, 1H), 5.52 – 5.42 (m, 1H), 3.70 (d, J = 12.5 Hz, 1H), 3.57 (d, J = 12.4 Hz, 1H), 3.16 (s, 1H), 3.10 (s, 1H), 3.02 (d, J = 12.4 Hz, 1H), 2.97 (dt, J = 6.8, 1.2 Hz, 2H), 2.93 (d, J = 12.4 Hz, 1H), 1.95 – 1.78 (m,

2H), 1.61 – 1.56 (m, 5H), 1.41 (s, 9H). Distinct minor *(E)*-isomer signals observed at δ 2.86 (d, J = 6.0 Hz, 2H). **^{13}C NMR** (126 MHz, $CDCl_3$) δ 156.10, 127.86, 126.81, 79.42, 58.48, 58.47, 50.93, 49.77, 49.19, 28.52, 25.34, 25.16, 13.23. Distinct minor *(E)*-isomer signals observed at δ 128.56, 128.48, 58.17, 55.17, 30.40, 29.77, 17.88. **HRMS** (ESI+) Calc: $[M+H]^+$ ($C_{15}H_{27}N_2O_2$) 267.2067; measured: 267.2064 = 1.1 ppm difference.

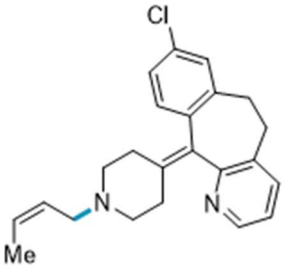

(Z)-11-(1-(but-2-en-1-yl)piperidin-4-ylidene)-8-chloro-6,11-dihydro-5H-benzo[5,6]cyclohepta[1,2-b]pyridine (2.29). Prepared from butene and Desloratadine; 68% NMR yield (10:1 Z:E) obtained by following General Procedure D and Workup A. **HRMS** (ESI+) Calc: $[M+H]^+$ ($C_{23}H_{25}ClN_2$) 365.1779; measured: 365.1776 = 0.8 ppm difference.

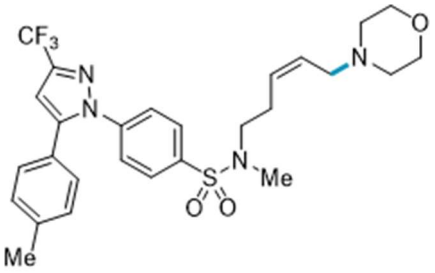

(Z)-N-methyl-N-(5-morpholinopent-3-en-1-yl)-4-(5-(p-tolyl)-3-(trifluoromethyl)-1H-pyrazol-1-yl)benzenesulfonamide (2.30). Prepared from N-methyl-N-(pent-4-en-1-yl)-4-(5-(p-tolyl)-3-(trifluoromethyl)-1H-pyrazol-1-yl)benzenesulfonamide (**A3**) and morpholine; 58% NMR yield (1:1 Z:E) obtained by following General Procedure C and Workup B. **HRMS** (ESI+) Calc: $[M+H]^+$ ($C_{27}H_{31}F_3N_4O_3S$) 549.2142 measured: 549.2140 = 0.4 ppm difference.

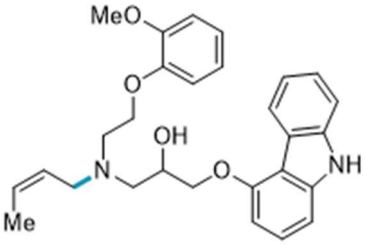

(Z)-1-((9H-carbazol-4-yl)oxy)-3-(but-2-en-1-yl(2-(2-methoxyphenoxy)ethyl)amino)propan-2-ol (2.31). Prepared from butene and Carvedilol; 103.3 mg (56% yield, 10:1 Z:E) obtained as a powder following General Procedure B and Workup C. **^{1}H NMR** (500 MHz, $CDCl_3$) δ 7.77 (d, J = 8.3, 1H), 8.26 (s, 1H), 7.39 – 7.33 (m, 2H), 7.29 (t, J = 8.0, 1H), 7.20 (ddd, J = 8.0, 5.8, 2.5 Hz, 1H), 7.00 (d, J = 8.1 Hz, 1H), 6.87 – 6.98 (m, 4H), 6.65 (d, J = 7.9 Hz, 1H), 5.53 – 5.73 (m, 2H), 4.28-4.34 (m, 2H), 4.21-4.26 (m, 1H), 4.11 – 4.18 (m, 2H), 3.83 (s, 3H), 3.38 (d, J = 6.7Hz, 2H), 3.15 (dt, J = 13.8, 6.1 Hz, 2H), 2.95 – 3.03 (m, 2H), 2.90 (dd, J = 13.0, 8.5 Hz, 1H), 1.64 – 1.68 (m, 3H). Distinctive minor *(E)*-isomer signals observed at δ 3.32 (d, J = 5.8 Hz, 2H). **^{13}C NMR** (126 MHz, $CDCl_3$) δ 155.36, 149.61, 149.58, 148.30, 141.06, 138.85, 129.49, 127.72, 126.88, 126.68, 123.13, 122.65, 121.45, 120.93, 119.56, 113.49, 112.74, 111.97, 111.91, 111.89, 110.08, 103.82, 101.12, 70.23, 67.37, 67.21, 57.69, 55.83, 53.43, 51.52, 13.23. Distinctive

minor *(E)*-isomer signals observed at δ 124.94, 127.47, 123.07, 121.40, 119.60, 113.41, 70.27, 67.27, 57.55, 53.12, 17.90. **HRMS** (ESI+) Calc: $[M+Na]^+$ ($C_{28}H_{32}N_2O_4$) 469.2098; measured: 469.2021; 1.4 ppm difference.

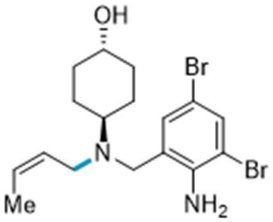

(1R,4R)-4-((2-amino-3,5-dibromobenzyl)((Z)-but-2-en-1-yl)amino)cyclohexan-1-ol (2.32). Prepared from butene and Ambroxol HCl; 38% NMR yield obtained by following General Procedure D and Workup C. No distinct minor isomers signals were observed by NMR spectroscopy. However, approximate selectivity of (8:1 Z:E) was determined using LC-MS analysis. **HRMS** (ESI+) Calc: $[M+H]^+$ ($C_{17}H_{24}Br_2N_2O$) 431.0328; measured: 431.0322 = 1.4 ppm difference.

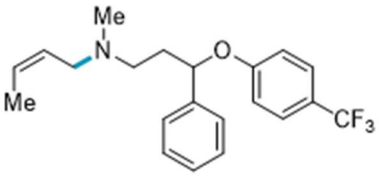

(Z)-N-methyl-N-(3-phenyl-3-(4-(trifluoromethyl)phenoxy)propyl)but-2-en-1-amine (2.33). Prepared from butene and Fluoxetine HCl salt; 97.3 mg (67% yield, 10:1 Z:E) obtained as an oil following General Procedure B and Workup A. **^{1}H NMR** (500 MHz, $CDCl_3$) δ 7.34 (d, J = 8.5 Hz, 2H), 7.30 – 7.21 (m, 4H), 7.21 – 7.13 (m, 1H), 6.82 (d, J = 8.6 Hz, 2H), 5.56-5.46 (m, 1H), 5.41-5.33 (m, 1H), 5.22 (dd, J = 8.3, 4.8 Hz, 1H), 2.96 (d, J = 6.9 Hz, 2H), 2.54-2.47 (m, 1H), 2.44-2.38 (m, 1H), 2.17 (s, 3H), 2.15 – 2.05 (m, 1H), 1.99 – 1.86 (m, 1H), 1.53 (dd, J = 6.9, 1.7 Hz, 3H). Distinctive minor *(E)*-isomer signals observed at δ 2.88 (t, J = 7.4 Hz, 2H), 2.16 (s, 3H). 13C NMR (126 MHz, $CDCl_3$) δ 160.73, 141.18, 128.75, 127.81, 127.40, 126.83, 126.71 (q, J = 3.77 Hz), 125.88, 124.43 (q, J = 271.07Hz), 122.72 (q, J = 32.7 Hz), 115.81, 78.52, 53.90, 53.20, 41.98, 36.48, 13.10. Distinctive minor *(E)*-isomer signals observed at δ 78.42, 59.97, 52.79, 41.85, 36.29, 13.57. **^{19}F NMR** (377 MHz, $CDCl_3$) δ -61.56. **HRMS** (ESI+) Calc: $[M+H]^+$ ($C_{21}H_{24}F_3NO$) 364.1883; measured: 364.1877 = 1.6 ppm difference.

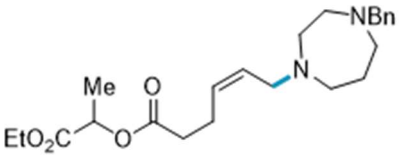

1-ethoxy-1-oxopropan-2-yl (Z)-6-(4-benzyl-1,4-diazepan-1-yl)hex-4-enoate (2.34). Prepared from 1-ethoxy-1-oxopropan-2-yl hex-5-enoate (**A4**) and 1-benzyl-1,4-diazepane; 80.4 mg (50% yield, 4:1 Z:E) obtained as an oil following General Procedure A (using 0.4 mmol, 1 equiv amine) and Workup B. **^{1}H NMR** (500 MHz, $CDCl_3$) δ 7.31 – 7.25 (m, 4H), 7.23 (dt, J = 7.0, 2.9 Hz, 1H), 5.78 – 5.67 (m, 2H), 4.97 (q, J = 7.1 Hz, 1H), 4.12 (qd, J = 6.9, 3.6 Hz, 2H), 3.67 (s, 2H), 3.61 – 3.51 (m, 2H), 3.37 – 2.63 (m, 8H), 2.54 – 2.28 (m, 4H), 2.28 – 1.80 (m, 2H), 1.41 (d, J = 7.0 Hz, 3H), 1.20 (t, J = 7.1 Hz, 3H). Distinct minor *(E)*-isomer signals observed at δ 5.86 – 5.78 (m, 2H), 3.44 (d, J = 7.1 Hz, 2H). **^{13}C NMR** (126 MHz, $CDCl_3$) δ 172.02, 170.64, 136.84, 136.25, 129.19, 128.65, 127.87, 120.95, 68.85, 62.26, 61.44, 54.31, 53.99, 53.52, 52.35, 49.81, 32.89, 23.83, 22.73, 16.90, 14.13. Distinct minor *(E)*-isomer signals observed at δ 171.93, 170.73, 129.15, 68.75, 61.37, 59.41, 52.35, 32.96, 22.23, 14.06. **HRMS** (ESI+) Calc: $[M+H]^+$ ($C_{23}H_{35}N_2O_4$) 403.2591 measured: 403.2585 = 1.5 ppm difference.

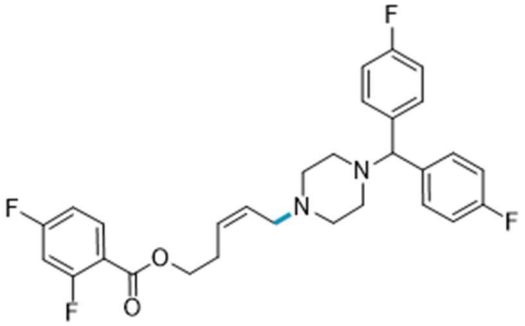

(Z)-5-(4-(bis(4-fluorophenyl)methyl)piperazin-1-yl)pent-3-en-1-yl 2,4-difluorobenzoate (2.35). Prepared from pent-4-en-1-yl 2,4-difluorobenzoate (**A5**) and 1-(bis(4-fluorophenyl)methyl)piperazine; 145.1 mg (71% yield, 2:1 Z:E) obtained as an oil following General Procedure A and Workup B. **^{1}H NMR** (500 MHz, $CDCl_3$) δ 7.96 (qd, J = 8.7, 6.5 Hz, 1H), 7.34 (ddd, J = 8.5, 5.4, 2.8 Hz, 4H), 7.01 – 6.95 (m, 4H), 6.94 – 6.87 (m, 1H), 6.87 – 6.79 (m, 1H), 5.71 – 5.58 (m, 2H), 4.36 (td, J = 6.6, 4.0 Hz, 2H), 4.22 (s, 1H), 3.06 (d, J = 5.3 Hz, 2H), 2.57 (q, J = 6.5 Hz, 1H), 2.68 – 2.09 (m, 7H), 1.68 (s, 2H). Distinct minor *(E)*-isomer signals observed at δ 4.21 (s, 1H), 2.97 (dd, J = 3.9, 1.6 Hz, 2H). **^{13}C NMR** (126 MHz, $CDCl_3$) δ 165.70 (dd, J = 256.5, 12.0 Hz), 163.49 (d, J = 4.1 Hz), 162.83 (dd, J = 263.3, 12.7 Hz), 162.79, 160.84, 138.25 (d, J = 3.3 Hz), 133.85 (dd, J = 10.5, 2.3 Hz), 129.24 (d, J = 7.8 Hz), 129.07, 127.86, 115.38 (d, J = 21.3 Hz), 111.55 (dd, J = 21.5, 4.0 Hz), 105.23 (dd, J = 25.7 Hz), 74.47, 64.55, 54.95, 53.34, 51.70, 31.86, 29.71, 27.16. Distinct minor *(E)*-isomer signals observed at δ 165.67 (dd, J = 256.5, 12.0 Hz), 163.40 (d, J = 4.1 Hz), 115.34 (d, J = 21.3 Hz), 111.52 (dd, J = 21.5, 4.0 Hz), 64.47, 60.63, 53.19, 51.62, 34.13, 30.33. **^{19}F NMR** (377 MHz, $CDCl_3$) δ -101.78 (dd, J = 38.9, 12.3 Hz, 1F), -103.78 (dd, J = 17.2, 12.4 Hz, 1F), -115.75 (d, J = 9.6 Hz, 2F). **HRMS** (ESI+) Calc: $[M+H]^+$ ($C_{29}H_{29}F_4N_2O_2$) 513.2160 measured: 513.2157 = 0.6 ppm difference.

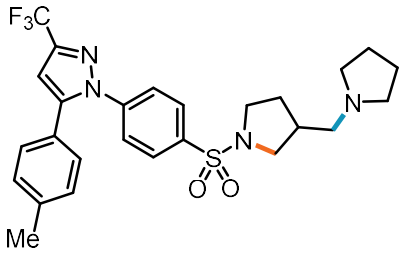

1-(4-((3-(pyrrolidin-1-ylmethyl)pyrrolidin-1-yl)sulfonyl)phenyl)-5-(p-tolyl)-3-(trifluoromethyl)-1H-pyrazole (2.36). Prepared from N-(but-3-en-1-yl)-4-(5-(p-tolyl)-3-(trifluoromethyl)-1H-pyrazol-1-yl)benzenesulfonamide and pyrrolidine; 90% NMR yield obtained by following General Procedure C and Workup B. Peaks assigned by analogy to **2.38**.

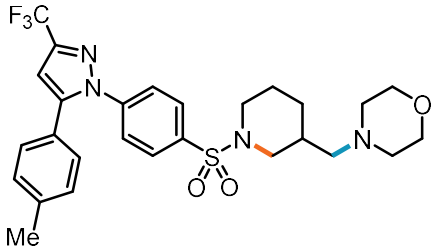

4-((1-((4-(5-(p-tolyl)-3-(trifluoromethyl)-1H-pyrazol-1-yl)phenyl)sulfonyl)piperidin-3-yl)methyl)morpholine (2.37). Prepared from N-(pent-4-en-1-yl)-4-(5-(p-tolyl)-3-(trifluoromethyl)-1H-pyrazol-1-yl)benzenesulfonamide and morpholine; 90% NMR yield obtained by following General Procedure C and Workup B. Peaks assigned by analogy to **2.38**.

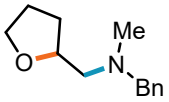

N-benzyl-N-methyl-1-(tetrahydrofuran-2-yl)methanamine (2.38). Prepared from ((pent-4-en-1-yloxy)methyl)benzene and N-methyl-1-phenylmethanamine; 56% NMR yield obtained by following General Procedure C and Workup B. Product was obtained as an oil for partial characterization. **^{1}H NMR** (500 MHz, $CDCl_3$) δ 7.28 – 7.11 (m, 5H), 3.98 (qd, J = 7.0, 4.9 Hz, 1H), 3.77 (dt, J = 8.3, 6.7 Hz, 1H), 3.66 (dt, J = 8.3, 6.9 Hz, 1H), 3.57 – 3.47 (m, 1H), 3.47 – 3.34 (m, 1H), 2.45 (dd, J = 12.8, 6.9 Hz, 1H), 2.41 – 2.27 (m, 1H), 2.20 (s, 3H), 1.96 – 1.84 (m, 1H), 1.83 – 1.70 (m, 2H), 1.52 – 1.38 (m, 1H); consistent with reported spectra (*Tetrahedron* **2006**, 62 (25), 5986–5994).

A6. Alkenylthianthrenium Salt Mechanistic Studies

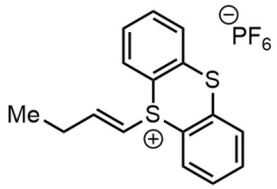

5-(but-1-en-1-yl)-5H-thianthren-5-ium hexafluorophosphate (2.39). Prepared from butene following procedure A except with no amine was added. Reaction was complete within 5 mins; 133.2 mg (32% yield, 1:1 E:Z) obtained as an oil. **^{1}H NMR** (500 MHz, $CDCl_3$) δ 8.16 (dt, J = 7.9, 1.7 Hz, 2H), 7.84 (dt, J = 7.9, 1.4 Hz, 2H), 7.75 (qd, J = 7.6, 1.4 Hz, 2H), 7.64 (tdd, J = 7.7, 4.4, 1.3 Hz, 2H), 7.20 (dt, J = 14.8, 6.3 Hz, 1H), 1H), 6.53 (dt, J = 14.8, 1.7 Hz, 1H), 2.29 (qdd, J = 7.4, 6.2, 1.7 Hz, 2H), 1.00 (t, J = 7.4 Hz, 3H). Distinctive minor *(Z)*-isomer signals observed at δ 6.79 (q, J = 8.0 Hz, 1H), 6.59 (dt, J = 8.6, 1.4 Hz), 2.73 (pd, J = 7.5, 1.4 Hz, 2H), 1.10 (t, J = 7.5 Hz, 2H). **^{13}C NMR** (126 MHz, $CDCl_3$) δ 158.77, 135.62, 134.69, 133.09, 130.38, 130.35, 120.24, 108.70, 53.55, 26.70, 11.29. Distinctive minor *(Z)*-isomer signals observed at δ 157.20, 135.74, 134.58, 132.65, 130.58, 130.36, 120.85, 110.67, 24.01, 12.68. **^{19}F NMR** (377 MHz, $CDCl_3$) δ -71.95, -73.83. **HRMS** (ESI+) Calc: $[M]^+$ ($C_{16}H_{15}S_2$) 271.0610; measured: 271.0605; 1.8 ppm difference.

Subjecting alkenylTT+ salt intermediate 2.39 to Substitution Reaction Conditions (Eq. 2.1)
Dissolved 5-(but-1-en-1-yl)-5H-thianthren-5-ium hexafluorophosphate (**2.39**) (1 equiv) in MeCN (0.05M). Added DIPEA (7 equiv), followed by N-methylbenzylamine (2 equiv). Let stir at room temperature for 3 hrs. Added in CH_2Br_2 as an internal standard and took an NMR aliquot to quantify NMR yield.

A7. NMR Spectra

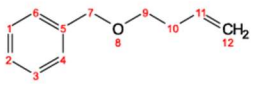

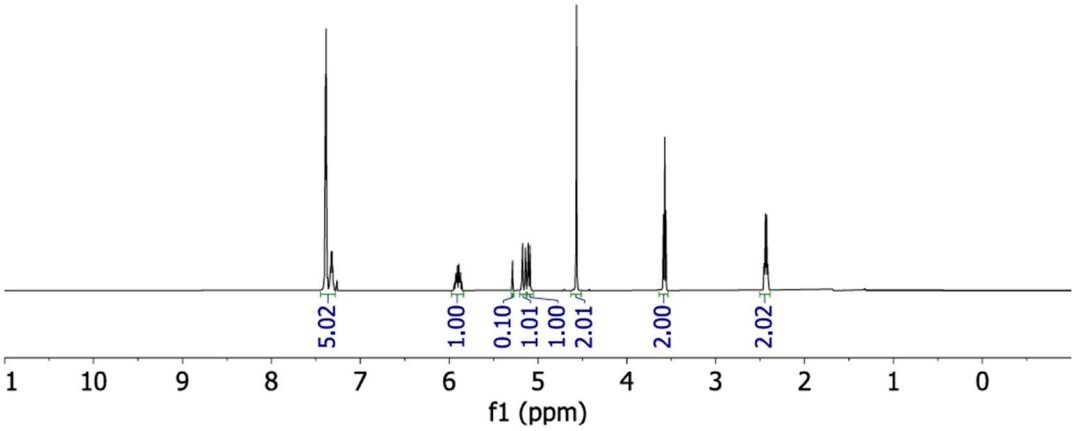

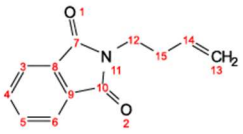

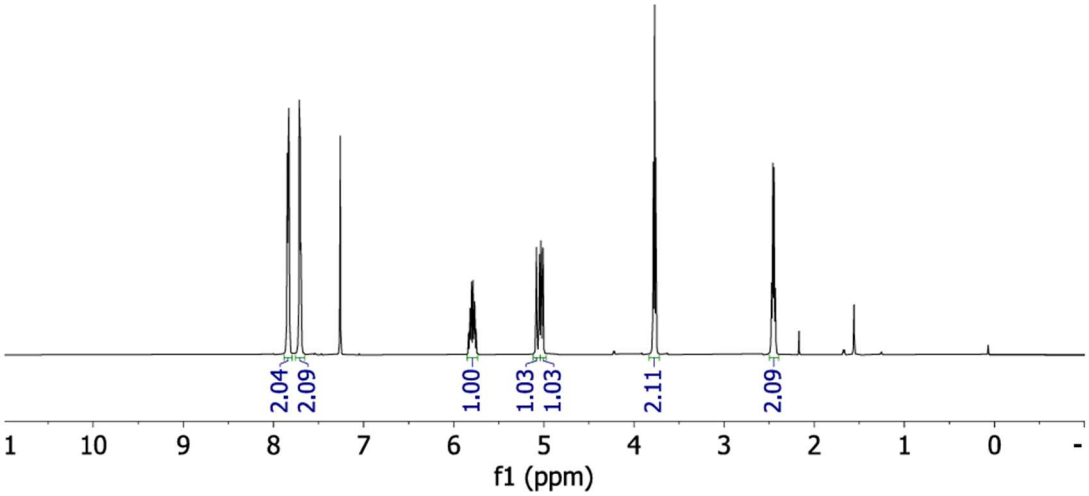

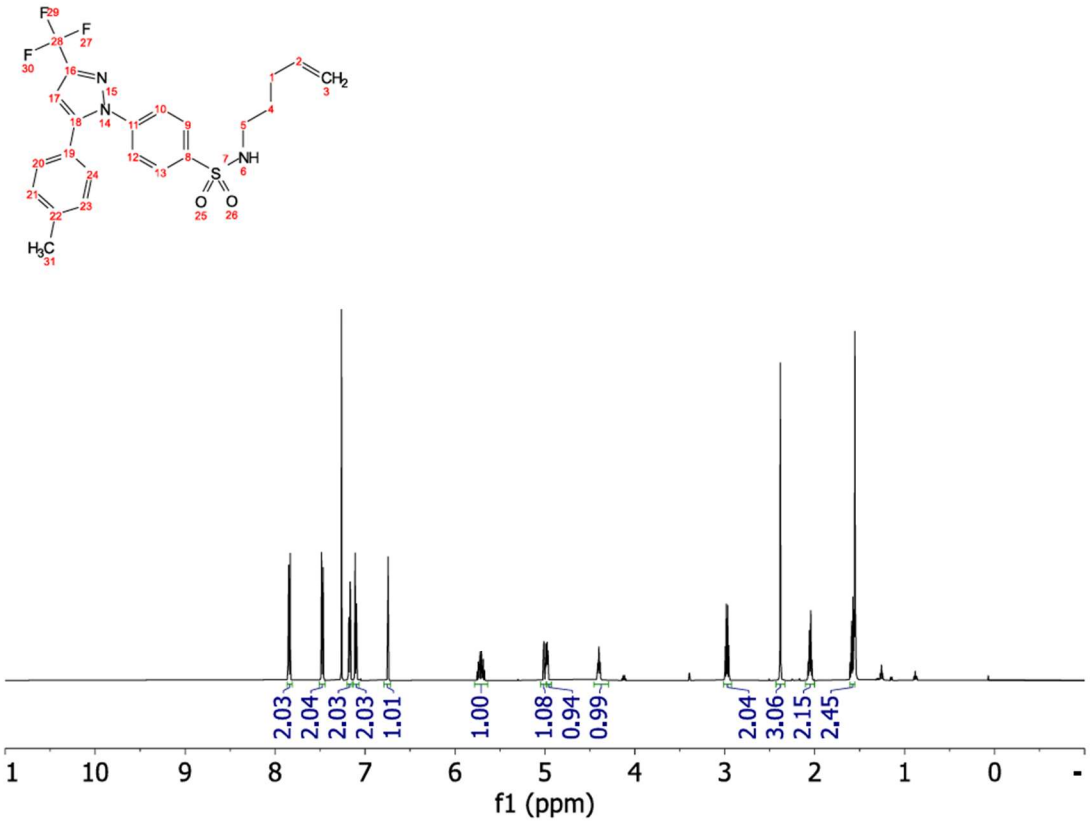
2.03
2.04
2.03
2.03
1.01
1.00
1.08
0.94
0.99
2.04
3.06
2.15
2.45
1 10 9 8 7 6 5 4 3 2 1 0 -
f1 (ppm)

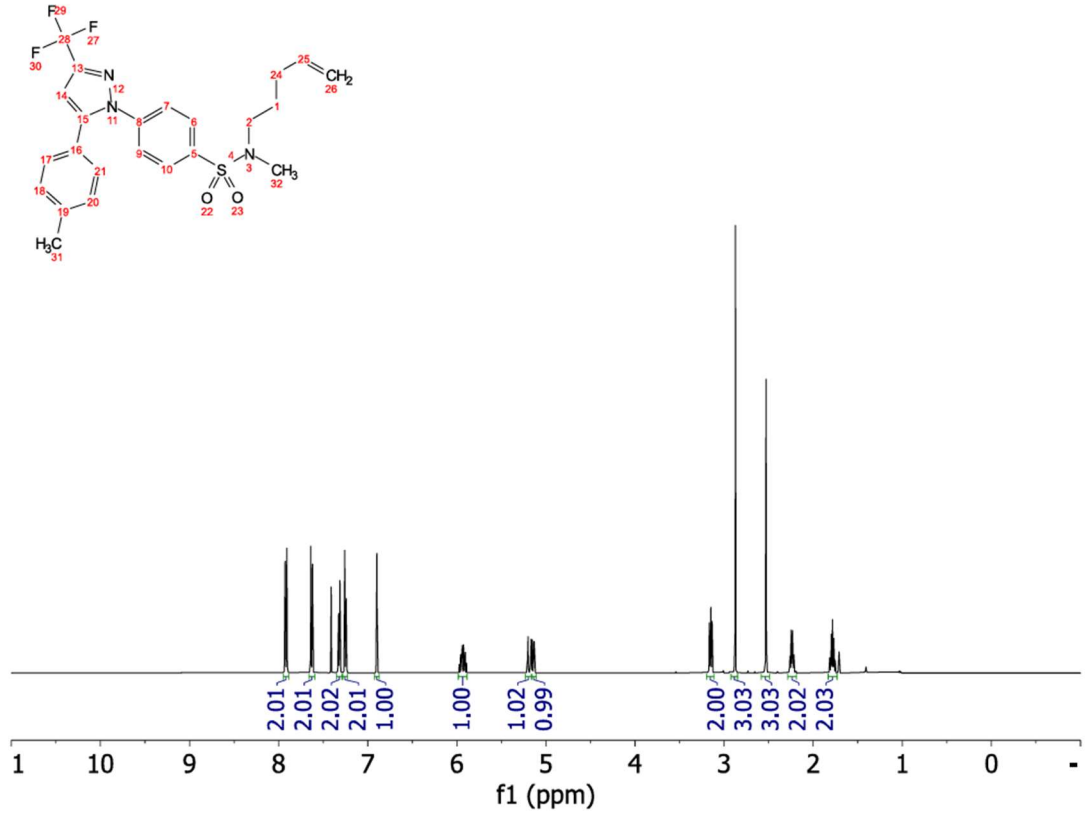
2.01
2.01
2.02
2.01
1.00
1.00
1.02
0.99
2.00
3.03
3.03
2.02
2.03
1 10 9 8 7 6 5 4 3 2 1 0 -
f1 (ppm)

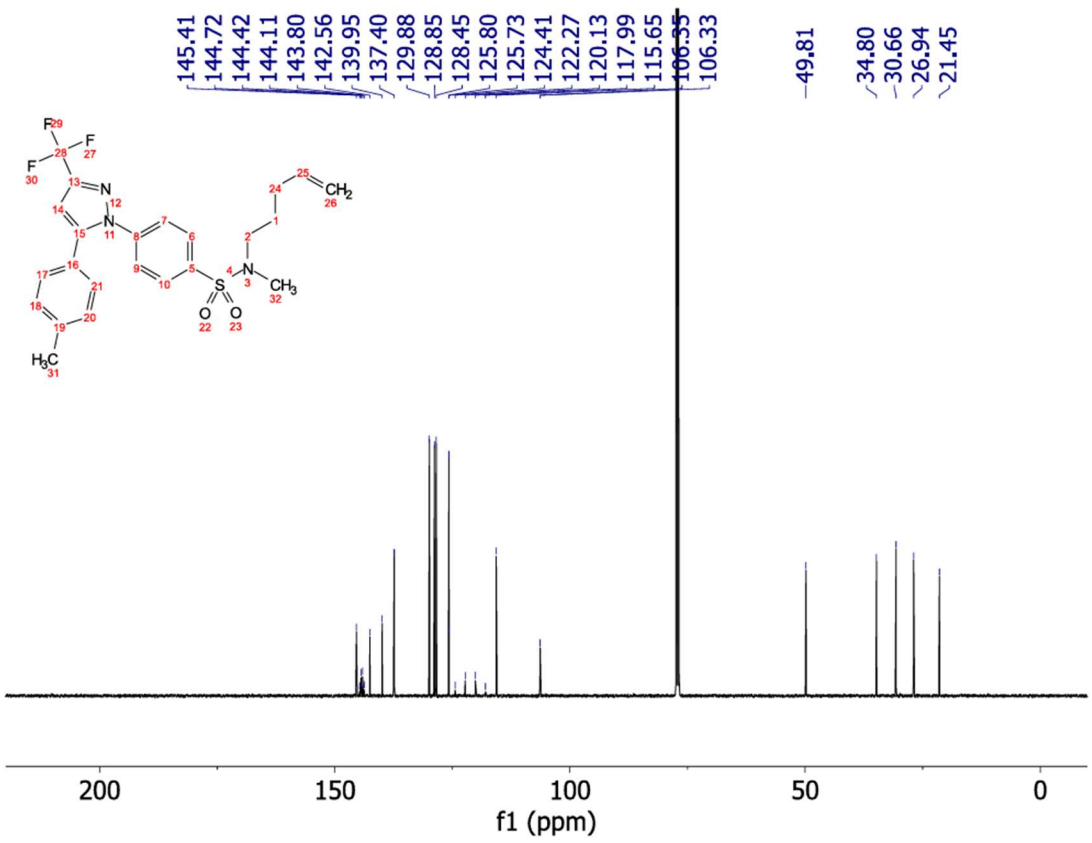
145.41
144.72
144.42
144.11
143.80
142.56
139.95
137.40
129.88
128.85
128.45
125.80
125.73
124.41
122.27
120.13
117.99
115.65
106.35
106.33
49.81
34.80
30.66
26.94
21.45
200
150
100
50
0
f1 (ppm)

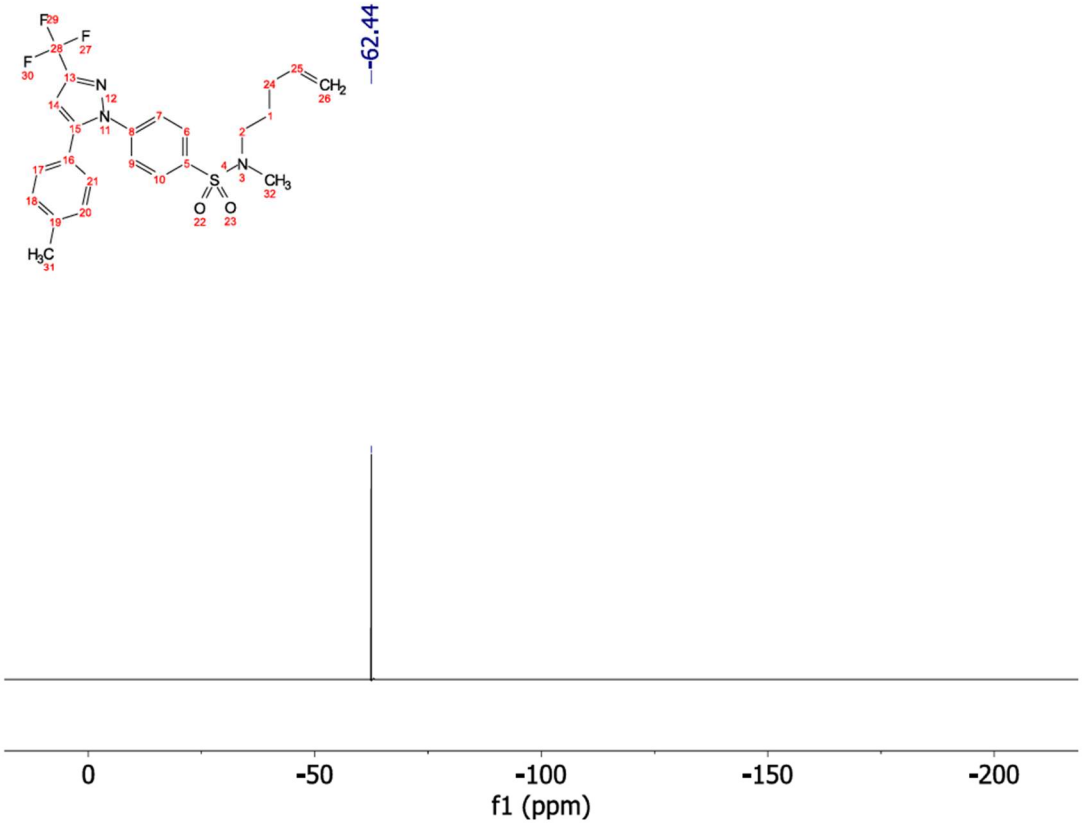
-62.44
0
-50
-100
-150
-200
f1 (ppm)

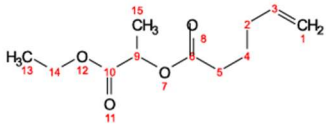

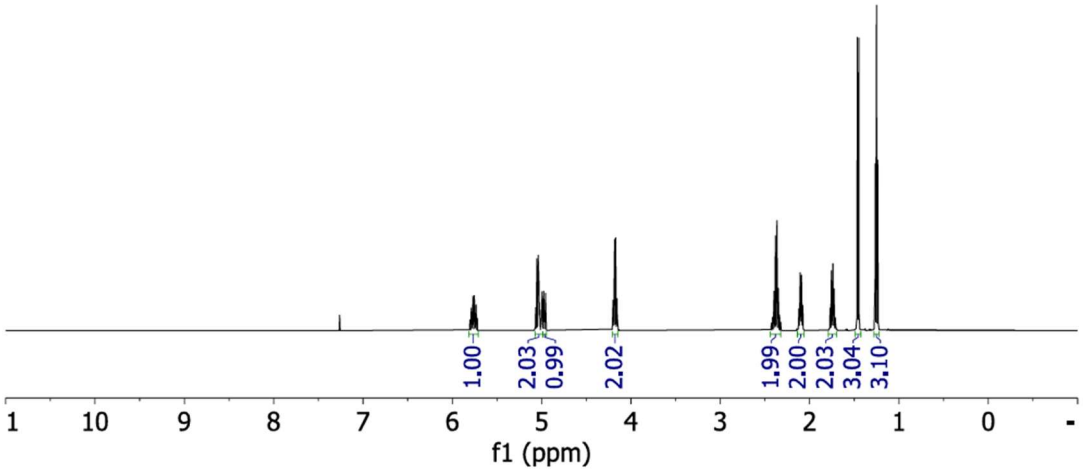
1.00
2.03
0.99
2.02
1.99
2.00
2.03
3.04
3.10
f1 (ppm)

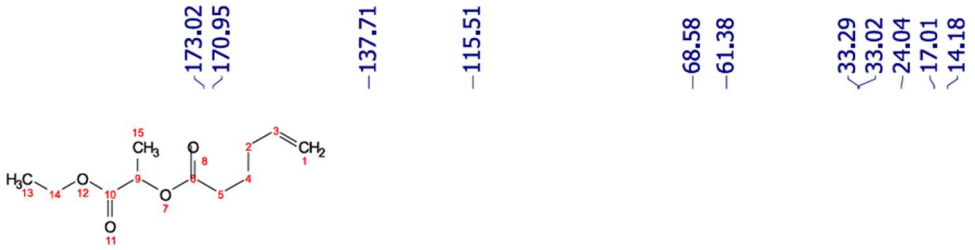
173.02
170.95
137.71
115.51
68.58
61.38
33.29
33.02
24.04
17.01
14.18

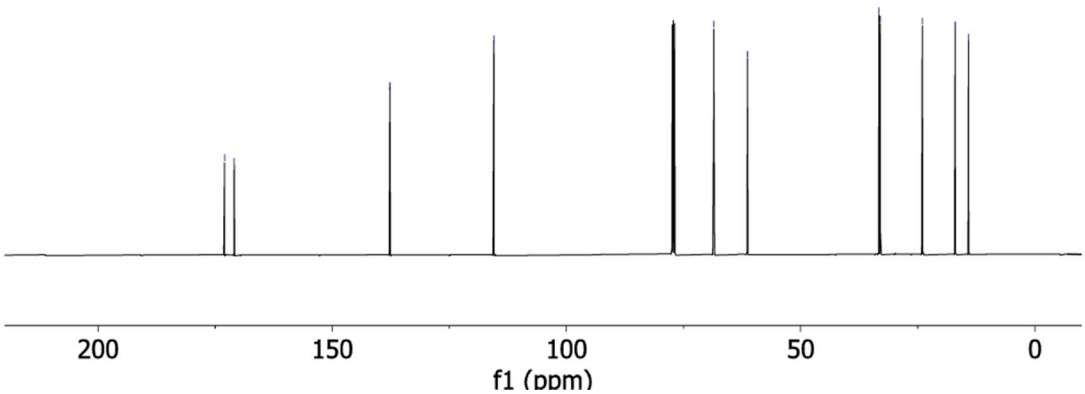
f1 (ppm)

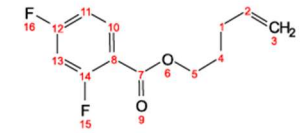

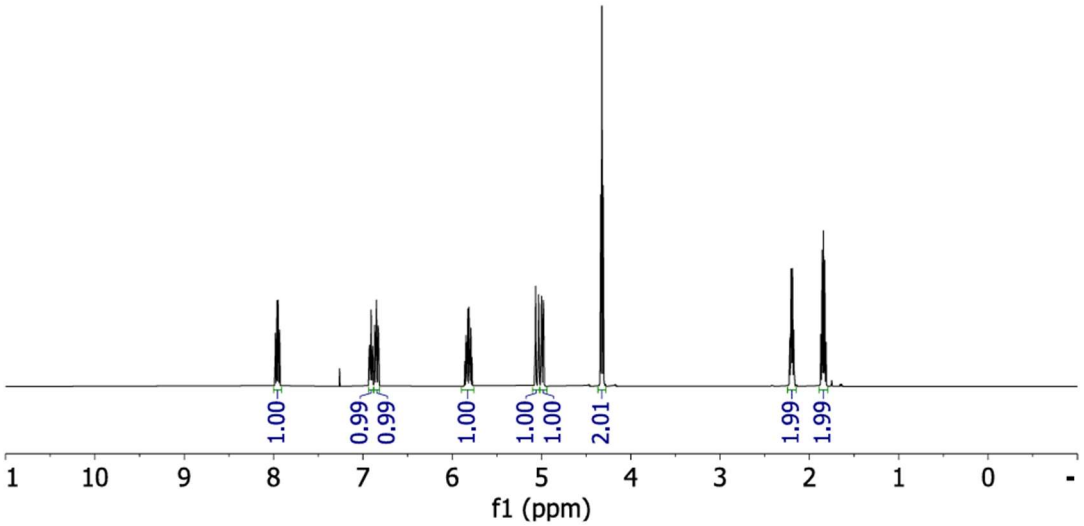

166.80
166.71
164.77
164.67
164.02
163.92
163.66
163.62
161.92
161.82
137.43
134.02
134.00
133.94
133.92
115.57
115.54
115.49
115.46
111.70
111.67
111.53
111.50
105.47
105.27
105.26
105.06
64.82
30.13
27.87

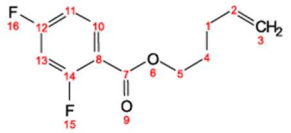

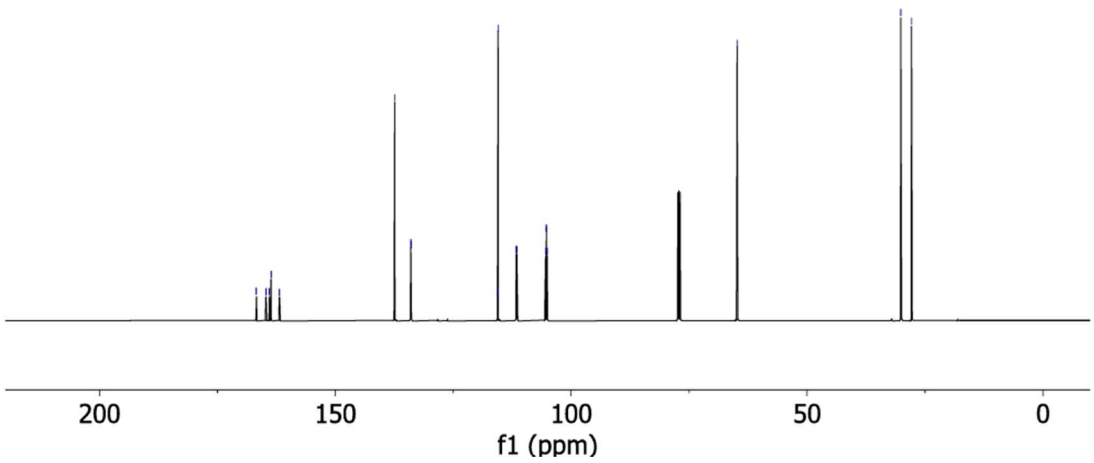

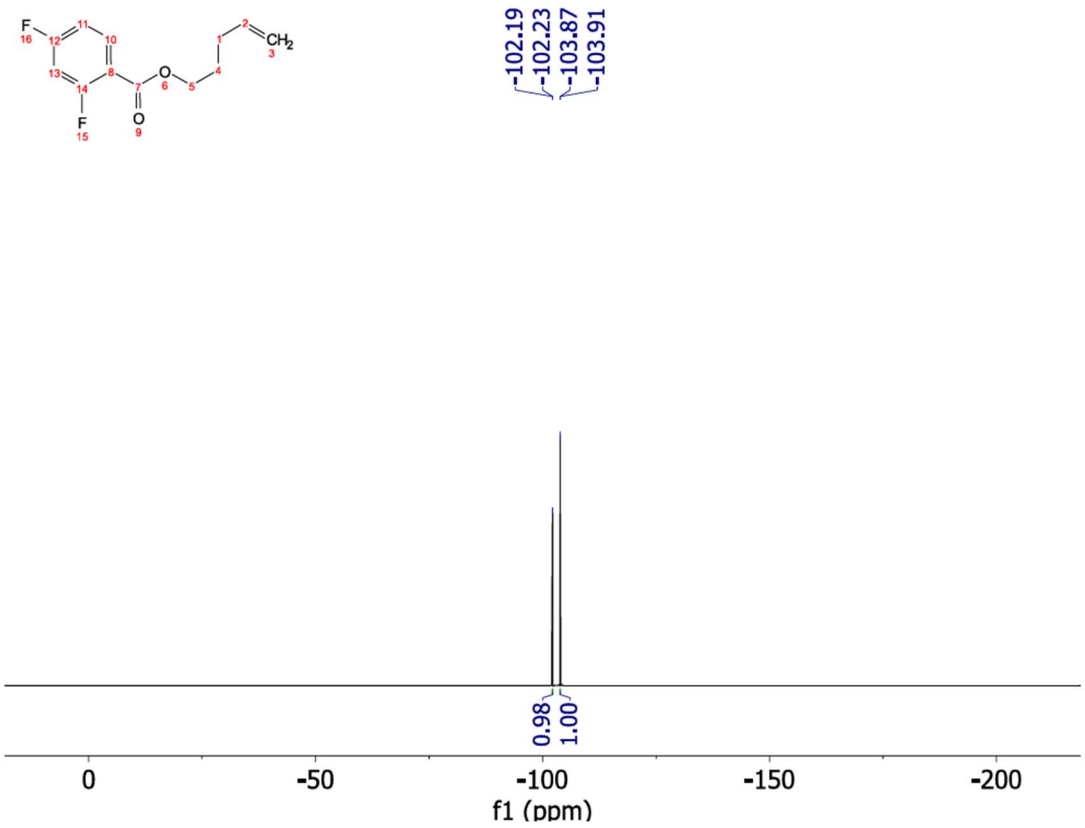

(blank space)

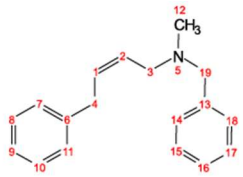
12
CH3
N
5
1
2
3
4
6
7
8
9
10
11
13
14
15
16
17
18
19

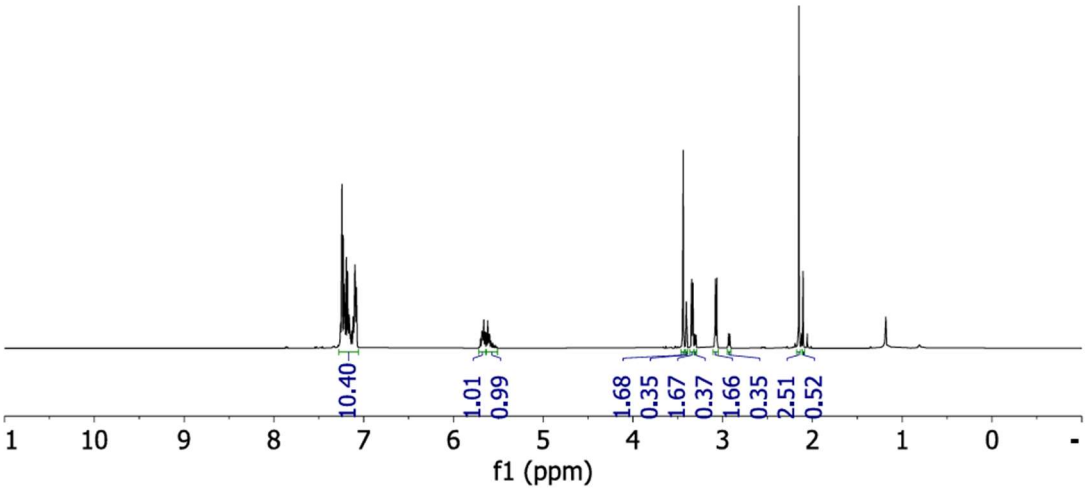
10.40
1.01
0.99
1.68
0.35
1.67
0.37
1.66
0.35
2.51
0.52
1
10
9
8
7
6
5
4
3
2
1
0
f1 (ppm)

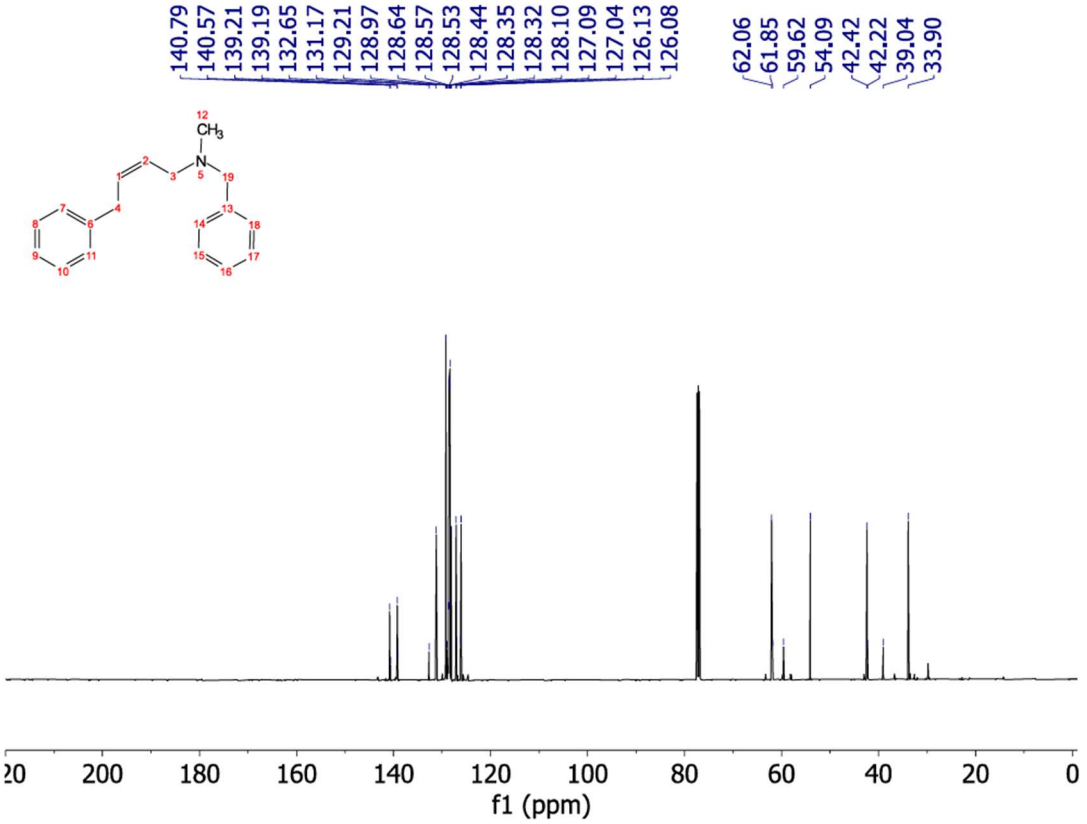
140.79
140.57
139.21
139.19
132.65
131.17
129.21
128.97
128.64
128.57
128.53
128.44
128.35
128.32
128.10
127.09
127.04
126.13
126.08
62.06
61.85
59.62
54.09
42.42
42.22
39.04
33.90
12
CH3
N
5
200
180
160
140
120
100
80
60
40
20
0
f1 (ppm)

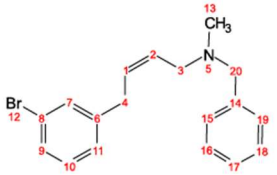
13
CH3
N
5
Br
12

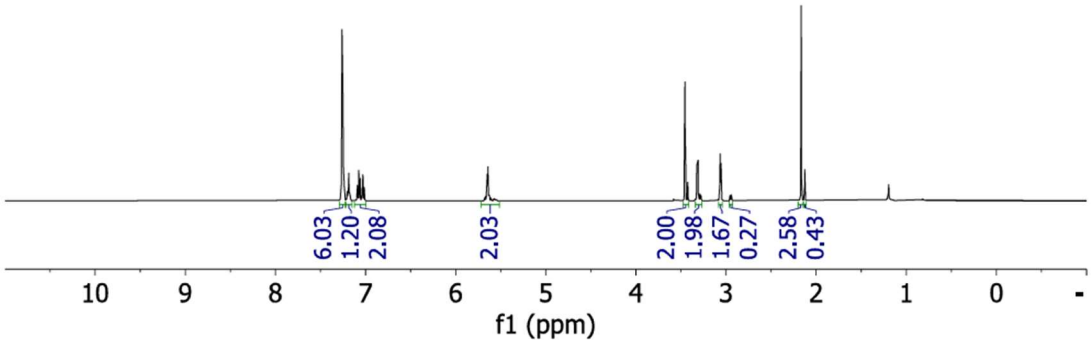
6.03
1.20
2.08
2.03
2.00
1.98
1.67
0.27
2.58
0.43
10
9
8
7
6
5
4
3
2
1
0
f1 (ppm)


143.12
142.92
139.10
139.08
131.73
131.67
131.54
130.22
130.11
130.09
129.76
129.29
129.23
129.22
128.85
128.39
128.36
127.32
127.16
127.10
122.66
122.63
62.11
61.90
59.49
54.00
42.45
42.25
38.61
33.49

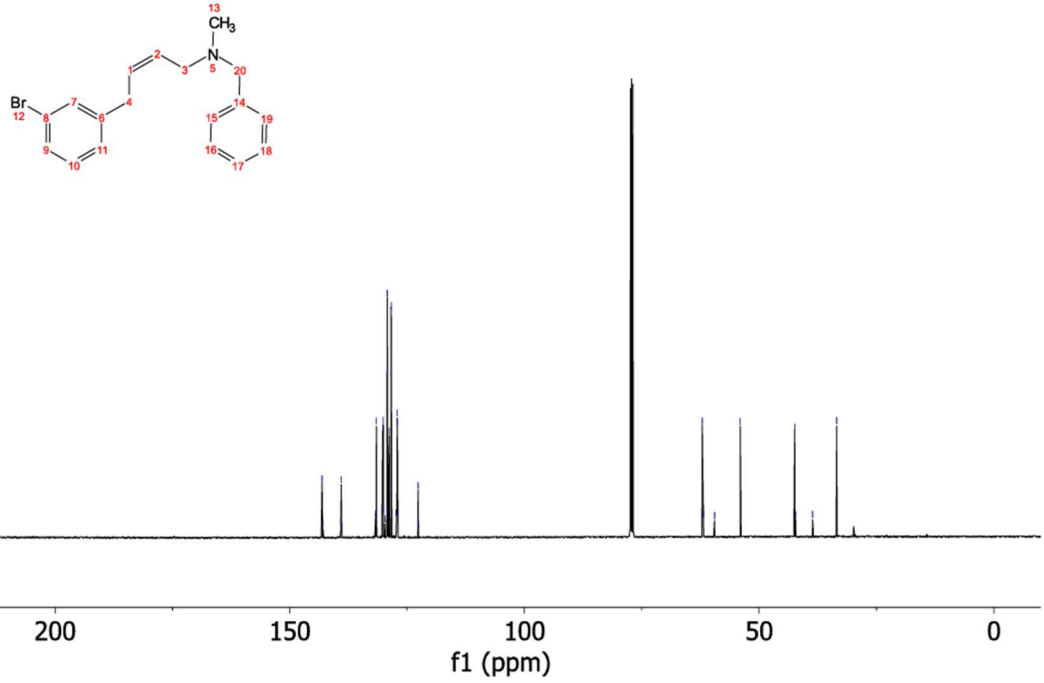
13
CH3
N
5
Br
12
200
150
100
50
0
f1 (ppm)

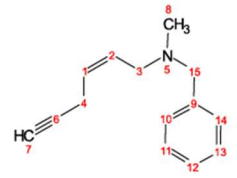
8
CH3
N
5
1
2
3
4
6
HC
7
15
9
10
11
12
13
14

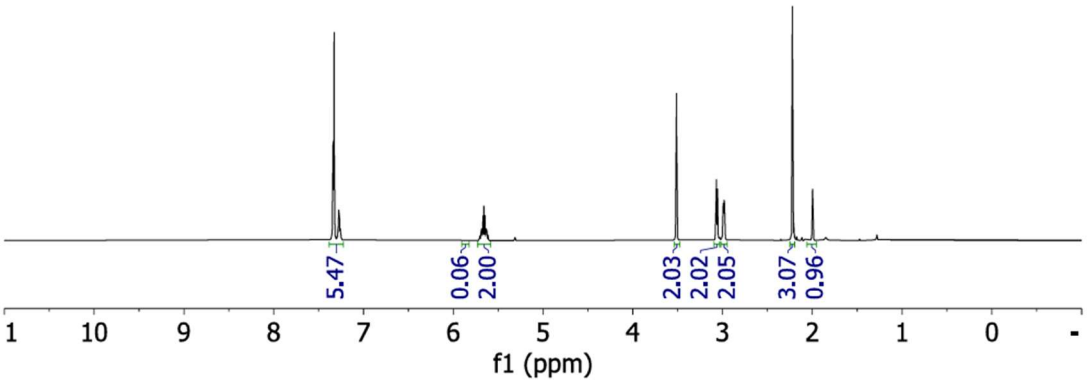
5.47
0.06
2.00
2.03
2.02
2.05
3.07
0.96
1
10
9
8
7
6
5
4
3
2
1
0
f1 (ppm)

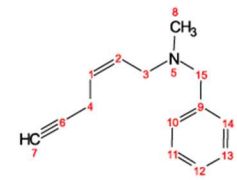
8
CH3
N
5
1
2
3
4
6
HC
7
15
9
10
11
12
13
14


139.02
129.70
129.27
129.20
128.37
128.34
127.15
126.67
82.44
70.30
68.41
61.97
61.86
59.20
53.79
42.37
42.22
17.34

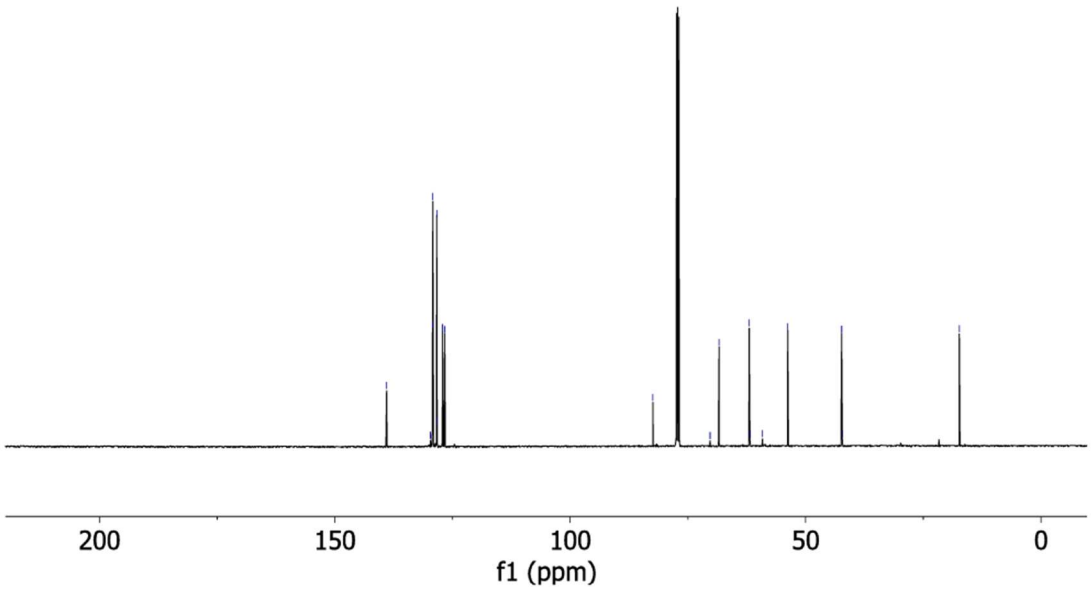
200
150
100
50
0
f1 (ppm)

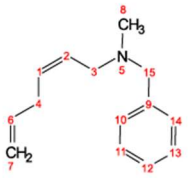

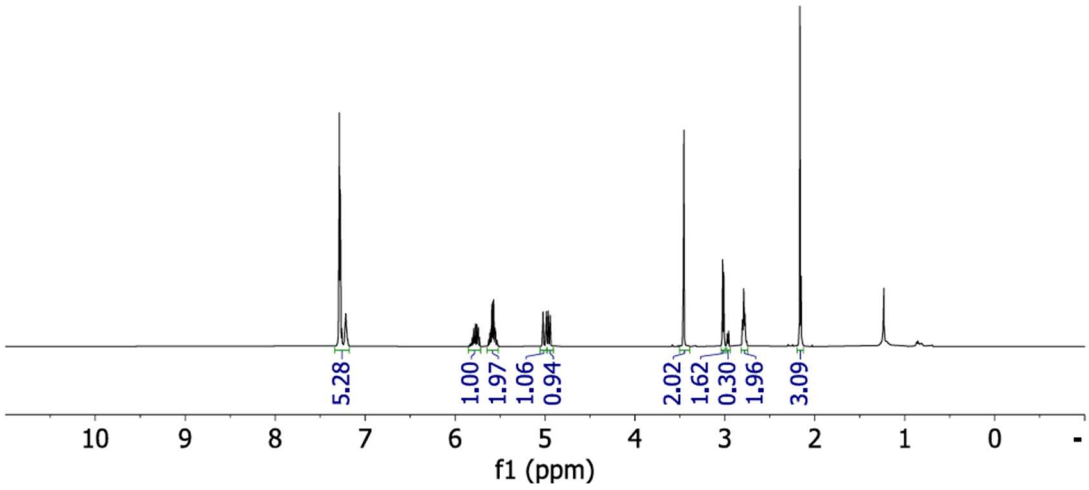
5.28
1.00
1.97
1.06
0.94
2.02
1.62
0.30
1.96
3.09
10
9
8
7
6
5
4
3
2
1
0
f1 (ppm)

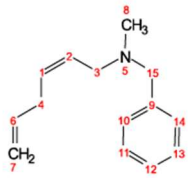

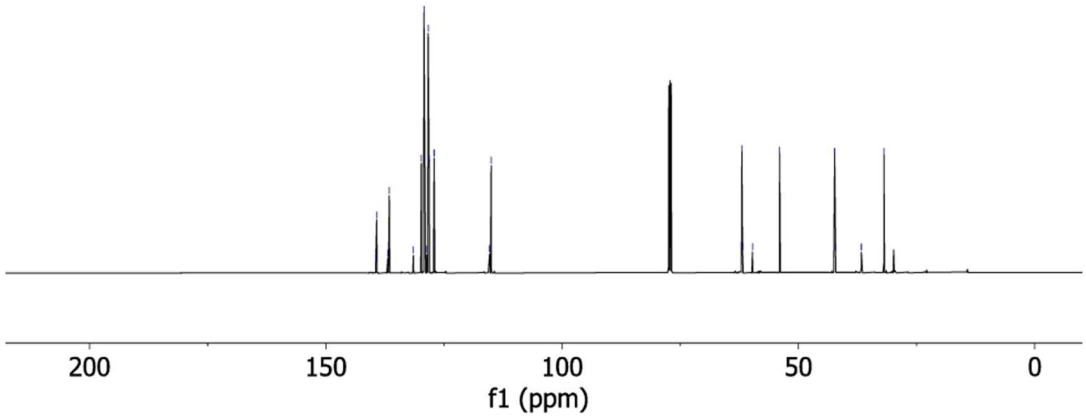
139.25
139.21
136.92
136.60
131.50
129.80
129.21
128.64
128.32
128.17
127.06
127.02
115.34
115.03
61.97
61.81
59.70
53.97
42.35
42.16
36.67
31.89
200
150
100
50
0
f1 (ppm)

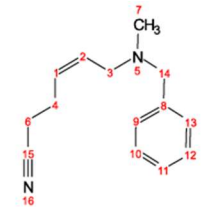

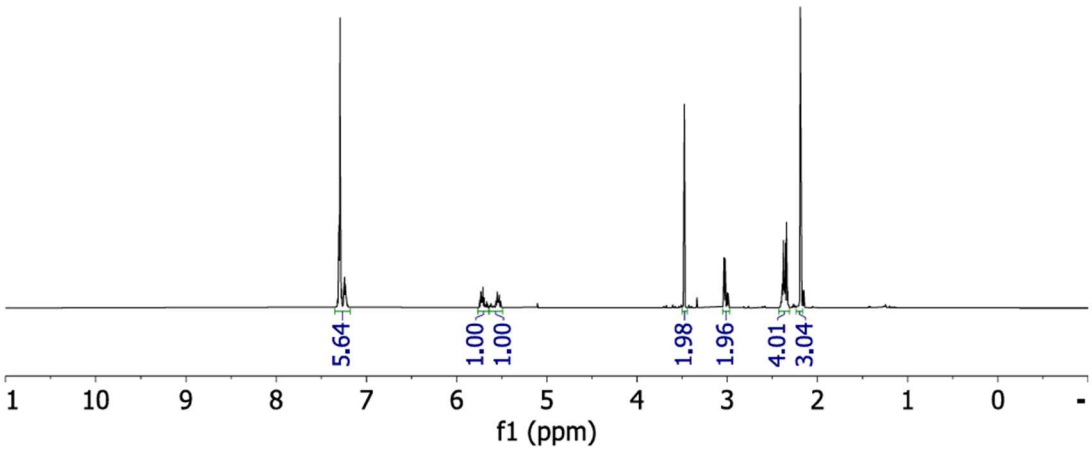
5.64
1.00
1.00
1.98
1.96
4.01
3.04
1 10 9 8 7 6 5 4 3 2 1 0 -
f1 (ppm)

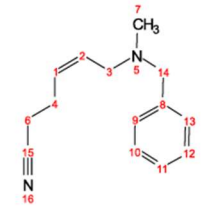

138.96
138.90
131.08
130.80
129.12
129.11
128.34
128.31
128.11
127.15
127.07
119.29
62.06
61.84
59.21
53.78
42.36
42.17
28.26
23.62
17.50
17.43
200 150 100 50 0
f1 (ppm)

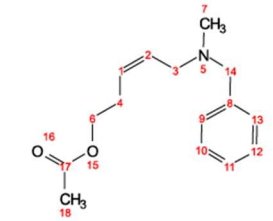

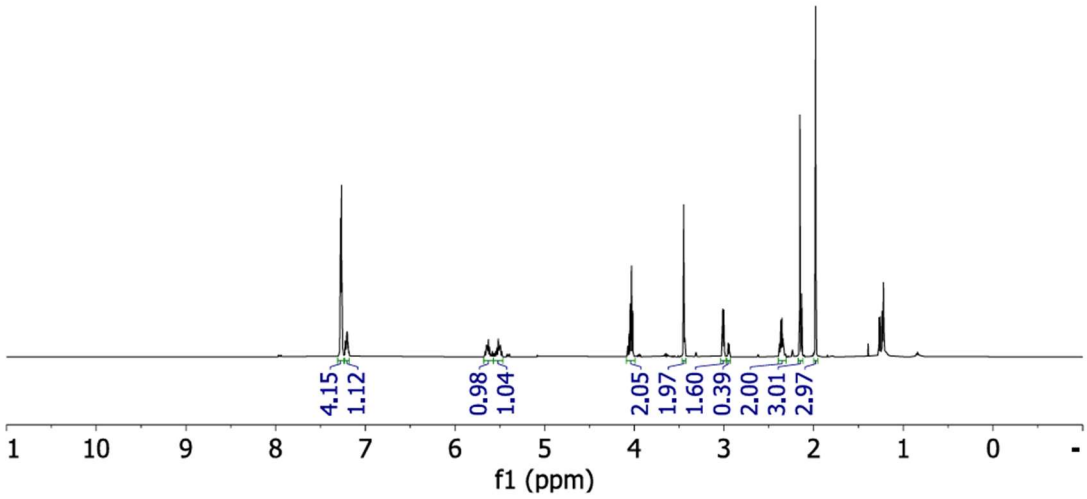
4.15
1.12
0.98
1.04
2.05
1.97
1.60
0.39
2.00
3.01
2.97
1
10
9
8
7
6
5
4
3
2
1
0
f1 (ppm)

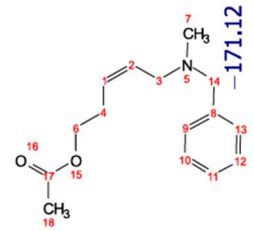

171.12
139.08
130.38
130.02
129.15
129.02
128.32
128.30
127.64
127.08
127.04
63.84
63.79
61.97
61.71
59.56
54.03
42.29
42.09
31.89
27.23
23.69
21.02
19.67
200
150
100
50
0
f1 (ppm)

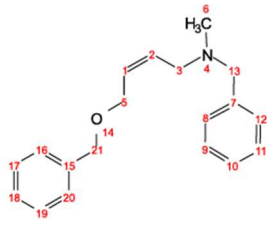

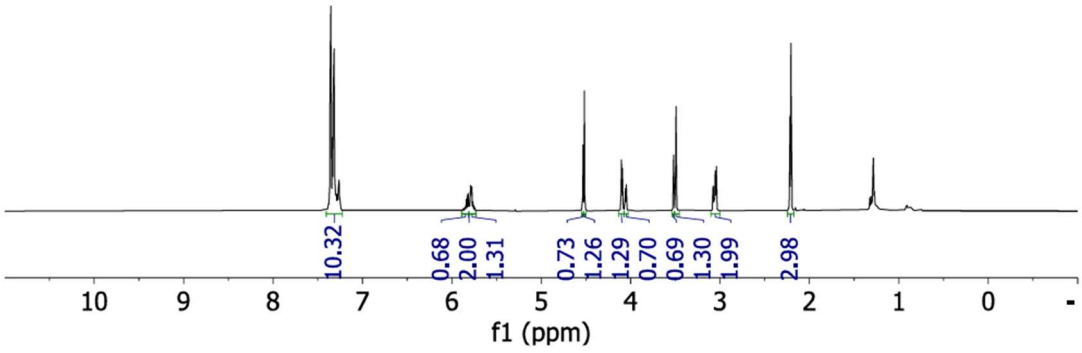
10.32
0.68
2.00
1.31
0.73
1.26
1.29
0.70
0.69
1.30
1.99
2.98
10
9
8
7
6
5
4
3
2
1
0
f1 (ppm)


139.00
138.91
138.37
138.30
131.15
130.48
129.67
129.16
129.10
129.08
128.43
128.41
128.26
127.80
127.78
127.66
127.61
127.05
127.00
72.31
72.07
70.46
65.90
61.88
61.79
59.19
54.06
42.24
42.19

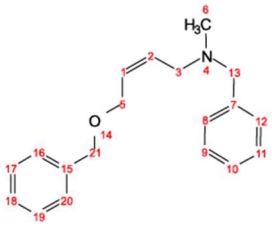

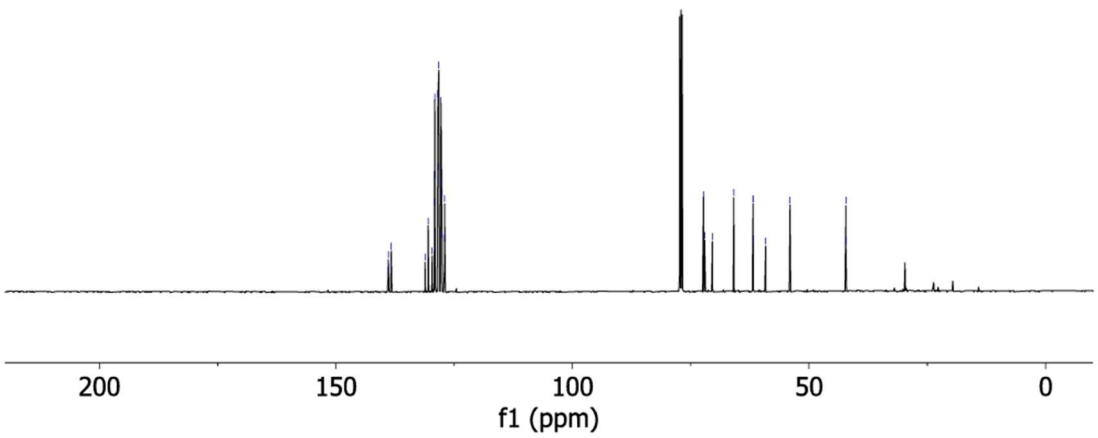
200
150
100
50
0
f1 (ppm)

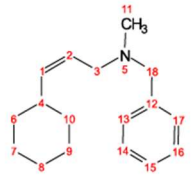
11
CH3
N
5
1
2
3
4
6
7
8
9
10
12
13
14
15
16
17
18

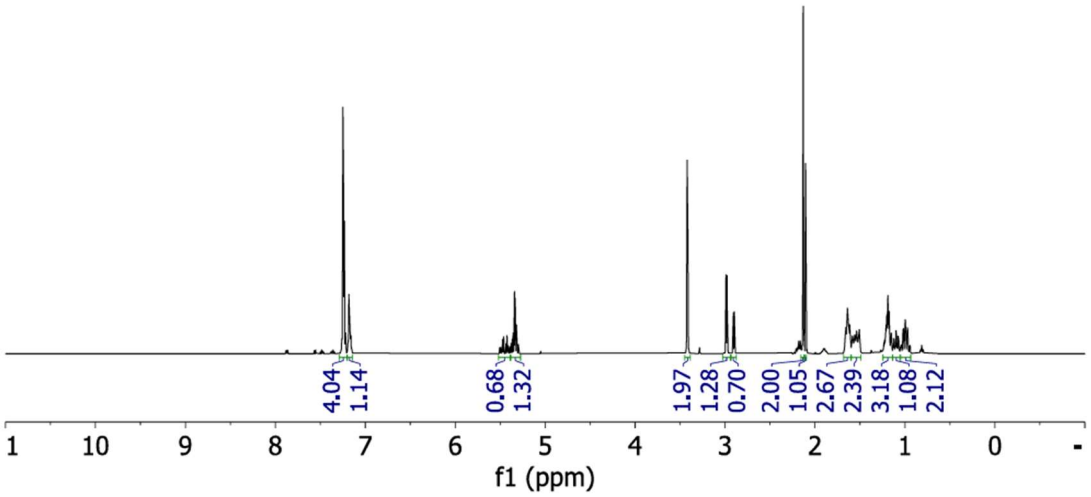
4.04
1.14
0.68
1.32
1.97
1.28
0.70
2.00
1.05
2.67
2.39
3.18
1.08
2.12
1
10
9
8
7
6
5
4
3
2
1
0
f1 (ppm)


140.40
139.13
138.99
129.21
129.14
128.21
128.20
126.95
126.93
124.75
124.29
61.74
61.48
59.78
54.15
42.20
41.92
36.55
33.16
33.01
26.22
26.06
26.03
25.89

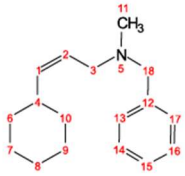
11
CH3
N
5
1
2
3
4
6
7
8
9
10
12
13
14
15
16
17
18

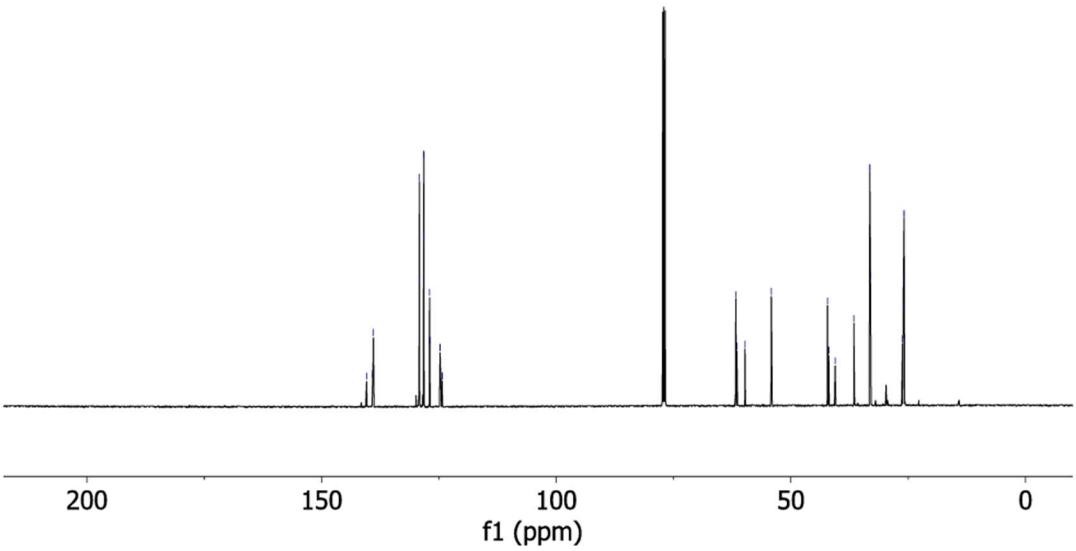
200
150
100
50
0
f1 (ppm)

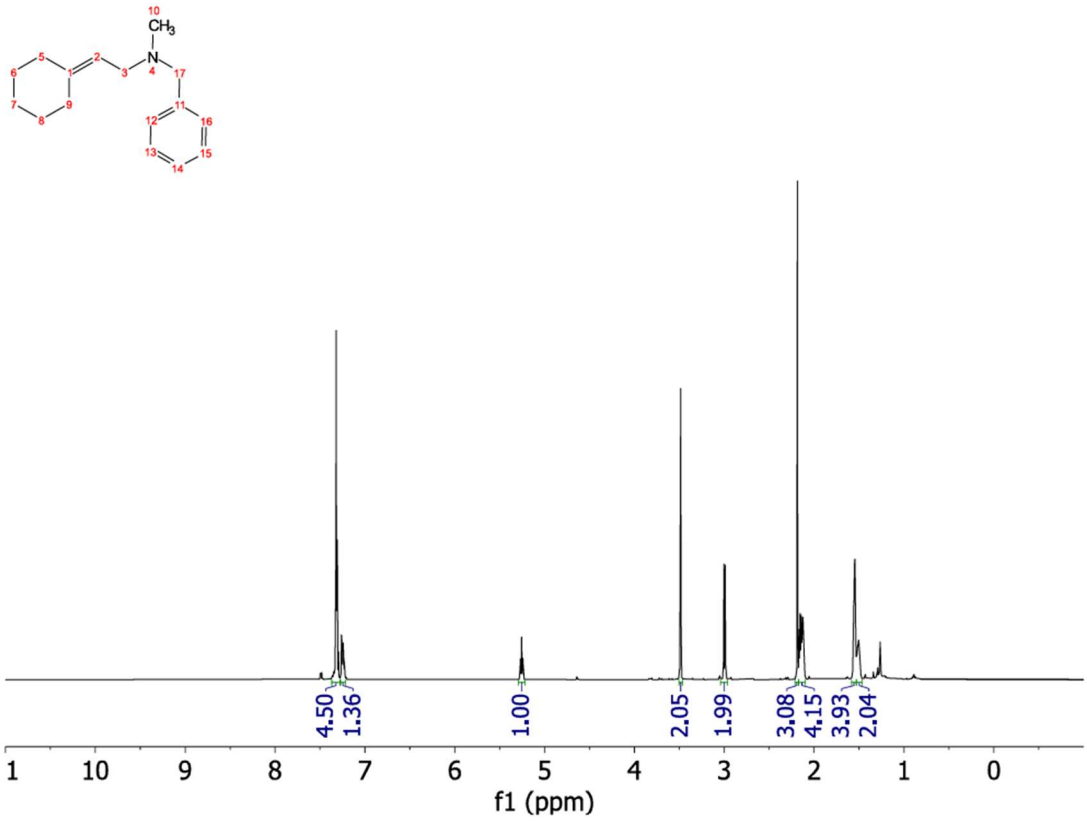
4.50
1.36
1.00
2.05
1.99
3.08
4.15
3.93
2.04
f1 (ppm)

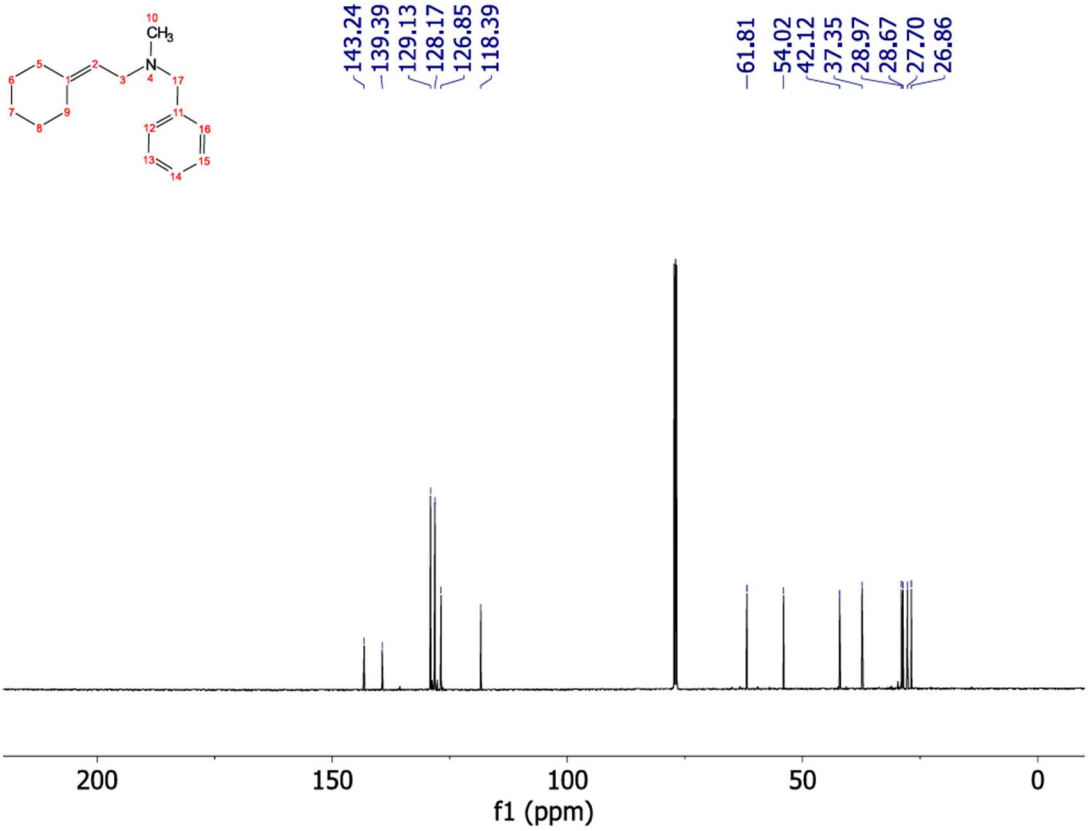
143.24
139.39
129.13
128.17
126.85
118.39
61.81
54.02
42.12
37.35
28.97
28.67
27.70
26.86
f1 (ppm)

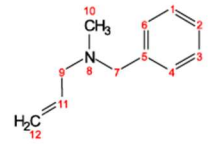
10
CH3
N
8
1
2
3
4
5
6
7
9
11
H2C
12

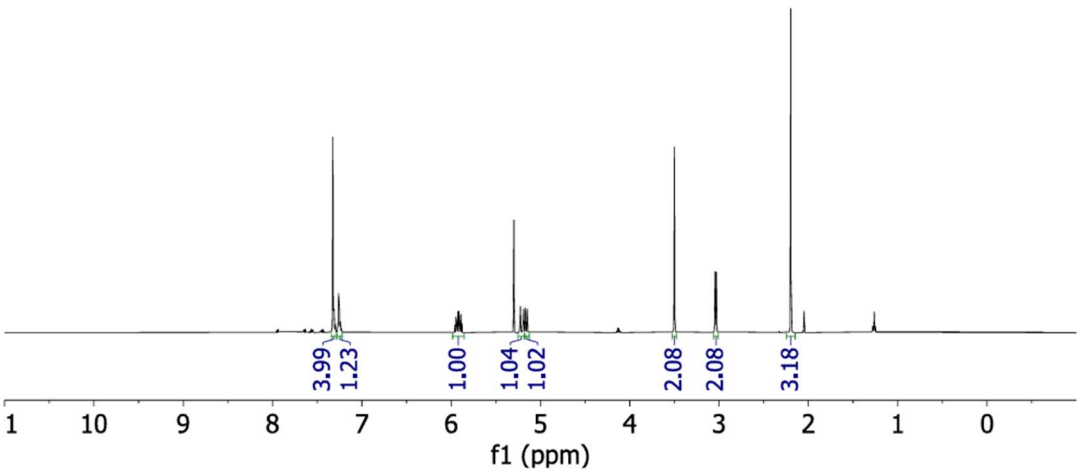
3.99
1.23
1.00
1.04
1.02
2.08
2.08
3.18
1
10
9
8
7
6
5
4
3
2
1
0
f1 (ppm)

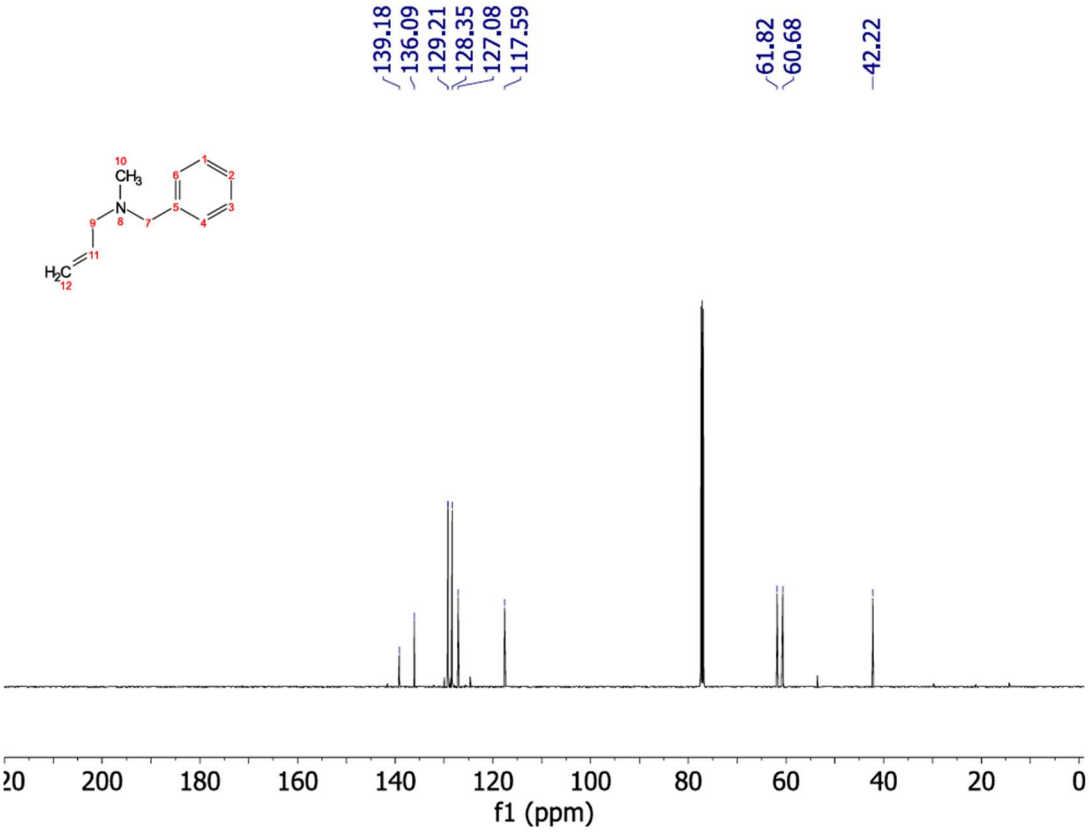
139.18
136.09
129.21
128.35
127.08
117.59
61.82
60.68
42.22
200
180
160
140
120
100
80
60
40
20
0
f1 (ppm)

10
CH3
N
8
1
2
3
4
5
6
7
9
11
H2C
12

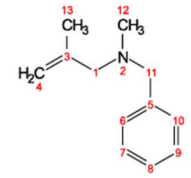
13
CH3
12
CH3
3
N
2
H2C
4
1
11
5
6
10
7
9
8

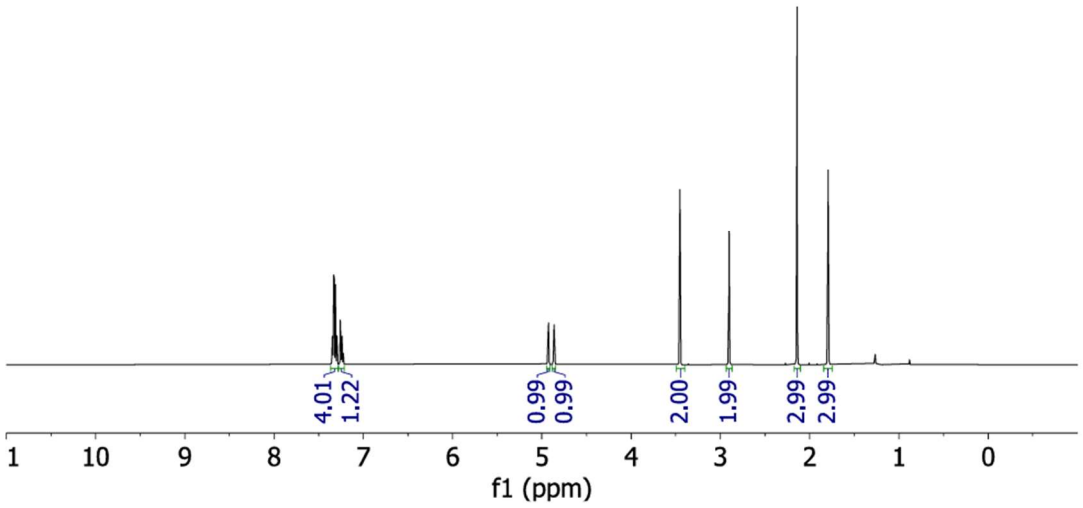
4.01
1.22
0.99
0.99
2.00
1.99
2.99
2.99
1
10
9
8
7
6
5
4
3
2
1
0
f1 (ppm)

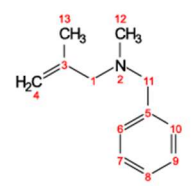
13
CH3
12
CH3
3
N
2
H2C
4
1
11
5
6
10
7
9
8

143.82
139.62
128.82
128.17
126.80
112.69
64.62
61.75
42.24
20.73
200
150
100
50
0
f1 (ppm)

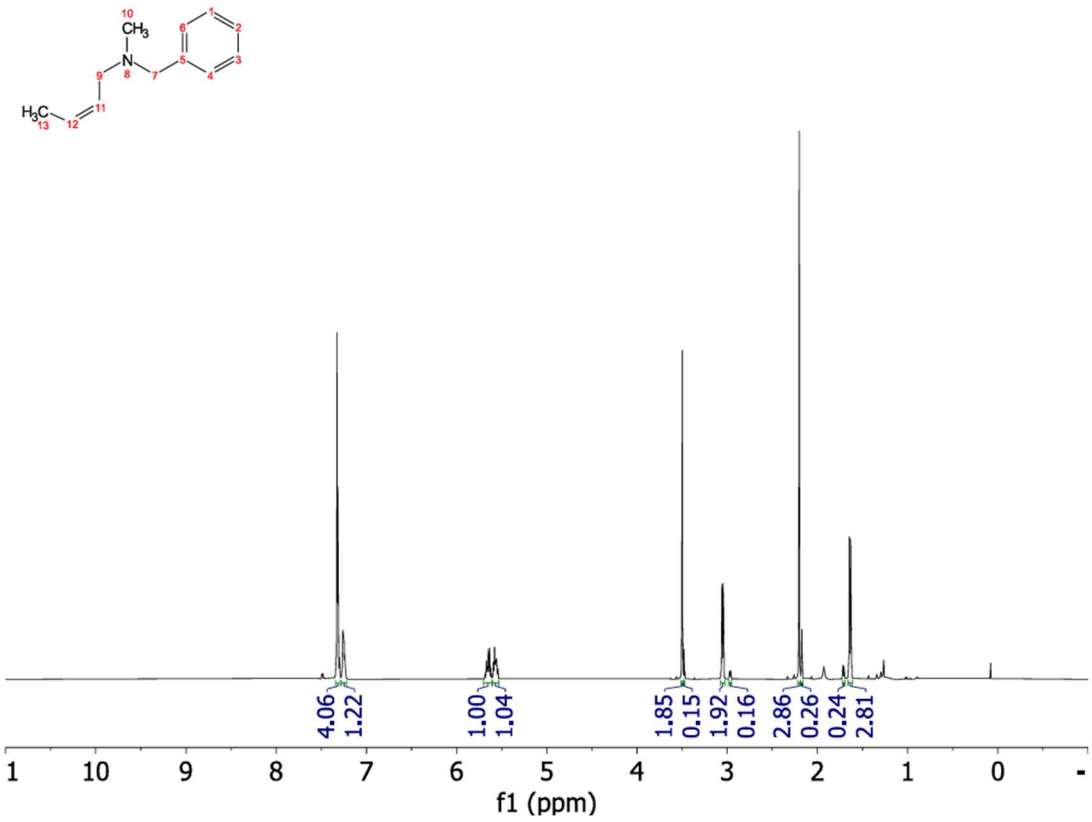
4.06
1.22
1.00
1.04
1.85
0.15
1.92
0.16
2.86
0.26
0.24
2.81
f1 (ppm)

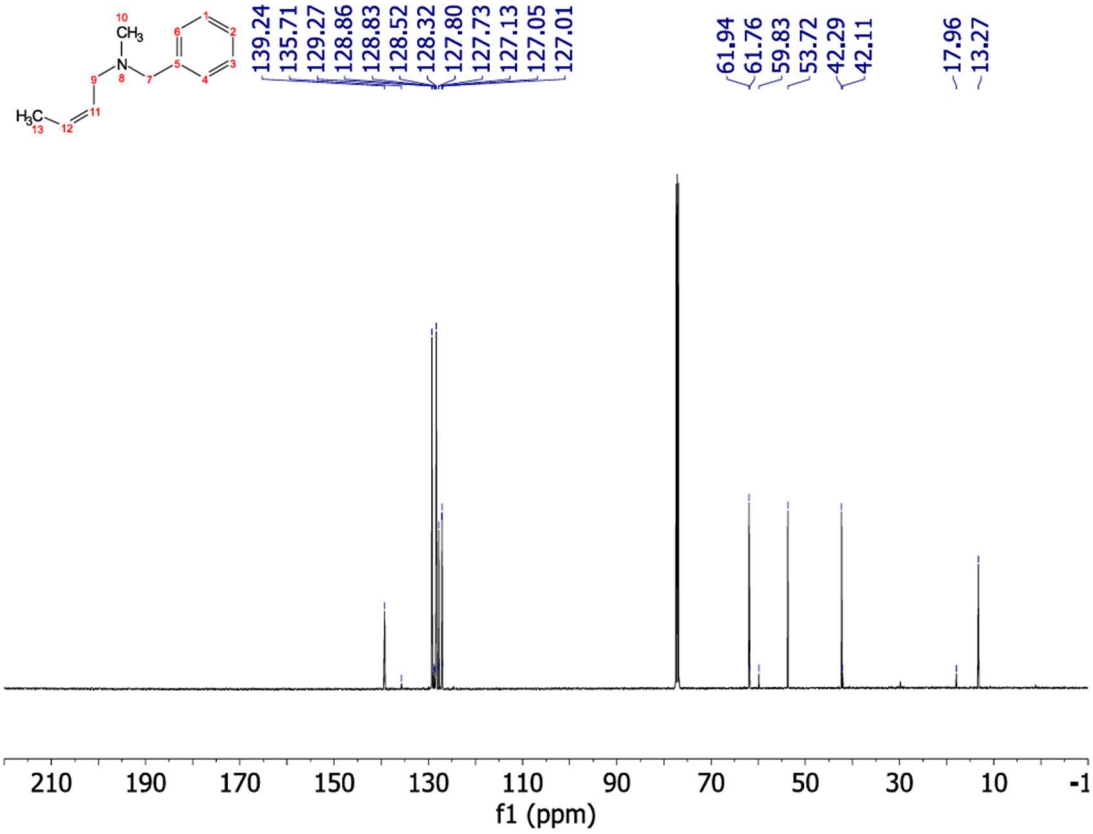
139.24
135.71
129.27
128.86
128.83
128.52
128.32
127.80
127.73
127.13
127.05
127.01
61.94
61.76
59.83
53.72
42.29
42.11
17.96
13.27
f1 (ppm)

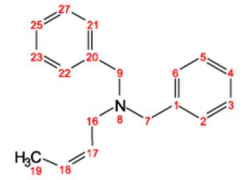

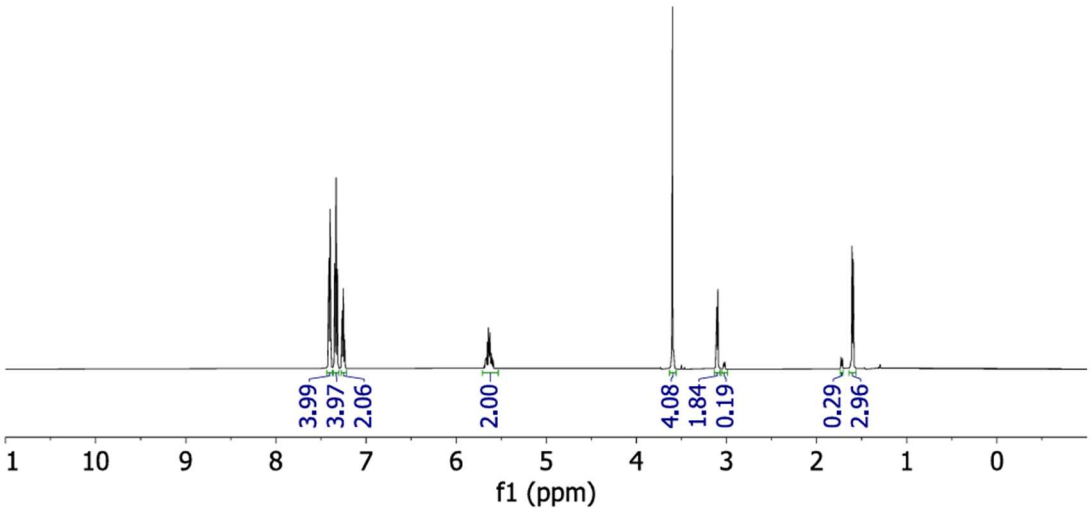
3.99
3.97
2.06
2.00
4.08
1.84
0.19
0.29
2.96
1 10 9 8 7 6 5 4 3 2 1 0
f1 (ppm)

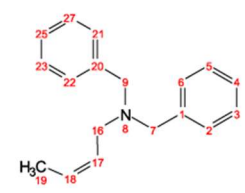

140.03
139.96
128.96
128.91
128.27
127.91
127.08
126.89
126.85
58.09
57.80
55.63
49.83
18.02
13.33
210 190 170 150 130 110 90 70 50 30 10 -1
f1 (ppm)

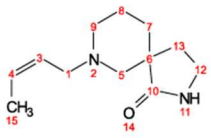
CH3
15
O
14
NH
11

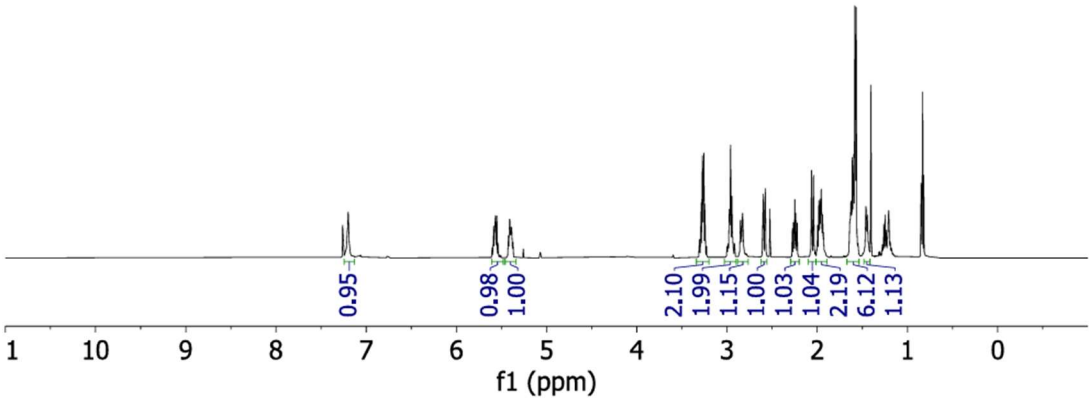
0.95
0.98
1.00
2.10
1.99
1.15
1.00
1.03
1.04
2.19
6.12
1.13
1
10
9
8
7
6
5
4
3
2
1
0
f1 (ppm)

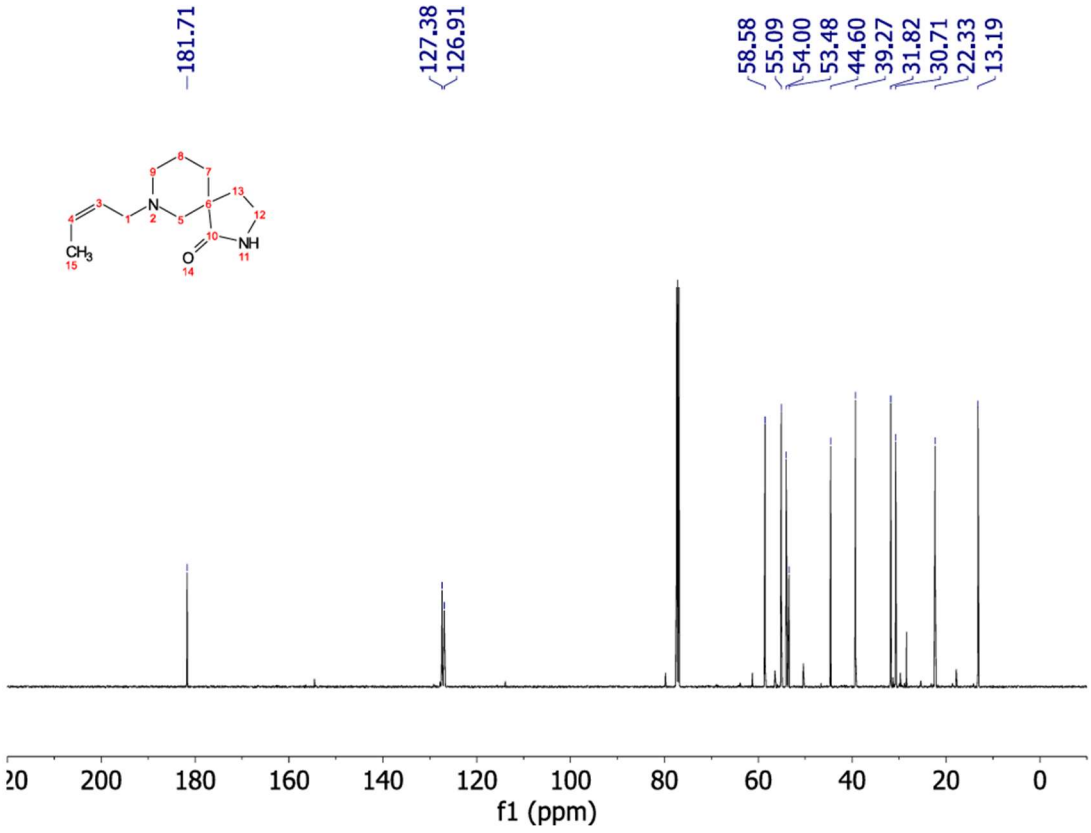
181.71
127.38
126.91
58.58
55.09
54.00
53.48
44.60
39.27
31.82
30.71
22.33
13.19
CH3
15
O
14
NH
11
200
180
160
140
120
100
80
60
40
20
0
f1 (ppm)

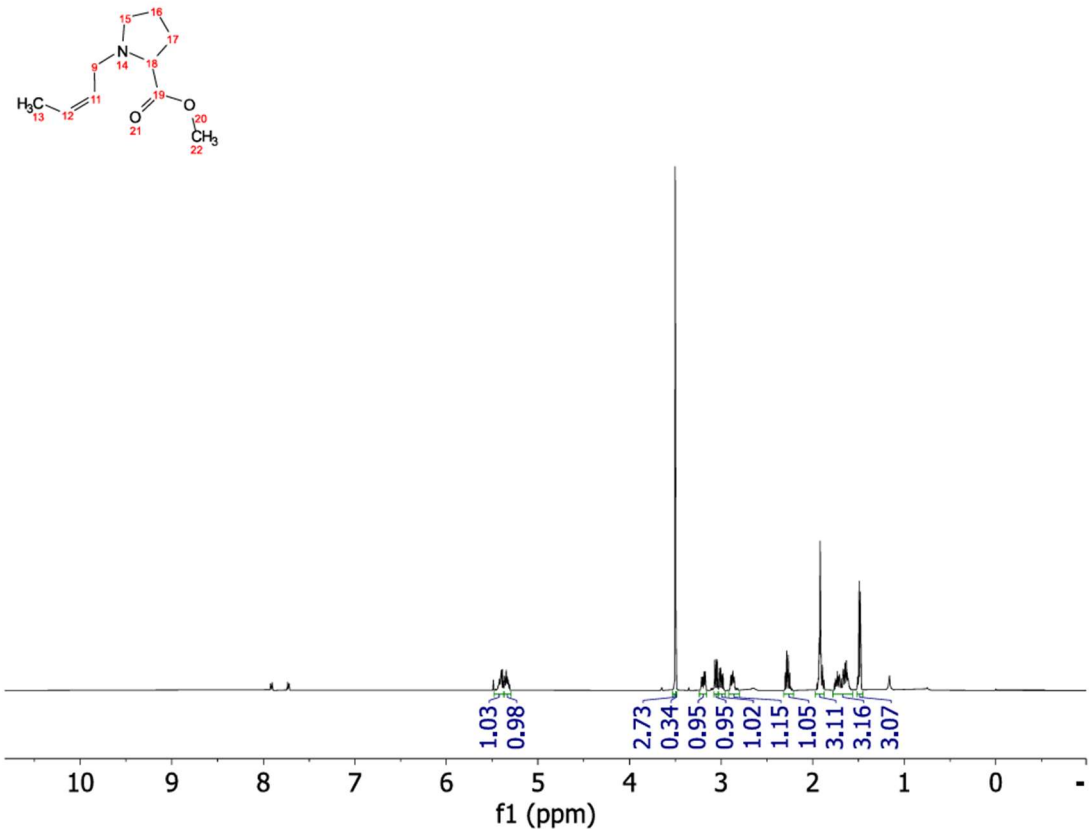
1.03
0.98
2.73
0.34
0.95
0.95
1.02
1.15
1.05
3.11
3.16
3.07
10
9
8
7
6
5
4
3
2
1
0
f1 (ppm)

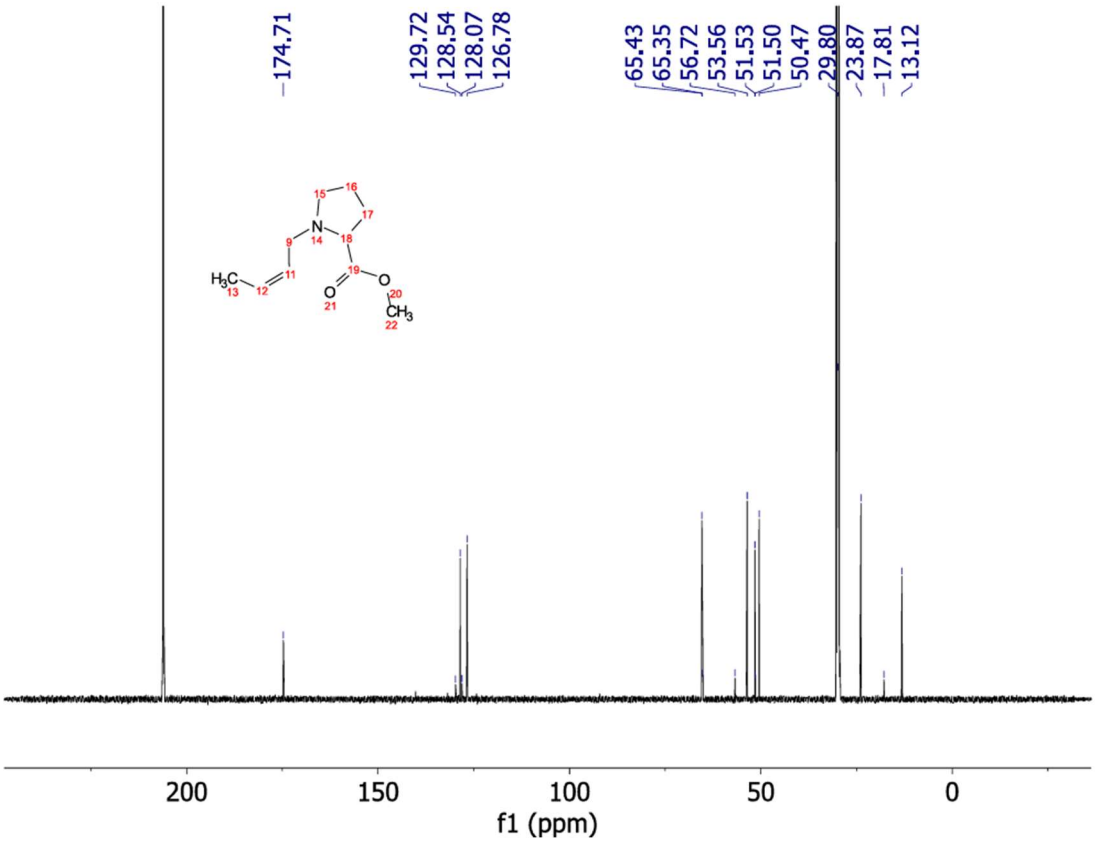
174.71
129.72
128.54
128.07
126.78
65.43
65.35
56.72
53.56
51.53
51.50
50.47
29.80
23.87
17.81
13.12
200
150
100
50
0
f1 (ppm)

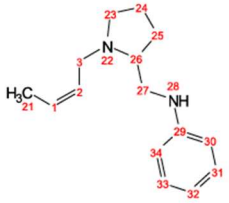
23
24
N
22
25
3
26
H3C
21
1
2
27
28
NH
29
30
34
33
31
32

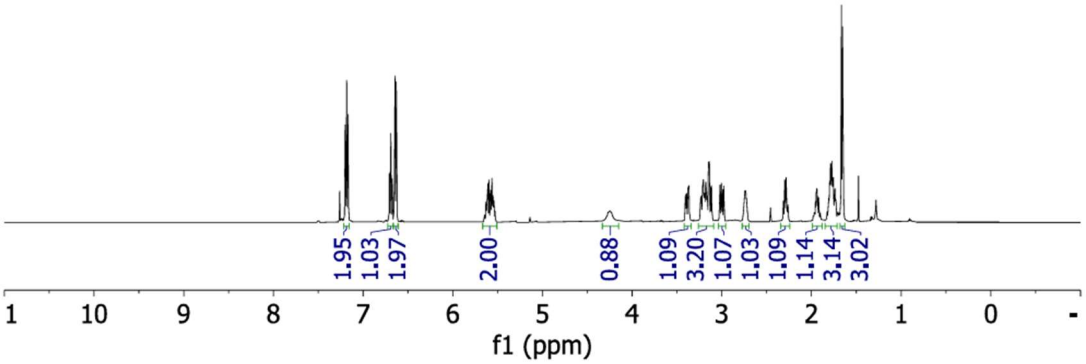
1.95
1.03
1.97
2.00
0.88
1.09
3.20
1.07
1.03
1.09
1.14
3.14
3.02
1
10
9
8
7
6
5
4
3
2
1
0
f1 (ppm)

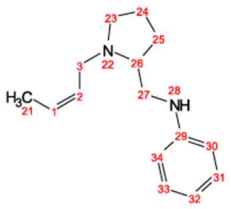
23
24
N
22
25
3
26
H3C
21
1
2
27
28
NH
29
30
34
33
31
32

148.97
129.36
127.57
126.61
117.01
112.86
62.61
54.43
50.24
45.46
28.83
22.90
13.21
200
180
160
140
120
100
80
60
40
20
0
f1 (ppm)

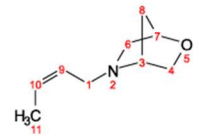

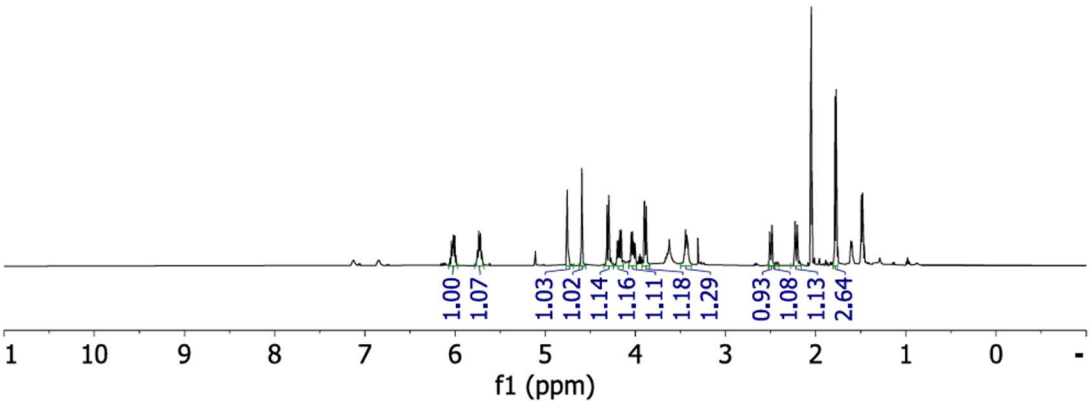
1.00
1.07
1.03
1.02
1.14
1.16
1.11
1.18
1.29
0.93
1.08
1.13
2.64
1 10 9 8 7 6 5 4 3 2 1 0 -
f1 (ppm)

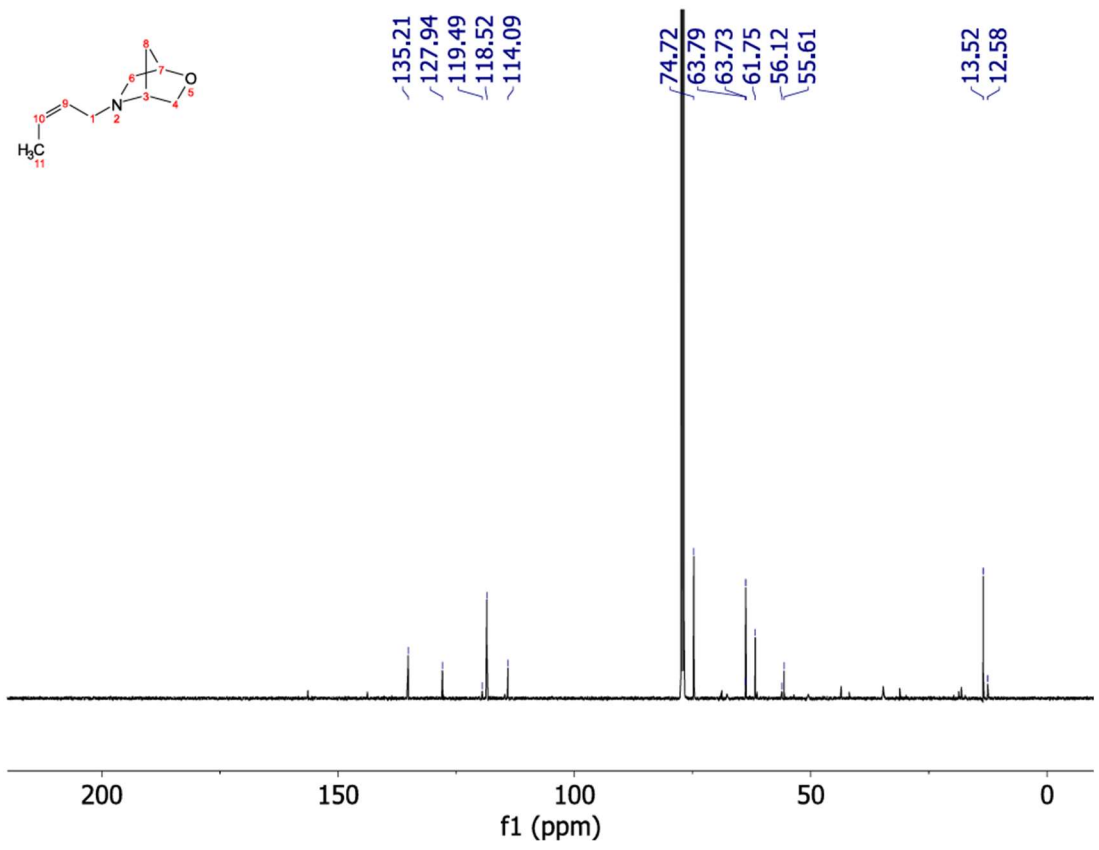
135.21
127.94
119.49
118.52
114.09
74.72
63.79
63.73
61.75
56.12
55.61
13.52
12.58
200 150 100 50 0
f1 (ppm)

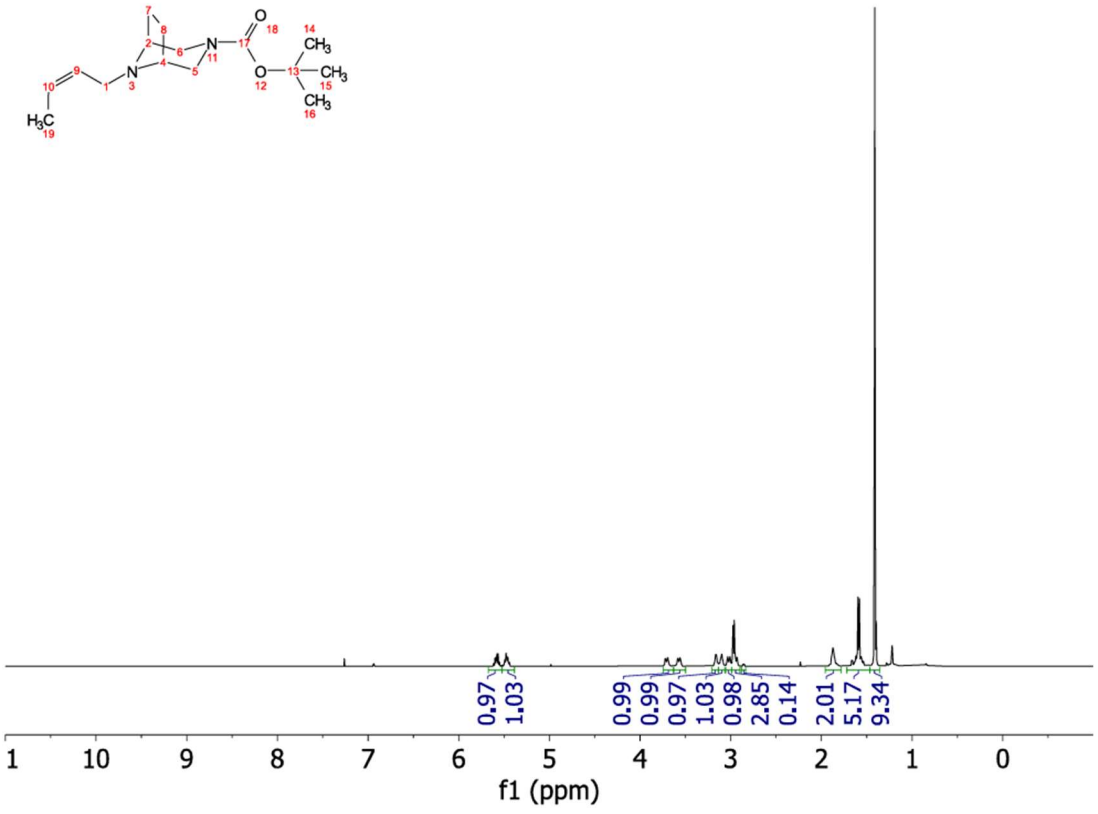
0.97
1.03
0.99
0.99
0.97
1.03
0.98
2.85
0.14
2.01
5.17
9.34
1
10
9
8
7
6
5
4
3
2
1
0
f1 (ppm)

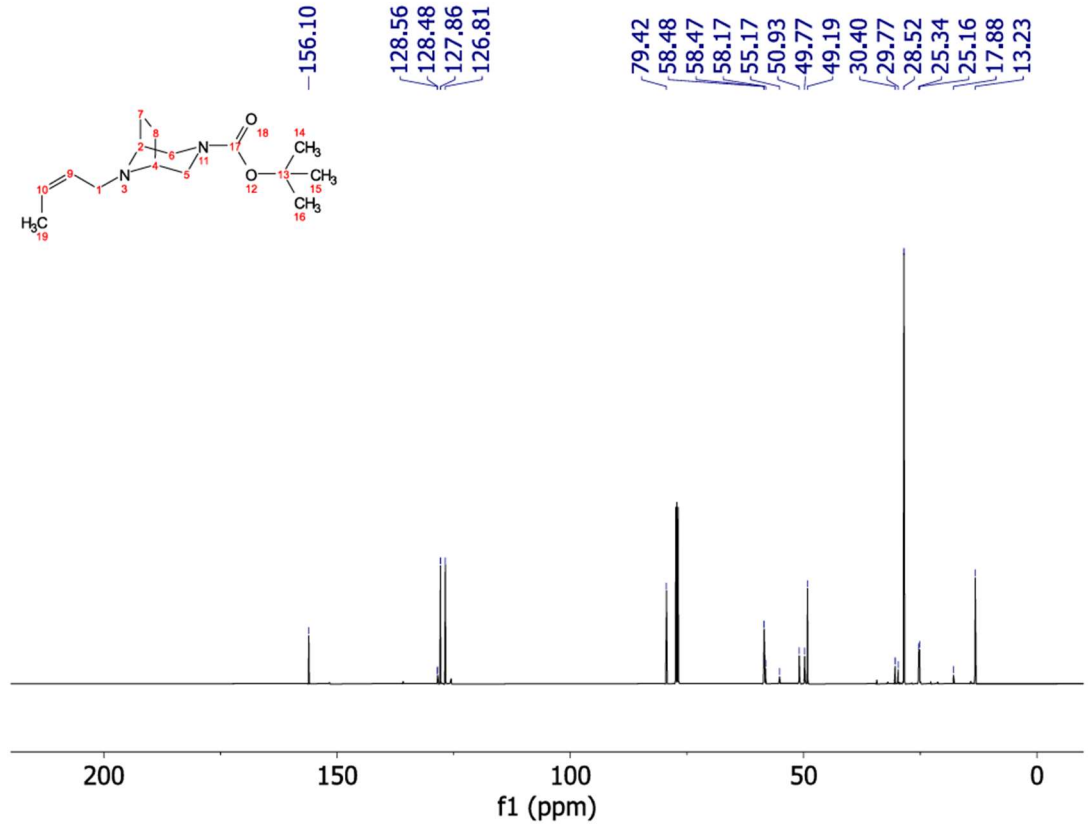
156.10
128.56
128.48
127.86
126.81
79.42
58.48
58.47
58.17
55.17
50.93
49.77
49.19
30.40
29.77
28.52
25.34
25.16
17.88
13.23
200
150
100
50
0
f1 (ppm)

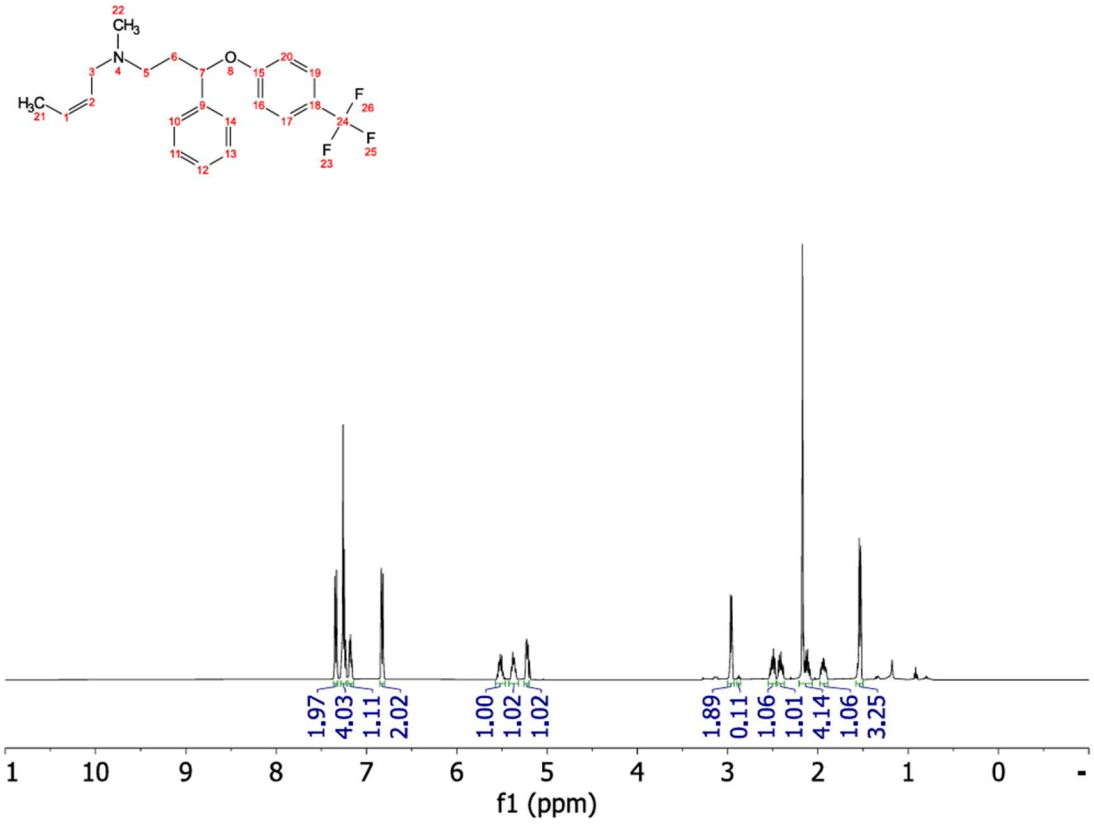
1.97
4.03
1.11
2.02
1.00
1.02
1.02
1.89
0.11
1.06
1.01
4.14
1.06
3.25
f1 (ppm)

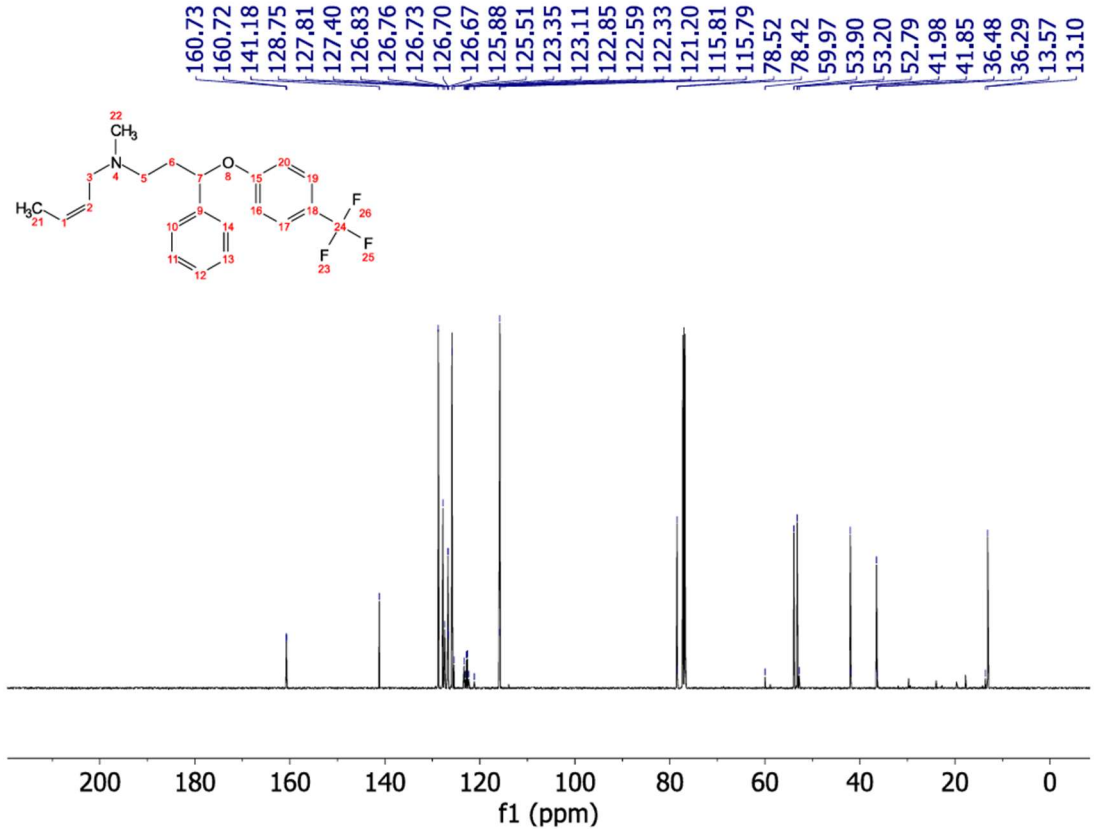
160.73
160.72
141.18
128.75
127.81
127.40
126.83
126.76
126.73
126.70
126.67
125.88
125.51
123.35
123.11
122.85
122.59
122.33
121.20
115.81
115.79
78.52
78.42
59.97
53.90
53.20
52.79
41.98
41.85
36.48
36.29
13.57
13.10
f1 (ppm)

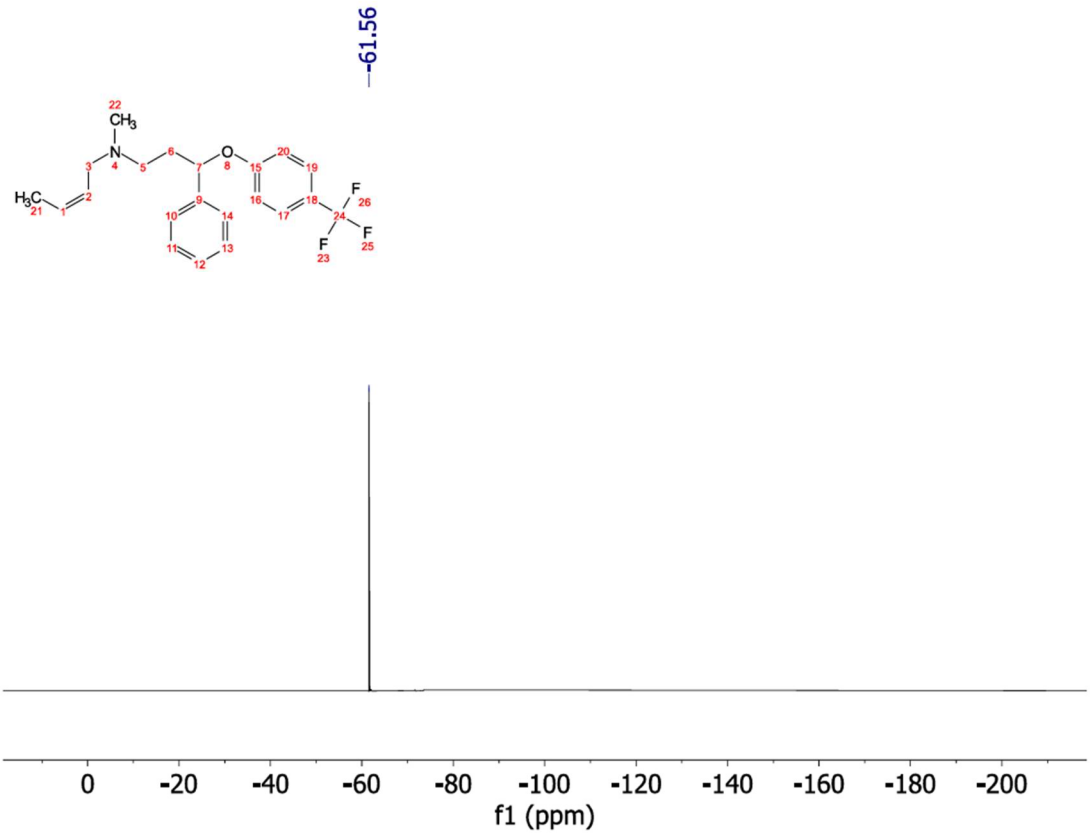

(blank space)

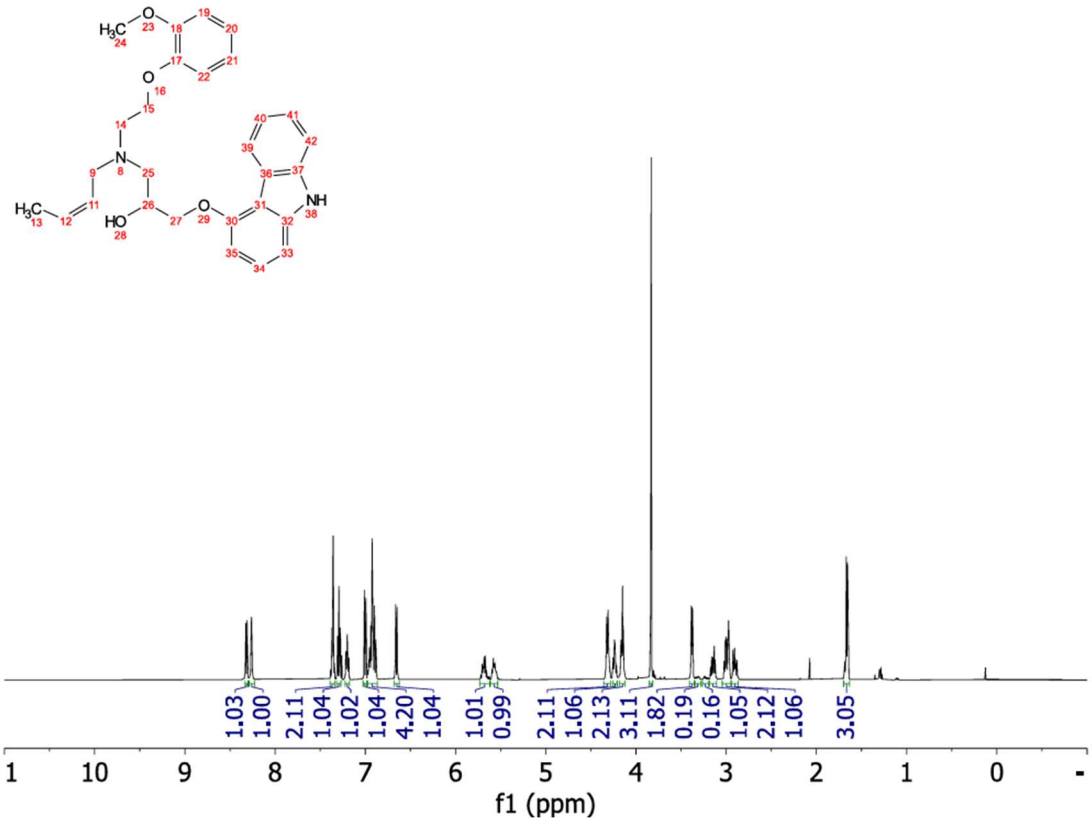
1.03
1.00
2.11
1.04
1.02
1.04
4.20
1.04
1.01
0.99
2.11
1.06
2.13
3.11
1.82
0.19
0.16
1.05
2.12
1.06
3.05
1
10
9
8
7
6
5
4
3
2
1
0
f1 (ppm)

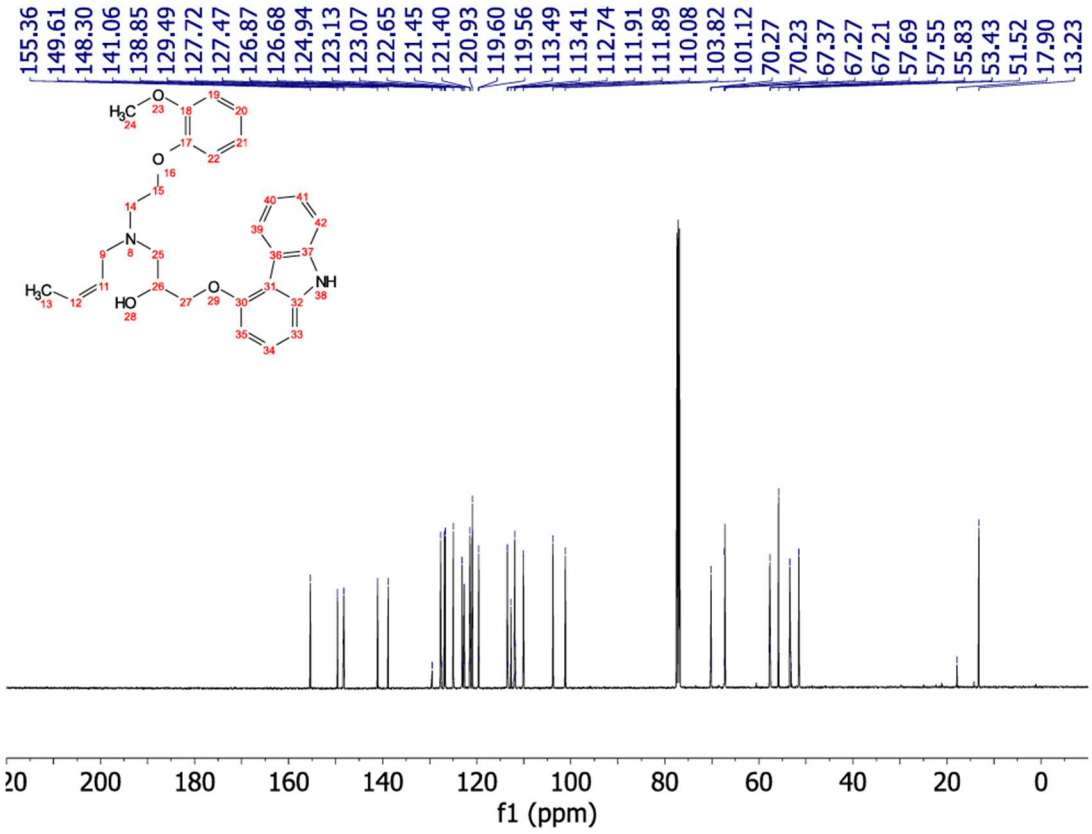
155.36
149.61
148.30
141.06
138.85
129.49
127.72
127.47
126.87
126.68
124.94
123.13
123.07
122.65
121.45
121.40
120.93
119.60
119.56
113.49
113.41
112.74
111.91
111.89
110.08
103.82
101.12
70.27
70.23
67.37
67.27
67.21
57.69
57.55
55.83
53.43
51.52
17.90
13.23
20
200
180
160
140
120
100
80
60
40
20
0
f1 (ppm)

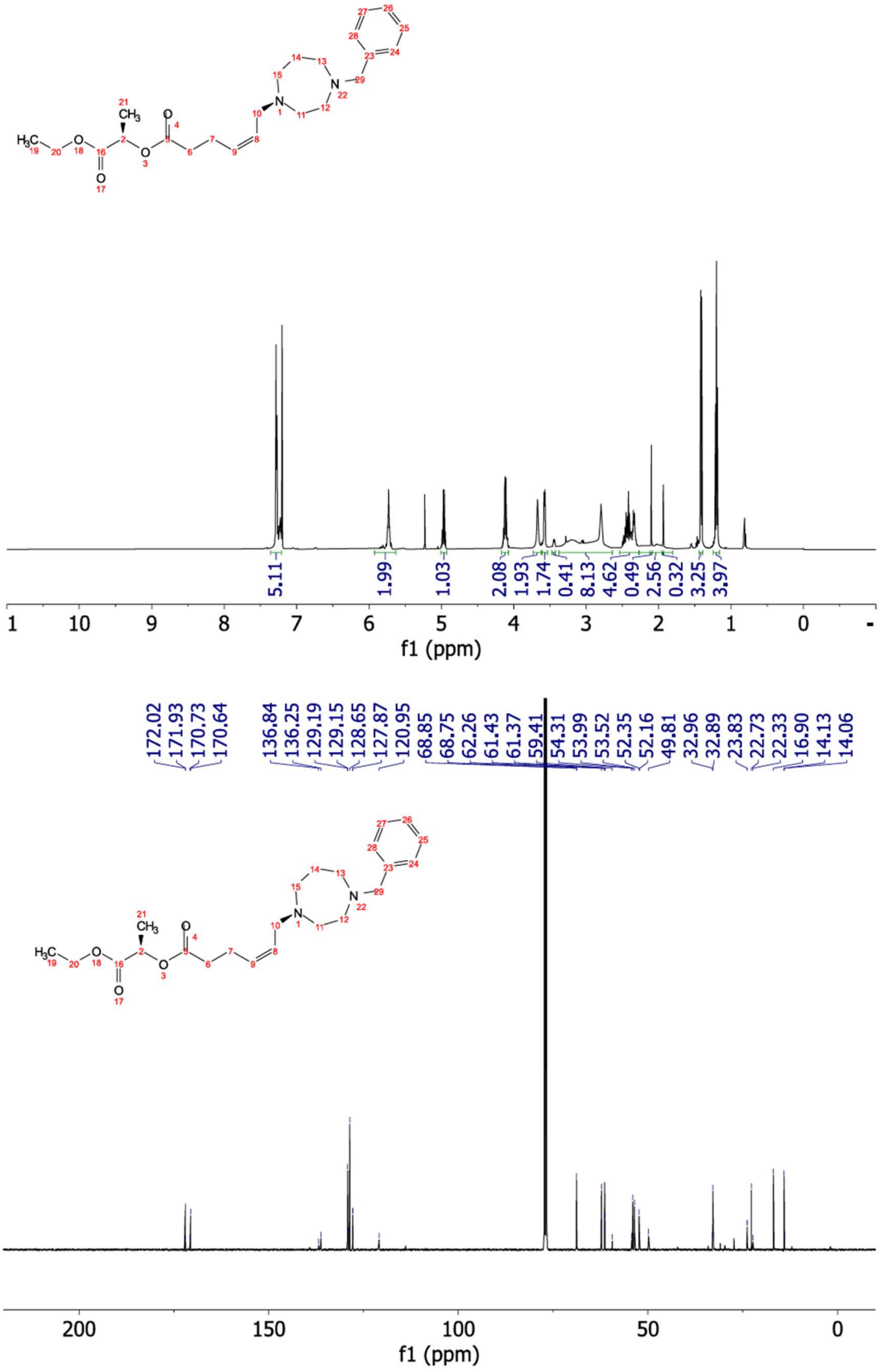
5.11
1.99
1.03
2.08
1.93
1.74
0.41
8.13
4.62
0.49
2.56
0.32
3.25
3.97
f1 (ppm)
172.02
171.93
170.73
170.64
136.84
136.25
129.19
129.15
128.65
127.87
120.95
68.85
68.75
62.26
61.43
61.37
59.41
54.31
53.99
53.52
52.35
52.16
49.81
32.96
32.89
23.83
22.73
22.33
16.90
14.13
14.06
f1 (ppm)

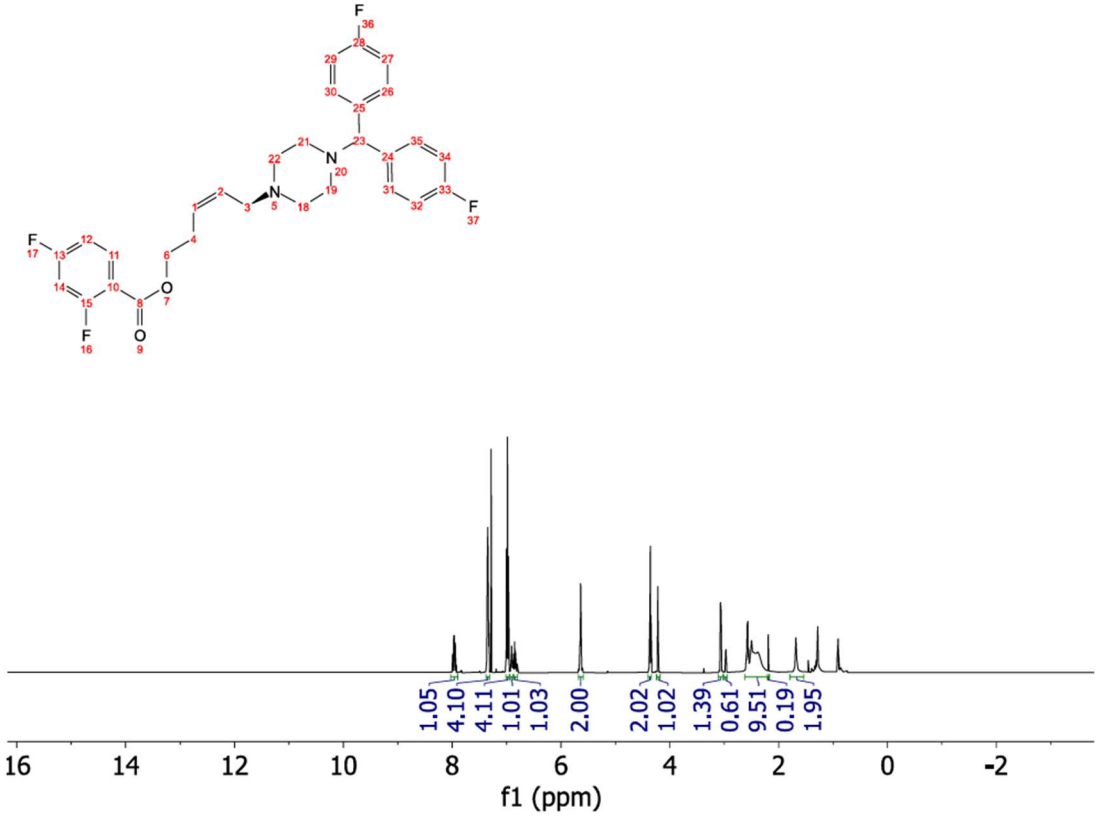
1.05
4.10
4.11
1.01
1.03
2.00
2.02
1.02
1.39
0.61
9.51
0.19
1.95
16
14
12
10
8
6
4
2
0
-2
f1 (ppm)

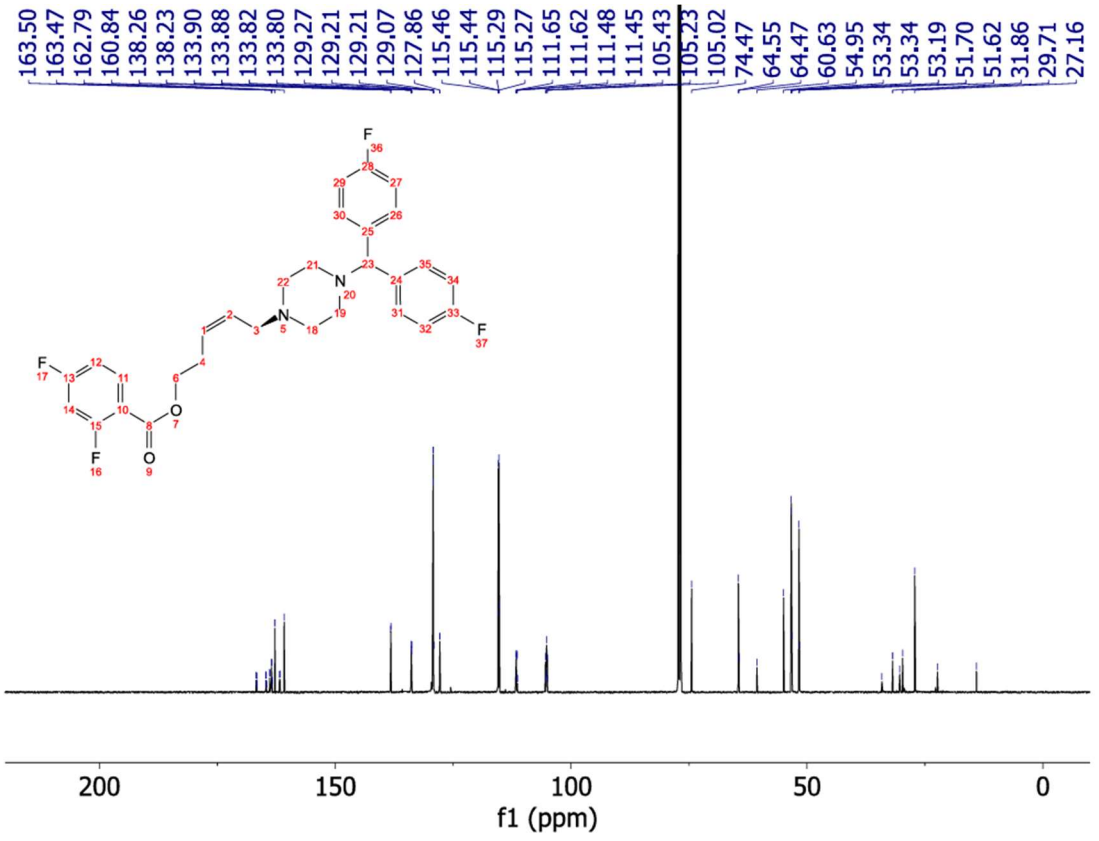
163.50
163.47
162.79
160.84
138.26
138.23
133.90
133.88
133.82
133.80
129.27
129.21
129.21
129.07
127.86
115.46
115.44
115.29
115.27
111.65
111.62
111.48
111.45
105.43
105.23
105.02
74.47
64.55
64.47
60.63
54.95
53.34
53.34
53.19
51.70
51.62
31.86
29.71
27.16
200
150
100
50
0
f1 (ppm)

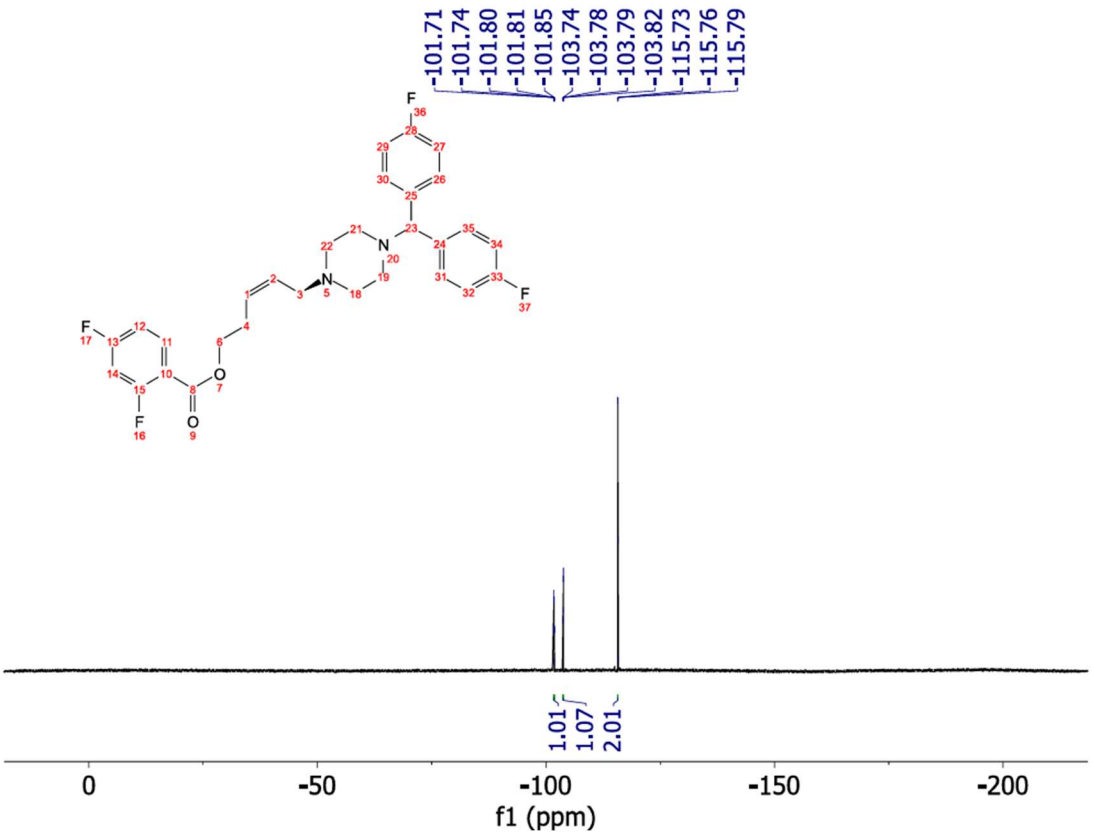
-101.71
-101.74
-101.80
-101.81
-101.85
-103.74
-103.78
-103.79
-103.82
-115.73
-115.76
-115.79
1.01
1.07
2.01
0
-50
-100
-150
-200
f1 (ppm)

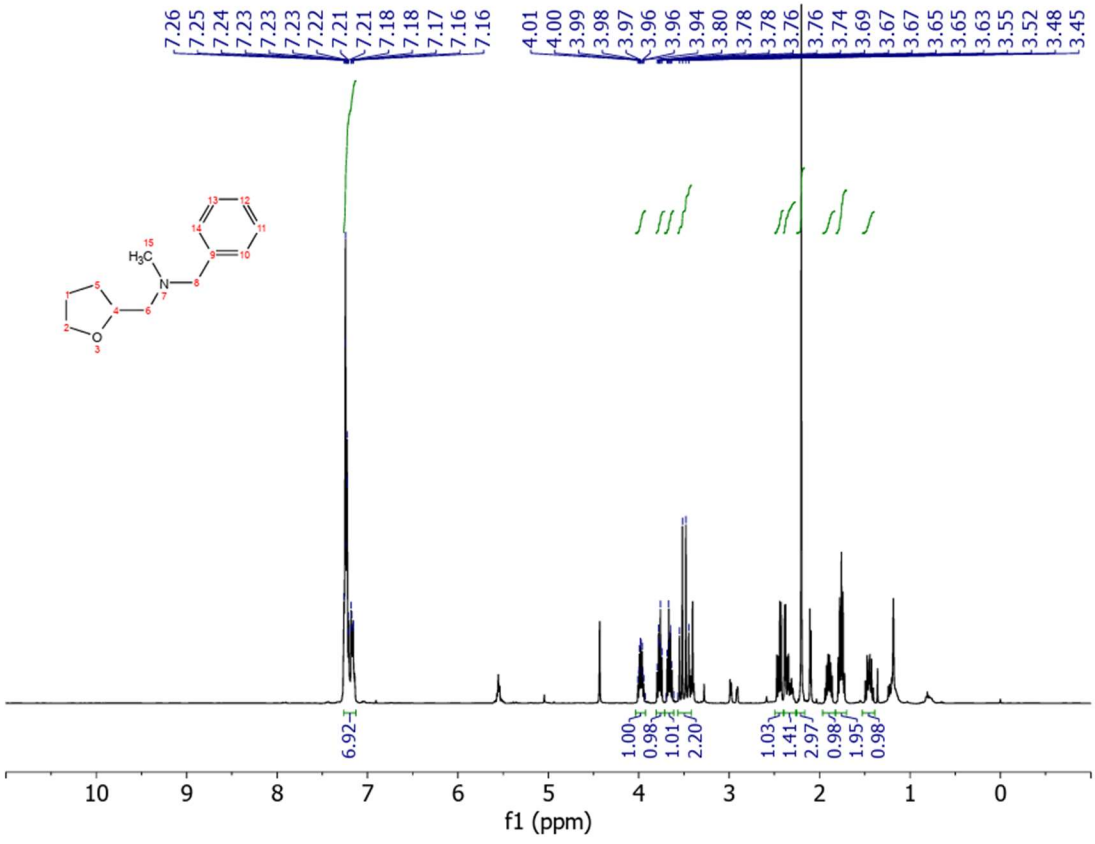
7.26
7.25
7.24
7.23
7.23
7.23
7.22
7.21
7.21
7.18
7.18
7.17
7.16
7.16
4.01
4.00
3.99
3.98
3.97
3.96
3.96
3.94
3.80
3.78
3.78
3.76
3.76
3.74
3.69
3.67
3.67
3.65
3.65
3.63
3.55
3.52
3.48
3.45
6.92
1.00
0.98
1.01
2.20
1.03
1.41
2.97
0.98
1.95
0.98
10
9
8
7
6
5
4
3
2
1
0
f1 (ppm)

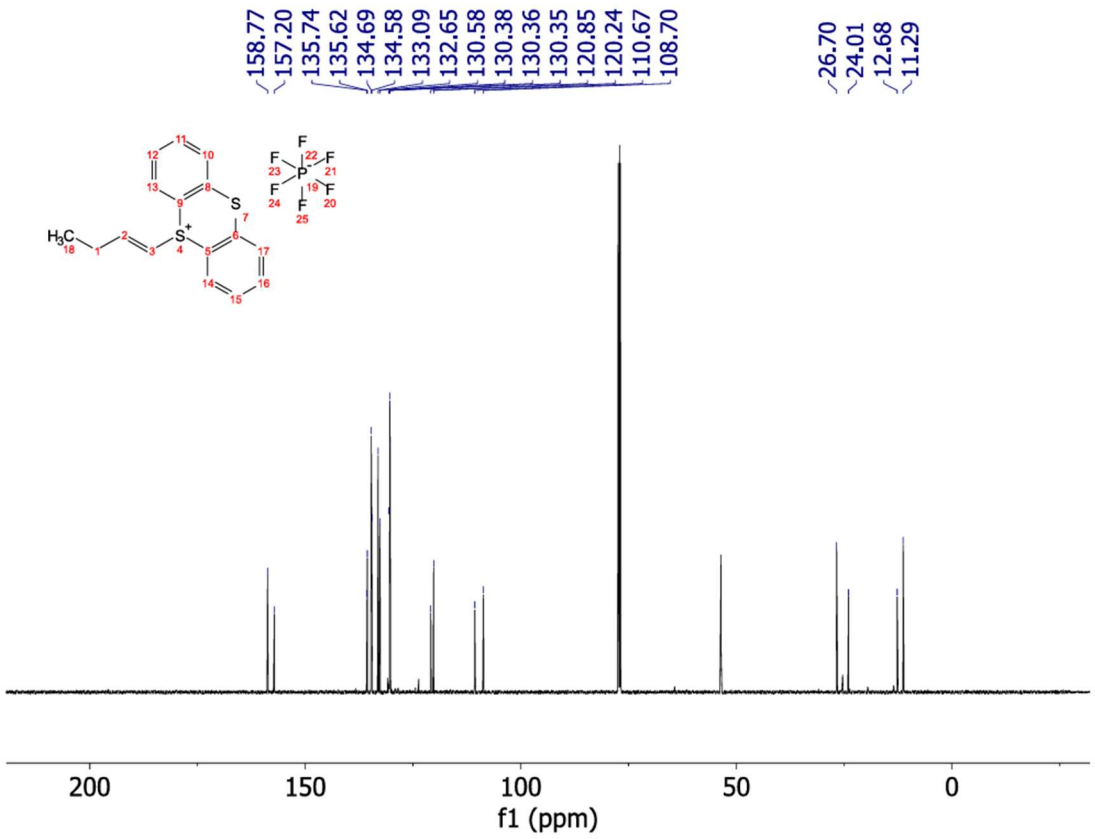
158.77
157.20
135.74
135.62
134.69
134.58
133.09
132.65
130.58
130.38
130.36
130.35
120.85
120.24
110.67
108.70
26.70
24.01
12.68
11.29
200
150
100
50
0
f1 (ppm)

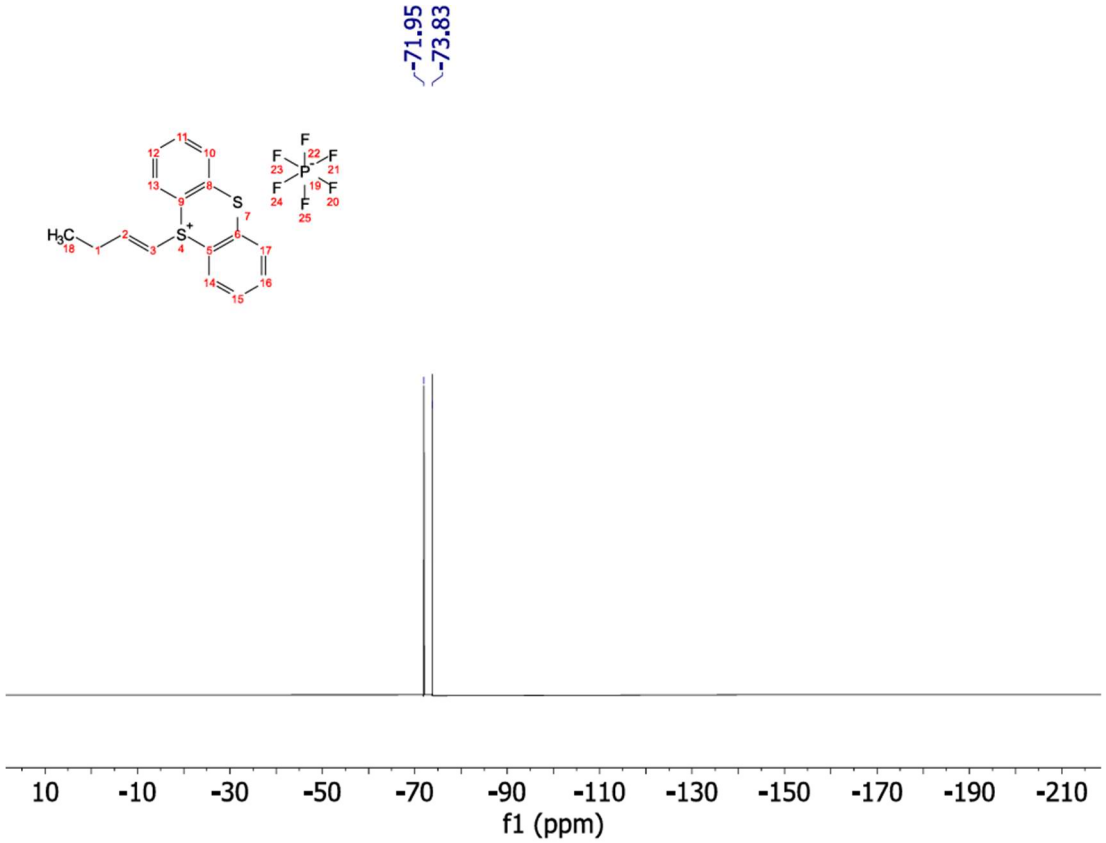
-71.95
-73.83
10
-10
-30
-50
-70
-90
-110
-130
-150
-170
-190
-210
f1 (ppm)

Appendix B: Supporting Information for Chapter 3 (Unraveling the Mechanism of *Z*-selective Allylic Functionalization *via* Thianthrenium Salts)

B1. General Methods and Materials

Unless otherwise noted, reactions were performed under air in an anhydrous solvent. MeCN and *i*-Pr_2NEt were purchased as a sureseal bottle and used as is. All liquid amines were distilled from CaH_2 prior to use. KPF_6 was dried under vacuum prior to use. Purity of 5-(4-phenylbut-1-en-1-yl)-5H-thianthren-5-ium hexafluorophosphate was verified prior to kinetic analysis, using ^1H NMR and ^{19}F NMR spectroscopy. Unless otherwise noted, other commercially-available reagents were used as received. Crude mixtures were evaluated by thin-layer chromatography using EMD/Merck silica gel 60 F254 pre-coated plates (0.25 mm) and were visualized by UV, Seebach, ninhydrin, or $KMnO_4$ staining. Flash chromatography was performed with a Biotage Isolera One automated chromatography system with re-packed silica columns (technical grade silica, pore size 60 Å, 230-400 mesh particle size, 40-63 particle size) or pre-packed Biotage Sfär Silica HC Duo 20µm 25g - High Capacity Column columns unless otherwise noted. Purified materials were dried in vacuo (0.050 Torr) to remove trace solvent. ^1H, ^{13}C, ^{19}F Spectra were taken using a Bruker Avance-400 with a BBFO Probe, a Bruker Avance-500 with a DCH Cryoprobe, or Bruker Avance III HD-500 with a TXO Cryoprobe. NMR data are reported relative to residual $CHCl_3$ (^1H, δ = 7.26 ppm), $CDCl_3$ (^{13}C, δ = 77.16 ppm) or residual CHD_2CN (^1H, δ = 1.96 ppm), CD_3CN (^{13}C, δ = 118.26 ppm). Data for ^1H NMR spectra are reported as follows: chemical shift (δ ppm) (multiplicity, coupling constant (Hz), integration). Multiplicity and qualifier abbreviations are as follows: s = singlet, d = doublet, t = triplet, q = quartet, m = multiplet, br = broad. All NMR yields were determined *via* reference against an internal standard (dibromomethane or mesitylene for ^1H). Mass spectrometry data was collected on a Thermo Scientific Q Exactive Plus Mass Spectrometer.

Abbreviations: Boc—tert-butyl carbamate, CFL—compact fluorescent lamps, CV—cyclic voltammetry, DCM—dichloromethane, DC—direct current, DFT—density functional theory, DMF—dimethyl formamide, DMSO—dimethylsulfoxide, Et—ethyl, EtOAc—ethyl acetate, *i*-Pr—isopropyl, Me—methyl, MeCN—acetonitrile, MeOH—methanol, NBO—natural bond orbital, KIE—kinetic isotop effect, *n*-Bu—butyl, *n*-Pr—propyl, RVC—reticulated vitreous carbon, PF_6—hexafluorophosphate, Ph—phenyl, PTFE—polytetrafluoroethylene, *t*-Bu—tert-butyl, THF—tetrahydrofuran, TEA—triethylamine, TFA—trifluoroacetic acid, TLC—thin layer chromatography

Electrochemical Methods and Materials

All chronoamperometric and chronopotentiometric measurements were performed at room temperature using a Pine WaveNowXV. Chronoamperometric and chronopotentiometric measurements were carried out in divided cells with RVC (8 × 6 × 6 mm, Ultramet, 80 ppi) as working electrodes affixed to a graphite pencil/wire assembly and with nickel foam (1.4 mm x 1.4 mm, MTI Corporation, Surface density: 350g/m^2) as counter electrodes affixed to stainless steel wire (see below). The potentials were measured versus an $Ag/AgNO_3$ (0.01 M in MeCN with 0.1 M n-Bu_4N•PF_6) reference electrode (all electrodes from Pine Research) and externally referenced *via* the ferrocene/ferrocenium couple. Bulk constant current electrolysis experiments were driven with a Dr. Meter HY3005M-L DC Power Supply or a custom–made low current power supply which was externally calibrated with a multimeter using a 10 or 1–Ohm resistor.

Low-Current Power Supply: Original design and fabrication by Dr. Blaise J. Thompson. Provides an operational range of ±0.01– 14.99 mA, tunable by variable resistor, delivering power to banana socket pair. The power supply is limited to ±15 V for bulk electrolysis and is powered by an 18 V wall wart. Circuitry is housed within an aluminum enclosure. For additional specifications, see: *J. Am. Chem. Soc.* **2020** 142, 2093–2099 and *Nature* **2021** 596, 74–79.

Figure B1. Divided cell with electrodes.

Divided Cell Set-up: Original design and fabrication by Tracy O. Drier. Porosity E diameter glass frit purchased from Ace Glass (7176-21). For additional specifications, see: *J. Am. Chem. Soc.* **2020** 142, 2093–2099 and *Fusion, Journal of the ASGS*, November 2020 issue, 19-26. Anode electrode assembled *via* affixing end of the metallic wire (Belden Hook-Up wire, item no. 83005 007100) around the pencil (JuneGold 2B graphite 2 mm) using conductive graphite adhesive (Alfa Aesar, 42465), wrapping in teflon tape to prevent exposure, then piercing RVC with pencil. Solvent exposed electrode surface area (2.1 cm^2) was calculated *via* manufacturer-supplied surface area/volume ratio measurements. PTFE tubing (Cole-Parmer; 1/32" ID, 1/16" OD, item number EW-06407-41) connects both sides of the divided cell to normalize pressure. Septa inner diameter 16 mm. Stainless steel purchased from Grainger; stainless steel lockwire, 0.025" diameter, item number 16Y043.

B2. Supplemental Data

General Procedure for Allylic Amination of Alkenylthianthrenium Salt: To a threaded vial equipped with a magnetic stir bar was added alkenylthianthrenium salt (0.05 mmol, 1.0 equiv.) and MeCN (0.5 mL). Then the amine nucleophile (0.05 mmol, 1.5 equiv.) followed by *i*-Pr_2NEt (45 µL, 0.25 mmol, 5.0 equiv.) were added. The reaction mixture was capped with a PTFE seal and stirred at room temperature until completion of the reaction (6 hours).

For NMR analyses – Reactions carried out using the above protocol were analyzed by ^1H NMR spectroscopy. Allylic amine product yield and *Z:E* were determined *via* ^1H NMR using CH_2Br_2 as an external standard.

B2.1. Monitoring Thianthrenium Salts During Allylic Amination (Scheme 3.1)

^{1}H NMR Monitoring of Dicationic Adduct Elimination: To an oven-dried divided electrochemical cell equipped with magnetic stir bars was added thianthrene (65 mg, 0.3 mmol, 1.5 equiv.) to the anode compartment and KPF_6 (147 mg, 0.8 mmol) to both compartments. The cell was equipped with two septa containing a stainless steel wire/Ni foam (12 x 6 mm) cathode assembly and a pencil/RVC (5 x 5 x 7 mm) anode assembly connected together with a teflon tubing to equalize pressure. CD_3CN (2 mL) was added to the cathode and anode compartments. But-3-en-1-ylbenzene (26 mg, 29.5 µL, 0.2 mmol, 1.0 equiv.) was added to the anode compartment. Trifluoroacetic acid (153 µL, 2.0 mmol, 10 equiv.) was added to the cathode compartment and both sides of the cell were stirred and electrolyzed under a constant current of 6.0 mA for 2.2 h (2.5 F/mol alkene). At completion of electrolysis, the electrode leads were disconnected, septa removed, and the anode RVC was pushed off the pencil into the reaction mixture. CH_2Br_2 (14.0 µL, 0.2 mmol, 1.0 equiv.) was added as an internal standard. To an oven-dried NMR tube was added 500 µL of the adduct solution (Figure B2).

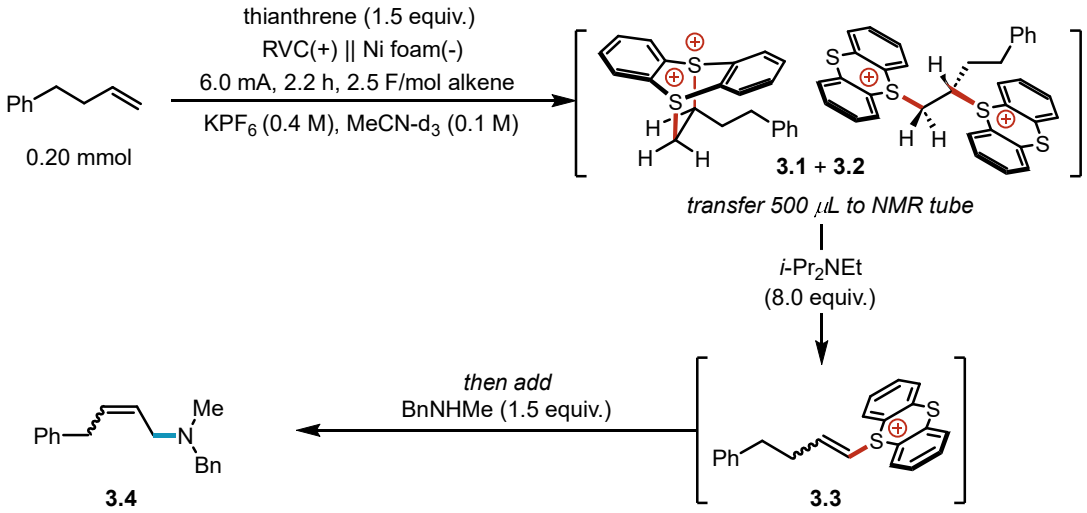

Figure B2. Reaction scheme for dicationic adducts **3.1** + **3.2** generation, base quench to **3**, and allylic amination to **3.4**.

Five initial ^{1}H NMR scans were taken over the course of five minutes before the addition of *i*-Pr_2NEt (70 µL, 0.40 mmol, 5.0 equiv.). Then the reaction was monitored by taking a spectrum every 15 seconds using 1 scan with a 1 second relaxation delay. Approximately five minutes after dicationic adducts were observed to be fully quenched, *N*-benzylmethylamine (9.7 µL, 0.075 mmol, 1.5 equiv.) was added and the reaction was monitored by taking a spectrum every 20 seconds using 1 scan with a 1 second relaxation delay.

Signals used for dicationic adducts **3.1** and **3.2** = 4.53 ppm (*mono*-adduct **3.1**; qd, J = 7.9, 5.6 Hz, 1H), 4.39 ppm (*mono*-adduct **3.1**; dd, J = 13.6, 8.6 Hz, 1H), 4.22 – 4.15 ppm (*bis*-adduct **3.2**; m, 1H), 4.10 ppm (*bis*-adduct **3.2**; dd, J = 13.6, 2.3 Hz, 1H), 3.87 ppm (*bis*-adduct **3.2**; dd, J = 13.6, 9.9 Hz, 1H), 3.73 ppm (*mono*-adduct **3.1**; dd, J = 13.6, 5.4 Hz, 1H); 5-(4-phenylbut-1-en-1-yl)-5H-thianthren-5-ium hexafluorophosphate **3.3** (alkenylTT)= 6.37 ppm (*E*-isomer; dt, J = 14.8, 1.4 Hz, 1H) and 6.69 ppm (*Z*-isomer; dt, J = 8.6, 1.4 Hz, 1H); *N*-benzyl-*N*-methyl-4-phenylbut-2-en-1-amine **3.4** (allylic amine product) = 5.81 – 5.53 ppm (m, 2H); and internal standard CH_2Br_2 = 5.10 ppm (s, 2H). See Figure B3.

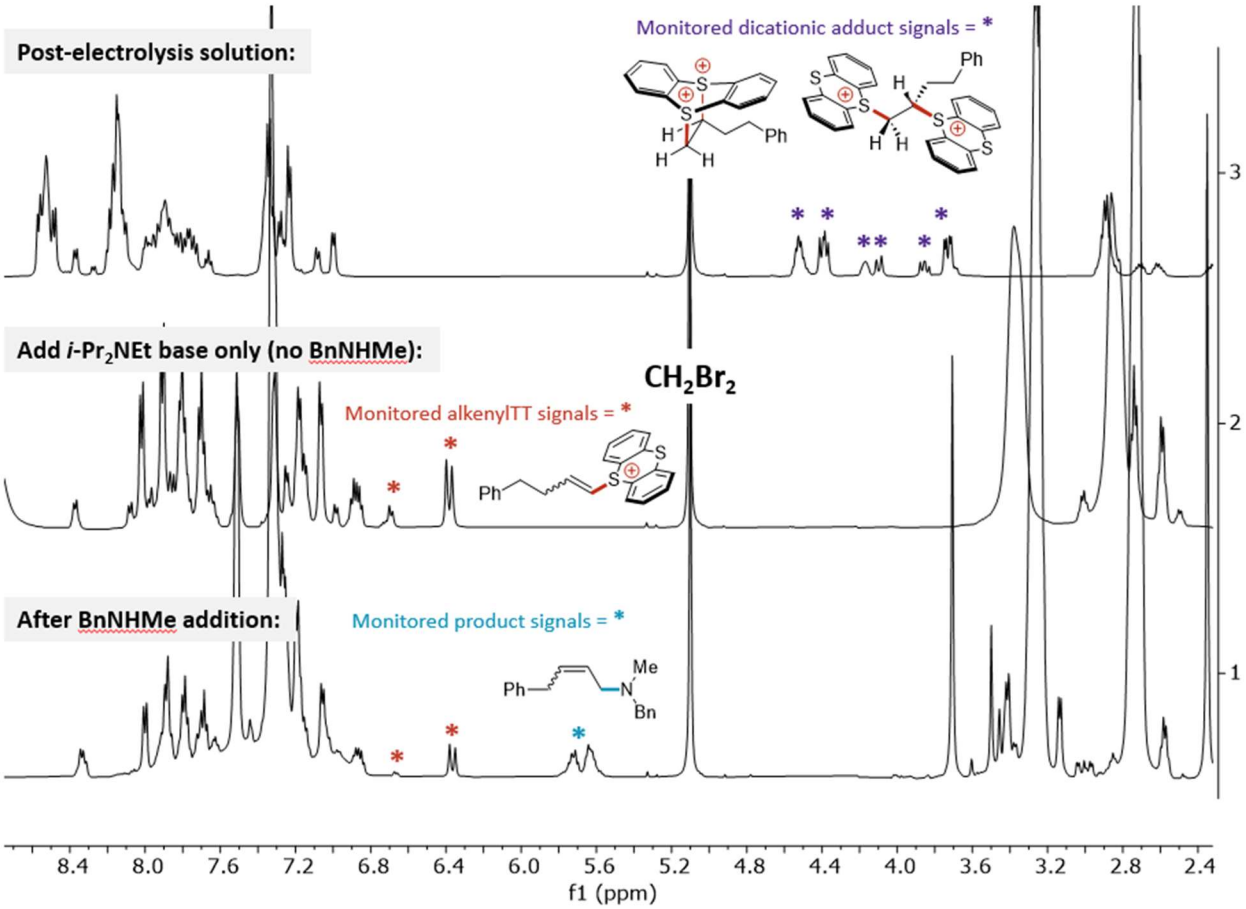

Figure B3. Example of ^{1}H NMR spectrum collected for monitoring the conversion of electrogenerated dicationic adducts **3.1** and **3.2** to alkenylTT **3.3** and subsequent formation of allylic amine product **3.4**. CH_2Br_2 was used as an internal standard (5.10 ppm, s, 2H).

Table B1. Data from Monitoring the Reaction using ^{1}H NMR Spectroscopy.

time (min)	[adducts 3.1 + 3.2] (mM)	[alkenylTT 3.3] (mM)	[allylic amine 3.4] (mM)
	Post-Electrolysis Solution		
0.00	80.00	0.00	0.00
1.07	77.00	0.00	0.00
2.13	78.00	0.00	0.00
3.18	77.00	0.00	0.00
4.25	78.00	0.00	0.00
5.30	77.00	0.00	0.00
	Add* i-*Pr*$_2$*NEt Base		
6.03	0.00	70.18	0.00
6.40	0.00	71.93	0.00

6.72	0.00	71.93	0.00
7.22	0.00	71.05	0.00
7.50	0.00	71.05	0.00
8.32	0.00	69.30	0.00
8.93	0.00	71.05	0.00
9.55	0.00	69.30	0.00
10.02	0.00	68.42	0.00
Add BnNHMe Nucleophile			
11.49	0.00	65.79	5.26
13.47	0.00	60.09	9.65
14.47	0.00	51.75	13.16
14.87	0.00	49.12	14.91
15.25	0.00	48.25	15.79
15.64	0.00	46.05	17.11
16.42	0.00	43.86	17.54
16.80	0.00	44.74	18.86
17.19	0.00	43.42	19.74
17.97	0.00	42.11	21.05
19.14	0.00	40.35	23.68
20.32	0.00	39.04	25.44
21.49	0.00	37.28	27.19
22.65	0.00	35.53	28.95
23.87	0.00	34.21	30.70
25.00	0.00	32.46	32.46
26.95	0.00	30.70	34.21
28.90	0.00	29.39	36.40
30.89	0.00	27.63	38.60
32.80	0.00	26.32	39.91
34.80	0.00	25.00	41.67
36.75	0.00	23.25	42.98
39.52	0.00	21.49	44.74

42.29	0.00	16.67	46.05
45.02	0.00	14.04	47.37
47.75	0.00	12.28	48.68
49.69	0.00	11.40	49.12

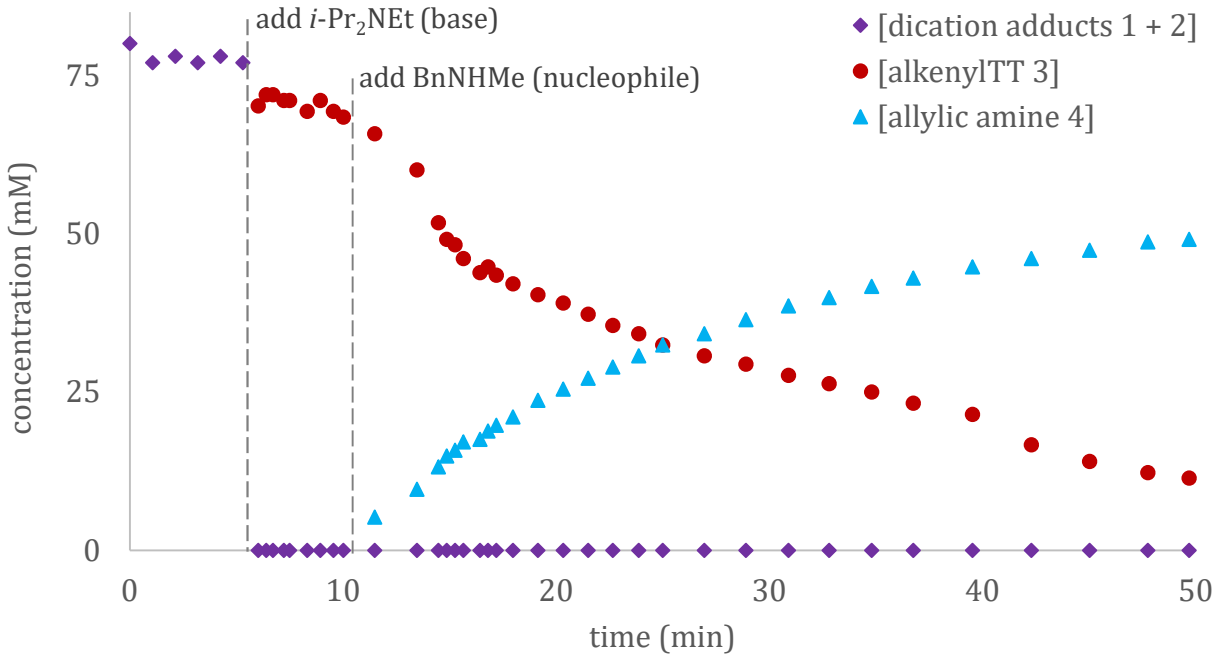

Figure B4. Data graphed from monitoring the dicationic adducts **3.1** and **3.2**, alkenylthianthrenium salt **3.3**, and allylic amine product **3.4** formation using ^{1}H NMR spectroscopy during sequential addition of reaction components (see Figure B2) for allylic amination. The decrease in [**3.3**] relative to [**3.1** + **3.2**] is due to the increased solution volume upon *i*-Pr$_2$NEt addition.

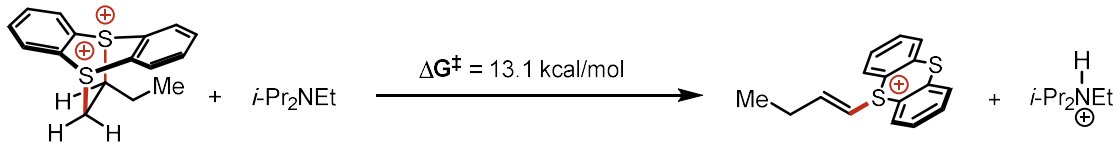

Figure B5. DFT calculations support that formation of alkenylthianthrenium salt from dicationic adducts is fast, exergonic, and irreversible. Transition state barrier $\Delta G^{\ddagger}$ for adduct deprotonation to alkenylthianthrenium salt is 13.1 kcal/mol ($t_{1/2}$ approx. 4.5 x 10^{-4} second) while the reverse $\Delta G^{\ddagger}$ for adduct reformation is 41.6 kcal/mol ($t_{1/2}$ approx. 1.1 x 10^{10} years). See Appendix B11 for computational details.

Conclusions: alkenylthianthrenium salt **3.3** is the only thianthrenium species detected by ^{1}H NMR spectroscopy during the allylic amination reaction. No detectable steady-state concentration of other thianthrenium species was observed. Experimental and computational data support the exothermic elimination step of dicationic adducts to alkenylthianthrenium salt under basic conditions. Furthermore, the rate of elimination from adducts to alkenylthianthrenium species is faster than allylic amination (see Figure B4). Based on these data, we chose to use alkenylthianthrenium salts to simplify subsequent mechanistic studies.

B2.2. Comparison of Aliphatic and Aryl Amine as Model Nucleophiles (Scheme 3.2)

The purpose of these experiments was to distinguish the ability of aliphatic and aryl amines to act as bases in allylic amination of thianthrenium salts. The reactivity of *N*-benzylmethylamine (aliphatic secondary amine) and *N*-methylaniline (aryl secondary amine) were evaluated by following the General Procedure for Allylic Amination of Alkenylthianthrenium Salts, *with the specified modification*: in addition to conducting the reactions with exogenous *i*-Pr_2NEt base, a set of control reactions were executed without the addition of *i*-Pr_2NEt.

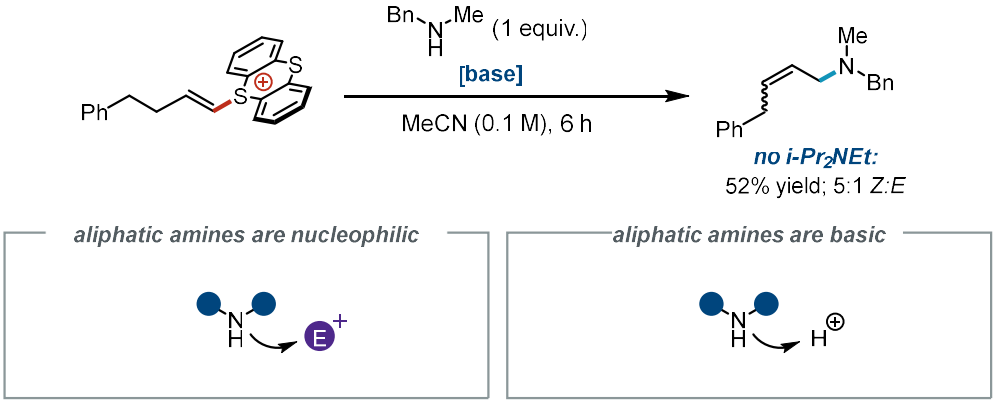

Figure B6. Secondary aliphatic amine convolutes kinetics analysis because it can be both a nucleophile and a base. For example, first order rate dependence on [BnNHMe] is observed, see Figure B15.

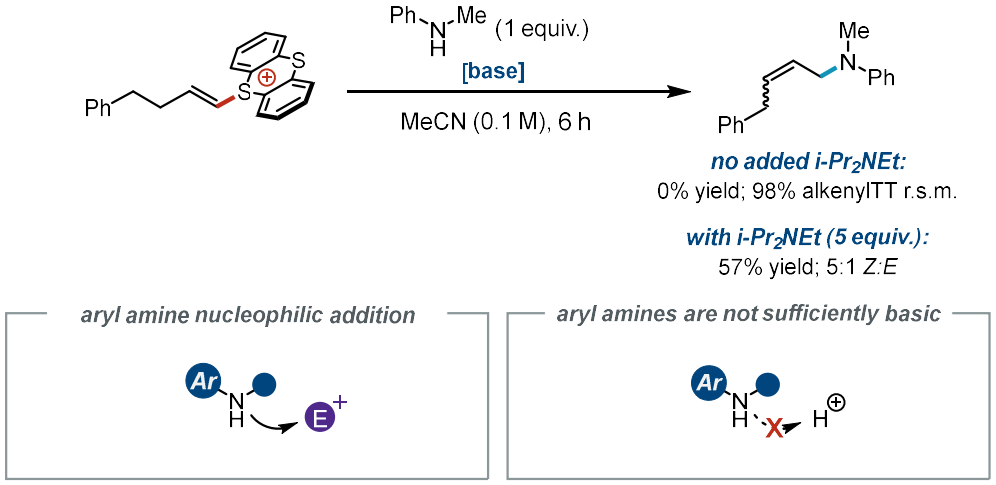

Figure B7. Secondary aryl amine nucleophile is sufficiently deactivated from acting as a base, but still undergoes allylic nucleophilic substitution with exogenous base. As such, secondary aryl amines clarify mechanistic investigation of allylic amination from alkenylthianthrenium salts. For example, zeroth order rate dependence on [PhNHMe] is observed, see Figure B19. r.s.m. = recovered starting material.

B2.3. Light Impact on *Z*-selectivity

One classic mechanism to induce *Z*-selectivity is contrathermodynamic photoisomerization that exploits photophysical differences between *E*-alkenes and *Z*-alkenes. Since alkenylthianthrenium salts have a conjugated π-system that can absorb visible light (for a UV-vis spectrum of vinylthianthrenium salt, see: *J. Am. Chem. Soc.* **2021**, 143, 33, 12992–12998), we questioned whether light (*e.g.* overhead from fume hood) could explain the observed *Z*-selectivity for allylic functionalization of thianthrenium-based intermediates. To this end, the General Procedure for Allylic Amination of Alkenylthianthrenium Salts was performed *with the specified modifications* in Figure B8 and the results are summarized in Table B2.

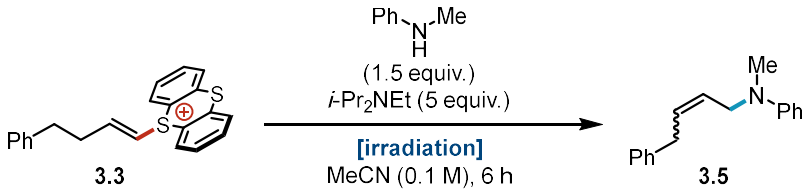

Figure B8. Allylic amination procedure conducted under various irradiation conditions.

Table B2. Influence of Light Source and Temperature on *Z*-selectivity of Allylic Amination.

Entry	Modification	Allylic amine 3.5 (%)	*Z:E*
1	None (fume hood, no precautions)	72	6.0:1
2	Dark (Al foiled)	70	6.0:1
3	CFL irradiation	71	6.0:1
4	40 °C (dark)	68	5.2:1

Conclusions: We observed no difference in reactivity or *Z*-selectivity in the dark or under CFL irradiation (Table B2, entries 1–3). Furthermore, heating the reaction resulted in an observable decrease in *Z*-selectivity (entry 4); this temperature dependence on *Z:E* is consistent with a kinetically-controlled process for the observed *Z*-selectivity.

B3. Reaction Kinetics

General Procedure for ^{1}H NMR Reaction Monitoring (for Kinetics and KIE Analyses): A stock solution of 5-(4-phenylbut-1-en-1-yl)-5H-thianthren-5-ium hexafluorophosphate **3.3** (0.1 M), *N*-methylaniline (0.15 M), and CH_2Br_2 internal standard (0.1 M) in MeCN-d_3 was prepared. To an oven-dried NMR tube was added 500 µL of the stock solution. An initial ^{1}H NMR scan was taken before the addition of *i*-Pr_2NEt (45 µL, 0.25 mmol, 5.0 equiv.) and then the reaction was monitored by taking a spectrum every 15–120 seconds using 1 scan with a 1 second relaxation delay. CH_2Br_2 was used as an internal standard and integrations compared to 5-(4-phenylbut-1-en-1-yl)-5H-thianthren-5-ium hexafluorophosphate **3.3** and product **5**. In each case, the reactions were monitored using several distinct signals for starting material and product. However, for clarity, a single signal shown throughout this appendix, however same outcome was observed for each signal. Signals used for 5-(4-phenylbut-1-en-1-yl)-5H-thianthren-5-ium hexafluorophosphate **3.3** (alkenylTT) = 8.01 ppm (dd, J = 8.0, 1.3 Hz, 2H) and 6.37 ppm (dt, J = 14.8, 1.4 Hz, 1H); *N*-methyl-*N*-(4-phenylbut-2-en-1-yl)aniline **3.5** (allylic amine product) = 5.82 – 5.68 ppm (m, 1H), 5.60 – 5.47 ppm (m, 1H), 4.08 ppm (*Z*-isomer; d, J = 6.8 Hz, 2H), 3.90 ppm (*E*-isomer; d, J = 5.4 Hz, 2H), 3.51 ppm (*Z*-isomer; d, J = 7.6 Hz, 2H), and 3.35 ppm (*E*-isomer; d, J = 6.9 Hz, 2H); and internal standard CH_2Br_2 = 5.10 ppm (s, 2H). See Figure B9.

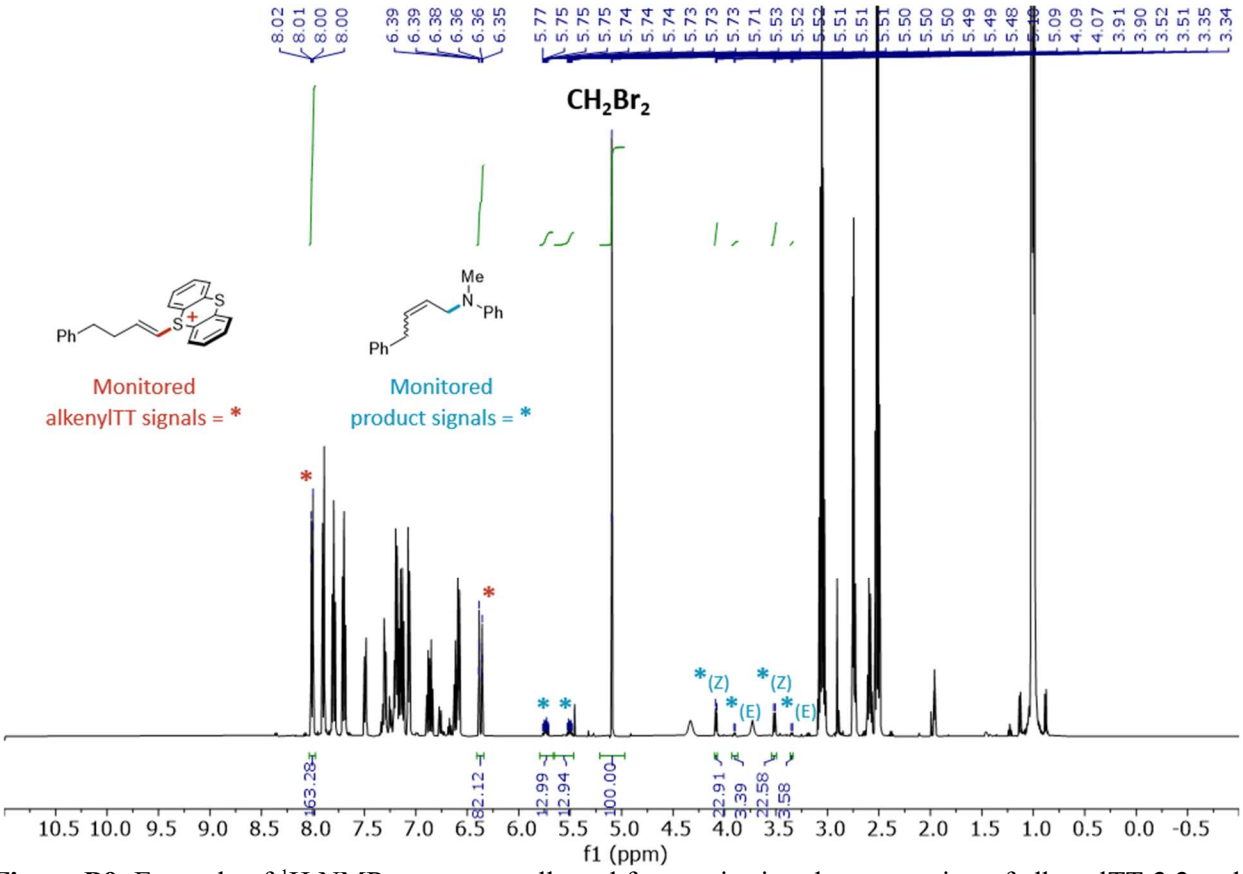

Figure B9. Example of ^{1}H NMR spectrum collected for monitoring the conversion of alkenylTT **3.3** and formation of allylic amine product **3.5**. CH_2Br_2 was used as an internal standard (5.10 ppm, s, 2H).

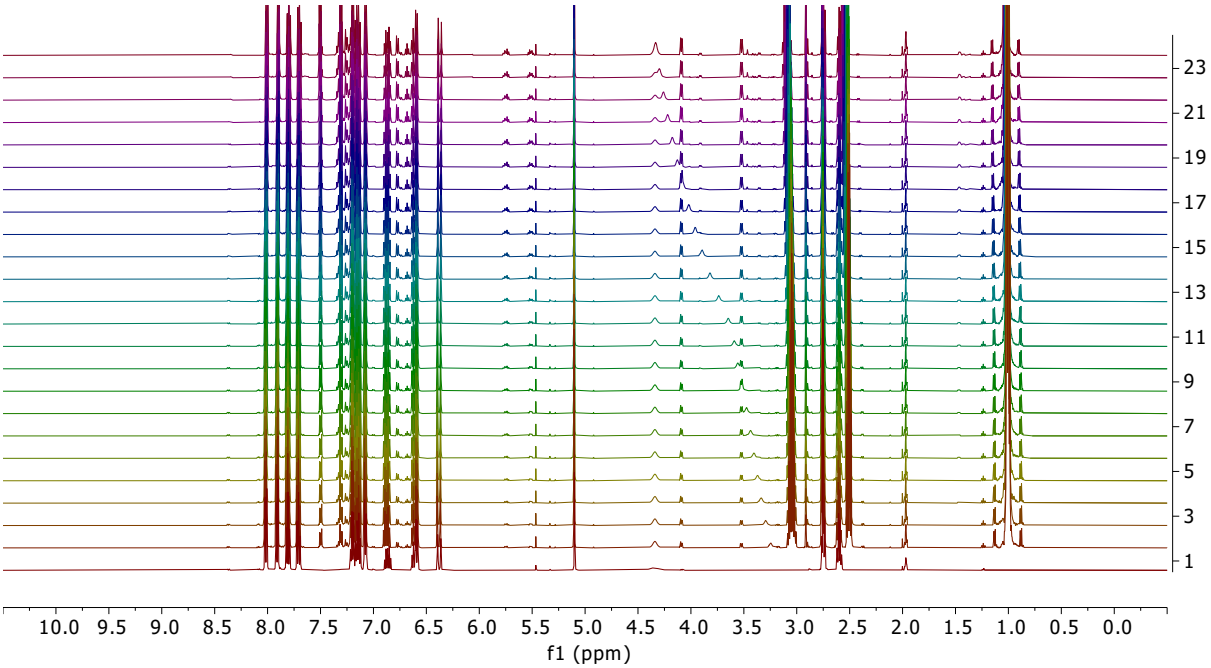

Figure B10. Example of ^{1}H NMR spectra collected over the course of the reaction monitoring the conversion of alkenylTT **3.3** and formation of allylic amine product **3.5**.

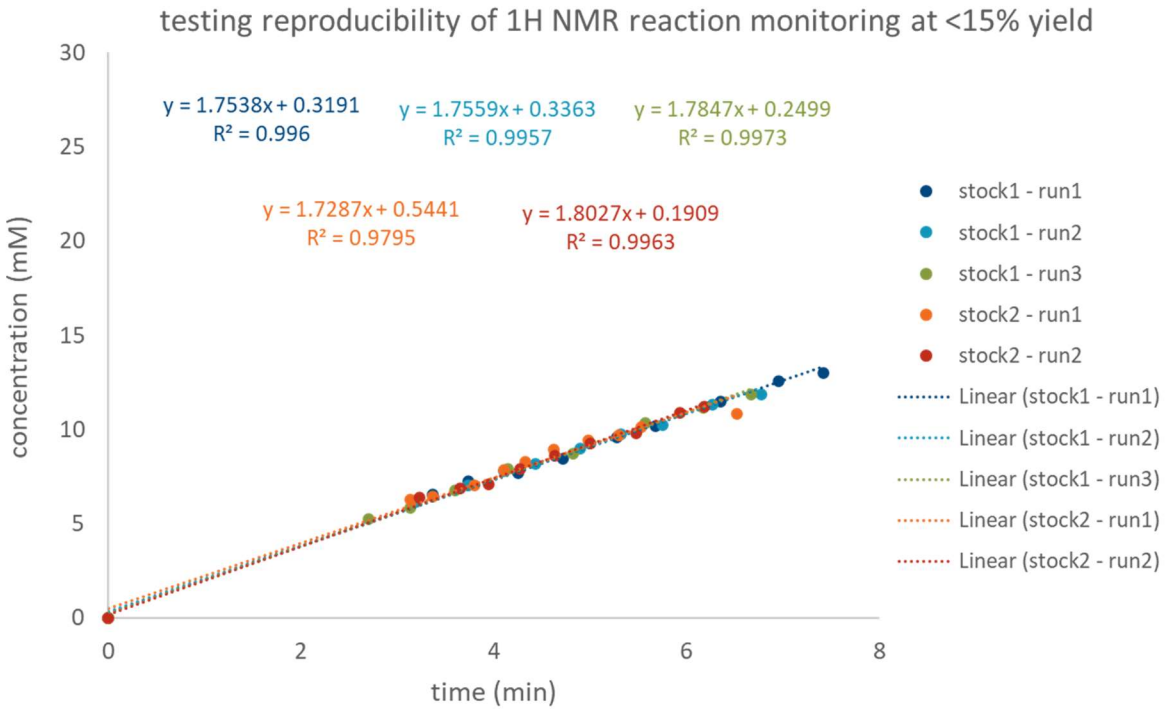

Figure B11. To evaluate the reproducibility of the initial reaction rate, stock solutions were prepared on separate days using the general procedure and replicates were found to have reproducible reaction rates. Monitoring allylic amine product **3.5** formation using the 5.82 – 5.68 (m, 1H) signal. Similar reproducibility was observed using other product signals *e.g.* 5.60 – 5.47 (m, 1H).

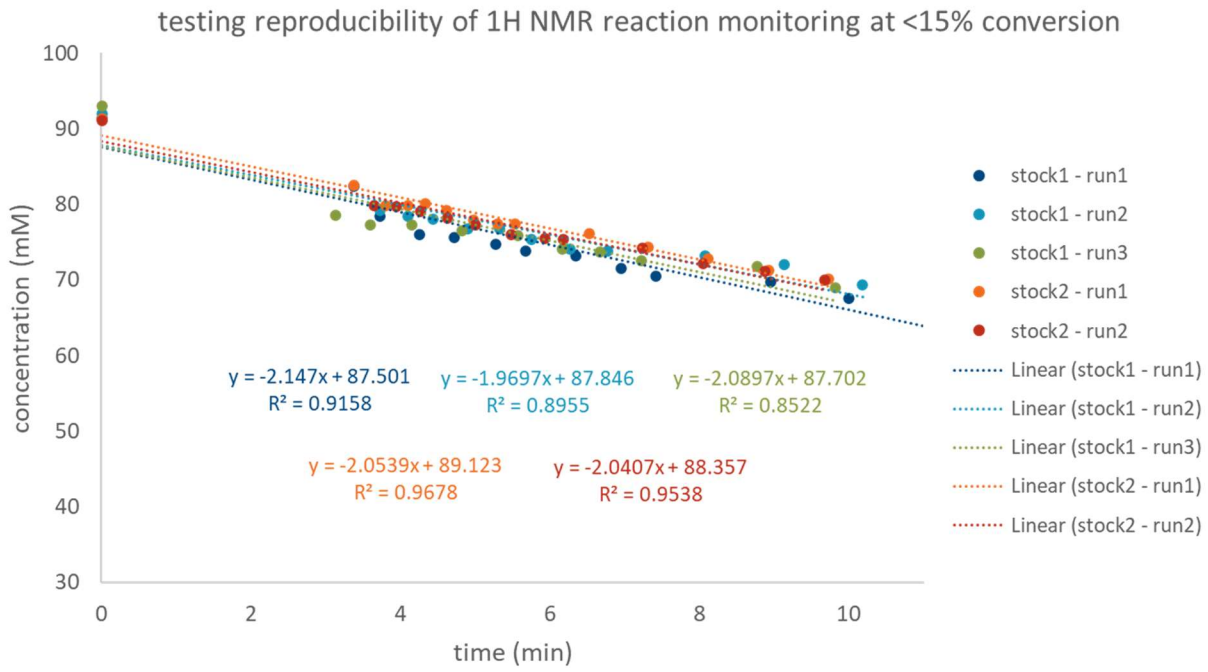

Figure B12. Stock solutions prepared on separate days using the general procedure led to reproducible reaction rates. Monitoring alkenylTT **3.3** conversion using the 8.01 ppm (dd, J = 8.0, 1.3 Hz, 2H) signal. Similar reproducibility was observed using other starting material signal 6.37 ppm (dt, J = 14.8, 1.4 Hz, 1H). The conversion rate of alkenylTT **3.3** is slightly higher than the rate of the formation of allylic amine product **3.5**. This observation is consistent with other minor pathways available to decompose the alkenylTT salt. Consequently, allylic amine product **3.5** formation rates will be used for quantitative analysis.

Error Propagation

For linear fit of a single trial, standard error of the slope (*e.g.* initial rate, rate constant extrapolation) was calculated using the Analysis ToolPak Regressions in Excel Data Analysis.

Fractional error was calculated for the average initial rates acquired from triplicate experiments. See *J. Am. Chem. Soc.* **1995**, 117, 36, 9357–9358; *J. Am. Chem. Soc.* **2017**, 139, 16, 5965–5972.

B3.1. Determination of the Reactant Order in *N*-Benzylmethylamine

The purpose of these experiments was to determine if the rate of allylic amination of thianthrenium salts is dependent on the secondary amine nucleophile (see, *J. Am. Chem. Soc.* **2021**, *143*, 21503–21510). Reaction monitoring was conducted using the General Procedure for ^{1}H NMR Reaction Monitoring *with the specified modifications*: *N*-benzylmethylamine was not added to the 0.1 M 5-(4-phenylbut-1-en-1-yl)-5H-thianthren-5-ium hexafluorophosphate (alkenylTT) **3.3** stock solution. Instead, *N*-benzylmethylamine (6.5 µL, 0.05 mmol, 1 equiv.; 13.0 µL, 0.10 mmol, 2 equiv.; or 19.0 µL, 0.15 mmol, 3.0 equiv.) was added *via* microsyringe to the NMR tube followed by *i*-Pr_2NEt (45 µL, 0.25 mmol, 5.0 equiv.). Signals used for *N*-benzyl-N-methyl-4-phenylbut-2-en-1-amine **3.4** (allylic amine product): 5.83 – 5.69 ppm (m, 1H) and 5.67 – 5.53 ppm (m, 1H).

Table B3. Data from Monitoring the Reaction Using ^{1}H NMR Spectroscopy for Varying Concentrations of BnNHMe.

0.0901 M BnNHMe		
time (min)	**[alkenylTT 3.3] (mM)**	**[allylic amine 3.4] (mM)**
0.00	87.04	0.00
3.30	76.16	10.88
5.00	69.81	13.60
6.10	67.09	15.87
7.15	63.46	18.59
0.1792 M BnNHMe		
time (min)	**[alkenylTT 3.3] (mM)**	**[allylic amine 3.4] (mM)**
0.00	86.02	0.00
3.58	67.20	17.47
4.75	63.62	17.47
5.30	59.14	19.71
6.75	52.87	25.99
0.2660 M BnNHMe		
time (min)	**[alkenylTT 3.3] (mM)**	**[allylic amine 3.4] (mM)**
0.00	81.56	0.00
3.23	58.51	20.83
3.52	54.96	21.28
3.78	54.08	22.61
4.07	52.30	23.94
4.35	50.53	24.82

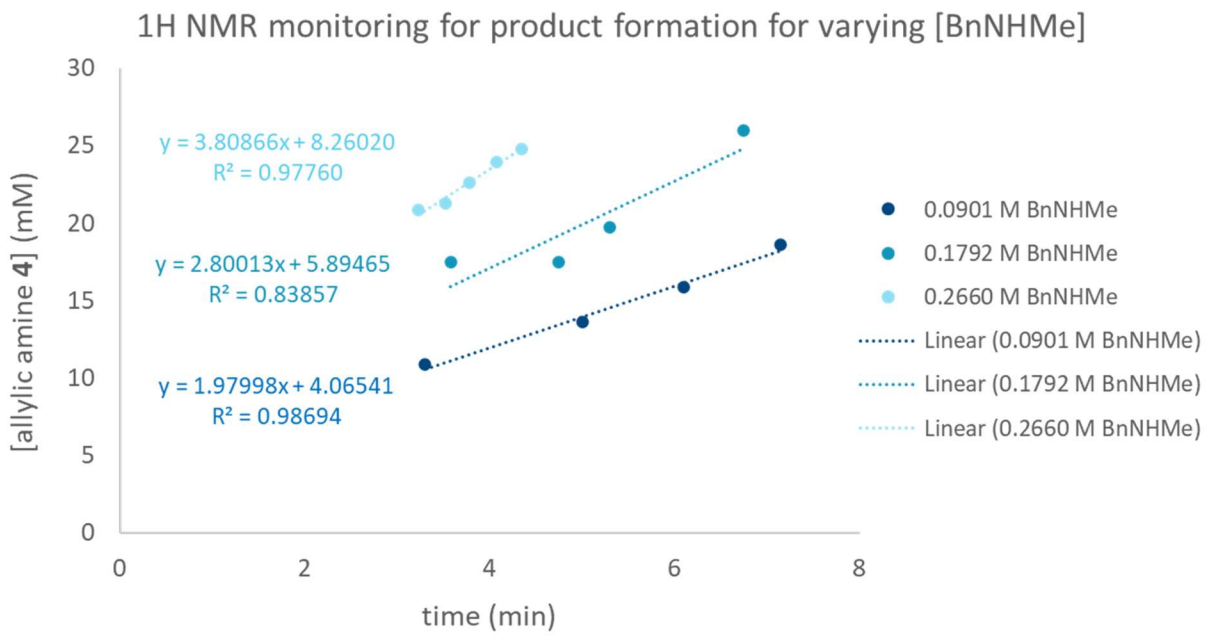

Figure B13. Data graphed from monitoring the allylic amine product **3.4** formation using ^{1}H NMR spectroscopy for varying concentrations of BnNHMe nucleophile.

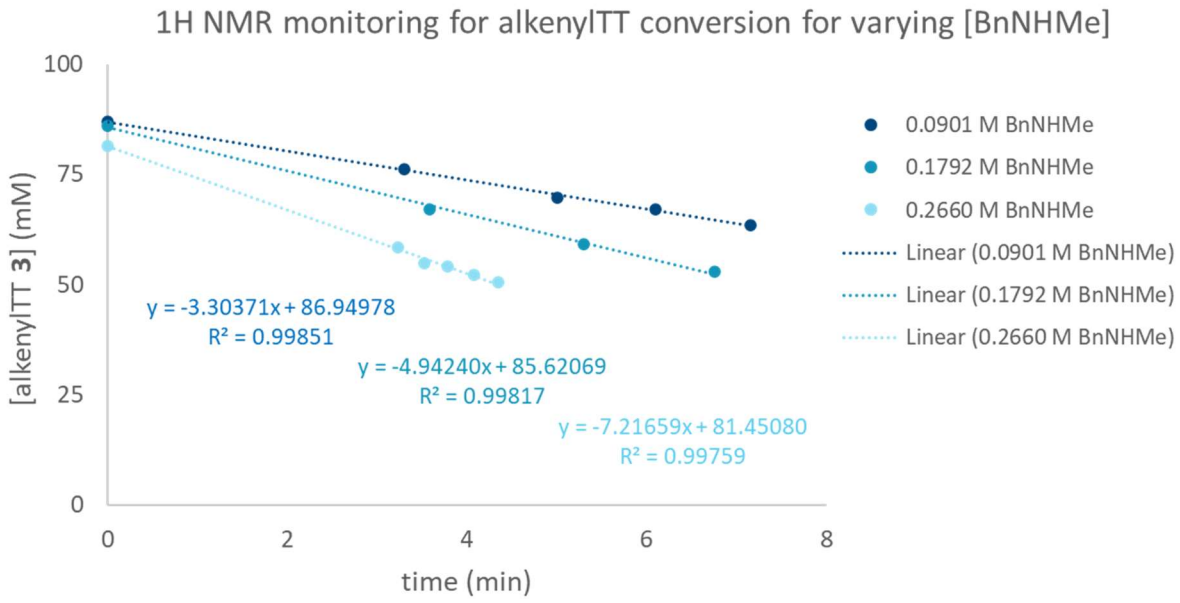

Figure B14. Data graphed from monitoring the alkenylTT **3.3** conversion using ^{1}H NMR spectroscopy for varying concentrations of BnNHMe nucleophile.

Table B4. Initial Rate Data for Varying Concentrations of BnNHMe.

using allylic amine 3.4 formation	
[BnNHMe] (M)	**initial rate (mM/min)**
0.09066	1.97998
0.1792	2.80013
0.26596	3.80866
using alkenylTT 3.3 conversion	
[BnNHMe] (M)	**initial rate (mM/min)**
0.09066	-3.30371
0.1792	-4.9424
0.26596	-7.21659

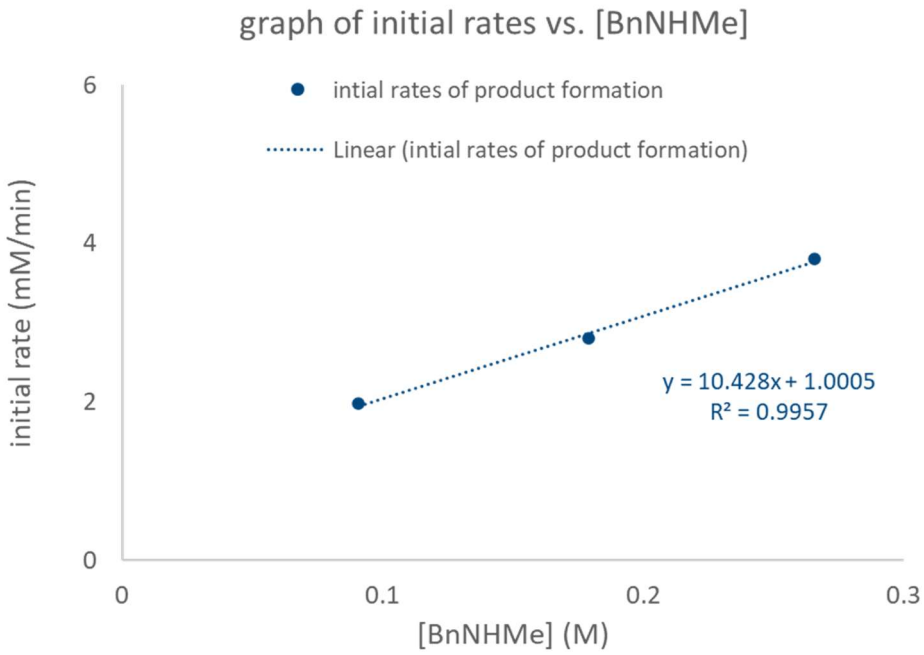

Figure B15. Linear fit (R^2 = 0.9957) for initial rate of allylic amine product **3.4** formation versus varying concentrations of BnNHMe nucleophile. First order rate dependence determined for BnNHMe during allylic amination.

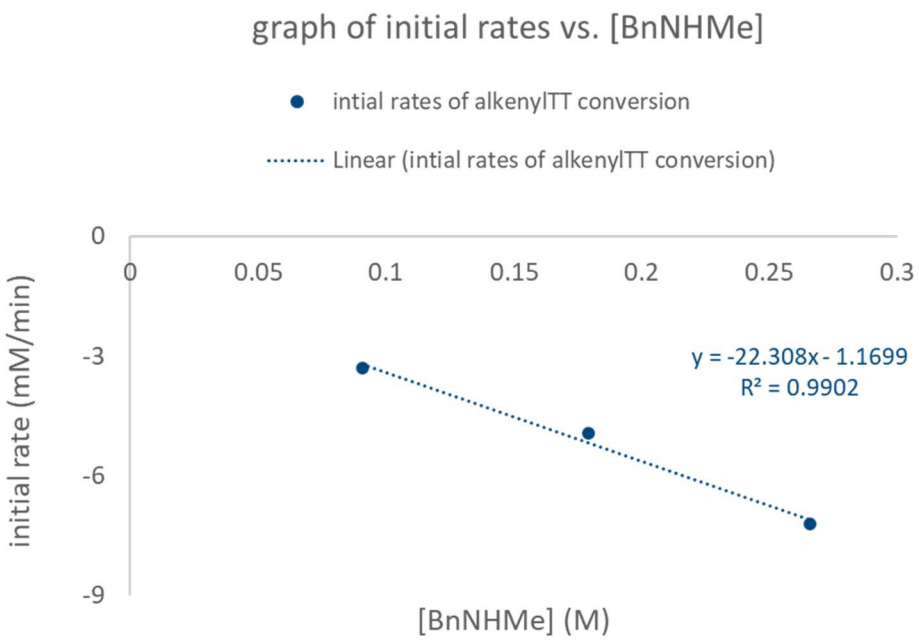

Figure B16. Linear fit (R^2 = 0.9902) for initial rate of alkenylTT **3.3** conversion versus varying concentrations of BnNHMe nucleophile. Qualitatively consistent with Figure B15 monitoring product formation: first order rate dependence determined for BnNHMe during allylic amination. The conversion rate of alkenylTT **3.3** is slightly higher than the rate of the formation of allylic amine product **3.4**. This observation is consistent with other minor pathways available to decompose the alkenylTT salt. Consequently, allylic amine product **3.4** formation rates will be used for quantitative analysis.

B3.2. Determination of the Reactant Order in *N*-Methylaniline Nucleophile (Figure 3.3A)

The purpose of these experiments was to determine if the rate of allylic amination of thianthrenium salts is dependent on the secondary aryl amine nucleophile. Reaction monitoring was conducted using the General Procedure for ^{1}H NMR Reaction Monitoring *with the specified modifications*: additional *N*-methylaniline (2.7 µL, 0.025 mmol, 0.5 equiv.; 5.4 µL, 0.05 mmol, 1.0 equiv.) was added *via* microsyringe to the NMR tube prepared from the stock solution described in the general procedure. A second stock solution with 0.1 M alkenylTT salt **3.3** and 0.1 M *N*-methylaniline was prepared and used according to the General Procedure for ^{1}H NMR Reaction Monitoring.

Table B5. Data from Monitoring the Reaction Using ^{1}H NMR Spectroscopy for Varying Concentrations of PhNHMe Nucleophile.

0.0917 M PhNHMe								
Run1			***Run2***			***Run3***		
Time (min)	**[alkenylTT 3.3] (mM)**	**[allylic amine 3.5] (mM)**	**Time (min)**	**[alkenylTT 3.3] (mM)**	**[allylic amine 3.5] (mM)**	**Time (min)**	**[alkenylTT 3.3] (mM)**	**[allylic amine 3.5] (mM)**
0.00	92.05	0.00	0.00	91.58	0.00	0.00	94.29	0.00
3.30	86.42	6.37	3.42	86.76	6.37	4.50	81.99	7.97
3.98	79.02	6.54	4.05	79.64	6.64	5.27	75.92	8.68
4.37	78.59	7.23	4.45	78.78	7.45	5.57	76.06	9.11
4.77	77.87	8.03	4.83	78.27	8.03	5.87	75.61	9.82
5.17	76.81	8.69	5.22	77.28	8.68	6.17	75.40	10.18
5.55	76.12	9.02	5.60	76.20	8.94	6.47	74.96	10.14
5.93	75.56	9.81	5.98	76.08	9.85	6.77	74.05	11.09
6.32	75.10	10.33	6.37	75.00	10.63	7.10	73.30	11.22
6.70	74.33	11.24	6.75	74.34	10.61	7.40	72.75	11.72
7.10	73.52	10.88	7.13	73.95	11.28	7.70	71.86	11.85
7.48	72.95	11.43	7.55	72.98	11.23	8.02	71.66	12.29
7.88	72.27	11.60	7.93	72.38	12.19	8.33	71.46	13.08
8.27	71.49	11.98	8.33	71.51	12.48	8.65	70.59	12.75
8.67	70.59	12.54	8.73	70.86	13.29	8.97	70.00	13.45
9.05	70.24	13.05	9.13	70.24	13.73	9.27	69.99	13.81
9.45	69.41	13.71	9.52	70.17	13.52	9.57	69.74	14.32
9.83	69.00	13.79	9.90	69.01	14.18	9.87	68.59	14.47
10.22	68.36	14.18	10.28	68.64	14.48	10.17	68.29	14.59
10.60	67.87	14.52	10.68	68.09	15.08	10.48	67.65	14.49
10.98	67.09	15.34	11.07	67.21	15.36	10.8	67.06	15.44
11.38	66.28	15.68	11.45	66.57	15.72	11.10	66.67	15.57
11.78	65.79	16.26	11.83	66.17	15.87	11.40	66.46	15.45

0.1376 M PhNHMe								
Run1			***Run2***			***Run3***		
Time (min)	**[alkenylTT 3.3] (mM)**	**[allylic amine 3.5] (mM)**	**Time (min)**	**[alkenylTT 3.3] (mM)**	**[allylic amine 3.5] (mM)**	**Time (min)**	**[alkenylTT 3.3] (mM)**	**[allylic amine 3.5] (mM)**
0.00	96.25	0.00	0.00	91.66	0.00	0.00	89.59	6.49
3.10	87.57	6.04	3.35	86.79	6.57	3.20	85.82	7.10
3.83	80.85	6.71	4.22	79.74	7.27	4.12	78.34	7.80
4.22	80.03	7.54	4.60	79.31	8.11	4.50	77.66	8.45
4.62	79.04	7.95	5.00	78.72	8.63	4.88	77.14	9.12
5.00	78.44	8.67	5.38	77.86	9.26	5.27	76.45	9.64
5.38	77.71	9.15	5.78	76.93	9.86	5.65	75.70	10.36
5.77	76.68	9.95	6.18	75.67	10.54	6.05	75.01	10.96
6.15	76.27	10.62	6.57	75.42	11.14	6.43	74.32	11.47
6.53	75.57	11.04	6.95	74.74	11.76	6.83	73.55	12.09
6.92	74.87	11.94	7.33	74.47	12.17	7.22	72.73	12.72
7.33	73.95	12.75	7.73	73.07	12.64	7.62	72.27	13.15
7.73	73.46	13.38	8.13	72.13	13.41	8.00	71.64	13.44
8.13	72.65	13.49	8.52	71.99	14.18	8.38	70.76	14.17
8.52	71.92	13.31	8.92	71.45	14.32	8.78	70.11	14.69
8.90	71.22	14.64	9.30	70.89	14.99	9.17	69.32	15.07
9.30	70.80	15.22	9.68	69.82	15.16	9.55	68.97	15.52
9.68	70.08	15.60	10.08	69.51	16.07	9.93	68.55	15.81
10.08	69.11	15.39	10.47	68.73	15.86	10.32	67.43	16.40
10.48	68.66	16.79	10.87	68.18	16.50	10.70	67.00	17.02
10.88	68.00	17.18	11.27	67.23	16.93	11.10	66.41	17.29
11.28	67.08	16.79	11.67	67.05	17.41	11.50	65.93	17.22
11.68	66.82	17.56	12.03	66.02	17.86	11.90	65.02	17.63

0.1826 M PhNHMe								
Run1			***Run2***			***Run3***		
Time (min)	**[alkenylTT 3.3] (mM)**	**[allylic amine 3.5] (mM)**	**Time (min)**	**[alkenylTT 3.3] (mM)**	**[allylic amine 3.5] (mM)**	**Time (min)**	**[alkenylTT 3.3] (mM)**	**[allylic amine 3.5] (mM)**
0.00	91.11	0.00	0.00	90.09	0.00	0.00	89.85	0.00
3.17	86.95	6.14	3.25	86.06	6.29	3.13	85.72	6.03
3.77	79.94	6.41	3.95	78.67	7.00	3.80	78.98	6.72
4.15	79.08	7.18	4.33	77.56	7.56	4.22	78.05	7.39
4.53	78.46	7.77	4.72	77.59	8.34	4.60	77.46	7.96
4.93	77.73	8.51	5.10	76.64	8.92	4.98	76.64	8.79
5.32	77.05	9.03	5.48	76.04	9.61	5.37	76.01	9.45
5.72	75.77	9.93	5.87	74.83	10.13	5.75	74.93	10.01
6.10	75.25	10.35	6.25	74.74	10.77	6.15	74.82	10.65
6.50	74.69	11.03	6.65	74.15	11.47	6.53	74.14	11.24
6.88	74.28	11.69	7.05	73.25	11.84	6.93	73.01	11.91
7.27	73.35	12.31	7.43	72.87	12.55	7.32	72.43	12.39
7.65	72.57	12.85	7.83	71.67	13.07	7.72	71.88	13.10
8.05	71.66	13.32	8.23	71.40	14.03	8.12	70.87	13.74
8.45	70.91	13.79	8.62	70.73	14.61	8.50	70.64	14.05
8.83	70.68	14.31	9.02	69.63	14.71	8.90	69.75	14.85
9.22	70.15	14.71	9.40	69.20	15.49	9.28	69.44	15.43
9.60	69.21	15.40	9.78	68.99	15.84	9.67	68.73	15.47
9.98	68.84	15.68	10.17	68.10	16.25	10.07	68.08	15.94
10.37	68.21	16.21	10.55	67.41	16.85	10.47	67.33	16.74
10.77	67.67	16.59	10.93	66.76	17.44	10.85	66.91	17.05
11.15	66.85	17.30	11.33	66.10	18.19	11.23	66.33	17.38
11.53	66.19	17.61	11.72	65.67	18.12	11.62	65.65	17.74

0.2271 M PhNHMe								
Run1			***Run2***			***Run3***		
Time (min)	**[alkenylTT 3.3] (mM)**	**[allylic amine 3.5] (mM)**	**Time (min)**	**[alkenylTT 3.3] (mM)**	**[allylic amine 3.5] (mM)**	**Time (min)**	**[alkenylTT 3.3] (mM)**	**[allylic amine 3.5] (mM)**
0.00	90.12	0.00	0.00	90.69	0.00	0.00	91.98	0.00
3.15	85.43	6.28	3.23	86.24	6.32	3.27	86.41	6.49
3.92	79.32	6.95	3.98	79.13	7.00	4.05	79.58	7.18
4.30	78.87	7.55	4.40	78.36	7.60	4.43	79.48	7.81
4.70	78.04	8.38	4.78	77.70	8.34	4.82	77.93	8.40
5.08	77.53	8.95	5.17	76.69	9.01	5.20	77.20	9.09
5.47	76.43	9.57	5.57	76.47	9.70	5.65	76.88	9.64
5.87	76.05	10.30	5.95	75.60	10.35	6.03	76.24	10.48
6.25	74.78	10.91	6.33	74.66	10.87	6.43	75.71	11.16
6.65	74.28	11.43	6.72	74.21	11.62	6.83	74.46	11.87
7.03	73.72	11.98	7.12	73.24	12.19	7.23	74.06	12.38
7.42	72.90	12.75	7.50	72.91	12.92	7.62	73.49	12.95
7.80	72.52	13.28	7.88	72.26	13.43	8.02	72.84	13.56
8.18	71.34	13.85	8.30	71.44	13.99	8.40	71.83	14.00
8.57	71.42	14.38	8.68	70.68	14.52	8.80	71.75	14.90
8.97	70.53	14.78	9.07	70.10	15.07	9.18	70.77	15.40
9.35	69.83	15.58	9.45	69.44	15.76	9.57	70.13	15.48
9.73	69.01	15.93	9.83	68.94	16.05	9.95	68.93	16.25
10.12	68.25	16.59	10.22	68.20	16.78	10.35	68.89	16.65
10.50	67.74	16.95	10.60	67.77	17.52	10.73	68.02	17.58
10.88	67.14	17.35	10.98	67.06	17.50	11.13	67.83	17.52
11.27	66.24	17.93	11.38	66.57	18.29	11.52	66.88	18.07
11.65	66.09	18.27	11.77	65.60	18.38	11.90	66.33	18.96

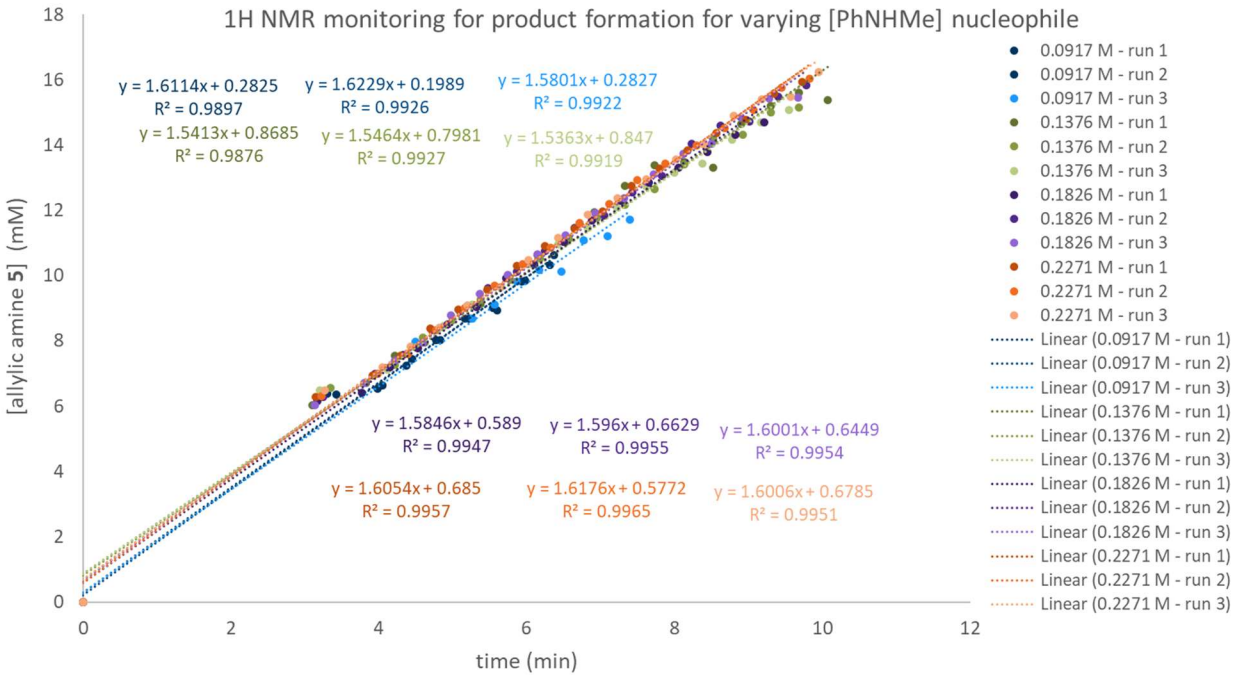

Figure B17. Data graphed from monitoring the allylic amine product **3.5** formation using ^{1}H NMR spectroscopy for varying concentrations of PhNHMe nucleophile.

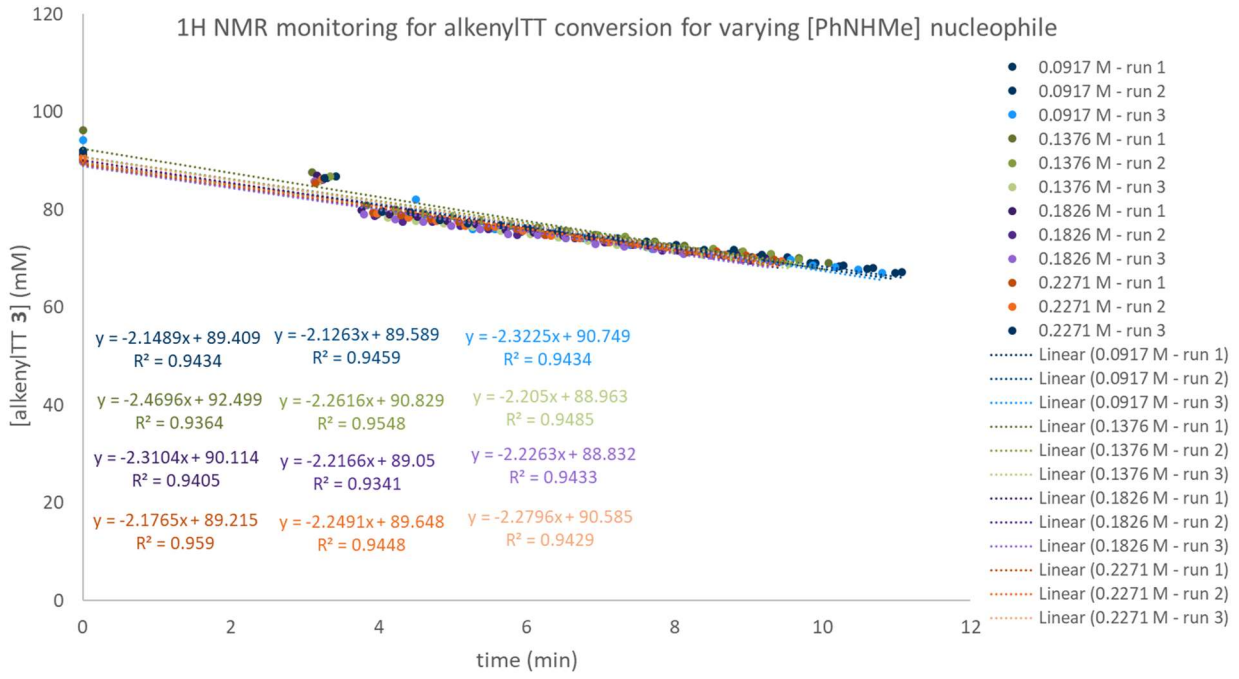

Figure B18. Data graphed from monitoring the alkenylTT **3.3** conversion using ^{1}H NMR spectroscopy for varying concentrations of PhNHMe nucleophile.

Table B6. Initial Rate Data for Varying Concentrations of PhNHMe Nucleophile.

using allylic amine 3.5 formation				
	initial rate (mM/min)			
[PhNHMe] (M)	***run1***	***run2***	***run3***	**average±error**
0.0917	1.6114±0.0621	1.6229±0.0531	1.5801±0.0495	1.6048±0.0954
0.1376	1.5413±0.0431	1.5464±0.0343	1.5363±0.0358	1.5413±0.0657
0.1826	1.5846±0.0300	1.5960±0.0268	1.6001±0.0272	1.5936±0.0486
0.2271	1.6054±0.0263	1.6176±0.0240	1.6142±0.0280	1.6124±0.0453

using alkenylTT 3.3 conversion				
	initial rate (mM/min)			
[PhNHMe] (M)	***run1***	***run2***	***run3***	**average±error**
0.0917	-2.1489±0.1565	-2.1263±0.1597	-2.3225±0.1848	-2.1992±0.2891
0.1376	-2.4696±0.0247	-2.2616±0.0237	-2.2050±0.0259	-2.3121±0.0431
0.1826	-2.3104±0.1500	-2.2166±0.1424	-2.2263±0.1316	-2.2511±0.2449
0.2271	-2.1765±0.1076	-2.2491±0.1310	-2.2796±0.1277	-2.2351±0.2117

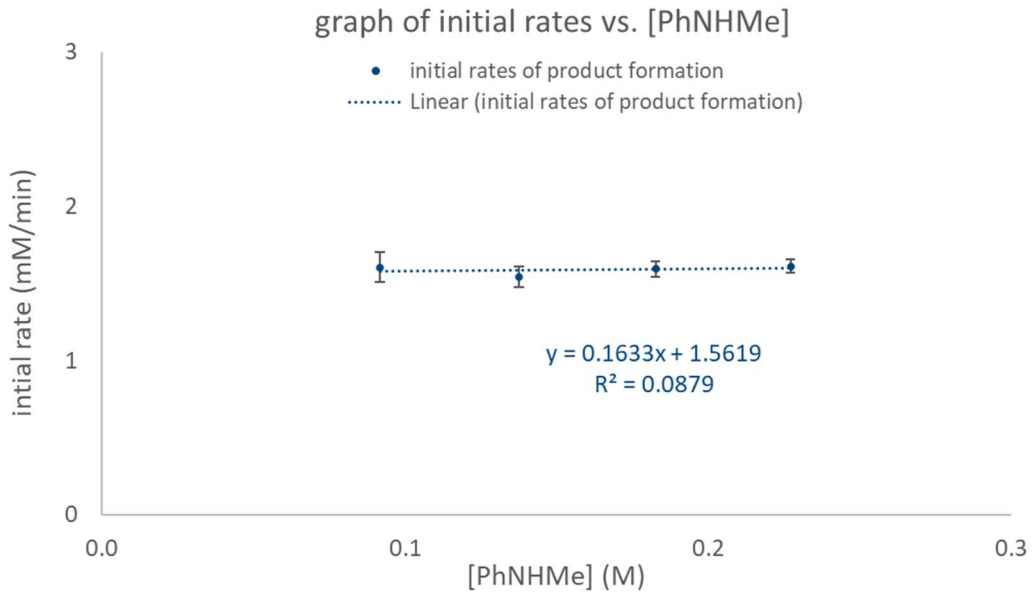

Figure B19. No linear fit ($R^2 = 0.0879$) for initial rate of allylic amine product **3.5** formation versus varying concentrations of PhNHMe nucleophile. Zeroth order rate dependence determined for PhNHMe nucleophile during allylic amination.

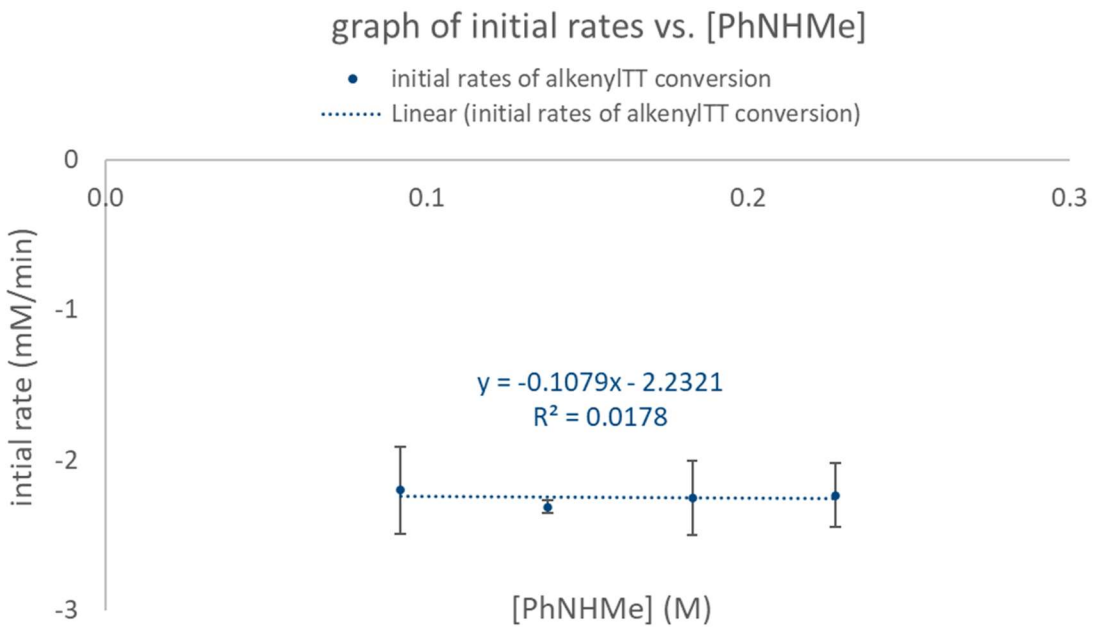

Figure B19. No linear fit (R^2 = 0.0178) for initial rate of alkenylTT **3.3** conversion versus varying concentrations of PhNHMe nucleophile. Consistent with Figure B18 monitoring product formation: zeroth order rate dependence determined for PhNHMe nucleophile during allylic amination. The conversion rate of alkenylTT **3.3** is slightly higher than the rate of the formation of allylic amine product **3.5**. This observation is consistent with other minor pathways available to decompose the alkenylTT salt. Consequently, allylic amine product **3.5** formation rates will be used for quantitative analysis.

B3.3. Determination of the Reactant Order in Alkenylthianthrenium Salt 3 (Figure 3.3B)

Reaction monitoring was conducted using the General Procedure for ^{1}H NMR Reaction Monitoring *with the specified modifications*: prepared separate stock solutions of 5-(4-phenylbut-1-en-1-yl)-5H-thianthren-5-ium hexafluorophosphate (alkenylTT) **3.3** (0.05 M, 0.1 M, 0.15 M, and 0.2 M), *N*-methylaniline (0.15 M), and CH_2Br_2 internal standard (0.1 M) in MeCN-d_3.

Table B7. Data from Monitoring the Reaction Using ^{1}H NMR Spectroscopy for Varying Concentrations of AlkenylTT 3.3.

0.0467 M alkenylTT 3.3								
Run1			***Run2***			***Run3***		
Time (min)	**[alkenylTT 3.3] (mM)**	**[allylic amine 3.5] (mM)**	**Time (min)**	**[alkenylTT 3.3] (mM)**	**[allylic amine 3.5] (mM)**	**Time (min)**	**[alkenylTT 3.3] (mM)**	**[allylic amine 3.5] (mM)**
0.00	45.92	0.00	0.00	46.88	0.00	0.00	47.25	0.00
3.07	43.67	3.13	3.35	43.86	3.22	2.95	43.87	2.94
4.45	39.69	3.58	3.85	40.59	3.62	4.13	40.70	3.16
5.27	39.28	4.41	4.15	39.77	4.21	4.95	39.92	3.94

0.0467 M alkenylTT 3.3								
Run1			***Run2***			***Run3***		
6.07	38.44	5.03	5.95	38.89	4.89	5.75	39.17	4.64
6.88	37.70	5.61	6.77	38.31	5.50	6.55	38.35	5.28
7.68	36.93	6.25	7.58	37.52	6.20	7.37	37.79	5.97
8.48	36.41	6.85	8.38	36.64	6.98	8.18	37.01	6.51
9.3	35.60	7.44	9.18	36.00	7.41	9.00	36.29	7.05

0.0914 M alkenylTT 3.3								
Run1			***Run2***			***Run3***		
Time (min)	**[alkenylTT 3.3] (mM)**	**[allylic amine 3.5] (mM)**	**Time (min)**	**[alkenylTT 3.3] (mM)**	**[allylic amine 3.5] (mM)**	**Time (min)**	**[alkenylTT 3.3] (mM)**	**[allylic amine 3.5] (mM)**
0.00	91.33	0.00	0.00	91.07	0.00	0.00	91.66	0.00
3.13	87.89	5.45	3.23	85.96	6.41	3.35	86.79	6.57
3.37	82.56	5.50	3.65	79.89	6.90	4.22	79.74	7.27
3.80	79.81	6.24	3.95	79.65	7.11	4.60	79.31	8.11
4.10	79.83	7.15	4.27	79.06	7.93	5.00	78.72	8.63
4.33	80.09	7.93	4.63	78.23	8.63	5.38	77.86	9.26
4.62	79.16	8.52	5.00	77.34	9.25	5.78	76.93	9.86
4.98	77.96	9.27	5.48	76.05	9.82	6.18	75.67	10.54
5.30	77.38	8.87	5.93	75.49	10.91	6.57	75.42	11.14
5.53	77.42	9.94	6.18	75.42	11.23	6.95	74.74	11.76
6.52	76.15	10.45	7.23	74.24	11.77	7.33	74.47	12.17
7.32	74.35	11.80	8.05	72.21	12.73	7.73	73.07	12.64
8.12	72.79	12.96	8.87	71.14	14.16	8.13	72.13	13.41
8.93	71.27	14.09	9.68	70.05	15.52	8.52	71.99	14.18
9.73	70.18	15.39	10.48	68.07	16.36	8.92	71.45	14.32
10.53	68.86	16.54	11.28	67.38	17.48	9.30	70.89	14.99
11.37	67.26	17.53	12.10	65.82	17.32	9.68	69.82	15.16

0.1371 M alkenylTT 3.3								
Run1			***Run2***			***Run3***		
Time (min)	**[alkenylTT 3.3] (mM)**	**[allylic amine 3.5] (mM)**	**Time (min)**	**[alkenylTT 3.3] (mM)**	**[allylic amine 3.5] (mM)**	**Time (min)**	**[alkenylTT 3.3] (mM)**	**[allylic amine 3.5] (mM)**
0.00	134.65	0.00	0.00	137.77	0.00	0.00	138.71	0.00
3.12	128.56	8.13	3.22	132.05	9.13	3.2	129.49	8.76
3.35	121.99	8.43	3.42	125.07	9.39	3.35	125.42	9.20
3.5	122.44	8.78	3.63	123.23	10.14	3.63	121.01	9.91
3.72	120.93	9.19	4.02	120.40	10.93	3.9	120.42	10.52
3.88	121.10	9.80	4.18	122.34	11.23	4.27	118.42	11.60
4.07	120.22	10.11	4.6	118.50	12.17	4.55	117.98	11.82
4.3	119.06	10.59	4.72	122.00	12.74	5.18	116.26	13.45
4.58	117.03	11.28	5.02	117.97	13.13	5.5	115.61	13.53
4.93	115.56	12.09	5.28	117.74	13.65	6.27	112.50	15.34
5.25	115.38	12.57	5.62	115.86	13.75	6.55	113.07	16.30
5.43	115.87	13.14	5.9	115.79	14.69	6.9	111.80	16.53
5.65	115.42	13.64	6.23	114.24	15.48	7.5	109.71	17.64

0.1874 M alkenylTT 3.3								
Run1			***Run2***			***Run3***		
Time (min)	**[alkenylTT 3.3] (mM)**	**[allylic amine 3.5] (mM)**	**Time (min)**	**[alkenylTT 3.3] (mM)**	**[allylic amine 3.5] (mM)**	**Time (min)**	**[alkenylTT 3.3] (mM)**	**[allylic amine 3.5] (mM)**
0.00	187.61	0.00	0.00	187.91	0.00	0.00	185.29	0.00
3.38	173.52	12.36	3.28	176.36	12.22	3.17	175.94	11.52
3.68	164.93	13.24	3.55	166.32	12.21	3.68	161.58	13.16
3.92	162.88	13.74	3.78	165.29	13.29	4.10	159.43	14.75
4.15	162.55	14.36	4.08	163.50	13.95	4.47	159.57	15.96
4.35	161.70	15.16	4.33	162.33	14.85	4.75	159.60	16.86

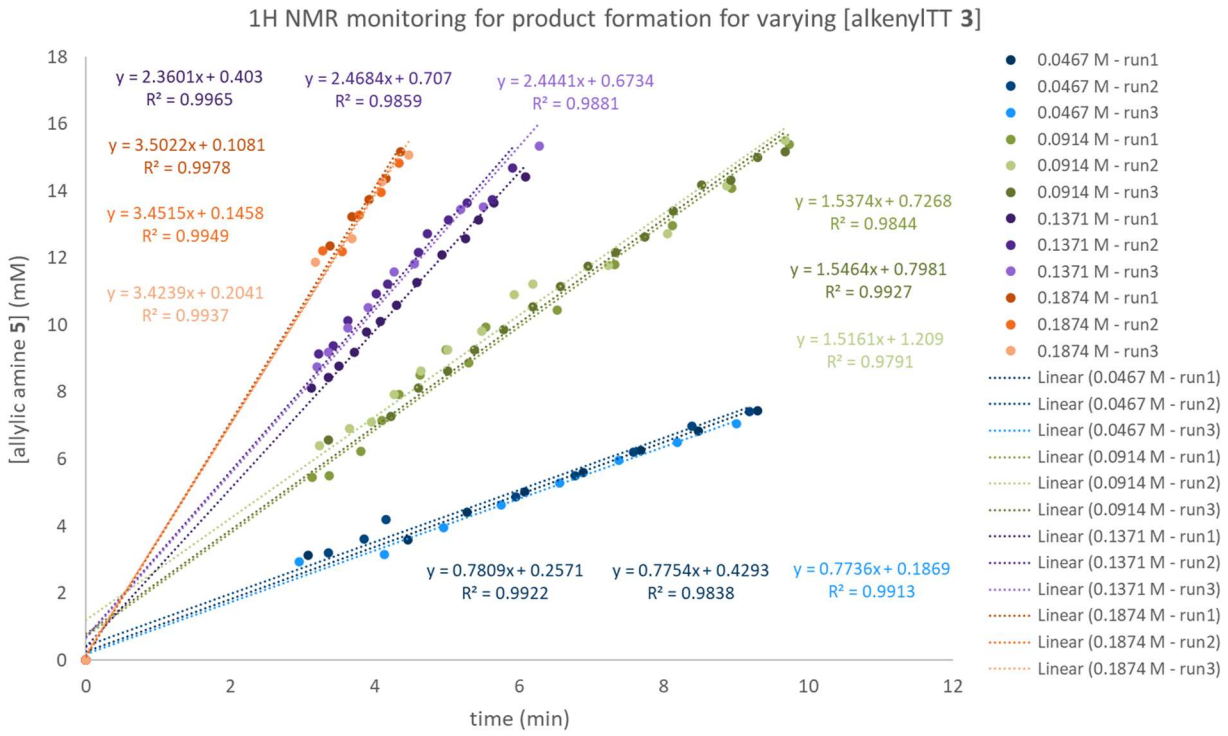

Figure B20. Data graphed from monitoring the allylic amine product **3.5** formation using ^{1}H NMR spectroscopy for varying concentrations of alkenylTT **3.3**.

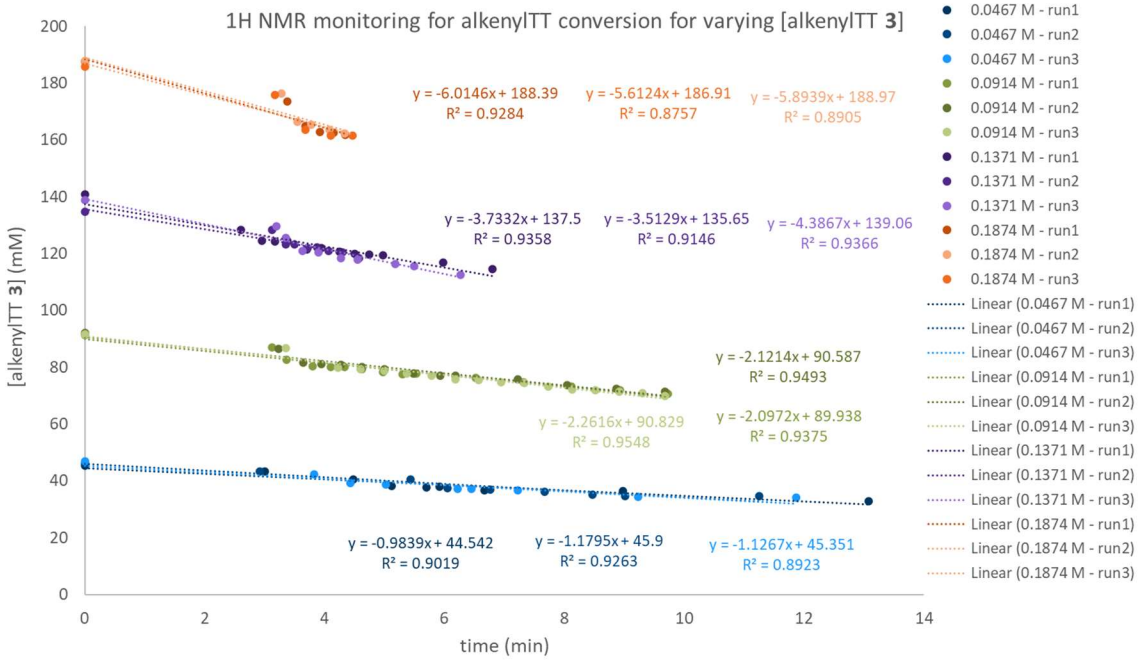

Figure B21. Data graphed from monitoring the alkenylTT **3.3** conversion using ^{1}H NMR spectroscopy for varying concentrations of alkenylTT **3.3.**

Table B8. Initial Rate Data for Varying Concentrations of AlkenylTT 3.3.

using allylic amine 3.5 formation				
	initial rate (mM/min)			
[alkenylTT 3.3] (M)	***run1***	***run2***	***run3***	**average±error**
0.0467	0.7809±0.0261	0.7554±0.0376	0.7736±0.0274	0.7766±0.0533
0.0914	1.5374±0.0536	1.5161±0.0639	1.5464±0.0343	1.5333±0.0905
0.1371	2.3601±0.0405	2.4684±0.0932	2.4441±0.0949	2.4242±0.1377
0.1874	3.5022±0.0828	3.4515±0.1234	3.4239±0.1575	3.4592±0.2175

using alkenylTT 3.3 conversion				
	initial rate (mM/min)			
[alkenylTT 3.3] (M)	***run1***	***run2***	***run3***	**average±error**
0.045872	-0.9839±0.1460	-1.1795±0.0837	-1.1267±0.1643	-0.7634±0.2410
0.091743	-2.1214±0.1502	-2.0972±0.1416	-2.2616±0.1271	-2.1601±0.2437
0.137615	-3.7332±0.2948	-3.5129±0.4057	-4.3867±0.4037	-3.8776±0.6493
0.183486	-6.0146±0.8349	-5.8939±0.5168	-5.6124±0.6105	-5.8403±1.1503

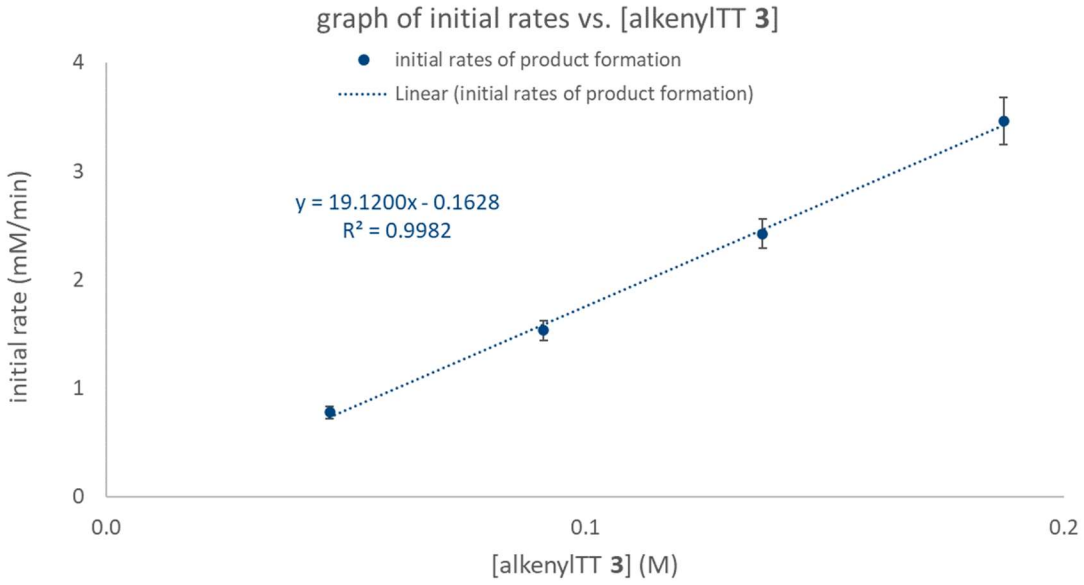

Figure B22. Linear fit (R^2 = 0.9982) for initial rate of allylic amine product **3.5** formation versus varying concentrations of alkenylTT **3.3**. First order rate dependence was determined for alkenylTT **3.3** during allylic amination.

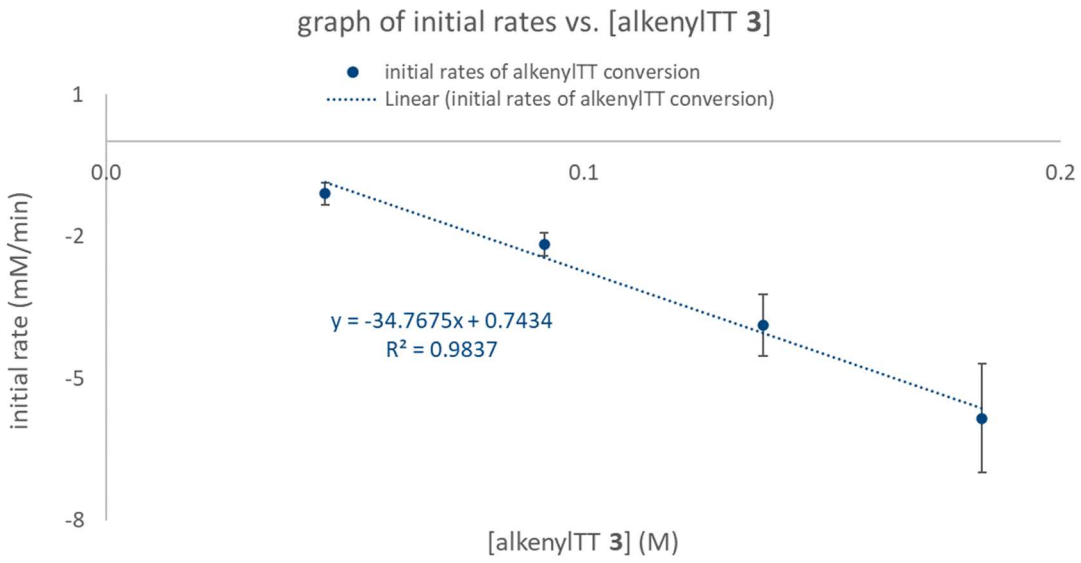

Figure B23. Linear fit (R^2 = 0.9837) for initial rate of alkenylTT **3.3** conversion versus varying concentrations of alkenylTT **3.3**. Consistent with Figure B22 monitoring product formation: first order rate dependence determined for alkenylTT **3.3** during allylic amination. The conversion rate of alkenylTT **3.3** is slightly higher than the rate of the formation of allylic amine product **5**. This observation is consistent with other minor pathways available to decompose the alkenylTT salt. Consequently, allylic amine product **3.5** formation rates will be used for quantitative analysis.

B3.4. Determination of the Reactant Order in *N,N*-Diisopropylethylamine Base (Figure 3.3C)

The purpose of these experiments was to determine if the rate of allylic amination of thianthrenium salts is dependent on the trialkylamine base. Reaction monitoring was conducted using the General Procedure for ^{1}H NMR Reaction Monitoring *with the specified modifications*: *i*-Pr_2NEt (13.5 µL, 0.075 mmol, 1.5 equiv.; 27.0 µL, 0.15 mmol, 3 equiv.; 45.0 µL, 0.25 mmol, 5 equiv.; or 62.0 µL, 0.345 mmol, 6.9 equiv.) was added *via* microsyringe to the NMR tube.

Table B9. Data From Monitoring the Reaction Using ^{1}H NMR Spectroscopy for Varying Concentrations of *i*-Pr_2NEt Base.

0.1461 M *i*-Pr_2NEt								
Run1			***Run2***			***Run3***		
Time (min)	**[alkenylTT 3.3] (mM)**	**[allylic amine 3.5] (mM)**	**Time (min)**	**[alkenylTT 3.3] (mM)**	**[allylic amine 3.5] (mM)**	**Time (min)**	**[alkenylTT 3.3] (mM)**	**[allylic amine 3.5] (mM)**
0.00	97.06	0.00	0.00	97.41	0.00	0.00	97.05	0.00
2.77	90.68	2.12	2.28	93.52	1.79	2.23	91.73	1.71
3.32	88.58	2.56	3.10	89.94	2.22	2.73	89.89	2.08

0.1461 M *i*-Pr$_2$NEt								
Run1			***Run2***			***Run3***		
4.03	87.16	2.84	3.78	89.13	2.65	3.37	88.32	2.59
4.80	86.89	3.33	4.30	88.74	3.08	3.87	89.36	2.75
5.75	86.82	3.88	5.00	87.57	3.51	4.28	88.58	3.10
8.03	86.65	4.23	5.68	87.43	4.19	4.85	87.96	3.60
10.12	84.11	5.61	6.23	87.06	4.52	5.45	87.79	3.89
12.18	82.63	6.68	7.15	86.58	5.02	6.07	86.64	4.32
14.23	81.78	8.53	9.47	86.14	5.84	6.78	86.39	4.63
16.28	80.06	9.62	11.52	84.76	6.68	9.08	86.90	5.00
18.33	78.76	10.81	13.58	83.07	8.49	11.13	84.66	6.21
20.40	77.89	11.80	15.65	81.89	9.68	13.18	83.26	7.40
22.45	76.69	12.76	17.72	80.17	10.03	15.23	82.26	8.65
24.50	75.26	13.73	19.78	78.60	11.76	17.30	80.88	10.57
26.57	74.53	14.68	21.83	77.49	13.03	19.38	79.37	11.63
28.62	73.30	15.87	23.88	76.04	14.10	21.43	78.35	11.86
30.67	72.36	16.71	25.93	75.23	15.11	23.50	76.94	13.81
32.75	70.30	17.35	28.02	74.07	16.11	25.55	76.22	14.94
34.80	69.71	18.21	30.08	72.31	17.10	27.62	74.46	15.99

0.2846 M *i*-Pr$_2$NEt								
Run1			***Run2***			***Run3***		
Time (min)	**[alkenylTT 3.3] (mM)**	**[allylic amine 3.5] (mM)**	**Time (min)**	**[alkenylTT 3.3] (mM)**	**[allylic amine 3.5] (mM)**	**Time (min)**	**[alkenylTT 3.3] (mM)**	**[allylic amine 3.5] (mM)**
0.00	94.46	0.00	0.00	95.09	0.00	0.00	95.06	0.00
3.08	87.29	3.83	2.73	89.60	3.64	3.15	90.68	4.16
3.53	81.79	4.35	3.33	84.07	4.25	3.38	87.29	4.31
4.15	80.98	4.95	3.80	84.12	4.86	3.97	84.47	4.88
4.88	79.96	5.94	4.60	81.90	5.64	4.45	83.68	5.26
5.47	78.98	6.36	5.15	82.00	6.36	4.95	83.46	6.05
6.05	78.98	6.93	5.98	81.11	7.06	5.33	82.59	6.83

0.2846 M *i*-Pr$_2$NEt								
Run1			***Run2***			***Run3***		
7.53	78.24	7.69	6.75	80.10	8.69	5.85	82.36	7.04
8.60	77.15	8.92	7.53	79.34	8.96	6.37	80.86	7.69
9.65	75.64	9.98	8.37	77.42	9.56	6.82	81.11	8.56
10.72	74.43	10.66	9.67	77.51	10.78	7.28	80.27	9.01
11.78	73.61	11.97	10.72	75.95	10.93	7.68	79.95	9.56
12.83	72.04	13.07	11.78	74.98	12.81	8.13	78.96	9.30
13.90	70.96	14.80	12.85	74.04	12.96	8.52	79.07	10.47
14.98	70.04	14.95	13.90	72.77	13.97	9.12	78.31	11.14
16.05	68.43	16.55	14.95	70.57	15.86	10.53	77.36	11.73
17.10	67.53	17.48	16.00	69.86	16.76	11.58	75.88	12.64
18.17	66.79	18.50	17.05	68.53	17.55	12.63	75.22	13.76
19.22	65.55	19.35	18.12	68.03	18.61	13.70	73.74	14.63
20.28	65.19	20.25	19.18	67.15	19.51	14.75	72.60	15.79

0.4587 M *i*-Pr$_2$NEt								
Run1			***Run2***			***Run3***		
Time (min)	**[alkenylTT 3.3] (mM)**	**[allylic amine 3.5] (mM)**	**Time (min)**	**[alkenylTT 3.3] (mM)**	**[allylic amine 3.5] (mM)**	**Time (min)**	**[alkenylTT 3.3] (mM)**	**[allylic amine 3.5] (mM)**
0.00	91.35	0.00	0.00	91.93	0.00	0.00	93.06	0.00
3.37	82.35	6.07	3.20	83.30	5.80	2.70	79.28	4.95
3.73	78.49	6.59	3.73	79.20	6.61	3.13	78.50	5.39
4.25	75.95	7.28	4.10	78.38	7.34	3.60	77.33	6.55
4.72	75.59	7.96	4.43	78.03	7.67	4.15	77.27	7.27
5.27	74.69	9.23	4.90	76.73	8.42	4.82	76.54	8.29
5.68	73.85	9.56	5.32	76.80	8.97	5.57	75.83	10.22
6.35	73.13	10.33	5.75	75.39	9.47	6.17	74.10	10.51
6.95	71.56	11.19	6.27	74.05	10.17	6.67	73.70	10.97
7.42	70.47	12.95	6.77	73.86	10.94	7.22	72.49	12.81
8.95	69.77	12.75	8.08	73.21	12.68	8.77	71.74	13.10

0.4587 M *i*-Pr$_2$NEt								
Run1			***Run2***			***Run3***		
10.00	67.55	15.03	9.13	72.02	14.13	9.82	68.95	14.50
11.05	65.86	15.47	10.18	69.32	15.50	10.88	68.07	16.53

0.6139 M *i*-Pr$_2$NEt								
Run1			***Run2***			***Run3***		
Time (min)	**[alkenylTT 3.3] (mM)**	**[allylic amine 3.5] (mM)**	**Time (min)**	**[alkenylTT 3.3] (mM)**	**[allylic amine 3.5] (mM)**	**Time (min)**	**[alkenylTT 3.3] (mM)**	**[allylic amine 3.5] (mM)**
0.00	88.64	0.00	0.00	89.35	0.00	0.00	89.07	0.00
3.28	78.60	7.28	3.38	78.28	7.19	2.95	77.38	6.78
3.52	75.76	7.74	3.65	74.53	7.74	3.20	76.35	6.90
3.75	74.55	8.20	3.87	74.83	7.83	3.55	75.04	7.99
3.98	74.11	8.84	4.10	74.39	8.42	3.87	74.39	7.88
4.33	72.94	9.43	4.30	73.57	8.86	4.30	73.35	9.61
4.55	73.02	10.04	4.50	72.74	9.34	4.77	72.39	9.56
4.80	71.76	10.48	4.68	73.03	9.70	5.17	70.86	11.25
5.08	71.31	11.14	4.90	72.29	10.02	5.62	70.63	12.26
5.43	70.18	11.48	5.13	71.98	10.60	6.35	69.94	12.92
6.38	68.85	12.49	6.03	69.64	11.32	6.92	68.94	14.02
6.93	67.78	13.27	6.58	68.23	12.88	7.48	67.05	14.82
7.48	66.73	14.48	7.13	67.27	12.94	8.03	66.25	15.62
8.05	65.52	15.27	7.70	66.44	14.95	8.58	63.93	16.39
8.62	64.10	16.49	8.23	64.87	15.89	9.13	63.36	17.51

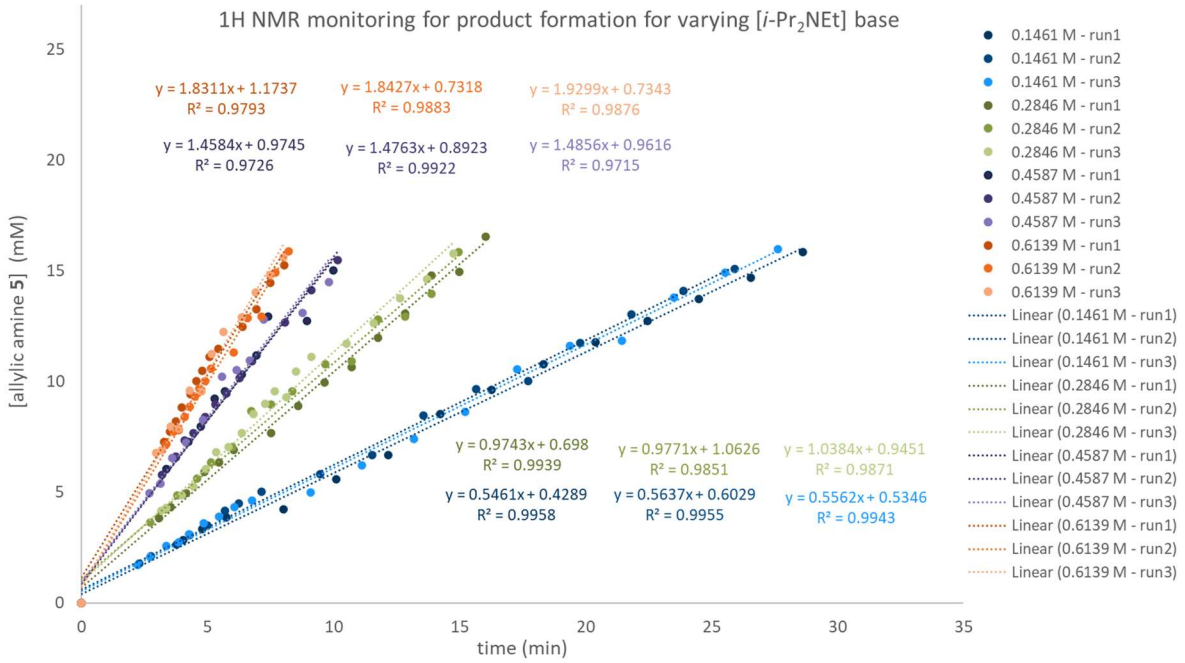

Figure B24. Data graphed from monitoring the allylic amine product **3.5** formation using ^{1}H NMR spectroscopy for varying concentrations of *i*-Pr$_2$NEt base.

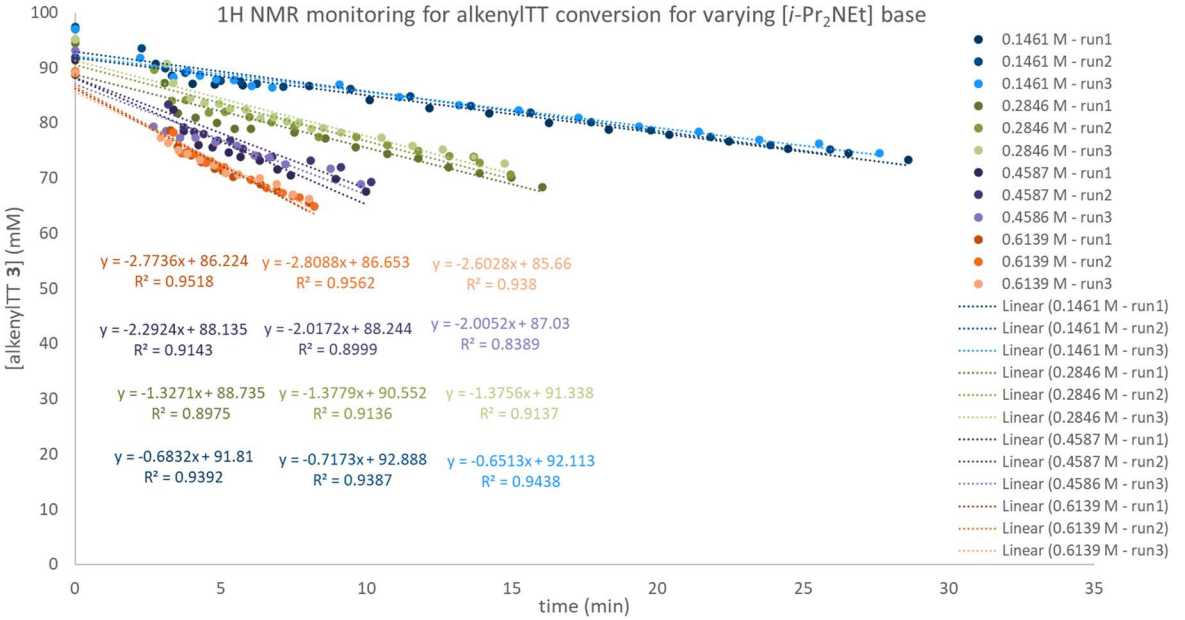

Figure B25. Data graphed from monitoring the alkenylTT **3.3** conversion using ^{1}H NMR spectroscopy for varying concentrations of *i*-Pr$_2$NEt base.

Table B10. Initial Rate Data for Varying Concentrations of *i*-Pr$_2$NEt Base.

using allylic amine 3.5 formation				
	initial rate (mM/min)			
[*i*-Pr$_2$NEt] (M)	*run1*	*run2*	*run3*	average±error
0.1461	0.5461±0.0095	0.5637±0.0097	0.5562±0.0100	0.5553±0.0168
0.2846	0.9743±0.0204	0.9971±0.0321	1.0384±0.0279	1.0033±0.0471
0.4587	1.4584±0.0774	1.4763±0.0396	1.4856±0.0805	1.4734±0.1185
0.6139	1.8311±0.0769	1.8427±0.0556	1.9299±0.0651	1.8679±0.1153

using alkenylTT 3.3 conversion				
	initial rate (mM/min)			
[*i*-Pr$_2$NEt] (M)	*run1*	*run2*	*run3*	average±error
0.1461	0.5461±0.0449	0.5637±0.0458	0.5562±0.0375	0.5553±0.0740
0.2846	0.9743±0.1198	0.9971±0.1132	1.0384±0.0997	1.0033±0.1931
0.4587	1.4584±0.2220	1.4763±0.2029	1.4856±0.0805	1.4734±0.3058
0.6139	1.8311±0.1802	1.8427±0.1666	1.9299±0.2018	1.8679±0.3199

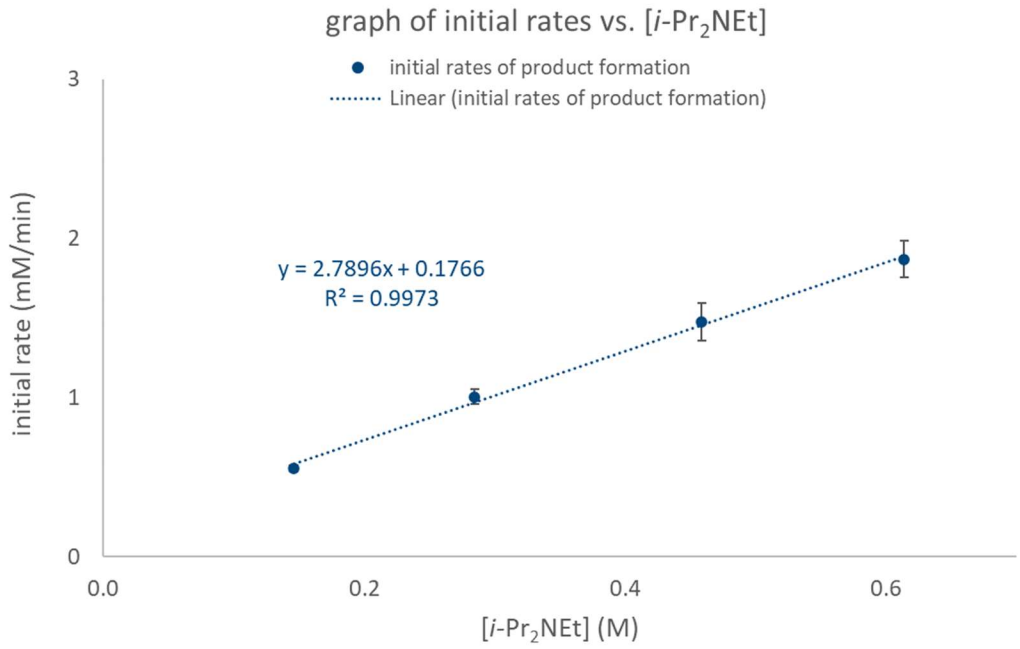

Figure B26. Linear fit (R^2 = 0.9973) for initial rate of allylic amine product **3.5** formation versus varying concentrations of *i*-Pr$_2$NEt base. First order rate dependence determined for *i*-Pr$_2$NEt base during allylic amination.

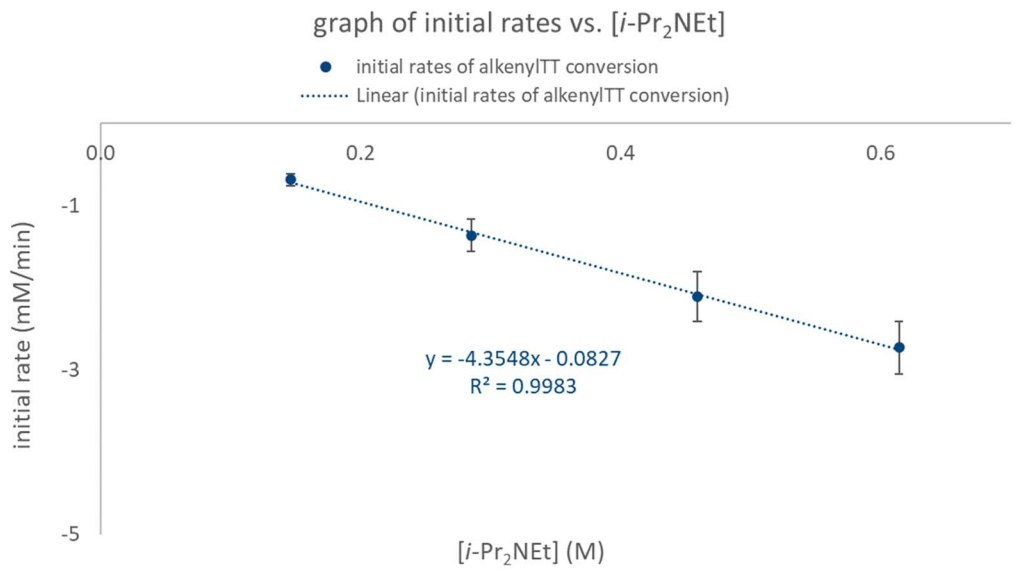

Figure B27. Linear fit (R^2 = 0.9983) for initial rate of alkenylTT **3.3** conversion versus varying concentrations of *i*-Pr_2NEt base. Consistent with Figure B26 monitoring product formation: first order rate dependence determined for *i*-Pr_2NEt base during allylic amination. The conversion rate of alkenylTT **3.3** is slightly higher than the rate of the formation of allylic amine product **3.5**. This observation is consistent with other minor pathways available to decompose the alkenylTT salt. Consequently, allylic amine product **3.5** formation rates will be used for quantitative analysis.

B3.5. Determination of the Reactant Order in *N,N*-Diisopropylethylamine Conjugate Acid (Figure 3.3D)

The purpose of these experiments was to determine if the rate of allylic amination of thianthrenium salts is dependent on the conjugate acid of the trialkylamine base. Reaction monitoring was conducted using the General Procedure for ^{1}H NMR Reaction Monitoring *with the specified modifications*: the stock solution was prepared with the specified concentration of *N*-ethyl-*N*-isopropylpropan-2-aminium hexafluorophosphate(V) (*i*-Pr_2NHEtPF_6).

Table B11. Data from Monitoring the Reaction Using ^{1}H NMR Spectroscopy for Varying Concentrations of *i*-Pr_2NHEtPF_6.

0 M *i*-Pr_2NHEtPF_6								
Run1			***Run2***			***Run3***		
Time (min)	**[alkenylTT 3.3] (mM)**	**[allylic amine 3.5] (mM)**	**Time (min)**	**[alkenylTT 3.3] (mM)**	**[allylic amine 3.5] (mM)**	**Time (min)**	**[alkenylTT 3.3] (mM)**	**[allylic amine 3.5] (mM)**
0.00	96.25	0.00	0.00	91.66	0.00	0.00	89.59	0.00
3.10	87.57	6.04	3.35	86.79	6.57	3.20	85.82	6.49
3.83	80.85	6.71	4.22	79.74	7.27	4.12	78.34	7.10
4.22	80.03	7.54	4.60	79.31	8.11	4.50	77.66	7.80

0 M *i*-$Pr_2NHEtPF_6$								
Run1			***Run2***			***Run3***		
4.62	79.04	7.95	5.00	78.72	8.63	4.88	77.14	8.45
5.38	77.71	9.15	5.38	77.86	9.26	5.27	76.45	9.12
5.77	76.68	9.95	5.78	76.93	9.86	5.65	75.70	9.64
6.15	76.27	10.62	6.18	75.67	10.54	6.05	75.01	10.36
6.53	75.57	11.04	6.57	75.42	11.14	6.43	74.32	10.96
6.92	74.87	11.94	6.95	74.74	11.76	6.83	73.55	11.47
7.33	73.95	12.75	7.33	74.47	12.17	7.22	72.73	12.09
7.73	73.46	13.38	7.73	73.07	12.64	7.62	72.27	12.72
8.13	72.65	13.49	8.13	72.13	13.41	8.00	71.64	13.15
8.52	71.92	13.31	8.52	71.99	14.18	8.38	70.76	13.44
8.90	71.22	14.64	8.92	71.45	14.32	8.78	70.11	14.17
9.30	70.80	15.22	9.30	70.89	14.99	9.17	69.32	14.69
9.68	70.08	15.60	9.68	69.82	15.16	9.55	68.97	15.07
10.08	69.11	15.39	10.08	69.51	16.07	9.93	68.55	15.52

0.0459 M *i*-$Pr_2NHEtPF_6$								
Run1			***Run2***			***Run3***		
Time (min)	**[alkenylTT 3.3] (mM)**	**[allylic amine 3.5] (mM)**	**Time (min)**	**[alkenylTT 3.3] (mM)**	**[allylic amine 3.5] (mM)**	**Time (min)**	**[alkenylTT 3.3] (mM)**	**[allylic amine 3.5] (mM)**
0.00	94.06	0.00	0.00	91.28	0.00	0.00	96.16	0.00
3.32	89.09	6.02	3.18	87.78	6.72	3.20	90.73	6.09
4.45	80.14	7.24	3.95	87.12	7.49	4.00	88.43	6.94
4.87	79.84	7.98	4.33	86.26	8.18	4.40	87.69	7.77
5.25	79.24	8.53	4.72	85.34	8.78	4.80	86.30	8.54
5.63	78.30	9.26	5.10	84.59	9.47	5.20	85.79	9.19
6.03	77.92	9.67	5.50	83.60	10.14	5.58	85.35	9.68
6.45	76.95	10.51	5.88	82.71	10.67	5.97	83.76	10.27
6.83	76.30	10.90	6.28	82.48	11.33	6.37	83.00	10.72
7.22	75.84	11.52	6.67	81.43	12.11	6.75	83.24	11.74

0.0459 M *i*-Pr$_2$NHEtPF$_6$								
Run1			***Run2***			***Run3***		
7.60	75.31	11.85	7.07	81.23	12.82	7.15	81.88	11.84
7.98	74.51	12.24	7.47	80.26	13.29	7.55	81.34	12.71
8.37	74.13	12.82	7.87	79.10	13.88	7.93	80.09	13.22
8.75	73.03	13.31	8.25	78.38	14.49	8.32	82.50	14.19
9.15	72.71	14.18	8.65	77.98	14.97	8.70	78.98	14.64
9.55	71.61	14.24	9.03	77.21	15.03	9.10	78.05	15.35
9.93	71.18	14.66	9.42	76.55	15.26	9.48	77.43	14.98
10.32	70.63	15.77	9.80	76.40	15.95	9.87	76.78	15.53

0.0917 M *i*-Pr$_2$NHEtPF$_6$								
Run1			***Run2***			***Run3***		
Time (min)	**[alkenylTT 3.3] (mM)**	**[allylic amine 3.5] (mM)**	**Time (min)**	**[alkenylTT 3.3] (mM)**	**[allylic amine 3.5] (mM)**	**Time (min)**	**[alkenylTT 3.3] (mM)**	**[allylic amine 3.5] (mM)**
0.00	91.08	0.00	0.00	88.20	0.00	0.00	90.05	0.00
3.57	87.05	6.24	3.27	83.44	5.19	3.53	83.05	6.06
4.32	80.60	6.99	3.80	81.01	5.60	4.48	76.98	6.86
4.70	79.88	7.37	4.18	79.18	6.11	4.87	76.97	7.29
5.10	79.17	8.20	4.57	77.99	7.12	5.27	76.97	7.71
5.48	78.79	8.89	4.97	76.90	7.63	5.65	77.60	8.79
5.88	78.51	9.60	5.35	77.29	7.87	6.03	75.90	9.28
6.28	76.96	9.81	5.75	75.52	8.67	6.42	76.21	10.13
6.67	76.59	10.29	6.13	75.88	9.16	6.80	75.54	10.69
7.07	76.06	10.97	6.53	75.35	10.15	7.18	75.19	11.18
7.47	74.89	11.40	6.92	73.49	10.44	7.60	74.00	11.85
7.87	74.26	12.48	7.32	73.85	11.31	7.98	73.81	12.34
8.25	73.68	13.09	7.70	72.56	11.41	8.38	72.56	13.01
8.63	73.14	13.11	8.10	71.76	12.23	9.17	71.75	14.30
9.03	72.20	14.13	8.48	71.89	12.87	9.57	71.00	14.77
9.42	71.57	14.64	8.88	71.10	12.99	9.95	70.04	15.05

0.0917 M *i*-Pr$_2$NHEtPF$_6$								
Run1			***Run2***			***Run3***		
9.80	71.24	14.61	9.27	70.16	13.83	10.33	69.74	15.58
10.20	70.52	15.12	9.67	69.91	14.46	10.73	69.18	16.08

0.1376 M *i*-Pr$_2$NHEtPF$_6$								
Run1			***Run2***			***Run3***		
Time (min)	**[alkenylTT 3.3] (mM)**	**[allylic amine 3.5] (mM)**	**Time (min)**	**[alkenylTT 3.3] (mM)**	**[allylic amine 3.5] (mM)**	**Time (min)**	**[alkenylTT 3.3] (mM)**	**[allylic amine 3.5] (mM)**
0.00	94.74	0.00	0.00	95.83	0.00	0.00	91.67	0.00
3.30	90.34	6.57	3.35	88.06	6.11	3.35	86.52	6.28
3.97	84.46	6.75	3.98	83.23	6.48	4.05	80.82	6.53
4.37	84.21	7.37	4.38	82.05	7.01	4.43	80.24	7.11
4.70	83.44	8.01	4.78	81.33	7.48	4.83	80.28	7.84
5.15	82.14	8.55	5.18	81.30	8.24	5.22	78.86	8.26
5.55	81.65	9.19	5.58	79.93	8.85	5.62	78.92	8.82
5.93	81.25	9.69	5.98	79.13	9.33	6.02	77.29	9.55
6.33	80.27	10.20	6.38	78.09	9.94	6.42	76.60	9.93
6.72	79.63	10.84	6.77	77.86	10.58	6.80	75.80	10.51
7.12	78.60	11.44	7.17	76.91	11.04	7.18	75.49	11.09
7.52	77.84	11.83	7.57	76.77	11.71	7.58	74.91	11.56
7.90	77.74	12.52	7.95	76.08	12.13	7.97	74.01	12.11
8.30	75.92	12.94	8.33	75.46	12.53	8.37	73.38	12.58
8.68	75.70	13.48	8.73	74.37	13.14	8.75	72.68	13.04
9.08	75.12	13.85	9.13	73.49	13.53	9.13	72.00	13.50

0.1835 M *i*-Pr$_2$NHEtPF$_6$								
Run1			***Run2***			***Run3***		
Time (min)	**[alkenylTT 3.3] (mM)**	**[allylic amine 3.5] (mM)**	**Time (min)**	**[alkenylTT 3.3] (mM)**	**[allylic amine 3.5] (mM)**	**Time (min)**	**[alkenylTT 3.3] (mM)**	**[allylic amine 3.5] (mM)**
0.00	95.60	0.00	0.00	91.32	0.00	0.00	93.77	0.00
3.10	91.33	6.75	3.57	86.06	7.15	3.82	88.05	5.57

0.1835 M *i*-Pr$_2$NHEtPF$_6$								
Run1			***Run2***			***Run3***		
3.80	85.48	7.00	4.48	78.93	8.00	4.63	84.24	6.24
4.18	84.77	7.37	4.87	79.40	8.54	5.02	81.71	6.96
4.57	83.80	8.04	5.27	78.91	9.20	5.42	81.40	7.27
4.97	83.36	8.89	5.65	77.81	9.87	5.82	80.69	7.94
5.35	82.70	9.44	6.07	76.29	10.49	6.20	79.73	8.82
5.73	81.88	10.03	6.45	76.72	10.93	6.60	79.48	9.59
6.13	81.00	10.53	6.83	75.78	11.60	6.98	78.46	10.02
6.53	81.60	11.24	7.22	75.52	12.35	7.37	77.73	10.42
6.93	79.52	11.68	7.60	73.79	12.73	7.77	77.05	11.24
7.33	78.77	12.28	8.00	73.16	13.22	8.15	77.85	12.17
7.73	78.26	12.97	8.38	72.60	13.81	8.53	75.44	12.36
8.12	78.11	13.56	8.77	71.85	13.99	8.92	75.08	12.83
8.52	76.62	13.92	9.15	71.23	14.89	9.32	74.56	13.57
8.90	76.14	14.21	9.53	71.58	15.18	9.72	73.72	14.53

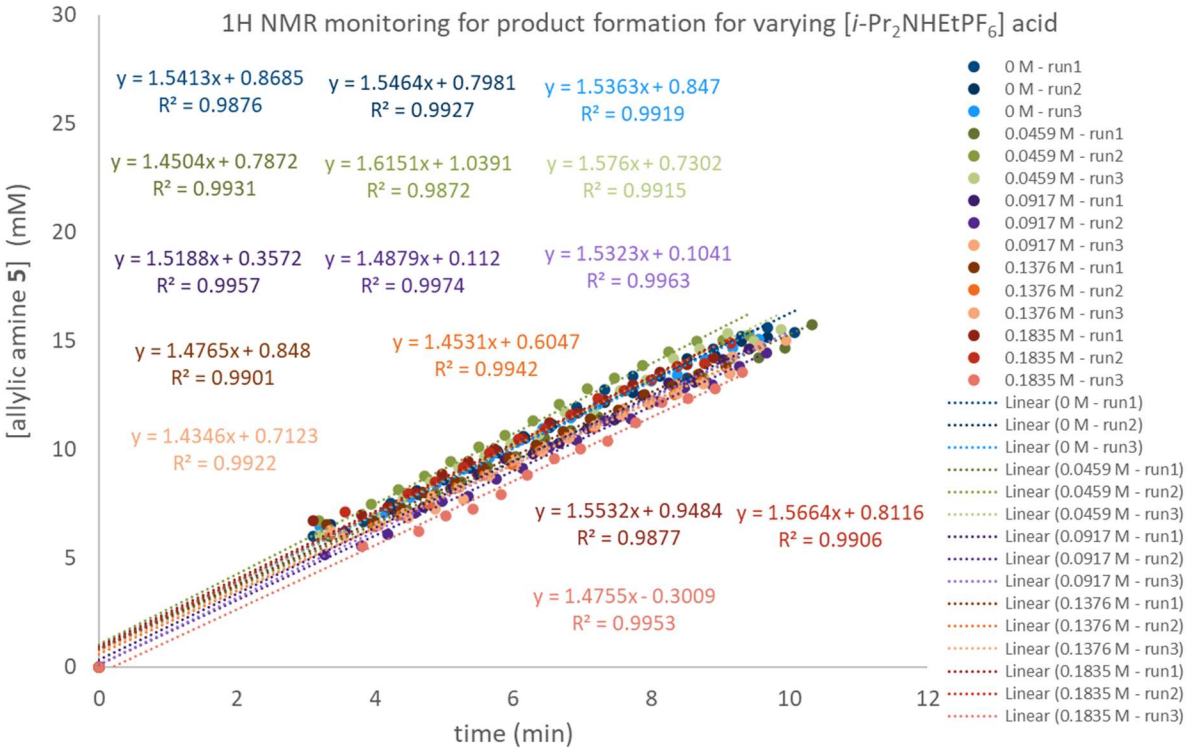

Figure B28. Data graphed from monitoring the allylic amine product **3.5** formation using ^{1}H NMR spectroscopy for varying concentrations of *i*-Pr$_2$NHEtPF$_6$.

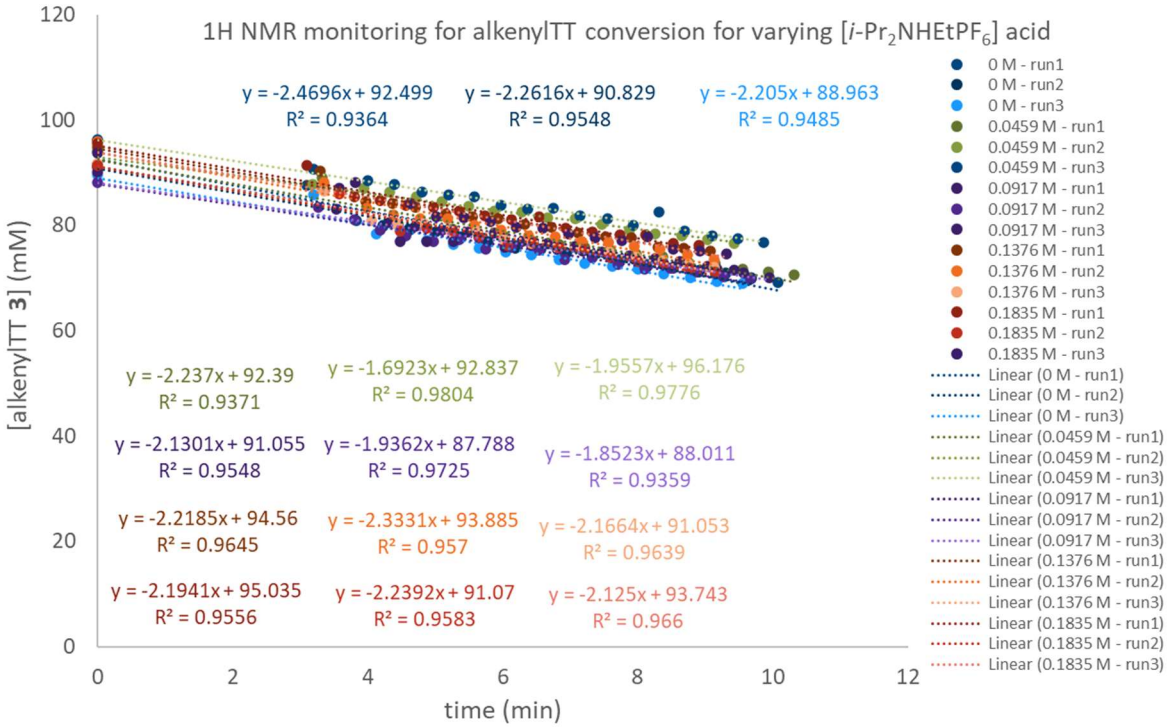

Figure B28. Data graphed from monitoring the alkenylTT **3.3** conversion using ^{1}H NMR spectroscopy for varying concentrations of *i*-$Pr_2NHEtPF_6$.

Table B12. Initial Rate Data for Varying Concentrations of *i*-$Pr_2NHEtPF_6$.

using allylic amine 3.5 formation				
	initial rate (mM/min)			
[*i*-$Pr_2NHEtPF_6$] (M)	***run1***	***run2***	***run3***	**average±error**
0	1.5413±0.0431	1.5464±0.0343	1.5363±0.0358	1.5413±0.0657
0.0459	1.4504±0.0302	1.6151±0.0475	1.5760±0.0364	1.5472±0.0662
0.0917	1.5188±0.0283	1.4879±0.0191	1.5323±0.0248	1.5130±0.0421
0.1376	1.4765±0.0395	1.4531±0.0297	1.5323±0.0341	1.4873±0.0600
0.1835	1.5532±0.0464	1.5664±0.0423	1.4755±0.0282	1.5317±0.0683

using alkenylTT 3.3 conversion				
	initial rate (mM/min)			
[*i*-$Pr_2NHEtPF_6$] (M)	*run1*	*run2*	*run3*	average±error
0	-2.4696±0.1609	-2.2616±0.1271	-2.2050±0.1326	-2.3121±0.2427
0.0459	-2.2370±0.1449	-1.6923±0.0618	-1.9557±0.0740	-1.9617±0.1637
0.0917	-2.1301±0.1149	-1.9362±0.0815	-1.8523±0.1295	-1.9729±0.1930
0.1376	-2.2185±0.138	-1.3331±0.1321	-2.1664±0.1120	-2.2393±0.2066
0.1835	-2.1941±0.1263	-2.2392±0.1296	-2.1250±0.1105	-2.1861±0.2116

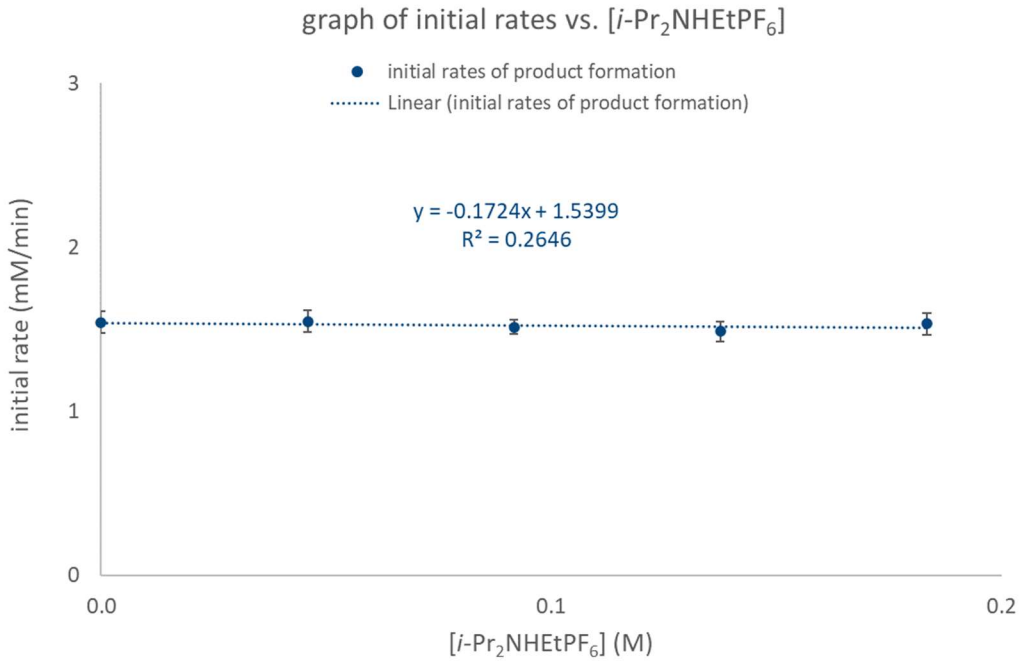

Figure B29. No linear fit ($R^2 = 0.2646$) for initial rate of allylic amine product **3.5** formation versus varying concentrations of *i*-$Pr_2NHEtPF_6$ acid. Zeroth order rate dependence is determined for *i*-$Pr_2NHEtPF_6$ acid during allylic amination.

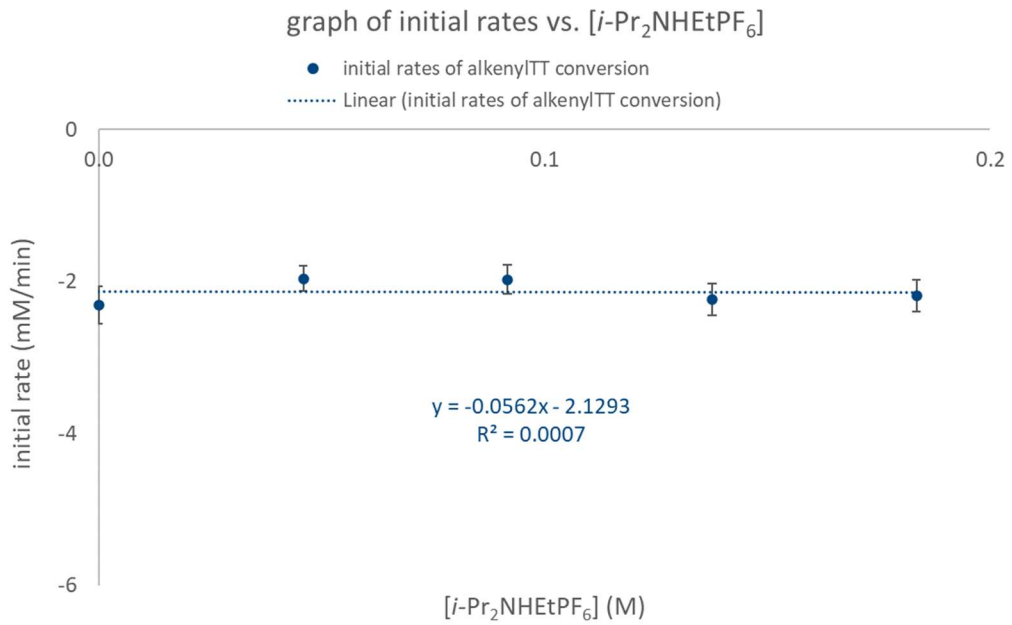

Figure B30. No linear fit (R^2 = 0.0007) for initial rate of alkenylTT **3.3** conversion versus varying concentrations of *i*-$Pr_2NHEtPF_6$ acid. Consistent with Figure B29 monitoring product formation: zeroth order rate dependence is determined for *i*-$Pr_2NHEtPF_6$ acid during allylic amination. The conversion rate of alkenylTT **3.3** is slightly higher than the rate of the formation of allylic amine product **3.5**. This observation is consistent with other minor pathways available to decompose the alkenylTT salt. Consequently, allylic amine product **3.5** formation rates will be used for quantitative analysis.

B3.6. Summary of Rate Law for Allylic Amination

To confirm the accuracy of the kinetics data, we compared the calculated rate constants, *k*, for the experiments and summarized the rate law for allylic amination of alkenylthianthrenium salts with *i*-Pr_2NEt base.

Zeroth order dependence was determined for PhNHMe nucleophile. The linear fit from these kinetic experiments afforded the equation:

initial rate *y*, mM/min = [0.1633 mM/(M*min)]*(*x* aniline concentration, M) + 1.5619 mM/min

As such, the *y*-intercept and first order dependence on alkenylTT **3.3** and *i*-Pr_2NEt base–where under the standard reaction conditions, [alkenylTT] = 0.0917 M and [*i*-Pr_2NEt] = 0.4587 M–can be used to determine the rate constant *k* for the allylic amination reaction. Where initial rate is k_{obs}

$$k_{obs} = k[\text{alkenylTT}][i\text{-}Pr_2NEt]$$

$$\text{rate (M/min)} = k * y\text{-intercept} = k(1.5619 \times 10^{-3}\ \text{M/min}) = k[\text{alkenylTT}][i\text{-}Pr_2NEt] =$$

$$k = 3.7 \times 10^{-2}\ M^{-1}min^{-1}$$

This value is consistent with the *k* values obtained from order determination in alkenylTT salt, *i*-Pr_2NEt base, and *i*-$Pr_2NHEtPF_6$ conjugate base (Table B13).

In the experiments varying [alkenylTT] or [*i*-Pr_2NEt], the slope rather than the *y*-intercept from the linear fit was used to determine the rate constant, *k*. A representative example:

$$\text{initial rate } y, \text{ mM/min} = [19.1200 \text{ mM/(M*min)}]*(x \text{ alkenylTT, M}) + 0.1628 \text{ mM/min}$$

Where,

$$\text{slope} = k[i\text{-}Pr_2NEt]$$

So under standard conditions where [*i*-Pr_2NEt] = 0.4587 M,

$$k = \text{slope}/[i\text{-}Pr_2NEt] = 4.2 \times 10^{-2}\ M^{-1}min^{-1}$$

Fractional errors were calculated using the errors for the average initial rates used to determine the linear fit equation.

Summary of rate law for allylic amination:

$$\text{rate} = (3.7 \pm 0.8) \times 10^{-2}\ M^{-1}min^{-1}\ [\text{alkenylTT}][i\text{-}Pr_2NEt]$$

Table B13. Summary of Kinetics Equations and Rate Constants Obtained from Order Determination in Reaction Components.

using allylic amine 3.5 formation			
Component	**Order**	**Linear fit equation**	***k* ($M^{-1}min^{-1}$)**
PhNHMe	0th	$y = 0.1633x + 1.5619$	$(3.7\pm0.3) \times 10^{-2}$
alkenylTT **3.3**	1st	$y = (19.1200\pm0.5806)x - (0.1628\pm0.0737)$	$(4.2\pm0.5) \times 10^{-2}$
i-Pr_2NEt	1st	$y = (2.7896\pm0.1028)x + (0.1766\pm0.0427)$	$(3.1\pm0.4) \times 10^{-2}$
i-$Pr_2NHEtPF_6$	0th	$y = -0.1724x + 1.5399$	$(3.7\pm0.3) \times 10^{-2}$
		average±error	$(3.7\pm0.8) \times 10^{-2}$

B4. Kinetic Isotope Effect (KIE) Experiments

Initial Rates Analysis and Error Propagation

For linear fit of a single trial, standard error of the slope (*i.e.* initial rate) was calculated using the Analysis ToolPak Regressions in Excel Data Analysis.

Fractional error was calculated for the average initial rates acquired from triplicate experiments. The error for kinetic isotope effects was calculated *via* propagation of these errors of the averaged initial rates. See *J. Am. Chem. Soc.* **1995**, 117, 36, 9357–9358; *J. Am. Chem. Soc.* **2017**, 139, 16, 5965–5972.

B4.1. Allylic Deprotonation Intermolecular KIE Effect *via* Initial Rates – Two Parallel Reactions (Scheme 3.3A)

The purpose of these experiments was to determine the KIE at the allylic C–H bonds of alkenylthianthrenium salts, for which allylic deprotonation is implicated as the rate determining step in allylic amination. Reaction monitoring was conducted using the General Procedure for ^{1}H NMR Reaction Monitoring *with the specified modifications:* in addition to the standard reaction, a second separate stock solution was prepared using 5-(4-phenylbut-1-en-1-yl-3,3-d2)-5H-thianthren-5-ium hexafluorophosphate(V) (alkenylTT-d_2) **3.3-d$_2$** instead of 5-(4-phenylbut-1-en-1-yl)-5H-thianthren-5-ium hexafluorophosphate (alkenylTT) **3.3**.

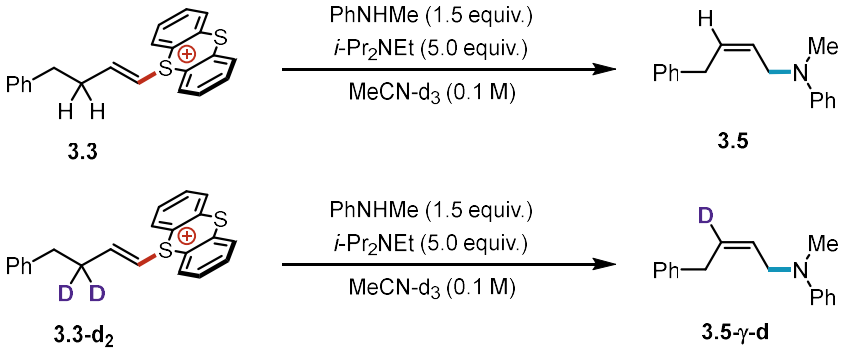

Figure B31. Reaction scheme for the two parallel experiments that compares the KIE of the allylic C–H/D bond deprotonation of alkenylthianthrenium salts.

Table B14. Data from Monitoring the Reaction Using ^{1}H NMR Spectroscopy for Allylic Amination of AlkenylTT 3.3 (Parallel Reactions Experiment).

Run1			***Run2***			***Run3***		
Time (min)	**[alkenylTT 3.3] (mM)**	**[allylic amine 3.5] (mM)**	**Time (min)**	**[alkenylTT 3.3] (mM)**	**[allylic amine 3.5] (mM)**	**Time (min)**	**[alkenylTT 3.3] (mM)**	**[allylic amine 3.5] (mM)**
0.00	91.35	0.00	0.00	91.93	0.00	0.00	93.06	0.00
3.37	82.35	6.92	3.20	83.30	6.66	2.70	79.28	5.51
3.73	78.49	7.05	3.73	79.20	6.97	3.13	78.50	6.03
4.25	75.95	7.73	4.10	78.38	7.57	3.60	77.33	6.86

Run1			*Run2*			*Run3*		
4.72	75.59	8.45	4.43	78.03	8.12	4.15	77.27	7.80
5.27	74.69	9.28	4.90	76.73	8.80	4.82	76.54	8.81
5.68	73.85	9.95	5.32	76.80	9.42	5.57	75.83	10.02
6.35	73.13	10.91	5.75	75.39	10.28	6.17	74.10	10.95
6.95	71.56	11.75	6.27	74.05	10.88	6.67	73.70	11.58

Table B15. Data from Monitoring the Reaction Using ^{1}H NMR Spectroscopy for Allylic Amination of AlkenylTT 3.3-d_2 (Parallel Reactions Experiment).

Run1			*Run2*			*Run3*		
Time (min)	**[alkenylTT 3.3-d_2] (mM)**	**[allylic amine 3.5-γ-d] (mM)**	**Time (min)**	**[alkenylTT 3.3-d_2] (mM)**	**[allylic amine 3.5-γ-d] (mM)**	**Time (min)**	**[alkenylTT 3.3-d_2] (mM)**	**[allylic amine 3.5-γ-d] (mM)**
0.00	91.79	0.00	0.00	92.41	0.00	0.00	92.63	0.00
3.02	92.35	0.32	2.95	93.47	0.61	2.97	93.00	0.29
7.03	86.61	0.67	6.50	87.26	0.73	6.55	87.51	0.45
10.10	85.88	1.38	8.55	86.03	1.29	9.62	86.29	1.32
13.00	84.89	1.91	12.60	85.68	1.91	12.67	85.02	1.92
16.20	83.49	2.54	15.65	84.56	2.47	15.72	84.63	2.40
19.27	83.09	3.04	18.72	83.84	2.98	18.77	84.16	2.98
22.32	82.21	3.71	21.78	82.92	3.46	21.83	83.10	4.15
24.37	81.72	4.24	24.85	82.39	4.01	24.88	82.21	4.01
28.42	81.26	5.36	27.92	81.82	5.51	27.95	81.59	4.71
31.47	80.18	5.96	30.98	81.29	6.13	31.02	80.62	5.95
34.53	79.47	6.73	34.07	79.98	6.69	34.07	80.14	6.56
37.60	78.89	7.06	37.13	79.37	7.19	37.13	79.54	7.25
40.67	78.25	7.68	43.25	78.28	8.34	40.18	78.85	7.78
46.78	76.97	9.01	46.32	77.58	8.80	43.25	78.33	8.30
49.85	76.35	9.34	49.37	76.99	9.24	46.30	77.54	8.68
52.92	75.95	9.90	52.42	75.92	10.00	49.35	77.16	9.34
55.98	75.28	10.41	55.48	75.77	10.34	52.40	76.30	9.84

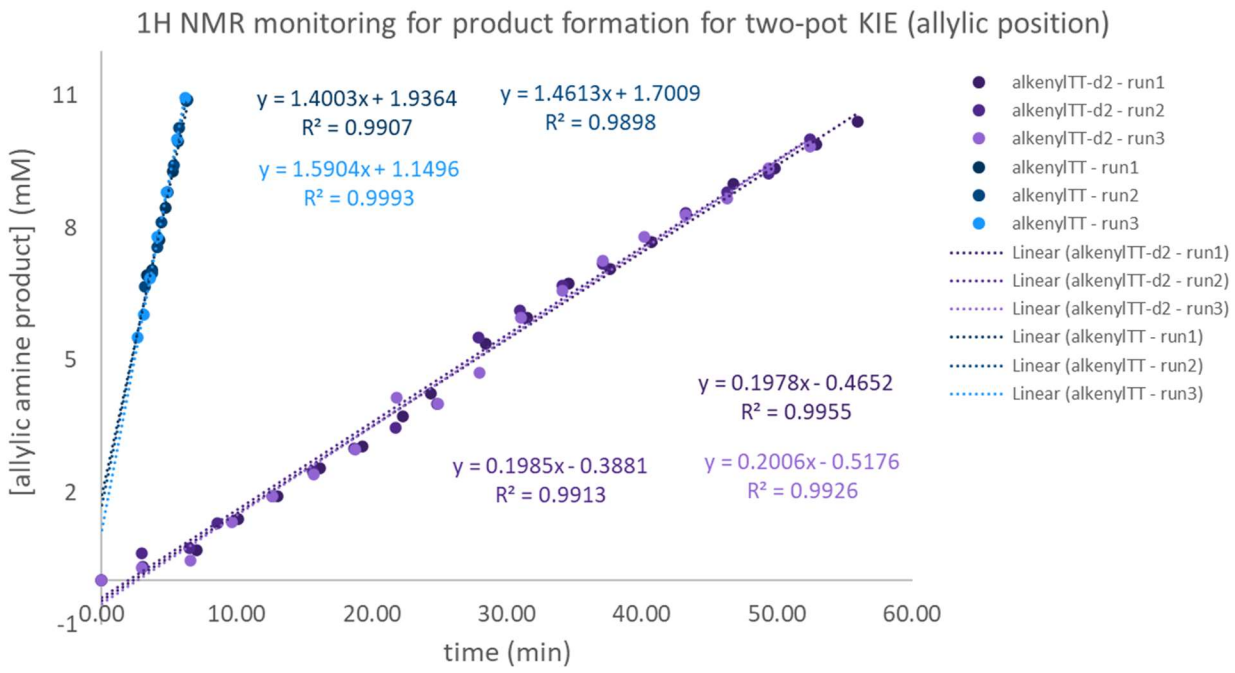

Figure B32. Data graphed from monitoring the allylic amine product **3.5** or **3.5-γ-d** formation using ^{1}H NMR spectroscopy with alkenylTT **3.3** or **3.3-d$_2$**, respectively (two parallel reactions). We have noted in our kinetic experiments that the conversion rate of alkenylTT **3.3** is slightly higher than the rate of the formation of allylic amine product **3.5**. This observation is consistent with other minor pathways available to decompose the alkenylTT salt. Consequently, allylic amine product **3.5** or **3.5-γ-d** formation rates will be used for quantitative analysis.

Table B16. Initial Rate Data for Two Parallel Reactions KIE at the Allylic Position using allylic amine 3.5 or 3.5-γ-d formation

	initial rate (mM/min)			
alkenylTT salt	***run1***	***run2***	***run3***	**average±error**
3.3	0.1978±0.0033	0.1985±0.0048	0.2006±0.0043	0.1990±0.0073
3.3-d$_2$	1.4003±0.0606	1.4613±0.0605	1.5904±0.01896	1.4840±0.0907
			k_H/k_D	7.46±0.53

B4.2. Allylic Deprotonation Intermolecular KIE Effect – Intermolecular Competition

The purpose of these experiments was to determine and validate the KIE at the allylic C–H bonds of alkenylthianthrenium salts, for which allylic deprotonation is implicated as the rate determining step in allylic amination. Reaction monitoring was conducted using the General Procedure for ^{1}H NMR Reaction Monitoring *with the specified modifications:* the stock solution was prepared with 5-(4-phenylbut-1-en-1-yl-3,3-d2)-5H-thianthren-5-ium hexafluorophosphate(V) (alkenylTT-d_2) **3.3-d$_2$** (0.05 M) and 5-(4-phenylbut-1-en-1-yl)-5H-thianthren-5-ium hexafluorophosphate (alkenylTT) **3.3** (0.05 M).

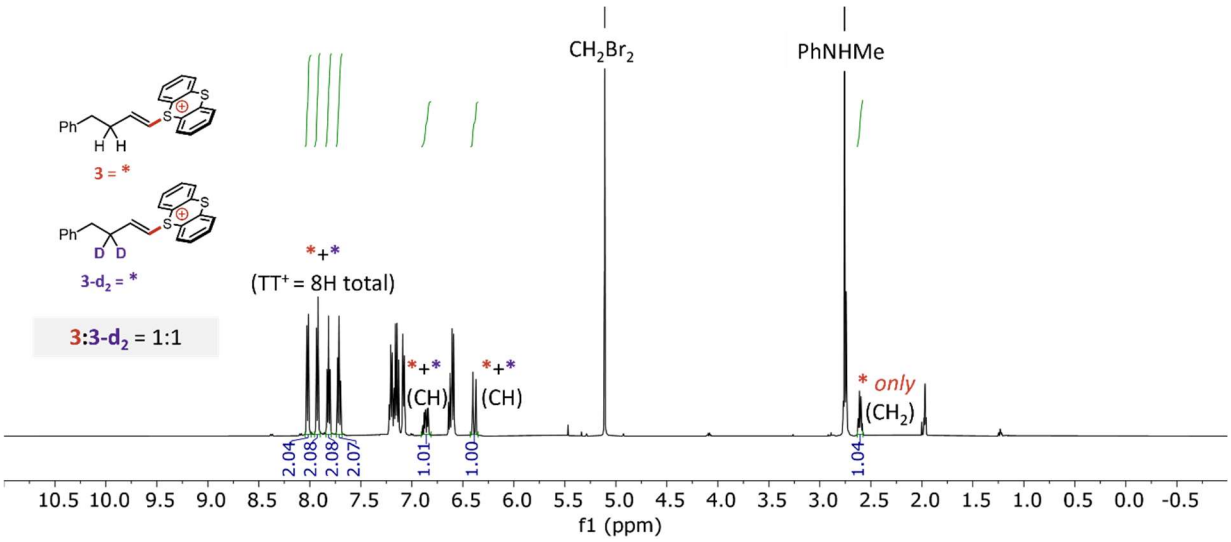

Figure B33. Representative ^{1}H NMR spectrum of the 1:1 alkenylTT **3.3: 3.3-d$_2$** stock solution prepared for the one-pot intermolecular KIE competition experiment. CH_2Br_2 was used as an internal standard (5.10 ppm, s, 2H).

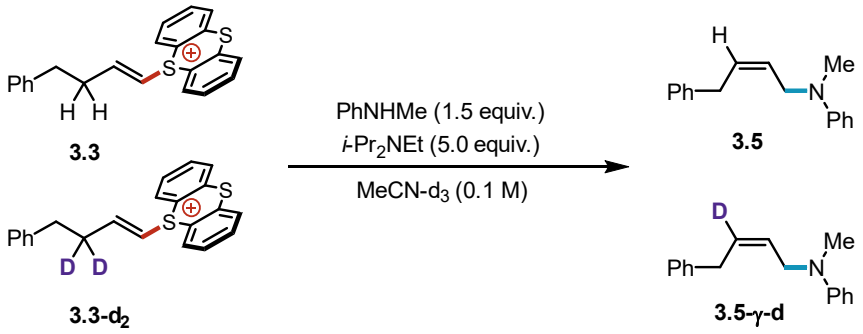

Figure B34. Reaction scheme for the one-pot intermolecular KIE competition for the allylic C–H/D bond deprotonation of alkenylthianthrenium salts. Concentration of **3.5-γ-d** was determined by subtraction of the annotated C–H signal of **3.5** (5.82 – 5.68 ppm, m, 1H) from the adjacent alkenyl proton signal common to both **3.5** and **3.5-γ-d** (5.60 – 5.47 ppm, m, 1H).

Table B17. Data from Monitoring the Reaction Using ^{1}H NMR Spectroscopy for Allylic Amination of AlkenylTT 3.3 and 3.3-d_2 (Intermolecular Competition).

Run1			
Time (min)	**[alkenylTT 3.3 + 3.3-d_2] (mM)**	**[allylic amine 3.5] (mM)**	**[allylic amine 3.5-γ-d] (mM)**
0.00	87.29	0.00	0.00
3.18	85.96	2.92	0.00
4.05	81.14	3.09	0.00
4.60	80.14	3.59	0.00
5.17	79.49	4.01	0.11
5.73	79.17	4.36	0.15
6.30	78.32	4.85	0.13
6.85	77.56	5.25	0.23
7.40	77.39	5.61	0.24
7.97	76.67	5.87	0.49
8.52	76.42	6.51	0.19
9.07	75.53	6.79	0.36
9.63	75.36	7.06	0.55
10.18	74.88	7.24	0.73
10.75	74.31	7.40	0.75
11.32	74.15	8.13	1.31

Run2			
Time (min)	**[alkenylTT 3.3 + 3.3-d_2] (mM)**	**[allylic amine 3.5] (mM)**	**[allylic amine 3.5-γ-d] (mM)**
0.00	90.02	0.00	0.00
3.32	86.83	2.97	0.00
4.17	81.28	3.06	0.00
4.75	81.35	3.71	0.00
5.30	80.08	4.03	0.00
5.85	79.43	4.40	0.09
6.40	79.11	4.88	0.25
6.95	78.09	5.23	0.33
7.52	77.98	5.64	0.37

Run2			
8.07	77.19	6.08	0.59
8.62	76.40	6.44	0.23
9.20	76.00	6.78	0.29
9.75	75.62	7.19	0.69
10.32	75.05	7.40	0.97
10.88	74.56	7.93	1.11
11.45	74.05	7.96	1.05

Run3			
Time (min)	**[alkenylTT 3.3 + 3.3-d_2] (mM)**	**[allylic amine 3.5] (mM)**	**[allylic amine 3.5-γ-d] (mM)**
0.00	89.36	0.00	0.00
3.62	87.12	2.92	0.00
4.60	81.73	3.09	0.00
5.17	81.10	3.59	0.00
5.72	80.34	4.01	0.11
6.27	79.99	4.36	0.15
6.83	80.06	4.85	0.13
7.38	78.91	5.25	0.23
7.93	77.91	5.61	0.24
8.48	78.00	5.87	0.49
9.05	77.11	6.51	0.19
9.60	77.03	6.79	0.36
10.17	76.25	7.06	0.55
10.73	75.62	7.24	0.73
11.28	75.28	7.40	0.75
11.83	74.53	8.13	1.31

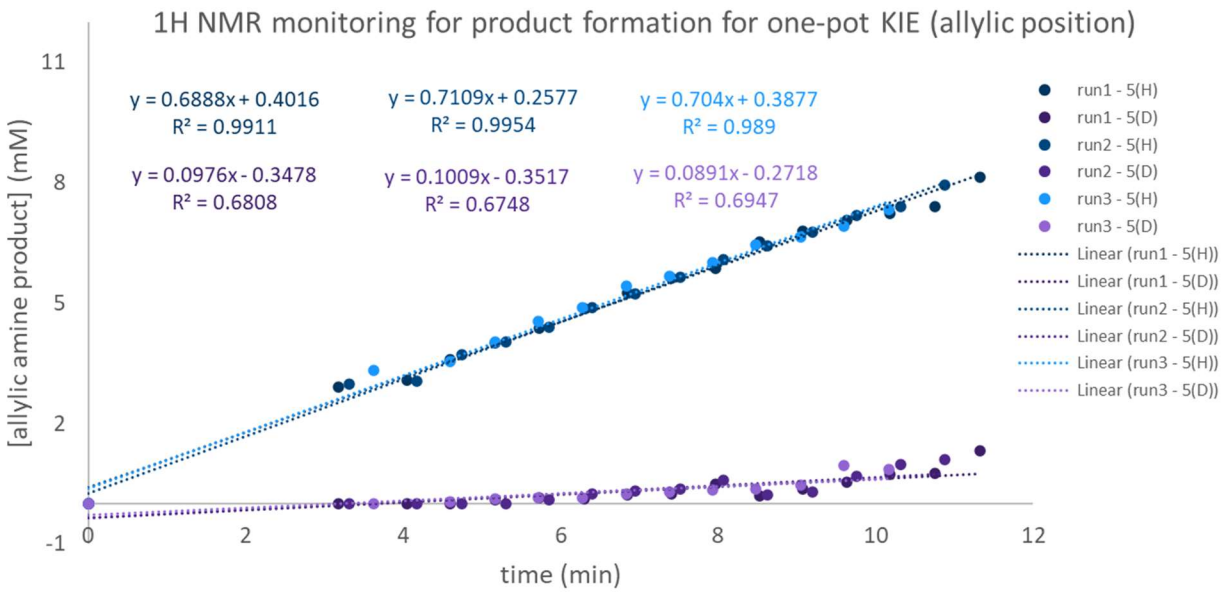

Figure B35. Data graphed from monitoring the allylic amine product **3.5** or **3.5-γ-d** formation using ^{1}H NMR spectroscopy with 1:1 alkenylTT **3.3** and **3.3-d$_2$**, respectively (intermolecular competition). We have noted in our kinetic experiments that the conversion rate of alkenylTT **3.3** is slightly higher than the rate of the formation of allylic amine product **3.5**. This observation is consistent with other minor pathways available to decompose the alkenylTT salt. Consequently, allylic amine product **3.5** or **3.5-γ-d** formation rates will be used for quantitative analysis.

Table B18. Initial Rate Data for Intermolecular Competition KIE at the Allylic Position using allylic amine 3.5 or 3.5-γ-d formation

	initial rate (mM/min)			
alkenylTT salt	***run1***	***run2***	***run3***	**average±error**
3.3	0.6888±0.0175	0.7109±.0135	0.7040±0.0223	0.7012±0.0314
3.3-d$_2$	0.0976±0.0089	0.1009±0.0097	0.0891±0.0089	0.0959±0.0159
			k_H/k_D	7.31±1.26

***Conclusion*:** Both the two parallel reactions and intermolecular one-pot competition experiments exhibit a large primary KIE of ~7. These data are consistent with breaking the C–H/D bond in the transition state structure of the rate determining step *i.e.* allylic deprotonation of the alkenylthianthrenium salt. See *Angew. Chem. Int. Ed.* **2012**, 51 (13), 3066–3072. Furthermore, the large primary KIE of 7.46±0.53 obtained from the two parallel reactions nears the maximum primary KIE (within error) for C–H bond dissociation at room temperature. This is consistent with high degree of C–H bond breaking in the late transition state for endothermic allylic deprotonation, see Appendix B11 for computational details.

B4.3. Intermolecular KIE Effect at Ylide Position *via* Initial Rates – Two Parallel Reactions

The purpose of these experiments was to determine the KIE at the ylide formation position of alkenylthianthrenium salts. Reaction monitoring was conducted using the General Procedure for ^{1}H NMR Reaction Monitoring *with the specified modifications:* in addition to the standard reaction, the stock solution was prepared using 5-(4-phenylbut-1-en-1-yl-1-d)-5H-thianthren-5-ium hexafluorophosphate(V) (alkenylTT-d) **3.3-d** instead of 5-(4-phenylbut-1-en-1-yl)-5H-thianthren-5-ium hexafluorophosphate (alkenylTT) **3.3**.

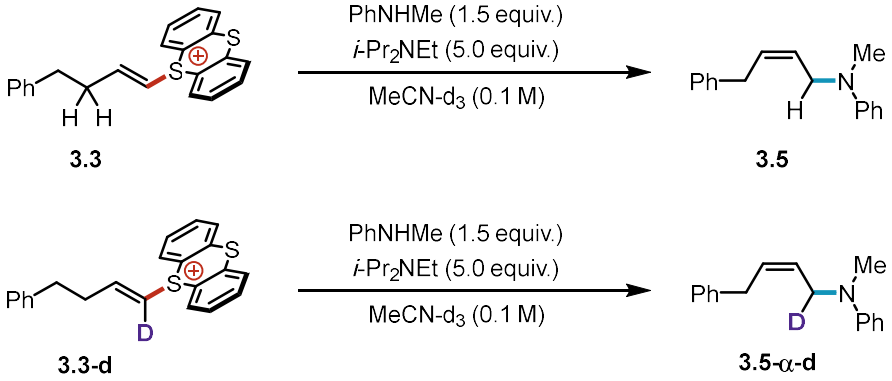

Figure B36. Reaction scheme for the two parallel experiments that compares the KIE of the alkenyl C–H/D bond that generates an ylide upon allylic deprotonation of alkenylthianthrenium salts.

Table B19. Data from Monitoring the Reaction Using ^{1}H NMR Spectroscopy for Allylic Amination of AlkenylTT 3.3 (Parallel Reactions Experiment).

Run1			***Run2***			***Run3***		
Time (min)	**[alkenylTT 3.3] (mM)**	**[allylic amine 3.5] (mM)**	**Time (min)**	**[alkenylTT 3.3] (mM)**	**[allylic amine 3.5] (mM)**	**Time (min)**	**[alkenylTT 3.3] (mM)**	**[allylic amine 3.5] (mM)**
0.00	86.97	0.00	0.00	87.36	0.00	0.00	86.80	0.00
3.47	81.43	5.57	3.02	83.10	4.92	3.53	82.44	5.92
4.13	75.77	6.69	3.67	77.50	5.93	3.92	76.44	6.52
4.37	76.06	7.00	4.03	76.93	6.82	4.55	74.91	7.35
4.65	75.10	7.33	4.52	75.93	7.36	4.78	75.34	7.70
5.07	74.14	8.18	5.08	74.79	8.23	5.32	73.38	9.13
5.45	73.31	9.35	5.58	74.06	9.12	5.85	72.31	9.78
5.85	72.43	9.85	6.12	72.67	10.37	6.38	71.26	10.65
6.28	71.64	9.99	6.68	71.63	10.34	6.83	70.85	11.45
6.55	71.70	10.44	7.12	70.84	11.14	7.22	69.65	11.89
6.93	70.91	10.86	7.52	70.28	11.34	0.00	86.80	0.00
7.32	69.80	11.33	8.12	69.14	13.16	3.53	82.44	5.92

Table B20. Data from Monitoring the Reaction Using ^{1}H NMR Spectroscopy for Allylic Amination of AlkenylTT 3.3-d (Parallel Reactions Experiment).

Run1			*Run2*			*Run3*		
Time (min)	**[alkenylTT 3.3-d] (mM)**	**[allylic amine 3.5-α-d] (mM)**	**Time (min)**	**[alkenylTT 3.3-d] (mM)**	**[allylic amine 3.5-α-d] (mM)**	**Time (min)**	**[alkenylTT 3.3-d] (mM)**	**[allylic amine 3.5-α-d] (mM)**
0.00	87.70	0.00	0.00	87.05	0.00	0.00	87.52	0.00
2.97	82.47	4.62	3.37	82.39	6.37	2.97	83.33	4.64
3.32	77.37	5.32	3.62	77.91	5.65	3.62	76.70	5.66
3.60	76.58	5.89	4.02	76.18	6.72	4.05	76.05	6.48
4.00	75.37	6.32	4.50	74.88	7.70	4.48	75.31	7.86
4.37	75.10	7.20	4.82	74.83	8.55	5.02	74.13	8.59
4.63	74.65	7.60	5.25	73.82	9.02	5.33	73.93	8.36
4.93	74.58	8.17	5.67	73.12	9.22	5.95	72.41	9.99
5.83	72.37	9.95	6.23	72.00	10.53	6.45	71.66	10.90
8.18	69.84	11.98	6.78	70.86	11.46	6.83	71.24	11.30

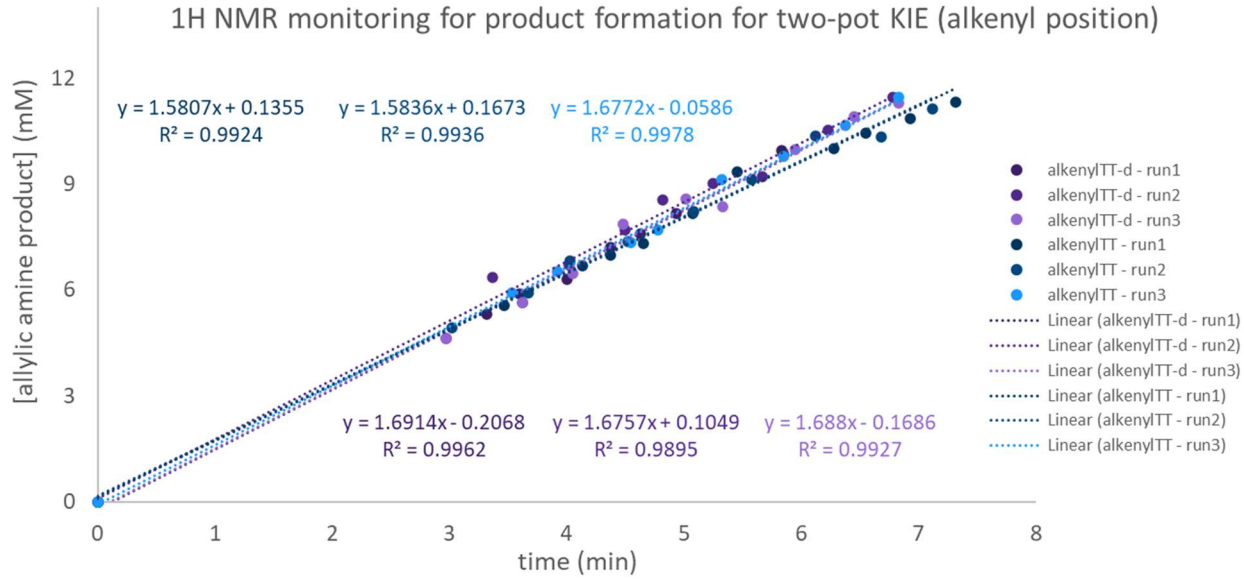

Figure B37. Data graphed from monitoring the allylic amine product **3.5** or **3.5-α-d** formation using ^{1}H NMR spectroscopy with 1:1 alkenylTT **3.3** and **3.3-d$_2$**, respectively (intermolecular competition). We have noted in our kinetic experiments that the conversion rate of alkenylTT **3.3** is slightly higher than the rate of the formation of allylic amine product **3.5**. This observation is consistent with other minor pathways available to decompose the alkenylTT salt. Consequently, allylic amine product **3.5** or **3.5-α-d** formation rates will be used for quantitative analysis.

Table B21. Initial Rate Data for Two Parallel Reactions KIE at the Alkenyl Position.

using allylic amine 3.5 or 3.5-α-d formation				
	initial rate (mM/min)			
alkenylTT salt	***run1***	***run2***	***run3***	**average±error**
3.3	1.5807±0.0438	1.5836±0.0451	1.6772±0.0296	1.6138±0.0702
3.3-d	1.6914±0.0396	1.6757±0.0611	1.6880±0.0513	1.6850±0.0891
			k_H/k_D	0.96 ±0.07

Conclusion: a minimal inverse secondary KIE that is within error of no KIE (k_H/k_D = 1) is observed at the position corresponding to the site of ylide formation. One potential rationalization for lack of KIE is minimal hybridization at the C–H bond upon allylic deprotonation of the alkenylthianthrenium salt, see Appendix B11 for computational details.

B5. Deuterium Oxide Labeling Experiments

B5.1. Stability of the Allylic Amine Product 3.5 Under Basic Conditions

To a threaded vial equipped with a magnetic stir bar was added *N*-methyl-*N*-(4-phenylbut-2-en-1-yl)aniline **5** (5.9 mg, 0.025 mmol, 1.0 equiv.) and MeCN (0.25 mL). Deuterium oxide (13.5 µL, 0.75 mmol, 30 equiv.) followed by *i*-Pr$_2$NEt (17.5 µL, 0.10 mmol, 4.0 equiv) were then added. The reaction mixture was capped with a PTFE seal and stirred at room temperature until completion of the reaction (6 hours). The reaction was analyzed by ^{1}H NMR spectroscopy using CH_2Br_2 as an external standard (Figure B38). The results and analysis are summarized in Figure B39.

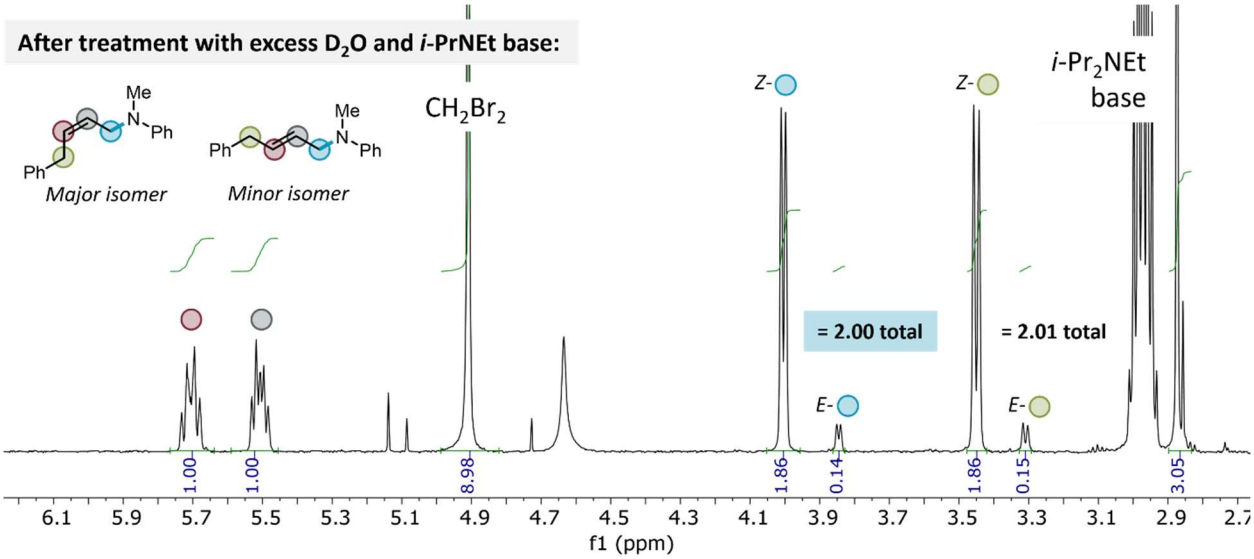

Figure B38. ^{1}H NMR spectrum of allylic amine **3.5** after treatment with *i*-Pr$_2$NEt base and D_2O.

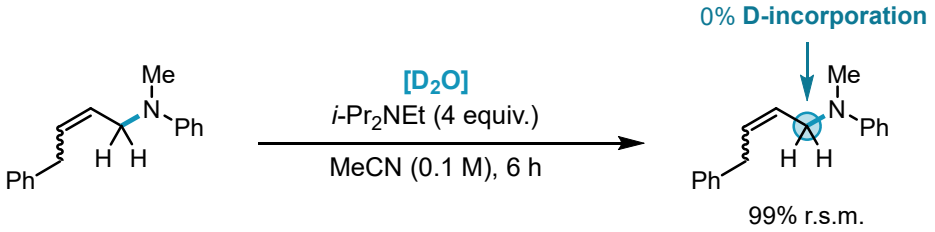

Figure B39. No deuterium incorporation is observed at the allylic position α to the *N*-amine (*N*-allylic signal) under the *i*-Pr_2NEt basic conditions used in the allylic amination of thianthrenium salts. r.s.m. = recovered starting material.

Conclusion: This control supports that the allylic position is stable upon product formation and that any incorporation of deuterium during allylic amination of thianthrenium salts can be attributed to deuteration of reaction intermediates.

B5.2. Probing the Deuteration of Reaction Intermediates (Scheme 3.3B)

The General Procedure for Allylic Amination of Alkenylthianthrenium Salts was performed *with the specified modifications*: the reaction was scaled to 0.20 mmol in alkenylthianthrenium salt **3.3** and deuterium oxide (119 µL, 6.6 mmol, 33 equiv.) was added prior to *N,N*-diisopropylethylamine addition. The reaction was first analyzed by ^{1}H NMR spectroscopy using CH_2Br_2 as an external standard, the yield and *Z:E* are summarized in Figure B40.

Upon completion, the reaction solution was then concentrated under reduced pressure. The residue was purified *via* flash column chromatography (hexanes/ethyl acetate) to afford allylic amine product **3.5** as an oil. For %H quantitation, six ^{1}H NMR (500 MHz) spectra were acquired with the following parameters: relaxation delay = 10 seconds, number of scans = 8 scans. Standard deviations of the integration averages are reported. Fractional error for percent deuterium incorporation was calculated *via* propagation of the average integration errors. The results and analyses are summarized in Table B22, Figure B42, and Figure B47.

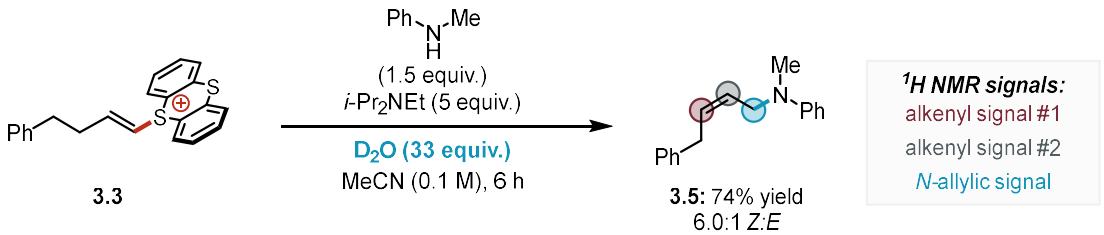

Figure B40. Deuterium labeling experimental results using D_2O. Protons being investigated for deuterium incorporation are annotated.

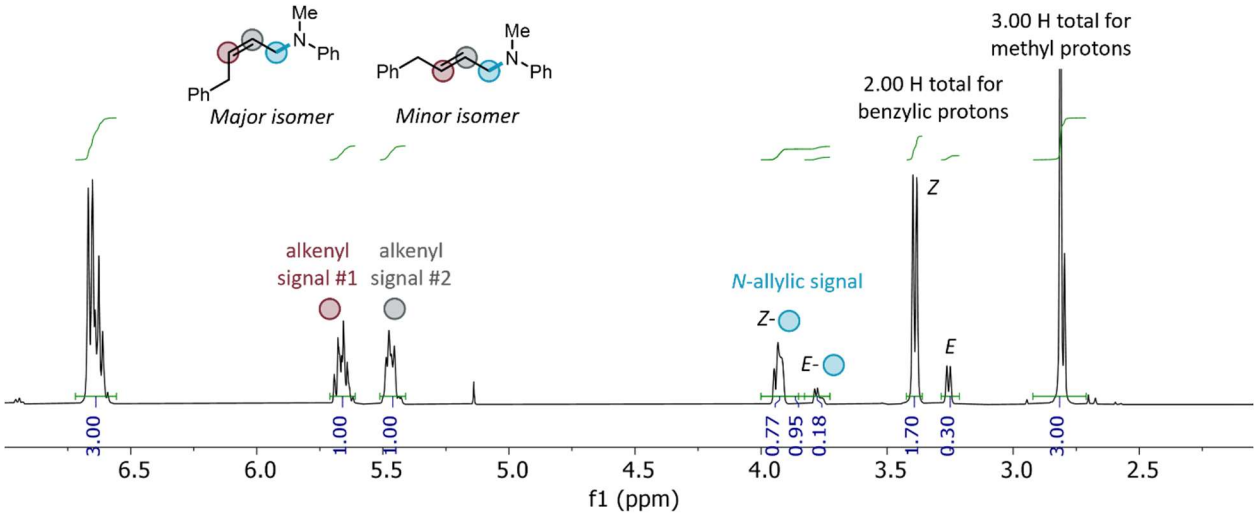

Figure B41. Example ^{1}H NMR spectrum of purified allylic amine product **3.5** for deuterium incorporation analysis. The benzylic (2.00 H) and *N*-methyl (3.00 H) signals were used for validation and comparison to determine the percent loss in proton signal of potentially reactive sites.

Table B22. ^{1}H NMR Integration Data for Alkenyl Signals and *N*-Allylic Signals. Integrations are Relative to 2.00 for the Benzylic Signal and 3.00 for the *N*-Methyl Signal.

Entry	**Alkenyl Signal #1** 5.71 – 5.61 ppm, 1H	**Alkenyl Signal #2** 5.51 – 5.44 ppm, 1H	***N*-allylic Signal** 3.97 – 3.73 ppm, 2H
1	1.00	1.00	0.95
2	1.01	1.00	0.95
3	1.00	0.99	0.94
4	1.01	1.01	0.96
5	1.00	1.00	0.94
6	1.00	1.00	.94
Average±StdDev	1.00±0.01	1.00±0.01	0.95±0.01
Percent Deuterium (%)	0.00±0.01	0.00±0.01	52.67±0.45

First, we looked at the deuterium incorporation at the *N*-allylic position (3.97 – 3.73 ppm, 2H) of the amine product **3.5**. Based on the proton signal of 0.95±0.01 for the expected 2H, the percent deuterium incorporation was calculated to be 52.67±0.45%. Mechanistically, either the ammonium conjugate acid (lower pKa) or D_2O (used in excess) can serve as the deuterium source. Since deuterium is incorporated into the site of sulfonium ylide formation, this supports the stipulation that deuterium from D_2O may wash into the conjugate acid of the amine base and that deuteration of anionic intermediates is feasible under these conditions.

Curiously, we observed lower deuterium incorporation for the *E*-isomer of the allylic amine product **5** than in the *Z*-isomer (Figure B42). This observation was found to be reproducible.

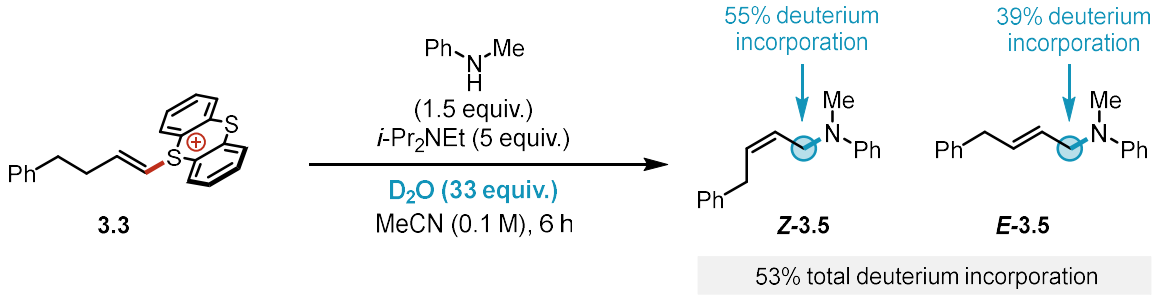

Figure B42. Deuterium labeling experimental results using D_2O. Protons being investigated for deuterium incorporation are annotated. Total deuterium incorporation for combined 74% yield (6.0:1 *Z:E*) of **3.5** is 53%. Greater deuterium incorporation was observed for ***Z*-3.5** than ***E*-3.5**.

Identifying the Source of Deuterium Incorporation Discrepancy for *Z*- and *E*-Isomers

We considered a scenario in which the allylic protons of the alkenylthianthrenium salt are giving rise to this observation. To probe this, General Procedure for Allylic Amination of Alkenylthianthrenium Salts was performed *with the specified modifications*: using 5-(4-phenylbut-1-en-1-yl-3,3-d2)-5H-thianthren-5-ium hexafluorophosphate(V) (alkenylTT-d_2) **3.3-d_2** instead of 5-(4-phenylbut-1-en-1-yl)-5H-thianthren-5-ium hexafluorophosphate (alkenylTT) **3.3**. The reaction was first analyzed by ^{1}H NMR spectroscopy using CH_2Br_2 as an external standard, the yield and *Z:E* are summarized in Figure B43.

Upon completion, the reaction solution was concentrated under reduced pressure. The residue was purified *via* flash column chromatography (hexanes/ethyl acetate) to afford allylic amine product **3.5-γ-d** as an oil. For %H quantitation, ^{1}H NMR (500 MHz) parameters: relaxation delay = 10 seconds, number of scans = 8 scans. The results and analyses are summarized in Figures B44 and B45.

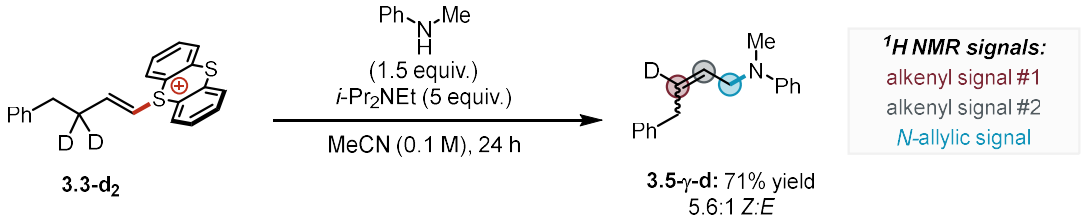

Figure B43. Deuterium labeling experimental results using alkenylTT-d_2 salt **3.3-d_2**. Protons being investigated for deuterium incorporation are annotated.

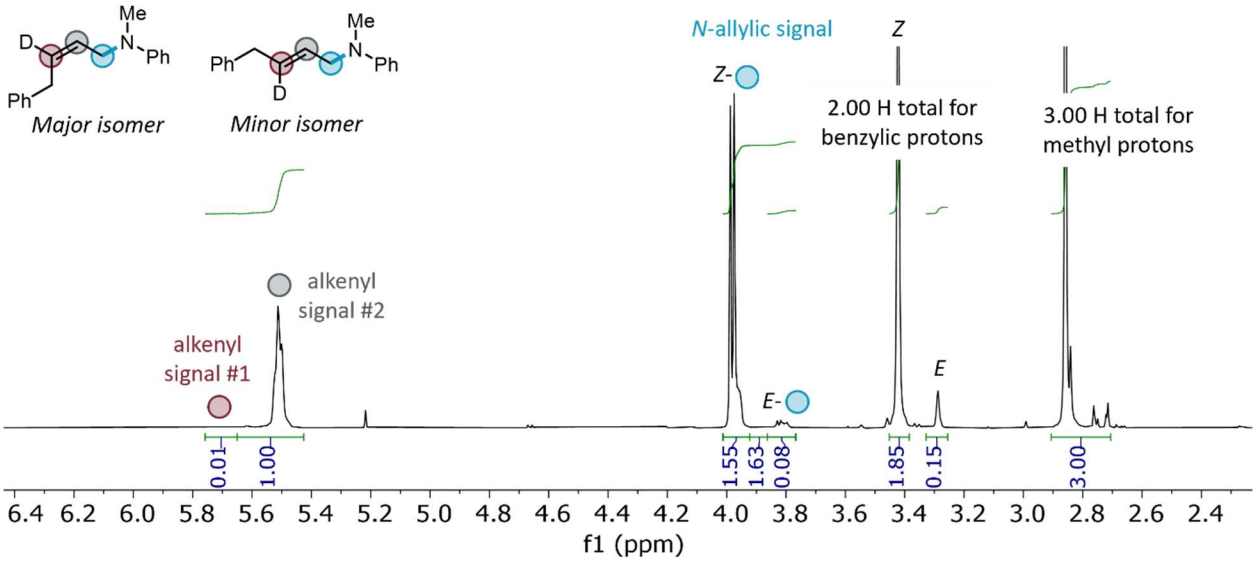

Figure B44. ^{1}H NMR spectrum of isolated allylic amine **3.5-γ-d** derived from allylic amination of alkenylTT-d$_2$ **3.3-d$_2$**. The benzylic and *N*-methyl signals were used for validation and comparison to determine the percent loss in proton signal of potentially reactive sites.

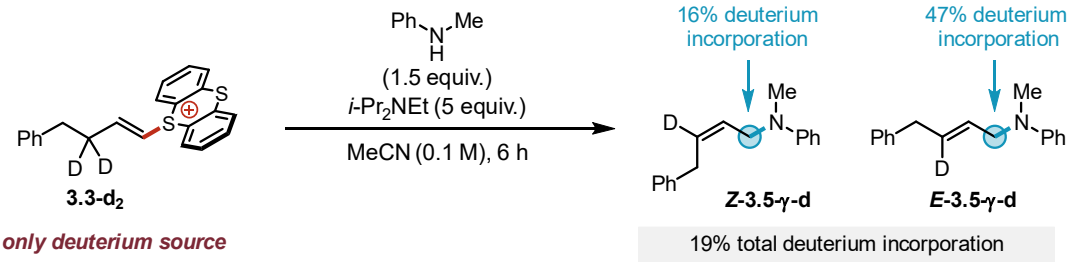

Figure B45. Deuterium labeling experimental results using alkenylTT-d$_2$ **3.3-d$_2$**. Protons being investigated for deuterium incorporation are annotated. Total deuterium incorporation for combined 71% yield (5.6:1 *Z:E*) of **3.5** is 19%. Lower deuterium incorporation was observed for ***Z*-3.5-γ-d** than ***E*-3.5-γ-d**.

Based on the *N*-allylic (3.97 – 3.73 ppm, 2H) signal of 1.63 for the expected 2H (see Figure B44), the total percent deuterium incorporation was calculated to be 19%. This total %D value was found to be less than statistical, which we attribute to proton contributions from exogenous water that may be present since no precautions to dry the reagents were taken. A similar analysis was applied to determine the %D in the *Z*- and *E*-isomers of **3.5-γ-d.** Importantly, this experiment shows that the *Z*-isomer of **3.5-γ-d** exhibits 16% deuteration while the *E*-isomer has significantly more at 47% deuteration. These results are the near inverse of observations made in the earlier experiment (Figure B40) and validates that the proton source in a sea of deuterium was coming from the alkenylthianthrenium salt **3.3** (Figure B42). We have formed a preliminary model to explain the difference in deuterium incorporation for the *Z*- and *E*-allylic products. Molecular dynamics computations suggest that allylic deprotonation of the *E*-alkene forming transition state may have contributions from a non-classical trajectory, see Appendix B11 for more details.

Evaluating the Reversibility of Allylic Deprotonation

Next, we looked at the alkenyl signals of the allylic amine product to determine if the allylic deprotonation of the alkenylthianthrenium salt was reversible or irreversible:

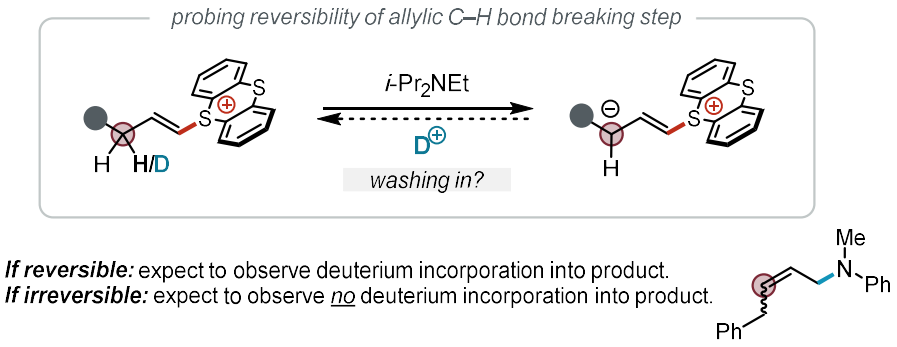

Figure B46. Mechanistic hypothesis tested by D_2O deuterium labelling experiment.

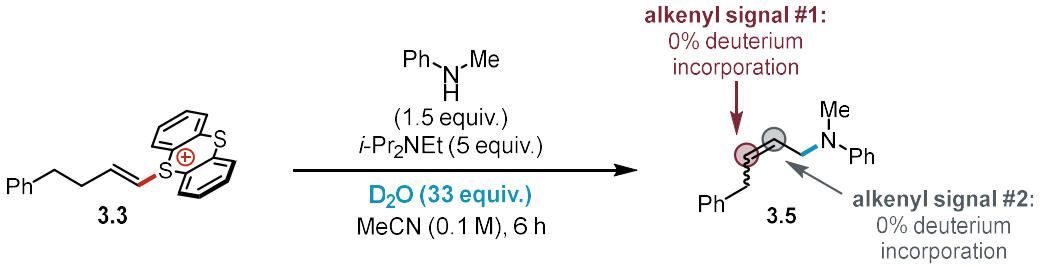

Figure B47. Deuterium labeling experimental results using D_2O. Protons being investigated for deuterium incorporation are annotated. Total deuterium incorporation for combined 74% yield (6.0:1 *Z:E*) of **3.5** is 0% at both alkenyl positions.

Since no deuterium incorporation is observed into the alkenyl positions (5.71 – 5.61 ppm, 1H and 5.51 – 5.44 ppm, 1H) of the allylic amine product **3.5**, this experiment supports irreversible deprotonation under allylic amination reaction conditions.

B5.3. Irreversibility of Allylic Deprotonation Under Reaction Conditions (Scheme 3.3C)

The purpose of this experiment was to validate the irreversibility of the allylic deprotonation during allylic amination conditions. To this end, the General Procedure for Allylic Amination of Alkenylthianthrenium Salts was performed *with the specified modification*: using 5-(4-phenylbut-1-en-1-yl-1-d)-5H-thianthren-5-ium hexafluorophosphate(V) (alkenylTT-d) **3.3-d** instead of 5-(4-phenylbut-1-en-1-yl)-5H-thianthren-5-ium hexafluorophosphate (alkenylTT) **3.3**. The reaction was first analyzed by ^{1}H NMR spectroscopy using CH_2Br_2 as an external standard, the yield and *Z:E* are summarized in Figure B48.

Upon completion, the reaction solution was concentrated under reduced pressure. The residue was purified *via* flash column chromatography (hexanes/ethyl acetate) to afford allylic amine product **3.5-α-d** as an oil. For %H quantitation, ^{1}H NMR (500 MHz) parameters: relaxation delay = 10 seconds, number of scans = 8 scans. Standard deviations of the integration averages are reported. Fractional error for percent deuterium incorporation was calculated *via* propagation of the average integration errors. The results and analyses are summarized in Table B23 and Figure B50.

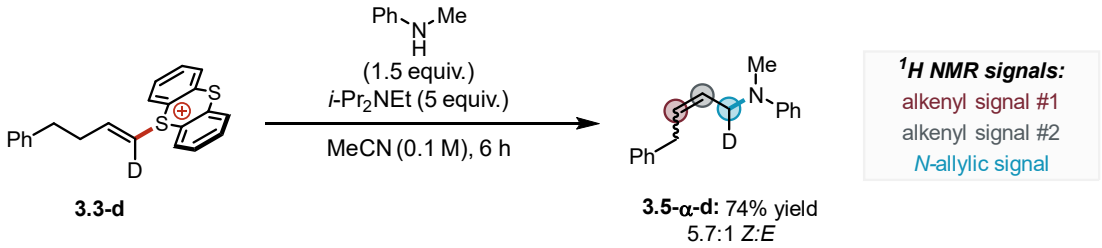

Figure B48. Deuterium labeling experimental results using alkenylTT-d **3.3-d**. Protons being investigated for deuterium incorporation are annotated.

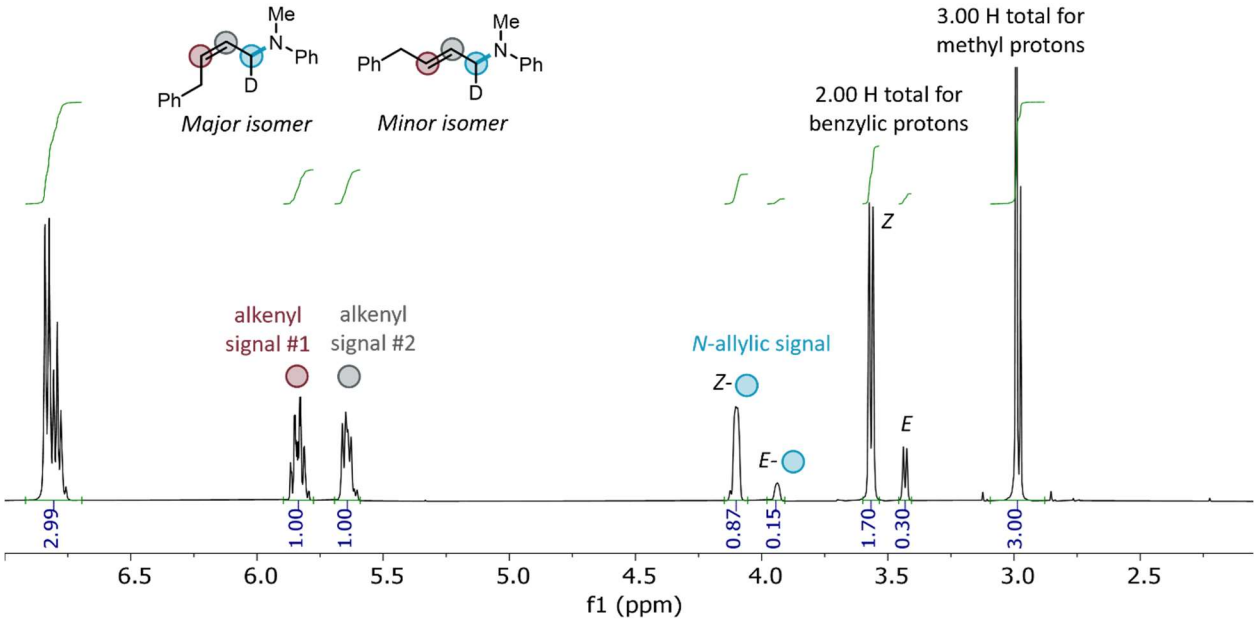

Figure B49. Example ^{1}H NMR spectrum of purified allylic amine product **3.5-α-d** for deuterium incorporation analysis. The benzylic and *N*-methyl signals were used for validation and comparison to determine the percent loss in proton signal of potentially reactive sites.

Table B23. ^{1}H NMR Integration data for Alkenyl Signals and *N*-Allylic Signals. Integrations are Relative to 2.00 for the Benzylic Signal and 3.00 for the *N*-Methyl Signal.

Entry	Alkenyl signal #1 5.71 – 5.61 ppm, 1H	Alkenyl signal #2 5.51 – 5.44 ppm, 1H	*N*-allylic signal 3.97 – 3.73 ppm, 2H
1	1.00	1.00	1.01
2	1.00	0.99	1.01
3	1.00	1.00	1.02
4	1.00	1.00	1.02

Entry	Alkenyl signal #1 5.71 – 5.61 ppm, 1H	Alkenyl signal #2 5.51 – 5.44 ppm, 1H	*N*-allylic signal 3.97 – 3.73 ppm, 2H
5	1.00	1.00	1.02
6	1.00	1.01	1.02
Average±StdDev	1.00±0.00	1.00±0.01	1.02±0.01
Percent Deuterium (%)	0.00±0.00	0.00±0.01	49.17±0.25

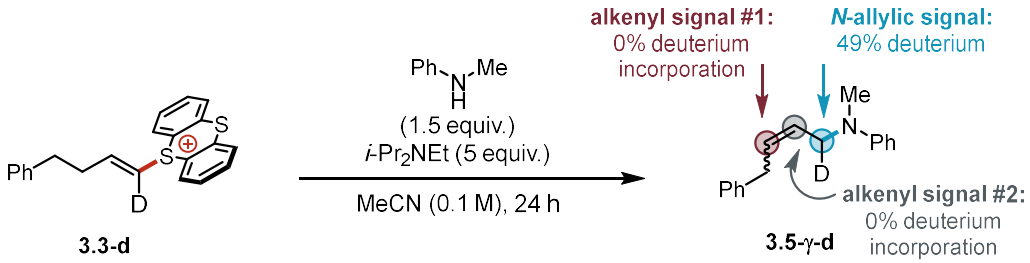

Figure B50. Deuterium labeling experimental results using alkenylTT-d **3.3-d**. Protons being investigated for deuterium incorporation are annotated. Total deuterium incorporation for combined 74% yield (5.7:1 *Z:E*) of **3.5-α-d** is 0% at both alkenyl positions, and there is 49% deuterium at the *N*-allylic position.

Conclusions: Given that the deuterium content of the alkenylTT-d **3.3-d** starting material is 98%, the 49% deuterium detected at the *N*-allylic position (3.97 – 3.73 ppm, 2H) of the amine product **3.5-α-d** indicates a 0% loss in deuterium. Taken together, these deuterium labelling experiments are consistent with irreversible allylic deprotonation under allylic amination conditions.

B6. Detection of an Allylic Thianthrenium Electrophile

During our *in situ* reaction monitoring of the allylic amination of alkenylthianthrenium salt (alkenylTT) **3.3** with *N*-methylaniline using *i*-Pr_2NEt base, no thianthrenium species other than alkenylTT **3.3** were detected. We questioned whether an allylic thianthrenium intermediate could be detected when using a bulkier nucleophile to decrease the rate of the substitution step. To this end, we utilized *i*-Pr_2NEt as both the base and nucleophile since we have observed allylic ammonium **B7** formation in the absence of a secondary amine. Reaction monitoring was conducted using the General Procedure for ^{1}H NMR Reaction Monitoring *with the specified modifications:* no *N*-methylaniline was added to the stock solution; then, *i*-Pr_2NEt (54.0 µL, 0.30 mmol, 6 equiv.) was added *via* microsyringe to the NMR tube.

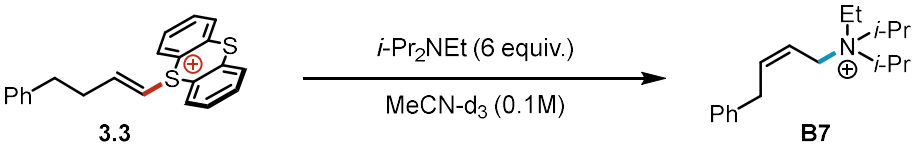

Figure B51. Reaction scheme for allylic amination using bulky *i*-Pr_2NEt as base and nucleophile.

Table B24. Data from Monitoring the Reaction Using ^{1}H NMR Spectroscopy for Allylic Amination of AlkenylTT 3.3 (Allylic Ammonium B7 Formation).

Time (min)	[alkenylTT 3.3] (mM)	[allylic ammonium B7] (mM)	Allylic ammonium *Z:E*	[allylic unknown] (mM) 4.73 ppm & 4.57 ppm	*Z:E* of unknown
0.00	91.16	0.00	--	0.00	--
3.00	86.64	3.16	71.43	2.71	83.33
5.60	79.42	5.87	69.23	2.71	83.33
6.70	77.62	7.22	75.00	3.16	85.71
7.75	75.81	8.57	78.95	3.16	85.71
8.80	73.10	9.93	81.82	3.16	85.71
9.90	71.30	12.18	77.78	3.16	85.71
11.00	70.40	13.54	80.00	3.16	85.71
12.00	68.59	14.89	81.82	3.16	85.71
13.00	66.79	16.25	83.33	3.16	85.71
14.00	64.98	17.15	84.21	2.71	83.33
15.10	64.08	19.40	81.40	2.71	83.33
16.25	62.27	20.76	82.61	2.26	80.00
21.50	55.96	27.08	83.33	2.26	80.00
26.80	50.54	32.49	86.11	2.26	80.00
32.10	45.13	37.45	85.54	1.81	75.00
37.40	40.61	42.42	85.11	1.81	75.00
42.75	37.00	46.03	86.27	1.81	75.00
48.00	33.39	49.64	85.45	1.35	66.67
53.30	29.78	52.80	86.32	1.35	66.67
58.50	27.08	56.41	85.60	1.35	66.67

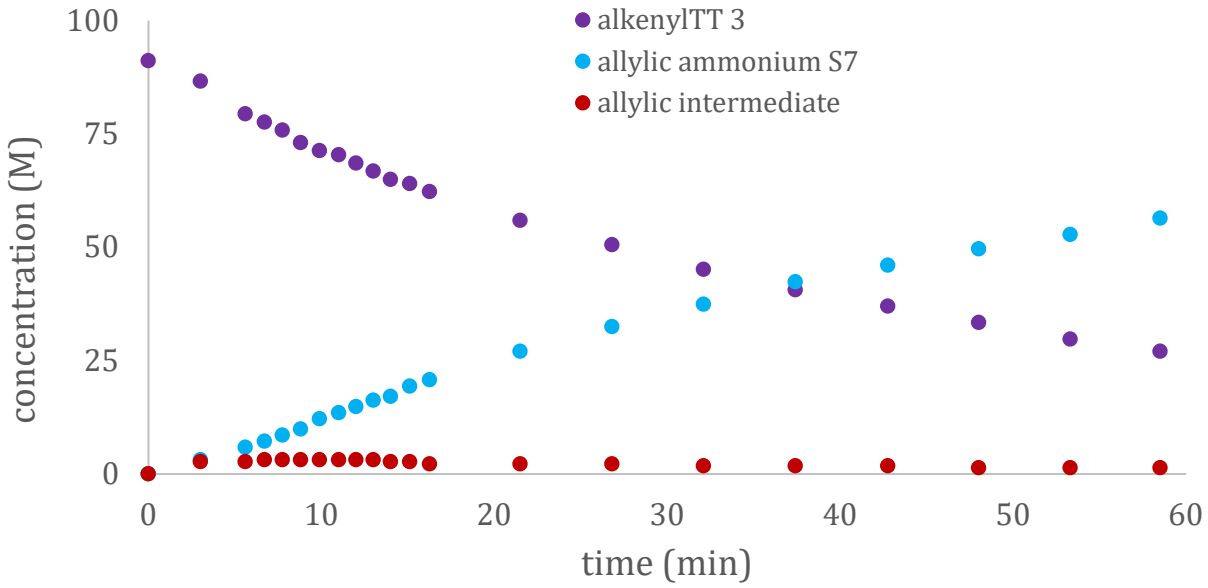

Figure B52. Data graphed from monitoring the allylic ammonium product **B7** formation using 1H NMR spectroscopy with alkenylTT **3.3** and *i*-Pr_2NEt. Unknown allylic intermediate is initially formed in low but detectable concentrations, then is fully consumed during the allylic amination.

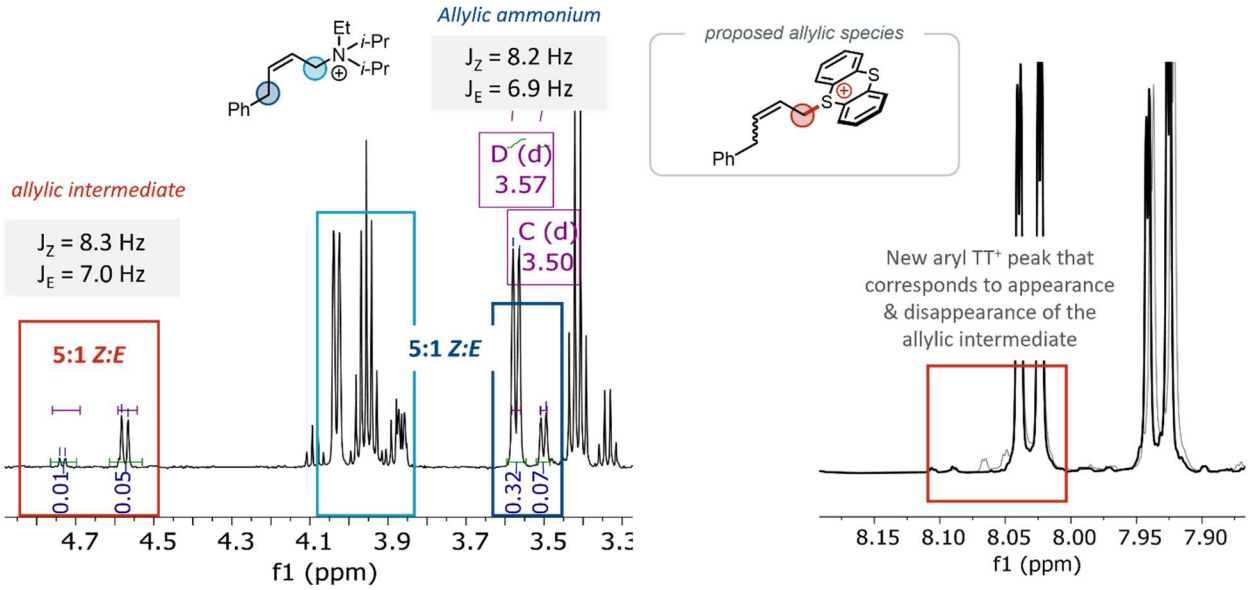

Figure B53. ^{1}H NMR detection of an allylic intermediate indicated by doublets at 4.57 and 4.73 ppm corresponding to potential *Z*- and *E*-isomers. Use of bulky *i*-Pr_2NEt as base and nucleophile gives rise to observation of this transient intermediate during allylic ammonium **B7** formation.

Conclusions: The coupling constants obtained for the new allylic intermediate signals (doublets at 4.57 and 4.73 ppm) correspond to those of the *Z*- and *E*-allylic ammonium product **B7**. Based on these J-values, the *Z:E* of the allylic intermediate corresponds to that of the allylic ammonium product **B7**. This species is detected in < 4% yield during the course of allylic amination with *i*-Pr_2NEt and is absent upon completion of the reaction. Lastly, the detection of new aryl thianthrenium signals that shoulder those of the alkenylTT **3.3** correspond to the detection of the unknown allylic signals. Taken together, we propose this allylic

intermediate corresponds to the allylic thianthrenium electrophile that is formed with Z-selectivity upon allylic deprotonation of the alkenylthianthrenium salt and protonation of the resultant ylide.

Stabilized allylic sulfonium salts are readily prepared (see *Chem. Lett.* **2003**, 32 (7), 626–627) and have been shown to undergo allylic substitution (see *Angew. Chem. Int. Ed.* **2023**, 62 (2), e202214096.). To the best of our knowledge, this marks the first report of detection of an unstablized allylic thianthrenium species with any stereochemical configuration (for studies regarding unsubstituted 5-allylthianthrenium salt, see *J. Org. Chem.* **1990**, 55 (9), 2702–2713).

B7. Discussion of Hypotheses Inconsistent with Mechanistic Data

B7.1. Inconsistent with Dication Formation from Alkenylthianthrenium Salt

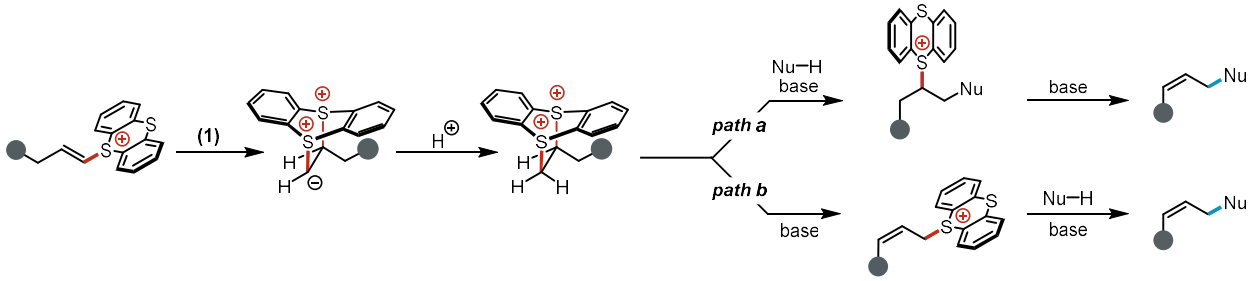

Figure B54. Potential pathways envisioned from dicationic adduct formation from alkenylthianthrenium salt that afford allylic functionalized products.

"Pathway a" is ruled out by the combination of a large primary KIE at the allylic C–H bonds of the alkenylTT salt rules and the reactant orders determined through kinetic experiments. This is because the primary KIE suggests the last step is the highest energetic barrier but, in this scenario, a second order in base as well as first order in nucleophile would be expected. However, experimentally a first order in *i*-Pr_2NEt base and zeroth order in PhNHMe nucleophile is observed.

On the other hand, "pathway b" is consistent with first order in base and zeroth order in nucleophile. However, a first order in acid would be expected since ylide protonation in "pathway b" occurs prior to rate determining allylic deprotonation, and this is inconsistent with experimentally determined zeroth order in *i*-$Pr_2NHEtPF_6$ acid.

While DFT calculations discussed prior (see Figure B5) indicate that mechanistic proposals involving the formation of dicationic adducts from alkenylthianthrenium salts, *i.e.* ylide formation (1) and protonation in Figure **S54**, are highly improbably at room temperature, we were motivated to experimentally exclude this sequence using phenoxathiin-derived alkenylsulfonium salt **B8**. Indeed, preparation of this alkenylsulfonium salt *via* sulfoxide de-oxygenation protocols that proceed through mono-adduct formation are ineffective (see *Angew. Chem.* **2020**, 132 (14), 5665–5669). We were able to prepare **B8** electrochemically in which exclusively bis-adduct *via* sulfur radical cation reactivity was detected.

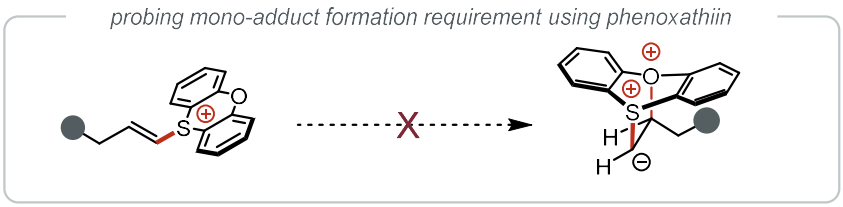

Figure B55. Mechanistic hypothesis tested by alkenylphenoxathiinium salt experiment.

With alkenylphenoxathiinium salt **B8** in hand, we were curious about the *Z*-selective allylic functionalization being unique to the thianthrene moiety, or if other sulfonium structures could be engaged in reactivity. General Procedure for Allylic Amination of Alkenylthianthrenium Salts was performed *with the specified modifications*: using 10-(4-phenylbut-1-en-1-yl)-10H-phenoxathiin-10-ium hexafluorophosphate(V) (alkenylPT) **B8** instead of 5-(4-phenylbut-1-en-1-yl)-5H-thianthren-5-ium hexafluorophosphate (alkenylTT) **3.3**. The yield and *Z:E* are summarized in Figure B56.

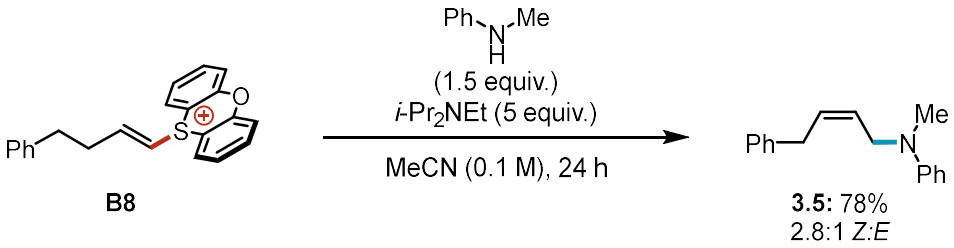

Figure B56. Allylic amination results using alkenylPT **B8**. Phenoxathiin is a competent sulfonium structure for *Z*-selective alyllic functionalization.

The purpose of these next experiments was to investigate the relative rates of allylic functionalization of the different alkenylsulfonium structures. Reaction monitoring was conducted using the General Procedure for ^{1}H NMR Reaction Monitoring *with the specified modifications:* in addition to the standard reaction, the stock solution was prepared using 10-(4-phenylbut-1-en-1-yl)-10H-phenoxathiin-10-ium hexafluorophosphate(V) (alkenylPT) **B8** instead of 5-(4-phenylbut-1-en-1-yl)-5H-thianthren-5-ium hexafluorophosphate (alkenylTT) **3.3**.

Table B25. Data From Monitoring the Reaction Using ^{1}H NMR Spectroscopy for Varying Alkenylsulfonium Structures.

Thianthrene			***Phenoxathiin***		
Time (min)	**[alkenylTT 3.3] (mM)**	**[allylic amine 3.5] (mM)**	**Time (min)**	**[alkenylS$^+$ B8] (mM)**	**[allylic amine 3.5] (mM)**
0.00	94.91	0.00	0.00	91.18	0.00
3.10	86.76	5.62	2.93	86.56	4.71
3.83	81.26	6.21	3.82	82.24	5.67
4.22	80.20	7.42	4.2	81.84	6.25
4.62	79.59	8.04	4.58	81.01	7.00
5.00	78.65	7.81	4.97	79.83	7.46

Thianthrene			*Phenoxathiin*		
5.38	78.12	8.62	5.37	79.42	8.01
5.77	76.38	9.69	5.77	78.48	8.65
6.15	76.62	10.33	6.15	78.02	9.18
6.53	75.69	11.11	6.55	77.55	10.03
6.92	75.02	11.68	6.95	76.54	10.56
7.33	73.78	12.43	7.35	75.83	11.07
7.73	73.63	12.95	7.75	74.93	11.20
8.13	72.66	13.44	8.15	74.54	12.09
8.52	71.64	14.17	8.53	73.92	12.71
8.90	71.22	14.59	8.93	73.66	12.94
9.30	70.60	15.17	9.32	72.87	13.86

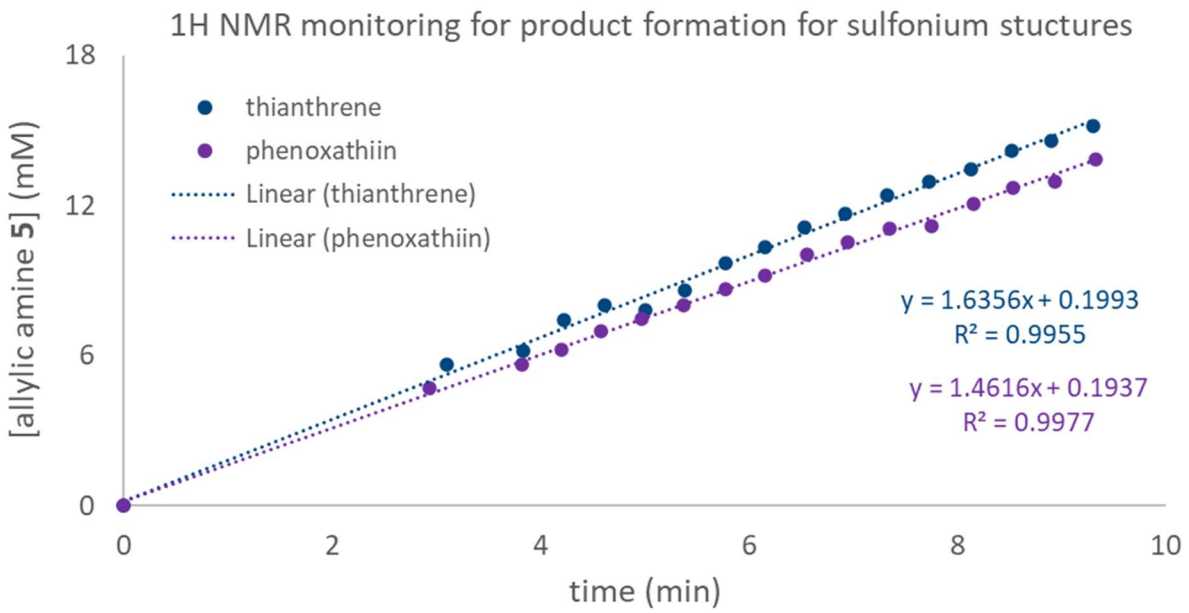

Figure B57. Data graphed from monitoring the allylic amine product **3.5** formation using ^{1}H NMR spectroscopy during allylic amination of alkenylTT **3.3** or alkenylPT **B8**.

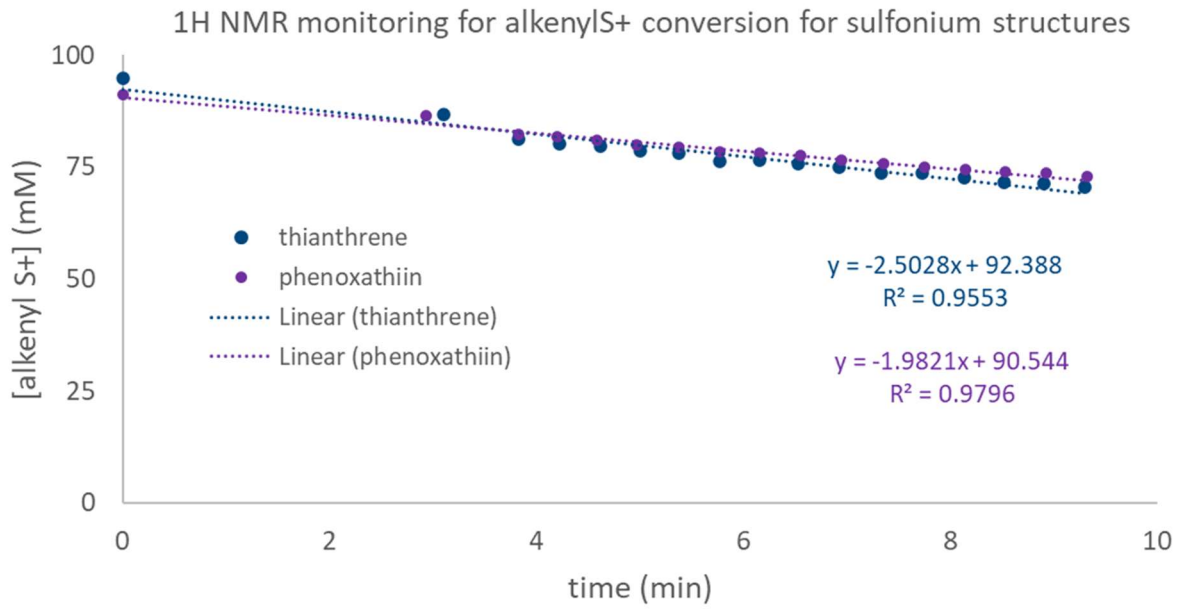

Figure B58. Data graphed from monitoring the alkenylTT **3.3** or alkenylPT **B8** conversion using ^{1}H NMR spectroscopy during allylic amination of alkenylTT **3.3** or alkenylPT **B8**.

Table B26. Initial Rate Data for Alkenylsulfonium Structures.

Sulfonium Structure =	Thianthrene	Phenoxathiin
k_{obs} (mM/min)	1.6356±0.0285	1.4616±0.0181

Conclusion: Allylic amination of alkenylPT salt **B8** proceeds with comparable yield of allylic amine product **5** and diminished Z-selectivity compared to alkenylTT **3.3**. Furthermore, the rate of allylic amination of alkenylPT salt **S8** is the same order of magnitude as that of alkenylTT **3.3**, with the rate of latter being slightly faster (1.1x). Taken together, these data suggest that alkenylsulfonium salts derived from phenoxathiin and thianthrene proceed through the same elementary steps for *Z*-selective allylic functionalization with amine nucleophiles. Altogether, we have excluded mechanistic hypotheses that invoke the formation of dicationic adduct from alkenylsulfonium salts and favor the proposed model in Figure 3.2.

B7.2. Inconsistent with Conjugate-type Addition Mechanisms

Recently, our group has developed a net diamination platform from electrogenerated dicationic adducts between thianthrene and alkenes (*J. Am. Chem. Soc.* **2023**, *145* (15), 8299–8307). Mechanistic studies revealed that adducts undergo elimination by potassium phthalimide to alkenylthianthrenium salt. Then, phthalimide anion engages with the alkenylthianthrenium intermediate by a conjugate-type addition then protonation sequence to generate a 1,2-phthalimidosulfonium salt. Furthermore, studies conducted within our lab demonstrated that, under certain basic conditions, this alkylthianthrenium salt can furnish *Z*-allylic products. We wondered if this conjugate-type addition reactivity could be operative for the allylic functionalization of alkenylthianthrenium salts.

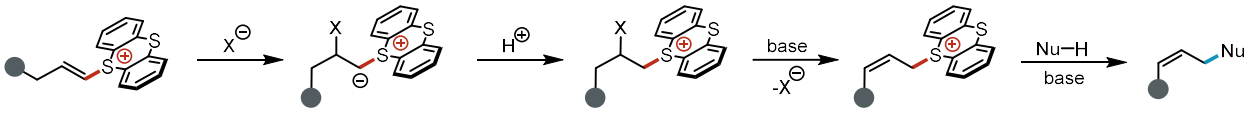

Figure B59. Potential pathways envisioned from conjugate-type addition into alkenylthianthrenium salt that afford allylic functionalized products.

At first glance, this hypothesis is consistent with large primary KIE at the allylic C–H bonds of the alkenylTT and first order in *i*-Pr_2NEt base. However, a first order in acid would be expected since ylide protonation occurs prior to rate determining deprotonation, and this is inconsistent with experimentally determined zeroth order in *i*-$Pr_2NHEtPF_6$ acid.

In our initial allylic amination disclosure, treatment of 1:1 *E:Z* alkenylTT salt furnished allylic amine in comparable yields and *Z*-selectivity as the one pot electrochemical protocol from adducts (*J. Am. Chem. Soc.* **2021**, *143* (51), 21503–21510). During studies in our group, we observed rapid isomerization of this mixture of *E*- and *Z*-alkenylTT salts upon addition of BnNHMe secondary amine. We propose the *Z*→*E* isomerization occurs through reversible conjugate-type addition into the alkenylTT that generates the thermodynamically favored *E*-isomer (*vide infra* Figure B62).

Along this line of reasoning, with regards to potential identities of **X** for the conjugate-type addition, we excluded PhNHMe amine since the reaction was experimentally determined to be zeroth order in PhNHMe nucleophile and the alkylthianthrenium salt was not detected during allylic amination, which excluded it as the lowest energy thianthrenium species. This would leave *i*-Pr_2NEt as **X** and, based on the large primary KIE, a second order dependence would be expected for steps involving *i*-Pr_2NEt prior to deprotonation, which is inconsistent with the experimentally determined first order in *i*-Pr_2NEt base.

We were curious to probe the ability of *i*-Pr_2NEt to engage in conjugate-type addition with alkenylthianthrenium salts. To this end, we prepared a 1:1 *E:*Z mixture of alkenylTT salt **B9** using the electrochemical conditions in our previous allylic amination study. We hypothesized that if reversible conjugate-addition was occurring, then *Z*→*E* isomerization would be observed faster than the rate of allylic functionalization. Reaction monitoring was conducted using the General Procedure for ^1H NMR Reaction Monitoring *with the specified modifications:* the stock solution was prepared using 5-(but-1-en-1-yl)-5H-thianthren-5-iumhexafluorophosphate(V) **B9** instead of 5-(4-phenylbut-1-en-1-yl)-5H-thianthren-5-ium hexafluorophosphate **3.3** and no *N*-methylaniline was added; then, *i*-Pr_2NEt (12.0 µL, 0.20 mmol, 2 equiv.) was added *via* microsyringe to the NMR tube. Allylic ammonium product derived from alkenylTT **B9** was assigned based on analogy to **B7**.

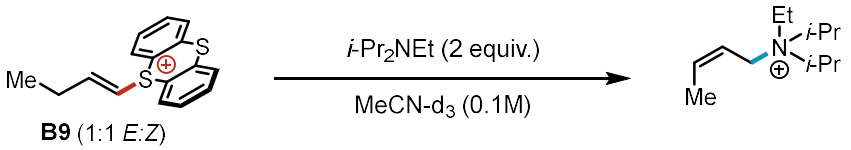

Figure B60. Reaction scheme for allylic amination of an *E:Z* alkenylTT mixture using *i*-Pr_2NEt as base and nucleophile.

Table B27. Data from Monitoring the Reaction Using ^{1}H NMR Spectroscopy for Allylic Amination of AlkenylTT B9 (*E:Z* mixture).

Time (min)	[alkenylTT *E*-B9] (mM)	[alkenylTT *E*-B9] (mM)	[allylic ammonium] (mM)
0.00	46.54	46.22	0.00
3.00	50.12	45.57	0.00
5.00	48.82	42.31	0.65
7.00	48.17	41.66	1.46
9.00	46.87	41.66	2.44
11.00	46.22	41.33	3.25
13.00	44.91	41.01	4.23
15.00	43.61	41.01	5.04
17.00	42.96	41.01	5.86
19.00	41.99	40.68	6.83
21.00	41.01	40.68	7.65
23.00	40.03	40.36	8.30
25.00	39.38	40.03	9.11
27.00	38.41	39.71	9.93
29.00	37.75	39.71	10.58
31.00	37.10	39.38	11.39
33.00	36.13	39.38	11.88
35.00	35.48	39.38	12.53
37.00	34.50	39.06	12.86
39.00	33.85	39.06	13.51
41.00	32.87	38.73	14.16
43.00	32.22	38.73	14.81
45.00	31.57	38.73	15.30
47.00	30.92	38.73	15.95

Time (min)	[alkenylTT *E*-B9] (mM)	[alkenylTT *E*-B9] (mM)	[allylic ammonium] (mM)
49.00	30.59	39.06	16.27
51.00	29.62	38.41	17.09
53.00	28.97	38.41	17.74
55.00	28.32	38.41	18.23
57.00	27.66	38.41	18.71
59.00	27.34	38.41	19.37
91.00	37.75	19.53	26.85
119.00	37.10	14.97	31.73
149.00	36.45	11.07	35.80
181.00	35.80	8.14	39.22
211.00	35.48	6.18	41.66
241.00	34.83	4.56	43.45
269.00	34.17	3.25	44.91
301.00	33.52	2.28	46.22
329.00	32.87	1.63	47.03
353.00	32.55	1.30	47.68
388.00	31.57	0.98	48.33
423.00	30.92	0.65	48.98
453.00	30.59	0.65	49.63
483.00	30.27	0.33	49.96
513.00	29.62	0.33	50.28

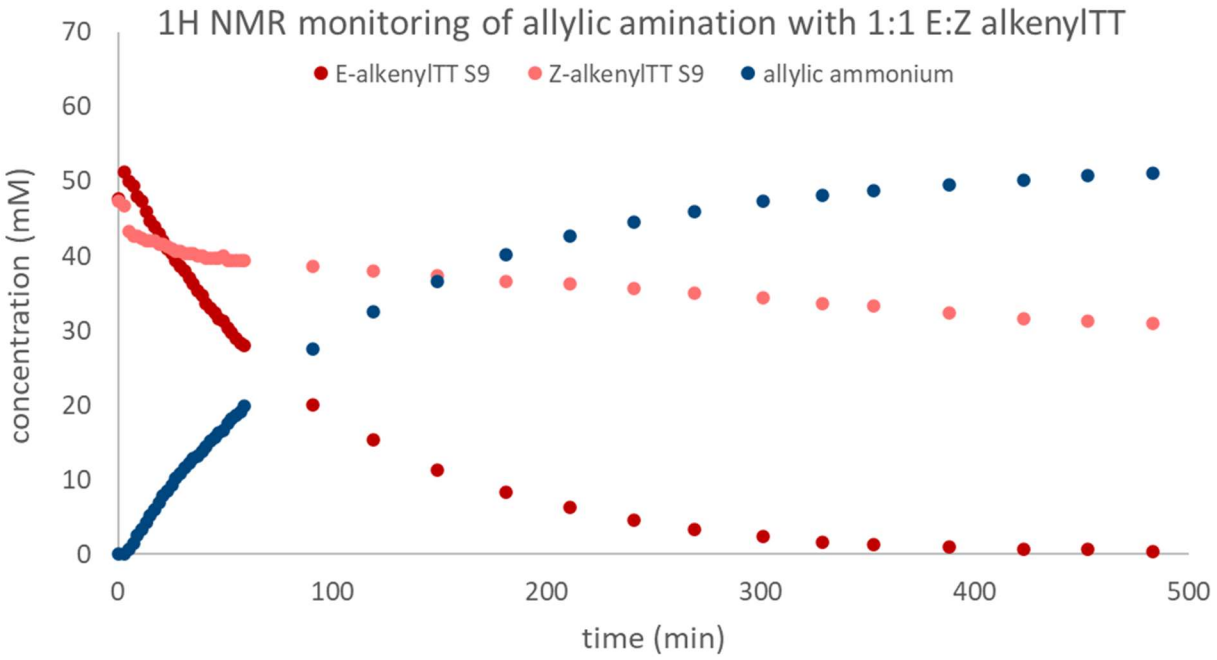

Figure B61. Data graphed from monitoring the 1:1 *E:Z* alkenylTT **B9** using ^{1}H NMR spectroscopy during allylic amination with *i*-Pr_2NEt as base and nucleophile.

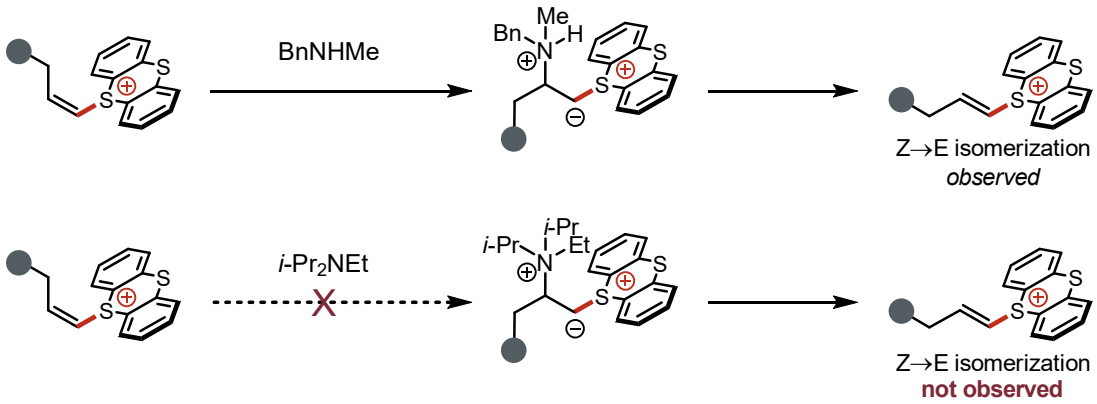

Figure B62. No alkenylTT Z→E isomerization is observed upon addition of *i*-Pr_2NEt, indicating that conjugate-addition is unlikely.

Conclusions: KIE and kinetics data are inconsistent with mechanistic hypotheses that invoke conjugate-type addition of base or amine nucleophiles into the alkenylthianthrenium species. Additionally, we have found that conjugate-type addition of bulky *i*-Pr_2NEt into alkenylthianthrenium salts is unlikely given the lack of Z→E isomerization, which is observed with less hindered secondary amine nucleophiles. These analyses rules out ammonium ylide formation or Hoffman elimination to explain the allylic functionalization of thianthrenium salts. In conclusion, we disfavor conjugate-addition mechanisms and favor the proposed model in Figure 3.2.

B8. Substrate Preparation

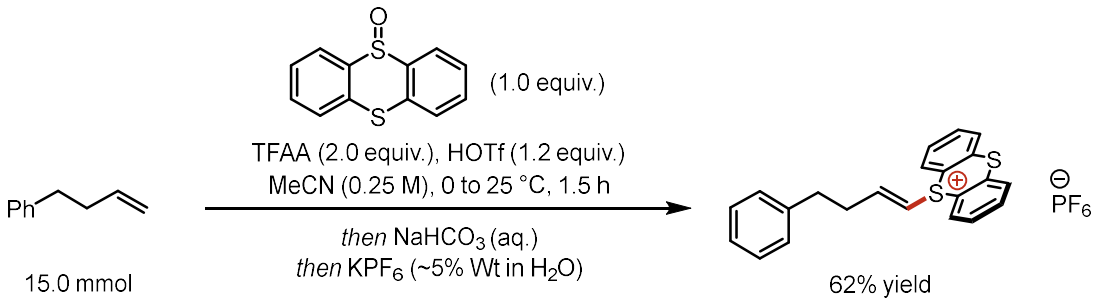

5-(4-phenylbut-1-en-1-yl)-5H-thianthren-5-ium hexafluorophosphate(V) (3.3). Under ambient atmosphere, to a 250-mL round bottom flask equipped with a magnetic stir bar was added but-3-en-1-ylbenzene (1.98 g, 2.25 mL, 15.0 mmol, 1.0 equiv.), thianthrene S-oxide (3.59 g, 15.5 mmol, 1.0 equiv.; prepared according to literature procedure: *Nature* **2019**, 567, 223), and MeCN (60 mL). After cooling to 0°C, 2,2,2-trifluoroacetic anhydride (6.30 g, 4.19 mL, 30.0 mmol, 2.0 equiv.) was added slowly, followed by dropwise addition of trifluoromethanesulfonic acid (2.70 g, 1.61 mL, 18.0 mmol, 1.2 equiv.). After stirring the resultant solution at 0 °C for 60 min followed by stirring at 25 °C for 30 min, the reaction mixture was concentrated under reduced pressure and subsequently diluted with DCM (200 mL). The DCM solution was poured slowly onto a saturated aqueous $NaHCO_3$ solution (200 mL). The combined mixture was poured into a separatory funnel, and the layers were separated. The DCM layer was collected, and the aqueous layer was further extracted with DCM (2 x 200 mL). The combined DCM solution was washed with aqueous KPF_6 solution (3 x 200 mL, 5% w/w). The DCM layer was dried over Na_2SO_4, filtered, and the solvent was removed under reduced pressure. The residue was diluted in a minimum amount of DCM and precipitated with EtOAc. The mixture was filtered and the solid was dried in vacuo to afford **3.3** as a solid (*E:Z* ≥ 20:1, 7.39 g, 9.3 mmol, 62% yield).
^{1}H NMR (500 MHz, CD_3CN) δ 8.02 (dd, J = 8.0, 1.4 Hz, 2H), 7.93 (dd, J = 7.9, 1.3 Hz, 2H), 7.82 (td, J = 7.7, 1.4 Hz, 2H), 7.71 (td, J = 7.7, 1.4 Hz, 2H), 7.25 – 7.18 (m, 2H), 7.18 – 7.12 (m, 1H), 7.11 – 7.05 (m, 2H), 6.86 (dt, J = 14.5, 7.1 Hz, 1H), 6.39 (dt, J = 14.8, 1.4 Hz, 1H), 2.75 (t, J = 7.2 Hz, 2H), 2.65 – 2.56 (m, 2H). Distinct minor *Z*-isomer signals observed at δ 6.71 (dt, J = 8.6, 1.3 Hz, 1H), 3.02 (q, J = 7.2 Hz, 2H), 2.87 (t, J = 7.0 Hz, 2H); **^{13}C NMR** (126 MHz, CD_3CN) δ 155.74, 140.88, 136.31, 135.38, 133.67, 131.24, 130.79, 129.38, 127.21, 121.25, 111.56, 35.02, 33.87; **^{19}F NMR** (377 MHz, CD_3CN) δ -71.85, -73.72; **^{31}P NMR** (162 MHz, CD_3CN) δ -144.58 (hept, J = 706.6 Hz). **HRMS** (ESI+) Calc: $[M]^+$ ($C_{22}H_{19}S_2^+$) 331.1151, measured: 331.1150; 0.3 ppm difference.

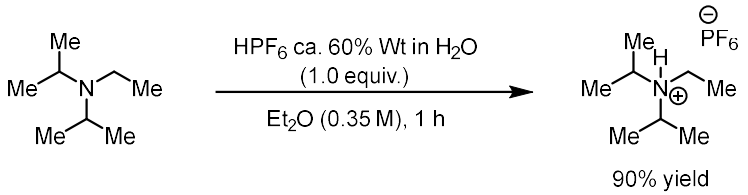

***N*-ethyl-*N*-isopropylpropan-2-aminium hexafluorophosphate(V) (B1).** To a 100 mL round bottom flask charged with a magnetic stir bar was added Et_2O (20 mL) and *N*-ethyl-*N*-isopropylpropan-2-amine (905 mg, 1.22 mL, 1.0 equiv., 7.00 mmol). Hexafluoro-l7-phosphane (1.76 g, 1.76 mL, 60% Wt, 1.0 equiv., 7.23 mmol) was slowly added. The solution was stirred under ambient conditions for an hour after which the reaction mixture was diluted with Et_2O (80 mL), filtered, and washed with excess Et_2O. The precipitate was dried under high vacuum to obtain 1.71 g (90% yield) of the desired ammonium salt **B1**.
^{1}H NMR (500 MHz, CD_3CN) δ 6.21 (broad t, J = 50.6 Hz, 1H), 3.68 (ddt, J = 9.5, 6.7, 2.8 Hz, 2H), 3.16 (qd, J = 7.4, 4.4 Hz, 2H), 1.60 – 1.12 (m, 15H); **^{13}C NMR** (126 MHz, CD_3CN) δ 56.01, 43.98, 18.61, 17.24, 12.88; **^{19}F NMR** (377 MHz, CD_3CN) δ -71.83, -73.71; **^{31}P NMR** (162 MHz, CD_3CN) δ -144.60 (hept, J = 706.3 Hz). **HRMS** (ESI^+) Calc: $[M]^+$ ($C_8H_{20}N^+$) 130.1590, measured: 130.1589; 0.8 ppm difference.

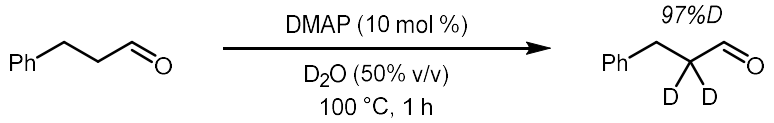

3-phenylpropanal-2,2-d$_2$ (B2). Distilled 3-phenylpropanal (2.68 g, 2.63 mL, 20.0 mmol, 1.0 equiv.) was added to a 25-mL round bottom flask charged D_2O (2.60 mL; 1 mL per 1 mL of aldehyde) and 4-(dimethylamino)pyridine (244 mg, 2.00 mmol, 0.1 equiv.). The mixture was heated to 100 °C for 1 hour. After the solution had cooled, biphasic solution was poured into a separatory funnel and extracted with DCM (2 x 20 mL). The combined DCM layers were washed with 1 M HCl (2 x 50 mL), saturated aqueous $NaHCO_3$ solution (50 mL), and brine (50 mL). The organic layer was dried over Na_2SO_4, filtered, and the solvent was removed under reduced pressure. The resulting crude was resubjected to the above procedure an additional two times. The product was purified via short path high-vacuum distillation to afford **B2** as an oil (1.02 g, 7.5 mmol, 37% yield; 97% total deuterium incorporation).
^{1}H NMR (500 MHz, $CDCl_3$) δ 9.83 (s, 1H), 7.33 – 7.28 (m, 2H), 7.25 – 7.18 (m, 3H), 2.96 (s, 2H); consistent with reported spectra (*J. Am. Chem. Soc.* **2018**, 140, 39, 12476–12483).

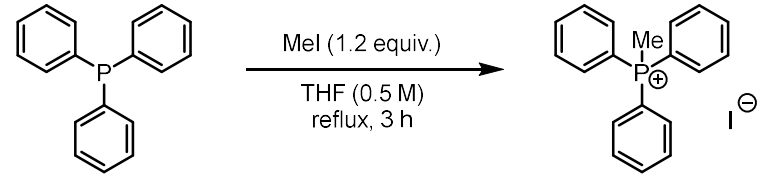

Iodo(methyl)triphenyl-l5-phosphane (B3). To a solution of triphenylphosphine (10.49 g, 40.0 mmol, 1.0 equiv.) in THF (80 mL) was added iodomethane (6.813 g, 2.99 mL, 48.0 mmol, 1.2 equiv.). The solution was refluxed (THF b.p. = 66 °C) for 3 hours, after which the reaction was allowed to cool to ambient temperature and stirred overnight. The reaction solution was filtered and the resultant precipitate was generously washed with toluene, followed by pentanes. The solid was collected and dried under high vacuum to provide iodo(methyl)triphenyl-l5-phosphane **B3** (15.76 g, 39.0 mmol, 97% yield).
^{1}H NMR (500 MHz, $CDCl_3$) δ 7.89 – 7.66 (m, 15H), 3.21 (d, J = 13.2 Hz, 3H); **^{31}P NMR** (162 MHz, $CDCl_3$) δ 21.54; consistent with reported spectra (*Tetrahedron*, **2023**, 135, 133321).

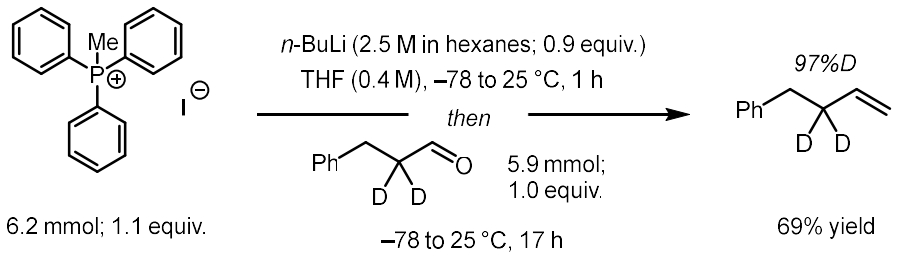

(but-3-en-1-yl-2,2-d2)benzene (B4). A solution of iodo(methyl)triphenyl-l5-phosphane **B3** (2.49 g, 6.17 mmol, 1.1 equiv) in THF (14.7 mL) was cooled to -78 °C. While stirring, *n*-butyllithium (352 mg, 2.20 mL, 2.5 molar in hexanes, 5.50 mmol, 0.9 equiv.) was added dropwise over 5 minutes. The ylide solution was stirred at -78 °C for 15 min, then warmed to room temperature (~22 °C) and stirred for an additional 50 min. The reaction mixture was cooled back down to -78 °C and 3-phenylpropanal-2,2-d$_2$ **B2** (800 mg, 785 µL, 5.87 mmol, 10 equiv.) was added dropwise over 5 minutes. After 1 hour, the solution was allowed to warm to room temperature and stirred for 16 hour. Upon completion, pentanes (~60 mL) was added to the reaction solution and the resultant mixture slurry was filtered. The residue was rinsed generously with

pentanes. The organic layer was concentrated in vacuo then purified by a short silica plug (100% pentanes) to afford **B4** as an oil (541 mg, 4.0 mmol, 69% yield; 97% total deuterium).
^{1}H NMR (400 MHz, $CDCl_3$) δ 7.35 – 7.28 (m, 2H), 7.25 – 7.16 (m, 3H), 5.92 – 5.83 (m, 1H), 5.07 (dd, J = 17.2, 2.0 Hz, 1H), 5.01 (dd, J = 10.2, 2.0 Hz, 1H), 2.73 (s, 2H); consistent with reported spectra (*ACS Catalysis* **2022**, 12, 1, 527–535).

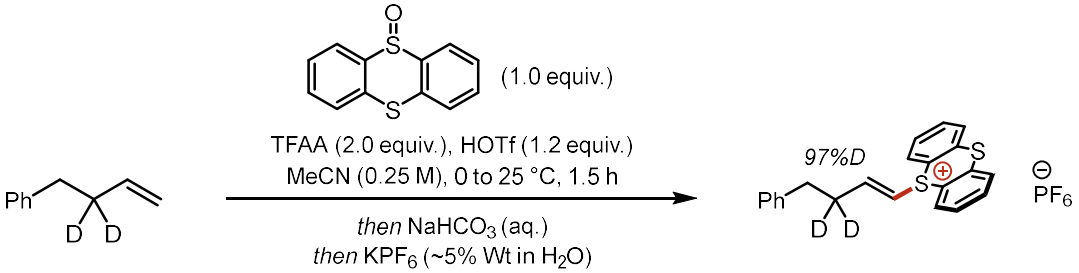

4.0 mmol 62% yield

5-(4-phenylbut-1-en-1-yl-3,3-d$_2$)-5H-thianthren-5-ium hexafluorophosphate(V) (3.3-d$_2$). Under ambient atmosphere, to a 50-mL round bottom flask equipped with a magnetic stir bar was added (but-3-en-1-yl-2,2-d$_2$)benzene **B4** (541 mg, 4.0 mmol, 1.0 equiv.), thianthrene S-oxide (965 mg, 4.15 mmol, 1.0 equiv.; prepared according to literature procedure: *Nature* **2019**, 567, 223), and MeCN (16 mL). After cooling to 0°C, 2,2,2-trifluoroacetic anhydride (1.69 g, 1.1 mL, 8.1 mmol, 2.0 equiv.) was added slowly, followed by dropwise addition of trifluoromethanesulfonic acid (726 mg, 432 µL, 4.8 mmol, 1.2 equiv.). After stirring the resultant solution at 0 °C for 60 min followed by stirring at 25 °C for 30 min, the reaction mixture was concentrated under reduced pressure and subsequently diluted with DCM (100 mL). The DCM solution was poured slowly onto a saturated aqueous $NaHCO_3$ solution (100 mL). The combined mixture was poured into a separatory funnel, and the layers were separated. The DCM layer was collected, and the aqueous layer was further extracted with DCM (2 x 100 mL). The combined DCM solution was washed with aqueous KPF_6 solution (3 x 100 mL, 5% w/w). The DCM layer was dried over Na_2SO_4, filtered, and the solvent was removed under reduced pressure. The residue was diluted in a minimum amount of DCM and precipitated with EtOAc. The mixture was filtered and the solid was dried in vacuo to afford **3.3-d$_2$** as a solid (*E:Z* ≥ 20:1, 1.31 g, 2.5 mmol, 62% yield; 97% total deuterium).
^{1}H NMR (500 MHz, CD_3CN) δ 8.02 (dd, J = 7.9, 1.3 Hz, 2H), 7.93 (dd, J = 7.9, 1.3 Hz, 2H), 7.81 (td, J = 7.7, 1.3 Hz, 2H), 7.71 (td, J = 7.7, 1.3 Hz, 2H), 7.22 – 7.18 (m, 2H), 7.18 – 7.13 (m, 1H), 7.10 – 7.05 (m, 2H), 6.85 (d, J = 14.8 Hz, 1H), 6.39 (d, J = 14.9 Hz, 1H), 2.74 (s, 2H); **^{13}C NMR** (126 MHz, CD_3CN) δ 155.66, 140.85, 136.28, 135.37, 133.66, 131.23, 130.79, 129.37, 127.18, 121.23, 111.62, 34.34 (t, J = 20.2 Hz), 33.73; **^{19}F NMR** (377 MHz, CD_3CN) δ -71.78, -73.66; **^{31}P NMR** (162 MHz, CD_3CN) δ -144.56 (hept, J = 706.7 Hz). **HRMS** (ESI+) Calc: $[M]^+$ ($C_{22}H_{18}DS_2^+$) 348.0986, measured: 348.0984; 0.6 ppm difference.

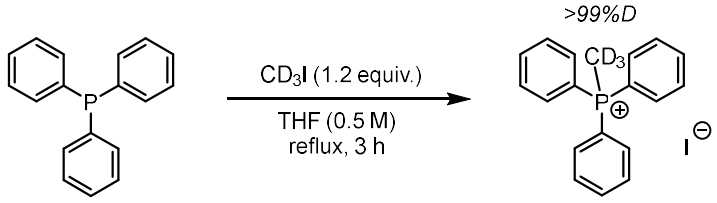

40.0 mmol 98% yield

Iodo(methyl-d$_3$)triphenyl-l5-phosphane (B5). To a solution of triphenylphosphine (10.49 g, 40.0 mmol, 1.0 equiv.) in THF (80 mL) was added iodomethane-d$_3$ (6.96 g, 3.00 mL, 48.0 mmol, 1.2 equiv.). The solution was refluxed (THF b.p. = 66 °C) for 3 hours, after which the reaction was allowed to cool to ambient temperature and stirred overnight. The reaction solution was filtered and the resultant precipitate was generously washed with toluene, followed by pentanes. The solid was collected and dried under high

vacuum to provide iodo(methyl-d3)triphenyl-l5-phosphane **B5** (15.89 g, 39.0 mmol, 98% yield; >99% total deuterium).
^{1}H NMR (400 MHz, $CDCl_3$) δ 7.86 – 7.65 (m, 15H); **^{31}P NMR** (162 MHz, $CDCl_3$) 21.58; consistent with reported spectra (*J. Am. Chem. Soc.* **2015**, 137, 25, 8054–8057).

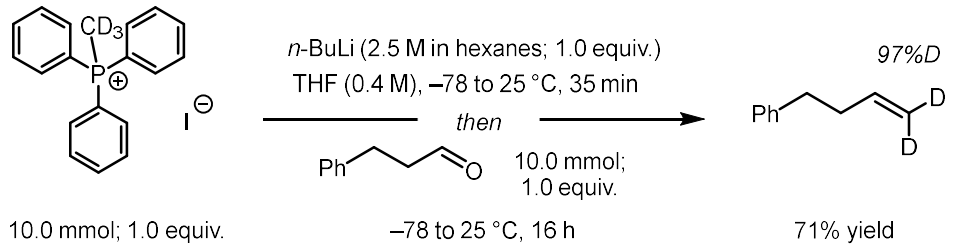

(but-3-en-1-yl-4,4-d$_2$)benzene (B6). A solution of iodo(methyl-d$_3$)triphenyl-l5-phosphane **S5** (4.07 g, 10.0 mmol, 1.0 equiv.) in THF (25 mL) was cooled to -78 °C. While stirring, *n*-butyllithium (641 mg, 4.0 mL, 2.5 molar in hexanes, 10.0 mmol, 1.0 equiv.) was added dropwise over 5 minutes. The ylide solution was stirred at -78 °C for 15 min, then warmed to room temperature (~22 °C) and stirred for an additional 20 min. The reaction mixture was cooled back down to -78 °C and distilled 3-phenylpropanal (1.34 g, 1.32 mL, 10.0 mmol, 1.0 equiv.) was added dropwise over 5 minutes. After 20 min, the solution was allowed to warm to room temperature and stirred for 16 hours. Upon completion, pentanes (~60 mL) was added to the reaction solution and the resultant mixture slurry was filtered. The residue was rinsed generously with pentanes. The organic layer was concentrated in vacuo then purified by a short silica plug (100% pentanes) to afford **B6** as an oil (956 mg, 7.1 mmol, 71% yield; 97% total deuterium incorporation).
^{1}H NMR (400 MHz, $CDCl_3$) δ 7.33 – 7.28 (m, 2H), 7.25 – 7.18 (m, 3H), 5.92 – 5.82 (m, 1H), 2.78 – 2.69 (m, 2H), 2.45 – 2.35 (m, 2H); consistent with reported spectra (*J. Am. Chem. Soc.* **2015**, 137, 25, 8054–8057).

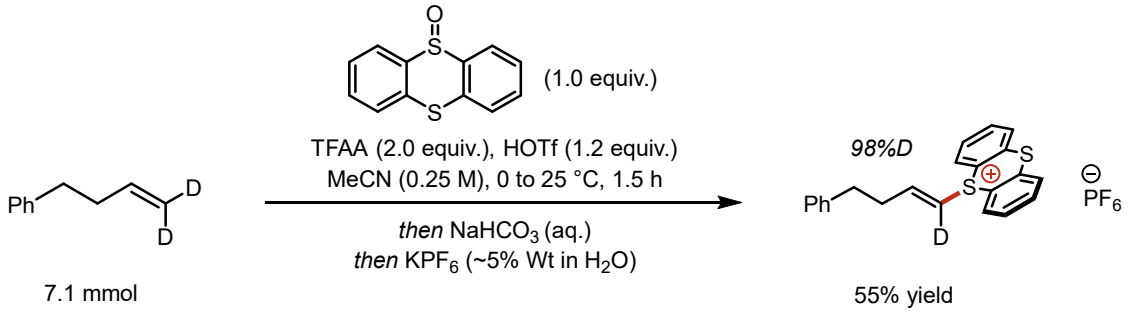

5-(4-phenylbut-1-en-1-yl-1-d)-5H-thianthren-5-ium hexafluorophosphate(V) (3.3-d). Under ambient atmosphere, to a 50-mL round bottom flask equipped with a magnetic stir bar was added (but-3-en-1-yl-2,2-d$_2$)benzene **S6** (956 mg, 7.1 mmol, 1.0 equiv.), thianthrene S-oxide (1.70 g, 7.3 mmol, 1.0 equiv.; prepared according to literature procedure: *Nature* **2019**, 567, 223), and MeCN (28 mL). After cooling to 0°C, 2,2,2-trifluoroacetic anhydride (2.99 g, 1.99 mL, 14.2 mmol, 2.0 equiv.) was added slowly, followed by dropwise addition of trifluoromethanesulfonic acid (1.28 g, 764 µL, 8.55 mmol, 1.2 equiv.). After stirring the resultant solution at 0 °C for 60 min followed by stirring at 25 °C for 30 min, the reaction mixture was concentrated under reduced pressure and subsequently diluted with DCM (100 mL). The DCM solution was poured slowly onto a saturated aqueous $NaHCO_3$ solution (100 mL). The combined mixture was poured into a separatory funnel, and the layers were separated. The DCM layer was collected, and the aqueous layer was further extracted with DCM (2 x 100 mL). The combined DCM solution was washed with aqueous KPF_6 solution (3 x 100 mL, 5% w/w). The DCM layer was dried over Na_2SO_4, filtered, and the solvent was removed under reduced pressure. The residue was diluted in a minimum amount of DCM and precipitated with EtOAc. The mixture was filtered and the solid was dried in vacuo to afford **3.3-d** as a solid (*E:Z* ≥ 20:1, 1.93 g, 3.9 mmol, 55% yield; 98% total deuterium).

^{1}H NMR (500 MHz, CD_3CN) δ 8.03 (dd, J = 8.0, 1.4 Hz, 2H), 7.94 (dd, J = 7.9, 1.3 Hz, 2H), 7.82 (td, J = 7.7, 1.4 Hz, 2H), 7.72 (s, 1H), 7.24 – 7.19 (m, 2H), 7.19 – 7.14 (m, 1H), 7.10 – 7.07 (m, 2H), 6.86 (tt, J = 7.2, 2.1 Hz, 1H), 2.76 (t, J = 7.2 Hz, 2H), 2.61 (q, J = 7.4 Hz, 2H). Distinct minor *Z*-isomer signals observed at δ 3.02 (q, J = 7.3 Hz, 2H), 2.87 (t, J = 7.0 Hz, 2H); **^{13}C NMR** (126 MHz, CD_3CN) δ 155.64, 140.88, 136.30, 135.38, 133.66, 131.24, 130.79, 129.38, 127.21, 121.25, 111.27 (t, J = 29.3 Hz), 34.98, 33.87; **^{19}F NMR** (377 MHz, CD_3CN) δ -71.85, -73.72; **^{31}P NMR** (162 MHz, CD_3CN) δ -144.58 (hept, J = 706.6 Hz). **HRMS** (ESI+) Calc: $[M]^+$ ($C_{22}H_{17}D_2S_2^+$) 349.1048, measured: 349.1046; 0.6 ppm difference.

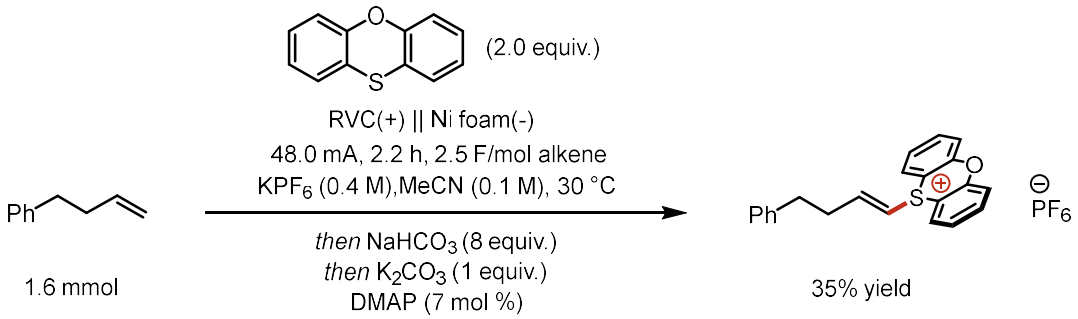

10-(4-phenylbut-1-en-1-yl)-10H-phenoxathiin-10-ium hexafluorophosphate(V) (B8).
Experimental procedure: To an oven-dried divided electrochemical cell (for fabrication details, see *J. Am. Chem. Soc.* **2023**, 145, 15, 8299–8307) equipped with magnetic stir bars was added phenoxathiine (641 mg, 3.2 mmol, 2.0 equiv.) to the anode compartment and KPF_6 (1.18 g, 6.4 mmol, 4.0 equiv.) to both compartments. The cell was equipped with two septa containing a stainless steel wire/Ni foam (1.6 x 1.2 cm) cathode assembly and a pencil/RVC (9 x 9 x 7 mm) anode assembly connected together with a teflon tubing to equalize pressure. MeCN (16 mL) was added to the cathode and anode compartments. But-3-en-1-ylbenzene (212 mg, 240 µL, 1.6 mmol, 1.0 equiv.) was added to the anode compartment. Trifluoroacetic acid (1.824 g, 1.2 mL, 16.0 mmol, 10.0 equiv.) was added to the cathode compartment and both sides of the cell were stirred at 30 °C and electrolyzed under a constant current of 48.0 mA for 2.2 h (2.5 F/mol). At completion of electrolysis, the electrode leads were disconnected, septa removed, and the anode RVC was pushed off the pencil into the reaction mixture. Solid $NaHCO_3$ (1.08 g, 12.8 mmol, 8.0 equiv.) was added to quench the anode compartment and the solution was stirred for 15 min. Then, K_2CO_3 (221 mg, 1.6 mmol, 1.0 equiv.) and 4-(dimethylamino)pyridine (14 mg, 0.1 mmol, 0.07 equiv.) were added and the reaction was stirred for another 15 min.
Purification: The anode solution was transferred to a flask and concentrated under reduced pressure. The crude residue was diluted with ~60 mL DCM, filtered, and concentrated under reduced pressure. The residue was purified via flash column chromatography (DCM/3:1 EtOAc:EtOH) to afford **B8** (*E:Z* = 11:1, 250 mg, 0.57 mmol, 35% yield) as a solid.
^{1}H NMR (500 MHz, CD_3CN) δ 7.87 (ddd, J = 8.6, 7.4, 1.6 Hz, 2H), 7.83 (dd, J = 8.0, 1.6 Hz, 2H), 7.58 (dd, J = 8.5, 1.2 Hz, 2H), 7.55 (td, J = 7.8, 1.2 Hz, 2H), 7.23 (dd, J = 8.2, 6.8 Hz, 2H), 7.19 – 7.13 (m, 1H), 7.14 – 7.07 (m, 2H), 7.04 (dt, J = 14.5, 7.2 Hz, 1H), 6.34 (dt, J = 14.6, 1.4 Hz, 1H), 2.77 (t, J = 7.2 Hz, 2H), 2.57 (q, J = 7.1 Hz, 2H). Distinct minor *)*-isomer signals observed at δ 7.46 (td, J = 7.7, 1.2 Hz, 2H), 7.41 (dd, J = 8.0, 6.1 Hz, 2H), 7.37 (dd, J = 6.8, 1.5 Hz, 2H), 7.34 (dt, J = 8.1, 1.7 Hz, 3H), 6.76 (q, J = 8.0 Hz, 1H), 6.45 (dt, J = 8.4, 1.4 Hz, 1H), 3.16 (q, J = 7.4 Hz, 2H), 2.98 (t, J = 6.8 Hz, 2H); **^{13}C NMR** (126 MHz, CD_3CN) δ 154.72, 152.10, 140.84, 137.45, 131.82, 129.40, 129.39, 127.88, 127.22, 121.06, 120.84, 106.32, 34.92, 33.78. Distinct minor *Z*-isomer signals observed at δ 153.30, 152.26, 141.06, 137.40, 131.46, 129.90, 129.83, 127.91, 127.70, 121.69, 121.15, 106.05, 34.45, 32.98; **^{19}F NMR** (377 MHz, CD_3CN) δ -71.82, -73.70; **^{31}P NMR** (162 MHz, CD_3CN) δ -144.57 (hept, J = 706.7 Hz). **HRMS** (ESI+) Calc: $[M]^+$ ($C_{22}H_{19}OS^+$) 347.0923, measured: 347.0921; 0.6 ppm difference.

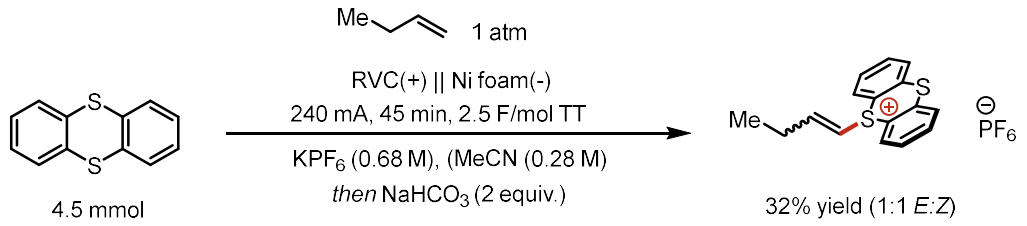

5-(but-1-en-1-yl)-5H-thianthren-5-iumhexafluorophosphate(V) (B9).

Experimental procedure: To an oven-dried divided electrochemical cell (for fabrication details, see *J. Am. Chem. Soc.* **2023**, 145, 15, 8299–8307) equipped with magnetic stir bars was added thianthrene (973.4 mg, 4.5 mmol, 1.0 equiv.) to the anode compartment and KPF_6 (1.99 g, 10.8 mmol, 2.4 equiv.) to both compartments. The cell was equipped with two septa containing a stainless steel wire/Ni foam (1.6 x 1.2 cm) cathode assembly and a pencil/RVC (9 x 9 x 7 mm) anode assembly connected together with a teflon tubing to equalize pressure. MeCN (16 mL) was added to the cathode and anode compartments, then the anode side was sparged with a balloon for 1-butene gas for 10 minutes. Trifluoroacetic acid (3.079 g, 2.1 mL, 27.0 mmol, 6.0 equiv.) was added to the cathode compartment and both sides of the cell were stirred at under ambient conditions and electrolyzed under a constant current of 240.0 mA for 45 min (2.5 F/mol). At completion of electrolysis, the electrode leads were disconnected, septa removed, and the anode RVC was pushed off the pencil into the reaction mixture. Solid $NaHCO_3$ (756.1 m g, 9.0 mmol, 2.0 equiv.) was added to quench the anode compartment and the solution was stirred for 15 min.

Purification: The anode solution was transferred to a flask and concentrated under reduced pressure. The crude residue was diluted with ~60 mL DCM, filtered, and concentrated under reduced pressure. The residue was purified via flash column chromatography (DCM/3:1 EtOAc:EtOH) to afford **B9** (*E:Z* = 1:1, 240 mg, 1.44 mmol, 32% yield) as a solid.

^{1}H NMR (500 MHz, CD_3CN) δ 8.13 (ddd, J = 8.1, 6.8, 1.4 Hz, 2H), 7.97 (ddd, J = 8.9, 7.9, 1.3 Hz, 2H), 7.83 (tdd, J = 7.8, 3.0, 1.4 Hz, 2H), 7.73 (tdd, J = 7.7, 4.2, 1.3 Hz, 2H), 6.97 (dt, J = 14.8, 6.4 Hz, 1H), 6.53 (dt, J = 14.8, 1.6 Hz, 1H), 2.34 – 2.27 (m, 2H), 1.01 (t, J = 7.4 Hz, 3H). Distinct *Z*-isomer signals observed at δ 6.84 (q, J = 8.0 Hz, 1H), 6.67 (dt, J = 8.6, 1.4 Hz, 1H), 2.68 (pd, J = 7.5, 1.4 Hz, 2H), 1.09 (t, J = 7.5 Hz, 3H); consistent with reported spectra (*J. Am. Chem. Soc.* **2021**, *143* (51), 21503–21510).

B9. Product Characterization

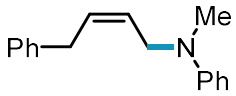

***(Z)-N*-methyl-*N*-(4-phenylbut-2-en-1-yl)aniline (3.5).** Prepared from 5-(4-phenylbut-1-en-1-yl)-5H-thianthren-5-ium hexafluorophosphate(V) (**5**) and *N*-methylaniline following General Procedure for ^{1}H NMR Reaction Monitoring. The crude reaction mixtures were combined, the solvent removed, and the residue purified *via* flash column chromatography (hexanes/ethyl acetate) to afford the allylic amine **3.5** as an oil. **^{1}H NMR** (500 MHz, $CDCl_3$) δ 7.39 – 7.34 (m, 2H), 7.32 – 7.19 (m, 5H), 6.90 – 6.73 (m, 5H), 5.88 – 5.79 (m, 1H), 5.69 – 5.59 (m, 1H), 4.11 (d, J = 5.9 Hz, 2H), 3.56 (d, J = 7.5 Hz, 2H), 2.99 (s, 3H). Distinct minor *E*-isomer signals observed at δ 3.95 (d, J = 5.7 Hz, 2H), 3.42 (d, J = 6.8 Hz, 2H), 2.97 (s, 3H); consistent with reported spectra (*Chem. Sci.*, **2022**, 13, 1003).

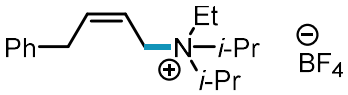

(Z)-*N*-ethyl-*N*,*N*-diisopropyl-4-phenylbut-2-en-1-aminium tetrafluoroborate (B7). To a threaded vial equipped with a magnetic stir bar was added 5-(4-phenylbut-1-en-1-yl)-5H-thianthren-5-ium tetrafluoroborate salt metathesized **3** (261 mg, 0.6 mmol, 1.0 equiv.) and MeCN (3 mL). Then the *i*-Pr_2NEt (323 µL, 1.80 mmol, 2.0 equiv.) was added. The reaction mixture was capped with a PTFE seal and stirred at room temperature until completion of the reaction (6 hours). The solvent was then removed, and the residue purified *via* flash column chromatography (hexanes/DCM) to afford the allylic ammonium **B7** as an oil. **^{1}H NMR** (500 MHz, CD_3CN) δ 7.40 – 7.32 (m, 2H), 7.30 – 7.22 (m, 3H), 6.13 – 6.04 (m, 1H), 5.80 (dtt, J = 11.0, 7.3, 1.8 Hz, 1H), 4.04 (dd, J = 7.2, 1.6 Hz, 2H), 3.97 (hept, J = 6.6 Hz, 2H), 3.57 (dd, J = 7.7, 1.7 Hz, 2H), 3.42 (q, J = 7.3 Hz, 2H), 1.50 – 1.45 (m, 12H), 1.41 – 1.33 (m, 3H). Distinct minor *E*-isomer signals observed at δ 6.26 – 6.17 (m, 1H), 5.77 – 5.70 (m, 1H), 3.92 – 3.82 (m, 3H), 3.71 (pd, J = 6.6, 3.9 Hz, 1H), 3.50 (d, J = 6.9 Hz, 2H), 3.35 (q, J = 7.3 Hz, 2H), 3.19 (qd, J = 7.4, 4.5 Hz, 1H), 1.45 – 1.41 (m, 12H); consistent with reported spectra of *Z*-allylic ammonium salts (*Chem. Sci.* **2022**, 13 (4), 1003–1008).

B10. NMR Spectra

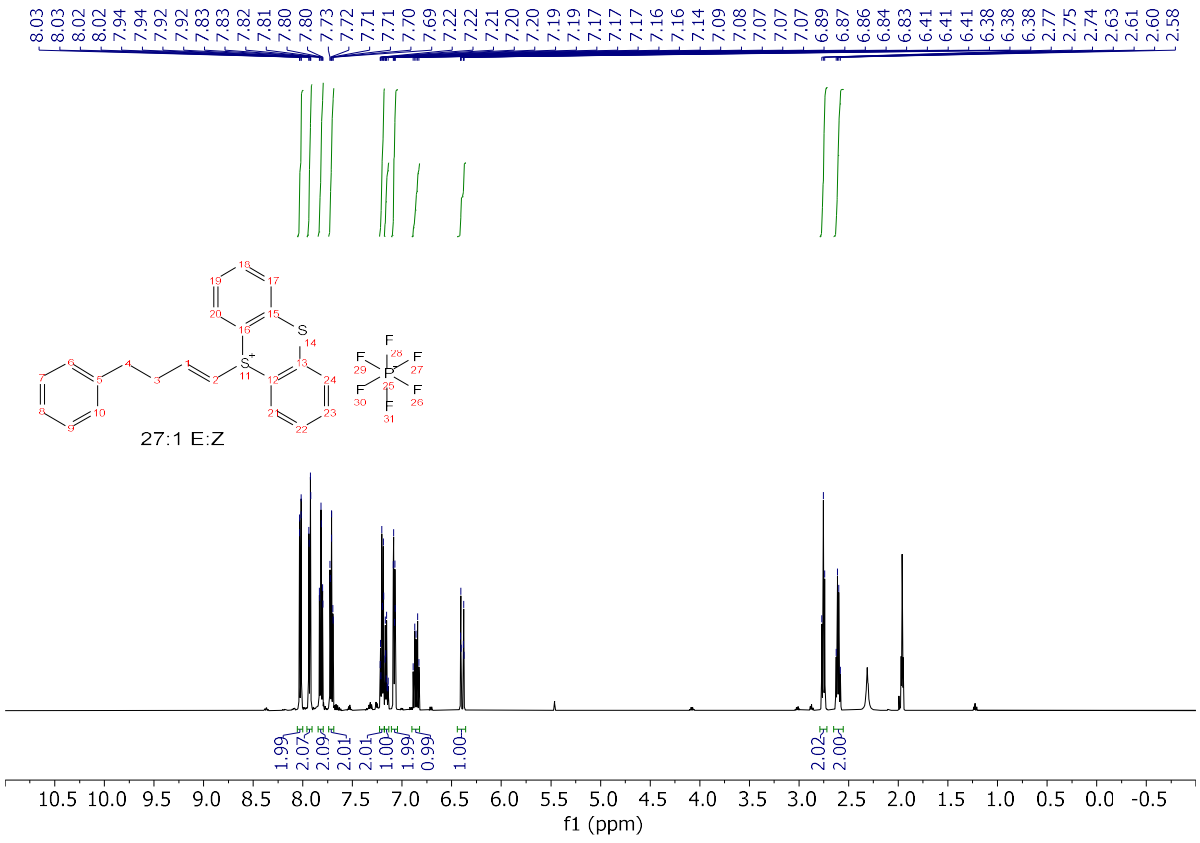

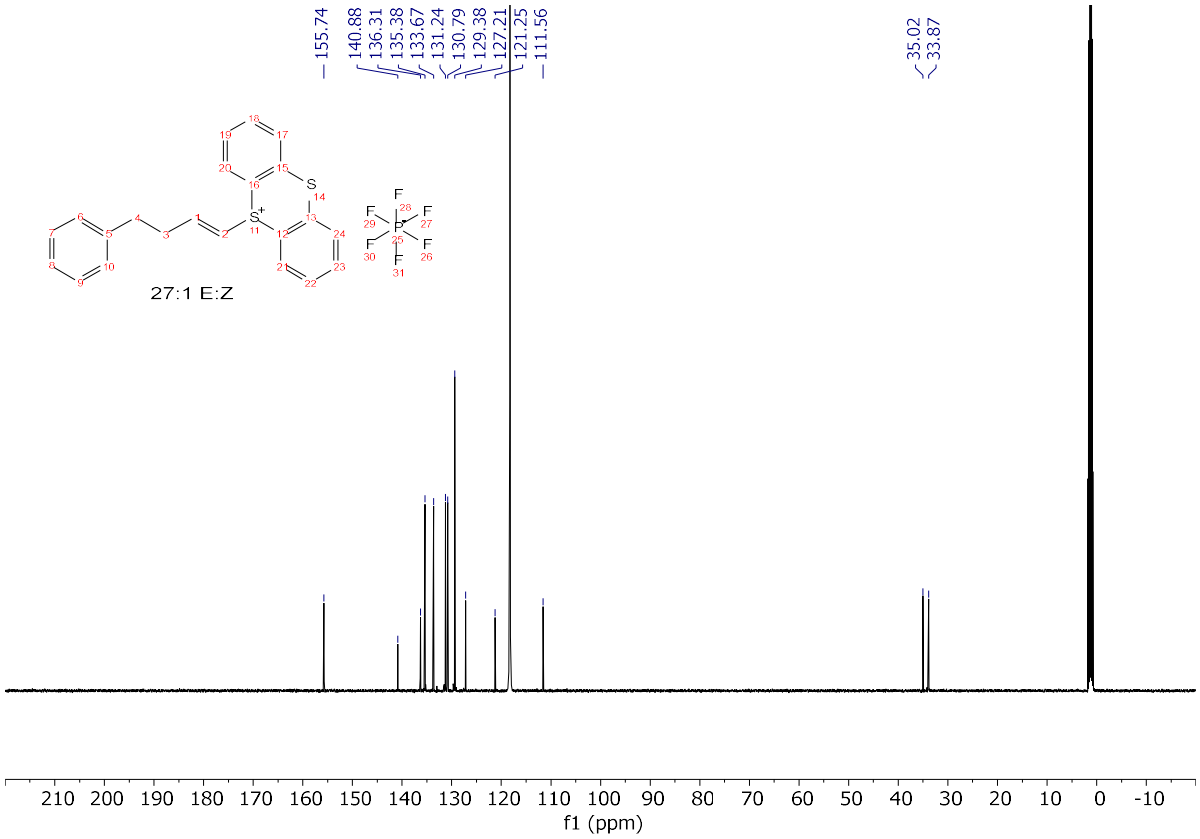
155.74
140.88
136.31
135.38
133.67
131.24
130.79
129.38
127.21
121.25
111.56
35.02
33.87
27:1 E:Z
f1 (ppm)

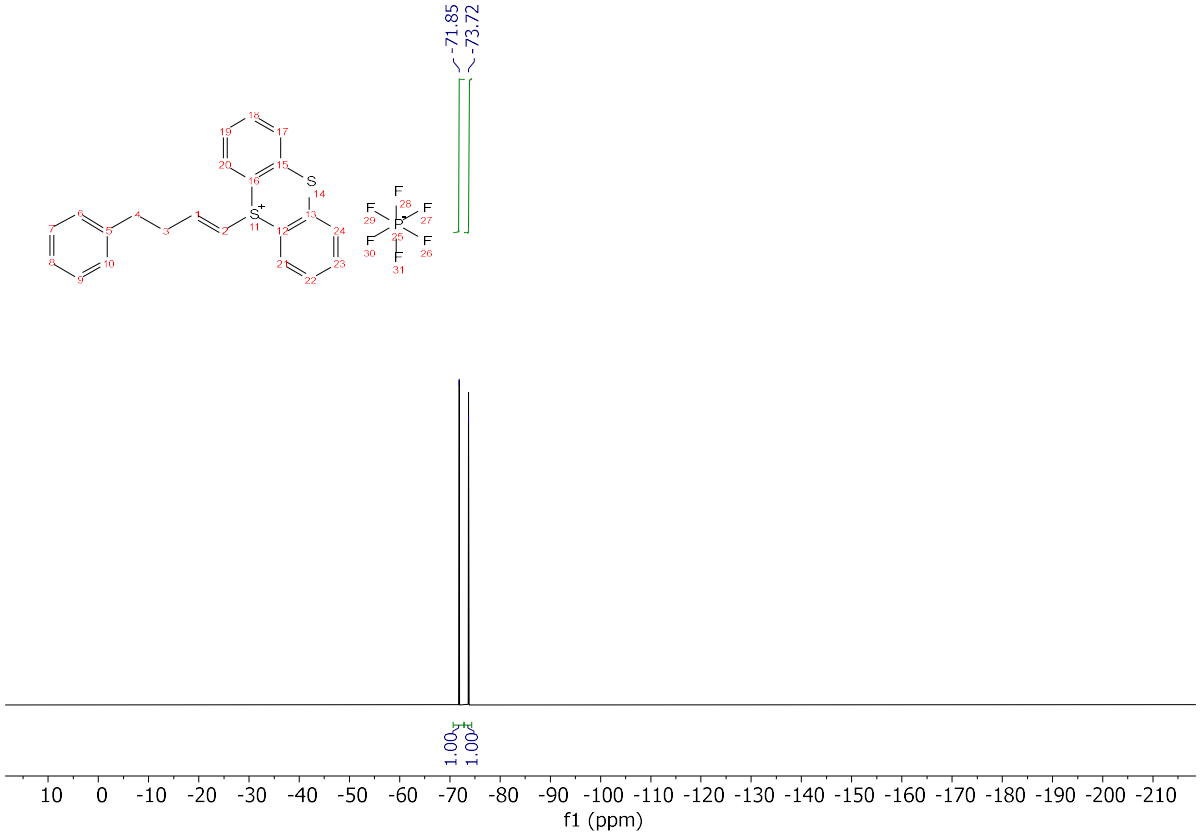
-71.85
-73.72
1.00
1.00
f1 (ppm)

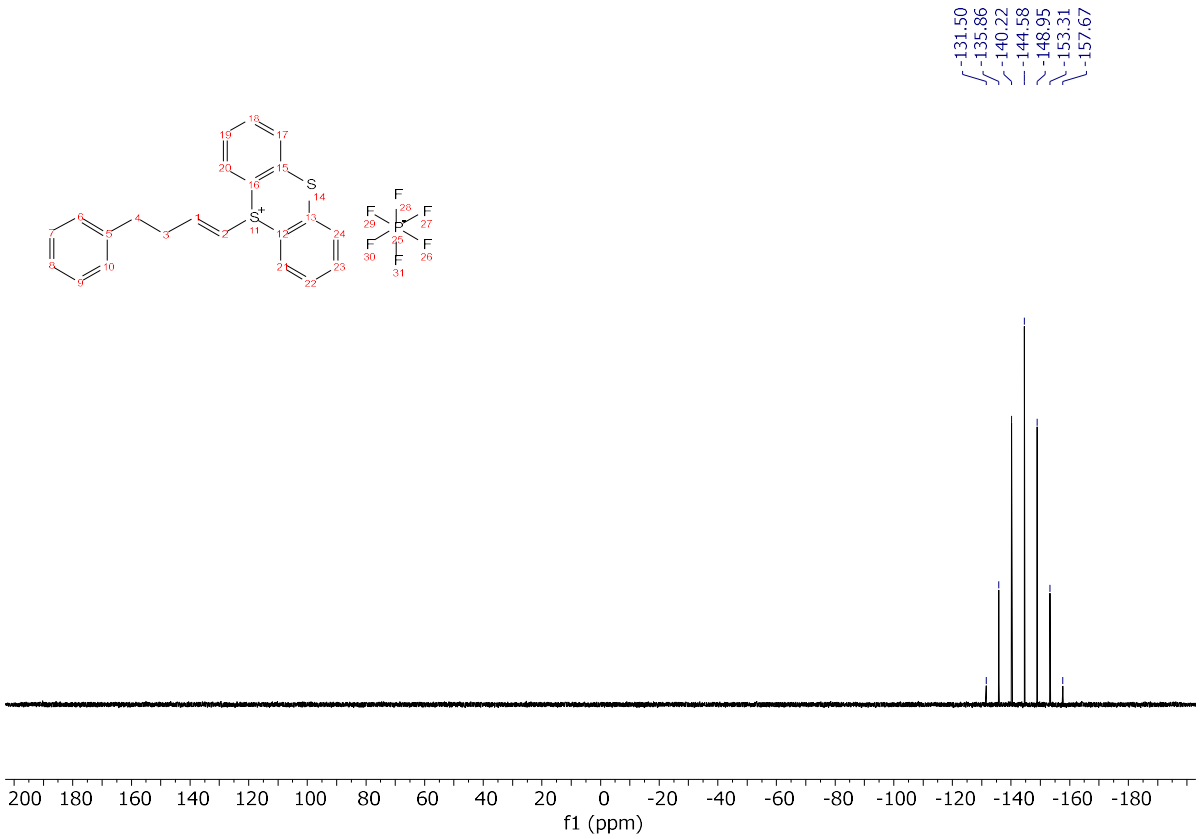
-131.50
-135.86
-140.22
-144.58
-148.95
-153.31
-157.67
200 180 160 140 120 100 80 60 40 20 0 -20 -40 -60 -80 -100 -120 -140 -160 -180
f1 (ppm)

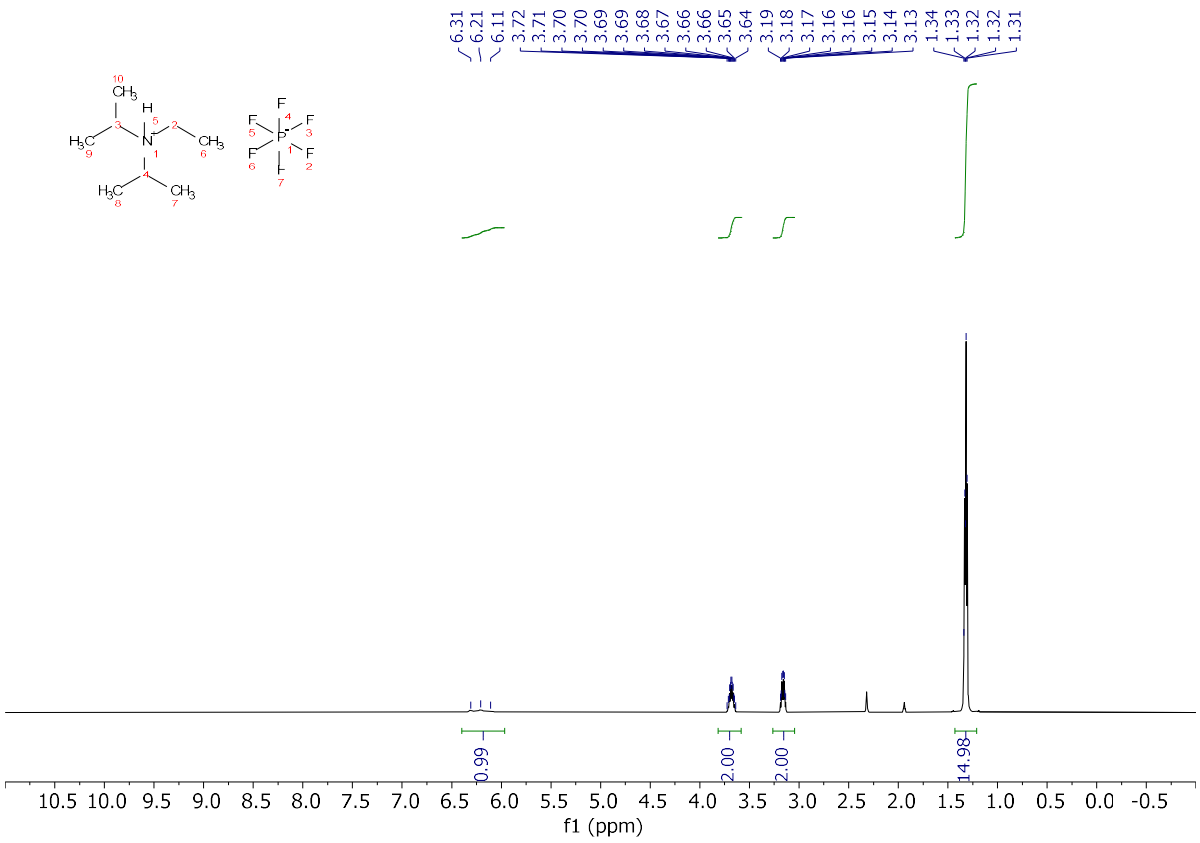
6.31
6.21
6.11
3.72
3.71
3.70
3.70
3.69
3.69
3.68
3.67
3.66
3.66
3.65
3.64
3.19
3.18
3.17
3.16
3.16
3.15
3.14
3.13
1.34
1.33
1.32
1.32
1.31
0.99
2.00
2.00
14.98
10.5 10.0 9.5 9.0 8.5 8.0 7.5 7.0 6.5 6.0 5.5 5.0 4.5 4.0 3.5 3.0 2.5 2.0 1.5 1.0 0.5 0.0 -0.5
f1 (ppm)

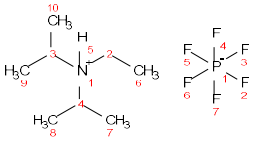

56.01
43.98
18.61
17.24
12.88
240 230 220 210 200 190 180 170 160 150 140 130 120 110 100 90 80 70 60 50 40 30 20 10 0 -10 -20
f1 (ppm)

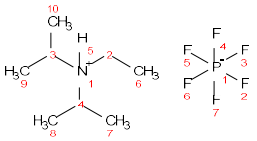

-71.83
-73.71
10 0 -10 -20 -30 -40 -50 -60 -70 -80 -90 -100 -110 -120 -130 -140 -150 -160 -170 -180 -190 -200 -210
f1 (ppm)

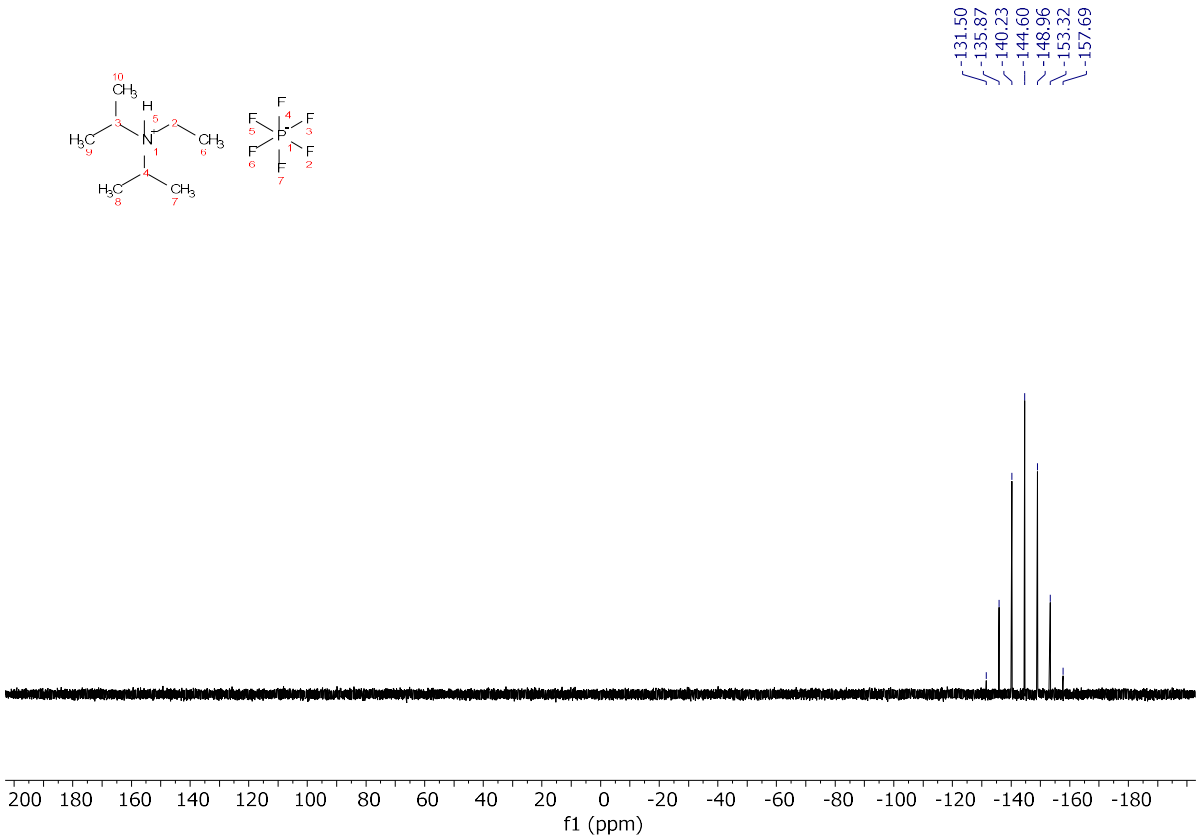
-131.50
-135.87
-140.23
-144.60
-148.96
-153.32
-157.69
f1 (ppm)

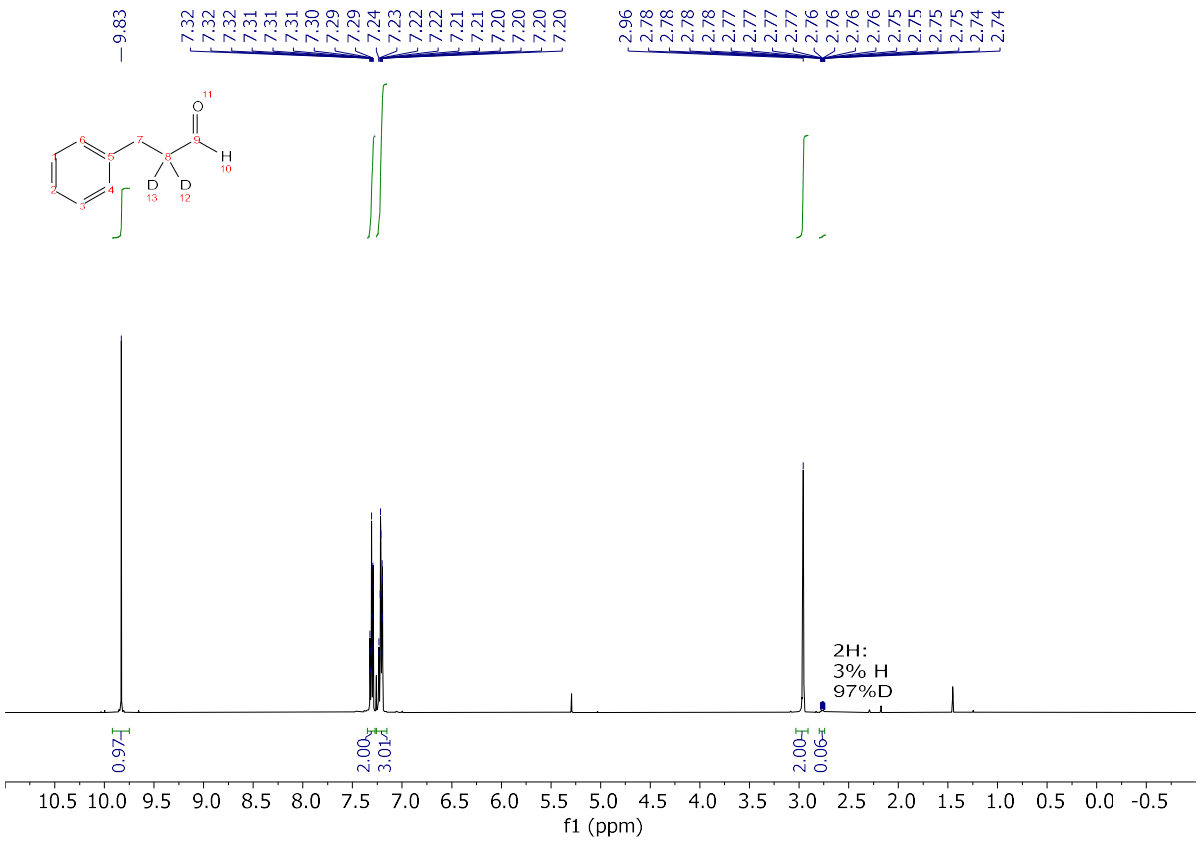
9.83
7.32
7.24
2.96
2.78
2.76
2H:
3% H
97%D
0.97
2.00
3.01
2.00
0.06
f1 (ppm)

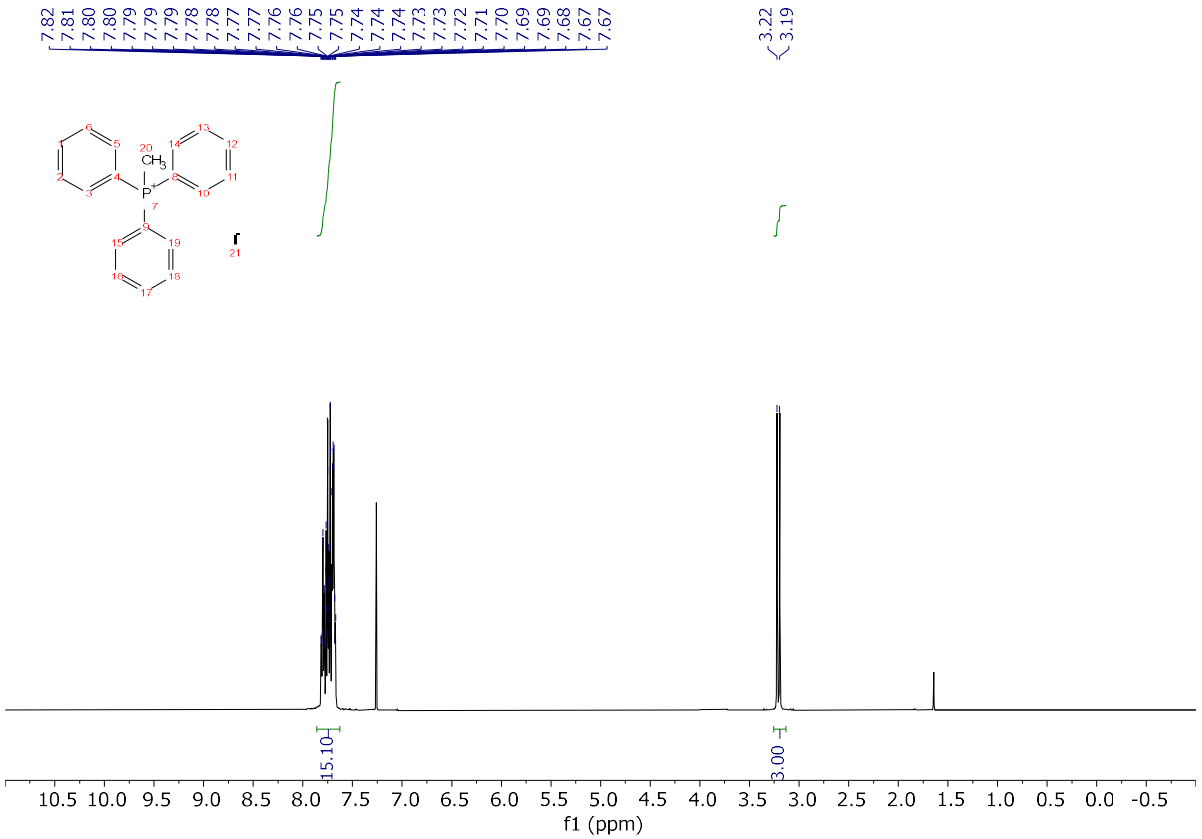
7.82
7.81
7.80
7.80
7.79
7.79
7.79
7.78
7.78
7.77
7.77
7.76
7.76
7.75
7.75
7.74
7.74
7.74
7.73
7.73
7.72
7.71
7.70
7.69
7.69
7.68
7.67
7.67
3.22
3.19
15.10
3.00
10.5 10.0 9.5 9.0 8.5 8.0 7.5 7.0 6.5 6.0 5.5 5.0 4.5 4.0 3.5 3.0 2.5 2.0 1.5 1.0 0.5 0.0 -0.5
f1 (ppm)

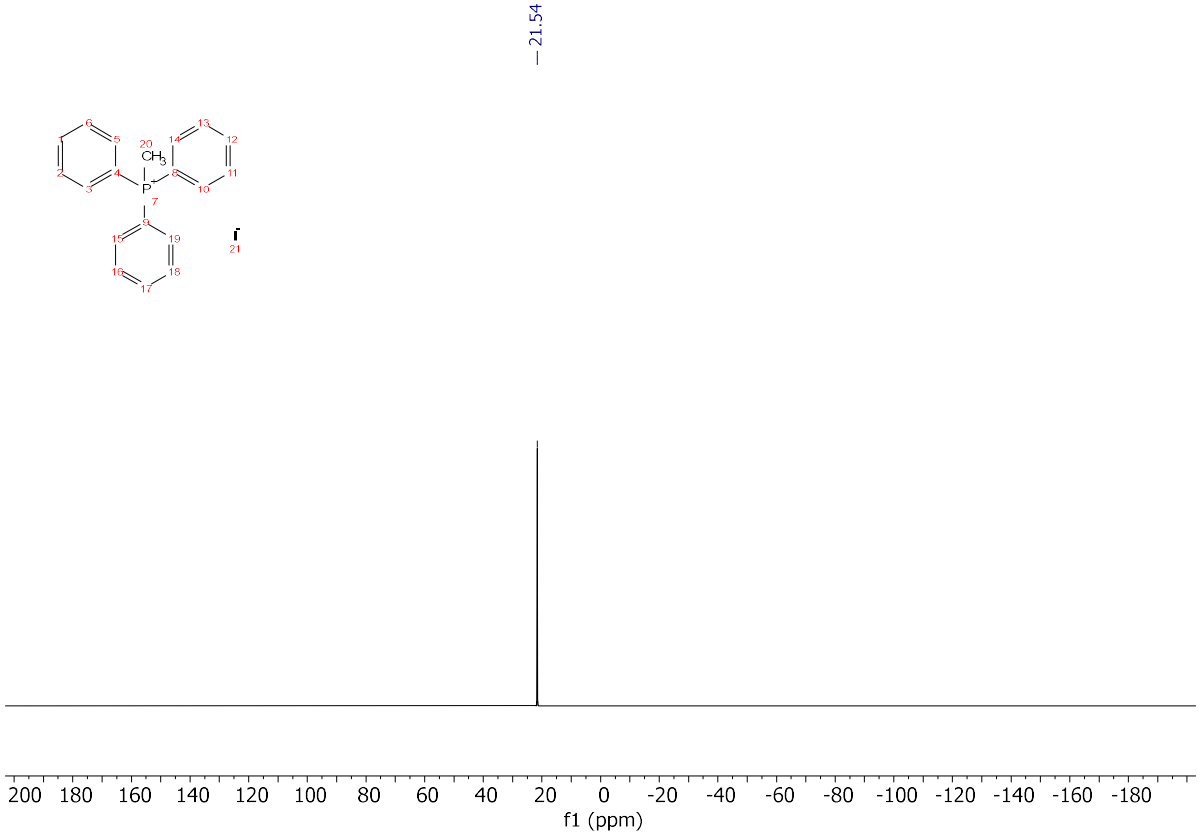
21.54
200 180 160 140 120 100 80 60 40 20 0 -20 -40 -60 -80 -100 -120 -140 -160 -180
f1 (ppm)

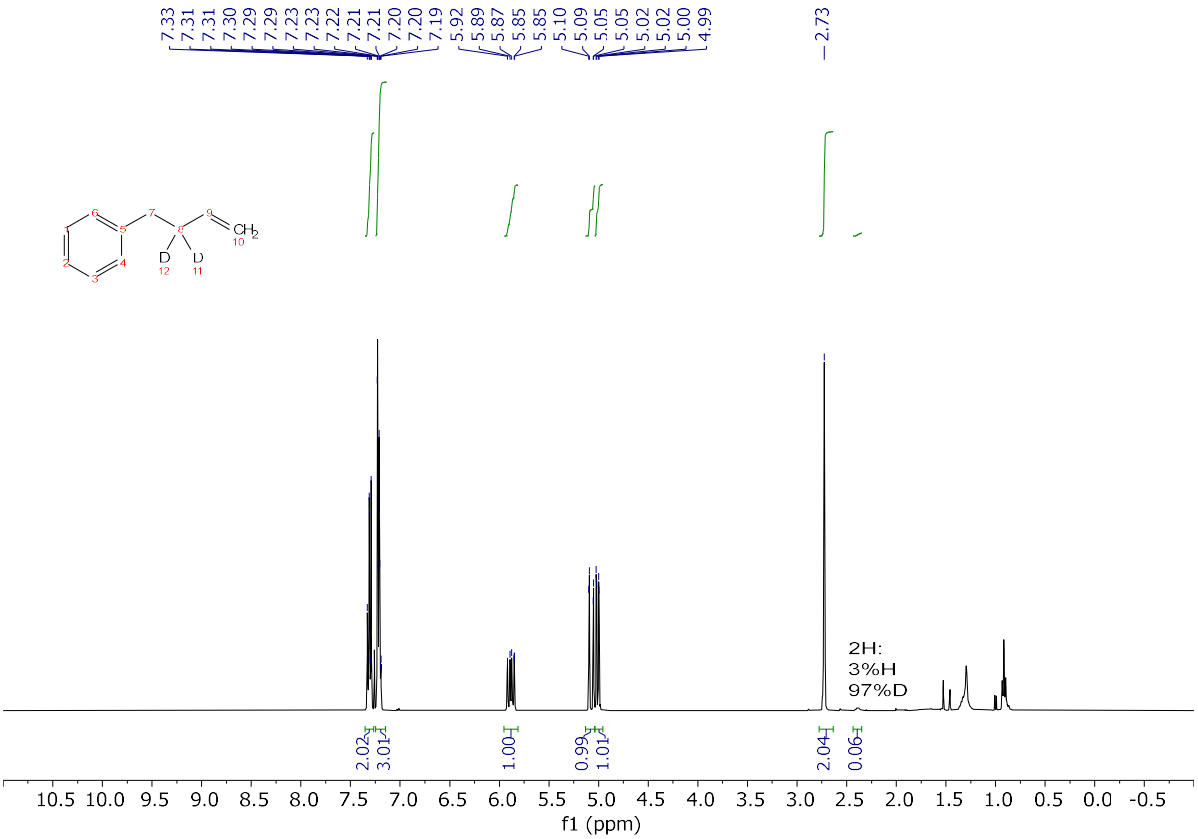
7.33
7.31
7.31
7.30
7.29
7.29
7.23
7.23
7.22
7.21
7.21
7.20
7.20
7.19
5.92
5.89
5.87
5.85
5.85
5.10
5.09
5.05
5.05
5.02
5.02
5.00
4.99
2.73
2H:
3%H
97%D
2.02
3.01
1.00
0.99
1.01
2.04
0.06
10.5 10.0 9.5 9.0 8.5 8.0 7.5 7.0 6.5 6.0 5.5 5.0 4.5 4.0 3.5 3.0 2.5 2.0 1.5 1.0 0.5 0.0 -0.5
f1 (ppm)

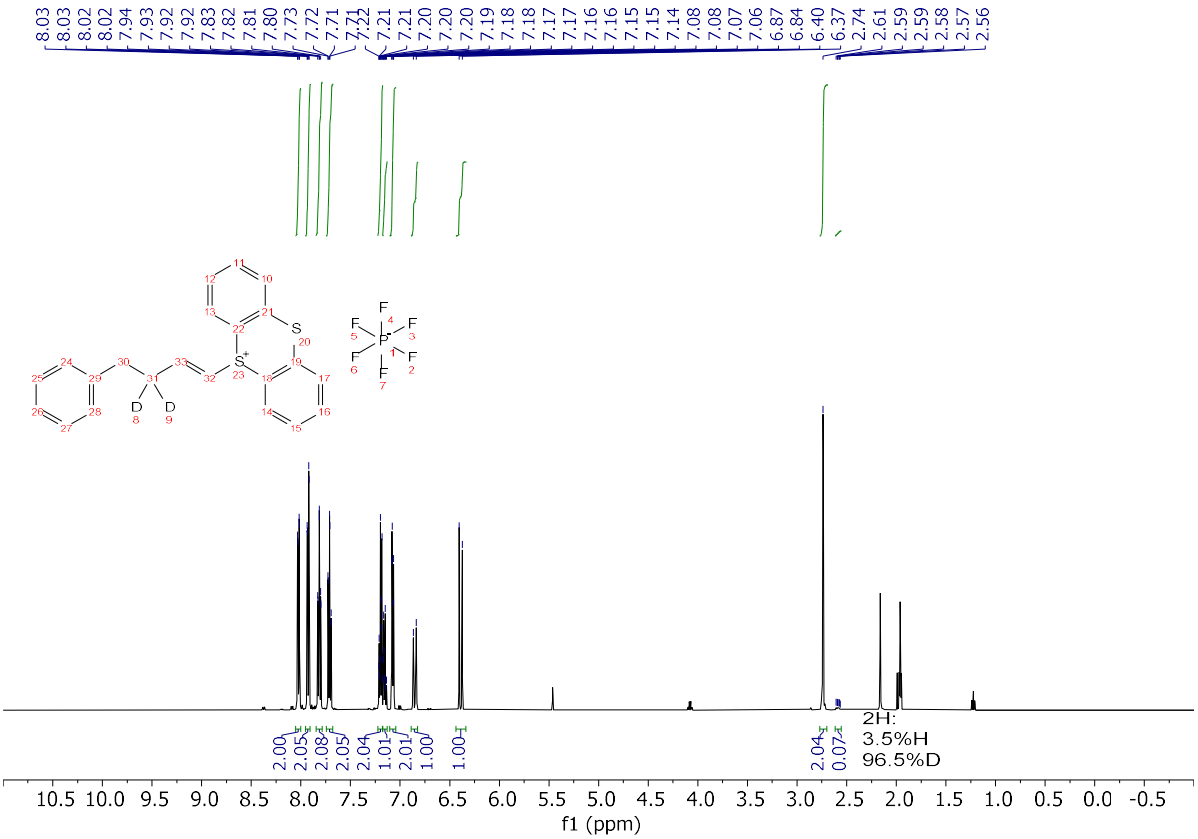
8.03
8.03
8.02
8.02
7.94
7.93
7.92
7.92
7.83
7.82
7.81
7.80
7.73
7.72
7.71
7.71
7.22
7.21
7.21
7.20
7.20
7.20
7.19
7.18
7.18
7.17
7.17
7.16
7.16
7.15
7.15
7.14
7.08
7.08
7.07
7.06
6.87
6.84
6.40
6.37
2.74
2.61
2.59
2.59
2.58
2.57
2.56
2H:
3.5%H
96.5%D
2.00
2.05
2.08
2.05
2.04
1.01
2.01
1.00
1.00
2.04
0.07
10.5 10.0 9.5 9.0 8.5 8.0 7.5 7.0 6.5 6.0 5.5 5.0 4.5 4.0 3.5 3.0 2.5 2.0 1.5 1.0 0.5 0.0 -0.5
f1 (ppm)

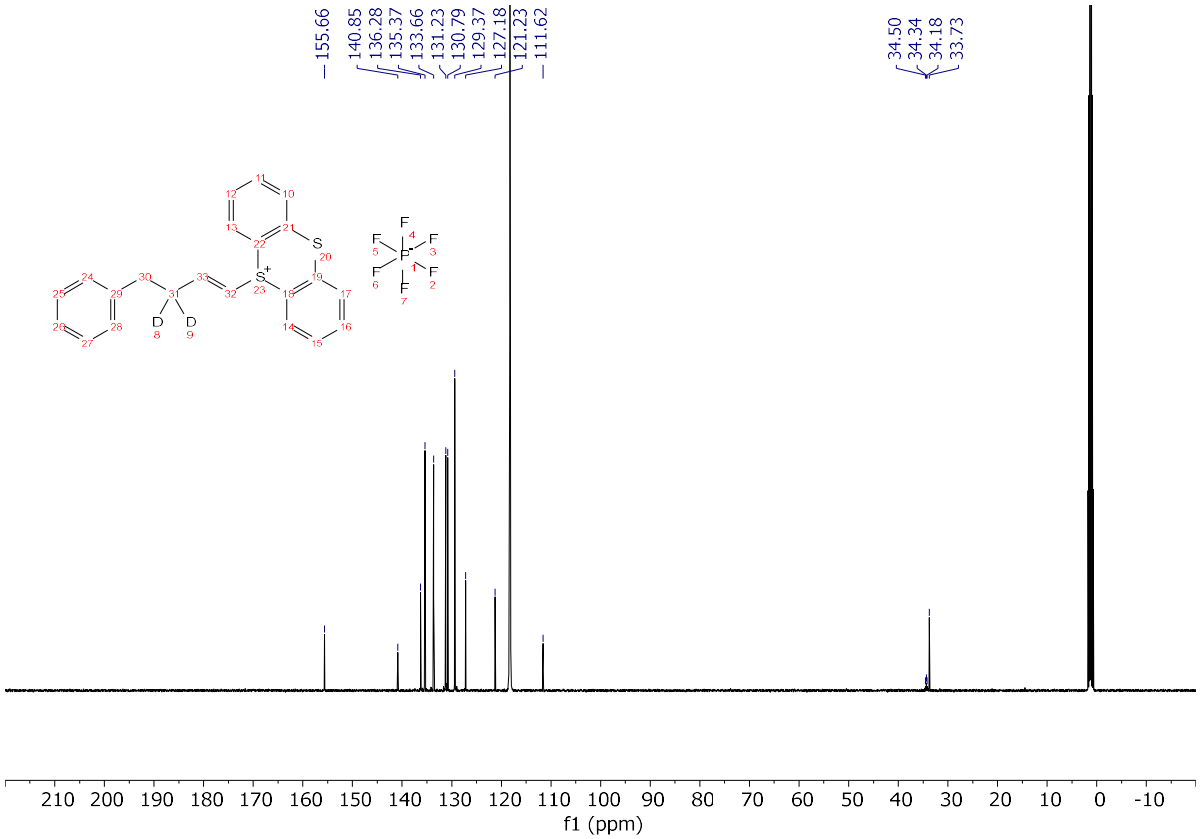
155.66
140.85
136.28
135.37
133.66
131.23
130.79
129.37
127.18
121.23
111.62
34.50
34.34
34.18
33.73
f1 (ppm)

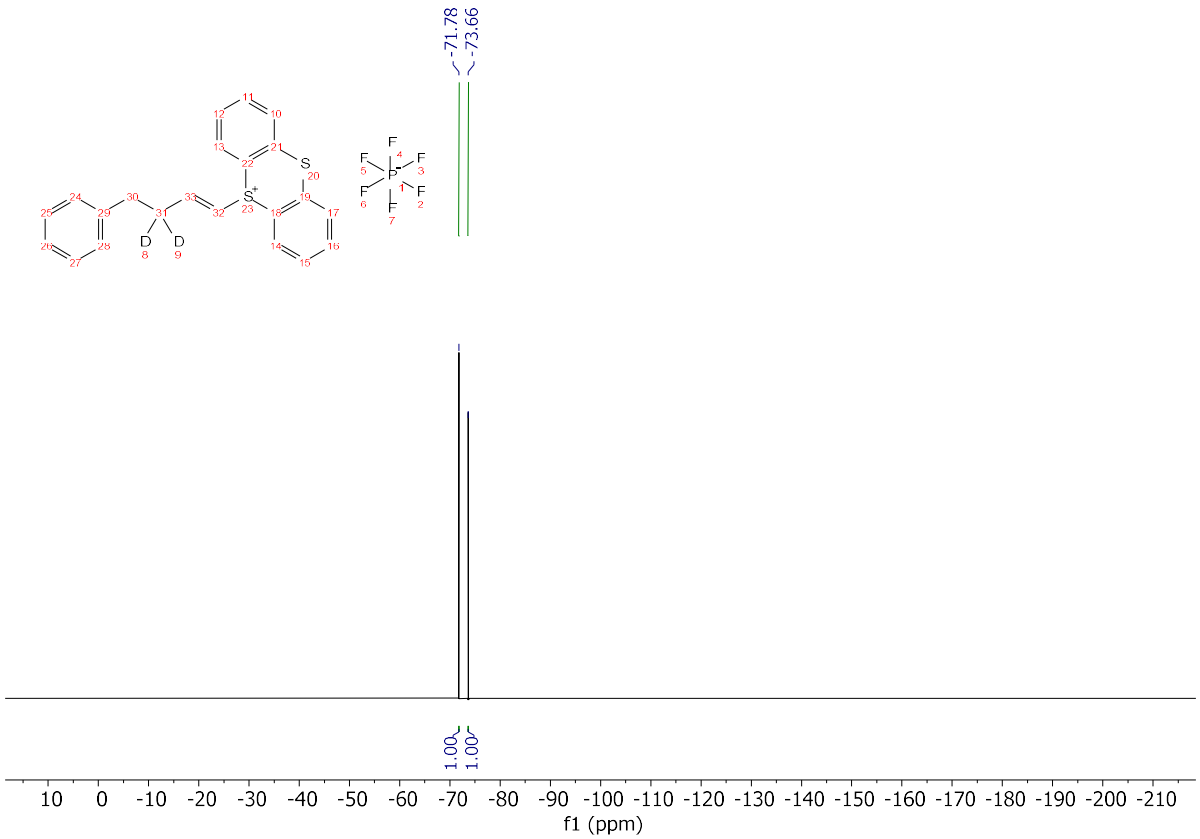
-71.78
-73.66
1.00
1.00
f1 (ppm)

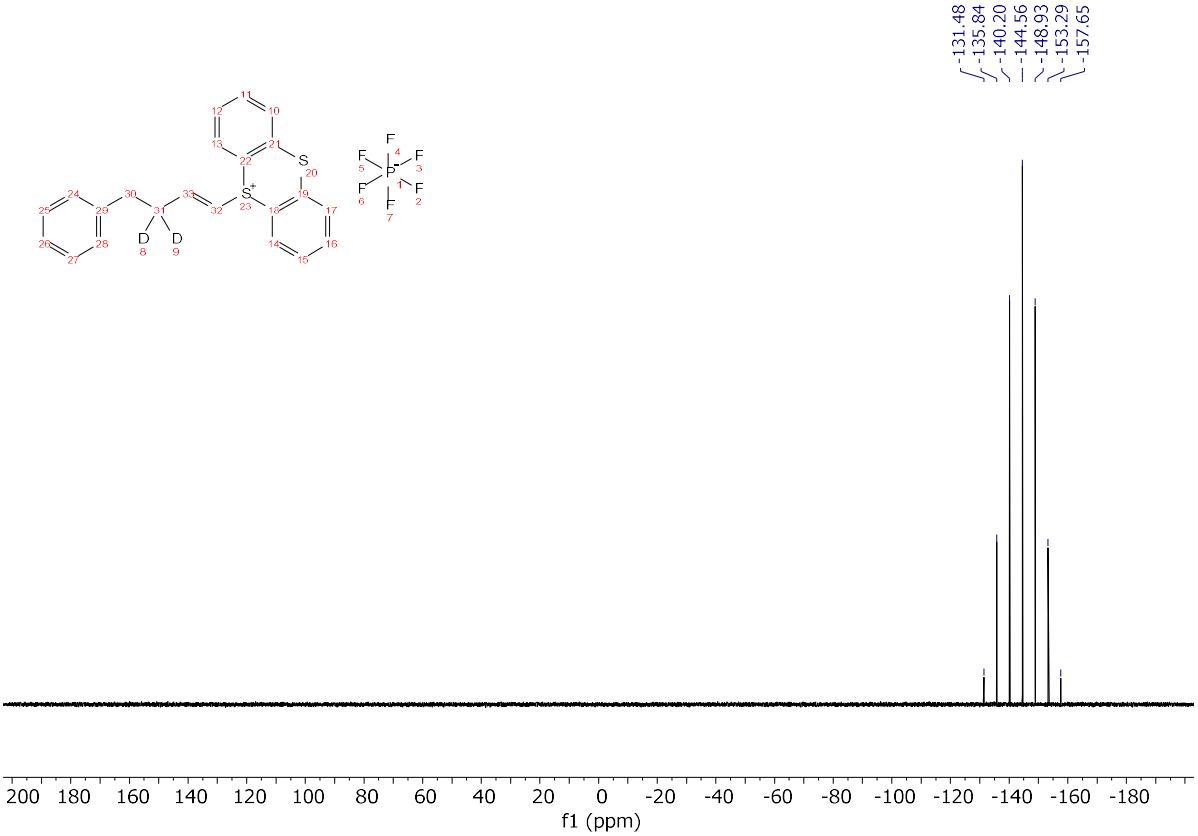
-131.48
-135.84
-140.20
-144.56
-148.93
-153.29
-157.65
f1 (ppm)

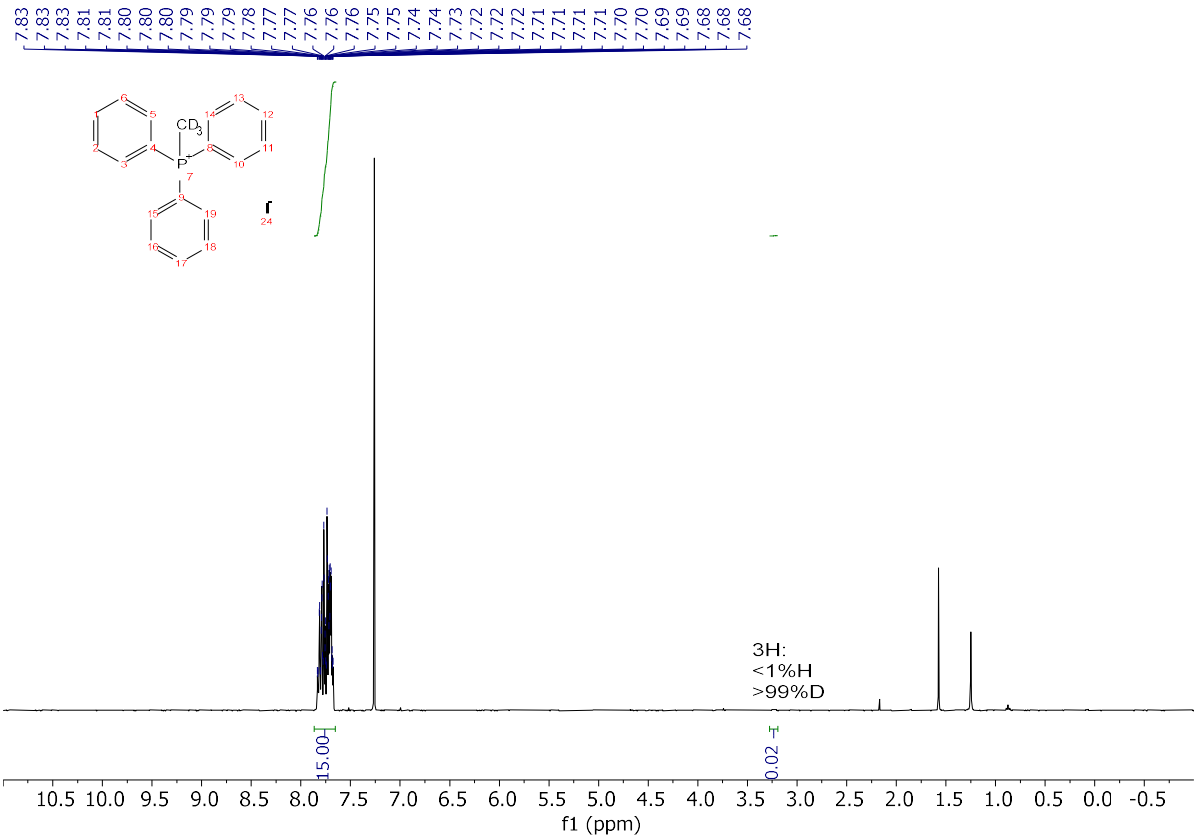
7.83
7.81
7.80
7.79
7.78
7.77
7.76
7.75
7.74
7.73
7.72
7.71
7.70
7.69
7.68
CD3
f
3H:
<1%H
>99%D
15.00
0.02
f1 (ppm)

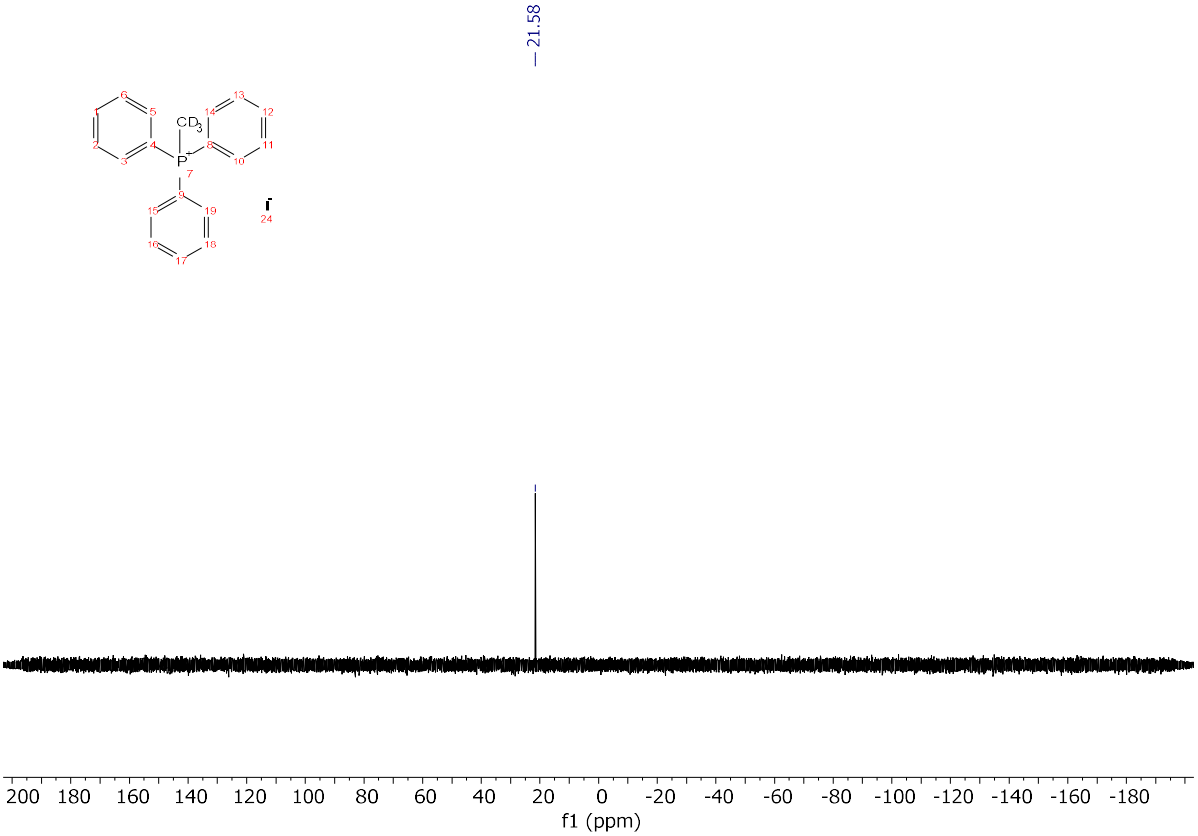
21.58
CD3
P+
f
200 180 160 140 120 100 80 60 40 20 0 -20 -40 -60 -80 -100 -120 -140 -160 -180
f1 (ppm)

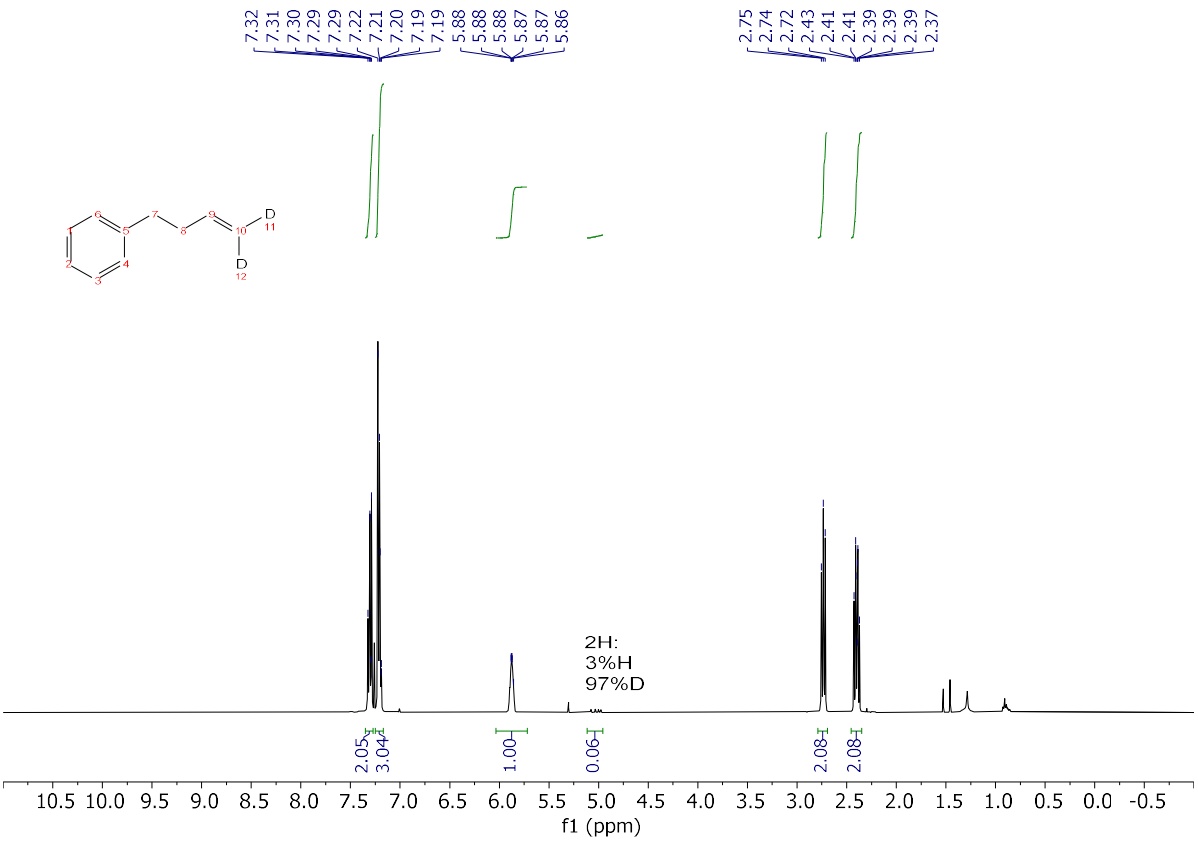
7.32
7.31
7.30
7.29
7.29
7.22
7.21
7.20
7.19
7.19
5.88
5.88
5.88
5.87
5.87
5.86
2.75
2.74
2.72
2.43
2.41
2.41
2.39
2.39
2.39
2.37
D
D
2H:
3%H
97%D
2.05
3.04
1.00
0.06
2.08
2.08
10.5 10.0 9.5 9.0 8.5 8.0 7.5 7.0 6.5 6.0 5.5 5.0 4.5 4.0 3.5 3.0 2.5 2.0 1.5 1.0 0.5 0.0 -0.5
f1 (ppm)

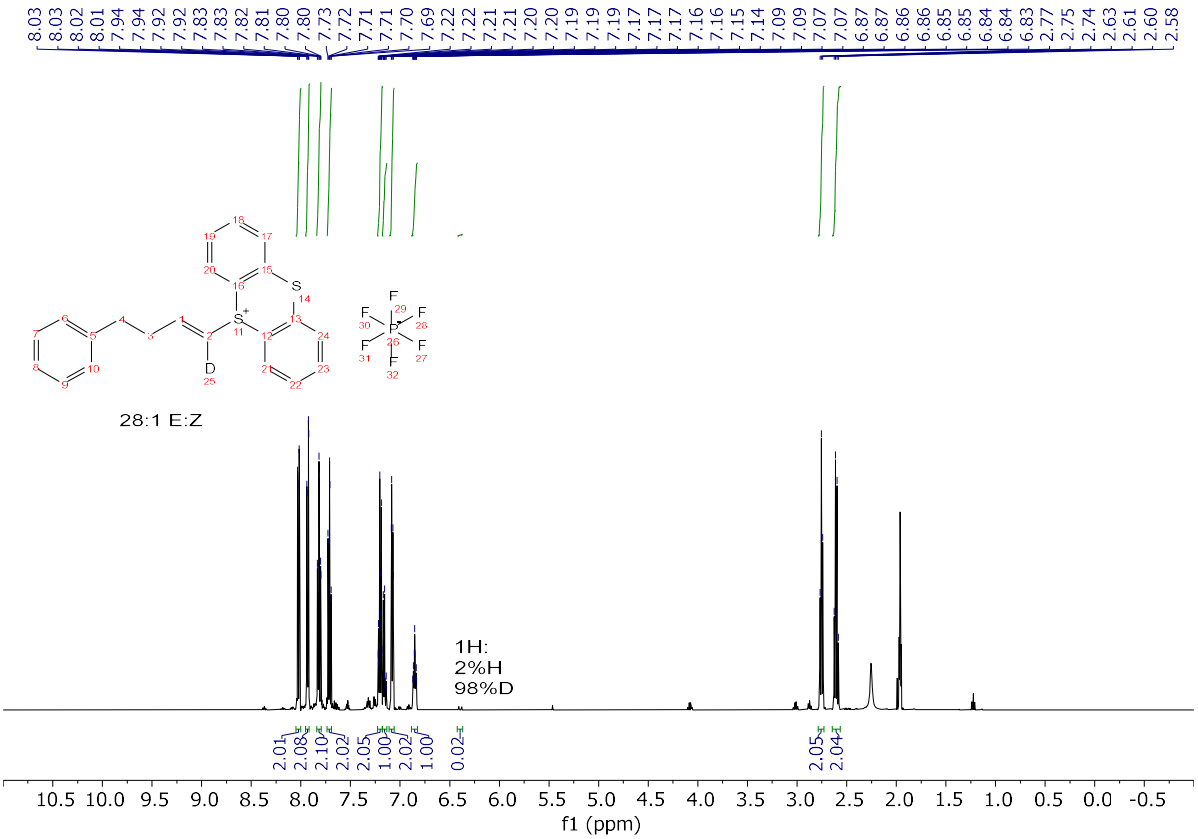
8.03 8.03 8.02 8.01 7.94 7.94 7.92 7.92 7.83 7.83 7.82 7.81 7.80 7.80 7.73 7.72 7.71 7.71 7.70 7.69 7.22 7.22 7.21 7.21 7.20 7.20 7.19 7.19 7.17 7.17 7.17 7.16 7.16 7.15 7.14 7.09 7.09 7.07 7.07 6.87 6.87 6.86 6.86 6.85 6.85 6.84 6.84 6.83 2.77 2.75 2.74 2.63 2.61 2.60 2.58
28:1 E:Z
1H:
2%H
98%D
2.01 2.08 2.10 2.02 2.05 1.00 2.02 1.00 0.02 2.05 2.04
10.5 10.0 9.5 9.0 8.5 8.0 7.5 7.0 6.5 6.0 5.5 5.0 4.5 4.0 3.5 3.0 2.5 2.0 1.5 1.0 0.5 0.0 -0.5
f1 (ppm)

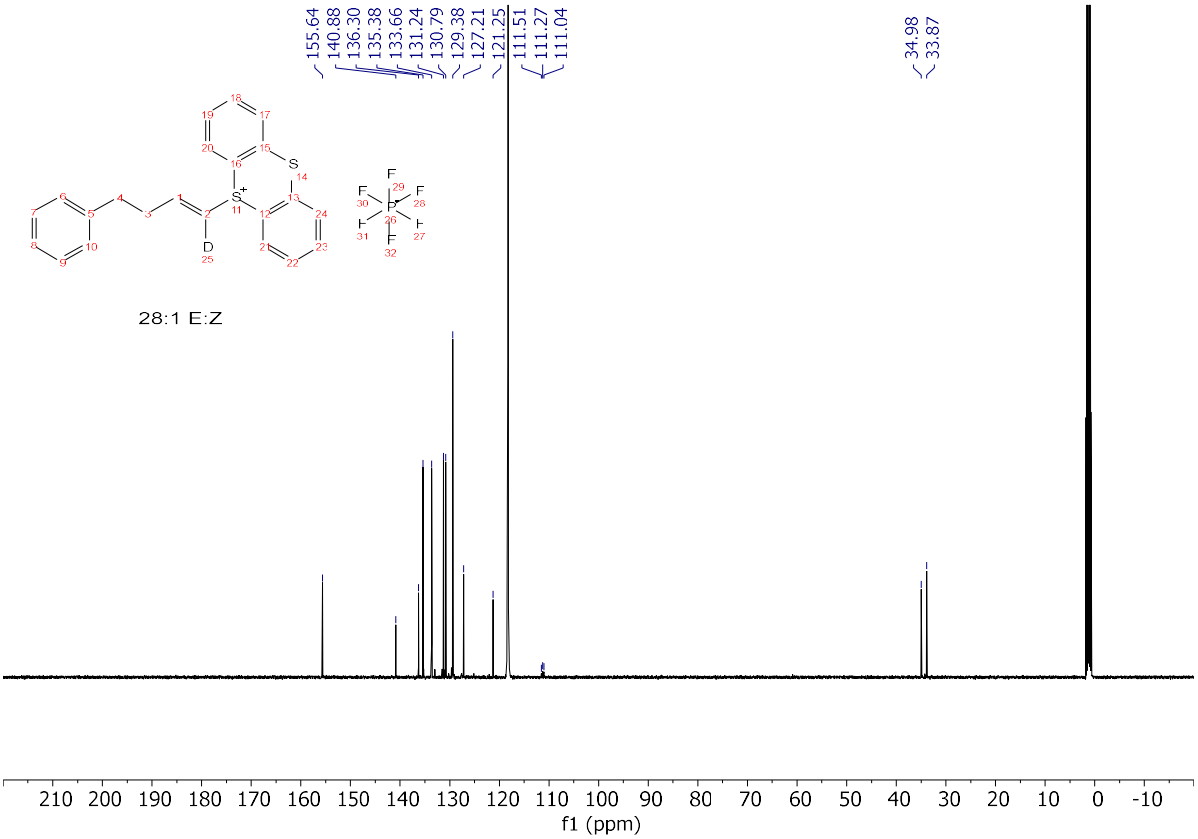
155.64 140.88 136.30 135.38 133.66 131.24 130.79 129.38 127.21 121.25 111.51 111.27 111.04
34.98 33.87
28:1 E:Z
210 200 190 180 170 160 150 140 130 120 110 100 90 80 70 60 50 40 30 20 10 0 -10
f1 (ppm)

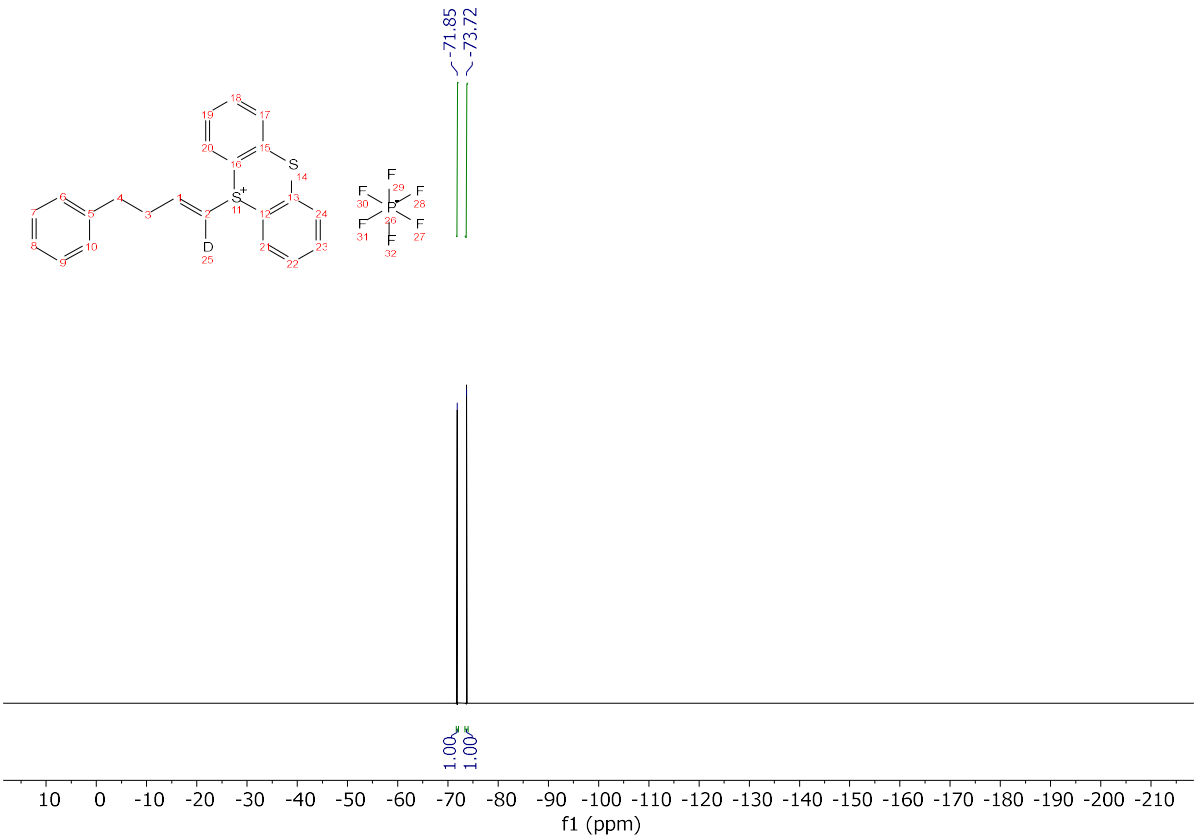
-71.85
-73.72
1.00
1.00
10 0 -10 -20 -30 -40 -50 -60 -70 -80 -90 -100 -110 -120 -130 -140 -150 -160 -170 -180 -190 -200 -210
f1 (ppm)

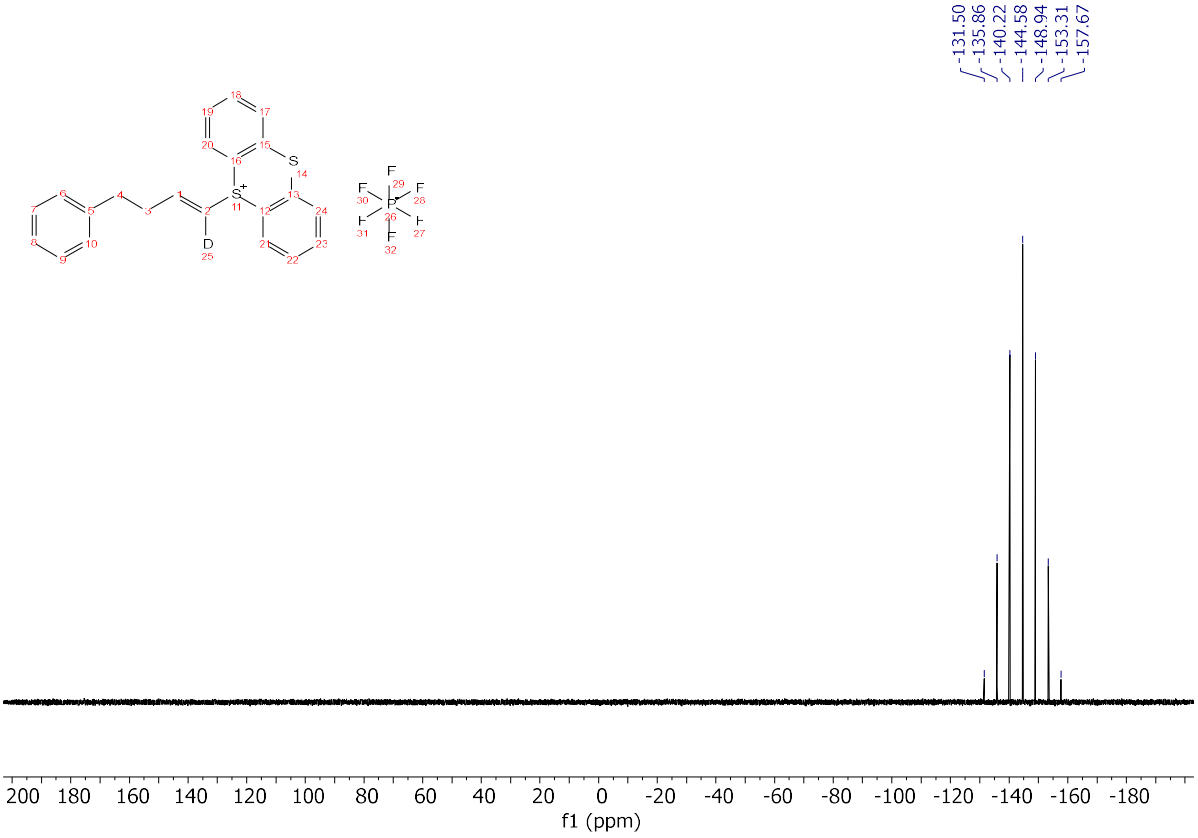
-131.50
-135.86
-140.22
-144.58
-148.94
-153.31
-157.67
200 180 160 140 120 100 80 60 40 20 0 -20 -40 -60 -80 -100 -120 -140 -160 -180
f1 (ppm)

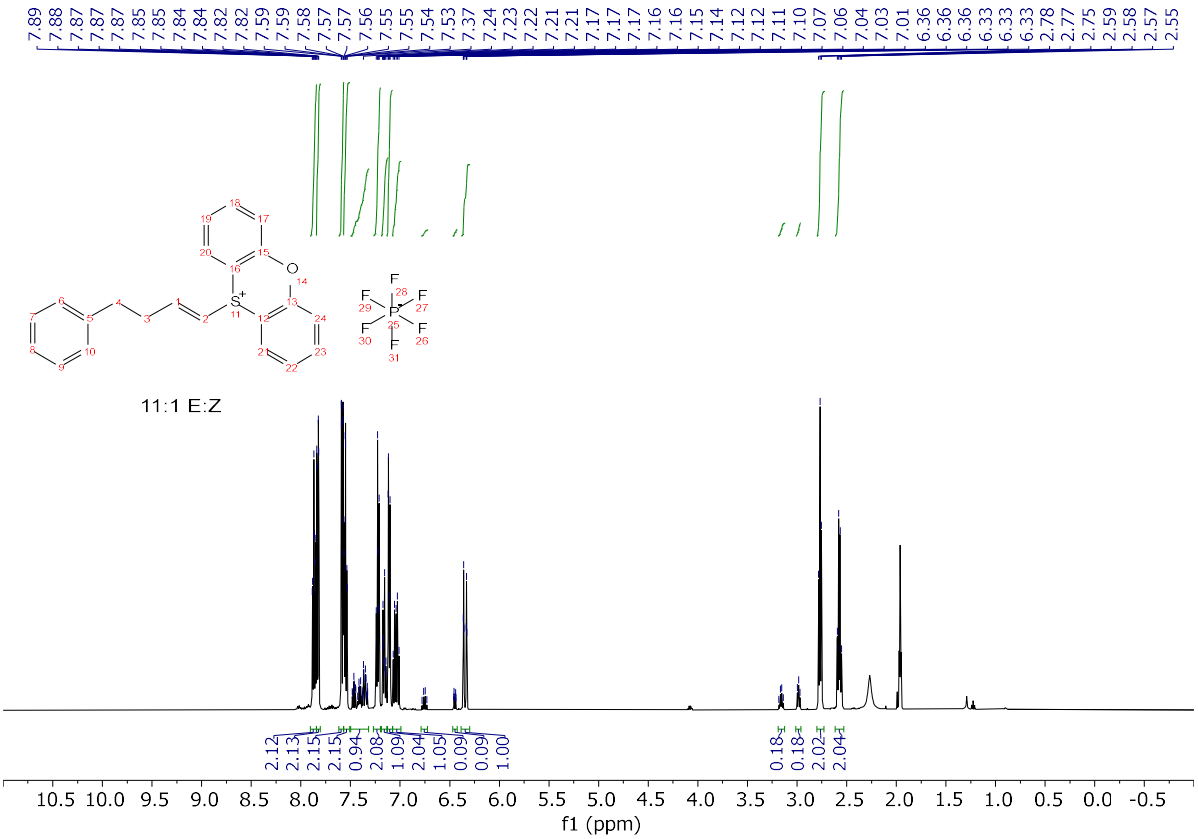
11:1 E:Z
f1 (ppm)

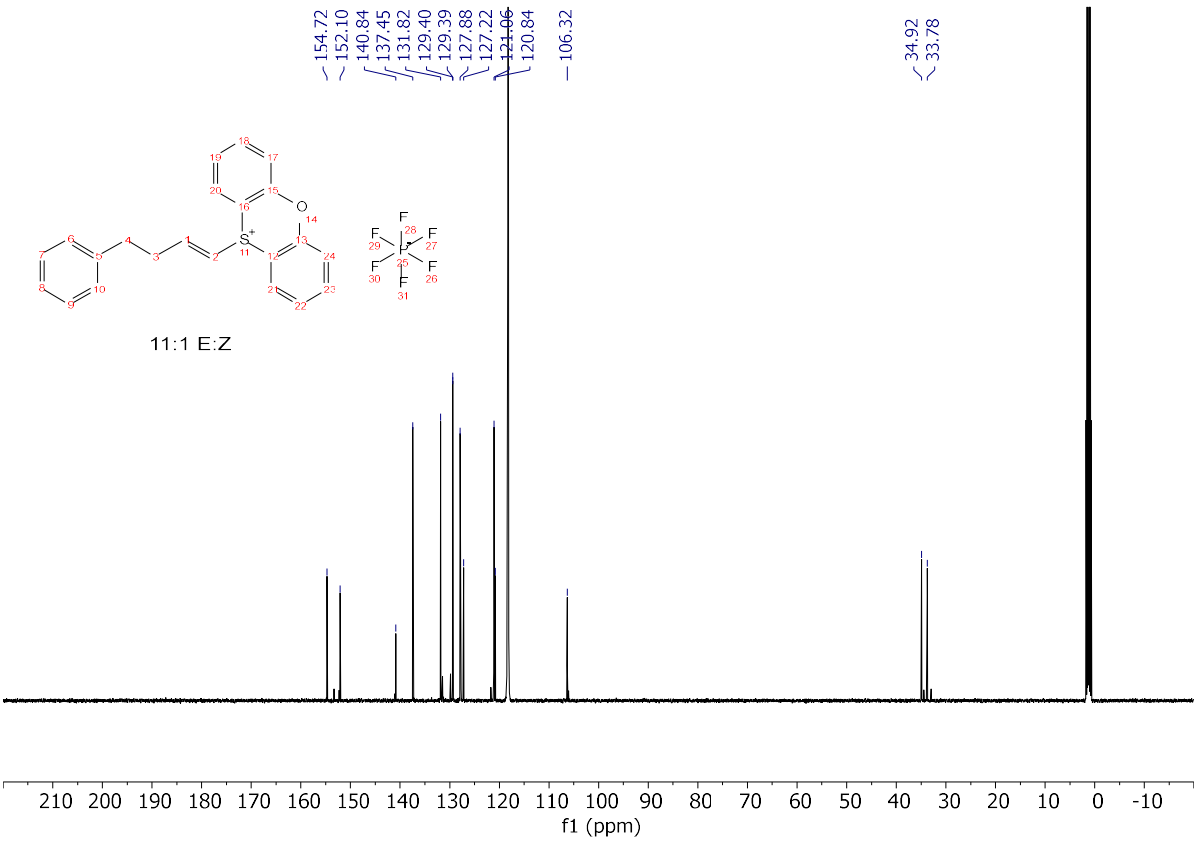
11:1 E:Z
f1 (ppm)

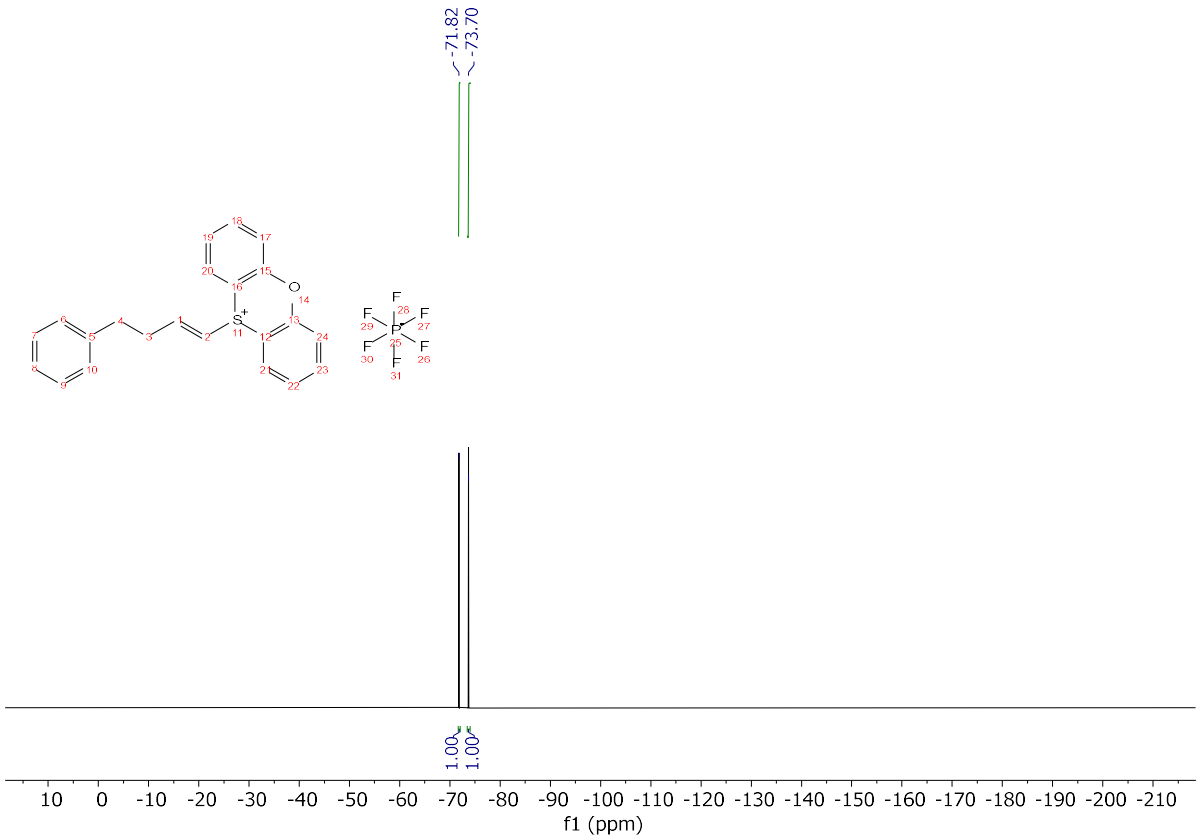
-71.82
-73.70
1.00
1.00
10 0 -10 -20 -30 -40 -50 -60 -70 -80 -90 -100 -110 -120 -130 -140 -150 -160 -170 -180 -190 -200 -210
f1 (ppm)

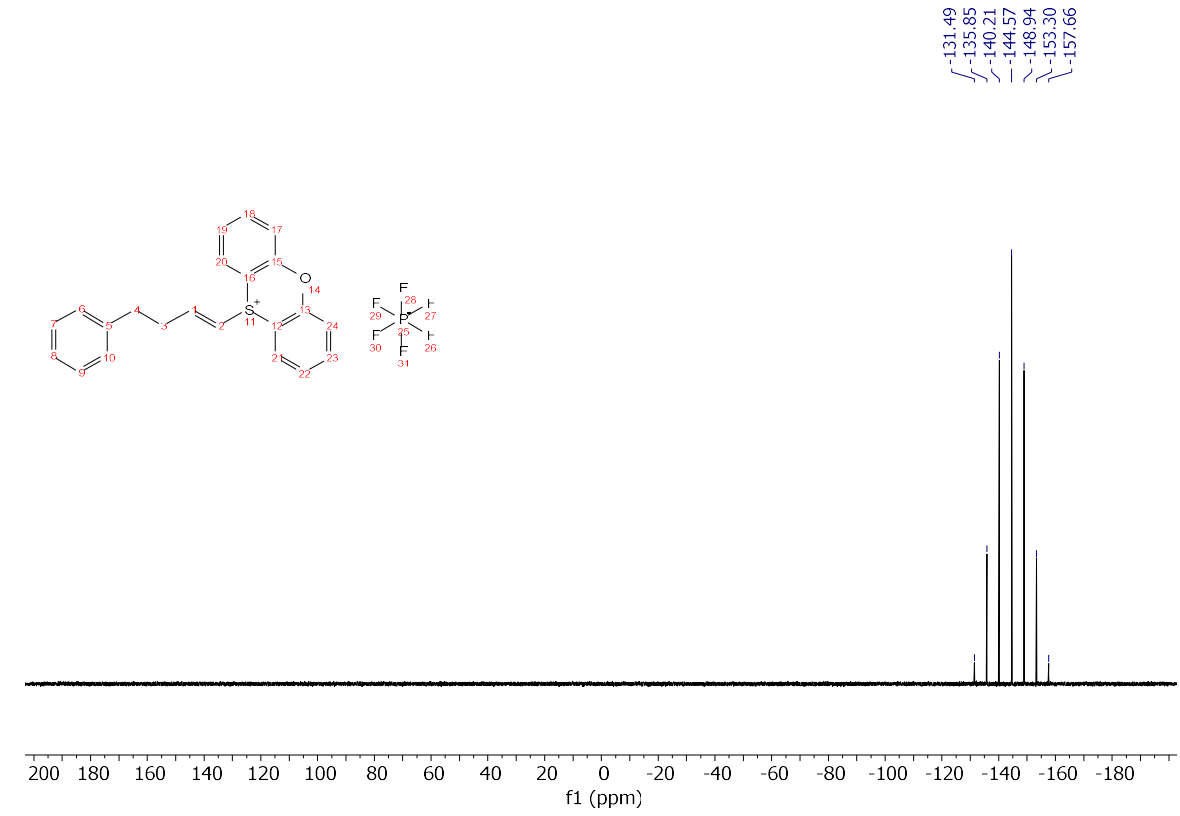
-131.49
-135.85
-140.21
-144.57
-148.94
-153.30
-157.66
200 180 160 140 120 100 80 60 40 20 0 -20 -40 -60 -80 -100 -120 -140 -160 -180
f1 (ppm)

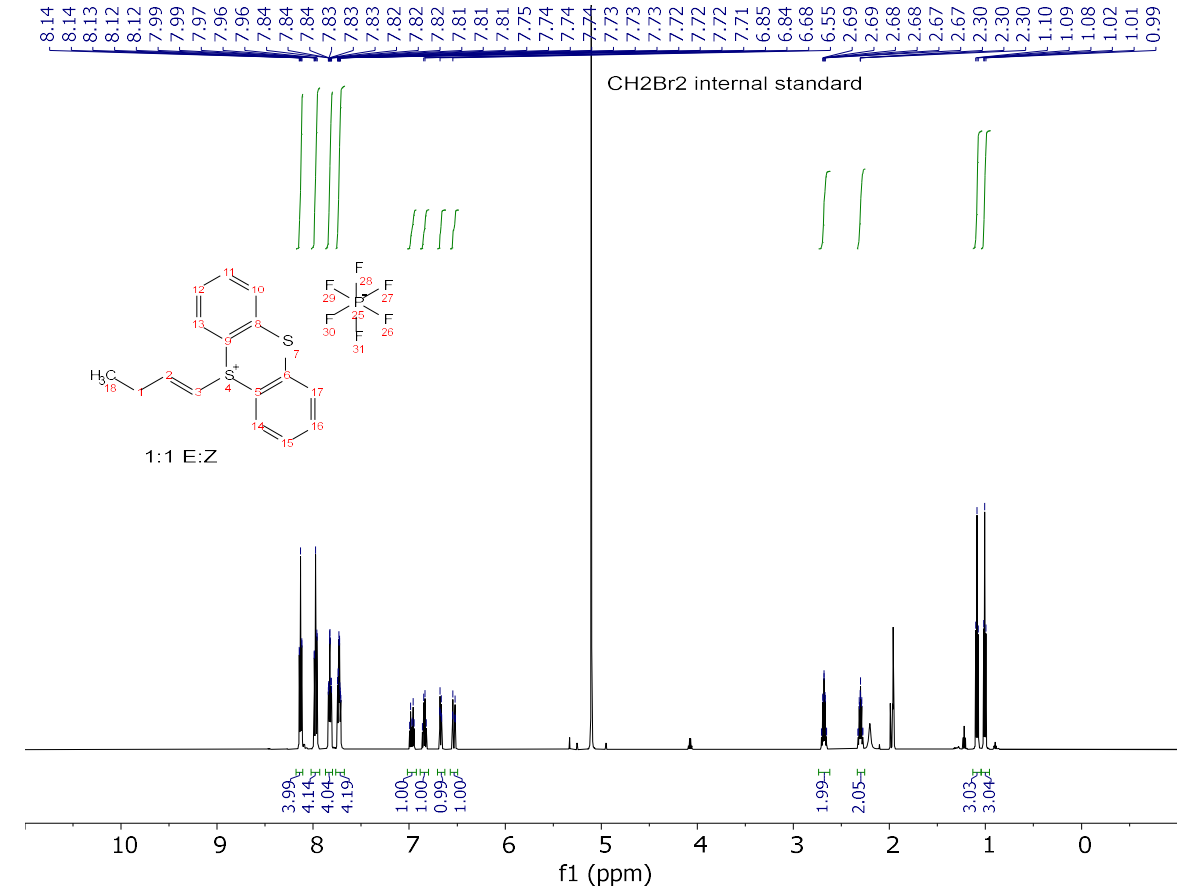
CH2Br2 internal standard
1:1 E:Z
f1 (ppm)

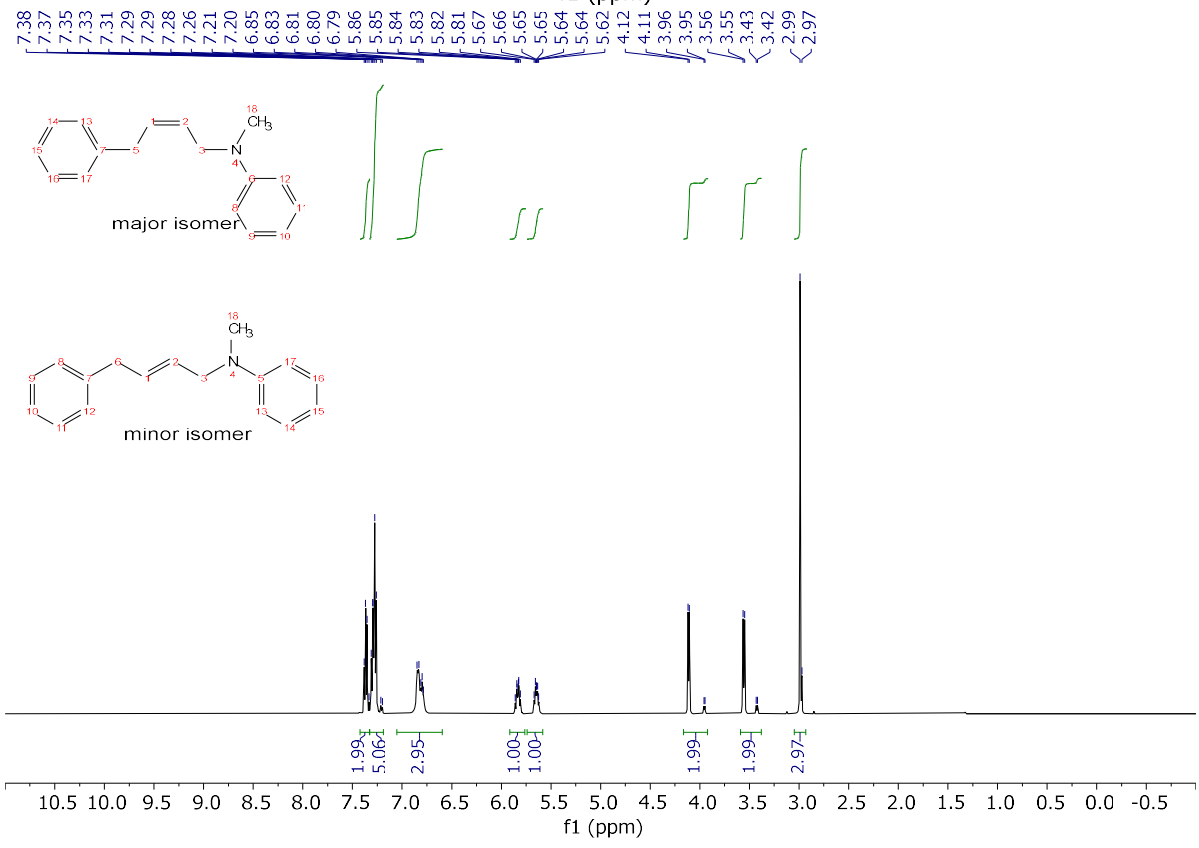
major isomer
minor isomer
f1 (ppm)

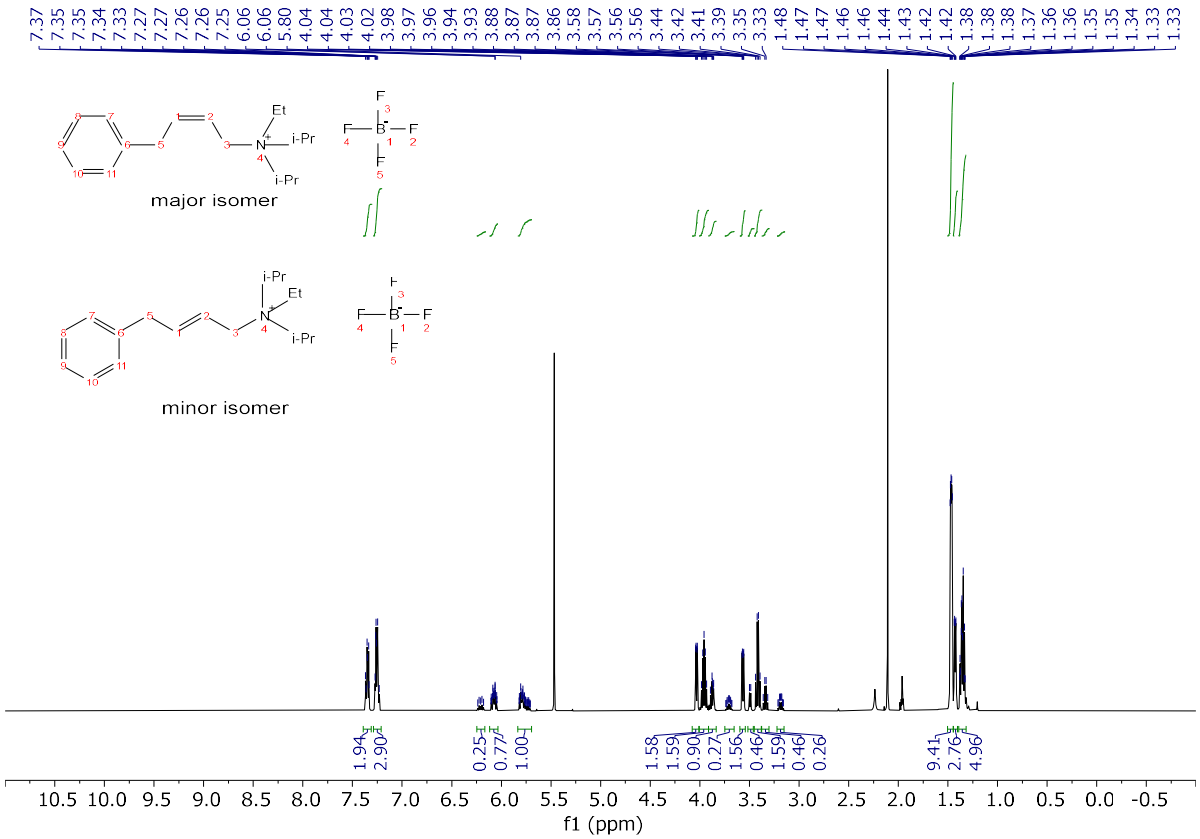

B11. Computational Details

All geometry optimizations of intermediates and transition states were achieved using spin-restricted RB3LYP[Ref1]-D3[Ref2]/def2-SVP[Ref3]method, in acetonitrile solvent using the CPCM solvent model[Ref4] with "opt=noeigen" and "guess=mix" keywords as implemented in Gaussian16[Ref5]. Frequency calculations were also conducted at the same level of theory to obtain vibrational frequencies to determine the identity of stationary points as intermediates (no imaginary frequencies) or transition states (only one imaginary frequency), as well as obtaining the thermochemistry: enthalpy (DH) and free energy (DG) at the temperature of 298 K. Single point calculations on the important structures were performed to ensure consistency in the energetic profile irrespective of the method employed. The methods employed for the single point calculations are: a) (RB3LYP-D3-def2tzvpp-CPCM(CH3CN)//RB3LYP-D3/def2svp-CPCM(CH3CN)) b) {RB3LYP-D3-6-311+G(d,p)-CPCM(CH3CN)//RB3LYP-D3/def2svp-CPCM(CH3CN)} c) [RB3LYP-D3-aug-cc-pvtz-CPCM(CH3CN)//RB3LYP-D3/def2svp-CPCM(CH3CN)]. All structural figures were generated with CYLview.[Ref6] Distances in structural figures are shown in Å and energies are in kcal/mol.

References for Computations

1. (a) Lee, C.; Yang, W.; Parr, R. G., Development of the Colle-Salvetti Correlation-Energy Formula into a Functional of the Electron Density. *Phys. Rev. B* **1988**, *37*, 785–789. (b) Becke, A. D., Density-Functional Thermochemistry. III. The Role of Exact Exchange. *J. Chem. Phys.* **1993**, *98*, 5648–5652.

2. (a) Grimme, S. Accurate description of van der Waals complexes by density functional theory including empirical corrections. *J. Comput. Chem.* **2004**, *25*, 1463-1473. (b) Grimme, S.; Antony, J.; Ehrlich, S.; Krieg, H. A consistent and accurate ab initio parametrization of density functional dispersion correction (DFT-D) for the 94 elements H-Pu. *J. Chem. Phys.* **2010**, *132*, 154104. (c) Grimme, S. Density functional theory with London dispersion corrections. *WIRES Comput. Mol. Sci.* **2011**, *1*, 211-228. (d) Ehrlich, S.; Moellmann, J.; Grimme, S. Dispersion-Corrected Density Functional Theory for Aromatic Interactions in Complex Systems. *Acc. Chem. Res.* **2012**, *46*, 916-926.

3. (a) Weigend, F.; Ahlrichs, R. Balanced basis sets of split valence, triple zeta valence and quadruple zeta valence quality for H to Rn: Design and assessment of accuracy. *Phys. Chem. Chem. Phys.* **2005**, *7*, 3297-3305. (b) Weigend, F. Accurate Coulomb-fitting basis sets for H to Rn. *Phys. Chem. Chem. Phys.* **2006**, *8*, 1057-1065.

4. (a) Klamt, A.; Schüürmann, G. COSMO: a new approach to dielectric screening in solvents with explicit expressions for the screening energy and its gradient. *J. Chem. Soc. Perkin Trans. 2* **1993**, *0*, 799-805. (b) Tomasi, J.; Persico, M. Molecular Interactions in Solution: An Overview of Methods Based on Continuous Distributions of the Solvent. *Chem. Rev.* **1994**, *94*, 2027-2094. (c) Andzelm, J.; Kölmel, C.; Klamt, A. Incorporation of solvent effects into density functional calculations of molecular energies and geometries. *J. Chem. Phys.* **1995**, *103*, 9312-9320. (d) Barone, V.; Cossi, M. Quantum Calculation of Molecular Energies and Energy Gradients in Solution by a Conductor Solvent Model. *J. Phys. Chem. A* **1998**, *102*, 1995-2001. (e) Cossi, M.; Rega, N.; Scalmani, G.; Barone, V. Energies, structures, and electronic properties of molecules in solution with the C-PCM solvation model. *J. Comput. Chem.* **2003**, *24*, 669-681.

5. Gaussian 16, Revision C.01, Frisch, M. J.; Trucks, G. W.; Schlegel, H. B.; Scuseria, G. E.; Robb, M. A.; Cheeseman, J. R.; Scalmani, G.; Barone, V.; Petersson, G. A.; Nakatsuji, H.; Li, X.; Caricato, M.; Marenich, A. V.; Bloino, J.; Janesko, B. G.; Gomperts, R.; Mennucci, B.; Hratchian, H. P.; Ortiz, J. V.; Izmaylov, A. F.; Sonnenberg, J. L.; Williams-Young, D.; Ding, F.; Lipparini, F.; Egidi, F.; Goings, J.; Peng, B.; Petrone, A.; Henderson, T.; Ranasinghe, D.; Zakrzewski, V. G.; Gao, J.; Rega, N.; Zheng, G.; Liang, W.; Hada, M.; Ehara, M.; Toyota, K.; Fukuda, R.; Hasegawa, J.; Ishida, M.; Nakajima, T.; Honda, Y.; Kitao, O.; Nakai, H.; Vreven, T.; Throssell, K.; Montgomery, J. A., Jr.; Peralta, J. E.; Ogliaro, F.; Bearpark, M. J.; Heyd, J. J.; Brothers, E. N.; Kudin, K. N.; Staroverov, V. N.; Keith, T. A.; Kobayashi, R.; Normand, J.; Raghavachari, K.; Rendell, A. P.; Burant, J. C.; Iyengar, S. S.; Tomasi, J.; Cossi, M.; Millam, J. M.; Klene, M.; Adamo, C.; Cammi, R.; Ochterski, J. W.; Martin, R. L.; Morokuma, K.; Farkas, O.; Foresman, J. B.; Fox, D. J. Gaussian, Inc., Wallingford CT, 2016.

6. Legault, C. Y. (2009) CYLview, 1.0b, Université de Sherbrooke: Sherbrooke, Canada, http://www.cylview.org.

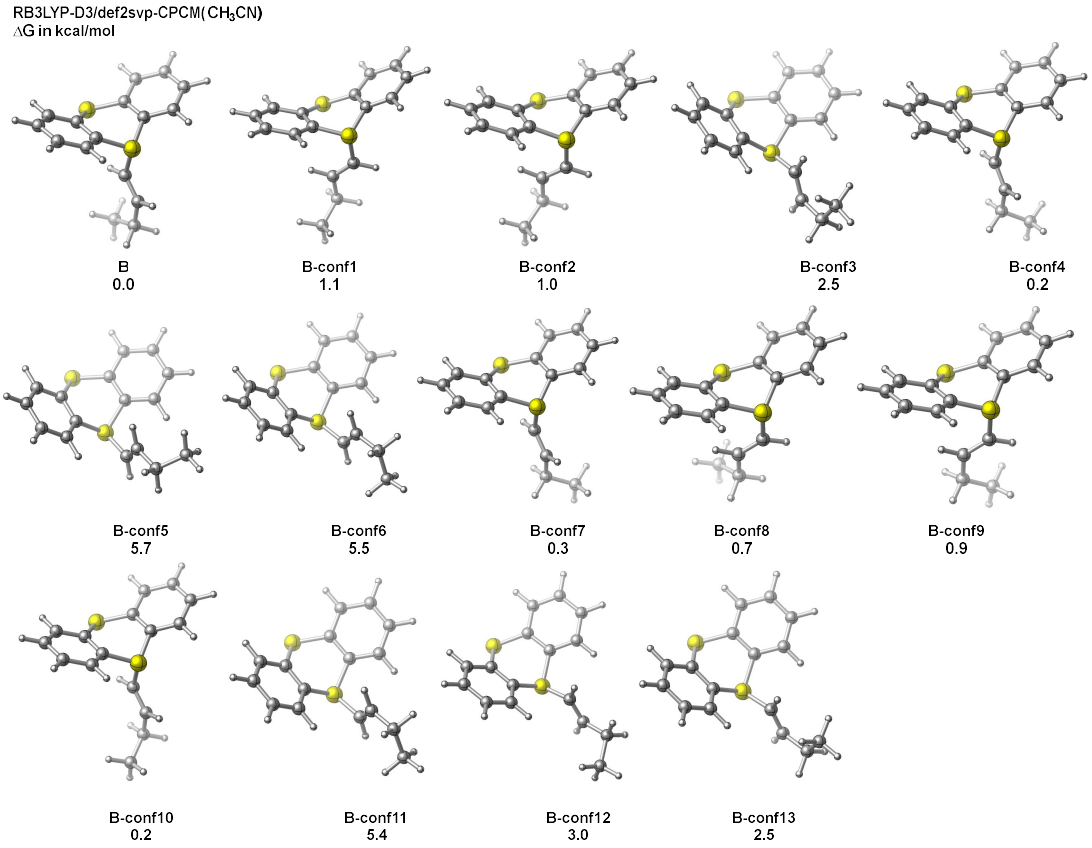

Figure B63. Conformational Analysis of species **3B** in its E configuration at RB3LYP-d3/def2-svp-CPCM(CH_3CN) level of theory. Gibbs free energies are in kcal/mol.

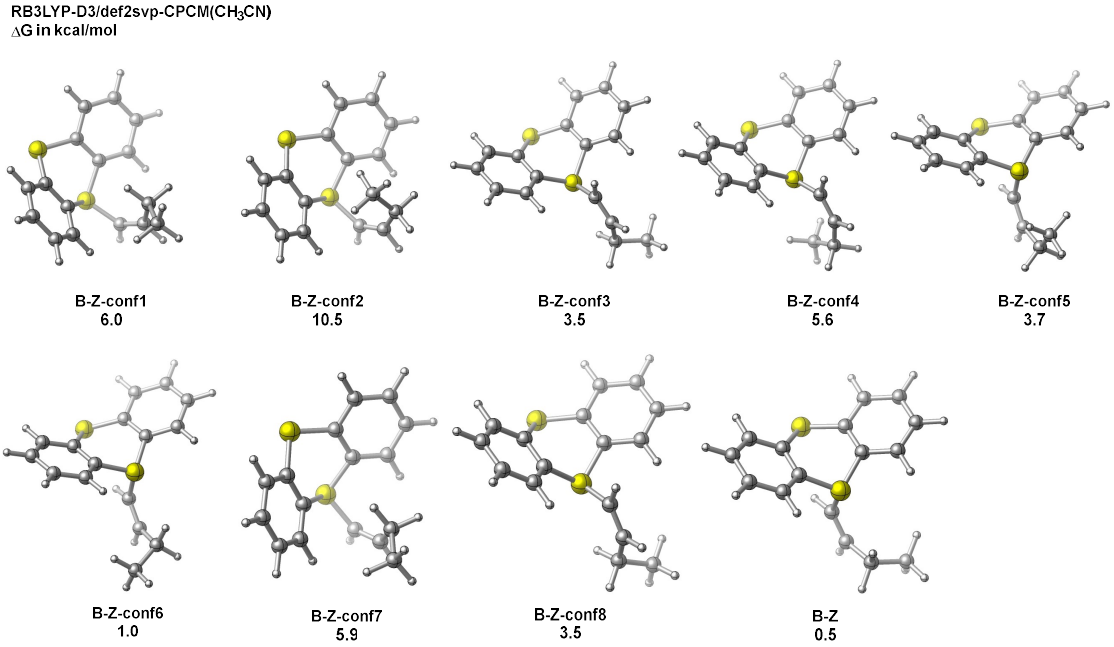

Figure B64. Conformational Analysis of species **3B** in its Z configuration at RB3LYP-d3/def2-svp-CPCM(CH_3CN) level of theory. Gibbs free energies are in kcal/mol.

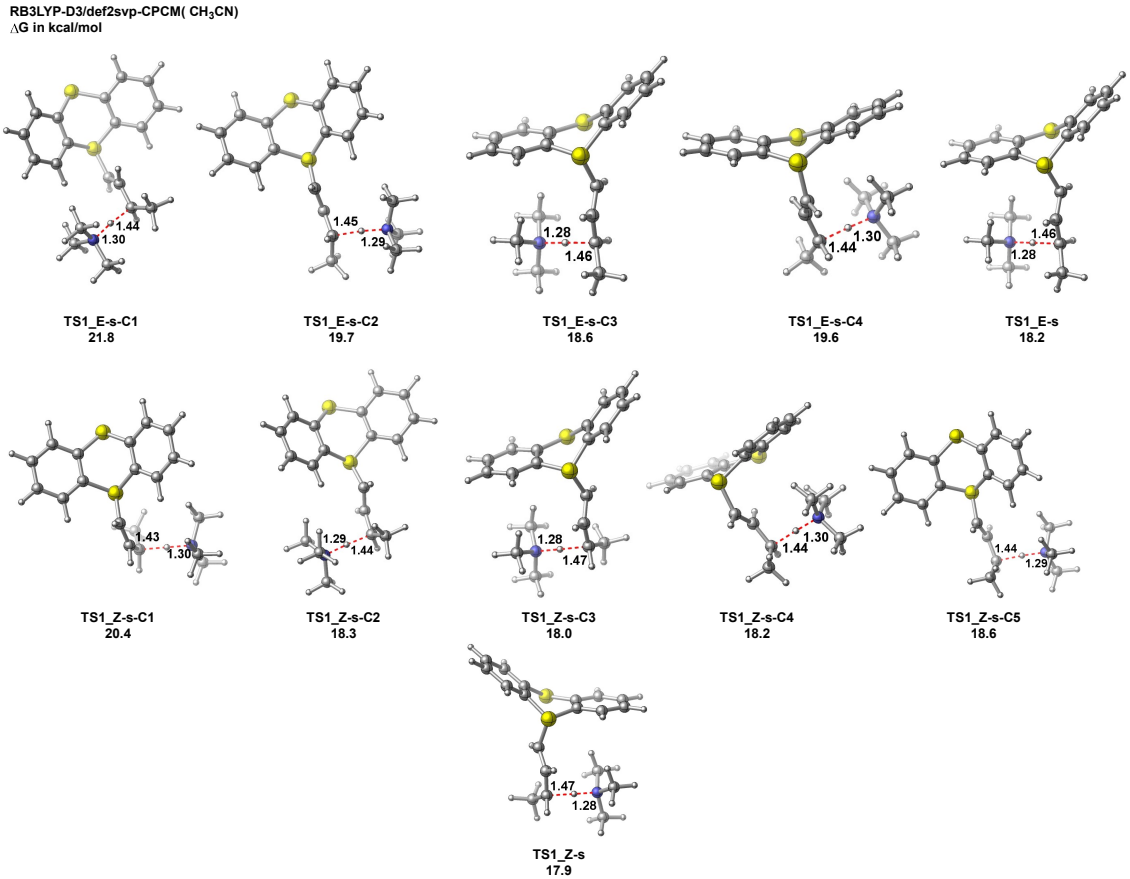

Figure B65. Conformational Analysis of species **TS3-1** leading to E and Z ylides using NMe_3 as the base at RB3LYP-d3/def2-svp-CPCM(CH_3CN) level of theory. Gibbs free energies are in kcal/mol.

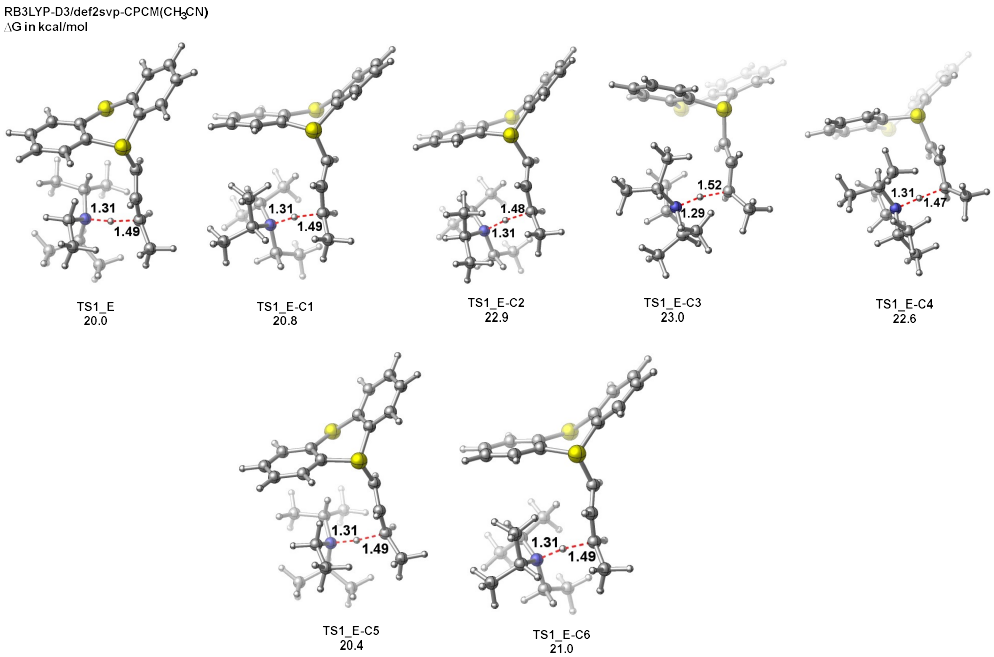

Figure B66. Conformational Analysis of species **TS3-1** leading to E-ylide (Species **3C_E**) using DIPEA as the base at RB3LYP-d3/def2-svp-CPCM(CH_3CN) level of theory. Gibbs free energies are in kcal/mol.

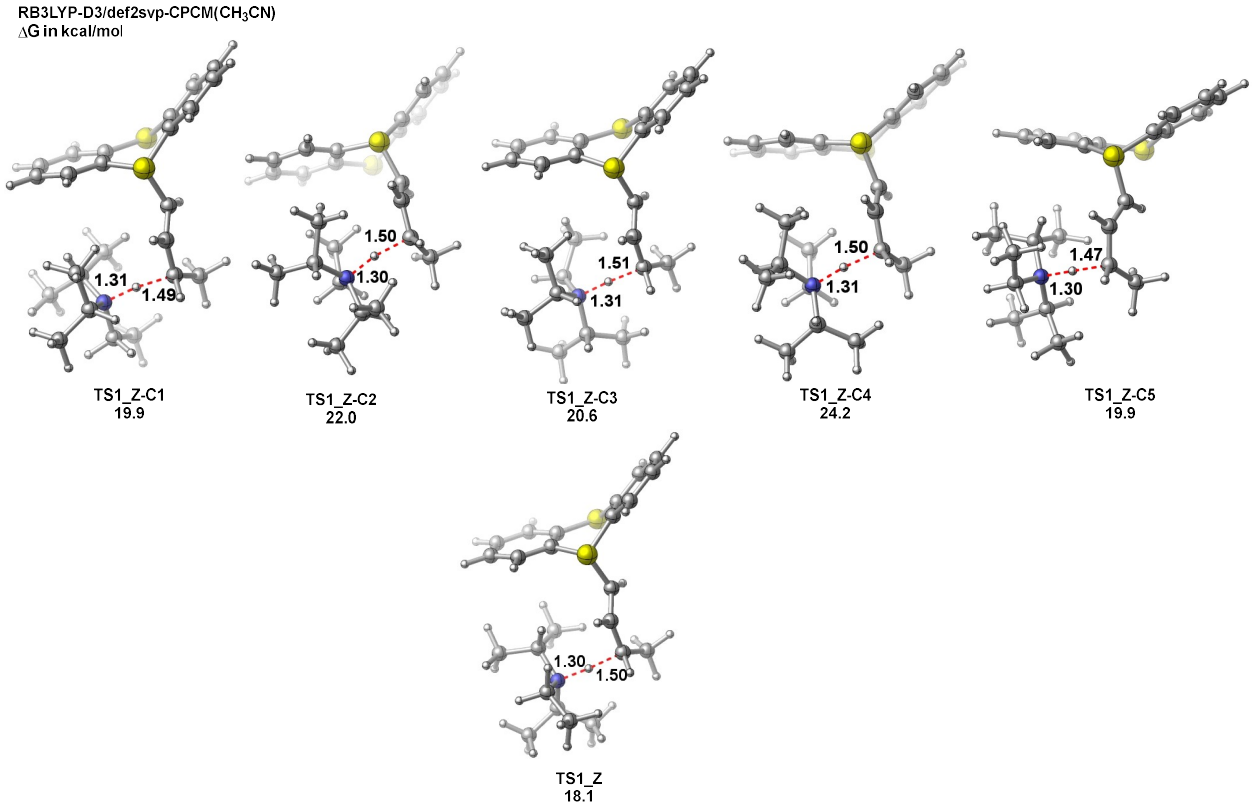

Figure B67. Conformational Analysis of species **TS3-1** leading to Z-ylide (Species **3C_Z**) using DIPEA as the base at RB3LYP-d3/def2-svp-CPCM(CH_3CN) level of theory. Gibbs free energies are in kcal/mol.

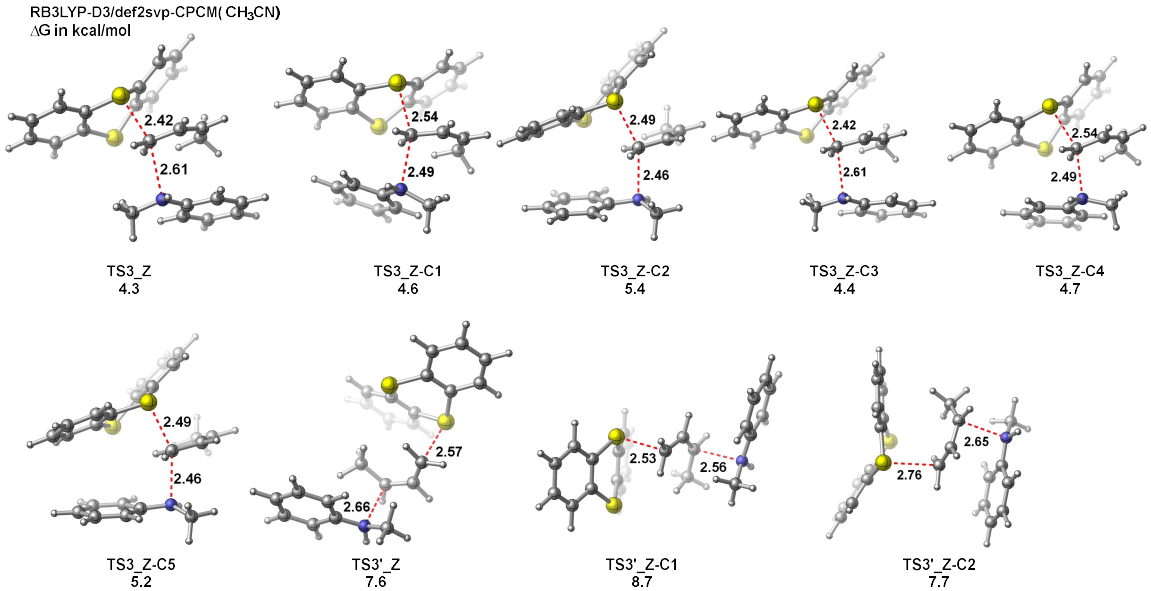

Figure B68. Conformational Analysis of species **TS3-1** and **TS3-1'** leading to S_N2 vs S_N2' product using N-Methyl-aniline as the nucleophile at RB3LYP-d3/def2-svp-CPCM(CH_3CN) level of theory. Gibbs free energies are in kcal/mol.

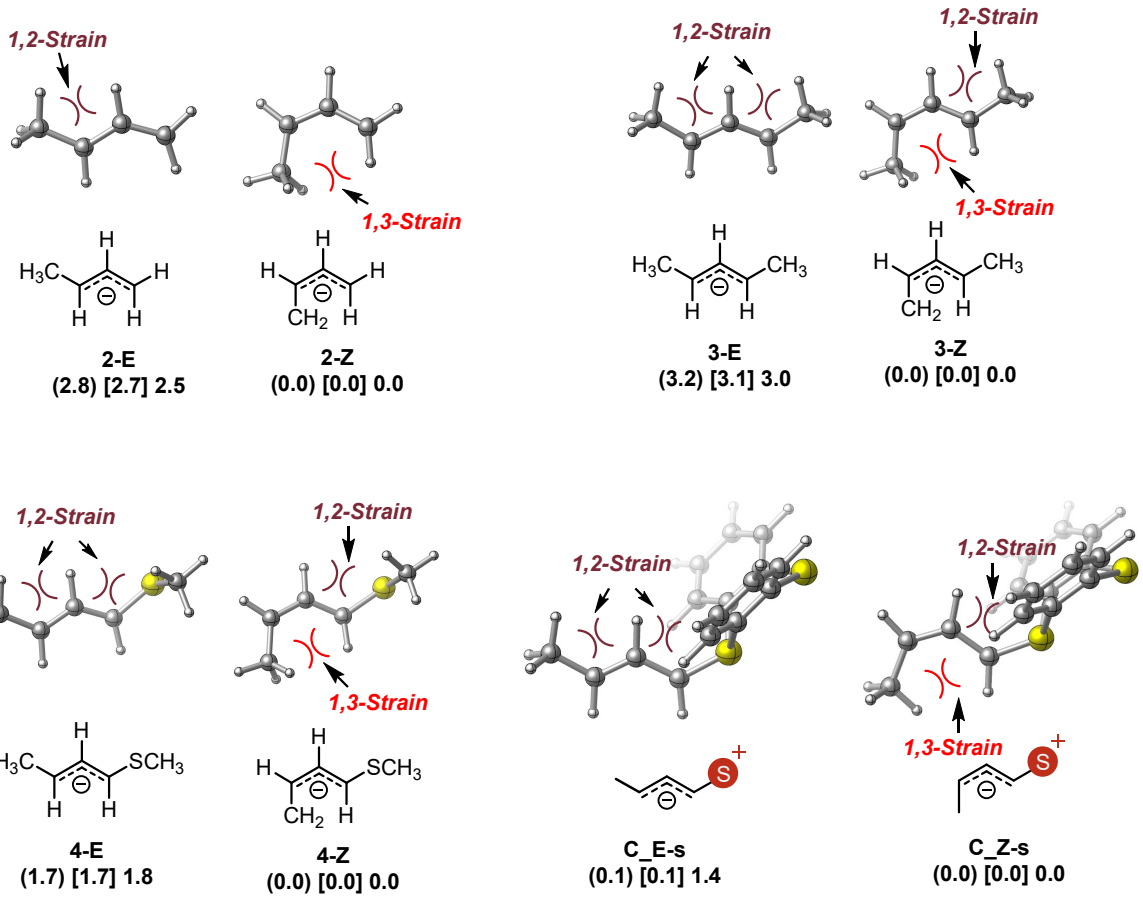

Figure B69. Thermodynamic feasibility analysis of E vs Z ylides of simple carbon systems and systems containing S hetero atoms at RB3LYP-D3/de2tzvpp-CPCM(CH_3CN)//RB3LYP-d3/def2-svp-CPCM(CH_3CN) level of theory. Gibbs free energies are in kcal/mol.

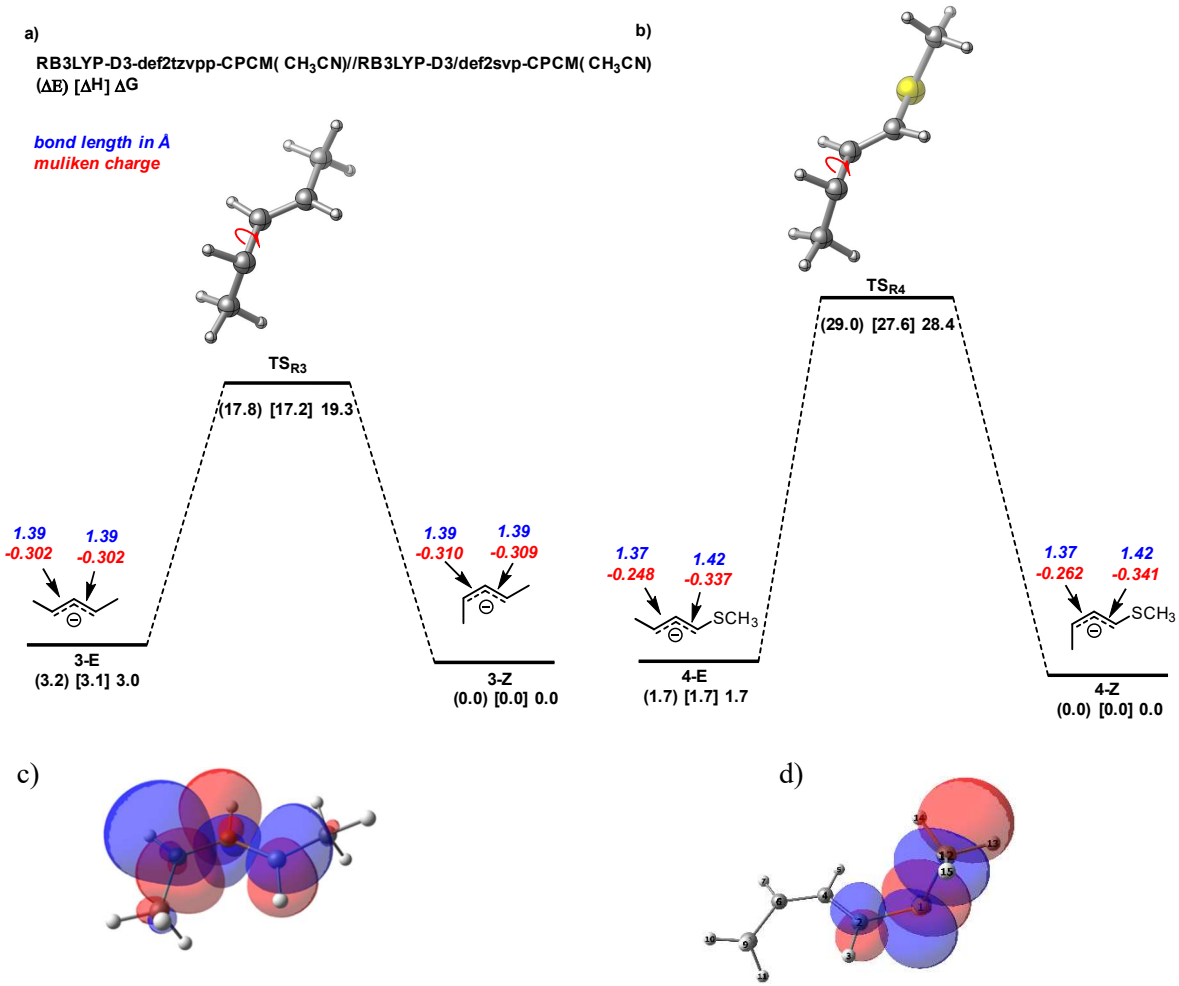

Figure B70. Rotation barrier between E and Z ylides of **a)** Five-membered simple carbon system and **b)** System containing S hetero atom **c)** NBO visualization of the orbitals containing the negative charge for species **3-Z** **d)** NBO visualization of the orbital containing the negative charge for species **4-Z** interacting with the C-S σ^* at RB3LYP-D3/de2tzvpp-CPCM(CH_3CN)//RB3LYP-d3/def2-svp-CPCM(CH_3CN) level of theory. Gibbs free energies are in kcal/mol.

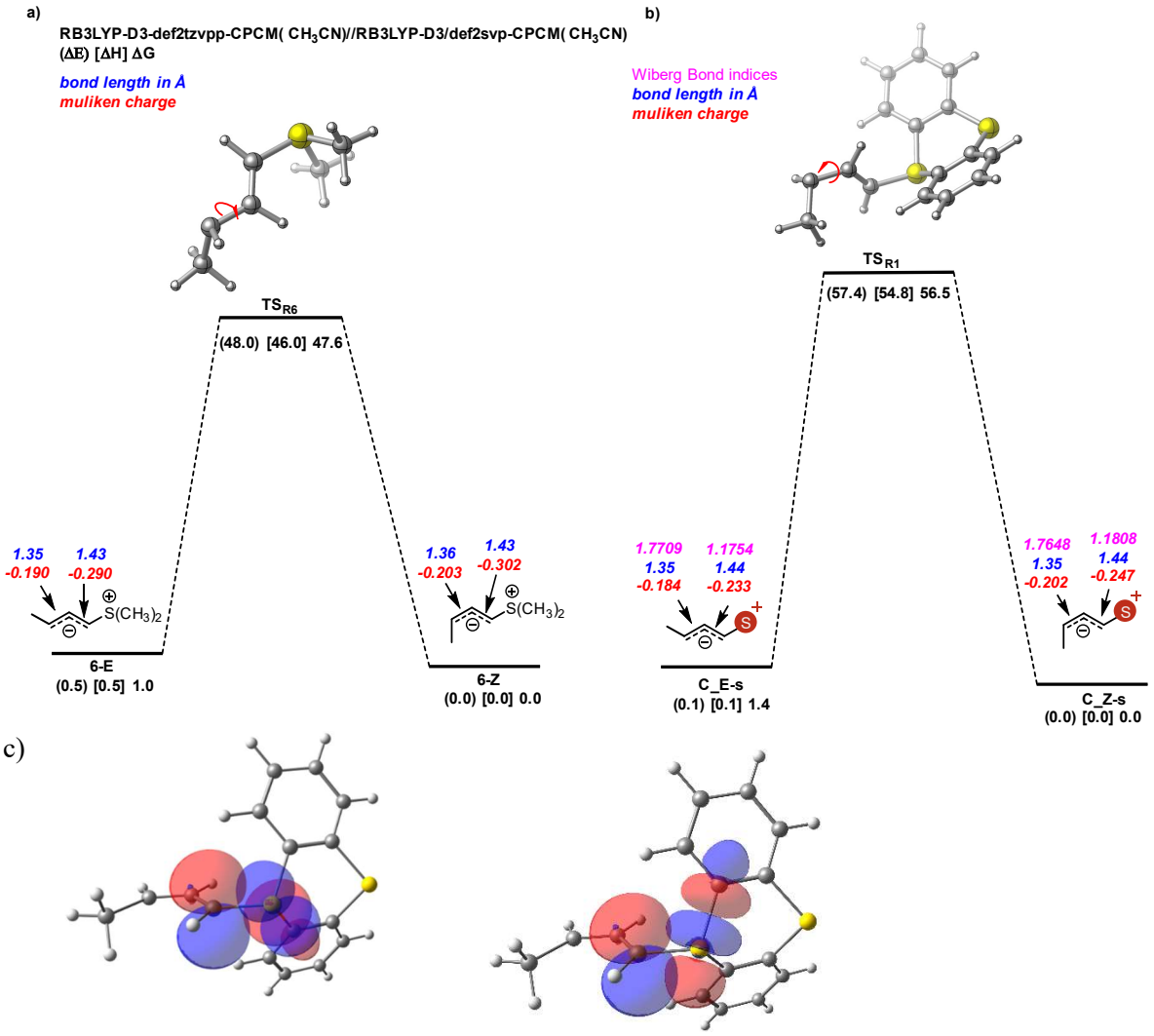

Figure B71. Rotation barrier between E and Z ylides of **a)** Cationic S system and **b)** Thianthrenium system **c)** NBO visualization of the orbital containing the negative charge for species **3C_Z-s** interacting with the C-S σ^* at RB3LYP-D3/de2tzvpp-CPCM(CH_3CN)//RB3LYP-d3/def2-svp-CPCM(CH_3CN) level of theory. Gibbs free energies are in kcal/mol.

RB3LYP-D3/def2svp-CPCM(CH_3CN)
(RB3LYP-D3-def2tzvpp-CPCM(CH_3CN)//RB3LYP-D3/def2svp-CPCM(CH_3CN))
{RB3LYP-D3-6-311+G(d,p)-CPCM(CH_3CN)//RB3LYP-D3/def2svp-CPCM(CH_3CN)}
[RB3LYP-D3-aug-cc-pvtz-CPCM(CH_3CN)//RB3LYP-D3/def2svp-CPCM(CH_3CN)]

ΔG in kcal/mol

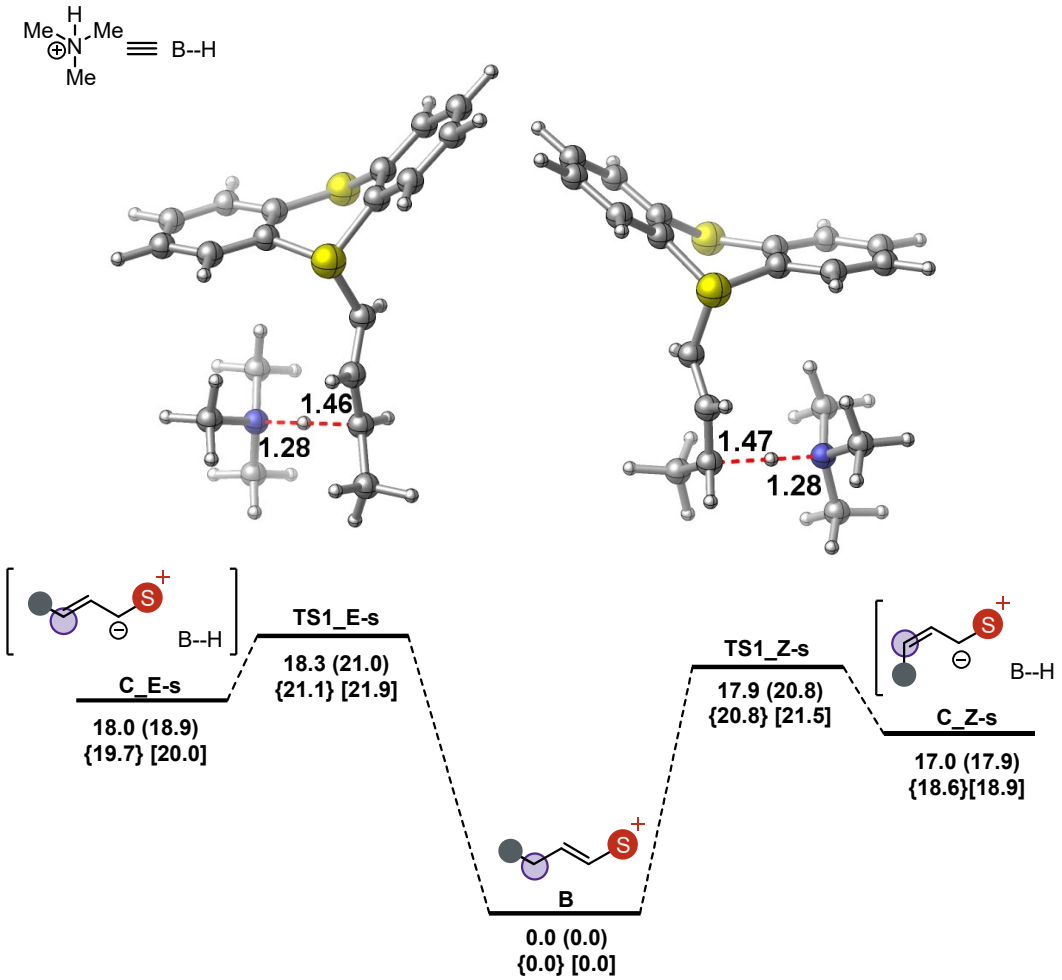

Figure B72. Deprotonation step of species **3B**, leading to E and Z ylide using NMe_3 as the base calculated at different levels of theory. Gibbs free energies are in kcal/mol.

RB3LYP-D3/def2svp-CPCM(CH_3CN)
(RB3LYP-D3-def2tzvpp-CPCM(CH_3CN)//RB3LYP-D3/def2svp-CPCM(CH_3CN))
{RB3LYP-D3-6-311+G(d,p)-CPCM(CH_3CN)//RB3LYP-D3/def2svp-CPCM(CH_3CN)}
[RB3LYP-D3-aug-cc-pvtz-CPCM(CH_3CN)//RB3LYP-D3/def2svp-CPCM(CH_3CN)]

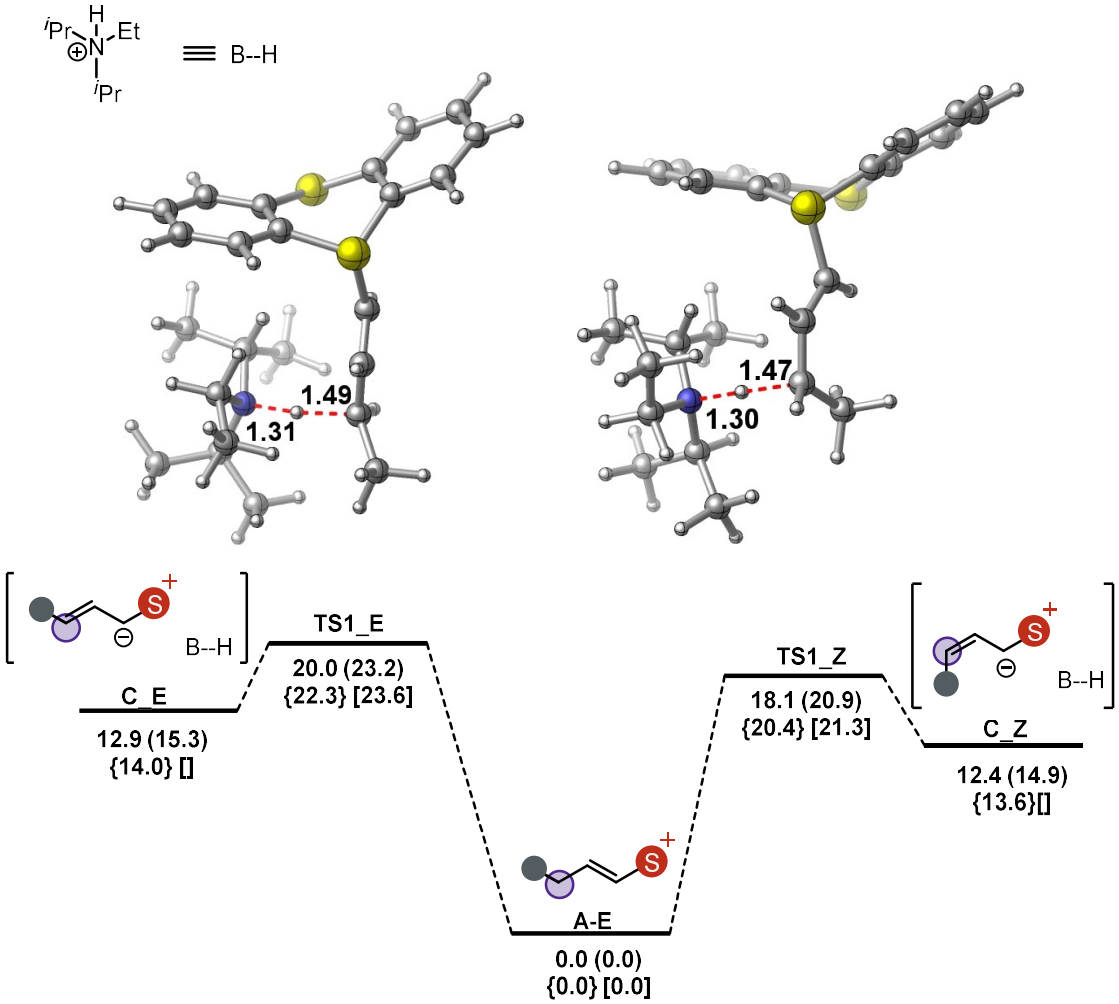

Figure B73. Deprotonation step of species **3B**, leading to E and Z ylide using DIPEA as the base calculated at different levels of theory. Gibbs free energies are in kcal/mol.

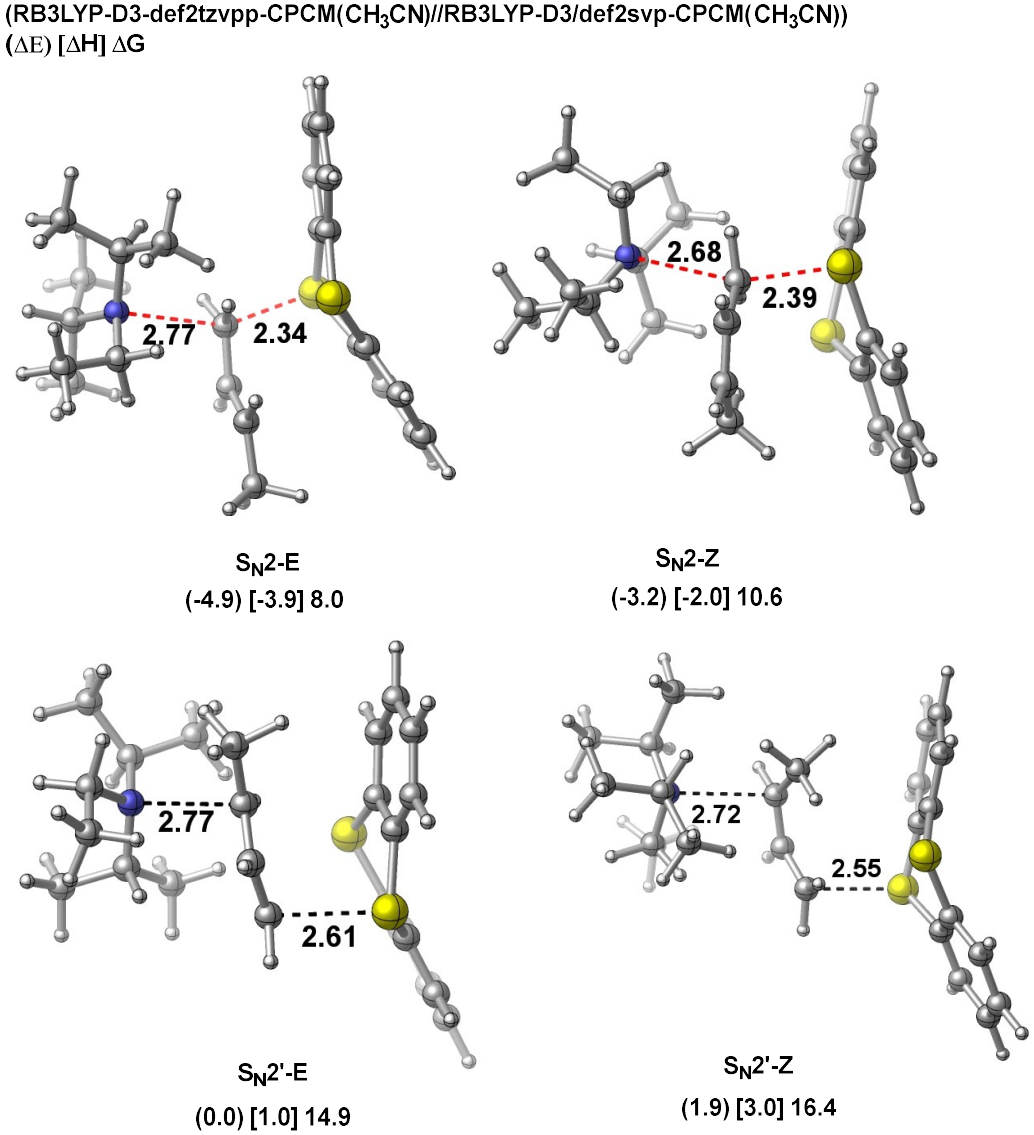

Figure B74. Barriers for S_N2 vs S_N2' using DIPEA as the nucleophile calculated at RB3LYP-D3/def2tzvpp-CPCM(CH_3CN)//RB3LYP-D3/def2svp-CPCM(CH_3CN) level of theory. Gibbs free energies are in kcal/mol.

Appendix C: Supporting Information for Chapter 4 (General *Z*-Selective Allylic Functionalization of Alkenes *via* Thianthrenium Salts)

C1. General Methods and Materials

Unless otherwise noted, reactions were performed under air in an anhydrous solvent. MeCN and *i*-Pr_2NEt were purchased as a sureseal bottle and used as is. KPF_6 was dried under vacuum prior to use. Unless otherwise noted, other commercially-available reagents were used as received. Crude mixtures were evaluated by thin-layer chromatography using EMD/Merck silica gel 60 F254 pre-coated plates (0.25 mm) and were visualized by UV, Seebach, ninhydrin, or KMnO4 staining. Flash chromatography was performed with a Biotage Isolera One automated chromatography system with re-packed silica columns (technical grade silica, pore size 60 Å, 230-400 mesh particle size, 40-63 particle size) or pre-packed Biotage Sfär Silica HC Duo 20µm 25g - High Capacity Column columns unless otherwise noted. Purified materials were dried in vacuo (0.050 Torr) to remove trace solvent. ^1H, ^{13}C, ^{19}F Spectra were taken using a Bruker Avance-400 with a BBFO Probe, a Bruker Avance-500 with a DCH Cryoprobe, or Bruker Avance III HD-500 with a TXO Cryoprobe. NMR data are reported relative to residual $CHCl_3$ (^1H, δ = 7.26 ppm), $CDCl_3$ (^{13}C, δ = 77.16 ppm) or residual CHD_2CN (^1H, δ = 1.96 ppm), CD_3CN (^{13}C, δ = 118.26 ppm). Data for ^1H NMR spectra are reported as follows: chemical shift (δ ppm) (multiplicity, coupling constant (Hz), integration). Multiplicity and qualifier abbreviations are as follows: s = singlet, d = doublet, t = triplet, q = quartet, m = multiplet, br = broad. All NMR yields were determined via reference against an internal standard (dibromomethane or mesitylene for ^1H). Mass spectrometry data was collected on a Thermo Scientific Q Exactive Plus Mass Spectrometer.

Abbreviations: Ac—acyl, Bn—benzyl, Boc—tert-butyl carbamate, *t*-Bu—tert-butyl, Cy—cyclohexyl, DCM—dichloromethane, DIPEA—*N,N*-Diisopropylethylamine, DMAP—4-dimethylaminopyridine, DMF—dimethyl formamide, EtOAc—ethyl acetate, *i*-Pr—isopropyl, Me—methyl, MeCN—acetonitrile, MeOH—methanol, Ms—mesyl, *n*-Pr—propyl, NPhth—phthalimido, Ns—nosyl, RVC—reticulated vitreous carbon, Ph—phenyl, TEA—triethylamine, Tf—triflyl, TFA—trifluoroacetic acid, Ts—tosyl.

Preparation of Sulfonamide Nucleophiles

If not commercially available, the *N*-alkyl and *N*-aryl sulfonamides used in this study were prepared according to literature procedures using either (1) the corresponding sulfonyl chloride and amine, or (2) alkylation of the NH_2 sulfonamide by the corresponding halide. The resultant sulfonamides were purified via flash column chromatography to yield the desired product. All ^1H NMR were consistent with reported spectra for the isolated compounds.

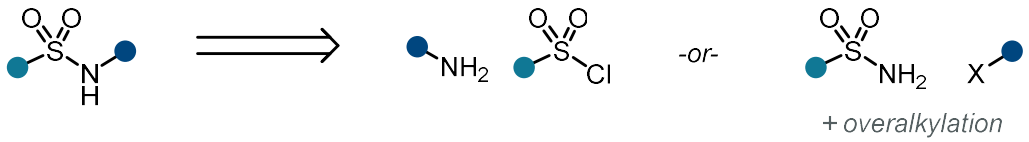

Figure C1. Sulfonamides were prepared using two synthetic strategies.

N-boc sulfonamides were prepared from the NH_2 sulfonamide and Boc_2O. Upon completion of the reaction mixture, the heterogeneous solution was filtered, and the collected solids were dried *in vacuo* to afford the desired compound in >95% mass purity. The most common impurity for this procedure was the di-Boc-protected sulfonamide. *Alternative purification:* a column can be performed to obtain >95% purity sulfonamide. All ^{1}H NMR were consistent with reported spectra for the isolated compounds.

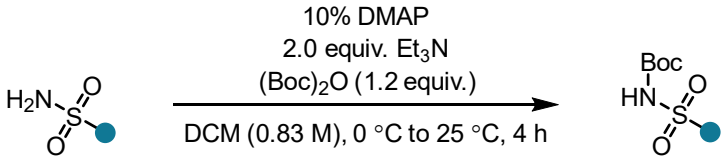

Figure C2. Preparation of *N*-boc sulfonamides.

N-triflyl sulfonamides were prepared according to literature procedures. See *J. Am. Chem. Soc.* **2018**, 140, 3202–3205. All ^{1}H NMR were consistent with reported spectra for the isolated compounds.

Electrochemical Methods and Materials

All chronoamperometric and chronopotentiometric measurements were performed at room temperature using a Pine WaveNowXV. Chronoamperometric and chronopotentiometric measurements were carried out in divided cells with RVC (8 × 6 × 6 mm, Ultramet, 80 ppi) as working electrodes affixed to a graphite pencil/silver wire assembly and with nickel foam (1.4 mm x 1.4 mm, MTI Corporation, Surface density: 350g/m^2) as counter electrodes affixed to stainless steel wire (see below). The potentials were measured versus an $Ag/AgNO_3$ (0.01 M in MeCN with 0.1 M n-Bu_4N•PF_6) reference electrode (all electrodes from Pine Research) and externally referenced via the ferrocene/ferrocenium couple. Bulk constant current electrolysis experiments were driven with a Dr. Meter HY3005M-L DC Power Supply or a custom–made low current power supply (see Scheme below) which was externally calibrated with a multimeter using a 10 or 1–Ohm resistor.

Figure C3. Divided cell with electrodes.

Divided cells were fabricated in-house. Glass frit purchased from Ace Glass (7176-36). Anode electrode assembled via affixing end of the silver wire (Belden Hook-Up wire, item no. 83005 007100) around the pencil (JuneGold 2B graphite 2 mm) using conductive graphite adhesive (Alfa Aesar, 42465), wrapping in teflon tape to prevent exposure, then piercing RVC with pencil. Solvent exposed electrode surface area (2.1 cm^2) was calculated via manufacturer-supplied surface area/volume ratio measurements. PTFE tubing (Cole-Parmer; 1/32" ID, 1/16" OD, item number EW-06407-41) connects both sides of the divided cell to normalize pressure. Septa inner diameter 16 mm. Stainless steel purchased from Grainger; stainless steel lockwire, 0.025" diameter, item number 16Y043.

Low-current Power Supply: Original design and fabrication by Dr. Blaise J. Thompson. Provides an operational range of ±0.01– 14.99 mA, tunable by variable resistor, delivering power to banana socket pair. The power supply is limited to ±15 V for bulk electrolysis and is powered by an 18 V wall wart. Circuitry is housed within an aluminum enclosure. For additional specifications, see: *J. Am. Chem. Soc.* **2020** 142, 2093–2099 and *Nature* **2021** 596, 74–79.

General Procedure for Allylic Functionalization of Alkenes via Electrochemical Thianthrenation

To an oven-dried divided electrochemical cell equipped with magnetic stir bars was added thianthrene (64.9 mg, 0.3 mmol, 3.0 equiv) to the anode compartment and KPF_6 (110 mg, 0.6 mmol) to both compartments. The cell was equipped with two septa containing a stainless steel wire/Ni foam cathode assembly and a pencil/RVC anode assembly connected together with a teflon tubing to equalize pressure. MeCN (2 mL) was added to the cathode and anode compartments. Alkene (0.2 mmol, 2.0 equiv) was added to the anode compartment. Trifluoroacetic acid (153 μL, 2.0 mmol, 20.0 equiv) was added to the cathode compartment and both sides of the cell were stirred at 30 ˚C and electrolyzed under a constant current of 6.0 mA (5.8 mA/cm^2) for 2.2 h (2.5 F/mol alkene). At completion of electrolysis, the electrode leads were disconnected, septa removed, and the anode RVC was pushed off the pencil into the reaction mixture. Dibromomethane was added as an internal standard to the anodic compartment. The solution was thoroughly stirred, and 50 μL of mixture was added to an NMR tube and diluted with MeCN-*d3*.

The cathode solution was removed from the cell via pipette. The anode solution was filtered over a pad of basic alumina (4 g, activated, basic, Brockmann I). The cathode compartment was washed with MeCN (2 mL) and pushed across the frit to rinse the frit. The anode compartment was further washed with MeCN (5 x 1 mL). The alumina pad was washed with MeCN (2 x 8 mL), taking care to fully disperse the alumina in solution using a spatula. The filtrate was concentrated in vacuo and then resuspended in MeCN (0.33 mL). Mesitylene was added as an internal standard to the resultant alkenylthianthrenium solution. The solution was thoroughly stirred, and 10 μL of mixture was added to an NMR tube and diluted with $CDCl_3$. Nucleophile (0.10 mmol, 1equiv.) was added to the reaction mixture followed by the (*i*-Pr)(*t*-Bu)NMe base (101 μL, 0.600 mmol, 6.0 equiv.). The solution was stirred for 3 h.

For NMR analyses – Reactions carried out using the above protocol were analyzed by ^1H NMR spectroscopy. NMR samples were prepared by diluting an aliquot of the reaction mixture in $CDCl_3$ and the allylic product yield were determined *via* ^1H NMR using mesitylene as an internal standard.

Preparation of Alkenylthianthrenium Salts

Alkenylthianthrenium salts were prepared by either (1) deoxygenative activation of thianthrene S-oxide, or (2) anodic oxidation of thianthrene in the presence of the corresponding alkene. See (1) *Angewandte Chemie International Edition* **2020**, 59, 5616–5620, and (2) *Nature* **2021**, 596, 74–79. Upon reaction completion, KPF_6 was used to prepare the alkenylthianthrenium PF_6 salts. The resultant alkenylthianthrenium salts were

purified either by flash column chromatography (DCM/3:1 EtOAc:EtOH) or dilution in a minimum amount of DCM followed by precipitation with EtOAc. All ^{1}H NMR were consistent with reported spectra for the isolated compounds. Purity of alkenylthianthrenium salts were verified using ^{1}H NMR and ^{19}F NMR spectroscopy.

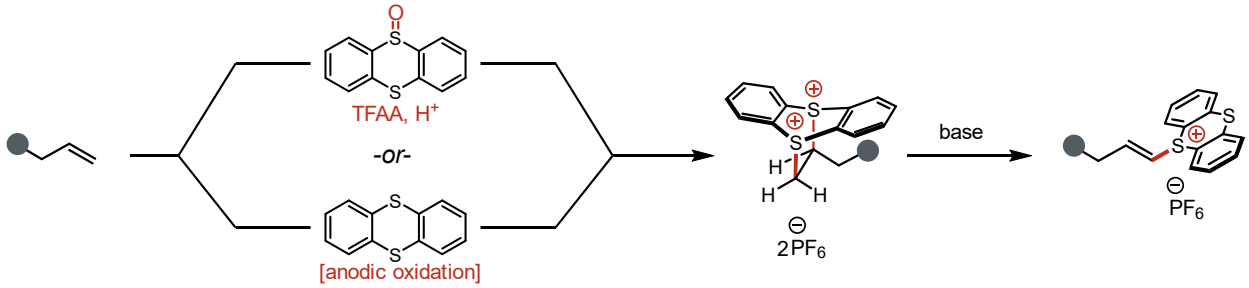

Figure C4. Preparation of isolated alkenylthianthrenium salts used in this study.

General Procedure for Allylic Functionalization of Alkenylthianthrenium Salts

To a threaded vial equipped with a magnetic stir bar was added alkenylthianthrenium salt (0.05 mmol, 1.0 equiv.) and MeCN (0.5 mL). Then the nucleophile (0.05 mmol, 1.5 equiv.) followed by either Cs_2CO_3 (49 mg, 0.15 mmol, 3.0 equiv.) or trialkylamine base (specified equiv. via microsyringe) were added. For investigation of the allylic functionalization with improved Z-selectivity, nucleophile was either added by slow addition using a syringe pump or by salt metathesis with KPF_6 (28 mg, 0.15 mmol, 3.0 equiv.). The reaction mixture was capped with a PTFE seal and stirred at room temperature until completion of the reaction (3 to 6 hours).

For NMR analyses – Reactions carried out using the above protocol were analyzed by ^{1}H NMR spectroscopy. NMR samples were prepared by diluting an aliquot of the reaction mixture in $CDCl_3$ and the allylic product yield and *Z:E* were determined *via* ^{1}H NMR using CH_2Br_2 as an external standard.

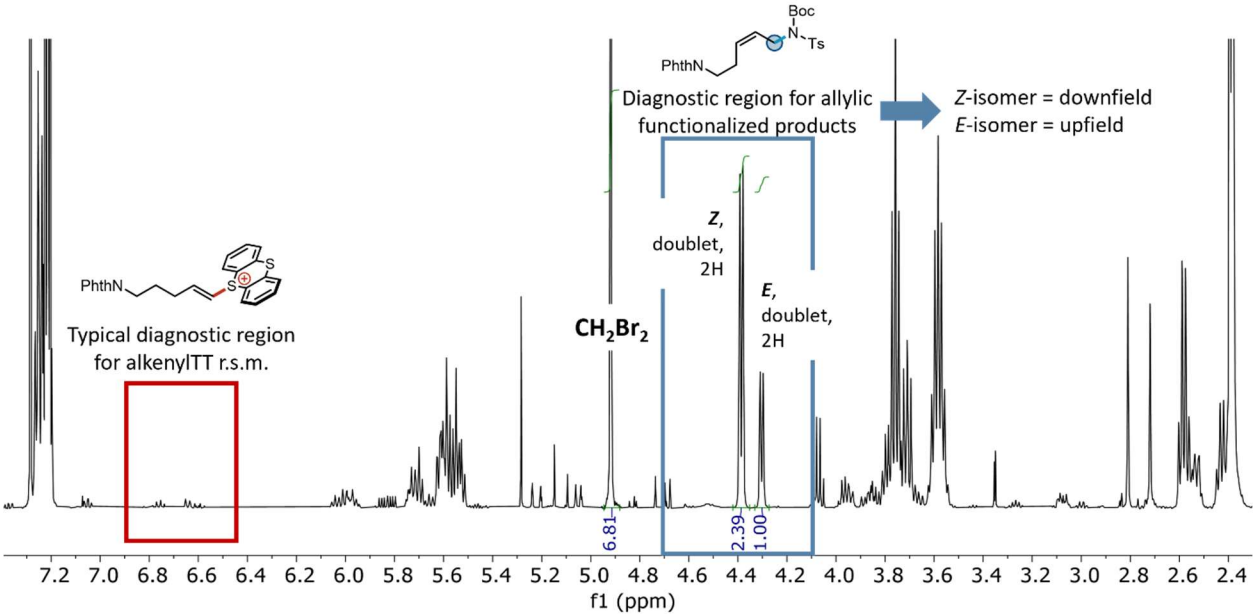

Figure C5. Example of ^{1}H NMR spectrum collected for allylic functionalization of alkene-derived thianthrenium salts. CH_2Br_2 (5.10 ppm, s, 2H) or mesitylene (6.82 ppm, s, 3H) was used as a ^{1}H NMR standard. r.s.m. = recovered starting material.

C2. Trialkylamine Base Concentration Impact on *Z*-selectivity

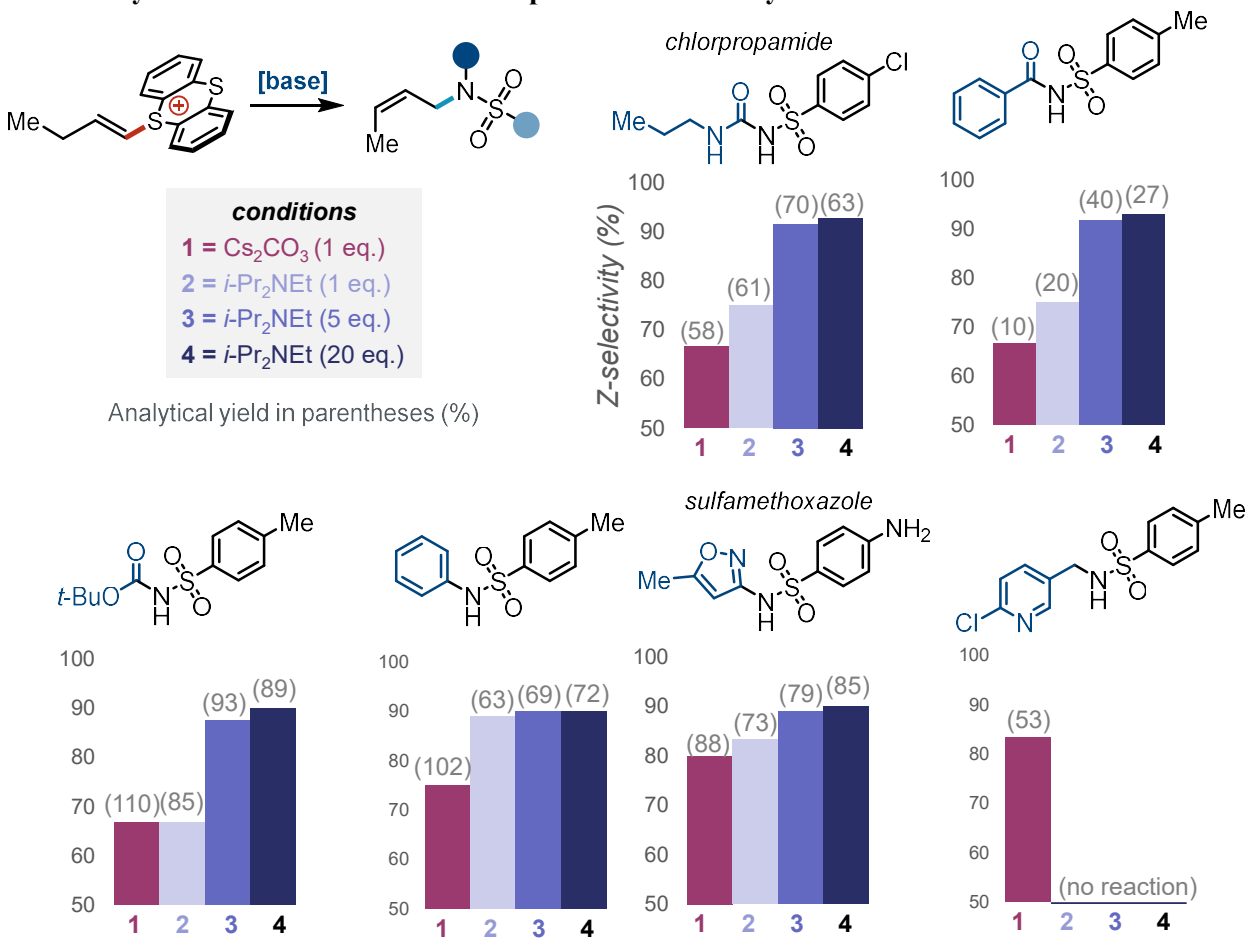

Figure C6. Higher Z-selectivity with acidic sulfonamide nucleophiles could be achieved by increasing the *i*-Pr$_2$NEt loading; however, selectivity remained modest, and yields were often diminished compared to when using carbonate base.

Appendix D: Supporting Information for Chapter 5 (Catalytic Base Enabled 1,2-Addition of *N*-Nucleophiles into Alkenylthianthrenium Salts)

D1. General Methods and Materials

Unless otherwise noted, reactions were performed under air in an anhydrous solvent. MeCN and *i*-Pr_2NEt were purchased as a sureseal bottle and used as is. KPF_6 was dried under vacuum prior to use. Unless otherwise noted, other commercially-available reagents were used as received. Crude mixtures were evaluated by thin-layer chromatography using EMD/Merck silica gel 60 F254 pre-coated plates (0.25 mm) and were visualized by UV, Seebach, ninhydrin, or KMnO4 staining. Flash chromatography was performed with a Biotage Isolera One automated chromatography system with re-packed silica columns (technical grade silica, pore size 60 Å, 230-400 mesh particle size, 40-63 particle size) or pre-packed Biotage Sfär Silica HC Duo 20µm 25g - High Capacity Column columns unless otherwise noted. Purified materials were dried in vacuo (0.050 Torr) to remove trace solvent. ^1H, ^{13}C, ^{19}F Spectra were taken using a Bruker Avance-400 with a BBFO Probe, a Bruker Avance-500 with a DCH Cryoprobe, or Bruker Avance III HD-500 with a TXO Cryoprobe. NMR data are reported relative to residual $CHCl_3$ (^1H, δ = 7.26 ppm), $CDCl_3$ (^{13}C, δ = 77.16 ppm) or residual CHD_2CN (^1H, δ = 1.96 ppm), CD_3CN (^{13}C, δ = 118.26 ppm). Data for ^1H NMR spectra are reported as follows: chemical shift (δ ppm) (multiplicity, coupling constant (Hz), integration). Multiplicity and qualifier abbreviations are as follows: s = singlet, d = doublet, t = triplet, q = quartet, m = multiplet, br = broad. All NMR yields were determined via reference against an internal standard (dibromomethane or mesitylene for ^1H). Mass spectrometry data was collected on a Thermo Scientific Q Exactive Plus Mass Spectrometer.

Abbreviations: Bn—benzyl, Boc—tert-butyl carbamate, *t*-Bu—tert-butyl, Cy—cyclohexyl, DCM—dichloromethane, DIPEA—*N,N*-Diisopropylethylamine, DMF—dimethyl formamide, EtOAc—ethyl acetate, *i*-Pr—isopropyl, Me—methyl, MeCN—acetonitrile, MeOH—methanol, Ns—nosyl, RVC—reticulated vitreous carbon, Ph—phenyl, TBA—tetrabutylammonium, TEA—triethylamine, TFA—trifluoroacetic acid, Ts—tosyl.

Preparation of Alkenylthianthrenium Salts

Alkenylthianthrenium salts were prepared by either (1) deoxygenative activation of thianthrene S-oxide, or (2) anodic oxidation of thianthrene in the presence of the corresponding alkene. See (1) *Angewandte Chemie International Edition* **2020**, 59, 5616–5620, and (2) *Nature* **2021**, 596, 74–79. Upon reaction completion, KPF_6 was used to prepare the alkenylthianthrenium PF_6 salts. The resultant alkenylthianthrenium salts were purified either by flash column chromatography (DCM/3:1 EtOAc:EtOH) or dilution in a minimum amount of DCM followed by precipitation with EtOAc. All ^1H NMR were consistent with reported spectra for the isolated compounds. Purity of alkenylthianthrenium salts were verified using ^1H NMR and ^{19}F NMR spectroscopy.

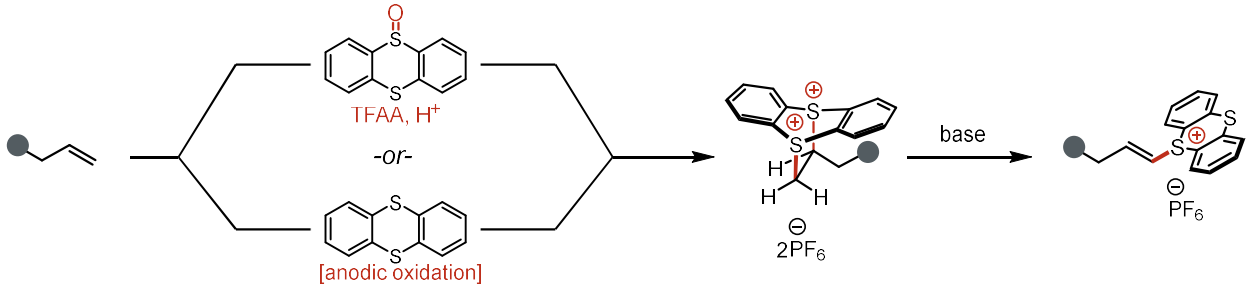

Figure D1. Preparation of isolated alkenylthianthrenium salts.

D2. Studies with Sulfonamide Nucleophiles

Preparation of Sulfonamide Nucleophiles

If not commercially available, the *N*-alkyl and *N*-aryl sulfonamides used in this study were prepared according to literature procedures using either (1) the corresponding sulfonyl chloride and amine, or (2) alkylation of the NH_2 sulfonamide by the corresponding halide. The resultant sulfonamides were purified via flash column chromatography to yield the desired product. All ^{1}H NMR were consistent with reported spectra for the isolated compounds.

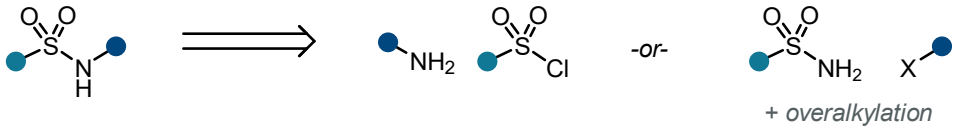

Figure D2. Sulfonamides were prepared using two synthetic strategies.

General Procedure for the Formation of *N*-sulfonamide-substituted Alkylthianthrenium Salts

To threaded vial equipped with a magnetic stir bar was added alkenylthianthrenium salt (0.05 mmol, 1.0 equiv.), sulfonamide (0.05 mmol, 1.0 equiv.) and cesium carbonate (1.0 mg, 0.0025 mmol, 0.05 equiv.) or proton sponge (10.7 mg, 0.05 mmol, 1.0 equiv.). MeCN (0.1 mL) was added and the reaction mixture was capped with a PTFE seal and stirred at room temperature until completion of the reaction (3 hours).

For NMR analyses – Reactions carried out using the above protocol were analyzed by ^{1}H NMR spectroscopy. NMR samples were prepared by diluting an aliquot of the reaction mixture in $CDCl_3$ and the sulfonamidoalkylthianthrenium product yield was determined *via* ^{1}H NMR using CH_2Br_2 as an external standard.

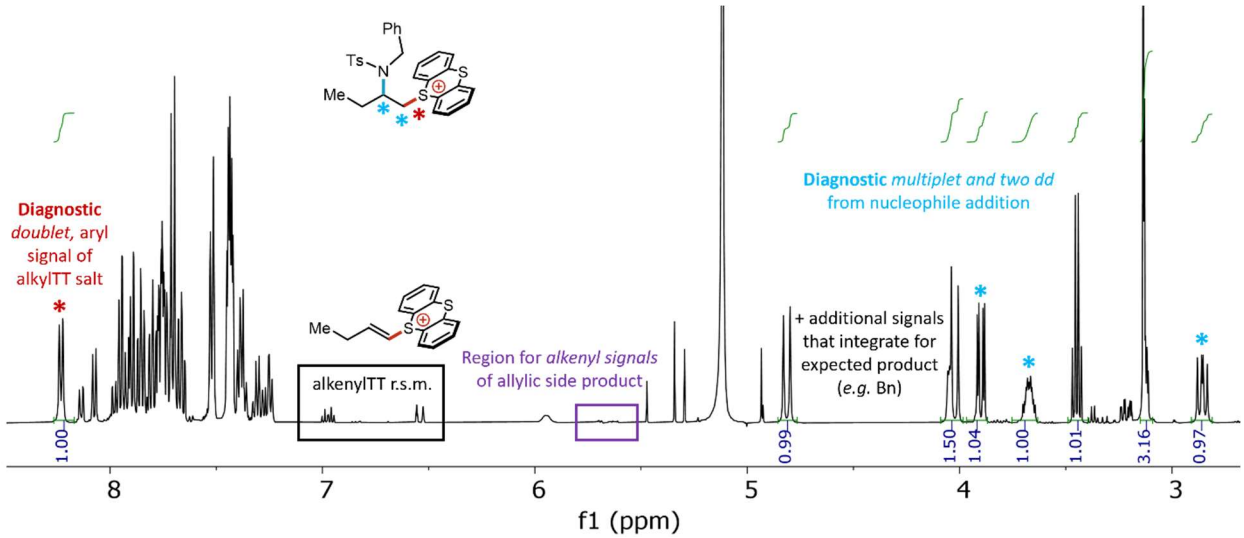

Figure D3. Representative ^{1}H NMR spectrum of crude reaction for NMR analyses of 1,2 sulfonamidosulfonium salt formation. CH_2Br_2 (5.10 ppm, s, 2H) was used as an external ^{1}H NMR standard. r.s.m. = recovered starting material.

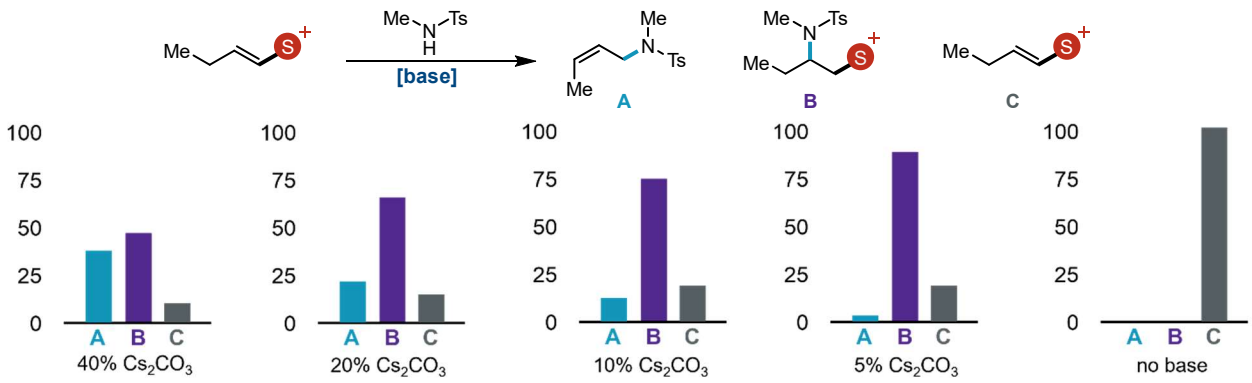

Figure D4. Catalytic base optimization for selective conjugate-type addition of sulfonamides into alkenylthianthrenium salts.

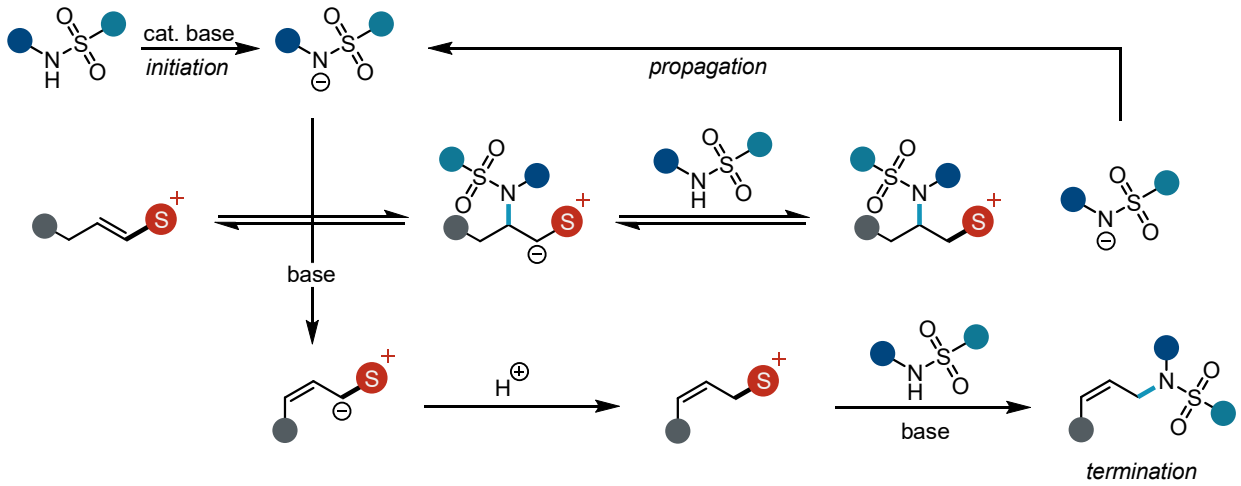

Figure D5. The proposed mechanism for catalytic base enabled 1,2-addition of sulfonamides into alkenylthianthrenium salts. Allylic functionalization pathway is ordered in base while conjugate-type addition is not. Selective addition of sulfonamides into alkenylthianthrenium salts can be achieved by considering optimal proton balance.

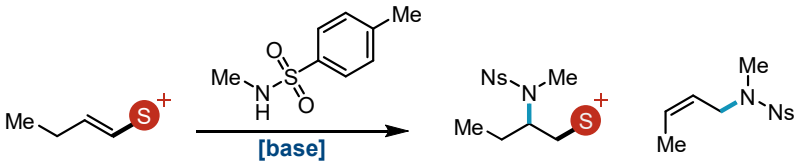

Cs_2CO_3 (5 mol %):	49%	11%
proton-sponge (1 equiv.):	46%	0%

Figure D6. Stoichiometric proton-sponge base for acidic sulfonamides minimizes allylic pathways.

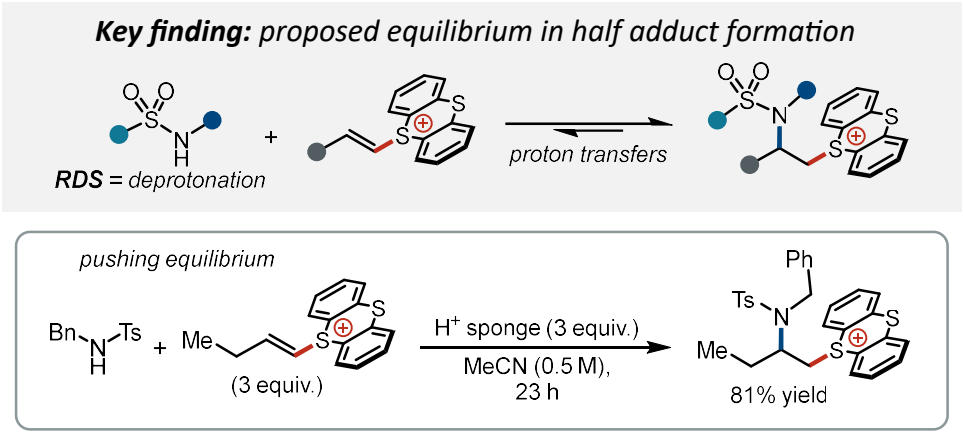

Figure D7. Equilibrium optimization of 1,2-sulfonamidosulfonium salt formation.

D3. Studies with Azole Nucleophiles

General Procedure for the Formation of *N*-heterocycle-substituted Alkylthianthrenium Salts

Experimental procedure: To threaded vial equipped with a magnetic stir bar was added alkenylthianthrenium salt (0.10 mmol, 1.0 equiv.), *N*-heterocycle nucleophile (0.10 mmol, 1.0 equiv.) and cesium carbonate (3.3 mg, 0.01 mmol, 0.1 equiv.). MeCN (2 mL) was added and the reaction mixture was capped with a PTFE seal and stirred at room temperature until completion of the reaction (3 hours).

For NMR analyses – Reactions carried out using the above protocol were analyzed by ^{1}H NMR spectroscopy. NMR samples were prepared by diluting an aliquot of the reaction in CD_3CN and the *N*-alkylated azole product yield and *N*-regioselectivity (by ^{19}F NMR if applicable) were determined *via* ^{1}H NMR using CH_2Br_2 as an external standard.

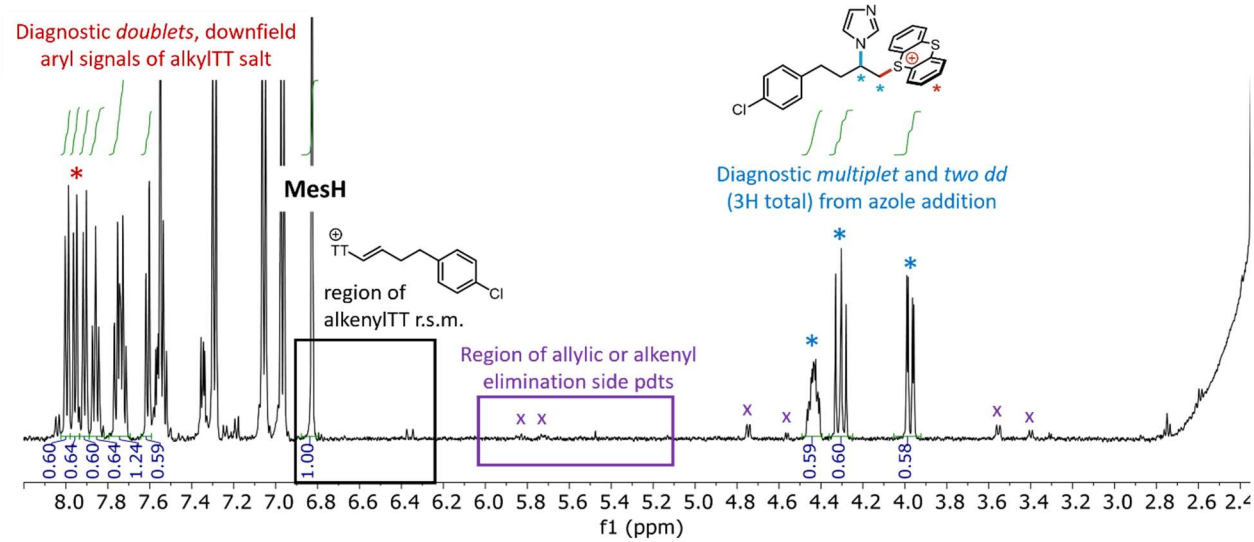

Figure D8. Representative ^{1}H NMR spectrum of crude reaction for NMR analyses of 1,2-azolosulfonium salt formation. CH_2Br_2 (5.10 ppm, s, 2H) or mesitylene (6.82 ppm, s, 3H) was used as an external ^{1}H NMR standard. r.s.m. = recovered starting material.

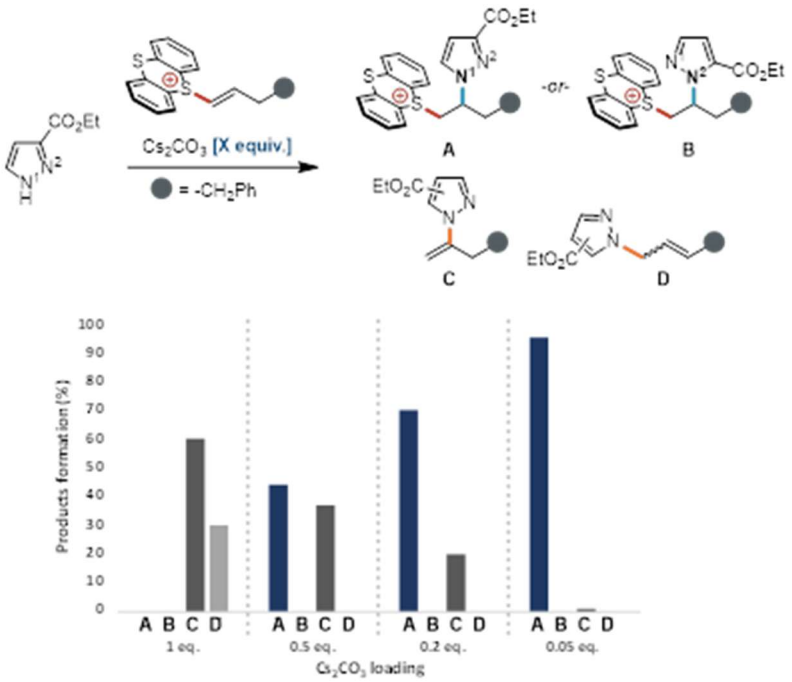

Figure D9. Optimization of catalytic base loading for asymmetric azole nucleophiles. Lower base loadings minimize base-induced elimination pathways such as allylic functionalization and azole vinylation (from deprotonation of 1,2-azolosulfonium product).

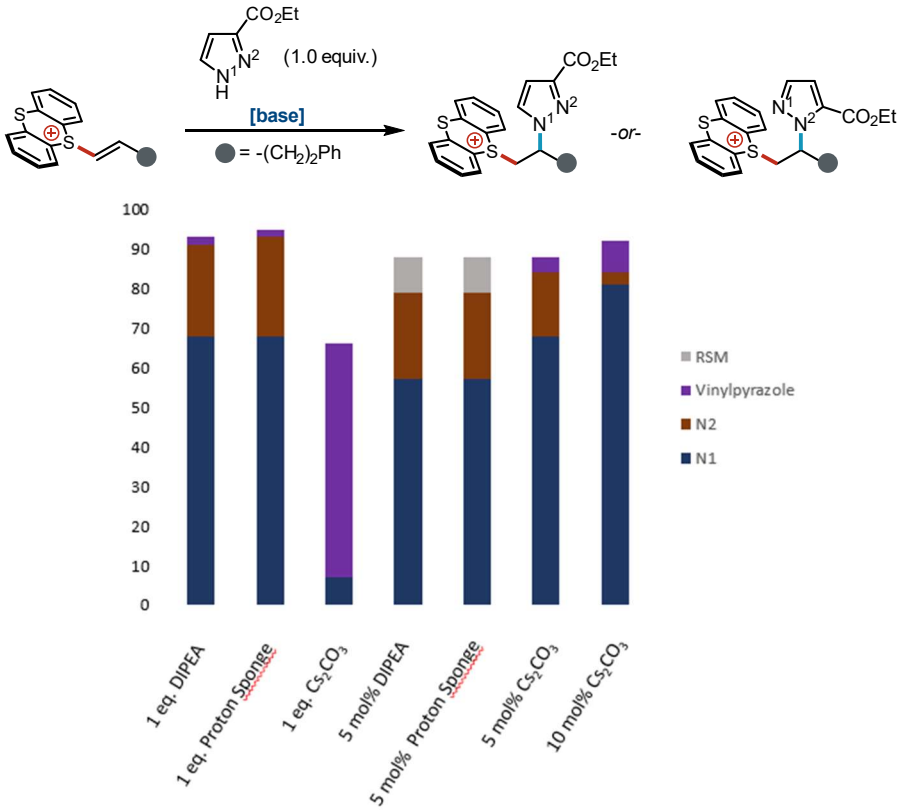

Figure D10. Optimization of base identity reveals base-dependence on *N*-regioselectivity.

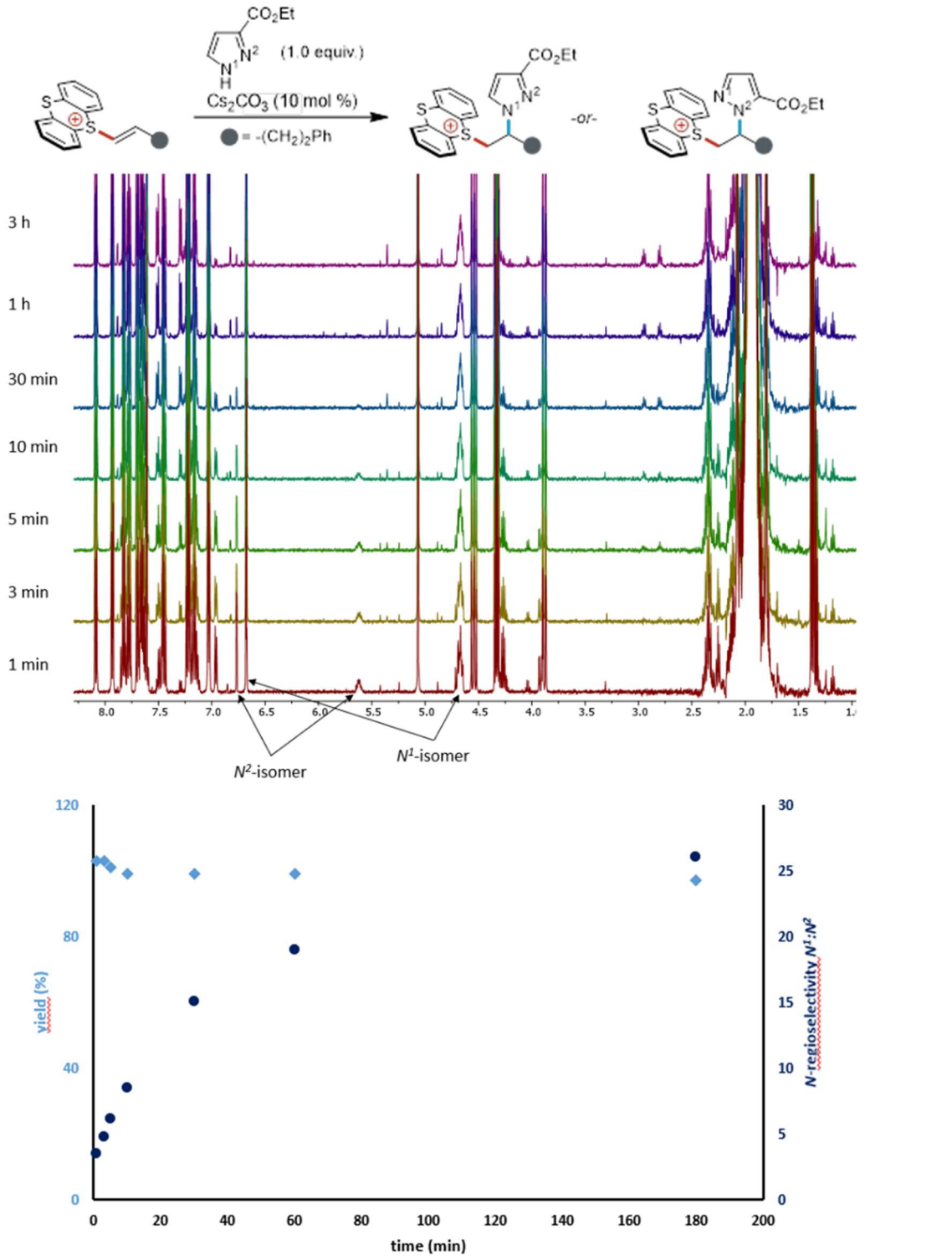

Figure D11. ^{1}H NMR time course of conjugate-type addition of asymmetric -CO_2Et azole into alkenylthianthrenium salt. Rapid and quantitative product formation occurs within the first minute of the reaction. Furthermore, complete conversion of the N^2-isomer in the ca. 3:1 N^1:N^2 regioisomeric mixture to the favored N^1-isomer is observed over time to achieve high ≥20:1 N^1:N^2 regioselectivity.

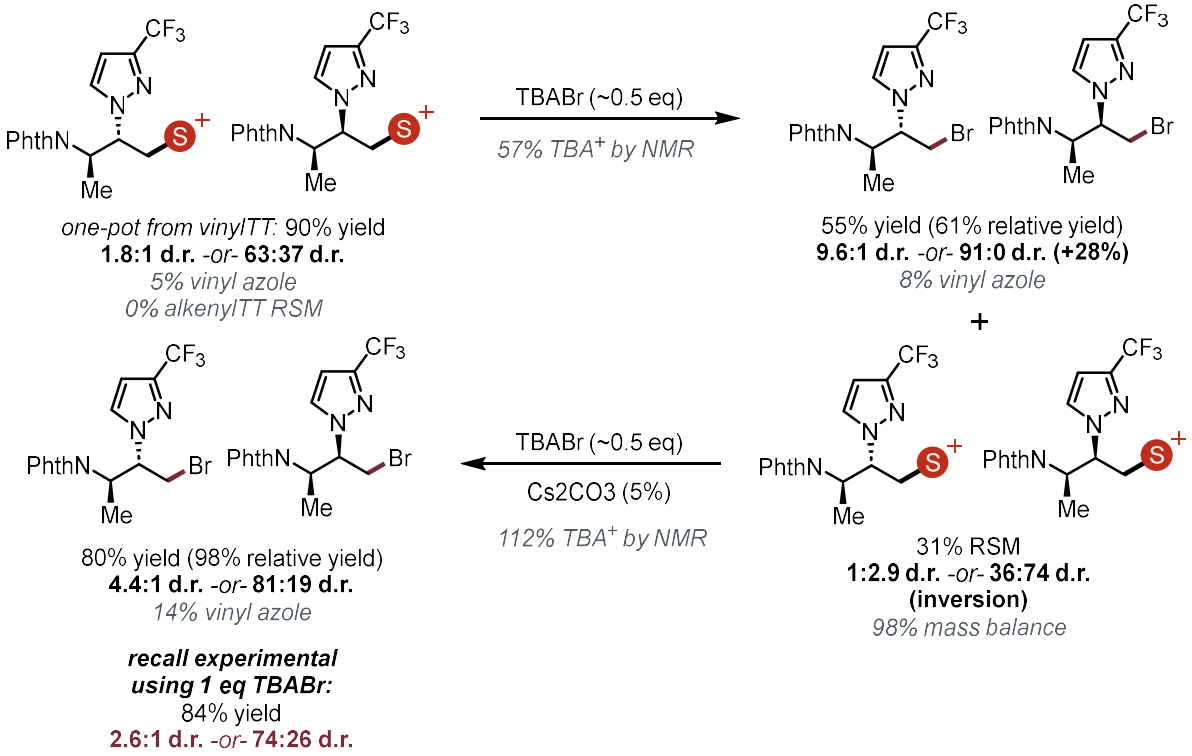

Figure D12. Addition of 0.5 equiv bromide to a diastereomeric mixture of 1,2-azolosulfonium salts. One diastereomer is selectively converted. Equilibration between diastereomers via reversible azole addition into alkenylthianthrenium salt enables a slight boost in final difunctionalized product d.r. compared to the alkylsulfonium intermediate d.r. This initial reactivity has been optimized to achieve up to 9:1 d.r. of the final bromo-substituted product.

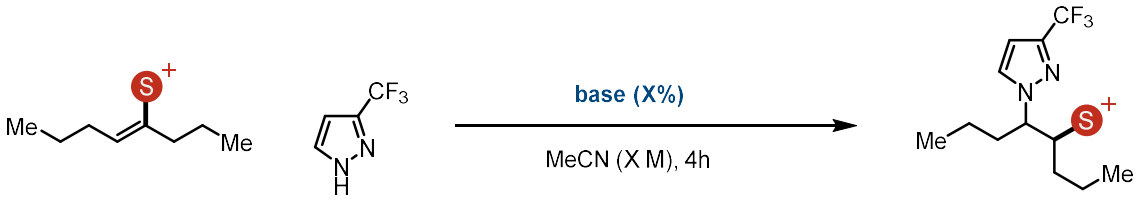

entry	conditions	time (h)	HA yield (%; d.r.)	alkenylTT RSM (%)	azole RSM (%)	vinyl azole (%)	allylic azole (%)	TT (%)
1	Cs_2CO_3 10%, 0.05M	4	**49 (3.0:1)**	26	37	12	3	19
2	above, **add 10%**	**+20**	**50 (2.7:1)**	15	28	21	3	28
3	Cs_2CO_3 **20%**, 0.05M	4	**49 (2.2:1)**	8	18	18	4	37
4	Cs_2CO_3 10%, 0.05M **2 equiv. alkenylTT**	4	**65 (3.4:1)**	52	18	14	5	21
5	Cs_2CO_3 10%, **0.5M**	4	**45 (3.8:1)**	29	36	14	1	17

Figure D13. Studies of 1,1-alkenylthianthrenium salt reactivity for 1,2-azolosulfonium product formation.

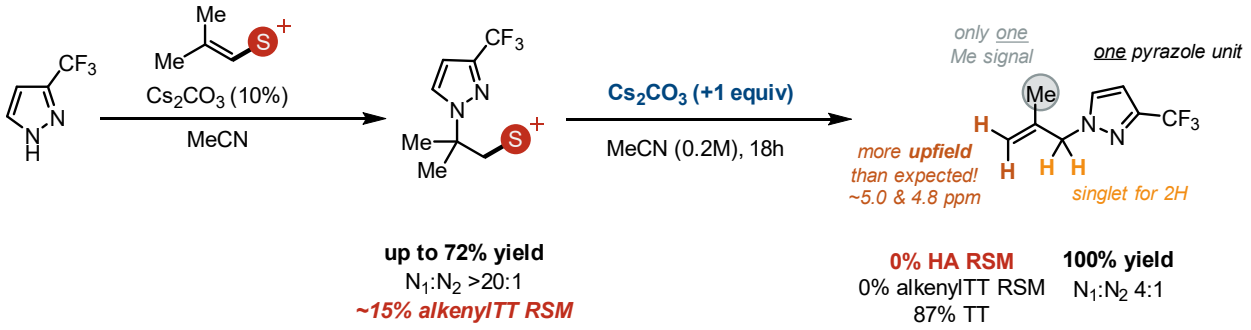

Figure D14. Treatment of α-tertiary azole sulfonium products with stoichiometric base. Outcome is quantitative elimination to allylic azole arising from reversible alkenylthianthrenium formation and allylic deprotonation and substitution by liberated azole nucleophile.

Preparation and Characterization of Alkenylthianthrenium Salts

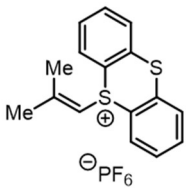

5-(2-methylprop-1-en-1-yl)-5H-thianthren-5-ium hexafluorophosphate(V) (5.41).
Experimental procedure: To an oven-dried 50-mL three-neck flask equipped with a magnetic stir bar was added KPF_6 (2.76 g, 15.0 mmol, 3.0 equiv) to the undivided cell. The side necks were equipped with two septa containing a stainless steel wire/Ni foam cathode assembly (2.9 x 1.6 cm) and a pencil/RVC anode assembly (1.6 x 0.6 x 0.7 cm). MeCN (36 mL) was added to the flask and sparged with a balloon of gaseous isobutene for 30 min. Thianthrene (1.08 g, 5.00 mmol, 1.0 equiv.) was added, followed by trifluoroacetic acid (2.82 mL, 50.0 mmol, 10.0 equiv) and trifluoroacetic anhydride (1.0 mL, 7.2 mmol, 1.4 equiv, 2% v/v) and the solution was stirred and electrolyzed under a constant current of 420 mA for 1.8 h (8.8 F/mol). The electrolysis was visually monitored until the solution turned from deep purple to light red.
Purification: At completion of electrolysis, the electrode leads were disconnected, septa removed, and the anode RVC was pushed off the pencil into the reaction mixture. The anode solution then was concentrated under reduced pressure. The crude residue was diluted with ~60 mL DCM, transferred to a separatory funnel, and quenched with saturated $NaHCO_3$ solution (150 mL) (*Caution:* excessive bubbling may occur). The aqueous layer was extracted with DCM (50 mL x 3) and the combined organic layers were washed with aqueous KPF_6 solution (3 × 100 mL, 5 % w/w), dried with anhydrous Na_2SO_4, filtered, and concentrated under reduced pressure. The residue was purified via flash column chromatography (DCM/3:1 EtOAc:EtOH). The collected fractions were triturated with DCM to afford 973.0 mg (47% yield) of **5.41**. *Alternative purification:* a second column can be performed to obtain >95% purity alkenylthianthrenium salt.
^{1}H NMR (500 MHz, CD_3CN) δ 8.08 (dd, J = 8.1, 1.3 Hz, 2H), 7.96 (dd, J = 7.9, 1.3 Hz, 2H), 7.80 (td, J = 7.7, 1.4 Hz, 2H), 7.71 (td, J = 7.7, 1.3 Hz, 2H), 6.52 (t, J = 1.3 Hz, 1H), 2.32 (d, J = 1.2 Hz, 3H), 2.04 (d, J = 1.3 Hz, 3H); **^{13}C NMR** (126 MHz, CD_3CN) δ13C NMR (126 MHz, CD3CN) δ 166.66, 135.99, 134.94, 132.54, 131.35, 130.74, 122.99, 105.07, 26.24, 21.67; **^{19}F NMR** (377 MHz, CD_3CN) δ -71.85, -73.72; **^{31}P NMR** (162 MHz, CD_3CN) δ -144.61 (hept, J = 706.7 Hz). **HRMS** (ESI+) Calc: $[M]^+$ ($C_{16}H_{15}S_2^+$) 271.0610, measured: 271.0606; 1.5 ppm difference.

Characterization of 1,2-Azolothianthrenium Salt 5.42

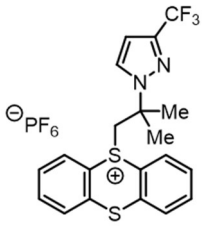

5-(2-methyl-2-(3-(trifluoromethyl)-1H-pyrazol-1-yl)propyl)-5H-thianthren-5-ium hexafluorophosphate(V) (5.42). Prepared from 3-(trifluoromethyl)-1H-pyrazole and 5-(2-methylprop-1-en-1-yl)-5H-thianthren-5-ium hexafluorophosphate(V) (**5.41**) 85% NMR yield (≥20:1 N^1:N^2) obtained by following the general procedure with the following modification: 16 h reaction using *i*-Pr_2NEt base (1 equiv.) instead of Cs_2CO_3. Peaks were assigned by partial isolation; regioselectivity determined by ^{19}F NMR.

Purification: The mixture was then filtered over a pad of celite and MeCN was removed under vacuum. The residue was diluted with DCM (~75 mL), filtered over a pad of celite and concentrated under vacuum. The residue was dissolved with a minimum amount of DCM, a stir bar added, and Et2O (~200 mL) was slowly added to precipitate a solid. If necessary, the mixture was left to stir overnight to ensure full precipitation. The precipitate was then filtered, the solid rinsed with Et2O (2x) and pentane (1x). The solids were collected into a vial and dried under high vacuum to afford the desired product. The funnel was rinsed with further portions of DCM, concentrated under reduced pressure, and collected into a vial to ensure complete collection of material.

^{1}H NMR (500 MHz, CD_3CN) δ 7.97 (dd, J = 8.1, 1.5 Hz, 2H), 7.95 (dd, J = 8.1, 1.3 Hz, 2H), 7.84 – 7.81 (1H), 7.78 (td, J = 7.7, 1.4 Hz, 2H), 7.64 (td, J = 7.7, 1.3 Hz, 2H), 6.60 (d, J = 2.5 Hz, 1H), 4.38 (s, 2H), 1.75 (s, 6H); **^{13}C NMR** (126 MHz, CD_3CN) δ 142.79 (q, *J* = 37.8 Hz), 137.71, 135.47, 134.45, 131.63, 130.77, 130.62, 122.23 (q, J = 268.0 Hz), 119.81, 106.24 (q, *J* = 2.2 Hz), 62.02, 54.50, 27.34; **^{19}F NMR** (377 MHz, CD_3CN) δ -62.07 (s, 3F), -71.96 (s, 3F), -73.83 (s, 3F); **^{31}P NMR** (162 MHz, CD_3CN) δ -144.62 (hept, J = 706.3 Hz). **HRMS** (ESI+) Calc: $[M]^+$ ($C_{20}H_{18}F_3N_2S_2^+$) 407.0858, measured: 407.0854; 1.0 ppm difference.

Characterization of Heterofunctionalization Products

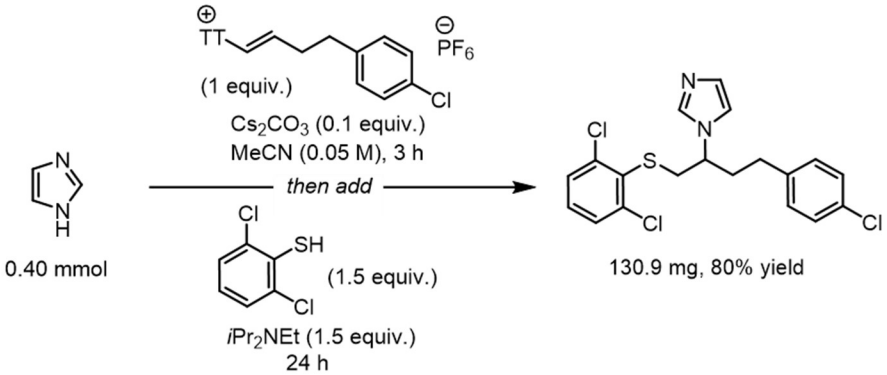

1-(4-(4-chlorophenyl)-1-((2,6-dichlorophenyl)thio)butan-2-yl)-1H-imidazole (5.21).

Experimental procedure: To threaded vial equipped with a magnetic stir bar were added 5-(4-(4-chlorophenyl)but-1-en-1-yl)-5H-thianthren-5-ium hexafluorophosphate(V) (210.8 mg, 0.40 mmol, 1.0 equiv.), imidazole (27.23 mg, 0.40 mmol, 1.0 equiv.), and cesium carbonate (13.03 mg, 0.04 mmol, 0.1 equiv.). MeCN (8 mL) was added and the reaction mixture was capped with a PTFE seal and stirred at room temperature until completion of the reaction (3 h). Then 2,6-dichlorobenzenethiol (107.4 mg, 0.60 mmol,

1.5 equiv.) followed by DIPEA (105 μL, 0.60 mmol, 1.5 equiv.) were added and the reaction mixture was allowed to stir for 24 h.

Purification: At completion, the reaction mixture was diluted with DCM (~60 mL) and washed with water (150 mL). The aqueous layer was then extracted with DCM (50 mL x 3). The combined organic layers were dried over Na_2SO_4, filtered and concentrated under reduced pressure. The residue obtained was then purified by flash column chromatography (DCM/acetone) to obtain 130.9 mg (80% yield) of **5.21**.

^{1}H NMR (500 MHz, $CDCl_3$) δ 7.52 (s, 1H), 7.32 (d, J = 8.1 Hz, 2H), 7.21 – 7.13 (m, 3H), 7.04 (s, 1H), 6.94 (d, J = 8.4 Hz, 2H), 6.89 (s, 1H), 4.00 (dt, J = 8.8, 3.4 Hz, 1H), 3.33 (dd, J = 13.9, 7.4 Hz, 1H), 3.15 (dd, J = 14.0, 6.0 Hz, 1H), 2.45 – 2.37 (m, 1H), 2.37 – 2.24 (m, 2H), 2.10 – 2.00 (m, 1H); **^{13}C NMR** (126 MHz, $CDCl_3$) δ 140.72, 138.30, 136.55, 132.04, 131.58, 130.24, 129.63, 129.60, 128.82, 128.62, 116.17, 57.69, 40.61, 35.99, 31.19. **HRMS** (ESI+) Calc: $[M+H]^+$ ($C_{19}H_{18}Cl_3N_2S$) 411.0251, measured: 411.0247; 1.0 ppm difference.

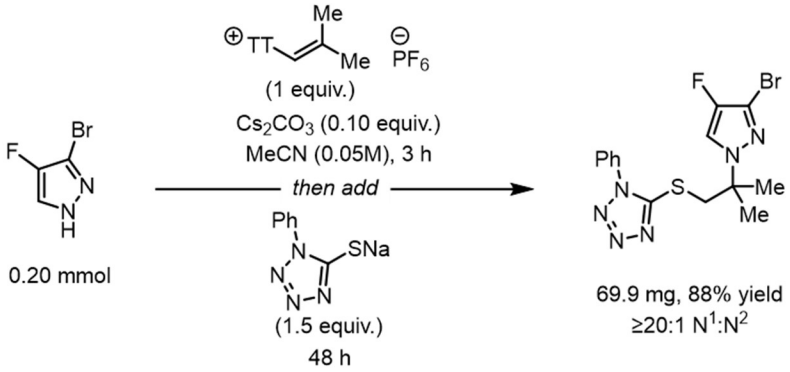

5-((2-(3-bromo-4-fluoro-1H-pyrazol-1-yl)-2-methylpropyl)thio)-1-phenyl-1H-tetrazole (5.47).

Experimental procedure: To threaded vial equipped with a magnetic stir bar were added 5-(2-methyl-2-(3-(trifluoromethyl)-1H-pyrazol-1-yl)propyl)-5H-thianthren-5-ium hexafluorophosphate(V) (**5.41**). (83.3 mg, 0.20 mmol, 1.0 equiv.), 3-bromo-4-fluoro-1H-pyrazole (33.0 mg, 0.20 mmol, 1.0 equiv.), and cesium carbonate (6.52 mg, 0.02 mmol, 0.1 equiv.). MeCN (4 mL) was added and the reaction mixture was capped with a PTFE seal and stirred at room temperature until completion of the reaction (3 h). Then sodium 1-phenyl-1H-tetrazole-5-thiolate (60.1 mg, 0.30 mmol, 1.5 equiv.) was added and the reaction mixture was allowed to stir for 48 h.

Purification: At completion, the reaction mixture was concentrated under reduced pressure. The residue obtained was then purified by flash column chromatography (DCM/ethyl acetate) to obtain 69.9 mg (88% yield, ≥20:1 N^1:N^2) of **5.47**. Regioisomer was determined using ^{13}C-^{1}H HSQC and ^{13}C-^{1}H HMBC NMR analysis.

^{1}H NMR (500 MHz, CD_3CN) δ 7.67 – 7.61 (m, 4H), 7.61 – 7.54 (m, 2H), 3.93 (s, 2H), 1.64 (s, 6H); **^{13}C NMR** (126 MHz, CD_3CN) δ 154.95, 147.33 (d, J = 245.7 Hz), 134.43, 131.49, 130.83, 125.45, 116.94 (d, J = 27.4 Hz), 112.30 (d, J = 16.3 Hz), 63.61, 45.07, 26.45; **^{19}F NMR** (377 MHz, CD_3CN) δ -175.46. **HRMS** (ESI+) Calc: $[M+H]^+$ ($C_{14}H_{15}BrFN_6S$) 397.2041, measured: 397.2037; 1.0 ppm difference.

D4. NMR spectra

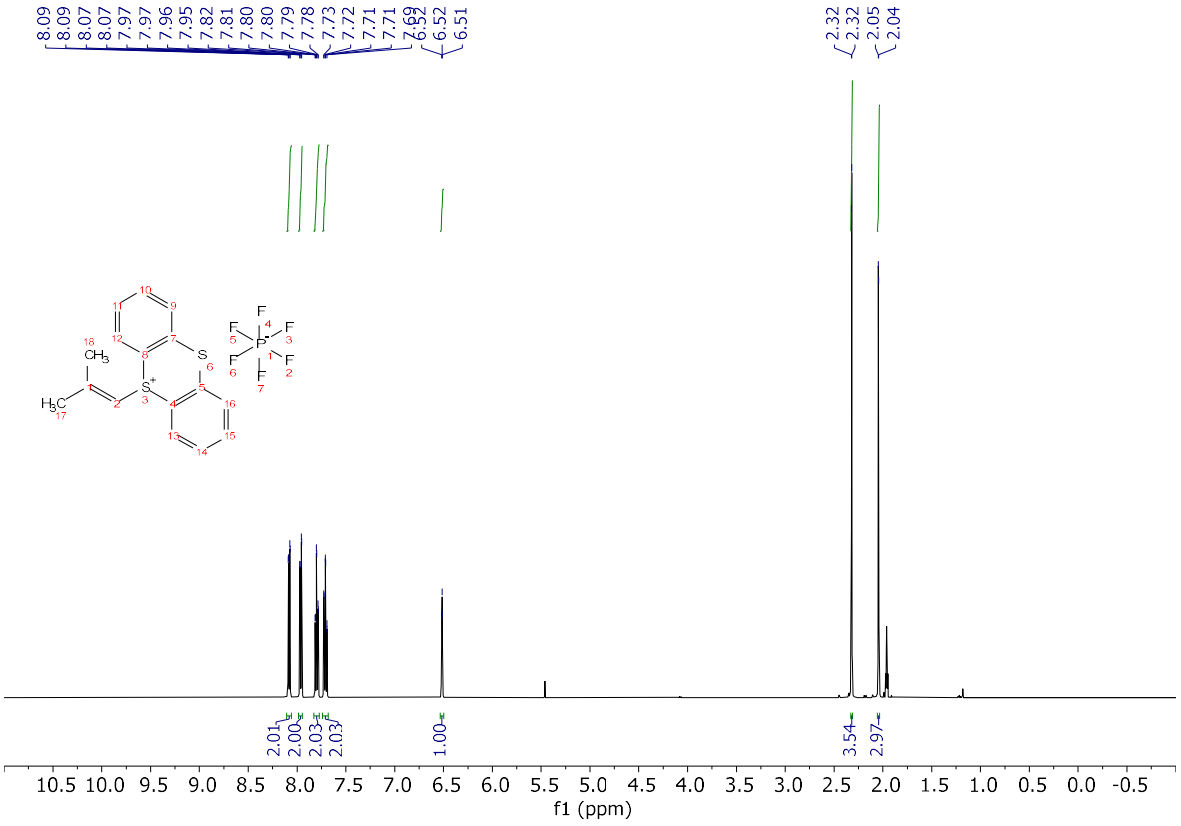

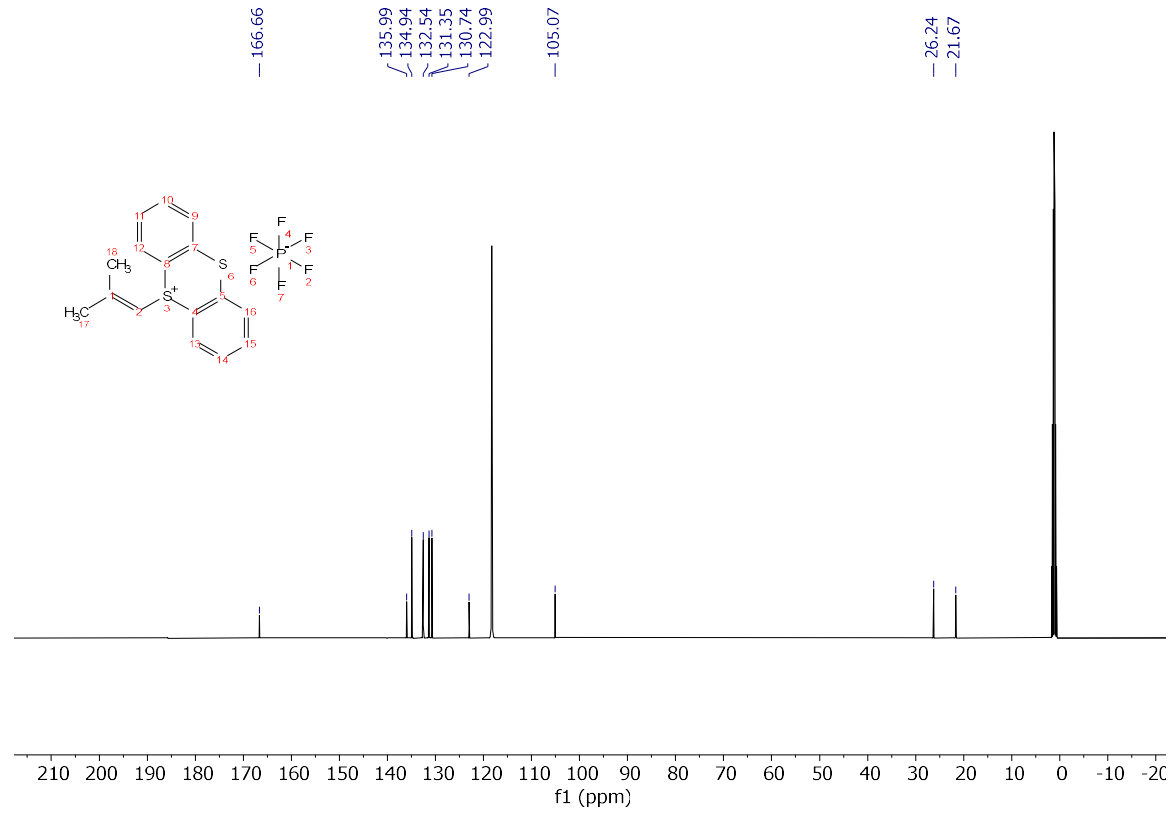

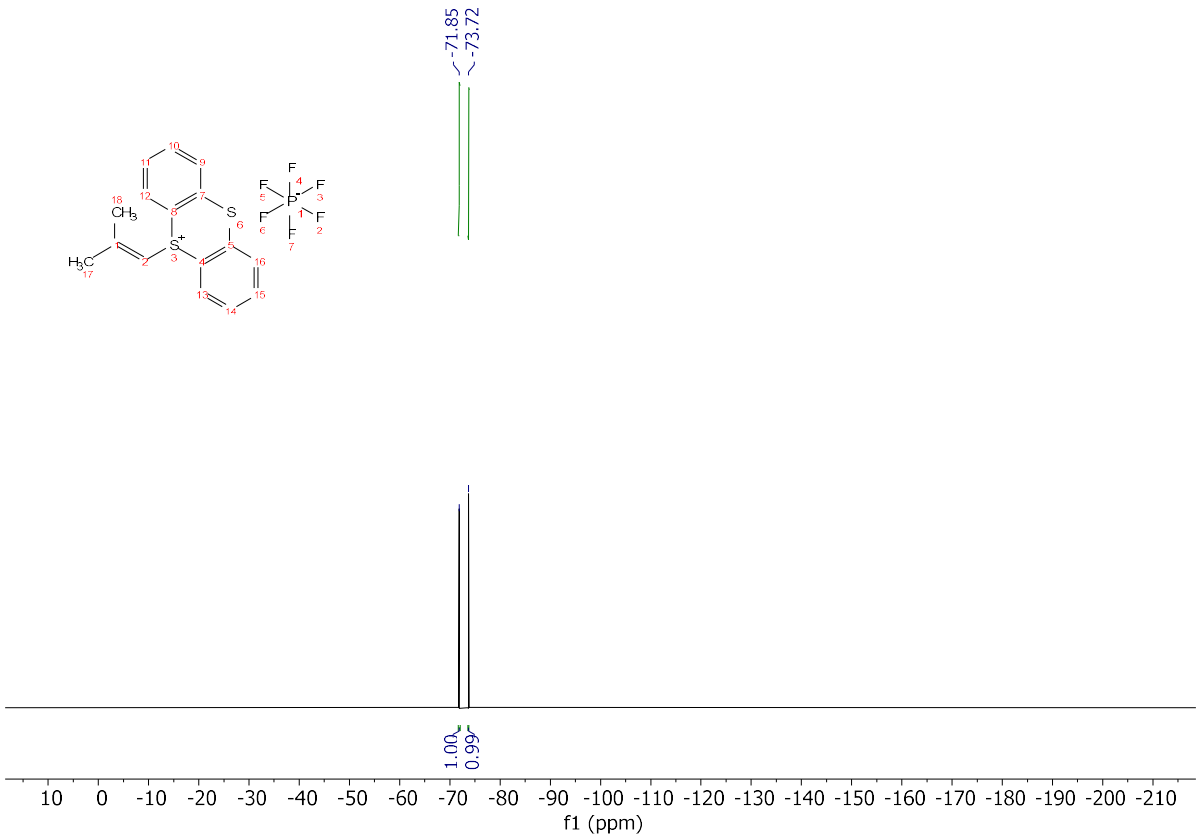
-71.85
-73.72
1.00
0.99
10 0 -10 -20 -30 -40 -50 -60 -70 -80 -90 -100 -110 -120 -130 -140 -150 -160 -170 -180 -190 -200 -210
f1 (ppm)

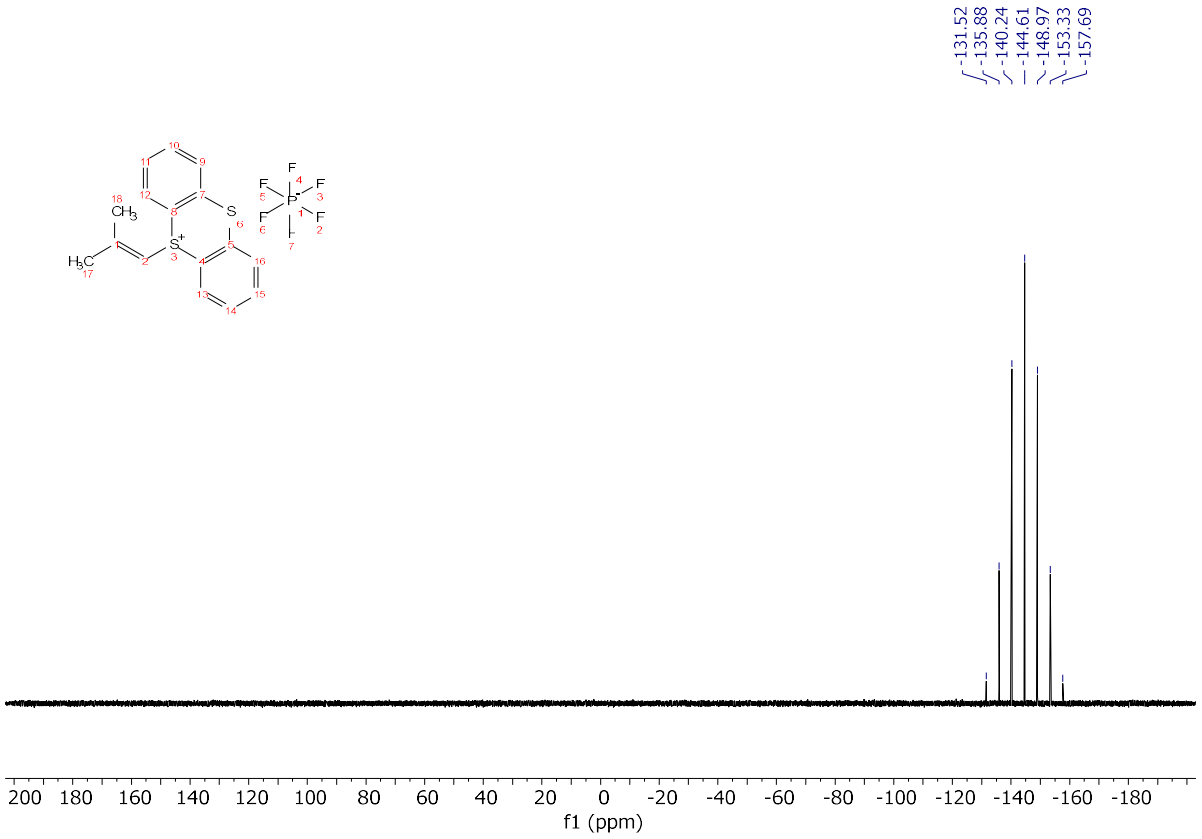
-131.52
-135.88
-140.24
-144.61
-148.97
-153.33
-157.69
200 180 160 140 120 100 80 60 40 20 0 -20 -40 -60 -80 -100 -120 -140 -160 -180
f1 (ppm)

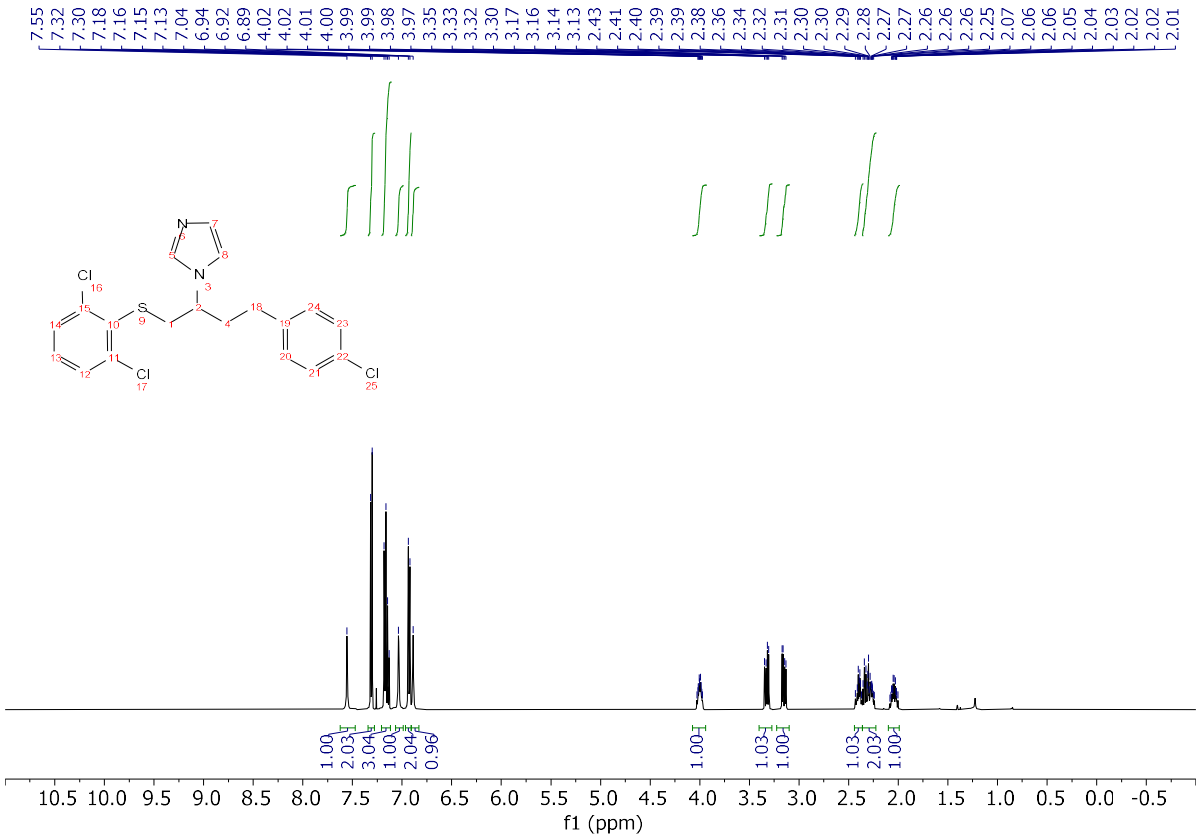
7.55 7.32 7.30 7.18 7.16 7.15 7.13 7.04 6.94 6.92 6.89 4.02 4.02 4.01 4.00 3.99 3.99 3.98 3.97 3.35 3.33 3.32 3.30 3.17 3.16 3.14 3.13 2.43 2.41 2.40 2.39 2.39 2.38 2.36 2.34 2.32 2.31 2.30 2.30 2.29 2.28 2.27 2.27 2.26 2.26 2.26 2.25 2.07 2.06 2.05 2.04 2.03 2.02 2.02 2.01
1.00 2.03 3.04 1.00 2.04 0.96 1.00 1.03 1.00 1.03 2.03 1.00
10.5 10.0 9.5 9.0 8.5 8.0 7.5 7.0 6.5 6.0 5.5 5.0 4.5 4.0 3.5 3.0 2.5 2.0 1.5 1.0 0.5 0.0 -0.5
f1 (ppm)

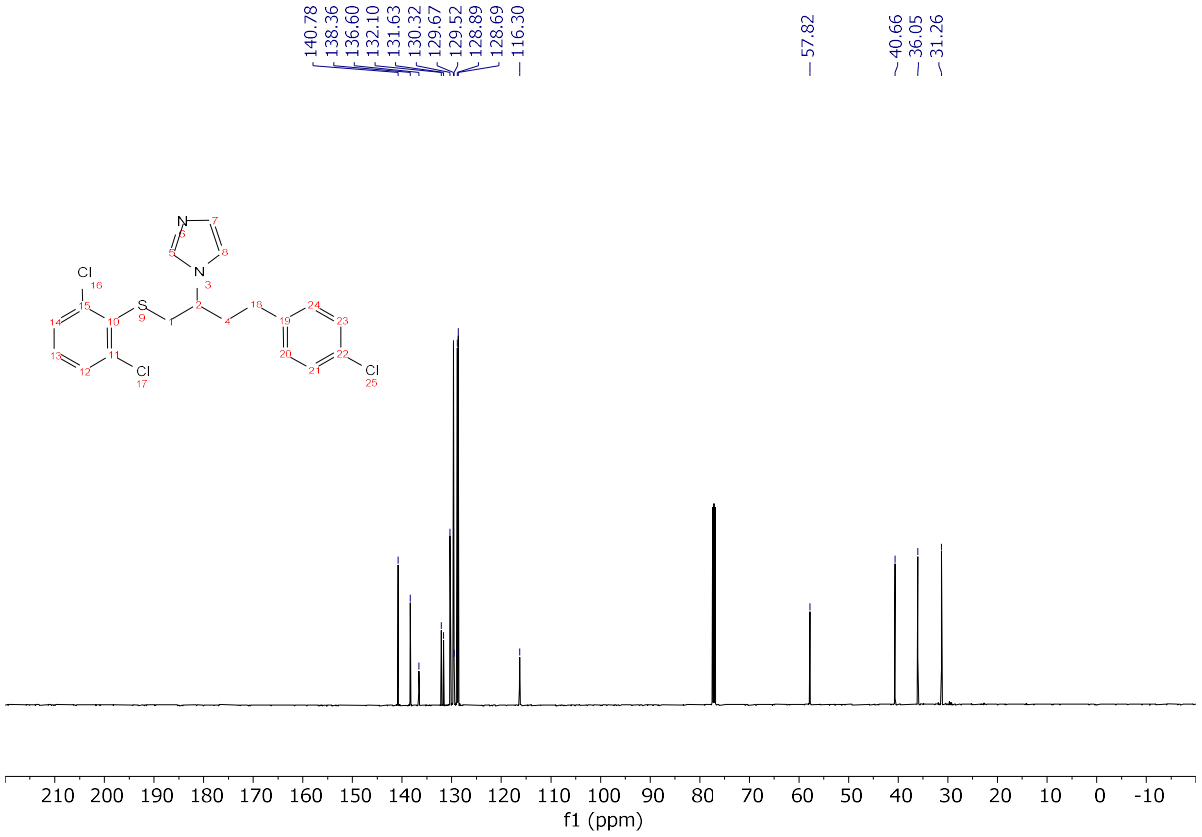
140.78 138.36 136.60 132.10 131.63 130.32 129.67 129.52 128.89 128.69 116.30 57.82 40.66 36.05 31.26
210 200 190 180 170 160 150 140 130 120 110 100 90 80 70 60 50 40 30 20 10 0 -10
f1 (ppm)

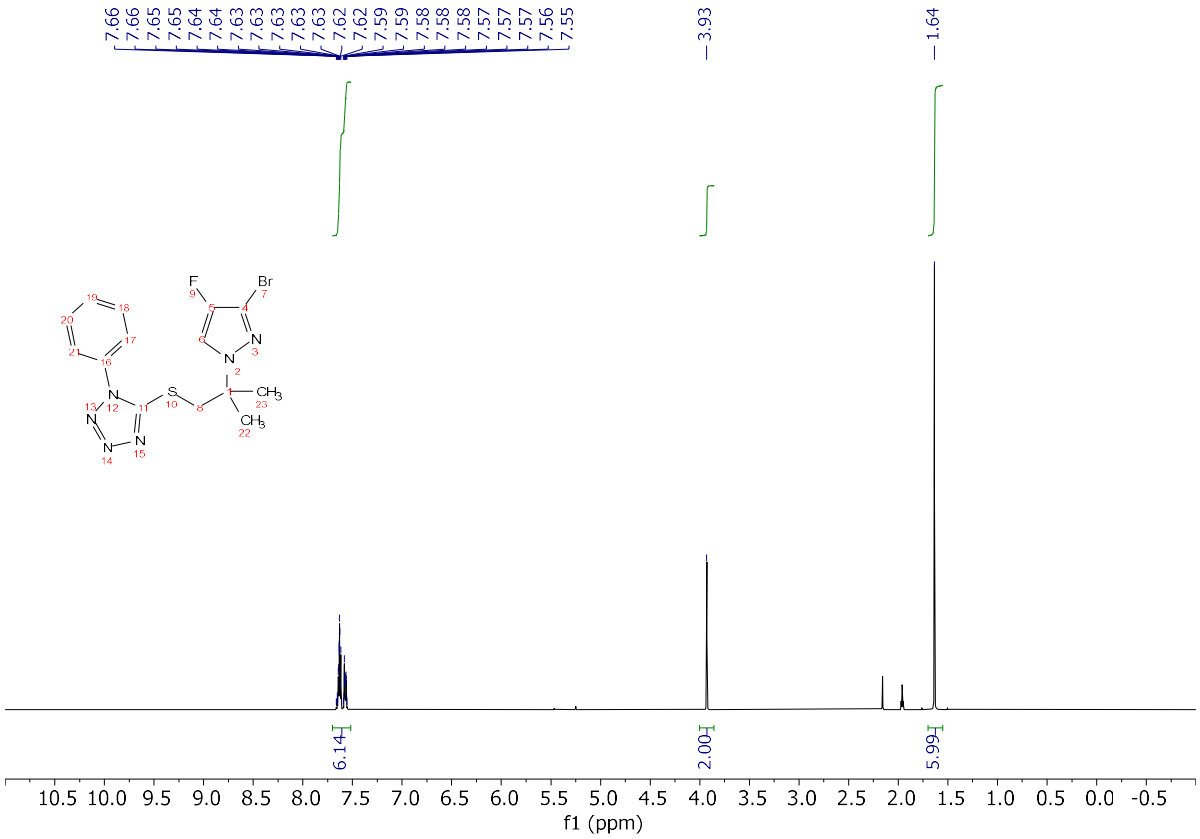
7.66
7.66
7.65
7.65
7.64
7.64
7.63
7.63
7.63
7.63
7.63
7.62
7.62
7.59
7.59
7.58
7.58
7.58
7.57
7.57
7.57
7.56
7.55
3.93
1.64
6.14
2.00
5.99
f1 (ppm)

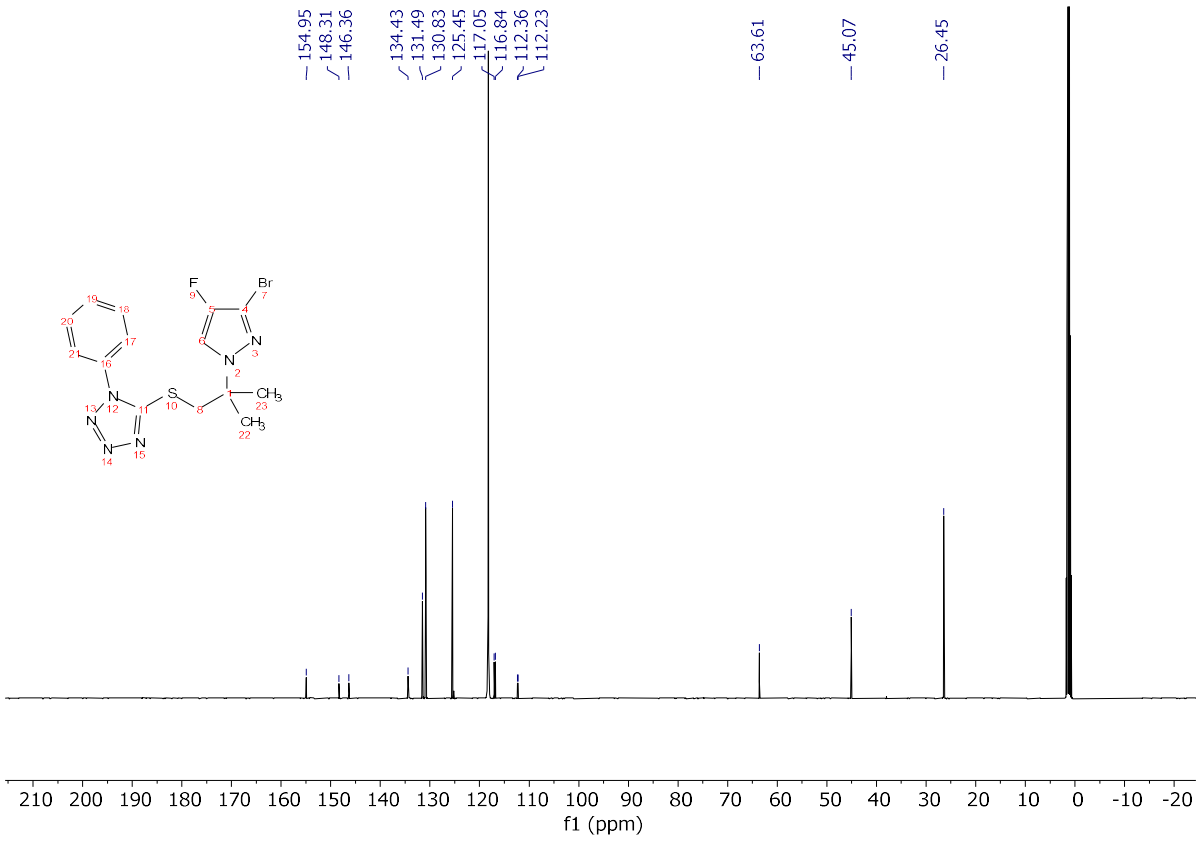
154.95
148.31
146.36
134.43
131.49
130.83
125.45
117.05
116.84
112.36
112.23
63.61
45.07
26.45
f1 (ppm)

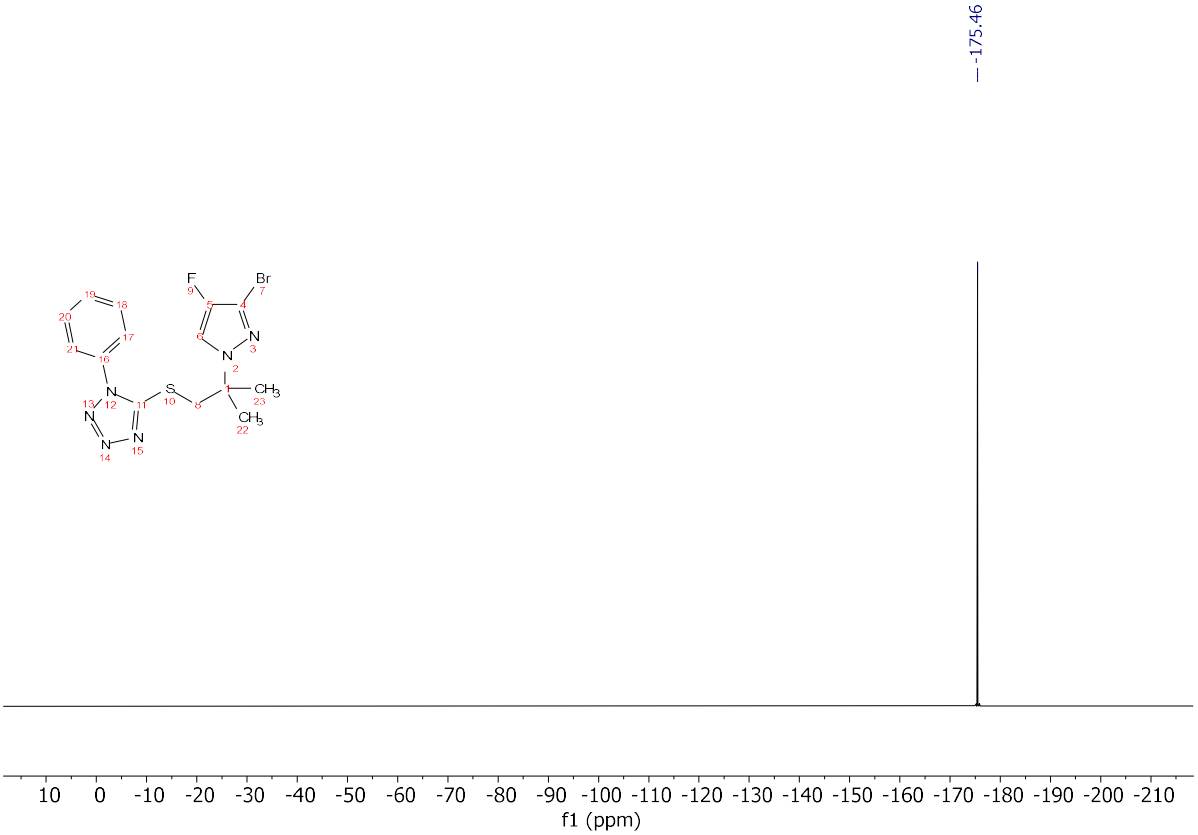
-175.46
10 0 -10 -20 -30 -40 -50 -60 -70 -80 -90 -100 -110 -120 -130 -140 -150 -160 -170 -180 -190 -200 -210
f1 (ppm)

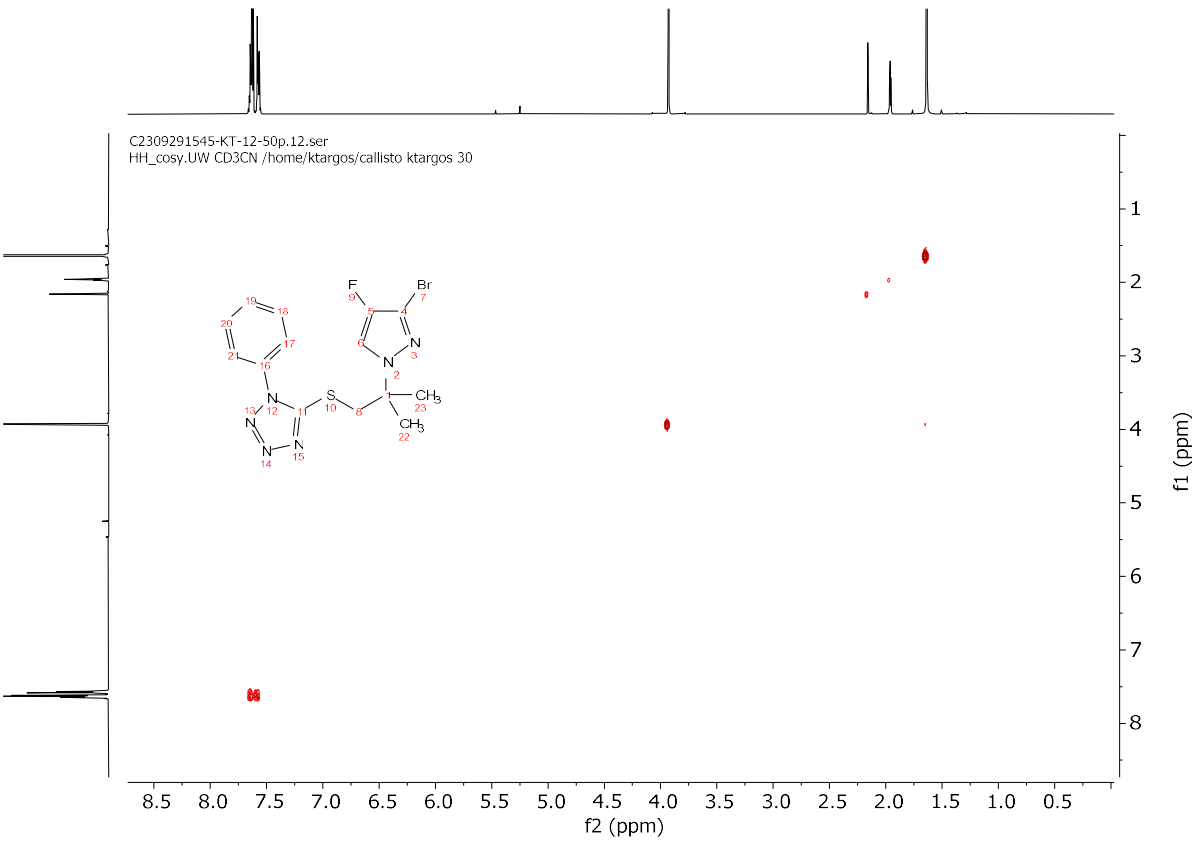
C2309291545-KT-12-50p.12.ser
HH_cosy.UW CD3CN /home/ktargos/callisto ktargos 30
8.5 8.0 7.5 7.0 6.5 6.0 5.5 5.0 4.5 4.0 3.5 3.0 2.5 2.0 1.5 1.0 0.5
f2 (ppm)
f1 (ppm)

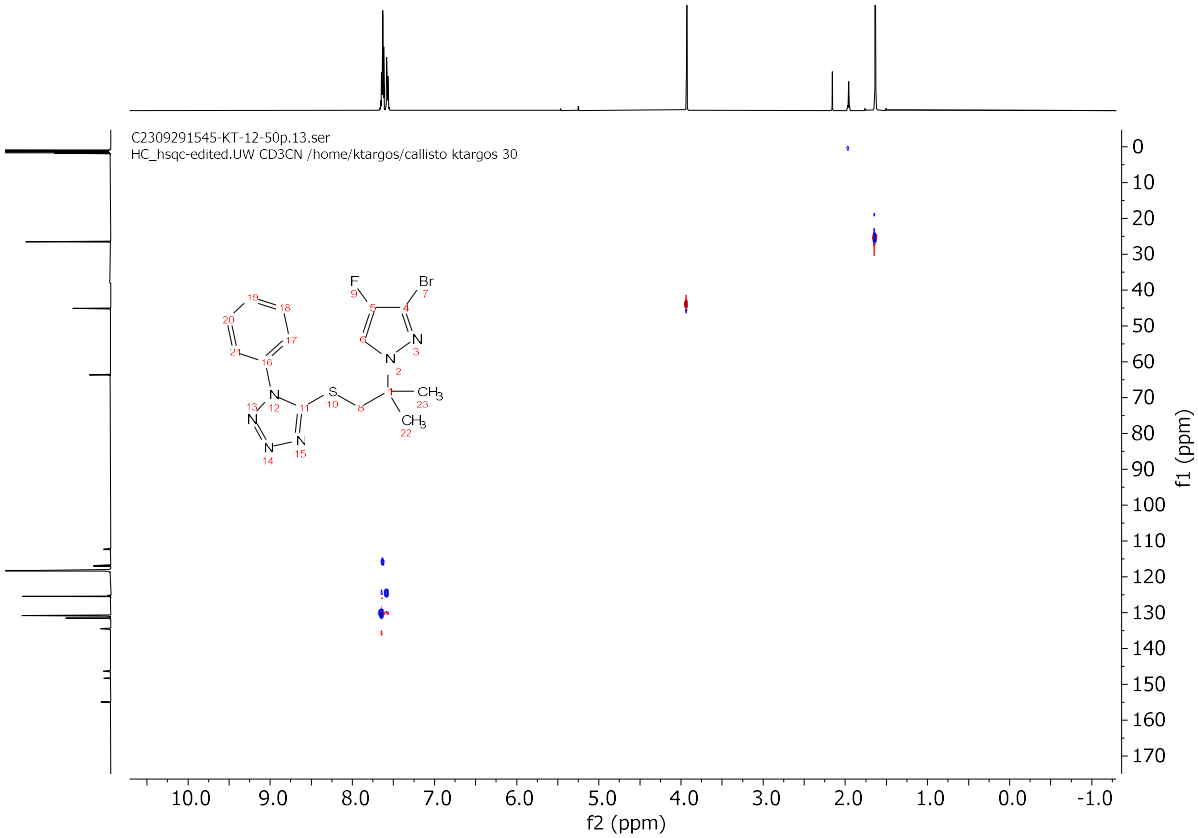
C2309291545-KT-12-50p.13.ser
HC_hsqc-edited.UW CD3CN /home/ktargos/callisto ktargos 30
f2 (ppm)
f1 (ppm)

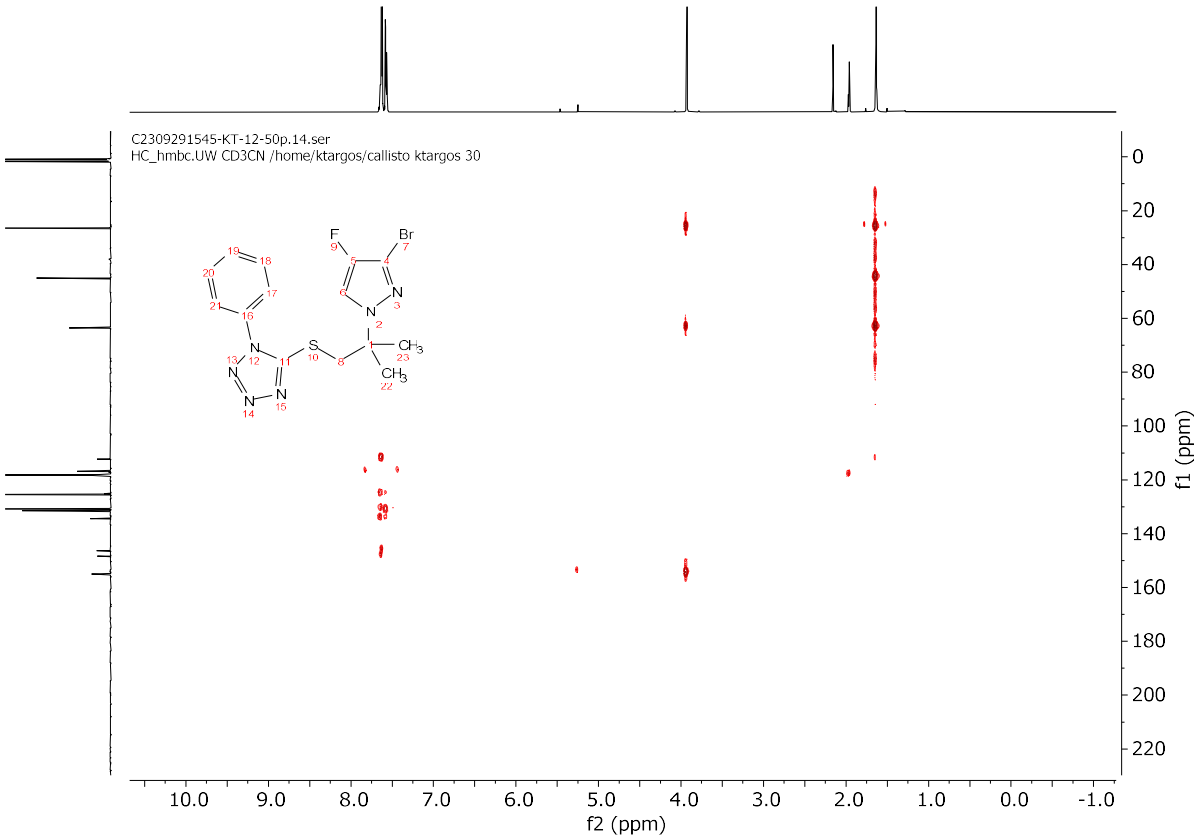
C2309291545-KT-12-50p.14.ser
HC_hmbc.UW CD3CN /home/ktargos/callisto ktargos 30
f2 (ppm)
f1 (ppm)

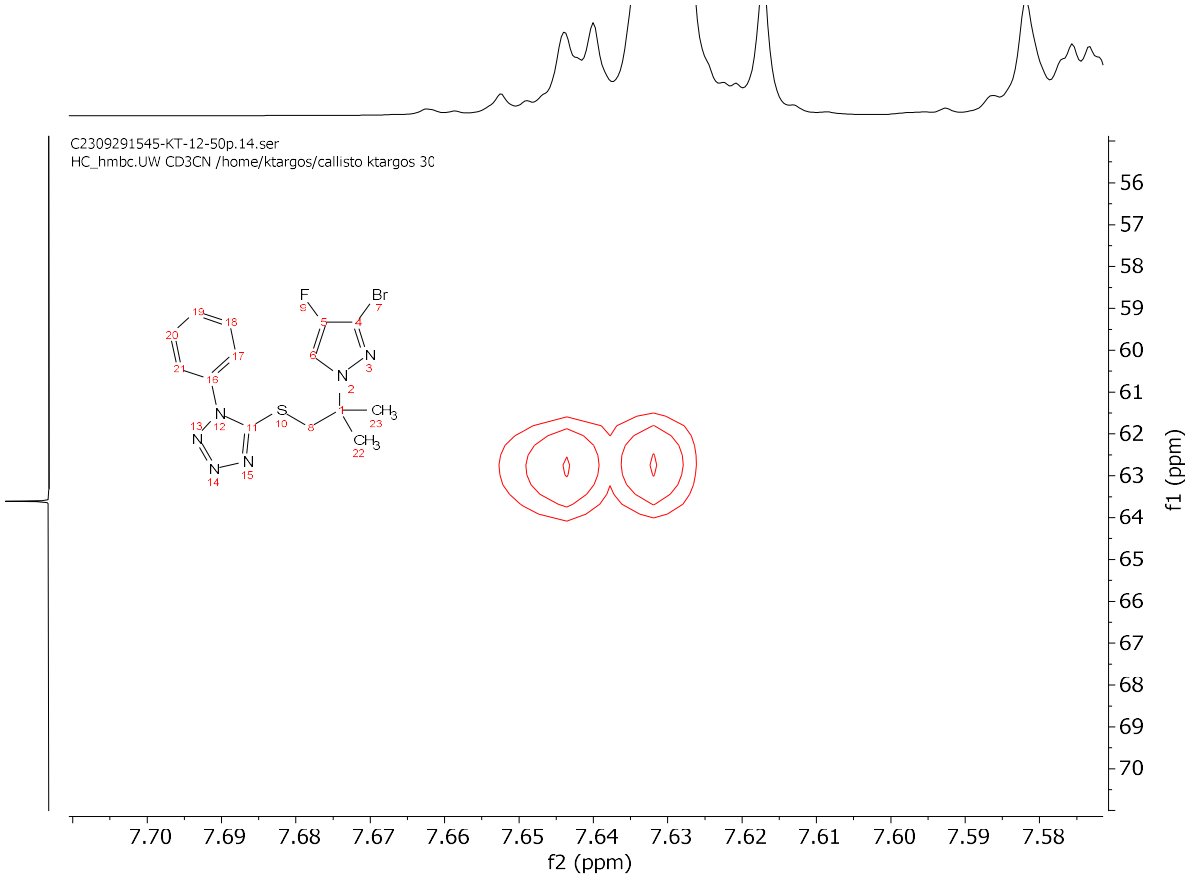
C2309291545-KT-12-50p.14.ser
HC_hmbc.UW CD3CN /home/ktargos/callisto ktargos 30
F
Br
N
S
CH3
CH3
7.70
7.69
7.68
7.67
7.66
7.65
7.64
7.63
7.62
7.61
7.60
7.59
7.58
f2 (ppm)
56
57
58
59
60
61
62
63
64
65
66
67
68
69
70
f1 (ppm)

Appendix E: Supporting Information for Chapter 6 (Diastereoselective Synthesis of Cyclopropanes from Carbon Pronucleophiles and Alkenes)

E1. General Methods and Materials

Unless otherwise noted, reactions were performed under air in an anhydrous solvent. MeCN and toluene were purchased as sureseal bottles and used as is. THF, DMF, DMSO, and DCM were dried by passing through activated alumina columns. Thianthrene was recrystallized from acetone prior to use. *n*-Bu_4NPF_6 was recrystallized three times from EtOAc prior to use. All liquid carbon pronucleophiles were distilled from CaH_2 prior to use. Unless otherwise noted, other commercially available reagents were used as received. Aluminum Oxide (activated, basic, Brockmann I) was purchased from Sigma-Aldrich and used for filtration. Crude reaction mixtures were evaluated by thin-layer chromatography using EMD/Merck silica gel 60 F254 pre-coated plates (0.25 mm) and were visualized by UV and/or Seebach, ninhydrin, or $KMnO_4$ staining. Flash chromatography was performed with a Biotage Isolera One automated chromatography system with re-packed silica columns (technical grade silica, pore size 60 Å, 230 - 400 mesh particle size, 40 - 63 particle size) or pre-packed Biotage Sfär Silica HC Duo 20µm 50g - High Capacity Column columns. Purified materials were dried in vacuo (0.050 Torr) to remove trace solvent. ^{1}H, ^{13}C, ^{19}F, and ^{31}P spectra were taken using a Bruker Avance-400 with a BBFO Probe, a Bruker Avance-500 with a DCH Cryoprobe, a Bruker Avance III HD-500 with a TXO Cryoprobe, or a Bruker Avance-600 with a TCI-F cryoprobe. NMR data are reported relative to residual $CHCl_3$ (1 H, δ = 7.26 ppm), $CDCl_3$ (13 C, δ = 77.16 ppm) or residual C_6H_6 (1 H, δ = 7.16), C_6H_6 (13C, δ = 128.06 ppm). Data for ^{1}H NMR spectra are reported as follows: chemical shift (δ ppm) (multiplicity, coupling constant (Hz), integration). Multiplicity and qualifier abbreviations are as follows: s = singlet, d = doublet, t = triplet, q = quartet, m = multiplet, br = broad. All NMR yields were determined via reference against an internal standard (dibromomethane or mesitylene for 1 H). Mass spectrometry data was collected on a Thermo Scientific Q Exactive Plus Mass Spectrometer. The crystal evaluation and data collections were performed on a Bruker D8 VENTURE PhotonIII four-circle diffractometer with Cu Kα (λ = 1.54178 Å) radiation with the detector to crystal distance of 4.0 cm (Bruker-AXS (2018). APEX3. Version 2018.1-0. Madison, Wisconsin, USA.). The reflections were indexed by an automated indexing routine built in the APEX3 program. Mercury was used for structural visualization.[1]

Abbreviations: OAc—acetate, Aq—aqueous, Boc—*tert*-butyl carbamate, *t*Bu—*tert*-butyl, DBU—1,8-Diazabicycl[5.4.0]undec-7-ene, DC—direct current, DCM— dichloromethane, DMF—dimethyl formamide, DMSO—dimethylsulfoxide, Et—ethyl, EtOAc—ethyl acetate, EtOH—ethanol, Me—methyl, MeCN—acetonitrile, MeOH—methanol, NBS—*N*-bromosuccinimide, NPhth—phthalimide, Ph—phenyl, PTFE—polytetrafluoroethylene, RVC—reticulated vitreous carbon, *n*-Bu_4—tetrabutyl, *n*-Oct_4—tetraoctyl, TBAB—tetrabutylammonium bromide, TEA—triethylamine, TFA— trifluoroacetic acid, THF—tetrahydrofuran, TLC—thin layer chromatography, TT—thianthrene.

Electrochemical Methods and Materials

Bulk constant current electrolysis experiments were driven with a Dr. Meter HY3005M-L DC Power Supply or a custom–made low current power supply which was externally calibrated with a multimeter using a 10 Ohm resistor. Original design and fabrication of low current power supply created by Dr. Blaise J. Thompson. Provides an operational range of ± 0.01 – 9.99 mA, tunable by variable resistor, delivering power to banana socket pair. The power supply is limited to ± 15 V for bulk electrolysis and is powered by an 18 V wall wart. Circuitry is housed within an aluminum enclosure. For additional specifications, see: *J. Am. Chem. Soc.* **2020** 142, 2093-2099 and *Nature* **2021** 596, 74-79.

Divided cell fabricated in house by Tracy Drier. Glass frit purchased from Ace Glass (7176-36). Anode electrode assembled via affixing end of the silver wire (Belden Hook-Up wire, item number 83005 007100) around the pencil (JuneGold 2B graphite 2 mm) and wrapping in teflon tape to prevent exposure, then piercing RVC (8 x 7 x 7 mm, Ultramet, 80 ppi) with pencil. Solvent exposed electrode surface area (22.4 cm^2) was calculated via manufacturer-supplied surface area/volume ratio measurements. Cathode electrode assembled via affixing nickel foam (1.4 x 1.4 cm, or 1.5 x 0.9 cm, MTI Corporation, Surface density: 350g/m^3) to the end of stainless steel wire (Grainger, stainless steel lockwire, 0.025" diameter, item number 16Y043). PTFE tubing (Cole-Parmer; 1/32" ID, 1/16" OD, item number EW-06407-41) connects both sides of the divided cell to normalize pressure. Septa inner diameter 16 mm.

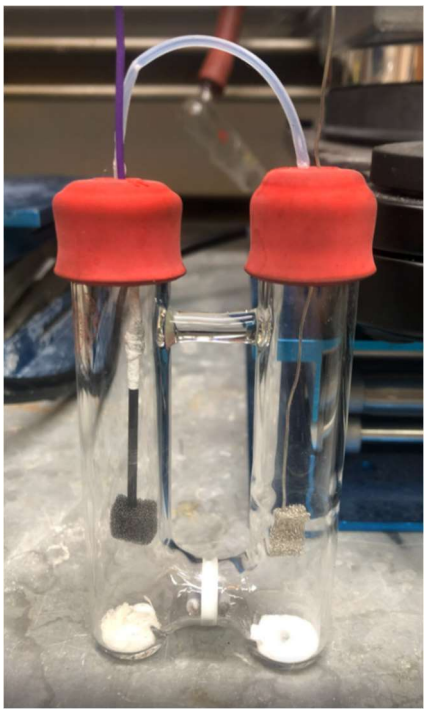

Figure E1. Picture of standard electrochemical H-cell used with electrode setup attached.

E2. Supplemental Data

E2.1. Cyclopropanation Comparison with Substitution of Vicinal Dihalide Starting Materials

A literature survey of different conditions varying base, solvents, and use of phase transfer reagents for cyclopropanation of dihaloethanes was found and applied to (3,4-dibromobutyl)benzene as a starting material. Results show minimal formation of cyclopropane product with mass balance favoring elimination side-products. For comparison, substitution of the 4-phenylbutene-derived dicationic adduct results in 85% yield for the desired cyclopropanation product.

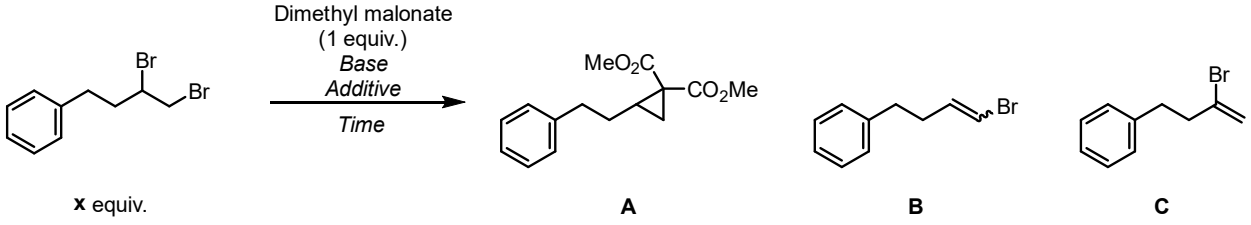

Table E1. Substitution of conventional vicinal dibromide dielectrophile for cyclopropanation.

Entry	Base (equiv.)	x equiv.	Additive (equiv.)	Solvent (M)	Time (h)	A (%)	B (%)	C (%)	SM (%)	Source
1	Cs_2CO_3 (2.5)	1.0	--	MeCN (0.3)	2	0	0	0	98*	Our work
2	NaOH (11)	1.5	TBAB (0.2)	Toluene:H_2O (1:1, 0.6)	4	0	54	82	0	Ref. 2
3	NaH (3.0)	1.5	--	DMSO (0.3)	16	0	63	80	0	Ref. 3
4	K_2CO_3 (2.5)	1.4	TBAB (0.05)	DMF (0.3)	16	15	21	26	56	Ref. 4
5	NaOH (25)	1.5	$BnEt_3NCl$ (1)	H_2O (0.5)	16	2	39	54	55	Ref. 5

* No further conversion was observed even after stirring overnight (16 h).

E2.2. Cyclopropanation of Vicinal Dibromide Dielectrophiles for Drug Intermediate Analog

Substitution conditions were taken from patent literature prepped by Vertex Pharmaceuticals[6] for the synthesis of 1-(2,2-difluorobenzo[d][1,3]dioxol-5-yl)cyclopropane-1-carbonitrile and applied to vicinal dibromide analogs of alkenes showcased in Scheme 6.3.

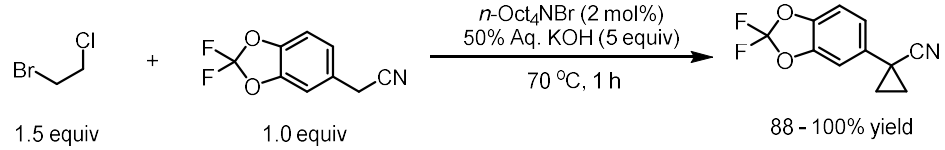

Scheme E1. Patented procedure for cyclopropanation of vicinal dihalide with 2-(2,2-difluorobenzo[d][1,3]dioxol-5-yl)acetonitrile.

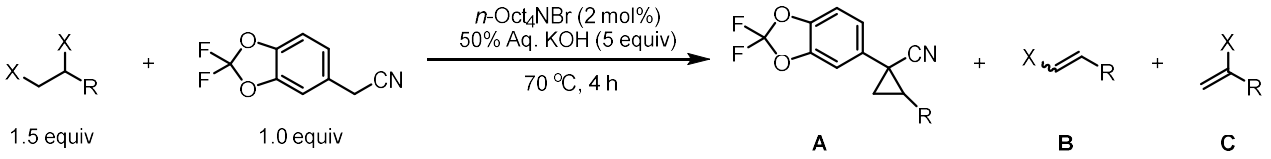

Table E2. Cyclopropanation of vicinal dibromide dielectrophiles targeting drug analog synthesis featured in Scheme 6.3.

Entry	Substrate	A (%)	B (%)	C (%)	SM (%)
1	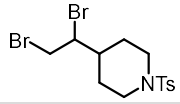	0	32	95	0
2*	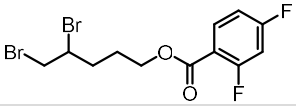	0	33	28	31
3	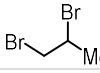	0	58	36	0

*Ester suffered from hydrolysis under basic conditions.

E3. Reaction Optimization

E3.1. Experimental Procedures with Cs_2CO_3 Quench

To an oven-dried divided electrochemical cell equipped with magnetic stir bars was added thianthrene (48.7 mg, 0.225 mmol, 1.5 equiv.) to the anode compartment and KPF_6 (110 mg, 0.6 mmol) to both compartments. The cell was equipped with two septa containing a stainless steel wire/Ni foam cathode assembly and a pencil/RVC anode assembly connected together with a teflon tubing to equalize pressure. MeCN (3 mL) was added to the cathode and anode compartments. 4-phenylbutene (23 µL, 0.15 mmol, 1 equiv.) was added to the anode compartment. TFA (116 µL, 1.5 mmol, 10 equiv.) was added to the cathode compartment and both sides of the cell were stirred at 30 °C and electrolyzed under a constant current of 4.5 for 2.5 h (2.5 F/mol). At completion of electrolysis, the electrode leads were disconnected, septa removed, and the anode RVC was pushed off the pencil into the reaction mixture.

Following electrolysis, dibromomethane was added as an internal standard to the anodic compartment. The solution was thoroughly stirred, and 50 µL of mixture mixture was added to an NMR tube prefitted with a glass-sealed NMR insert filled with MeCN-*d3*. The NMR tube was diluted with 0.2 mL MeCN and an NMR of adduct was taken.

The cathode solution was removed from the cell via pipette and a fresh septum was added to the cathode department to prevent equilibration. 2-(6-chloropyridin-3-yl)acetonitrile (22.9 mg, 0.15 mmol, 1 equiv.) was added to the anode compartment followed by Cs_2CO_3 (varying equiv.). To the anode compartment was added a septum pierced with a needle to prevent pressurizing. After pressure equilibration, the needle was removed, and the anode solution was stirred in the cell for 2.5 h.

Following the Cs_2CO_3 quench, upon substitution reaction completion, the reaction mixture was taken up in an NMR tube for NMR yield.

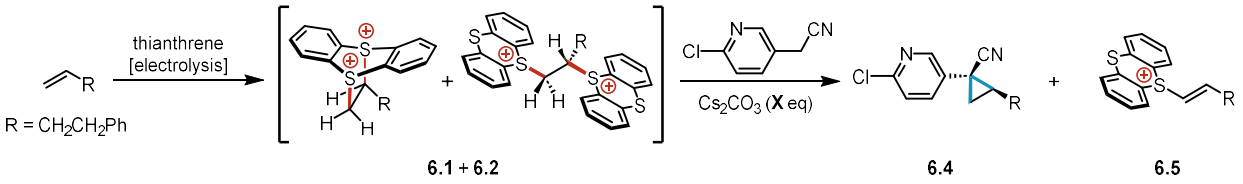

Table E3. Base equivalence screening yields.

Cs_2CO_3 (equiv.)	6.1 + 6.2 (%)	6.4 (%)	6.5 (%)
1	88	0	90
2	81	0	83
3	89	5	80
4	85	19	56
5	83	32	43
6	84	67	0
8	78	71	0
10	86	80	0

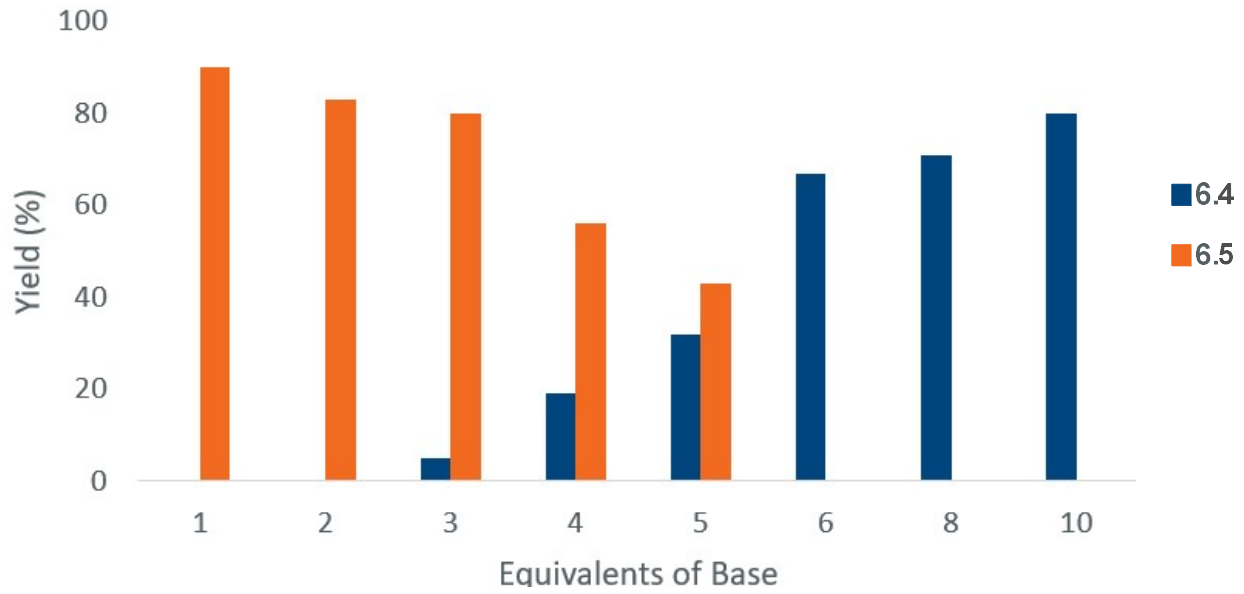

Figure E2. Base equivalence screening for cyclopropanation yield via dication pool.

E3.2. Experimental Procedures for Reaction Time Course Study for Substitution

To an oven-dried divided electrochemical cell equipped with magnetic stir bars was added thianthrene (48.7 mg, 0.225 mmol, 1.5 equiv.) to the anode compartment and KPF_6 (110 mg, 0.6 mmol) to both compartments. The cell was equipped with two septa containing a stainless steel wire/Ni foam cathode assembly and a pencil/RVC anode assembly connected together with a teflon tubing to equalize pressure. MeCN-*d3* (3 mL) was added to the cathode and anode compartments. 4-phenylbutene (23 µL, 0.15 mmol, 1 equiv.) was added to the anode compartment. TFA (116 µL, 1.5 mmol, 10 equiv.) was added to the cathode compartment and both sides of the cell were stirred at 30 °C and electrolyzed under a constant current of 4.5 mA for 2.5 h (2.5 F/mol). At completion of electrolysis, the electrode leads were disconnected, and dibromomethane was added as an internal standard and the reaction was stirred for an additional minute. Then, 0.5 mL of the anode solution was transferred to an oven-dried NMR tube directly using a syringe. Initially, the concentration of thianthrenium dicationic adducts was quantified via ^{1}H NMR using dibromomethane as an internal standard (NS = 1, Bruker Avance 600, TCI-F cryoprobe) with shimming. (**Note:** the reaction time was tracked relative to collection of the first spectrum.) Following initial scans, the NMR tube was removed from the spectrometer, and 2-(6-chloropyridin-3-yl)acetonitrile (0.025 mmol, 3.81 mg, 1 equiv. relative to solution in NMR tube) was added to the NMR tube. After a couple shakes, the NMR tube was placed in the NMR spectrometer and a series of spectra were gathered (NS = 1, no lock, no shimming). The NMR tube was again removed from the spectrometer, and Cs_2CO_3 (0.250 mmol, 81.5 mg, 10 equiv. relative to solution in NMR tube) was added to the NMR tube through a glass pipette to prevent solid sticking to the side of the tube. Without mixing, the solid was allowed to sink to the bottom, and the NMR tube was placed in the NMR spectrometer and a series of spectra were gathered (NS = 1, no lock, no shimming). Starting around 18 minutes after initial spectrum was taken, the NMR tube was removed from the spectrometer and mixed by hand in increasing increments of time (0.5, 1, 2, 4 mins). Spectra were collected after each mixing event (NS = 1, no lock, no shimming). Starting around 35 minutes after initial spectrum was taken, the NMR tube was removed from the spectrometer and mixed attached to a rotary evaporator and spun at lowest setting (approximately 10 full revolutions per minute). At varying times during the reaction, mixing was stopped, and spectra were collected to determine the concentration of alkenylthianthenium salt and final cyclopropane product using dibromomethane as an internal standard.

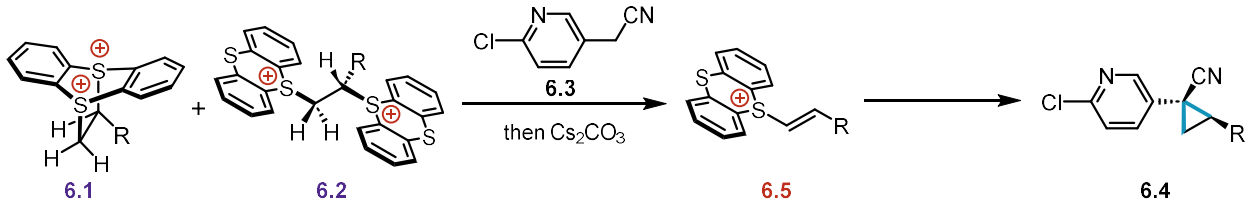

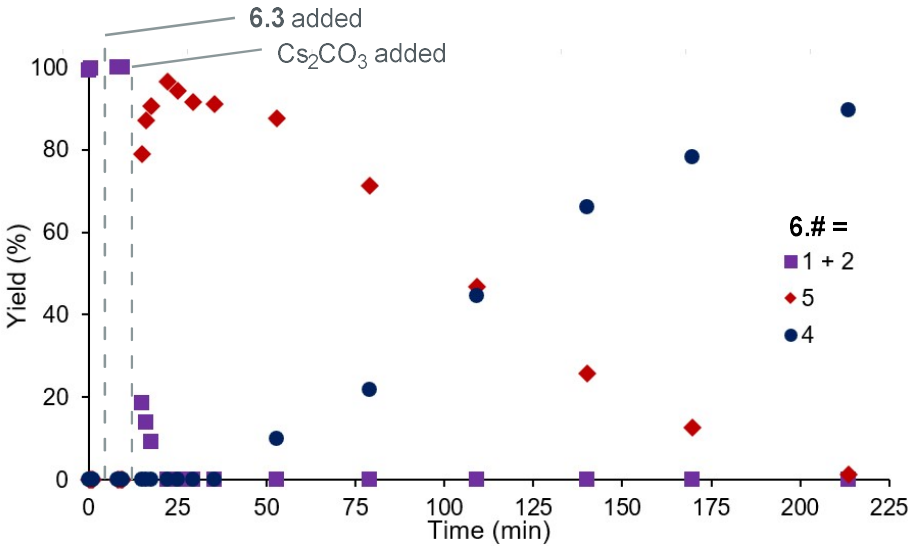

Figure E3. Reaction profile of substitution step with 10 equiv. of Cs_2CO_3. (R = CH_2CH_2Ph).

Table E4. Full time course data for cyclopropanation via dication pool.

Time (mins)	1 + 2	5	4
0	99	0	0
9	100	0	0
15	19	79	0
16	14	87	0
18	9	91	0
22	0	96	0
25	0	94	0
29	0	91	0
35	0	91	0
53	0	88	10
79	0	71	22
109	0	47	45
140	0	26	66
170	0	13	78
214	0	1	90

This ^{1}H NMR time course supports facile elimination of adducts **1** and **2** to form alkenyl thianthrenium **5**, which serves as a key intermediate en route to cyclopropane product **4**. Similarly, mechanistic studies for other transformations via the dication pool also support alkenyl thianthrenium as competent intermediates for both aziridination[7] (see below for data) and allylic amination.[8]

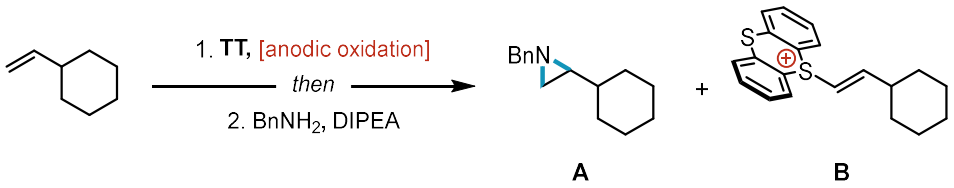

Table E5. Time course of aziridination via the dication pool.

Time (h)	A	B
0.5	17	48
3	23	53
18	0	83

E3.3. Testing Effect of Nitrile vs Ester Groups on Diastereoselectivity

To a 1 dram vial was added a stir bar and (*E*)-5-(4-phenylbut-1-en-1-yl)-5H-thianthren-5-ium hexafluorophosphate (43.4 mg, 0.100 mmol) followed by MeCN (2 mL). Then either 2-(6-chloropyridin-3-yl)acetonitrile (15.3 mg, 100 µmol, 1 equiv.) or ethyl-2-(6-chloropyridin-3-yl)acetate (20.0 mg, 15.5 µL, 100 µmol, 1 equiv.) was added, followed by Cs_2CO_3 (65.2 mg, 200 µmol, 2 equiv.). The solution was stirred for 2.5 h. Dibromomethane was added as an internal standard and an aliquot for NMR yield was taken. Cyclopropane coupling product yield and d.r. was determined via ^{1}H NMR. See Reaction Optimization section for characterization of products.

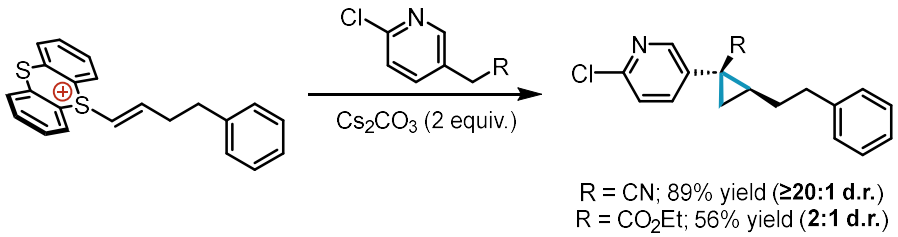

Scheme E2. Cyclopropanation of alkenyl-TT$^+$ as starting material. Distinct d.r. is observed based on steric profile for substituents on acidic methylene carbon pronucleophile.

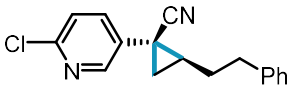

1-(6-Chloropyridin-3-yl)-2-phenethylcyclopropane-1-carbonitrile (6.4): Following procedures outlined above afforded an NMR yield of 81% yield, mixture of diastereomers, ≥20:1 d.r. Structural configuration assigned via analogy with compound **6.25**. **^{1}H NMR** (500 MHz, $CDCl_3$) δ 8.23 (d, *J* = 2.6 Hz, 1H), 7.49 (dd, *J* = 8.4, 2.7 Hz, 1H), 7.29 (dd, *J* = 8.0, 6.3 Hz, 3H), 7.24 – 7.18 (m, 3H), 3.01 – 2.76 (m, 2H), 2.16 – 2.00 (m, 2H), 1.61 (dd, *J* = 8.0, 4.7 Hz, 1H), 1.58 – 1.49 (m, 2H). Distinct minor diastereomer signals observed at δ 8.17 (d, *J* = 2.7 Hz, 0H), 2.58 (td, *J* = 7.9, 4.2 Hz, 1H), 1.74 (dd, *J* = 9.3, 6.3 Hz, 0H), 1.43 (dd, *J* = 7.2, 5.3 Hz, 0H), 1.33 (dd, *J* = 7.4, 5.9 Hz, 1H). **^{13}C NMR** (126 MHz, $CDCl_3$) δ 150.88, 147.18, 140.52, 136.67, 131.74, 128.76, 128.66, 126.52, 124.37, 119.64, 34.90, 33.09, 30.34, 24.20, 17.80. **HRMS** (ESI+) Calc: $[M+H]^+$ ($C_{17}H_{15}ClN_2$) 283.0997, measured: 283.0994; 1.1 ppm difference.

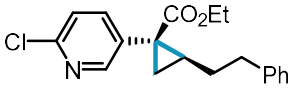

Ethyl 1-(6-chloropyridin-3-yl)-2-phenethylcyclopropane-1-carboxylate (E1): Following procedure outlined above afforded an NMR yield of 56% yield, mixture of diastereomers, 2.4:1 d.r. Structural configuration assigned via analogy with compound **6.29**. **^{1}H NMR** (500 MHz, $CDCl_3$) δ 8.27 (d, *J* = 2.4 Hz, 1H), 7.51 (dd, *J* = 8.2, 2.6 Hz, 1H), 7.30 (dd, *J* = 8.2, 6.9 Hz, 2H), 7.25 – 7.18 (m, 4H), 4.19 – 4.04 (m, 2H), 2.75 (td, *J* = 7.4, 2.4 Hz, 2H), 2.08 – 1.93 (m, 2H), 1.66 (dd, *J* = 7.5, 4.7 Hz, 1H), 1.55 – 1.45 (m, 1H), 1.28 (dd, *J* = 9.0, 4.7 Hz, 1H), 1.17 (t, *J* = 7.1 Hz, 3H). Distinct minor diastereomer signals observed at δ 8.27 (dd, *J* = 2.5, 0.7 Hz, 1H), 7.51 (dd, *J* = 8.2, 2.4 Hz, 1H), 7.29 – 7.22 (m, 3H), 7.20 – 7.13 (m, 1H), 7.10 – 7.04 (m, 2H), 4.16 – 4.00 (m, 2H), 2.75 – 2.62 (m, 2H), 1.91 (tdd, *J* = 9.2, 6.9, 4.9 Hz, 1H), 1.79 (ddd, *J* = 9.0, 4.4, 0.7 Hz, 1H), 1.67 (dddd, *J* = 13.6, 8.7, 6.8, 4.8 Hz, 1H), 1.16 (t, *J* = 7.1 Hz, 3H), 1.06 (dd, *J* = 6.9, 4.4 Hz, 1H), 0.83 (dtd, *J* = 13.9, 9.0, 6.6 Hz, 1H). **HRMS** (ESI+) Calc: $[M+H]^+$ ($C_{19}H_{20}ClNO_2$) 330.1255, measured: 330.1253; 0.6 ppm difference.

E3.4. Experimental Procedures with Basic Alumina Filtration Quench

To an oven-dried divided electrochemical cell equipped with magnetic stir bars was added thianthrene (130 mg, 0.600 mmol, 1.5 equiv.) to the anode compartment and KPF_6 (294 mg, 1.60 mmol) to both compartments. The cell was equipped with two septa containing a stainless steel wire/Ni foam cathode assembly and a pencil/RVC anode assembly connected together with a teflon tubing to equalize pressure. MeCN (8 mL) was added to the cathode and anode compartments. 4-phenylbutene (60 µL, 0.400 mmol, 1 equiv.) was added to the anode compartment. TFA (308 µL, 4.00 mmol, 10 equiv.) was added to the cathode compartment and both sides of the cell were stirred at 30 °C and electrolyzed under a constant current of 12.0 mA for 2.25 h (2.5 F/mol alkene). At completion of electrolysis, the electrode leads were disconnected, septa removed, and the anode RVC was pushed off the pencil into the reaction mixture.

Following electrolysis, dibromomethane was added as an internal standard to the anodic compartment. The solution was thoroughly stirred, and 50 µL of mixture mixture was added to an NMR tube pre-fitted with a glass-sealed NMR insert filled with MeCN-*d3*. The NMR tube was diluted with 0.2 mL MeCN and an NMR of adduct was taken.

The cathode solution was removed from the cell via pipette and a fresh septum was added to the cathode department to prevent equilibration. The anode solution was filtered over a pad of basic alumina (8 g, activated, basic, Brockmann I). The cathode compartment was washed with MeCN (2.0 mL) and pushed across the frit to rinse the frit. The anode compartment was further washed with MeCN (5 x 1.2 mL). The alumina pad was washed with MeCN (2 x 8 mL), taking care to fully disperse the alumina in solution using a spatula. The filtrate was concentrated in vacuo and then resuspended in MeCN (1.5 mL). 2-(6-chloropyridin-3-yl)acetonitrile or (61.0 mg, 0.400 mmol, 1 equiv.) was added to the reaction mixture followed by Cs_2CO_3 (261 mg, 0.800 mmol, 2 equiv.). The solution was stirred for 2.5 h.

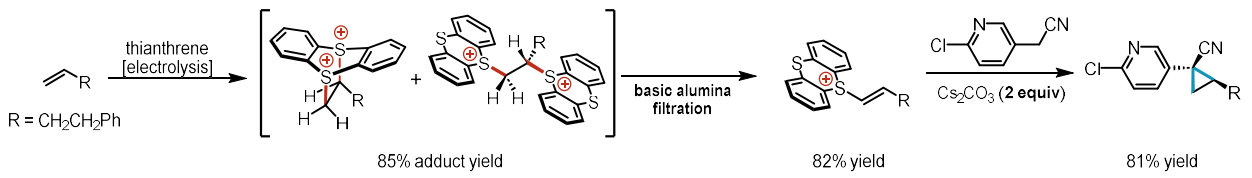

Scheme E3. Cyclopropanation via the dication pool using a basic alumina quench.

E4. Substrate Preparation

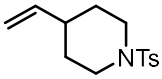

1-Tosyl-4-vinylpiperidine (E3) – prepared in three steps according to *Angew. Chem. Int. Ed.* **2018**, 57, 13096-13100.

Step 1: synthesis of *tert*-Butyl 4-vinylpiperidine-1-carboxylate (E2): An oven-dried round bottom flask under N_2 was charged with $MePPh_3I$ (28.9 g, 71.5 mmol, 1.3 equiv.) and THF (275 mL, 0.2 M). KOtBu (8.64 g, 77.0 mmol, 1.4 equiv.) was added to the suspension at 0 °C. The resulting mixture was allowed to warm to room temperature and stirred for 1 h. The yellow suspension was then cooled to 0 °C and *tert*-butyl-4-formylpiperidine-1-carboxylate (11.7 g, 55.0 mmol, 1 equiv.) was added. The reaction was allowed to warm to room temperature and stirred overnight. Following completion monitored via TLC, the reaction mixture was concentrated under reduced pressure and then diluted with ether (~ 100 mL) to precipitate triphenylphosphine oxide. The mixture was filtered, and the solid was washed 5x with ether. The filtrate was collected, concentrated under reduced pressure, and the reside was purified via flash column chromatography (EtOAc/hexanes) to give 11.1 g (96%) of **E2** as a liquid. **^{1}H NMR** (400 MHz, $CDCl_3$) δ 5.77 (ddd, J = 17.0, 10.5, 6.4 Hz, 1H), 4.98 (m, 2H), 4.08 (m, 2H), 2.72 (m, 2H), 2.11 (m, 2H), 1.68 (d, J = 13.2, Hz, 2H), 1.45 (s, 9H), 1.28 (m, 2H). **^{13}C NMR** consistent with reported spectra (*Angew. Chem. Int. Ed.* **2018**, 57, 13096-13100).

Step 2: synthesis of 1-Tosyl-4-vinylpiperidine (E3): An oven-dried round bottom flask was charged with **E2** (9.80 g, 46.4 mmol, 1 equiv.) and 1:1 DCM:TFA (60 mL, 0.8 M). The reaction was stirred at room temperature and monitored for completion via TLC (~ 1 h). Then NEt_3 (70mL), DMAP (567 mg, 4.64 mmol, 0.1 equiv.), and tosyl chloride (10.6 g, 55.7 mmol, 1.2 equiv.) were added to the reaction mixture. The mixture was stirred at room temperature for 16 h. The mixture was then quenched with water (250 mL). The organic layer was separated, and the aqueous layer was extracted with DCM (3 x 250 mL). The combined organic layers were dried over anhydrous Na_2SO_4, filtered, and concentrated under reduced pressure. The residue was purified via flash column chromatography (conditions) to give 10.1 g (82% yield) of **E3** as a solid. **^{1}H NMR** (400 MHz, $CDCl_3$) δ 7.64 (d, J = 8.3 Hz, 2H), 7.32 (d, J = 7.9 Hz, 2H), 5.71 (ddd, J = 17.1, 10.5, 6.4 Hz, 1H), 4.96 (m, 2H), 3.76 (dt, J = 11.9, 3.3 Hz, 2H), 2.43 (s, 3H), 2.28 (td, J = 11.9, 2.6 Hz, 2H), 1.88 (m, 1H), 1.74 (m, 2H), 1.49 (m, 2H). ^{13}C NMR consistent with reported spectra (*Angew. Chem. Int. Ed.* **2018**, 57, 13096-13100).

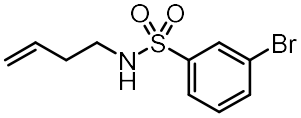

3-bromo-*N*-(but-3-en-1-yl)benzenesulfonamide (E4): To a solution of 3-bromobenzenesulfonyl chloride (2.56 g, 10.0 mmol, 1.1 equiv.) in DCM (10 mL) at 0 °C was added NEt_3 (1.4 mL, 10.0 mmol, 1.1 equiv.) followed by 3-buten-1-amine (0.84 mL, 9.09 mmol, 1 equiv.). The mixture was allowed to warm to room temperature overnight. 1 N HCl (~20 mL) was added to the reaction mixture and the layers were separated. The aqueous layer was extracted with DCM (~40 mL x3). The combined organic layers were dried with anhydrous Na_2SO_4, filtered, and evaporated under reduced pressure. The residue was purified via flash column chromatography (EtOAc/hexanes) to give 2.00 g (76 % yield) of **E4** as a white fluffy solid. **^{1}H NMR** (400 MHz, $CDCl_3$) δ 8.01 (t, J = 1.9 Hz, 1H), 7.79 (ddd, J = 7.9, 1.8, 1.0 Hz, 1H), 7.71 (ddd, J = 8.0, 1.9, 1.0 Hz, 1H), 7.40 (t, J = 7.9 Hz, 1H), 5.63 (ddt, J = 17.1, 10.3, 6.9 Hz, 1H), 5.16 – 5.01 (m, 2H), 4.47 (t, J = 6.4 Hz, 1H), 3.07 (q, J = 6.4 Hz, 2H), 2.28 – 2.20 (m, 2H). ^{13}C NMR consistent with reported spectra (*Nature* **2021**, 596, 74-79).

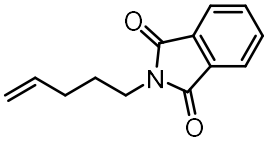

2-(pent-4-enyl)-isoindoline-1,3-dione (E5): To a mixture of potassium phthalimide (11.11 g, 60.0 mmol, 1.5 equiv.) in DMF (80 mL) was added 5-brompent-1-ene (4.74 mL, 40.0 mmol, 1 equiv.). The reaction mixture was heated to 60 °C and stirred overnight (18 h). At completion, the mixture was cooled to room temperature and poured into a saturated brine solution (~200 mL). The aqueous layer was extracted with Et_2O (3 x 150 mL). The combined organic layers were washed with aqueous 10% LiCl solution (2 x 20 mL), dried over anhydrous Na_2SO_4, filtered, and concentrated under reduced pressure. The residue was purified via flash column chromatography (EtOAc/hexanes) to give 4.66 g (54% yield) of **E5** as a solid. **^{1}H NMR** (500MHz, $CDCl_3$) δ 7.82 (dd, J = 5.4, 3.0 Hz, 2H), 7.69 (dd, J = 5.5, 3.0 Hz, 2H), 5.80 (ddt, J = 16.9, 10.2, 6.6 Hz, 1H), 5.03 (dd, J = 17.1, 1.7 Hz, 1H), 4.96 (dd, J = 10.3, 1.4 Hz, 1H), 3.68 (t, J = 7.4 Hz, 2H), 2.14 – 2.06 (m, 2H), 1.77 (ddd, J = 14.7, 8.1, 6.8 Hz, 2H); ^{13}C NMR consistent with reported spectra (*JACS* **2009**, 131, 9670–9685).

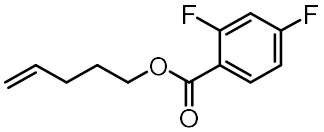

Pent-4-en-1-yl 2,4-difluorobenzoate (E6). A mixture of 2,4-difluorobenzoic acid (1.11 g, 7.0 mmol, 1 equiv.), N-(3-Dimethylaminopropyl)-N′-ethylcarbodiimide hydrochloride (1.74 g, 9.1 mmol, 1.3 equiv.), and 4-(dimethylamino)pyridine (86 mg, 0.7 mmol, 0.1 equiv.) in DCM (28 mL) was stirred at 0 °C for 20 min. Pent-4-en-1-ol (724 mg, 8.4 mmol, 0.87 mL, 1.1 equiv.) was added and the reaction mixture was allowed to warm to room temperature. At completion as monitored by TLC, the mixture was diluted with DCM and extracted with 1N HCl solution (~80 mL). The organic layer was washed with brine solution (~50 mL), dried over anhydrous MgSO4, filtered, and concentrated under reduced pressure. The residue was purified via flash column chromatography (EtOAc/hexanes) to give 1.14 g (72% yield) of **E6** as an oil. **^{1}H NMR** (500MHz, $CDCl_3$) δ 7.95 (td, J = 8.5, 6.5 Hz, 1H), 6.91 (dddd, J = 8.7, 7.6, 2.5, 1.0 Hz, 1H), 6.85 (ddd, J = 11.1, 8.9, 2.5 Hz, 1H), 5.82 (ddt, J = 16.9, 10.2, 6.6 Hz, 1H), 5.05 (dq, J = 17.1, 1.7 Hz, 1H), 5.01 – 4.96 (m, 1H), 4.32 (t, J = 6.5 Hz, 2H), 2.24 – 2.15 (m, 2H), 1.84 (dq, J = 8.1, 6.6 Hz, 2H). ^{13}C NMR consistent with reported spectra (*JACS* **2021**, 143, 21503-21510).

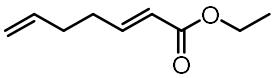

(E)-ethyl hepta-2,6-dienoate (E7): In a flame-dried 1L round-bottom flask, oxalyl chloride (9.77 g, 6.8 mL, 77.0 mmol, 1.1 equiv.) was dissolved in DCM (240 mL). The reaction mixture was cooled to -78 °C. DMSO (13.1 g, 11.9 mL, 168 mmol, 2.4 equiv.) was added, and the reaction was stirred at -78 °C for 10 min. Pent-4-en-1-ol (6.03 g, 7.2 mL, 70.0 mmol, 1 equiv.) was added dropwise, and the reaction was stirred at -78 °C for 30 min before warming to room temperature. (Carbethoxymethylene)triphenylphosphorane (36.6 g, 105 mmol, 1.5 equiv.) dissolved in DCM (55 mL) was added. The reaction was stirred at room temperature for 2 h. Water (100 mL) was added to the reaction mixture and the layers were separated. The aqueous layer was extracted with DCM (50 mL x 3). The combined organic layers were washed with brine (40 mL), dried with anhydrous $MgSO_4$, filtered, and evaporated under reduced pressure. The residue was purified via flash column chromatography (EtOAc/hexanes) to give 8.53 g (79 % yield) of **E7** as an oil. **^{1}H NMR** (400 MHz, $CDCl_3$) δ 6.96 (dt, J = 15.6, 6.7 Hz, 1H), 5.87 – 5.74 (m, 2H), 5.09 – 4.97 (m, 2H), 4.18 (q, J = 7.1 Hz, 2H), 2.35-– 2.36 (m, 2H), 2.25 – 2.18 (m, 2H), 1.28 (t, J = 1.3 Hz, 3H). ^{13}C NMR consistent with reported spectra (*Australian Journal of Chemistry* **2000**, 53, 659-664).

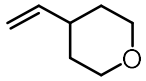

4-vinyltetrahydro-2H-pyran (E8): Sodium hydride (60% oil dispersion, 973 mg, 24 mmol, 1.2 equiv.) was washed with 3 portions of hexanes under an inert atmosphere to remove oil. THF (82 mL) was then added followed by methyltriphenylphosphonium iodide (9.8 g, 24 mmol, 1.2 equiv.). The reaction mixture was then heated to reflux for 2 h. The solution was then cooled to room temperature. Tetrahydro-2H-pyran-4-carbaldehyde (2.3 g, 20 mmol, 1.0 equiv.) was slowly added and the reaction was allowed to stir for an additional 24 h. Upon reaction completion, saturated aqueous $NaHCO_3$ (40 mL) was added and the mixture was extracted with Et_2O (80 mL). The organic layer was then washed with water and brine, dried over $MgSO_4$, and concentrated. (Note: Due to the volatility of the product, the rotavap bath was kept at 0 °C.) The product was purified via column chromatography (Et_2O/pentane) to yield 800 mg (35% yield) of the **E8** as an oil. **^{1}H NMR** (500 MHz, $CDCl_3$) δ 5.78 (ddd, J = 17.0, 10.4, 6.3 Hz, 1H), 5.00 (dt, J = 17.3, 1.6 Hz, 1H), 4.96 (dt, J = 10.5, 1.5 Hz, 1H), 3.97 (ddd, J = 11.5, 4.6, 2.0 Hz, 2H), 3.42 (td, J = 11.7, 2.2 Hz, 2H), 2.26 – 2.15 (m, 1H), 1.63 (ddq, J = 13.2, 4.2, 2.2 Hz, 2H), 1.46 (dtd, J = 13.3, 11.6, 4.4 Hz, 2H). **^{13}C NMR** (126 MHz, CDCl3) δ 142.81, 112.71, 67.70, 38.70, 32.21. **HRMS** (ESI+) Calc: $[M+H]^+$ ($C_7H_{13}O$) 113.0961, measured: 113.0960.

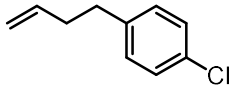

1-(but-3-en-1-yl)-4-chlorobenzene (E9): Allylmagnesium bromide (1 M in THF, 25.8 mL, 25.8 mmol, 1.29 equiv.) was added to a solution of 4-chlorobenzyl bromide (4.11 g, 20 mmol) in Et2O (30 mL) at 0 °C under an inert atmosphere. The reaction was allowed to come to room temperature and stirred for 2 h. Upon reaction completion, the reaction was quenched with saturated aqueous NH_4Cl. The aqueous layer was extracted with DCM, and the combined organic layers were dried over $MgSO_4$, filtered through celite, and concentrated. The crude mixture was purified via flash column chromatography followed by distillation to yield 2.04 g (61% yield) of **E9** as an oil. **^{1}H NMR** (400 MHz, $CDCl_3$) δ 7.27 (dt, *J* = 9.0, 2.1 Hz, 2H), 7.18 – 7.10 (m, 2H), 5.85 (ddt, *J* = 16.9, 10.2, 6.6 Hz, 1H), 5.10 – 4.96 (m, 2H), 2.70 (dd, *J* = 8.8, 6.7 Hz, 2H), 2.37 (tdt, *J* = 7.8, 6.5, 1.4 Hz, 2H). ^{13}C NMR consistent with reported spectra (*Chem. Commun.* **2013**, *49* (95), 11230-11232).

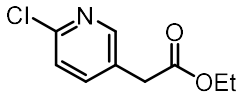

Ethyl 2-(6-chloropyridin-3-yl)acetate (E10): (6-chloropyridin-3-yl)acetonitrile (1.00 g, 6.55 mmol) was added to a mixture of EtOH (12.2 mL) and concentrated sulfuric acid (4.54 mL, 85.2 mmol), and the mixture was stirred under reflux for 45 h. The reaction mixture was slowly added dropwise while stirring to a mixture of $NaHCO_3$ (16.0 g, 190 mmol) and water (100 mL). The aqueous phase was extracted with DCM (5 x 200 mL). The combined organic phases were dried over Na_2SO_4, filtered, and evaporated under reduced pressure. The crude mixture was purified via column chromatography (EtOAC/hexanes) to yield 1.15 g (88% yield) of the **E10** as an oil. **^{1}H NMR** (500 MHz, $CDCl_3$) δ 8.31 – 8.27 (m, 1H), 7.62 (dd, *J* = 8.2, 2.6 Hz, 1H), 7.30 (dd, *J* = 8.2, 0.6 Hz, 1H), 4.17 (q, *J* = 7.1 Hz, 2H), 3.60 (s, 2H), 1.26 (t, *J* = 7.2 Hz, 3H). ^{13}C NMR consistent with reported spectra (*Chem. Med. Chem.* **2018**, 13 (10), 988–1003).

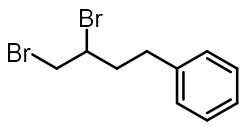

(3,4-Dibromobutyl)benzene (S11): 4-Phenylbutene (5.3 mL, 35.0 mmol, 1.0 equiv.) and DMSO (3.0 mL, 42.0 mmol, 1.2 equiv.) were dissolved in EtOAc (140 mL). The reaction mixture was heated to 60 °C. Aqueous HBr (48%, 9.6 mL, 84.0 mmol, 2.4 equiv.) was added. The reaction was stirred at 60 °C for 30

min. After cooling to room temperature, the reaction mixture was concentrated under reduced pressed. The crude mixture was purified via column chromatography (EtOAc/hexanes) to yield 9.96 g (98% yield) of **S11** as an oil. ^{1}**H NMR** (500 MHz, $CDCl_3$) δ 7.33 (m, 2H), 7.25 (m, 3H), 4.13 (tdd, J = 9.6, 4.5, 3.0 Hz, 1H), 3.87 (dd, J = 10.3, 4.4 Hz, 1H), 3.66 (t, J = 10.0 Hz, 1H), 2.96 (ddd, J = 13.9, 0.3, 4.7 Hz, 1H), 2.78 (ddd, J = 13.8, 9.2, 7.2 Hz, 1H), 2.50 (dddd, J = 14.7, 9.2, 7.2, 3.0 Hz, 1H), 2.11 (dtd, J = 14.3, 9.3, 4.7 Hz, 1H). ^{13}C NMR consistent with reported spectra (*Green Chem.* **2015**, *17*, 3285-3289.)

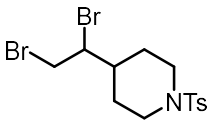

4-(1,2-Dibromoethyl)-1-tosylpiperidine (E12): N-Bromosuccinimide (1.07 g, 6.00 mmol, 3.0 equiv.) and DMSO (0.43 mL, 6.00 mmol, 3.0 equiv.) were dissolved in DCM (24 mL), and the reaction mixture was let stir until NBS completely dissolved. 1-Tosyl-4-vinylpiperidine (**S3**) was added, and the reaction mixture was stirred at room temperature for 30 min. The crude mixture was purified via column chromatography (EtOAc/hexanes) to yield 510 mg (60% yield) of **E12** as a solid. ^{1}**H NMR** (500 MHz, $CDCl_3$) δ 7.65 (d, J = 8.3 Hz, 2H), 7.33 (d, J = 8.1 Hz, 2H), 4.11 (dt, J = 9.7, 4.2 Hz, 1H), 3.93 – 3.85 (m, 2H), 3.82 (dd, J = 10.7, 4.7 Hz, 1H), 3.66 (d, J = 10.7, 9.7 Hz, 1H), 2.42 (s, 3H), 2. 28 (dtd, J = 15.1, 12.1, 2.9 Hz, 2H), 1.88 – 1.70 (m, 3H), 1.67 – 1.53 (m, 2H). **^{13}C NMR** (126 MHz, CDCl3) δ 143.75, 133.25, 129.83, 127.86, 57.01, 46.07, 45.95, 37.90, 33.72, 30.13, 25.78, 21.67. **HRMS** (ESI+) Calc: $[M+H]^+$ ($C_{14}H_{19}Br_2NO_2S$) 423.9576, measured: 423.9571; 1.2 ppm difference.

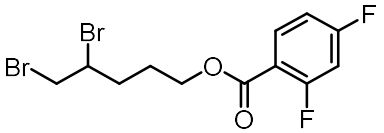

4,5-Dibromopentyl 2,4-difluorobenzoate (E13): N-Bromosuccinimide (1.07 g, 6.00 mmol, 3.0 equiv.) and DMSO (0.43 mL, 6.00 mmol, 3.0 equiv.) were dissolved in DCM (24 mL), and the reaction mixture was let stir until NBS completely dissolved. Pent-4-en-1-yl 2,4-difluorobenzoate (**S6**) was added, and the reaction mixture was stirred at room temperature for 30 min. The crude mixture was purified via column chromatography (EtOAc/hexanes) to yield 368 mg (48% yield) of **E13** as an oil. ^{1}**H NMR** (500 MHz, $CDCl_3$) δ 8.00 – 7.94 (m, 1H), 6.96 – 6.90 (m, 1H), 6.90 – 6.84 (m, 1H), 4.42 – 4.34 (m, 2H), 4.25 – 4.19 (m, 1H), 3.87 (dd, J = 10.3, 4.3 Hz, 1H), 3.63 (t, J = 10.2 Hz, 1H), 2.43 – 2. 31 (m, 1H), 2.13 – 2.02 (m, 1H), 1.98 – 1.85 (m, 2H). **^{13}C NMR** (126 MHz, CDCl3) δ 165.85 (dd, J = 256. 4, 12.0 Hz), 163.60 (d, J = 4.2 Hz), 162.97 (dd, J = 263.4, 12.7 Hz), 134 (dd, J = 10.5, 2.3 Hz), 115.25 (dd, J = 9.9, 3.7 Hz), 111.74 (dd, J = 21.6, 3.9 Hz), 105.38 (t, J = 25.7 Hz), 64.42, 52.04, 36.02, 32.85, 26.26. **^{19}F NMR** (377 MHz, $CDCl_3$) δ -101.73 (d, J = 12.5 Hz, 1F), -103.58 (d, J = 12.6 Hz, 1F). **HRMS** (ESI+) Calc: $[M+H]^+$ ($C_{12}H_{12}Br_2F_2O_2$) 384.9245, measured: 384.9240; 1.3 ppm difference.

E5. General Experimental Procedures

CAUTION: Although there is no known toxicology data on these dicationic adducts and no issues were encountered during these experiments, we suspect, based on analogy to other dielectrophiles, that these adducts are toxic. Isolation or storage of the adducts was avoided.

General Procedure A: Electronically Neutral Alkenes

To an oven-dried divided electrochemical cell equipped with magnetic stir bars was added thianthrene (130 mg, 0.6 mmol, 1.5 equiv.) to the anode compartment and *n*-Bu_4NPF_6 (620 mg, 1.6 mmol, 4 equiv.) to both compartments. The cell was equipped with two septa containing a stainless steel wire/Ni foam cathode assembly and a pencil/RVC anode assembly connected together with a teflon tubing to equalize pressure. MeCN (8 mL) was added to the cathode compartment and the glass frit was allowed to become saturated (<1 min). MeCN (8 mL) was added to the anode compartment, followed by alkene (0.4 mmol, 1 equiv.). (Electrode depth: 2 cm). TFA (306 µL, 4.0 mmol, 10 equiv.) was added to the cathode compartment and both sides of the cell were stirred at 30 °C and electrolyzed under a constant current of 12 mA for 2.25 h (2.5 F/mol). At completion of electrolysis, the electrode leads were disconnected, septa removed, and the anode RVC was pushed off the pencil into the anode reaction mixture. To the anode compartment was added a septum pierced with a needle to prevent pressurizing. After pressure equilibration, the needle was removed, and the cathode solution was removed from the cell via pipette. The anode solution was filtered through activated basic alumina (8 g, Brockmann I). The cathode compartment was washed with MeCN (1 mL) and pushed across the frit to rinse the frit. The anode compartment was further washed with MeCN (5 x 1 mL). The alumina pad was washed with MeCN (3 x 8 mL), taking care to fully disperse the alumina in solution using a spatula. The filtrate was concentrated under reduced pressure. Then a stir bar and MeCN (1.5 mL) was added to the flask, followed by carbon pronucleophile (0.4 mmol, 1 equiv.) then Cs_2CO_3 (326 mg, 1.0 mmol, 2.5 equiv.). The solution was stirred for 2 h. At completion, the mixture was diluted with DCM (60 mL) and water (150 mL). The aqueous layer was extracted with DCM (50 mL x 3). The combined organic layers were washed with saturated NaCl solution (40 mL), dried with anhydrous Na_2SO_4, filtered, and concentrated under reduced pressure. The residue was purified via flash column chromatography to yield the pure cyclopropane product.

General Procedure B: Electron Deficient Alkenes

Followed General Procedure A but modified electrolysis by stirring both sides of the cells and electrolyzing under a constant current of 14.4 mA for 2.25 h (3.0 F/mol). Otherwise, procedure A was followed as written.

General Procedure C: Gaseous Alkenes

To an oven-dried divided electrochemical cell equipped with magnetic stir bars was added thianthrene (216 mg, 1.0 mmol, 2.5 equiv.) to the anode compartment and *n*-Bu_4NPF_6 (620 mg, 1.6 mmol) to both compartments. The cell was equipped with two septa containing a stainless steel wire/Ni foam cathode assembly and a pencil/RVC anode assembly connected together with a teflon tubing to equalize pressure. In a separate 10 mL-round bottom flask, MeCN (8 mL) was sparged with a balloon of gaseous alkene for 10 min. Alkene-saturated MeCN (4 mL) was transferred to the cathode and anode compartments via Teflon cannula. TFA (460 µL, 6.0 mmol, 15 equiv.) was added to the cathode compartment and both sides of the cell were stirred at ambient temperature and electrolyzed under a constant current of 30.0 mA for 1.5 h (1.7 F/mol TT). At completion of electrolysis, the electrode leads were disconnected, septa removed, and the anode RVC was pushed off the pencil into the reaction mixture. To the anode compartment was added a septum pierced with a needle to prevent pressurizing. After pressure equilibration, the needle was removed, and the cathode solution was removed from the cell via pipette. The anode solution was filtered through activated basic alumina (8 g, Brockmann I). The cathode compartment was washed with MeCN (1 mL) and pushed across the frit to rinse the frit. The anode compartment was further washed with MeCN (5 x 1 mL). The alumina pad was washed with MeCN (2 x 8 mL), taking care to fully disperse the alumina in solution

using a spatula. The filtrate was concentrated under reduced pressure. Then a stir bar and MeCN (1.5 mL) was added to the flask, followed by carbon pronucleophile (0.4 mmol, 1 equiv.) then Cs_2CO_3 (261 mg, 0.8 mmol, 2.0 equiv.). The solution was stirred for 16 h. At completion, the mixture was diluted with DCM (60 mL) and water (150 mL). The aqueous layer was extracted with DCM (50 mL x 3). The combined organic layers were washed with saturated NaCl solution (40 mL), dried with anhydrous Na_2SO_4, filtered, and concentrated under reduced pressure. The residue was purified via flash column chromatography to yield the pure cyclopropane product.

General Procedure D: Ethylene

Followed General Procedure C but modified substitution by using DBU (121 µL, 0.8 mmol, 2.0 equiv.) instead of Cs_2CO_3. Otherwise, procedure C was followed as written.

General Procedure E: NMR Yield

Following General Procedure A, but with the following modification: following stirring with carbon pronucleophile and Cs_2CO_3 for 2 h, cyclopropane product yield was determined via ^1H NMR using mesitylene or dibromomethane as an internal standard.

E6. Adduct/alkenyl-TT$^+$/Product Yield Breakdown

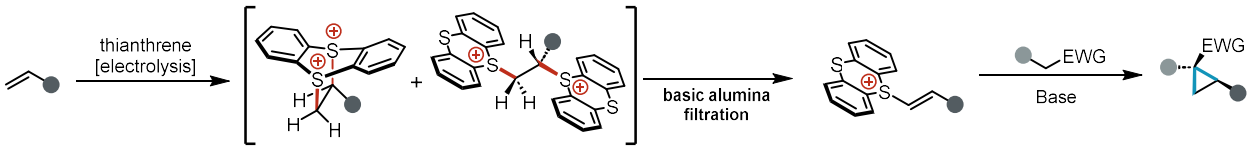

Table S6. Telescoped yields for adduct, alkenyl-TT$^+$, and cyclopropane yield for each substrate. All yields reported relative to carbon pronucleophile as limiting reagent.

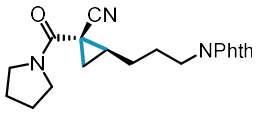

6.6
75% adduct
75% alkenylTT$^+$
70% product

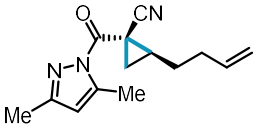

6.7
76% adduct
73% alkenylTT$^+$
61% product

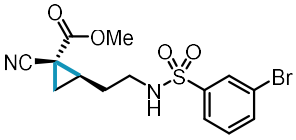

6.8[a]
107% adduct
78% alkenylTT$^+$
54% product

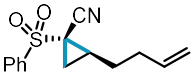

6.9
78% adduct
78% alkenylTT$^+$
74% product

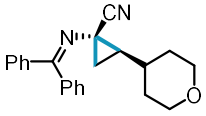

6.10
69% adduct
69% alkenylTT$^+$
68% product

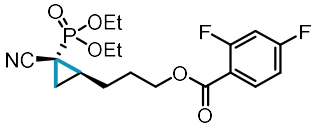

6.11
85% adduct
85% alkenylTT$^+$
68% product

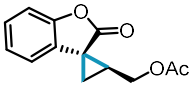

6.12[b]
150% adduct
72% alkenylTT$^+$
54% product

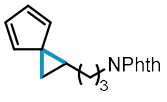

6.13
85% adduct
74% alkenylTT$^+$
45% product

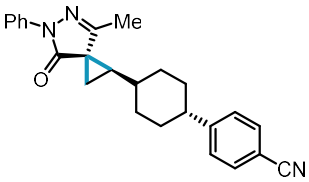

6.14
78% adduct
78% alkenylTT^{+}
69% product

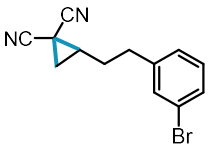

6.15
77% adduct
77% alkenylTT^{+}
67% product

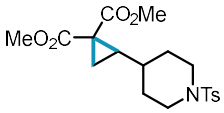

6.16
80% adduct
80% alkenylTT^{+}
74% product

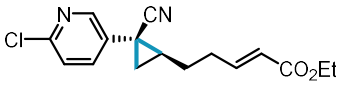

6.17
64% adduct
65% alkenylTT^{+}
54% product

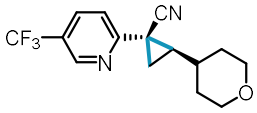

6.18
75% adduct
76% alkenylTT^{+}
63% product

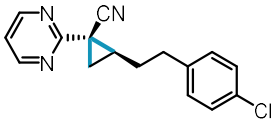

6.19
80% adduct
80% alkenylTT^{+}
78% product

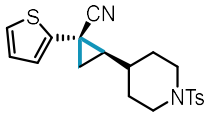

6.20
85% adduct
84% alkenylTT^{+}
74% product

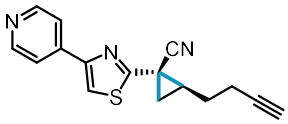

6.21
--
61% alkenylTT^{+}
61% product

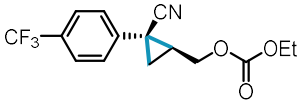

6.22^{b}
166% adduct
68% alkenylTT^{+}
70% product

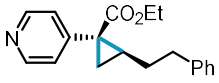

6.23
72% adduct
72% alkenylTT^{+}
66% product

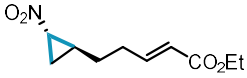

6.24
71% adduct
61% alkenylTT^{+}
55% product

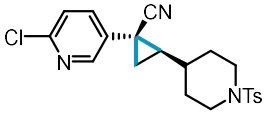

6.25
79% adduct
78% alkenylTT^{+}
74% product

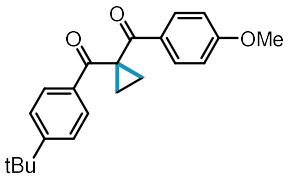

6.26^{c}
--
150% alkenylTT^{+}
76% product

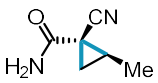

6.27^{c}
--
121% alkenylTT^{+}
74% product

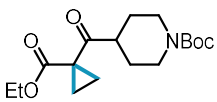

6.28^{c}
--
152% alkenylTT^{+}
95% product

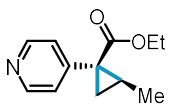

6.29^{c}
--
117% alkenylTT^{+}
83% product

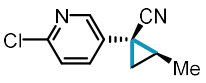

6.30^{c}
--
124% alkenylTT^{+}
95% product

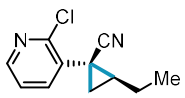

6.31^{c}
--
141% alkenylTT^{+}
99% product

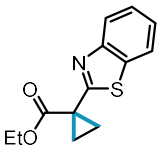

6.32^{c}
--
143% alkenylTT^{+}
67% product

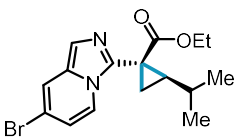

6.33^{c}
--
125% alkenylTT^{+}
50% product

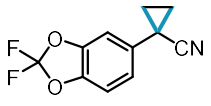

6.34[c]
--
148% alkenylTT$^+$
87% product

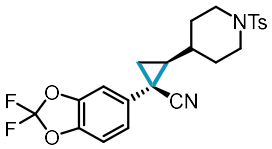

6.35
80% adduct
82% alkenylTT$^+$
75% product

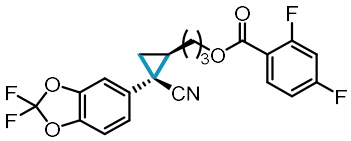

6.36
83% adduct
79% alkenylTT$^+$
66% product

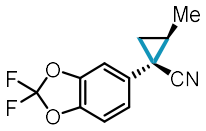

6.37[c]
--
128% alkenylTT$^+$
74% product

[a]1.5 equiv. alkene used; [b]2.0 equiv. alkene used; [c]1 atm alkene used.

Unsuccessful Substrates

Alkenes that failed to form dicationic adduct under electrolysis conditions.

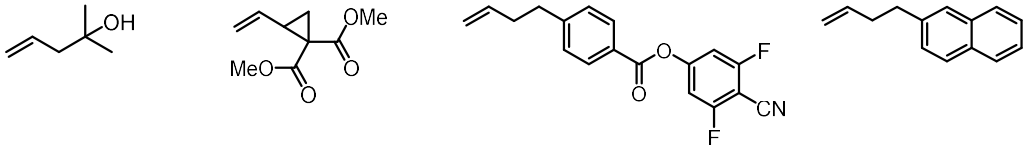

Alkenes that formed adduct but failed to cleanly eliminate to a alkenylthianthrenium salt upon basic workup.

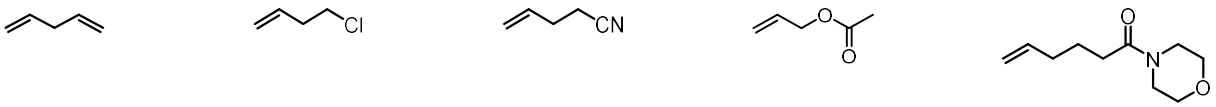

Alkenes that smoothly converted to alkenyl thianthrenium salts but resulted in poor yield of cyclopropane product under substitution conditions.

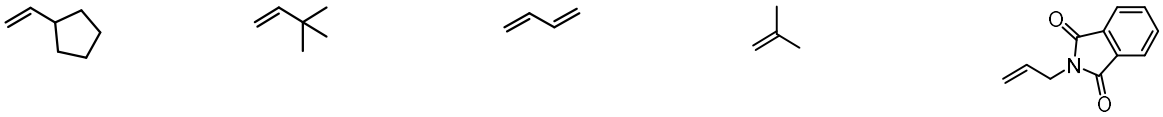

Carbon pronucleophiles that failed to deliver cyclopropane products under substitution conditions.

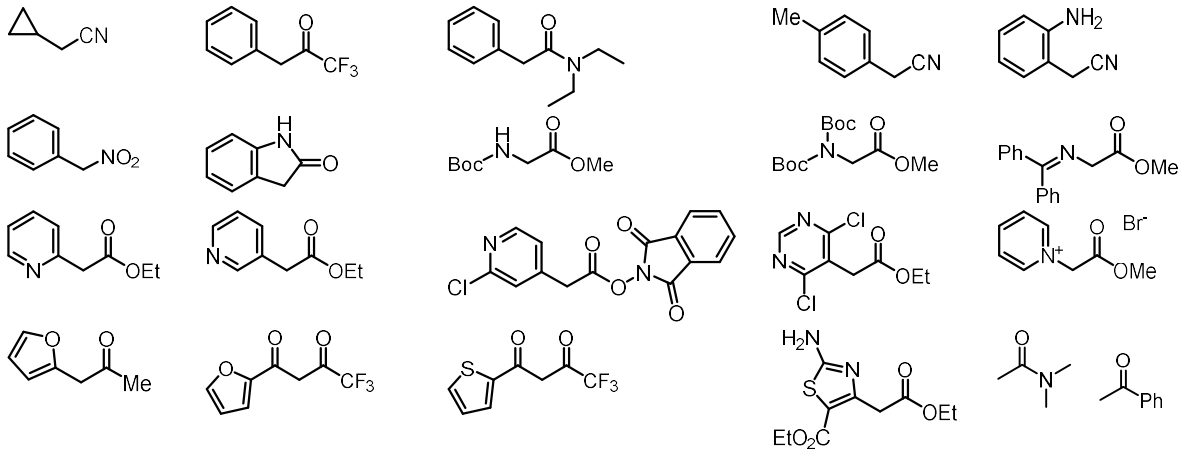

Fig. E4. Alkene and carbon pronucleophile coupling partners that presented challenges for the dication pool.

E7. Product Characterization

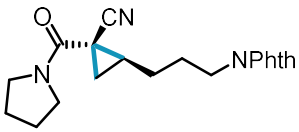

2-(3-(1,3-dioxoisoindolin-2-yl)propyl)-1-(pyrrolidine-1-carbonyl)cyclopropane-1-carbonitrile (6.6). Following General Procedure B afforded one detectable diastereomer in 98.3 mg (70% yield, ≥20:1 d.r.) as an oil. $\mathbf{R_f}$ = 0.14 (20% acetone/hexanes). Structural configuration assigned via analogy with compound **27**. **^{1}H NMR** (500 MHz, $CDCl_3$) δ 7.82 (dd, J = 5.4, 3.0 Hz, 2H), 7.70 (dd, J = 5.5, 3.0 Hz, 2H), 3.82 (dt, J = 10.2, 7.0 Hz, 1H), 3.74 (td, J = 7.1, 1.7 Hz, 3H), 3.45 (t, J = 7.0 Hz, 2H), 2.00 (p, J = 6.8 Hz, 2H), 1.95 – 1.79 (m, 6H), 1.77 – 1.68 (m, 1H), 1.67 – 1.58 (m, 1H), 1.23 (q, J = 2.6 Hz, 1H). **^{13}C NMR** (126 MHz, $CDCl_3$) δ 168.41, 162.75, 134.06, 132.14, 123.33, 118.65, 47.74, 47.66, 37.37, 27.85, 27.82, 27.72, 26.55, 24.06, 22.82, 19.83. **HRMS** (ESI+) Calc: $[M+H]^+$ ($C_{20}H_{22}N_3O_3$) 352.1656, measured: 352.1654; 0.6 ppm difference.

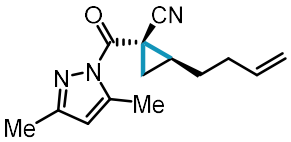

2-(but-3-en-1-yl)-1-(3,5-dimethyl-1H-pyrazole-1-carbonyl)cyclopropane-1-carbonitrile (6.7). Following General Procedure E with KPF_6 instead of n-Bu_4NPF_6 afforded an NMR yield of 68%. Structural configuration assigned via analogy with compound **6.27**. **^{1}H NMR** (500 MHz, $CDCl_3$) δ 5.95 (d, J = 1.1 Hz, 1H), 5.79 (ddt, J = 17.1, 10.2, 6.8 Hz, 1H), 5.00 (dq, J = 17.1, 1.7 Hz, 1H), 4.94 (ddd, J = 10.2, 2.1, 1.0 Hz, 1H), 2.41 (s, 3H), 2.45 – 2.18 (m, 2H), 2.22 (s, 3H), 2.03 (dd, J = 9.0, 5.0 Hz, 1H), 1.90 – 1.72 (m, 3H), 1.37 (dd, J = 7.3, 4.7 Hz, 1H). **HRMS** (ESI+) Calc: [M+H]+ (C14H17N3O) 244.1444, measured: 244.1442; 0.8 ppm difference.

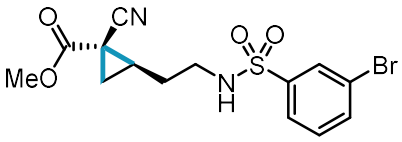

Methyl 2-(2-((3-bromophenyl)sulfonamido)ethyl)-1-cyanocyclopropane-1-carboxylate (6.8). Following General Procedure B using 1.5 equiv. alkene and 21.6 mA for 2.25 h (3.0 F/mol) afforded one detectable diastereomer in 124.5 mg (54% yield, ≥20:1 d.r.) as an oil. $\mathbf{R_f}$ = 0.12 (20% acetone/hexanes). Structural configuration assigned via NOESY. **^{1}H NMR** (500 MHz, $CDCl_3$) δ 8.00 (t, J = 1.9 Hz, 1H), 7.79 (ddd, J = 7.8, 1.8, 1.0 Hz, 1H), 7.71 (ddd, J = 8.0, 1.9, 1.0 Hz, 1H), 7.41 (t, J = 7.9 Hz, 1H), 5.06 (t, J = 6.4 Hz, 1H), 3.81 (s, 3H), 3.15 (q, J = 6.6 Hz, 2H), 1.99 (dtd, J = 8.9, 7.8, 6.4 Hz, 1H), 1.93 – 1.83 (m, 2H), 1.79 (ddt, J = 14.4, 7.9, 6.5 Hz, 1H), 1.39 (dd, J = 7.9, 4.9 Hz, 1H). **^{13}C NMR** (126 MHz, $CDCl_3$) δ 167.93, 141.85, 135.98, 130.93, 130.02, 125.68, 123.32, 117.26, 53.76, 42.02, 30.77, 28.48, 24.76, 19.36. **HRMS** (ESI+) Calc: $[M+NH_4]^+$ ($C_{14}H_{19}BrN_3O_4S$) 404.0274, measured: 404.0273; 0.2 ppm difference.

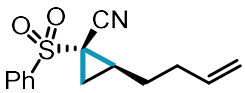

2-(but-3-en-1-yl)-1-(phenylsulfonyl)cyclopropane-1-carbonitrile (6.9). Following General Procedure A afforded one detectable diastereomer in 77.0 mg (74% yield, ≥20:1 d.r.) as an oil. $\mathbf{R_f}$ = 0.34 (20% acetone/hexanes). Structural configuration assigned via NOESY. **^{1}H NMR** (500 MHz, $CDCl_3$) δ 7.96 (dd, J = 8.4, 1.3 Hz, 2H), 7.78 – 7.70 (m, 1H), 7.66 – 7.59 (m, 2H), 5.72 (ddt, J = 17.0, 10.3, 6.7 Hz, 1H), 5.08 – 4.90 (m, 2H), 2.20 (dtd, J = 9.5, 8.1, 6.2 Hz, 1H), 2.11 (dddd, J = 13.2, 8.1, 6.6, 1.4 Hz, 2H), 2.07 – 2.01 (m, 1H), 1.74 (ddt, J = 14.5, 8.0, 6.6 Hz, 1H), 1.55 (dtd, J = 14.3, 8.0, 6.2 Hz, 1H), 1.43 (dd, J = 7.9, 5.6

Hz, 1H). **^{13}C NMR** (126 MHz, $CDCl_3$) δ 137.35, 136.22, 134.92, 129.70, 128.84, 116.44, 114.94, 38.38, 32.17, 29.24, 27.72, 22.25. **HRMS** (ESI+) Calc: $[M+NH_4]^+$ ($C_{14}H_{19}N_2O_2S$) 279.1162, measured: 279.1157; 1.8 ppm difference.

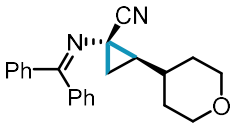

1-((diphenylmethylene)amino)-2-(tetrahydro-2H-pyran-4-yl)cyclopropane-1-carbonitrile (6.10). Following General Procedure A afforded 89.9 mg (68% yield, mixture of diastereomers, 2:1 d.r.) as a solid. **R_f** = 0.27 (10:1:89 ethyl acetate:NEt_3:hexanes). Structural configuration assigned via analogy with compound **6.18**. **^{1}H NMR** (500 MHz, $CDCl_3$) δ 7.55 (m, 5H), 7.43 (m, 1H), 7.35 (m, 4H), 4.04 (m, 2H), 3.47 (tdd, J = 11.6, 6.7, 2.4 Hz, 2H), 1.95 (m, 1H), 1.89 (1H), 1.75 (dd, J = 9.3, 5.1 Hz, 1H), 1.63 (m, 4H), 1.27 (dd, J = 7.6, 5.1 Hz, 1H). Distinct minor diastereomer signals observed at δ 3.98 (dddd, J = 13.5, 11.7, 4.7, 2.1 Hz, 2H), 3.37 (tdd, J = 11.7, 5.0, 2.4 Hz, 2H), 1.83 (m, 1H), 1.38 (m, 1H), 1.33 (m, 1H). **^{13}C NMR** (126 MHz, $CDCl_3$) δ 171.91, 139.56, 135.95, 130.83, 129.89, 128.63, 128.60, 128.27, 67. 92, 67.69, 37.52, 37.16, 34.49, 32.42, 32.04, 25.03. Distinct minor diastereomer signals observed at δ 171.16, 139.39, 136.03, 130.80, 129.81, 128.59, 128.57, 128.19, 67.70, 67.52, 37.13, 36.66, 34.20, 31.90, 31.73, 26.34. **HRMS** (ESI+) Calc: $[M+H]^+$ ($C_{22}H_{22}N_2O$) 331.1805, measured: 331.1798; 2.1 ppm difference.

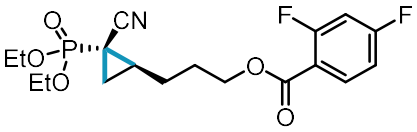

3-(2-cyano-2-(diethoxyphosphoryl)cyclopropyl)propyl 2,4-difluorobenzoate (6.11). Following General Procedure B afforded separable diastereomers, providing 89.2 mg of major diastereomer as an oil and 19.7 mg of minor diastereomer as an oil, 108.9 mg total isolated (68% yield, 5:1 d.r.). Structural configuration assigned via analogy with compound **6.9**.

Major diastereomer: **R_f** = 0.19 (20% acetone/hexanes). **^{1}H NMR** (500 MHz, $CDCl_3$) δ 7.98 (td, J = 8.5, 6.5 Hz, 1H), 6.98 – 6.91 (m, 1H), 6.87 (ddd, J = 11.0, 8.8, 2.5 Hz, 1H), 4.40 (t, J = 6.2 Hz, 2H), 4.26 – 4.16 (q, J = 7.1 Hz, 4H), 2.07 – 1.92 (m, 2H), 1.91 – 1.81 (m, 2H), 1.79 – 1.70 (m, 2H), 1.39 (t, J = 7.1 Hz, 6H), 1.29 (ddd, J = 9.1, 6.7, 4.7 Hz, 1H). **^{13}C NMR** (126 MHz, $CDCl_3$) δ 165.91 (dd, J = 256.5, 12.0 Hz), 163.64 (d, J = 4.2 Hz), 163.01 (dd, J = 263.2, 12.7 Hz), 134.12 (dd, J = 10.6, 2.3 Hz), 117.48 (d, J = 4.4 Hz), 115.25 (dd, J = 9.9, 3.7 Hz), 111.79 (dd, J = 21.5, 3.8 Hz), 105.40 (dd, J = 26.0, 25.9 Hz), 64.39, 64.02 (d, J = 6.8 Hz), 63.97 (d, J = 6.8 Hz), 27.72, 27.11 (d, J = 1.3 Hz), 25.46 (d, J = 2.3 Hz), 20.67 (d, J = 3.0 Hz), 16.45 (d, J = 1.9 Hz), 16.47 (d, J = 1.9 Hz), 10.71 (d, J = 200.2 Hz). **^{31}P NMR** (162 MHz, $CDCl_3$) δ 18.64. **^{19}F NMR** (377 MHz, $CDCl_3$) δ -101.76 (d, J = 12.5 Hz), -103.78 (d, J = 12.7 Hz). **HRMS** (ESI+) Calc: $[M+H]^+$ ($C_{18}H_{23}F_2NO_5P$) 402.1276, measured: 402.1270; 1.5 ppm difference.

Minor diastereomer: **R_f** = 0.16 (20% acetone/hexanes). **^{1}H NMR** (500 MHz, $CDCl_3$) δ 7.98 (td, J = 8.5, 6.5 Hz, 1H), 6.93 (dddd, J = 8.8, 7.6, 2.5, 1.0 Hz, 1H), 6.87 (ddd, J = 11.1, 8.8, 2.5 Hz, 1H), 4.37 (q, J = 6.0 Hz, 2H), 4.23 (ddt, J = 15.2, 8.2, 7.0 Hz, 4H), 2.07 – 1.83 (m, 5H), 1.72 (ddd, J = 8.3, 7.0, 4.5 Hz, 1H), 1.58 (ddd, J = 14.4, 7.2, 4.7 Hz, 1H), 1.41 (t, J = 7.1 Hz, 3H), 1.38 (t, J = 7.1 Hz, 3H). **^{13}C NMR** (126 MHz, $CDCl_3$) δ 165.88 (dd, J = 256.4, 12.0 Hz), 163.67 (d, J = 4.1 Hz), 162.99 (dd, J = 263.2, 12.5 Hz), 134.10 (dd, J = 10.6, 2.4 Hz), 119.79 (d, J = 4.6 Hz), 115.33 (dd, J = 9.9, 3.7 Hz), 111.78 (dd, J = 21.5, 3.8 Hz), 105.27 (dd, J = 26.2, 25.2 Hz), 64.73, 63.88 (d, J = 6.1 Hz), 63.60 (d, J = 6.9 Hz), 29.24 (d, J = 2.4 Hz), 28.17, 24.55 (d, J = 3.5 Hz), 20.96 (d, J = 2.1 Hz), 16.47 (d, J = 6.2 Hz), 16.39, 9.67 (d, J = 199.8 Hz). **^{31}P NMR** (162 MHz, $CDCl_3$) δ 17.87. **^{19}F NMR** (377 MHz, $CDCl_3$) δ -102.91 (d, J = 12.0 Hz), -104.88 (d, J = 12.3 Hz). **HRMS** (ESI+) Calc: $[M+H]^+$ ($C_{18}H_{23}F_2NO_5P$) 402.1276, measured: 402.1273; 0.7 ppm difference.

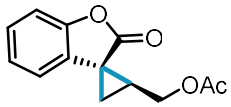

(2-Oxo-2H-spiro[benzofuran-3,1'-cyclopropan]-2'-yl)methyl acetate (6.12). Following General Procedure A using 2.0 equiv. alkene and 29 mA for 2.25 h (3.0 F/mol) afforded 49.7 mg (54% yield, mixture of diastereomers, 6:1 d.r.; estimated 4:1 d.r. in crude ^{1}H NMR spectrum prior to purification) as an oil. $\mathbf{R_f}$ = 0.30 (20% acetone/hexanes). Structural configuration of major diastereomer assigned via NOESY. **^{1}H NMR** (500 MHz, $CDCl_3$) δ 7.35 – 7.27 (m, 1H), 7.24 – 7.12 (m, 2H), 6.87 (dd, J = 7.5, 1.3 Hz, 1H), 4.70 (ddd, J = 12.0, 6.0, 1.5 Hz, 1H), 4.38 (ddd, J = 12.0, 8.8, 1.1 Hz, 1H), 2.36 (qd, J = 8.5, 5.8 Hz, 1H), 2.04 (s, 3H), 1.92 (d, J = 8.1 Hz, 2H). Distinct minor diastereomer signals observed at δ 7.03 (dd, J = 7.6, 1.4 Hz, 1H), 4.52 (dd, J = 12.3, 6.5 Hz, 1H), 4.21 (dd, J = 12.3, 8.3 Hz, 1H), 2.10 (dd, J = 9.3, 5.0 Hz, 1H), 1.99 (s, 3H), 1.65 (dd, J = 7.8, 5.0 Hz, 1H). **^{13}C NMR** (126 MHz, $CDCl_3$) δ 175.30, 171.04, 153.40, 128.83, 127.98, 124.22, 118.87, 110.80, 61.09, 32.26, 28.29, 24.72, 20.97. Distinct minor diastereomer signals observed at δ 176.75, 170.88, 154.04, 128.19, 125.79, 124.14, 121.09, 111.11, 61.74, 31.37, 29.17, 23.41, 20.83. **HRMS** (ESI+) Calc: $[M+Na]^+$ ($C_{13}H_{12}O_4Na$) 255.0628, measured: 255.0622; 2.4 ppm difference.

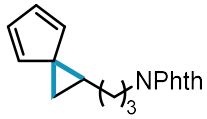

2-(3-(Spiro[2.4]hepta-4,6-dien-1-yl)propyl)isoindoline-1,3-dione (6.13). Following General Procedure B afforded 50.4 mg (45% yield) as a solid. $\mathbf{R_f}$ = 0.29 (26% Ether/Hexanes). **^{1}H NMR** (500 MHz, $CDCl_3$) δ 7.83 (dd, *J* = 5.5, 3.1 Hz, 2H), 7.70 (dd, *J* = 5.5, 3.1 Hz, 2H), 6.54 (ddd, *J* = 5.2, 2.1, 1.4 Hz, 1H), 6.42 (ddd, *J* = 5.0, 2.3, 1.4 Hz, 1H), 6.22 (ddd, *J* = 5.2, 2.1, 1.4 Hz, 1H), 6.05 (dt, *J* = 5.0, 1.8 Hz, 1H), 3.72 – 3.61 (m, 2H), 2.16 – 2.06 (m, 1H), 1.79 (dd, *J* = 8.6, 4.0 Hz, 1H), 1.78 – 1.67 (m, 3H), 1.64 – 1.58 (m, 1H), 1.57 (dd, *J* = 7.3, 4.0 Hz, 1H). **^{13}C NMR** (126 MHz, $CDCl_3$) δ 168.39, 139.83, 135.31, 133.90, 132.15, 130.62, 128.04, 123.19, 42.94, 37.52, 30.04, 28.48, 27.73, 19.98. **HRMS** (ESI+) Calc: $[M+H]^+$ ($C_{18}H_{17}NO_2$) 280.1332, measured: 280.1330; 0.7 ppm difference.

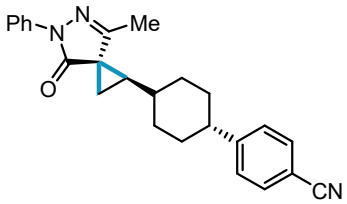

4-(4-(4-methyl-7-oxo-6-phenyl-5,6-diazaspiro[2.4]hept-4-en-1-yl)cyclohexyl)benzonitrile (6.14). Following General Procedure A afforded 105.5 mg (69% yield, mixture of diastereomers, 3:1 d.r.) as a solid. $\mathbf{R_f}$ = 0.24 (20% ethyl acetate/hexanes). Structural configuration assigned via x-ray crystallography. **^{1}H NMR** (500 MHz, $CDCl_3$) δ 7.94 (dd, J = 8.8, 1.2 Hz, 2H), 7.57 (t, J = 8.8 Hz, 2H), 7.42 – 7.37 (m, 2H), 7.29 (d, J = 8.4 Hz, 1H), 7.27 (d, J = 8.4 Hz, 1H), 7.17 (td, J = 7.4, 1.1 Hz, 1H), 2.51 (tt, J = 12.2, 3.4 Hz, 1H), 2.14 – 2.07 (m, 1H), 2.04 – 1.98 (m, 1H), 1.96 (s, 3H), 1.88 (dd, J = 8.5, 3.7 Hz, 1H), 1.85 – 1.73 (m, 3H), 1.72 – 1.60 (m, 1H), 1.52 (dqd, J = 23.3, 12.8, 3.5 Hz, 2H), 1.36 (tt, J = 12.3, 6.3 Hz, 2H), 1.17 (qd, J = 12.7, 3.5 Hz, 1H). Distinct minor diastereomer signals observed at δ 7.95 (dd, J = 8.8, 1.1 Hz, 2H), 2.58 (td, J = 11.5, 9.8, 5.6 Hz, 1H). **^{13}C NMR** (126 MHz, $CDCl_3$) δ 171.53, 159.65, 152.76, 138.95, 132.36, 128.92, 127.77, 124.85, 119.21, 118.89, 109.91, 44.55, 39.88, 37.14, 33.58, 33.47, 33.20, 33.10, 32.96, 32.73, 24.32, 12.60. Distinct minor diastereomer signals observed at δ 172.58, 158.57, 152.31, 138.80, 132.40, 128.95, 127.72, 119.13, 118.65, 110.10, 44.15, 42.82, 38.61, 38.02, 33.50, 33.23, 32.94, 25.70, 16.01. **HRMS** (ESI+) Calc: $[M+H]^+$ ($C_{25}H_{26}N_3O$) 384.2070, measured: 384.2065; 1.3 ppm difference.

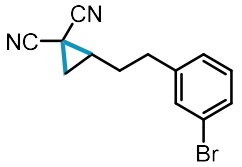

2-(3-bromophenethyl)cyclopropane-1,1-dicarbonitrile (6.15). Following General Procedure A afforded 73.7 mg (67% yield) obtained as an oil. **^{1}H NMR** (400 MHz, $CDCl_3$) δ 7.42 – 7.34 (m, 2H), 7.21 (t, *J* = 7.6 Hz, 1H), 7.17 – 7.12 (m, 1H), 2.84 (tt, *J* = 14.0, 7.6 Hz, 2H), 2.03 – 1.87 (m, 4H), 1.50 (td, *J* = 5.4, 1.3 Hz, 1H). **^{13}C NMR** (126 MHz, $CDCl_3$) δ 141.93, 131.63, 130.51, 130.05, 127.26, 122.98, 115.36, 113.76, 33.91, 31.83, 30.51, 24.73, 4.03. **HRMS** (ESI+) Calc: $[M+H]^+$ ($C_{13}H_{11}BrN_2$) 275.0178, measured: 275.0175; 1.1 ppm difference.

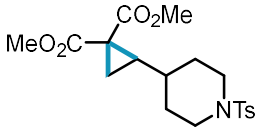

Dimethyl 2-(1-tosylpiperidin-4-yl)cyclopropane-1,1-dicarboxylate (6.16). Following General Procedure B afforded 116.7 mg (74% yield) as a solid. **R_f =** 0.22 (20% acetone/hexanes). **^{1}H NMR** (500 MHz, $CDCl_3$) δ 7.60 (d, J = 8.2 Hz, 2H), 7.30 (d, J = 8.0 Hz, 2H), 3.77 – 3.73 (m, 1H), 3.71 – 3.67 (m, 1H), 3.69 (s, 3H), 3.68 (s, 3H), 2.42 (s, 3H), 2.20 (td, J = 11.8, 2.7 Hz, 1H), 2.11 (td, J = 11.8, 2.7 Hz, 1H), 1.82 – 1.66 (m, 3H), 1.59 – 1.45 (m, 2H), 1.34 (ddd, J = 20.5, 8.4, 4.7 Hz, 2H), 0.74 (qt, J = 11.1, 3.7 Hz, 1H). **^{13}C NMR** (126 MHz, $CDCl_3$) δ 170.36, 168.71, 143.59, 133.05, 129.70, 127.74, 52.76, 52.62, 46.15, 46.02, 35.37, 33.79, 33.26, 31.14, 30.84, 21.56, 19.88. **HRMS** (ESI+) Calc: $[M+H]^+$ ($C_{19}H_{26}NO_6S$) 396.1475, measured: 396.1471; 1.0 ppm difference.

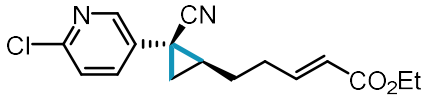

Ethyl (E)-5-(2-(6-chloropyridin-3-yl)-2-cyanocyclopropyl)pent-2-enoate (6.17). Following Following General Procedure B afforded one detectable diastereomer with an NMR yield of 54%. Structural configuration assigned via analogy with compound **6.25**. **^{1}H NMR** (500 MHz, $CDCl_3$) δ 8.27 (d, J = 2.7 Hz, 1H), 7.56 (dd, J = 8.4, 2.7 Hz, 1H), 7.31 (d, J = 8.5 Hz, 1H), 7.01 – 6.92 (m, 1H), 5.86 (dq, J = 15.6, 1.5 Hz, 1H), 4.17 (q, J = 7.1 Hz, 2H), 2.54 – 2.38 (m, 2H), 1.96 – 1.88 (m, 2H), 1.74 – 1.61 (m, 1H), 1.60 – 1.48 (m, 2H), 1.27 (t, J = 7.1 Hz, 3H). Distinct minor diastereomer signals observed at δ 6.77 (m, 1H), 5.75 (m, 1H). **HRMS** (ESI+) Calc: $[M+H]^+$ ($C_{16}H_{14}ClN_3$) 305.1051, measured: 305.1049; 0.7 ppm difference.

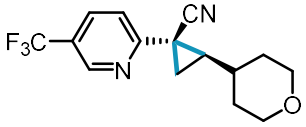

2-(Tetrahydro-2H-pyran-4-yl)-1-(5-(trifluoromethyl)pyridin-2-yl)cyclopropane-1-carbonitrile (6.18). Following General Procedure B afforded one detectable diastereomer in 74.7 mg (63% yield, ≥20:1 d.r.) as a solid. **R_f =** 0.26 (10% acetone/hexanes). Structural configuration assigned via x-ray crystallography. **^{1}H NMR** (500 MHz, $CDCl_3$) δ 8.73 – 8.69 (m, 1H), 7.92 (dd, *J* = 8.3, 2.5 Hz, 1H), 7.83 (d, *J* = 8.2 Hz, 1H), 4.03 (ddd, *J* = 11.6, 4.6, 2.4 Hz, 1H), 3.97 (ddd, *J* = 11.3, 4.3, 2.4 Hz, 1H), 3.49 – 3.39 (m, 2H), 2.06 (dd, *J* = 8.7, 4.4 Hz, 1H), 1.98 – 1.91 (m, 1H), 1.87 (dq, *J* = 9.6, 2.3 Hz, 1H), 1.80 – 1.73 (m, 1H), 1.69 – 1.58 (m, 2H), 1.58 – 1.46 (m, 2H). **^{13}C NMR** (126 MHz, $CDCl_3$) δ 158.94, 146.78 (q, J = 4.1 Hz), 134.11 (q, J = 3.5 Hz), 125.21 (q, J = 33.2 Hz), 123.53 (q, J = 272.2 Hz), 120.51, 119.93, 67.73, 67.60, 38.49, 38.09, 32.20, 32.02, 26.02, 21.42. **^{19}F NMR** (377 MHz, $CDCl_3$) δ -62.28. **HRMS** (ESI+) Calc: $[M+H]^+$ ($C_{15}H_{15}F_3N_2O$) 297.1209, measured: 297.1206; 1.0 ppm difference.

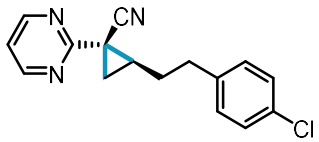

2-(4-Chlorophenethyl)-1-(pyrimidin-2-yl)cyclopropane-1-carbonitrile (6.19). Following General Procedure A afforded one detectable diastereomer in 84.8 mg (75% yield, ≥20:1 d.r.) as an oil. $\mathbf{R_f}$ = 0.29 (30% EtOAC/Hexanes). Structural configuration assigned via analogy with compound **6.18**. **^{1}H NMR** (500 MHz, C_6D_6) δ 7.97 (d, *J* = 4.9 Hz, 2H), 7.03 (d, *J* = 8.4 Hz, 1H), 6.70 (d, *J* = 8.3 Hz, 2H), 6.11 (t, *J* = 4.9 Hz, 1H), 2.46 (ddd, *J* = 14.0, 8.6, 5.6 Hz, 1H), 2.33 (ddd, *J* = 13.7, 8.2, 6.6 Hz, 1H), 1.82 – 1.60 (m, 4H), 1.04 (dd, *J* = 6.7, 4.2 Hz, 1H).). Distinct minor diastereomer signals observed at δ 6.53 (d, *J* = 8.3 Hz, 1H). **^{13}C NMR** (126 MHz, $CDCl_3$) δ 166.10, 156.95, 139.67, 132.14, 130.17, 128.79, 128.25, 128.06, 127.87, 119.04, 118.87, 34.18, 32.68, 32.24, 26.37, 24.23. **HRMS** (ESI+) Calc: $[M+H]^+$ ($C_{16}H_{14}ClN_3$) 284.0949, measured: 284.0944; 1.8 ppm difference.

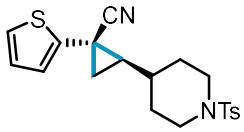

1-(Thiophen-2-yl)-2-(1-tosylpiperidin-4-yl)cyclopropane-1-carbonitrile (6.20). Following General Procedure B afforded separable diastereomers, providing 101.9 mg of major diastereomer as a solid and 12.4 mg of minor diastereomer as a solid, 114.3 mg total isolated (74% yield, 8:1 d.r.). Structural configuration assigned via analogy with compound **6.22**.

Major diastereomer: $\mathbf{R_f}$ = 0.22 (20% acetone/hexanes). **^{1}H NMR** (500 MHz, $CDCl_3$) δ 7.68 – 7.60 (m, 2H), 7.37 – 7.29 (m, 2H), 7.19 (dd, *J* = 5.2, 1.2 Hz, 1H), 6.99 (dd, *J* = 3.6, 1.3 Hz, 1H), 6.93 (dd, *J* = 5.2, 3.7 Hz, 1H), 3.85 (ddd, *J* = 7.0, 4.7, 2.4 Hz, 2H), 2.44 (s, 3H), 2.25 (dtd, *J* = 22.1, 12.1, 2.8 Hz, 2H), 2.12 (d, *J* = 13.4 Hz, 1H), 1.84 (d, *J* = 13.3 Hz, 1H), 1.70 – 1.57 (m, 3H), 1.46 – 1.35 (m, 2H), 1.15 – 1.03 (m, 1H). **^{13}C NMR** (126 MHz, $CDCl_3$) δ 143.83, 140.25, 132.85, 129.84, 127.86, 127.42, 126.02, 120.25, 46.31 (d, *J* = 1.9 Hz), 38.51, 36.15, 30.81, 30.58, 24.56, 21.66, 15.72. **HRMS** (ESI+) Calc: $[M+NH_4]^+$ ($C_{20}H_{22}N_2O_2S_2$) 404.1461, measured: 404.1460; 0.2 ppm difference.

Minor diastereomer: $\mathbf{R_f}$ = 0.20 (20% acetone/hexanes). **^{1}H NMR (**500 MHz, $CDCl_3$) δ 7.58 (d, *J* = 8.2 Hz, 2H), 7.28 (d, *J* = 8.2 Hz, 2H), 7.21 (dd, *J* = 5.2, 1.4 Hz, 1H), 6.99 (dd, *J* = 3.5, 1.4 Hz, 1H), 6.94 (dd, *J* = 5.2, 3.5 Hz, 1H), 3.72 (dtd, *J* = 11.7, 3.9, 1.9 Hz, 1H), 3.64 (dtd, *J* = 11.7, 3.9, 1.9 Hz, 1H), 2.41 (s, 3H), 2.16 (td, *J* = 11.7, 3.1 Hz, 1H), 1.99 (td, *J* = 11.8, 2.9 Hz, 1H), 1.81 (dd, *J* = 9.3, 5.6 Hz, 2H), 1.70 – 1.46 (m, 4H), 1.31 (dd, *J* = 7.5, 5.6 Hz, 1H), 0.58 (dtd, *J* = 15.1, 11.1, 4.0 Hz, 1H). **^{13}C NMR** (126 MHz, $CDCl_3$) δ 143.65, 135.73, 133.37, 129.78, 128.62, 127.49, 126.18, 122.22, 45.96, 45.70, 34.90, 34.44, 30.72, 30.45, 20.38, 14.12. **HRMS** (ESI+) Calc: $[M+H]^+$ ($C_{20}H_{22}N_2O_2S_2$) 387.1196, measured: 387.1194; 0.5 ppm difference.

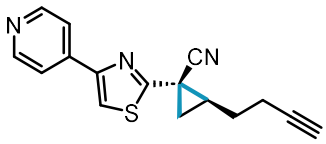

2-(But-3-yn-1-yl)-1-(4-(pyridin-4-yl)thiazol-2-yl)cyclopropane-1-carbonitrile (6.21). Following General Procedure A afforded an NMR yield of 61% (5:1 d.r.). Structural configuration assigned via analogy with compound **6.18**. **^{1}H NMR** (500 MHz, $CDCl_3$) δ 8.66 (d, *J* = 5.4 Hz, 2H), 7.71 (d, *J* = 6.1 Hz, 2H), 7.61 (s, 1H), 2.48 (tdd, *J* = 6.9, 2.6, 1.0 Hz, 2H), 2.37 – 2.25 (m, 1H), 2.22 (m, 1H), 2.11 – 1.99 (m,

2H), 1.99 – 1.89 (m, 0H), 1.82 – 1.68 (m, 1H). **HRMS** (ESI+) Calc: $[M+H]^+$ ($C_{16}H_{15}N_3S$) 280.0903, measured: 280.0902; 0.4 ppm difference.

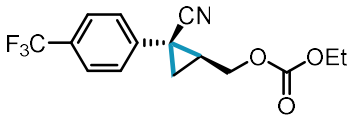

(2-Cyano-2-(4-(trifluoromethyl)phenyl)cyclopropyl)methyl ethyl carbonate (6.22). Following General Procedure A using 2.0 equiv. alkene and 29 mA for 2.25 h (3.0 F/mol) afforded one detectable diastereomer in 88.4 mg (70% yield, ≥20:1 d.r.) as an oil. $\mathbf{R_f}$ = 0.24 (20% acetone/hexanes). Structural configuration assigned via NOESY. **^{1}H NMR** (500 MHz, $CDCl_3$) δ 7.62 (d, J = 8.1 Hz, 2H), 7.42 (d, J = 8.1 Hz, 2H), 4.55 (dd, J = 12.0, 6.0 Hz, 1H), 4.29 (dd, J = 12.0, 8.4 Hz, 1H), 4.23 (q, J = 7.1 Hz, 2H), 2.10 – 2.01 (m, 1H), 1.77 – 1.70 (m, 2H), 1.32 (t, J = 7.2 Hz, 3H). **^{13}C NMR** (126 MHz, $CDCl_3$) δ 154.93, 139.33 (q, *J* = 1.5 Hz), 130.50 (q, *J* = 32.9 Hz), 126.40, 126.17 (q, *J* = 3.7 Hz), 123.87 (q, *J* = 272.2 Hz), 119.15, 67.40, 64.62, 28.45, 22.05, 19.82, 14.32. **^{19}F NMR** (377 MHz, $CDCl_3$) δ -62.73. **HRMS** (ESI+) Calc: $[M+Na]^+$ ($C_{15}H_{14}F_3NO_3Na$) 336.0818, measured: 336.0813; 1.5 ppm difference.

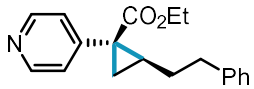

Ethyl 2-phenethyl-1-(pyridin-4-yl)cyclopropane-1-carboxylate (6.23). Following General Procedure A afforded 77.8 mg (66% yield, mixture of diastereomers, 3:1 d.r.) as an oil. $\mathbf{R_f}$ = 0.31 (20% acetone/hexanes). Structural configuration assigned via analogy with compound **6.29**. **^{1}H NMR** (500 MHz, $CDCl_3$) δ 8.54 – 8.51 (m, 2H), 7.37 – 7.13 (m, 7H), 4.16 (dddd, J = 17.9, 10.9, 7.1, 3.8 Hz, 2H), 2.81 – 2.73 (m, 2H), 2.05 – 1.93 (m, 2H), 1.67 (dd, J = 7.4, 4.7 Hz, 1H), 1.59 (dq, J = 9.1, 7.2 Hz, 1H), 1.29 (dd, J = 8.9, 4.7 Hz, 1H), 1.23 – 1.10 (m, 3H). Distinct minor diastereomer signals observed at δ 8.58 – 8.56 (m, 2H), 7.09 – 6.99 (m, 2H), 4.10 – 4.05 (m, 1H), 2.72 – 2.63 (m, 2H), 1.74 (dd, J = 9.0, 4.5 Hz, 1H), 1.13 (dd, *J* = 6.9, 4.5 Hz, 1H), 0.89 (dtd, J = 13.9, 9.0, 6.7 Hz, 1H). **^{13}C NMR** (126 MHz, $CDCl_3$) δ 171.09, 149.90, 149.65, 141.53, 128.55, 128.54, 126.14, 124.88, 61.42, 35.69, 34.05, 29.56, 29.12, 20.79, 14.31. Distinct minor diastereomer signals observed at δ 173.02, 149.56, 145.47, 141.43, 128.49, 128.46, 126.50, 126.10, 35.34, 33.39, 32.33, 28.42, 20.67, 14.19. **HRMS** (ESI+) Calc: $[M+H]^+$ ($C_{19}H_{22}NO_2$) 296.1645, measured: 296.1642; 1.0 ppm difference.

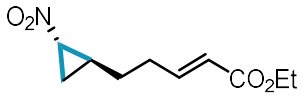

Ethyl (*E*)-5-(2-nitrocyclopropyl)pent-2-enoate (6.24). Following General Procedure B afforded one detectable diastereomer in 41.9 mg (49% yield) obtained as an oil and afforded an NMR yield of 55%. Structural configuration assigned via NOESY. **^{1}H NMR** (400 MHz, $CDCl_3$) δ 6.92 (dt, *J* = 15.6, 7.0 Hz, 1H), 5.85 (dt, *J* = 15.7, 1.6 Hz, 1H), 4.19 (q, *J* = 7.2 Hz, 2H), 4.10 – 4.03 (m, 1H), 2.35 (qd, *J* = 7.3, 1.6 Hz, 2H), 1.99 (dqd, *J* = 10.2, 7.3, 2.9 Hz, 1H), 1.86 (ddd, *J* = 10.2, 5.8, 3.5 Hz, 1H), 1.66 – 1.41 (m, 3H), 1.29 (t, *J* = 7.1 Hz, 3H), 1.08 (td, *J* = 7.3, 5.8 Hz, 1H). **^{13}C NMR** (126 MHz, $CDCl_3$) δ166.46, 146.77, 122.79, 60.56, 59.79, 31.22, 29.91, 25.60, 18.54, 14.44. **HRMS** (ESI+) Calc: $[M+Na]^+$ ($C_{10}H_{15}NO_4$) 236.0893, measured 236.0890; 1.3 ppm difference.

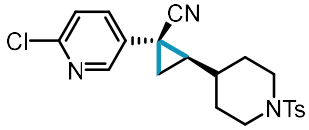

1-(6-chloropyridin-3-yl)-2-(1-tosylpiperidin-4-yl)cyclopropane-1-carbonitrile (6.25). Following scaleup setup and procedures afforded 3.3 g (72% yield, ≥20:1 d.r.) as solid. $\mathbf{R_f}$ = 0.32 (15% EtOAC/Hexanes). Structural configuration assigned via NOESY. **^{1}H NMR** (500 MHz, $CDCl_3$) δ 8.28 (d, J

= 2.7 Hz, 1H), 7.63 (d, J = 8.3 Hz, 2H), 7.52 (dd, J = 8.4, 7.8 Hz, 1H), 3.92 – 3.79 (m, 2H), 2.44 (s, 3H), 2.25 (dtd, J = 15.0, 12.0, 2.8 Hz, 2H), 2.11-2.04 (m, 1H), 1.90-1.83 (m, 1H), 1.68-1.55 (m, 3H), 1.49 (dd, J = 7.4, 5.9 Hz, 1H), 1.35 (ddd, J = 10.1, 8.7, 7.4 Hz, 1H), 1.15 (ddt, J = 15.3, 11.4, 5.8 Hz, 1H). Distinct minor diastereomer signals observed at δ 8.26 (d, J = 2.8 Hz, 1H), 7.69 (dd, J = 8.3, 2.7 Hz, 1H), 7.55 (d, J = 8.2 Hz, 2H), 3.73 (d, J = 12.2 Hz, 1H), 3.59 (d, J = 12.0 Hz, 1H), 2.41 (s, 3H). **^{13}C NMR** (126 MHz, $CDCl_3$) δ 151.22, 147.43, 143.89, 136.66, 132.80, 131.17, 129.85, 127.83, 124.57, 119.56, 46.26, 46.21, 38.60, 35.23, 30.84, 30.60, 23.04, 21.65, 17.26. **HRMS** (ESI+) Calc: $[M+Na]^+$ ($C_{21}H_{22}ClN_3O_2S$) 438.1013, measured: 438.1011; 0.5 ppm difference.

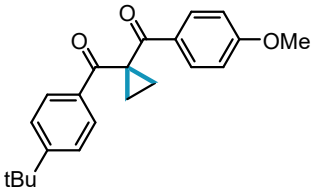

(1-(4-(*tert*-butyl)benzoyl)cyclopropyl)(4-methoxyphenyl)methanone (6.26). Following General Procedure D afforded 102.3 mg (76% yield) obtained as an oil. **R_f** = 0.27 (5% EtOAc/hexanes). **^{1}H NMR** (500 MHz, $CDCl_3$) δ 7.81 (d, J = 8.9 Hz, 2H), 7.76 (d, J = 8.6 Hz, 2H), 7.30 (d, J = 8.6 Hz, 2H), 6.76 (d, J = 8.9 Hz, 2H), 3.77 (s, 3H), 1.66 (s, 4H), 1.24 (s, 9H). **^{13}C NMR** (126 MHz, $CDCl_3$) δ 197.80, 196.42, 164.30, 157.65, 135.72, 132.13, 131.46, 129.74, 126.41, 114.66, 56.35, 41.44, 36.01, 31.94, 16.43. **HRMS** (ESI+) Calc: $[M+H]^+$ ($C_{22}H_{24}O_3$) 359.1618, measured: 359.1612; 1.7 ppm difference.

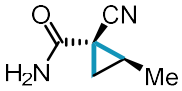

1-cyano-2-methylcyclopropane-1-carboxamide (6.27). Following General Procedure C afforded one detectable diastereomer in 36.8 mg (74% yield, ≥20:1 d.r.) obtained as an white solid. **R_f** = 0.25 (50% EtOAc/hexanes). Structural configuration assigned via x-ray crystallography. **^{1}H NMR** (500 MHz, $CDCl_3$) δ 6.42 (br s, 1H), 6.21 (br s, 1H), 1.95 (ddq, J = 8.8, 7.7, 6.2 Hz, 1H), 1.83 (dd, J = 8.8, 4.3 Hz, 1H), 1.36 (d, J = 6.2 Hz, 3H), 1.25 (dd, J = 7.8, 4.4 Hz, 1H). **^{13}C NMR** (126 MHz, $CDCl_3$) δ 168.17, 119.00, 25.62, 25.27, 20.31, 15.22. **HRMS** (ESI+) Calc: $[M+H]^+$ ($C_6H_8N_2O$) 147.0529, measured: 147.0527; 1.4 ppm difference.

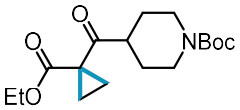

***tert*-Butyl 4-(1-(ethoxycarbonyl)cyclopropane-1-carbonyl)piperidine-1-carboxylate (6.28)**. Following General Procedure D afforded 123.3 mg (95% yield) obtained as an oil. **R_f** = 0.29 (10% EtOAc/hexanes). **^{1}H NMR** (500 MHz, $CDCl_3$) δ 4.17 (q, J = 7.2Hz, 2H), 4.04 (br s, 2H), 3.29 (tt, J = 11.3, 3.6Hz, 1H), 2.75 (t, J = 12.7Hz, 2H), 1.80 (d, J = 13.2Hz, 2H), 1.48 (dtd, J = 13.4, 11.8, 4.3Hz, 1H), 1.40 (s, 9H), 1.24 (t, J = 7.1Hz, 3H). **^{13}C NMR** (126 MHz, $CDCl_3$) δ 206.71, 171.00, 154.62, 79.46, 61.26, 47.12, 33.76, 28.37, 18.18, 14.07. **HRMS** (ESI+) Calc: $[M+H]^+$ ($C_{17}H_{27}NO_2$) 326.1962, measured: 326.1955; 2.1 ppm difference.

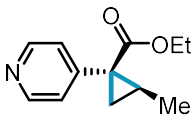

Ethyl 2-methyl-1-(pyridin-4-yl)cyclopropane-1-carboxylate (6.29). Following General Procedure C afforded 70.76 mg (67.7% yield, mixture of diastereomers, 4:1 d.r.) as an oil. **R_f** = 0.21 (70% Et_2O/hexanes). Structural configuration assigned via NOESY. **^{1}H NMR** (500 MHz, $CDCl_3$) δ 8.51 (m, 2H), 7.21 (m, 2H), 4.14 (m, 2H), 1.60 (m, 2H), 1.30 (d, J = 5.8 Hz, 2H), 1.26 (m, 1H), 1.19 (t, J = 7.1 Hz, 3H). Distinct minor

diastereomer signals observed at δ 8.56 (m, 2H), 7.18 (m, 2H), 4.06 (m, 2H), 1.93 (m, 1H), 1.75 (dd, J = 9.0, 4.4 Hz, 1H), 1.15 (t, J = 7.1 Hz, 3H), 1.08 (dd, J = 6.8, 4.4 Hz, 1H), 0.80 (d, J = 6.3 Hz, 3H). **^{13}C NMR** (126 MHz, $CDCl_3$) δ 171.04, 150.05, 149.79, 124.61, 61.32, 34.32, 23.57, 14.38, 13.12. Distinct minor diastereomer signals observed at δ 173.29, 149.65, 145.48, 126.71, 61.37, 33.36, 23.13, 22.00, 15.32, 14.23. **HRMS** (ESI+) Calc: $[M+H]^+$ ($C_{12}H_{15}NO_2$) 206.1176, measured: 206.1176; <0.1ppm ppm difference.

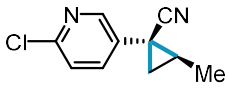

1-(6-chloropyridin-3-yl)-2-methylcyclopropane-1-carbonitrile (6.30). Following General Procedure C afforded one detectable diastereomer in 73.3 mg (95% yield, ≥20:1 d.r.) obtained as an oil. **R_f** = 0.25 (10% acetone/hexanes). Structural configuration assigned via analogy with compound **25**. **^{1}H NMR** (500 MHz, $CDCl_3$) δ 8.39-8.36 (m, 1H), 7.65 (dd, J = 7.6, 2.2Hz, 1H), 7.27-7.23 (m, 1H) 1.59-1.48 (m, 5H), 1.48-1.43 (m, 1H). **^{13}C NMR** (126 MHz, $CDCl_3$) δ 153.40, 149.54, 139.68, 131.34, 122.66, 119.20, 23.13, 23.09, 19.12, 15.62. **HRMS** (ESI+) Calc: $[M+H]^+$ ($C_{10}H_9ClN_2$) 193.0527, measured: 193.0527; <0.1 ppm difference.

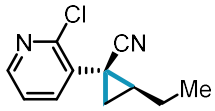

1-(2-chloropyridin-3-yl)-2-ethylcyclopropane-1-carbonitrile (6.31). Following General Procedure C afforded one detectable diastereomer in 82.1 mg (99% yield, ≥20:1 d.r.) obtained as an oil. **R_f** = 0.23 (15% acetone/hexanes). Structural configuration assigned via analogy with compound **25**. **^{1}H NMR** (500 MHz, $CDCl_3$) δ 8.31 (dd, J = 4.8, 1.9Hz, 1H), 7.62 (dd, J = 7.6, 1.9Hz, 1H), 7.21 (dd, J = 7.6, 4.7Hz, 1H), 1.84 (dq, J = 14.4, 7.2Hz, 1H), 1.66 (tt, J = 14.2, 7.3Hz, 1H), 1.52-1.39 (m, 3H), 1.16 (t, J = 7.4Hz, 3H). **^{13}C NMR** (126 MHz, $CDCl_3$) δ 152.99, 149.49, 139.93, 131.24, 122.78, 119.35, 29.90, 24.41, 22.34, 18.71, 13.03. **HRMS** (ESI+) Calc: $[M+H]^+$ ($C_9H_7ClN_2$) 207.0684, measured: 207.0681; 1.4 ppm difference.

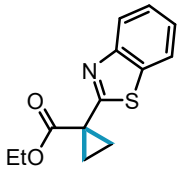

***tert*-butyl 4-(1-(ethoxycarbonyl)cyclopropane-1-carbonyl)piperidine-1-carboxylate (6.32)**. Following General Procedure C afforded 67.1 mg (68% yield) obtained as an oil. **R_f** = 0.39 (5% acetone/hexanes). **^{1}H NMR** (500 MHz, $CDCl_3$) δ 7.90 (dt, J = 8.1, 0.9Hz, 1H), 7.86 (dt, J = 7.9, 1.0Hz, 1H), 7.43 (ddd, J = 8.3, 7.2, 1.3Hz, 1H), 7.34 (ddd, J = 8.2, 7.2, 1.2Hz, 1H), 4.27 (q, J = 7.1Hz, 2H), 1.94 (m, 4H), 1.31 (t, J = 7.1Hz, 3H). **^{13}C NMR** (126 MHz, $CDCl_3$) δ 171.86, 168.75, 151.86, 135.94, 125.72, 124.52, 122.44, 121.21, 61.57, 27.89, 22.76, 14.14. **HRMS** (ESI+) Calc: $[M+H]^+$ ($C_{13}H_{13}NO_2S$) 248.0740, measured: 248.0734; 2.4 ppm difference.

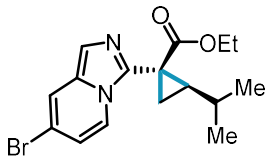

Ethyl 1-(7-bromoimidazo[1,5-a]pyridin-3-yl)-2-isopropylcyclopropane-1-carboxylate (6.33). Following General Procedure C afforded one detectable diastereomer in 70.76 mg (50% yield, ≥20:1 d.r.) obtained as a solid. **R_f** = 0.28 (20% EtOAc/hexanes). Structural configuration assigned via analogy with compound **6.18**. **^{1}H NMR** (500 MHz, $CDCl_3$) δ 8.23 (dd, J = 2.0, 0.9 Hz, 1H), 7.74 (d, J = 7.7, 0.7 Hz, 1H), 7.42 (dt, J = 9.5, 0.9 Hz, 1H), 7.17 (dd, J = 9.5, 1.9 Hz, 1H), 4.15 (m, 2H), 1.81 (dd, J = 7.5, 4.1 Hz, 1H),

1.75 (dd, J = 9.1, 4.1 Hz, 1H), 1.67 (td, J = 9.3, 7.5, 1H), 1.23 (t, J = 7.1 Hz, 3H), 0.97 (t, J = 6.3 Hz, 3H), 0.91 (m, 1H), 0.80 (d, J = 6.3 Hz, 3H). **^{13}C NMR** (126 MHz, $CDCl_3$) δ 173.59, 143.13, 142.22, 127.35, 125.43, 118.05, 113.64, 106.79, 61.10, 39.50, 29.18, 28.01, 22.47, 21.78, 20.41, 14.36. **HRMS** (ESI+) Calc: $[M+H]^+$ ($C_{16}H_{19}BrN_2O_2$) 351.0703, measured: 351.0699; 1.1 ppm difference.

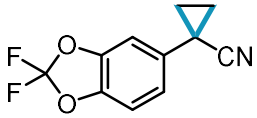

1-(2,2-difluorobenzo[d][1,3]dioxol-5-yl)cyclopropane-1-carbonitrile (6.34). Following General Procedure D afforded 82.9 mg (87% yield) obtained as an white solid. **R_f =** 0.25 (40% Et_2O/hexanes). **^{1}H NMR** (500 MHz, $CDCl_3$) δ 7.08 (dd, J = 8.4, 1.9 Hz, 1H), 7.03 (m, 2H), 1.73 (m, 2H), 1.37 (m, 2H). **^{13}C NMR** (126 MHz, $CDCl_3$) δ145.18, 144.28, 133.31, 132.66 (t, J = 256.4Hz), 123.03, 110.67, 108.98, 18.86, 14.81. **^{19}F NMR** (376 MHz, $CDCl_3$) δ -49.90. **HRMS** (ESI+) Calc: $[M+H]^+$ ($C_{11}H_7F_2NO_2$) 224.0518, measured: 225.0515; 1.3 ppm difference.

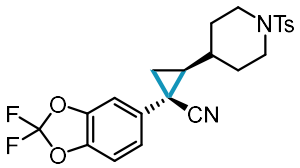

1-(2,2-Difluorobenzo[d][1,3]dioxol-5-yl)-2-(1-tosylpiperidin-4-yl)cyclopropane-1-carbonitrile (6.35). Following General Procedure B afforded one detectable diastereomer in 138.2 mg (74% yield, ≥20:1 d.r.) as a solid. **R_f** = 0.34 (20% acetone/hexanes). Structural configuration assigned via NOESY. **^{1}H NMR** (500 MHz, $CDCl_3$) δ 7.64 (d, *J* = 8.4 Hz, 2H), 7.36 – 7.31 (m, 2H), 7.05 – 6.97 (m, 2H), 6.96 (d, *J* = 1.7 Hz, 1H), 3.86 (dddt, *J* = 9.3, 6.6, 4.1, 2.4 Hz, 2H), 2.44 (s, 3H), 2.25 (dtd, *J* = 20.3, 12.1, 2.7 Hz, 2H), 2.10 (ddd, *J* = 13.0, 3.7, 2.1 Hz, 1H), 1.86 (ddd, *J* = 13.1, 3.8, 2.2 Hz, 1H), 1.68 – 1.57 (m, 2H), 1.55 (dd, *J* = 5.6, 3.1 Hz, 1H), 1.40 (dd, *J* = 7.2, 5.7 Hz, 1H), 1.29 (ddd, *J* = 10.2, 8.7, 7.3 Hz, 1H), 1.12 (tdt, *J* = 11.6, 9.9, 3.7 Hz, 1H). **^{13}C NMR** (126 MHz, $CDCl_3$) δ 144.38, 143.87, 143.51, 133.86, 132.82, 132.36, 131.82, 129.85, 129.77, 127.86, 122.14, 120.50, 109.93, 108.19, 46.33, 46.29, 38.57, 34.96, 30.93, 30.66, 22.80, 21.66, 19.70. **^{19}F NMR** (377 MHz, $CDCl_3$) δ -49.83. **HRMS** (ESI+) Calc: $[M+H]^+$ ($C_{23}H_{22}F_2N_2O_4S$) 461.1341, measured: 461.1335; 1.3 ppm difference.

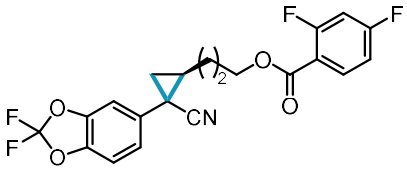

3-(2-cyano-2-(2,2-difluorobenzo[d][1,3]dioxol-5-yl)cyclopropyl)propyl 2,4-difluorobenzoate (6.36). Following General Procedure B afforded one detectable diastereomer in 110.9 mg (66% yield, ≥20:1 d.r.) as a solid. **R_f =** 0.43 (20% acetone/hexanes). Structural configuration assigned via analogy with compound **6.35**. **^{1}H NMR** (500 MHz, $CDCl_3$) δ 7.98 (td, J = 8.6, 6.5 Hz, 1H), 7.07 – 6.98 (m, 3H), 6.93 (dddd, J = 8.8, 7.6, 2.4, 1.0 Hz, 1H), 6.86 (ddd, J = 11.1, 8.8, 2.5 Hz, 1H), 4.43 (td, J = 6.2, 1.0 Hz, 2H), 2.08 (dtd, J = 14.0, 6.4, 2.3 Hz, 1H), 2.05 – 1.98 (m, 1H), 1.96 – 1.84 (m, 2H), 1.62 – 1.54 (m, 2H), 1.52 – 1.45 (m, 1H). **^{13}C NMR** (126 MHz, $CDCl_3$) δ 165.92 (dd, J = 256.6, 12.0 Hz), 163.71 (d, J = 4.2 Hz), 162.98 (dd, J = 263.2, 12.5 Hz), 144.35 (t, J = 1.1 Hz), 143.33 (t, J = 1.1 Hz), 134.11 (dd, J = 10.5, 2.3 Hz), 132.85, 131.81 (t, J = 256.4 Hz), 121.88, 120.43, 115.24 (dd, J = 9.9, 3.7 Hz), 111.81 (dd, J = 21.5, 3.8 Hz), 109.81, 107.87, 105.40 (dd, J = 26.2, 25.7 Hz), 64.68, 30.04, 28.16, 27.90, 24.08, 20.18. **^{19}F NMR** (377 MHz, $CDCl_3$) δ 49.89, -101.67 (d, J = 12.7 Hz), -103.75 (d, J = 12.5 Hz). **HRMS** (ESI+) Calc: $[M+NH_4]^+$ ($C_{21}H_{19}F_4N_2O_4$) 439.1276, measured: 439.1270; 1.4 ppm difference.

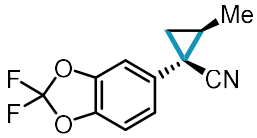

1-(2,2-difluorobenzo[d][1,3]dioxol-5-yl)-2-methylcyclopropane-1-carbonitrile (6.37). Following General Procedure C afforded 72.0 mg (74% yield, ≥20:1 d.r.) obtained as an oil. Structural configuration assigned via analogy with compound **6.35**. $\mathbf{R_f}$ = 0.25 (40% Et_2O/hexanes). **^{1}H NMR** (500 MHz, $CDCl_3$) δ 7.05 (dd, J = 8.4, 1.8Hz, 1H), 7.02 (d, J = 7.0Hz, 1H), 6.99 (d, J = 1.9Hz, 1H), 1.59-1.52 (m, 2H), 1.48 (d, J = 5.6Hz, 3H), 1.43-1.37 (m, J = 1H). **^{13}C NMR** (126 MHz, $CDCl_3$) δ144.17, 143.07, 133.05, 131.66 (t, J = 256.3Hz), 121.59, 120.40, 109.59, 107.65, 25.08, 25.00, 20.43, 15.92. **^{19}F NMR** (376 MHz, $CDCl_3$) δ -49.95. **HRMS** (ESI+) Calc: $[M+H]^+$ ($C_{12}H_9F_2NO_2$) 238.0674, measured: 238.0670; 1.7 ppm difference.

E8. Scale-Up Batch Electrolysis Setup and Procedures

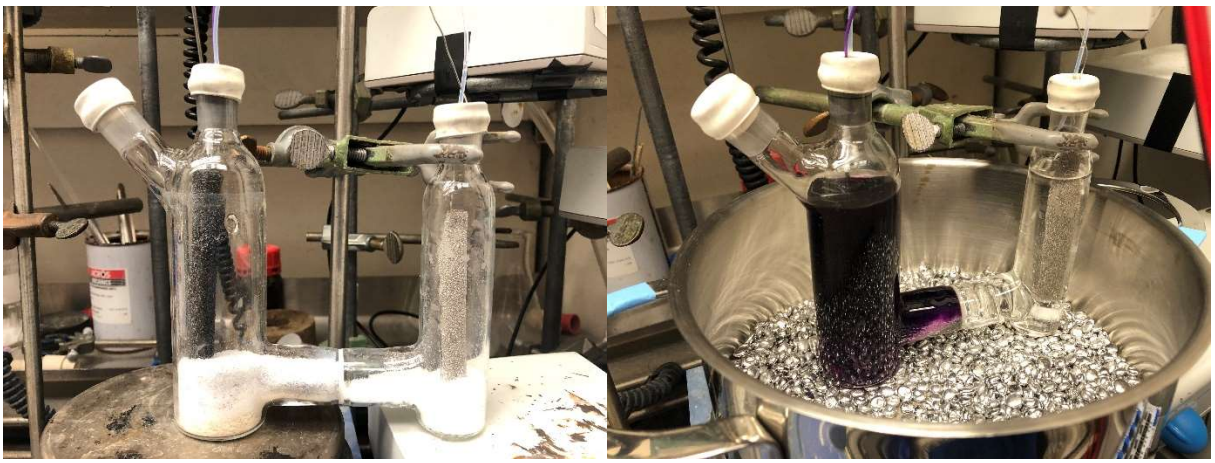

Figure E4. *Left:* Large scale divided cell batch assembly prior to addition of solvent. *Right:* Large scale divided cell batch assembly 5 minutes into electrolysis.

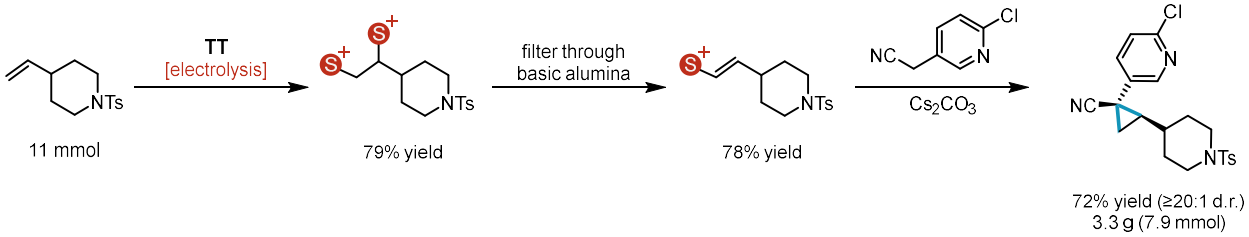

Scheme E4. Scale-up reaction for cyclopropanation via dication pool.

Procedure (11 mmol scale) - To an oven-dried large scale divided electrochemical cell equipped with magnetic stir bars was added thianthrene (3.57 g, 16.5 mmol, 1.5 equiv.), 1-tosyl-4-vinylpiperidine (2.92 g, 11 mmol, 1 equiv.), and *n*-Bu_4NPF_6 (17.0 g, 44.0 mmol, 4.0 equiv.) to the anode compartment and *n*-Bu_4NPF_6 (8.50 g, 22 mmol, 2.0 equiv.) to the cathode compartment. The cell was equipped with two septa containing a large scale stainless steel wire/Ni foam cathode assembly (electrode dimensions: 8x4.5 cm, rolled into a tube) and a pencil/RVC anode assembly (electrode dimensions: 8.5x1x1 cm) connected together with a teflon tubing to equalize pressure. MeCN (46 mL) and TFA (8.5 mL, 110 mmol, 10 equiv.) was added to the cathode compartment at the same time that MeCN (110 mL) was added to the anode compartment as to equalize solvent level in both compartments. The cathode septa was pierced with an outlet needle to avoid pressurization from hydrogen evolution. Both sides of the cell were then stirred at

30 °C and electrolyzed under a constant current of 175 mA for 5.1 h (3.0 F/mol). At completion of electrolysis, the electrode leads were disconnected, septa removed, and the anode RVC was pushed off the pencil into the reaction mixture. Dibromomethane was added as an internal standard and an NMR aliquot was taken to assess adduct formation. To the anode compartment was added a septum pierced with a needle to prevent pressurizing. After pressure equilibration, the needle was removed, and the cathode solution was removed from the cell via pipette. The anode solution was filtered through activated basic alumina (110 g, Brockmann I). The cathode compartment was washed with MeCN (40 mL) and pushed across the frit to rinse the frit. The anode compartment was further washed with MeCN (5 x 40 mL). The alumina pad was washed with MeCN (3 x 320 mL), taking care to fully disperse the alumina in solution using a spatula. The filtrate was concentrated under reduced pressure until ~50mL MeCN remains. Mesitylene was added as an internal standard and an NMR aliquot was taken to assess alkenyl-TT+ yield. Then a stir bar was added to the flask, followed by 2-chloro-5-(cyanomethyl)pyridine (1.68 g, 11.0 mmol, 1 equiv.) then Cs_2CO_3 (8.96 g, 27.5 mmol, 2.5 equiv.). The solution was stirred for 16 h. At completion, the mixture was diluted with DCM (200 mL) and water (600 mL). The aqueous layer was extracted with DCM (200 mL x 3). The combined organic layers were dried with anhydrous Na_2SO_4, filtered, and concentrated under reduced pressure. The residue was purified via flash column chromatography to yield the pure cyclopropane product.

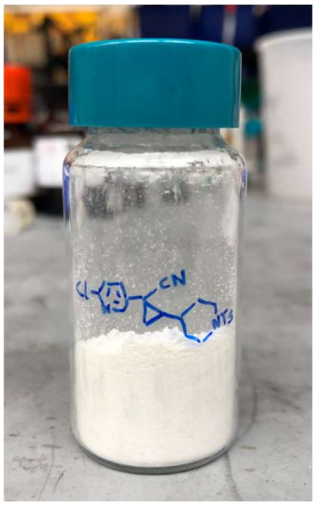

Figure E5. Gram-scale synthesis of cyclopropane via dication pool.

E9. X-Ray Diffraction Data

Data Collection (6.18)

A colorless crystal with approximate dimensions 0.18 × 0.18 × 0.15 mm^3 was selected under oil under ambient conditions and attached to the tip of a MiTeGen MicroMount©. The crystal was mounted in a stream of cold nitrogen at 100(1) K and centered in the X-ray beam by using a video camera.

The crystal evaluation and data collection were performed on a Bruker D8 VENTURE PhotonIII four-circle diffractometer with Cu Kα (λ = 1.54178 Å) radiation and the detector to crystal distance of 4.5 cm.[9]

The initial cell constants were obtained from a 180° φ scan conducted at a 2θ = 50° angle with an exposure time of 1 second per frame. The reflections were successfully indexed by an automated indexing routine built into the APEX3 program. The final cell constants were calculated from a set of 9394 strong reflections from the actual data collection.

The data were collected by using a full sphere data collection routine to survey reciprocal space to the extent of a full sphere to a resolution of 0.78 Å. A total of 24922 data were harvested by collecting 22 sets of frames with 1.0º scans in ω and φ with exposure times of 0.75–4 sec per frame. These highly redundant datasets were corrected for Lorentz and polarization effects. The absorption correction was based on fitting a function to the empirical transmission surface as sampled by multiple equivalent measurements.[10]

Structure Solution and Refinement (6.18)
The systematic absences in the diffraction data were uniquely consistent for the space group $P2_1/c$ that yielded chemically reasonable and computationally stable results of refinement.[11–16]

A successful solution by intrinsic phasing provided most non-hydrogen atoms from the *E*-map. The remaining non-hydrogen atoms were located with an alternating series of least-squares cycles and difference Fourier maps. The atomic structure factors were determined by DFT calculations, using the B3LYP hybrid functional and the 6-31G(d) basis set, in the NoSpherA2 extension of the olex2.refine program.[17–19] All atoms were refined with anisotropic displacement coefficients.

In the stereoisomer shown in Figure 1 both chiral centers (C7 and C10) are *R*. The *S,S*-stereoisomer is also present in the crystal structure. The *R,R* molecule was chosen arbitrarily.

The final least squares refinement of 325 parameters against 3021 data resulted in residuals *R* (based on F^2 for $I \geq 2\sigma$) and *wR* (based on F^2 for all data) of 0.0216 and 0.0478, respectively. The final difference Fourier map was featureless.

Data Collection (6.14)
A colorless crystal with approximate dimensions 0.168 × 0.08 × 0.076 mm^3 was selected under oil under ambient conditions and attached to the tip of a MiTeGen MicroMount©. The crystal was mounted in a stream of cold nitrogen at 100(1) K and centered in the X-ray beam by using a video camera.

The crystal evaluation and data collection were performed on a Bruker D8 VENTURE PhotonIII four-circle diffractometer with Cu Kα (λ = 1.54178 Å) radiation and the detector to crystal distance of 4.5 cm.[9]

The initial cell constants were obtained from a 180° φ scan conducted at a 2θ = 50° angle with the exposure time of 1 second per frame. The reflections were successfully indexed by an automated indexing routine built in the APEX3 program. The final cell constants were calculated from a set of 9365 strong reflections from the actual data collection.

The data were collected by using the full sphere data collection routine to survey the reciprocal space to the extent of a full sphere to a resolution of 0.80 Å. A total of 128377 data were harvested by collecting 34 sets of frames with 0.9º scans in ω and φ with an exposure time 1–6 sec per frame. These highly redundant datasets were corrected for Lorentz and polarization effects. The absorption correction was based on fitting a function to the empirical transmission surface as sampled by multiple equivalent measurements.[10]

Structure Solution and Refinement (6.14)
The systematic absences in the diffraction data were uniquely consistent for the space group $P2_1/n$ that yielded chemically reasonable and computationally stable results of refinement.[11–16]

A successful solution by intrinsic phasing provided most non-hydrogen atoms from the *E*-map. The remaining non-hydrogen atoms were located in an alternating series of least-squares cycles and difference Fourier maps. All non-hydrogen atoms were refined with anisotropic displacement coefficients. All hydrogen atoms were included in the structure factor calculation at idealized positions and were allowed to ride on the neighboring atoms with relative isotropic displacement coefficients.

The compound crystallizes as a racemate. The enantiomer shown in Figure 1 (C8 – *S*, C12 – *S*) was chosen arbitrarily.

There are two symmetry-independent molecules with identical compositions, handedness, and very similar conformations in the asymmetric unit.

The final least-squares refinement of 525 parameters against 8466 data resulted in residuals *R* (based on F^2 for $I \geq 2\sigma$) and *wR* (based on F^2 for all data) of 0.0371 and 0.0990, respectively. The final difference Fourier map was featureless.

Data Collection (6.27)

A colorless crystal with approximate dimensions 0.09 x 0.07 x 0.06 mm^3 was selected under oil under ambient conditions and attached to the tip of a MiTeGen MicroMount©. The crystal was mounted in a stream of cold nitrogen at 100(1) K and centered in the X-ray beam by using a video camera.

The crystal evaluation and data collection were performed on a Bruker D8 VENTURE PhotonIII four-circle diffractometer with Cu Kα (λ = 1.54178 Å) radiation and the detector to crystal distance of 4.5 cm.[9]

The initial cell constants were obtained from a 180° φ scan conducted at a 2θ = 50° angle with an exposure time of 1 second per frame. The reflections were successfully indexed by an automated indexing routine built into the APEX3 program. The final cell constants were calculated from a set of 9522 strong reflections from the actual data collection.

The data were collected by using a full sphere data collection routine to survey reciprocal space to the extent of a full sphere to a resolution of 0.80 Å. A total of 11798 data were harvested by collecting 20 sets of frames with 0.9º scans in ω and φ with exposure times of 10-30 sec per frame. These highly redundant datasets were corrected for Lorentz and polarization effects. The absorption correction was based on fitting a function to the empirical transmission surface as sampled by multiple equivalent measurements[10]

Structure Solution and Refinement (6.27)

The systematic absences in the diffraction data were uniquely consistent for the space group $P2_1/n$ that yielded chemically reasonable and computationally stable results of refinement.[11–16]

A successful solution by intrinsic phasing provided most non-hydrogen atoms from the *E*-map. The remaining non-hydrogen atoms were located with an alternating series of least-squares cycles and difference Fourier maps. All atoms were refined with anisotropic displacement coefficients. The atomic form factors were computed with NoSpherA2[17] at the B3LYP/def2-SVP level of theory.

This compound crystallizes as a racemate. The molecule shown in the first diagram was chosen arbitrarily, with chiral atoms C2 and C4 in the *S*,*S* conformation. However, the *R*,*R* enantiomer is also present in the structure.

The final least-squares refinement of 154 parameters against 1309 data resulted in residuals *R* (based on F^2 for $I \geq 2\sigma$) and *wR* (based on F^2 for all data) of 0.0157 and 0.0393, respectively. The final difference Fourier map was featureless.

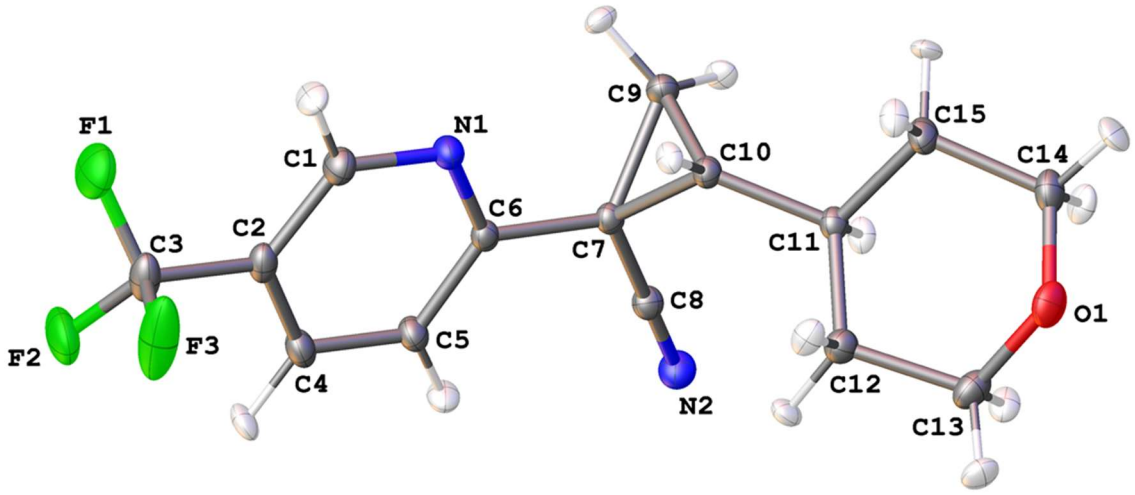

Figure E6. A molecular drawing of the asymmetric unit in compound **6.18** shown with 50% probability ellipsoids.

Table E7. Crystal data and structure refinement for (6.18)

Identification code	wickens06
Empirical formula	$C_{15}H_{15}F_3N_2O$
Formula weight	296.294
Temperature/K	100.00
Crystal system	monoclinic
Space group	$P2_1/c$
a/Å	6.1884(5)
b/Å	9.2955(10)
c/Å	24.5282(19)
α/°	90
β/°	91.250(5)
γ/°	90
Volume/Å^3	1410.6(2)
Z	4
ρ_{calc}g/cm^3	1.395
μ/mm^{-1}	0.993
F(000)	618.5
Crystal size/mm^3	0.18 × 0.18 × 0.15
Radiation	Cu Kα (λ = 1.54178)
2Θ range for data collection/°	7.2 to 158.26
Index ranges	$-7 \leq h \leq 7$, $-11 \leq k \leq 11$, $-31 \leq l \leq 27$
Reflections collected	24922
Independent reflections	3021 [R_{int} = 0.0236, R_{sigma} = 0.0151]
Data/restraints/parameters	3021/0/325
Goodness-of-fit on F^2	1.101
Final R indexes [I>=2σ (I)]	R_1 = 0.0216, wR_2 = 0.0475
Final R indexes [all data]	R_1 = 0.0221, wR_2 = 0.0478
Largest diff. peak/hole / e Å^{-3}	0.36/-0.26

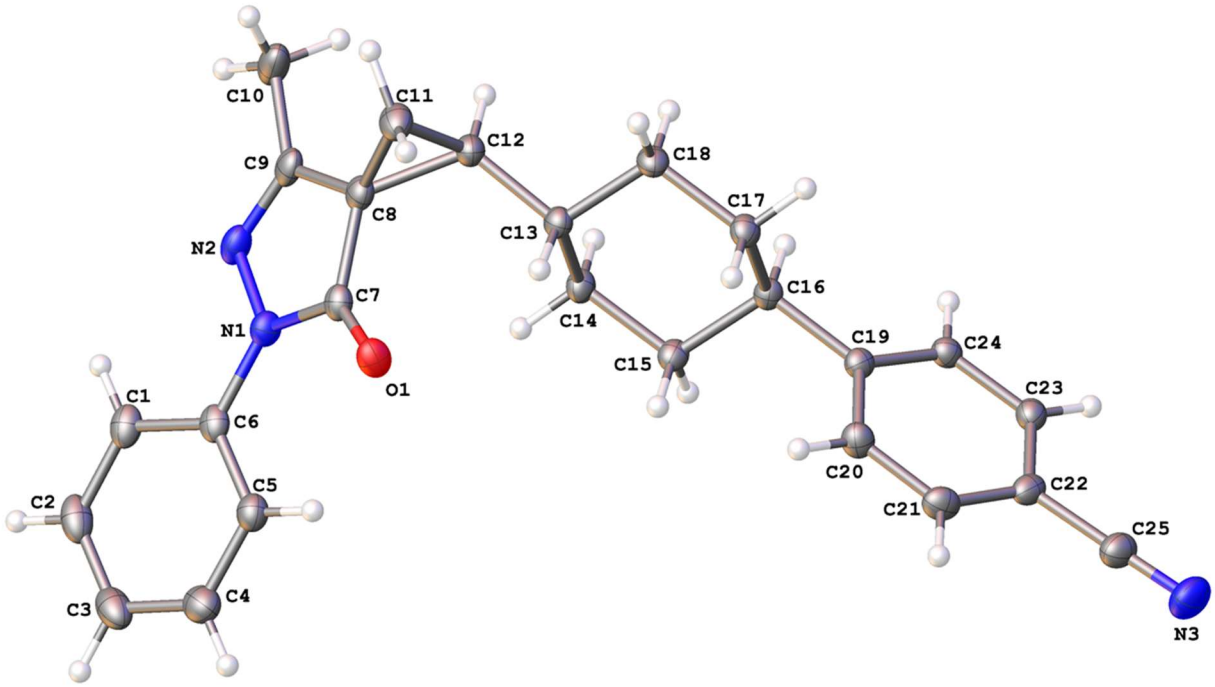

Figure E7. A molecular drawing of the first symmetry-independent molecules of compound **6.14** shown with 50% probability ellipsoids.

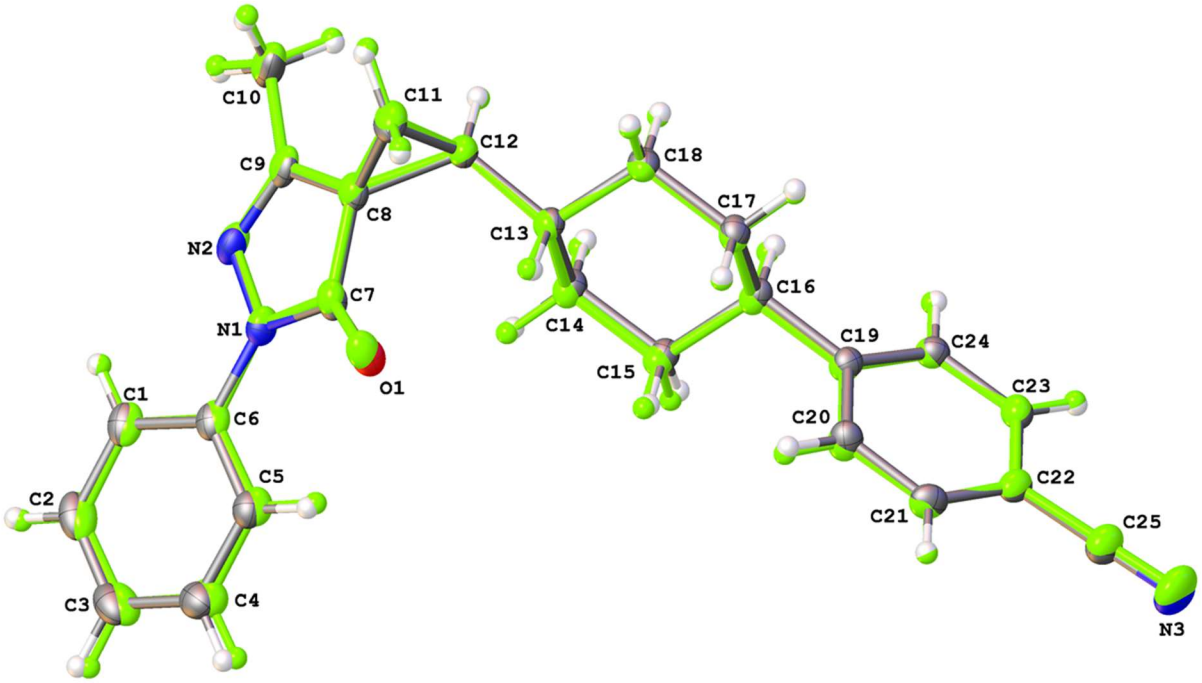

Figure E8. A superposition of the two symmetry-independent molecules of compound **6.14** shown with 50% probability ellipsoids. The second molecule is green.

Table E8. Crystal data and structure refinement for (16.4).

Identification code	Wickens07
Empirical formula	$C_{25}H_{25}N_3O$
Formula weight	383.48
Temperature/K	100.00
Crystal system	monoclinic
Space group	$P2_1/n$
a/Å	15.3630(10)
b/Å	10.4765(6)
c/Å	26.2845(17)
α/°	90
β/°	99.916(5)
γ/°	90
Volume/Å^3	4167.3(5)
Z	8
ρ_{calc}g/cm^3	1.222
μ/mm^{-1}	0.593
F(000)	1632.0
Crystal size/mm^3	0.168 × 0.08 × 0.076
Radiation	Cu Kα (λ = 1.54178)
2Θ range for data collection/°	6.236 to 149.198
Index ranges	$-19 \leq h \leq 19$, $-13 \leq k \leq 12$, $-32 \leq l \leq 32$
Reflections collected	128377
Independent reflections	8466 [R_{int} = 0.0331, R_{sigma} = 0.0126]
Data/restraints/parameters	8466/0/525
Goodness-of-fit on F^2	1.086
Final R indexes [I>=2σ (I)]	R_1 = 0.0371, wR_2 = 0.0974
Final R indexes [all data]	R_1 = 0.0393, wR_2 = 0.0990
Largest diff. peak/hole / e Å^{-3}	0.28/-0.21

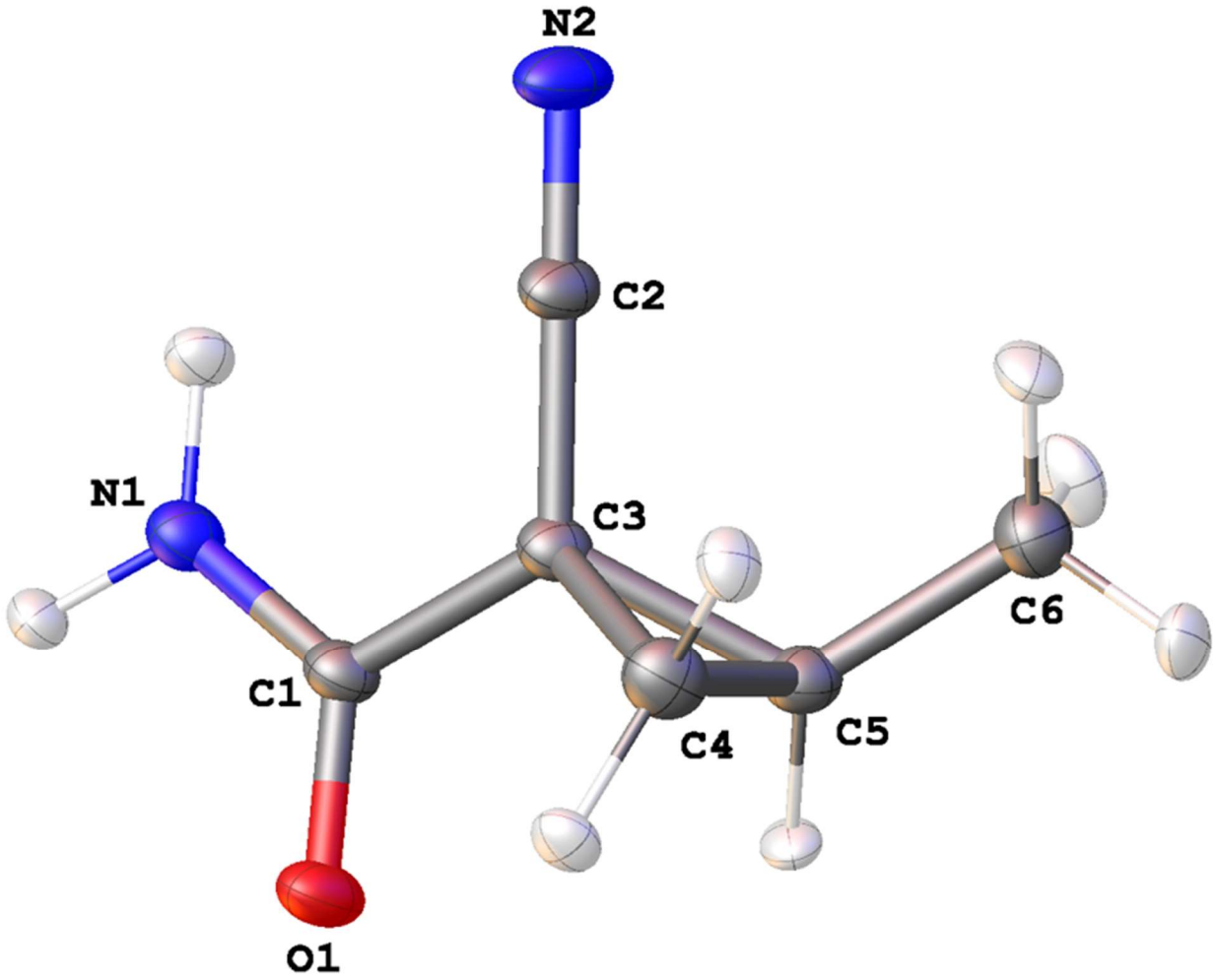

Figure E9. A molecular drawing of the molecule in compound **6.27** shown with 50% probability ellipsoids. The molecule shown was chosen arbitrarily, with chiral atoms C2 and C4 in the S,S conformation. However, this compound crystallizes as a racemate, thus the R,R enantiomer is also present.

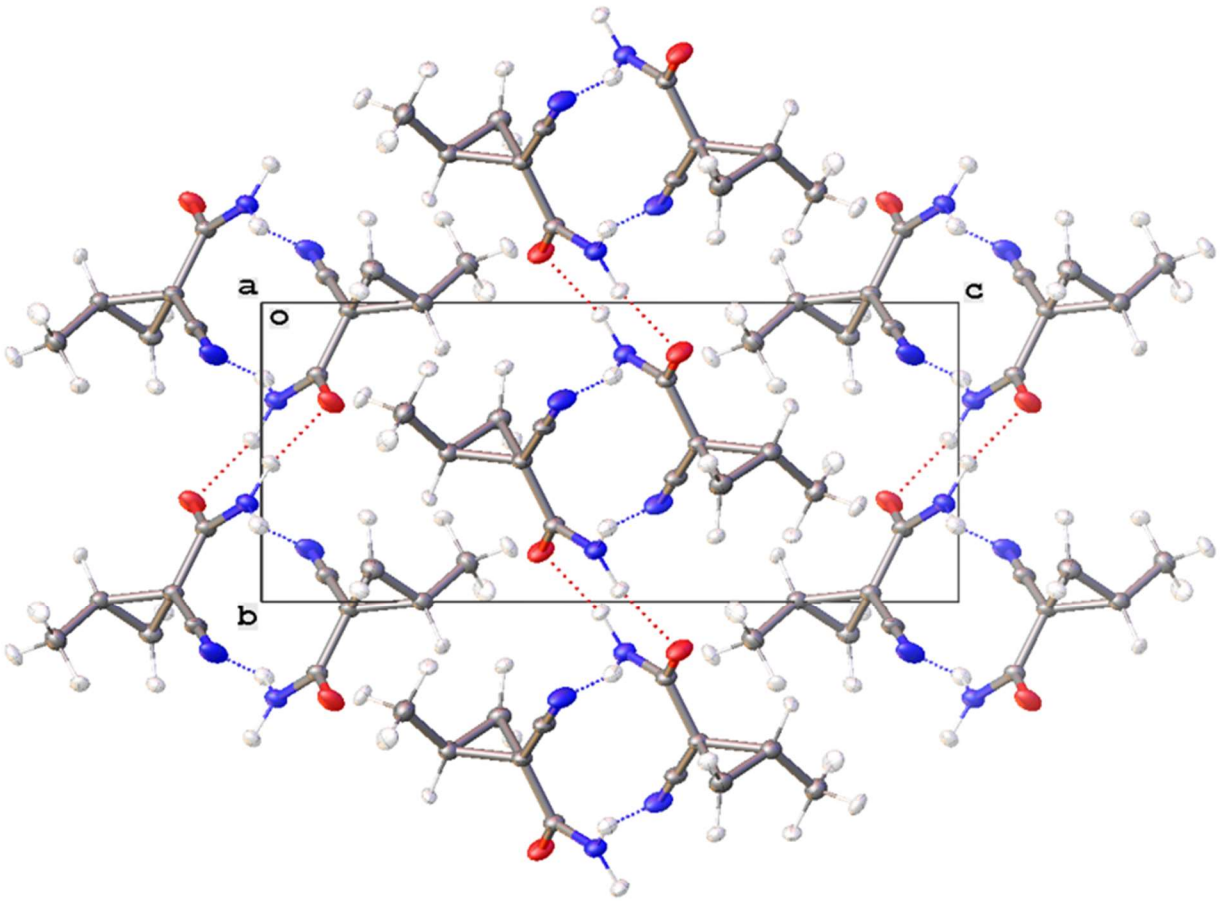

Figure E10. A packing diagram of compound **6.27** shown along the a axis with 50% probability ellipsoids.

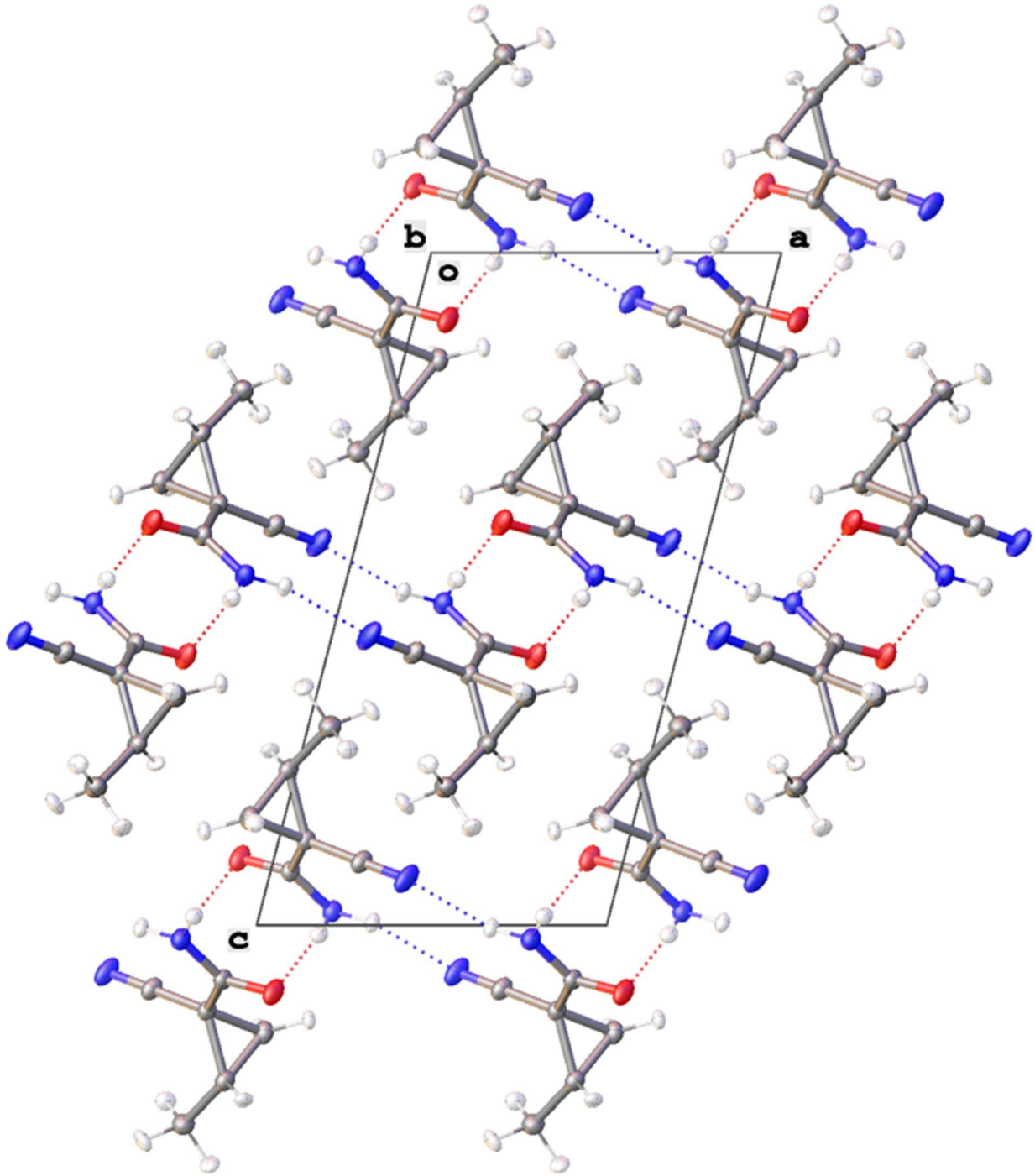

Figure E11. A packing diagram of compound **6.27** shown along the b axis with 50% probability ellipsoids.

Table E9. Crystal data and structure refinement for compound 6.27.

Identification code	wickens08
Empirical formula	$C_6H_8N_2O$
Formula weight	124.143
Temperature/K	100.00
Crystal system	monoclinic
Space group	$P2_1/n$
a/Å	7.4137(7)
b/Å	6.1089(6)
c/Å	14.7286(14)
α/°	90
β/°	104.550(4)
γ/°	90
Volume/Å^3	645.66(11)
Z	4
ρ_{calc}g/cm^3	1.277
μ/mm^{-1}	0.740
F(000)	264.9
Crystal size/mm^3	0.09 × 0.07 × 0.06
Radiation	Cu Kα (λ = 1.54178)
2Θ range for data collection/°	12.34 to 149.06
Index ranges	$-9 \leq h \leq 9$, $-7 \leq k \leq 7$, $-18 \leq l \leq 18$
Reflections collected	11382
Independent reflections	1309 [R_{int} = 0.0259, R_{sigma} = 0.0180]
Data/restraints/parameters	1309/0/154
Goodness-of-fit on F^2	1.296
Final R indexes [I>=2σ (I)]	R_1 = 0.0157, wR_2 = 0.0389
Final R indexes [all data]	R_1 = 0.0165, wR_2 = 0.0393
Largest diff. peak/hole / e Å^{-3}	0.11/-0.08

E10. References

(1) Macrae, C. F.; Edgington, P. R.; McCabe, P.; Pidcock, E.; Shields, G. P.; Taylor, R.; Towler, M.; Streek, J. van de. Mercury: Visualization and Analysis of Crystal Structures. *J Appl Cryst* **2006**, *39* (3), 453–457. https://doi.org/10.1107/S002188980600731X.

(2) Peretto, I.; Radaelli, S.; Parini, C.; Zandi, M.; Raveglia, L. F.; Dondio, G.; Fontanella, L.; Misiano, P.; Bigogno, C.; Rizzi, A.; Riccardi, B.; Biscaioli, M.; Marchetti, S.; Puccini, P.; Catinella, S.; Rondelli, I.; Cenacchi, V.; Bolzoni, P. T.; Caruso, P.; Villetti, G.; Facchinetti, F.; Del Giudice, E.; Moretto, N.; Imbimbo, B. P. Synthesis and Biological Activity of Flurbiprofen Analogues as Selective Inhibitors of β-Amyloid1-42 Secretion. *J. Med. Chem.* **2005**, *48* (18), 5705–5720. https://doi.org/10.1021/jm0502541.

(3) Okaniwa, M.; Hirose, M.; Imada, T.; Ohashi, T.; Hayashi, Y.; Miyazaki, T.; Arita, T.; Yabuki, M.; Kakoi, K.; Kato, J.; Takagi, T.; Kawamoto, T.; Yao, S.; Sumita, A.; Tsutsumi, S.; Tottori, T.; Oki, H.; Sang, B.-C.; Yano, J.; Aertgeerts, K.; Yoshida, S.; Ishikawa, T. Design and Synthesis of Novel DFG-Out RAF/Vascular Endothelial Growth Factor Receptor 2 (VEGFR2) Inhibitors. 1. Exploration of [5,6]-Fused Bicyclic Scaffolds. *J. Med. Chem.* **2012**, *55* (7), 3452–3478. https://doi.org/10.1021/jm300126x.

(4) Chang, X.-W.; Han, Q.-C.; Jiao, Z.-G.; Weng, L.-H.; Zhang, D.-W. 1-Aminoxymethylcyclopropanecarboxylic Acid as Building Block of β N–O Turn and Helix: Synthesis and Conformational Analysis in Solution and in the Solid State. *Tetrahedron* **2010**, *66* (51), 9733–9737. https://doi.org/10.1016/j.tet.2010.10.037.

(5) Rancourt, J.; Cameron, D. R.; Gorys, V.; Lamarre, D.; Poirier, M.; Thibeault, D.; Llinàs-Brunet, M. Peptide-Based Inhibitors of the Hepatitis C Virus NS3 Protease: Structure−Activity Relationship at the C-Terminal Position. *J. Med. Chem.* **2004**, *47* (10), 2511–2522. https://doi.org/10.1021/jm030573x.

(6) Altshuler, D. M.; Anderson, C. D.; Chen, W. G.; Clemens, J. J.; Cleveland, T.; Coon, T. R.; Frieman, B.; GROOTENHUIS (deceased), P.; Ruah, S. S. H.; Hare, B. J.; KEWALRAMANI, R.; Mccartney, J.; Miller, M. T.; PARASELLI, P.; Pierre, F.; ROBERTSON, S. M.; SOSNAY, P. R.; SWIFT, S. E.; Zhou, J. Methods of Treatment for Cystic Fibrosis. WO2020102346A1, May 22, 2020. https://patents.google.com/patent/WO2020102346A1/en?oq=WO2020%2f102346 (accessed 2022-12-30).

(7) Holst, D. E.; Wang, D. J.; Kim, M. J.; Guzei, I. A.; Wickens, Z. K. Aziridine Synthesis by Coupling Amines and Alkenes via an Electrogenerated Dication. *Nature* **2021**, *596* (7870), 74–79. https://doi.org/10.1038/s41586-021-03717-7.

(8) Wang, D. J.; Targos, K.; Wickens, Z. K. Electrochemical Synthesis of Allylic Amines from Terminal Alkenes and Secondary Amines. *J. Am. Chem. Soc.* **2021**, *143* (51), 21503–21510. https://doi.org/10.1021/jacs.1c11763.

(9) *Bruker-AXS (2019). APEX3. Version 2019.11-0. Madison, Wisconsin, USA.*

(10) Krause, L.; Herbst-Irmer, R.; Sheldrick, G. M.; Stalke, D. Comparison of Silver and Molybdenum Microfocus X-Ray Sources for Single-Crystal Structure Determination. *J Appl Cryst* **2015**, *48* (1), 3–10. https://doi.org/10.1107/S1600576714022985.

(11) *Sheldrick, G. M. (2013b). XPREP. Version 2013/1. Georg-August-Universität Göttingen, Göttingen, Germany.*

(12) *Sheldrick, G. M. (2013a). The SHELX homepage, http://shelx.uni-ac.gwdg.de/SHELX/.*

(13) Sheldrick, G. M. SHELXT – Integrated Space-Group and Crystal-Structure Determination. *Acta Cryst A* **2015**, *71* (1), 3–8. https://doi.org/10.1107/S2053273314026370.

(14) Sheldrick, G. M. Crystal Structure Refinement with SHELXL. *Acta Cryst C* **2015**, *71* (1), 3–8. https://doi.org/10.1107/S2053229614024218.

(15) Dolomanov, O. V.; Bourhis, L. J.; Gildea, R. J.; Howard, J. a. K.; Puschmann, H. OLEX2: A Complete Structure Solution, Refinement and Analysis Program. *J Appl Cryst* **2009**, *42* (2), 339–341. https://doi.org/10.1107/S0021889808042726.

(16) *Guzei, I. A. (2007-2022). Programs Gn. University of Wisconsin-Madison, Madison, Wisconsin, USA.*

(17) Kleemiss, F.; Dolomanov, O. V.; Bodensteiner, M.; Peyerimhoff, N.; Midgley, L.; Bourhis, L. J.; Genoni, A.; Malaspina, L. A.; Jayatilaka, D.; Spencer, J. L.; White, F.; Grundkötter-Stock, B.; Steinhauer, S.; Lentz, D.; Puschmann, H.; Grabowsky, S. Accurate Crystal Structures and Chemical Properties from NoSpherA2. *Chem. Sci.* **2021**, *12* (5), 1675–1692. https://doi.org/10.1039/D0SC05526C.
(18) Bourhis, L. J.; Dolomanov, O. V.; Gildea, R. J.; Howard, J. a. K.; Puschmann, H. The Anatomy of a Comprehensive Constrained, Restrained Refinement Program for the Modern Computing Environment – Olex2 Dissected. *Acta Cryst A* **2015**, *71* (1), 59–75. https://doi.org/10.1107/S2053273314022207.
(19) Neese, F. Software Update: The ORCA Program System, Version 4.0. *WIREs Computational Molecular Science* **2018**, *8* (1), e1327. https://doi.org/10.1002/wcms.1327.

E11. NMR Spectra

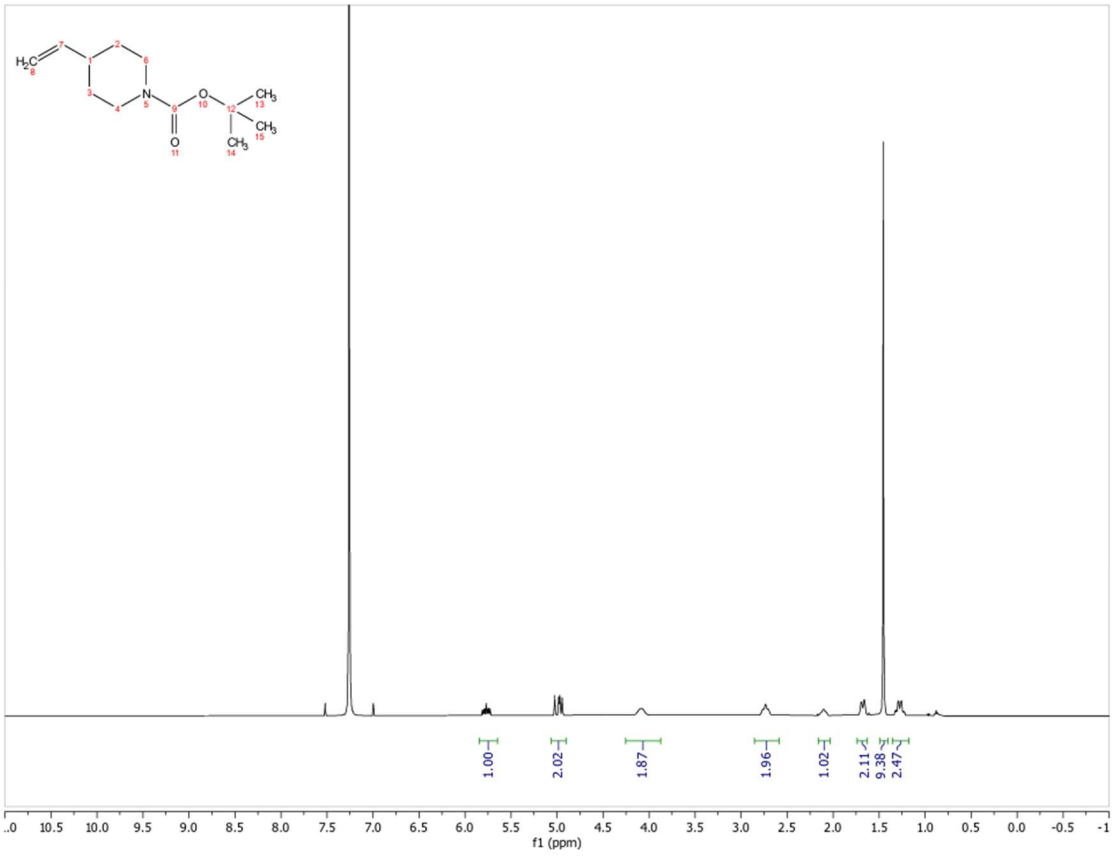

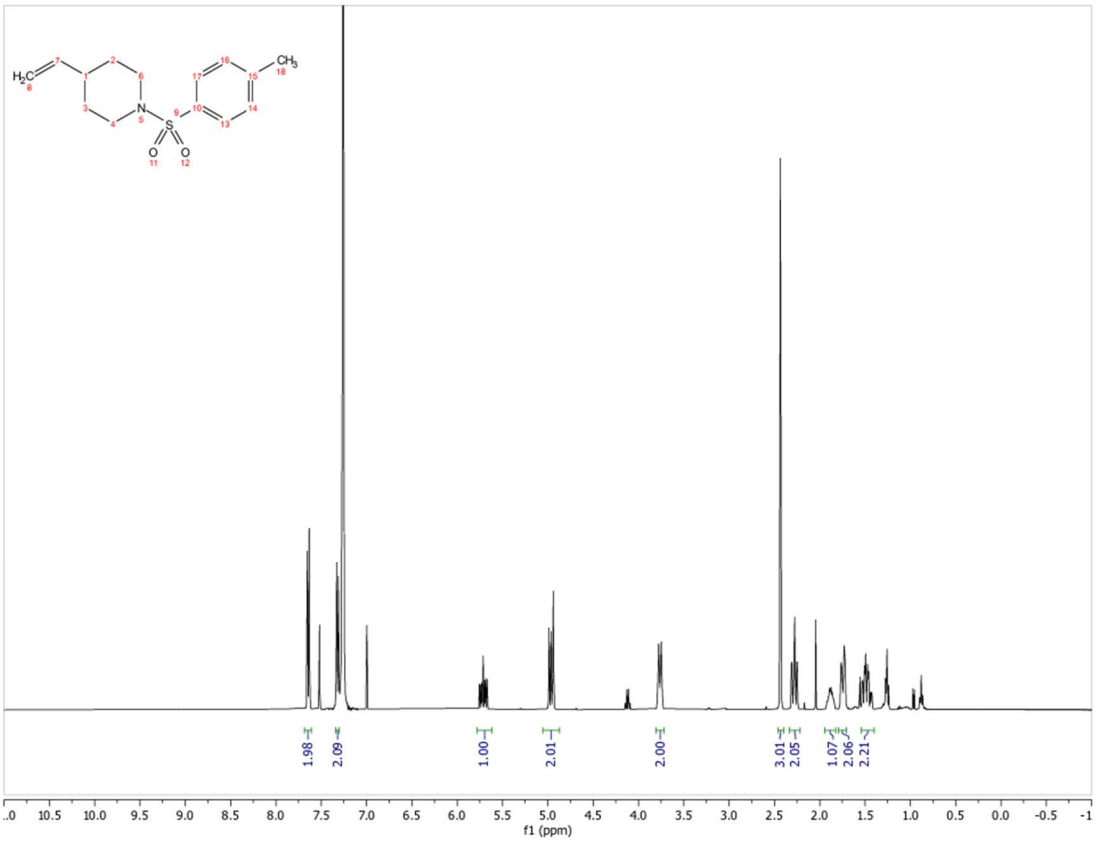
1.98
2.09
1.00
2.01
2.00
3.01
2.05
1.07
2.06
2.21
f1 (ppm)

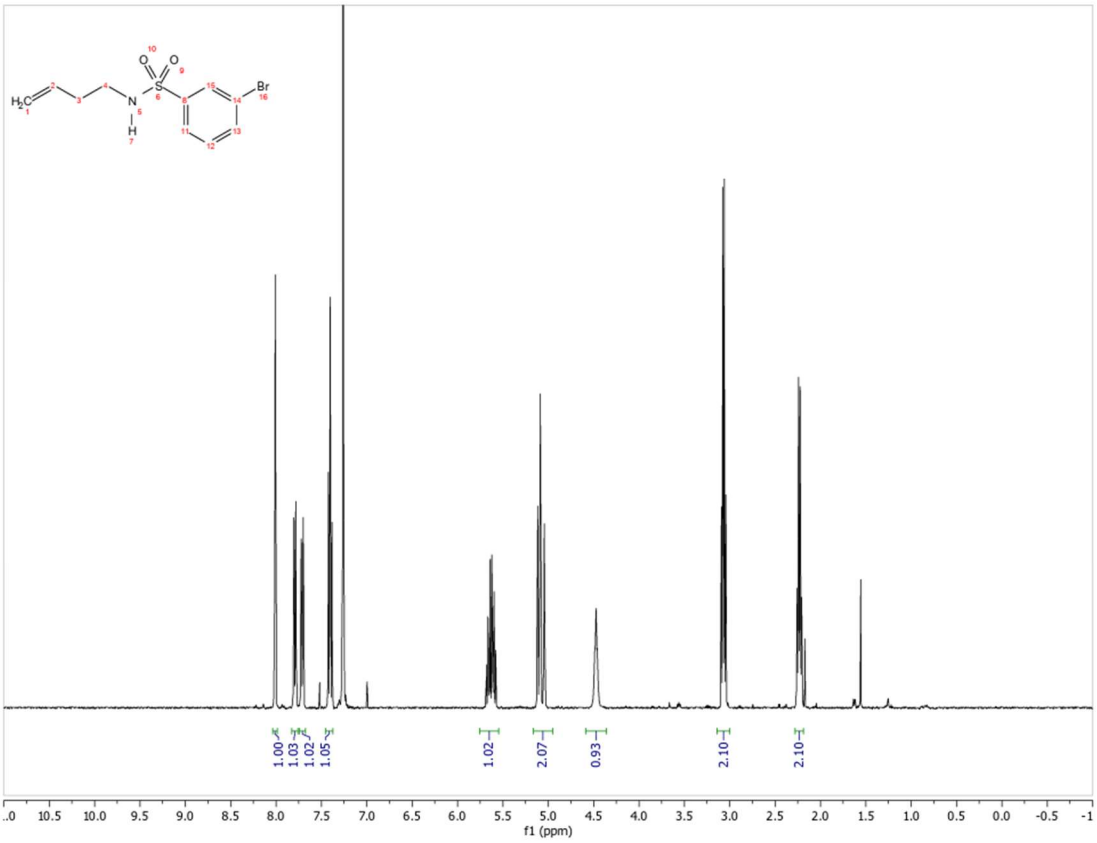
1.00
1.03
1.02
1.05
1.02
2.07
0.93
2.10
2.10
f1 (ppm)

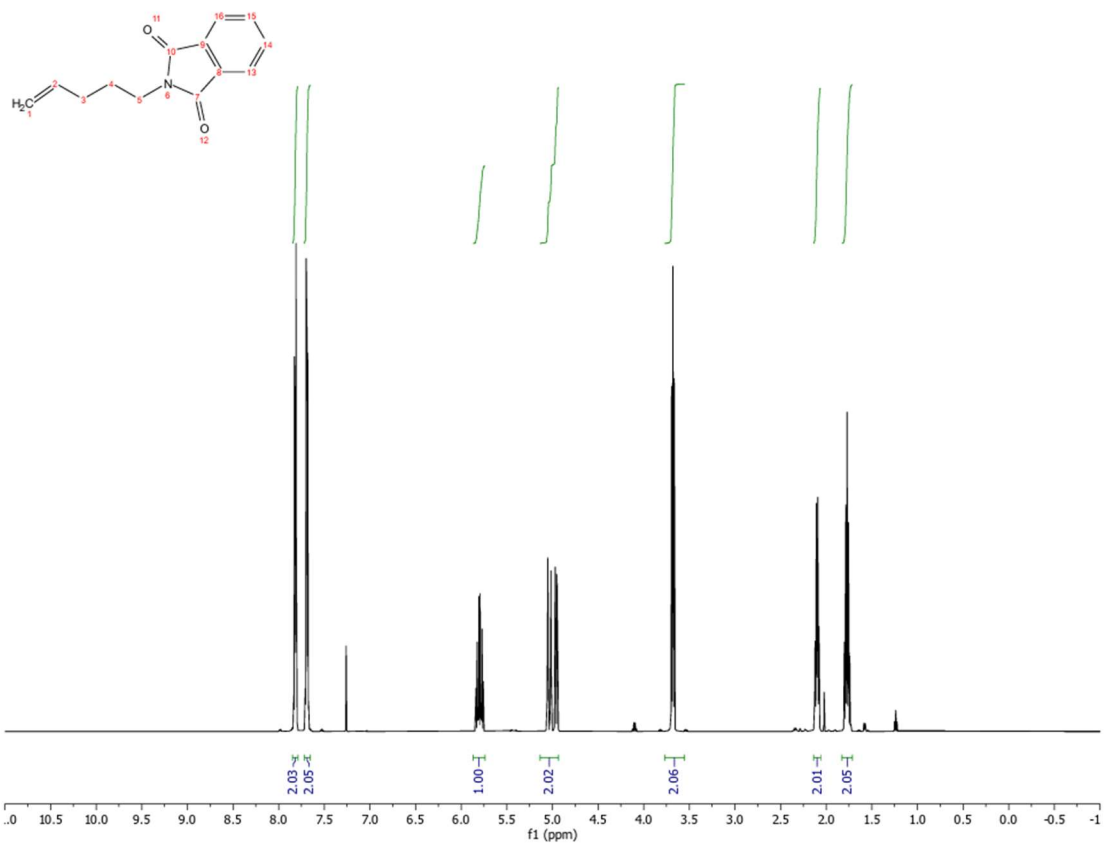
2.03
2.05
1.00
2.02
2.06
2.01
2.05
f1 (ppm)

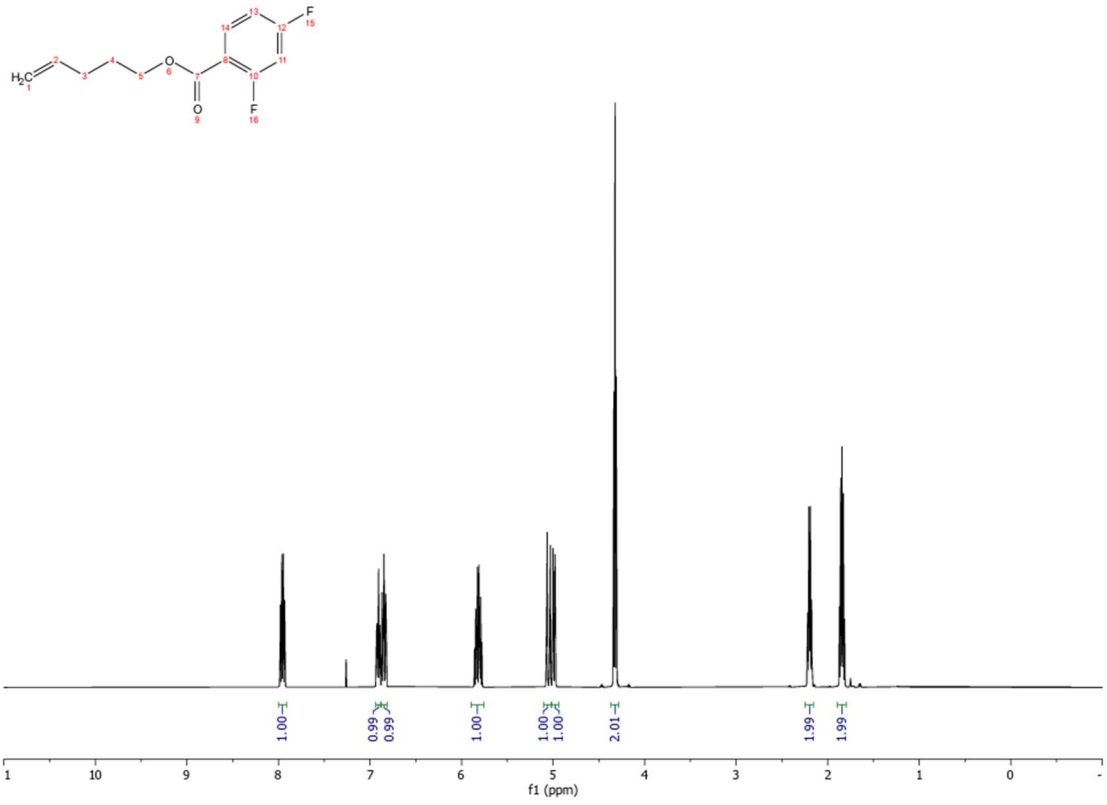
1.00
0.99
0.99
1.00
1.00
1.00
2.01
1.99
1.99
f1 (ppm)

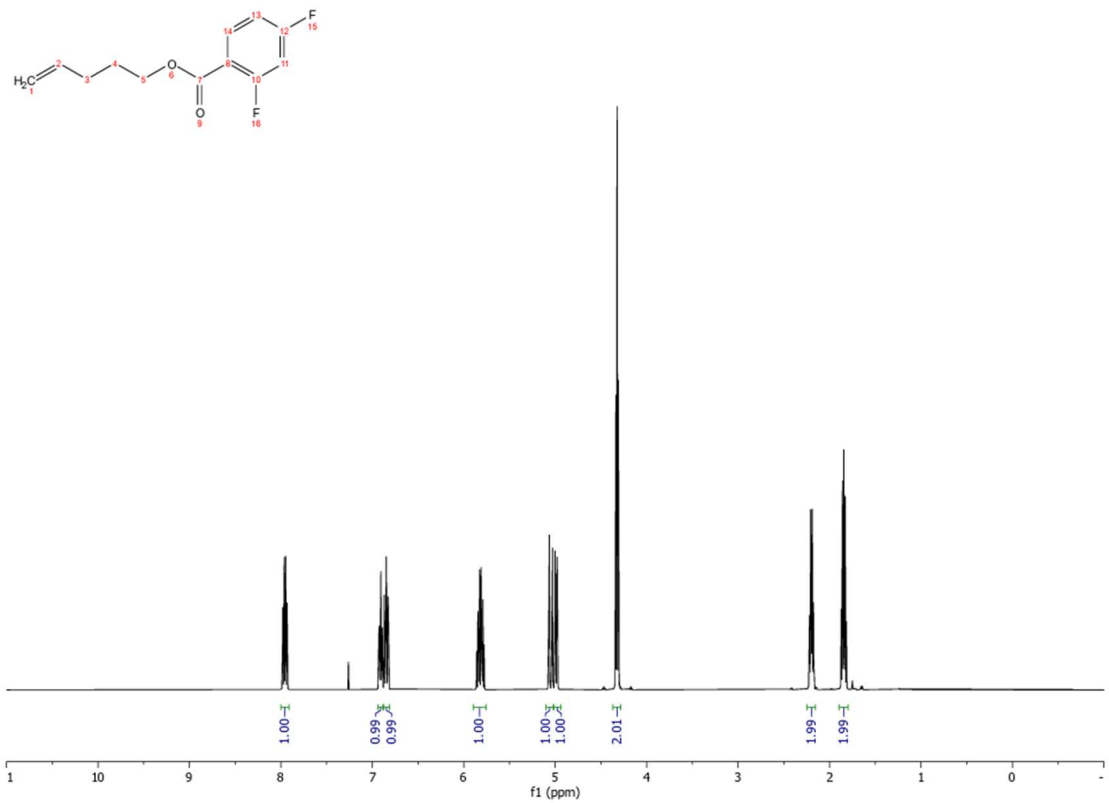
1.00
0.99
0.99
1.00
1.00
1.00
2.01
1.99
1.99
f1 (ppm)

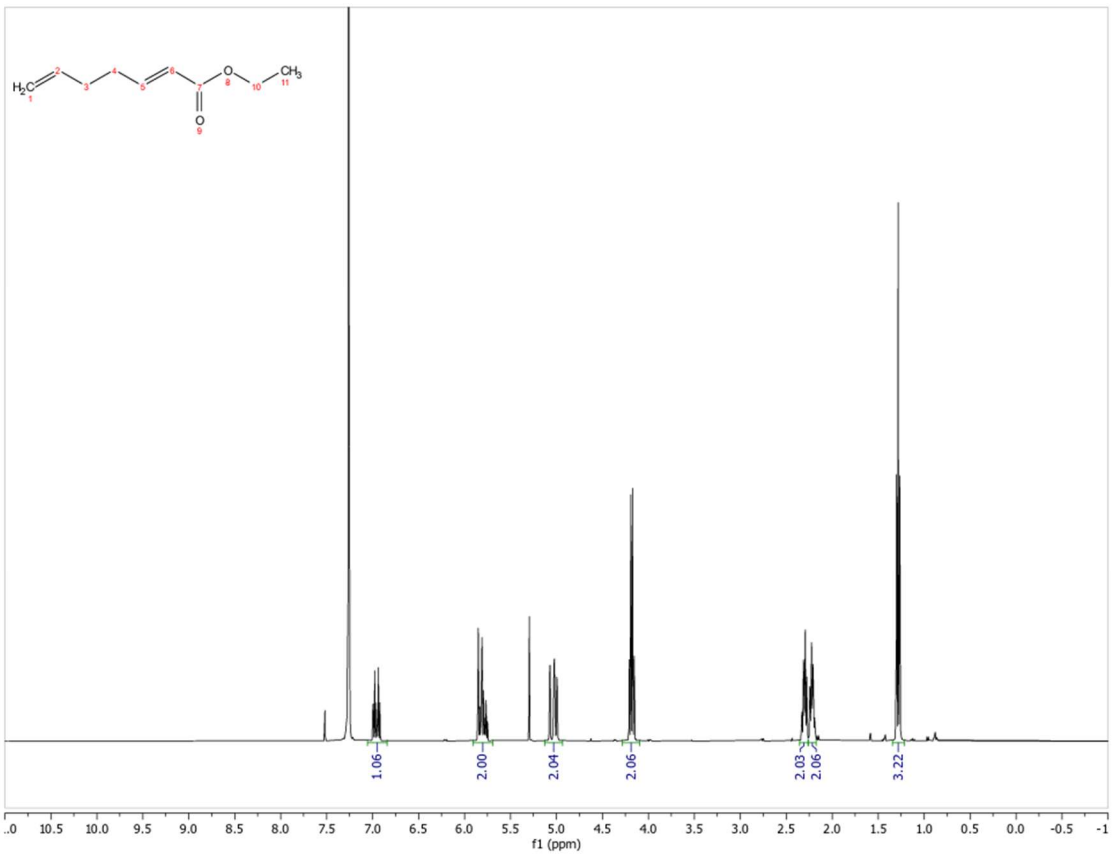
1.06
2.00
2.04
2.06
2.03
2.06
3.22
f1 (ppm)

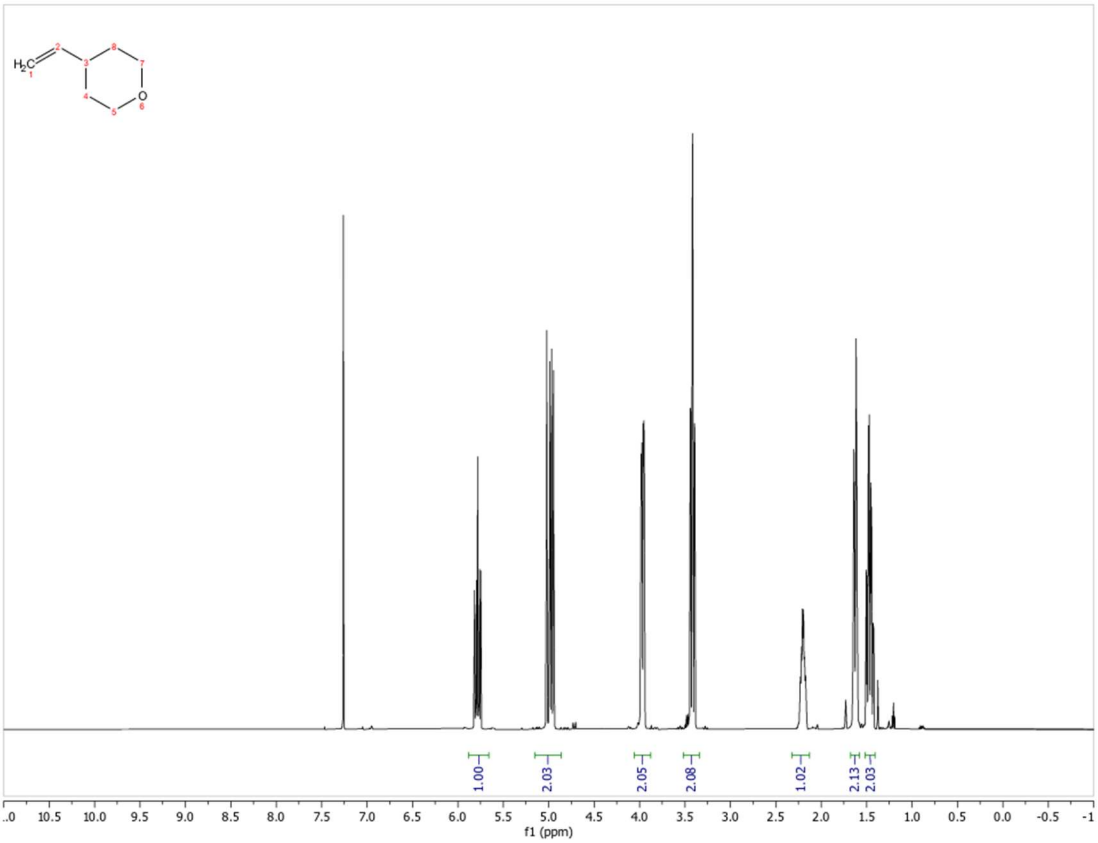
1.00
2.03
2.05
2.08
1.02
2.13
2.03
f1 (ppm)

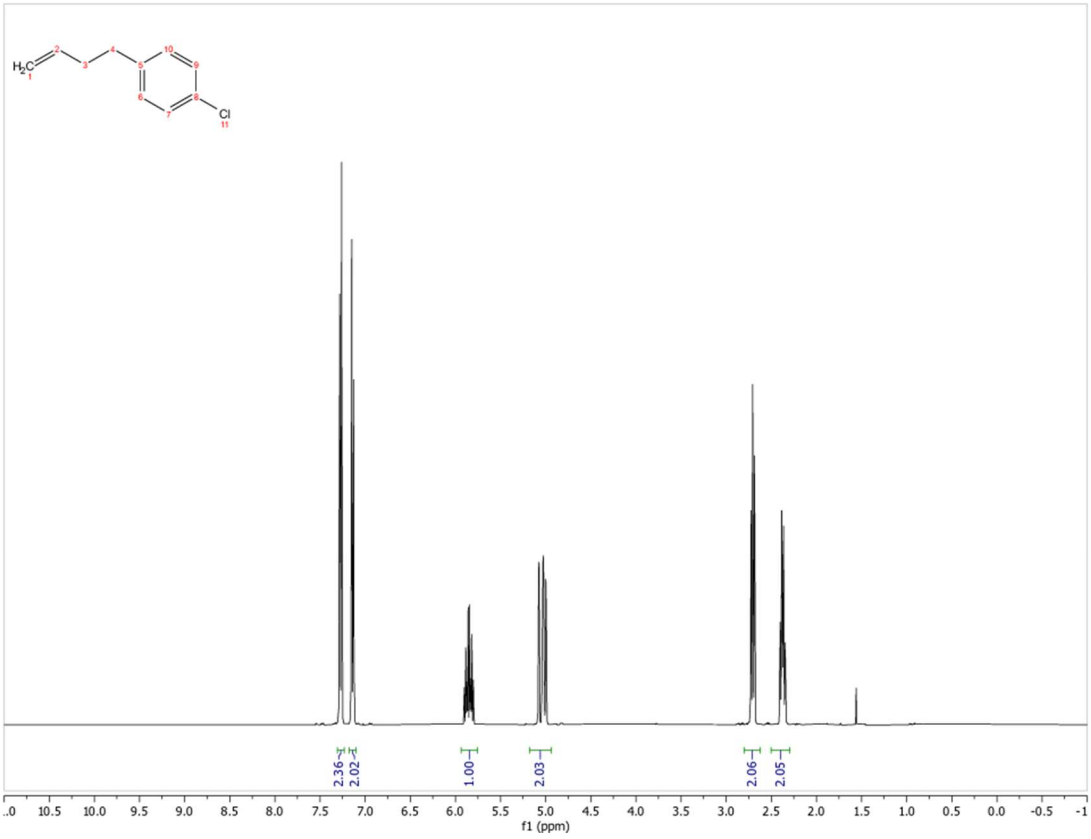
Cl
2.36
2.02
1.00
2.03
2.06
2.05
f1 (ppm)

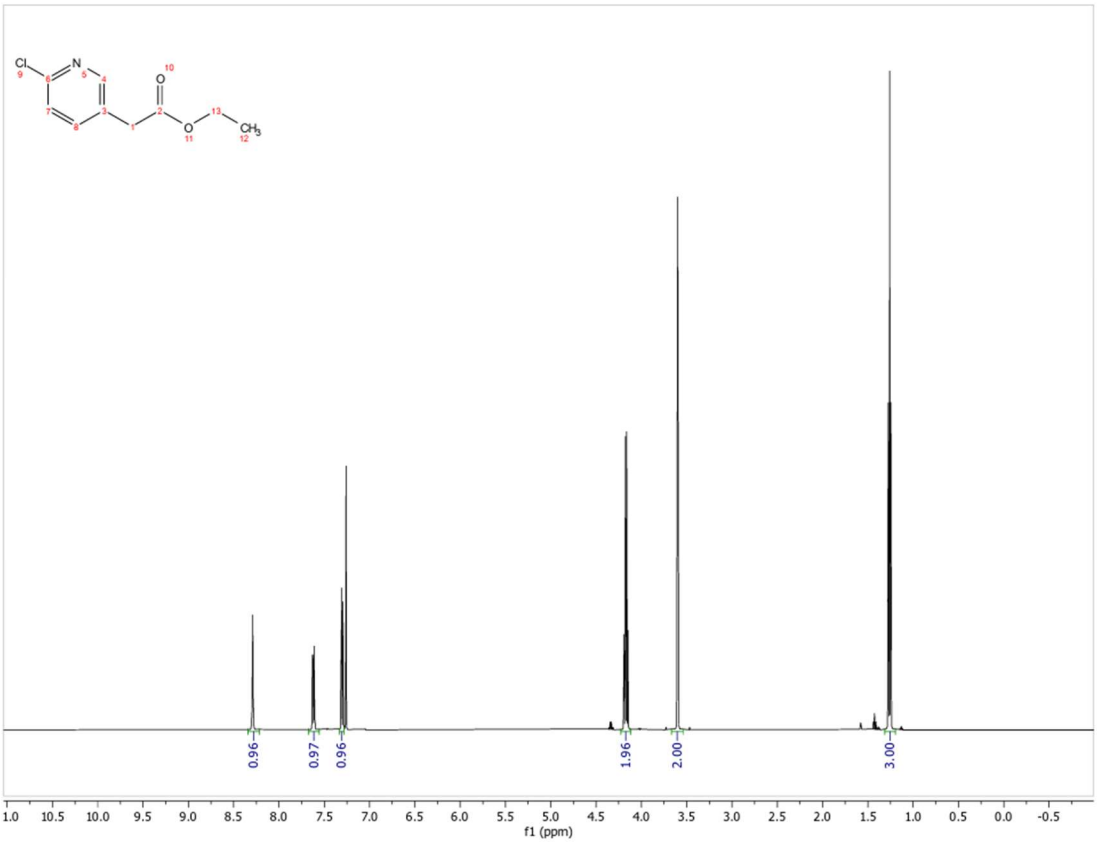
0.96
0.97
0.96
1.96
2.00
3.00
f1 (ppm)

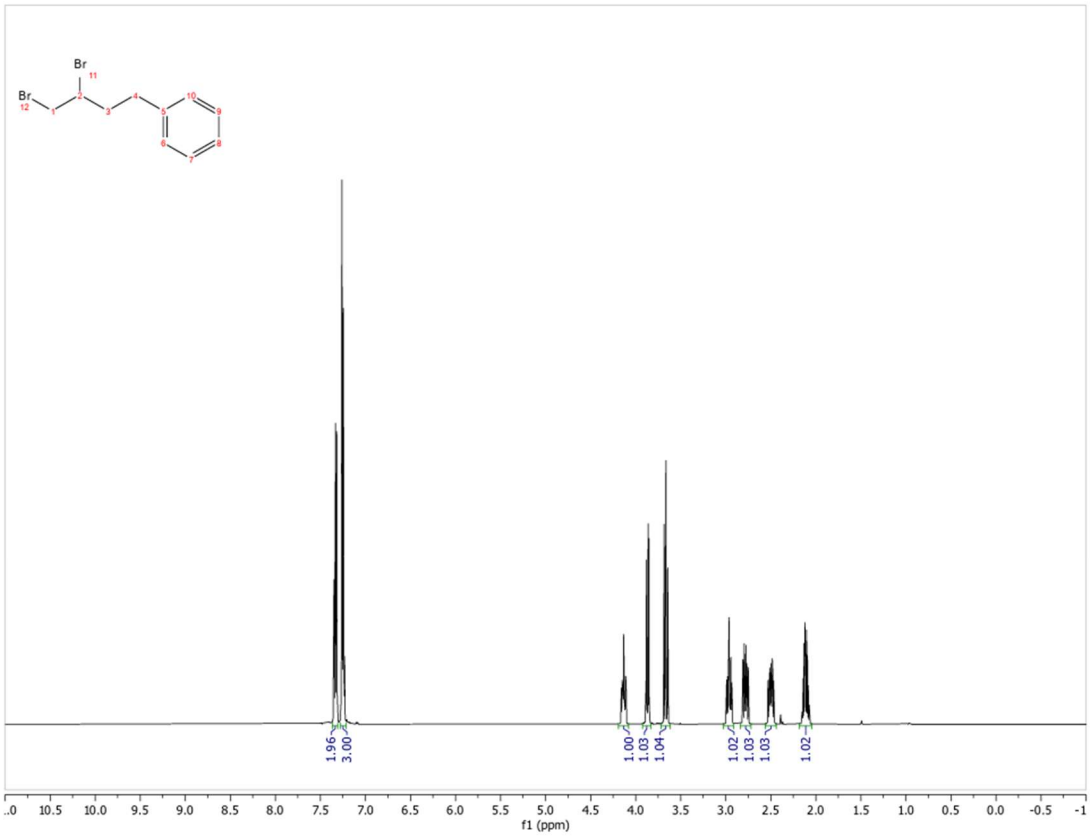
1.96
3.00
1.00
1.03
1.04
1.02
1.03
1.03
1.02
f1 (ppm)

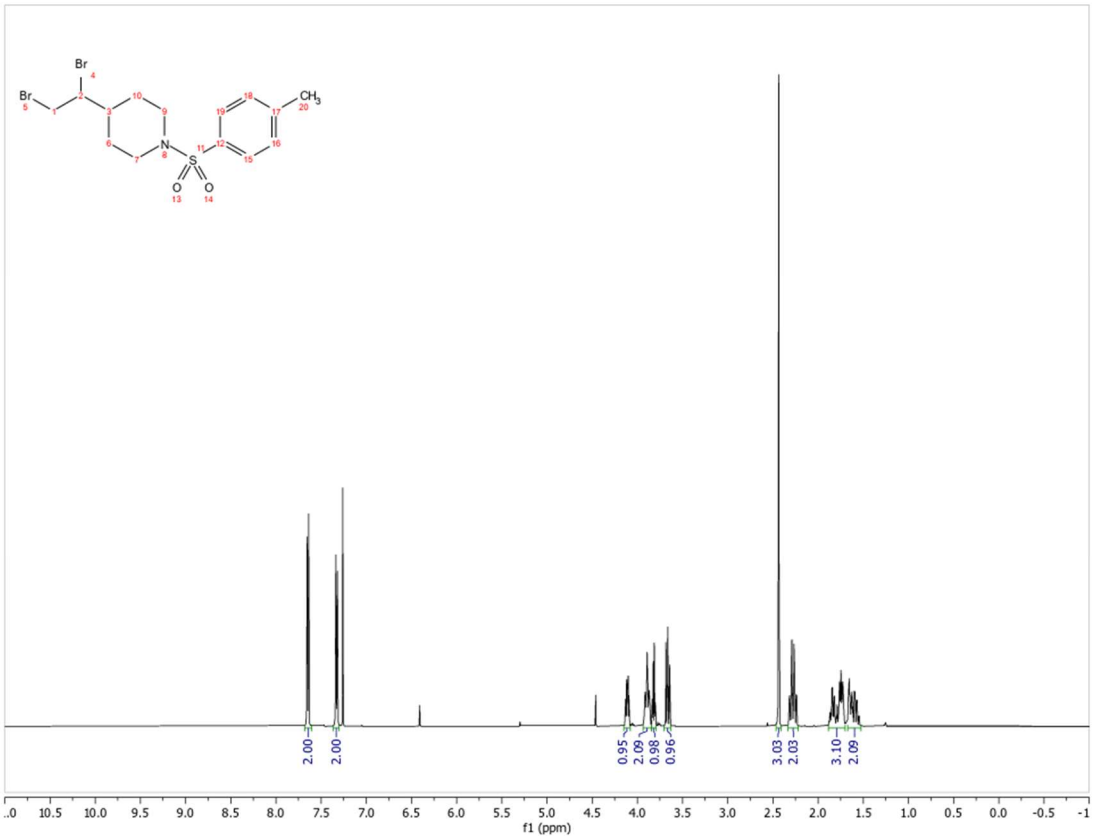
Br
Br
CH3
N
S
O
O
2.00
2.00
0.95
2.09
0.98
0.96
3.03
2.03
3.10
2.09
f1 (ppm)

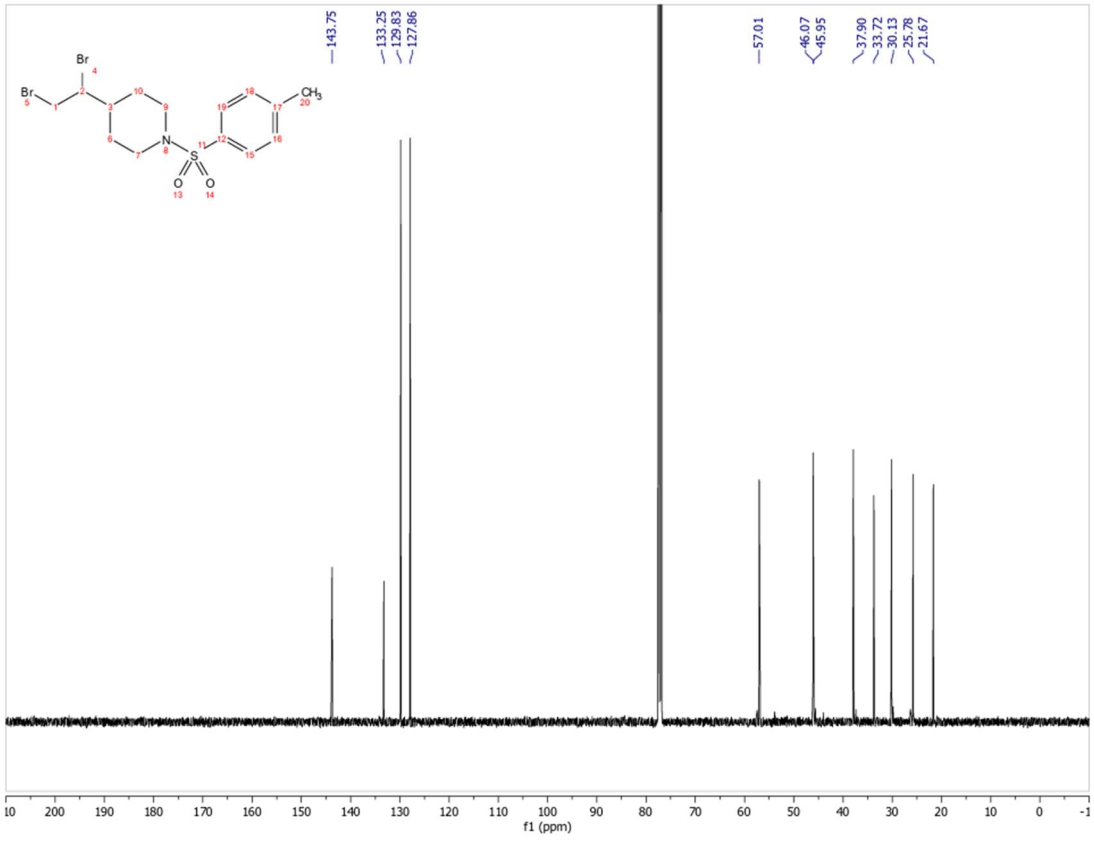
143.75
133.25
129.83
127.86
57.01
46.07
45.95
37.90
33.72
30.13
25.78
21.67
Br
Br
CH3
N
S
O
O
f1 (ppm)

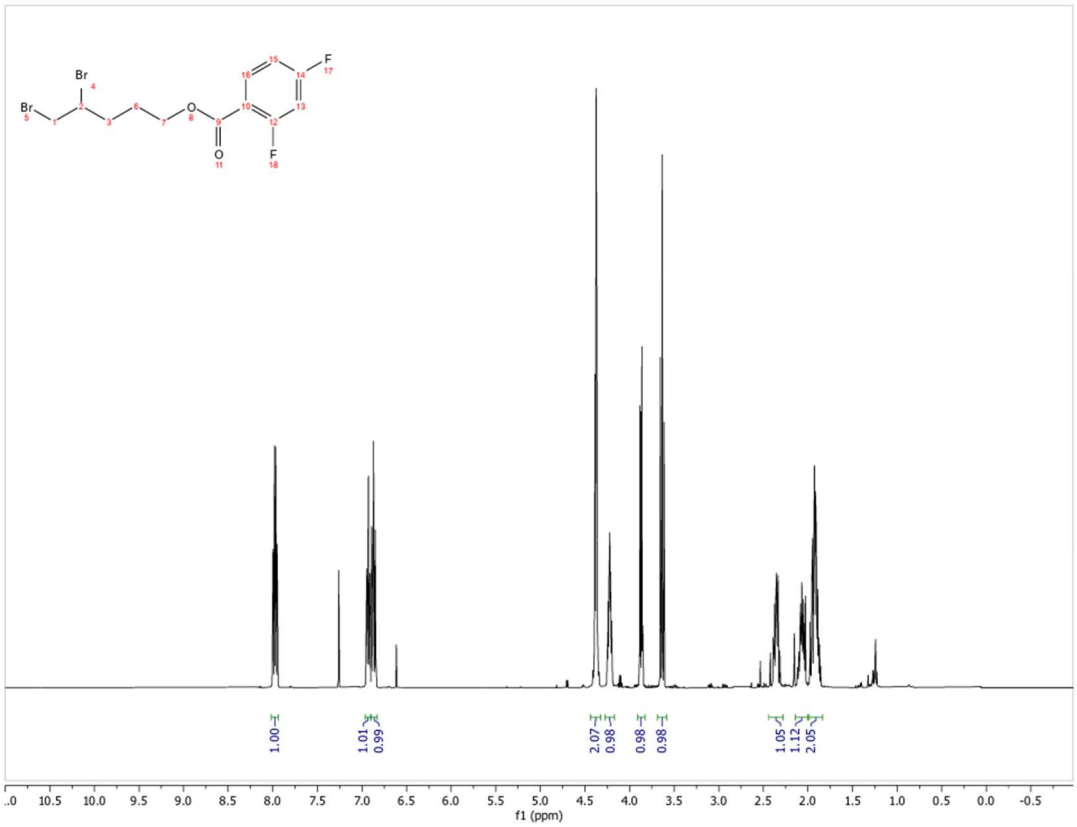
Br
F
O
F
1.00
1.01
0.99
2.07
0.98
0.98
0.98
1.05
1.12
2.05
f1 (ppm)

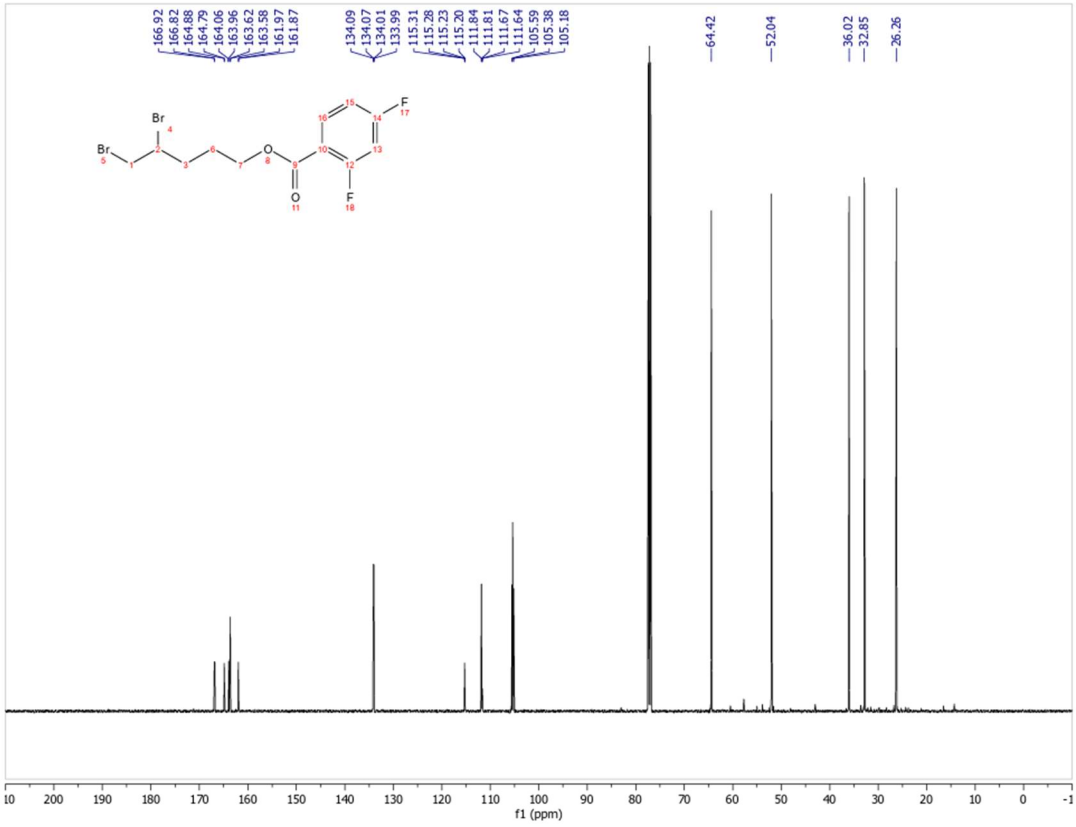
166.92
166.82
164.88
164.79
164.06
163.96
163.62
163.58
161.97
161.87
134.09
134.07
134.01
133.99
115.31
115.28
115.23
115.20
111.84
111.81
111.67
111.64
105.59
105.38
105.18
64.42
52.04
36.02
32.85
26.26
Br
F
O
F
f1 (ppm)

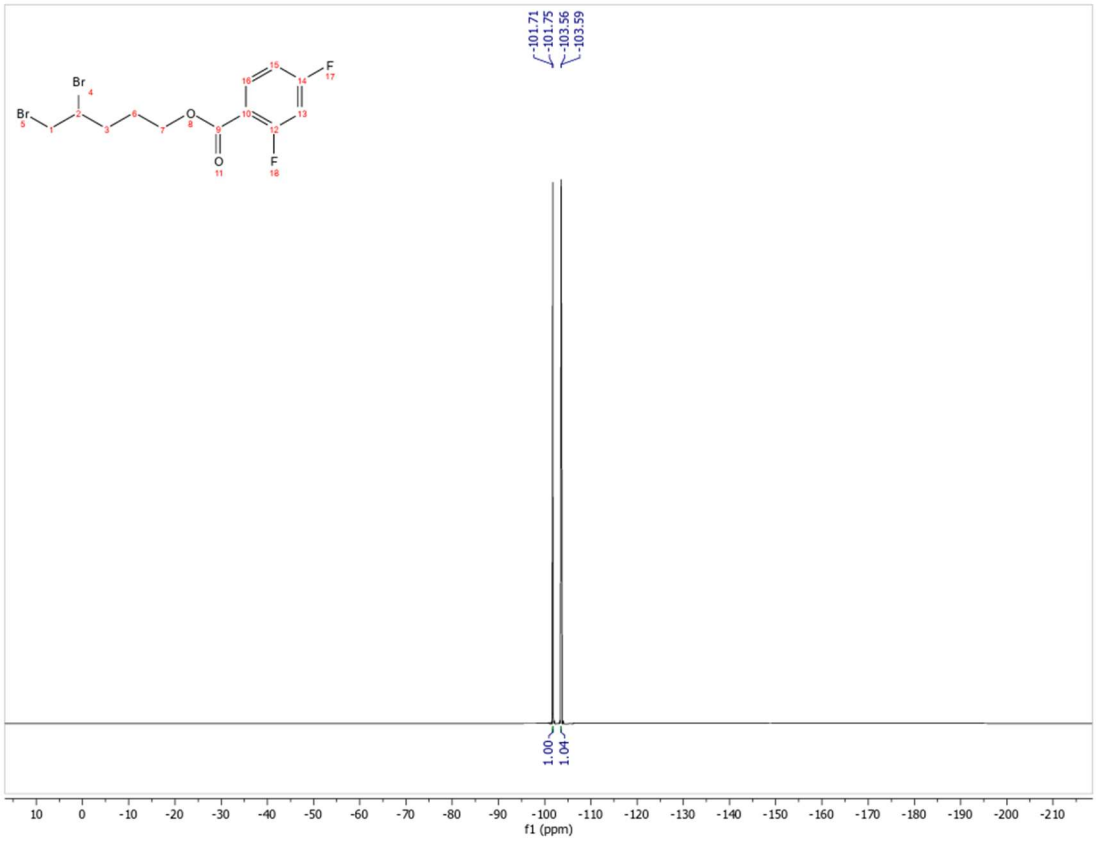
-101.71
-101.75
-103.56
-103.59
1.00
1.04
10 0 -10 -20 -30 -40 -50 -60 -70 -80 -90 -100 -110 -120 -130 -140 -150 -160 -170 -180 -190 -200 -210
f1 (ppm)

(blank space)

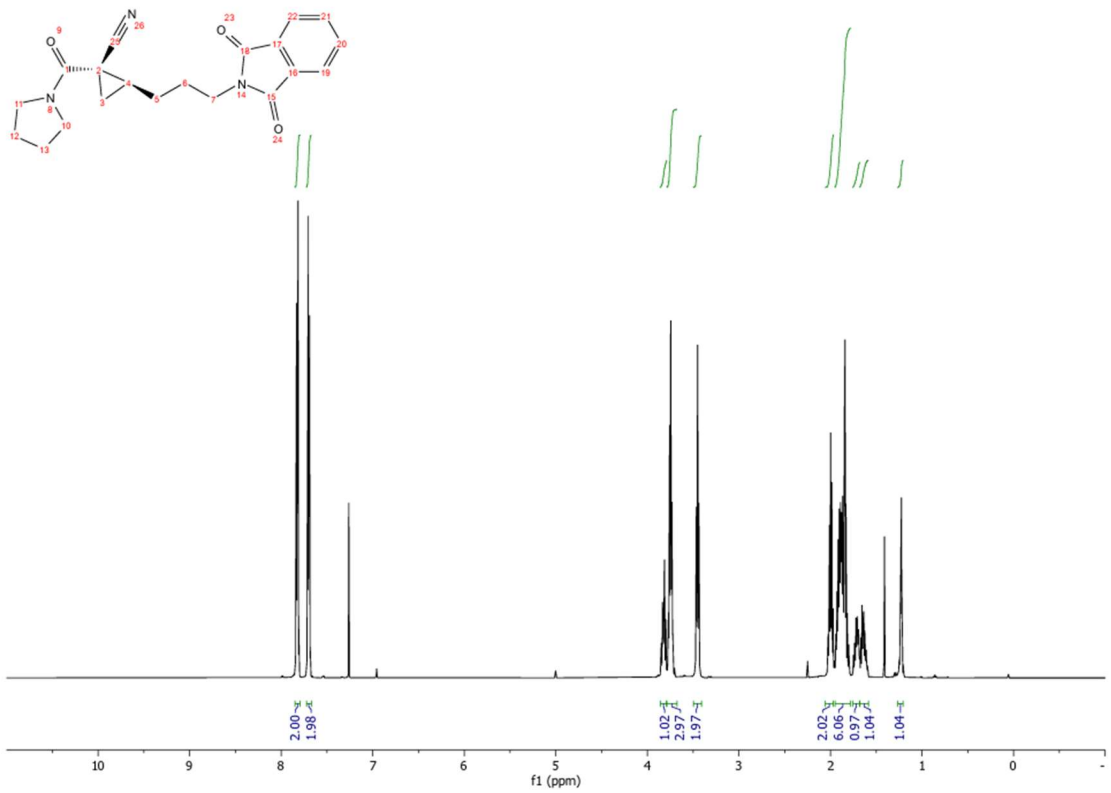
2.00
1.98
1.02
2.97
1.97
2.02
6.06
0.97
1.04
1.04
f1 (ppm)

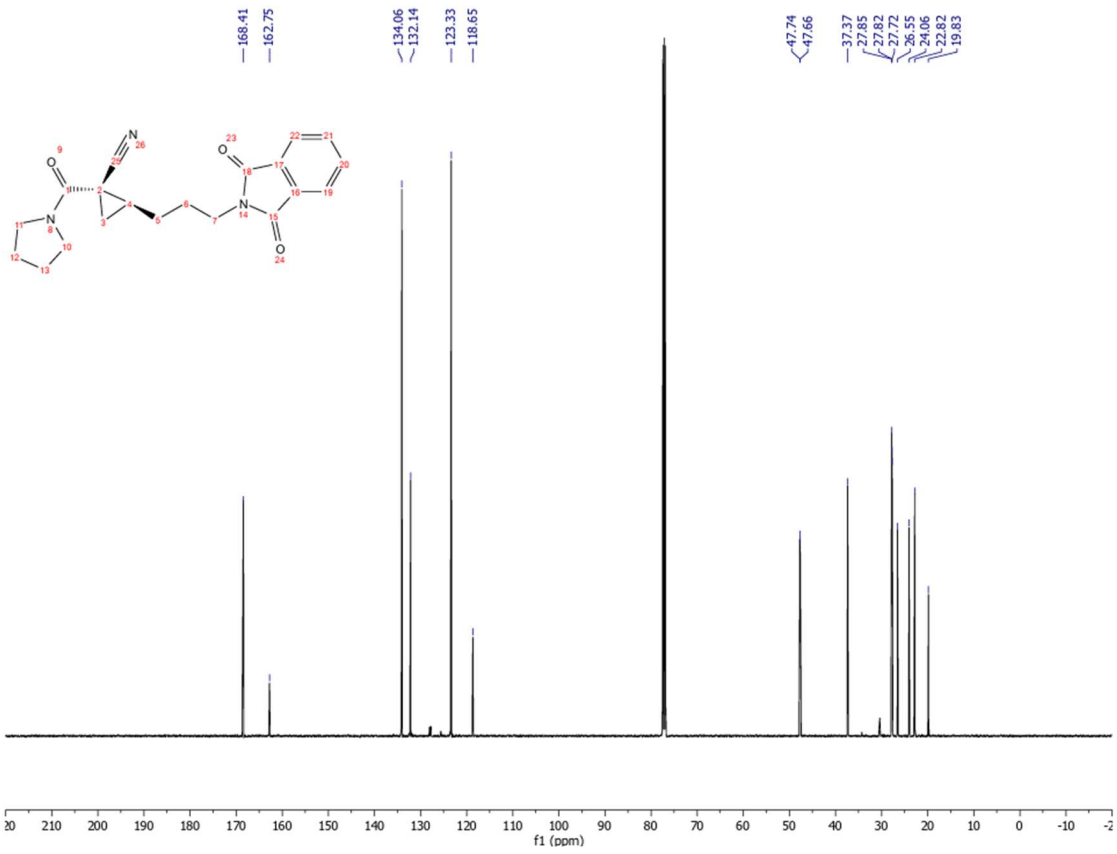
168.41
162.75
134.06
132.14
123.33
118.65
47.74
47.66
37.37
27.85
27.82
27.72
26.55
24.06
22.82
19.83
f1 (ppm)

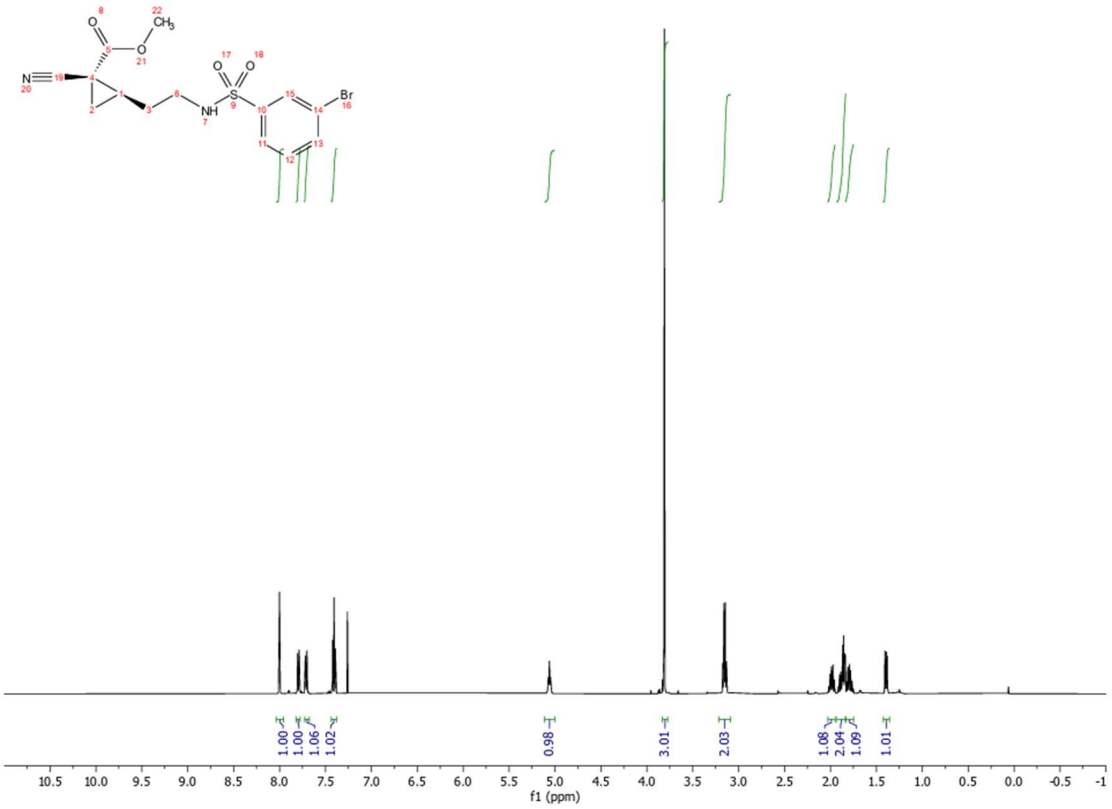
1.00
1.00
1.06
1.02
0.98
3.01
2.03
1.08
2.04
1.09
1.01
f1 (ppm)

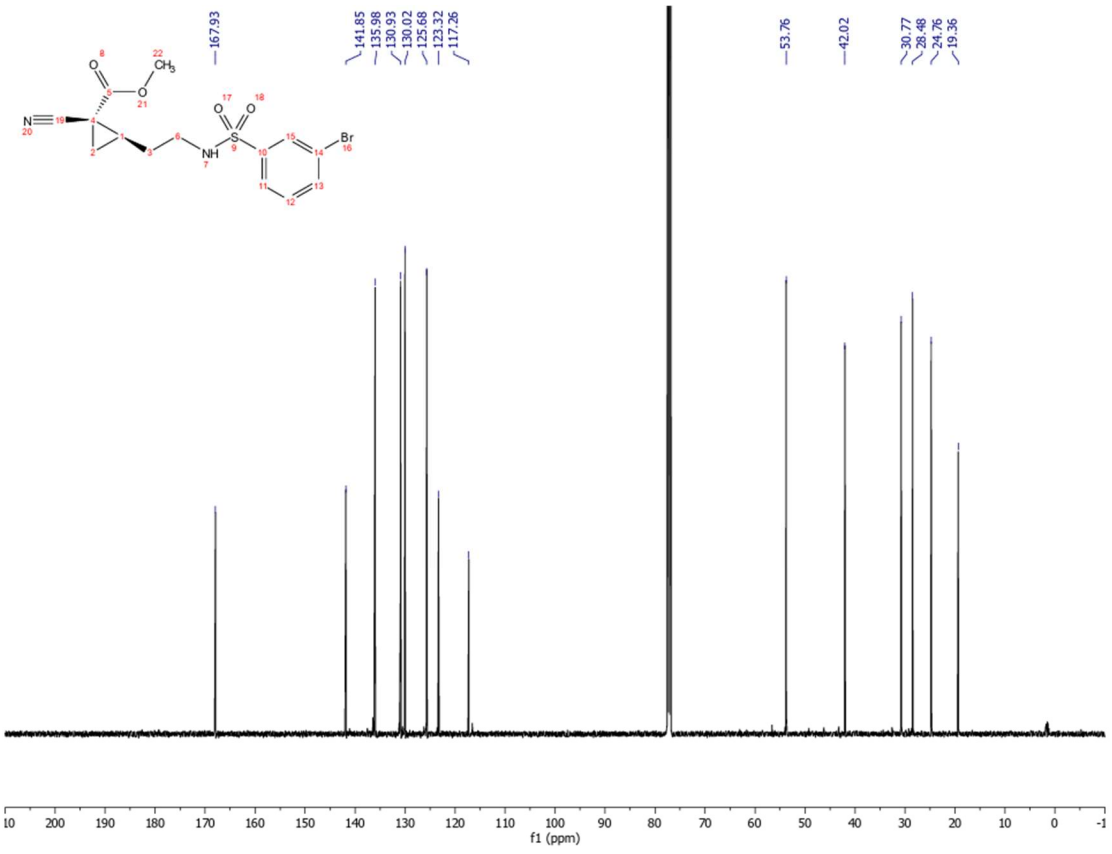
167.93
141.85
135.98
130.93
130.02
125.68
123.32
117.26
53.76
42.02
30.77
28.48
24.76
19.36
f1 (ppm)

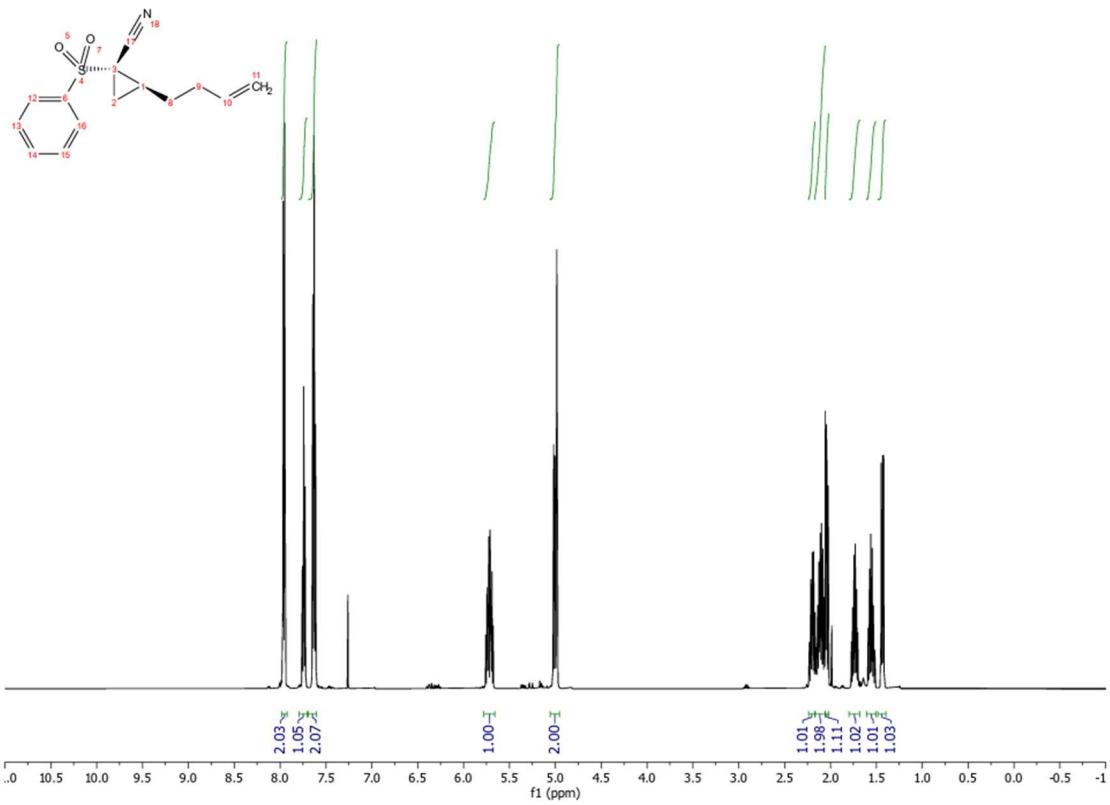
2.03
1.05
2.07
1.00
2.00
1.01
1.98
1.11
1.02
1.01
1.03
f1 (ppm)

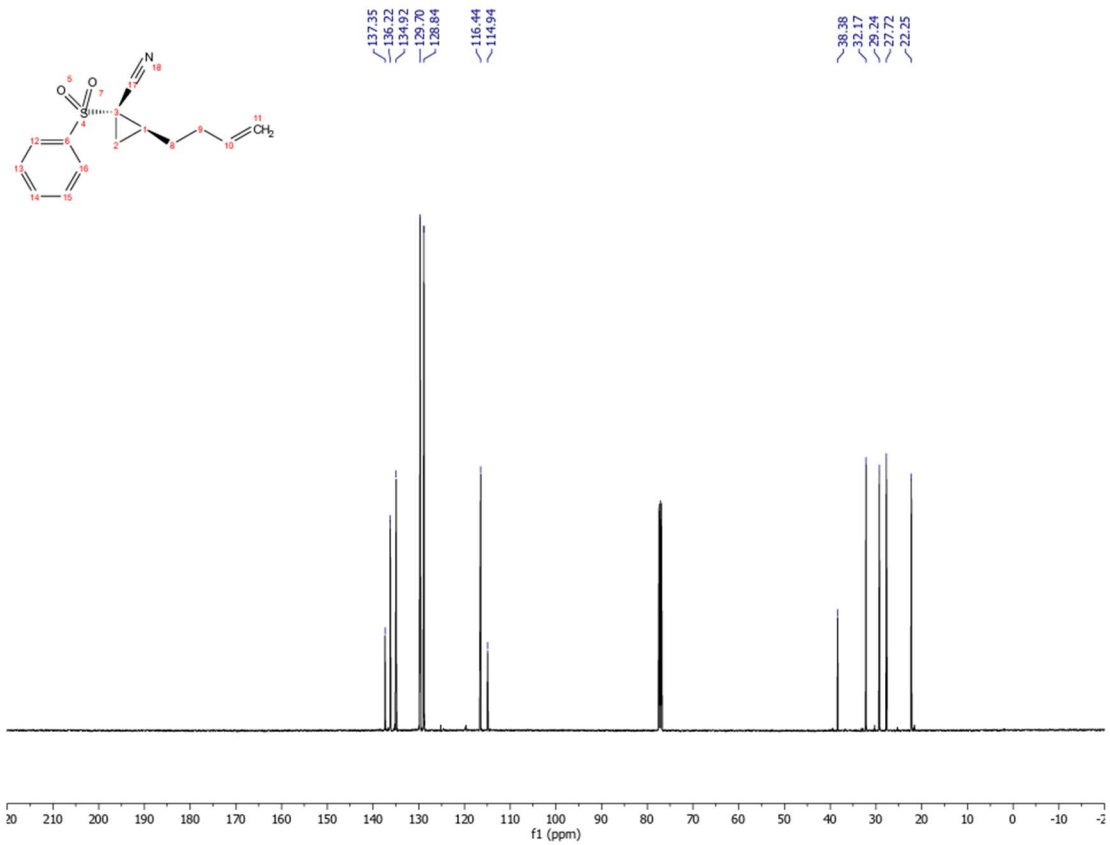
137.35
136.22
134.92
129.70
128.84
116.44
114.94
38.38
32.17
29.24
27.72
22.25
f1 (ppm)

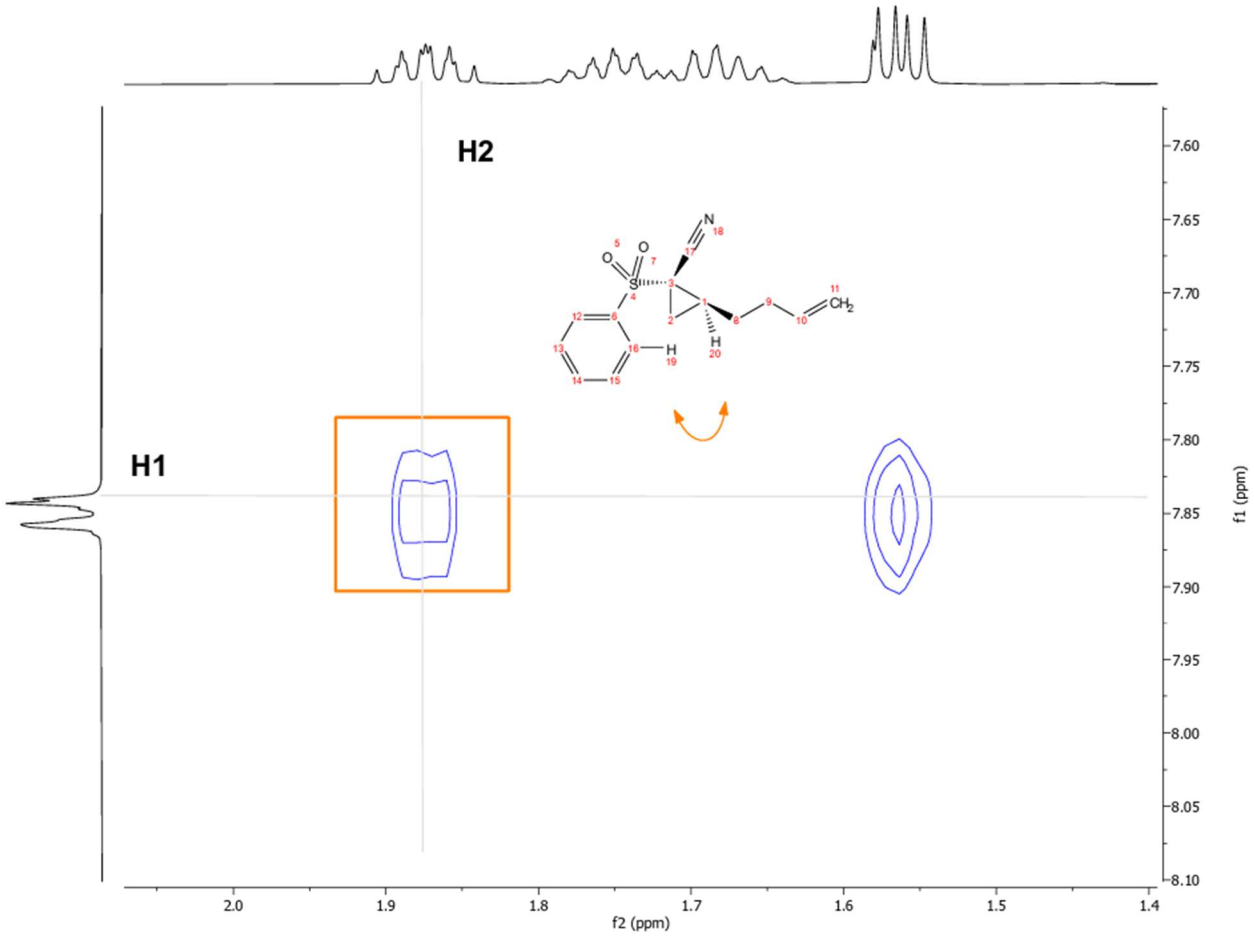
H2
H1
f2 (ppm)
f1 (ppm)
2.0
1.9
1.8
1.7
1.6
1.5
1.4
7.60
7.65
7.70
7.75
7.80
7.85
7.90
7.95
8.00
8.05
8.10

(blank space)

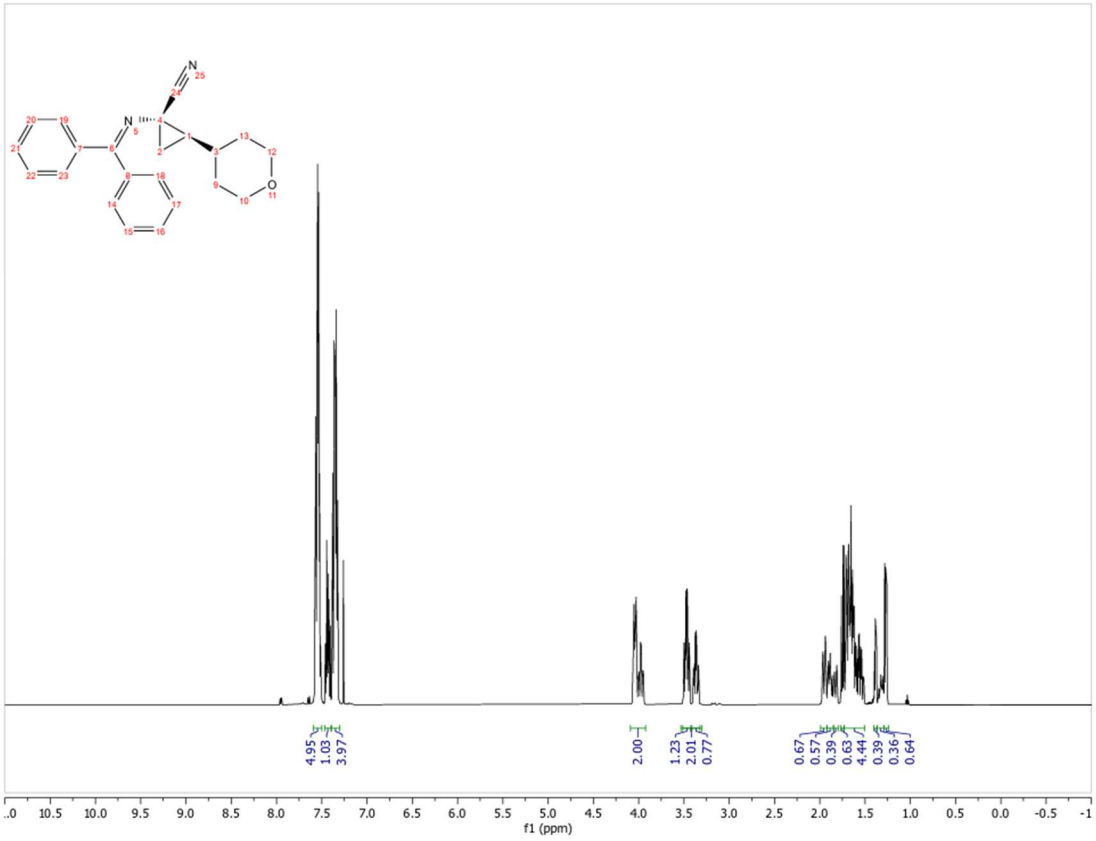
4.95
1.03
3.97
2.00
1.23
2.01
0.77
0.67
0.57
0.39
0.63
4.44
0.39
0.36
0.64
f1 (ppm)

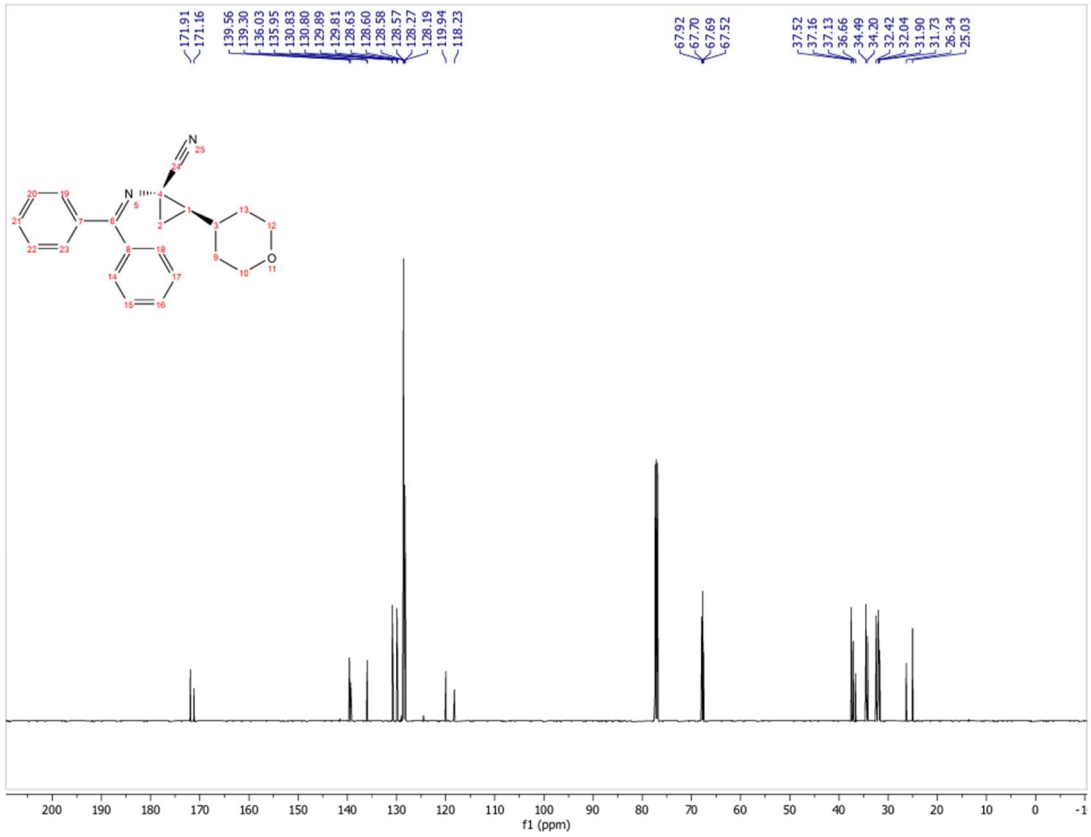
171.91
171.16
139.56
139.30
136.03
135.95
130.83
130.80
129.89
129.81
128.63
128.60
128.58
128.57
128.27
128.19
119.94
118.23
67.92
67.70
67.69
67.52
37.52
37.16
37.13
36.66
34.49
34.20
32.42
32.04
31.90
31.73
26.34
25.03
f1 (ppm)

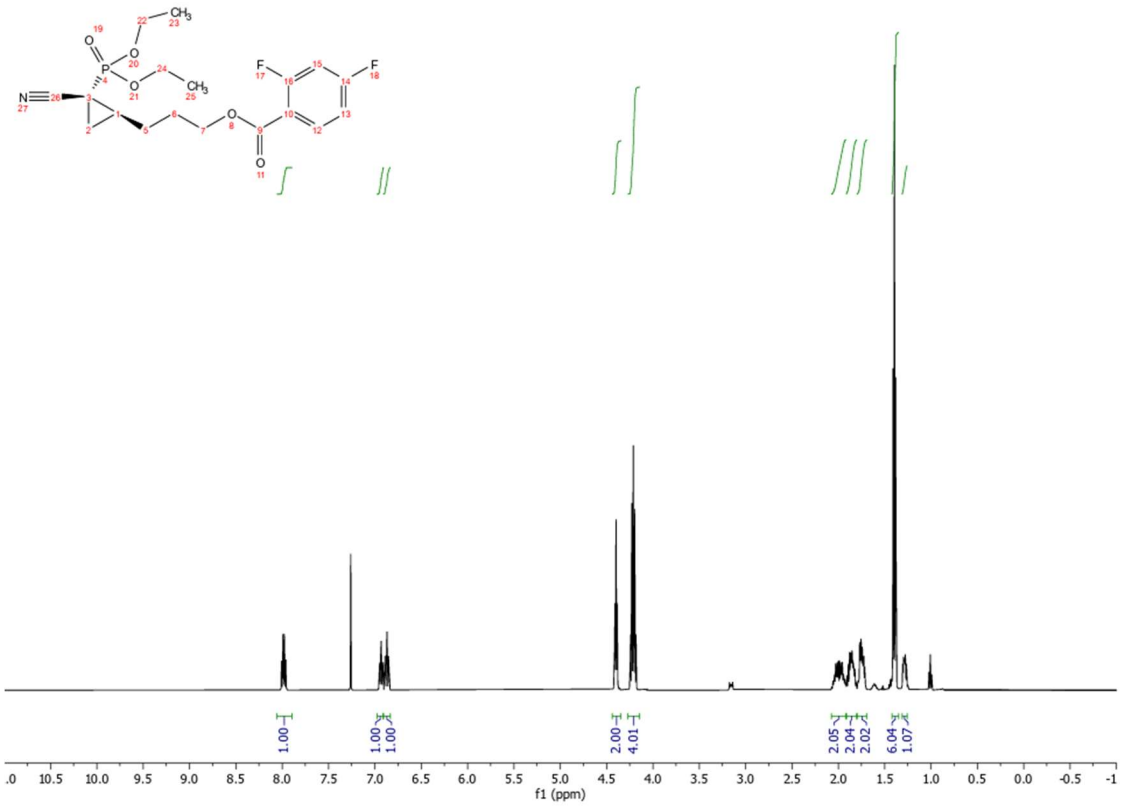
1.00
1.00
1.00
2.00
4.01
2.05
2.04
2.02
6.04
1.07
f1 (ppm)

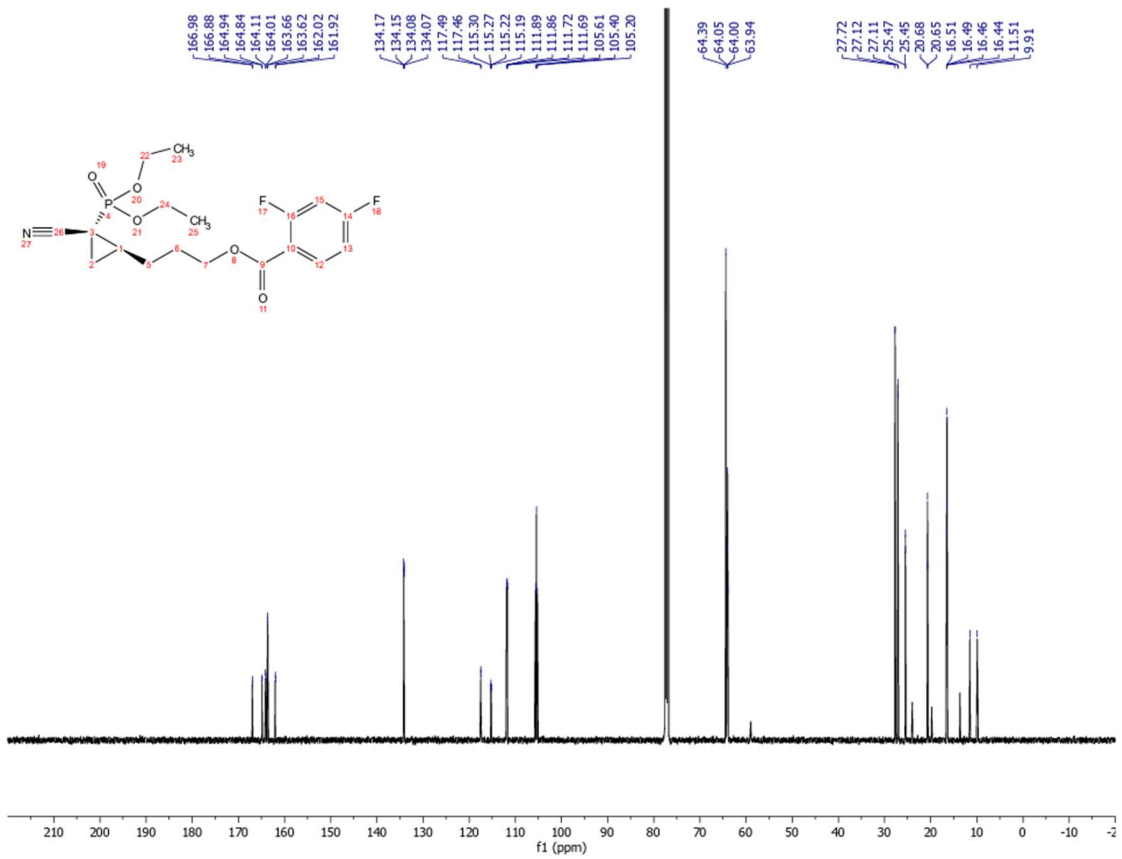
166.98
166.88
164.94
164.84
164.11
164.01
163.66
163.62
162.02
161.92
134.17
134.15
134.08
134.07
117.49
117.46
115.30
115.27
115.22
115.19
111.89
111.86
111.72
111.69
105.61
105.40
105.20
64.39
64.05
64.00
63.94
27.72
27.12
27.11
25.47
25.45
20.68
20.65
16.51
16.49
16.46
16.44
11.51
9.91
f1 (ppm)

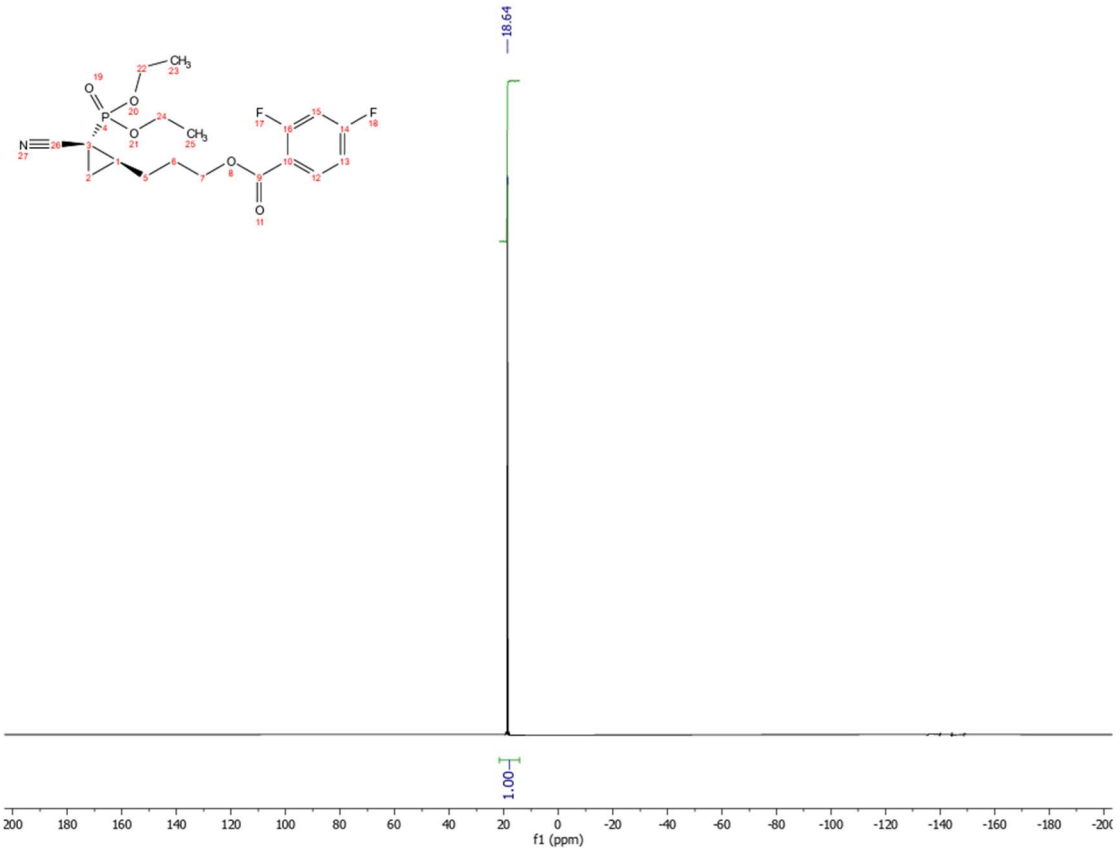
18.64
1.00
f1 (ppm)

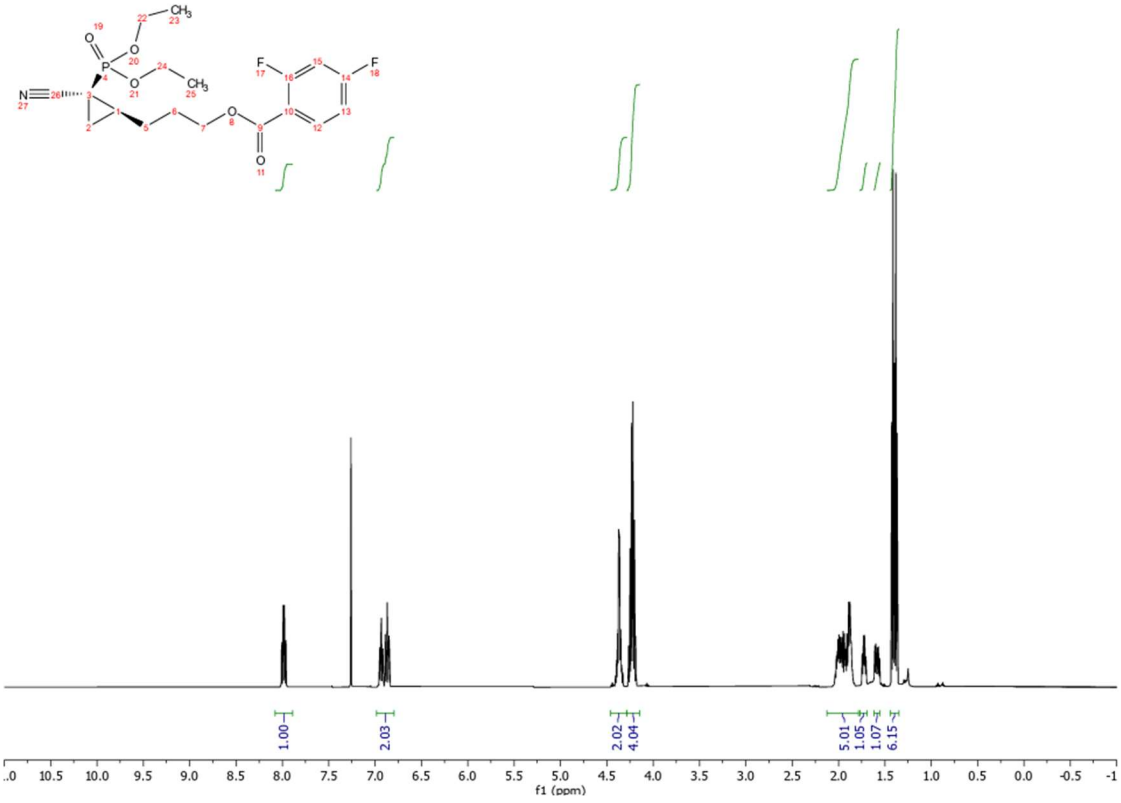
1.00
2.03
2.02
4.04
5.01
1.05
1.07
6.15
f1 (ppm)

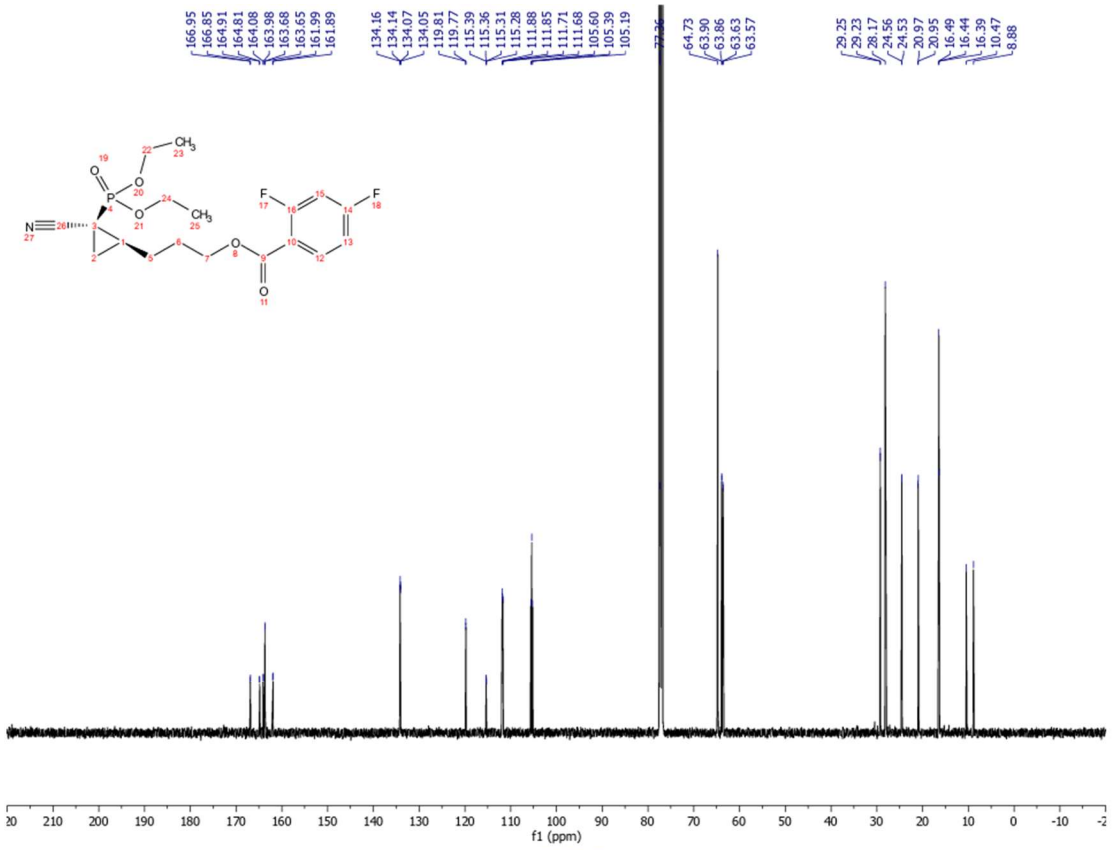
166.95
166.85
164.91
164.81
164.08
163.98
163.68
163.65
161.99
161.89
134.16
134.14
134.07
134.05
119.81
119.77
115.39
115.36
115.31
115.28
111.88
111.85
111.71
111.68
105.60
105.39
105.19
77.36
64.73
63.90
63.86
63.63
63.57
29.25
29.23
28.17
24.56
24.53
20.97
20.95
16.49
16.44
16.39
10.47
8.88
f1 (ppm)

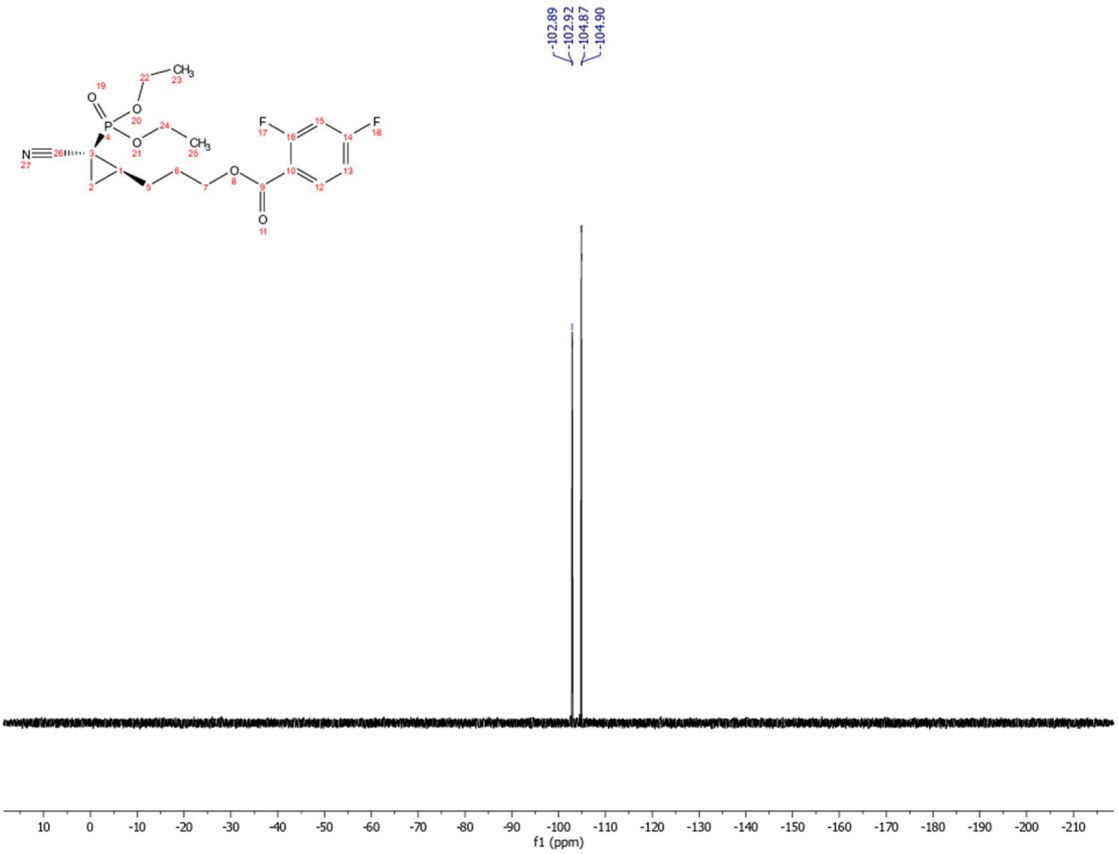
-102.89
-102.92
-104.87
-104.90
f1 (ppm)

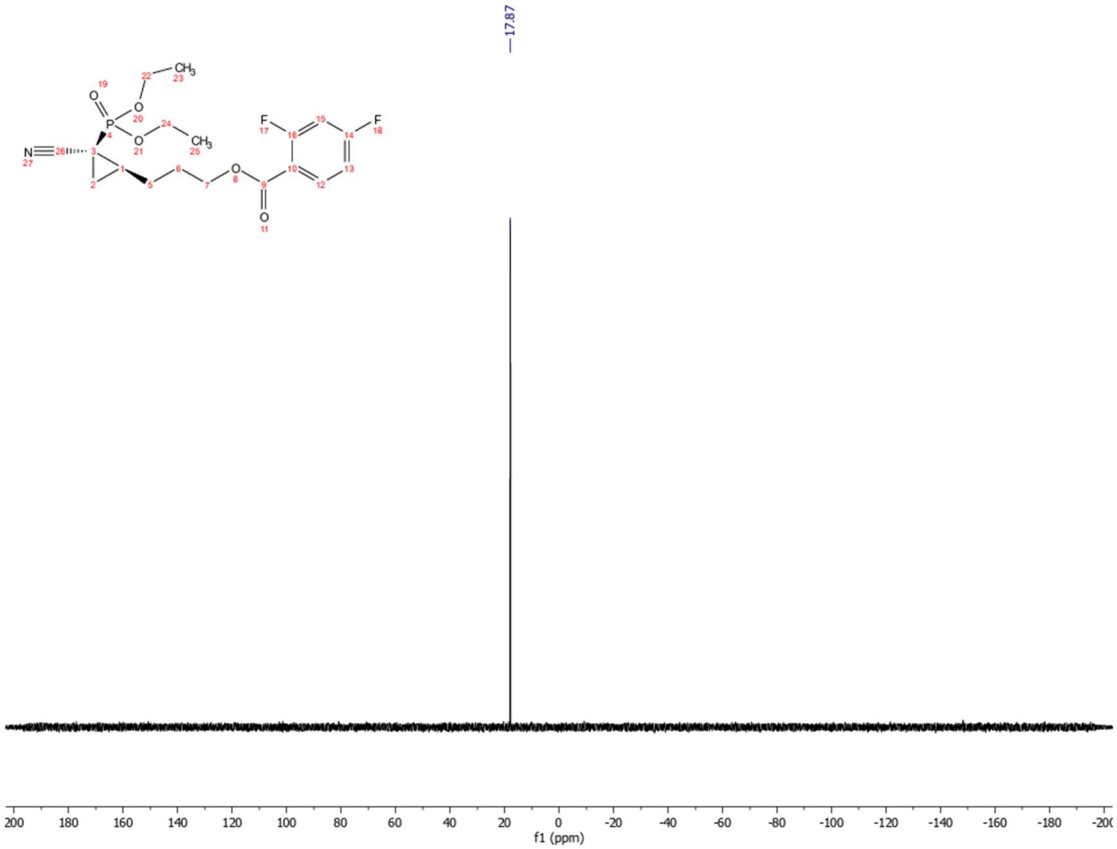
17.87
200
180
160
140
120
100
80
60
40
20
0
-20
-40
-60
-80
-100
-120
-140
-160
-180
f1 (ppm)

(blank space)

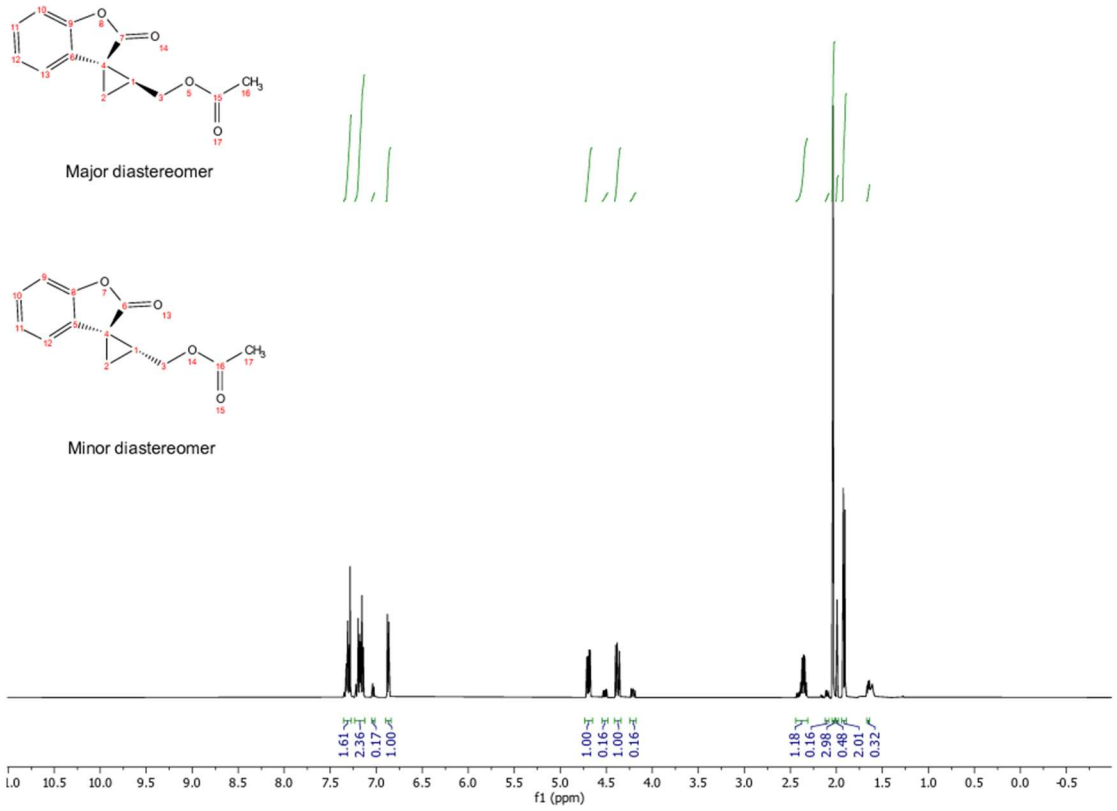
Major diastereomer
Minor diastereomer
1.61
2.36
0.17
1.00
1.00
0.16
1.00
0.16
1.18
0.16
2.98
0.48
2.01
0.32
f1 (ppm)

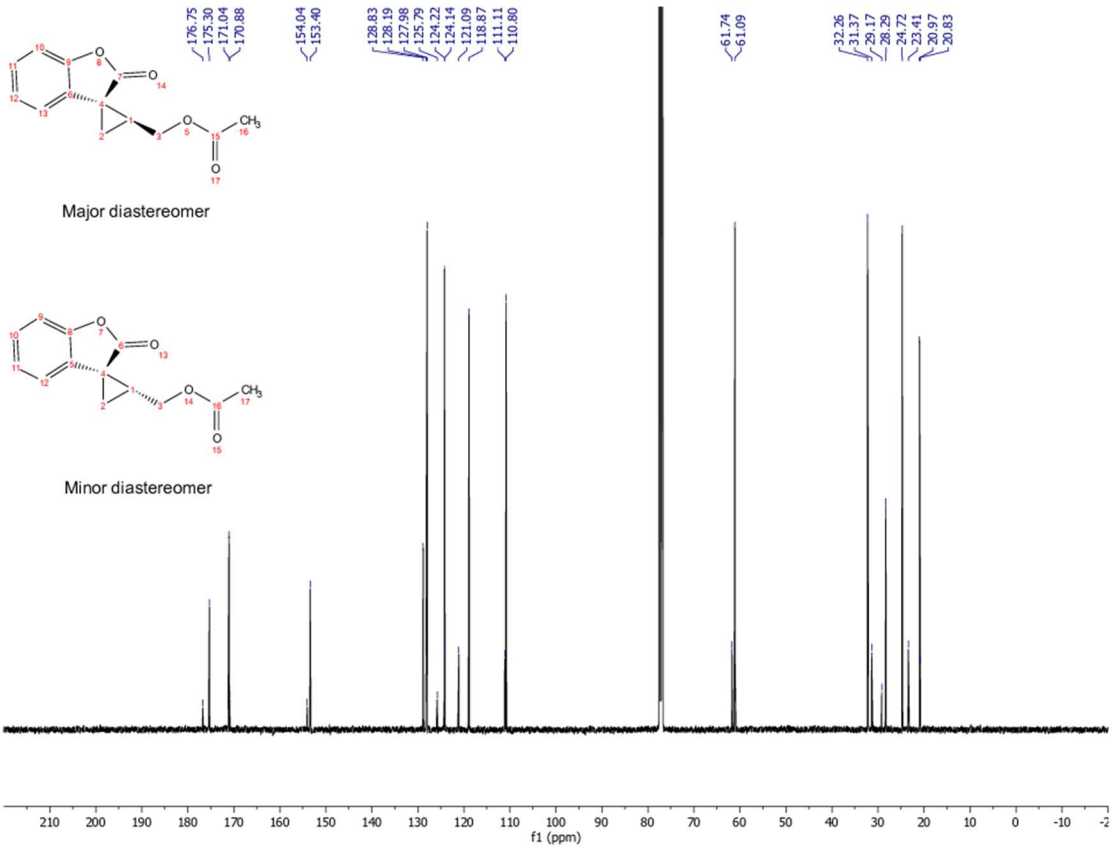
176.75
175.30
171.04
170.88
154.04
153.40
128.83
128.19
127.98
125.79
124.22
124.14
121.09
118.87
111.11
110.80
61.74
61.09
32.26
31.37
29.17
28.29
24.72
23.41
20.97
20.83
Major diastereomer
Minor diastereomer
f1 (ppm)

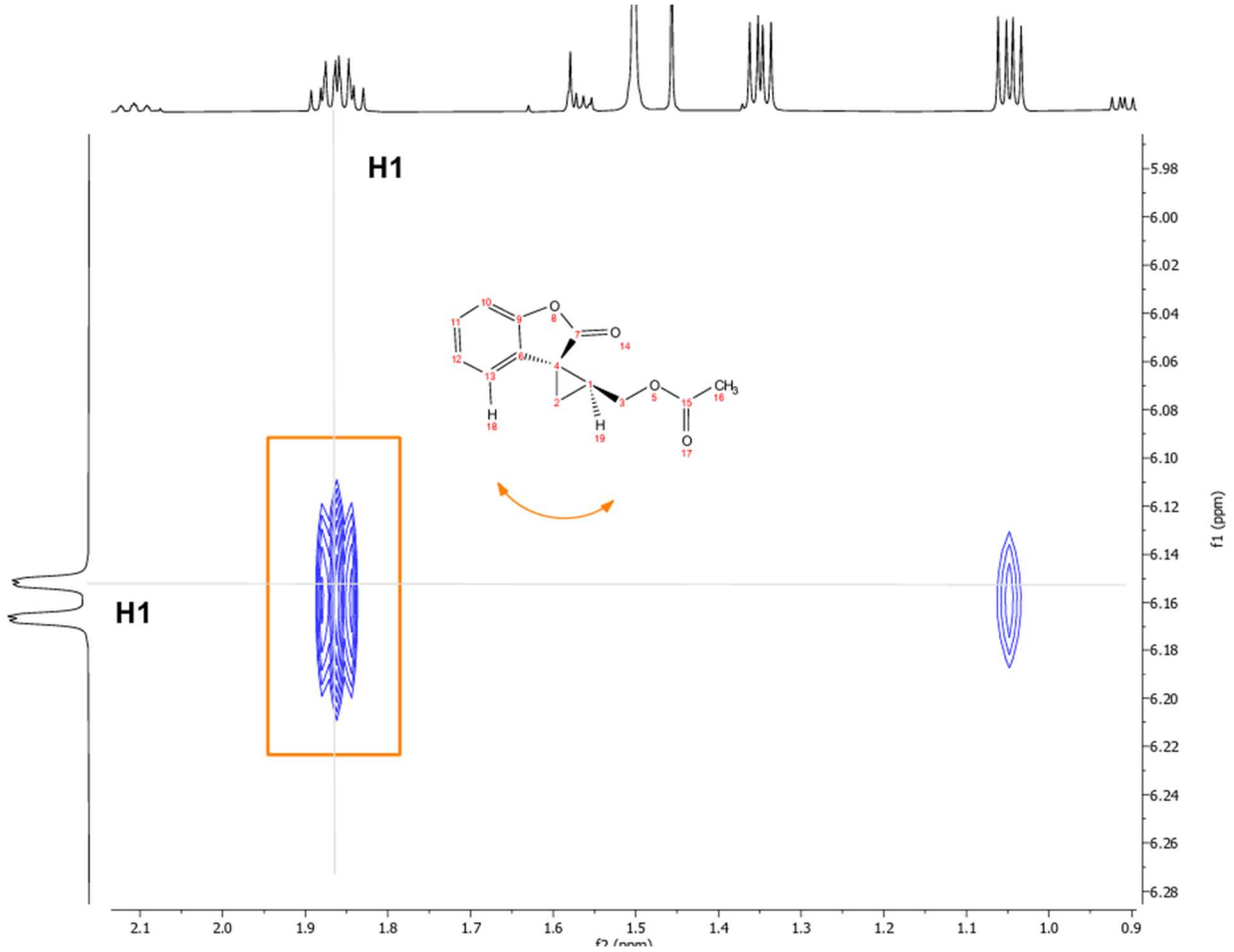
H1
H1
f1 (ppm)
5.98
6.00
6.02
6.04
6.06
6.08
6.10
6.12
6.14
6.16
6.18
6.20
6.22
6.24
6.26
6.28
2.1
2.0
1.9
1.8
1.7
1.6
1.5
1.4
1.3
1.2
1.1
1.0
0.9

(blank space)

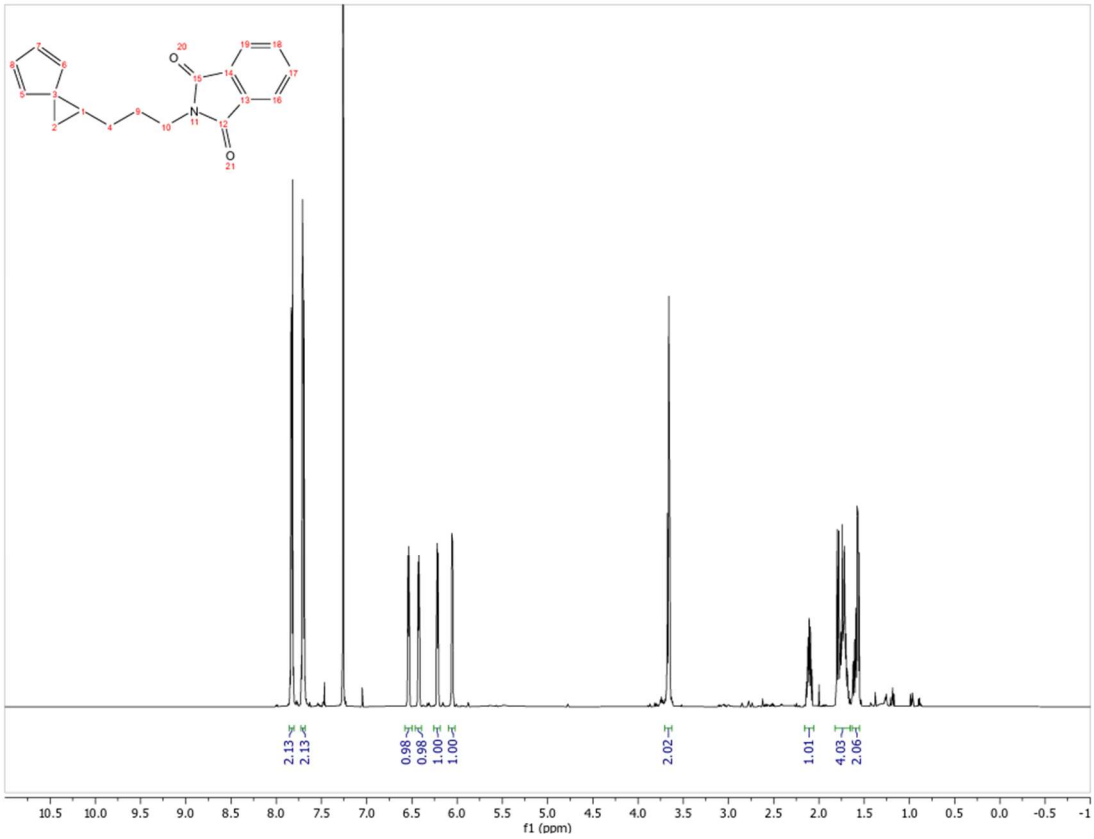
2.13
2.13
0.98
0.98
1.00
1.00
2.02
1.01
4.03
2.06
f1 (ppm)

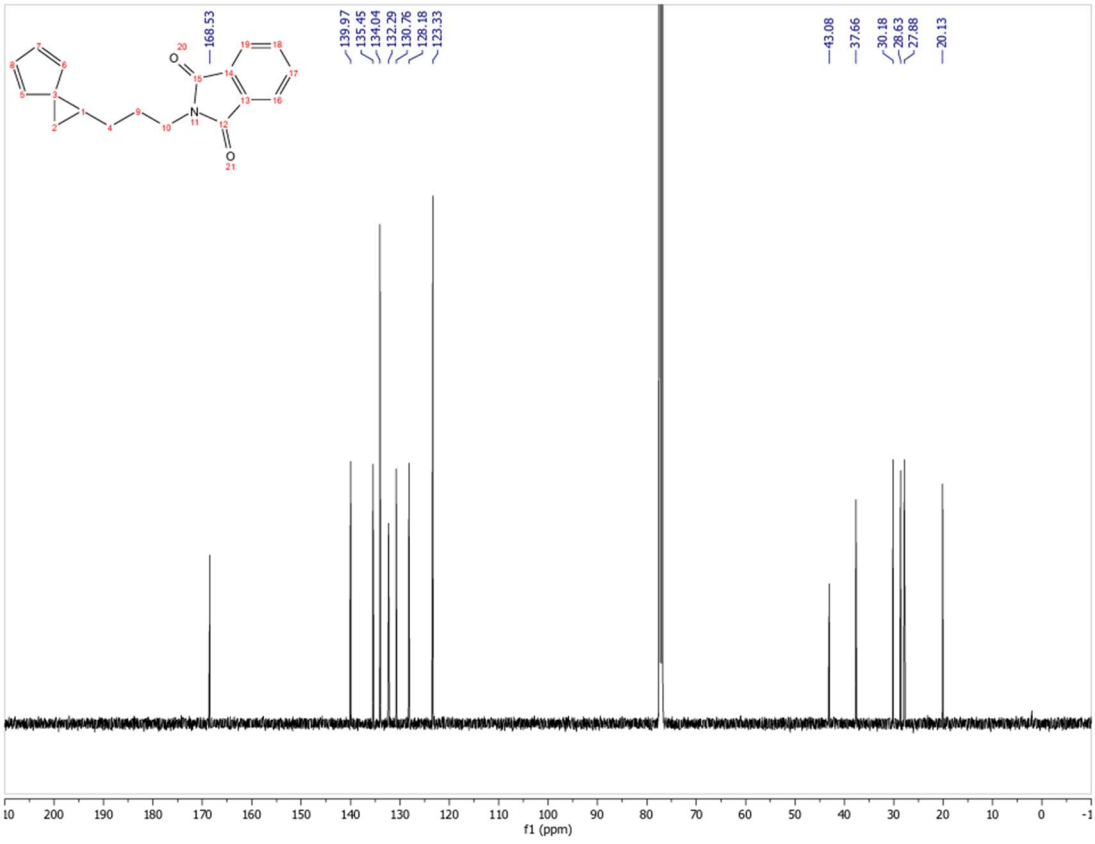
168.53
139.97
135.45
134.04
132.29
130.76
128.18
123.33
43.08
37.66
30.18
28.63
27.88
20.13
f1 (ppm)

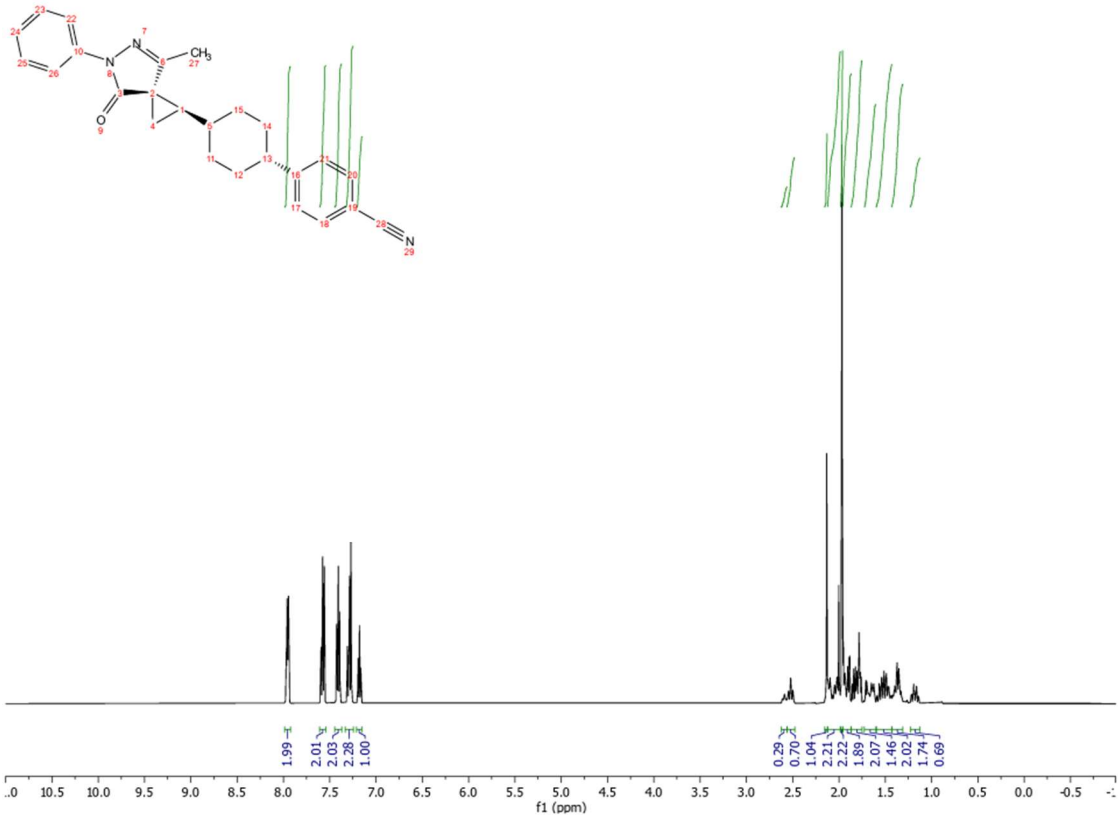
1.99
2.01
2.03
2.28
1.00
0.29
0.70
1.04
2.21
2.22
1.89
2.07
1.46
2.02
1.74
0.69
f1 (ppm)

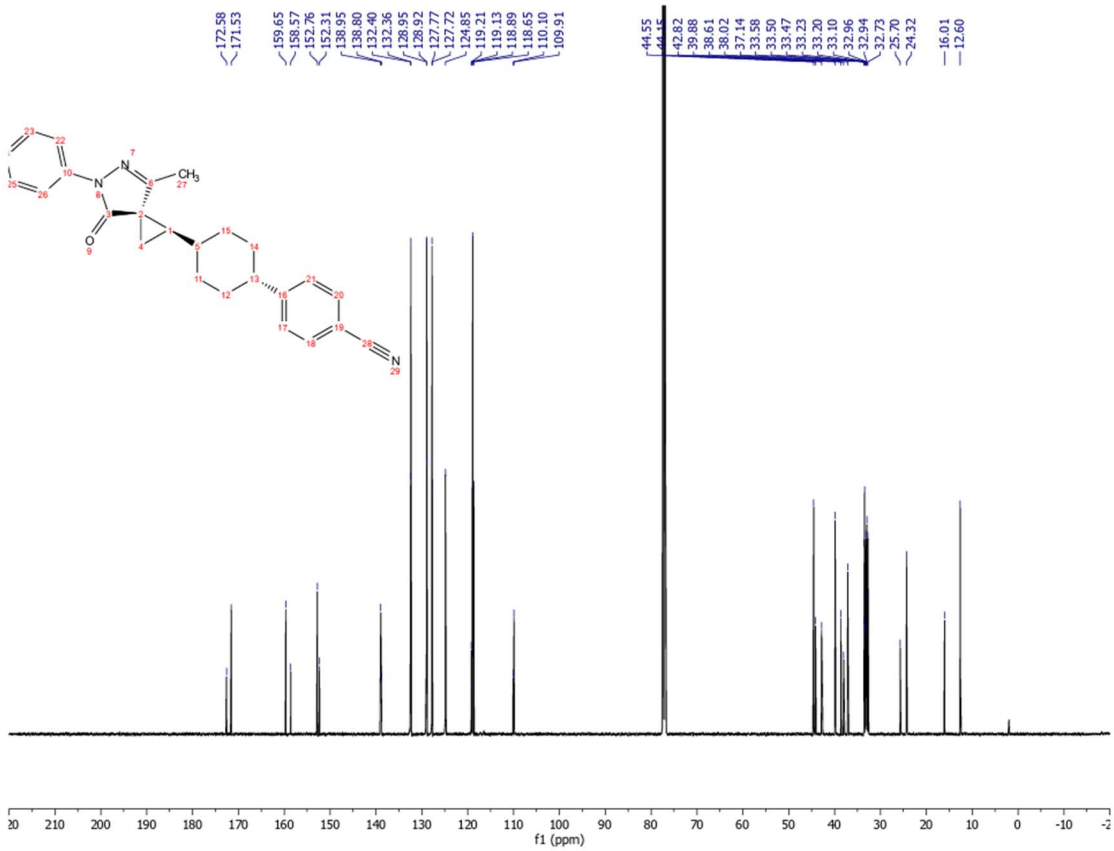
172.58
171.53
159.65
158.57
152.76
152.31
138.95
138.80
132.40
132.36
128.95
128.92
127.77
127.72
124.85
119.21
119.13
118.89
118.65
110.10
109.91
44.55
44.15
42.82
39.88
38.61
38.02
37.14
33.58
33.50
33.47
33.23
33.20
33.10
32.96
32.94
32.73
25.70
24.32
16.01
12.60
f1 (ppm)

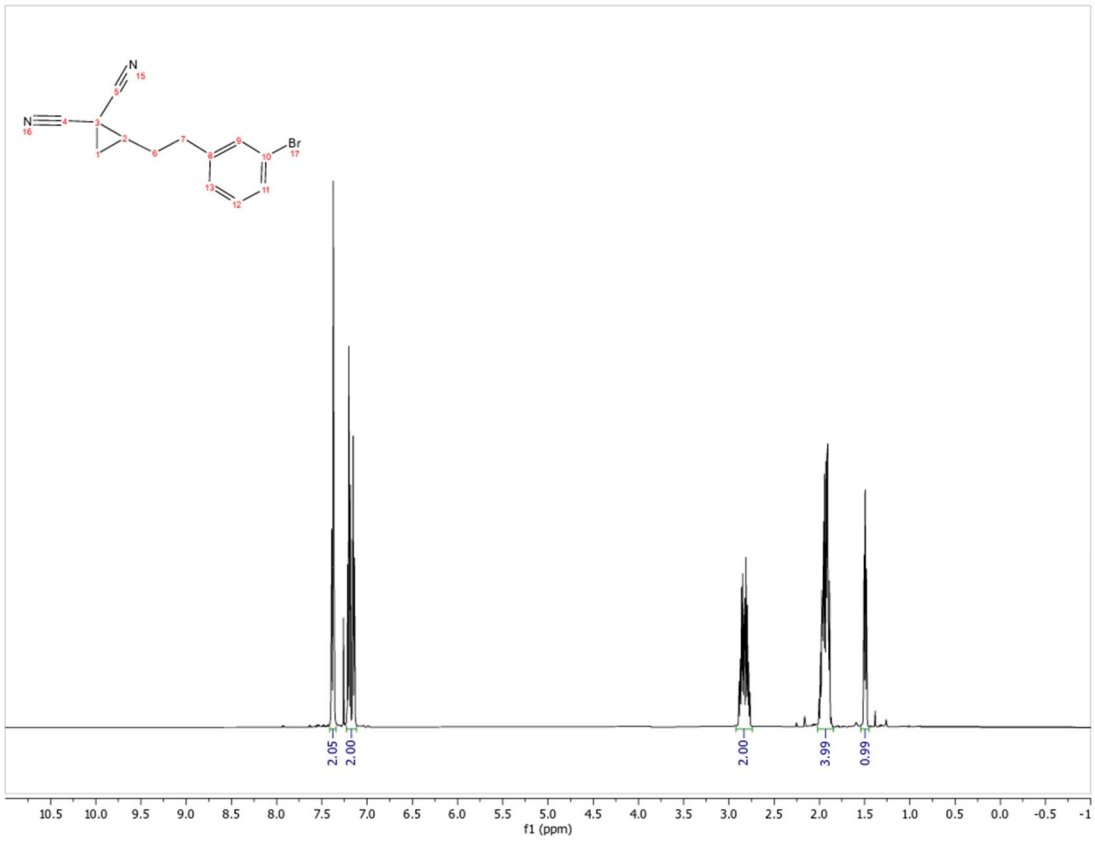
2.05
2.00
2.00
3.99
0.99
f1 (ppm)

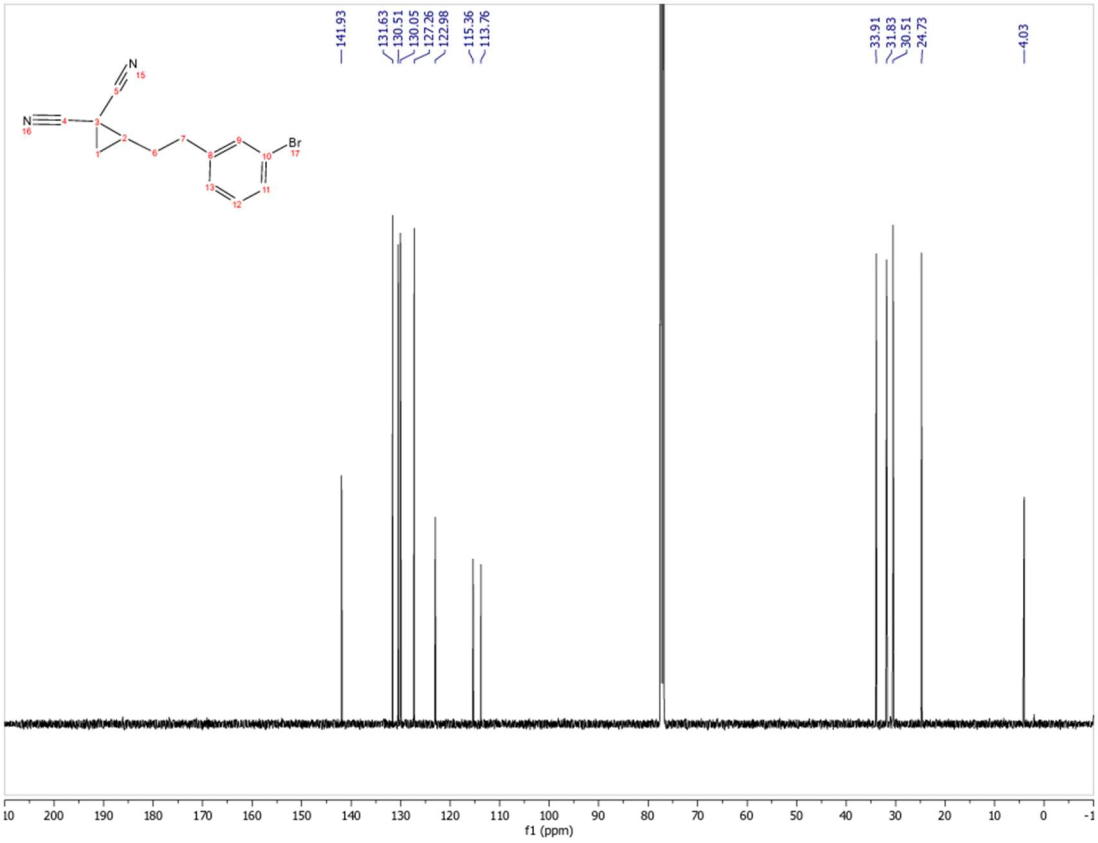
141.93
131.63
130.51
130.05
127.26
122.98
115.36
113.76
33.91
31.83
30.51
24.73
4.03
f1 (ppm)

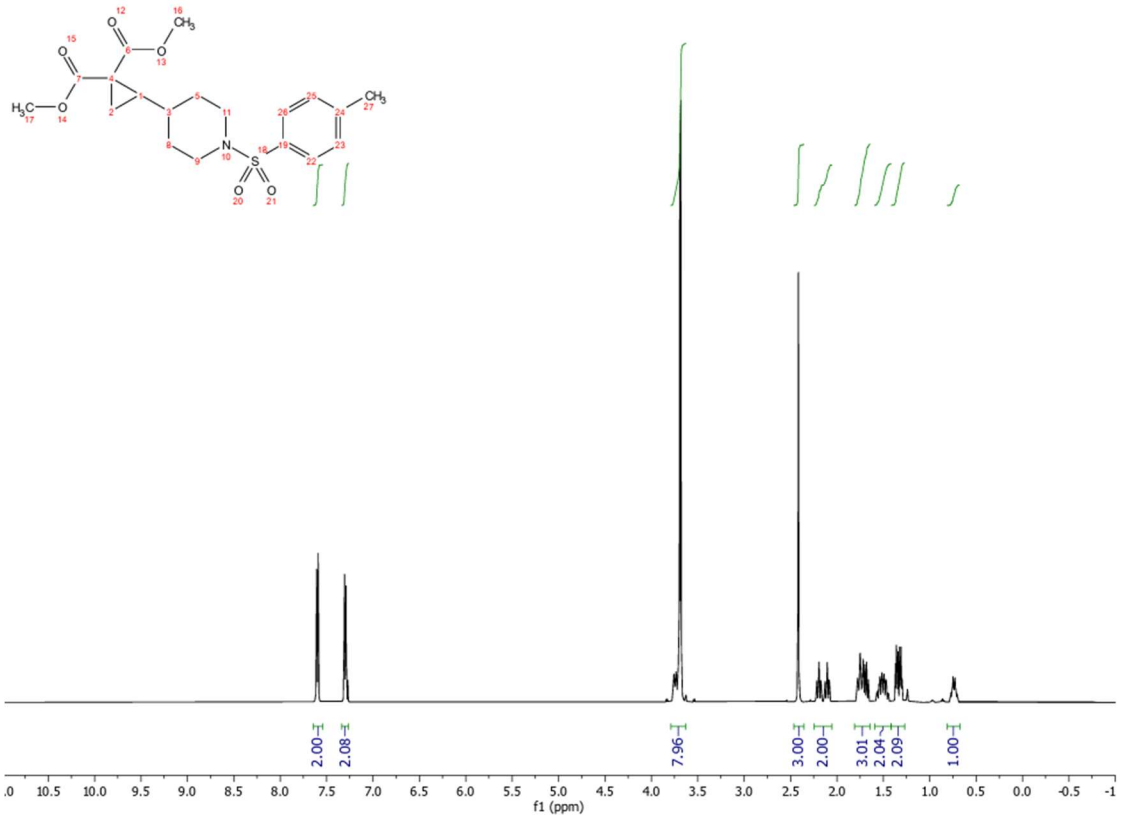
2.00
2.08
7.96
3.00
2.00
3.01
2.04
2.09
1.00
f1 (ppm)

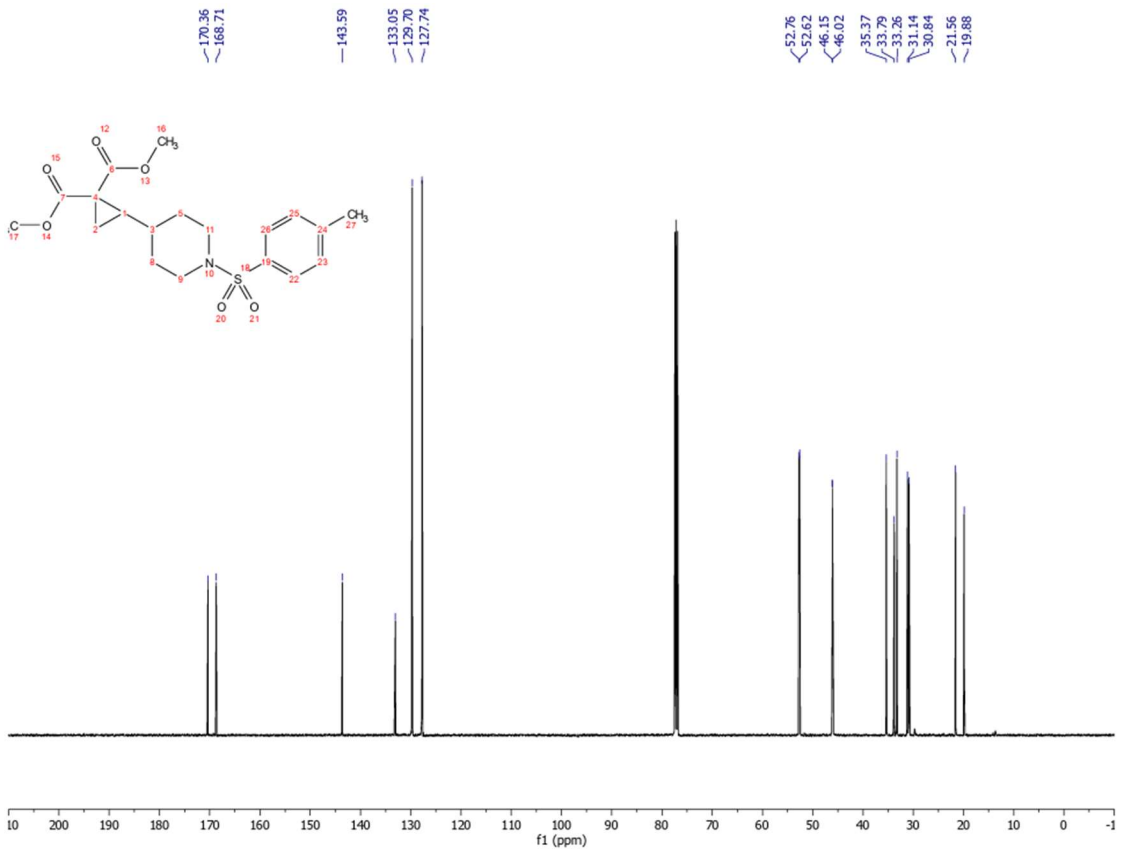
170.36
168.71
143.59
133.05
129.70
127.74
52.76
52.62
46.15
46.02
35.37
33.79
33.26
31.14
30.84
21.56
19.88
f1 (ppm)

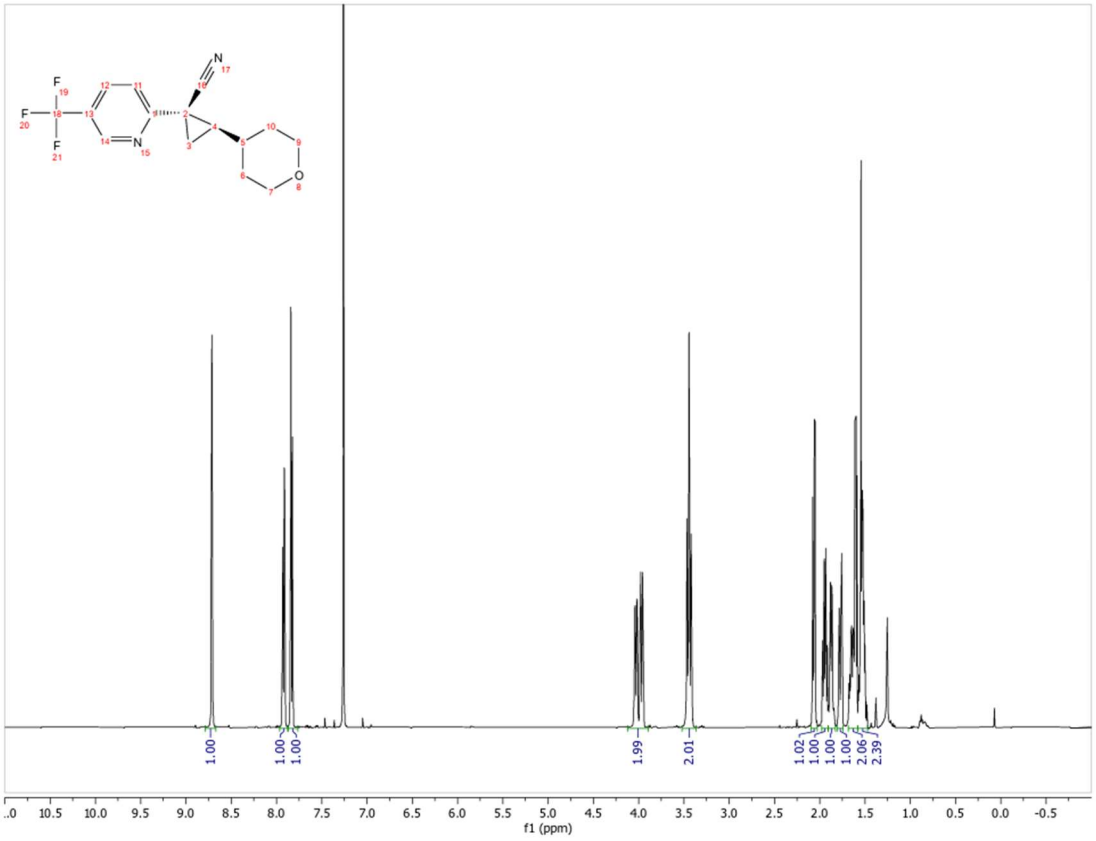
1.00
1.00
1.00
1.99
2.01
1.02
1.00
1.00
1.00
2.06
2.39
f1 (ppm)

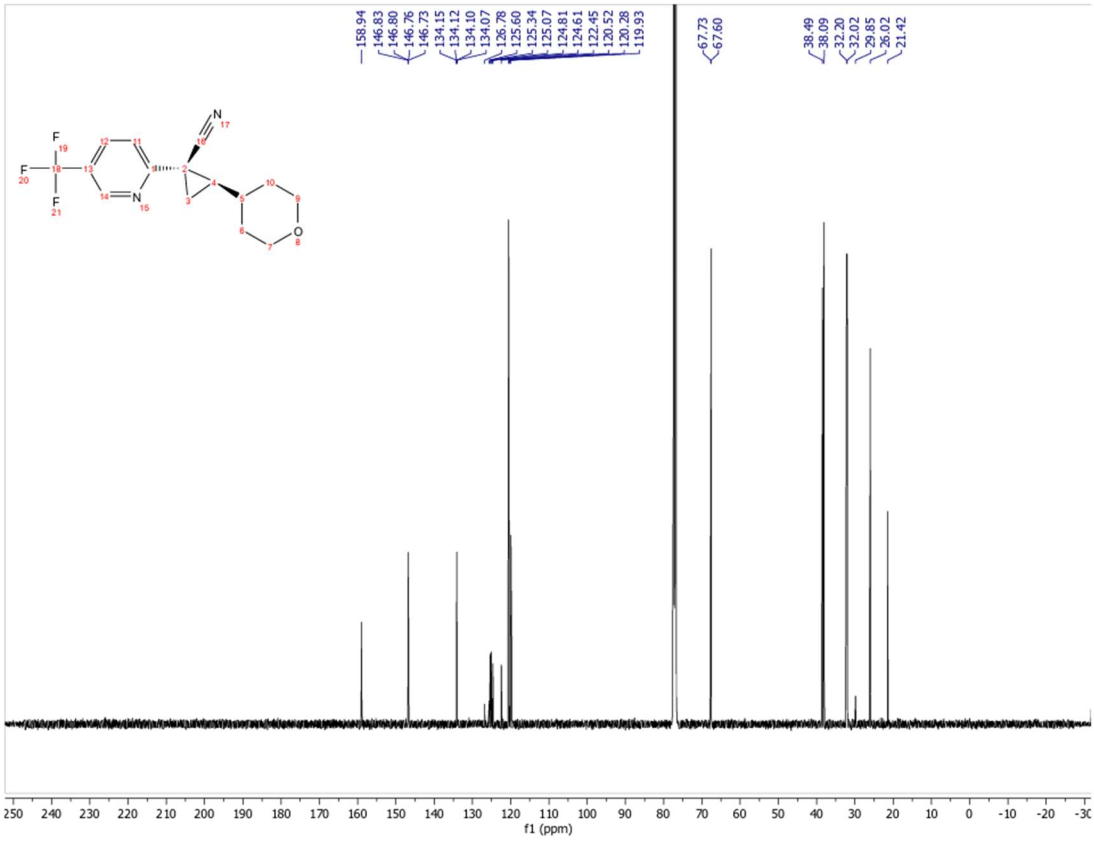
158.94
146.83
146.80
146.76
146.73
134.15
134.12
134.10
134.07
126.78
125.60
125.34
125.07
124.81
124.61
122.45
120.52
120.28
119.93
67.73
67.60
38.49
38.09
32.20
32.02
29.85
26.02
21.42
f1 (ppm)

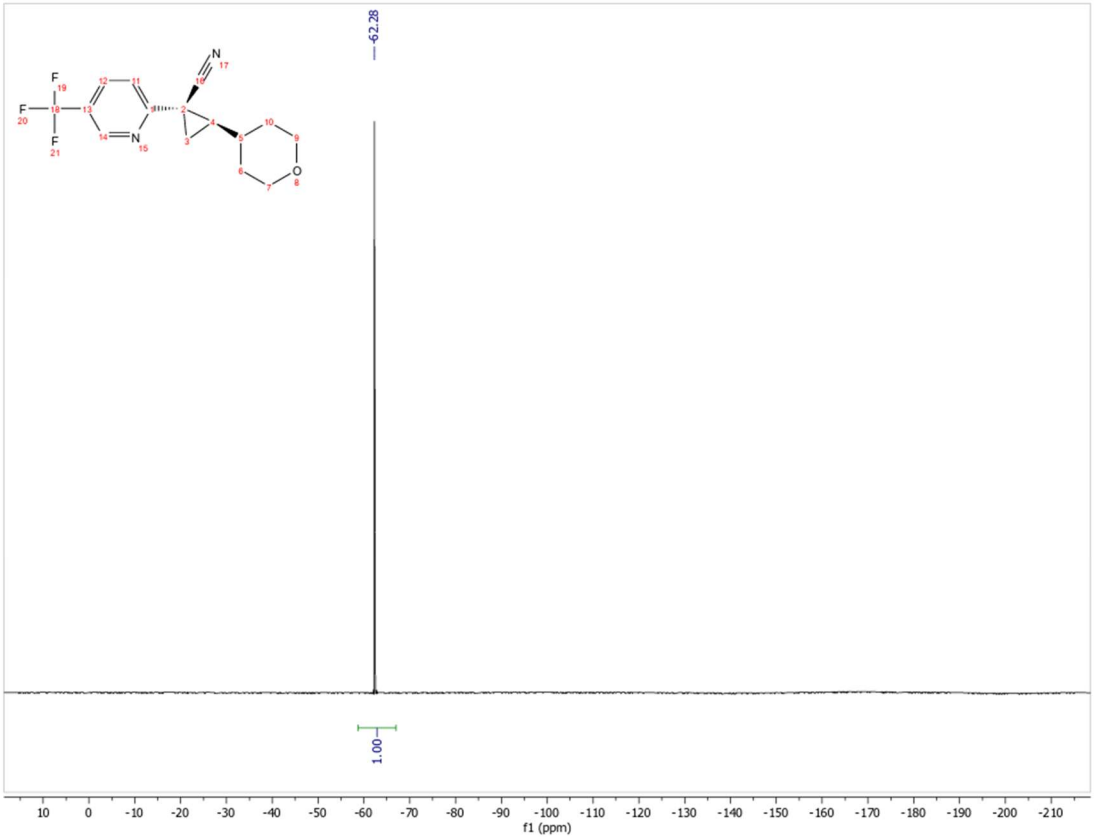
-62.28
1.00
10 0 -10 -20 -30 -40 -50 -60 -70 -80 -90 -100 -110 -120 -130 -140 -150 -160 -170 -180 -190 -200 -210
f1 (ppm)

(blank space)

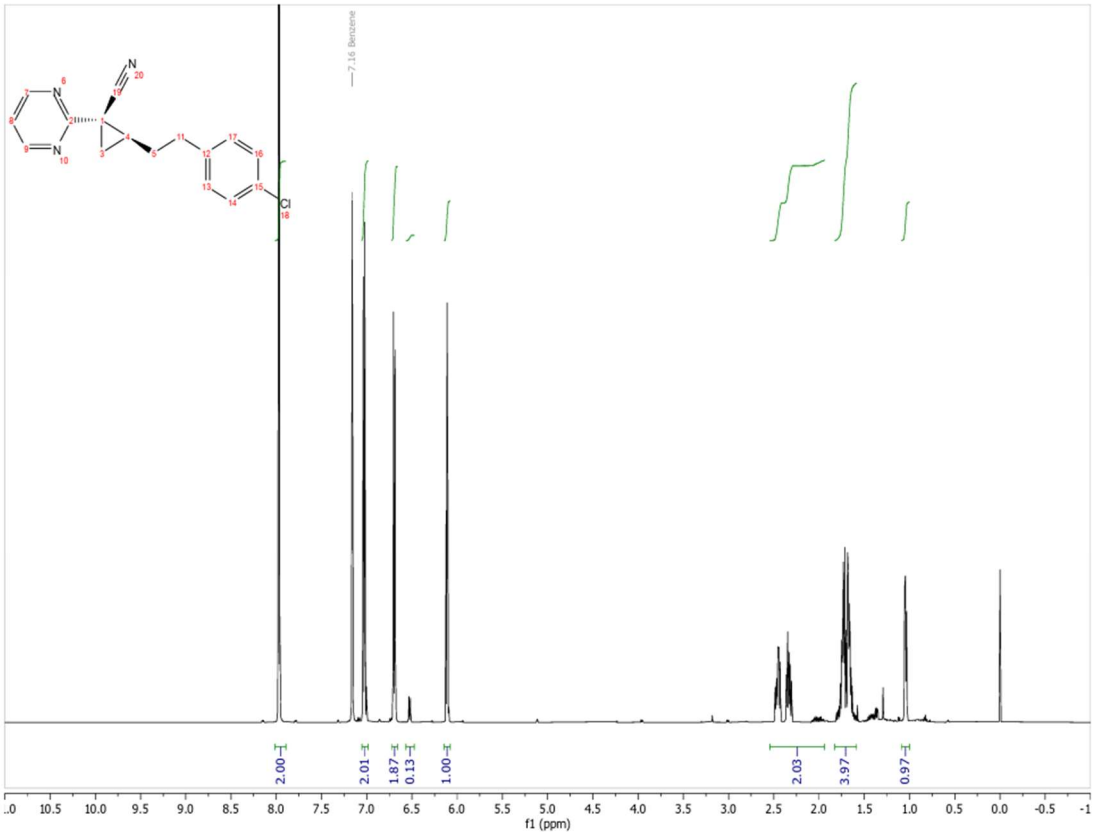
7.16 Benzene
2.00
2.01
1.87
0.13
1.00
2.03
3.97
0.97
f1 (ppm)

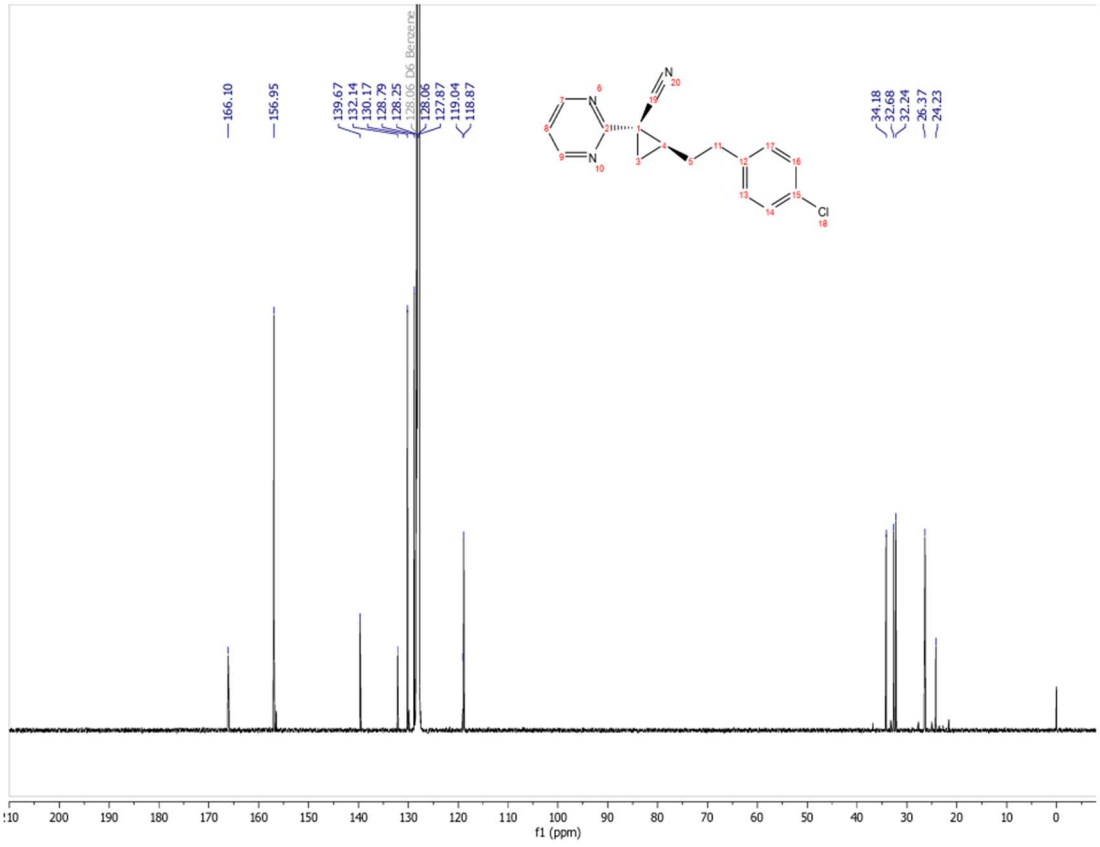
166.10
156.95
139.67
132.14
130.17
128.79
128.25
128.06 D6 Benzene
127.87
119.04
118.87
34.18
32.68
32.24
26.37
24.23
f1 (ppm)

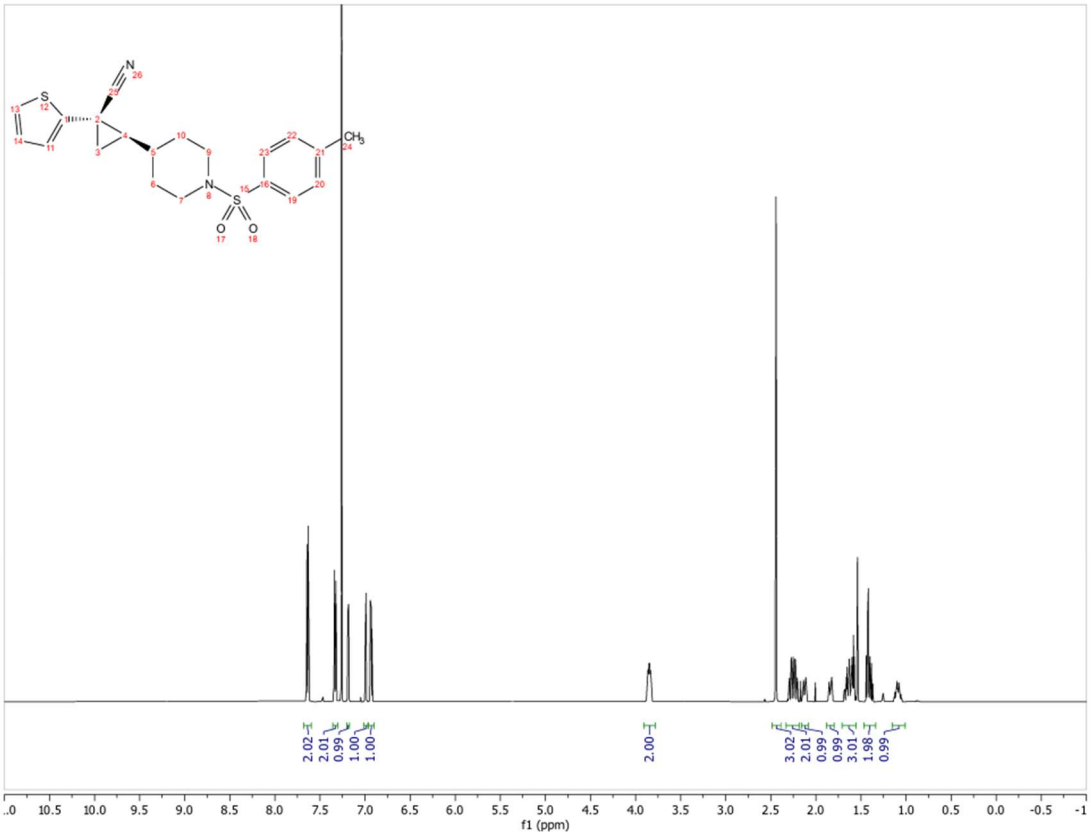
2.02
2.01
0.99
1.00
1.00
2.00
3.02
2.01
0.99
0.99
3.01
1.98
0.99
f1 (ppm)

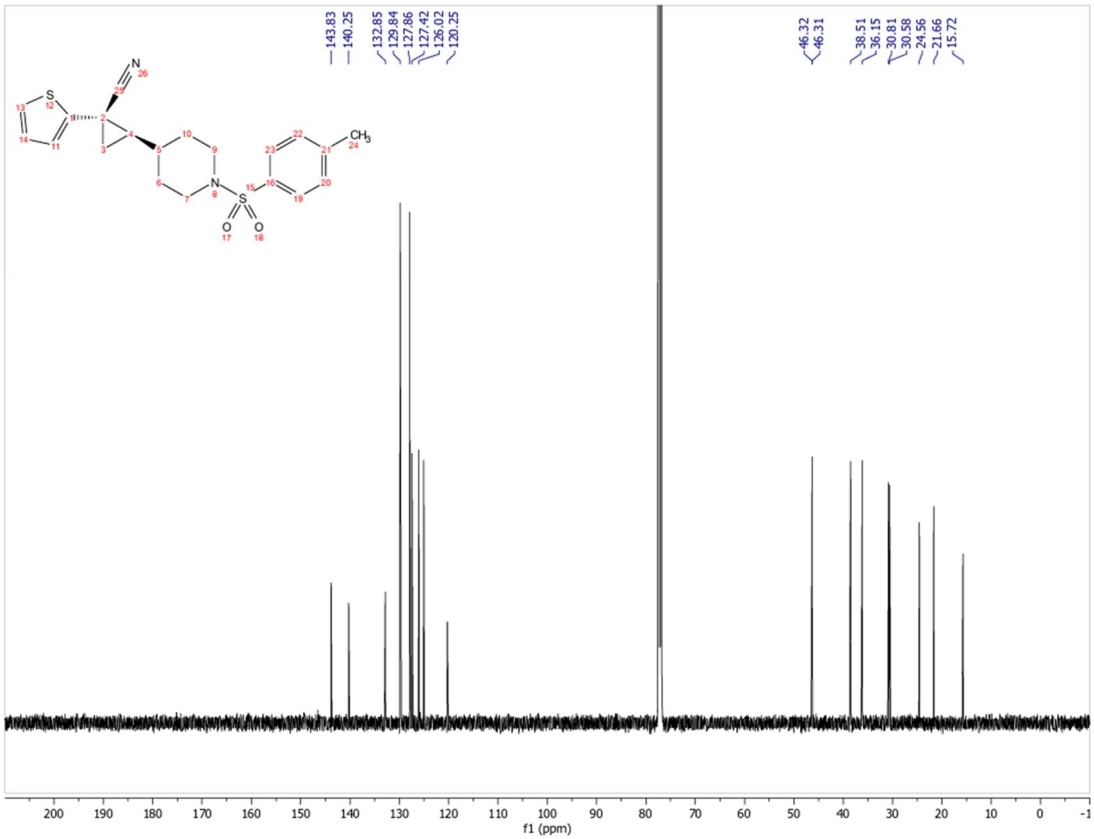
143.83
140.25
132.85
129.84
127.86
127.42
126.02
120.25
46.32
46.31
38.51
36.15
30.81
30.58
24.56
21.66
15.72
f1 (ppm)

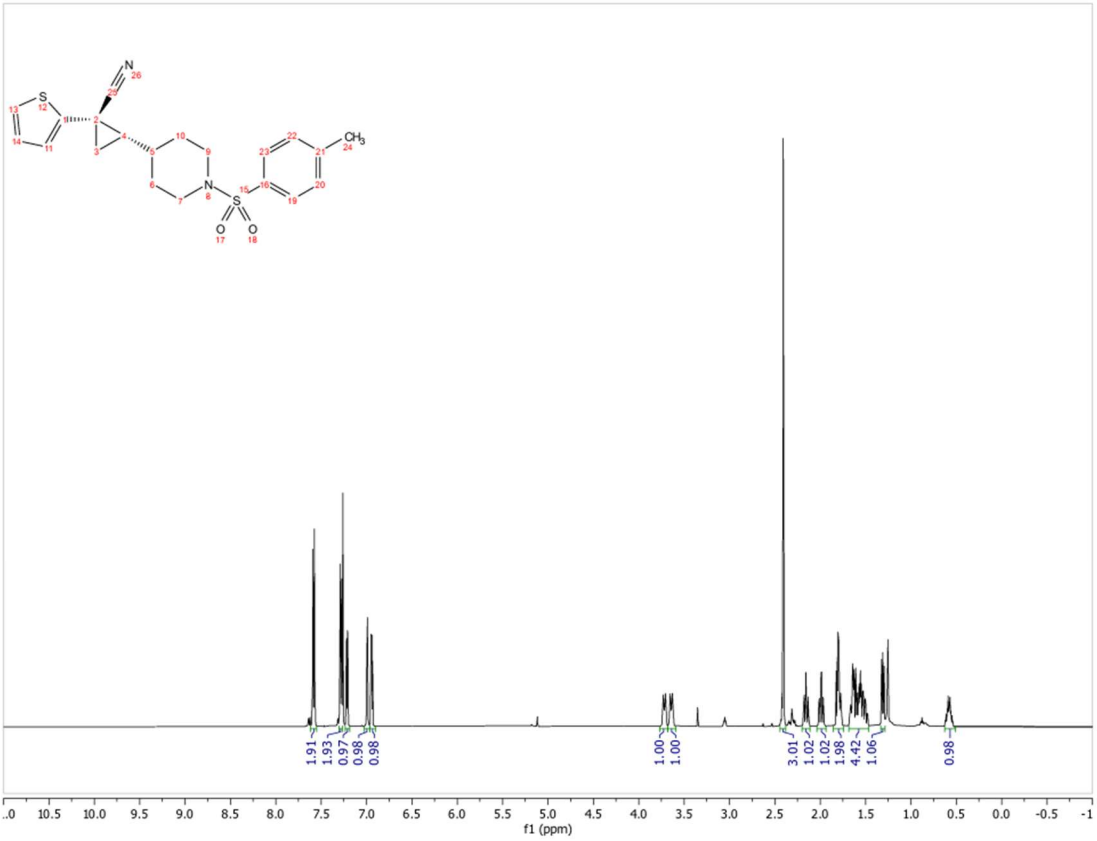
1.91
1.93
0.97
0.98
0.98
1.00
1.00
3.01
1.02
1.02
1.98
4.42
1.06
0.98
f1 (ppm)

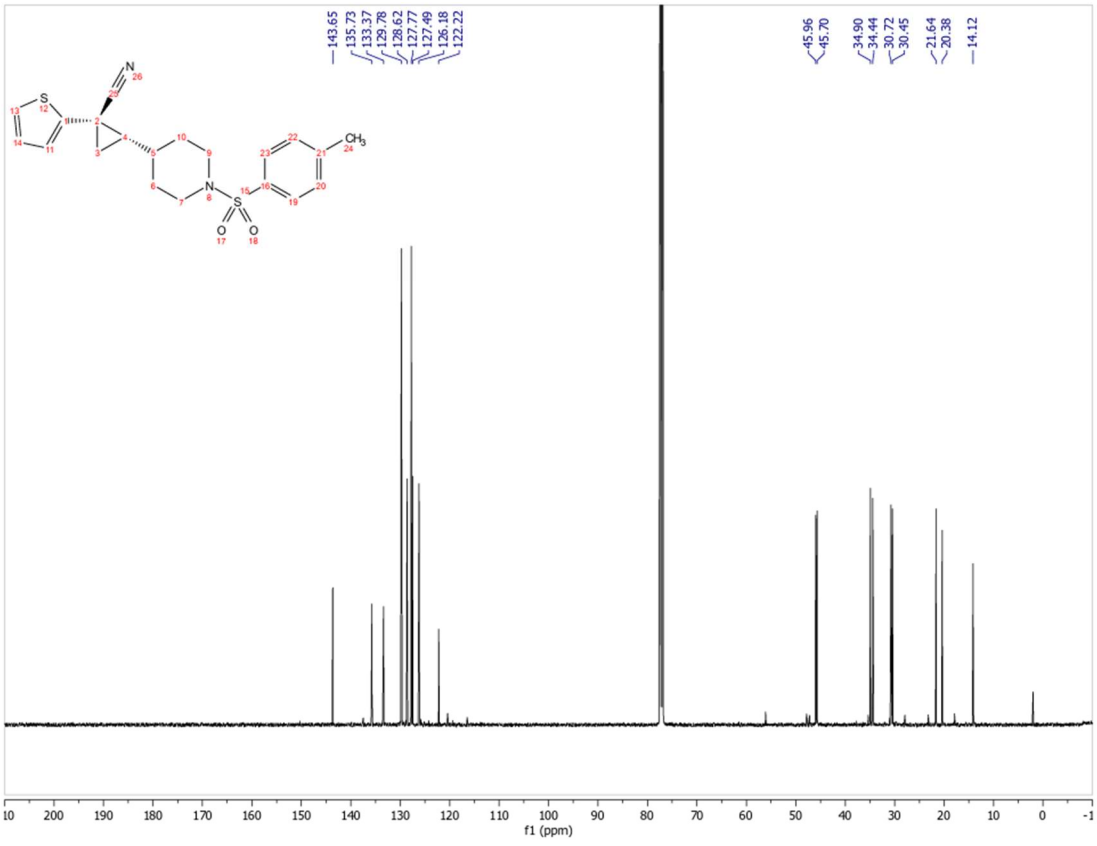
143.65
135.73
133.37
129.78
128.62
127.77
127.49
126.18
122.22
45.96
45.70
34.90
34.44
30.72
30.45
21.64
20.38
14.12
f1 (ppm)

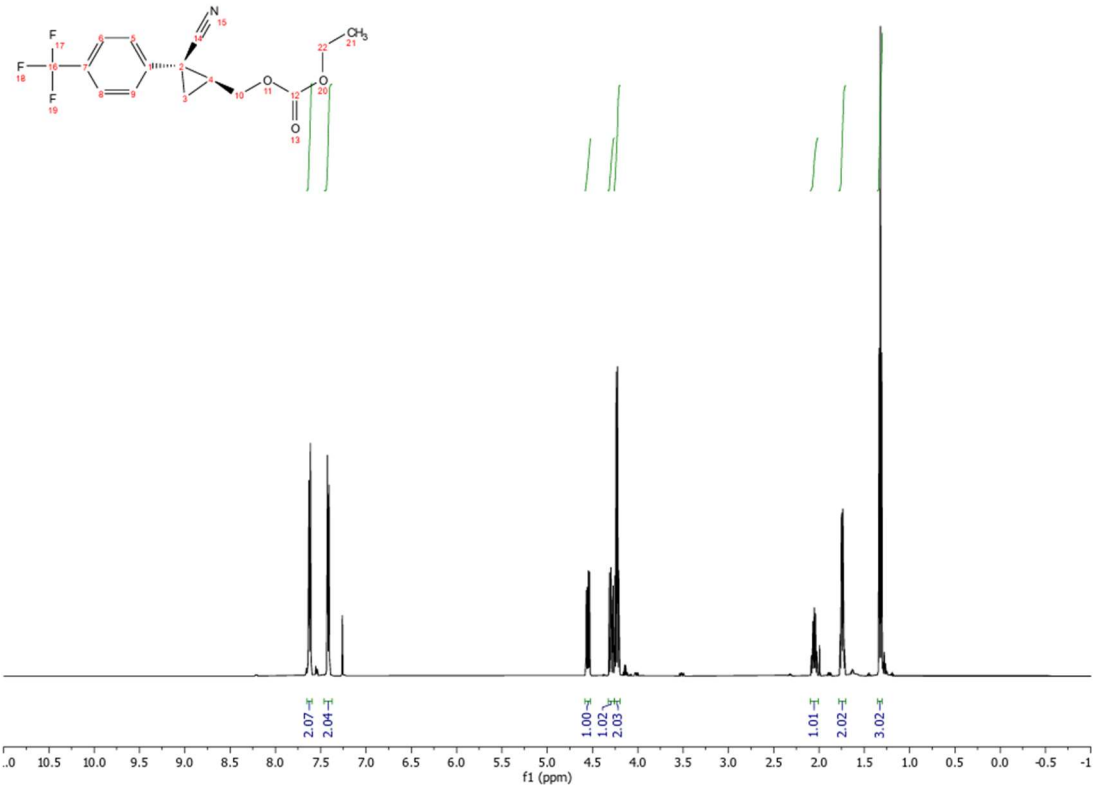
2.07
2.04
1.00
1.02
2.03
1.01
2.02
3.02
f1 (ppm)

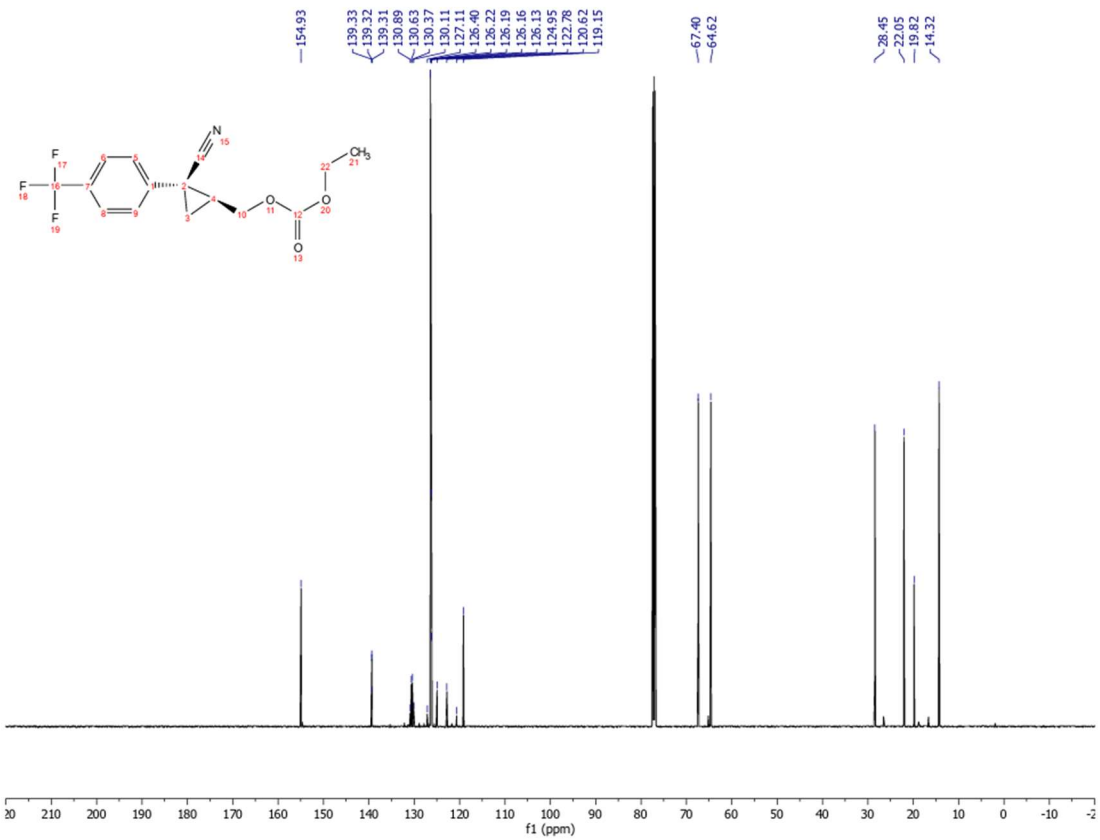
154.93
139.33
139.32
139.31
130.89
130.63
130.37
130.11
127.11
126.40
126.22
126.19
126.16
126.13
124.95
122.78
120.62
119.15
67.40
64.62
28.45
22.05
19.82
14.32
f1 (ppm)

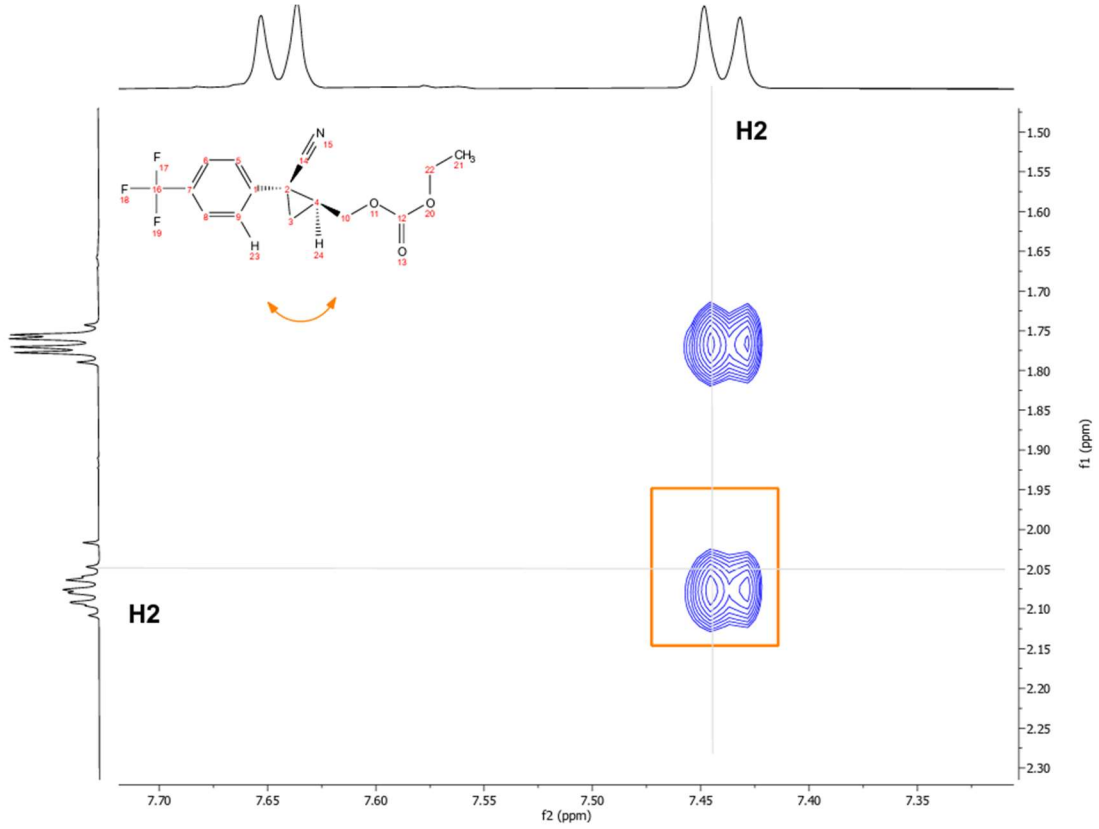
H2
H2
f1 (ppm)
f2 (ppm)

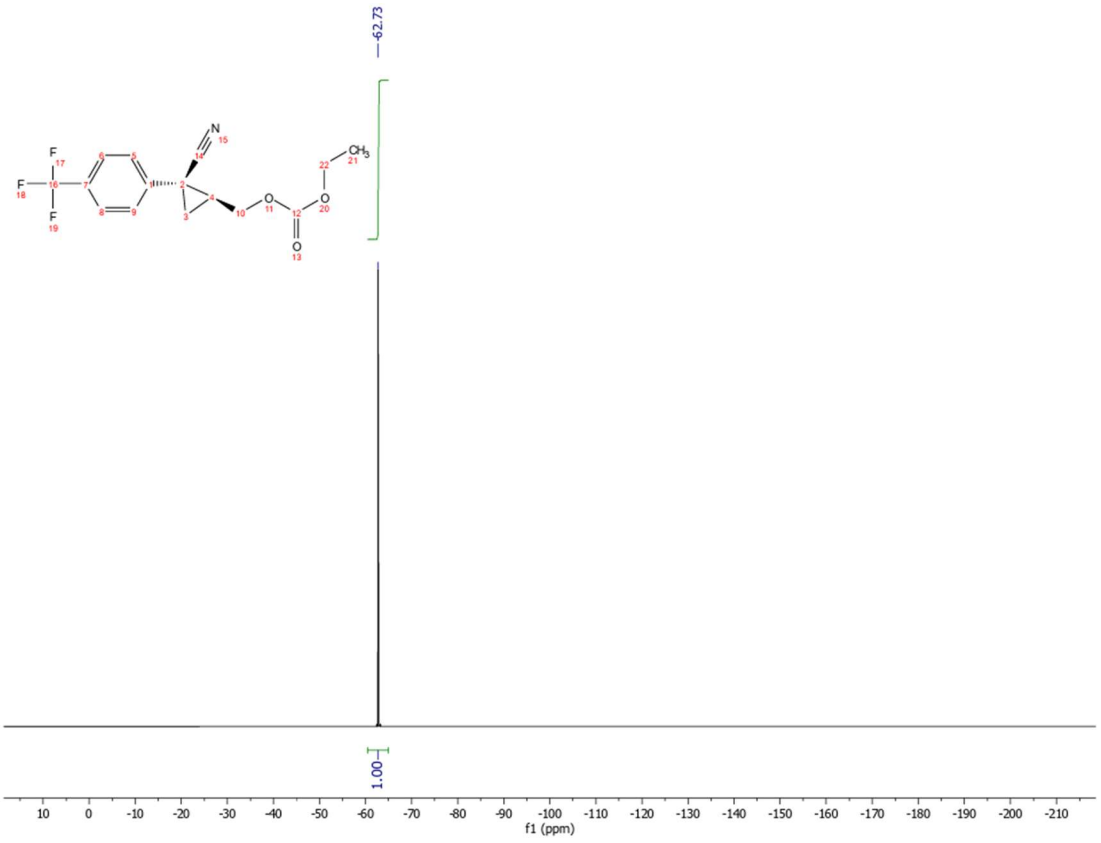
-62.73
1.00
f1 (ppm)

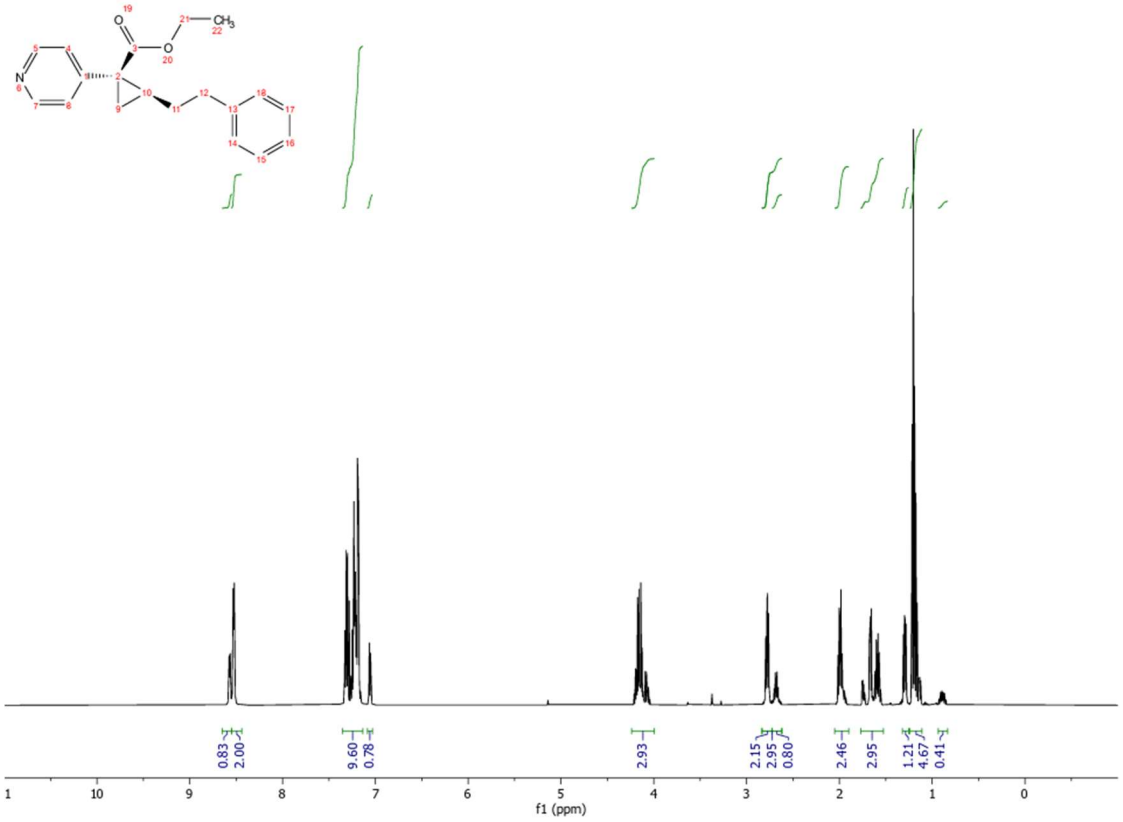
0.83
2.00
9.60
0.78
2.93
2.15
2.95
0.80
2.46
2.95
1.21
4.67
0.41
f1 (ppm)

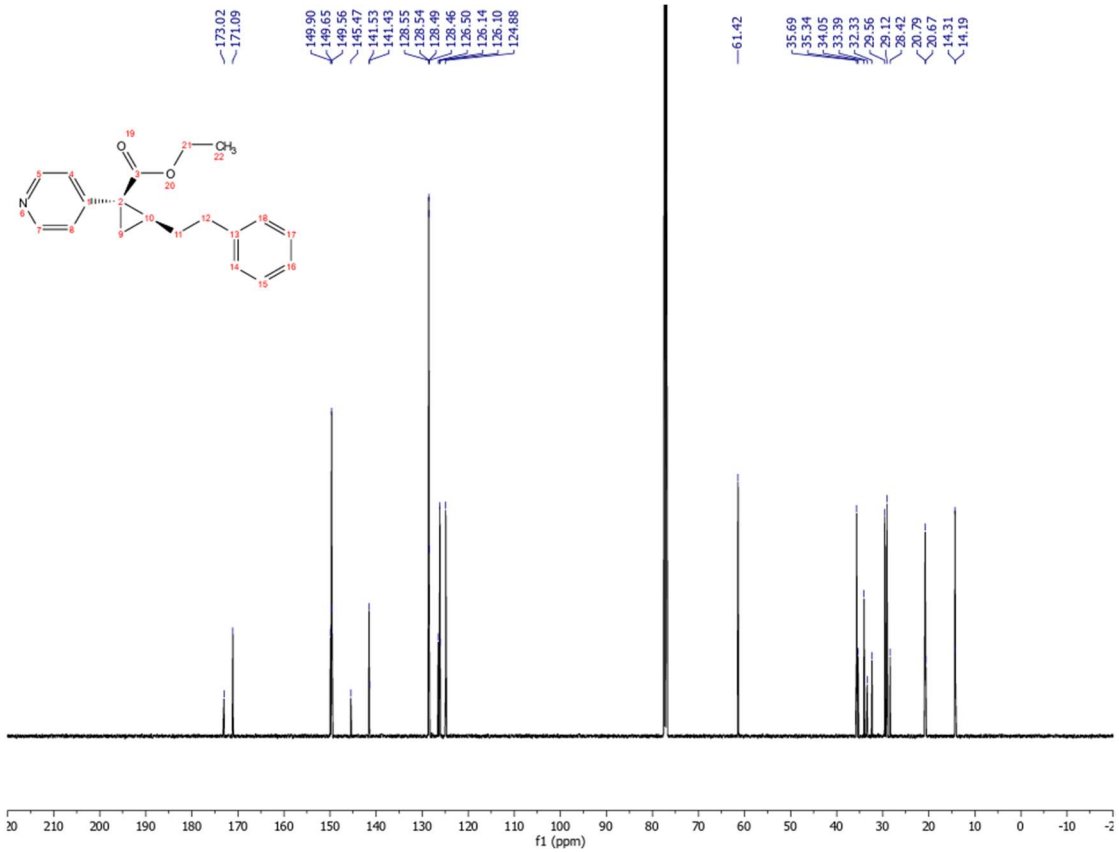
173.02
171.09
149.90
149.65
149.56
145.47
141.53
141.43
128.55
128.54
128.49
128.46
126.50
126.14
126.10
124.88
61.42
35.69
35.34
34.05
33.39
32.33
29.56
29.12
28.42
20.79
20.67
14.31
14.19
f1 (ppm)

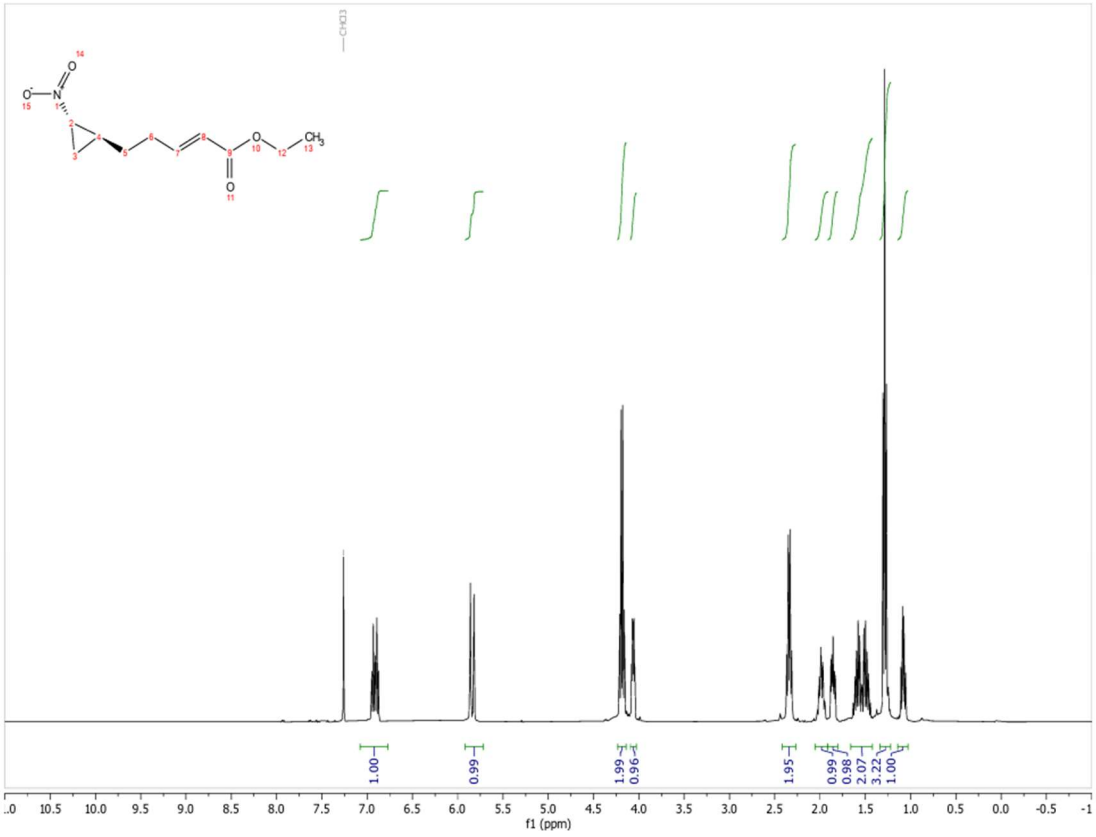
1.00
0.99
1.99
0.96
1.95
0.99
0.98
2.07
3.22
1.00
f1 (ppm)

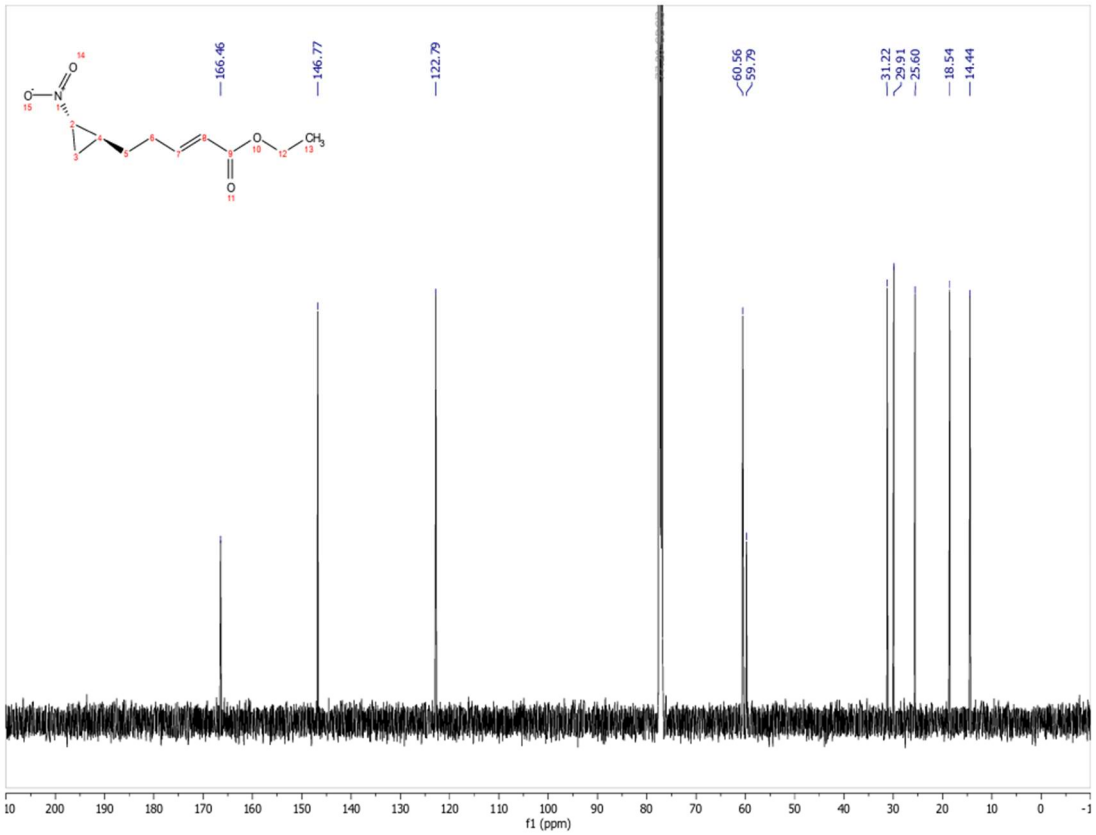
166.46
146.77
122.79
60.56
59.79
31.22
29.91
25.60
18.54
14.44
f1 (ppm)

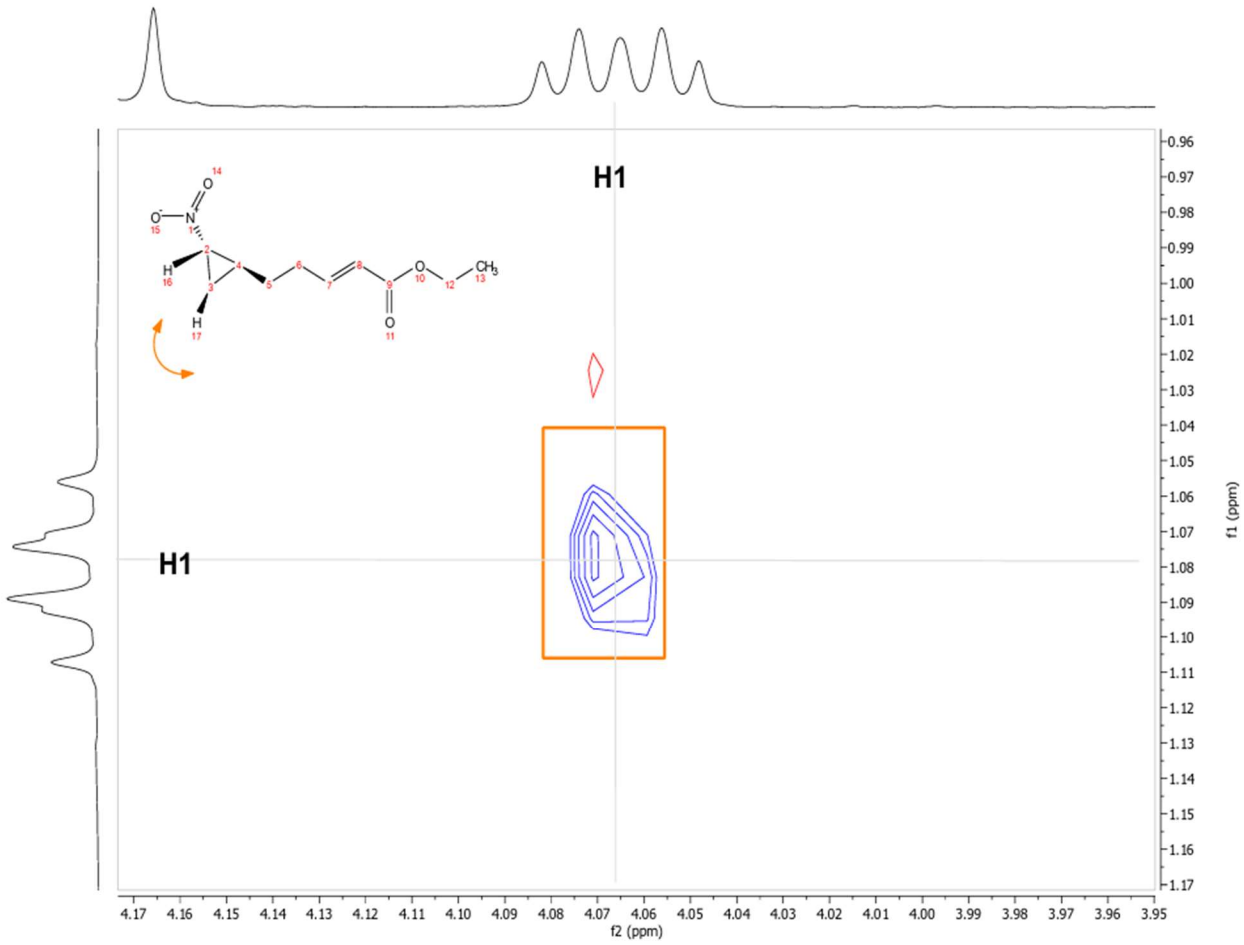

(blank space)

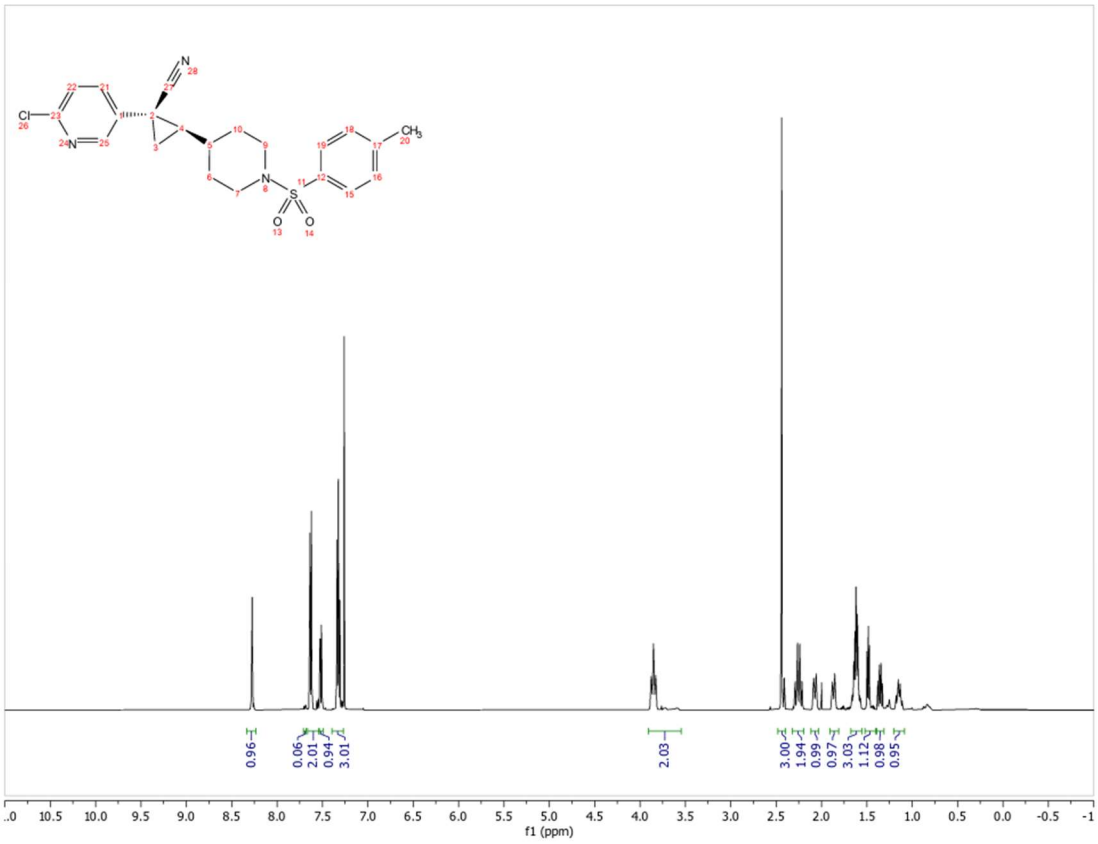
0.96
0.06
2.01
0.94
3.01
2.03
3.00
1.94
0.99
0.97
3.03
1.12
0.98
0.95
f1 (ppm)

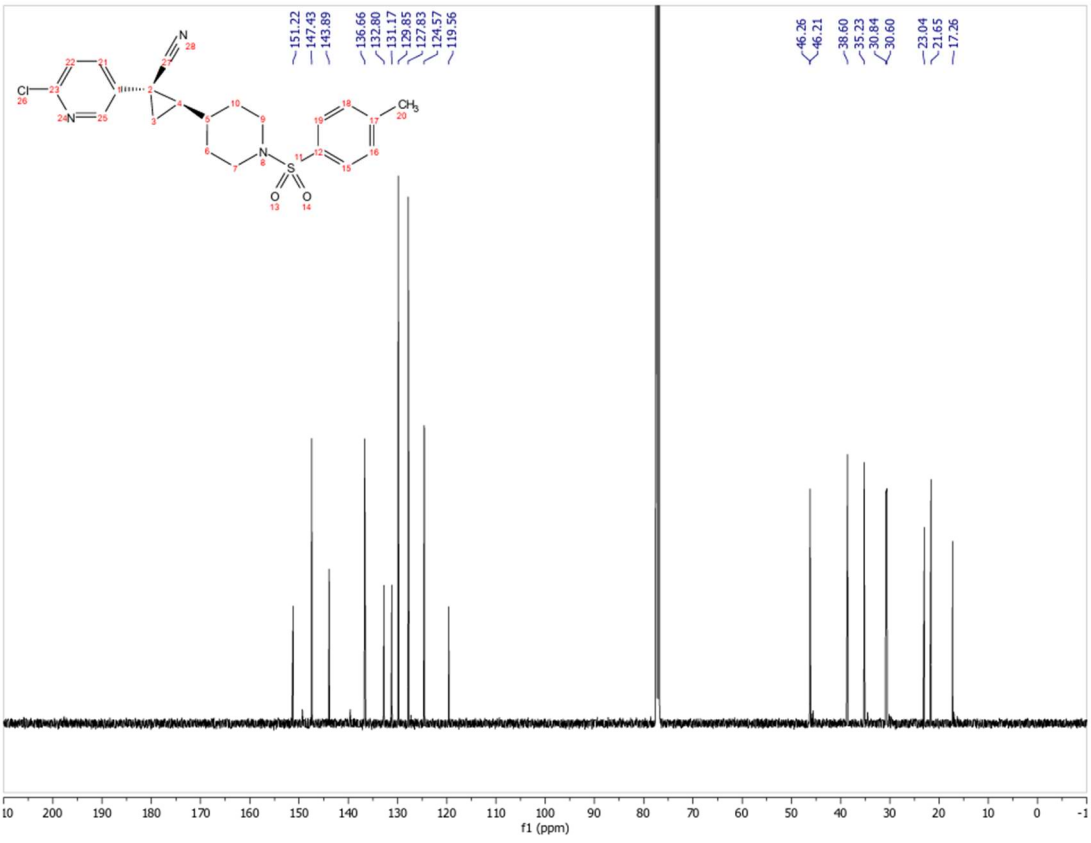
151.22
147.43
143.89
136.66
132.80
131.17
129.85
127.83
124.57
119.56
46.26
46.21
38.60
35.23
30.84
30.60
23.04
21.65
17.26
f1 (ppm)

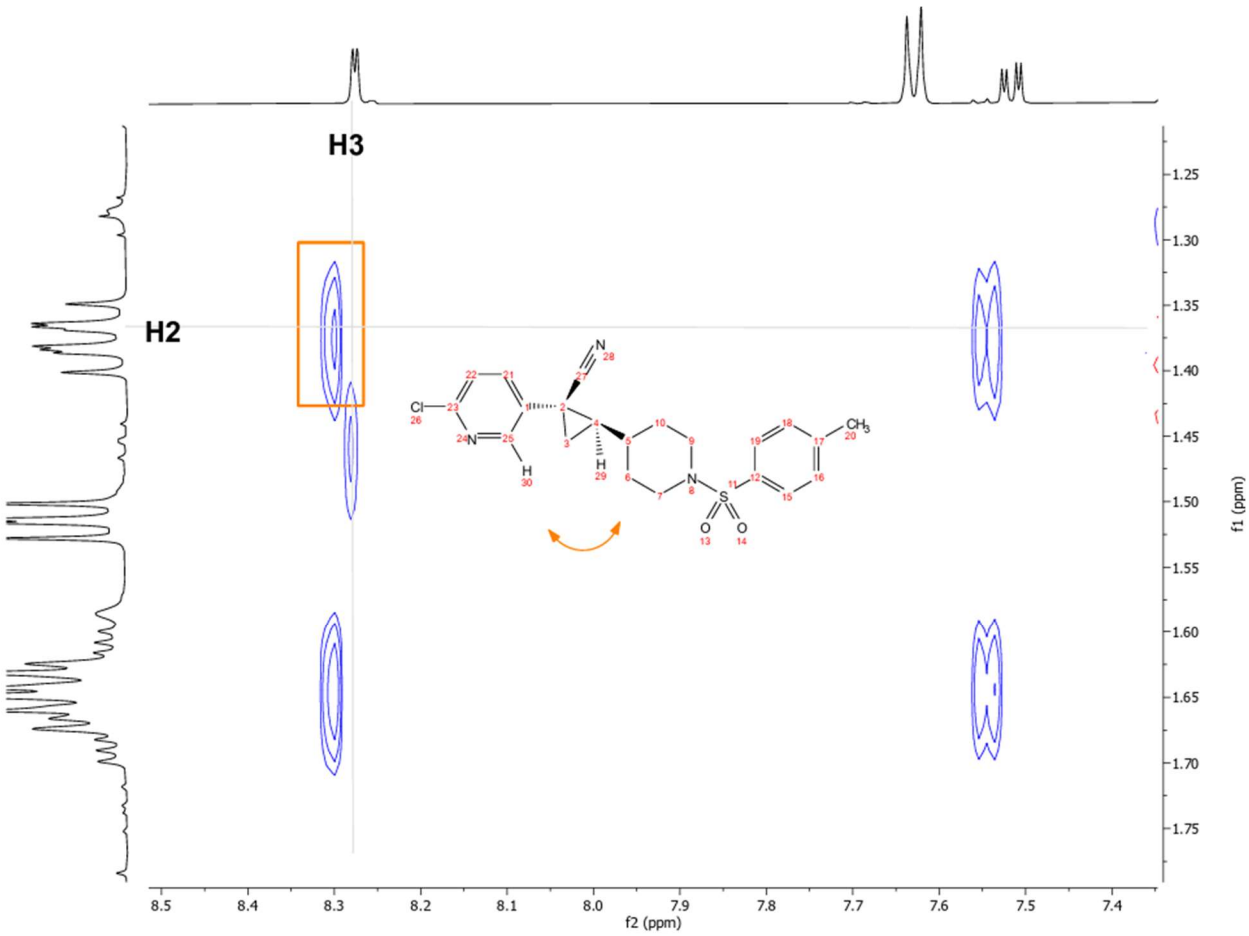
H3
H2
f2 (ppm)
f1 (ppm)
8.5
8.4
8.3
8.2
8.1
8.0
7.9
7.8
7.7
7.6
7.5
7.4
1.25
1.30
1.35
1.40
1.45
1.50
1.55
1.60
1.65
1.70
1.75
Cl
N
S
O
H
CH3

(blank space)

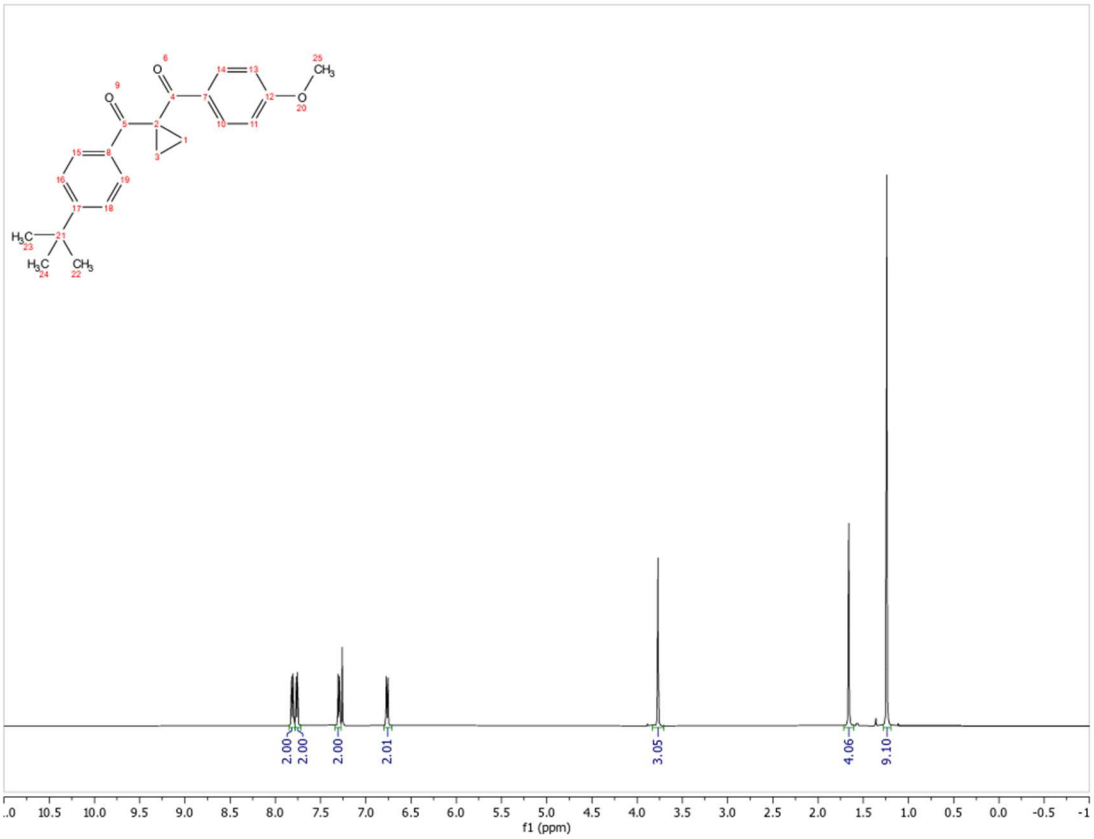
2.00
2.00
2.00
2.01
3.05
4.06
9.10
f1 (ppm)

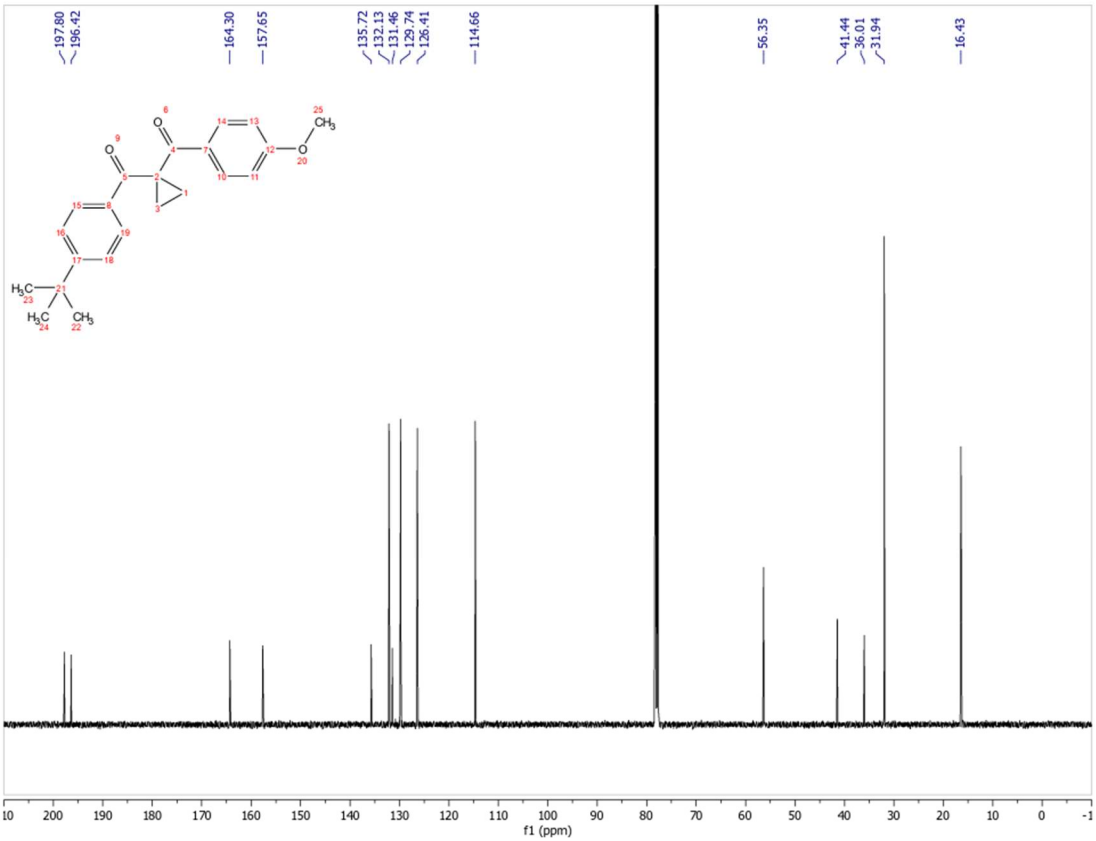
197.80
196.42
164.30
157.65
135.72
132.13
131.46
129.74
126.41
114.66
56.35
41.44
36.01
31.94
16.43
f1 (ppm)

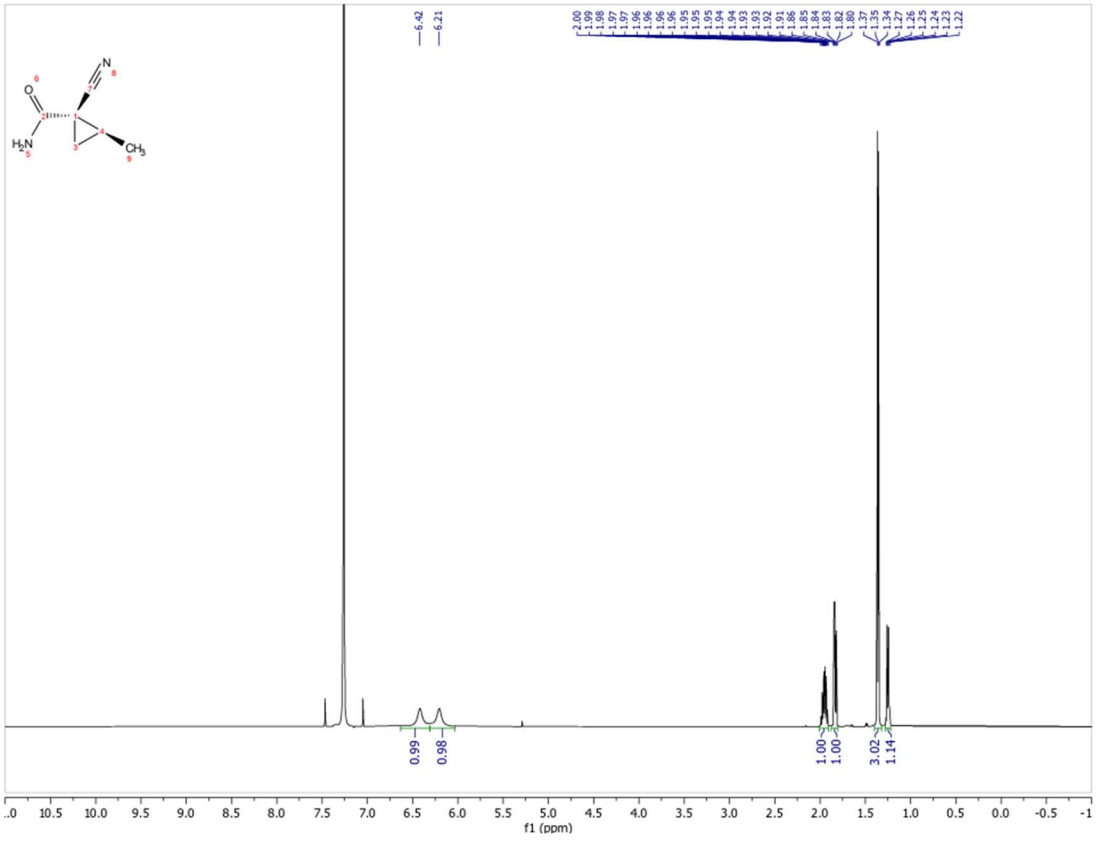
6.42
6.21
0.99
0.98
1.00
1.00
3.02
1.14
f1 (ppm)

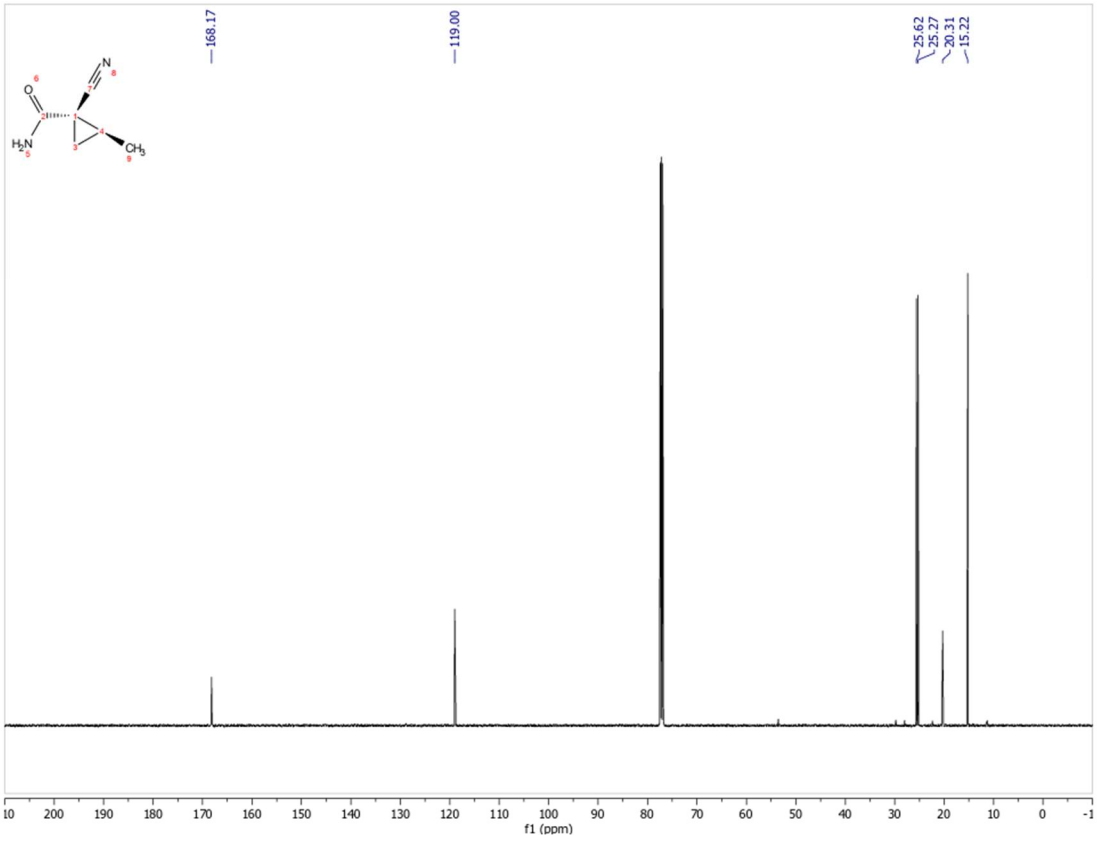
168.17
119.00
25.62
25.27
20.31
15.22
f1 (ppm)

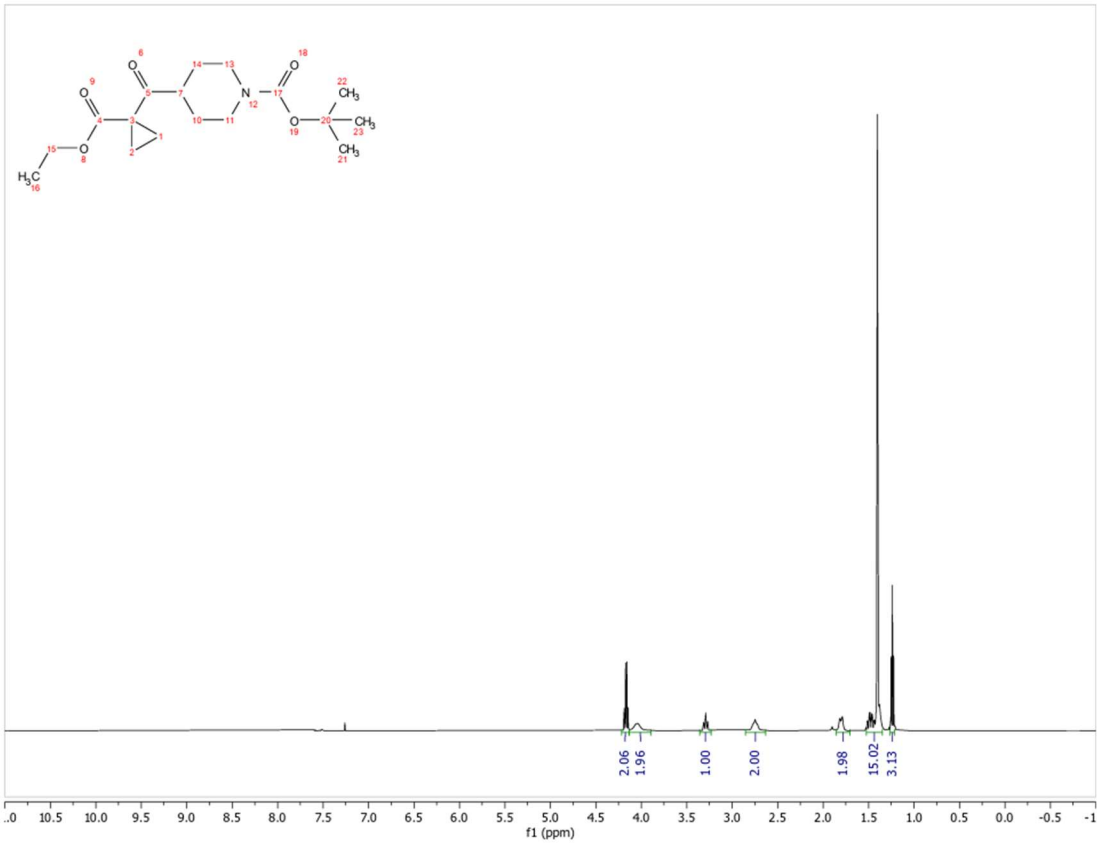
2.06
1.96
1.00
2.00
1.98
15.02
3.13
f1 (ppm)

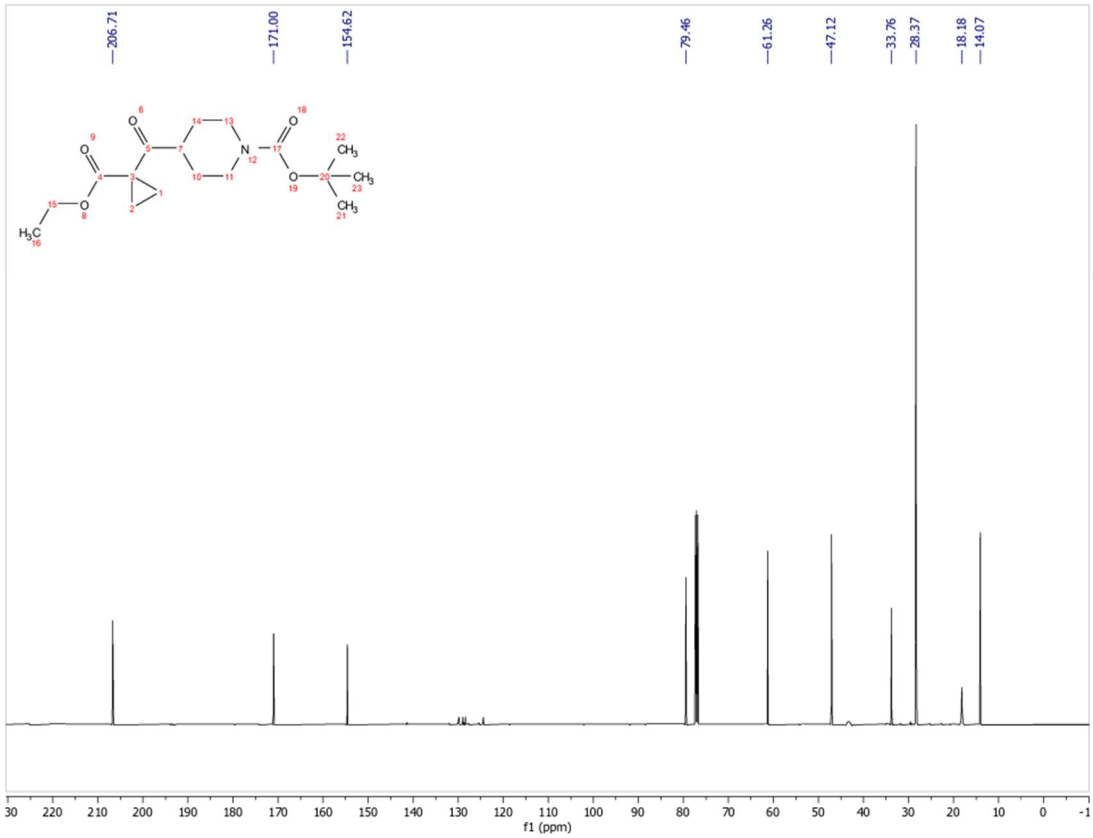
206.71
171.00
154.62
79.46
61.26
47.12
33.76
28.37
18.18
14.07
f1 (ppm)

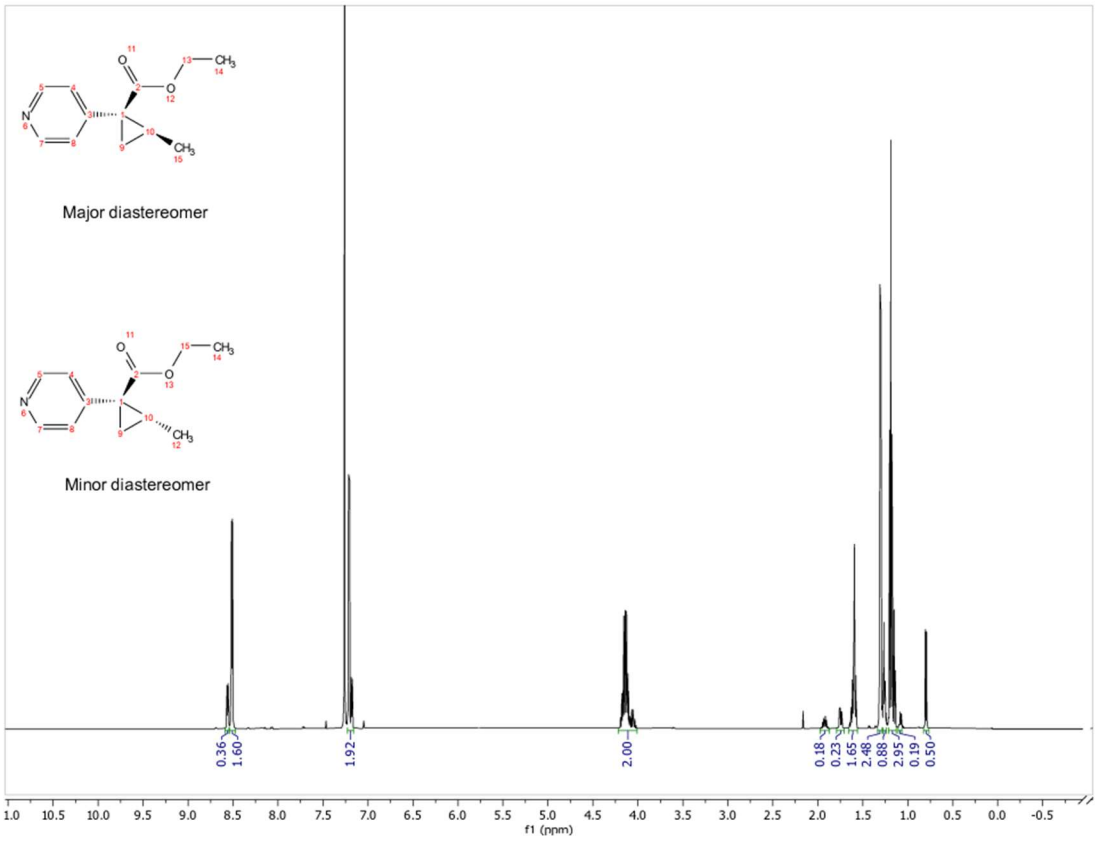
Major diastereomer
Minor diastereomer
0.36
1.60
1.92
2.00
0.18
0.23
1.65
2.48
0.88
2.95
0.19
0.50
f1 (ppm)

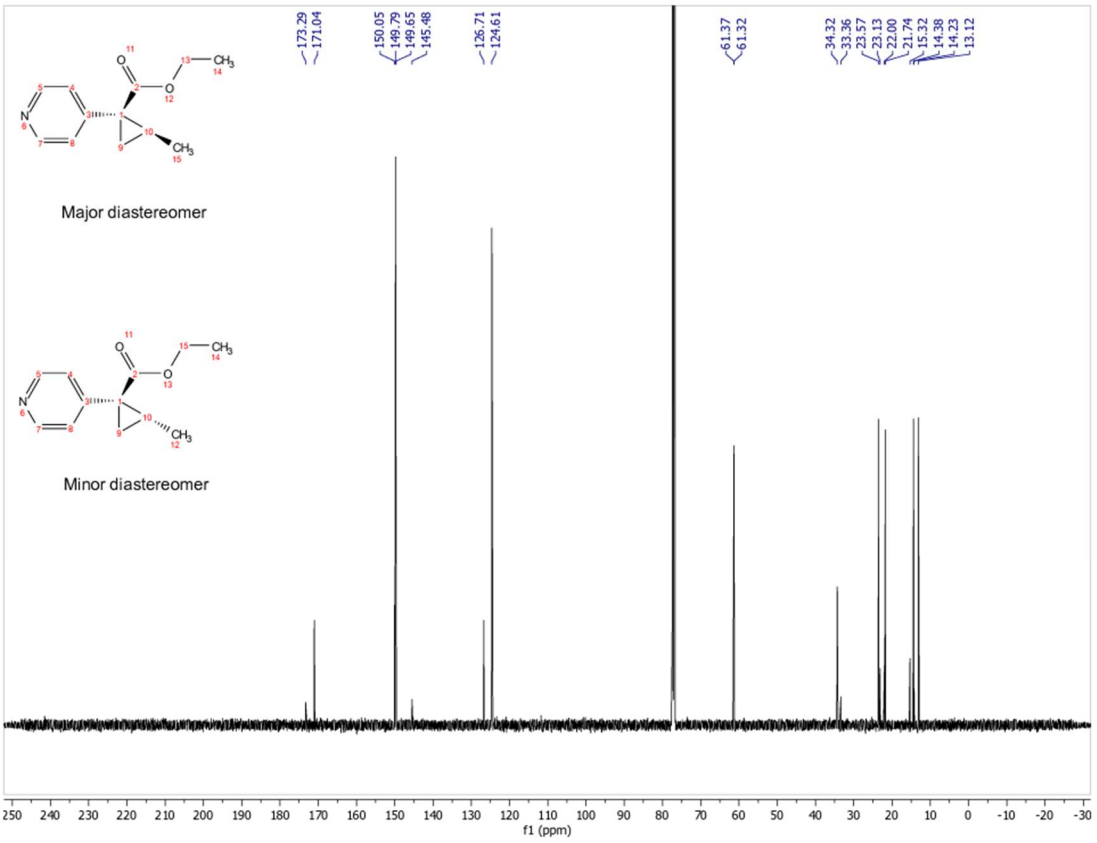
Major diastereomer
Minor diastereomer
173.29
171.04
150.05
149.79
149.65
145.48
126.71
124.61
61.37
61.32
34.32
33.36
23.57
23.13
22.00
21.74
15.32
14.38
14.23
13.12
f1 (ppm)

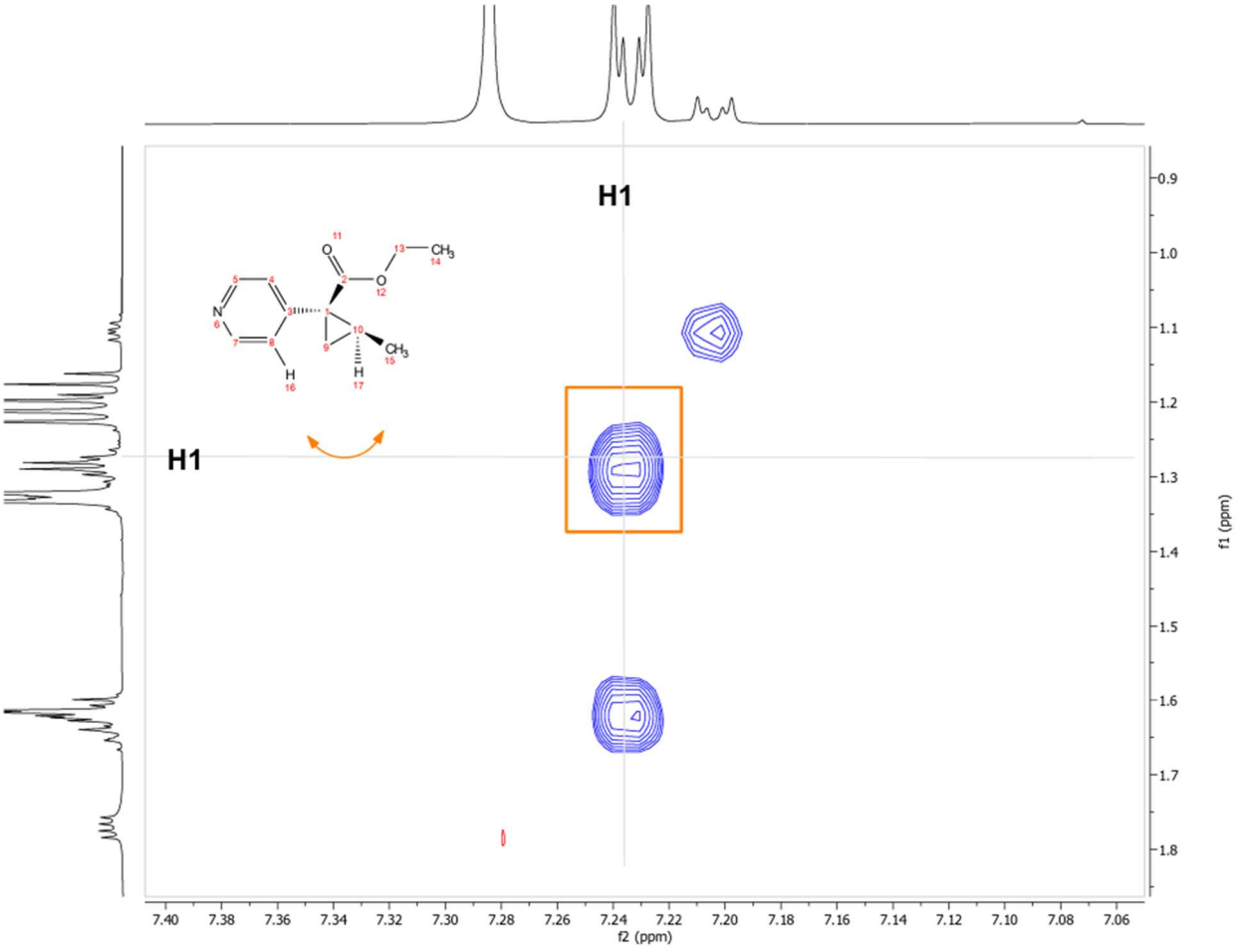

(blank space)

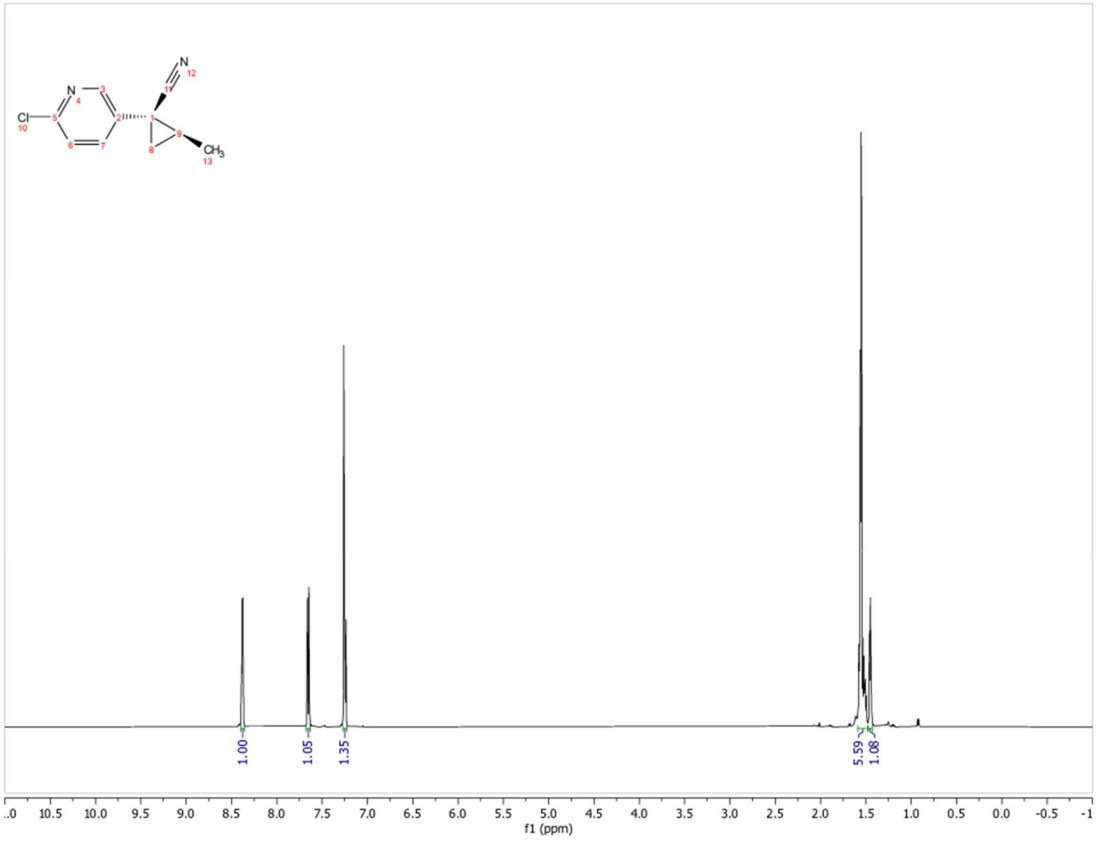
1.00
1.05
1.35
5.59
1.08
f1 (ppm)

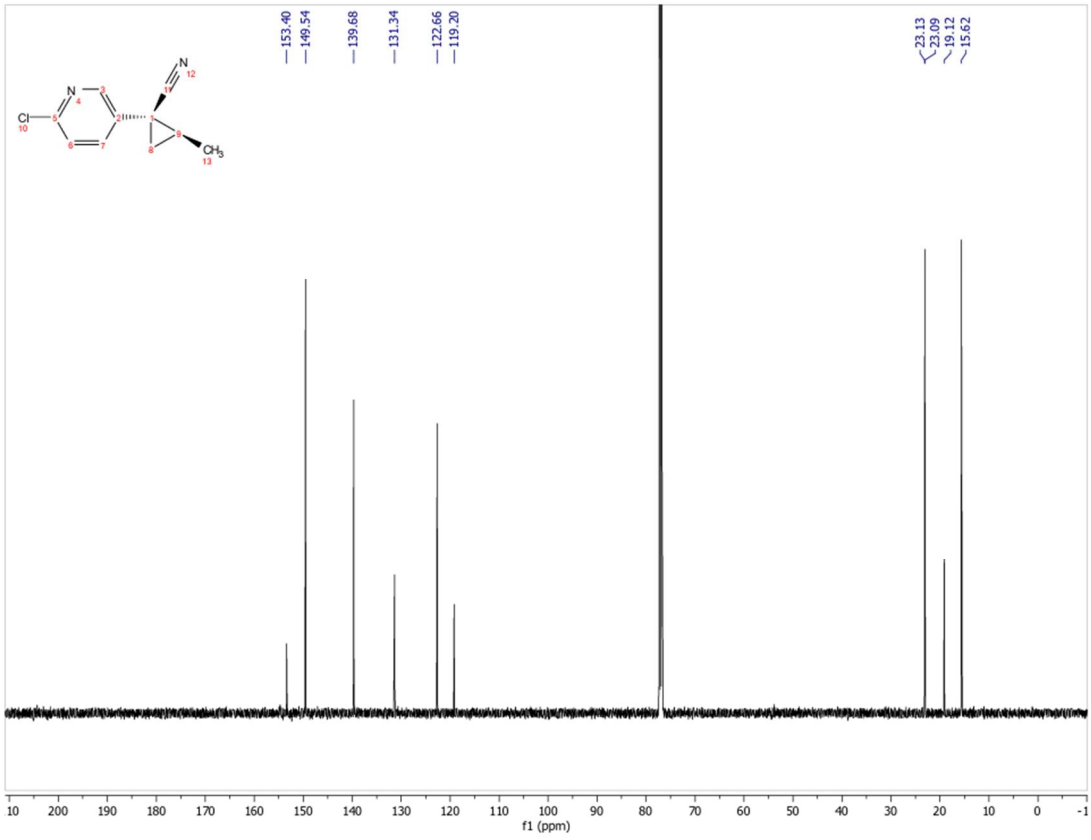
153.40
149.54
139.68
131.34
122.66
119.20
23.13
23.09
19.12
15.62
f1 (ppm)

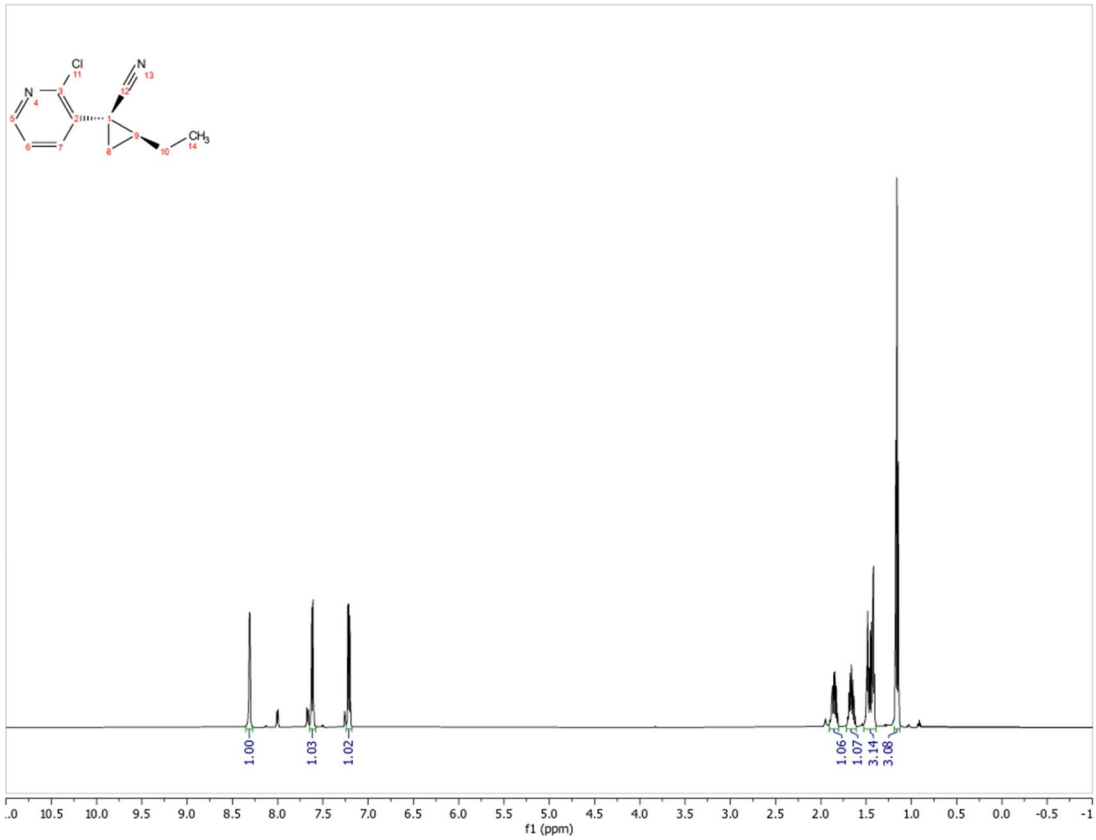
Cl
11
N
13
N
4
CH3
14
1.00
1.03
1.02
1.06
1.07
3.14
3.08
f1 (ppm)

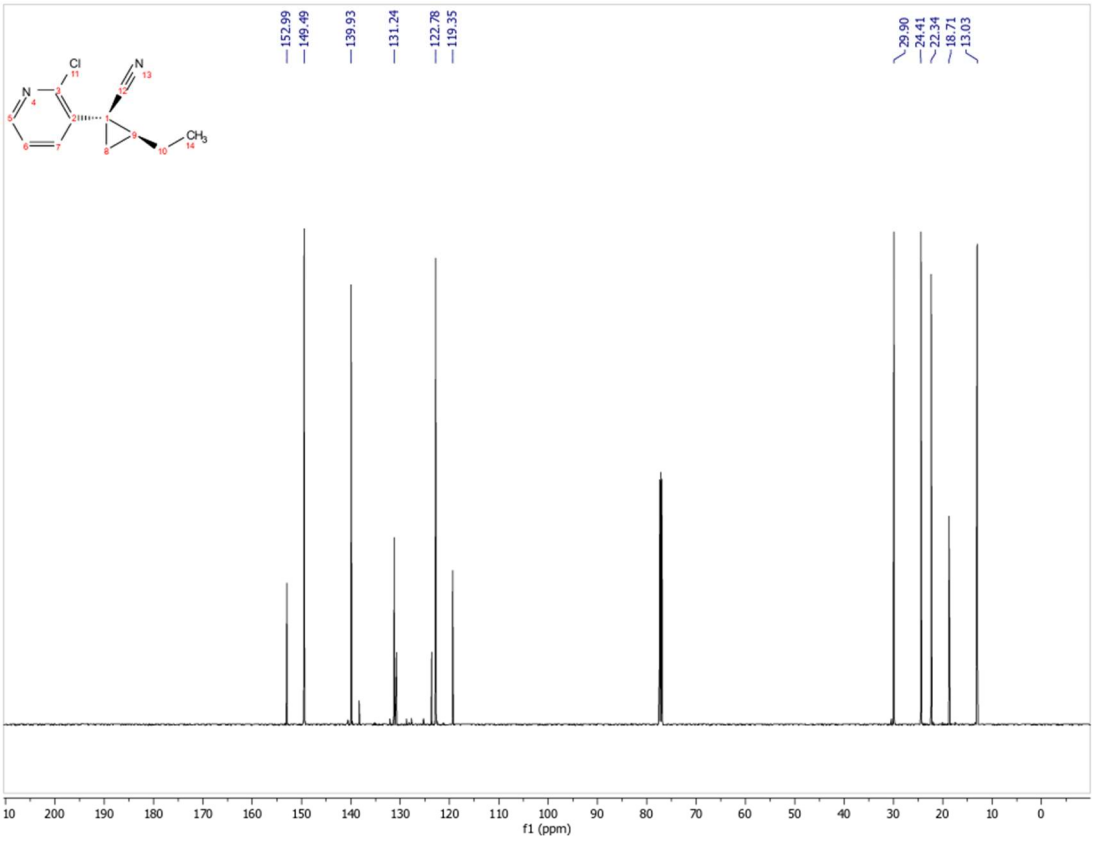
Cl
11
N
13
N
4
CH3
14
152.99
149.49
139.93
131.24
122.78
119.35
29.90
24.41
22.34
18.71
13.03
f1 (ppm)

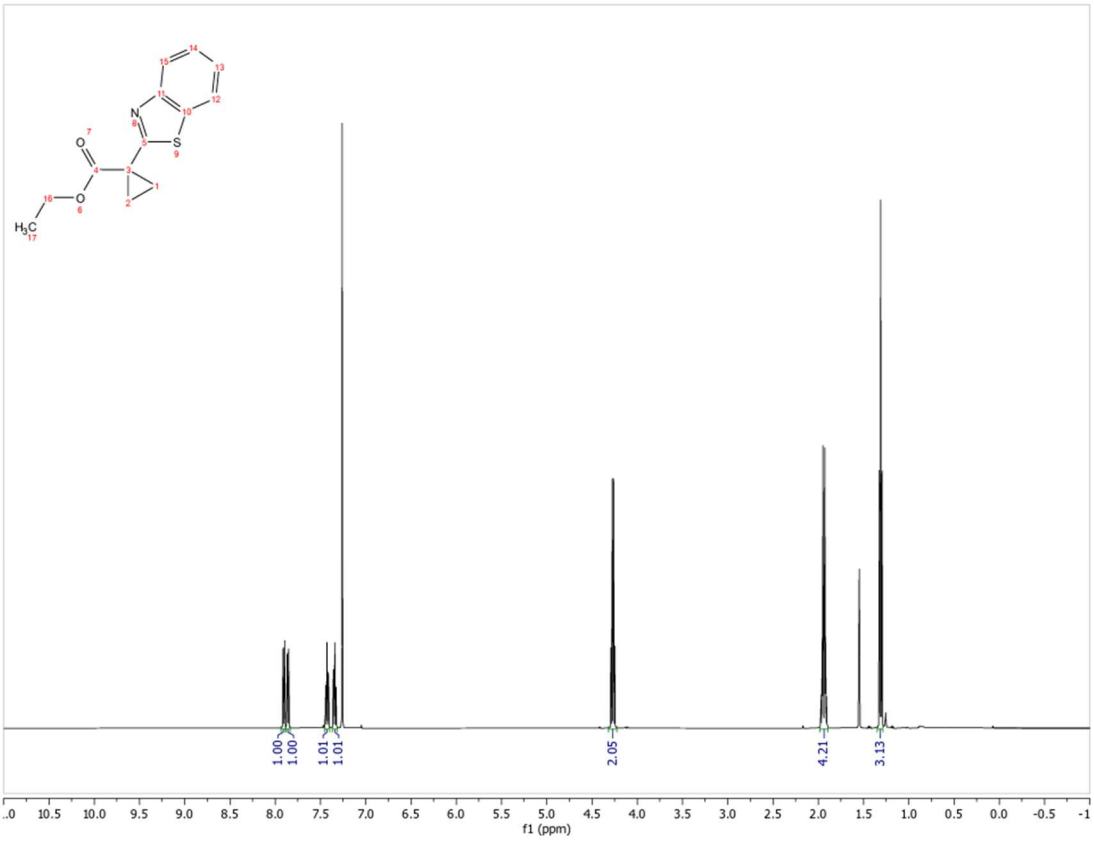
1.00
1.00
1.01
1.01
2.05
4.21
3.13
f1 (ppm)

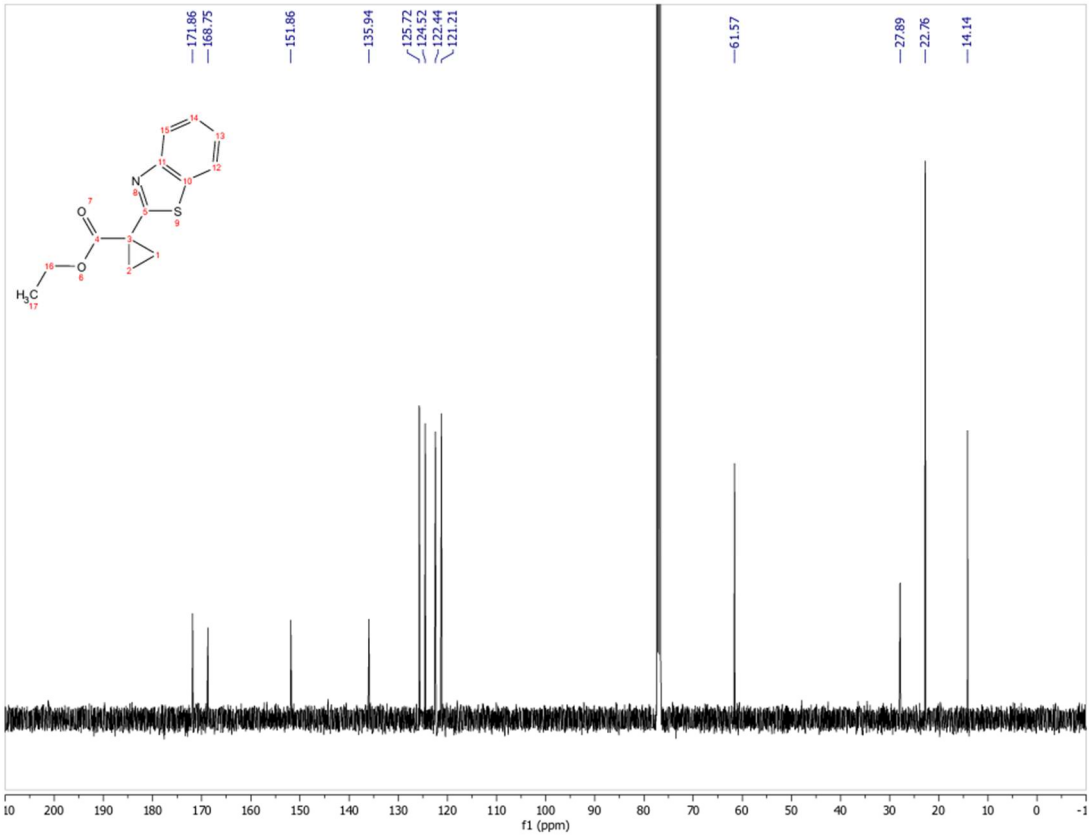
171.86
168.75
151.86
135.94
125.72
124.52
122.44
121.21
61.57
27.89
22.76
14.14
f1 (ppm)

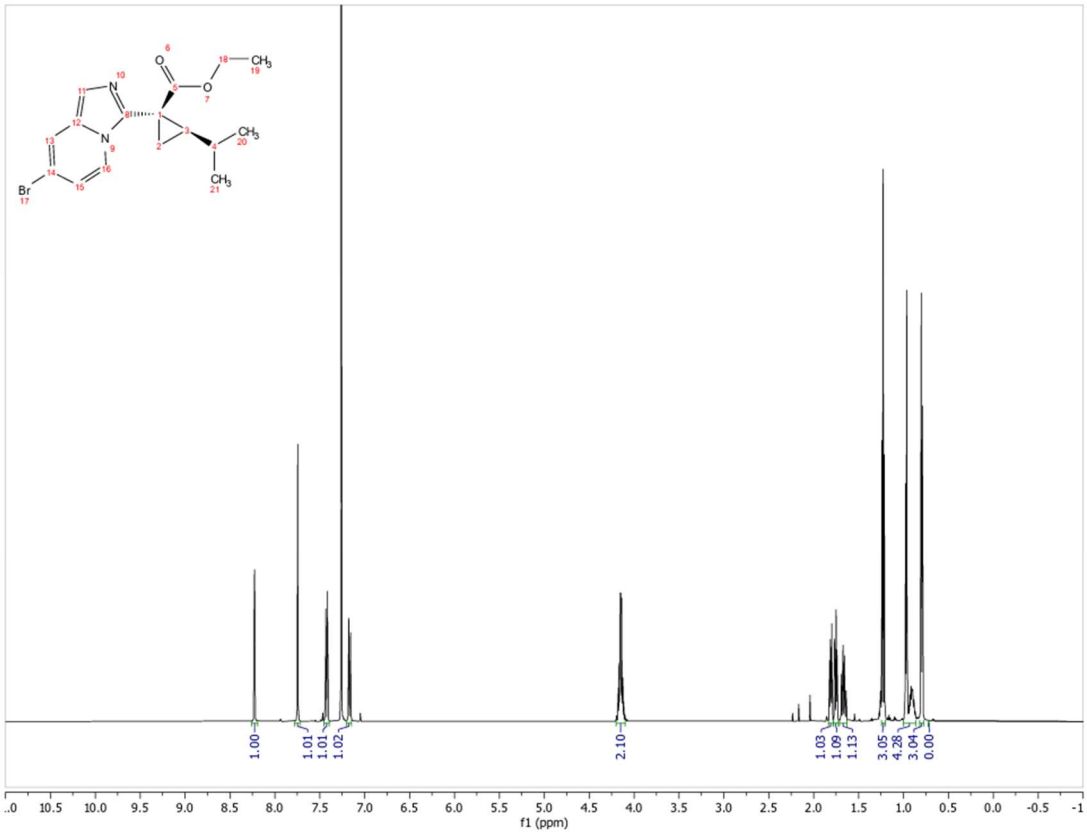
1.00
1.01
1.01
1.02
2.10
1.03
1.09
1.13
3.05
4.28
3.04
0.00
f1 (ppm)

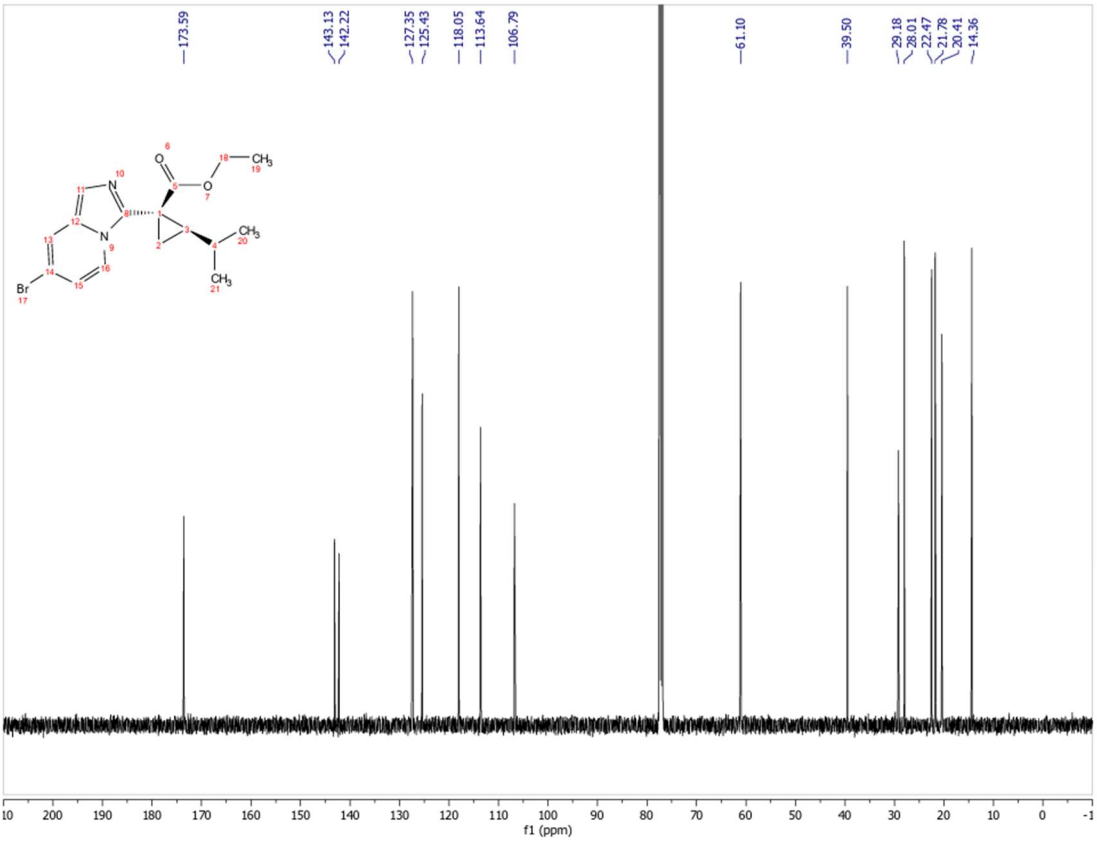
173.59
143.13
142.22
127.35
125.43
118.05
113.64
106.79
61.10
39.50
29.18
28.01
22.47
21.78
20.41
14.36
f1 (ppm)

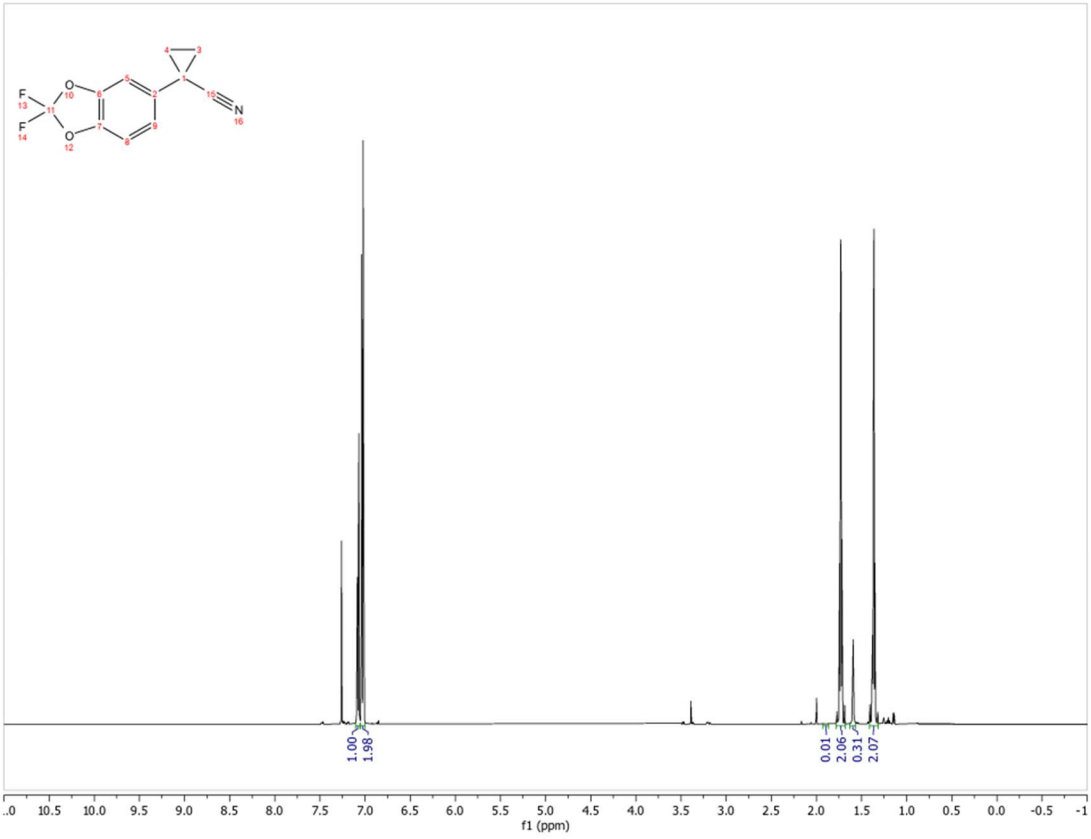
1.00
1.98
0.01
2.06
0.31
2.07
f1 (ppm)

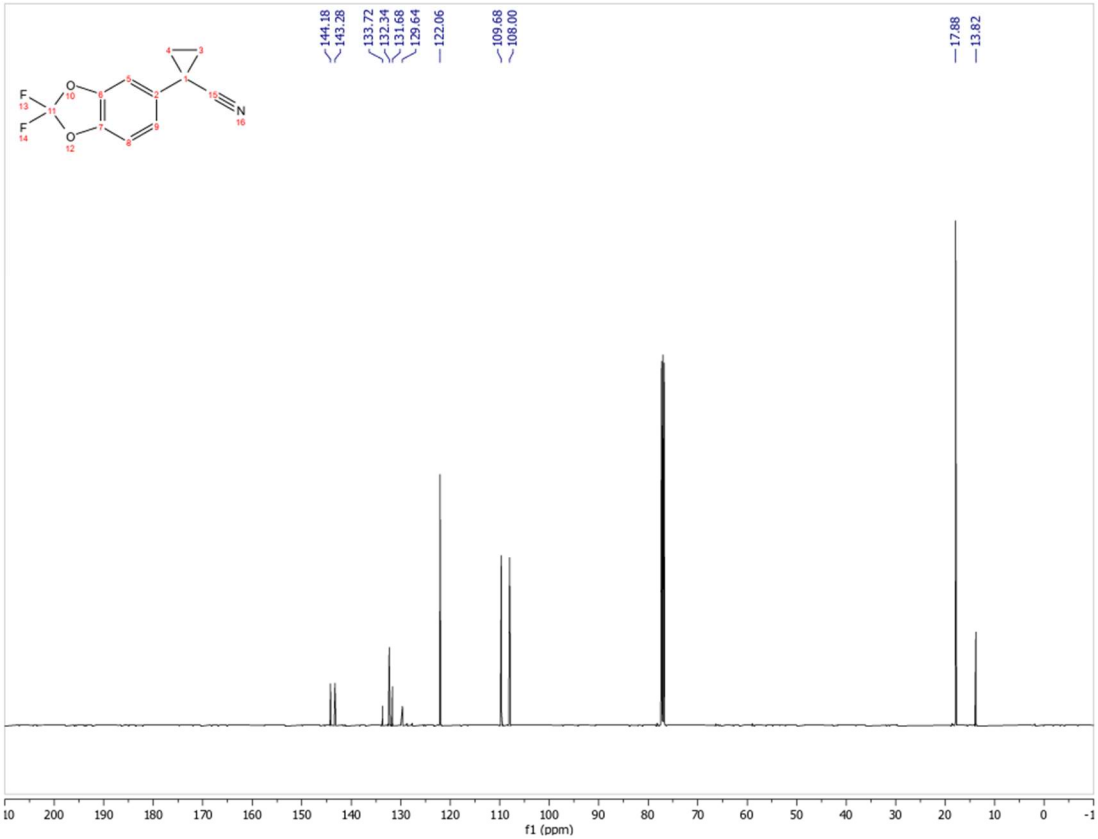
144.18
143.28
133.72
132.34
131.68
129.64
122.06
109.68
108.00
17.88
13.82
f1 (ppm)

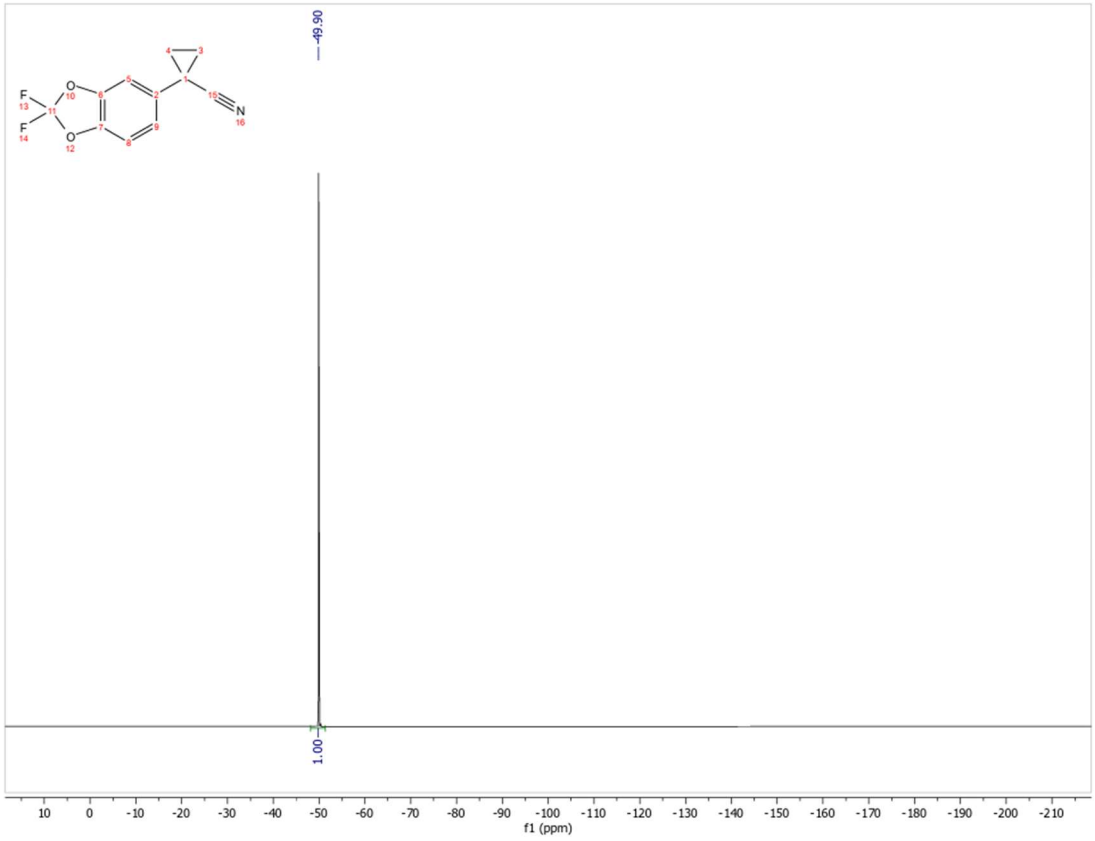
-49.90
1.00
10 0 -10 -20 -30 -40 -50 -60 -70 -80 -90 -100 -110 -120 -130 -140 -150 -160 -170 -180 -190 -200 -210
f1 (ppm)

(blank space)

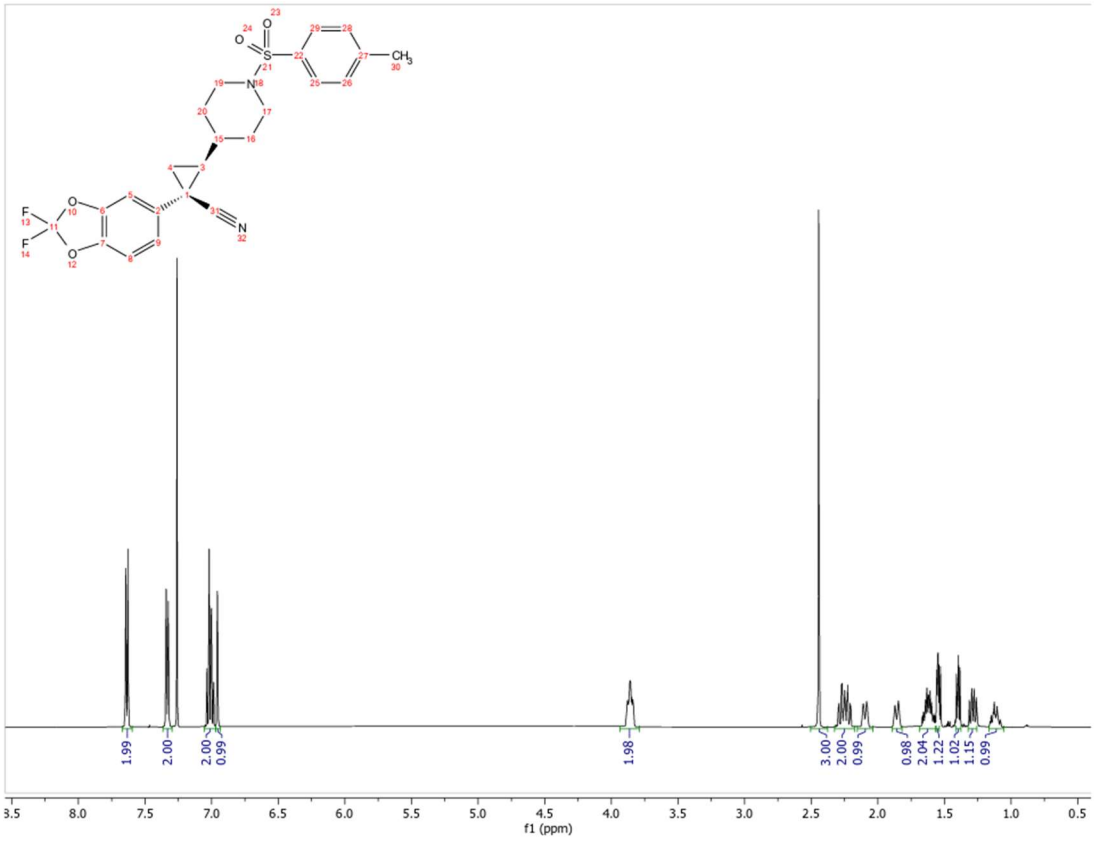
1.99
2.00
2.00
0.99
1.98
3.00
2.00
0.99
0.98
2.04
1.22
1.02
1.15
0.99
f1 (ppm)

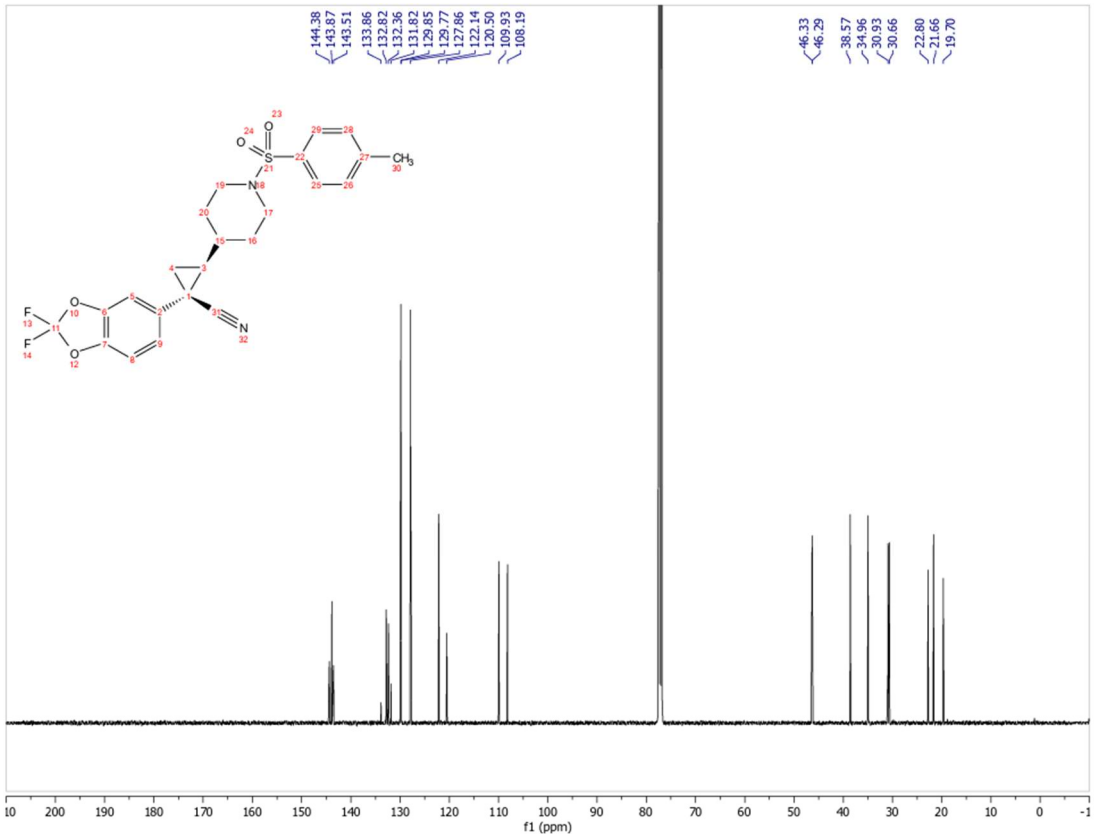
144.38
143.87
143.51
133.86
132.82
132.36
131.82
129.85
129.77
127.86
122.14
120.50
109.93
108.19
46.33
46.29
38.57
34.96
30.93
30.66
22.80
21.66
19.70
f1 (ppm)

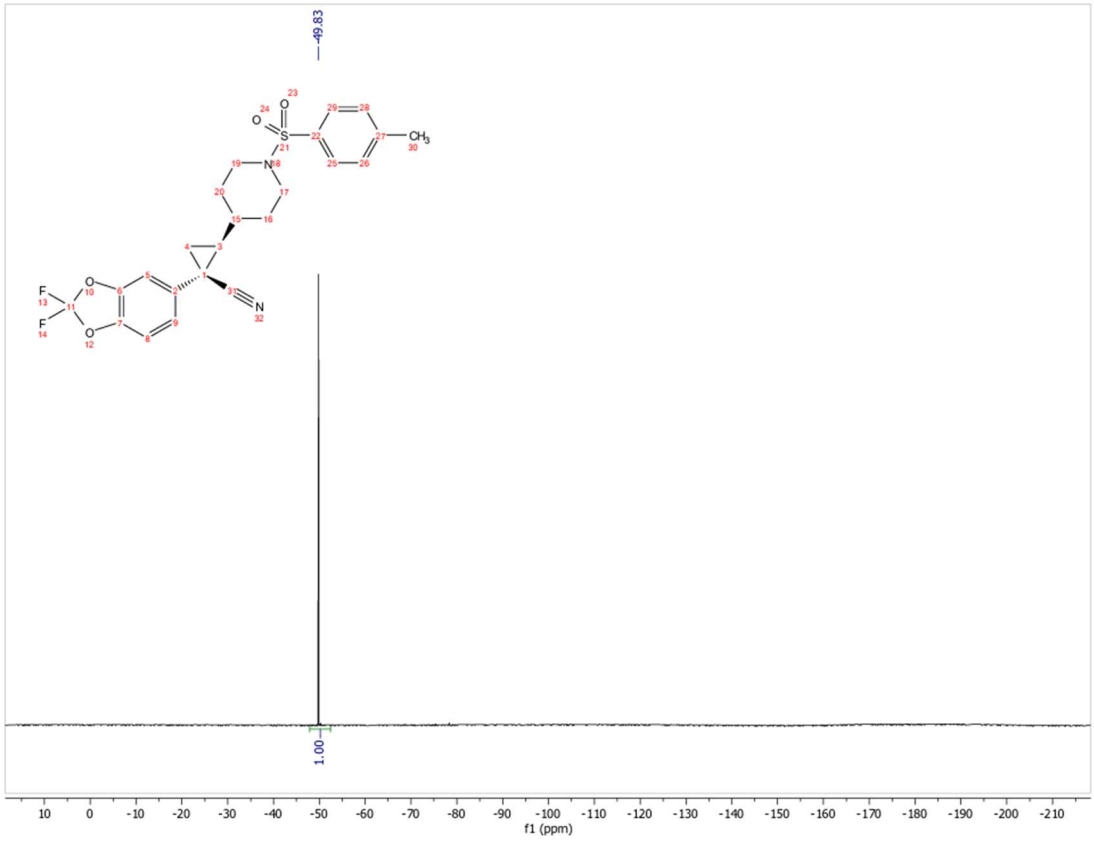
-49.83
1.00
10 0 -10 -20 -30 -40 -50 -60 -70 -80 -90 -100 -110 -120 -130 -140 -150 -160 -170 -180 -190 -200 -210
f1 (ppm)

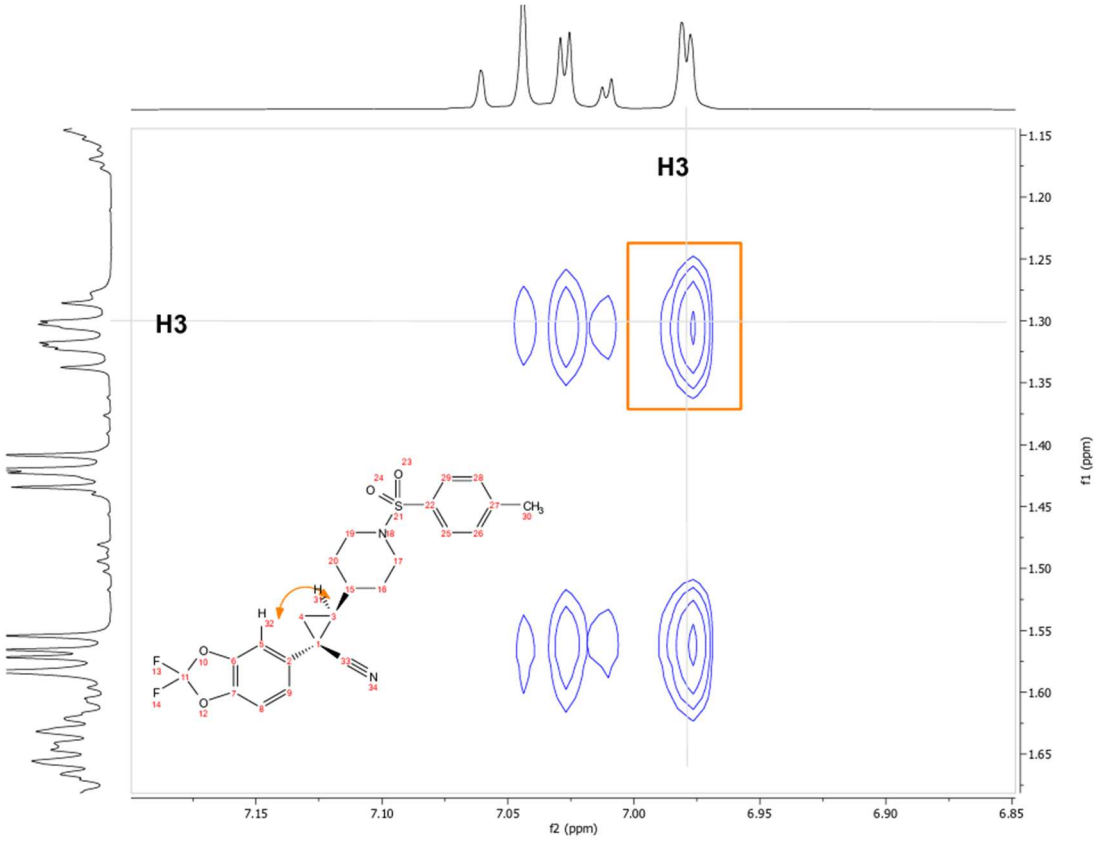
H3
H3
7.15 7.10 7.05 7.00 6.95 6.90 6.85
f2 (ppm)
1.15 1.20 1.25 1.30 1.35 1.40 1.45 1.50 1.55 1.60 1.65
f1 (ppm)

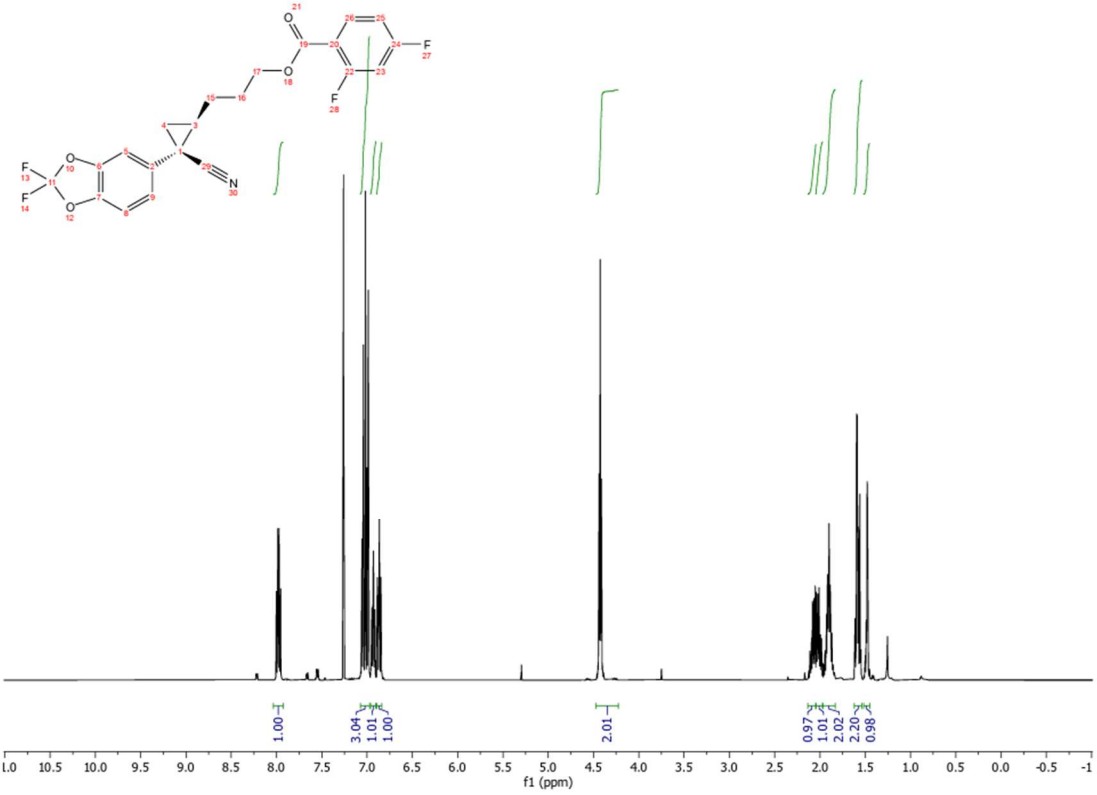
1.00
3.04
1.01
1.00
2.01
0.97
1.01
2.02
2.20
0.98
f1 (ppm)

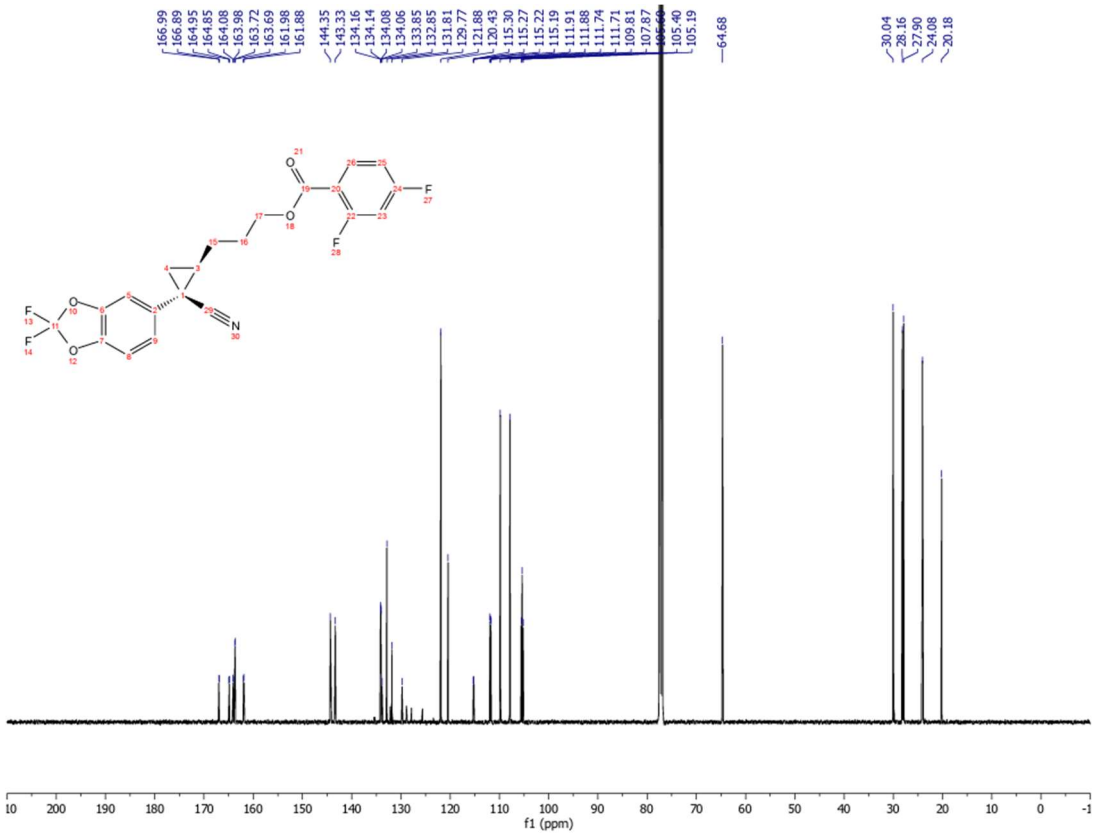
166.99
166.89
164.95
164.85
164.08
163.98
163.72
163.69
161.98
161.88
144.35
143.33
134.16
134.14
134.08
134.06
133.85
132.85
131.81
129.77
121.88
120.43
115.30
115.27
115.22
115.19
111.91
111.88
111.74
111.71
109.81
107.87
105.40
105.19
64.68
30.04
28.16
27.90
24.08
20.18
f1 (ppm)

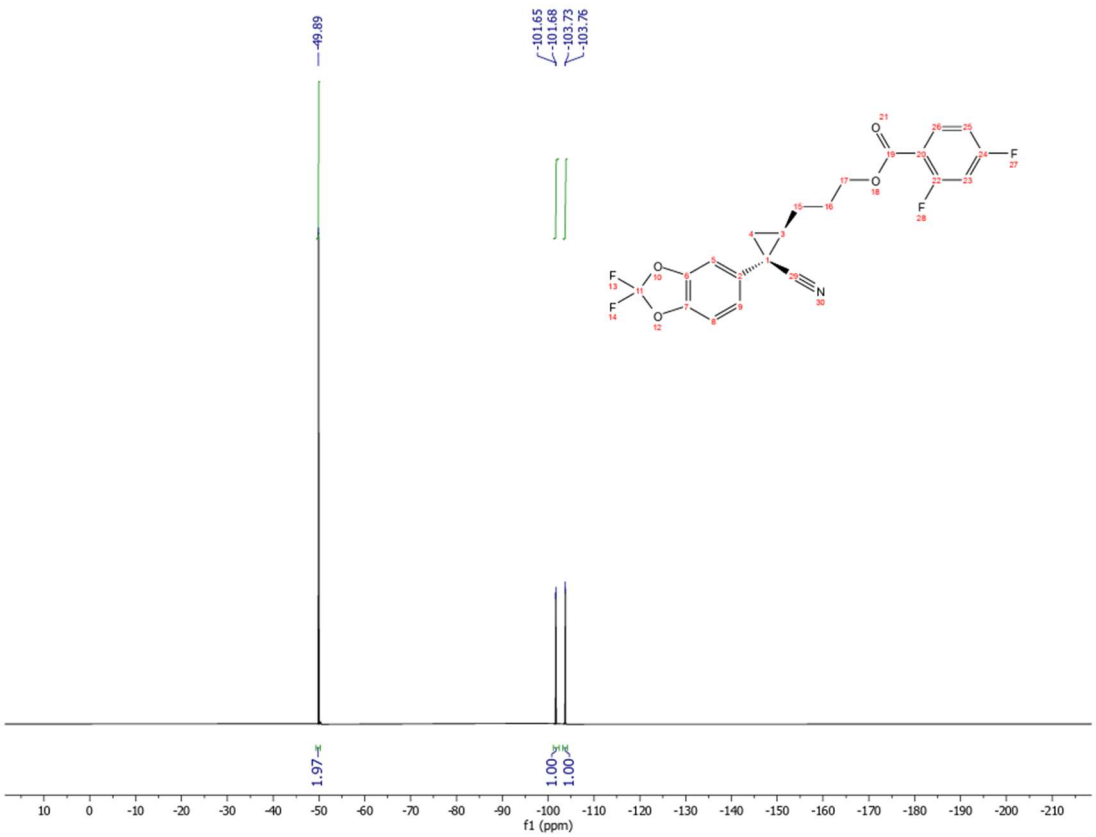

(blank space)

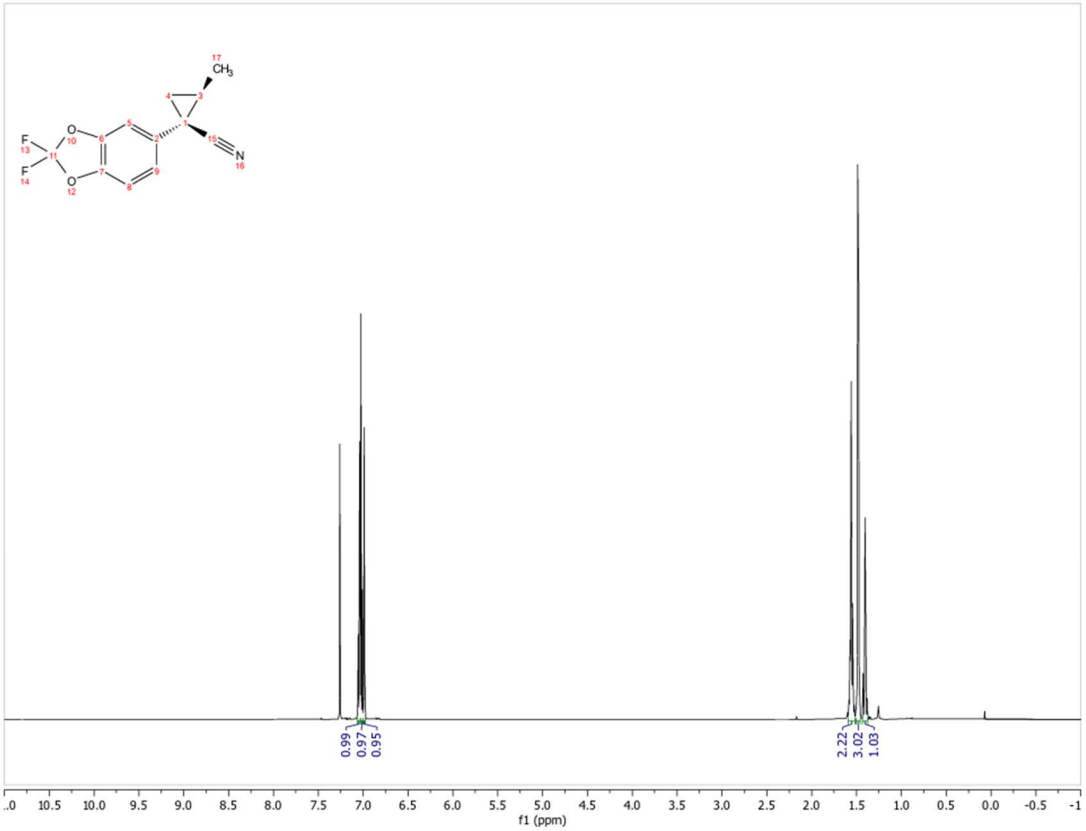
0.99
0.97
0.95
2.22
3.02
1.03
f1 (ppm)

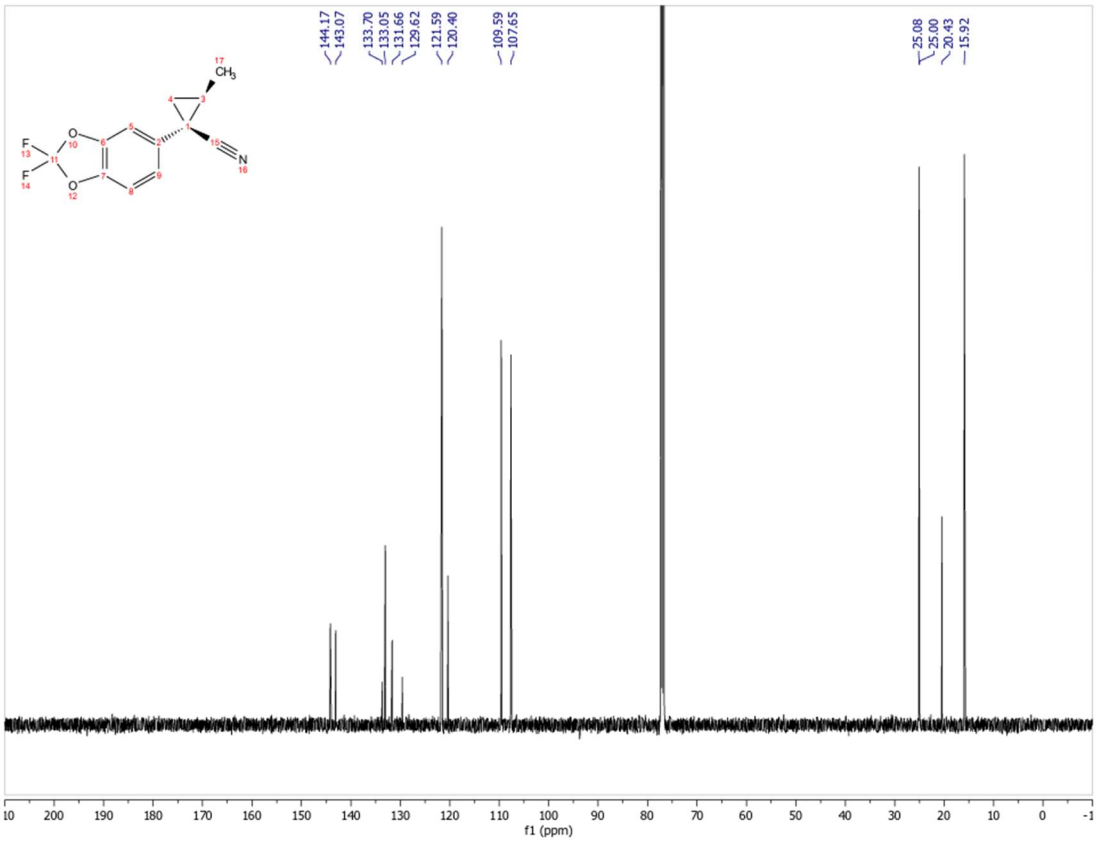
144.17
143.07
133.70
133.05
131.66
129.62
121.59
120.40
109.59
107.65
25.08
25.00
20.43
15.92
f1 (ppm)

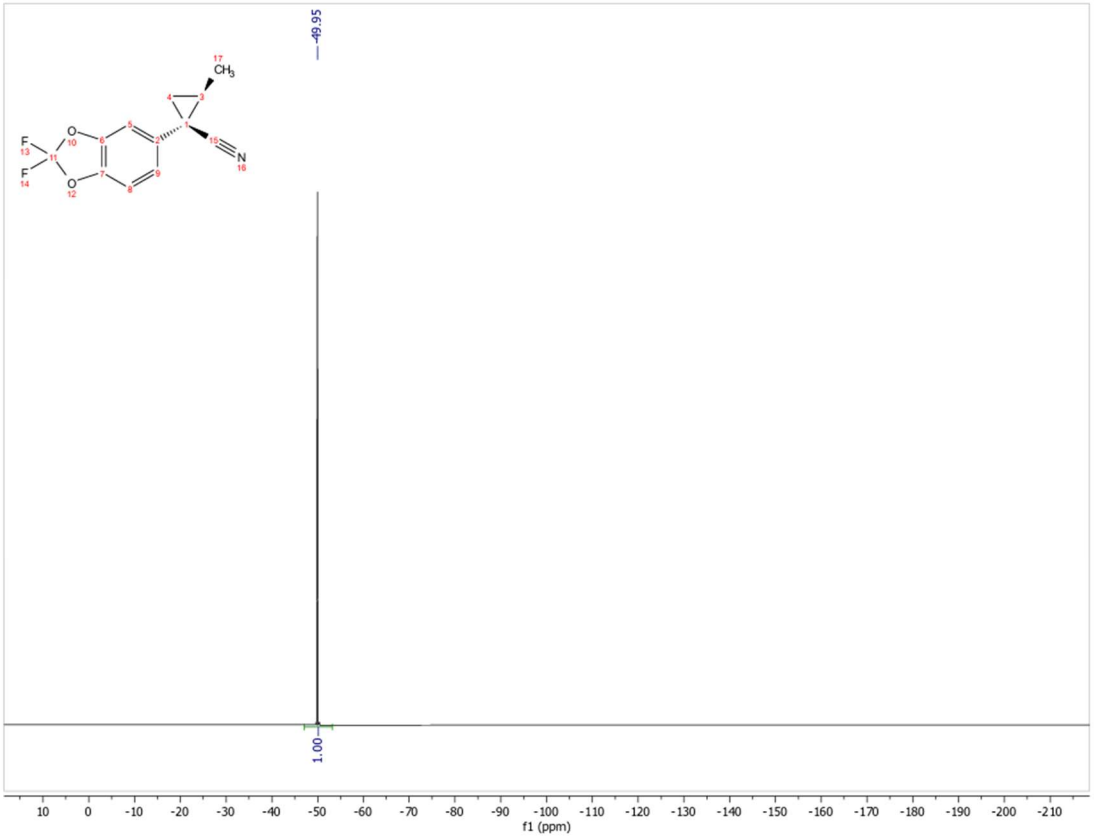
-49.95
1.00
10
0
-10
-20
-30
-40
-50
-60
-70
-80
-90
-100
-110
-120
-130
-140
-150
-160
-170
-180
-190
-200
-210
f1 (ppm)

Appendix F: Supporting Information for Chapter 7 (Electrochemical *Z*-selective C(sp^2)–H Functionalization of Alkenes)

F1. General Methods and Materials

Unless otherwise noted, reactions were performed under air in an anhydrous solvent. MeCN and *i*-Pr_2NEt were purchased as a sureseal bottle and used as is. KPF_6 was dried under vacuum prior to use. Unless otherwise noted, other commercially-available reagents were used as received. Crude mixtures were evaluated by thin-layer chromatography using EMD/Merck silica gel 60 F254 pre-coated plates (0.25 mm) and were visualized by UV, Seebach, ninhydrin, or KMnO4 staining. Flash chromatography was performed with a Biotage Isolera One automated chromatography system with re-packed silica columns (technical grade silica, pore size 60 Å, 230-400 mesh particle size, 40-63 particle size) or pre-packed Biotage Sfär Silica HC Duo 20µm 25g - High Capacity Column columns unless otherwise noted. Purified materials were dried in vacuo (0.050 Torr) to remove trace solvent. ^1H, ^{13}C, ^{19}F Spectra were taken using a Bruker Avance-400 with a BBFO Probe, a Bruker Avance-500 with a DCH Cryoprobe, or Bruker Avance III HD-500 with a TXO Cryoprobe. NMR data are reported relative to residual $CHCl_3$ (^1H, δ = 7.26 ppm), $CDCl_3$ (^{13}C, δ = 77.16 ppm) or residual CHD_2CN (^1H, δ = 1.96 ppm), CD_3CN (^{13}C, δ = 118.26 ppm). Data for ^1H NMR spectra are reported as follows: chemical shift (δ ppm) (multiplicity, coupling constant (Hz), integration). Multiplicity and qualifier abbreviations are as follows: s = singlet, d = doublet, t = triplet, q = quartet, m = multiplet, br = broad. All NMR yields were determined via reference against an internal standard (dibromomethane or mesitylene for ^1H). Mass spectrometry data was collected on a Thermo Scientific Q Exactive Plus Mass Spectrometer.

Abbreviations: Ac—acyl, Bn—benzyl, Cy—cyclohexyl, DCM—dichloromethane, DIPEA—*N,N*-diisopropylethylamine, DMAP—4-dimethylaminopyridine, DME—dimethoxyethane, DMF—dimethyl formamide, DMSO—dimethyl sulfoxide, EtOAc—ethyl acetate, HER—hydrogen evolution reaction, HFIP—hexafluoroisopropanol, H+ sponge—1,8-bis(dimethylamino)naphthalene, *i*-Pr—isopropyl, Me—methyl, MEK—methyl ethyl ketone, MeOH—methanol, MeCN—acetonitrile, NPhth—phthalimido, RVC—reticulated vitreous carbon, Ph—phenyl, TFA—trifluoroacetic acid, TFAA—trifluoroacetic acid anhydride, THF—tetrahydrofuran.

Electrochemical Methods and Materials

All chronoamperometric and chronopotentiometric measurements were performed at room temperature using a Pine WaveNowXV. Chronoamperometric and chronopotentiometric measurements were carried out in divided cells with RVC (8 × 6 × 6 mm, Ultramet, 80 ppi) as working electrodes affixed to a graphite pencil/silver wire assembly and with nickel foam (1.4 mm x 1.4 mm, MTI Corporation, Surface density: 350g/m^2) as counter electrodes affixed to stainless steel wire (see below). The potentials were measured versus an $Ag/AgNO_3$ (0.01 M in MeCN with 0.1 M n-Bu_4N•PF_6) reference electrode (all electrodes from Pine Research) and externally referenced via the ferrocene/ferrocenium couple. Bulk constant current electrolysis experiments were driven with a Dr. Meter HY3005M-L DC Power Supply or a custom–made low current power supply (see Scheme below) which was externally calibrated with a multimeter using a 10 or 1–Ohm resistor.

Divided cells were fabricated in-house. Glass frit purchased from Ace Glass (7176-36). Undivided cell was prepared using an anode electrode assembled via affixing end of the silver wire (Belden Hook-Up wire, item no. 83005 007100) around the pencil (JuneGold 2B graphite 2 mm) using conductive graphite adhesive (Alfa Aesar, 42465), wrapping in teflon tape to prevent exposure, then piercing RVC with pencil. Solvent exposed electrode surface area (2.1 cm^2) was calculated via manufacturer-supplied surface area/volume ratio measurements. PTFE tubing (Cole-Parmer; 1/32” ID, 1/16” OD, item number EW-06407-41) connects both sides of the divided cell to normalize pressure. Septa inner diameter 16 mm. Stainless steel purchased from Grainger; stainless steel lockwire, 0.025" diameter, item number 16Y043.

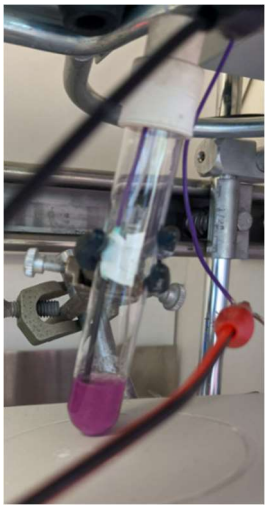

Figure F1. Undivided cell with submerged RVC and Ni foam electrodes.

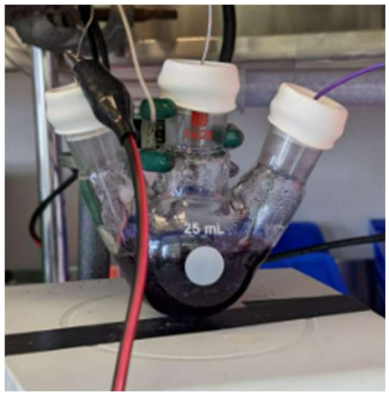

Figure F2. Undivided cell set-up for gaseous electrolysis.

Figure F3. Divided cell electrolysis for dicationic adducts studies.

Low-current Power Supply: Original design and fabrication by Dr. Blaise J. Thompson. Provides an operational range of ±0.01– 14.99 mA, tunable by variable resistor, delivering power to banana socket pair. The power supply is limited to ±15 V for bulk electrolysis and is powered by an 18 V wall wart. Circuitry is housed within an aluminum enclosure. For additional specifications, see: *J. Am. Chem. Soc.* **2020** 142, 2093–2099 and *Nature* **2021** 596, 74–79.

F2. Development of Undivided Cell Electrolysis

General Procedure for Undivided Electrolysis Studies

Limiting thianthrene with gaseous alkenes:
To an oven-dried 25-mL three-neck flask equipped with a magnetic stir bar was added KPF_6 (552 g, 3.0 mmol, 3.0 equiv) to the undivided cell. The side necks were equipped with two septa containing a stainless-steel wire/Ni foam cathode assembly (2.9 x 1.6 cm) and a pencil/RVC anode assembly (1.6 x 0.6 x 0.7 cm). MeCN (10 mL) was added to the flask and sparged with a balloon of gaseous alkene for 10 min. Thianthrene (216 mg, 1.0 mmol, 1.0 equiv.) was added, followed by trifluoroacetic acid (0.77 mL, 10.0 mmol, 10.0 equiv.) and trifluoroacetic anhydride (0.2 mL, 2% v/v, 1.0 mmol, 1.0 equiv.) and the solution was stirred and electrolyzed under a constant current of 84 mA for 3.75 h (11.8 F/mol). The electrolysis was visually monitored until the solution turned from deep purple to light red. At completion of electrolysis, the electrode leads were disconnected, septa removed, and the anode RVC was pushed off the pencil into the reaction mixture. Dibromomethane was added as an internal standard to the anodic compartment. The solution was thoroughly stirred, and 50 µL of mixture was added to an NMR tube and diluted with MeCN-d_3.

Limiting alkene:
To an oven-dried 16 x 100 mm fraction tube equipped with magnetic stir bars was added thianthrene (86.5 mg, 0.4 mmol, 2.0 equiv) and dried KPF_6 (110 mg, 0.6 mmol, 3.0 equiv.). The cell was equipped with a septum containing a stainless-steel wire/Ni foam cathode assembly (7 x 8 mm) and a pencil/RVC anode assembly (9 × 3 × 3 mm) connected together with a teflon-wrapped, hollowed 1mL syringe body to prevent the electrodes from making contact (electrode depth: 1 cm, electrode distance 0.5 cm). The cell was placed under active N_2 atmosphere and degassed MeCN (2 mL) was added. Alkene (0.2 mmol, 1.0 equiv.) was added to the undivided cell followed by trifluoroacetic acid (153 µL, 2.0 mmol, 10.0 equiv.) and trifluoroacetic anhydride (40 µL, 2% v/v, 0.3 mmol, 1.4 equiv.). The cell were stirred at ambient temperature and electrolyzed under a constant current of 7.4 mA for 17 h (23.5 F/mol alkene). At completion of electrolysis, the electrode leads were disconnected, septa removed, and the anode RVC was pushed off the pencil into the reaction mixture. Dibromomethane was added as an internal standard to the anodic compartment. The solution was thoroughly stirred, and 50 µL of mixture was added to an NMR tube and diluted with MeCN-d_3.

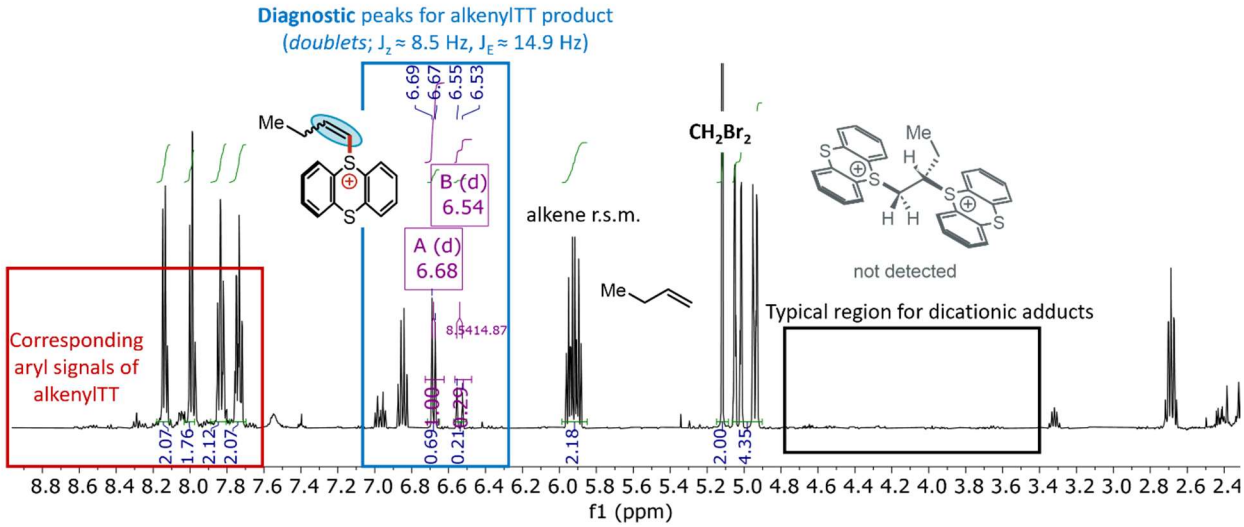

Figure F4. Example of ^{1}H NMR spectrum collected after undivided cell electrolysis to prepare alkenylthianthrenium salts with *Z*-selectivity. CH_2Br_2 (5.10 ppm, s, 2H) was used as a ^{1}H NMR standard. r.s.m. = recovered starting material.

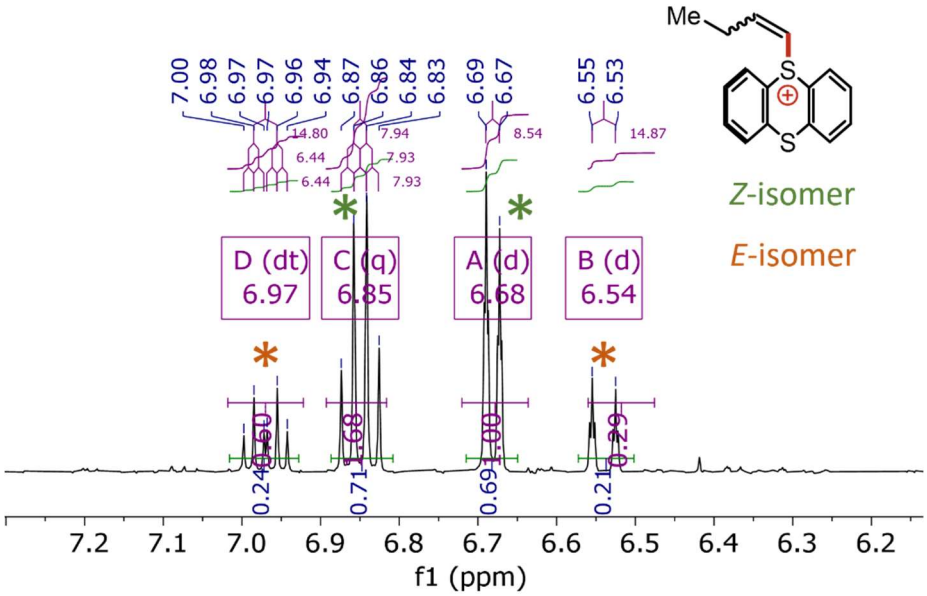

Figure F5. Coupling constant analysis of ^{1}H NMR alkenyl signals of alkenylthianthrenium salts to assign the *Z*- and *E*-isomers.

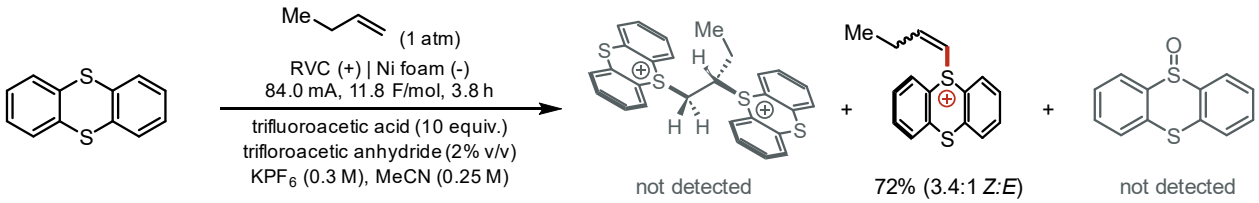

Figure F6. Initial undivided cell reactivity for *in situ* dicationic adduct formation and elimination to afford alkenylthianthrenium salts. *Z*-selectivity was observed for gaseous 1-butene derived alkenylTT salt.

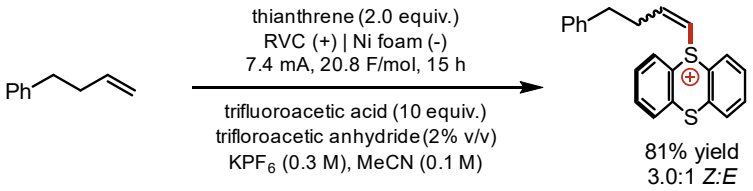

Table F1. Translation of undivided cell reactivity and Z-selectivity to limiting alkene electrolysis conditions.

entry	variation	alkenylTT (%)	*Z:E*	alkene r.s.m. (%)
1	none	81	3.0:1	8
2	"fast" electrolysis 18 mA, 21.3 F/mol (6.6 h)	81	2.9:1	10
3	2.7 V constant cell potential (15 h)	77	2.9:1	13
4	No TFAA	63	3.1:1	31

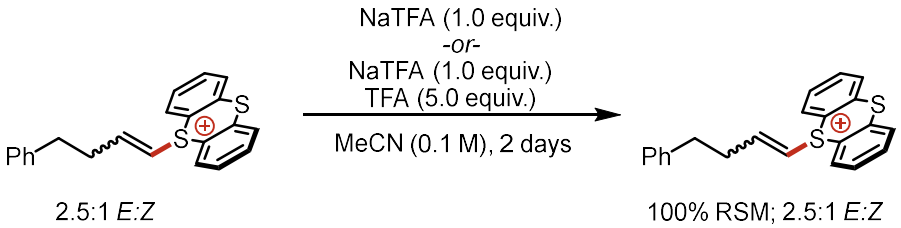

Figure F7. Trifluoroacetate base does not isomerize or react with alkenylthianthrenium salt. This anion is the electrogenerated base in undivided cell electrolysis. RSM = recovered starting material.

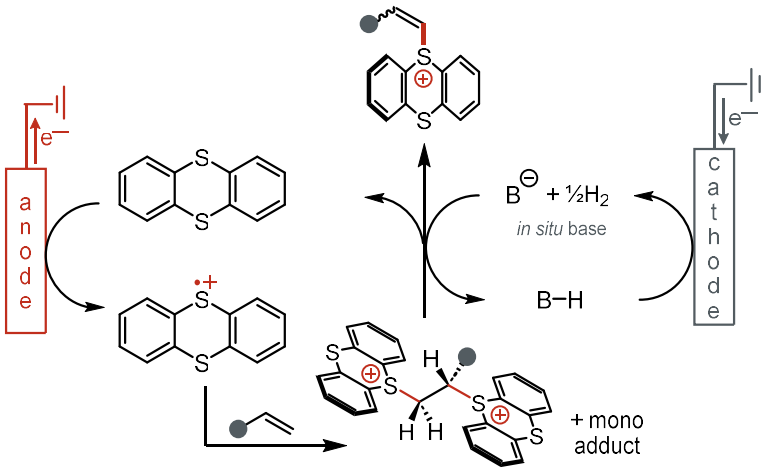

Figure F8. Proposed mechanism for alkenylthianthrenium salt formation in an undivided cell. Anodic oxidation of thianthrene leads to dicationic adduct formation with alkene substrate. Cathodic HER of TFA generates trifluoroacetate which acts as an electrogenerated base to eliminate adducts *in situ*, generating alkenylTT salt with observed *Z*-selectivity. Unlike divided cell electrolysis, undivided cell enables Z-selective preparation of alkenylTT salts through the liberation of thianthrene from *bis*-adduct deprotonation and cathodic reduction of oxidized thianthrenium species, both of which keep neutral thianthrene concentration high to promote selective *bis*-adduct formation via radical pathways.

F3. Dicationic Adduct Elimination Studies

General Procedure for Dicationic Adduct Pool Studies

To an oven-dried divided electrochemical cell equipped with magnetic stir bars was added thianthrene (64.9 mg, 0.3 mmol, 3.0 equiv) to the anode compartment and KPF_6 (110 mg, 0.6 mmol) to both compartments. The cell was equipped with two septa containing a stainless steel wire/Ni foam cathode assembly and a pencil/RVC anode assembly connected together with a teflon tubing to equalize pressure. MeCN (2 mL) was added to the cathode and anode compartments. Alkene (0.2 mmol, 2.0 equiv) was added to the anode compartment. Trifluoroacetic acid (153 µL, 2.0 mmol, 20.0 equiv) was added to the cathode compartment and both sides of the cell were stirred at 30 °C and electrolyzed under a constant current of 6.0 mA (5.8 mA/cm^2) for 2.2 h (2.5 F/mol alkene). At completion of electrolysis, the electrode leads were disconnected, septa removed, and the anode RVC was pushed off the pencil into the reaction mixture. Dibromomethane was added as an internal standard to the anodic compartment. The solution was thoroughly stirred, and 50 µL of mixture was added to an NMR tube and diluted with MeCN-*d3*. The dicationic adduct yield and *mono:bis* were determined *via* ^{1}H NMR using dibromomethane as an external standard.

To a threaded vial equipped with a magnetic stir bar was added 1 mL of the dicationic adduct solution followed by sodium trifluoroacetate (54 mg, 0.4 mmol, 4.0 equiv.). Rapid quenching of purple thianthrene radical cation was observed upon addition of base and an NMR sample was prepared within a minute of the quench. NMR samples were prepared by diluting an aliquot of the reaction solution in CD_3CN or $CDCl_3$ and the alkenylthianthrenium salt yield and *E:Z* were determined *via* ^1H NMR using dibromomethane as an internal standard.

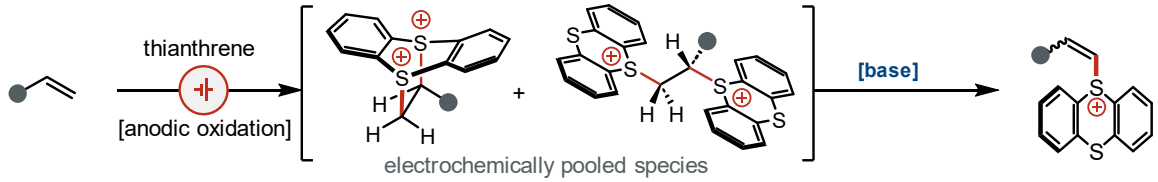

Figure F9. General reaction flow for *mono-* and *bis-* dicationic adduct generation studies and subsequent addition of base for adduct elimination to alkenylthianthrenium salts with *E:Z* stereochemistry.

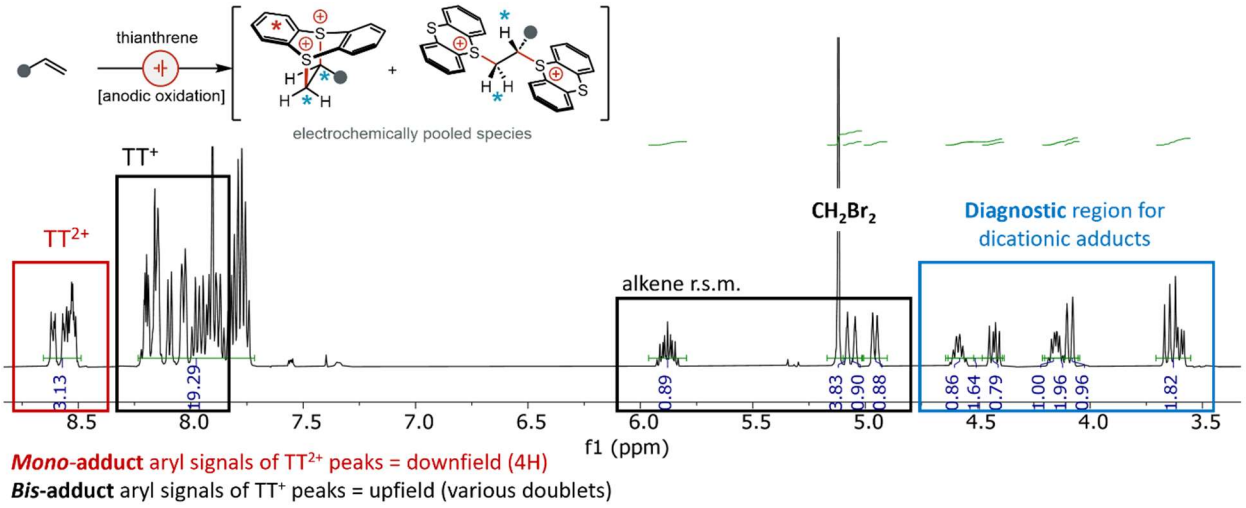

Figure F10. Example of ^1H NMR spectrum collected after divided cell electrolysis to prepare *mono-* and *bis*-dicationic adducts between thianthrene and alkene substrate. CH_2Br_2 (5.10 ppm, s, 2H) was used as a ^1H NMR standard. r.s.m. = recovered starting material.

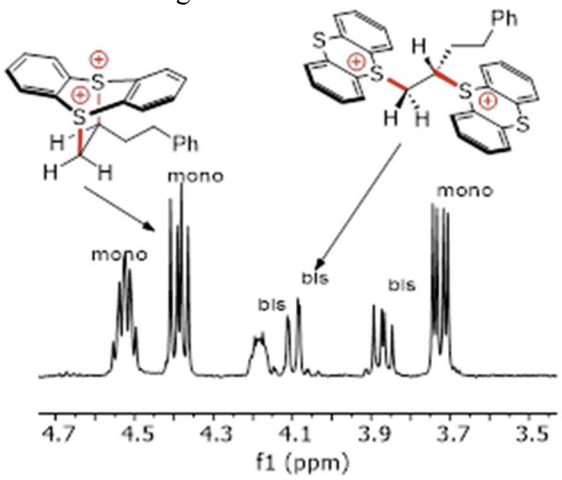

Figure F11. Analysis of ^1H NMR alkyl sulfonium signals of dicationic adducts to assign the *mono-* and *bis*-adducts. Each peak in this 3.5 to 4.8 ppm region corresponds to 1H, where each adduct has 3H alkylthianthrenium signals in total. If possible, these signals are correlated to the aryl region >8.5 ppm to support the assignment of the *mono*-adduct. See Figure F10 above.

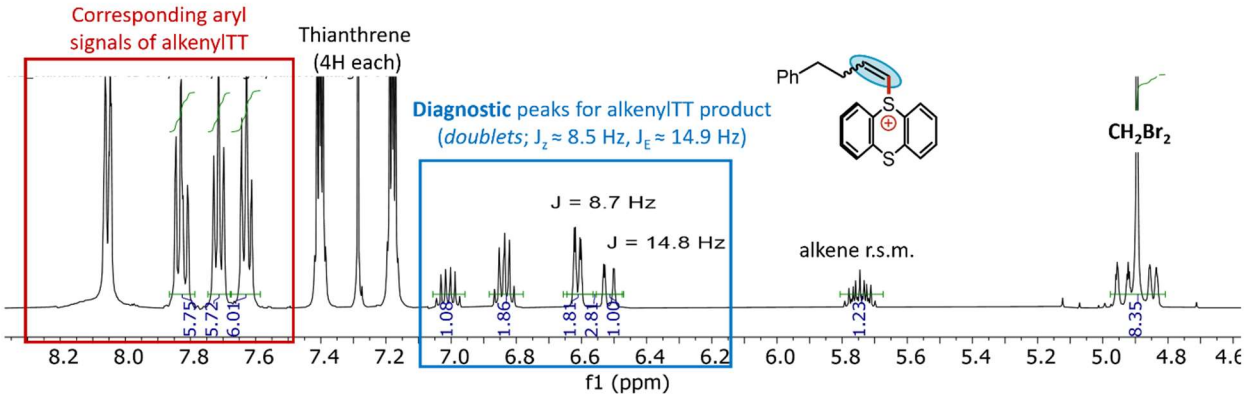

Figure F12. Example of ^{1}H NMR spectrum collected after base addition to quench *mono*- and *bis*-dicationic adducts electrogenerated from thianthrene and alkene substrate in divided cell electrolysis. The result is elimination to alkenylthianthrenium salt with a mixture of *E*- and *Z*-stereochemistry. CH_2Br_2 (5.10 ppm, s, 2H) was used as a ^{1}H NMR standard. r.s.m. = recovered starting material.

F3.1. Solvent Screen for Z-selectivity of *Bis*-adduct Elimination

For solvent screen experiments, dicationic adducts were prepared according to the general procedure for divided cell electrolysis with the corresponding sulfur heterocycle. Then the resultant electrochemical solution was transferred into separate vials (1 mL, 0.1 M) and concentrated *in vacuo*. When all the MeCN solvent was removed based on visual inspection, the crude residue was re-dissolved in 1 mL of the specific solvent and NaTFA base was added. For thianthrene-based adducts, the *bis*-adduct *Z*-selectivity was calculated assuming ≥20:1 *E:Z* of alkenylthianthrenium derived from the *mono*-adduct elimination. See *Angewandte Chemie International Edition* **2020**, 59, 5616–5620.

Table F2. Solvent screen data for thianthrene-based dicationic adducts.

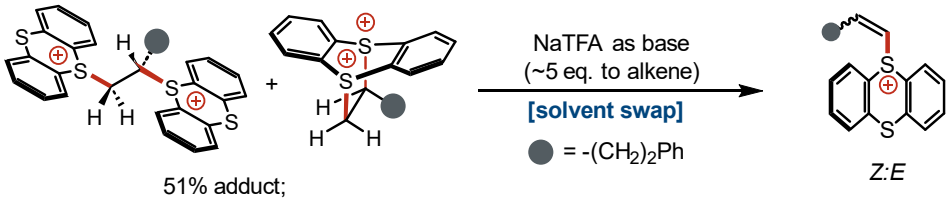

solvent	*Z:E*	calc' bis *Z*-selectivity	solvent	*Z:E*	calc' bis *Z*-selectivity
diMeCarbonate	71:29	≥20:1 *Z:E*	MeCN	68:32	≥20:1 *Z:E*
THF	66:34	≥20:1 *Z:E*	$MeNO_2$	66:34	≥20:1 *Z:E*
DCM*	only Z detected*	≥20:1 *Z:E*	MEK	68:32	≥20:1 *Z:E*
5:1 DCM*:MeCN	69:31	≥20:1 *Z:E*	DMF	69:31	≥20:1 *Z:E*
MeOH	68:32	≥20:1 *Z:E*	PhCN	73:27	≥20:1 *Z:E*

*note that NaTFA & dicationic adducts insoluble

Generally the *bis:mono* translates to *Z:E*, suggesting that *bis*-adduct elimination *Z*-selectivity seems high across solvents for thianthrenium salts. Sometimes, the *Z*-isomer ratio is notably higher (>5% out of 100) than *bis*-adduct max (PhCN & dimethyl carbonate), suggesting that *mono*-adduct may be less *E*-selective (6:1 to 9:1 E:Z) in these solvents. Other sources of errors for the increased %Z such as analytical, or slightly different solubilities of *Z*- and *E*-alkenylTT cannot be excluded.

Table F3. Solvent screen data for phenoxathiin-based dicationic adducts.

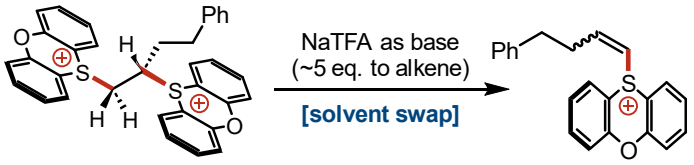

solvent	Z:E	solvent	Z:E
diMeCarbonate	3.2 : 1	MeCN	1.9 : 1
THF	2.4 : 1	PhNO2	1.9 : 1
DME	2.4 : 1	MeNO2	1.7 : 1
9:1 PhCl:MeCN	2.4 : 1	MEK	1.6 : 1
DCM	2.1 : 1	DMF	1.6 : 1
chloroform*	2.0-2.4 : 1*	PhCN	1.4 : 1
MeOH	2.1 : 1	DMSO	1.4 : 1
		HFIP	1.4 : 1

*signal intensity low, solubility issues?

F3.2. Base Screen for Z-selectivity of 1-Butene-Dervied Dicationic Adducts Elimination

For base screen experiments, electrogenerated dicationic adducts (mixture of *mono*- and bis-species) were prepared using 1-butene gas. For literature procedure, see *J. Am. Chem. Soc.* **2021**, 143, 51, 21503–21510. Exclusive *mono*-adduct was prepared by thianthrene S-oxide activation in the presence of 1-butene alkene substrate. For literature procedure, see *J. Am. Chem. Soc.* **2021**, 143, 33, 12992–12998. Then the resultant adduct solutions were transferred into separate vials (1 mL, 0.1 M) and the specified base was added.

Table F4. Base screen data for quenching of electrogenerated 1-butene-derived dicationic adducts.

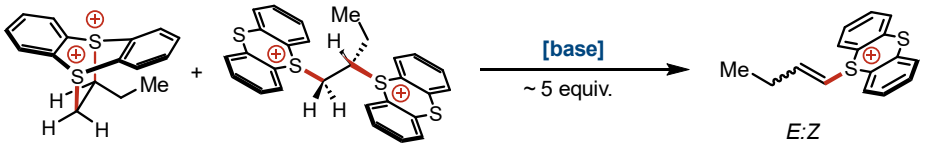

generated *via* electrolysis
1.4:1 *m:b*

Cs_2CO_3	K_2CO_3	K_2PO_4	Al quench	KOH	$NaHCO_3$
3.6:1 *E:Z*	2.4:1 *E:Z*	2.2:1 *E:Z*	4.0:1 *E:Z*	1.4:1 *E:Z*	1.3:1 *E:Z*

$NaHCO_3$ (aq)	*i*-Pr_2NEt	pyridine	2,6-lutidine	DMAP	H^+ sponge
1.2:1 *E:Z*	1.5:1 *E:Z*	1.5:1 *E:Z*	1.4:1 *E:Z*	2.6:1 *E:Z*	1.5:1 *E:Z*

85% half adduct

Table F5. Base screen data for quenching of S-oxide prepared 1-butene-derived *mono*-adduct.

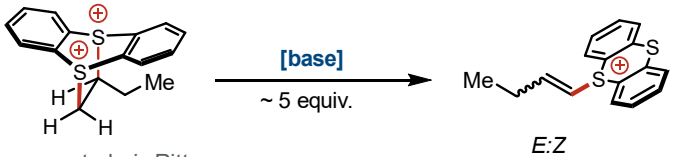

generated *via* Ritter
only *mono* detected

$NaHCO_3$ (aq)	*i*-Pr_2NEt	pyridine	H^+ sponge
≥20:1 *E:Z*	≥20:1 *E:Z*	≥20:1 *E:Z*	5.7:1 *E:Z*

Mono-adduct elimination appears to be highly *E*-selective. Curiously, the apparent selectivity of the elimination step is dependent on the identity of the base. Adducts *mono:bis* ratio typically translate to the alkenylthianthrenium species *E:Z* ratio when using weaker bases for the elimination whereas erosion of *Z*-selectivity was observed with stronger bases such as carbonate. This could be a consequence of either (1) changing the stereoselectivity of the elimination step, or (2) isomerization of *Z*-isomer to *E*-isomer via reversible conjugate addition of nucleophilic bases. More mechanistic experiments will need to be conducted to distinguish the two possibilities. Out studies show with *i*-Pr_2NEt base, the stereoselectivity of the *mono:bis* elimination occurs with high fidelity to the *E:Z* of the alkenylTT, and that this hindered trialkylamine base does not isomerze the alkenylTT.

F3.3. Dicationic Adduct Interconversion and Elimination Time Courses

For adduct time course studies, dicationic adducts were prepared using the general procedure for divided cell electrolysis. Adduct conversion was monitored by taking an aliquot of the solution to prepare an NMR sample at the specific time point. For the *in situ* quenching to alkenylthianthrenium salts, the adduct solution was electrolyzed in CD_3CN. Then 0.5 mL of the solution was transferred to an NMR tube. After acquiring a ^1H NMR spectrum of the meta-stable adducts, solid NaTFA (approx 20 mg) was added to the NMR sampel. Spectra were immediately collected approx. every 10-15 s using the following ^1H NMR parameters: 1 scan, 1 s relaxation delay.

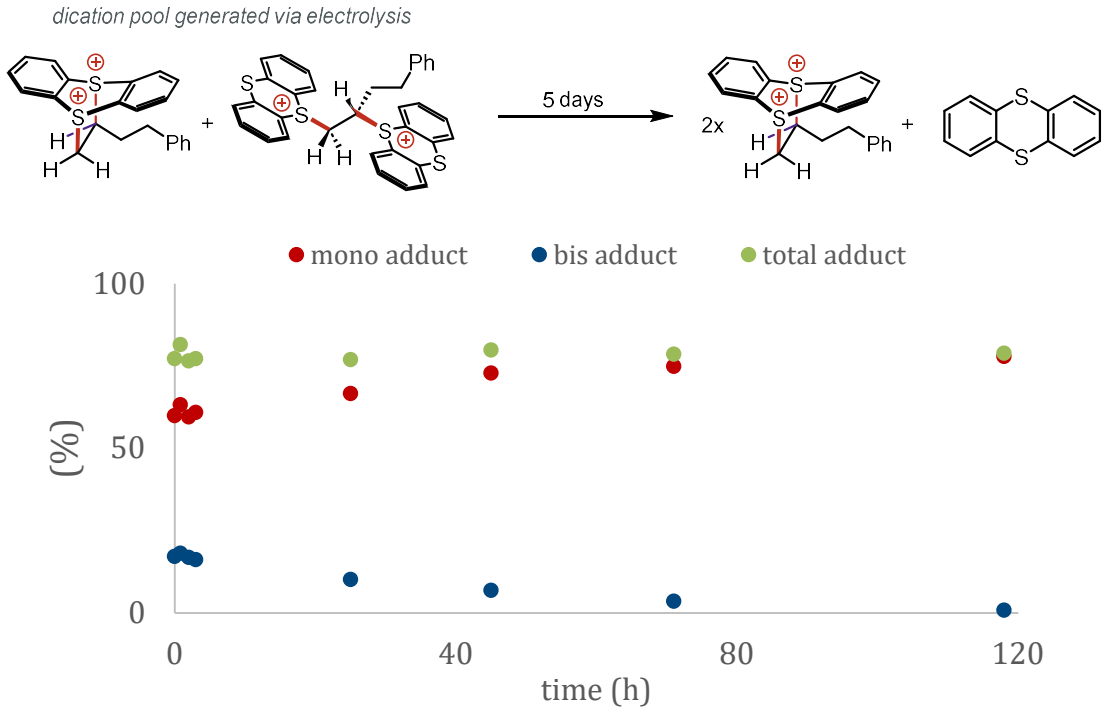

Figure F13. While *bis*-adduct converts quantitatively to *mono*-adduct over extended period (several days), minimal interconversion within 3 hours. The origin of this interconversion is not fully understood. Light promoted interconversion has been excluded since this *bis*- to *mono*-adduct conversion is still observed when the solution is kept in the dark, and the rate is minimally impacted when the solution is intentionally irradiated. Two alternative potential explanations include (1) the formation of *mono*-adduct is thermodynamically favorable, or (2) insolubility of thianthrene drives the equilibrium to favor *mono*-adduct formation.

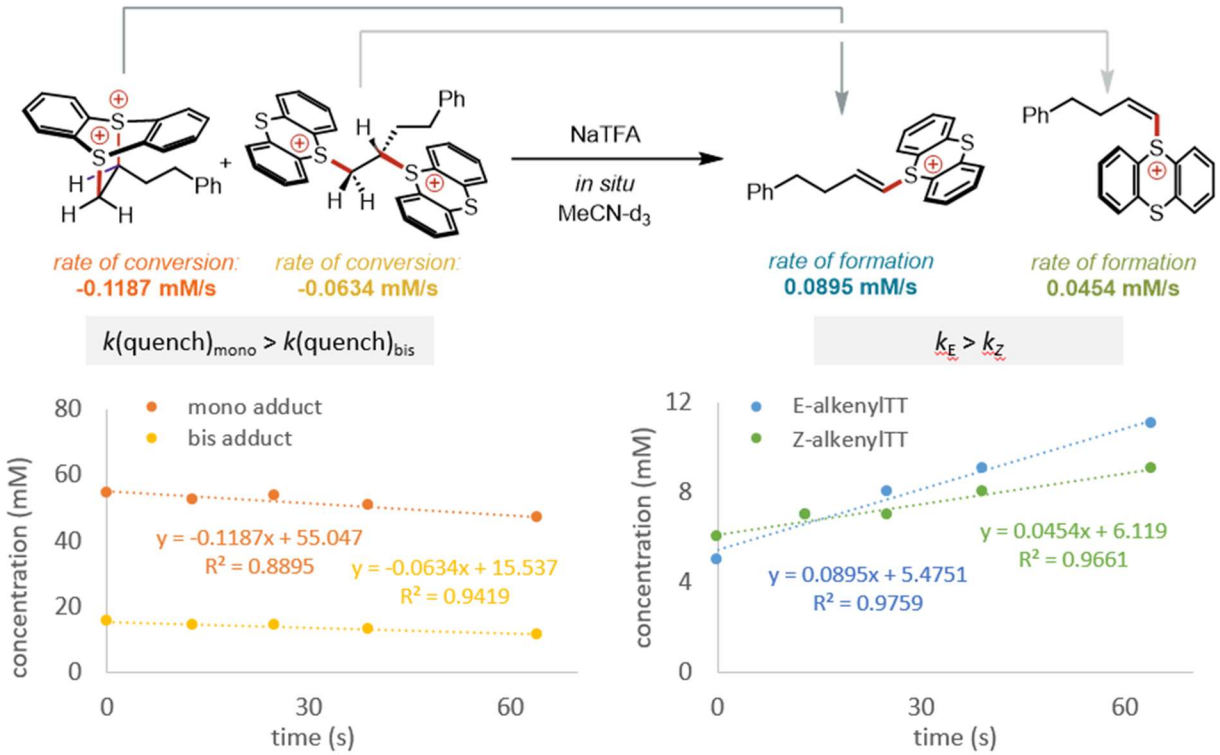

Figure F14. Dicationic adduct quenching with trifluoroacetate is fast. Qualitatively, *mono*-adduct appears to quench at a slightly faster rate than *bis*-adduct. The formation of *E*-alkenylTT salt is slightly faster than that of *Z*-alkenylTT salt. These data are consistent with *mono*-adduct eliminating with *E*-selectivity and *bis*-adduct eliminating with *Z*-selectivity.

F3.4. Evaluation of Sulfonium Activating Group Structures

Thianthrene derivatives were prepared according to literature procedures. All ^{1}H NMR were consistent with reported spectra for the isolated compounds.

Dicationic adducts with thianthrene derivatives were generated according to the general procedure for divided cell electrolysis with the specified modification: alkene concentration was 0.05 M instead of 0.1 M, and *i*-Pr$_2$NEt base (8 equiv. to alkene) was used instead of NaTFA. We have observed that this sterically hindered trialkylamine base does not impact the *mono:bis* to *E:Z* conversion of 1-butene derived adducts. The dicationic adducts and alkenylsulfonium salts of thianthrene derivatives were assigned by analogy to those of parent thianthrene using ^{1}H NMR spectroscopy, described in Figures 10–12.

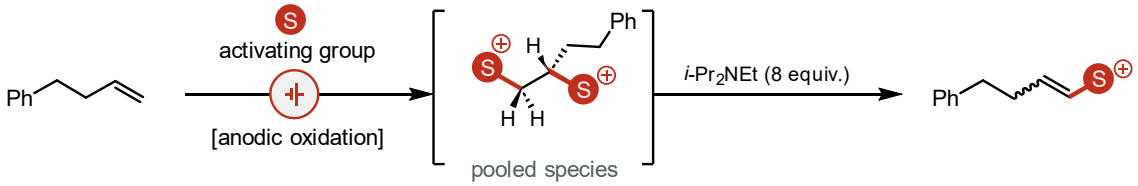

Figure F15. General reaction flow for *mono*- and *bis*- dicationic adduct generation studies and subsequent addition of base for adduct elimination to alkenylsulfonium salts with *E:Z* stereochemistry.

Characterization of Z-Alkenylthianthrenium Salt 7.6

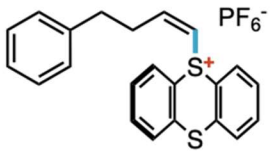

(*Z*)-5-(4-phenylbut-1-en-1-yl)-5*H*-thianthren-5-ium hexafluorophosphate (**7.6**): ^{1}H-NMR (500 MHz, CD_3CN) δ 7.95 (dd, J = 7.95, 1.26 Hz, 2H), 7.84 (dd, J = 7.97, 1.32 Hz, 2H), 7.80 (td, J = 7.70, 1.37 Hz, 2H), 7.67 (td, J = 7.73, 1.29 Hz, 2H), 7.35 – 7.24 (m, 5H), 6.92 (dt, J = 8.66, 7.83 Hz, 1H), 6.72 (dt, J = 8.58, 1.36 Hz, 1H), 3.03 (m, 2H), 2.88 (t, J = 7.01 Hz, 2H). ^{13}C-NMR (125 MHz, CD_3CN) δ 155.42, 140.49, 135.80, 134.86, 132.62, 131.10, 130.55, 129.30, 129.28, 127.21, 121.65, 112.42, 33.84, 32.62. ^{19}F-NMR (500 MHz, CD_3CN) δ -72.85 (d, J = 706.59, 6F). ^{31}P-NMR (500 MHz, CD_3CN) δ -144.61 (hept, J = 706.56, 1P).

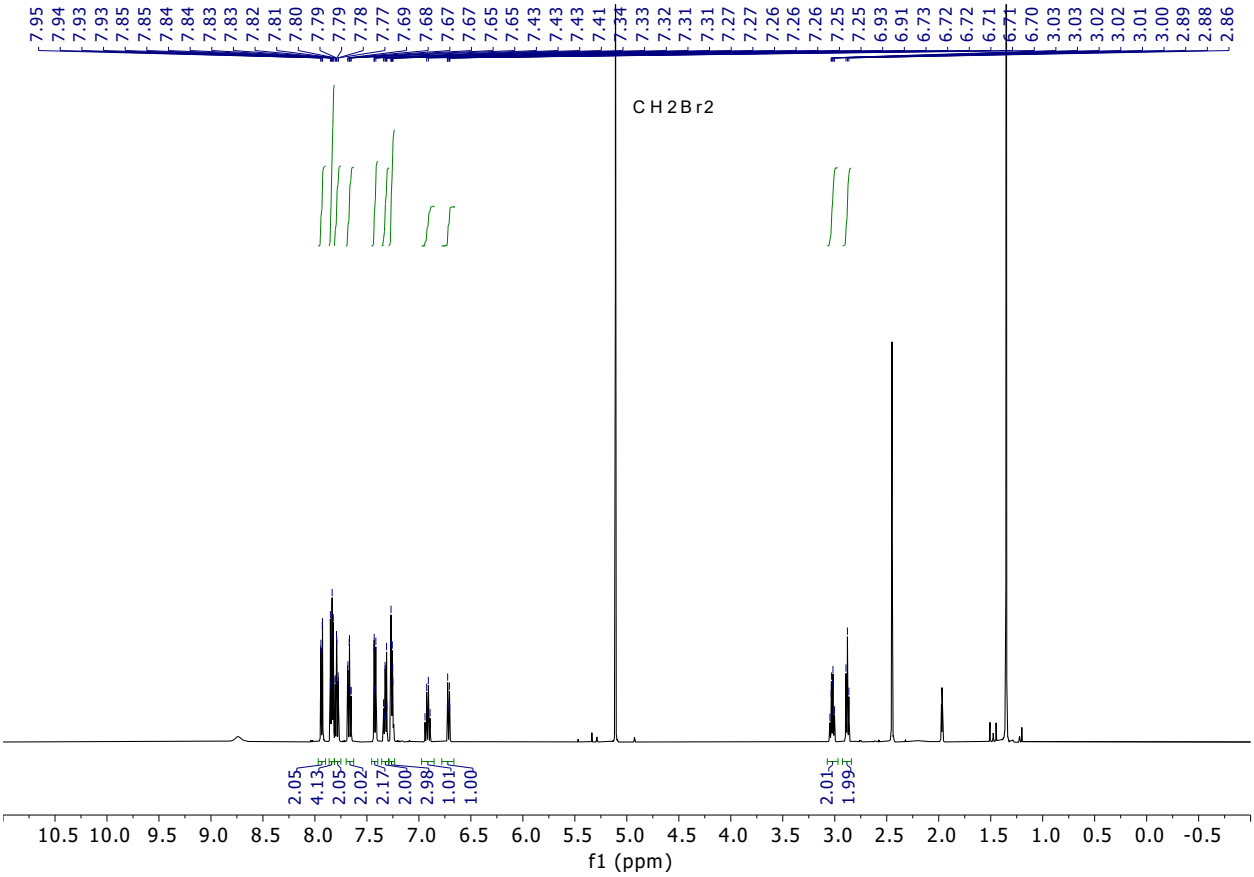

Appendix G: Supporting Information for Chapter 8 (Unveiling Potent Photooxidation Behavior of Catalytic Photoreductants)

G1. General Methods and Materials

Unless otherwise noted, reactions were performed under 1 atm O_2 in an anhydrous solvent. MeCN was dried by passing through activated alumina columns. Unless otherwise noted, commercially-available reagents were used as received. $LiClO_4$ was recrystallized from MeCN and dried under vacuum. Irradiation of photochemical reactions was carried out using Kessil LED lamps (390 nm [KSPR160L-390]; Tuna Blue [A160WE]). Crude mixtures were evaluated by thin-layer chromatography using EMD/Merck silica gel 60 F254 pre-coated plates (0.25 mm) and were visualized by UV. Flash chromatography was performed with a Biotage Isolera One automated chromatography system with re-packed silica columns (technical grade silica, pore size 60 Å, 230-400 mesh particle size, 40-63 particle size). Purified materials were dried *in vacuo* (0.050 Torr) to remove trace solvent. ^1H and ^{13}C Spectra were collected using a Bruker Avance-400 with a BBFO Probe, Bruker Avance-500 with a DCH Cryoprobe, or a Bruker Avance-600 with a TCI-F Cyroprobe. NMR data are reported relative to residual $CHCl_3$ (^1H, δ = 7.26 ppm), $CDCl_3$ (^{13}C, δ = 77.16 ppm), DMSO-d_6 (^1H, δ = 2.50 ppm), C_6D_6 (^1H, δ = 7.16 ppm), or MeCN-d_3 (^1H, δ = 1.94 ppm). Data for ^1H NMR spectra are reported as follows: chemical shift (δ ppm) (multiplicity, coupling constant (Hz), integration). Multiplicity and qualifier abbreviations are as follows: s = singlet, d = doublet, t = triplet, q = quartet, m = multiplet, br = broad. All NMR yields were determined via reference against an internal standard (dibromomethane for ^1H NMR). GC traces were taken on an Agilent 7890A GC with dual DB-5 columns (20 m ×180 μμm × 0.18 μm), dual FID detectors, and hydrogen as the carrier gas. A sample volume of 1 μL was injected at a temperature of 300 °C and a 100:1 split ratio. The initial inlet pressure was 20.3 psi but varied as the column flow was held constant at 1.8 mL/min for the duration of the run, FID temperature was 325 °C.

Abbreviations: BET–back electron transfer, DCM–dichloromethane, EtOAc–ethyl acetate, HFIP–1,1,1,3,3,3-hexafluoro-2-propanol, MeCN–acetonitrile, Mes–mesityl, Ph–phenyl, PTH–10-phenyl-10H-phenothiazine, TFE–2,2,2-trifluoroethanol, TFA–trifluoroacetate, GC–gas chromatography.

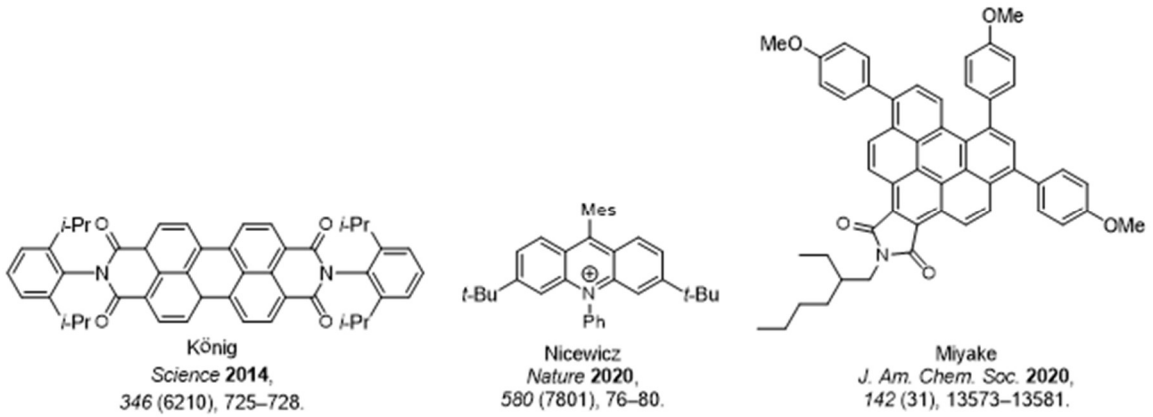

Figure G1. Established multi-photon photoreductants; complete catalyst structures for Figure 8.1.

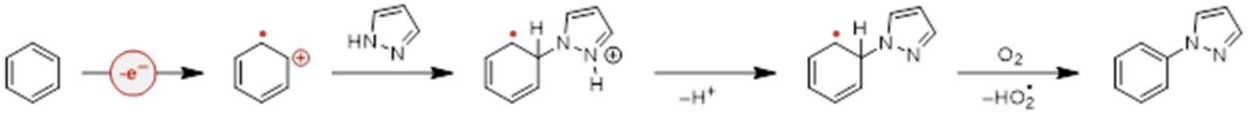

Scheme G1. Proposed mechanism for pyrazole *N*-arylation under photooxidation conditions.

G2. Photochemical Experimental Set-Ups

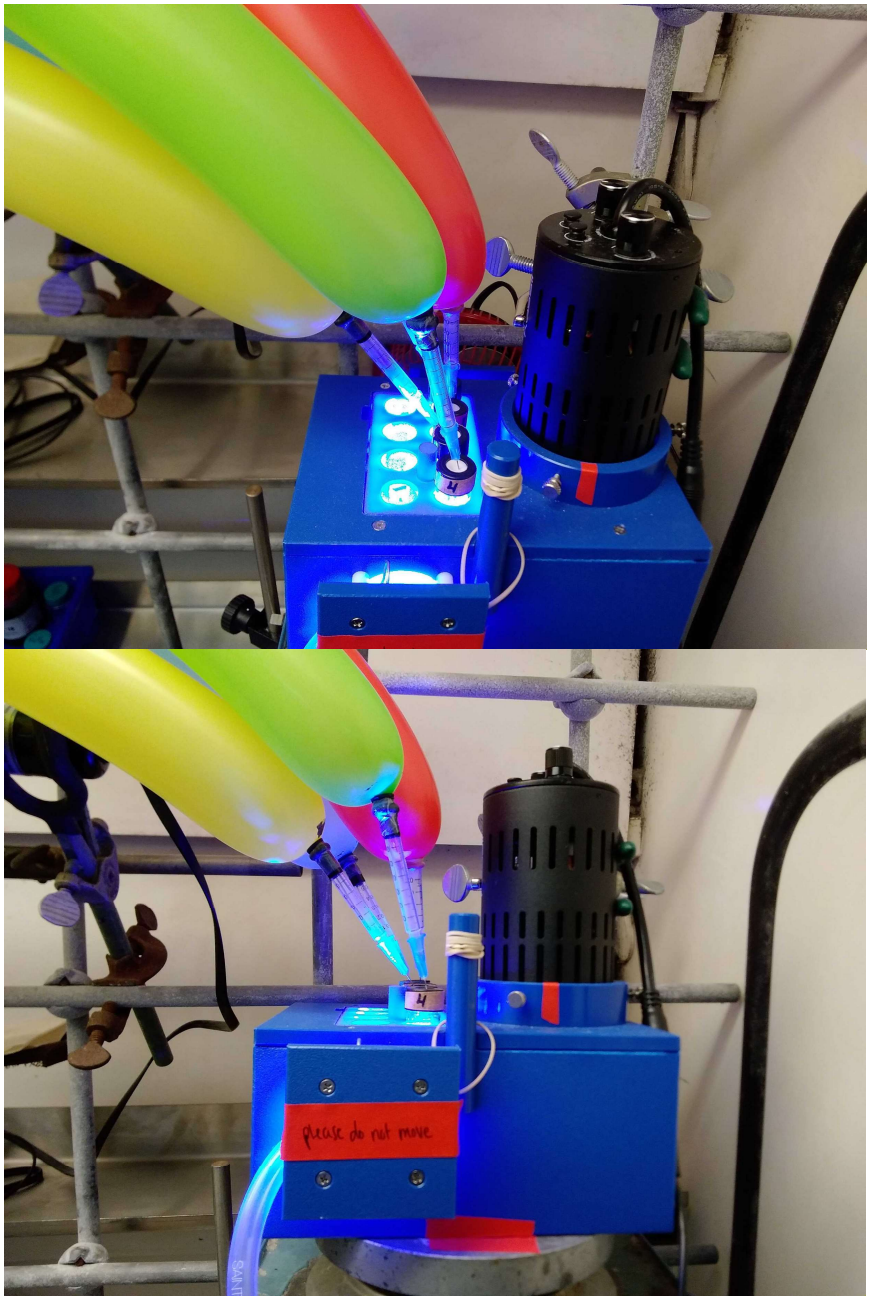

Figure G2. Photochemical experimental set-up for reaction optimization experiments using a HepatoChem EvoluChem™ PhotoRedOx Box [HCK1006-01-016] fitted with a Kessil LED lamp and compressed air cooling.

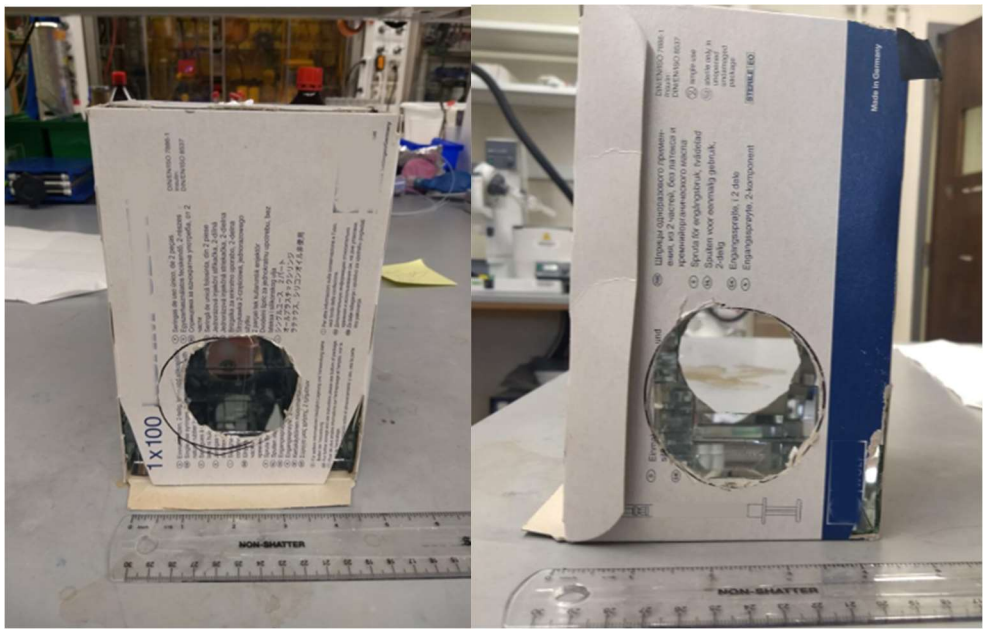

Figure G3. Homemade photobox for scaling up reactions. Circular cut-out in front "door" and triangular slits on side and top for fan cooling and air flow; two circular openings fit Kessil LED lamps for side-on irradiation; angled mirrors at top to reflect light downwards; rectangular opening in back wall for clamp to hold reaction tube; circular hole on top for balloon needle.

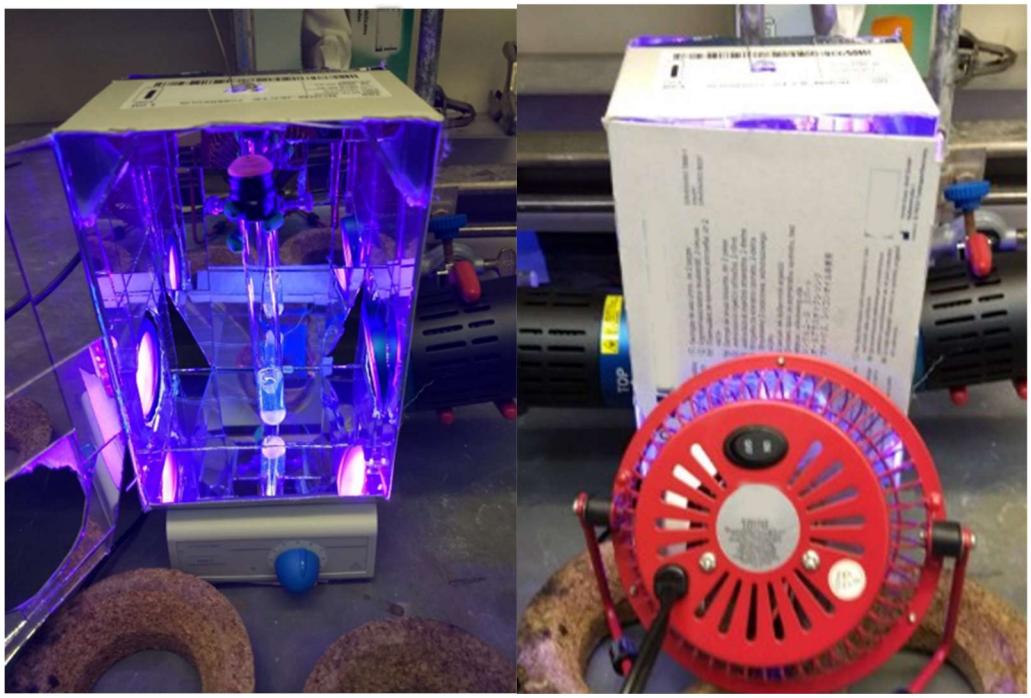

Figure G4. Scale up photobox in action. End reactions measure ca. 35°C.

G3. Preparation of Ester Pyrazole 8.1

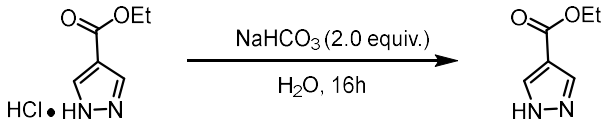

8.1
99% yield

Ethyl 1H-pyrazole-4-carboxylate hydrochloride (2.649 g, 15.0 mmol, 1.0 equiv.) and sodium bicarbonate (2.520 g, 30.0 mmol, 2.0 equiv) were dissolved in water (160 mL). The reaction mixture was stirred under ambient conditions for 16 h. The aqueous phase was extracted with 3 × 200 mL DCM. The combined organic phases were dried over Na_2SO_4, filtered, and the solvent evaporated to afford ester pyrazole **8.1** as a white solid (2.0877 g, 99%). **^{1}H NMR** (500 MHz, CDCl3) δ 11.68 (br s, 1H), 8.09 (s, 2H), 4.33 (qd, J = 7.1, 0.8 Hz, 2H), 1.36 (td, J = 7.1, 0.9 Hz, 3H). Consistent with reported spectra (*Synthetic Communications*, **2008**, 38, 5, 674 - 683).

G4. Preparation of Photocatalysts

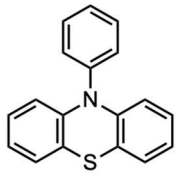

10-phenyl-10H-phenothiazine (PTH) – prepared according to *Beilstein J. Org. Chem.* **2019,** 15, 52–59. 10H-phenothiazine (1.49 g, 7.50 mmol, 1.0 equiv), potassium tert-butoxide (1.09 g, 9.67 mmol, 1.29 equiv), tri-tert-butylphosphoniumtetrafluoroborate (131 mg, 450 µmol, 0.06 equiv), and bis(dibenzylideneacetone)palladium (129 mg, 225 µmol, 0.03 equiv) were combined and placed under an atmosphere of nitrogen. The solids were then dissolved in anhydrous toluene (14 mL). Bromobenzene (1.44 g, 964 µL, 9.15 mmol, 1.22 equiv) was added. The reaction mixture was stirred under reflux for 20 h. After reaching room temperature, the reaction contents were filtered, then 200 mL EtOAc and 100 mL water were added to the reaction mixture. After phase separation, the aqueous phase was extracted additionally with 3 × 200 mL EtOAc followed by 1 x 100 mL brine. The combined organic phases were dried over Na_2SO_4, the solvent evaporated, and the crude product purified by column chromatography (2.01 g, 97%); **^{1}H NMR** (400 MHz, DMSO) δ 7.67 (t, *J* = 7.6 Hz, 2H), 7.54 (t, *J* = 7.5 Hz, 1H), 7.45 – 7.38 (m, 2H), 7.08 (dd, *J* = 7.5, 1.6 Hz, 2H), 6.93 (ddd, *J* = 8.4, 7.3, 1.7 Hz, 2H), 6.89 – 6.81 (m, 2H), 6.16 (dd, *J* = 8.1, 1.3 Hz, 2H); consistent with reported spectra (*Eur. J. Org. Chem., **2019**: 5807-5811*)

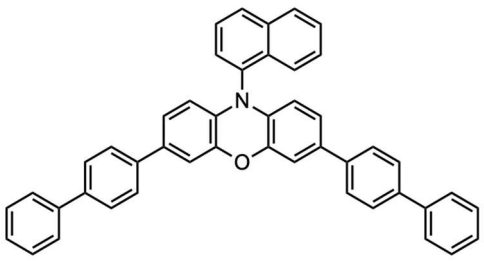

3,7-di([1,1′-biphenyl]-4-yl)-10-(naphthalen-1-yl)-10H-phenoxazine (**PC-8.1**) – prepared in three steps according to *J. Am. Chem. Soc.* **2016**, 138, 35, 11399–11407.

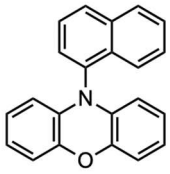

Step 1: Synthesis of 1-Naphthalene-10-phenoxazine – A stir bar was placed into a 100 mL storage flask, flame dried under vacuum and then back filled with nitrogen three times. The flask was then charged with 10H-phenoxazine (500 mg, 2.73 mmol, 1.0 equiv), sodium tert-butoxide (525 mg, 5.46 mmol, 2.0 equiv,), 2-dicyclohexylphosphino-2',6'-diisopropoxybiphenyl (RuPhos, 38.2 mg, 81.9 µmol, 0.03 equiv), (2-dicyclohexylphosphino-2',6'-diisopropoxy-1,1'-biphenyl)[2-(2'-amino-1,1'-biphenyl)]palladium(II) methanesulfonate (RuPhos Pd G3, 68.5 mg, 81.9 µmol, 0.03 equiv), 1,4-dioxane (3 mL), and 1-bromonaphthalene (1.13 g, 764 µL, 5.46 mmol, 2.0 equiv). The flask was heated at 130 ºC while stirring for 48 hours. The flask was then cooled to room temperature, diluted with CH_2Cl_2, and the solution was washed with water three times, brine once, dried over $MgSO_4$ and purified by recrystallization from CH_2Cl_2 layered with hexanes on top at -25ºC to yield the product as yellow crystals (615 mg, 73% yield). **^{1}H NMR** (400 MHz, $CDCl_3$) δ 8.08 (dt, *J* = 8.2, 1.0 Hz, 1H), 8.02 – 7.95 (m, 2H), 7.65 (dd, *J* = 8.3, 7.2 Hz, 1H), 7.59 – 7.51 (m, 2H), 7.47 (ddd, *J* = 8.2, 6.8, 1.3 Hz, 1H), 7.26 (s, 1H), 6.73 (dd, *J* = 7.9, 1.5 Hz, 2H), 6.63 (td, *J* = 7.7, 1.5 Hz, 2H), 6.49 (td, *J* = 7.7, 1.5 Hz, 2H), 5.70 (dd, *J* = 8.0, 1.5 Hz, 2H); consistent with reported spectra (*J. Am. Chem. Soc.* **2016**, 138, 35, 11399–11407)

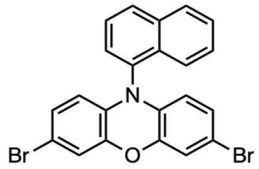

Step 2: Synthesis of 3,7-Dibromo-1-Naphthalene-10-phenoxazine – 10-(naphthalen-1-yl)-10H-phenoxazine (515 mg, 1.66 mmol, 1.0 equiv) was dissolved in chloroform (51.5 mL). Acetic acid (51.5 mL) was then added to the stirring mixture. Aluminum foil was thoroughly wrapped around to cover the reaction vial, blocking out light. In the dark, powdered *N*-bromosuccinimide (607 mg, 3.41 mmol, 2.05 equiv) was added in small portions over a 20 minute period. After 2 hours at room temperature the reaction mixture was concentrated under vacuum. The resulting solid was washed three times with water, brine, then dried with $MgSO_4$. A light tan powder (688 mg, 88% yield) was collected. This was used for the Suzuki coupling without further purification. **^{1}H NMR** (400 MHz, C_6D_6) δ 7.82 (d, *J* = 8.4 Hz, 1H), 7.58 (dd, *J* = 19.0, 8.2 Hz, 2H), 7.20 (d, *J* = 7.4 Hz, 1H), 7.13 – 7.07 (m, 2H), 6.90 (d, *J* = 7.2 Hz, 1H), 6.84 (d, *J* = 2.3 Hz, 2H), 6.37 (dd, *J* = 8.6, 2.3 Hz, 2H), 5.31 (d, *J* = 8.4 Hz, 2H); consistent with reported spectra (*J. Am. Chem. Soc.* **2016**, 138, 35, 11399–11407)

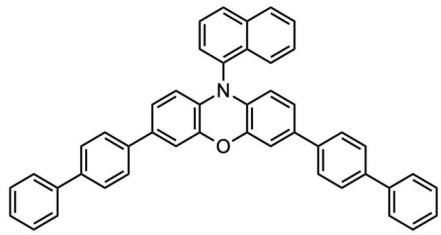

Step 3: Synthesis of 3,7-Di(4-biphenyl) 1-Naphthalene-10-Phenoxazine (**PC-8.1**) – A 200 mL schlenk flask was flame dried, filled with nitrogen, and equipped with a stir bar and reflux condenser before 3,7-dibromo-10-(naphthalen-1-yl)-10H-phenoxazine (225 mg, 482 µmol, 1.0 equiv), [1,1'-biphenyl]-4-ylboronic acid (382 mg, 1.93 mmol, 4.0 equiv) was added, then dissolved in 20 mL of THF. 6 mL of aqueous K_2CO_3 (2M) was syringed into the solution and then heated to 80 °C and stirred for 20 minutes.

After which, tetrakis(triphenylphosphine)-palladium(0) (167 mg, 144 µmol, 0.3 equiv) in a 20 mL solution of THF was added then heated to 100 °C and left to run for 24 hours. Once complete, the reaction was concentrated under vacuum, dissolved in DCM, and washed with water two times, brine, then dried with $MgSO_4$. A bright yellow powder was collected (128 mg, 43% yield) after recrystallization in DCM/MeOH. **^{1}H NMR** (400 MHz, C_6D_6) δ 8.18 (d, *J* = 8.3 Hz, 1H), 7.69 (d, *J* = 8.6 Hz, 2H), 7.68 – 7.63 (m, 1H), 7.61 – 7.54 (m, 1H), 7.54 – 7.49 (m, 4H), 7.46 (s, 8H), 7.36 (d, *J* = 2.0 Hz, 2H), 7.25 (td, *J* = 7.8, 7.3, 4.9 Hz, 8H), 6.73 (dd, *J* = 8.3, 2.1 Hz, 2H), 5.88 (d, *J* = 8.3 Hz, 2H); consistent with reported spectra (*J. Am. Chem. Soc.* **2016**, 138, 35, 11399–11407).

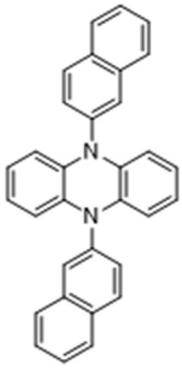

N,N-5,10-di(2-naphthalene)-5,10-dihydrophenazine (**PC-8.2**) – Commercially available material from MilliporeSigma was used. For preparation, see *Science*, **2016**, 352, 6289, 1082-1086.

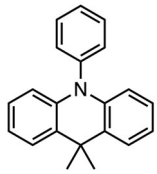

[9,9-dimethyl-10-phenyl-9,10-dihydroacridine] (**PC-8.3**) – In a three-neck flask, bromobenzene (0.23 mL, 2.2 mmol, 1.1 equiv), 9-dimethyl-9,10-dihydroacridine (419 mg, 2.0 mol), and sodium tert-butoxide (577 mg, 6.0 mol, 3.0 equiv) were introduced. Everything was kept under an inert atmosphere and the solids were dissolved in 10 mL of toluene. The catalyst was prepared in a flask, by mixing $Pd(dba)_2$ (73.3 mg, 0.08 mmol, 0.04 equiv) and $HP(tBu)_3$ BF_4 (46.4 mg, 0.16 mmol, 0.08 equiv) in 2 ml of toluene. This catalyst solution was added to the reaction medium and heated overnight at reflux. After complete conversion, the reaction medium was filtered through a celite pad and the solvent was removed under vacuum. The crude product purified by column chromatography (550 mg, 96%); **^{1}H NMR** (400 MHz, $CDCl_3$) δ 7.63 (t, *J* = 7.6 Hz, 2H), 7.51 (t, *J* = 7.5 Hz, 1H), 7.46 (dd, *J* = 7.5, 1.8 Hz, 2H), 7.34 (d, *J* = 7.0 Hz, 2H), 6.97 (td, *J* = 8.0, 7.6, 1.8 Hz, 2H), 6.92 (td, *J* = 7.4, 1.5 Hz, 2H), 6.26 (dd, *J* = 7.9, 1.5 Hz, 2H), 1.70 (s, 6H); consistent with reported spectra (*Organic Electronics* **2018**, *57*, 327–334).

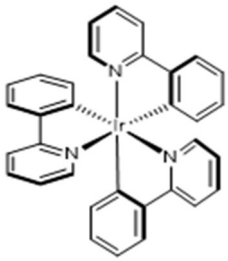

Ir(ppy)$_3$ - sample generously donated from the Yoon group. For preparation see *J. Am. Chem. Soc.* **2003**, 125, 24, 7377–7387.

G5. Preparation of PTH•PF_6 Radical Cation

Preparation adapted from *ChemCatChem* **2018**, 10, 2955 –2961. In a Schlenk tube 82.5 mg (0.300 mmol, 1.00 equiv) 10-phenyl-10H-phenothiazine was dissolved in 1mL anhydrous MeCN. Then the mixture was cooled to 0 °C and 47.2 mg (0.270 mmol, 0.90 equiv) $NOPF_6$ was slowly added to the mixture as a concentrated MeCN solution. The mixture turned deep red immediately and was stirred for a further 20 min. The mixture was freeze-pump-thawed for three cycles to remove the generated NO. Then the mixture was let come to room temperature and the solvent removed. The solid was then dissolved in DCM. A red solid precipitated upon addition of hexanes. The red solid was washed with hexanes three times to remove excess PTH then dried under reduced pressure. PTH•PF_6 radical cation was characterized by its absorption spectrum.

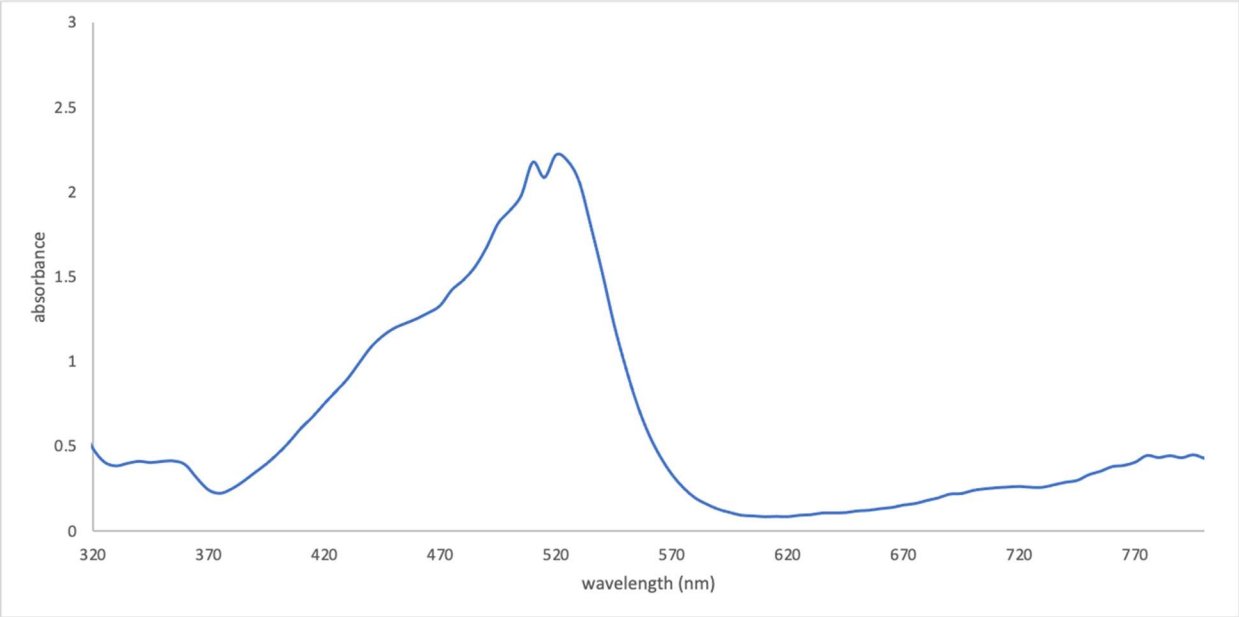

Spectrum and distinct feature at 520 nm is consistent with literature (*Bulletin of the Chemical Society of Japan*, **1999**, vol. 72, # 2, p. 253 - 257). ^{1}H NMR confirmed no residual PTH, although a trace amount of PTH S-oxide is observed.

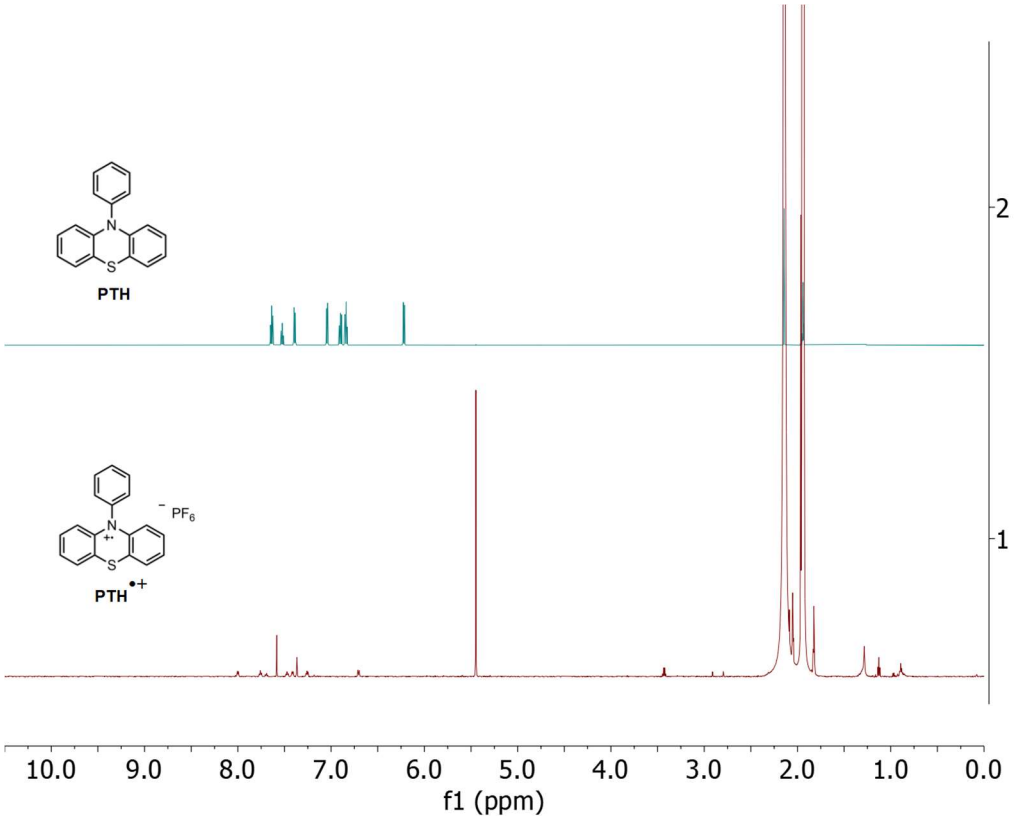

Figure G5. ^{1}H NMR (600 MHz, MeCN-d_3) spectrum shows no residual PTH.

G6. General Experimental Procedures for Redox-Primed Photocatalysis

General Procedure A – Add PTH (5.5 mg, 0.02 mmol, 5 mol %) and $LiClO_4$ (1.1 mg, 0.08 mmol, 20 mol %) to a 16x150 mm fraction tube equipped with a stir bar. If a solid, add pyrazole (0.4 mmol, 1.0 equiv.) to the tube. Add arene (8 mL), TFE (7.2 mL), and HFIP (0.8 mL) to the tube. Affix the reaction vessel to the photoreactor (see fig. G3 and G4 photobox description). Sparge the solution for 20 minutes with oxygen from a balloon (1 atm). If liquid, add pyrazole (0.4 mmol, 1.0 equiv.) to the tube. Irradiate using two 390 nm Kessil lamps for 20 h under 1 atm O_2 and with fan cooling. Concentrate crude product for purification by flash chromatography with silica.

General Procedure B – Following General Procedure A, but with the following modification: following irradiation, concentrate crude product. Add dibromomethane internal standard to the residue and dilute with $CDCl_3$. Take up the solution in an NMR tube. Cross coupling product yield was determined via ^{1}H NMR using dibromomethane as an internal standard.

General Procedure C – Add PTH (5.5 mg, 0.02 mmol, 5 mol %) to a 16x150 mm fraction tube equipped with a stir bar. If a solid, add pyrazole (0.4 mmol, 1.0 equiv.) to the tube. Add arene (8 mL), MeCN (4 mL), and HFIP (4 mL) to the tube. Affix the reaction vessel to the photoreactor (see fig. S3 and S4 photobox description). Sparge the solution for 20 minutes with oxygen from a balloon (1 atm). If liquid, add pyrazole (0.4 mmol, 1.0 equiv) to the tube. Add *t*-dodecyl mercaptan (9.4 µL, 0.04 mmol, 10 mol %) to the tube. Irradiate using two 390 nm Kessil lamps for 20h under 1 atm O_2 and with fan cooling. Concentrate crude product for purification by flash chromatography with silica.

General Procedure D – Add PTH (5.5 mg, 0.02 mmol, 5 mol %) to a 16x150 mm fraction tube equipped with a stir bar. If a solid, add pyrazole (0.4 mmol, 1.0 equiv) to the tube. Add MeCN (2 mL) and HFIP (2 mL) to the tube. Affix the reaction vessel to the photoreactor (see fig. G3 and G4 photobox description). Sparge the solution for 7 minutes with oxygen from a balloon (1 atm). If liquid, add pyrazole (0.4 mmol, 1.0 equiv) to the tube. Add *t*-dodecyl mercaptan (9.4 µL, 0.04 mmol, 10 mol %) to the tube. Irradiate using two 390 nm Kessil lamps for 20h under 1 atm O_2 and with fan cooling. Concentrate crude product for purification by flash chromatography with silica.

G7. Reaction Optimization and Control Experiments (Tables 8.1 and 8.2)

Add solid reaction components (catalyst, pyrazole, co-catalyst) to a 1-dram vial equipped with a stir bar. Add arene (1 mL) and solvent (1 mL) to the vial. Seal with a septum-containing cap. Pierce septum with a needle attached to a balloon filled with the gas of choice and purge the headspace of the vial for two minutes. Tighten the cap and place the vial into the photobox, which itself is on a magnetic stirring plate. Commence the reactions by turning on the Kessil lamp and compressed air cooling. Experiments performed on a 0.05 mmol scale with the pyrazole as the limiting reagent.

For NMR analyses – Following irradiation, concentrate crude product. Add dibromomethane internal standard to the residue and dilute with $CDCl_3$. Take up the solution in an NMR tube. Oxidative coupling product yield was determined via ^1H NMR using dibromomethane as an internal standard.

For GC analyses – Following irradiation, add dodecane internal standard to crude reaction and remove a 0.1 mL aliquot. Filter the aliquot through a celite plug pre-wetted with EtOAc to remove solids and dilute the filtrate (0.2 mL) with ethyl acetate (1.0 mL).

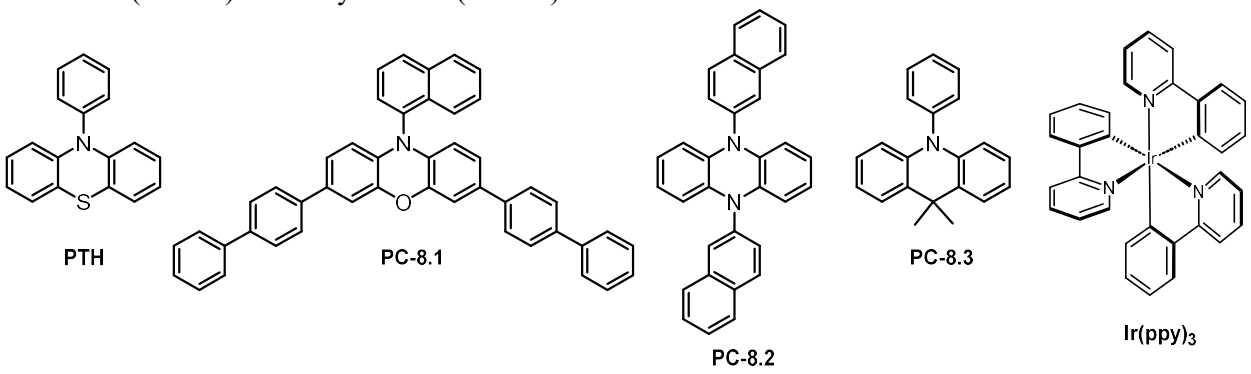

Figure G6. Catalysts used for reaction development.

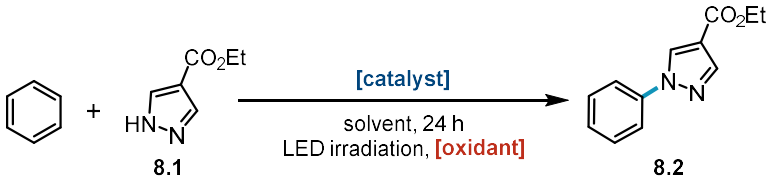

Table G1. Optimization of photocatalyst and terminal oxidant for oxidative coupling of benzene with pyrazole 8.1.[a-d]

entry	catalyst	solvent	oxidant	yield (%)
1	**PTH** (5%)	MeCN	none	n.d.
2	**PTH** (5%)	MeCN	PhI (2 equiv)	n.d.

3	**PTH** (5%)	MeCN	PhBr (2 equiv)	2%
4	**PTH** (5%)	MeCN	CH_2Br_2 (2 equiv)	5
5	**PTH** (5%)	MeCN	$NOPF_6$ (2 equiv)	12
6	**PTH** (5%)	MeCN	$Cu(TFA)_2$ (2 equiv)	n.d.
7	**PTH** (5%)	MeCN	O_2 (1 atm)	14
8	**PTH** (5%)	TFE	O_2 (1 atm)	31
9[e]	**PTH** (5%)	9:1 TFE:HFIP	O_2 (1 atm)	89
10	**PC-8.1** (5%)	MeCN	PhI (2 equiv)	<2%
11	**PC-8.1** (5%)	MeCN	PhBr (2 equiv)	<2%
12	**PC-8.1** (5%)	MeCN	CH_2Br_2 (2 equiv)	<2%
13	**PC-8.1** (5%)	MeCN	$NOPF_6$ (2 equiv)	4
14	**PC-8.1** (5%)	MeCN	$Cu(TFA)_2$ (2 equiv)	n.d.
15	**PC-8.1** (5%)	MeCN	O_2 (1 atm)	n.d.
16	**PC-8.1** (5%)	TFE	O_2 (1 atm)	<2%
17[e]	**PC-8.1** (5%)	9:1 TFE:HFIP	O_2 (1 atm)	<2%
18	**PC-8.2** (5%)	MeCN	PhI (2 equiv)	n.d.
19	**PC-8.2** (5%)	MeCN	PhBr (2 equiv)	<2%
20	**PC-8.2** (5%)	MeCN	CH_2Br_2 (2 equiv)	<2%
21	**PC-8.2** (5%)	MeCN	$NOPF_6$ (2 equiv)	3
23	**PC-8.2** (5%)	MeCN	$Cu(TFA)_2$ (2 equiv)	n.d.
24	**PC-8.2** (5%)	MeCN	O_2 (1 atm)	6
25	**PC-8.2** (5%)	TFE	O_2 (1 atm)	<2%
26[e]	**PC-8.2** (5%)	9:1 TFE:HFIP	O_2 (1 atm)	<2%
27[f]	**PC-8.2** (5%)	MeCN	$NOPF_6$ (2 equiv)	<2%
28[f]	**PC-8.2** (5%)	MeCN	O_2 (1 atm)	<2%
29[f]	**PC-8.2** (5%)	TFE	O_2 (1 atm)	2%
30[e,f]	**PC-8.2** (5%)	9:1 TFE:HFIP	O_2 (1 atm)	8%

31[f,g]	**PC-8.3** (5%)	MeCN	O_2 (1 atm)	37%
32	$Ir(ppy)_3$ (1%)	MeCN	PhI (2 equiv)	n.d.
33	$Ir(ppy)_3$ (1%)	MeCN	PhBr (2 equiv)	n.d.
34	$Ir(ppy)_3$ (1%)	MeCN	CH_2Br_2 (2 equiv)	<2%
35	$Ir(ppy)_3$ (1%)	MeCN	$NOPF_6$ (2 equiv)	6
36	$Ir(ppy)_3$ (1%)	MeCN	$Cu(TFA)_2$ (2 equiv)	n.d.
37	$Ir(ppy)_3$ (1%)	MeCN	O_2 (1 atm)	n.d.
38	$Ir(ppy)_3$ (1%)	TFE	O_2 (1 atm)	n.d.
39[e]	$Ir(ppy)_3$ (1%)	9:1 TFE:HFIP	O_2 (1 atm)	<2%

[a]**PTH** irradiated using 390 nm Kessil lamp; **PC-8.1**, **PC-8.2**, and $Ir(ppy)_3$ irradiated using Tuna Blue Kessil lamp. [b]Conducted under an argon atmosphere (1 atm) unless noted otherwise. [c]GC yields. [d]n.d. = not detected. [e]20 mol % $LiClO_4$. [f]390 nm Kessil lamp used. [g]10% *t*-dodecyl mercaptan.

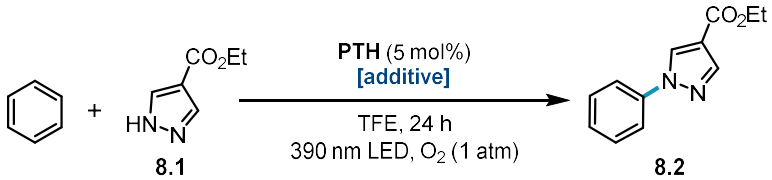

Table G2. effect of superoxide and optimization of Li additive.[a]

entry	additive	yield (%)
1	none	31
2	KO_2 (5 mol %)	<2%
3	$LiClO_4$ (1 equiv)	86
4	$LiClO_4$ (20 mol %)	73
5	$TBAClO_4$ (20 mol %)	29
6	$LiPF_6$ (20 mol %)	64
7	LiOTf (20 mol %)	56
8[b]	**$LiClO_4$ (20 mol %)**	**89**

[a]GC yields. [b]9:1 TFE:HFIP solvent.

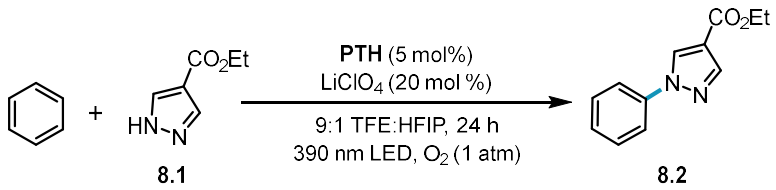

Table G3. control experiments for optimized reaction condition.[a,b]

entry	variation	yield (%)
1	no change	89
2	no catalyst	n.d.
3	no irradiation	n.d.
4[c,d]	no oxidant	n.d.
5	air instead of O_2 balloon	21
6[c]	no $LiClO_4$	33
7	0.1 M instead of 0.025 M	45

[a]NMR yields. [b]n.d.=not detected. [c]GC yield using dodecane internal standard. [d]Conducted under an argon atmosphere (1 atm).

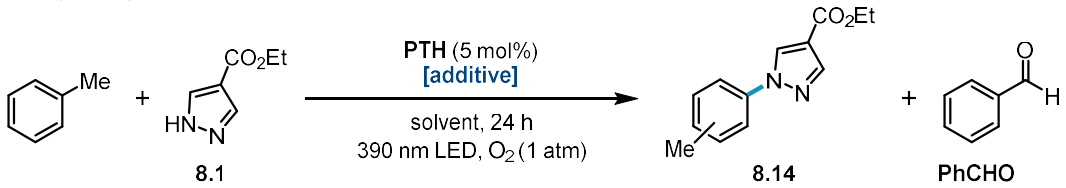

Table G4. optimization oxidative coupling of toluene as model alkyl arene.[a,b]

entry	solvent	additive	yield (%) (*p:o*)	PhCHO (%)[c]
1	9:1 TFE:HFIP	$LiClO_4$ (20%)	70 (1:1)	91
2	1:1 MeCN:HFIP	$LiClO_4$ (1 equiv)	73 (1:1)	55
3	1:1 MeCN:HFIP	*t*-dodecyl mercaptan (10%)	75 (1:1)	31

[a]Reactions conducted using 0.4 mmol of pyrazole **1**, 8 mL of toluene, and irradiated with two 390 nm Kessil lamps for 24h with fan cooling. [b]NMR yields. [c]Relative to pyrazole **1**.

The optimized conditions for benzene applied to alkyl arenes afforded significant oxygenation of the benzylic position (Table G10, entry 1). We found increasing the $LiClO_4$ to stoichiometric quantity and adjusting the solvent system decreased undesired reactivity in the presence of O_2 atmosphere (entry 2). However, we wondered if other additives might serve the co-catalytic role of Li in catalyzing the decomposition of reduced O_2 byproducts arising from catalyst photooxidative activation. Addition of co-catalytic thiol decreased benzylic oxygenation side products while retaining oxidative coupling product yield (entry 3). Superoxide may undergo HAT with thiol to generate hydroperoxy radical and thus prevent BET to deactivate catalyst. The resulting thiyl radical may formally abstract a hydrogen atom from the distonic radical cation adduct between pyrazole and benzene to regenerate the thiol co-catalyst and form the final product. Alternative roles of thiol are also possible.

G8. BET ^{1}H NMR Experiment (Figure 8.2)

Add PTH•PF_6 (9.0 mg, 0.021 mmol) and KO_2 (3.3 mg, 0.046 mmol, 2.2 equiv) to a 1-dram vial equipped with a stir bar. Add MeCN-d_3 (2 mL) and stir for 40 min. Transfer 0.5 mL of the solution to an NMR tube. ^{1}H NMR spectra were acquired 5 h after sample preparation.

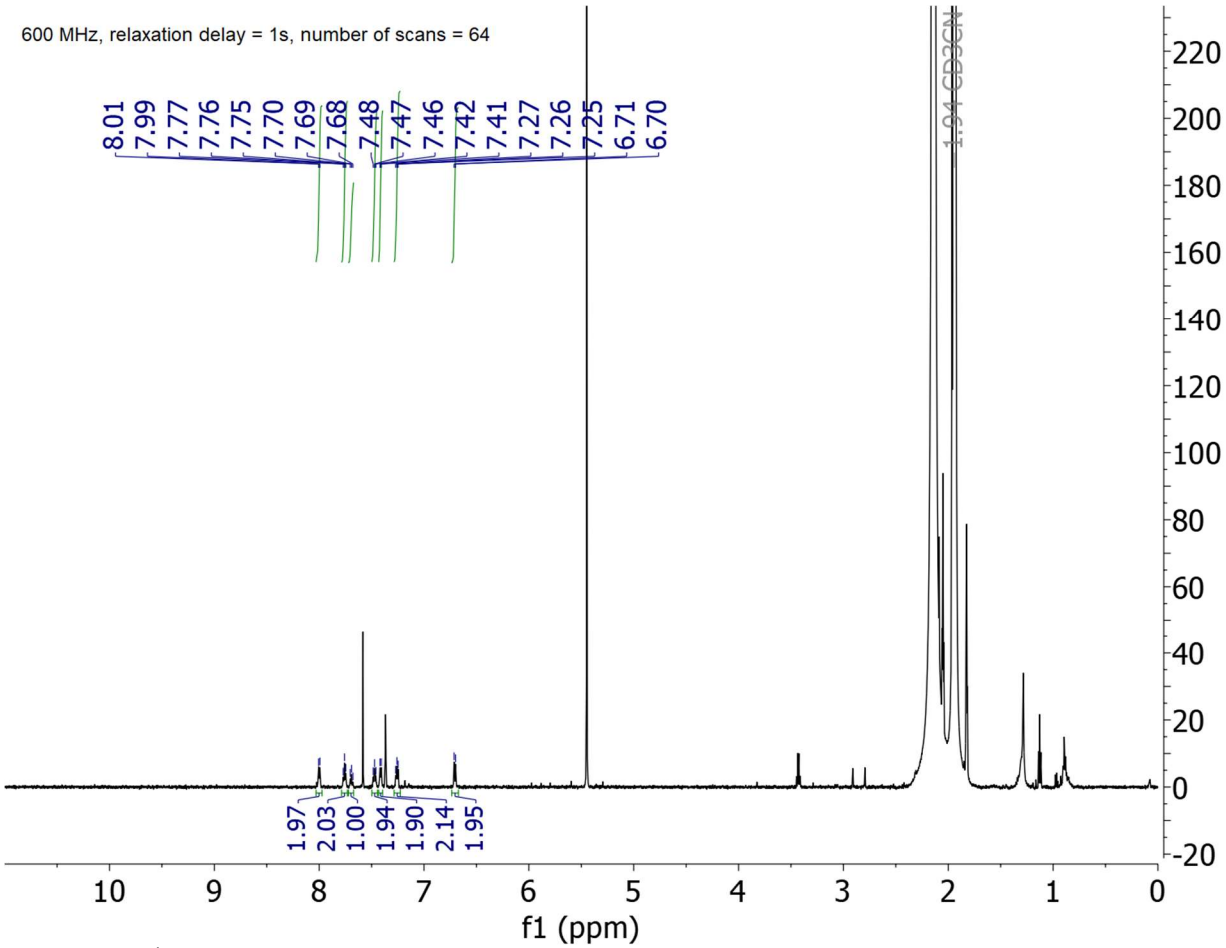

Figure G7. ^{1}H NMR spectrum of prepared PTH•PF_6 shows that paramagnetic PTH radical cation is ^{1}H NMR silent. The observed and integrated signals were assigned as the PTH S-oxide formed from residual water. **^{1}H NMR** (600 MHz, CD_3CN) δ 8.00 (d, J = 7.4 Hz, 2H), 7.76 (t, J = 7.3 Hz, 1H), 7.69 (t, J = 7.6 Hz, 1H), 7.47 (t, J = 7.7 Hz, 1H), 7.41 (d, J = 7.4 Hz, 1H), 7.29 – 7.23 (m, 1H), 6.71 (d, J = 8.5 Hz, 1H); consistent with reported spectra *(J. Chem. Soc., Perkin Trans. 1*, **1995**, No. 8, 1057-1064).

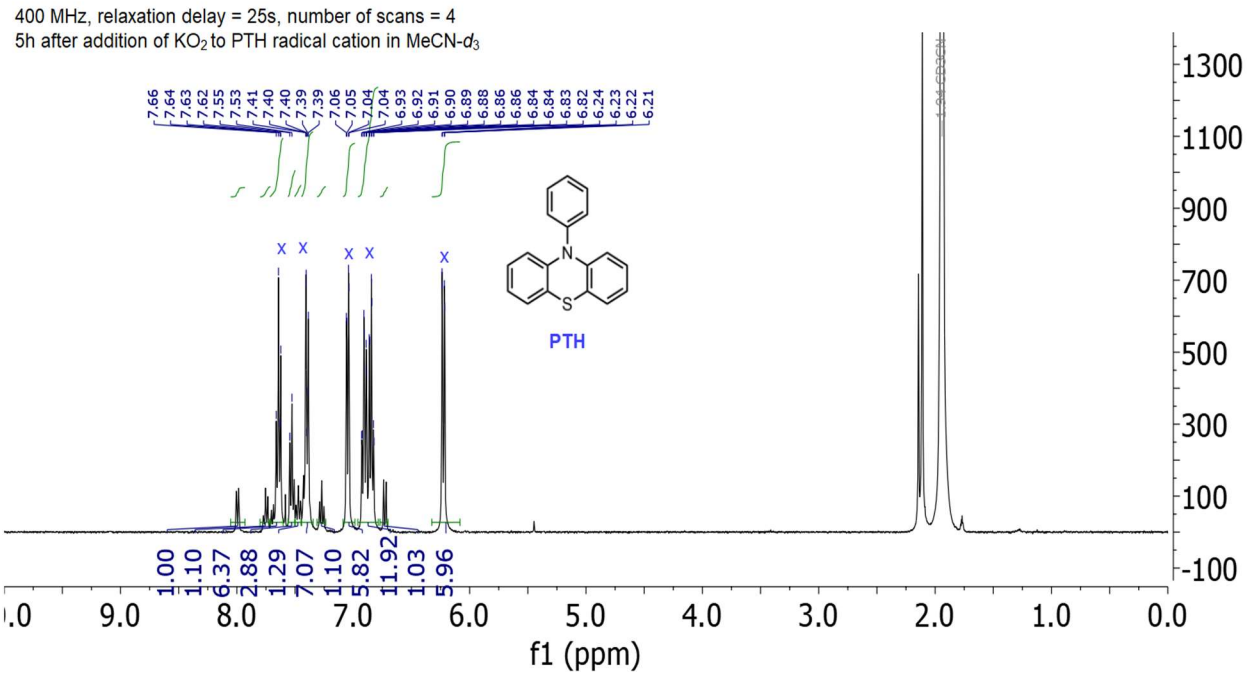

Figure G8. Formation of closed-shell PTH from PTH•PF_6 in MeCN-d_3 upon addition of KO_2.

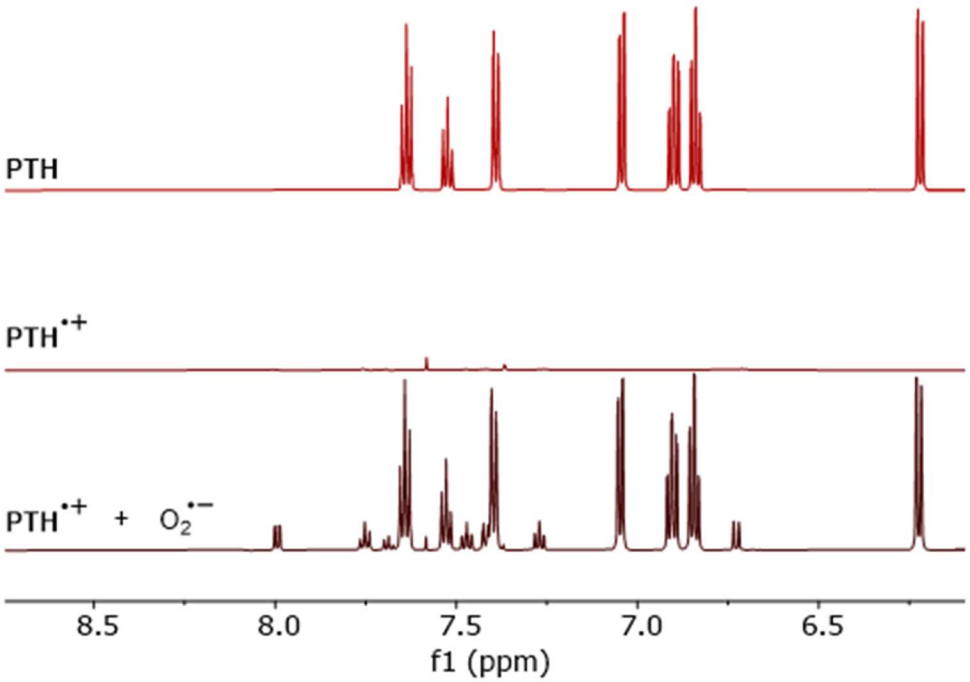

Figure G9. ^{1}H NMR spectroscopic evidence supporting the working model for catalyst deactivation pathways by superoxide.

G9. Time Course Experiments

Add ester pyrazole 8.**1** (7.0 mg, 0.05 mmol, 1.0 equiv.), PTH (0.7 mg, 0.0025 mmol, 5 mol %), and $LiClO_4$ (1.1 mg, 0.01 mmol, 20 mol %) to a 1-dram vial equipped with a stir bar and septum-containing cap. Add benzene (1 mL), TFE (0.9 mL), and HFIP (0.1 mL). Piece the septum with a needle attached to an O_2 balloon. Purge the headspace for 2 min by partially opening the cap of the vial while stirring the solution. Add dodecane (10 µL, 0.044 mmol) via microsyringe and tighten the cap to maintain an O_2 atmosphere. Place vial into a HepatoChem EvoluChem™ PhotoRedOx Box [HCK1006-01-016] and irradiate with a 390 nm Kessil lamp for the duration of the time course experiment.

For GC analyses – Remove 10 µL of reaction solution via microsyringe through the septum cap. Filter the aliquot through a celite plug pre-wetted with EtOAc to remove salts and dilute the filtrate (0.2 mL) with ethyl acetate (1.0 mL).

Figure G10. Time course experimental set up.

Figure G11. reaction vial in designated position for reproducibility.

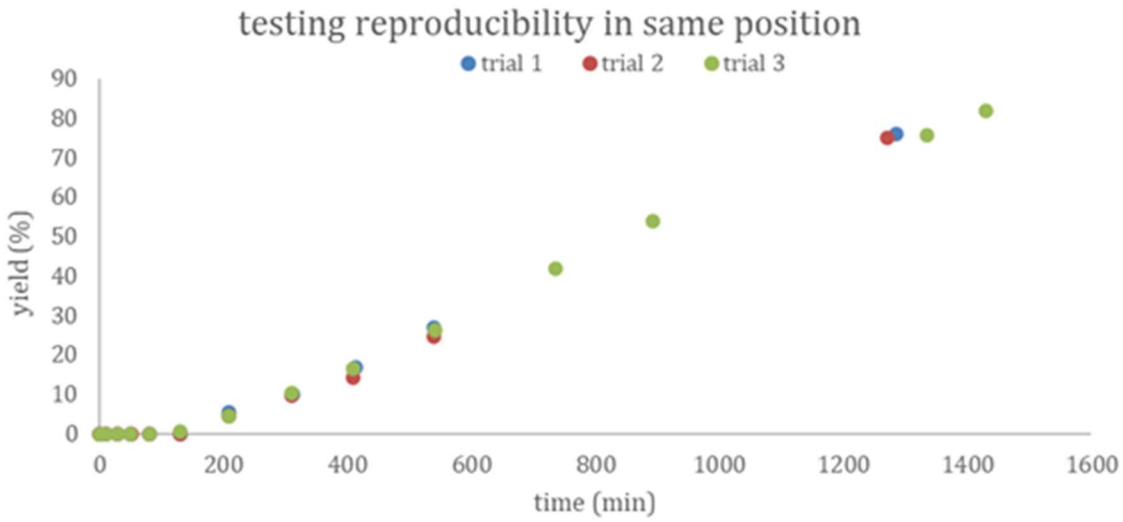

Figure G12. Three trials prepared on separate days using the general procedure led to reproducible reaction rates and final yields.

G10. Light Dependence Experiments (Scheme 8.1)

The procedure for time course experiments was followed, except for the following: during the designated "dark" time points, the reaction vial was wrapped in aluminum foil and kept in the photobox. After the dark period, the foil was removed, and the reaction was allowed to proceed with irradiation.

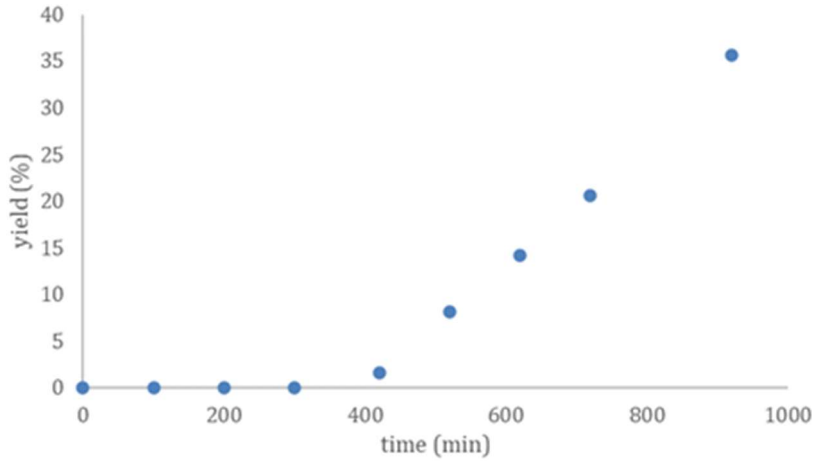

Figure G13. 200 min of dark time during the induction period. Reactions shielded from light between 100 min and 300 min. The induction period lengthened accordingly.

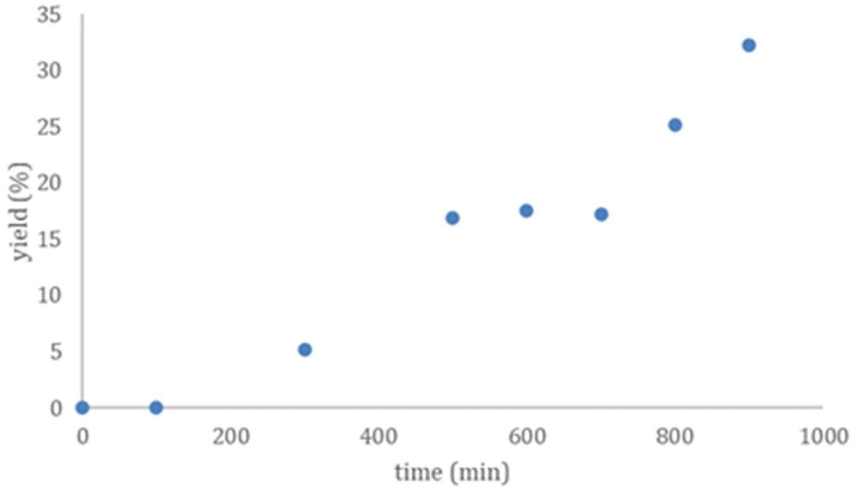

Figure G14. 200 min of dark time during product formation. Reactions shielded from light between 500 min and 700 min. The percent yield of the coupling product did not increase without irradiation.

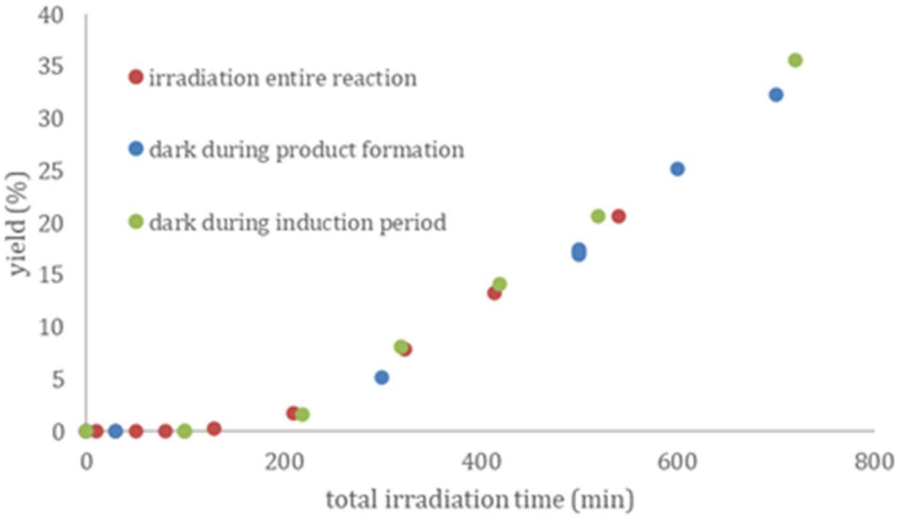

Figure G15. When accounting for total irradiation time (by subtraction of the dark periods), the dark control experiments during the induction period and product forming phase overlay with the standard reaction profile during which irradiation is continuous. This indicates both the induction period and product formation involve light dependent processes.

G11. Oxygen Uptake Experiment

Oxygen uptake experiments were performed on an apparatus developed by the Stahl lab – A stock solution of ethyl 1H-pyrazole-4-carboxylate (0.025 M) and $LiClO_4$ (0.005 M) in 9:1:10 TFE:HFIP:benzene was prepared as well as a stock solution of PTH in benzene (0.00125 M). A heavy walled tube equipped with a stir bar of known volume was attached to a pressure transducer, evacuated and refilled with 1 atm O2 three times, and then pressurized to 1 atm. The tube was clamped above a stir plate and 2 mL of the ethyl 1H-pyrazole-4-carboxylate stock solution (0.05 mmol) was added to the tube through a thick rubber septum. Magnetic stirring and fan cooling were begun and the 390 nm Kessil lamp was turned on to allow for thermal equilibration over 20 min. Pressure monitoring was commenced, then 0.1 mL of PTH containing stock solution (0.0025 mmol PTH) was injected into the tube through the septum. To facilitate analysis, the uptake was normalized after the 0.1 mL catalyst injection. After pressure monitoring, the final yield of the reaction was measured via gas chromatography using dodecane as an internal standard. The data points were plotted over time to determine the amount of O2 consumed during different phases of the reaction.

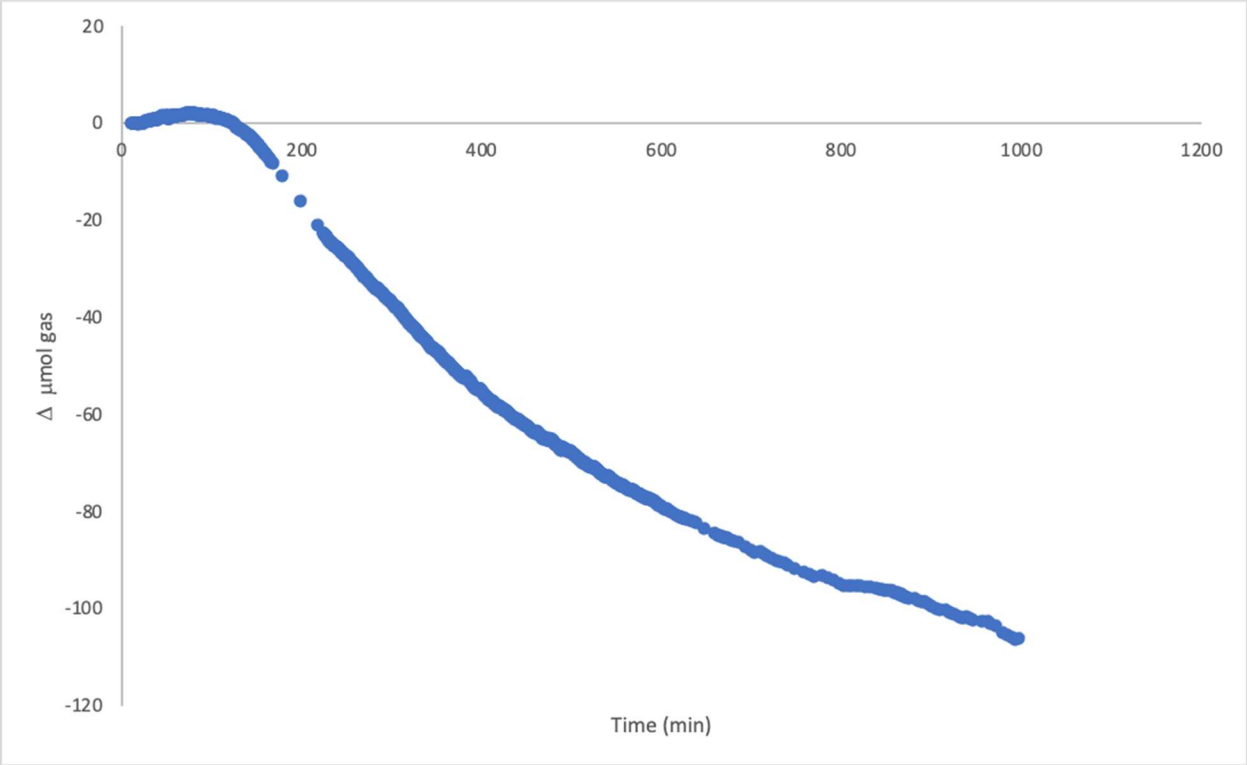

Figure G16. Change in µmol of O_2 over the course of the reaction.

The reaction was run on a 50 µmol scale. 46.5 µmol of product was determined via GC, and 106 µmol of O_2 were consumed during the reaction. Collectively, this indicates that approximately 2.3 equivalents of O_2 are consumed relative to product. Furthermore, this experiment reveals that there is minimal change in pressure during the induction period. However, due to the slightly positive slope (consistent with modest heating from the light source and the system thermally equilibrating), precise quantification of how much O_2 is consumed during catalyst activation is not feasible. Drawing analogy to time course experiments, O_2 is only significantly consumed during the product forming phase of the reaction.

G12. Lithium Saturation Curve Experiments (Scheme 8.2)

The general procedure for time course experiments was followed, except for the following: $LiClO_4$ concentrations lower than 0.005 M (20 mol%) were prepared from stock solutions.

Figure G17. Reaction profiles for varying $LiClO_4$ concentrations (0 to 40 mol % loading).

Figure G18. Linear fit of zeroth order product formation regime for varying $LiClO_4$ concentrations (0 to 40 mol % loading). Slope is the rate of the reaction.

Table G5. Reaction rate for varying Li concentrations. Li = $LiClO_4$.

mol % Li^+	$[Li^+]$ (mM)	rate (10^{-5} M*s^{-1})
40	10	2.701
20	5	2.677
10	2.5	2.485
5	1.25	2.264
2.5	0.625	1.962
0	0	1.233

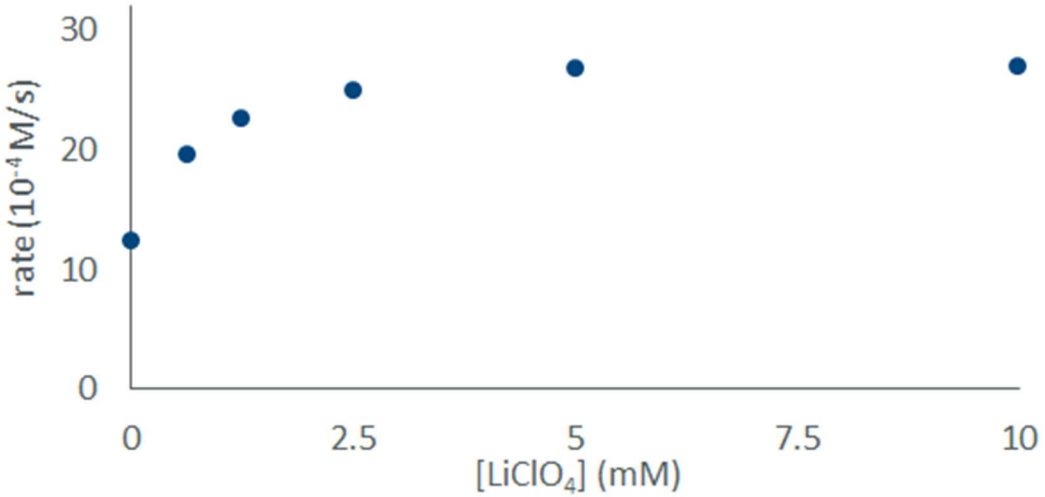

Figure G19. Plot of Li^+ concentration versus reaction rate reveals saturation in Li^+ co-catalyst.

G13. Superoxide Inhibition (Scheme 8.3)

The general procedure for time course experiments was followed, except for the following: working quickly, prepare a stock solution of KO_2 (0.05 M) in TFE and immediately add 50 µL via microsyringe to the reaction solution that was irradiated for 9.3h (560 min). Continue monitoring the reaction using GC aliquots. No change in reaction outcome is observed due to addition of 50 µL TFE.

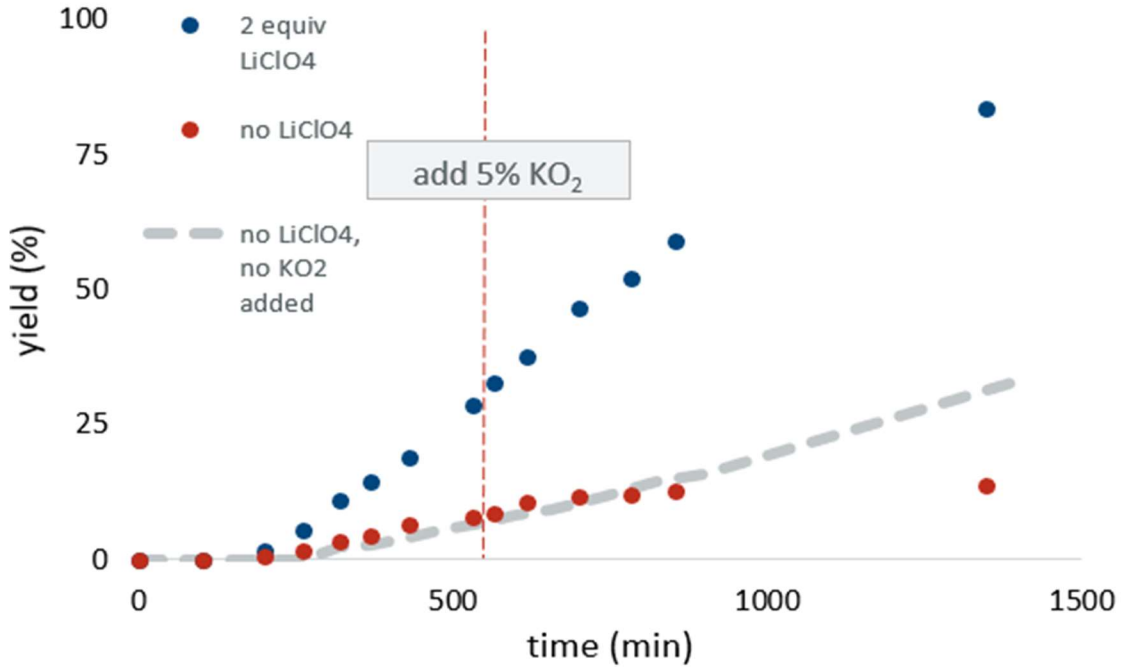

Figure G20. Addition of 5% KO2 shows an inhibitory effect on product formation (red points vs. grey dash). The presence of sufficient $LiClO_4$ protects the reaction from KO_2 inhibition (blue points).

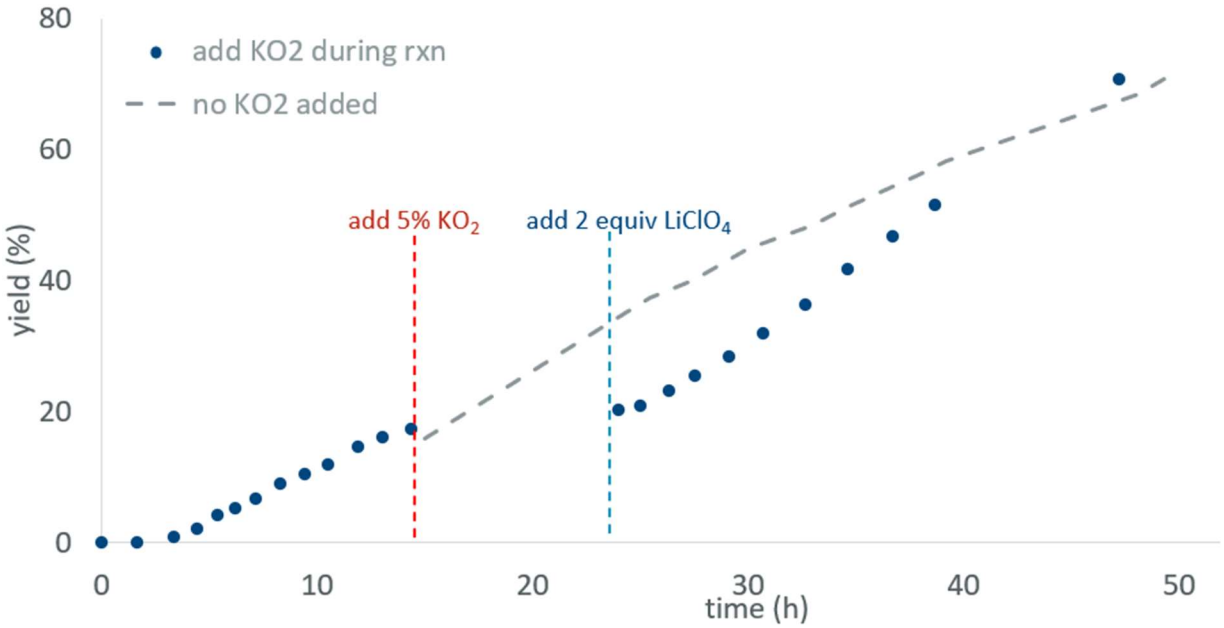

Figure G21. A reaction with no $LiClO_4$ present is stalled by addition of 5% KO_2 compared to when no KO_2 is added (grey dash); the addition of $LiClO_4$ restarts the reaction and recovers product formation (blue points).

GC Calibration Curves

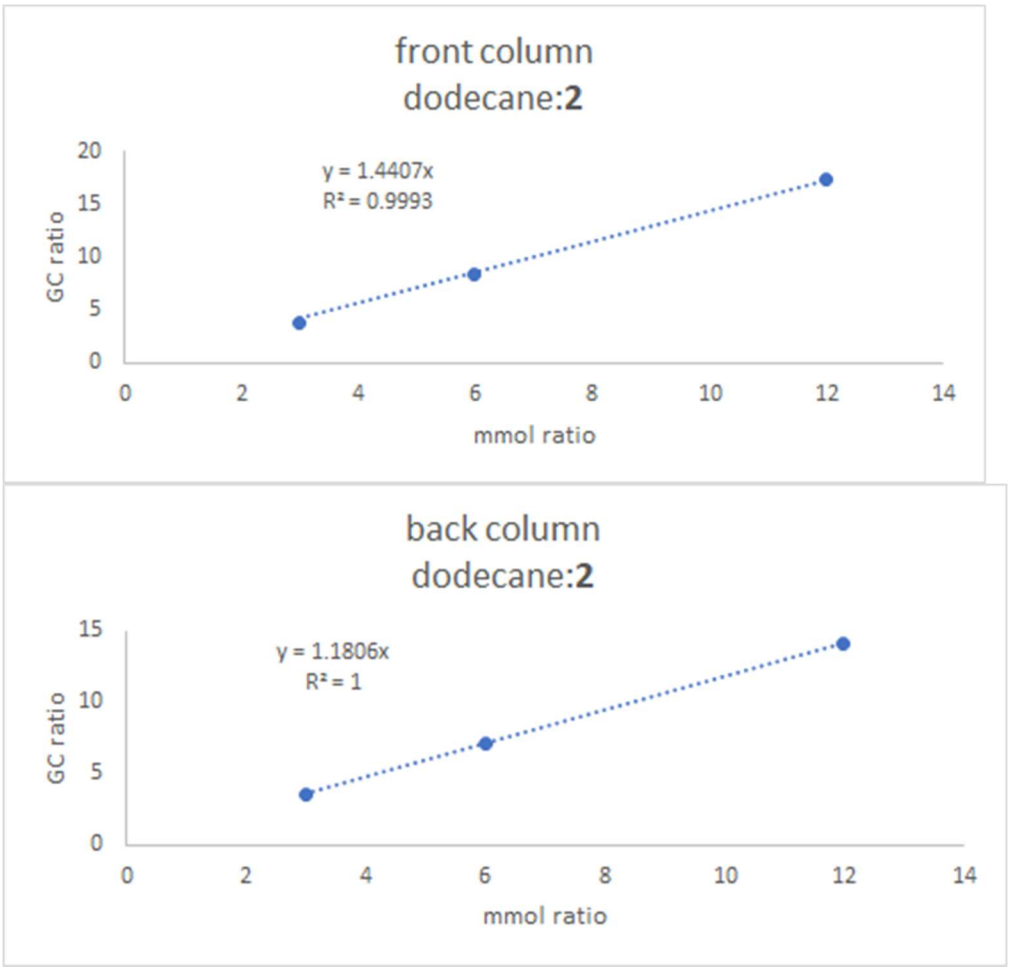

G14. Investigation of Charge Transfer Complex Formation via UV-Vis

All absorbance spectra were measured on a Varian Cary 50 UV-Vis spectrophotometer instrument using quartz cuvettes. Baseline corrections were made using blanks containing solvent only.

A 50 μM solution of PTH•PF_6 in TFE was prepared and its absorbance spectrum collected. Absorbance spectra of the same sample were sequentially measured after addition of 100, 1000, and 10000 equivalents of benzene (1.34, 12, 120 μL). The spectra in Figure S22 did not provide definitive evidence of a charge transfer complex between PTH radical cation and benzene. The observed decrease in absorbance is more consistent with either dilution or medium effects than a discrete complex between PTH radical cation and benzene.

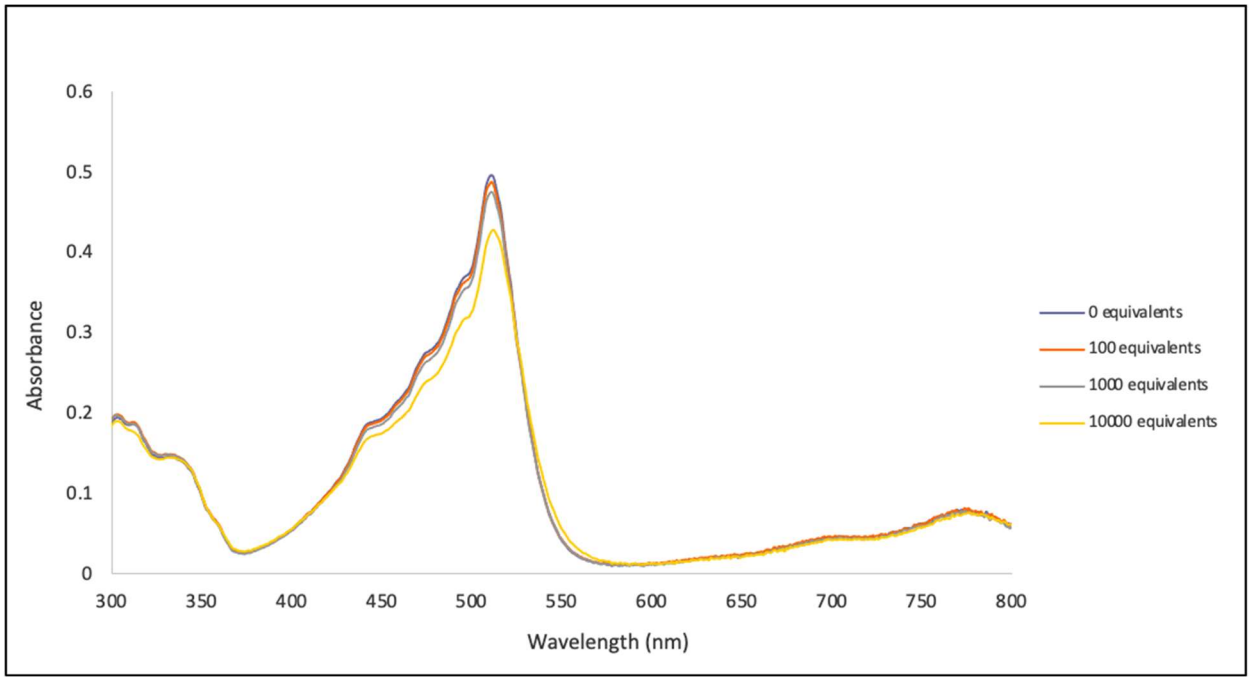

Figure G22. Absorption spectra of PTH radical cation with increasing equivalents of benzene.

Next, to control for dilution, two cuvettes containing a 50 μM PTH•PF_6 in TFE solution were prepared. To one was added 10000 equivalentes of benzene (134 μL), and to the other an equal volume of TFE. A third cuvette containing a 50 μM PTH•PF_6 solution in 1:2 TFE:benzene was also prepared. Under these conditions, no clear feature consistent with a charge transfer complex was observed (Figure S23). Based on these data, we conclude that the observed spectral changes are most consistent with a change in solvation.

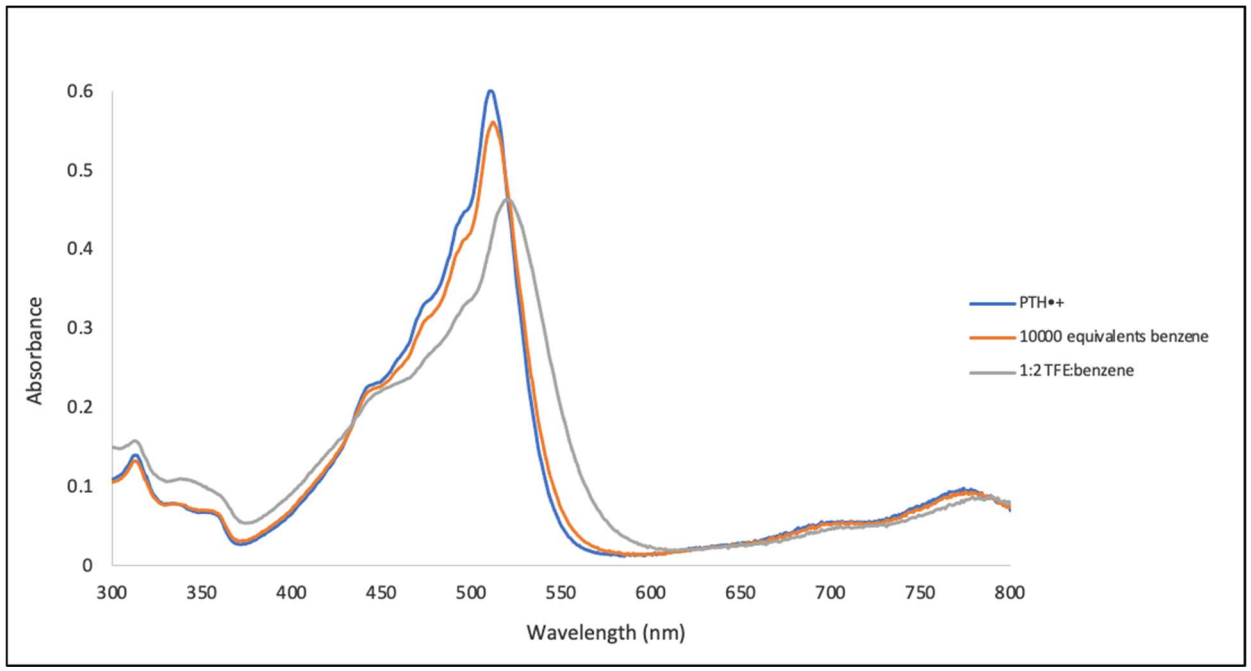

Figure G23. Absorption spectrum of 50 μM PTH radical cation in the presence (orange trace) and absence (blue trace) of benzene. Absorption spectrum of PTH radical cation with benzene as a co-solvent (grey trace).

Finally, UV-Vis spectra of PTH radical cation and mesitylene were collected given that a smaller excess of mesitylene was amenable in the reaction. A 50 μM stock solution of PTH•PF_6 in MeCN was prepared. To one cuvette was added 10 equivalents of mesitylene (1.50 μmol), via stock solution, and to the other an equal volume of MeCN. No significant change was observed upon addition of mesitylene (Figure S24). Overall, these data (Figures S22–24) are inconsistent with an exergonic association between PTH radical cation and the arene substrates.

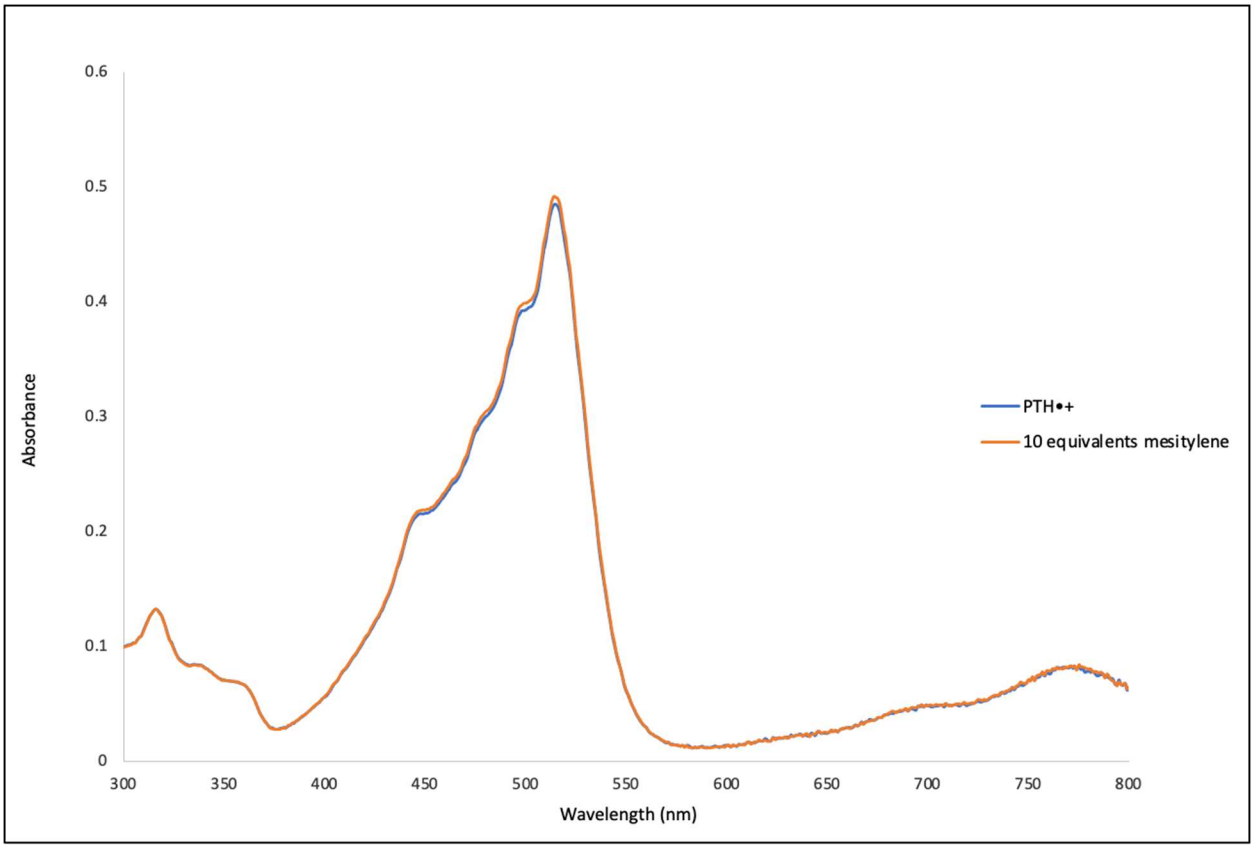

Figure G24. Absorption spectrum of 50 μM PTH radical cation in the presence (orange trace) and absence (blue trace) of mesitylene.

G15. Product Isolation and Characterization

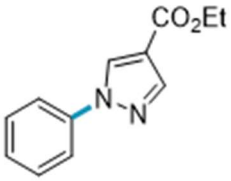

Ethyl 1-phenyl-1H-pyrazole-4-carboxylate (8.2): Prepared from benzene and ethyl 1H-pyrazole-4-carboxylate; 86.5 mg (81% yield) obtained following General Procedure A. **^{1}H NMR** (500 MHz, $CDCl_3$) δ 8.41 (s, 1H), 8.10 (s, 1H), 7.74 – 7.68 (m, 2H), 7.52 – 7.44 (m, 2H), 7.36 (td, *J* = 7.4, 1.3 Hz, 1H), 4.34 (q, *J* = 7.2 Hz, 2H), 1.38 (t, *J* = 7.1 Hz, 3H); consistent with reported spectra (*Angew. Chem. Int. Ed.,* **2019***, 58*, 13318–13322).

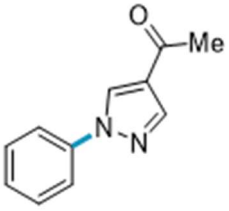

1-(1-phenyl-1H-pyrazol-4-yl)ethanone (8.3): Prepared from benzene and 1-(1H-pyrazol-4-yl)ethanone; 66.0 mg (88% yield) obtained following General Procedure A using 20 mol % $LiPF_6$. **^{1}H NMR** (500 MHz, $CDCl_3$) δ 8.32 (s, 1H), 8.03 (s, 1H), 7.67 – 7.62 (m, 2H), 7.46 – 7.40 (m, 2H), 7.33 – 7.28 (m, 1H), 2.44 (s, 3H); consistent with reported spectra (*Angew. Chem. Int. Ed.,* **2019***, 58*, 13318–13322).

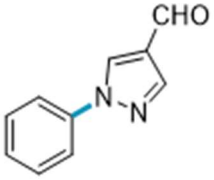

1-phenyl-1H-pyrazole-4-carbaldehyde (8.4): Prepared from benzene and 1H-pyrazole-4-carbaldehyde; 49.2 mg (71% yield) obtained following General Procedure A using 1:1 HFIP:PhH solvent mixture. **^{1}H NMR** (500 MHz, $CDCl_3$) δ 9.96 (s, 1H), 8.44 (s, 1H), 8.16 (s, 1H), 7.74 – 7.68 (m, 2H), 7.50 (t, J = 8.0 Hz, 2H), 7.42 – 7.35 (m, 1H); consistent with reported spectra (*Angew. Chem. Int. Ed.,* **2019***, 58*, 13318–13322).

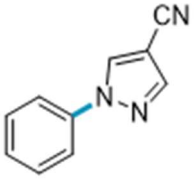

1-phenyl-1H-pyrazole-4-carbonitrile (8.5): Prepared from benzene and 1H-pyrazole-4-carbonitrile; 58.6 mg (87% yield) obtained following General Procedure A. **^{1}H NMR** (500 MHz, $CDCl_3$) δ 8.32 (s, 1H), 8.00 (s, 1H), 7.71 – 7.65 (m, 2H), 7.52 (dd, J = 8.7, 7.3 Hz, 2H), 7.42 (td, J = 7.2, 1.3 Hz, 1H); consistent with reported spectra (*Org. Lett.*, **2015***, 17*, 2886–2889).

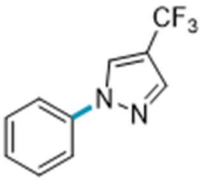

1-phenyl-4-(trifluoromethyl)-1H-pyrazole (8.6): Prepared from benzene and 4-(trifluoromethyl)-1H-pyrazole; 59.0 mg (70% yield) obtained following General Procedure A. **^{1}H NMR** (500 MHz, $CDCl_3$) δ

8.19 (s, 1H), 7.92 (s, 1H), 7.72 – 7.66 (m, 2H), 7.50 (dd, J = 8.6, 7.4 Hz, 2H), 7.39 (td, J = 7.3, 1.3 Hz, 1H); ^{1}H and ^{19}F NMR are consistent with reported spectra (*RSC Advances,* **2019**, *9*, 30952–30956).

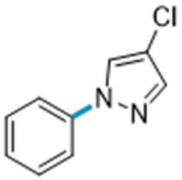

4-chloro-1-phenyl-1H-pyrazole (8.7): Prepared from benzene and 4-chloro-1H-pyrazole; 58% yield obtained following General Procedure B; consistent with reported spectra (*Angew. Chem. Int. Ed.,* **2019***, 58*, 13318–13322).

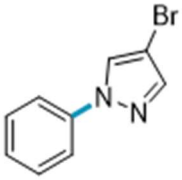

4-bromo-1-phenyl-1H-pyrazole (8.8): Prepared from benzene and 4-bromo-1H-pyrazole; 40.2 mg (45% yield) obtained following General Procedure A using 20 mol % $LiPF_6$. **^{1}H NMR** (500 MHz, $CDCl_3$) δ 7.94 (s, 1H), 7.68 (s, 1H), 7.67 – 7.62 (m, 2H), 7.51 – 7.42 (m, 2H), 7.35 – 7.31 (m, 1H); consistent with reported spectra (*Chem. - Eur. J.,* **2015**, *21*, 11976–11979).

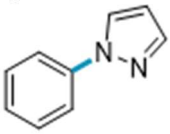

1-phenylpyrazole (8.9): Prepared from benzene and pyrazole; 38% yield obtained following General Procedure B; consistent with reported spectra (*Tetrahedron,* **2013**, *69* (30), 6230–6233).

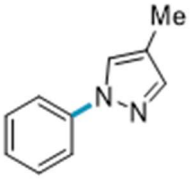

4-methyl-1-phenyl-1H-pyrazole (8.10): Prepared from benzene and 4-methyl-1H-pyrazole; 13.6 mg (22% yield) obtained following General Procedure A. **^{1}H NMR** (500 MHz, $CDCl_3$) δ 7.71 (s, 1H), 7.70 – 7.63 (m, 2H), 7.54 (s, 1H), 7.48 – 7.40 (m, 2H), 7.29 – 7.22 (m, 1H), 2.17 (s, 3H); consistent with reported spectra (*Chemistry – A European Journal*, **2019***, 26* (1), 155–159).

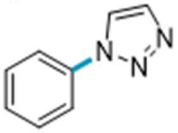

1-phenyl-1,2,3-triazole (8.11): Prepared from benzene and 1,2,3-triazole; 22.1 mg (38% yield) obtained following General Procedure A. **^{1}H NMR** (500 MHz, $CDCl_3$) δ 8.00 (d, *J* = 1.1 Hz, 1H), 7.86 (d, *J* = 1.1 Hz, 1H), 7.80 – 7.72 (m, 2H), 7.58 – 7.50 (m, 2H), 7.49 – 7.42 (m, 1H); consistent with reported spectra (*Angew. Chem. Int. Ed.* **2020**, *59*, 1181).

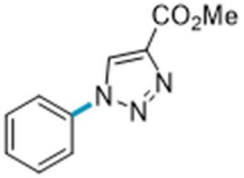

8.12a;

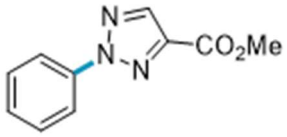

8.12b;

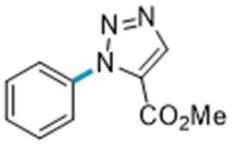

8.12c

Methyl 1-phenyl-1H-1,2,3-triazole-4-carboxylate (8.12a), methyl 2-phenyl-2H-1,2,3-triazole-4-carboxylate (8.12b), and methyl 1-phenyl-1H-1,2,3-triazole-5-carboxylate (8.12c): Prepared from benzene and methyl 1,2,3-triazole-4-carboxylate; 45.9 mg (55% combined yield, 4:1:9 **8.12a** to **8.12b** to **8.12c** ratio) obtained as a separable mixture following General Procedure A.

8.12a: ^{1}H NMR (500 MHz, $CDCl_3$) δ 8.52 (s, 1H), 7.79 – 7.73 (m, 2H), 7.62 – 7.53 (m, 2H), 7.53 – 7.47 (m, 1H), 4.00 (s, 3H); consistent with reported spectra (*Green Chem.*, **2016**, *18*, 2534-2541).

8.12b: ^{1}H NMR (500 MHz, $CDCl_3$) δ 8.25 (s, 1H), 8.18 – 8.12 (m, 2H), 7.55 – 7.47 (m, 2H), 7.46 – 7.39 (m, 1H), 4.01 (s, 3H); consistent with reported spectra (*J. Org. Chem.*, **2014**, *79*, 6105−6112).

8.12c: ^{1}H NMR (500 MHz, $CDCl_3$) δ 8.27 (s, 1H), 7.57 – 7.51 (m, 3H), 7.51 – 7.46 (m, 2H), 3.85 (s, 3H); consistent with reported spectra (*Adv. Synth. Catal.* **2018**, *360*, 3117).

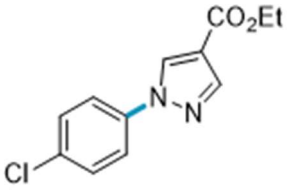

8.13a;

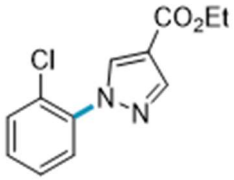

8.13b

Ethyl 1-(4-chlorophenyl)-1H-pyrazole-4-carboxylate (8.13a) and ethyl 1-(2-chlorophenyl)-1H-pyrazole-4-carboxylate (8.13b): Prepared from chlorobenzene and ethyl 1H-pyrazole-4-carboxylate; 21.8 mg (22% combined yield, 3:1 **8.13a** to **8.13b** ratio) obtained as a separable mixture following General Procedure A.

8.13a: ^{1}H NMR (400 MHz, $CDCl_3$) δ 8.37 (s, 1H), 8.09 (s, 1H), 7.70 – 7.62 (m, 2H), 7.49 – 7.39 (m, 2H), 4.34 (q, J = 7.1 Hz, 2H), 1.38 (t, J = 7.1 Hz, 3H).; consistent with reported spectra (*Angew. Chem. Int. Ed.,* **2020**, *59*, 658).

8.13b: ^{1}H NMR (400 MHz, $CDCl_3$) δ 8.35 (s, 1H), 8.13 (s, 1H), 7.63 – 7.50 (m, 2H), 7.46 – 7.34 (m, 2H), 4.34 (q, J = 7.2 Hz, 2H), 1.38 (t, J = 7.1 Hz, 3H); consistent with reported spectra (*ChemRxiv* **2020**, https://doi.org/10.26434/chemrxiv.13140053.v1).

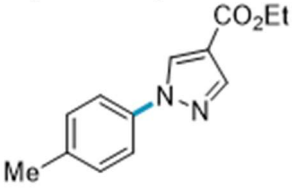

8.14a;

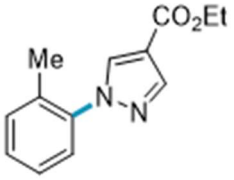

8.14b

Ethyl 1-(4-methylphenyl)-1H-pyrazole-4-carboxylate (8.14a) and ethyl 1-(2-methylphenyl)-1H-pyrazole-4-carboxylate (8.14b): Prepared from toluene and ethyl 1H-pyrazole-4-carboxylate; 71.1 mg (77% yield, 2:1 **8.14a** to **8.14b** ratio) obtained as an intractable mixture following General Procedure C.

8.14a: ^{1}H NMR (500 MHz, $CDCl_3$) δ 8.29 (s, 1H), 8.01 (s, 1H), 7.53 – 7.47 (m, 2H), 7.32 – 7.17 (m, 2H), 4.26 (q, J = 7.1 Hz, 2H), 2.32 (s, 3H), 1.30 (t, J = 7.1 Hz, 3H); consistent with reported spectra (*Org. Lett.,* **2015**, *17*, 872–875).

8.14b: ^{1}H NMR (500 MHz, $CDCl_3$) δ 8.03 (s, 1H), 8.01 (s, 1H), 7.55 – 7.49 (m, 1H), 7.51 – 7.46 (m, 1H), 7.37 (t, J = 7.8 Hz, 1H), 7.18 (d, J = 7.6 Hz, 1H), 4.26 (q, J = 7.1 Hz, 2H), 2.17 (s, 3H), 1.30 (t, J = 7.1 Hz, 3H); consistent with reported spectra (*Org. Lett.,* **2015**, *17*, 872–875).

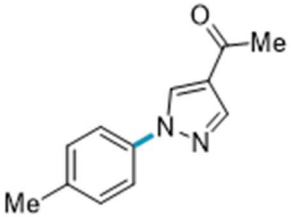

8.15a;

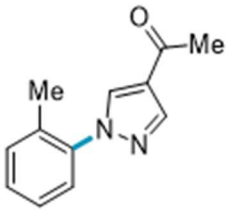

8.15b

1-[1-(4-methylphenyl)pyrazol-4-yl]ethanone (8.15a) and 1-[1-(2-methylphenyl)pyrazol-4-yl]ethanone (8.15b): Prepared from toluene and 1-(1H-pyrazol-4-yl)ethanone; 49.2 mg (61% yield, 2:1 **8.15a** to **8.15b** ratio) obtained as an intractable mixture following General Procedure C. **^{1}H NMR** (500 MHz, $CDCl_3$, mixture of **15a** and **15b**) δ 8.31 (s, 1H), 8.06 (s, 1H), 8.03 (s, 2H), 7.57 – 7.50 (m, 2H), 7.36 – 7.20 (m, 6H), 2.45 (s, 6H), 2.36 (s, 3H), 2.21 (s, 3H). **^{13}C NMR** (126 MHz, $CDCl_3$, mixture of **8.15a** and **8.15b**) δ 192.23, 192.15, 141.42, 141.05, 139.08, 137.85, 137.14, 133.76, 133.09, 131.57, 130.22, 130.16, 129.36, 129.05, 128.49, 126.86, 126.03, 125.51, 124.85, 119.73, 77.36, 77.10, 76.85, 28.10, 28.08, 21.06, 18.02. **HRMS** (ESI+) Calc: $[M+H]^+$ ($C_{12}H_{13}N_2O$) 201.1028; measured: 201.1022 = 0.6 ppm difference.

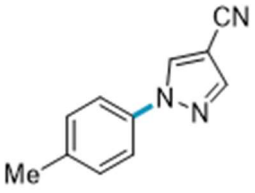

8.16a;

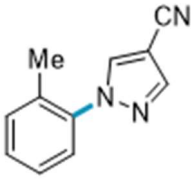

8.16b

1-(4-methylphenyl)-1H-pyrazole-4-carbonitrile (8.16a) and 1-(2-methylphenyl)-1H-pyrazole-4-carbonitrile (8.16b): Prepared from toluene and 1H-pyrazole-4-carbonitrile; 52.8 mg (72% yield, 2:1 **8.16a** to **8.16b** ratio) obtained as an intractable mixture following General Procedure C.

8.16a: ^{1}H NMR (500 MHz, $CDCl_3$) δ 8.26 (s, 1H), 7.98 (s, 1H), 7.60 – 7.54 (m, 2H), 7.34 – 7.29 (m, 2H), 2.42 (s, 3H).

8.16b: ^{1}H NMR (500 MHz, $CDCl_3$) δ 8.29 (s, 1H), 7.99 (s, 1H), 7.54 – 7.50 (m, 1H), 7.46 (dd, J = 7.8, 2.3 Hz, 1H), 7.39 (t, J = 7.8 Hz, 1H), 7.23 (ddt, J = 7.5, 1.7, 0.9 Hz, 1H), 2.45 (s, 3H).

^{13}C NMR (126 MHz, $CDCl_3$, mixture of **8.16a** and **8.16b**) δ 143.20, 143.13, 140.18, 138.54, 136.66, 131.90, 131.75, 130.37, 129.66, 129.19, 120.77, 119.97, 117.08, 113.22, 113.16, 94.32, 94.18, 77.35, 77.10, 76.85, 21.52, 21.11. **HRMS** (ESI+) Calc: $[M+H]^+$ ($C_{11}H_{10}N_3$) 184.0875; measured: 184.0869 = 0.6 ppm difference.

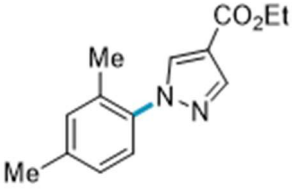

8.17a;

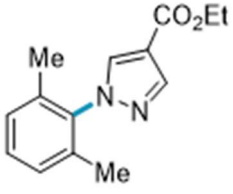

8.17b

Ethyl 1-(2,4-dimethylphenyl)-1H-pyrazole-4-carboxylate (8.17a) and ethyl 1-(2,6-dimethylphenyl)-1H-pyrazole-4-carboxylate (8.17b): Prepared from m-xylene (490 µL, 4 mmol, 10.0 equiv) and ethyl 1H-pyrazole-4-carboxylate; 72.1 mg (74% yield, 4:1 **8.17a** to **8.17b** ratio) obtained as an intractable mixture following General Procedure D.

8.17a: ^{1}H NMR (500 MHz, $CDCl_3$) δ 8.11 (s, 1H), 8.07 (s, 1H), 7.21 (d, J = 8.0 Hz, 1H), 7.18 – 7.14 (m, 1H), 7.10 (dd, J = 8.0, 2.0 Hz, 1H), 4.35 (q, J = 7.1 Hz, 2H), 2.39 (s, 3H), 2.21 (s, 3H), 1.37 (t, fJ = 7.1 Hz, 3H); consistent with reported spectra (*Org. Lett.,* **2015***, 17*, 872–875).

8.17b: ^{1}H NMR (500 MHz, $CDCl_3$) δ 8.16 (s, 1H), 7.98 (s, 1H), 7.29 (t, J = 8.0 Hz, 1H), 7.18 – 7.14 (m, 2H), 4.36 (q, J = 7.2 Hz, 2H), 2.04 (s, 6H), 1.38 (t, J = 7.1 Hz, 3H); consistent with reported spectra (*ChemRxiv* **2020***,* https://doi.org/10.26434/chemrxiv.13140053.v1).

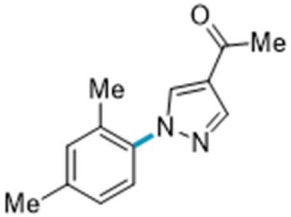
8.18a; 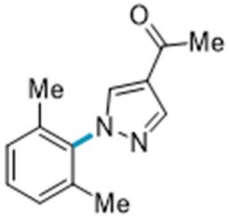 **8.18b**

1-[1-(2,4-dimethylphenyl)pyrazol-4-yl]ethanone (8.18a) and 1-[1-(2,6-dimethylphenyl)pyrazol-4-yl]ethanone (8.18b): Prepared from m-xylene (490 µL, 4 mmol, 10.0 equiv) and 1-(1H-pyrazol-4-yl)ethanone; 75% yield (4:1 **8.18a** to **8.18b** ratio) obtained following General Procedure B; peaks assigned by analogy to **8.17a** and **8.17b**.

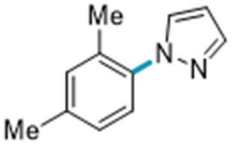
8.19a; 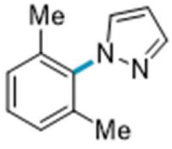 **8.19b**

1-(2,4-dimethylphenyl)-1H-pyrazole (8.19a) and 1-(2,6-dimethylphenyl)-1H-pyrazole (8.19b): Prepared from m-xylene (490 µL, 4 mmol, 10.0 equiv) and pyrazole; 26.5 mg (38% yield, 14:1 **8.19a** to **8.19b** ratio) obtained as an intractable mixture following General Procedure D.

8.19a: ^{1}H NMR (500 MHz, $CDCl_3$) δ 7.70 (d, *J* = 1.8 Hz, 1H), 7.56 (d, *J* = 2.3 Hz, 1H), 7.20 (d, *J* = 7.9 Hz, 1H), 7.12 (d, *J* = 2.1 Hz, 1H), 7.10 – 7.04 (m, 1H), 6.42 (t, *J* = 2.1 Hz, 1H), 2.37 (s, 3H), 2.19 (s, 3H); consistent with reported spectra (*Angew. Chem. Int. Ed.,* **2019***, 58*, 13318–13322).

8.19b: ^{1}H NMR (500 MHz, $CDCl_3$) δ 7.74 (d, *J* = 1.9 Hz, 1H), 7.46 (d, *J* = 2.3 Hz, 1H), 7.25 – 7.22 (m, 2H), 7.14 (s, 1H), 6.45 (t, *J* = 2.1 Hz, 1H), 2.01 (s, 6H); consistent with reported spectra (*Angew. Chem. Int. Ed.,* **2019***, 58*, 13318–13322).

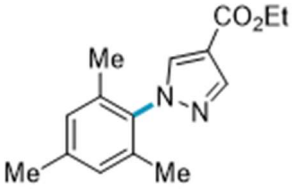

Ethyl 1-mesityl-1H-pyrazole-4-carboxylate (8.20): Prepared from mesitylene (278 µL, 2 mmol, 5.0 equiv) and ethyl 1H-pyrazole-4-carboxylate; 80.5 mg (78% yield) obtained following General Procedure D. **^{1}H NMR** (500 MHz, $CDCl_3$) δ 8.13 (s, 1H), 7.94 (s, 1H), 6.96 (s, 2H), 4.34 (q, J = 7.1 Hz, 2H), 2.35 (s, 3H), 1.99 (s, 6H), 1.38 (t, J = 7.1 Hz, 3H); consistent with reported spectra (*Angew. Chem. Int. Ed.,* **2019***, 58*, 13318–13322).

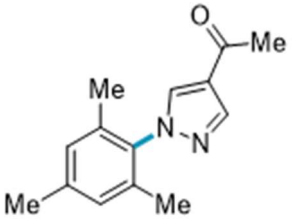

1-(1-mesityl-1H-pyrazol-4-yl)ethanone (8.21): Prepared from mesitylene (278 µL, 2 mmol, 5.0 equiv) and 1-(1H-pyrazol-4-yl)ethanone; 63.7 mg (70% yield) obtained following General Procedure D. **^{1}H NMR** (500 MHz, $CDCl_3$) δ 8.12 (s, 1H), 7.93 (s, 1H), 6.96 (s, 2H), 2.50 (s, 3H), 2.34 (s, 3H), 1.98 (s, 6H); consistent with reported spectra (*Angew. Chem. Int. Ed.,* **2019***, 58*, 13318–13322).

G16. NMR Spectra

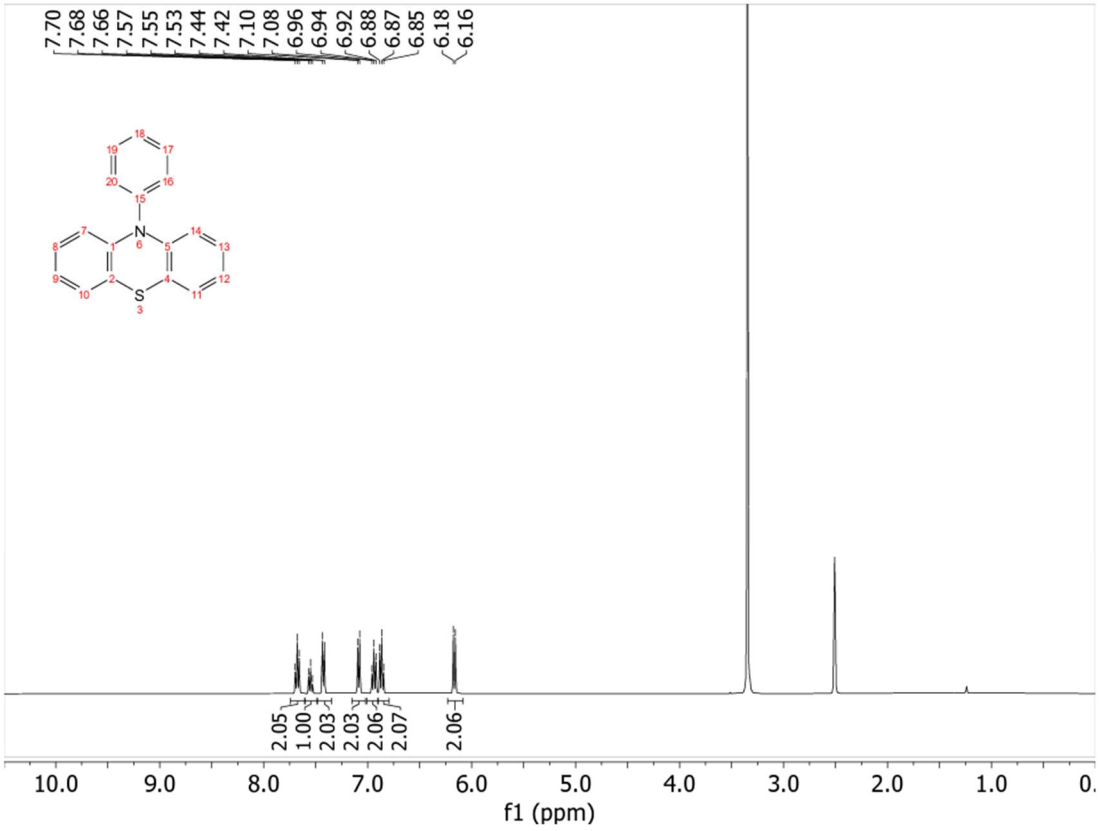

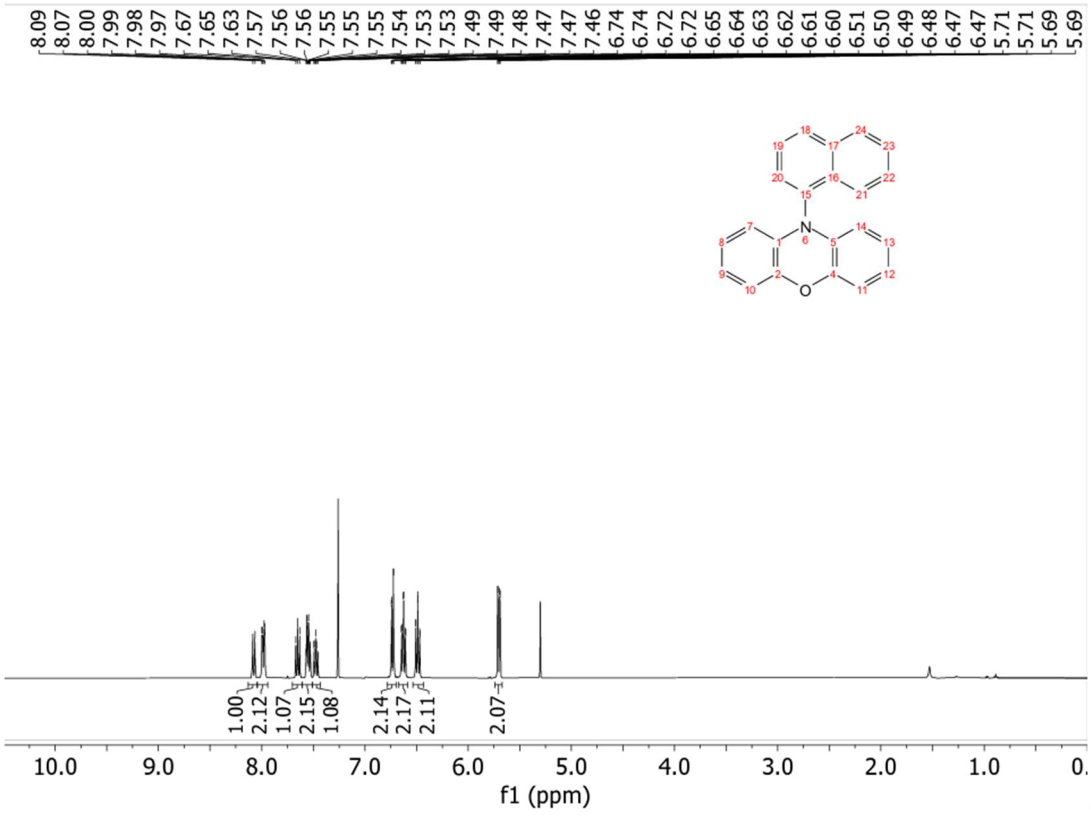

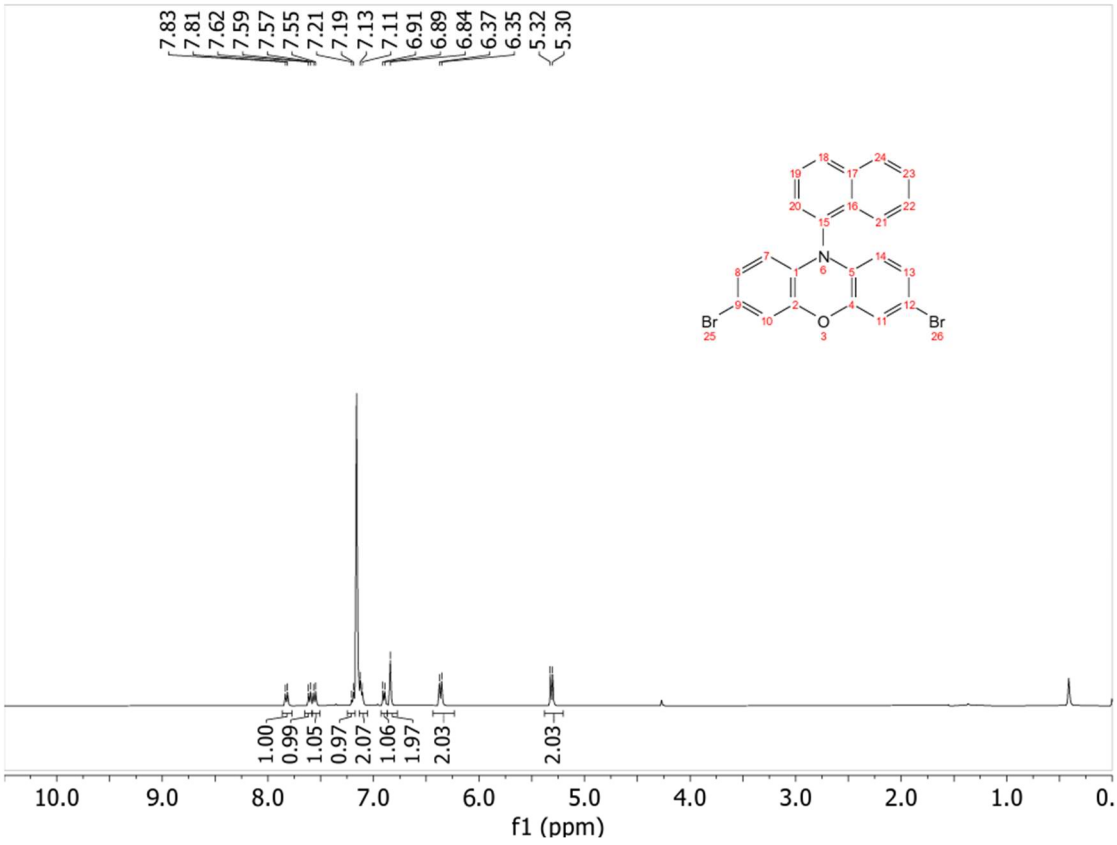
7.83
7.81
7.62
7.59
7.57
7.55
7.21
7.19
7.13
7.11
6.91
6.89
6.84
6.37
6.35
5.32
5.30
Br
Br
1.00
0.99
1.05
0.97
2.07
1.06
1.97
2.03
2.03
10.0
9.0
8.0
7.0
6.0
5.0
4.0
3.0
2.0
1.0
f1 (ppm)

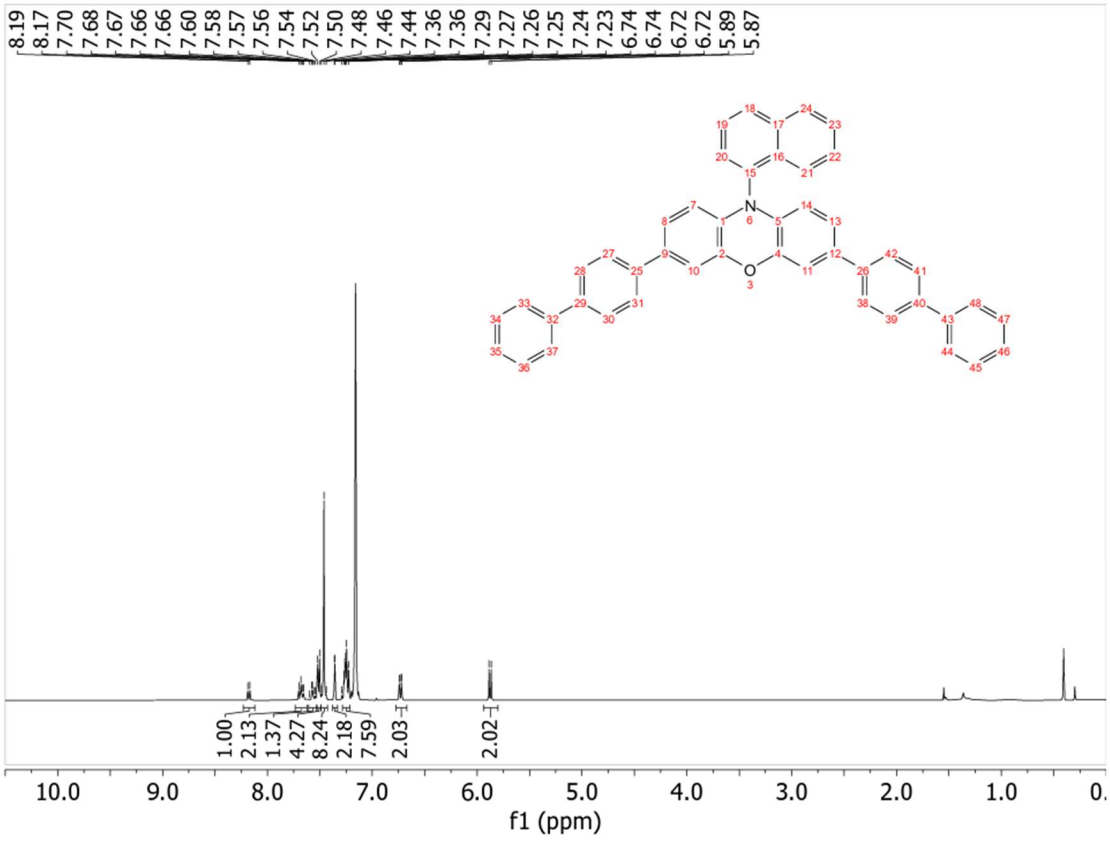
8.19
8.17
7.70
7.68
7.67
7.66
7.66
7.60
7.58
7.57
7.56
7.54
7.52
7.50
7.48
7.46
7.44
7.36
7.36
7.29
7.27
7.26
7.25
7.24
7.23
6.74
6.74
6.72
6.72
5.89
5.87
1.00
2.13
1.37
4.27
8.24
2.18
7.59
2.03
2.02
10.0
9.0
8.0
7.0
6.0
5.0
4.0
3.0
2.0
1.0
f1 (ppm)

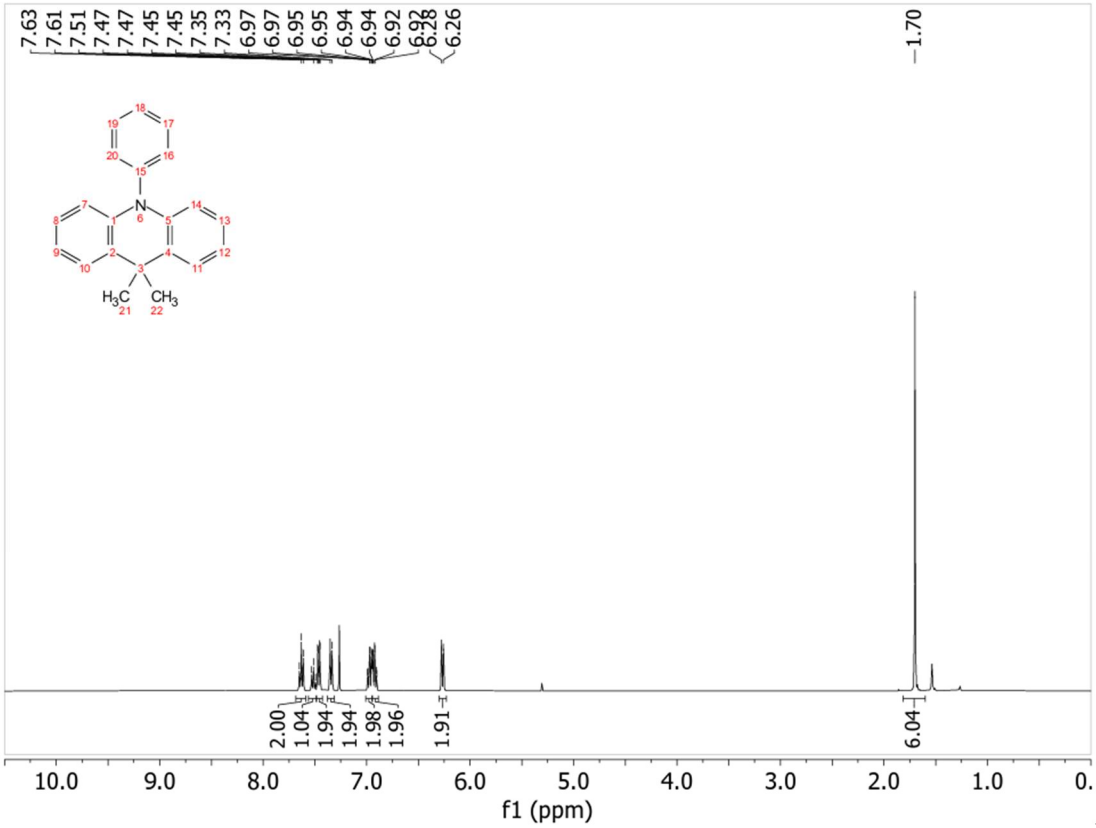
7.63
7.61
7.51
7.47
7.47
7.45
7.45
7.35
7.33
6.97
6.95
6.95
6.94
6.94
6.92
6.28
6.26
1.70
2.00
1.04
1.94
1.94
1.98
1.96
1.91
6.04
10.0
9.0
8.0
7.0
6.0
5.0
4.0
3.0
2.0
1.0
f1 (ppm)

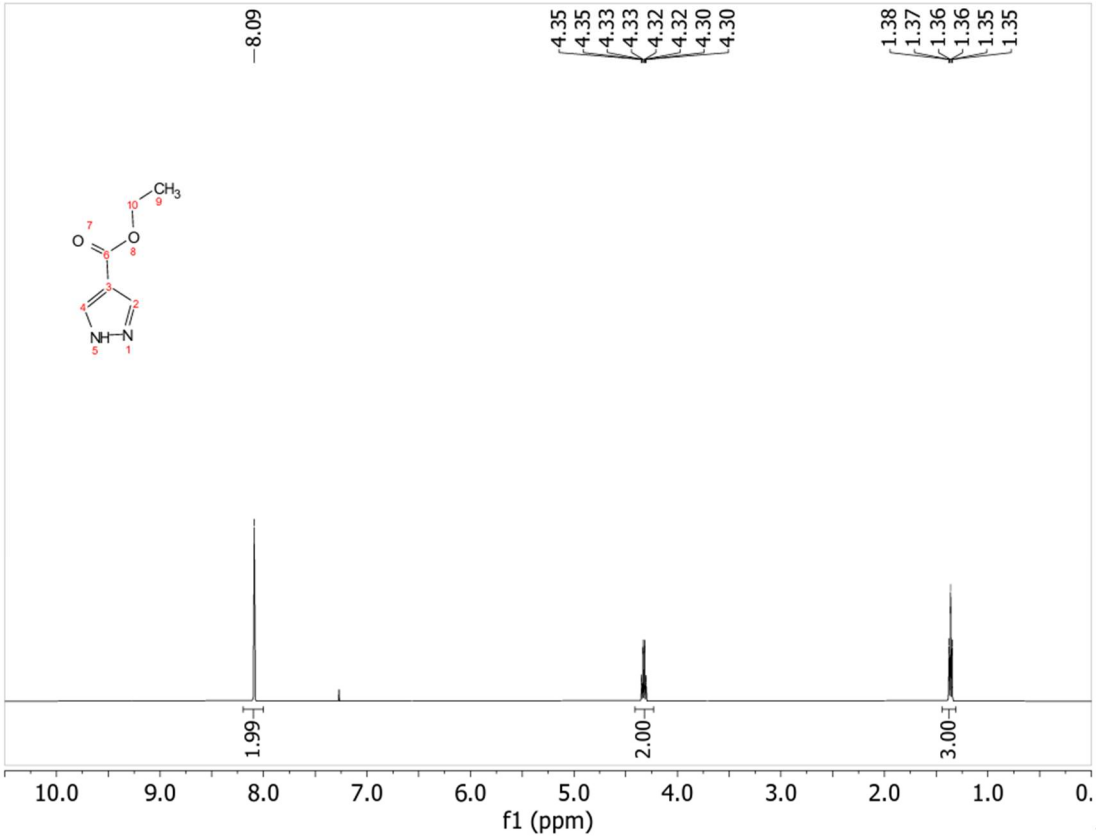
8.09
4.35
4.35
4.33
4.33
4.32
4.32
4.30
4.30
1.38
1.37
1.36
1.36
1.35
1.35
1.99
2.00
3.00
10.0
9.0
8.0
7.0
6.0
5.0
4.0
3.0
2.0
1.0
f1 (ppm)

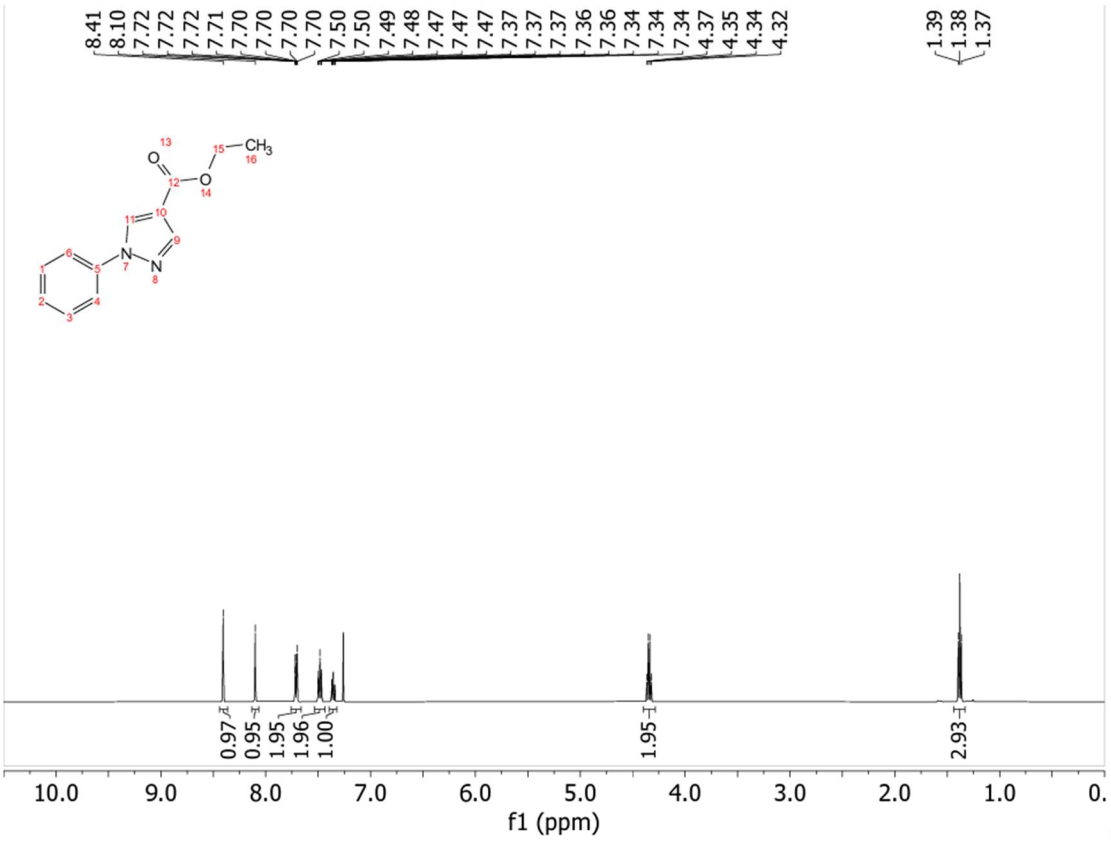
8.41
8.10
7.72
7.72
7.72
7.71
7.70
7.70
7.70
7.70
7.50
7.50
7.49
7.48
7.47
7.47
7.47
7.37
7.37
7.37
7.36
7.36
7.34
7.34
7.34
4.37
4.35
4.34
4.32
1.39
1.38
1.37
0.97
0.95
1.95
1.96
1.00
1.95
2.93
10.0
9.0
8.0
7.0
6.0
5.0
4.0
3.0
2.0
1.0
f1 (ppm)

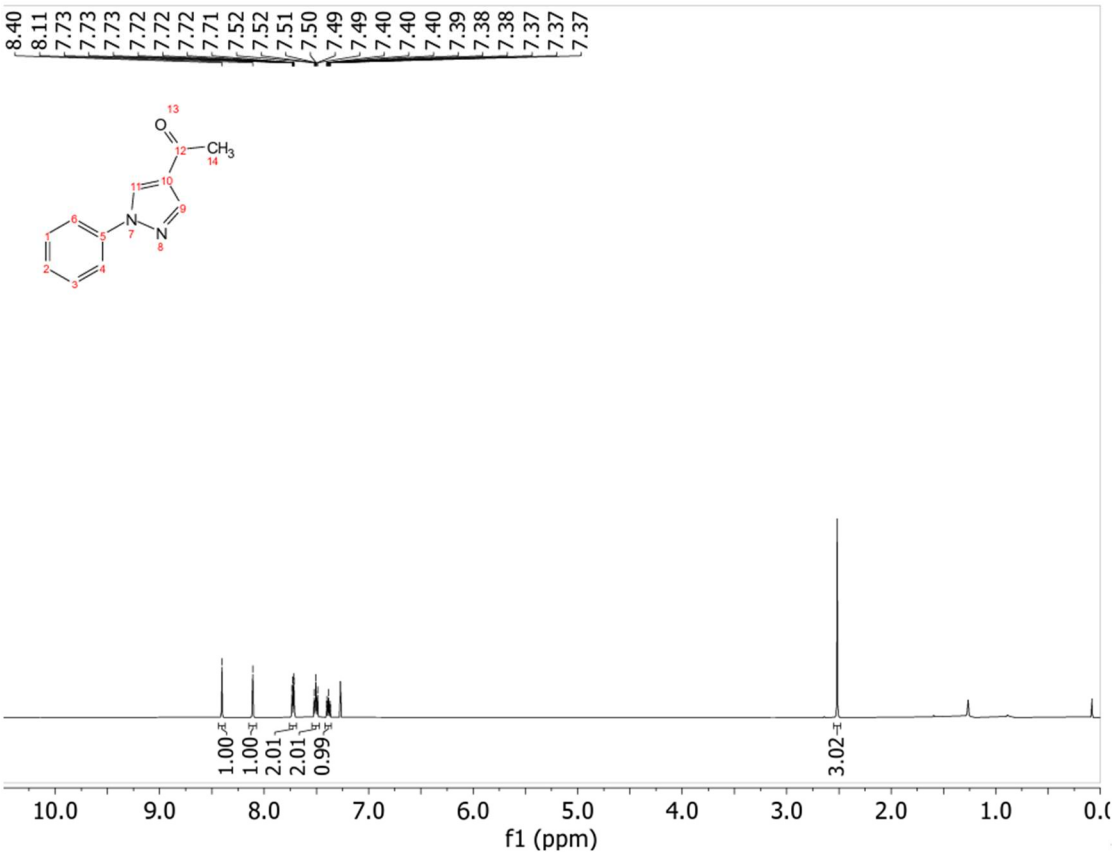
8.40
8.11
7.73
7.73
7.73
7.72
7.72
7.72
7.71
7.52
7.52
7.51
7.50
7.49
7.49
7.40
7.40
7.40
7.39
7.38
7.38
7.37
7.37
1.00
1.00
2.01
2.01
0.99
3.02
10.0
9.0
8.0
7.0
6.0
5.0
4.0
3.0
2.0
1.0
f1 (ppm)

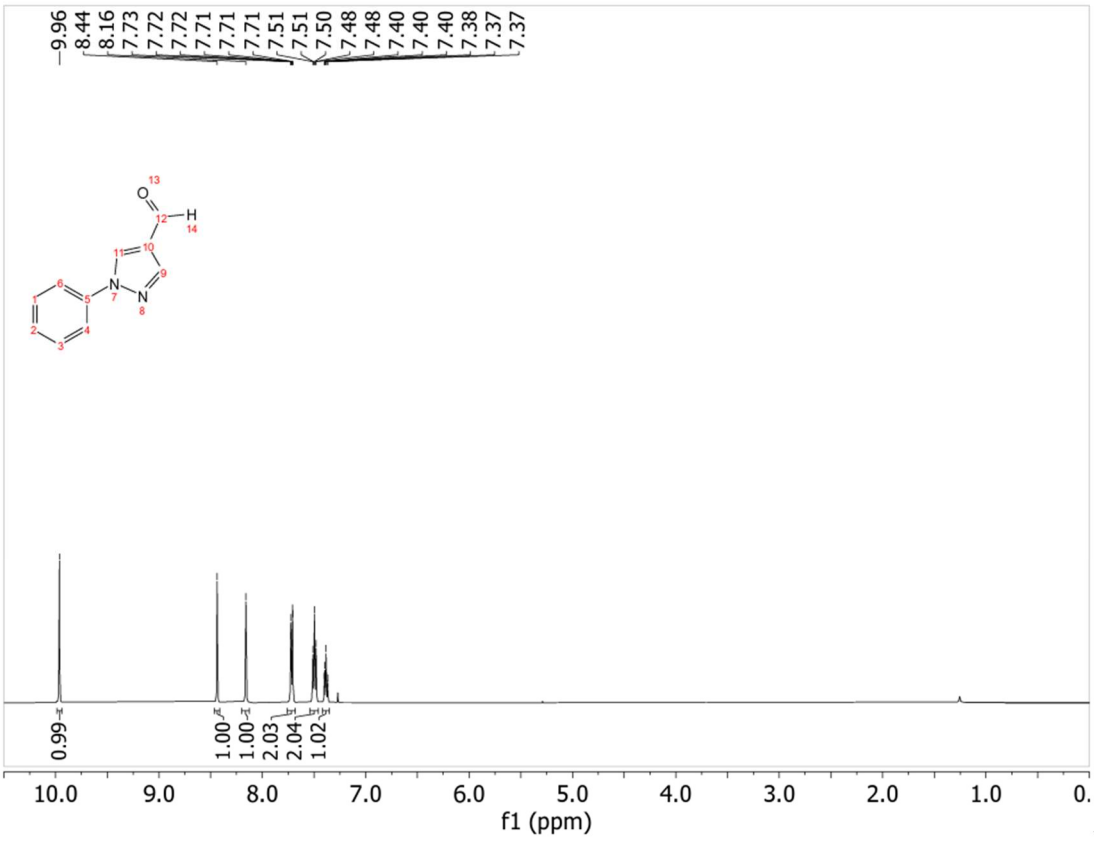
9.96
8.44
8.16
7.73
7.72
7.72
7.71
7.71
7.71
7.51
7.51
7.50
7.48
7.48
7.40
7.40
7.40
7.38
7.37
7.37
0.99
1.00
1.00
2.03
2.04
1.02
10.0
9.0
8.0
7.0
6.0
5.0
4.0
3.0
2.0
1.0
f1 (ppm)

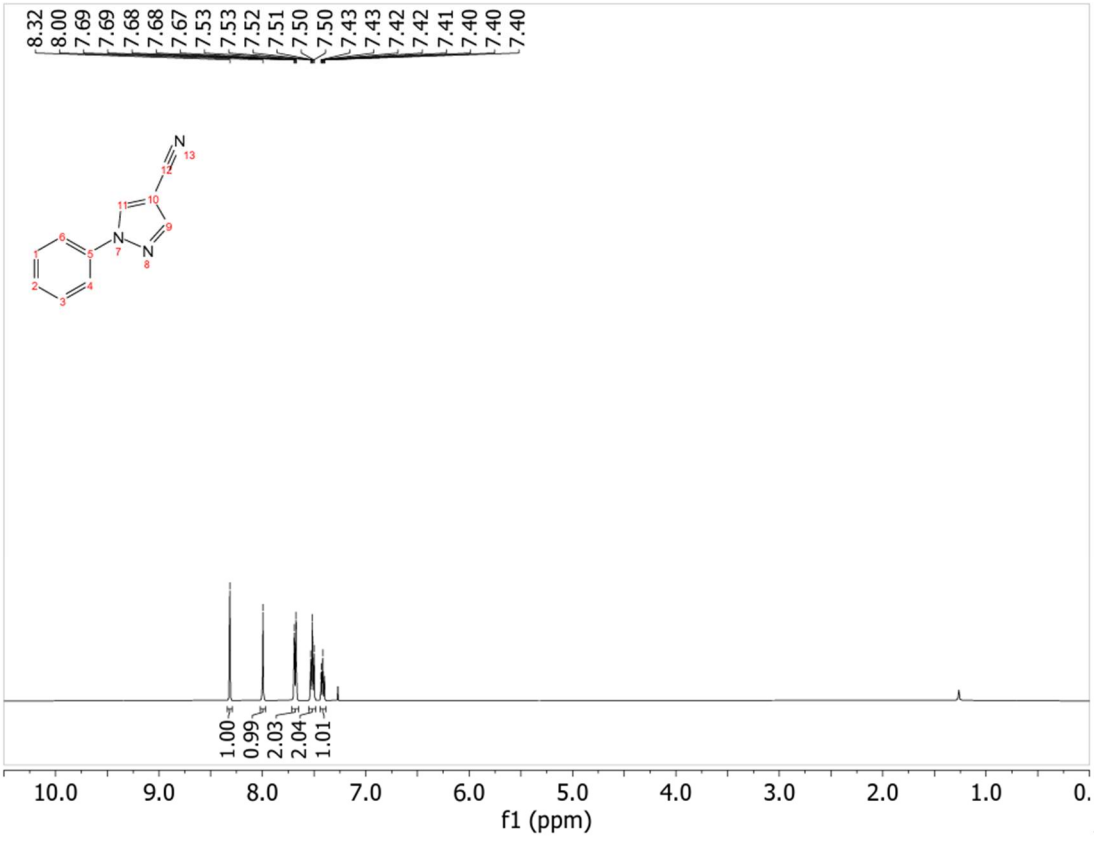
8.32
8.00
7.69
7.69
7.68
7.68
7.67
7.53
7.53
7.52
7.51
7.50
7.50
7.43
7.43
7.42
7.42
7.41
7.40
7.40
1.00
0.99
2.03
2.04
1.01
10.0
9.0
8.0
7.0
6.0
5.0
4.0
3.0
2.0
1.0
f1 (ppm)

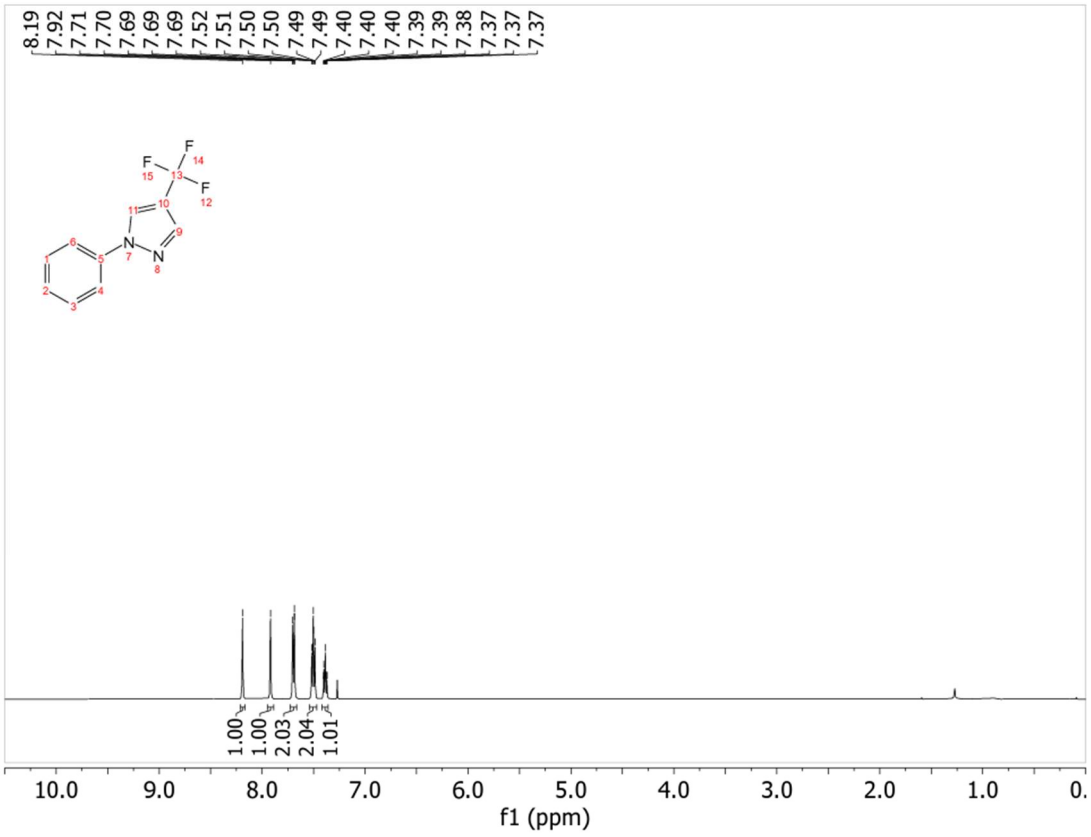
8.19
7.92
7.71
7.70
7.69
7.69
7.69
7.52
7.51
7.50
7.50
7.49
7.49
7.40
7.40
7.40
7.39
7.39
7.38
7.37
7.37
7.37
F
F
F
1.00
1.00
2.03
2.04
1.01
10.0
9.0
8.0
7.0
6.0
5.0
4.0
3.0
2.0
1.0
f1 (ppm)

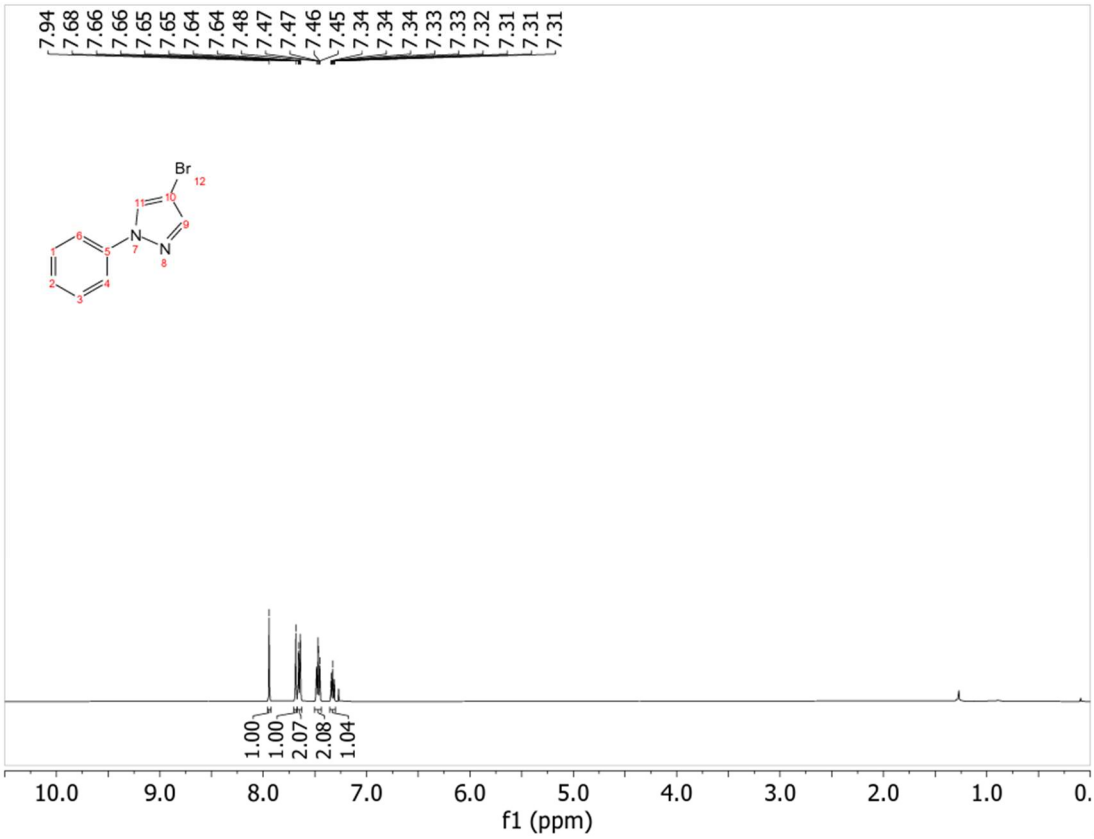
7.94
7.68
7.66
7.66
7.65
7.65
7.64
7.64
7.48
7.47
7.47
7.46
7.45
7.34
7.34
7.34
7.33
7.33
7.32
7.31
7.31
7.31
Br
1.00
1.00
2.07
2.08
1.04
10.0
9.0
8.0
7.0
6.0
5.0
4.0
3.0
2.0
1.0
f1 (ppm)

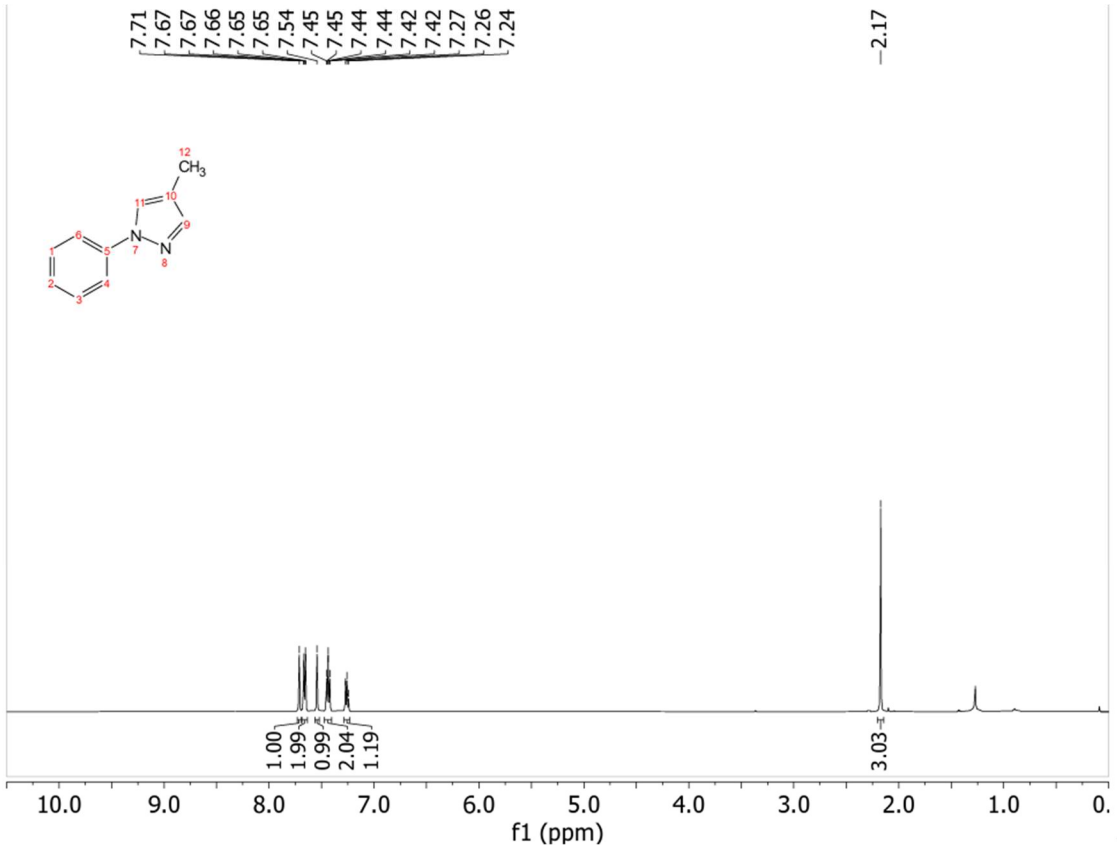
7.71
7.67
7.67
7.66
7.65
7.65
7.54
7.45
7.45
7.44
7.44
7.42
7.42
7.27
7.26
7.24
2.17
12
CH3
10
11
9
6
5
N
7
N
8
1
2
3
4
1.00
1.99
0.99
2.04
1.19
3.03
10.0
9.0
8.0
7.0
6.0
5.0
4.0
3.0
2.0
1.0
0.
f1 (ppm)

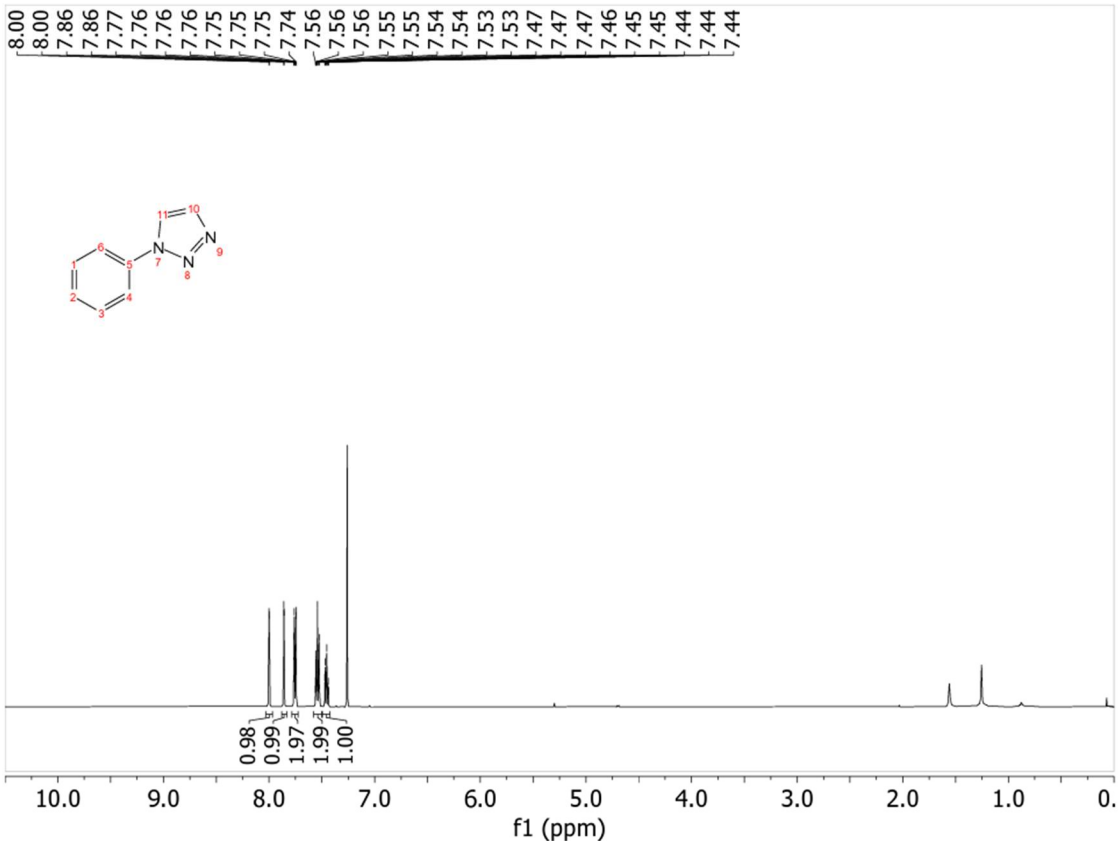
8.00
8.00
7.86
7.86
7.77
7.76
7.76
7.76
7.75
7.75
7.75
7.74
7.56
7.56
7.56
7.55
7.55
7.54
7.54
7.53
7.53
7.47
7.47
7.47
7.46
7.45
7.45
7.44
7.44
7.44
10
11
9
6
5
N
7
N
8
1
2
3
4
0.98
0.99
1.97
1.99
1.00
10.0
9.0
8.0
7.0
6.0
5.0
4.0
3.0
2.0
1.0
0.
f1 (ppm)

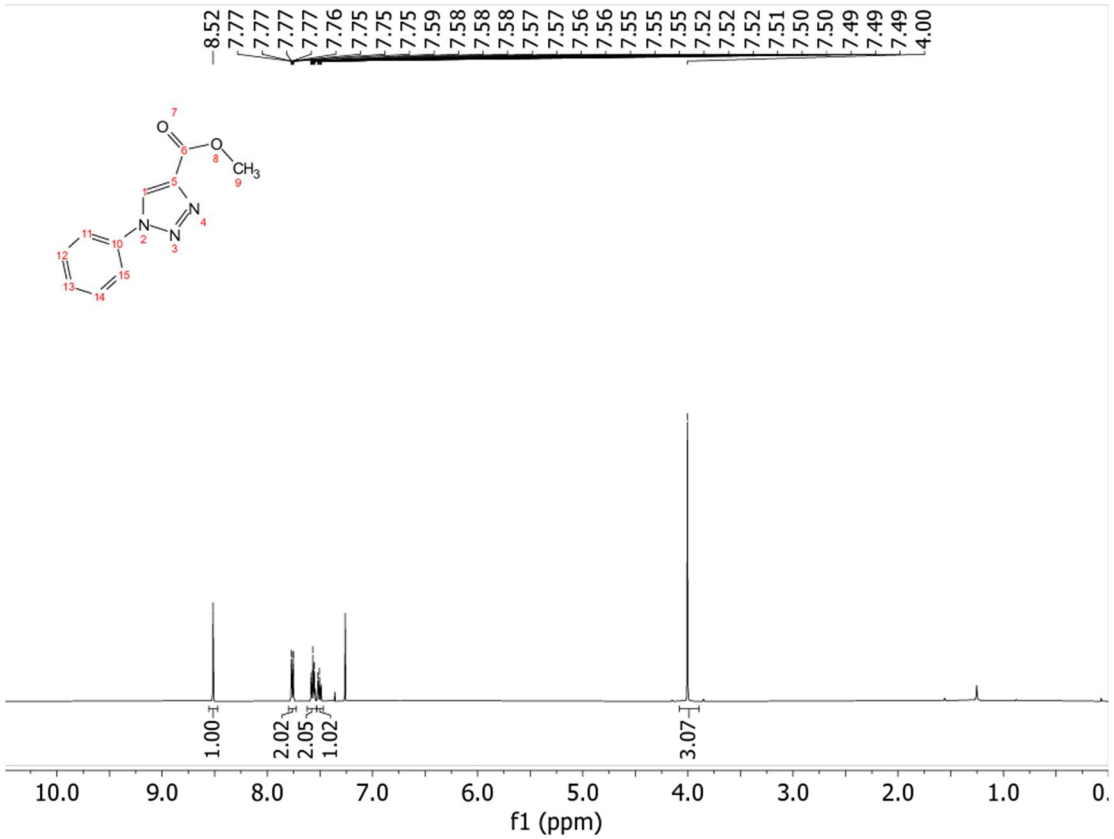
8.52
7.77
7.77
7.77
7.77
7.76
7.75
7.75
7.75
7.59
7.58
7.58
7.58
7.57
7.57
7.56
7.56
7.55
7.55
7.55
7.52
7.52
7.52
7.51
7.50
7.50
7.49
7.49
7.49
4.00
1.00
2.02
2.05
1.02
3.07
10.0
9.0
8.0
7.0
6.0
5.0
4.0
3.0
2.0
1.0
f1 (ppm)

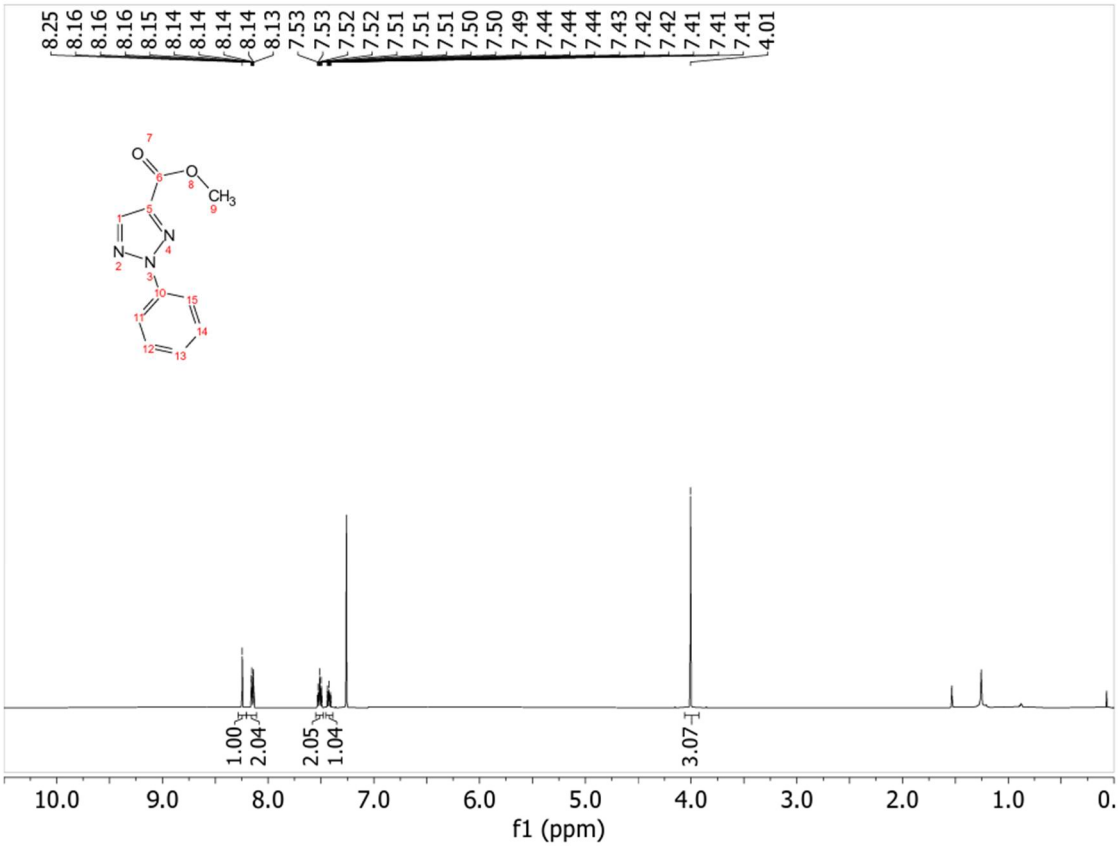
8.25
8.16
8.16
8.16
8.15
8.14
8.14
8.14
8.14
8.13
7.53
7.53
7.52
7.52
7.51
7.51
7.51
7.50
7.50
7.49
7.44
7.44
7.44
7.43
7.42
7.42
7.41
7.41
7.41
4.01
1.00
2.04
2.05
1.04
3.07
10.0
9.0
8.0
7.0
6.0
5.0
4.0
3.0
2.0
1.0
f1 (ppm)

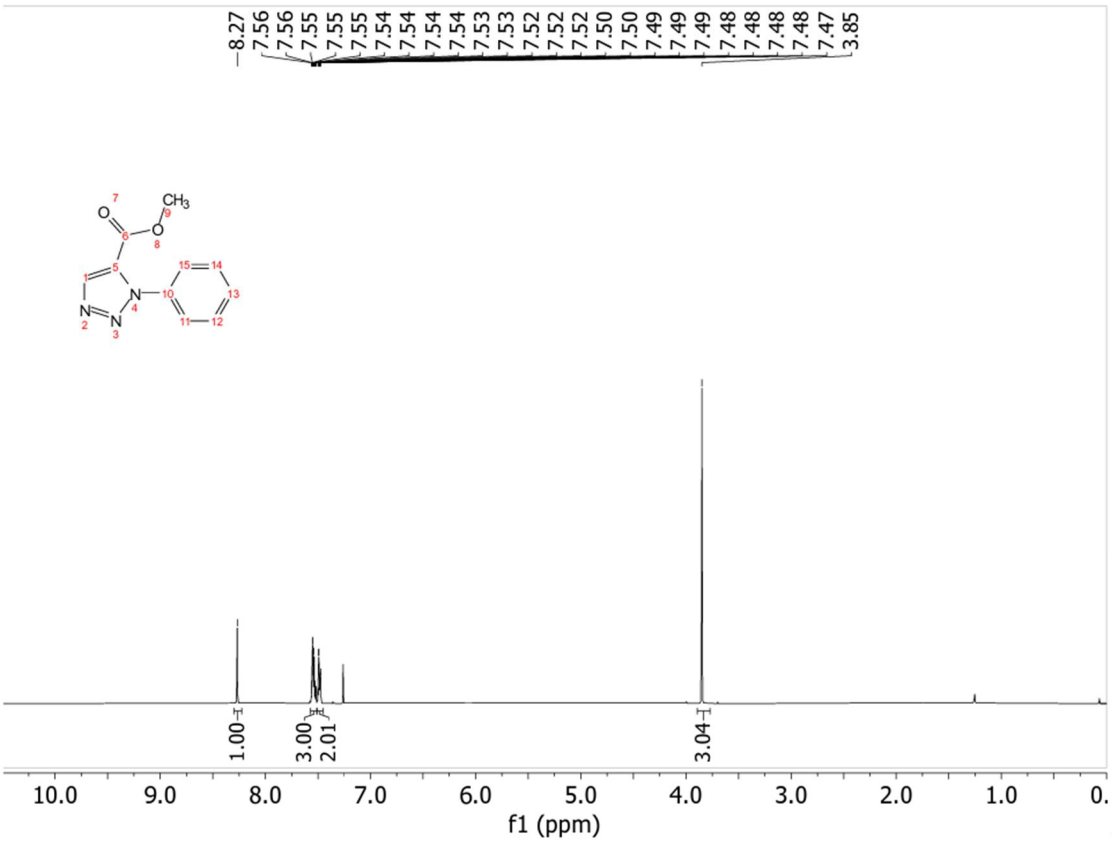
8.27
7.56
7.56
7.55
7.55
7.55
7.54
7.54
7.54
7.54
7.53
7.53
7.52
7.52
7.52
7.50
7.50
7.49
7.49
7.49
7.48
7.48
7.48
7.47
3.85
1.00
3.00
2.01
3.04
10.0
9.0
8.0
7.0
6.0
5.0
4.0
3.0
2.0
1.0
0.
f1 (ppm)

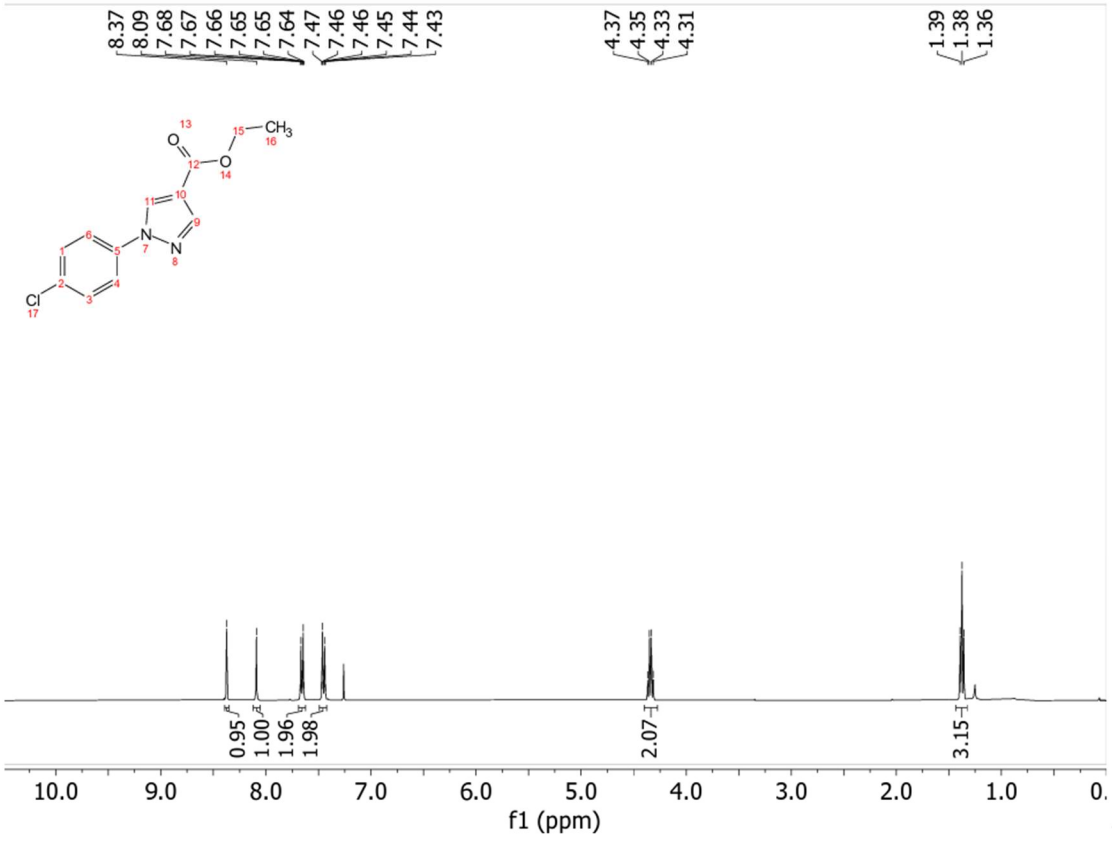
8.37
8.09
7.68
7.67
7.66
7.65
7.65
7.64
7.47
7.46
7.46
7.45
7.44
7.43
4.37
4.35
4.33
4.31
1.39
1.38
1.36
0.95
1.00
1.96
1.98
2.07
3.15
10.0
9.0
8.0
7.0
6.0
5.0
4.0
3.0
2.0
1.0
0.
f1 (ppm)

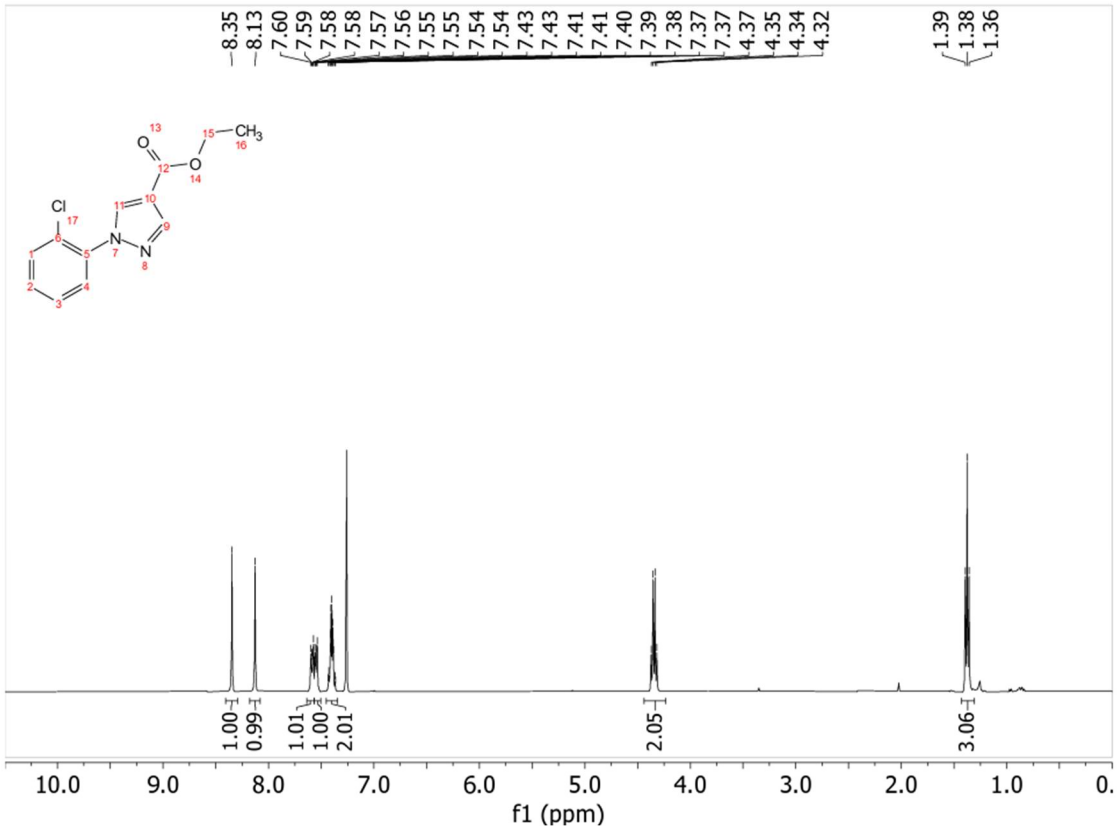
8.35
8.13
7.60
7.59
7.58
7.58
7.57
7.56
7.55
7.55
7.54
7.54
7.43
7.43
7.41
7.41
7.40
7.39
7.38
7.37
7.37
4.37
4.35
4.34
4.32
1.39
1.38
1.36
Cl
1.00
0.99
1.01
1.00
2.01
2.05
3.06
10.0
9.0
8.0
7.0
6.0
5.0
4.0
3.0
2.0
1.0
f1 (ppm)

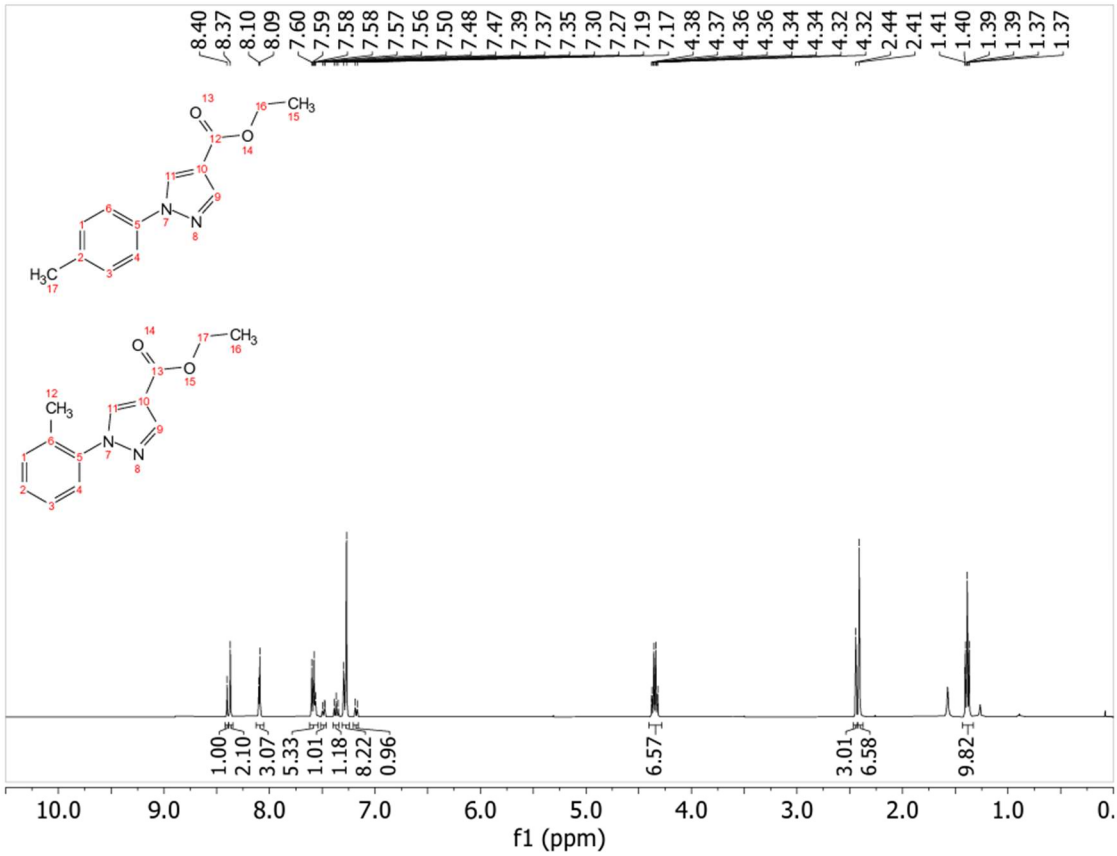
8.40
8.37
8.10
8.09
7.60
7.59
7.58
7.58
7.57
7.56
7.50
7.48
7.47
7.39
7.37
7.35
7.30
7.27
7.19
7.17
4.38
4.37
4.36
4.36
4.34
4.34
4.32
4.32
2.44
2.41
1.41
1.40
1.39
1.39
1.37
1.37
H3C
CH3
1.00
2.10
3.07
5.33
1.01
1.18
8.22
0.96
6.57
3.01
6.58
9.82
10.0
9.0
8.0
7.0
6.0
5.0
4.0
3.0
2.0
1.0
f1 (ppm)

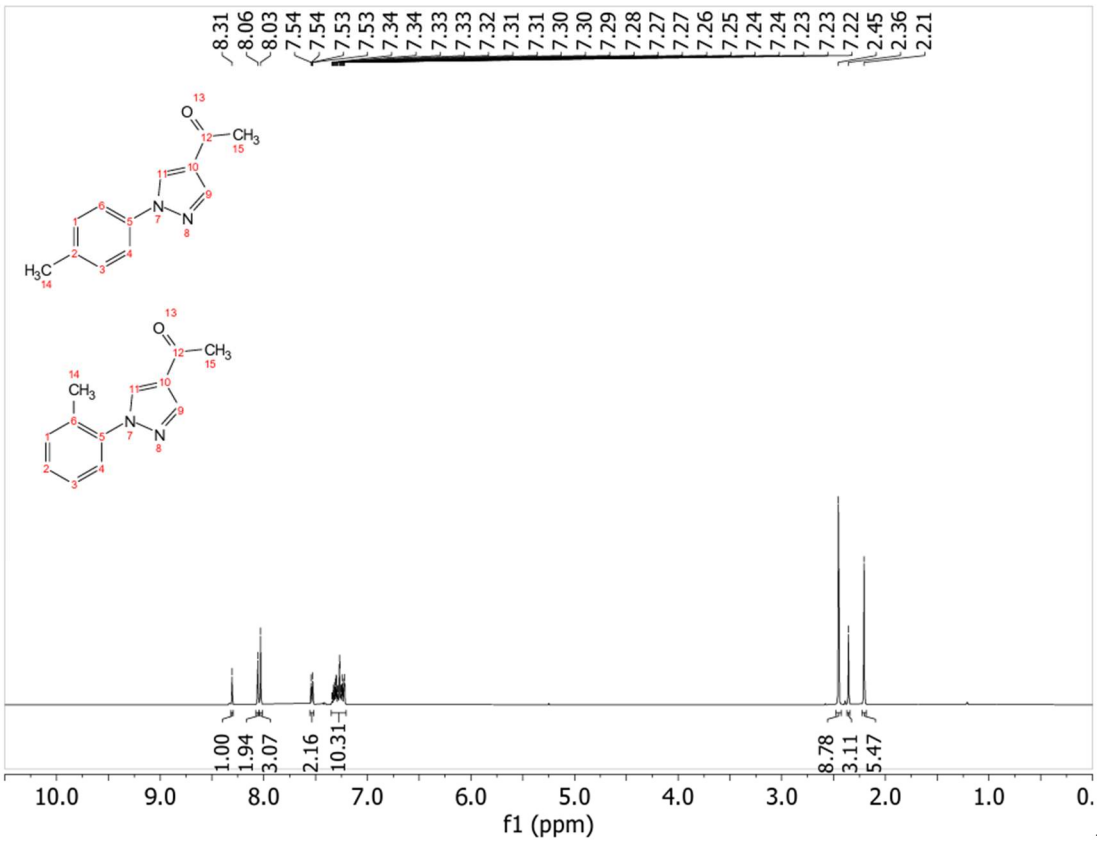
8.31
8.06
8.03
7.54
7.54
7.53
7.53
7.34
7.34
7.33
7.33
7.32
7.31
7.31
7.30
7.30
7.29
7.28
7.27
7.27
7.26
7.25
7.24
7.24
7.23
7.23
7.22
2.45
2.36
2.21
1.00
1.94
3.07
2.16
10.31
8.78
3.11
5.47
10.0
9.0
8.0
7.0
6.0
5.0
4.0
3.0
2.0
1.0
f1 (ppm)

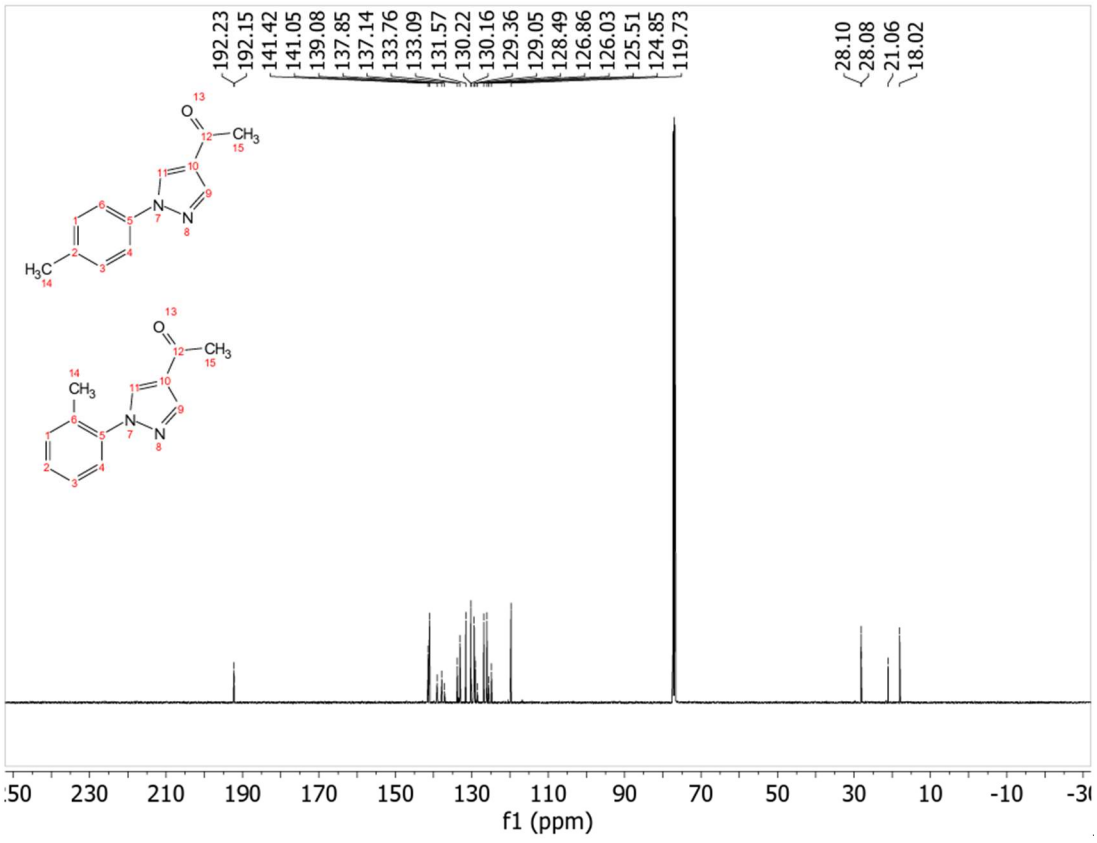
192.23
192.15
141.42
141.05
139.08
137.85
137.14
133.76
133.09
131.57
130.22
130.16
129.36
129.05
128.49
126.86
126.03
125.51
124.85
119.73
28.10
28.08
21.06
18.02
230
210
190
170
150
130
110
90
70
50
30
10
-10
f1 (ppm)

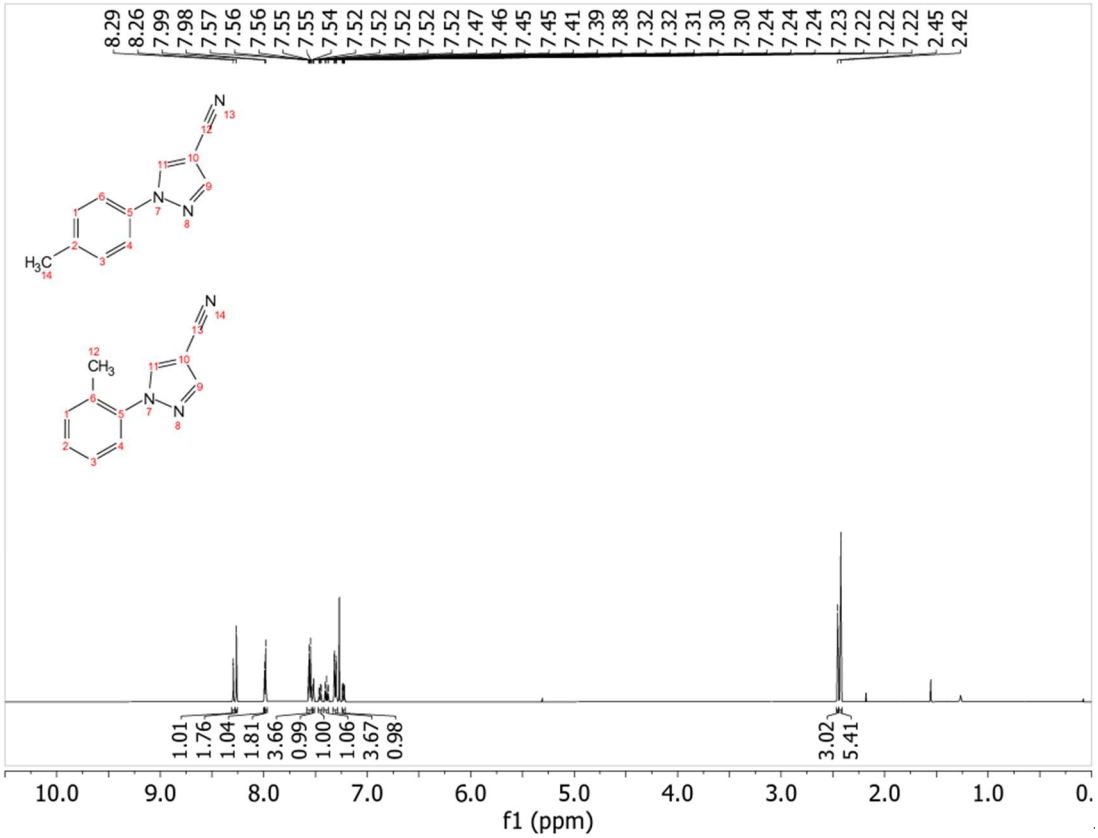
8.29
8.26
7.99
7.98
7.57
7.56
7.56
7.55
7.55
7.54
7.52
7.52
7.52
7.52
7.52
7.47
7.46
7.45
7.45
7.41
7.39
7.38
7.32
7.32
7.31
7.30
7.30
7.24
7.24
7.24
7.23
7.22
7.22
7.22
2.45
2.42
1.01
1.76
1.04
1.81
3.66
0.99
1.00
1.06
3.67
0.98
3.02
5.41
10.0
9.0
8.0
7.0
6.0
5.0
4.0
3.0
2.0
1.0
f1 (ppm)

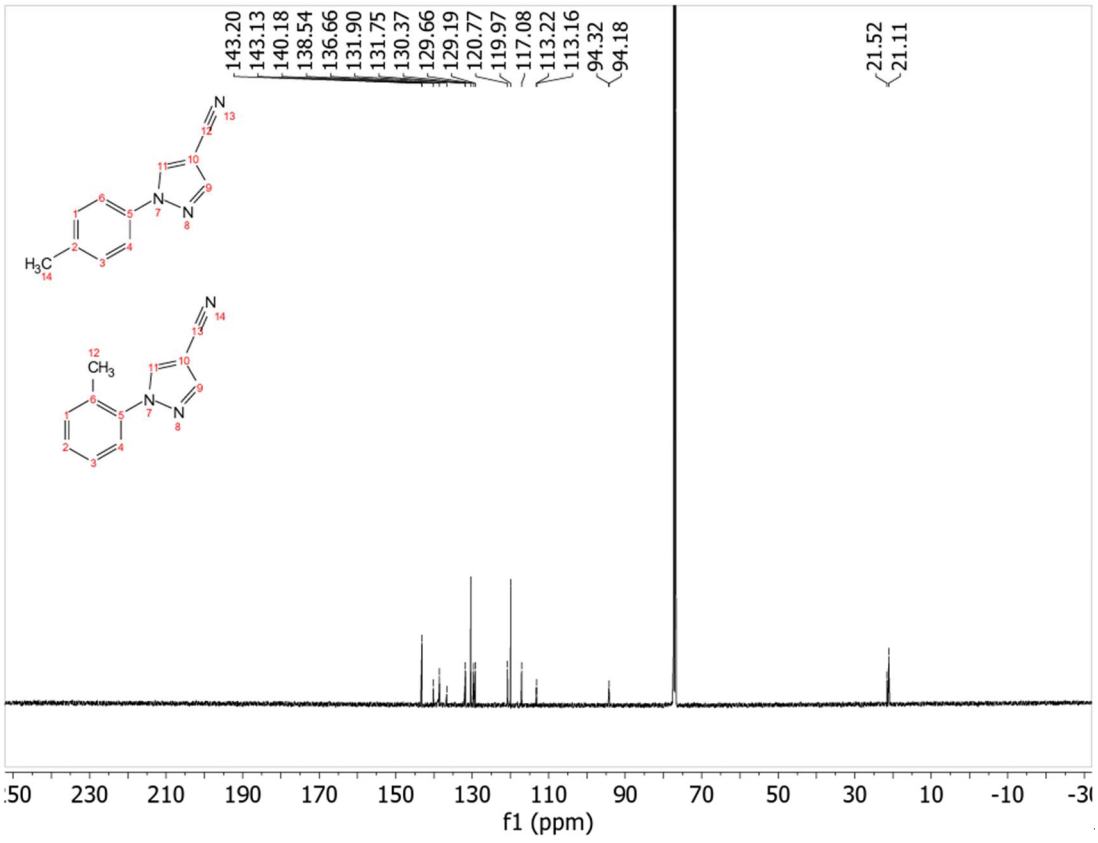
143.20
143.13
140.18
138.54
136.66
131.90
131.75
130.37
129.66
129.19
120.77
119.97
117.08
113.22
113.16
94.32
94.18
21.52
21.11
230
210
190
170
150
130
110
90
70
50
30
10
-10
f1 (ppm)

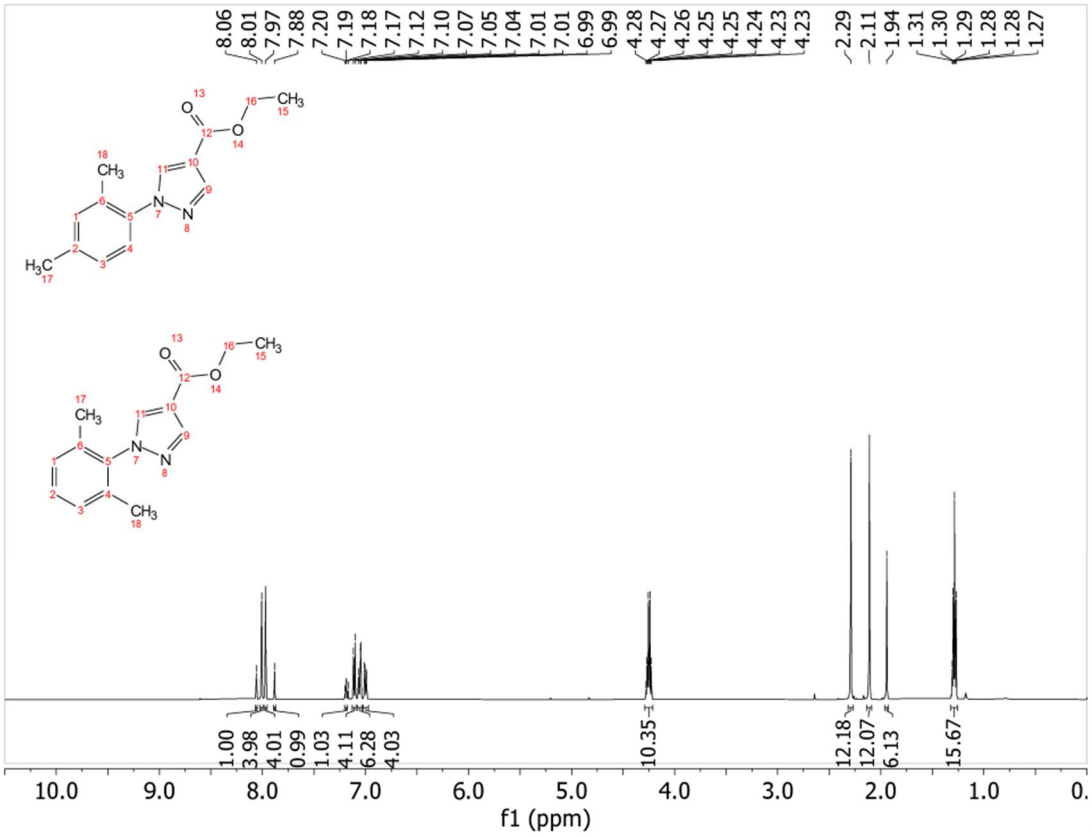
8.06
8.01
7.97
7.88
7.20
7.19
7.18
7.17
7.12
7.10
7.07
7.05
7.04
7.01
7.01
6.99
6.99
4.28
4.27
4.26
4.25
4.25
4.24
4.23
4.23
2.29
2.11
1.94
1.31
1.30
1.29
1.28
1.28
1.27
1.00
3.98
4.01
0.99
1.03
4.11
6.28
4.03
10.35
12.18
12.07
6.13
15.67
10.0
9.0
8.0
7.0
6.0
5.0
4.0
3.0
2.0
1.0
f1 (ppm)

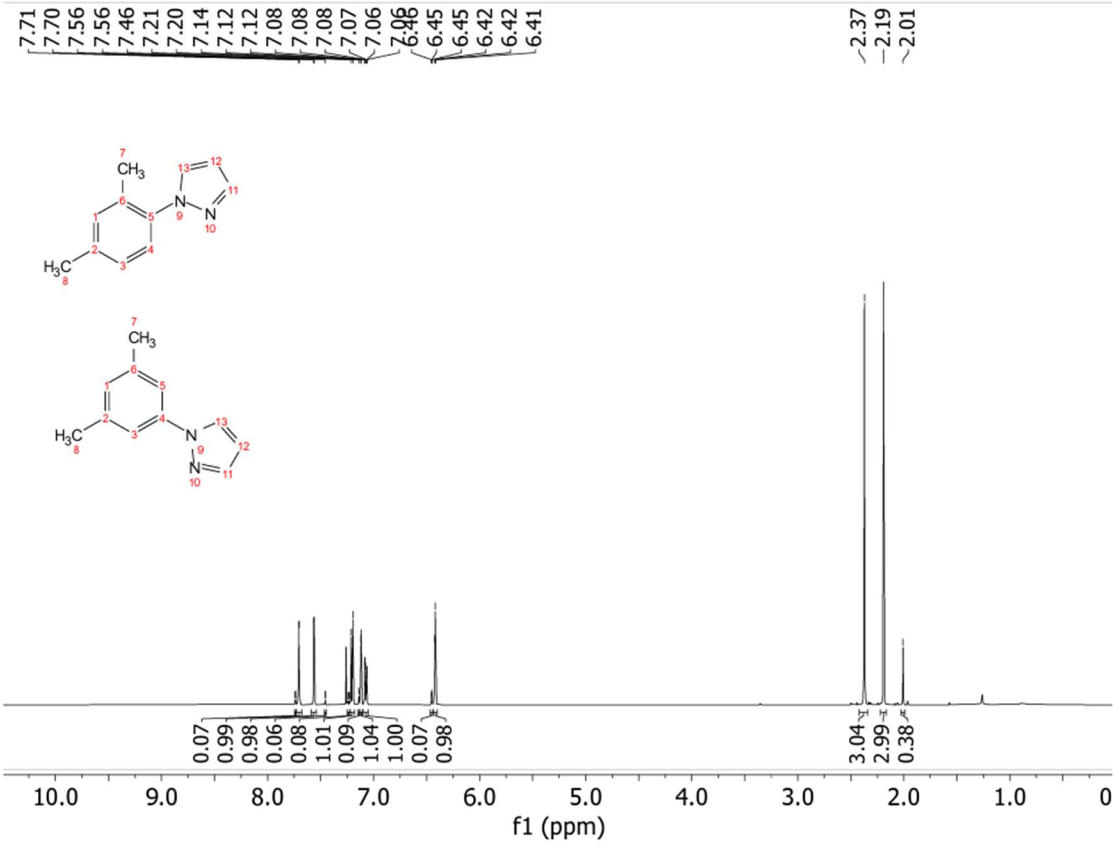
7.71
7.70
7.56
7.56
7.46
7.21
7.20
7.14
7.12
7.12
7.08
7.08
7.08
7.07
7.06
6.45
6.45
6.42
6.42
6.41
2.37
2.19
2.01
0.07
0.99
0.98
0.06
0.08
1.01
0.09
1.04
1.00
0.07
0.98
3.04
2.99
0.38
10.0
9.0
8.0
7.0
6.0
5.0
4.0
3.0
2.0
1.0
0
f1 (ppm)

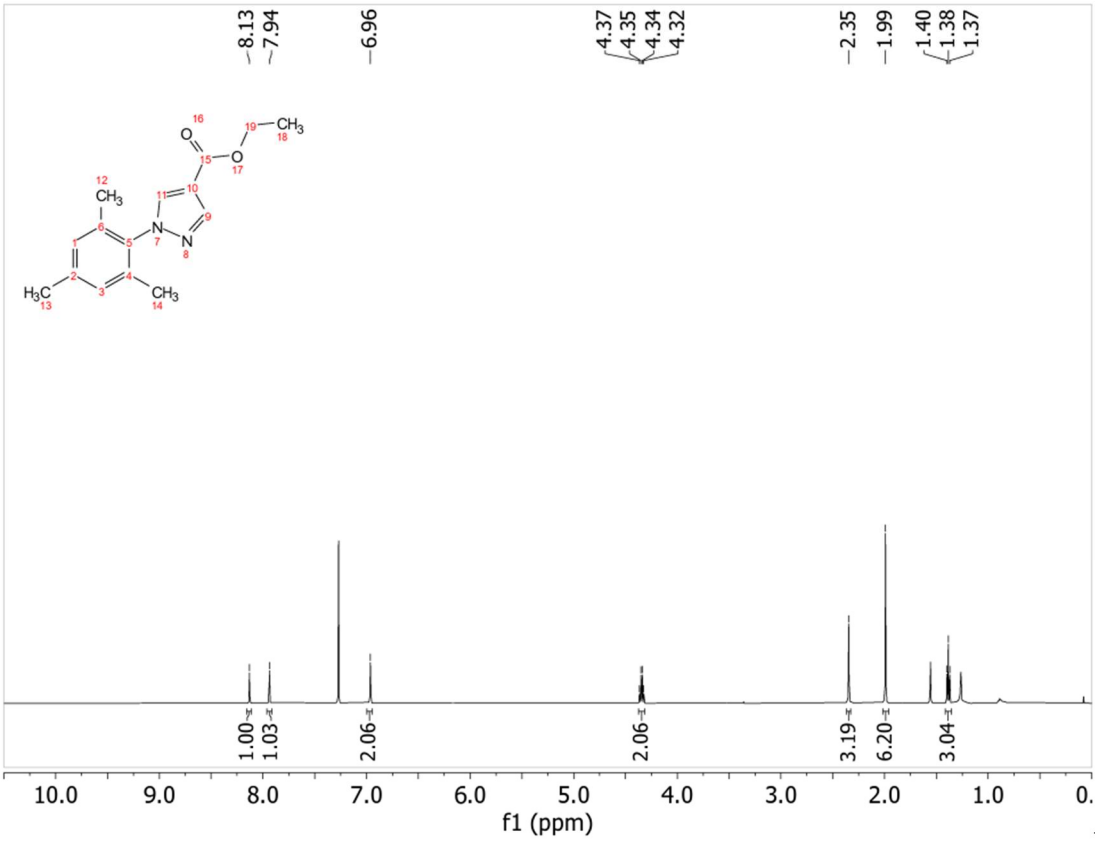
8.13
7.94
6.96
4.37
4.35
4.34
4.32
2.35
1.99
1.40
1.38
1.37
1.00
1.03
2.06
2.06
3.19
6.20
3.04
10.0
9.0
8.0
7.0
6.0
5.0
4.0
3.0
2.0
1.0
f1 (ppm)

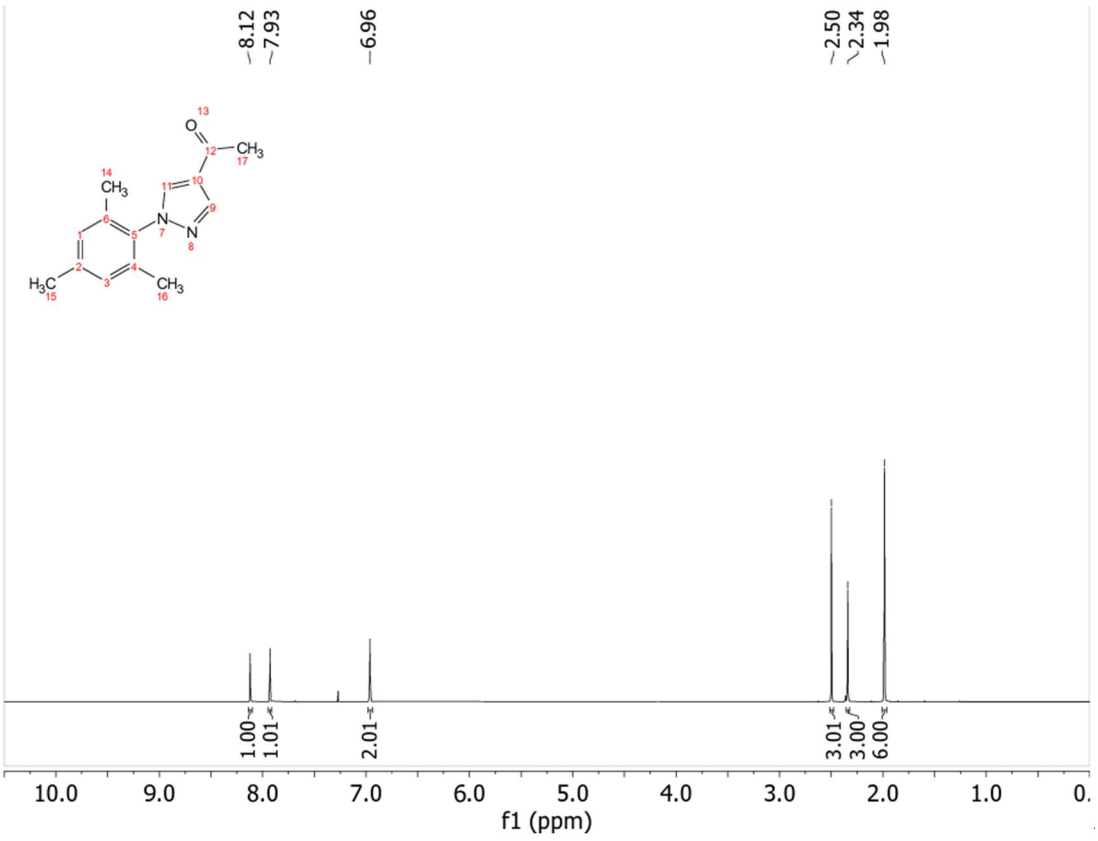
8.12
7.93
6.96
2.50
2.34
1.98
1.00
1.01
2.01
3.01
3.00
6.00
10.0
9.0
8.0
7.0
6.0
5.0
4.0
3.0
2.0
1.0
f1 (ppm)